SPONSORS

Main Sponsor

Philips Medical Systems

PHILIPS

Sponsors

Development Corporation City of Rotterdam (OBR)

OBR
Development Corporation
City of Rotterdam

Port of Rotterdam Authority

Port of Rotterdam
Havenbedrijf Rotterdam N.V.

Boston Scientific

Boston Scientific

OLDelft

Oldelft Ultrasound

Special Grants

Interuniversity Cardiology Institute of the Netherlands (ICIN)

ICIN

The Dutch Foundation for Ultrasound in Medicine & Biology (SUGB)

SUGB

TABLE OF CONTENTS

SYMPOSIUM ORGANIZING COMMITTEE

General Chair

Ton van der Steen
Erasmus University Medical Centre, Rotterdam, The Netherlands
a.vandersteen@erasmusmc.nl

Technical Program Chair

John Hossack
University of Virginia, Charlottesville, VA, USA
hossack@ieee.org

Short Course/Tutorial Chair

Nico de Jong
Erasmus University Medical Centre, Rotterdam, The Netherlands
n.dejong@erasmusmc.ml

Finance Chair

Herman van de Vaart
vdv@ieee.org

Publicity Chair

Sorah Rhee
MEGGITT Endevco, San Juan, Capistrano, CA, USA
soray.rhee@ieee.org

Editorial Chair

Marj Yuhas
Industrial Measurement Systems Inc., Aurora, IL USA
myuhas@imsysinc.com

Exhibit/Sponsor Chair

Chris de Korte
Nijmegen University Medical Centre, Nijmegen, The Netherlands
cldekorte@ieee.org

Awards Chair

Reinhard Lerch
Friedrich-Alexander-Universitat, Erlangen, Germany
reinhard.lerch@lse.eei.uni-erlangen.de

TECHNICAL PROGRAM COMMITTEE

GROUP 1: Medical Ultrasonics

Vice Chair: **Stanislav Emelianov**: University of Texas of Austin, USA
Olivier Basset: INSA, France
Geneviève Berger: Laboratorie Imagerie Parametrique, France
Richard Chiao: Ultrasound Group, Siemens Medical Solutions, USA
Lawrence A. Crum: University of Washington, USA
Emad Ebbini: University of Minnesota, USA
Helmut Emert: Electrical Engineering Department, Ruhr University, Germany
David Evans: Department of Medical Physics, Leicester Royal Infirmary, UK
Kathy Ferrara: Biomedical Engineering, University of California, USA
Stuart Foster: Department of Medical Physics, Sunnybrook Health Sciences Centre, Canada
James Greenleaf: Ultrasound Research, Mayo Clinic, USA
John Hossack, Department of Biomedical Engineering, School of Engineering & Applied Sciences, University of Virginia, USA
Kullervo Hynynen: Brigham and Women's Hospital, USA
Peter Hoskins: Senior Research Fellow, Medical Physics, The University of Edinburgh, Scotland
Michael F. Insana: Biomedical Engineering, University of California, USA
Jorgen Jensen: Department of Information Technology, Technical University of Denmark
Nico de Jong: Biomedical Engineering, Erasmus University Rotterdam, The Netherlands
Hiroshi Kanai: Tohoku University, Japan
Jian-yu Lu: The University of Toledo, USA
Leonardo Masotti: Dipartimento di Ingegneria Elettronica, University di Firenze, Italy
James G. Miller: Physics Department, Washington University, USA
Kathy Nightingale: Biomedical Engineering Department, Duke University, USA
William O'Brien: Director of Bioacoustics Research Lab, Department of Electrical & Computer Engineering, University of Illinois, USA
Helen Routh: Philips Research, USA
Ton van der Steen: Head of Biomedical Engineering, Erasmus University Rotterdam, The Netherlands

Tom Thomas: Siemens
Kai Thomenius: GE CRD, USA
Peirro Tortoli: Electronic Engineering Department, University of Florence, Italy
Keith Wear: FDA Center for Devices and Radiological Health, USA

GROUP 2: Sensors, NDE, and Industrial Applications

Vice Chair: **Jafar Saniie**: Department of Electrical & Computer Engineering, Illinois Institute of Technology, USA
Robert C. Addison: Rockwell Science Center, USA
Walter Arnold: Fraunhofer Institute for Nondestructive Testing, Germany
Narendra K. Batra
Eric S. Furgason: School of Electrical & Computer Engineering, Purdue University, USA
Donna C. Hurley: National Institute of Standards & Technology, USA
David A. Hutchins: School of Engineering, University of Warwick, England
Bernhard Jakoby: Institute of Industrial Electronics and Material Science, Vienna University of Technology, Austria
Lawrence W. Kessler: Sonoscan Inc., USA
Pierre T. Khuri-Yakub: Stanford University, USA
Jun-ishi Kushibike: Department of Electrical Engineering, Graduate School of Engineering, Tohoku University, Japan
Lawrence C. Lynnworth: Chief Technologist, GE Panametrics, USA
Roman Gr. Maev: Professor & Director, Center for Imaging Research & Advanced Material Characterization, Department of Physics, University of Windsor, Canada
Massimo Pappalardo: Lab of Acustoelectronics, Dipartimento di Ingegneria Elettronica, University di Roma TRE, Italy
Tony Sinclair: Professor of Mechanical & Industrial Engineering, Department of Mechanical Engineering, University of Toronto, Canada
Bernhard R. Tittman: Department of Engineering & Mechanics, Pennsylvania State University, USA
Jiromaru Tsujino: Faculty of Engineering, Kanagawa University, Japan
Donald E. Yuhas: Industrial Measurement Systems, Inc., USA
John F. Vetelino: Lab for Surface Science & Technology, University of Maine, USA

GROUP 3: Physical Acoustics

Vice Chair: **Kenneth Lakin**: TFR Technologies, Inc., USA
Art Ballato: Chief Scientist, US Army CECOM RDEC AMSEL-RD-CS, USA
Mack Brezaeale: Department of Physics, University of Mississippi, USA
Jan Brown: JB Consulting, USA
David Hecht
Fred Hickernell
Amit Lal: Assistant Professor, School of Electrical & Computer Engineering, Cornell University, USA
John Larson
Moises Levy: Department of Physics, Naples, Florida, USA
George Mansfield: Institute of Radio Engineering and Electronics, Russian Academy of Sciences, Russia
Kiyoshi Nakamura: Department of Electrical & Communication Engineering, Graduate School of Engineering, Tohuku University, Japan
Valeri Proklov: Institute of Radio Engineering & Electricity, Russia
Edgar Schmidhammer
Susan Schnieder: Department of Electrical & Computer Engineering, Marquette University, USA
Bikash Sinha, Schlumberger-Doll Research, USA
Yook-Kong Yong: Department of Civil & Environmental Engineering, Rutgers University, USA
John Vig: US Army CECOM, AMSEL-RD-C2-PT, USA
Smaine Zeroug: Program Manager, Schlumberger-Doll Research, USA

GROUP 4: Surface Acoustic Waves

Vice Chair: **Don Malocha**, School of Electrical Engineering & Computer Science, University of Central Florida, USA
Benjamin Abbott: Sawtek Inc., USA
Ali Bagi-Wadji: Vienna University of Technology, Austria
Kushal Bhattacharjee: Clarisay, USA
Serguey Biryukov: Surfaces and Interfaces Department, Leibniz Institute for Solid State and Materials Research Dresden (IFW), Germany
Yasuo Cho: Research Institute of Electrical Communications, Tohoku University, Japan
Yasuo Ebata: Director of SAW Core Technology, Fujitsu Media Device Ltd., Japan
Ken-ya Hashimoto: Department of Electronic & Mechanical Engineering, Chiba University, Japan

Daniel Hauden: CNRS_LPMO, France
Mitsutaka Hikita: Communications Systems Research Department, Central Research Laboratory, Hitachi, Ltd., Japan
William D. Hunt: School of Electrical & Computer Engineering, Georgia Institute of Technology, USA
Shen Jen: RF Monolithics Inc., USA
John A. Kosinski: US Army RDE Command, USA
David Morgan: Impulse Consulting, UK
Mauricio Pereira da Cunha: Assistant Professor, Department of Electrical & Computer Engineering, University of Maine, USA
Viktor Plesski: SAW Design Bureau, Thomson Microsonics, Switzerland
Bob R. Potter: Vectron International, USA
Arne Ronnekleiv: Division of Physical Electronics, Norwegian Institute of Technology, Norway
Clemens C. W. Ruppel: EPCOS AG - SAW RD SAM, Germany
Peter Smith: McMaster University, Canada
Robert Weigel: University of Erlangen-Nuremberg, Germany

GROUP 5: Transducers and Transducer Materials

Vice Chair: **Scott Smith**, GE Corporate Research & Development, USA
Levent Degertekin: Woodruff School of Mechanical Engineering, Georgia Institute of Technology, USA
Jean-Francois Gelly: Thomson Microsonics, France
Hal Kunkel: Philips Ultrasound, USA
Reinhard Lerch: Friedrich-Alexander-Universitat Erlangen-Nurnberg Lehrstuhl fur Sensorik, Germany
Geoff Lockwood: Stirling Hall, Department of Physics, Queen's University, Canada
Clyde Oakley: Vice-president of Probe Development, Tetrad Corporation, USA
Mark E. Schafer: Sonic Tech Inc., USA
K. Kirk Shung: Bioengineering Department, Pennsylvania State University, USA
Stephen W. Smith: Department of Biomedical Engineering, Duke University, USA
Wallace A. Smith: Materials Division, Office of Naval Research, USA
Yasuhito Takeuchi: Professor, Department of Information & Computer Science, Faculty of Engineering, Kagoshima University, Japan
Roger H. Tancrell: Aimar Technology Corporation, USA
Vasandara Varadan: Pennsylvania State University, USA

Qiming Zhang: Materials Research Lab, Pennsylvania State University, USA
Yongrae Roh: Kyungpook National University, Korea
Thomas Shrout: Materials Research Lab, Pennsylvania State University, USA
Christopher Daft: Sensant Corporation, USA

2005 UFFC-S ADMINISTRATIVE COMMITTEE

SOCIETY OFFICERS

PRESIDENT Gerald V. Blessing
Natl. Institute of Standards & Tech (retired)

PRESIDENT-ELECT Art Ballato
U. S. Army RDECOM CERDEC HQ

VP, FERROELECTRICS Susan Trolier-McKinstry
The Pennsylvania State University

VP, FREQUENCY CONTROL Lute Maleki
Jet Propulsion Laboratory

VP, ULTRASONICS Clemens C. Ruppel
EPCOS AG

VP, PUBLICATIONS Donald Yuhas
Industrial Measurement Systems Inc.

SECRETARY-TREASURER Jacqueline H. Hines
J. H. Hines Consulting

ELECTED ADMINISTRATIVE COMMITTEE MEMBERS

2003 - 2005
Thomas R. Shrout, *Pennsylvania State University*
2003 - 2005
Mathias Fink, *Universite Denis Diderot*
2003 - 2005
Kullervo Hynynen, *Brigham and Women's Hospital Harvard Medical School*
2003 - 2005
Mike Garvey, *Symmetricom Inc.*
2004 - 2006
Victor P. Plessky, *GVR Trade SA*
2004 - 2006
Nava Setter, *EPFL Swiss Federal Institute of Technology in Lausanne*
2004 - 2006
Peter M. Smith, *McMaster University*
2004 - 2006
Daniel S. Stevens, *Vectron International*
2005 - 2007
Ruyan Guo, *Pennsylvania State University*
2005 - 2007
Massimo Pappalardo, *University of Roma Tre*
2005 - 2007
Leonhard M. Reindl, *Albert-Ludwigs-University of Freiburg*
2005 - 2007
Mark E. Schafer, *Sonic Tech, Inc.*

INVITED SPEAKERS

GROUP 1:

Patrick W. Serruys: 'Biomedical Engineering in the Catheterization Laboratory'

Timothy Leighton: 'Bubble Acoustics: from Seas to Surgeries'

Peter Wells: 'Lord Rayleigh'

Jaques Souquet: 'Telemedicine: What is in Place Today? What are the Challenges for the Future?'

Kathy Ferrara: 'Targeted Ultrasound Imaging and Drug Delivery'

Ralph Sinkus: 'Dynamic MR-Elastography as a Non-Invasive Imaging Modality: In Vivo Application to Breast, Liver, and Brain'

GROUP 2:

Chris Lowe: 'Novel Acoustic Biosensors'

K. Yamanaka: 'Diffraction-Free Propagation of Collimate Surface Acoustic Wave on a Sphere Applied for Innovative Gas Sensors'

Ute Rabe: 'Surface Characterization Using Ultrasonic Vibration Modes of Atomic Force Microscope Cantilevers'

GROUP 3:

Paul Muralt: 'Is There a Better Material for Thin Film BAW Applications than AIN?'

S. V. Krishnaswamy: 'Piezoelectric/Ferroelectric Films for Microwave/MEMS Application - Historical Perspective'

E. V. Charnaya: 'Ionic Conductivity in Acoustic Crystals'

GROUP 4:

Meirion F. Lewis: 'SAW and Optical Signal Processing'

Peter Wright: 'Trends in Integrated Front-End Modules for Cellular Handsets'

GROUP 5:

Christopher Daft: 'cMUTs and Electronics for 2-D and 3-D Imaging: Monolithic Integration, In-Handle Chip Sets and System Implications'

Stephen M. Fry: 'A Glimpse into the Future of Intravascular Ultrasound Technology'

Tim Proulx: 'Advances in Catheter-Based Ultrasound Imaging'

Jie Chen: 'Commercialization of Piezoelectric Single Crystals for Medical Imaging Applications'

SHORT COURSES

All courses are Sunday, September 18.

1 - Medical Ultrasound Transducers

8:00 a.m. – 12:00 p.m.
Douglas G. Wildes and L. Scott Smith
GE Global Research Center - Niskayuna, NY, USA

This course will provide an introduction to the design, fabrication, and testing of medical ultrasound transducers. Starting from an overview of the basic types of phased-array transducers (linear, convex, sector), we will discuss how the design for a probe is derived from its target application and how equivalent-circuit, finite-element, and acoustic field models can be used to optimize the design and accurately predict performance. A discussion of the structure of an ultrasound probe will lead to a survey of the different types of materials used in probes and their critical properties. Typical fabrication processes will be introduced and common problems in probe manufacturing will be summarized. Methods for evaluating completed transducers will be discussed. The course will highlight recent developments in probe technology, including. single crystal piezoelectrics, cMUT transducers, multi-row and 2D arrays, and electronics in probes, and will discuss performance advantages and fabrication difficulties which may be associated with each.

Douglas G. Wildes is a physicist with GE Global Research. He earned an A.B. in physics and mathematics from Dartmouth College and a Ph.D. in low-temperature physics from Cornell University, then joined GE in 1985. Since 1991, Dr. Wildes' research has focused on aperture design, fabrication processes, and high-density interconnect technology for multi-row and 2D transducers for medical ultrasound. Dr. Wildes has 19 issued patents and 18 external publications. He is a member of the American Physical Society and a Senior Member of the IEEE.

L. Scott Smith is a physicist with GE Global Research. He earned B.S. and Ph.D. degrees in physics from the University of Rochester and the University of Pennsylvania respectively. Joining GE in 1976, he developed phased array probes for medical ultrasound. More recently, he examined novel probe materials and led projects on pediatric endoscopes and adaptive acoustics. Dr. Smith has 37 issued patents and over 35 refereed publications. He is a member of the American Physical Society and a Senior Member of the IEEE where he serves as Vice Chair for Transducers on the Ultrasonics Symposium's Technical Program Committee.

2 - Elasticity Imaging: Principles, Systems, Approaches and Applications

8:00 a.m. – 12:00 p.m.
Stanislav Emelianov
University of Texas - Austin, Texas, USA

Elasticity imaging is rapidly evolving into a new diagnostic and treatment-aid tool. The primary purpose of this course is to provide both a broad overview and comprehensive understanding of elasticity imaging, and, as such, it is well suited for both newcomers and active researchers in the field. Starting with a historical introduction to elasticity imaging, we begin to lay a foundation for static and dynamic approaches in elasticity imaging with a brief discussion of theory of elasticity including both the equation of equilibrium and the wave equation. We will also review the mechanical properties of soft tissues. Then, experimental aspects of elasticity imaging will be discussed with emphasis on data capture, signal and image processing algorithms to measure internal tissue motion induced by either internally or externally applied forces. Motion tracking methods will be introduced, and techniques to increase and optimize signal-to-noise ratio in strain imaging will be overviewed. Finally, tech-

niques to map elasticity and other mechanical properties of tissue will be presented and discussed. Following an overview of elasticity imaging, the ultrasound elasticity imaging techniques and their biomedical and clinical applications will be presented. Advantages and limitations of each approach will be discussed and contrasted with other elasticity imaging techniques such as MRI or optical elastography. The course will conclude with overview of several experimental and commercial systems capable of ultrasound elasticity imaging, and discussion of current and potential clinical applications of elasticity imaging.

Stanislav Emelianov received the B.S. and M.S. degrees in physics and acoustics in 1986 and 1989, respectively, from the Moscow State University, and the Ph.D. degree in physics in 1993 from Moscow State University, and the Institute of Mathematical Problems of Biology of the Russian Academy of Sciences, Russia. In 1989, he joined the Institute of Mathematical Problems of Biology, where he was engaged in both mathematical modeling of soft tissue biomechanics and experimental studies of noninvasive visualization of tissue mechanical properties. Following his graduate work, he moved to the University of Michigan, Ann Arbor, as a post-Doctoral Fellow in the Bioengineering Program, and Electrical Engineering and Computer Science Department. From 1996 to 2002, Dr. Emelianov was a Research Scientist at the Biomedical Ultrasonics Laboratory at the University of Michigan. During his tenure at Michigan, Dr. Emelianov was involved primarily in the theoretical and practical aspects of elasticity imaging. Dr. Emelianov is currently an Assistant Professor of Biomedical Engineering at the University of Texas, Austin. His research interests are in the areas of medical imaging for therapeutics and diagnostic applications, ultrasound microscopy, elasticity imaging, photoacoustical imaging, cellular/molecular imaging, and functional imaging.

3 - Ultrasound Contrast Agents: Theory and Experimental Results

8:00 a.m. – 12:00 p.m.
Nico de Jong and Michel Versluis
Erasmus MC - Rotterdam, the Neth. & University of Twente - Enschede, the Netherlands.

The course consists of 6 main topics: a) First an overview will be presented of the (clinical and pre-clinical available) contrast agents, including the properties and characteristics of the gas inside the bubble and the shell surrounding it. b) Models of the behavior of small bubbles in a ultrasound field will be discussed. Simple models based on a one dimensional mass-spring system and more complicated models including gas and shell properties. c) Experimental ultrasound methods for UCA will be presented for characterizing the bubbles in a UCA, like harmonic and subharmonic scattering, absorption and attenuation. Also the influence of ambient pressure, temperature and gas concentration will be discussed. d) Experimental optical methods for characterizing individual bubbles. e) Imaging methods for contrast agents, like fundamental, harmonic, subharmonic and superharmonic and multi-pulse methods like pulse inversion, power modulation etc. and new methods like chirp excitation. f) Ultrasound mediated drug delivery: Interaction between mammalian cells and ultrasound in the vicinity of bubbles will be discussed.

Nico de Jong graduated from Delft University of Technology, The Netherlands, in 1978. He got his M.Sc. in the field of pattern recognition. Since 1980, he has been a staff member of the Thoraxcenter of the Erasmus University Medical Center, Rotterdam, The Netherlands. At the Dept. of Biomedical Engineering, he developed linear and phased array ultrasonic probes for medical diagnosis, especially compound and transesophageal transducers. In 1986 his interest in ultrasound applications shifted toward the theo-

retical and practical background of ultrasound contrast agents. In 1993 he received his Ph.D. for “Acoustic properties of ultrasound contrast agents.” Currently he is interested in the development of 3-D transducers and fast framing camera systems. De Jong is the project leader of STW and FOM projects on ultrasound contrast imaging and drug delivery systems. Together with Folkert ten Cate, MD, he is organizer of the annual European Symposium on Ultrasound Contrast Imaging, held in Rotterdam and attended by approximately 175 scientists from all over the world. Since 2003 Nico de Jong is part-time professor at the University of Twente.

Michel Versluis graduated in Physics in 1988 at the University of Nijmegen, the Netherlands, with a special interest in Molecular Physics and Astrophysics. Later, he specialized in the application of intense tunable UV lasers for flame diagnostics resulting in a successful defense of his PhD thesis in 1992. Michel Versluis is now a lecturer at the University of Twente, the Netherlands, in the Physics of Fluids group working on the experimental study of bubbles and jets in multiphase flows and granular flows. He also works on the use of microbubbles as a tool for medical diagnosis and therapy. Dr. Versluis teaches various courses in Fluid Mechanics, one of them focusing on the physics of bubbles.

4 - Recent Trends in Beamformation in Medical Ultrasound

1:00 p.m. – 5:00 p.m.
Kai Thomenius
General Electric’s Corporate R&D - Niskayuna, NY, USA

The goal of this introductory course is to review the design of ultrasound front ends and beamformers from a linear systems point of view including transduction, beamformation, and image formation functions. We will dis-

cuss analytical methods used in developing the design of a typical beamformer in use in diagnostic ultrasound today. The key points to be covered deal with methods of analysis of arrays and beamformers, the interaction of transmit and receive beams with clinically relevant targets, and how this interaction is used in image formation. The means by which these analytical methods contribute to a beamformer design and the trade-offs involved are reviewed. The techniques developed for such analysis will be applied to topics of current interest involving beamformation such as system miniaturization, 2D arrays, synthetic aperture techniques, and aberration correction.

Kai E. Thomenius is a Chief Technologist in the Imaging Technologies Organization at General Electric's Global Research facility in Niskayuna, NY. His focus is on Ultrasound and Biomedical Engineering. Previously, he has held senior R&D roles at ATL Ultrasound, Inc., Interspec Inc., Elscint, Inc., Inc as well as several other ultrasound companies, and is currently an Adjunct Professor in the Electrical, Computer, and Systems Engineering Department at Rensselaer Polytechnic Institute where he teaches a course in general imaging. Dr. Thomenius' academic background is in electrical engineering with a minor in physiology; all of his degrees are from Rutgers University. His long-term interests have been in ultrasound beamformation and miniaturization of ultrasound scanners, propagation of acoustic waves in inhomogeneous media such as tissue, the potential of bioeffects due to those acoustic beams, and determination of additional diagnostic information from the echoes that arise from such beams. Recently he has contributed to work on coherent beamformers in millimeter wave radar applications. He is a Fellow of the American Institute of Ultrasound in Medicine.

5 - Micromachined Ultrasonic Sensors and Actuators

1:00 p.m. – 5:00 p.m.
Ville Kaajakari, Amit Lal, and Richard White
Cornell University - Ithaca, NY and University of California - Berkeley, CA

Part A: The goal of this part is to introduce the fundamentals of micromachining, and the way they affect the design and performance of ultrasonic sensors and actuators. We will cover established micromachining techniques, such as bulk micromachining and surface micromachining on silicon. Material on thin film deposition and foundries will be presented. The relevant acoustic and ultrasonic properties of materials used in MEMS will be discussed for predictable device design. Nonlinearities, material property gradients, and internal stresses will be covered to describe their effect on design.

Part B: Case studies of sonic MEMS will be presented. These include (1) electrostatic actuation of micromachined membranes, nonlinearities and effective electromechanical coupling, (2) comparison of PZT and thin-film piezoelectric actuation of silicon bulk and surface micromachined structures (silicon horn design, microphones, speakers, flexural plate waves, FBARS), and (4) nonlinear ultrasound in microfluidic devices, and (5) Micro resonators for RF communications.

Amit Lal is an associate professor of electrical and computer engineering at Cornell University. He received his Ph. D. in electrical engineering from the University of California, Berkeley in 1996, and the B.S. degree from the California Institute of Technology in 1990. Amit Lal is the leader of the SonicMEMS group at Cornell University, which focuses on ultrasonics, micromachining, modeling of piezoelectric systems, use of radioactive energy sources in microsystems, and design and analysis of integrated circuits. He has published papers on ultrasonic sensors and actuators at confer-

ences in ultrasonics and micromachining. He serves on the Technical Committee on Physical Acoustics in the IEEE Ultrasonics, Ferroelectrics, and Frequency Control Society. He holds patents on micromachined acoustic sources/receivers, and silicon-based high-intensity ultrasonic actuators. He is also the recipient of the NSF CAREER award for research on applications of ultrasonic pulses to MEMS.

Richard M. White is a professor of EECS and a founding co-director of the Berkeley Sensor & Actuator Center at the University of California at Berkeley, Dick White has concentrated on ultrasonics and microsensors. He has published on thermoelastic wave generation, SAW transduction, and flexural plate-wave sensors. He has co-authored three books - a text for freshmen, a book on solar cells, and the reference book “Acoustic Wave Sensors”. White is a member of the National Academy of Engineering, and has received awards for his contributions to ultrasonics from the IEEE and the Ultrasonics and Frequency Control societies of the UFFC. His present research interests include ultrasonic airborne particulate monitoring and wireless passive proximity metering of AC power use in dwellings.

Ville Kaajakari received his M.S. and Ph.D. degrees in electrical and computer engineering fromUniversity of Wisconsin-Madison in 2001 and 2002, respectively. He is currently Senior Research Scientist at VTT Information Technology, Finland, where his research interest is RF-MEMS.

6 - Clinical Applications of Diagnostic Ultrasound

1:00 p.m. – 5:00 p.m.
Folkert ten Cate and Juiry W. Wladimiroff
Erasmus MC - Rotterdam, the Netherlands

The goal of this introductory course is to review the clinical applications of ultrasound imaging in cardiology. The pre-

sentation will be illustrated with realtime 2D and 3D Echoimages.

Folkert J ten Cate, M.D., is director of the clinical echolaboratory of the Thoraxcenter , Erasmus MC in Rotterdam.His main interest is in cardiomyopathies and ultrasound contrast both for diagnosis and treatment. He is a Fellow of the American College of Cardiology and the European Society of Cardiology.

Professor ***Juiry W. Wladimiroff*** was born in The Hague. He graduated from the school of medicine in Leiden in 1965 and was Board certified in Obstetrics and Gynecology in 1972. After some initial endeavours, Wladimiroff soon went down to London to study with Professor Stuart Campbell at the Post-graduate Institute at the Queen Charlotte's Hospital. In the late 1970s he field tested Organon Teknika's original real-time equipments from the Netherlands (in collaboration with Nicolaas Bom, the original inventor) and demonstrated the usefulness of the MiniVisor in the rapid measurement of the biparietal diameter at the bedside. His research at Queen Charlotte's started with the measurement of fetal urinary production rate, which he continued to expand after returning to the Netherlands, looking at fetal urinary production under a variety of physiological and pathological situations. From then on Professor Wladimiroff became particularly interested in the physiology and pathophysiology of pregnancy and the fetus and his group was very productive in researches pertaining to fetal cardiology, fetal vascular and cerebral function and fetal blood flow as assessed by doppler velocimetry. In 1974, he received his PhD at the University of Nijmegen with a thesis on fetal monitoring. In 1973, he started work as a consultant at the department of obstetrics and gynecology of Erasmus University Rotterman at Dijkzigt Hospital; in 1977, he was appointed reader at this department, and in 1980 full professor. Since 1984, he was head of the division of prenatal diagnosis and since 1996, when the two divisions were merged, head of the division of obstetrics and prenatal diag-

nosis at Rotterdam University Hospital. In 1981, his group reported fetal left ventricular volume determination from a study of two-dimensional measurement of real-time ultrasonic images of the left ventricle. Their group was the first to describe doppler studies of the middle cerebral arteries and the carotid carteries, and popularizing the carotid artery/umbilical artery PI ratio for the assessment of fetal compromise. Professor Wladimiroff was the President of the Dutch Society of Obstetrics and Gynecology from 1993 to 1995 and was the Chairman of the National Liason Committee for Medical Research Committees in the Netherlands. He has organized numerous National and International Scientific meeetings and Symposia and was the Chairman of the Education Committee of the International Society for Ultrasound in Obstetrics and Gynecology (ISUOG). He is also a board member of the Society of the "Fetus as a Patient" and executive board member of the European Board and College of Obstetrics and Gynecology and has carried out visitations in departments from Slovenia to Portugal. Professor Wladimiroff has produced over 300 important scientific papers and contributed to over 20 books and monographs. He is well regarded by his colleagues as a great teacher and investigator. Since 1977, he has supervised 25 PhDs on many different aspects of prenatal diagnosis, of obstetrical, gynecological and Doppler ultrasound, and of fetal monitoring. His PhD students came from Holland, Switzerland, Britain, Indonesia and Austria. In recognition of his contributions to the advancement of ultrasound in Obstetrics and Gynecology, he was presented the Ian Donald Gold Medal by the ISUOG in 1997. In 1999 he received the Gold Medal from the Drs. Haackert Foundation for "Lifetime Achievements in the field of Prenatal Diagnosis and Therapy".

7 - Non-linear Acoustics and Harmonic Imaging

6:00 p.m. – 10:00 p.m.
Victor Humphrey
Southampton University - Southampton, UK

This course will provide an introduction to the origins of non-linear propagation, and its consequences and applications in medical ultrasound.

The first section will review the basic physics of non-linear propagation, and discuss the propagation of plane waves as a means of introducing non-linear acoustics terminology. This will be followed by a discussion of the techniques used to numerically model non-linear propagation and the specific problems of performing measurements in high amplitude fields with their associated distortion and harmonic content.

The effects of diffraction and attenuation on non-linear propagation will then be introduced by considering the fields of transducers and arrays, and the fields they generate in tissue; this will be illustrated by a combination of experimental results and model predictions. This will lead on to a discussion of the consequences for medical ultrasound of non-linear propagation. Finally the application to harmonic imaging will be described.

Victor Humphrey is a Professor of Acoustics at the Institute of Sound and Vibration Research (ISVR) in Southampton, U.K. He received his BSc and PhD degrees from the University of Bristol in 1975 and 1981 respectively. He then moved to the School of Physics at the University of Bath where was promoted to Senior Lecturer. In 2004 he took up his current position at ISVR. His initial research was in the area of laboratory applications of non-linear parametric arrays in underwater acoustics. For this work he was awarded the Institute of Acoustics A.B. Wood Medal 1988. Subsequently he helped to develop a research programme on the non-linear propagation of ultrasound in medical fields that investigated these fields both numerically and experimentally. He was awarded the University of Bath Mary Tasker Award for excellence in teaching in 1995.

8 - Finite Element Modelling of Ultrasound Applications

6:00 p.m. – 10:00 p.m.
Paul Reynolds and John Mould
Weidlinger Associates Inc - Los Altos, USA

Finite Element Modelling (FEM) of ultrasound devices has been growing since its early use in the late 1980s and early 1990s. It is now common, and likely soon to be universal, to find industrial and academic groups with a significant ultrasound research component to utilize computer simulations of one form or another in their work. While the researchers are experts in their own field of ultrasound, they rarely have such extensive knowledge of the field of finite element modelling and consequently often have difficulty in making appropriate choices and decisions regarding their modelling needs and approach. It is the aim of this course to educate the ultrasound expert in the important considerations with regards to the finite element modelling of ultrasound applications, with particular emphasis on phenomena occurring in front of the transducer. By the end of the course, it is our intention that the attendees will have the basic information on finite element simulations, and several common but varied applications, with which to make informed decisions in regards to simulating their own particular problems, and therefore make best use of the resources available to them. The course will be divided in four parts.

Part 1: Finite Element Basics

The first section will involve an introduction to the field of finite element modelling, in order to ensure that all participants are aware of the basic assumptions inherent in the various modelling approaches. Common terminology, types of analysis (harmonic, transient etc), types of solution methods (implicit, explicit), types of numerical solver (direct, iterative), and typical boundary conditions, such as symme-

try and infinite element (e.g. absorbers and PML), validation and verification methods will be detailed.

Part 2: Wave Propagation

The second section will concentrate on the modelling of wave propagation through various media. Initial consideration will be given to the simple, linear, elastic cases and then moving to include the effects of long distance propagation, material discontinuities, frequency dependant attenuation, and non-linearity (such as is prominent in higher-harmonic imaging).

Part 3: Ultrasound Applications

The third section will consider a variety of ultrasound applications. This includes accidental or intentional tissue heating (such as with HIFU). Appropriate and accurate calculation of thermal generation (sometimes called the Bioheat Equation) and its application as a load to a thermal model will be detailed. Aspects of ultrasound/thermal coupling will be compared to acoustic radation force calculation, which bear significant resemblance in approach.

Part 4: Efficient Application of Modelling Software on Available Hardware

The ability to economically answer the questions posed often marks the difference between a successful and a failed project. We cover simple and effective approaches for ensuring maximum return on time invested in FEM, and important considerations for ensuring sufficiently accurate answers. This will then extend to discussion of numerical optimization techniques, and the relative costs compared to the potential benefits considered. We will discuss common computer architectures, the 32 to 64 bit transition, and multiprocessing, in order to leave the potential user somewhat more comfortable in this rapidly changing and bewildering field.

Paul Reynolds received B.Eng in Electrical and Mechanical Engineering from the University of Strathclyde, Scotland, in 1994, and Ph.D in 1998 for his work on finite element modelling of piezoelectric transducers. Since 1999 he has worked at WAI using the PZFlex finite element package to model a wide range of ultrasound and piezoelectric applications, including medical imaging, therapeutics, SONAR, and sensors.

John Mould received B.Sc. and M.Sc. in Civil Engineering from Virginia Tech in 1978 and 1979 respectively. He received a Ph.D. in Civil Engineering from the University of Colorado in 1983. Since joining WAI in 1983 he has been an analyst and a major contributor to the development of the entire FLEX family of codes for Nonlinear Solids, Acoustics, Thermal, Piezoelectric and Electromagnetic analyses.

9 - Flow Measurements and Doppler

6:00 p.m. – 10:00 p.m.
Hans Torp
Norwegian University of Science and Technology - Trondheim, Norway

This course provides basic understanding of physical principles and signal processing methods for flow measurements and visualization; with emphasis on Doppler methods and blood flow applications. The course starts with an overview of currently used techniques for velocity estimation in pulsed and continuous wave Doppler and color flow imaging. Statistical models for the received signal, as well as commonly used velocity and flow estimators are developed. Several different simulation methods for ultrasound signals from moving blood and clutter signals will be discussed. This includes fast simulation methods, as well as full 3D point scatter models using spatial impulse response techniques or k-space analysis. Efficient simulation tools to

explore estimator properties are derived, and examples on implementation in Matlab will be shown. Methods to suppress clutter signals from slowly moving targets, including regression filter will be discussed. Elements from classical estimation theory will be applied to develop minimum variance velocity estimators in the presence of clutter noise. The performance will be compared with commonly used approaches for clutter rejection and velocity estimation, and practical implementations will be discussed. Velocity components transversal to the ultrasound beam can not be measured by Doppler techniques. However, several approaches to overcome this limitation has been proposed, including speckle tracking, transit time measurements, and lateral beam modulation. Principles and practical limitations will be discussed. Methods for visualisation of 2D vector flow information will be shown.

Hans Torp received the MS degree in mathematics in 1978, and the Dr. Techn. degree in electrical engineering in 1992; both from the University of Trondheim, Norway. Since 1980 he has been working with ultrasound technology applied to blood flow measurements and imaging at the university of Trondheim, in cooperation with GE-Vingmed Ultrasound. He is currently professor of medical technology at the Norwegian University of Science and Technology, and has since 1987 given courses on ultrasound imaging and blood flow measurements for students in electrical engineering and biophysics. His research interests includes statistical signal- and image processing with applications in medical ultrasound imaging.

PLENARY SESSION

Monday, September 19
Willem Burger Zaal
8:30 a.m.-10:00 a.m.

Welcome
Ton van der Steen, General Chair
John Hossack, Technical Program Chair

Awards and Recognitions
Achievement Award
Distinguished Service Award
Rayleigh Award
Outstanding Paper Award
Fellow Awards
Distinguished Lecturer Award
David Sarnoff Award

Nanoscience, From Single-Molecule Science to Applications Cees Dekker
Delft University of Technology, Kavli Institute of NanoScience,
Lorentzweg 1, 2628 CJ Delft, The Netherlands
http://www.mb.tn.tudelft.nl/

Prof.dr. Cees Dekker (1959) is a professor in Molecular Biophysics at the Technical University Delft. His research takes place at the boundaries of nanotechnology, biology and physics. His work in carbon nanotubes is most famous, but his current interests have diverted to nanotechnology of living cells. He published more than 130 peer reviewed papers, of which more than 20 in Nature en Science. In 2003 he was appointed as a member of the Royal Dutch Academy of Arts and Sciences. Dekker received several honours

and awards, including the 2001 Agilent Europhysics Prize, the 2003 Spinoza Award of the Netherlands Organization for Scientific Reasearch and an honorate doctorate in Diepenbeek, Belgium. Further information can be found on: www.mb.tn.tudelft.nl/user/dekker/index.htm

This talk will give a broad introduction and overview of nanoscience and nanotechnology. I will illustrate the excitement and potential of this emerging field by focusing on a number of examples, in particular carbon nanotubes for nanoelectronics and single-molecule techniques for biophysics of DNA-enzyme interactions.

EXHIBITS

Time: Daily from 8 a.m. to 6 p.m.

Location: Foyer room 2, Jurriaanse Zaal (first floor)
Foyer room 3, Van der Mandele Zaal (first floor)

Acqiris SA-Data Conversion Instruments
Advanced Modular Sputtering, Inc. (AMS)
Ferroperm Piezoceramics A/S
HITACHI Medical Systems
HONDA Electronics Co. Ltd.
IEEE-UFFC Society
Imasonic
Lecoeur Electronique
Microfine Materials Technologies PTE LTD
Precision Acoustics Ltd.
Smart Material GmbH
Sonora Medical Systems, Inc.
Sound Technology, Inc.
Valpey Fisher Corporation
W. L. Gore & Associates

MONDAY, SEPTEMBER 19, 2005

*Author presenting paper

POSTER SESSIONS

Session: PS
STUDENT PAPER FINALISTS
Chair: Helen Routh, Philips Medical Systems, and Tom Thomas, Siemens Medical Solutions

PS-1
HIGH FREQUENCY ULTRASOUND CHARACTERIZATION OF THE BLOOD CLOTTING PROCESS: INTRA- AND INTER-INDIVIDUAL VARIATIONS.

R. LIBGOT*[1], F. OSSANT[1,2], Y. GRUEL[2], and F. PATAT[1,2], [1]LUSSI FRE 2448 CNRS, Tours, France, [2]Bretonneau University Hospital, Tours, France.
Corresponding e-mail: libgot_r@med.univ-tours.fr

In a previous study [1], we presented a device capable to simultaneously estimate high frequency ultrasound parameters both in double-transmission mode (DT-mode) and in backscattering mode (BSC-mode). Sound velocity was estimated in DT-mode and BSC coefficient (from which the integrated BSC coefficient (IBC) and the effective scatterer size (ESS) were estimated) in BSC-mode. We used a 45 MHz single element transducer for the DT-mode, and a real time high frequency echographic devices allowing spectral analysis of signals in the frequency range 10-30 MHz (Dermcup 2020TM). We showed that BSC-mode and DT-mode parameters were complementary to give a fine description of blood coagulation process in terms of mechanical properties (blood solidification) and spatial distribution of blood components (formation RBC aggregates).

In the present paper, our purpose was to estimate interindividual and intraindividual variations of these ultrasound parameters in order to assess the clinical potential of this technique. Blood samples were collected from 10 healthy donors to study interindividual variations. To study intraindividual variations, blood samples were collected 3 times over 24 hours from each volunteer. Several protocols were then conducted: samples were taken in 3.5 ml sodium citrate tubes and placed in a temperature controlled chamber (37°C ± 0.1) for 15 and 30 minutes before the start of the experiment (tcit), the coagulation process was initiated by adding 100 and 200 µl of CaCl2 (with concentration of 0.5M). The hematocrit and fibrin concentration were determined for each blood sample. During the blood clotting process (two hours' observation), the entire set of acoustic parameters was measured with 15 seconds time resolution for the DT-mode and 30 seconds for the BSC-mode.

In the DT-mode, the results were focused on the variation kinetics of the acoustic velocity. Three characteristics could be considered to differentiate these kinetics: the time t0 at which the velocity increased strongly (typically between 20 to 50 minutes), the slope S of this increase (typically between 0.013 and 0.029 m/s^2) and the final increase I of the velocity (typically between 20 and 35 m/s). In the BSC-mode, the IBC varied as the fourth power of the frequency (Rayleigh scattering) during the first few minutes of the process and then decreased, from 4 to 2.5, as the clot formed (corresponding to ESS values between 0 and 25 μm for a Gaussian model).

Preliminary results from RF-signals in the frequency range 30-60 MHz with a 50 MHz center frequency probe were also obtained and compared to those obtained for 10-30 MHz. Histological analysis of the clots were performed and several acoustic parameters values were analyzed in relation to clot structures.

Finally, the kinetics of high frequency ultrasound parameters, for instance the acoustic velocity, during blood clotting process is a promise technique to characterize clotting properties of whole blood.

1:Ossant and al., High frequency ultrasound characterization of the coagulation process of whole blood, Ultrasonics Symposium, 2004 IEEE pp846-849

PS-2
ULTRASONIC DETECTION OF THE ANISOTROPY OF PROTEIN CROSS LINKING IN MYOCARDIUM.

S. BALDWIN*, M. YANG, K. MARUTYAN, K. WALLACE, M. HOLLAND, and J. MILLER, Washington University in St. Louis, St. Louis, MO.
Corresponding e-mail: slb@hbar.wustl.edu

BACKGROUND: Diastolic dysfunction may arise, in part, because of an increase in myocardial stiffness from cross-linking of extracellular matrix proteins such as collagen. Studies by others indicate that high-frequency (30 MHz to 50 MHz) ultrasound can detect chemically-induced increases in protein cross-linking (C. S. Hall et al., “High-Frequency Ultrasound Detection of the Temporal Evolution of Protein Cross-Linking in Myocardial Tissue,” IEEE Trans. Ultrason., Ferroelect., Freq. Contr., vol. UFFC-47, pp.1051-1058, 2000).

OBJECTIVE: The goal of the current study was to measure, as a function of the angle of insonification relative to that of the predominant myofiber orientation, changes in myocardial attenuation resulting from increased protein cross-linking.

METHODS: Through-transmission radiofrequency-based measurements of the attenuation coefficient (3 MHz to 7 MHz), for angles of insonification over a complete rotation relative to the predominant myofiber orientation in 5 degree increments, were performed at room temperature on 36 specimens from 12 freshly excised lamb hearts. These specimens were then fixed in formalin to induce protein cross-linking. After sufficient time had elapsed to ensure that the process of cross-linking had reached completion, measurements were repeated on the identical specimens.

RESULTS: For both freshly excised and formalin-fixed myocardium, the attenuation coefficient was found to increase as a function of frequency in an

approximately linear manner. The attenuation varied systematically as a function of angle of insonification, with a minimum perpendicular to, and a maximum parallel to, the direction of the myofibers. Increased protein cross-linking inferred from fixation resulted in a maximum increase in attenuation at perpendicular insonification. For angles near perpendicular to the predominant direction of the myofibers, the measured slope of attenuation increased from 0.52 ± 0.07 dB/(cm·MHz) (mean ± one standard deviation) for freshly excised to 0.85 ± 0.08 dB/(cm·MHz) for formalin-fixed myocardium. In contrast, for parallel insonification uncertainties exhibit considerable overlap (1.88 ± 0.17 for freshly excised and 1.75 ± 0.19 dB/(cm·MHz) for formalin-fixed myocardium).

CONCLUSION: This study indicates that effects of fixation, and therefore presumably protein cross-linking, in myocardium can be anisotropic, suggesting that the response of the extracellular collagenous matrix to changes in cross-linking is directionally dependent. The anisotropy of ultrasonic attenuation may thus provide an approach for the noninvasive monitoring of the extent and progression of myocardial disease associated with changes in protein cross-linking.

NIH R37 HL40302

PS-3
DETECTION OF THE MYOCARDIAL BOUNDARY IN THE LEFT VENTRICLE FROM SIMULTANEOUSLY ACQUIRED TRIPLANE ULTRASOUND IMAGES USING MULTI VIEW ACTIVE APPEARANCE MOTION MODELS.

J. HANSEGÅRD*[1], S. URHEIM[2], E. STEEN[4], H. TORP[3], B. OLSTAD[3], S. MALM[3], and S. RABBEN[4], [1]University of Oslo, Oslo, Norway, [2]Rikshospitalet University Hospital, Oslo, Norway, [3]The Norwegian University of Science and Technology, Trondheim, Norway, [4]GE Vingmed Ultrasound, Horten, Norway.
Corresponding e-mail: jogerh@ifi.uio.no

We report a new algorithm for detecting the myocardial boundary in the left ventricle (LV) from simultaneously acquired triplane ultrasound (US) image sequences using Multi View Active Appearance Motion Models (MVAAMM). Coupled boundary detection in three planes can potentially increase the accuracy of LV volume measurements, and also increase the robustness of the boundary detection over traditional methods.

The MVAAMM is an extension of the Active Appearance Motion Models (AAMM) and is capable of generating LV triplane image sequences. The parameters of the model are optimized iteratively to fit the patient data set, and the myocardial boundary is then extracted from the fitted model. Shape and texture are coupled between the image planes, while the model pose is fitted independently.

A database of triplane image sequences from full cardiac cycles, including the standard apical four chamber, two chamber, and long axis views were established from 20 volunteers, including 12 healthy persons and 8 persons suffering from heart disease. Patient cases with asynchronies were not included. A Vivid 7 scanner (GE Vingmed Ultrasound, Horten) was used for acquisition of the data sets. For each dataset the LV myocardial boundary was manually outlined, and

the end diastolic (ED) and end systolic (ES) frames were determined visually for phase normalization of the cycles.

Evaluation of the MVAAMM was done by detecting the LV myocardial boundaries in the test sets. Variation within the data sets is critical when training the model. Therefore, a leave one out approach was used for evaluation, resulting in 20 models where one case was left out from each model. The point distance between the automatically detected myocardial boundary and the manually outlined boundary was found as the mean of the distances between corresponding points along the contours. The detected volumes at ED, mid systole and ES (VolC) were compared to manually determined volumes (VolM). Based on the ED and ES volumes, the Ejection Fraction (EF) was calculated.

Table 1 shows the mean and 1 standard deviation of the point distance, volume error, volume fractional error, EF error, and also the regression line for VolC as a function of VolM. The detected volumes at ED, mid systole and ES correlate well with the manually determined volumes ($R^2 = 0.87$). The correlation between detected EFs and manually determined EFs was poor ($R^2 = 0.29$), this is probably caused by the method's tendency to identify an average motion pattern.

Dropouts are handled well by the MVAAMM, because the shapes and textures of the three planes are coupled. The views with the largest point distances have one or more foreshortened views, resulting in a suboptimal detection. Adding more samples to the training database or coupling of the model's pose parameters between the views may improve the performance in such cases.

Table 1: MVAAMM Results

Mean Point distance (mm)	4.1 ± 1.9
Error (VolM - VolC) (ml)	7.0 ± 14
Volume fractional error (1 - VolC/VolM) (%)	13 ± 12
Volume regression (y - VolM) (ml)	y = 1.0 x - 11
Volume correlation coefficient (R^2)	0.87

We wish to acknowledge Jan Yee at GE Vingmed Ultrasound for gathering ultrasound data. The project is supported by The Research Council of Norway.

PS-4

3D PERFUSION MAPPING IN THE INTACT MOUSE HEART AFTER MYOCARDIAL INFARCTION USING MYOCARDIAL CONTRAST ECHOCARDIOGRAPHY.

Y. LI*, Z. YANG, B. A. FRENCH, and J. A. HOSSACK, University of Virginia, Charlottesville, VA.
Corresponding e-mail: yinbo@virginia.edu

Due to the widespread availability of transgenics and knock-outs, the murine species provides a very useful and robust model in which to study human

cardiovascular disease. Myocardial contrast echocardiography (MCE) using microbubbles as contrast agent has been shown to be an effective tool in characterizing myocardial perfusion in vivo, and it has been employed previously for two-dimensional (2D) myocardial perfusion analysis in mice. However, three-dimensional (3D) analysis, fully encompassing the entire left ventricle (LV), is required for a more complete understanding of the relationship between LV perfusion and function after myocardial infarction (MI). In this work, we studied an intact mouse model of surgically-induced MI resulting from a Left Anterior Descending (LAD) occlusion. Healthy mice which underwent a similar invasive procedure but with no occlusion were also studied as controls. Imaging was performed at 14 MHz using a non-destructive, contrast-specific, imaging mode ('Contrast Pulse Sequences' [1]). The infusion of contrast agent was accomplished at a slow and steady flow rate using a syringe pump driving a 1ml syringe. For each mouse heart, MCE images were acquired in parallel short axis cross-sections of the heart at 1 mm elevational increments. For accurate 3D reconstructions, calibrated ECG gating and a tri-axial adjustable micro-manipulator were used for temporal and spatial registration, respectively. Perfusion analysis was conducted by analyzing the local refilling processes within the LV myocardium. This analysis indicated a significantly slower flow rate in areas of perfusion defects compared to normal areas. MCE images acquired during steady-state perfusion of each 1mm slice of the LV were color-coded to indicate relative perfusion, with blue corresponding to well-perfused areas and red corresponding to perfusion defects. As a standard for comparison, post-mortem tissue was stained with Phthalo blue and TTC red dyes to identify perfused and ischemic yet viable LV myocardium, respectively. A good correlation ($R^2 > 0.87$) was observed between the MCE-based, in vivo measurements and the tissue-based, ex vivo measurements of % perfused area in each tissue slice. 3D multi-slice models and 3D volumetric models of the distribution of perfusion in each LV were created for improved visualization and quantification of the 3D extent of the perfusion defects. These models demonstrated a promising match with the results of post-mortem tissue staining.

[1] P. Phillips, "Contrast Pulse Sequences (CPS): Imaging non-linear microbubbles," Proceedings of the 2001 IEEE Ultrasonics Symposium, vol. 2, pp. 1739-1745, 2001.

NIH grants EB001826. EB002349, Siemens Medical Solutions, Mountain View, CA and Vermon SA, France.

PS-5
APPLYING *IN VITRO* ELASTICITY IMAGING RESULTS TO OPTIMIZE *IN VIVO* BREAST LESION CHARACTERIZATION USING A COMBINED 3D US/ DIGITAL X-RAY SYSTEM.

R. BOOI*[1], P. CARON[1], R. ERKAMP[1], H. XIE[1], A. KAPUR[2], G. LECARPENTIER[1], M. ROUBIDOUX[1], J. FOWLKES[1], and M. O'DONNELL[1], [1]University of Michigan, Ann Arbor, [2]General Electric Global Research Center, Schenectady, NY.
Corresponding e-mail: rbooi@engin.umich.edu

Ultrasound-based reconstructive elasticity imaging has great potential for diagnosis and characterization of breast lesions. Applying external strain with a mammographic paddle as part of a combined 3D US/Digital X-ray system provides more uniform deformation and breast stability, offering opportunities to improve image fidelity. In this study, we examined *in vitro* and *in vivo* strain image quality with three GE transducers (M12L, 10L, 7L) each operating at several frequencies between 5-10 MHz and four TPX paddle thicknesses to predict optimal *in vivo* results with the combined system. Out-of-plane motion was measured by translating an ultrasonic transducer across a breast phantom (ATS, model BB-1) in 50μm steps over 400μm. Each image was correlated to the first in the sequence using conventional 2D phase-sensitive speckle tracking techniques to determine the rate of elevational decorrelation. Next, in-plane, strain-limited decorrelation was evaluated by compressing the phantom at 0.15% increments up to 5% strain. Images were correlated at step sizes 0-7 (0-1.05% mean strain) using two-pass 2D speckle tracking algorithms and estimated displacements were accumulated. Adaptive strain estimation (ASE) was applied to maximize CNR throughout the final strain image. Overall, the 10L transducer caused the least decorrelation due to out-of-plane motion (R = 0.97 at 7.5MHz and 400μm elevational translation). In-plane decorrelation was also primarily strain-limited with the 10L transducer at 7.5MHz, with R = 0.9 for a 1.6% strain step. Accumulated strain images after ASE demonstrated a CNR = 3.8 with the M12L transducer at 10 MHz. Using the same post-processing techniques, the 10L transducer at 7.5 MHz demonstrated a CNR = 4.7. Of the four TPX paddle thicknesses (0, 0.25, 1.0, 2.5 mm) used in the *in vitro* study, the 2.5mm paddle created clearer strain images with less artifacts than the thinner paddles under the same experimental conditions, providing more uniform deformation during compression by bowing less than the thinner paddles. Next, we evaluated sources of *in vivo* chest wall motion in 7 subjects to minimize patient motion during the scan. Patients were asked to breathe shallowly during exams as it caused less decorrelation due to chest wall motion (Ravg = 0.96 over 91 frames) than holding their breath (Ravg = 0.93). *In vivo* results were acquired with the 10L at 7.5 MHz and TPX 2.5mm paddle using continuous compression over 2.1 seconds. Strain images clearly distinguished between tissue types when accumulated up to 4% strain and ASE was applied. *In vivo* results are limited by out-of-plane motion and CNR but are expected to improve significantly with full 3D tracking. These early successes indicate that using elasticity imaging with the combined system shows great potential for characterizing breast lesions that might be malignant, reducing the need for biopsies.

This work was supported in part by NIH grant RO1 CA 091713.

PS-6
STRESS FIELD FORMATION FOR MULTIFREQUENCY VIBRO-ACOUSTOGRAPHY.

M. URBAN*[1], G. SILVA[2], R. KINNICK[1], M. FATEMI[1], and J. GREENLEAF[1], [1]Mayo Clinic College of Medicine, Rochester, MN, [2]Universidade Federal de Alagoas, Maceio, AL, Brazil.
Corresponding e-mail: urban.matthew@mayo.edu

Background: Vibro-acoustography is a recently developed method that uses the dynamic radiation force (stress) of ultrasound to locally excite an object. Presently, to form the stress field we typically use two ultrasound beams whose frequencies differ by Δf, typically in the kilohertz range. The two beams interfere at the system focus creating the radiation stress at the difference frequency Δf. The system point spread function (PSF) is given as a function of the radiation stress. The object response to the radiation stress may vary significantly as Δf changes due to its internal resonances. Thus, acquiring images with multiple Δf values in one scan would provide more information than using one difference frequency. **Methods:** We propose a multifrequency vibro-acoustography method that uses a multifrequency radiation stress produced by an array transducer driven with N ultrasound frequencies. The N ultrasound beams interfere at the focus of the transducer producing up to $N(N\text{-}1)/2$ unique difference frequencies in the radiation stress. This method can produce a multifrequency image at the different $N(N\text{-}1)/2$ frequencies with only one scan of the region of interest, increasing the information of the scanned region by a factor of $N(N\text{-}1)/2$. The objective of this paper is to present the image formation theory in multifrequency vibro-acoustography systems with experimental validation. The radiation stress generated by sector array and annular array transducer systems is analyzed theoretically. For experimental validation, an eight element sector array transducer driven with four different ultrasound frequencies is used to produce a PSF with six components at different Δf values. A stainless steel sphere with diameter 0.51 mm embedded in a gelatin phantom was scanned to obtain a measurement of the PSF. A Doppler laser vibrometer is used to measure the vibration velocity of the sphere, which is proportional to the radiation stress upon the sphere. The detected signal was processed using a bandpass filter and lock-in amplifier to extract each of six PSF components. In another configuration, the raw signal from the laser was digitized for off-line digital filtering to insure that each PSF component can be extracted from the raw data set. We compared the measured and the theoretical PSF components through their spatial distribution, mainlobe width at -6 dB, and sidelobe levels. Lastly, we used a computer phantom with small spheres to demonstrate the usefulness of multifrequency vibro-acoustography for microcalcification detection in breast imaging. **Results:** The main lobe width numerically evaluated for a PSF component is 0.91 x 2.06 mm, while the experimental measurement yields 0.98 x 1.94 mm. The theoretical and measured sidelobe levels are -7.29 dB and -7.67 dB, respectively. **Conclusion:** The proposed method holds the potential for a large gain of information with no increase in same scanning time when applied to conventional vibro-acoustography systems.

This study was supported in part by grants EB002640, EB002167, and EB00535-03 from National Institutes of Health, and DCR2003.013 from FAPEAL/CNPq, Brazil.

PS-7

A LATERAL FIELD EXCITED ACOUSTIC WAVE PESTICIDE SENSOR.

W. PINKHAM*, L. FRENCH, D. FRANKEL, and J. VETELINO, University of Maine, Orono, ME.
Corresponding e-mail: wade.pinkham@umit.maine.edu

Organophosphate pesticides are commonly used worldwide to control pests in fruits and vegetables. Although these pesticides serve their purpose in protecting crops, excessive pesticide use can have adverse effects on the environment and also jeopardize the health of the consumer. Government agencies in the U.S. limit the amount of pesticides that may be used, however many agricultural products are imported from countries where pesticide use may not be regulated. Therefore, to minimize environmental effects and protect the health of consumers, a need exists for a low-cost portable sensor that will detect harmful pesticide levels. Recently a lateral field excited (LFE) acoustic wave sensor on AT-cut quartz has been developed [1] which is capable of detecting both mechanical and electrical property changes in a film which selectively sorbs a target analyte. In the LFE sensor the transverse shear mode (TSM) is excited by electrodes on the reference surface and the sensing surface is unmetallized and coated only with the target analyte selective film, resulting in a much simpler structure than the standard AT-cut quartz crystal microbalance (QCM). In the present work a polyepichlorohydrin (PECH) film is evenly spun onto the sensing surface of an LFE sensor to detect the organophosphate pesticide, phosmet ($C_{11}H_{12}NO_4PS_2$), in an aqueous environment with a flow through system. When comparing the LFE sensor to the standard QCM as a pesticide sensor, results show that the LFE sensor has at least 25% greater sensitivity with a lower limit in the parts per billion (ppb) range, 12% shorter response times and more consistent reproducibility. The improvement in sensitivity, response time and reproducibility is most likely due to the absence of the gold film on the sensing surface. In particular the electric field associated with the TSM is able to penetrate directly into the analyte selective film and monitor film electrical property changes resulting in higher sensitivity. Quicker response times and better reproducibility may also be attributed to the absence of the gold film and any aging effects associated with the film. In conclusion, the simplicity in structure and improved sensing properties of the LFE sensor results in a sensor platform which may replace the standard QCM in a wide range of applications.

[1] Y. Hu, L. A. French Jr., K. Radecsky, M. Pereira da Cunha, P. Millard, and J. F. Vetelino. “A Lateral Fiield Excited Acoustic Wave Sensor.” IEEE Transactions on Ultrasonics, Ferroelectrics, and Frequency Control, Vol. 15, No. 11, pp. 1373-1380, November 2004.

**This work is supported by the National Science Foundation under grant 0330100.*

PS-8

MORPHO-MECHANICAL ANALYSIS OF THE DENTIN-CEMENT INTERFACE STRENGTH USING A SCANNING ACOUSTIC MICROSCOPE.

E. BAKULIN*[1], L. DENISOVA[2], R. MAEV[1], F. RUSANOV[2], A. DENISOV[2], D. GAVRILOV[2], F. SEVERIN[1], and G. GRAYSON[3], [1]Windsor University, Windsor, Ontario, Canada, [2]Institute for Biochemical Physics, Moscow, Russian Federation, [3]Ultradent Clinical Research Ltd., Windsor, Ontario, Canada.
Corresponding e-mail: deniso@com2com.ru

Up to now caries stays one of the most widely spread human diseases. A carious tooth treatment as a rule includes restoration of the pathologically changed tissue with a dental material cement, amalgam, resin etc. Therefore a restored tooth is a small complicated construction formed of biological tissues and an artificial restorative material. Mechanical strength of such a construction depends of many factors, and one of the most significant is adhesive strength of the contact zone between dentin and dental cement. Cement shrinkage, pores, cavities and voids inside restoration and, particularly, in the interface between dentin and restoration can dramatically influence upon the quality of the treatment. The aim of the present study is to develop experimental approaches to evaluate dentin-cement interface quality using a scanning acoustic microscope.

Human teeth extracted by orthodontic reasons in dental clinics have been used. Special model samples imitating good and failed adhesion have been prepared. The study has been performed with scanning acoustic microscopes Sonix (Sonoscan, USA) and Tessonix (R.G.Maev et al). The acoustic lens providing ultrasound frequency 50 MHz (lateral resolution about 30 microns) has been used. Following the investigation in an acoustic microscope, the teeth and prepared samples have been sectioned in accordance with the scanning position and the results, obtained with acoustic microscope have been verified using a light microscope.

Acoustic impedance of the dental materials, which we use in the study, is quite similar to that of dentin. Therefore in the case of a good bonding strength between the cement and dentin almost all acoustic energy of the focused ultrasound passes from the restoration into dentin. This is why we obtain practically no reflected signal from this interface. If due to the shrinkage there is a void (filled with tissue liquid or with air) in the cement-dentin interface, then the ultrasound signal is reflecting not from dentin, but from the media with comparatively low acoustic impedance; so the largest part of the acoustic energy will be reflected and registered. In this case the interface between cement and dentin will became visible in acoustic images, formed in B- or C-scan mode. A series of the acoustic images of the restored teeth and experimental models demonstrate the difference between the imaging of the good and failed adhesion in the cement-dentin interface.

The morphological data obtained non-destructively in the acoustic microscopes are in a good agreement with the results of the examining of the same samples after sectioning in the optic microscope. The experimental approaches developed in the present study can serve as a basis for the development of new instruments and methods for dental clinical practice.

Keywords: acoustic microscopy, focused ultrasound, dental cement, cement-dentin adhesion, nondistructive evoluation

PS-9
PARAMETRIC MODELING OF WAVE PROPAGATION IN GAS MIXTURES - A SYSTEM IDENTIFICATION APPROACH.

J. MARTINSSON* and J. E. CARLSON, Lulea University of Technology / EISLAB, Lulea, Sweden.
Corresponding e-mail: Jesper.Martinsson@ltu.se

Using ultrasonic techniques, the measurable properties of a gas are characterized by the frequency dependent attenuation and speed of sound. The properties are directly related to the bulk modulus by the wave number. For a non-attenuating and non-dispersive gas the bulk modulus is a real-valued constant containing the equilibrium density and the thermodynamic speed of sound. For dispersive gases, the relationship between the acoustic pressure and the condensation is dynamic, and the bulk modulus connecting these two quantities is both complex-valued and frequency dependent.

The standard approach to describe the dynamics of the bulk modulus is to parameterize it given the physical knowledge of the gas properties under investigation. However, for gas mixtures with complex dynamic behavior and/or unknown components, a complete physical description of the bulk modulus is generally not available. For these situations a common approach is to use non-parametric methods to describe the dynamics. Although non-parametric techniques are easy to apply, they give only moderately accurate descriptions. To obtain higher accuracy, parametric models must be used. When choosing the model structure, two things are desirable: First, the model should capture the dynamics of the system and second, the model parameters should give information about the underlying physical properties.

In this paper, the bulk modulus is parameterized using a rational transfer function (spring-dashpot model). This structure has a well-known connection to some physical properties, while still keeping the number of parameters reasonably low. We use system identification techniques to estimate the parameters and cross-validation to prevent over-parameterization. The model is validated by analyzing the prediction errors which show that the prediction errors are uncorrelated with the measured echoes. This means that the parametric model is able to capture the dynamics of the true system.

The proposed method is compared with standard non-parametric techniques using pulse-echo measurements in ethane, oxygen, and mixtures of the two. The experimental results show that the variances of the estimates are considerably smaller using the proposed method compared to non-parametric methods, especially for noisy data.

Generous grants from the Swedish Energy Agency and the Kempe Foundation are gratefully acknowledged.

PS-10

INTERMEDIATE FREQUENCY RESONATORS USING LAMB WAVES CO-INTEGRATED WITH BULK ACOUSTIC WAVE RESONATORS.

A. VOLATIER*[1,3], G. CARUYER[1,3], E. DEFAY[2], D. PELLISSIER TANON[1], P. ANCEY[1], and B. DUBUS[3], [1]STMicroelectronics, Crolles, France, [2]CEA-LETI/DIHS/LCRF, Grenoble, France, [3]IEMN, Lille, France.
Corresponding e-mail: volatieral@chartreuse.cea.fr

Bulk Acoustic Wave (BAW) resonators exhibit attractive properties in term of power handling capacity and on-chip integration to realize filters in the GHz range. In a BAW resonator, a thin piezoelectric layer (a few μm) deposited between two electrodes is driven in its thickness extensional mode of vibration. To get a high quality factor, this structure is decoupled from the substrate by a multilayer Bragg reflector (Solidly Mounted Resonator: SMR) or a surface micro-machining membrane (Film Bulk Acoustic Resonator: FBAR). A current problem in the design of BAW resonators is the existence of spurious resonances due to Lamb waves propagation close to the thickness extensional mode which generate ripple in the filter passband.

In this work, it is demonstrated that Lamb wave resonances can be used to realize resonators in the 30-250 MHz range with high quality factor by using specific electrode design and electrical excitation.

1D simulation (based on Mason model) is usually sufficient for the design of BAW resonators. In our case, two dimensions behaviour of Lamb waves is modelled using finite element ATILA code. Design of Lamb wave resonators are performed using modal and harmonic analysis. Typical dimensions of resonator are 100 μm width and 450 μm length (clamped-clamped beam). Influence of electrode geometry and type of excitation (one- or two-phase) upon coupling of fundamental or higher harmonic resonances will be emphasized.

Lamb wave resonators are realized using a surface micro-machining process compatible with Above IC integration. Sacrificial layer is first deposited, patterned and encapsulated by SiN film (600 nm). AlN thin film are elaborated by DC pulsed sputtering and the active stack of the resonator is made of Ti (50 nm) / Pt (100 nm) / AlN (550 nm) / Pt (200 nm). Lateral dimension of resonators is defined by etching of AlN and SiN thin films. The release of the structure is made using dioxygen plasma. According to a completely similar process Film Bulk Acoustic Resonators (FBAR) are processed at the same time.

Symmetrical S0 Lamb wave resonances ranging from 30 MHz to 250 MHz are measured for different electrode geometries and electrical excitations (network analyzer HP 8753E). High quality factors (Q_s and Q_p) of 2000 and k^2~0.8% (k coupling coefficient) are obtained at 92 MHz for 3rd harmonic resonator. These electrical measures agree well with 2D simulations previously described. As for Bulk Acoustic Wave resonators, thickness extensional resonance is measured at 2.4 GHz.

The electrical characteristics of Lamb wave resonator are potentially suitable for channel filtering or oscillator applications and co-integrating Lamb wave and FBAR resonators in one single Above IC process promises to offer great potential

for design of resonators and filters in the field of Intermediate (IF) and Radio Frequency (RF) applications.

PS-11
CALIBRATION OF ACOUSTIC RADIATION PRESSURE FIELD INSIDE MICROCHANNELS USING MICROPARTICLE ZETA POTENTIAL MEASUREMENT.

M. ARAZ* and A. LAL, Cornell University, Ithaca, NY.
Corresponding e-mail: mka22@cornell.edu

We have previously presented a low power, small scale ultrasonic excitation of bending waves on a glass capillary microfluidic system by a laser-cut PZT plate [1]. Complex acoustic force field generated by the inertial coupling of standing flexural waves on the capillary body can be used to collect and manipulate cells, silica or polystyrene beads suspended in the fluid. As focusing of particles from 300nm to 10 μm (or larger) size range is possible, separation of particles with respect to size or acoustic impedance is also possible by 2-D radiation pressure fields [1]. While the FEM, and analytical modeling of the actuator dispersion relationships agree with the experimental results for a broad range of frequency regime of the actuation [2], nonlinear affects due to excessive bending leads to parametric excitation of multiple modes, making modeling of acoustic radiation pressure difficult. Since two of the possible proposed applications of the device are controlled biological assays and cell growth in 3-D, a quantitative understanding of the distribution of the radiation force inside the capillary is needed.

Related to the problem given above, we present a new method to estimate the acoustic field inside the capillary. It is known that acoustic radiation force on a spherical object is related to its radius. While radiation force decreases by the size of the particle, small particles collected inside the channel tend to disperse due to Brownian motion and electrostatic interactions of the Debye layer surrounding them. The Debye layer interaction can be quantified by measuring the zeta potential of the suspended particle. While Brownian motion will be only related to the temperature and the viscosity of the suspension, varying the pH of the solution enables control of the zeta potential around the particles. Although, zeta potential change has negligible affect on the acoustic field, it changes the electrostatic interaction between the particles depending on the value of the pH change. In this sense possibility of calculating the dispersion force due to the repelling of charged particles and Brownian motion can be used to estimate the counter balancing ultrasonic force produced by the acoustic field. Our preliminary results show that 500 nm silica beads suspended in pH 7 solution, having about -30mV of measured zeta potential tend to collect in a broader range forming a cloudy structure compared to the same particles in pH 3 solutions. The tightly packed structures form due to smaller zeta potential. The size of the radiation-induced force induced clusters is a sensitive function of the zeta function. Since the radiation force experiments can be run on samples with different zeta potentials, a quantitative value for the radiation forces can be extracted. This extraction procedure and analysis of the limits of the procedure will be presented.

1) M.K.Araz, C.H.Lee, A.Lal, “Ultrasonic Separation in Microfluidic Capillaries” IEEE UFFC, Honolulu, 2003

2) M.K.Araz, C.H.Lee, A.Lal, “Finite Element Modeling of Ultrasonic Separation at the Microscale”,IEEE UFFC, Montreal, 2004

PS-12
CANTILEVER RESONANCE INDUCED IN SITU BY MAGNETOSTRICTION FOR ACTIVE FLOW CONTROL.

O. DUCLOUX*[1], N. TIERCELIN[1], Y. DEBLOCK[1], P. PERNOD[1], V. PREOBRAZHENSKY[1,2], and A. MERLEN[3], [1]LEMAC / IEMN-DOAE – UMR CNRS 8520, Ecole Centrale de Lille, Cité Scientifique - Av Poincaré, Villeneuve d’Ascq, France, [2]LEMAC / Wave Research Center - GPI-RAS, Moscow, Russia, [3]LEMAC / LML UMR CNRS 8107, Villeneuve d’Ascq, France.
Corresponding e-mail: olivier.ducloux@iemn.univ-lille1.fr

Active flow control is at the intersection between the needs of the aerospace industry and the possibilities of microactuators. By controlling the flow on air wings for example, one may decrease dramatically aircraft fuel consumption and/or noise. Such a control can be achieved for example by pulsed air blowing through submillimetric holes distributed at specific locations of the wings of the airplane [1]. To achieve such pulsed jets, a microvalve containing an internal resonant cantilever actuated by a magnetostrictive film has been designed, fabricated and characterized. The microvalve is fed by a pressurized source of air and the resonating cantilever acts as a deflector on the internal fluid flow addressed alternatively to the output hole on the wing’s surface or to a recycling output.

Magnetostrictive films were chosen as actuating means for they can provide high induced stress compared to other kinds of active materials, and also because of their remote actuation capability. In this device, artificially nanostructured TbCo/FeCo multilayers were used: in these layers, a large magnetoelastic coupling can be kept while having a well-defined in-plane magnetic anisotropy, with a relatively low saturation field. These characteristics allow the induction of a Spin Transition Reorientation (SRT) state in the layer: the SRT corresponds to a magnetic instability that is used to increase dramatically the magnetoelastic sensitivity[2] and make it compatible with silicon Microsystems : that way, the field produced by the two microcoils is sufficient for the dynamic actuation.

The actual microsystem consists in a 1000 µm long and 1.5 µm thick polysilicon cantilever on which a nanostructured magnetostrictive film is deposited by RF Sputtering: (TbCo/FeCo)xn, total thickness 0.5 µm to 1µm. On each edge of the cantilever, one microcoil has been processed with 4 windings and a wire thickness of 20 µm. Each coil produces the 20 Oe dynamic magnetic field necessary for the actuation. The magnetic field is then transmitted from one coil to the other via the magnetostrictive film, enabling the cantilever’s resonance at a 2 kHz frequency.

Characterization of the resonance frequency, amplitude and magnetoelastic coefficient are achieved by interferometric means. Outcoming flow is visualized by conventional strioscopy method using He / Air optical indice difference. The results of these characterizations are presented

[1] Kumar, S.M.; Reynolds, W.C.; Kenny, T.W.; “MEMS based transducers for boundary layer control”, Micro Electro Mechanical Systems, 1999. MEMS ’99. Twelfth IEEE International Conference on 17-21 Jan. 1999 Page(s):135 - 140

[2] N. Tiercelin, V. Preobrazhensky, P.Pernod, H. Le Gall, J. Ben Youssef, “Nonlinear actuation of cantilevers using giant magnetostrictive thin films”, Ultrasonics 38(2000) 64-66

PS-13

DOUBLE-RESONANCE SAW FILTERS.

J. MELTAUS*[1], V. P. PLESSKY[2,1], and S. S. HONG[3], [1]Helsinki University of Technology, Espoo, Finland, [2]GVR Trade SA, Bevaix, Switzerland, [3]Samsung Electro-Mechanics Co., Ltd., Suwon, Korea.
Corresponding e-mail: johanna.meltaus@hut.fi

We present SAW filters based on a double resonance appearing in structures consisting of long interdigital transducers (IDT) separated by a λ/4-gap. This type of device was proposed by Plessky et al in 1996 [1]; it was called degenerated coupled resonator filter (CRF) because its topology combines characteristics of CRF and impedance elements. Although COM modeling showed filter response with low loss and small standing wave ratio, experimental results [1] gave unsatisfactory performance with 6-8 dB insertion loss. We show that the loss was caused by scattering and attenuation in the gap, prominent in this type of device with resonant energy concentrated in the gap. Replacing the gap with a distributed gap will radically decrease the loss level [2]. To achieve low loss, the anti-resonance frequency of the synchronous resonance of the long IDTs must coincide with the frequency of the hiccup resonance arising in the gap. The anti-resonance of the IDTs cancels the static capacitance of the structure, self-matching the filter. We describe three variants: a single-ended 2-IDT filter, a 3-IDT filter with balanced output, and a 3-IDT filter with cascaded characteristics.

Topologically, the structures studied here resemble a standard CRF. The operation, however, is not similar to that of a CRF. Long structures give rise to strong reflections that prevent acoustic propagation in the device. In a 2-IDT device, electrical signal is transmitted from input to output by excitation of a synchronous resonance in the first IDT and a hiccup resonance in the gap. Gap resonance transmits a part of the acoustic energy to the second IDT, creating a voltage in the bus bars and a synchronous resonance in the IDT. The hiccup resonance is spatially localized in the gap, as opposed to CRF where resonance modes are distributed over the length of the device. Therefore, we feel that it is more precise to call the structure a double-resonance filter.

Above-described scheme of operation can be applied to situation with more than one gap; e.g., for 3 IDTs separated by 2 distributed gaps, transmission of signal from input at first IDT via center IDT to output at third IDT is possible, if the central transducer is left open-circuited. The characteristics of such a filter are similar to that of two 1-gap filters cascaded. Grounding the center IDT eliminates the uniform resonance in this part of the structure and prevents the transfer of the signal from input to output.

The 3-IDT structure can operate with input in the center and output at sides, typical of a standard CRF. In this case, the resonances in the two gaps are connected in parallel, and the skirts will not be as steep as for the cascaded variant. Such a symmetric structure can be employed with unbalanced input and balanced output.

Measurements confirm the simulations of the described scheme of operation, and experimental data will be presented. The structures described here are ideal for filters with 1...1.5 % bandwidth requiring extremely low loss and small standing wave ratio.

[1] V. P. Plessky et al, 1996 IEEE Ultrasonics Symposium, pp. 25-28.
[2] W. Wang et al, 2004 IEEE Ultrasonics Symposium, pp. 1363-1366.

PS-14

IDENTIFICATION OF NEW LTO HVPSAW ORIENTATIONS CONSIDERING FINITE THICKNESS ELECTRODES.

T. KENNY* and M. PEREIRA DA CUNHA, University of Maine, Orono.
Corresponding e-mail: mdacunha@eece.maine.edu

The continuing trend towards higher operating frequencies in RF communications has strained SAW filter fabrication capabilities, focusing recent efforts on identifying low-attenuated high velocity pseudo-surface acoustic wave (HVPSAW) orientations of quartz, lithium niobate (LNO), lithium tantalate (LTO), and lithium tetraborate (LBO). In particular, LTO is a well established SAW substrate widely used for wireless applications, due to its relatively high electromechanical coupling and moderate temperature sensitivity in comparison to the other substrates previously mentioned. Although HVPSAW propagation directions have been recently identified in the literature for these materials, several show diminished coupling or prohibitively high propagation losses. Others imply the use of heavy mechanical loading by the use of thick electrodes to achieve reduced device loss.

This paper reports on the investigation of LTO HVPSAW excitation and propagation properties, including: phase velocity, propagation loss per wavelength (λ), and electromechanical coupling (K^2) for arbitrary orientations under periodic aluminum (Al), gold (Au), and platinum (Pt) electrodes. The harmonic admittance of periodic electrodes is calculated using orthogonal Chebyshev basis functions in conjunction with the finite element method. The determination of well defined complex poles in the harmonic admittance curve as a function of crystal rotation leads to the identification of low-attenuated and high coupled HVPSAW orientations. For example, along selected orientations of the LTO (0°,120°,ψ) plane, HVPSAWs are identified which exhibit phase velocities around 5000 m/s, propagation losses as low as 0.04 dB/λ, and K^2=0.74 %, for Al and Au electrodes with thicknesses h/λ=9% and h/λ=3%, respectively. For the same electrode materials and thicknesses, the HVPSAWs propagating under a uniform film layer show propagation losses around 0.3 dB/λ, using matrix method calculations. Therefore, the resulting decrease in propagation loss by more than one order of magnitude demonstrates the importance of the grating

structure in achieving low loss operational HVPSAW devices. The reported work identifies new LTO HVPSAW orientations, exhibiting high phase velocity, low propagation loss, and high electromechanical coupling, suitable for high frequency, low loss communication and sensor applications.

This work was conducted with support from the National Science Foundation (grants ECS-0233463 and ECS-0134335).

PS-15

HEXAGONAL SAW DEVICES FOR ENHANCED SENSING.

S. CULAR*[1], V. BHETHANABOTLA[1], and D. BRANCH[2], [1]University of South Florida, Tampa, FL, [2]Sandia National Laboratories, Albuquerque, NM.
Corresponding e-mail: cular@eng.usf.edu

We present the design, fabrication and testing of a novel, hexagonal array based on 36° YX lithium tantalate for non destructive evaluation of thin inorganic and biological films. Propagation along the x-axis generates the leaky shear horizontal (SH) mode where off axis propagation excites Rayleigh type surface acoustic waves (SAW). Our approach permits rapid and simultaneous extraction of multiple film parameters. Given that SAW devices are in widespread use for chemical and biological sensing; a need exists to rapidly interrogate the interface for several parameters. This is especially relevant in biological applications when the sample quantity can be very limited. Our design allows for the simultaneous extraction of multiple properties (film material density or thickness, Lamé and shear moduli, sheet conductivity) of a thin film material to achieve a more complete characterization than when a single SAW device is utilized. In sensor applications, this capability translates to better discrimination of the analyte and possibly more accurate determination of the concentration. We present this device as an alternative to a SAW sensor array configuration that does not allow for simultaneous probing and which would require larger devices and packaging. These cost advantages are significant when working with novel piezoelectric materials. The device is based on a double split finger delay-line with widths of 4 μm and a delay path of 197λ. The individual delay path of each hexagonal device intersects in the center of the die producing a single region for sensor analysis. Additionally, the central region where the acoustic waves intersect is shorted to reduce the number of modes of waves traversing the surface. Initial testing has shown the pass band frequency of the individual delay paths to be centered around 97 MHz. The acoustic velocities of the rotated device have been measured to be 3452 m/s, 3161 m/s, and 3331 m/s, which correspond to the theoretical range of all acoustic waves in the crystal of velocities 3290-4160 m/s. This variation is sufficient to allow for the simultaneous solution of the same wave parameter dependent equation that will allow for the multiple properties of the sensing film to be extracted.

We would like to thank Nancy Saldanha and Dr. Don Malocha of the University of Central Florida for the use of fabrication equipment and insightful discussions. Support for this work has been provided by NSF grant number DGE-0221681 and the University of South Florida CERC.

PS-16

A HIGH FREQUENCY VARIABLE FOCUS ULTRASONIC TRANSDUCER USING POLYUREA THIN FILM.

M. NAKAZAWA*[1], T. KOSUGI[1], K. NAKAMURA[1], S. UEHA[1], A. MAEZAWA[2], and Y. HIRAO[3], [1]Tokyo Institute of Technology, Yokohama, Japan, [2]Konica Minolta, Tokyo, Japan, [3]Kobayashi Institute of Physical Research, Tokyo, Japan.
Corresponding e-mail: nakazawa@sonic.pi.titech.ac.jp

Polyurea thin film has useful characteristics as a high frequency ultrasonic transducer material such as a low acoustic impedance of seventy percentages of that of PVDF, considerably high piezoelectric constants compatible with conventional piezoelectric polymers, and a higher Curie temperature. Fabrication on curved surfaces and multi-layer lamination are possible by vapor deposition polymerization. However, few studies have been made on the application for ultrasonic transducers.

This report presents fabrications and experimental evaluations of the non-focusing, the line/point-focusing, and the variable focus transducers with polyurea thin films. First, the vapor deposition polymerization process using two monomers is briefly reviewed, and the temperature condition for higher piezoelectric constants is explored. Flat polyurea thin film transducers of about 1 μm thickness are deposited on polyimide films of 25 μm, while focusing transducers are fabricated on spherical plano-concave optical lenses with diameters of 20 mm and radius curvatures of 25 mm, 50 mm, 80 mm, and 100 mm. Here, the polyurea layer of 1 - 100 μm is sandwiched by two aluminum electrodes.

The resonant frequency, the mechanical Q, and the electromechanical coupling factor were evaluated through the electrical measurement with an impedance analyzer. Pulse transmitting/receiving experiments were carried out at the resonant frequencies to determine focusing parameters. These experiments show that the polyurea transducer works effectively at over 100 MHz and is suitable for a high frequency diagnostic ultrasound transducer.

A line focusing transducer with the variable focal length was also prototyped. A polyurea thin film of 5 - 7 μm is deposited on a flexible polymer film as a transducer element. The film transducer is attached in the gap between two mechanical sliders, so that the transducer may be bent and its radius of curvature may be mechanically controlled by the gap width. The continuous change of the focal length from 0.8 mm to 2.54 mm was successfully demonstrated in the pulse transmitting/receiving experiments.

A high resolution B-mode imaging of living tissue using the polyurea focusing transducer will be discussed as a preliminary study for fabrication high density array transducers.

PS-17

3-D ULTRASOUND IMAGING USING FORWARD-VIEWING CMUT RING ARRAYS FOR INTRAVASCULAR AND INTRACARDIAC APPLICATIONS.

D. YEH*[1], O. ORALKAN[1], I. WYGANT[1], M. O'DONNELL[2], and B. KHURI-YAKUB[1], [1]Stanford University, Stanford, CA, [2]University of Michigan, Ann Arbor.
Corresponding e-mail: dtyeh@stanford.edu

Forward-viewing intravascular ultrasound enables new procedures in medicine such as diagnosing severely occluded blood vessels or guiding the placement of stents. Using a forward-viewing transducer in catheter-based applications requires clearance in the center of the transducer for the guidewire, and requires the development of a ring array. It is challenging to design and fabricate piezoelectric transducers of the dimensions needed for forward-looking ring arrays. However, Capacitive Micromachined Ultrasonic Transducers (CMUTs) can be used to develop such arrays. This paper presents the first full synthetic phased array volumetric images from CMUT ring arrays with integrated electronics.

CMUTs offer several advantages over piezoelectric transducers for use in medical imaging. Microlithography is used to make CMUTs and routinely yields the finely controlled dimensions required for high frequency ring arrays. In addition, the CMUT can be switched on-demand between its two modes of operation during the imaging procedure, thereby providing a choice between the low frequency conventional mode for navigation and the high frequency collapse mode for diagnosis.

The CMUT ring array demonstrated in this paper has the following parameters: ring diameter, 2 mm; number of elements, 64; element pitch, 102 μm; element size, 100$\times$100 μm; cells per element, 9; cell membrane radius, 13 μm.

The imaging setup consists of the CMUT mounted in a 209-pin PGA package with the array elements wire bonded to 64 transmit/receive channels in a bank of four integrated circuits. The full synthetic phased array data set was collected by exciting one element at a time, and acquiring signals from the entire array for each transmit element. Each A-scan was acquired at a sampling rate of 500 MS/s for both collapse and conventional modes, with 16 averages, and without averaging. The imaging phantom consists of three steel wires 0.30 mm in diameter. A-scan data indicates that the transducer operates conventionally at 7.5 MHz with a 6-dB bandwidth of 8.5 MHz, and in collapse mode at 19 MHz with a bandwidth of 13 MHz. A conical volume was reconstructed offline from the complete 64$\times$64 set of A-scans, weighted for full-aperture resolution and cosine apodization. The wires are clearly visible in images reconstructed from data taken with no averaging, and demonstrate the good SNR of the CMUT. Because of higher operating frequency and reduced crosstalk, collapse mode produces images with a narrower main lobe than conventional mode imaging.

We have demonstrated 3-D ultrasound imaging with a forward-viewing CMUT ring array using the first full synthetic phased array data taken using a ring array. A fully integrated system with flip-chip bonded electronics will further

improve performance and SNR. These results show that forward-looking probes for intravascular ultrasound are well on their way to becoming reality.

This work is funded by the National Institutes of Health. David Yeh is supported by a National Defense Science and Engineering Graduate Fellowship.

PS-18
ANALYSIS AND DESIGN OF DUAL-ELECTRODE CAPACITIVE MICROMACHINED ULTRASONIC TRANSDUCERS.

R. O. GULDIKEN* and F. L. DEGERTEKIN, Georgia Institite of Technology, Atlanta.
Corresponding e-mail: gtg181u@mail.gatech.edu

Although ultrasound imaging arrays based on conventional Capacitive Micromachined Ultrasonic Transducers (CMUTs) have been shown to have adequate performance, the flexibility offered by microfabrication techniques can be exploited to further enhance the capabilities of CMUT arrays. With multiple electrodes embedded in dielectric CMUT membrane, dual-electrode CMUTs that can be considered an example of this approach improving both transmit and receive performance of the CMUTs without relying on collapsed membrane operation [1]. Simple parallel-plate electrical equivalent circuit model suggests that the electromechanical transformer ratio close to collapse depends only on the gap thickness but not on the absolute value of the collapse voltage. The advantage of the dual-electrode structure in the receive mode becomes apparent when non-zero DC bias is applied to the side electrodes reducing the effective gap for the center receive electrode. However, in contrast to the ideal parallel plate CMUT, the maximum improvement with gap thickness reduction is limited in CMUTs with dielectric membranes. As predicted by coupled finite element analysis, when the bias voltage applied to the side electrodes is increased over a certain value, the bottom of the silicon nitride membrane underneath the center electrode makes contact with the bottom surface before the device is forced into unstable collapse region and reach the maximum possible receive sensitivity. Therefore, minimizing the dielectric layer thickness between the receive electrode and the bottom electrode, e.g. eliminating the isolation layer over the bottom electrode, helps improve the receive performance. These predictions are verified by experimental data obtained on dual-electrode CMUTs by recording receive signal amplitude as a function of side and center electrode bias voltage. Dual-electrode CMUT design for transmit performance improvement involves placement of side electrodes and shaping the silicon nitride membrane to increase maximum volume displacement. For example, using 0.4μm deep, 1μm wide notches between 4μm wide center and side electrodes in a 0.9μm thick 20μm wide rectangular silicon nitride membrane improves the overall performance of CMUT by 10.7dB over conventional CMUT. This is achieved while reducing the required maximum (collapse) voltage levels from 90V to 50V for center receive electrode when 70V is applied to the side electrodes. Analysis methods, experimental results, and optimal dual-electrode CMUT designs are discussed in detail in this paper.

[1] R.O. Guldiken, J. McLean and F.L. Degertekin, “CMUTs with Dual-electrode Structure for Improved Transmit and Receive Performance,” submitted to IEEE Trans. Ultrason., Ferroelect., Freq. Contr., 2005.

Session: P1A

BLOOD FLOW
Chair: E. Ebbni
University of Minnesota

P1A-1
SYNTHETIC APERTURE FLOW ANGLE ESTIMATION ON IN-VIVO DATA FROM THE CAROTID ARTERY.

N. ODDERSHEDE* and J. A. JENSEN, Center for Fast Ultrasound Imaging, Technical University of Denmark, Denmark.
Corresponding e-mail: no@oersted.dtu.dk

In conventional ultrasound velocity estimation systems only the velocity projected onto the direction of the steered ultrasound beam is found. It has previously been shown how true blood flow velocity magnitudes can be found using synthetic transmit aperture imaging. The method is based on cross-correlation between lines beamformed along the flow direction. This method assumes the direction of flow is known.

Jensen (2004) presented a method for estimating the direction of flow. The angle determination method is based on a search for the maximum normalized cross-correlation as a function of angle. It assumes the largest correlation is seen for the angle of flow. Previously, this method has only been validated using data from a circulating flow rig. This paper presents an In-Vivo investigation of the method.

Real time data covering a full cardiac cycle of the carotid artery of a healthy 34-year old male volunteer is acquired and then processed off-line using a large computer cluster.

Data are acquired using our RASMUS experimental ultrasound scanner and a 128 element 7 MHz linear array transducer with λ pitch. A 20 μs chirp was used during emission and virtual transmit sources were created in front of the transducer using 64 transmitting elements. Data from 9 transmissions with each 64 receiving elements are beamformed and coherently summed to create high resolution lines at different angles for a set of points within the region of flow. The pulse repetition frequency was set to 16.5 kHz.

The direction of flow is estimated using the above mentioned method. It is compared to the flow angle of 110° with respect to the axial direction, determined visually from the B-mode image. For a point in the center of the common carotid artery, the flow angle is estimated with a bias of -2.2° and a standard deviation of 20.5° over time.

Blood velocity magnitudes along the individual angle estimates are found and compared to velocities estimated along the visually determined direction. The

velocity difference had a bias of 0.0014 m/s and a standard deviation of 0.14 m/s. The peak systolic velocity was around 1 m/s.

Full color flow maps from different parts of the cardiac cycle are presented, including vector arrows indicating both estimated flow direction and velocity magnitude.

This work was supported by grant 26-04-0024 from the Danish Science Foundation and by B-K Medical A/S.

P1A-2

REAL-TIME ADAPTIVE CLUTTER REJECTION FILTERING IN COLOR FLOW IMAGING USING POWER METHOD ITERATIONS.

L. LOEVSTAKKEN*[1], S. BJAERUM[2], K. KRISTOFFERSEN[2], and H. TORP[1], [1]Norwegian University of Science and Technology, Trondheim, Norway, [2]GE Vingmed Ultrasound, Horten, Norway.
Corresponding e-mail: lasse.lovstakken@medisin.ntnu.no

The removal of signal from stationary and moving tissue is a necessity and a challenge in ultrasound Color Flow Imaging (CFI) and related techniques. This task has conventionally been performed by using fixed response temporal high-pass filters prior to blood flow parameter estimation. By adapting the clutter rejection filter to the clutter signal statistics, better attenuation of the clutter signal can be achieved in normal as well as more extreme cases of clutter movement and acceleration. This improvement can provide a better detection of blood flow and ensure less biased velocity estimates, which in the clinical setting can translate to a more clear diagnosis of patients with abnormal flow patterns related to pathology.

We propose a new algorithm for real-time adaptive clutter rejection filtering in CFI related techniques, based on the eigenvector decomposition of the signal correlation matrix in image regions of uniform clutter statistics. The filtering is performed by projecting the signal vector for a given sample volume onto the complement of an eigenvector basis representing the clutter signal subspace. This method has previously been shown to be superior to conventional fixed response high-pass filtering, but has until now been considered too computationally demanding for real-time processing in general higher frame rate modalities.

By using packet acquisition with interleaving, the acquisition time is short between neighbouring beams, and sampling of uniform clutter statistics by averaging in the lateral as well as the radial direction of the image can be properly obtained. A rectangular averaging grid coinciding with the interleave group size determines the number of filters that need to be estimated for each frame. Using the iterative power method technique, the dominant eigenvalues and corresponding eigenvectors within each averaging region can effectively be estimated. The power method converges rapidly when the dominant eigenvalue is large relative the remaining eigenvalues. This is shown to be the case when clutter is present, and by using the convergence rate of the power method as a criterion for deciding if there is remaining clutter, a clutter subspace basis can be found.

The real-time performance of the algorithm is sufficient on standard CPUs used in desktop computers today, and a filter prototype has been implemented on a GE Vingmed Vivid 7 ultrasound system. By using the number of algorithmic floating point instructions (flops) as a measure of performance, the algorithm has been compared to that of FIR and polynomial regression filtering. For a representative example, the flop count for filtering one packet frame using the new algorithm was 2.7 Mflops, compared to 1.2 Mflops for polynomial regression filtering, and 0.50 Mflops for FIR filtering. Images of real-time scanning using the new algorithm will be given, showing the superiority of adaptive filtering for detection of blood flow and for removing clutter artifacts.

P1A-3
A NEW EIGEN-BASED FLOW ESTIMATOR USING THE MATRIX PENCIL APPROACH.

A. YU*[1], L. MO[2], R. WARRINER[1], and R. COBBOLD[1], [1]University of Toronto, Toronto, ON, Canada, [2]ZONARE Medical Systems, Mountain View, CA.
Corresponding e-mail: cobbold@ecf.utoronto.ca

In color flow imaging, velocity estimation is often performed by applying a clutter filter to remove low-frequency components in the slow-time signal and then using a correlation-based strategy to find the mean flow velocity. However, the clutter filter may distort the flow spectrum and lead to significant estimation biases when the flow spectrum is near the filter cutoff frequency. As such, our aim is to develop a more consistent flow estimation strategy that performs well in various flow regimes.

In this paper, we describe a new eigen-based flow estimation strategy that can be directly applied to the slow-time signal without prior clutter filtering. Our new estimator, which is based on a framework originally developed for system pole estimation, works by exploiting the algebraic properties of a mathematical entity called matrix pencil and in turn treating flow estimation as a generalized eigenvalue problem. Similar to a previously reported eigen-based estimator [1] known as MUSIC, the Matrix Pencil can be considered as a principal spectral component estimator whose eigenstructure is assumed to be the set of dominant complex exponentials in the slow-time signal. Hence, by including the clutter harmonics as part of its eigenstructure, this new estimator can extract the mode flow velocity in the presence of clutter. In comparison to MUSIC, the Matrix Pencil should give more consistent flow estimates since it does not rely on covariance matrix statistics. Also, because its formulation does not involve eigenroot searches after eigendecomposition, it should be more computationally efficient.

We studied the Matrix Pencil estimator using raw color flow data acquired with a 5 MHz linear-array scanner and a steady flow phantom (5 mm tube diameter). For this study, the clutter-to-blood signal ratio near the vessel wall was estimated to be between 20-30 dB. As well, the Matrix Pencil assumed that the slow-time signal has two principal complex exponentials: one corresponding to the clutter harmonic and the other to the flow harmonic. For comparison, flow estimation was separately performed using an autocorrelator with a Chebyshev-I high-pass filter (5th order, step initialized, and normalized cutoff frequency of 0.1).

Our results indicate that the estimates from the Matrix Pencil were comparable to the ones obtained from the autocorrelator. In particular, given a 14-point ensemble length and a center line velocity of 70 cm/s, the average estimation difference between the two approaches was only 2.4 cm/s. Also, our spectral analysis of individual color flow pixels show that the two mode frequency estimates from the Matrix Pencil were close in location with the two largest Fourier coefficients of the slow-time power spectrum.

We anticipate that the Matrix Pencil can be applied to various flow scenarios such as the microcirculation. Indeed, this new estimator should be particularly useful in micro-flow studies because the presence of tissue motion near the microcirculation would considerably increase the complexity of clutter suppression.

Reference: [1] Vaitkus and Cobbold, IEEE Trans. UFFC, pp. 939-954, 1998.

P1A-4

DETERMINATION OF VELOCITY VECTOR ANGLES FOR THE DIRECTIONAL CROSS-CORRELATION METHOD.

J. KORTBEK*[1,2] and J. JENSEN[1], [1]Center for Fast Ultrasound Imaging, Technical University of Denmark, Denmark, [2]B-K Medical, Herlev, Denmark.
Corresponding e-mail: jk@oersted.dtu.dk

For conventional blood velocity estimation systems the velocity estimate is a projection of the true velocity onto the ultrasound beam. It is thus impossible to detect transverse flow, and these systems rely on knowledge of the angle between the flow vector and the direction of the ultrasound beam, which traditionally is determined visually from B-mode image.

In this paper a method is suggested for determining both velocity magnitude and angle in any direction in the image plane without using B-mode image and with a computational demand which permits implementation in a conventional scanner. Beamforming along a given direction creates spatial signals denoted directional signals. These signals are focused along the velocity direction, and a cross-correlation is used for finding the correct velocity magnitude. The angle is found from beamforming directional signals in a number of directions and then selecting the flow angle as the direction with the highest normalized correlation value between consecutive directional signals.

The focusing of directional signals is a key element in this method. Different ways of calculating the time-of-flight and the influence on the estimation results are presented. The standard deviation for the angle estimation for a flow angle of 60° improves from 4.5° to 2.8°, when the transmit time-of-flight is calculated using a virtual source instead of between transmit aperture center and focusing point.

The approach is investigated using Field II simulations and data from the experimental ultrasound scanner, RASMUS. A 7 MHz linear array transducer is used with a normal transmission of a focused ultrasound field. The performance of the velocity and the angle estimator is presented for parabolic flow at angles

45°, 60°, 75° and 90° with a peak velocity of 0.3 m/s. Not more than 20 pulse-echo emissions are used for the estimations.

For the velocity magnitude estimation, a mean relative bias and standard deviation are calculated over the profile. In simulations the bias and standard deviation for the velocity magnitude are all 1% for flow at 45° and 60°. At 75° and 90°, the bias is 4% in both cases and the standard deviations are 2% and 7%, respectively. For the angle estimation, a probability of having estimates within the range ± 15° from the true angle is calculated. The bias and standard deviation of the angle estimation are calculated from the estimates that are within that range. In simulations the bias and standard deviation are between 0.3° and 2.3° and the probabilities are above 99%. Measurements are made with the experimental scanner RASMUS, and for velocity estimation the standard deviation is between 2.5% and 14% for flow between 45° and 90°. For angle estimation the bias and standard deviation at 60° to 90° are between 1.0° and 3.4° and the probabilities are above 98%.

This work was supported by grant 9700883, 9700563 and 26-04-0024 from the Danish Science Foundation and by B-K Medical.

P1A-5
BLOOD VELOCITY ESTIMATION USING SPATIO-TEMPORAL ENCODING BASED ON A FREQUENCY DIVISION APPROACH.

F. GRAN*, S. NIKOLOV, and J. A. JENSEN, Center for Fast Ultrasound Imaging, Technical University of Denmark, Copenhagen, Denmark.
Corresponding e-mail: fg@oersted.dtu.dk

This paper investigates the possibility for flow estimation using spatio-temporal encoding of the transmissions based on a frequency division approach in synthetic transmit aperture imaging (STA).

In STA, a major disadvantage is that only a single transmitter (denoting single transducer element or a virtual source) is used in every transmission. The transmitted acoustic energy will be low compared to a conventional focused transmission where a large part of the aperture is used. By using several transmitters simultaneously the transmitted energy can be increased.

However, to focus the data properly, the information originating from the different transmitters must be separated. To do so, the pass band of the transducer is divided into a number of sub-bands with disjoint spectral support. At every transmission, each transmitter is assigned one of the sub-bands. In receive, the signals are separated using a simple filtering operation. To attain high axial resolution, broad-band spectra must be synthesized for each of the transmitters. By multiplexing the different waveforms on different transmitters over a number of transmissions this can be accomplished. To further increase the transmitted energy, the waveforms are designed as linear frequency modulated signals implying that the full excitation amplitude can be utilized during most of the transmission.

The method has been evaluated for blood velocity estimation for several different velocities and incident angles. The program Field II was used. A 128 element transducer with a center frequency of 7 MHz was simulated. 64 transmitting element were used as the transmitting aperture and 128 elements were used as the receiving aperture. Four virtual sources were created in every transmission. Each virtual source was created by 16 transducer elements focused 5 mm in front of the transducer. To generate a smooth broad-band spectrum for each virtual source, eight excitation waveforms had to be designed. Every transmission yields a temporally narrow-band low resolution image for every virtual source. By multiplexing the waveforms for the different virtual sources and combining the result of several transmissions, broad band excitation waveforms are synthesized for each virtual source. By beamforming lines in the flow direction, directional data was extracted and correlated. Hereby, the velocity of the blood was estimated. The pulse repetition frequency was 16 kHz.

Three different setups were investigated with flow angles of 45, 60 and 75 degrees with respect to the acoustic axis. Four different velocities were simulated for each angle at 0.10, 0.25, 0.50 and 1.00 m/s. The mean relative bias with respect to the peak flow for the three angles was 2.34, 2.61 and 4.85% and the mean relative standard deviation with respect to the peak flow was 0.98, 0.86 and 1.27% respectively.

This work was supported by grant 9700883, 9700563 and 26-01-0178 from the Danish Science Foundation and by B-K Medical A/S, Denmark.

P1A-6
DESTRUCTION-MODE OPTOACOUSTIC FLOW MEASUREMENTS WITH GOLD NANORODS.

P.-C. LI*[1], S.-W. HUANG[1], C.-W. WEI[1], and C. R. WANG[2], [1]Department of Electrical Engineering, National Taiwan University, Taipei, Taiwan, ROC, [2]Department of Chemistry and Biochemistry, National Chung Cheng University, Chia-Yi, Taiwan, ROC.
Corresponding e-mail: paichi@cc.ee.ntu.edu.tw

Time-intensity based blood flow measurements have been widely applied in various imaging modalities. In optoacoustic imaging, we have previously tested the hypothesis that gold nanospheres can be used for quantitative flow estimation based on wash-out analysis. In this study, a wash-in flow analysis method using gold nanorods is developed. Specifically, the proposed technique makes use of the shape dependence of the optical absorption wavelength of gold nanorods and their shape transformation after pulsed laser irradiation. Gold nanorods have unique optical properties based on their surface plasma absorption and the transformation results in a shift in the peak absorption wavelength. The shape transformation property does not exist on gold nanospheres. Also, the photon-induced shape transformation of the gold nanorod system exhibits mainly a rod-to-sphere conversion. Therefore, with pulsed laser irradiation at a wavelength that corresponds to the peak optical absorption of the original shape of the gold nanorods, the particles that undergo shape changes can be viewed as being destructed by laser irradiation at that wavelength. A series of laser pulses with lower laser energy can then be applied to monitor the acoustic

intensities as a function of time as new gold nanorods wash in the region of interest. Quantitative flow information can then be derived from the temporal intensity data. Based on this property, a destruction-mode technique was developed. With this technique, a destruction laser pulse is followed by a series of observation pulses. Phantom experiments were conducted. 0.26 nM of gold nanorods were injected into a vessel with a diameter of 5 mm connected to a polyvinyl alcohol phantom. The gold nanorods had an optical absorption peak at 1018 nm. A Nd:YAG laser operating at 1064 nm with a pulse duration of 5 ns was used for optical illumination. The laser radiation power was 73.1 mW for the destruction pulse and 11.3 mW for the observation pulse. The pulse repetition rate was 15 Hz. An ultrasonic single element transducer with a center frequency of 1 MHz was employed to detect the acoustic signals. After detection, the acoustic waveforms were amplified and sampled at 100 MHz by a data acquisition card housed in a personal computer on which subsequent data analysis was performed. Laser irradiation was from the top of the vessel and the acoustic detection was from the side. To prevent recirculation of the nanoparticles back in the phantom, the water only passed through the phantom once. The flow velocity ranged from 0.1 mm/s to 2.3 mm/s. The linear regression results show that the correlation coefficient between the measured velocities and the true values was close to unity (0.96), thus demonstrating the feasibility of the proposed destruction-mode technique for quantitative flow estimation in optoacoustic imaging.

P1A-7

A SIMPLE METHOD TO REDUCE ALIASING ARTIFACTS IN COLOR FLOW MODE IMAGING.

J. UDESEN*[1,2], S. I. NIKOLOV[1], and J. A. JENSEN[1], [1]Center for Fast Ultrasound Imaging, Technical University of Denmark, Lyngby, Denmark., [2]B-K Medical A/S,, Herlev, Denmark.
Corresponding e-mail: ju@oersted.dtu.dk

It is a well known limitation in conventional blood velocity estimation using a phase estimation approach, that aliasing artifacts are present, when the blood velocities exceed a value determined by half of the pulse repetition frequency (the Nyquist frequency) of the ultrasound system. In this paper we propose a simple method to increase the aliasing limit to twice the Nyquist frequency.

The method is based on a conventional autocorrelation estimator. Normally N=8 to N=16 emissions in the same direction are used to estimate the axial velocity. In the suggested method N/2 emissions are fired at a pulse repetition period Tprf. After a time period of 1.5 Tprf the N/2 emissions are repeated. All N emissions are used to determine the mean phase vector P1 for emissions separated Tprf in time. To determine whether aliasing is present, another phase vector P2 is estimated for the two emissions N/2 and N/2+1. The sign of the angle θ between P1 and P2 is used to determine whether aliasing occurs. θ is found by estimating the angle to the vector P = P1* P2, where (*) denotes complex conjugate. The method is limited to angles where $-\pi<\theta<\pi$. This corresponds to Doppler frequencies smaller than twice the Nyquist frequency 1/(2Tprf) of the system. To increase signal to noise ratio on the estimates, RF-averaging is performed over a pulse length in the axial direction.

The method is tested in simulations using the Field II program. A virtual 7 MHz linear array transducer is used to scan a virtual blood vessel of radius 6.7 mm, situated at a depth of 40 mm at an angle of 70 deg to the ultrasound beam. Hanning apodization is applied both in transmit and receive. The pulse repetition time Tprf of the system is 0.5 msec, and the scatters are moved, so that parabolic flow is simulated with a maximum velocity of 0.4 m/s. These values give aliasing at the center of the vessels inside a radius of 3.15 mm. The velocity is found along one axial line where N=8 emissions are used for each velocity estimate, and 24 velocity profiles are found along the axial line. The proposed method gives a mean standard deviation and a mean bias of the axial velocity over the vessel of 1.3%, and 3.5%, respectively. This should be compared to the case where a conventional autocorrelation estimator is used to find the axial velocity. Here the mean bias over the vessel is 23.3%, and the mean standard deviation is 5.3%. The large bias of 23.3% is due to the aliasing.

The method is tested experimentally using the ultrasound scanner RASMUS and a circulating flowrig with parabolic flow. All the setup parameters are kept the same as in the Field II simulation. When the proposed method is used, the mean bias over the vessel is 1.2%, and the mean standard deviation is 4.8%. This should be compared to the conventional case, where the mean bias over the vessel is 20.0%, and the mean standard deviation is 3.9%.

This work was supported by grant 9700883,9700563 and 26-01-0178 from the Danish Science Foundation, the Ministry of Science, Technology and Development, and by B-K Medical A/S, Denmark.

Session: P1B

ELASTOGRAPHY
Chair: P.-C. Li
National Taiwain University

P1B-1

ANALYSIS OF TRANSIENT SHEAR WAVE GENERATION FOR REAL-TIME SHEAR ELASTOGRAPHY IN-VIVO.

S. YAGI*[1], A. SANUGA[1], Y. KONDO[2], K. TAMURA[2], and M. SATO[3], [1]Meisei University, Oume, Tokyo, Japan, [2]Aloka Co., Ltd., Oume, Tokyo, Japan, [3]Microsonic Co., Ltd., Tokyo, Japan.
Corresponding e-mail: yagi@con.ei.meisei-u.ac.jp

We developed a numerical analysis of transient shear wave generation and experimentally verified the results using our customly modified real-time displacement tomography for real-time imaging of dynamic absolute shear modulus in vivo.

FDTD analysis: For real-time evaluation of the transient shear wave generation Finite-Difference Time-Domain analysis of elastic wave field is utilized, in which the separation of compressional and shear waves, dynamical analysis of shear

wave across the near-field and the inversion approaches to absolute shear modulus can be implemented. According to the compressional and shear wave velocities in liver tissue (1500 m/s and 1 m/s), 2-dimensional spatial mesh size and time step are set to 1mm $\times$ 1mm and 0.33 ms respectively. The FDTD analysis is performed through the 150mm $\times$ 150mm area surrounded by perfect matching layer to absorb reflected waves. Since the spatio-temporal impulse response by vertical stress on the tissue surface clearly demonstrates the split bi-directional shear wave profiles separated by vector velocity potentional, as the far field directivity by Miller and Pursey in1954, non-splitting transient profile by the vertical stress distribution are evaluated by adjusting band-limited temporal driving function. After the successive experimental analysis it is confirmed that the vertical stress distribution by superposing each separated reverse-polar raised-cosine can generate a continuous shear wave front in circular phase after the end of temporal driving by raised-cosine. The spatial separation and width of raised-cosine and the applied driving time are focused on 10mm, 20mm and 50ms in this tissue model, respectively.

Experiments: To verify the performance of transient shear wave generation a conventional ultrasonic tomography was modified to real-time imaging of longitudinal displacement between successive RF echo frames (12-bit. 4 times the center-frequency of transducer). These spatio-temporal data are processed by the parallel architecture of flexible Field Programmable Gate Array modules for real-time local cross-correlation and its statistical phase. After the scan-line conversion the real-time tissue movement is superposed upon B-mode image at the same frame rate. The measuring accuracy was verified by the shear wave profile across a liver tissue in vivo, in which the displacement by heartbeat was less than 10 μm per frame interval and the boundary traveled at 1 m/s or so. The experimental stress pulse on the surface of tissue phantom with 1 to 5 % gelatin concentration clearly demonstrated the predicted shear wave generation and propagation with velocity of 0.5 to 3 m/s across the phantom medium.

This is partly supported by JHPF research grant 2004.

P1B-2

A PARAMETRIC STUDY ON PROCESSING PARAMETERS FOR TWO-DIMENSIONAL CARDIAC STRAIN ESTIMATION: AN IN-VIVO STUDY.

S. LANGELAND*, P. F. WOUTERS, H. A. LEATHER, P. CLAUS, B. BIJNENS, and J. D'HOOGE, Catholic University of Leuven, Leuven, Belgium.
Corresponding e-mail: stian.langeland@uz.kuleuven.be

In the last years, two-dimensional (2D) myocardial strain estimation has been evolving as a method that could replace todays 1D strain estimation and solve several of its limitations. The 2D strain estimation is typically based on 2D displacement tracking of spatial features in the gray-scale (GS) or radio-frequency (RF) data using either 1D or 2D kernels. All approaches have specific advantages and disadvantages but a trade-off between accuracy and computational cost generally has to be made. Although some studies have been presented in the

literature on the effect of these parameters, these have been limited to simulated or tissue mimicking phantom setups.

The aim of this study was therefore to evaluate the influence of these parameters on the strain estimate in an in-vivo setting in order to optimize of computation time.

Methods: B-mode IQ data sets were acquired from the inferolateral wall of 4 open chest sheep using a parasternal long axis view. The data were aquired at 4.5 MHz at a sampling rate of 10 MHz using a Toshiba

PowerVision 6000 equipped with an RF interface. The framerate was 168 Hz with a sector angle of 45 degrees and 60 image lines. The images were interpolated by a factor of 10 in the azimuth direction. 2D displacements were calulated in each data set based on a sum of squared differences estimator using different parameters. The investigated parameters were: axial and azimuth kernel size (2 and 3 wave lengths and 1, 3 and 5 beams respectively), axial sampling frequency (40 and 80 MHz) and the tracking was performed both on GS and RF images. Myocardial radial (R) and longitudinal (L) strain were simultaneously estimated using a previously described methodology based on 2D motion gradients. Four segment-length sonomicrometry crystals (SM) were placed in a tetrahedral configuration just lateral to the imaging plane giving a continuous reference for the L and R strain. As an error measure, the mean absolute difference between ultrasound and SM strain was calulated over the cardiac cycle for all data sets and all processing parameters. Differences in average error (DAE) between methods were statistically tested using ANOVA.

Results: No statistically significant differences were found for the different kernel sizes in neither axial or azimuth direction (mean DAE 1D vs. 2D kernel = 0.1%, p=NS). Similarly, neither sampling frequency (mean DAE = 0.4%, p=NS) nor GS vs. RF tracking (mean DAE = 0.4% ,p=NS) had a significant influence on the mean error. However, for all parameters L strain errors were significantly smaller than the R ones (mean DAE = 3% ,$p < 0.01$).

Conclusion: Although it has been shown in the literature that under ideal conditions the variance in the strain estimator reduces using a 2D kernel, these results did not reproduce in this in-vivo setting. This might be due to an increased sensitivity of 2D kernels to myocardial shear. Similarly, sampling frequency and GS vs. RF tracking had no significant impact on accuracy. 1D kernels might thus be better for 2D strain estimation in vivo since they give a similar accuracy at a reduced computional cost.

P1B-3
ELASTOGRAPHIC PARAMETERS BY SURFACE WAVE ANALYSIS.

N. BENECH, C. A. NEGREIRA*, and I. NUÑEZ, Facultad de Ciencias, Montevideo. Uruguay.
Corresponding e-mail: nbenech@fisica.edu.uy

Ultrasonic elastography has proved to be a useful means to obtain quantitative information about the viscoelastic parameters of soft tissue. This information is used to diagnose pathologies like cirrhosis or carcinomas surrounded of healthy

tissue in the breast. The analysis of surface waves in an elastographic experience can be very useful and complementary in the diagnosis carried out starting from the shear waves in the bulk of the medium. Previous work in this area is limited although it is potentially useful as a diagnostic tool.This fact is due that surface waves, as the shear waves, are very dependent of the viscoelastic parameters of the medium. In this work we make a study of surface waves using the optic method of desfocusing in a homogeneous phantom. We have made a sweeping in frequencies from 40 up to 500 Hz, obtaining by this way a dispersion curve in function of the medium's viscosity. We discriminated the Rayleigh waves from the Lamb waves by the speed dependance of the frequency. The speed of the surface wave and the attenuation are compared with those obtained with transient elastography from the shear waves in the interior of the phantom. For speed values in the 1-5 m/s range we obtained a 2% agreement for this comparison. In a second stage, we studied an heterogeneous phantom (a hard inclusion surrounded of soft tissue). The lesion is detected through the amplitude variations of the surface wave and this result was compared with elastographic image made from the local shear wave speed. In this study we also determine the exploration depth that this method allows in function of the excitation frequency.

This work was supported by Programa para el Desarrollo de las Ciencias Básicas (PEDECIBA-URUGUAY) and project PROCISUR.

P1B-4
MEASUREMENT SPATIAL DISTRIBUTION OF HEART WALL MOTION GENERATED BY REMOTE PERTURBATION OF INNER PRESSURE.

H. KANAI*, H. HASEGAWA, and K. IMAMURA, Tohoku University, Sendai, Japan. Corresponding e-mail: hkanai@ecei.tohoku.ac.jp

Background: Though the myocardial movability is important to diagnosis of the heart diseases, a noninvasive method for estimation of the movability has never been developed. If the heart wall is sinusoidally actuated using a low frequency actuator directly attached to the chest wall, the bending vibration (mode-2) dominantly occurs in the heart wall. For the vibration with mode-2, however, there are 8 nodes which remain still on the heart wall. Thus, it is necessary to distinguish the nodes from the other points to avoid underestimating the movability of the regional myocardium. **Method:** By attaching an actuator to the brachium artery and driving it by sinusoidal wave of f_0 Hz, the inner pressure of the artery is perturbed and the perturbation propagates along the artery to the left ventricle (LV) of the heart. Then, the perturbation of the LV inner pressure is generated. Using ultrasound-based method (Kanai et al. IEEE Trans UFFC 43, 1996), the resultant minute motion on the heart wall can be measured. Since the *vibration mode* of the heart wall depend on the actuated frequency, the vibration mode and the positions of the nodes can be identified from the measurement of the spatial distribution of the heart wall motions by scanning the ultrasonic beam (Kanai et al. Ultrasound Med Biol 27, 2001). Finally, from the resultant strain and the delay of the strain to the applied pressure, the instantaneous myocardial movability and its transition property during one cardiac cycle are noninvasively estimated. **Basic experiments:** As a model of the heart,

a spherical shell (outer diameter=45 mm, thickness=7.5 mm) made of silicone rubber was set in a water tank and a silicone rubber tube (50 cm in length) was connected to the spherical shell. By remotely actuating the tube with a sinusoidal vibration of f_0 Hz, the internal pressure of the shell was perturbed with several mmHg. From the measured spatial distribution of the vibrations on the shell surface, the vibration-mode was identified. For 7-8 Hz, the vibration-mode is 0, which shows to the homogeneous expansion and contraction without node. For 12 Hz, the mode is 1, which shows the parallel displacement of the whole shell. For 16-17 Hz, the mode is 2. From its distribution, the positions of the nodes were identified. **In vivo experiments:** By applying external remote actuation to the brachial artery, the LV internal pressure was successfully perturbed for the first time. The motions in and on the heart wall were measured with ultrasound from the chest wall. For the actuation frequency of 26 Hz, the minute velocity components of 0.01 m/s due to the perturbation of the inner pressure were superposed on the spontaneous myocardial motion of about 0.1 m/s. **Conclusion:** This study proposes a novel method to noninvasively perturb the LV internal pressure by remotely actuating the brachium artery with the sinusoidal vibration. By measuring the spatial distribution of the heart wall motion using ultrasound, the vibration mode is identified, which has a potential to noninvasively evaluate the movability and its transition property during one cardiac cycle.

P1B-5
TRANSIENT ULTRASOUND ELASTOGRAPHY FOR BREAST CANCER DIAGNOSIS USING IMPULSIVE RADIATION FORCE: AN IN VITRO STUDY.

D. MELODELIMA*[1], J. BAMBER[1], F. DUCK[2], and J. SHIPLEY[2], [1]Royal Marsden NHS trust and Institute of Cancer Research, Sutton, Surrey, UK, [2]Royal United Hospital MHS trust, Bath, UK.
Corresponding e-mail: David.MelodeLima@icr.ac.uk

Alternative imaging methods are needed to improve the effectiveness of breast cancer detection and diagnosis. As a result, the development of imaging systems capable of evaluating the mechanical properties of tissues with high resolution is being carried out by numerous research teams. Several groups are studying acoustic radiation force-based imaging modalities. However, to date these have been largely based on the detection, by various means, of signals that are proportional to the displacement induced by radiation force, whereas in pseudo-static elastography it is generally strain that is imaged, as a surrogate for inverse stiffness. The imaging of strain generated by radiation force from a focused ultrasound transducer has never been suggested, and may be of interest to improve breast cancer detection.

In this study, a focused ultrasound transducer of f-number 1.3 was driven at an operating frequency of 1.7 MHz, and was used to apply localised radiation force to a small volume of tissue mimic. Images were created using a single “pushing” burst at each location, of duration 8 ms. A linear array with a centre frequency of 7.5 MHz was used to obtain echo signals. The focused transducer and the linear array were aligned such that the focus was in the plane of imaging. The time-dependent transient strains resulting from the impulsive radiation force were

mapped using a least-squares strain estimator and ultrasound RF correlation-based displacement tracking methods.

Gelatine phantoms containing cylindrical stiff inclusions were used. Experimental results demonstrate that strain on the order of 0.04% can be generated and detected with a resolution of about 1 mm. A stiffer region exhibits lower strain than a more compliant region. The instantaneous strain immediately following cessation of the radiation force varies approximately linearly with the Young's modulus of the material. Good agreement was obtained between the size of the inclusion seen macroscopically and measurements made using transient radiation force elastography.

Strain imaging using impulsive radiation force offers several advantages. The highly localised and transient strain that is produced by focused and impulsive radiation force may permit the sensing of changes in tissue elastic properties that are difficult to detect with conventional elastography, due to greater independence from boundary conditions and a resulting improved global contrast-to-noise ratio. For example, the characteristic, bi-directional, high strain artefacts due to stress concentration, often seen with static elastography at the tissue-inclusion interface, do not appear using the transient radiation force strain imaging technique. It is also possible to utilize a single pushing burst, strongly focused in two dimensions, that acts as a spatially localised impulse, and to use low frequencies to supply radiation force more efficiently to deeper-lying tissues.

This work was supported by funding from the UK Department of Health (NEAT D008).

P1B-6

THE EFFECT OF SURROUNDING GELATIN ON ULTRASOUND GENERATED SHORT PULSE WAVE PROPAGATION IN ARTERIES.

X. ZHANG* and J. GREENLEAF, Mayo Clinic College of Medicine, Rochester, MN.
Corresponding e-mail: zhang.xiaoming@mayo.edu

Background: Pulse wave velocity (PWV) is widely used for estimating the stiffness of an artery. It is well known that a stiffened artery can be associated with various diseases and with aging. Usually, PWV is measured using the "foot-to-foot" method. The "foot" of the pressure wave is not clear due to reflected waves and blood noise. Also, PWV is an average indicator of artery stiffness between the two measuring points, and therefore does not identify local stiffness variations. In a series of recent studies, we propose producing a bending wave in the arterial wall using low frequency localized ultrasound radiation force and measuring the wave velocity along the arterial wall [X. Zhang et al., Proc. 2003 Ultrason. Symp., 1883-1886], [X. Zhang et al., Proc. 2004 SPIE, Medical Imaging]. The wave velocity can be measured accurately over a few millimeters.

Objective: PWV is directly related to the Young's modulus in the circumferential direction of the artery by the well known Moens-Korteweg equation. However, in this famous equation, PWV only relates to the artery properties and blood density,

but does not relate to the surrounding tissue. The objective of this paper is to develop method for studying the surrounding tissue effect on the arterial waves.

Method: An excised artery was tested in a water tank. The artery was pressurized internally with saline. A short pulse wave in the artery was generated by ultrasound. The wave velocity was measured with laser. Then the artery was embedded in a tissue-mimicking gelatin. The wave velocity of the artery embedded in gelatin was measured.

Results: The short pulse wave velocity of the artery without gelatin is measured 5.6 m/s, while the short pulse wave velocity of the artery with gelatin is measured 10 m/s.

Conclusion: The short pulse wave generated by ultrasound in the artery travels faster if the artery is embedded in gelatin. This means that the gelatin stiffens the artery. Further research will be developing method for studying the effect of surrounding tissue on artery stiffness.

This study is supported by grant EB 02640 from the National Institutes of Health. The authors thank R. R. Kinnick for experimental support.

Session: P1C
TISSUE CHARACTERIZATION
Chair: E. Biagi
University of Florence

P1C-1
BREAST TUMOR CLASSIFICATION BASED ON IMAGE SEQUENCE ANALYSIS DURING COMPRESSION.

K.-H. LEE[1], Y.-H. CHOU[2], C.-M. CHEN[3], and P.-C. LI*[1], [1]Department of Electrical Engineering, National Taiwan University, Taipei, Taiwan, ROC, [2]Veterans General Hospital, Taipei, Taiwan, ROC, [3]Institute of Biomedical Engineering, National Taiwan University, Taipei, Taiwan, ROC.
Corresponding e-mail: paichi@cc.ee.ntu.edu.tw

Tumor contour features have been used for classification of breast tumors. Typically such computer aided diagnosis systems are based on analysis of a single image. In this paper, we investigate performance of breast tumor classification using image features from a breast image sequence acquired when the breast is under increasing compression. The motivation is to incorporate features that are related to tissue elastic properties into classification. Also, these features can be combined with the original contour features from a single image to further improve the accuracy. Specifically, the features used in this study included (1) area changing rate, (2) changing rate of the equivalent ellipse parameters (long axis dimension, short axis dimension and inclination angle), and (3) the mean displacement of the contour. The B-spline model was employed to define the contour. By using this model, the analysis can be done efficiently and classification can be performed in real time. 20 clinical image sequences were obtained from the Taipei Veterans General Hospital and separated into

two categories by an experienced physician. Among the 20 cases, 7 were classified as malignant nodules and the others were classified as benign nodules. A linear support vector machine with the leave-one-out method was used for training and classification. A success rate of 17/20 (85%) was achieved. The method can be combined with existing single image contour features to further improve the accuracy. In addition, it is a robust method because it is not sensitive to the detailed structures of the contour. Finally, since only B-mode images are needed, the proposed method can be more easily integrated with current clinical systems than other elasticity imaging methods that require access to the radio frequency data.

P1C-2

ULTRASOUND BASED ASSESSMENT OF GEOMETRICAL PARAMETERS INVOLVED IN LUMEN PRESERVATION DURING ATHEROSCLEROTIC PLAQUE BUILD UP.

J. WENTZEL, A. DHARAMPAL, F. GIJSEN*, J. SCHUURBIERS, G. RODRIGUEZ-GRANILLO, A. VAN DER STEEN, P. DE FEYTER, and C. SLAGER, Erasmus MC, Rotterdam, the Netherlands.
Corresponding e-mail: j.wentzel@erasmusmc.nl

BACKGROUND The presence of atherosclerotic plaques in human coronary arteries is mostly identified by X-ray based angiography. However, during the late eighties it became clear that the true atherosclerotic plaque burden is not reflected in the dimensions of the lumen because of plaque compensation mechanisms of the vessel wall, i.e. vascular remodeling. At the time, intravascular ultrasound (IVUS) was the only tool to assess the true plaque burden of the atherosclerotic plaques taking the total wall thickness into consideration. IVUS studies showed that atherosclerotic plaques are often eccentric, implying that the wall, including the endothelium, is only partially diseased. Mechanisms responsible for remodeling of the vessel wall are thought to be dependent on healthy endothelium. Therefore, we hypothesize that the plaque free wall (PFW), having functional endothelium, controls the local arterial capacity of vascular remodeling. We studied by IVUS whether reduction in PFW, presumable because of plaque extension at the shoulders, attributes to lumen narrowing.

METHODS Coronary arteries of 5 patients (<50% angiographic stenosis) were studied at baseline and at 4 years follow up applying an ECG gated stepwise IVUS pullback (30 Mhz, CVIS, Boston Scientific). IVUS images were matched carefully using anatomic landmarks. Only cross sections in between side branches were studied. From the IVUS images the lumen and external elastic membrane contours were semi automatically delineated to assess local wall thickness (WT), lumen area (LA), lumen diameter, media bounded area (MBA) and plaque area (PA) of successive cross sections at 0.5 mm intervals. WT smaller than 0.2*lumen diameter was defined as normal and was used to determine the per cross section the arc of PFW. Cross sections showing increase in plaque area were selected and divided into 2 groups based on the median of the change in PFW(ΔPFW).

RESULTS In total 202 out of 336 cross sections showed increase in plaque area over the 4 years follow up. The average increase in plaque area was 26%. The median of the ΔPFW was -27.5°. Cross sections showing decrease in PFW (-103.2°±$68.8°, p<0.05, n =101), presented with 15% lumen narrowing (p<0.05) and still a minor increase in MBA of 2.5% (p<0.05). For cross sections showing some extension in PFW (11.5°±32.7°, p<0.05, n=101) LA was preserved (+1.5%, p=NS) and MBA increased (7.8%, p<0.05) more than the group with loss of PFW. For both groups progression in plaque area was similar.

CONCLUSION IVUS derived plaque progression accompanied with decrease in plaque free vessel wall, presumably because of plaque fissuring at the shoulders, is related to lumen narrowing at 4 years follow up. These results imply a potential role for the plaque free vessel wall in the process of lumen preservation.

P1C-3

A NOVEL METHOD FOR AUTOMATIC CONTOUR EXTRACTION OF ULTRASONIC BREAST LESIONS.

C.-K. YEH*[1], Y.-S. CHEN[1], and W.-S. CHEN[2], [1]Department of Electrical Engineering, Yuan Ze University, Taiwan, Chung-Li, Taiwan, [2]Department of Physical Medicine and Rehabilitation, National Taiwan University Hospital, Taiwan, Taipei, Taiwan.
Corresponding e-mail: yehck@ntu.edu.tw

Automatically detecting tumors and extracting lesion boundaries in ultrasound images is difficult due to the variance in shape and the interference from speckle noise. Previous research works primarily focused on lesion classification with manual delineation of the tumor boundaries. In this study, we present a novel algorithm to automatically find lesion contours in ultrasonic breast images. With inherent property of ultrasound image embedding speckle noise, the image can be regarded as degraded paint character (DPC) image containing closure noise, which is well known in perceptual organization of psychology. An effective scheme of removing closure noise using iterative disk expansion method has been addressed in our previous work and it has been successfully applied to many applications. The contour extraction of ultrasonic breast lesions can be equivalent to the removal of speckle noise. In our method, the brightness equalization and adaptive thresholding schemes are first used for converting the original ultrasound image into a binary image, which is similar to DPC image. Then, applying disk expansion method to the binary image, we can obtain a significant radius-based image where the radius for each pixel represents the corresponding disk covering the specific object information. Based on the cumulative distribution function analysis on the radius-based image, the significant lesion region can be easily located. Finally, a signal transmission process is used for searching the complete breast lesion region and thus the desired lesion contour can be effectively and automatically extracted. In this study, simulations and clinical images were performed to evaluate the performance of the proposed algorithm. Several types of cysts with different contours and contrast resolutions images were simulated with speckle characteristics. The results show that the mean normalized true positive area overlap between simulated contour and contour

obtained by the proposed algorithm is 87.5%. There is a strong correlation between experienced physicians manual and automated contour extraction in clinical breast images (R=0.90). The algorithm is also able to simultaneously contour multiple lesions in a single image. Comparison with conventional snake contour extraction algorithm, the proposed algorithm does not position any initial seed point within the lesion and thus it can be viewed as a fully automatic process. Furthermore, due to running time for contour extraction in a single breast lesion image was 0.06 s on a 3.0-GHz Intel Xeon machine, the algorithm is feasible to be implemented in a real-time ultrasound imaging system.

The authors acknowledge the National Science Council of ROC (NSC 93-2218-E-155-002-) for providing support.

P1C-4
EVALUATION OF A MODIFIED AUTOCORRELATION METHOD WHEN APPLIED TO CARDIAC STRAIN RATE IMAGING.

A. BLOMBERG*[1], A. HEIMDAL[2], S. I. RABBEN[2], J. D'HOOGE[3], and A. AUSTENG[4], [1]University of Oslo, Oslo, Norway, [2]GE Vingmed Ultrasound, Oslo, Norway, [3]University Hospital Gasthuisberg, Leuven, Belgium, [4]University of Oslo, Oslo, Norway.
Corresponding e-mail: a.e.a.blomberg@fys.uio.no

Background: Strain rate imaging is an ultrasound method suitable for quantitative assessment of regional myocardial function. More precisely, strain rate measures the rate of local deformation within a defined region of interest. Myocardial strain rate imaging involves computing spatial gradients in tissue velocities. Since the gradient-operation is noise-sensitive, accurate velocity estimates are essential.

When estimating tissue velocities using the conventional autocorrelation method (AM), the ultrasound center frequency is assumed constant and equal to the demodulation frequency, while in the modified autocorrelation method (MAM) the former is continuously estimated together with the phase shift from pulse to pulse. The AM is unbiased only if the demodulation frequency is equal to the received center frequency. This assumption is not necessarily valid.

The MAM has shown promising results with respect to estimator variance and bias when implemented in simulated environments.

Aim: The purpose of this work has been to evaluate the performance of the MAM compared to the AM, when applied to myocardial strain rate estimation.

Method and results: Both methods have been implemented and evaluated in two different environments, namely simulated RF-data from an analytic model of the human heart and experimental data acquired from human hearts scanned with a specially programmed Vivid 7 scanner (GE Vingmed Ultrasound).

When applied to simulated RF-data, the MAM demonstrated superior performance with respect to estimator variance (43%-81% improvement compared to the AM) and bias, as well as an over all slightly higher degree of correlation with the true strain rate of the analytic model ($r=0.98$-0.99 vs. 0.97-0.99, $p<0.0001$).

When estimating strain rate using experimental data, a previously presented spectral strain rate method was used as a reference. In this case the MAM did not show superior performance. On the contrary, the AM demonstrated a lower estimator variance (by 46% -49%) and bias, as well as an over all higher degree of correlation with the mean value of the strain rate spectrogram (r = 0.73-0.90 vs. 0.62-0.86, p<0.001).

There are several possible contributing factors to the degraded performance of the MAM when applied to experimental data, including spatial scatterer distribution and acoustic noise. In an attempt to explain the degraded performance of the MAM, filtered white noise modeling reverberation noise was added to the simulated RF-data before processing. SNRs ranging from infinity (no added noise) to 5 dB were simulated.

Discussion: As expected, both methods displayed degraded performance in the presence of noise. Interestingly, the MAM degraded more quickly. As the SNR decreases, the performance of the MAM approaches that of the AM. For an SNR of 5 dB, both methods display similar results.

In conclusion, the MAM shows promising results in simulated environments with high SNR. Under heavy noise conditions and in experimental data, however, it displays similar or poorer performance compared to the AM.

Session: P1D
BEAMFORMER IMPLEMENTATION
Chair: J.-Y. Lu
University of Toledo

P1D-1
"SYNTHETIC AXIAL ACQUISITION" FULL RESOLUTION C-SCAN ULTRASONIC IMAGING.

Y. LI*, T. BLALOCK, W. WALKER, and J. HOSSACK, University of Virginia, Charlottesville, VA.
Corresponding e-mail: jh7fj@virginia.edu

Previously, we described various components for a low cost approach for enabling C-Scan beamforming using a fully sampled 2D array and very short element data records. In the Directly Sampled In-phase and Quadrature (DSIQ) approach, we use as few as one complex sample per array element. However, there is a penalty in terms of reduced final image spatial and contrast resolution when using DSIQ as opposed to conventional techniques using finite length time records and delay / sum beamforming. In the 'Synthetic Axis Acquisition' (SAA) approach, we take advantage of the fact that we use an unfocused transmit beam (plane wave) and are imaging primarily shallow and slowly moving, or even static, tissue regions. This allows us to acquire, over a set of approximately 25 serial transmit / receive firings, each with the receive sampling trigger delay offset by the equivalent of one digital sampling interval, a per channel data record of sufficient length to enable an approximation to conventional full record delay and sum beamforming. The penalty for taking this approach is encountered

in several areas. Firstly, the opportunity to increase SNR by averaging is reduced. Secondly, the performance of the approach degrades as a function of tissue motion. Additionally, it is readily evident that this version of a C-Mode imaging device requires more extensive hardware and signal processing. However, depending on choice of beamforming condition (center frequency, aperture size and focal depth), the SAA approach yields an improvement in lateral resolution by a factor of approximately two over that achievable with DSIQ. FIELD II based simulations were initially performed for the parameters appropriate for our next generation of 'Sonic Window' that we intend to present in another paper at this conference. These parameters are: 5 MHz Center Frequency, 60 $\times$ 60 fully sampled 2D array with 0.3 mm pitch. The imaging depth was 20 mm and the assumed pulse repetition interval was 40 microseconds. Assuming a required final equivalent sampling rate of 40 MHz necessitated 25 Synthetic Axial Acquisitions ('pulse-echos') to form sufficiently long data records. Our numeric simulations have been performed for a variety of target velocities occurring during the process of acquiring the full data record. It has been observed lateral target velocities of 50 mm/s or more are tolerable with no significant (i.e. greater than 1-2 dB at approximately the -20 dB level) impact on beamplot performance. As might be anticipated, the approach is more sensitive to degradation due to axial target motion. However, even in this case an axial velocity of 50 mm/s has an impact of approximately 3-4 dB at the -20 dB level. A variety of both simulation-based and experimental data results will be presented. Further improvements based on using aperiodic pulsing as an approach to enable faster acquisition are also discussed.

NIH EB002349, EB001826

P1D-2
A HARDWARE EFFICIENT BEAMFORMER FOR SMALL SIZE ULTRASOUND SCANNERS.

J. Y. LEE*, H. S. KIM, and T. K. SONG, Sogang University, Seoul, South Korea. Corresponding e-mail: powerjun77@sogang.ac.kr

Digital receive beamformer is one of the most important parts governing the performance and complexity of a medical ultrasound imaging system. In this presentation, we present a hardware efficient digital beamformer for small size ultrasound scanners, which is advantageous over the two most widely used beamforming schemes, interpolation beamformer and phase rotation beamformer, in terms of hardware complexity and performance. In the interpolation beamformer, the rf data are sampled at a rate not smaller than 4fo and the sample rate is increased by a factor of 4 to achieve the required time delay resolution of 1/16fo, which requires a multi-tap interpolation filter for each channel. In the phase rotation beamformer, the inter-channel delay compensation is done by shifting the phase of inphase and quadrature components of the input rf data, which only requires 4multipliers. However, the phase rotation beamformer requires an I/Q demodulator for each channel, consisting of two mixers and two multi-tap LPFs. Moreover, accurate delay compensation can be done only at the center frequency.

The proposed beamformer is identical to the interpolation beamformer except that it uses fractional delay(FD) filters to generate the delayed samples, instead of the interpolation filters. To obtain the 1/16f0 delay resolution, each FD filter should be capable of providing a programmable fractional delay D, which has the ideal response H(w)=exp(-jwD), D=0,0.25,0,5,0.75, and |H(w)|=1, for all w. A 4tap FD filter was designed using maximally flat filter design constraints and least square error method. It was shown that its phase response error increases with frequency: For a sampling rate of 40MHz, the group delay error is 0.001 at 3.5MHz, 0.0015 at 5MHz, 0.0208 at 7.5MHz, and 0.0756 at 10MHz. It was also shown that the magnitude response error, which also increases with frequency, has less effect on the accuracy of the delayed samples compared with the phase response error.

To evaluate the proposed method, computer simulations were performed with Gaussian signals of 50% 6dB bandwidth and the signal to noise ratios(SNR), defined as the ratio of true sample value to the difference between the true and delayed sample values, of different schemes were compared. The SNR of the proposed FD beamformer decreases with frequency (58dB at 3.5MHz, 55dB at 5MHz, 37dB at 7MHz and 22dB at 10MHz), whereas the phase rotation beamformer has SNR lower than 20dB at all frequencies. In addition, the phase rotation beamformer requires 36multipliers: 2 for mixers, 32 for two LPFs and 4 for phase rotation. It was also observed that the SNR of the interpolation beamformer is lower than that of the FD beamformer by 20dB at 5MHz and 6dB at 10MHz, when 4multiplier polyphase filter is used to implement a 16tap interpolation filter. In order for the interpolation beamformer to have the same SNR as the FD beamformer, its hardware complexity should increase by from 25% to 300% depending on the imaging frequency. These results show that the FD beamformer outperforms the phase rotation beamformer and interpolation beamformer in terms of both performance and hardware complexity.

P1D-3
MODERN IMPLEMENTATION OF A REALTIME 3D BEAMFORMER AND SCAN CONVERTER SYSTEM.

K. WALL* and G. LOCKWOOD, Queen's University, Kingston, Ontario, Canada. Corresponding e-mail: kwall@physics.queensu.ca

We have developed a scalable high-speed beamformer and scan converter for real-time 3D imaging. The beamformer uses 4 Field Programmable Gate Array (FPGA) devices (Xilinx Spartan3 series), each chip processing the data received from 72 of the 288 transducer elements. Internally, the FPGAs are divided into a series of element processing units. Each unit handles the data processing from a single transducer element, storing the received data in a circular buffer. An internal calculator then determines the appropriate delay samples required for each target point, pulls them from this buffer, interpolates and apodizes them. The summed result is transferred to the PC for display. For a high-speed FPGA based beamformer, two areas typically consume the largest amount of the available resources: look-up table storage ROM, and resources used to switch signals between the internal processing units. For our application, the beamformer is required to generate a 60 degree sector format image. Storing

the focusing delays associated with the range of steering angles used to form the sector format image, takes a huge amount of memory. An exponential reduction in the size of this table is possible by modifying the beamformer to generate scan lines that are perpendicular to the array in much the same way a linear array image is formed. This greatly reduces the size of the look-up table since the same set of delays can be shared for all the image lines. This choice also allows a significant reduction in switching resources by allowing table data to be passed between the internal data processing units, rather than distributed from a single source. To further reduce the size of the stored data, compression techniques are applied. Storing only the second order derivative of the data allows a 10:1 reduction in storage. The beamformed data is transferred to a PC through the PCI bus. A PCI bus controller integrated into the FPGA code provides a DMA transfer into the computer's RAM. When each transfer block is complete, a PC side program coded in C# .NET begins a second DMA transfer onto the video card, where all scan conversion logic is implemented. Offloading scan conversion processing to the Graphics Processing Unit (GPU) provides a huge increase in performance as the GPU is designed for handling massive parallel data processing. It also leverages the built in graphics functions, such as interpolation, anti-aliasing, and alpha blending. The scan conversion, log compression, and display are all coded in a High Level Shader Language program, using Pixel Shader 3.0. The FPGA design has been tested using the Xilinx XST synthesis engine. Functional testing using Modelsim generates 100% agreement with theoretical Matlab simulation results, and shows secondary lobe suppression of at least 55 dB. The beamformer can sustain processing for 7,500 transmit pulses/sec, internally calculating more than 3,840 beamformed points per pulse. Volume frame rates far exceeding 30fps are easily achievable by the GPU scan converter, with very low CPU dependence.

P1D-4

ABOUT THE POSSIBILITY TO IMPLEMENT A NONUNIFORM OVERSAMPLING RECEIVE BEAMFORMER IN A FPGA.

L. LIE* and M. E. TANASE, Politehnica University of Timisoara, Timisoara, Timis, Romania.
Corresponding e-mail: ioan.lie@etc.utt.ro

A hardware implementation is presented in a context of receive beamforming based on nonuniform oversampling techniques. Using these techniques is possible to obtain image quality similar to those obtained using multi-bit digital beamforming techniques, in the conditions of significant complexity, size and cost reduction. The beamformers based on delta-sigma modulators have two major advantages over traditional multi-bit methods: simplifying the ADC structure and ensure precise delays by manipulating the samples taken with a high rate.

The digital beamformers that are based on non-uniform sampling create the dynamic focusing by sampling the echo samples at specific moments that ensure the coherent summing operation at the reception.

From a structural point-of-view, the digital beamformer with a nonuniform oversampling is made up of two sections:

- An analogue section containing the delta-sigma modulators.

- A digital section consisting of the following entities: Digital controller, FIFO, Adder and decimating filter.

The central entity of our design is the digital controller, which generate the non-uniform sampling clocks for command the delta-sigma modulators and load the FIFO buffers, and ensures the signals for download the FIFO buffers and for synchrony the adding block and the decimating filter.

In order to generate the non-uniform sampling clock we have taken into account the possibility of iterative “in circuit” calculating for the delay information, based on the “midpoint” algorithm applied to one of the equations that derives from the focusing geometry.

The design has been simulated in the ALTERA QUARTUS environment and the resulting structure of has been implemented in the largest FLEX10K circuit EPF10K250ABC600. The device utilization shows that it can host the sampling clock generators for an array with 64 elements. Therefore, it is possible to implement in a single FPGA, which contains memory blocks, every digital blocks of a beamformer: the digital controller and FIFO memory for each channel, the adder for n (64, 128,...) channels and the decimating filter.

The beamformer was tested using ultrasonic data acquired with a multi-bit converter. Using a MATLAB routine the original signal was converted into delta-sigma format. The resulting signal was used like test signal for the FPGA implemented beamformer. The filtered signal was captured in a MATLAB script for comparative analyse in time and frequency domain with the original signal in order to validate the implementation.

The results shows the possibility to build in the future a “single chip” receive beamformer using programmable analogue / digital structures.

P1D-5

PHASED SUBARRAYS FOR LOW COST C-SCAN APPLICATIONS.

Y. LI*, T. BLALOCK, W. WALKER, and J. HOSSACK, University of Virginia, Charlottesville, VA.
Corresponding e-mail: jh7fj@virginia.edu

The performance of subarray beamformer processing as a means of reducing overall beamforming computational load for a low cost C-Scan imaging device is analyzed. Unlike the case encountered in B-Mode imaging, the C-Scan format is characterized by a large channel count ($64 \times 64 = 4096$ in this case) and very short data record lengths. Additionally, unlike the case in B-Mode, there is no essential need for realtime processing of ‘streaming’ received channel data. Thus, the C-Scan image format benefits greatly from a subarray processing approach in which partial sums are ‘reused’ with modified differential delays to form multiple beamformed image pixels. It is shown that the beamforming computational load for our previously described low-cost C-Scan imaging device

('Sonic Window'), measured in terms of delay and sum operations, may be reduced by approximately 50 fold with a 1-3 dB impact on sidelobe level at the -30dB level. Subarrays with dimensions of 2, 4, 8 and 16 elements per side have been investigated. Larger subarrays requires fewer calculations but exhibit higher sidelobes. Subarrays with side dimensions of 2 and 4 elements do not have significant image performance advantages over a subarray size of 8 but require more significantly more computational effort. Consequently, for the array / target geometries of interest to us (5 MHz and an aperture / focal depth corresponding to f/number = 1), a subarray dimension of 8×8 is favored. The impact of subarrays on performance along the diagonal directions (worst case) and also the benefits of optimal (i.e. hexagonal) beam spatial sampling are also considered. Additionally, results using both conventional full record length and single complex sample ('Directly Sampled In-phase and Quadrature' - DSIQ) are presented. The potential computational savings is less when using DSIQ because imaging resolution is inferior and consequently relatively fewer image samples are required to fully sample the image plane without aliasing. Initial results have been obtained using FIELD II simulations. Experimental results, obtained with our prototype 'Sonic Window', are also presented.

NIH EB002349, EB001826

P1D-6
AN ARBITRARY WAVEFORM TRANSMITTER USING BIPOLAR PULSERS BASED ON A HIGH ORDER MODIFIED SIGMA DELTA MODULATION.

H. H KIM*, H. S HAN, and T. K SONG, Sogang university, Seoul, South Korea. Corresponding e-mail: kh2_brian@sogang.ac.kr

Coded excitation has been studied to improve the SNR with the limited excitation voltage, to increase the imaging frame rate, to improve the performance of ultrasound imaging with contrast agents, and so forth. However, it requires a complicated arbitrary waveform transmitter for each active channel that customarily uses a multi-bit DAC and a linear power amplifier(LPA). Not only does the LPA increase the cost and size of a transmitter block, but it consumes much power, increasing the system complexity further and causing a heating-up problem, which is critical in some cases.

We present an efficient arbitrary waveform generation scheme, which is based on modified sigma-delta modulation(SDM) methods suitable for coded excitation techniques relying on correlation based pulse compression. The proposed arbitrary waveform transmitter is composed of a 1bit DAC to generate single-bit SDM waveforms, a bipolar pulser to produce their high voltage versions, and a simple LC filter connected to array elements, resulting in a great reduction in the hardware size and cost. At the present work, the modified sigma-delta modulator has been designed to produce a weighted chirp signal with a center frequency of 5MHz and 6dB bandwidth of 3MHz. It was assumed that the Nyquist rate for this chirp is 20MHz. Customary methods to obtain a high SQNR in single-bit SDM are to use a high oversampling ratio(OSR) and to add dither noise to the quantizer input. In ultrasound imaging, however, high OSR should

be avoided since for example an OSR of 16 requires high voltage pulsers that should operate at switching rate as high as 320MHz. Our design goal is to achieve a low OSR of 4 (i.e., 80MHz switching rate), while the peak sidelobe level of the compressed waveform on receive should be smaller than -45dB. To achieve such a low OSR, a modified 4th order SDM is employed, which also eliminates the necessity of using dither noise. Its noise transfer function(NTF) is chosen to obtain an optimal stability and to suppress the inband quantization noise, using a linear coefficient comparison method and root locus method for stability analysis. For this purpose, the two coefficient sets of the modified SDM are selected such that the NTF has the poles and zeros of the 4th order Butterworth and Chebyshev type 2 highpass filters, with the cutoff frequencies of 8MHz and 6MHz, respectively.

To evaluate the proposed scheme, the 80MHz single-bit SDM waveform was passed through a 4th order Butterworth LC lowpass filter with a cutoff frequency of 7MHz, yielding the demodulated SDM signal with a SQNR of 25dB. The demodulated signal was then correlated with the original weighted chirp and compared with the ideally compressed signal, i.e., the autocorrelation of the original chirp. The peak sidelobe of the compressed waveform in the proposed method was -45.0dB, whereas the ideally compressed one exhibits the peak sidelobe level of -46.5dB, both with the same mainlobe width. The results showed that the proposed scheme can be used to reduce the hardware complexity of the coded excitation imaging without sacrificing the image resolution.

Session: P1E

MEDICAL IMAGING
Chair: J d'Hooge
University of Leuven

P1E-1

PHASE BASED LIVER MOTION COMPENSATION OF HARMONIC IMAGES.

A. KISSI*[1], A. BOUAKAZ[1], L. POURCELOT[1], S. CORMIER[2], and F. TRANQUART[1], [1]INSERM Unity 619, Tours, France, [2]LERI CRESTIC, Reims, France.
Corresponding e-mail: kissi_a@med.univ-tours.fr

Background: The use of ultrasound contrast agents allows to image liver perfusion in real time.

This visualization provides important information for the diagnosis of various diseases as well as for characterization of tumors. By using the slopes of the rise in activity during the arterial phase of liver enhancement, an perfusion index value β is computed. This index allows us to characterize lesions. However, artefacts, such as respiratory or cardiac motions often limits this quantification. A preliminary motion compensation is thus needed.

Method: In this context, we present a new method for compensating motion in order to estimate the perfusion index, over a sliding window, in order to accurately

characterize liver lesions from harmonic ultrasound sequences. The differential motion estimation technique used in this study is the phase-based optical flow. The local phase gradient, intensity-amplitude invariant, is first calculated by using Gabor quadrature filters. From the output of these filters, the component of lateral and transversal motion are computed by minimization procedure. This components are thus used to compensate motion.

Results: This method has been tested off-line five sequences of 160 non compressed images, using a Siemens Acuson Sequoia 512 with a 4C1 probe, after Sonovue injection (Bracco SpA imaging, Italy). The study was in CPS mode with an mechanical index of 0.21.

Our process eliminates some errors in positioning and thus in the calculated intensity from a given lesion. Our results show that, for solitary metastasis, there is an improvement of lesion quantification of 15%: the perfusion index β=0,21.

This study is funded by the International Rotary Club. This is gratefully acknowledged.

P1E-2
SPECTROSCOPIC THREE-DIMENSIONAL IMAGING OF LIGHT SCATTERING MEDIUM BY DETECTION OF ULTRASONIC VELOCITY CHANGE DUE TO LIGHT ILLUMINATION.

H. HORINAKA*[1], T. URA[1], Y. NAKATANI[1], K. WADA[1], and T. MATSUNAKA[2], [1]Osaka Prefecture University, Sakai,Osaka,Japan, [2]Aloka Co. Ltd., Mitaka,Tokyo,Japan.
Corresponding e-mail: horinaka@pe.osakafu-u.ac.jp

Optical tomography using near-infrared light is theoretically capable of imaging not only soft tissue information but also metabolic information of a living body using spectroscopic method. However, it was very difficult to construct the optical image of deep region of the body because the near-infrared light is scattered severely inside the soft tissue. We have already proposed a new optical tomography for medical diagnosis based on the interaction between the light and the ultrasonic wave. The 2D (two-dimensional) optical absorption image was constructed by detecting the ultrasonic velocity change due to the thermal agitation of light scattering medium. In this study, to apply diagnosis of physiological activities and pathological defects we performed experiments to construct the spectroscopic 3D (three-dimensional) optical images of the highly scattering phantom by developing 2D optical image construction. An ultrasonic transducer with the center frequency of 5 MHz and the beam width of 1.9mm in water was used for the experiments. Two oval spheres (about 30x20x20mm) which were made of agar included many small pieces of plastic thin film (0.1mm in thickness and 3 to 5mm in width) were prepared as experimental phantoms: one was transparent and the other was colored with the black ink. They were mounted in a transparent container filled with aqueous solution of the 10% “Intralipid” which has the scattering coefficient of 16cm^{-1} equivalent to the reported value of biomedical tissue. The transducer emitted ultrasonic pulses in water and received echo pulses from the phantom. The light from a laser diode (810nm)

were guided around the container by optical fibers and illuminated the phantoms for thermal agitation. The waveforms of echo pulses with and without light illumination were detected and time delay between two pulses were measured. The ultrasonic velocity shift was detected under the illumination intensity of 0.2W/cm^2(the skin exposure limit of continuous wave diode laser in the ANSI Z 136.1 Safe Use of Lasers standard). The 2D images of the ultrasonic amplitude and the velocity shift due to illumination were measured to construct the 3D images when the transducer was shifted every 1mm. The ultrasonic amplitude 3D image showed the contour of two oval spheres in the scattering medium. On the other hand, the ultrasonic velocity 3D image showed only the oval sphere made of colored agar. It was confirmed that the spatial information of optical absorption was obtained in highly scattering medium by our method.

P1E-3

MULTITONE NONLINEAR CODING.

A. NOWICKI*, J. WÓJCIK, and W. SECOMSKI, Institute of Fundamental Technological Research, Polish Academy of Sciences, Warsaw, Poland.
Corresponding e-mail: anowicki@ippt.gov.pl

A new method termed multitone nonlinear coding that utilizes nonlinear properties of acoustic tissue to improve ultrasound image resolution is presented. It is well known that under nonlinear propagation conditions field distribution for compressional and rarefactional portion of the wave is different. If $P^+(x,t)$ is a solution of the linear propagation equation fulfilling the boundary condition $P^+(x,t)=P^+(S(x),t)$ for x at S(x) where S(x) is the surface of the source then $P^-(x,t)=-P^+(x,t)$ is also the solution of the same equation for boundary condition with reverse phase $P^-(S(x),t) =-P^+(S(x),t)$ and $P^+(x,t)+P^-(x,t)= 0$. For nonlinear propagation the sum of P^+ and P^- is not equal to 0 despite the fact that, $P^+(S(x),t)+P^-(S(x),t)=0$.

In our novel method the acoustic source is activated with two tones burst (2.5 and 5 MHz) with specially designed polarization of the adjacent tone burst. This new approach is called nonlinear multi tone coding NMC because the choice of polarization of the adjacent tones (and their amplitudes) allowing optimization of the receiving properties depends on the nonlinear properties of the tissue. The calculations were done for two tone burst propagating in the tissue-like lossy medium comprising of spheres of different diameters and cylinders with inhomogeneous acoustic impedance, average absorption 7 Np/m•MHz. Comparison of the spatial field distribution obtained using conventional harmonic imaging approach, in which 2-nd harmonic is used to reconstruct the image, and field distributions corresponding to each of the excitation frequencies and differential frequency are presented.

The received signal comprises the similar amount of harmonics as in the standard pulse inversion method, however, in comparison with the last it has also fundamental component enhancing the image content close and distant to the transducer, where harmonics are limited.

Conclusions: In conventional harmonic imaging a single tone burst is applied to the acoustic source and the 2-nd harmonic signal is utilized to generate the resolution improved image. However, in the standard harmonic imaging only

half of the transducer bandwidth is employed, whereas in the proposed multitone nonlinear coding full bandwidth of the ultrasound imaging transducer is utilized. The results indicate that in comparison with conventional harmonic the acoustic energy available for image construction when using multitone nonlinear coding is enhanced by the factor of 2 with the corresponding increase in signal-to-noise ratio.

P1E-4
ULTRASOUND BLADDER SCANNER BASED ON 2D CONCAVE PROBE.

S. DERROUICH*, J. OYAMA, T. HIGUCHI, and T. ABE, Nagasaki University, Nagasaki City, Japan.
Corresponding e-mail: derrouich_salah@ieee.org

The medical reports in Japan show that around 1 of 5 senior citizens suffers from urine incontinence. Although the humidity sensor installed inside the diapers is a valuable measure for those patients, it is still a subjective system of only *reporting* the fact that the diaper is wet. In the context of this background, there is a need to develop a *warning* sensor system to evaluate the quantity of urine while still inside the bladder.

The abdominal scans are performed using a sector probe in both longitudinal and transverse planes. The bladder may also be seen using a trans-vaginal or trans-rectal approach with an intracavitary probe; these probes have to be attached to an ultrasound machine for visualization. Those types of scanners are impractical for bladder volume estimation because they are large, heavy, table top and expensive devices.

In this framework, the key bladder-scanner related challenges are the following: periodic and automatic scanning, portable, small size, light and affordable.

The bladder scanner presented in this paper uses A-mode approach and a limited number of UT; using A-mode approach with a small number of Ultrasonic Transducers (UT) is the only reasonable way to deal with all the above mentioned challenges. Our scanner is certainly not the first bladder scanner that makes use of A-mode approach with a small number of UT. However the existing bladder-scanner uses either one-dimension (1D) linear or circular array probe; these probes can sometimes fail to detect the bladder efficiently, especially in case of a small Pubis-Peritoneum-Window (PPW) or the absence of symmetry when the bladder is shifted to the right or left side of the body.

Inspired by the Pinhole-Camera-Model, our probe has been geometrically associated to constitute a 2D concave probe. The potency of this assembly subsists in the arrangement of 12 UT in a 4x3 matrix, the UT are angled in a way to face the center of the PPW. The probe increases scan rate, precision and reliability, it is also capable of sensing even in both cases of small PPW and bladder-asymmetry, and allowing different part of the bladder to be reached by a maximum number of used transducers; then shape of the bladder is estimated and approximated for volume calculation. By setting the system to scan automatically and periodically, when the bladder reaches a preset threshold a warning alarm is activated.

The probe has been designed, produced, tested and used with a developed algorithm for experiments on human-like model filled with water, targeting a bladder-like balloon. Experiments are conducted and results are compared with 'Yuririn USH-052' and 'Aloka ProSound SSD 3500' particularly in case of small PPW and bladder-asymmetry.

The results show a better performance of our scanner in critical conditions. An optimum size, weight and price are expected in the final product. Furthermore, conducting experiments directly on human body is the framework of our future research

This work is supported in part by the Cooperation of Innovative Technology and Advanced Research in Evolution Area, Toshi Area Project.

This work is registered for Japanese Patent No. 2005-126558.

P1E-5
DESIGN AND EVALUATION OF A LOW COST PC CARD USED FOR AN ACOUSTIC RADIATION FORCE BASED MECHANICAL CHARACTERIZATION SYSTEM.

M. SANTY*, T. BLALOCK, and W. WALKER, University of Virginia, Charlottesville, VA.
Corresponding e-mail: mks3k@virginia.edu

A growing area of ultrasound research is the use of acoustic radiation force to characterize mechanical properties of soft tissues. In acoustic radiation force imaging, the transfer of momentum related to the propagation of an acoustic wave through a dissipative medium is used to generate small and localized displacements within tissues. These displacements are then tracked using time delay estimation techniques. Images of viscoelastic properties are formed by processing temporal changes in displacement.

In this paper we describe the development of a new system that consists of a custom printed circuit board housed in and controlled by a standard PC. All transmit and receive electronics, prior to digitization, are placed on one PCI bus compatible card. PCI bus interaction is performed by a PCI interface chip (ASIC Design Services, PCILite chip, Midrand, South Africa). The front end electronics consist of transmit and timing circuitry. The transmit circuitry is a bipolar transmit circuit, composed of a cascade of paired N- and P-type mosfets, with programmable on and off times operating at a maximum transmit voltage of 121V and up to frequencies of 25MHz. The timing circuitry, controlled by a Complex Programmable Logic Device (CPLD) (Xilinx Inc., XCR3512XL), controls the length of the pulse, the number of pulses and transmissions, and the pulse repetition frequency. The receive electronics consist of two stages, a protection and an amplification stage. The protection stage is composed of multiple diode pairs configured to clip high voltages, protecting downstream electronics. The amplification stage consists of two non-inverting opamp based amplifiers with a total gain of 60dB. After the amplification stage, the data is sampled at 50MHz using a PC card (Gage Applied, Compuscope 12100 A/D card, Lachine, Quebec, Canada). This sampling is synchronized with the transmit pulse to assure timing accuracy on the order of picoseconds. The digitized data is then processed

using MATLAB (The Mathworks, Inc. Natick, MA). We are currently developing an easy to use interface for users who do not have extensive ultrasound expertise.

The PC card is fully assembled and being tested for functionality. All circuitry is being characterized to ensure timing accuracy of transmit and receive signals. We have also performed a series of experiments in a water tank. A half cycle of a 60Vpp, 8.3MHz sinusoid was transmitted using a single piston transducer. A 2.2V echo was successfully received and digitized. Experimental data is in relative agreement with simulation results performed in PSpice. A number of experiments are currently being performed to evaluate the potential of using this custom system to characterize tissue properties. We present experimental results and displacement curves from water tank and various soft tissue experiments. This system has the capability to transmit and receive acoustic pulses that can be processed to determine mechanical data of various soft tissues.

We acknowledge support from the Whitaker Foundation.

P1E-6
HIGH-FREQUENCY HIGH FRAME RATE ULTRASOUND IMAGING SYSTEM FOR SMALL ANIMAL IMAGING WITH LINEAR ARRAYS.

X.-C. XU*, C.-H. HU, L. SUN, J. YEN, and K. SHUNG, University of Southern California, Los Angeles,CA.
Corresponding e-mail: xiaochex@usc.edu

Small animal imaging is needed by biological and pharmaceutical research. Currently both Micro-CT and Micro-PET were developed and used. But their cost effectiveness and real-time capability are still of a great concern. Especially due to the fast heart rate of a mouse (>400/min), cardiovascular research utilizing mice requires imaging modalities with high frame rate capability (>100 Frame/sec), which can not be realized by Micro-CT and Micro-PET at present. High-frequency ultrasound imaging on the other hand is capable of achieving a better spatial resolution at an affordable price. Single element transducer based ultrasound backscatter microscopies (UBM) have been used in small animal research. Recently, high frequency ultrasonic arrays (>30MHz), which provide clinical convenience, reduce imaging time, and offer dynamic focusing, have been developed successfully. Comparing to current UBMs, a linear array based high-frequency ultrasound imaging system would alleviate many of these problems.

In this paper, we report the development of a high-frequency high frame rate ultrasound imaging system using 30~35MHz linear arrays. A pulser is dedicated to each element so that only low voltage trigger signals are necessary to drive 16 to 48 demultiplexers. A microprocessor (89S8252) based control board is used to generate all the necessary control signals for multiplexers and demultiplexers in the tranceiver board and analog delaylines in the beamforming board. A 40-60 dB TGC amplifier is applied to echoes from each channel before they are aligned by a cross-point switch and analog delaylines. One channel beamformed echo signals are digitized by a 500MS/s 8-bit PCI A/D card in PC. Finally the acquired data are processed and B-mode images are displayed in

real time by Labview based software. The system can display 30 images per second and acquire over 100 images per second for slow motion playback by using a 48 element linear array with center frequency at 30MHz. By replacing with more powerful microcontrollers and more efficient C++ based software, it should be possible to acquire images at a much higher frame rate.

Rabbit eyeball images and mouse heart images have been obtained in vitro and in vivo to demonstrate the potential of this system in biomedical applications.

P1E-7
ULTRASOUND-BASED AIR BUBBLE TRAPPING SYSTEM FOR HAEMODIALYSIS.

P. PALANCHON*[1], A. BOUAKAZ[2], L. POURCELOT[3], and F. TRANQUART[2], [1]CIT, CHU Bretonneau, Tours, France, [2]INSERM U619, Tours, France, [3]Ultrasound and Nuclear Medecine, CHU Bretonneau, Tours, France.
Corresponding e-mail: palanchon@med.univ-tours.fr

Background: Microembolization in patients undergoing chronic haemodialysis sessions is considered as a potential source of severe pulmonary side-effects. Previous experimental and clinical studies indicated that several air bubbles were generated by the haemodialysis system but they were not always trapped by the air filter. The goal of this study was to develop an air bubble trapper using ultrasound waves to remove any bubble from the tubing system before they reach the patient.

Method: A home-made bubble trapper was developed in the laboratory. It consists of a Perspex block containing a main channel connected to the tubing of a haemodialysis machine and a second sub channel perpendicularly positioned to the main one. The sub-channel is used to trap the air bubbles. The bubbles flowing in the main channel were insonifed through an acoustic window with an ultrasound wave, pulsed (8 to 20 cycles) or continuous, at a frequency of 500 kHz generated by a single element transducer positioned 3cm away from the main flow. The generated acoustic pressure was kept below 1MPa. The radiation force induced by the ultrasound beam acts directly on the flowing air emboli, by pushing them into the sub-channel. Two Doppler probes operating both at 2.5 MHz, connected to a DWL Doppler machine were placed before and after the bubble trapper to count simultaneously the number of embolic events. The flow of the machine was varied between 200ml/min and 500ml/min.

Results : Depending on the flow velocity, the number of microembolic signals (MES) detected by the Doppler probes before and after the trapping system was identical and ranged 5 to 150 MES/min in absence of the ultrasound irradiation. When the air bubble trapper was activated, a reduction of the number of MES detected by the second Doppler probe of up to 70% was observed. According to the Doppler recordings, the circulating bubbles were either fragmented into smaller bubble fragments or directly got pushed into the second sub-channel where they were collected.

Conclusions: This simple approach using an ultrasound-based trapping system showed to operate adequately with the current settings and can be used to neutralize air emboli.

P1E-8

VERSATILE ASSESSMENT OF 3D PROSTATE ANATOMY AND ELASTIC ANOMALIES.

Y LI*, C. D. GARSON, and J. A. HOSSACK, University of Virginia, Charlottesville, VA.
Corresponding e-mail: yinbo@virginia.edu

Prostate cancer is the second most prevalent malignant cancer among men in the US with approximated 220,000 new cases and 29,000 deaths per year [1]. Unfortunately, current prostate cancer screening approaches using digital rectal examination and Prostate Specific Antigen (PSA) blood testing, yield disappointing diagnostic sensitivity and specificity. In this work, we use a modified transrectal transducer operating in the 'I-Beam' mode [2]. Auxiliary tracking arrays provide image frame to frame measurement of offset and rotation facilitating later reconstruction into a 3D image data set. This particular approach to 3D positioning is especially well suited to this application since the 3D positioning device is adjacent to the B-scan imaging transducer at the tip of the transducer probe. This avoids the numeric ill-conditioning that may be encountered when the position measurement device and image plane are physically separated as they would be if the position measurement device is in the handle of a transrectal transducer. Additionally, the I-Beam approach senses relative tissue motion and thus any bulk tissue motion during the scan is at least partially compensated out in the final reconstruction. The approach is also compatible with the generally preferred freehand scanning technique (as opposed to approaches based on using a mechanized stage). In 3D reconstructions of lesions in a realistic prostate phantom we have achieved linear dimensional accuracy of 5% in the reconstructed (elevational) dimension and lesion volume measurement accuracy of 11%. The modified transducer is also fitted with a water injection port to facilitate a technique that we refer to as 'Synthetic Digital Rectal Examination'. (This approach was independently conceived by Alam et al. and described at the 2004 IEEE Ultrasonics Symposium. [3]) The latex sheath over the transducer is inflated using a syringe pump. In prototype phantom testing, we have verified our ability to detect $3 \times 3 \times 5$mm lesions via the computed elastographic image at a depth of 2 cm. Thus, we believe that we are able to detect and quantify lesions that are small smaller and deeper than those that may be practically palpated using conventional digital rectal examination.

[1] American Cancer Society, "Prostate Cancer Statistics from www.cancer.org," 2003.

[2] J. A. Hossack, T. Sumanaweera, S. Napel, and J. Ha, "Quantitative 3D Diagnostic Ultrasound Imaging Using a Modified Transducer Array and an Automated Image Tracking Technique," IEEE Transactions on Ultrasonics Ferroelectrics & Frequency Control, vol. 49, pp. 1029-1038, 2002

[3] S. Alam, E. Fellepa, A. Kalisz, S. Ramchandran, R. Ennis, F. Lizzi, C.-S. Wuu, and J. Ketterling, "In vivo Prostate Elastography: Preliminary Results," Proceedings of IEEE Ultrasonics Symposium, 2004.

This work supported in part by US Army Grant W81XWH-04-1-0240.

P1E-9

A STUDY OF MOTION ARTIFACTS OF FOURIER-BASED IMAGE CONSTRUCTION.

J. WANG* and J.-Y. LU, Ultrasound Lab, Dept. of Bioengineering, The University of Toledo, Toledo, OH.
Corresponding e-mail: jilu@eng.utoledo.edu

Based on high frame rate method developed in our lab, a Fourier based imaging method with a variable frame rate was developed recently. In this method, multiple steered plane waves are used to obtain ultrasound echo signals. Images are constructed based on Fourier transformation. Because multiple transmissions may be used to obtain a frame of image to reduce sidelobe and increase resolution, it is important to study the effects of motion on the method for fast moving objects such as the mitral valve of the heart, and compare the results with those of conventional delay-and-sum method.

In this paper, we performed experiments with the Fourier based method by using our high frame rate imaging system to obtain radio frequency (RF) data. A point scatterer was placed in the imaging plane, moving perpendicularly to the axis of a 2.5MHz, 19.2mm aperture, and 128 element array transducer at a velocity of 210 mm/s which is about the peak velocity of the mitral valve of a heart. Experiments were repeated with the point scatterer placed on axis but with different depths (30, 46, 50, 70 and 90mm) from the transducer surface. At each depth, data from different numbers of transmissions (1, 11, 19, and 91) were used to construct images with the Fourier-based method (frame rates of 5346, 486, 281, and 59 frames/s, respectively). As a comparison, images were also constructed with conventional delay-and-sum method with and without dynamic focusing in transmission. (For delay-and-sum, the frame rate is about 59 frames/s with a fixed transmission focal distance at 70 mm. For dynamic focusing at all depths in transmission, the frame rate would be very low but the image quality would be high.) To study the image contrast changes, an ATS539 tissue mimicking phantom was in place of the point scatterer with the center of its six 15mm diameter cylinders located at a depth of 46mm. Images constructed without object motion were also obtained and were used as bases to calculate corresponding percentage changes of resolution, sidelobe, and contrast.

The results show that for 1, 11, and 19 transmissions, the percentage changes for the Fourier-based method are smaller than those of delay-and-sum method without dynamic focusing. For 91 transmissions, the percentage changes are larger in small depths but are comparable with the delay-and-sum method when distance increases. In conclusion, the Fourier-based method is not very sensitive to the motion except when the number of transmissions is large (lower frame rate) and the depth is small.

The authors would like to thank Mr. Jiqi Cheng for his help in doing the experiments and providing the image construction programs. This work was supported in part by a grant HL 60301 from the National Institute of Health.

Session: P1F

ACOUSTIC SENSORS
Chair: P. Khuri-Yakub
Stanford University

P1F-1

INVESTIGATION OF PRECISION SOUND VELOCITY MEASUREMENT METHODS AS REFERENCE FOR ULTRASONIC GAS FLOW METERS.

P. NORLI*[1], P. LUNDE[1], and M. VESTRHEIM[2], [1]Christian Michelsen Research AS (CMR), Bergen, Norway, [2]University of Bergen, Dept. of Physics and Technology, Bergen, Norway.
Corresponding e-mail: pnorli@cmr.no

Ultrasonic gas flow meters for volumetric flow rate fiscal metering of natural gas (USMs) may today also be used for mass and energy flow rate measurement, based on velocity of sound (VOS) measurement. To establish the accuracy of the VOS measurements given by the USM, and for traceability purposes, an independent and high-accuracy VOS measurement cell may be used as reference. To include relevant effects of dispersion, the cell should preferably work in the operational frequency range of USMs, 100-200 kHz, with natural gas under high pressure. VOS measurement cells with extreme accuracy are available in the audio frequency range, for which uncertainties down to 1 ppm have been reported. Less work is however identified at a sufficient accuracy level in the frequency range 100-200 kHz.

Three different candidate transient methods have been tested and analyzed with respect to measurement uncertainty, and they are seen to have several common experimental uncertainty sources. In the present work, a *two-distance method* is discussed in more detail as an example, and some results from measurements in an insulated chamber with air at 1 atm and ca. 25 °C are presented.

The relative expanded measurement uncertainty was estimated according to ISO guidelines to approximately 264 ppm (95% conf. level). One major source of uncertainty in these measurements was experienced to be small convection currents in the chamber. Without these, the expanded measurement uncertainty would have been about 126 ppm. Such convection effects are however expected to be strongly reduced in a properly designed measurement cell.

The VOS measurement results were compared with predictions from Cramer's VOS model for standard air, including dispersion [J. Acoust. Soc. Am. **93** (5), pp. 2510-2516, 1993], resulting in a mean deviation of -18 ppm with a two standard deviation spread in the data of 190 ppm.

P1F-2

A CONTROLLED INVESTIGATION OF THE SPATIAL DISTRIBUTION OF ACOUSTIC CAVITATION ACTIVITY GENERATED IN A STANDING WAVE FIELD PRODUCED BY A 40 KHZ CLEANING VESSEL TRANSDUCER.

M. HODNETT*, M. CHOI, P. GELAT, and B. ZEQIRI, Quality of Life Division, National Physical Laboratory, Teddington, Middlesex, UK.
Corresponding e-mail: mark.hodnett@npl.co.uk

High power ultrasound has found significant utility in a wide range of applications, from healthcare, through sonochemistry, to cleaning and industrial processing. The phenomenon of cavitation is the principal driver behind many of these applications, yet quantification techniques for cavitation are still not widely available. Access to such measurement methods, and their establishment into a standards infrastructure would undoubtedly lead to process improvements and enhanced technology take-up.

The work reported describes work carried out at NPL to provide a facility against which the performance of NPL's patented novel cavitation sensors may be tested on a quantitative, reproducible basis. It therefore comprises the results of a systematic measurement programme carried out on a 40 kHz single transducer system, built around a stressed-stack piezoelectric transducer typical of the type used in ultrasonic cleaning systems. Both a conventional sonar hydrophone (B & K type 8103) and NPL cavitation sensors have been used to measure the distribution of acoustic pressure and cavitation activity generated by the 40 kHz transducer in a cylindrical vessel. Repeat measurements show that the acoustic pressure amplitude, even under cavitating conditions, is reproducible to ±15%. Cavitation activity, defined as the broadband acoustic emissions from bubble oscillation and collapse integrated over the frequency range 1 - 3 MHz, is reproducible to ±20%. Both cavitation activity and acoustic pressure measurements have been carried out for a range of water column heights and transducer drive voltages, and the results illustrate clearly the evolution of cavitation activity with increasing applied acoustic pressure, and its enhancement when standing waves are established.

To predict the acoustic pressure distribution in the cylindrical vessel, a detailed Finite-Element (FE) model was set up of the transducer and vessel combination. Results from this show good agreement with experiment in terms of the locations of acoustic field maxima and minima, and the model has thus been used to refine the experimental protocol adopted when testing sensors experimentally.

Finally, the motion of the emitting face of the 40 kHz transducer in water has been probed experimentally using a Polytec scanning laser vibrometer. The results obtained show that the vibration characteristics of the 40 kHz transducer are approximately piston-like, but that future FE models will need to consider a more detailed approach to transducer construction, in particular allowing for the effects of the tensioning bolt.

The authors acknowledge the financial support of the National Measurement System Directorate of the UK Department of Trade and Industry.

P1F-3

INVESTIGATION ON VISCOELASTICITY OF SILICONE RUBBER USING IMPEDANCE CHANGE OF A QUARTZ-CRYSTAL TUNING-FORK TACTILE SENSOR.

H. ITOH* and Y. YAMADA, Shinshu University, Nagano, Japan.
Corresponding e-mail: rokuro1@gipwc.shinshu-u.ac.jp

It is well known that viscoelastic data of silicone rubber measured by rotating viscometer or DMA (Dynamic Mechanical Analysis) is quite different each other. Viscoelastic data strongly depends on measurement equipment. In this paper, viscoelasticity of silicone rubber has been investigated experimentally by use of a quartz-crystal tuning-fork tactile sensor. The quartz-crystal tuning-fork tactile sensor makes use of its impedance or frequency change at resonant vibration 32.48 kHz when its base gets brought into contact with an object. The quartz-crystal tactile sensor has many advantages. It is capable of distinguishing a wide variety of materials from soft to hard ones by use of the impedance change of the quartz-crystal tactile sensor. Their quality and surface roughness are also distinguished. The experiments were done for eight kinds of silicone rubbers (the values of rubber hardness tester are JIS85, 70, 65, 60, 50, 45, 40, and 35). Rubber hardens as the value of rubber hardness tester increases. The impedance change (ΔR) was calculated between the sensor in contact with an object and in no contact at room temperature. The impedance change increases according to the value of rubber hardness tester. At the same time, the impedance change increases according to acoustic impedance ρC (ρ: density of an object, C: sound velocity of longitudinal acoustic wave in silicone rubber) because the impedance change has been proportional to the transmitting energy resulting from the difference between silicone rubber and the base of the quartz-crystal tuning fork in acoustic impedance of the longitudinal plane wave. We compare two cases of impedance change characteristics: one is obtained by C calculated by Young's modulus measured by tensile meter, the other is calculated by complex Young's modulus measured by rotating viscometer. In the range of low ρC of silicone rubber compared to metals, the impedance change is almost proportional to ρC. The correlation coefficient of linearity between ΔR and ρC for the former case is 0.89 and for the latter case is 0.929. It is found that the impedance change of a quartz-crystal tuning-fork tactile sensor correlates closely with complex Young's modulus of silicone rubber because silicone rubber is intrinsic viscoelasticity and includes the information of viscoelasticity of silicone rubber as its complex Young's modulus.

P1F-4

INFLUENCE OF RECEIVER NOISE PROPERTIES ON RESOLUTION OF PASSIVE WIRELESS RESONANT SAW SENSORS.

V. KALININ*, Transense Technologies plc, Upper Heyford, Bicester, Oxon., UK.
Corresponding e-mail: victor.kalinin@transense.co.uk

Wireless or contactless sensors based on SAW resonators and delay lines working as passive back-scatterers have found application in the areas where

temperature and mechanical strain need to be measured on rotating parts. As an example, resonant SAW sensors are used in automotive tire pressure monitoring systems (TPMS), they are being developed for torque measurements in electrical power assisted steering systems, driveline control and engine management systems.

Resolution is one of the most important characteristics of the passive wireless SAW sensor. It is mainly determined by noise in the measured value, which in its turn depends on the loaded Q factor of the SAW resonator, noise properties of the receiver and the algorithm used for spectrum estimation. Several publications investigated theoretical limit for the resolution that is set by additive noise of the receiver. It was shown that the potentially achievable resolution could be very high. For instance, the standard deviation of the measured strain can be as small as 0.02 microstrain at a distance of 1 m for the interrogation power of 10 mW at 433 MHz, the receiver bandwidth of 0.5 MHz, noise figure of 5 dB and the loaded Q = 6000 of the resonator made on ST-X cut quartz. However in reality the achievable resolution is considerably worse. This paper investigates additional limitations on the SAW sensor resolution that are imposed by the phase noise of the local oscillator of the receiver.

The problem is studied by means of stochastic simulations on the basis of information on the realistic phase noise of the receiver synthesiser used in the wireless interrogation unit. It is shown that the additive noise determines the resolution only at a distance larger than 3 m in the free space. This situation may be typical for TPMS where the received signal power can be as low as -80 dBm. The received signal in torque sensors is much stronger, typically from -20 to -10 dBm. In this case or in the case of shorter distances for TPMS it is mainly the phase noise that determines the resolution. For a typical value of the phase noise of -90 dBc/Hz at 10 kHz offset the predicted standard deviation of measured strain is 25 times larger than the one determined only by additive noise. This figure is much closer to experimental results.

The paper also studies variation of the dynamic range of the wireless resonant SAW sensor with interrogation distance and the number of coherently accumulated SAW responses. Practically achievable dynamic range for the torque sensor is close to 60 dB.

P1F-5
PIEZOELECTRIC BIMORPH MICROCANTILEVER: A NEW GAS PRESSURE SENSOR.

V. MORTET*[1], R. PETERSEN[2], K. HAENEN[1,2], and M. D'OLIESLAEGER[1,2],
[1]Universiteit Hasselt, Institute for Materials Research, Diepenbeek, Belgium,
[2]IMEC vzw, Division IMOMEC, Diepenbeek, Belgium.
Corresponding e-mail: vmortet@yahoo.fr

Since the development of the atomic force microscope (AFM), the interest in micro-fabricated cantilevers has grown. Micro-machined cantilevers are extremely sensitive, miniature, mass produced and low cost sensors. Cantilevers are excellent micro-mechanical sensors. Micro-cantilevers sensors operate by detecting changes either in resonance frequency, amplitude, Q-factor or

deflection caused by mass loading, surface stress variation, or changes in damping conditions. In this work, we used a non-symmetric piezoelectric bimorph cantilever as a wide range pressure sensor. The sensor detects the change in the resonance frequency of the micro cantilever with a piezoelectric film (ZnO). In contrary to common cantilever sensor systems, which use either optical, integrated piezo-resistive, integrated piezoelectric, or integrated capacitance detections, the piezoelectric film of the bimorph cantilever acts as both a sensor and an actuator. The frequency characterization of the piezoelectric bimorph cantilever was accomplished by measuring the bimorph's admittance using an impedance/gain-phase analyzer.

In this communication, we report the experimentally measured changes in the cantilever's resonant frequencies versus the gas pressure (up to 7 bar), the type of the gas and the temperature (up to 60°C) and we discuss the optimisation of both mechanical and geometrical properties of the cantilever for pressure measurement.

The cantilever exhibits several resonance frequencies. We have measured variation of the two first resonance modes at f_1 =46kHz and f_2 =913.4kHz (at room temperature and atmospheric pressure). Both resonance frequencies show a linear variation as a function of the pressure and they exhibit the same variation as a function of the temperature. The frequency shift as function of the pressure is -0.00421 /bar for the first mode and -0.00319 /bar for the second mode. These experimental results show that a simple cantilever can be use to measure both pressure and temperature simultaneously.

P1F-6
A NOVEL DOPPLER BASED ULTRASONIC SURFACE ROUGHNESS MEASUREMENT.

J. REZANEJAD GATABI*[1] and I. REZANEJAD GATABI[2], [1]Iran University of Science and Technology, Tehran-Tehran-Iran, [2]Khajeh Nasir Toosi-University of Technology, Tehran-Tehran-Iran.
Corresponding e-mail: irezanejad@yahoo.com

Surface topography is of great importance in specifying the function of a surface. A significant proportion of component failure starts at the surface due to either an isolated manufacturing discontinuity or gradual deterioration of the surface quality. Typical, these problems of lower surface integrity, lead to in service stress corrosion and fatigue failure. The most important parameter describing surface integrity is surface roughness.

In the manufacturing industry, surface must be within certain limits of roughness. Therefore, measuring surface roughness is vital to quality control of machining workpiece, especially if it is non-contact method compared to the direct conventional method; which uses stylus type devices.

In this paper, a novel Doppler based ultrasonic sensor has been proposed for high-precision surface roughness measurement. Despite conventional non-contact ultrasonic techniques which use the ultrasonic travel time to measure the distance of the undertest surface from the sensor to describe the roughness parameters, the proposed sensor implements the Doppler effect on the

continuously emitted ultrasonic bursts for surface roughness measurement.

When an object is ready to undergo roughness testing, it is mounted on a motor rotating at a constant velocity of ω. The device comprises an ultrasonic transmitter emitting sound pulses travel across to the undertest object. The sonic wave is reflected diffusely on the object where it is separated into many weak sounds, a few of which are received by the receiver. The Doppler effect causes the frequency of the received signal to be shifted with respect to the roughing depth and its shape. The relationship between the rate of change of the frequency of the received signal and the peak-to-valley height and the roughing shape is mathematically analyzed.

After amplification, the received signal is applied to a high-pass filter and therefore to a rectifier stage. Of its frequency response, the circuit provides an output voltage related to the frequency of the received signal. Analysis of the output voltage by a processor allows the parameters of the surface roughness to be calculated.

Since the sonic speed changes in various environmental situations, it may cause some errors in transit-time based sensors. Using Doppler effect, these problems are avoided and therefore a more precise measurement is achieved. Also the continuous ultrasonic emission allows the processor to sample the surface at any point where needed.

The proposed method also can be applied for vibration analysis of the rotating fans. The fabrication of a prototype sensor and experimental verification of the analytical results are reported. The experimental results agree well with the theory.

With specially thanks to following people for their assistance and encouragement: 1- Dr. F. Forouzbakhsh- University of Tehran 2- Mr. A. Araghi- University of Mazandaran

P1F-7

INTERACTION OF SURFACE ACOUSTIC WAVES WITH PARTICLES.

J. KONDOH*[1], T. OYAMA[1], Y. MATSUI[1], and S. SHIOKAWA[2], [1]Faculty of Engineering, Shizuoka University, Hamamatsu-shi, Shizuoka , Japan, [2]SAW&SPR-Tech, Hamamatsu-shi, Shizuoka, Japan.
Corresponding e-mail: j-kondoh@sys.eng.shizuoka.ac.jp

This paper presents interaction of surface acoustic waves (SAW) and particles. Liquid-phase sensor is realized by using a shear horizontal SAW (SH-SAW). Measurements of particles in liquid are important application for biosensor, process monitoring, and so on. The detection mechanisms of the SAW are mechanical and electrical perturbations. For simultaneous detection of both perturbations, three-channel SH-SAW sensor was proposed. Several particles, such as pigments, guard gel (diameter is 10 micron), and steel ball, are measured. The results indicate that it is difficult to detect particles in liquid based on the mechanical perturbation. We have concluded that the penetration depth of the shear horizontal displacement is not enough to detect particles, because it is about 80 nm, when water is loaded on 50 MHz SH-SAW sensor. As the viscous

penetration depth increases with decreasing sensor frequency and increasing viscosity, the steel balls are immersed in 80 wt.% glycerol/water mixture. The results show that the high sensitive detection is realized with 30 MHz SH-SAW sensor.

The measurements of mass loading effect in gas phase are performed by using the steel balls. The steel balls, whose weight is a few grams, are loaded on the SH-SAW propagating surface. Whereas the mass loading effects in liquid are not observed, phase, i.e. frequency, increment phenomenon is observed in the gas phase. On the other hand, amplitude of the SH-SAW is not changed. Increment of phase corresponds to increase of the phase velocity. The same phenomenon is observed by using Rayleigh-SAW sensor. Based on these results, we have assumed that the elastic constants of the piezoelectric crystal increase by loading of the steel ball. This assumption agrees of a pressure sensor based on the acoustic wave sensor. The results suggest that a threshold exist between the mass loading effect and pressure effect.

This work is supported by Human Frontier Science Program.

P1F-8
ORGANIC VAPOR SENSING AND DISCRIMINATION USING ENHANCED SENSITIVITY THICKNESS SHEAR MODE DEVICES.

R. WILLIAMS, S. CULAR*, A. UPADHYAYULA, and V. BHETHANABOTLA, University of South Florida, Tampa, FL.
Corresponding e-mail: willia15@gmail.com

Thickness shear mode (TSM) resonators, also known as quartz crystal microbalances (QCM) are a class of acoustic wave sensors that have been used for gas/vapor sensing and for determining liquid properties. Fast and sensitive chemical vapor sensing, specifically of hydrocarbon vapors, has attracted recent attention. The TSM sensors typically used have a lower sensitivity compared with other acoustic wave sensors. This paper describes the development of high sensitivity organic vapor sensors using polymer thin film coatings of polyisobutylene (PIB) on TSM devices. Commercially available AT-quartz TSM devices were milled to 17 μm, leaving a thin quartz membrane surrounded by a 50 μm thick outer ring. This resulted in an increased frequency and a consequent increase in sensitivity, as described by device models. TSM devices with fundamental mode resonant frequencies of 10, 20 MHz were compared to the milled 96 MHz devices. The organic vapors studied were benzene, toluene, hexane, cyclohexane, heptane, dichloroethane, dichloromethane, and chloroform at levels ranging from less than 1 to over 10 volume percentage in nitrogen gas. The Butterworth-VanDyke (BVD) equivalent circuit model was used to model both the perturbed and unperturbed TSM resonator. Monitoring the sensor response through the equivalent circuit model allowed for discriminating between the organic vapors. In particular, changes in the resistance parameter due to softening and relaxation of the PIB film allowed for this vapor discrimination. For instance, it was found that vapor discrimination of benzene vapors was possible at over 4.74 % levels which corresponded to resistance changes over 5 ohms.

We present results of tests conducted to demonstrate increase in sensitivity for higher fundamental frequency TSM devices. We also evaluate and compare the performance of each sensor in terms of detection limit and noise level.

Inverse mesa resonators were fabricated at MTronPTI, Orlando Florida. The authors acknowledge the significant contributions of Shibendra Pobi, Krishnan Srinivasan, and Tom Payne.

Session: P1G
NDE MODELING AND MEASUREMENTS
Chair: N. Bilgutay
Drexel University

P1G-1
STUDIES ON EFFECTIVE AND STABLE ABSORBING BOUNDARY CONDITIONS IN ULTRASONIC WAVE MODELING.

H. ZHAO[1], X. WANG[1,2], and H. ZHANG*[1], [1]Institute of Acoustics, Haidian District, Beijing, China, [2]CSIRO Petroleum, Bently, WA, Australia.
Corresponding e-mail: xiuming.wang@csiro.au

In ultrasonic wave numerical modeling for inhomogeneous material, it is impossible to allow numerical simulation of ultrasonic wave propagation in unbounded medium with a limited computation model. Usually the ultrasonic waves in an unbounded medium are simulated using bounded models through imposing artificial boundaries. These artificial boundaries, if not treated properly, may cause spurious unwanted reflections that affect the accuracy of numerical solutions. Thus, effective and stable absorbing boundary conditions (ABCs) to reduce or eliminate artificial reflections from these artificial boundaries are needed. The perfectly matched layer (PML) has been applied to both acoustic and elastic problem for simulating wave propagation. It is known that apparent reflections occur at the interface between inner normal regions and PML regions are reduced greatly.

In this paper, in order to conduct effective ultrasonic wave numerical experiment in inhomogeneous material for perfect artificial reflection absorptions, a high-order staggered-grid finite-difference scheme, with velocity-strain equation systems is proposed. This algorithm uses the PML method, the damping factor method, and the Liao's method that are considered to be more efficient than the others. These three ABCs are carefully implemented in a staggered-grid finite-difference, and studied in detail. Numerical examples for the three kinds of absorption boundary conditions are run, and the related numerical results are compared with each other. The related algorithms are implemented by means of calculating reflection coefficient in the case of the discrete condition. The results both in time and in space domains show that the PML ABC is better than either of damping factor ABC and Liao's ABC for all of the reflected angles. When the Lao's and damping factor methods are used, the reflections become much stronger as reflected angle is larger than 50 degree. In addition, we also

draw a conclusion that the PML is highly efficient in absorbing the surface waves particularly.

P1G-2

MEASUREMENT METHOD OF LONGITUDINAL ACOUSTIC PROPERTIES FOR SOLID SPECIMENS USING THIN LAYER WATER COUPLANT IN UHF RANGE.

H. ODAGAWA*, M. ARAKAWA, K. MORIOKA, and J. KUSHIBIKI, Tohoku University, Sendai, Japan.
Corresponding e-mail: odagawa@ecei.tohoku.ac.jp

High frequency and wide band ultrasonic measurement methods are required in ultrasonic material characterization to evaluate velocity dispersion and frequency characteristics of attenuation coefficient. Generally, measurements for solid specimen are performed in the ultrasonic composite transmission line, consisting of a buffer rod with an ultrasonic transducer on one end, a couplant and a specimen. Pure water is usually used as the couplant, because precise acoustic properties was obtained: no velocity dispersion at least 1GHz, known attenuation coefficient (α/f^2=22.3$\times$10^{-15} s^2/m) and velocity (V=1491.23 m/s) at 23°C. However, because of large attenuation of an ultrasonic wave in the water, it is difficult to use it in UHF range by the conventional method. A method using salol (phenyl salicylate) as a solid couplant has been reported for UHF range measurement. However, this method has a complexity that the acoustic characteristics of the salol couplant depend on the solidification condition. Therefore if the water couplant can be applied in UHF range, it is very useful to characterize the acoustic properties of materials.

In this paper, we will describe a measurement method of UHF-range longitudinal acoustic properties for solids using a thin water layer as a couplant. The thickness of the couplant t is reduced to around 1μm to reduce the propagation attenuation. It is approximately half wavelength of the center frequency of the measurement range. Consequently, multiple reflections of the acoustic waves are occurred in the couplant. Reflection coefficient at the water couplant from the buffer rod becomes minimum in the frequency f_d satisfying a condition of $f_d = V/(2t)$. We can determine the accurate value of t by measuring f_d. Considering them, we develop an analysis method using a fitting technique. In this measurement, a RF pulse signal and complex mode are used.

In order to confirm a validity of this method, some measurements have been demonstrated for synthetic silica glass which has no velocity dispersion in VHF and UHF ranges; T-4040 (Toshiba Ceramics Co.) and N-ES (Nippon Silica Glass Co.) were measured 300-750 MHz and 450-1100 MHz, respectively. We made several ultrasonic devices, which had piezoelectric ZnO thin film transducers on the one side of the buffer rods and spacers made by ZnO thin film on the opposite side. The spacers kept the thickness of the water couplant constant as well as the parallelism of the thin layer. The devices and specimens were put in a small chamber, which soaked in a temperature controlled water bath. The results showed a good agreement with the value measured by our conventional

methods in VHF and UHF ranges. Velocities of T-4040 and N-ES were 5953.4±0.2 m/s and 5927.2±0.1 m/s, respectively. The deviations from the previous results was less than ±0.004%, and they exhibit no velocity dispersion up to 1GHz. Measured α/f^2 of these specimen were 1.2-1.4$\times10^{-16}$ s^2/m (previous results: 1.3$\times10^{-16}$ s^2/m). Therefore, we confirmed that this method was very useful and powerful for characterizing solid materials.

P1G-3
APPLICATION OF THE FDTD TF/SF METHOD TO ANALYSIS OF THE SCATTERING PHENOMENA OF THE ELASTIC WAVE FIELDS IN SOLIDS.

M. SATO*, Akita University, Akita, Akita, Japan.
Corresponding e-mail: ma-sato@ed.akita-u.ac.jp

Scattering phenomena of the elastic wave fields in solids is the most critical aspect to be clarified in the non-destructive evaluation (NDE) of solids using ultrasonic waves. In order to obtain the desired information from the echo signals of elastic waves reflected from the flaws in solid materials, the relation between the signals and the flaws should be clarified. For this objective, analysis by numerical simulation represents the most versatile tool available because of the difficulties in investigating by other analytical and experimental methods. By using numerical methods such as the finite difference method (FDM), finite element method (FEM) and boundary element method (BEM), researchers have clarified various characteristics of the scattered elastic waves.

The present author and colleagues have previously reported the application of a Finite-Difference Time-Domain (FDTD) numerical method to the elastic wave fields in solids. The FDTD method has the unique characteristic that it can separately calculate the far field scattered waves and near field total waves at the same time, where total waves refer to a mixture of incident plane waves and scattering waves. This formulation is called the total-field/scattered-field (TF/SF) formulation and is very effective for the analysis of scattering problems in NDE.

Generally, perfect plane waves are difficult to realize in numerical calculations. If we input the plane-like wave in the analysis region, both of the sides of the wave will be diffracted. Also, if we realize the plane wave by adopting some boundary conditions at the truncated boundary, we will not be able to absorb the scattering waves at the boundary. The TF/SF formulation, however, can realize perfect plane waves that are incident to the scattering objects.

To date, the TF/SF formulation has only been applied to scalar wave fields and electromagnetic wave fields. Application to the elastic wave fields in solids has not yet been attempted.

In this report, a TF/SF formulation of the elastic wave fields in solids is described. Specifically, scalar and vector potentials are used for the formulation. Using these potentials is beneficial for two reasons. First, the longitudinal waves and shear waves are initially separated. Therefore the scattering phenomenon can be clearly recognized. Second, it is facile to use the potentials for setting the absorbing boundaries. Generally, it is not simple to implement the absorbing

boundaries of the elastic wave fields in solids. Because, the two waves, longitudinal and shear waves, exist in the solid material and the waves have different characteristics, it is difficult to match the absorbing boundaries to both waves at the same time. However, if we use the potentials, we can divide the waves perfectly and set the boundary to each wave separately such as in a scalar wave.

The FDTD TF/SF formulation has been proved effective in analysis of the scattering phenomenon of a longitudinal plane wave incident to a square hole.

P1G-4

STUDY OF THE TIME-DEPENDENCE OF THE MECHANICAL PROPERTIES OF DOUGHS FOR FLOUR STRENGTH EVALUATION.

J. GARCIA-ALVAREZ*, J. M. RODRIGUEZ, Y. YAÑEZ, A. TURO, J. A. CHAVEZ, M. J. GARCIA, and J. SALAZAR, Technical University of Catalonia (UPC), Barcelona, Spain.
Corresponding e-mail: javier.garcia-alvarez@upc.edu

Both flour strength and dough processing affect the dough consistency that determines its potential for breadmaking purposes. Quick identification of poor dough quality would reduce problems with dough handling during further stages of the process and maximise productivity. Maintaining consistent production would contribute to better control of product quality and consequently lead to high levels of customer satisfaction.

Ultrasonic measurements have already been carried out to characterise dough properties. The ultrasonic wave parameters generally measured include the velocity of propagation and the attenuation of the acoustic wave travelling through the sample. These measurements can be related to both viscoelastic and physical properties of the sample, providing the flour strength. However, due to the time-dependent nature of dough accurate measurements of the ultrasonic velocity and attenuation are sometimes difficult to attain especially in highly attenuating materials like dough. Furthermore, due to viscoelastic properties of dough when a sample is placed between both transducers it slowly flows away from the transducer surface producing changes in the values of the ultrasonic velocity and attenuation with time. The greater these changes are the softer the dough is. This makes necessary a settling time in order to get an accurate measurement.

In this work, an alternative method for evaluating the flour strength using low intensity ultrasound is shown. The evolution with time of both velocity and attenuation is monitored and then related to the flour strength. Main advantage of this novel approach is that changes in time of ultrasonic velocity and attenuation are easy to monitor than carry out accurate measurements of them after a settling time. Experimental results on doughs with different flour strength are presented, compared and discussed.

This work was supported by a CRAFT Project under contract no. QLK1-CT-2001-70377. Also, the authors would like to thank the baking and Cereal Processing section of CCFRA for dough preparation, bread baking and bread assessment.

P1G-5

DESIGNING AND SIGNAL PROCESSING OF INTELLIGENT INSPECTION PIG APPLYING ULTRASONIC A-SCAN.

C. TIANLU*, Q. PEIWEN, J. TAO, and Z. ZHIGANG, Dept. of Information Measurement technology and Instrument, Shanghai Jiaotong University, Shanghai, P. R. China.
Corresponding e-mail: chentianlu@sjtu.edu.cn

Pipeline safety evaluation is an issue of great concern in China. Several types of NDE methods have been tried and tested for inspecting pipelines. Great success has been achieved using ultrasonic A-scan to size and locate defects in oil and gas pipelines. An ultrasonic inspection system (intelligent pig) is designed to inspect pipelines of different diameters. The overall architecture, hardware configuration, and signal processing strategy are discussed.

The intelligent pig (2400mm long, 60 kg weight) includes six parts: driver robot, system controller, power supply, ultrasonic sensors, ultrasonic data processor, and position tracer. The robot can drive the pig to climb in pipeline from 150 mm to 350 mm diameter with speed about 15-20 mm/s. 128 ultrasonic transducers, a humidity sensor, a temperature sensor and a pressure sensor are fixed on special sensor carriers and arranged scientifically to ensure that the stand-off and the transmission angle of the sensors are fixed and the whole pipeline wall can be covered. The CAN bus communication network inside the pig is represented by a block diagram. Multi-channel parallel inspection procedure and the sensor trigger sequence are introduced. Inspected signals are digitized, selected, compressed by data processors and stored in four hard disks for off-line analysis. The position data generated by the odometer is stored together with corresponding A-scan signal.

In lab, we use the pig to inspect samples which have same material and size with Chinese offshore pipelines. Defects as flaw, crack and corrosion with different size made by electricity-sparkle are prepared. The inspection signal analysis procedure is described in detail step by step. Downloaded and decompressed raw signals are firstly de-noised and compensated by wavelet theory. Then, defect characters such as size, location and type can be extracted through temporal and spatial alignment, association, and wavelet neural network fusion. They are stored in defect character database. Full three-dimensional profiles of defects are given. Finally, fuzzy ARTMAP is used to classify defects into five risk levels according to ASME B31G. The classifier is trained by pipeline defects information provided by Shengli Petroleum Bureau of China.

Experiments show that the preprocessing and character extraction strategies are effective. The defects recognizing error rate is less than 0.5%. The result is satisfying since the pig's inspection precision is 10mm. 98% defects can be assigned to correct levels.

We would like to acknowledge the State Key Laboratory of Ocean Engineering for the opportunity to have experiments, and with a special thanks to Shengli Petroleum Bureau offering correlative pipeline information and samples. This work was supported by China National High-Tech Research and Development Program #2001AA602021.

P1G-6
ULTRASONIC MONITORING OF PAPER COATING BULK MODULUS DURING LAYER FORMATION.

T. KARPPINEN*, I. LASSILA, and E. HAEGGSTROM, Dept. Physical Sciences, Univ. of Helsinki, Helsinki, Uusimaa, Finland.
Corresponding e-mail: edward.haeggstrom@helsinki.fi

We report on efforts to monitor, in real-time, the bulk modulus in the thickness-direction of pigmented industrial grade paper coatings during layer formation. The formation of this multiphase dispersion (latex-pigment-thickener-water) determines largely the coating structure that has a significant impact on the printability and the strength of paper.

The ultrasonic probing was conducted with a pitch-catch set-up. A broadband 20MHz ultrasonic longitudinal pulse propagated orthogonally towards the coating through an aluminum slab on top of which coating paste was applied and reflected from the aluminum-paste and coating-air interfaces. The longitudinal modulus of the coating was calculated from the time-of-flight of the received signal and the density of the coating that was obtained from a contemporaneous laser distance measurement of the layer thickness.

Four different, 200 um thick, coatings were investigated in a controlled environment. These were: 1) a typical coating consisting of calcium carbonate, latex, and carboxy-methyl cellulose (CMC); and simplified versions of it, i.e. 2) calcium carbonate and latex, 3) calcium carbonate and CMC, and 4) pure calcium carbonate. The maximum bulk modulus for these sample kinds was 6 GPa. This first and second critical concentration stages of the drying process were identified.

Keywords: ultrasound, bulk modulus, longitudinal waves, pigment, paper coating, nondestructive evaluation

We gratefully acknowledge Oy Keskuslaboratorio-Centrallaboratorium Ab for providing us with samples.

P1G-7
HIGH PRECISION TUNING FORK SENSOR FOR LIQUID PROPERTY MEASUREMENTS.

L. MATSIEV*, J. BENNETT, and O. KOLOSOV, Symyx Technologies, Santa Clara, CA.
Corresponding e-mail: lmatsiev@symyx.com

It was shown in [1] that if the piezoelectric resonator is immersed in a certain liquid the changes in the resonator electrical impedance produced by a liquid environment can be measured and used to independently calculate viscosity, density, dielectric constant and conductivity of the liquid. The measurement procedure described in [2], allows for precision of the data comparable to the precision of reference analytical equipment, and can exceed the requirements of ASTM D-445. The sensor based on this principle is currently being commercialized for lubrication monitoring and other applications.

The equivalent circuit of a piezoelectric resonator with electrodes capacitance and mechanical arms connected in parallel is a proven way of explaining the interaction of such resonator with the environment. The fringing electric field from the electrodes passes through surrounding liquid, which makes the capacitance sensitive to the dielectric constant of the liquid. The mechanical arm consists of the sequentially connected equivalent capacitance, resistance and inductance. In [1] it was shown that for a flexural resonator the additional impedance produced by surrounding liquid is connected sequentially to the mechanical arm and the value is given by a sum of two terms, one of which is proportional to the product of frequency and liquid density and the second one is proportional to the square root of the product of frequency, viscosity and density. Since these two impedance terms and the impedance of the electrodes capacitance are orthogonal functions of the frequency, viscosity, density and dielectric constant can be calculated independently from the total impedance of the resonator measured at three different frequencies. In practice, it can be advantageous to sweep the frequency within certain range and use the whole impedance curve. Liquid properties are extracted from the curve by fitting it using the least square method [3] with the liquid property values being free variables. In this case the average error in the free variable can be related to the error of impedance through an integral equation over the frequency range. The impedance partial derivatives under the integrals serve as natural weighting functions allowing for better averaging of the impedance errors acquired in the course of frequency sweep. This method of the errors calculation helps analyzing the contribution of various error sources: measurement system noise, non-linearity, frequency instability, etc.

Experimental studies were performed using a quartz tuning fork and the technique described above. The results of viscosity and density measurements for a set of Cannon™ standard oils are shown in Table 1. The method demonstrated excellent reproducibility (< 1%) in all samples the viscosities of which varied between 2 and 30 cP.

References:
1. L. Matsiev Application of Flexural Mechanical Resonators to High Throughput Liquid Characterization. Proc. of 2000 IEEE Ultrasonics Symposium. v.1, 427-434
2. L. Matsiev, J. Bennett, E. McFarland US Patent 6393895, 05/28/2002
3. O. Kolosov, L. Matsiev, M. Spitkovsky, V. Gammer US Patent Application 2004/0107055A1

Table 1. Peak-to-peak scatter in 10 sequential measurements at 50C°

CannonÔ Standard	Viscosity, cP	Scatter, %	Density, g/ccm	Scatter, %
S3	2.008	0.352	0.8403	0.144
S6	3.757	0.407	0.8559	0.196
S20	10.65	0.187	0.8458	0.064
N35	18.25	0.298	0.8492	0.041
S60	29.72	0.256	0.8566	0.098

P1G-8
AN ULTRASONIC FLOWMETER IN PRODUCTION BOREHOLES OF OILFIELDS.

H. ZHANG*[1], W. LIN[1], C. ZHANG[1], D. WANG[1], and T. LU[2], [1]Institute of Acoustics, Chinese Academy of Sciences, Beijing, China, [2]China Oilfield Services Limited, Tianjing, China.
Corresponding e-mail: zhanghl@mail.ioa.ac.cn

In petroleum exploitation, it is desirable to monitor the flow in cased production and injection boreholes for full borehole injection and production profiling. This is especially true to have a picture of the flow variation with borehole depths, from which the outflow from each layer of formations can be evaluated in determining oil and water output production profiles. Traditional techniques for the flow measurement, including ultrasonic flowmeters used for the flow measurement inside a pipe, are not suitable for the situation. In this paper, a prototype of an ultrasonic flowmeter used in a cased borehole is introduced. The possibility to develop an effective ultrasonic flowmeter, similar to popular well logging system, has been studied in the laboratory. The proposed tool is made up mainly a steel cylinder pipe with a diameter in 60mm and a length in 1 meter, two ultrasonic transducers, and an electric circuit part. During the measurement, the tool is put in a simulated borehole and kept on the borehole axis. The ultrasonic pulse transmitted by one transducer is obliquely impinged on the side wall of the borehole from which it is reflected several times and eventually is received by the other transducer. The received signal is transmitted through a cable to the ground for further processing. The time of the propagation of the ultrasonic pulse is dependent on the velocity of the flow inside the borehole. The relation between the time lag and the flow velocity in various conditions is studied and is used in data analysis to extract the flow velocity. Both of the two ultrasonic transducers act as transmitter and receiver alternatively and the date for both of the propagation directions is compared to improve the measurement precision. In our laboratory a system of 1 MHz is implemented and tested. The precision is better than 10mm/s. The effect of the tool on the flow measurement results is studied and a special treatment in reducing this effect is adopted in the signal processing. In order to use this measurement system in real borehole environments, all of the transducers and electric circuits are packed within a thin pipe. This system is tested and it works well at the temperature up to 120°.

P1G-9
LAMB WAVE PROPAGATION IN A PIEZOELECTRIC PLATE SUBJECTED TO CONDUCTIVE AND VISCOUS FLUID LOADINGS.

S.-H. KUO* and Y.-C. LEE, Nation Cheng Kung University, Tainan,Taiwan.
Corresponding e-mail: n1890118@ccmail.ncku.edu.tw

Leaky Lamb wave is an interesting problem in the area of NDE and ultrasonic sensor technology. When the lamb wave propagates on the plate surrounded by a fluid, not only the mass loading effect but also the viscosity of the fluid will

cause the mode-shifting in the dispersing curve of leaky lamb wave. Furthermore, when the plate is a piezoelectric material, the conductivity of the fluid also disturbs the dispersion curve and this is known as dielectric loading effect. All these three effects added up together make leaky lamb wave propagation a very complicated problem in physical acoustics. In the last two decades, many people have been investigated in this phenomenon and most of them have been using a theoretical analysis method called partial wave theory. However, there are very limited experiment results being reported in the literature and hence make it difficult to verify this theoretical model.

In this paper, the leaky Lamb wave problem will be re-examined with theoretical analysis as well as experimental measurements. First of all, the partial wave theory is used to analyze the corresponding velocity shifting and attenuation of leaky Lamb waves induced by the conductivity and viscosity. Secondly, a PVDF lens-less acoustic microscopy measurement system is established to measure the leaky Lamb waves using tone burst acoustic signals. It is basically an acoustic interfering measurement system and can obtain V(z) curves at a selected frequency. In comparison to the time-resolved or time-domain PVDF lens-less acoustic microscopy, this tone burst measurement system can greatly improve the accuracy in measurements of dispersion curves over a specific frequency range.

Based on the V(z) curve measurements, the velocity shifting in leaky Lamb wave can be accurately determined and then compared with theoretical data calculated from partial wave theory. Good agreements between experimental data and numerical results are observed, which verifies the analytic model of the leaky Lamb wave. For a x-cut $LiNbO_3$ sample plate, a significant dielectric loading effect along a particular orientation has been identified by the partial wave analysis and numerical calculation, and verified experimentally by the V(z) measurement. This could be very useful for further development of dielectric or conductivity sensors based on Lame wave propagation.

Key Words: Leaky Lamb Wave, Dispersion Curve, Fluid-Loading, Conductivity, Viscosity, V(z) curve measurement

P1G-10
MECHANICAL CHARACTERIZATION OF TA AND TAN DIFFUSION BARRIER LAYERS USING LASER ACOUSTICS.

D. M. PROFUNSER*[2,1], J. VOLLMANN[1], and J. DUAL[1], [1]ETH Zurich, Center of Mechanics, Zurich, Switzerland, [2]Hokkaido University, Graduate School of Engineering, Sapporo, Japan.
Corresponding e-mail: vollmann@imes.mavt.ethz.ch

The usage of copper as replacement of aluminium in integrated circuits leads to new technological challenges which are caused by its mechanical properties on the one hand side and by is tendency to migrate into dielectric and/or semiconducting layers on the other hand. To prevent such diffusion processes, very thin layers consisting of tantalum and tantalum nitride are deposited.

A non-contact, non-destructive, short-pulse-laser-acoustic method is used to determine the mechanical properties of the barrier layers and of the copper layer. High frequency mechanical pulses are excited and detected using laser pulses of 70 fs duration. For metals this leads to wavelengths of about 10 to 20 nm and the corresponding frequencies amount to 0.3 to 0.6 THz. Thin film measurements of buried diffusion layers are provided and compared with Scanning Electron Microscopy measurements (SEM) and Rutherford Backscattering Spectroscopy measurements (RBS). Limits of the presented method are discussed.

Keywords: Laser acoustic thin film metrology, Diffusion barrier measurement, Photo acoustic detection, in-depth profiling

P1G-11
EVALUATION OF LOW-LIGHT ABSORPTION MATERIAL BY PHOTOACOUSTIC MICROSCOPE.

A. MINAMIDE*[1], N. NAOE[1], and Y. TOKUNAGA[2], [1]Kanazawa Technical College, Kanazawa, Japan, [2]Kanazawa Institute of Technology, Ishikawa, Japan.
Corresponding e-mail: minamide@kanazawa-tc.ac.jp

A photoacoustic microscope can be used for the nondestructive evaluation and imaging of cracks and defects in opaque materials. Unfortunately, conventional photoacoustic microscopes are difficult to use for the evaluation of low absorption materials, such as transparent materials and metal thin films, since these materials do not form a strong heat source because they have high transparency or high reflectivity for visible light.

In this paper, a new evaluation method for low-light absorption materials by a photoacoustic microscope with low laser power is proposed. In the evaluation of the transparent epoxy adhesive, the laser light is absorbed by an opaque substrate under the adhesive, and a heat source is formed. A method to estimate the thermal diffusivity of the adhesive that used the thermal wave from the heat source is proposed.

In addition, attention is given to the remarkable behavior of the surface plasmon generated on the boundary plane between metal and air as one possibility for generating a strong heat source. If the surface plasmon forms on the boundary plane of metal and air, it could be converted into heat for electron-phonon interaction. Therefore, the surface plasmon may be used as a source of thermal wave generation, a method that is called Surface Plasmon Thermal Wave Microscopy (SPTWM). In this work, a basic system of SPTWM was constructed and used in experiments that generated a strong heat source from the surface plasmon in metal thin films. The Kretschmann configuration was used for the excitation of the surface plasmon, and a microphone was used to measure the photoacoustic signal generated from the heat source. The experimental results obtained using a thin film of silver showed that the SPTWM was about 20 times more effective than conventional methods for observing photoacoustic signals.

This work was partially supported by a Grant-in-Aid for Scientific Research from the Japanese Ministry of Education, Culture, Sports, Science, and Technology.

P1G-12

ULTRASONIC TESTING OF THE TIME EVOLUTION PROPERTIESOF ORANGES.

F. CAMARENA*, J. A. MARTÍNEZ-MORA, M. ARDID, J. RAMIS, and V. ESPINOSA, EPSG-UPV, Gandía, Valencia, Spain.
Corresponding e-mail: fracafe@fis.upv.es

Valencian region in Spain is one of the greater producers of citrus fruits of the world. In this context, the capability to store them in good conditions is very relevant. Classical measurements used in orange factories in order to obtain information related to the quality of the fruit are dehydration and oil-gland break stress, but those measurements are costly and destructive. The quality and evolution with the storage time of the fruits properties inside the refrigeration chambers can be tested by means of the use of ultrasounds. In this study we report the techniques, experimental set up, measurement procedures and results obtained to relate classical measurements (destructive) with the ultrasonic ones, in order to test the possibility to design a non-destructive ultrasonic device able to give information as turgidity and hydration of the oranges. Two different ultrasonic experimental set-ups have been built: a destructive one to test the properties of the orange skin and a non-destructive one to test the properties of the whole orange. A sample of 200 oranges Navelina has been measured during two months at normal conditions. Wave aluminium transformers have been used to focalize the ultrasonic wave into the orange skin as well as for the subsequent detection of the acoustic signal once crossed the peel. The design studies of the transformers, the correct way to do the measurements, the effect of the pressure, and the dispersion reached are described. Correlation between classical, ultrasonic and impact test measurements has been obtained. We show that the ultrasonic magnitudes change with the dehydration of the fruit and the control procedure test can be carried out with ultrasound techniques. Finally, an absolute calibration table allows us to estimate the hydration and turgidity of the oranges using non-destructive ultrasonic techniques.

This study was supported by Generalitat Valenciana (GV04B/368) and Productos Citrosol.

Session: P1H

ULTRASONIC MOTORS/LAB ON A CHIP

Chair: S. Bhave

Cornell University

P1H-1

A NEW SCHEME FOR EXPERIMENTAL-BASED MODELING OF A TRAVELING WAVE ULTRASONIC MOTOR.

H. MOJALLALI[1], R. AMINI*[2], R. IZADI-ZAMANABADI[2], A. A. JALALI[1], and J. POSHTAN[1], [1]Iran University of Science and Technology, Tehran, Iran, [2]Aalborg

University, Aalborg, Denmark.
Corresponding e-mail: mojallali@iust.ac.ir

In recent years, piezoelectric structures have been widely used in small scale actuators specifically motors and new implementations have exhibited high torque densities and similar efficiencies in comparison with conventional electro-magnetic motors. As in the case of the traditional electromagnetic motors, the experimental investigations, which highlight the behavior of the piezoelectric motor, are used to derive the model of the motor as the first stage of speed and position control.

In this paper, a new and high precision method for experimental modeling of rotary piezoelectric ultrasonic motors by equivalent circuit approach is presented in a thorough manner and examined on a Sashida USR60 piezoelectric motor as the case study.

As the first step, an improved equivalent circuit model for free stator modeling of traveling wave piezoelectric motor has been presented where the elements of the circuit are complex. The circuit elements are derived through a new iterative approach for determining the piezoelectrical material constants in the transverse mode. The usage of complex values which considers the information of the magnitude and phase of the admittance together, accounts the losses of the piezoelectric vibrator with more precision. The new approach uses only the measurements of five data points of admittance measurement. Comparison between the obtained circuit model and real data illustrates the accuracy and precision of the method.

In the next step, a model of the no load motor is derived through a new approach by considering the correspondent effect between the free stator, rotor-stator contact and rotor. A new method for compensating the effect of the rotor on changing the resonance and anti-resonance frequencies and the overall admittance of the un-loaded motor is presented which is based on altering the complex values of the circuit elements of free stator model. At this stage, a nonlinear parameter estimation method based on levenberg-marquardt algorithm is used to find the best complex values for the equivalent circuit. Also a current source is added to introduce the effect of the pressure of the rotor on the stator and the resultant speed change. The value of this current source is determined by using the theoretical relation between the tangential vibrting speed and the rotary speed of the unload motor. It is shown that the admittance of this new model agrees with the admittance measurements of the unloaded motor.

The paper continues by adding the model of the effect of the load. The loading torque interfere on the model as a torque-dependant current source.

Simulation of the speed under various torques shows that this models meets the results of the experiment.

Finally, the effect of the temperature on changing the resonance frequency of the motor is modeled. The result of this simulation is shown and verified with the experiments.

Comparison between the obtained circuit model and real data illustrates the accuracy of the new equivalent circuit modeling method as an experimental method for modeling of ultrasonic piezoelectric motors and specifically Sashida USR60 as a case study.

P1H-2
TRAPPING AND EXTRACTION OF SMALL PARTICLES BY VIBRATING SHARP EDGES.

J. HU*, J. YANG, J. XU, C. TAY, and Y. CAI, Nanyang Technological University, Singapore.
Corresponding e-mail: ejhhu@ntu.edu.sg

Manipulations of small particles have applications in biotechnology and many other areas. In this report, we present the methods of trapping and extracting small particles by ultrasonic actuators, which employ one or two tapered metal plates operating at the flexural vibration mode. Small particles can be trapped on the sharp edges of the metal plates. By the pumping effect in the gap between two tapered metal plates in vibration, lighter particles can be extracted from a mixture of particles. The capability of trapping and extracting small particles was measured for different particles, electric input and vibration velocity. The results show that the methods are effective in collecting particles in water and air, and extracting particles from a mixture of particles in air.

P1H-3
FLOW-BIREFRINGENCE SPECTROSCOPY OF MOLECULAR ORIENTATION WITH QUADRAPOLE PIEZO-ACTUATOR SYSTEM.

M. HOSODA*[1], K. HORII[2], H. OGAWA[1], K. TAKAGI[2], H. NOMURA[1], and K. SAKAI[2], [1]Tokyo Denki University, Saitama, Japan, [2]University of Tokyo, Tokyo, Japan.
Corresponding e-mail: mhosoda@frontier.dendai.ac.jp

We are interested in the physical properties of the soft condensed matters, including those liquids of polymers, molecules of potential liquid crystals, and self-assembling micelles. In particular, these liquids have different internal degrees of freedom, and the coupling among them plays an important role in the dynamics that characterizes the complex nature of the matter. Oscillatory flow birefringence has been the common technique to observe the coupling between the translational and rotational degrees of freedom of molecules. However, the experimental difficulty in inducing the quickly alternating shear flow of layered-mode has limited the frequency range of observation to 1kHz.

We recently developed a new spectroscopic technique of flow birefringence induced with a set of four piezo-actuators in a quadrapole position surrounding the sample chamber of 1mm square in size. One pair of them facing each other is driven in a countering motion, while the other pair is also countering but in the opposite phase. In this configuration, the liquid is activated into a periodical shear deformation of completely pure mode without volume change. The induced dynamic birefringence is observed by the optical ellipsometry technique. A laser beam passing through the sample under the shear deformation suffers from the modulation in its polarization, which is analyzed in the conventional way with the wavelength plates. The ellipsometry signal thus obtained gives information on the coupling between the molecular orientation and the shear deformation.

We chose the isotropic phase of 6CB as a typical sample that changes into nematic phase below the critical point, and examined the performance of the present system. The result showed that we could observe the coupling dynamics between the shear flow and the orientation over the frequency up to 100 kHz. The mechanical resonance of the actuators and their surroundings determines this limiting frequency at present. A piezo-actuator system with smaller dimension would improve the higher-frequency operation. The experimental system was applied to the aqueous solutions of CTAB in the phase of wormlike micelle and the spectroscopic study was made. We successfully observed the relaxation effect of the orientational order at around 100 Hz, which agrees well with the previous result obtained by the ultrasonic birefringence method.

P1H-4
ULTRASONIC MMICROMANIPULATION OF LIQUID DROPLETS FOR A LAB-ON-A-CHIP.

M. TAKEUCHI* and K. NAKANO, Faculty of Engineering, Tamagawa University, Machida, Tokyo, Japan.
Corresponding e-mail: takeuchi@eng.tamagawa.ac.jp

Noncontact and nondestructive techniques for manipulation of micron-sized particles in liquids, such as transportation, trapping, and separation, are of considerable interest for biotechnology and micromachining. Previously we have proposed ultrasonic micromanipulation (UMM) techniques based on the radiation forces of very-high-frequency (VHF) ultrasound. Recently, with the emergence of the so called Lab-on-a-Chip (LOC), various chemical processes such as transport, reaction, separation, purification and detection are now integrated on glass and plastic substrates of with dimensions of several centimeters. Further development of LOC requires new microfluidic technology to process liquid droplets of a very small size (0.5~60μl) without requiring complicated pumps and tubes. In this paper, we report two types of ultrasonic micromanipulators for use in liquid droplet processing. The first type of manipulator uses a single phase unidirectional interdigital transducer on a piezoelectric Lamb waveguide. The second type of manipulator uses wedge type transducers on an isotropic glass plate. Experiments using a frequency of about 6MHz confirm one-dimensional and two-dimensional transportation of water droplets. Experimental results are given for the relationship between the moving speed and the volume of the water droplet. Also presented is work in progress on the development of visual feedback techniques.

P1H-5
SMART SEPARATION DEVICES FOR PARTICLE CONCENTRATION IN WATER USING ULTRASONIC STANDING WAVE.

Y.-S. LEE* and J. KWON, Smart Measurement Group, Korea Research Institute of Standards and Science, Daejeon, South Korea.
Corresponding e-mail: highfield@naver.com

This paper presents the theory, design, manufacture, experiment and evaluation of smart devices for enhanced separability of tiny particles in water. The smart devices take advantage of the ultrasonic standing wave, which was generated by the operation of piezoceramic PZT patches installed on the separation devices. Since the devices were developed for the concentration of plant cells, the design and manufacture of them were targetted to the improvement of conventional separation processes.

The details of the device design including the electro-acoustical modelling for separation and PZT transducers are described at first. Two different ultarsonic wavelengths in half (1/2) for a nodal line in the middle and quarter (1/4) for a nodal line at the boundary of each separation channel respectively were applied in the design to compare their separation performance of the cells. Each separation channel has 370 micrometers width with the operating frequencies of 1 MHz and 2 MHz. Based on this design, the separation devices were analyzed with finite element approach to confirm the design parameters and to predict the acoustic pressure field in the separation channels of the devices.

Results of the experiment showed that the quarter wavelength in the separation channel gave a better performance in concentration of plant cells rather than the half wavelength one. Also the electric impedances of the PZT patches bonded on the separation devices were measured to compare with theoretical analysis.

P1H-6
FREE STATOR ANALYTICAL MODELING OF A NOVEL LOW VOLTAGE MULTILAYER PIEZOELECTRIC MOTOR.

H. MOJALLALI[1], R. AMINI*[2], R. IZADI-ZAMANABADI[2], A. A. JALALI[1], and J. POSHTAN[1], [1]Iran University of Science and Technology, Tehran, Iran, [2]Aalborg University, Aalborg, Denmark.
Corresponding e-mail: mojallali@iust.ac.ir

In recent years, many research activities in the field of ultrasonic motors and piezoelectric actuators have been done because of their attractive features. Most of developed ultrasonic motors operate at a high voltage which is a demerit in the application areas of ultrasonic motors.

In this paper, at first we introduce a novel and small rotary piezoelectric ultrasonic motor based on the well known traveling wave principle, the dimensions of which are 15.0 mm in diameter and 5.0 mm in thickness. The usage of multilayer ceramic in the stator structure of the piezoelectric motor has led to low drive voltage, quick response time, large generative force and high electromechanical coupling.

Then, a novel analytical model, which deals with the electromechanical behavior of multilayer structure of free stator, is derived. In this model, a new form for the constitutive equations of multilayered structure of stator is presented where the electromechanical coupling is as an additional stiffness matrix. This matrix shows properties of the piezoelectric structure and is not dependent on mechanical boundary conditions. But some of the parameters in this analytical model such as stiffness, modal mass and damping coefficients should be determined through

experiments on the multilayer structure. This identification performs by the aid of an equivalent circuit model of the free stator which is recently introduced in our previous published works. This hybrid approach for determining the free stator unknown parameters results a high precision model from the combination of the analytical and experimental modeling approaches.

Finally, the validity and accuracy of the free stator model is verified by simulation and comparison to the real data obtained from the multilayer rotary piezoelectric motor.

P1H-7
DEVELOPMENT OF GYRO-MOMENT MOTOR.

Y. TOMIKAWA*, T. TAKANO, and M. AOYAGI, Yamagata University, Yamagata Japan.
Corresponding e-mail: tomikawa@yz.yamagata-u.ac.jp

This paper deals with developmental research of the gyro-moment motor. This motor is a construction of a pizoelectric vibratory motor, which was named a gyro-moment motor by one of authors(Y.Tomikawa). The gyro-moment motor was composed of a stator vibrator of a thin rectangular plate and a T-type rotor set on the center point of the plate stator vibrator. The stator vibrator was electrically driven by the piezo-ceramics bonded on it. As mentioned above, this vibratory motor was of a new concept which nobody might think of before. In our previous papers(1), (2), the fundamental principle and some measured characteristics of a such motor were reported to show that the rotor of T-type was merely made to rotate by such a motor construction and what sizes of rotors should be chosen to rotate with a high speed. However, the gyro-moment motor of a trial production was a littel big; that is, sizes of the stator vibrator were 160mm(length)x30mm(width)x0.5mm(thickness), which might not be suitable for a practical use. Therefore, after previous works, we have further developed the gyro-moment motor in order to make clear its operation and to improve weak points of its characterisitics through experiments. That is, in this paper, we would like to present the experimental results.

Main points of the experimental works of this timeare followings: 1) A smaller sized motor construction than the previous motor was dealt with , 2) A self-oscilated-type gyro-moment motor was tried, because the previous motors needed an external punching-force in its starting of rotation.

The experimental results proved that this problem could be solved by somewhat modification of T-type rotor. 3) As another motor construction, we also devised the gyro-moment motor which can be called a stator-vertically-set type. It was found clear that this motor might be applied as a kind of toy. We think this will be useful for physical excercise of senior persons, too.

References :

(1) K. Kanauchi and Y.Tomikawa; “Gyro-Moment Motor”, ACTUATOR 2000 19-21 June 2000, Bremen, Germany No.B2.2 pp.246-249.

(2) Y.Tomikawa and Y.Matsuzaka; “Characterisitcs of Gyro-moment motor”, ACTUATOR 2002, 10-12 June 2002, Bremen, Germany, No.P15 pp.450-453.

Session: P1I
PIEZOELECTRICAL TRANSFORMERS/MOTORS
Chair: M. Kurosawa
Tokyo Institute of Technology

P1I-1
EFFECTS OF ELECTRIC LOAD ON VIBRATION DISTRIBUTION OF A PIEZOELECTRIC TRANSFORMER OPERATING AT THE THICKNESS SHEAR MODE.

J. DU*, J. HU, and K. J. TSENG, Nanyang Technological University, Shcool of EEE, Singapore.

Corresponding e-mail: djl@pmail.ntu.edu.sg

In this study, a theoretical model for analyzing the effect of electric load on the vibration distribution of a piezoelectric transformer operating at the thickness shear mode was developed. The relationship between the vibration distribution and load resistance of the transformer was analyzed by this model. The vibration of output part decreases along the direction of vibration transmission. The larger the difference between the load resistance and the matching load is, the more the vibration of output part decreases. The theoretical conclusions were justified by experiment measurement and FEM analyses. The model provides guidelines of optimizing the transformer and explains some important phenomena in piezoelectric transformers, such as a higher temperature at the input part of almost all piezoelectric transformers.

The authors would like to acknowledge the financial support by Academic Research Fund RG4/102 from the Ministry of Education, Singapore.

P1I-2
MODELING AND CHARACTERISTICS COMPARISON OF TWO DIFFERENT PIEZOELECTRIC TRANSFORMERS.

J. M. FERNANDEZ* and Y. PERRIARD, Ecole Polytechnique Fédérale de Lausanne, Lausanne, Switzerland.
Corresponding e-mail: jose.fernandezlopez@epfl.ch

Recent progress on electrical power applications, particularly in the domain of the miniaturization of both electrical and electromechanical devices, has enabled envisaging the development of very compact systems (microcomputers, microsystems, cellular telephones, etc.). The supply, storage and transformation of electrical power in these systems must respect this trend. However, the miniaturization of classical electromagnetic transformers raises certain problems such as manufacture both the coils and the magnetic core, increase in magnetic leak and especially electromagnetic pollution of the environment. One interesting solution consists of using a piezoelectric transformer. This will insure an electrical-mechanical and mechanical-electrical double conversion of energy with a transformation ratio that allows adapting the output voltage being used. This

kind of transformer, which is more compact, lends itself better to miniaturization, in addition to displaying the attractive characteristics of immunity to the magnetic field. In this paper a Rosen-type structure of piezoelectric transformer has been initially studied. The first approach consists of performing an analytical model. This approach is inspired by the technique used in electroacoustics and allows to build an electric equivalent circuit of the vibrating structure. The second approach deals with numerical finite element method using ANSYS software. The 3D structure has been simulated and the validity of the hypotheses done in the equivalent circuit method has been proved. In order to validate the models, experiments on two different multi-layer piezoelectric transformers, one from Noliac and the other from Transoner have been performed. Measures of the global transformation ratio versus frequency under different values of the load resistance have been obtained. As an example, for a load resistance of 200kΩ, the voltage transfer ratio is about 100 at the resonance frequency (132kHz) for the Noliac type and about 80 (at 66kHz) for the Transoner type. With regard to the output power, it varies from 1.5W in the first case to 5W for the second one. Then, a piezoelectric transformer using radial extensional vibration mode has been studied and characterized. An analytical model has been investigated using linear piezoelectric equations combined with the theory of elasticity, and an equivalent circuit model has been deduced. A three-dimensional finite element model has been then simulated using ANSYS to find out the resonance frequency but also to determine the transformation ratio as a function of the frequency for several values of the load resistance. The models are then validated through experimental results using a Transoner radial type piezoelectric transformer.

Finally, voltage gain, output power and efficiency of both piezoelectric transformer types are compared taking into account their characteristics. This will allow a case study depending on the application, especially in the pre-study process, where one of these two different piezoelectric transformers is to be chosen.

P1I-3
A POWER ULTRASONIC ACTUATOR BASED ON A DISPLACEMENT AMPLIFIER VIBRATING IN FLEXURAL MODE.

A. IULA*[1], L. PARENTI[1], N. LAMBERTI[2], and M. PAPPALARDO[1], [1]University Roma Tre, Roma, Italy, [2]University of Salerno, Salerno, Italy.
Corresponding e-mail: iula@uniroma3.it

Commonly used high displacement ultrasonic actuators are composed of a power vibration generator (the Langevin transducer) and of a displacement amplifier. This structure is employed in a large variety of industrial applications, as well as in the biomedical field as an ultrasonic bystoury.

Among possible displacement amplifiers, sectional ultrasonic concentrators, made from rods of variable and constant cross section, are those that have been mainly exploited in applications. Basically, sectional concentrators are designed to resonate in length-extensional mode at the same frequency of the Langevin transducer and the displacement amplification depends on the ratio between the back and the front sections.

In this work a new type of ultrasonic actuator has been proposed. It is composed of a symmetrical Langevin transducer working in a length-extensional mode joined to a displacement amplifier that is designed to vibrate in flexural mode.

The displacement amplifier is composed of: a cylinder shaped base with the same radius of the Langevin transducer, of four arms, and of a thin disk acting as a displacement collector.

This kind of structure is able to transform the almost flat displacement provided by the Langevin transducer into a flexural deformation of the arms. This deformation is transmitted to the collector. In this way, an axial symmetric flexural mode can be excited in the collector. In this case, the maximum value of the axial displacement occurs at the centre of the collector.

In analogy to classical actuators that use sectional concentrators, the Langevin transducer and the flexural amplifier have been separately designed to work at the same frequency. Design and analysis of the actuator have been performed by using a FEM commercial package (ANSYS).

Performances of the proposed actuator have been compared with that of a classical stepped horn actuator designed to work at the same frequency (about 50 kHz) and with the front section equal to the total section of the areas of the arms.

Simulated results have shown that the proposed concentrator exhibits a displacement amplification about 50 % higher than the stepped horn. Furthermore, by joining the two concentrators to the same Langevin transducer, and driving the two actuators with the same current amplitude, the proposed actuator is able to absorb a higher electrical power than the classical one.

Due to superposition of these two effects, the proposed actuator has shown a maximum displacement that is about twice the maximum displacement of the classical actuator.

In order to validate numerical results, two prototypes have been manufactured by following FE design. Measurements of the maximum displacement carried out on the two actuators are in a good agreement with simulation results, proving that the proposed actuator is more suitable than the classical stepped horn in application where high displacements are required. As an example, due to the flexural deformation of the front surface, the proposed actuator could be exploited as a mirror with variable bend radius to deflect laser beams in optical applications.

P1I-4
AN ULTRASONICALLY LEVITATED NON-CONTACT SLIDING TABLE WITH THE TRAVELING VIBRATIONS ON FINE-CERAMIC BEAMS.

D. KOYAMA*, T. IDE, J. FREND, K. NAKAMURA, and S. UEHA, Precision and Intelligence Laboratory, Tokyo Institute of Technology, Yokohama, Japan.
Corresponding e-mail: dkoyama@sonic.pi.titech.ac.jp

This report presents a new design and its performance test for a non-contact sliding table by ultrasonic levitation. A slider is levitated by an acoustic radiation

force emitted from two vibrating guide rails, and a flexural traveling wave propagated along the rail guides allows a non-contact transportation of the slider. The reduction of the abrasion and dust generation, high cost performance and simple structure are expected. The profile of the sliding table was designed using the finite element method (FEM) for high levitation and transportation efficiency. The twist mode and the in-phase flexural mode were selected and tested.

The prototype sliding table made of alumina ceramics for obtaining higher machining accuracy and rigidity. A structure consists of a pair of 152-mm-long beams with a triangle cross-section, two bolt-clamped Langevin transducers with the diameter of 11 mm and cross-shaped vibration direction converters to permit low height of 11 mm. A slider with the length of 40 mm was designed to fit the two rail guides.

The vibration modes of the guide rail were investigated with a laser Doppler vibrometer. The experimental results showed that the modes designed by FEM were successfully excited near the expected. The flexural mode standing wave was observed along the guide rail at the resonance frequencies of 89.4 kHz, and the levitation of the slider could be confirmed even if the levitation distance is less than 10 μm. The levitation distance of the slider was measured with increasing the slider's weight, and the levitation force, the levitation rigidity and the displacement amplitude of the levitating slider in the vertical direction were measured to be 4.8 kN/m2, 2.5 kN/μm/m2 and under ±1 μm, respectively, in the case of the levitation distance of 2.2 μm.

The non-contact transporting of the slider was achieved with the phased drive difference of two transducers. By controlling the phase difference, the slider transportation direction could be switched. The maximum thrust and the transportation speed were 1.3 mN and 34.6 mm/s, respectively, in the case of the slider's weight of 107 g.

P1I-5

MINI-DRIVER FOR ULTRASONIC MOTOR BASED ON CPLD.

L.. HUAFENG* and Z. CHUNSHENG, Nanjing Univ. of Aeronautics and Astronautics, Nanjing, China.
Corresponding e-mail: lihuaf@sina.com

As a novel motor, UltraSonic Motors (USM) exhibit advantages over conventional electromagnetic motors. For example, USM can produce a relative high torque at a low speed with a high efficiency, and the torque produced per unit weight is high. These features are useful for utilizing as gearless actuators or direct servo drives. The motors have recently been applied as direct drive actuators for articulated robots, actuators for control valves and a positioning table of machine tools because they require quick response and precise position control of actuators. Some experts even predict that USMs will replace micro electro-magnetic motors in certain special areas in the future.

But in order to drive the USM, a special driver is required, which has been an obstacle for replacement of traditional motors by USMs. If the driver has a big

volume, the promotion of USM would be more difficult. Therefore, on the premise of meeting the basic requirements, the volume of the driver must be reduced to the greatest extent, so as to exploit the particular advantages of USMs in more areas.

In order to fulfill this command, a new CPLD based mini-driver for ultrasonic motor is presented in this work. Since the square-wave outputted by transformer is filter to sine-wave to drive the USM, there must be a most suitable duty cycle. So, the relation between the output voltage and energy efficiency of ultrasonic motor driver and the duty cycle of driving pulse is analyzed in details firstly. The rationality of 37% duty cycle is proved based on the analysis. Then a mini-driver based on CPLD for ultrasonic motor is designed and manufactured. The driver is applied to a TRUM-45 type traveling-wave ultrasonic motor, which is developed by our Research Center. Experimental results show that this scheme is valid and feasible. Compared with original driver composed by separate logical circuit, this mini-driver can be reduced by 66% in volume and 40% in element numbers, which fulfils the demand of practicability for general engineering.

This work is sponsored by Key Project of National Natural Science Foundation of China (Project No.50235010)

P1I-6
DEVELOPMENT OF A MINIATURE ULTRASONIC MOTOR USING A HELICAL COIL AS A STATOR.

T. MORIYA*[1], Y. FURUKAWA[2], Y. AKANO[1], and A. NAKAJIMA[2], [1]Tokyo Metropolitan University, Hachioji-shi, Tokyo, Japan, [2]Tokyo University of Agriculture & Technology, Koganei-shi, Tokyo, Japan.
Corresponding e-mail: moriya@eei.metro-u.ac.jp

Preliminary results for the development of a miniature ultrasonic motor using a helical coil as a stator are described. The coil was constructed using an acoustic waveguide such as stainless steel wire. A rotor can be placed in or outside of the coil. An ultrasonic transducer was attached at the end of the waveguide.

The basic principle of the motor is that of the traveling wave type ultrasonic motor. That is, when the Lamb waves were transmitted along the coil, the waves cause the elliptical motion on the surface of the waveguide, which is transmitted to the rotor.

The group and phase velocities of the Lamb wave propagating along the waveguide were analyzed using PZFLEX, and compared with the experiments. The waveguides with a rectangular cross section ranging from 0.1 mm x 0.1 mm to 1 mm x 1 mm were used for the analysis. The experiments were conducted using stainless steel wires that have a circular cross section. Reasonable agreements between the simulations and the experiments were obtained.

The principle of the motor was confirmed experimentally. The wire diameter, the number of turns, the height and radius of the coil were 0.3 mm, 7, 3 mm, 1.1 mm, respectively. A stainless steel wire with 0.5 mm in diameter was used as a rotor. The motor was operated at 50 kHz. The rotation frequency ranged approximately from 500 rpm to 1000 rpm according to the applied ultrasonic power. The torque was estimated to be less than 100 nN-m. The motor worked at 200 kHz, and 400 kHz.

This motor has several features as follows. (1) Since the rotor can be placed outside or inside of the stator, a motor with a hollow axis can be constructed. (2) Since the motor works under water condition, it can be used for medical blood vessel devices such as a motor driving a mirror of IVUS. (3)Since no preload spring is required, an extremely miniature motor can be constructed. (4)Any axial-symmetrical object can be rotated. (5)Linear motion can be realized.

This work was supported in part by Grant in Aid for Scientific Research from the Ministry of Education, Science and Culture(Grant No.1526013)

Session: P1J

SIMULATION OF SAW DEVICES

Chair: L. Reindl

University of Freiburg

P1J-1

REFINEMENT OF THE COM PARAMETER EVALUATION.

B. SVESHNIKOV* and V. CHEREDNICK, Nizhny Novgorod State University, Russia.

Corresponding e-mail: bvs@ieee.org

This abstract does not appear in the online abstracts at the author's request.
It will appear in the print version.

P1J-2

THE K-MODEL - GREEN'S FUNCTION BASED ANALYSIS OF SURFACE ACOUSTIC WAVE DEVICES.

J. H. KUYPERS*, D. A. EISELE, and L. M. REINDL, University of Freiburg, Freiburg, Germany.
Corresponding e-mail: jan@mems.mech.tohoku.ac.jp

We have developed a new model for the precise simulation of surface acoustic wave devices (SAW), as applied to filters, sensors [1][2], and ID tags [1]. The model relates the potential adherent to a surface wave propagating on a piezoelectric substrate and applied transducer potentials. Each electrode is hereby represented by a 3-port element, comprising two acoustic terminals and one electrical terminal, just as found for the P-matrix [3]. The underlying charge model is based on the Green's Function [4] and is computed making use of the Method of Moments (MoM) as shown by [5]. At this point the model neglects the coupling to bulk waves, which can be included by either modelling their losses at the electrode edges or by including their excitation by performing a post-processing step, as discussed by Ruppel et al. [3]. The inclusion of all important secondary effects into the model, as electrical loading, mass loading [6], electrode resistance, damping, dispersion and diffraction enables the accurate simulation and design of e.g. SAW based sensor and identification systems. In order to evaluate the ability of our model, reflective delay line sensors and transversal transducer structures were fabricated on 128° LiNbO3, designed for an operation in the ISM frequency band from 2400 MHz to 2483.5 MHz. The very good agreement of measurements and simulation thus recommend our model for the development of SAW devices on high coupling substrates featuring low bulk wave conversion and operating up to several gigahertz. This model was applied to the development of a reflection compensated single electrode transducer, which in turn lead to the fabrication of low loss SAW reflective delay line sensors. The desired transducer input impedance of 50 Ω was achieved by 3.3 Ω. The measured values of the equivalent circuit elements at the centre frequency of 2441.75 MHz in comparison to the simulated ones in brackets yielded, 53.3 Ω (49.2 Ω), 0.76 pF (0.76 pF) and 5.57 nH (5.62 nH) for the input impedance, susceptance (static capacitance and acoustic susceptance), and computed

parallel matching inductance. The deviation between simulated and measured centre frequency was found to be 0.11 %.

References

[1] L. Reindl et al., “SAW Device as Wireless Passive Sensors”, Proc. IEEE Ultrason. Symp. 1996, pp. 363-367

[2] A. Pohl, “A Review of Wireless SAW Sensors”, IEEE Trans. Ultrason., Ferroelect., Freq. Contr., vol. 47, no. 2, 2000, pp. 317-332

[3] C. W. Ruppel et al., “Review of Models for Low-Loss Filter Design and Applications”, Proc. IEEE Ultrason. Symp. 1994, pp. 313-324

[4] R. F. Milsom, “Analysis of Generation and Detection of Surface and Bulk Acoustic Waves by Interdigital Transducers”, IEEE Trans. Sonics Ultrason., vol. SU-24, no. 3, 1977, pp. 147-166

[5] A. R. Baghai-Wadji et al., “Analysis and Measurement of Transducer End Radiation in SAW Filters on Strongly Coupling Substrates”, IEEE Trans. Microwave Theory Tech., vol. 37, no. 1, 1989, pp. 150-158

[6] K. Ibata et al., “Polynomial Expressions for SAW Reflection by Aluminium Gratings on 128°YX-LiNbO3”, Proc. IEEE Ultrason. Symp. 1998, pp. 193-197

P1J-3

CLOSED-FORM COM MODELING OF REFLECTIVE SAW TRANSDUCERS WITH ARBITRARY POLARITY SEQUENCE AND APODIZATION.

A. S. RUKHLENKO*, Institute of Microtechnology, Neuchatel, Switzerland.
Corresponding e-mail: rukhlenko@bluewin.ch

A new closed-form Coupling-of-Modes (COM) model of reflective polarity-weighted and/or apodized surface acoustic wave (SAW) transducers has been developed. The results are presented in the form of the complete mixed scattering matrix comprising the acoustoelectric and electroacoustic conversion functions and transducer admittance (radiation conductance and susceptance). The solution is found in terms of the normal modes in the infinite periodic grating which are two counter-propagating waves. Acoustic fields are described by the coupled fundamental and the first backward spatial harmonics, with the additional terms accounting for the electrical excitation of the interdigital array. The normal modes of the infinite array are superimposed to satisfy the boundary conditions at the SAW transducer ends (acoustic ports). Two important model parameters are to be determined a priori: 1) wave propagation constant in the grating; 2) the coupling factor between the fundamental and the first backward spatial harmonics. The former is found from the dispersion equation for the short-circuit infinite grating. The latter is related to the reflection factor of the semi-infinite periodic grating. Given a strip reflection coefficient, the coupling factor is deduced in the closed-form by applying the Morgan′s reflective array model equation to the extreme case of the periodic array with the infinite number of the strips. The classical COM equations follow from the theory in the particular case of a solid-finger SAW transducer with a regular sign alternation. The equations are general

comprising reflective apodized SAW transducers. They allow to accurately predict SAW reflections at the transducers ends even for split-finger apodized SAW transducers. In the case of reflectionless SAW transducers, the theory is reduced to the regular quasi-static approximation equations. The analysis results for solid-finger withdrawal-weighted SAW transducers are presented which agree well with the published results (reflective array model) and experimental data.

P1J-4
EMPIRICAL EQUATION FOR THE TEMPERATURE COEFFICIENT OF FREQUENCY DERIVED FOR LEAKY SAW DEVICES.

S. SABAH*[1], E. CHILLA[1], and D.- P. CHEN[2], [1]VI Telefilter, Teltow, Brandenburg, Germany, [2]Vectron International, Hudson, NH.
Corresponding e-mail: sabah@telefilter.com

Temperature dependence has been proved to be a significant design parameter for the development of SAW devices. It is well known that many critical parameters are temperature dependent, e.g. velocity, reflection coefficient, transduction coefficient, electro-static capacitance and resistance.

Thus the performance of SAW filters, in particularly centre frequency, insertion loss, group delay, input and output impedance, varies with temperature. However, the temperature behavior is even more complicated since it is not only dependent on material constants but also on the filter structure itself, e.g. type of configuration, film thickness to wavelength ratio, mark to period ratio, as well as the wave (Rayleigh wave, leaky SAW, STW) and mode (transverse or longitudinal modes) utilized.

This paper reports on the determination of the temperature coefficient of frequency (TCF). We present experimental data of leaky materials like LiTaO3 and LiNbO3 and derive an empirical equation for TCF. The agreement between the measured and the calculated values is within 2 ppm/K. We found that the TCF is mainly dependent on the film thickness to wavelength ratio and compared the measured data with numerical calculations.

P1J-5
TRANSMISSION AND REFLECTION COEFFICIENTS OF SAW IN BASIC CELLS OF SPUDT.

R. TAZIEV*, Institute of Semiconductor Physics of Russian Academy of Sciences, Novosibirsk, Novosibirsk, Russia.
Corresponding e-mail: taziev@thermo.isp.nsc.ru

In the previous paper [1] we suggested a scanning window technique in SPUDT filter optimization, where we used 15 different basic cells for construction of SPUDT filter structure. The purpose of the presented paper is to simulate accurately transmission and reflection coefficients of SAW, taking into account bulk wave losses, in the basic cells of such irregular, nonperiodic structure of

SPUDT by rigorous combined finite element and boundary element (FEM/BEM) method. For every basic cell, which consists of 3 or 4 electrodes with different width and finite height, electrically grounded or open-circuited, we simulate transmission and reflection coefficients of SAW and bulk wave losses. That allows us to evaluate P-matrix parameters of every cell properly, and compute the characteristics of SPUDT on YZ $LiNbO_3$. The results obtained were compared with exact analysis of the same SPUDT structure by rigorous FEM/BEM software, similar to [2].

[1] E.Bausk, R.Taziev and L.C.An. Scanning window technique in SPUDT optimization, 2004 IEEE Ultrasonics Symposium Proceedings, pp.145-149.

[2] P. Ventura, J.M.Hode and B. Lopes. Rigorous analysis of finite SAW devices with arbitrary electrode geometries, 1995 IEEE Ultrasonics Symposium Poceedings,pp.257-262.

P1J-6

ANALYSIS OF SAW DEVICES USING FEM/BEM METHOD AND PARALLEL COMPUTING.

X. PEROIS*, T. PASTUREAUD, P.-A. GIRARD, and R. LARDAT, Temex, Sophia Antipolis, Fance.
Corresponding e-mail: xavier.perois@temex.fr

The main work for the SAW designer is to improve the filter performances, keeping simulation and prototyping time as short as possible. In order to avoid costly and time-consuming technological iterations, a very accurate simulation tool is required.

Finite transducer FEM/BEM models give very accurate predictions for synchronous or asynchronous structures like resonators or DMS on various piezoelectric materials. A wide range of phenomena is taken into account through the Green function and the Finite Elements formulation: mechanical effects like Leaky SAW conversion into bulk waves or mechanical losses in materials (electrodes or piezoelectric), or electrical effects like resistive losses in the electrodes or ground plane influence through a special treatment of the Green function.

The drawback of this approach is a very time and memory consuming model that can be incompatible with short design time and cost effective computing system. In order to reduce computation time and extend memory capacity, the simulation software was modified for parallel computing using Message Passing Interface standard and run on a multiprocessors PC's cluster. Two different ways were used to optimize the parallel software performances. The first one shares the large FEM/BEM matrix over the memory of the computation nodes, allowing to solve large problems, but the network communications limits the computation time performance. The second one distributes every frequency computation, allowing a quasi-linear acceleration of the computation time, but the FEM/BEM matrix must be small enough for the memory of one computation node.

[1] P. Ventura, J.M. Hodé, M. Solal, J. desbois J.Ribbe, "Numerical methods for SAW propagation characterization",1998 IEEE Ultrasonics Symp. proc., pp 175-186

[2] N. Finger, G. Kovacs, J Schöberl, U. Langer, „Accurate FEM/BEM simulation of SAW filters“, 2004 . IEEE Ultrasonics Symp. proc

The authors are grateful to A. Mazari and N. Béreux-Vialle (CMAP, Palaiseau), for the software development and help-ful support on the cluster configuration

P1J-7
FINITE-DIFFERENCE TIME-DOMAIN SIMULATION OF DISPERSIVE LAYERED SAW FILTERS INCLUDING ELECTRODE MASSLOADING.

K. Y. WONG* and W. Y. TAM, The Hong Kong Polytechnic University, Hong Kong.
Corresponding e-mail: kingyuen.wong@polyu.edu.hk

A number of analytical and numerical techniques have been developed to simulate the frequency response of a SAW filter. However, due to the future wireless communication applications, the present modelling schemes are difficult to accurately predict the characteristics of SAW filters with complex interdigital transducer (IDT) and fabricated on multilayered substrates. Furthermore, none of them except the direct finite element method (FEM) can accurately predict the performance of SAW filters for high frequency applications when second order effects become significant.

Our goal in this paper is to extend the finite-difference time-domain (FDTD) technique to analyze the frequency response of dispersive layered surface acoustic wave (SAW) filters. The massloading effects of the IDT are also considered. In this method, the partial derivatives of quasi-static Maxwell′s equations and equation of motion are discretized to centered finite-differences. Furthermore, the perfectly matched layer (PML) boundary condition is applied to reduce the spurious reflections.

The main advantages of this technique are that the characteristics of the wave propagating in inhomogeneous and non-linear media can be calculated. Furthermore, with FDTD, specifying a new structure to be modelled is reduced to a problem of mesh generation rather than the potentially complex reformulation of an integral equation. Moreover, the update algorithm in the FDTD method is efficient because it is based on the past field values at nearest neighbour components, and unlike other numerical techniques such as FEM, requires no matrix inversion. This technique is particularly suitable for the broadband analysis because the frequency response of the wide frequency band can be computed from a wideband Gaussian impulse excitation. In addition, FDTD method generating time-marched arrays of field quantities are suitable for using the computer visualization to illustrate the field dynamics[1,2].

In this paper, the proposed model is applied to analyze the frequency response of a ZnO/Diamond/Si layered SAW filter including the massloading effects of IDT. The wave-front images of the acoustic waves are simulated and the phase velocities of the Rayleigh and 1st Sezawa waves are extracted from the time domain responses by using the Prony′s method. The simulated results are in good agreement with the existing experimental data, indicating that the FDTD method is an appropriate approach for modeling layered SAW filters.

Index Terms - FDTD methods, surface acoustic wave filters and frequency response.

[1]A. Taflove, and S.C. Hagness, *Computational electrodynamics: the finite-difference time-domain method,*2nd Edition, Artech House, 2000.

[2]P.M. Smith, and Wei Ren,′Finite-difference time domain techniques for SAW device analysis,′ in *IEEE Ultrasonics Symp.,* vol. 1, Oct. 2002, pp. 325-328.

The work described in this paper was partially supported by a grant from the Research Grants Council of the Hong Kong Administrative Region, China (Project No. PolyU 5135/02E).

P1J-8
FAST AND PRECISE MULTI-PURPOSE P-MATRIX SIMULATION TOOL: BUILT-IN FEATURES AND APPLICATION EXAMPLES.

R. LARDAT*, T. PASTUREAUD, and W. STEICHEN, TEMEX.
Corresponding e-mail: raphael.lardat@temex.fr

The need for time to market products has increased due to the reduction of the market's growth for SAW components in RF telecommunication. To reach the challenging goal of designing SAW filters quickly with good characteristics, one needs a fast and precise filter response simulation tool. This tool can then be used inside an optimisation loop to achieve customer's requirements in a short period of time.

The aim of the presented tool is to simulate the following phenomena: fast and precise capacitive computation, ohmic losses, P-Matrix dispersive parameters, SAW directivity, multi-modes simulation used for transverse modes and continuum.

It is based on P-Matrix model [1] coupled with a fast electrostatic solver that computes the capacitive admittance taking into account for the real geometry and polarities of the filter. This 2D BEM solver may use semi-infinite substrate or can take into account for mass planes either on back surface or above active area representing the package metallic lid. This 2D BEM solver uses spatial electrostatic Green function and Chebishev polynomial for a reduced number of unknowns (typically only 3 dof per electrode). For very large SAW devices, one can accelerate the resolution by using "windowing" technique over a limited number of electrodes.

Ohmic losses are modelled by adding a serial resistance at each electrode connecting point. This leads to the construction of a linear problem whose size is the number of electrodes. Exact resolution of such problem is time consuming and an approached solution can be found using the knowledge of the capacitive mutual admittance.

The P-Matrix parameters take into account for directivity in addition to usual phenomena (SAW velocity under the grating, reflection coefficient, propagation losses, coupling factor) and they may be frequency dependant for simulating dispersive phenomena [2] which is well adapted for SAW devices using Pseudo SAW.

The P-Matrix model may have an unlimited number of both electrical and acoustical ports. This enables, for instance, the simulation of transverse modes and continuum as an approach for diffraction [3].

In addition to filter admittance matrix, this tool may produce the charge distribution due to capacitive coupling and the acoustic power representation along the simulated device. The latter option enables an easy understanding of longitudinal acoustical modes present, for instance, in Double Modes SAW devices.

Examples of various applications will be given: filters on Tantalate 42 and Niobate 41 for dispersive PSAW, high Q resonators on Quartz ST with slanted propagation vs. X axis showing directivity and guided modes.

[1] J.M. Hode et al, “SPUDT- Based filters: Design Principles and Optimization”, 1995 IEEE Ultra. Symp.

[2] T. Pastureaud, “Evaluation of the P-Matrix parameters frequency variation using periodic FEM/BEM analysis”, 2004 IEEE Ultra. Symp.

[3] M. Solal et al, “A P-Matrix based Model for SAW Grating Waveguides taking into account Modes Conversion at the Reflexion”, 2003 IEEE Ultra. Symp.

P1J-9
COM MODEL OF THE IMPEDANCE-LOADED SAW SENSOR.

Q. FU*, W.-J. FISCHER, and H. STAB, Dresden University of Technology, Dresden, Sachsen, Germany.
Corresponding e-mail: fu@ihm.et.tu-dresden.de

The wirelessly requestable RF passive impedance-loaded surface acoustic wave (SAW) sensor consists of one transmitting/receiving inter-digital transducer (IDT), one or more programmable reflectors and a classical sensor connected to one of the reflectors. In the last decade, many researchers have made great efforts researching such devices and succeeded in simulating impedance-loaded SAW sensors based on scattering parameters of a realized SAW delay line measured by a vector network analyzer. In this work, the coupling-of-modes (COM) model of SAW IDT is used to form a model of the RF impedance-loaded SAW sensor, which does not require any measured data. This model is suitable for designing and optimizing impedance-loaded SAW sensors, because it consumes less computing time and it is much easier to obtain the relationship between SAW response and the impedance variation of sensors. Some key parameters for this model are determined by the software FEMSDA, in which the finite element method (FEM) is used to simulate the mechanical properties of the electrodes and spectral domain analysis (SDA) is used to model the substrate. SAW devices have been designed, fabricated and measured. The simulation results agree well with the experimental results. The applications for capacitive and resistive sensors are presented.

This work is mainly funded by the German Research Council (DFG—Graduiertenkolleg Sensorik). The authors are thankful to the research group of Prof. Ken-ya Hashimoto for their free software FEMSDA.

P1J-10

A QUASI-COM MODEL FOR 2-DIMENSIONAL SURFACE WAVE AND SIMULATION FOR LEAKY SURFACE WAVE DEVICES.

X. ZHANG[1], J. LIN[2], W. WANG*[1], H. WANG[1], H. WU[1], and Y. SHUI[1], [1]Nanjing University, Nanjing, Jiangsu, China, [2]Department of Communication and Information Engineering, Guili, Guangxi, China.
Corresponding e-mail: wbwang@nju.edu.cn

In SAW device design, extraction of COM parameters and simulation of SAW devices by P matrix calculation has been extensively used to optimize the structure of the devices, because this method is fast and efficient. The presupposition of COM model is 1-dimensional wave propagation in a periodical medium. However, SAW is a kind of 2- dimensional wave, whose vibration distribution along depth direction is not uniform and varies with frequency. Therefore, SAW device does not fit the presupposition of COM model. The error brought by this difference is not significant in case of Rayleigh wave devices. But in the case of leaky surface wave, especially for 36°-42°YX-$LiTaO_3$, the error between actual curve and simulation by COM model cannot be ignored. So, it is necessary to improve the COM model, when leaky surface wave devices are simulated. We still use the form of COM model, but take the COM parameters as frequency dependent and with propagation attenuation, to represent the bulk wave radiation varying with frequency, and the frequency dependent excitation and dispersion. We use a new method (virtual phase shift excitation method) to extract all the COM parameters as function of frequency. By using the model, a synchronous resonator and a DMS filter are simulated. The calculation used by Green's function combine with finite element method/boundary element method for finite electrodes is taken as standard for comparison. The results are in good agreement in a wide frequency range.

The paper is supported by Natural Science Foundation, China, No. 60261003

Session: P1K

SAW DEVICES I
Chair: R. Potter
Vectron International

P1K-1

TUNABLE EDGE REFLECTORS IN SAW FILTERS.

V. CHEREDNICK[1], M. DVOESHERSTOV[1], V. REUT[2], and B. SVESHNIKOV*[1], [1]Nizhny Novgorod State University, Russia, [2]AEC Design, St.-Petersburg, Russia.
Corresponding e-mail: bvs@ieee.org

This abstract does not appear in the online abstracts at the author's request.
It will appear in the print version.

P1K-2

DESIGN AND FABRICATION OF THIN FILM LAMB WAVE RESONATORS UTILIZING A LONGITUDINAL WAVE TRANSDUCER.

V. YANTCHEV* and I. KATARDJIEV, Uppsala University, The Angstrom Laboratory, Uppsala, Sweden.
Corresponding e-mail: veya@angstrom.uu.se

Highly c-oriented aluminum nitride (AlN) thin piezoelectric films have been grown on low resistive silicon by pulsed direct-current (DC) magnetron reactive sputter deposition. The films were deposited at room temperature and had typical full width half maximum (FWHM) value of the rocking curve of around 2 degrees.

Resonant membrane devices were designed and micro-machined using standard photolithography and deep silicon etching. The devices were designed to operate with the high velocity symmetric Lamb mode excited by means of longitudinal wave (LW) transducers. SAW based designs having varying cavity lengths and transducer topology were fabricated and characterised. Quality factors well in excess of 2000 have been demonstrated at a frequency of around 850 MHz. The Lamb excitation by means of LW transducers demonstrated high efficiency. These results indicate that LW transducers represent a competitive alternative to the commonly used interdigital transducers since they offer reduced transducer size minimizing thus the device area.

This work is supported by the Swedish Foundation for Strategic Research (SSF) through the ICTEA program in microelectronics.

P1K-3

AMPLITUDE AND PHASE MEASUREMENT OF SURFACE ACOUSTIC WAVES WITHIN A SAW FILTER HAVING FAN-SHAPED TRANSDUCERS AND NUMERICAL SIMULATIONS.

T. CHIBA*, Meisei University, Hino, Tokyo, Japan.
Corresponding e-mail: chiba@ee.meisei-u.ac.jp

Several authors have reported optical measurement of surface acoustic waves within a SAW filter having fan-shaped transducers. P. Dufilie et al [1] and K. Kokkonen et al [2] investigated the X-112Y $LiTaO_3$ substrate, and H. Yatsuda et al [4] the Y-Z $LiNbO_3$ and 128Y-X $LiNbO_3$ substrates. Numerical simulations have also been performed for the field distributions of surface acoustic waves and electrical frequency characteristics of SAW filters; P. Dufilie et al [1] and K. Kokkonen et al [2] using the equivalent circuit model, and H. Yatsuda et al [3][4] using the angular spectrum method. However, the behavior of surface acoustic waves has still not been clarified in detail, for example, with regard to fan-shaped transducers and their diffraction effect.

In this paper, we apply a new method of laser heterodyne interferometry to measuring and processing data for the phase measurement of surface acoustic waves within a SAW filter having fan-shaped transducers on a 128Y-X $LiNbO_3$ substrate. The following results for the wave motion and the diffraction effect are clarified. That is, standing waves inside the fan-shaped transducers are found to move towards the open end of the fan, which is perpendicular to the propagation direction of the main beam, and to cause several diffraction beams.

Furthermore, a simple numerical simulation concerning the wave motion and electrical characteristics of a SAW filter having fan-shaped transducers is proposed. The method uses a parabolic approximation, where the propagation direction of the wave is corrected by the power flow angle. Numerical simulations are applied to the field distributions of surface acoustic waves, the wave motion inside fan-shaped transducers, and the amplitude- and group-delay-frequency characteristics of the SAW filter. Good agreements are obtained between the simulations and the experiments.

References:

[1] P. Dufilie, L.Kopp, J.V. Knuuttila, J.Vartiainen and M.M. Salomaa, IEEE Ultras. Symp. Proc., pp. 41-44, Oct. 2001. [2] K. Kokkonen, P. Dufilie, J.V. Knuuttila and M.M. Salomaa, IEEE Ultras. Symp. Proc., pp. 1339-1342, Aug. 2004. [3] H. Yatsuda, IEEE Ultrasonic Symposium Proc., pp. 173-176, Oct. 2000. [4] H. Yatsuda, S. Kamiseki and T. Chiba, IEEE Ultras. Symp. Proc., pp. 13-17, Oct. 2001.

P1K-4

DESIGNING CAPACITIVELY COUPLED MICROELECTROMECHANICAL FILTERS.

A. ALASTALO* and V. KAAJAKARI, VTT Information Technology, Espoo, Finland. Corresponding e-mail: ari.alastalo@vtt.fi

Miniature mechanical resonators, fabricated with microelectromechanical-systems (MEMS) technology, are a potential replacement of off-chip filters (such as SAW and FBAR) as they are compact in size and integratable with IC electronics [1]. The demonstrated quality factors of MEMS resonators, Q>100 000 at 10 MHz [2] and Q>1000 at 1 GHz [3], are comparable to their macroscopic counterparts. While the mechanical properties of microresonators are very promising, obtaining a low-enough electrical impedance is challenging, especially for high frequency resonators. To obtain low impedance levels with electrostatic coupling, a narrow electrode gap (< 200 nm) is needed. This introduces higher harmonics due to the inverse relationship between the electrode capacitance and the gap spacing.

In filters, signal intermodulation due to odd-order nonlinearities is especially detrimental as it can lead to unwanted frequency components within the filter passband. For example, cubic mixing of two signals having frequencies f1 and f2 results in third-order intermodulation products at frequencies 2f1-f2 and 2f2-f1. If f1 = f0 + df and f2 = f0 + 2df, the IM product at 2f1 - f2 is at the passband center frequency f0 corrupting the desired signal. We have derived analytic closed-form equations to estimate the third-order intermodulation in MEMS filters and validated the theoretical results in measurements [4,5].

In this paper, we formulate a design procedure for MEMS filters. Central characteristics, such as insertion loss, bandwidth and filter distortion, are related to basic parameters, such as center frequency, mechanical resonator geometry, supply voltage and receiver architecture, for a single-stage MEMS filter. It is shown that it is extremely challenging for MEMS filters to operate in the 50 ohm source and load terminated environments, where FBAR filters are replacing SAW filters and becoming integrable with CMOS electronics. We show this by considering the lower limit for the smallest achievable electrode gap spacing set by intermodulation distortion, electromechanical instability (pull-in) and field-emission breakdown. The maximum electrode gap, on the other hand, is given by the insersion-loss specification that set the required mechanical impedance. These two requirements for the minimum and maximum gap may not be simultaneously met at GHz frequencies. It is concluded that MEMS filters are more suited for novel integrated receiver architectures where the impedance

levels at both sides of the filter can be much higher than 50 ohm and where the resonator Q value can be utilized for voltage gain.

[1] C. T.-C. Nguyen, IEEE Trans. Microwave Theory Tech., 47(8), pp. 1486-1503, Aug. 1999.

[2] V. Kaajakari, T. Mattila, A. Oja, J. Kiihamäki, and H. Seppä, IEEE Electron Device Lett., 25(4), pp. 173 - 175, Apr. 2004.

[3] J. Wang, Z. Ren, and C. T.-C. Nguyen, IEEE Trans. Ultrason., Ferroelect., Freq. Contr., 51(12), pp. 1607 - 1628, Dec. 2004.

[4] A. T. Alastalo and V. Kaajakari, IEEE Electron Device Letters, 26(5), pp. 289 – 291, May 2005.

[5] A. T. Alastalo and V. Kaajakari, IEEE Journal of Microelectromechanical Systems, submitted.

P1K-5
THIRD-ORDER INTERMODULATION DISTORTION IN CAPACITIVELY-DRIVEN VHF MICROMECHANICAL RESONATORS.

Y.-W. LIN*, S.-S. LI, Z. REN, and C. T.-C. NGUYEN, University of Michigan, Ann Arbor, MI.
Corresponding e-mail: ywlin@umich.edu

Substantial increases by more than 25dB in the third-order input intercept points (IIP_3) of capacitively-transduced MEMS-based vibrating micromechanical resonators have been attained by using contour-mode disk geometries to replace previous clamped-clamped beam versions [Navid, et al., MEMS 2001]. Specifically, a 160-MHz contour-mode disk resonator with Q = 20,500 exhibits a measured IIP_3 = 22.11dBm, which is substantially better than the -3dBm previously measured for a 10-MHz clamped-clamped beam resonator, and which now erases any lingering skepticism regarding the linearity of micro-scale mechanical resonators. Indeed, with IIP_3's greater than 20dBm, high Q communication filters using the micromechanical resonators of this work should now be able to replace present-day receive path filters with little degradation (only 0.11dB) in cumulative receiver IIP_3.

The 160-MHz micromechanical contour-mode disk resonator measured in this work was fabricated via a fully planar wafer-level surface-micromachining process and consists of a 3μm-thick, 17μm-radius polysilicon disk suspended by a stem at its center, and enclosed by two polysilicon capacitive transducer electrodes spaced 70nm from the disk perimeter. To operate the device, a dc-bias voltage is applied across its electrode-to-resonator capacitive gaps, and an ac excitation applied to the electrodes. Together, these voltages drive the disk into a vibration mode shape where it expands and contracts uniformly around its perimeter. The disk motion creates dc-biased time-varying electrode-to-resonator capacitors, which then source output currents that are linear for small motions, but that can contain distortion components when vibration amplitudes are large enough to instigate capacitive transducer nonlinearity. In particular, when two electrical interferer tones at f_o-200kHz and f_o-400kHz are applied to two separate

input electrodes, these signals and their induced mechanical displacements can interact to generate third-order intermodulation forces within the resonator passband, that then generate third-order intermodulation output distortion components, and thus, lower the IIP_3.

The IIP_3 = 22.11dBm measured using the above "two tone" test for a 160-MHz contour-mode disk with Q = 20,500 under a dc-bias of 7V is quite close to the value of 19.07dBm predicted by a model derived via harmonic balance analysis to be expanded upon in the full paper. Among the IIP_3 dependencies correctly predicted by this model are: (1) an increase in power IIP_3 with increasing resonator dc-bias voltage, verified by measured IIP_3's of 19.6dBm, 21.9dBm, and 24.7dBm for a 100-MHz contour-mode disk resonator under dc-biases of 3V, 5V, and 7V, respectively; (2) an increase in power IIP_3 with decreasing electrode-to-resonator gap spacing; and (3) an increase in power IIP_3 with increasing resonator size, verified by measured of IIP_3's of 25.0dBm, 21.9dBm, and 20.1dBm for 60-MHz, 100-MHz, and 160-MHz contour-mode disk resonators with radii of 44μm, 26μm, and 17μm, respectively. The model further predicts clear paths towards even better IIP_3's, perhaps up to 20dB better.

P1K-6

CHARGE-BIASED VIBRATING MICROMECHANICAL RESONATORS.

S.-S. LI*, Y.-W. LIN, Y. XIE, Z. REN, and C. T.-C. NGUYEN, University of Michigan, Ann Arbor, Michigan.
Corresponding e-mail: ssli@umich.edu

MEMS-based capacitively-transduced micromechanical disk resonators have been demonstrated that dispense with conventional high voltage source direct dc-biasing and instead use stored charge on their resonant structures to achieve equivalent performance. In particular, a 100-MHz micromechanical contour-mode disk resonator has been demonstrated with the same Q (~25,000) and series motional resistance when charge-biased, as when biased via a dc voltage source directly connected to its resonant structure. In removing the need for a dc voltage source, charge-biasing affords several important advantages, including: (1) better immunity against power supply variations, which should greatly facilitate integration into mixed-signal analog-digital communication circuits; (2) an ability to supply an effective bias voltage higher than the system power supply without the need for power hungry charge pumping; and (3) removal of the interconnects that would normally be needed to supply the dc-bias voltage to the resonant structure. These advantages stand to greatly simplify the use of micromechanical resonator technology in portable systems.

The micromechanical disk resonator used in this work to compare charge- and direct dc-biased performance comprise 26μm-diameter doped-polysilicon disks suspended 650nm from the substrate by stems at their centers, with two doped-polysilicon electrodes spaced 80nm from the disk edges, each covering half of the disk's circumference. Under conventional operation, a direct dc-bias voltage is applied to the suspended structure through an electrode connected to its conductive stem, and an ac excitation v_i is applied to one electrode. The two voltages combine to generate a force at the frequency of v_i that drives the disk

into a resonance mode shape where it expands and contracts, generating a time-varying electrode-to-resonator capacitance. An output current then ensues that traces out a very high *Q* bandpass biquad transfer function as the input frequency is swept.

In this work, the lead from the resonant structure to the dc-bias voltage source is abruptly broken, leaving charge on the resonator structure to maintain its bias state. Since the resonator is electrically well isolated from its surroundings, this charge leaks out very slowly, to the point where the resonator is still operational for long periods. The operational period can be made even longer by tying a capacitor in parallel with the resonator structure, which can increase the amount of charge available by several orders of magnitude, hence increase the operational lifetime by the same order. For a stand-alone charge-biased resonator, leaky discharging of the resonant structure in vacuum attenuates the output signal by 3dB after 900s. If a 0.18μF capacitor is charged and attached to the floating resonant structure, the resonator can operate for more than 8.5 days before its signal is attenuated by 3dB, which clearly illustrates the long-term efficacy of this charge-biasing approach. Frequency shifts caused by discharge-induced bias shifts are less than 2.5 ppm per hour, making plausible a “charge-and-refresh” operating mode with one-hour refresh intervals.

P1K-7
LAYER MODE DEVICES ON EPITAXIALLY GROWN GAN FILMS ON AL_2O_3.

K. HOHKAWA*[1], C. KANESHIRO[1], K. KOH[1], K. NISHIMURA[2], and N. SHIGEKAWA[2], [1]Kanagawa Institute of Technology, Kanagawa , Japan, [2]Nippon Telegraph & Telephone Co., Kanagawa, Japan.
Corresponding e-mail: chinami@ele.kanagawa-it.ac.jp

The layer modes on thin film, such as Sezawa mode, have an advantage over the Rayleigh mode, because they provide higher frequency devices using the same inter-digital transducers. However, these modes have the velocity dispersion, which might deteriorates device characteristics, especially on wide bandwidth devices. Device characteristics also tend to be dispersed by many factors on fabrication processes. This paper investigates a feasibility of layer mode devices with a high frequency and a wide bandwidth using present process technologies available for us, and tries to investigate a simple design method for these devices.

We have fabricated a simple delay line on some kinds of GaN films (including a commercially available film) and measured device characteristics of layer modes around a few GHz frequency range. We have adopted the film thickness of shorter than the periodic length of IDT (less than 1/1.6). In this condition the layer modes are seriously affected by an isotropy of Al_2O_3 substrate, we selected propagation directions along the main axis of sapphire and its perpendicular direction. We have measured device characteristics focused on amplitude and delay. The results have shown that the device characteristics are affected seriously by the difference on the propagation direction and residual stresses in film. We obtained many interesting results, such as the propagation wave along

main axis has shown a negative dispersion characteristics (the delay time decreases when operation frequency increases).

Based on these results, we clarify a condition suitable for device application. We also propose a simple design method for layer mode device, based on the impulse response model and discuss its feasibility.

P1K-8
DEVELOPMENT OF HIGH-SPEED LASER PROBE SYSTEM BASED ON KNIFE-EDGE METHOD FOR DIAGNOSIS OF RF SAW DEVICES.

H. KAMIZUMA*, T. OMORI, K. HASHIMOTO, and M. YAMAGUCHI, Chiba University, Chiba-shi, Japan.
Corresponding e-mail: k.hashimoto@ieee.org

This paper describes the development of a high-speed laser probe system for diagnosis of RF surface acoustic wave (SAW) devices. A fast scanning rate of 2.5 kS/s is realised, making it possible to visualise an SAW field consisting of 2,620×410 data points in approximately 40 min.

For the optical detection, the phase-sensitive knife-edge method was employed. This makes the system very insensitive to low-frequency mechanical vibrations caused by the fast stage translation. A prism mirror was used as a knife-edge and combined with a high-speed photo diode (PD) for system operation in GHz range.

A heterodyne receiver system was newly developed for the synchronous detection of the PD output and the high-speed data acquisition described below.

For the fast measurement, the following scanning technique was applied: the mechanical stage is translated continuously instead of the conventional “inch worm” action, and the detector output is acquired successively by a high-speed data-logger. Trigger pulses are generated from the output of a high-precision linear-scale installed in the translation stage and fed to the data-logger to synchronise with the stage movement. Then the translation stage can be driven in its maximum speed of 1 mm/s without degradation of the measured result.

After describing the system setup in details, the system is applied for the characterisation of spurious resonance modes in SAW resonators on ST-cut quartz and 15°YX-$LiNbO_3$. In conjunction with skillful use of image processing in wavenumber domain, it is shown how the present system is effective in the diagnosis and development of SAW devices.

P1K-9

NONSTANDARD ELECTROSTATIC PROBLEM FOR SAW INTERDIGITAL TRANSDUCER IN EXTERNAL ELECTRIC FIELD.

Y. TASINKEVYCH* and E. DANICKI, Institute of Fundamental Technological Research, Polish Academy of Sciences, Warsaw, Poland.
Corresponding e-mail: yurijtas@ippt.gov.pl

The nonstandard electrostatic problem for the system of strips making IDT placed in external electric field is solved by a novel method. It is based on earlier presented approach [1] exploiting the special template functions constructed in spectral domain and satisfying the electric boundary conditions on the strips. The functions can be effectively evaluated numerically with sufficient accuracy [2]. What is most important, the same functions and analogous approach exploiting them can be applied in the analysis of the electrostatic problems for anisotropic media, and also numerous problems of electromagnetic and elastic wave scattering by strips or planar cracks.

In contrast to standard electrostatics, here we construct solutions in the spectral domain. Note that the field spatial distribution is the least important in applications: measured are either the mutual strip capacitances depending on the total strip charges (the integrals of the charge distribution), or the spatial spectrum (in the scattering cases, like Bragg scattering by strips or frequency characteristics of surface wave transducers). The solution constructed in spectral domain with satisfactory accuracy is advantageous as compared with the standard evaluation of spatial charge distribution at least in the latter case, because of high sensitivity of the charge spectrum on the charge distribution details over the entire system. Having the spatial spectrum, one can easily evaluate the spatial distribution and its integral (in order to evaluate the measured total charges of strips) with similar high accuracy, what is not true in the reverse way. Moreover, the inverse Fourier transformation yields the tool for verification of the spectral results, lacking in the standard analysis.

1] E. Danicki, “Strip electrostatics - spectral approach”, 1996 IEEE Ultras. Symp. Proc. (1996) 193-196.

[2] Y.Tasinkevych, “Numerical efficiency of interdigital transducers charge spatial spectrum evaluation methods”, PhD Thesis, Polish Acad. of Sci., IFTR, Warsaw, 2004.

Present work was sponsored by State Committee of Scientific Research, Grant 3 T11B 046 26.

Session: P1L

MATERIALS FOR TRANSDUCERS

Chair: T. Shrout

The Pennsylvania State University

P1L-1

TEMPERATURE EVALUATION OF SOFT AND HARD PZT TRANSDUCERS FOR ULTRASONIC TRAPPING IN A MICROFLUIDIC PLATFORM.

L. JOHANSSON*[1], M. NILSSON[2], T . LILLIEHORN[1], M. ALMQVIST[2], J. NILSSON[2], T. LAURELL[2], and S. JOHANSSON[1], [1]Uppsala University, Uppsala, Sweden, [2]Lund University, Lund, Sweden.
Corresponding e-mail: linda.johansson@angstrom.uu.se

This paper reports a comparison of soft and hard piezoceramic transducer materials used for ultrasonic standing wave particle trapping in a microfluidal bioanalytical platform. The investigation is made with the objective to obtain high acoustic forces with a minimum of temperature increase. Temperature is a critical parameter for bioassays and most often needed to be kept below a certain level to allow handling of cells and proteins. The main conclusions in this paper are that it is possible to get efficient trapping with a temperature increase of only a few degrees and that a soft piezoceramic material has advantages in an application such as this.

Several groups have reported using acoustic forces in fluidic systems for separation or trapping of particles and cells in macro-scale resonators. In our group, a micro-scale system has been developed using higher frequencies and thus stronger trapping force. The platform with an array of individually controlled trapping sites offers a versatile system for various bioassays.

Miniature PZT-ultrasound transducers are integrated in the bottom of a microchannel and are designed to work as acoustic resonators at a frequency of around 12 MHz. Properly matched channel height allows a standing wave to be formed between each transducer and a glass-reflector with a local pressure minimum in the center of the channel defining the trapping site. Temperature rise in the channel is caused by mechanical and dielectric loss in the PZT transducers. At resonance and at the conditions suitable for efficient trapping, the standard measurements of dielectric loss $\tan\delta$ and mechanical loss Q^{-1} are insufficient for predictions of what material is the most favourable with respect to both temperature and trapping force in our device. To be able to select the optimal transducer material, the acoustic output and the fluid temperature has to be measured.

The piezoelectric materials (EDO EC-69 and EC-76) have different piezoelectric constants and the acoustic pressure is therefore measured, with a miniature hydrophone and at a distance of 35 wavelengths from the transducer, and the drive voltage adjusted to give the same output. For these drive voltages, fluid temperature in channel is evaluated by measuring fluorescence intensity of temperature sensitive Rhodamine B dissolved in the fluid.

The piezoelectrically softer material delivers more than twice as high output pressure for a drive voltage of 7 V. For both materials, series resonance gives about 10 % higher pressure than parallel resonance. Taking temperature also into account, the soft material gives a lower temperature increase (2 ° C) than the hard material (7 ° C). At anti-resonance however, the hard material is more favourable (plus 3 ° C) than the soft material (plus 5 ° C). So most favourable is to run the soft material at resonance frequency followed by hard material at anti-resonance frequency. The loss mechanisms in these transducer materials are complex and the paper presents some of the issues that have to be considered in these ultrasonic trapping devices.

P1L-2

MULTILAYER PIEZOELECTRIC COPOLYMER TRANSDUCERS.

T. LILLIEHORN*[1], T. BLOM[1], M. NILSSON[2], M. ALMQVIST[2], U. SIMU[1], and S. JOHANSSON[1], [1]Uppsala University, Uppsala, Sweden, [2]Lund Institute of Technology, Lund, Sweden.
Corresponding e-mail: tobias.lilliehorn@angstrom.uu.se

This contribution, for the first time at an international conference, presents process technology to fabricate multilayer ultrasonic transducers of the piezoelectric copolymer poly(vinylidene fluoride-trifluoroethylene) (P(VDF-TrFE)) by spin-coating. Multilayer technology is used to be able to subject the polymer material to high electrical fields at low drive voltages, and to increase the capacitance of the transducers for impedance matching purposes. Multilayer transducers become increasingly important in miniaturized systems, due to the low permittivity of the piezoelectric polymer material. The outlook of the present work is to investigate if miniaturized polymer transducers can be used to produce continuous wave acoustic energy high enough to be able to manipulate particles in a microfluidic system by acoustic radiation forces in an acoustic standing wave.

Multilayer transducers, 6 mm in diameter, have been fabricated on electroded glass substrates by spin-coating of a solution of P(VDF-TrFE) with a molar ratio of 65:35 and methyl ethyl ketone (MEK). Each spin-coated layer was 17 μm thick, and each transducer consisted of three polymer layers. After each layer, the substrate was annealed at 120°C for three hours, followed by the deposition of an evaporated electrode layer. The annealing of each layer was critical to being able to deposit another layer on top without dissolving the underlying polymer material and destroying the intermediate electrode layer. Single layer transducers were fabricated by a similar process scheme, but with electrodes deposited only on the substrate and on top of the third spun polymer layer. The transducers were polarized at peak electric fields between 19-76 V/μm, to analyze the effect of varying polarization.

The electrical impedance spectra of the transducers clearly showed the resonances in the glass substrate. The center frequency of the transducers was found to be 10.4 MHz, and the impedance of the multilayer transducer at this frequency was 50 Ω, compared to 400 Ω for the single layer transducer, being better matched to 50 Ω electronics. The transducers were characterized by

pitch-catch measurements, using polymer transducers as both transmitters and receivers. The round-trip insertion loss ($IL=20\log(V_D/V_P)$) was calculated from the peak-peak voltage of the drive signal (V_D), and the peak value of the pitch-catch response (V_P). The results were corrected for the gain in the receiving electronics and for the dampening in the medium. The IL decreased with 12.5 dB when increasing the poling field of the multilayer transducers from 19 V/μm to 76 V/μm. At 50 V/μm polarization, the IL was 11.7 dB less for the multilayer transducers when compared to the single layer transducers.

To conclude, multilayer polymer transducers have successfully been fabricated by a process technology based on spin-coating. The multilayer transducers have been evaluated by pitch-catch measurements, and have shown to outperform similar single-layer transducers.

P1L-3
MODELLING OF ULTRASONIC WAVE PROPAGATION IN INTEGRATED PIEZOELECTRIC STRUCTURES UNDER RESIDUAL STRESS.

M. LEMATRE*, G. FEUILLARD, and M. LETHIECQ, LUSSI GIP Ultrasons Université F. Rabelais, EIVL Blois France.
Corresponding e-mail: gfeuillard@univ-tours.fr

The development of piezoelectric integrated structures is mostly based on thin or thick film technology. In this case, the piezoelectric layer is laid down on a substrate and submitted to thermal treatment. In particular, after the sintering process, due to the difference of thermal expansion coefficients between the film and the substrate, a non uniform shrinkage appears that leads to a degradation of the functional properties of the structure through residual stress. Thus, it has become necessary to understand the role of residual stress in piezoelectric layers in order to predict the performance of integrated structures.

In a first part, a bulk piezoelectric material with internal stress is considered. For this, Christoffel's equation for a piezoelectric material is modified to take into account a uniform residual stress on a given cross-section. A numerical study of its influence is led on the slowness curves and coupling coefficients of a PZT-based material. It is showed that a lateral residual stress could couple pure transverse mode to piezoelectricity because of a slight rotation of the polarisation vector. In a second part, modified Cristoffel tensor is used to calculate the dispersion curves of Lamb waves in a piezoelectric plate. The Lamb modes are found to be sensitive to the residual stress. In particular, we show how the behaviour of the first Lamb modes is modified with residual stress.

In a third part, these results have been extended to a piezoelectric film laid down on a substrate in order to model the importance of these phenomena on the behaviour of an integrated structure.

This work was supported by the European community: MINUET Project NMP2-CT-2004-505657

P1L-4
NET-SHAPE CERAMIC MANUFACTURING AS AN AID TO REALIZE ULTRASONIC TRANSDUCERS FOR HIGH RESOLUTION MEDICAL IMAGING.

T. BUTTON*[1], S. COCHRAN[2], K. KIRK[2], K. MCDONALD[2], C. MEGGS[1], D. RODRIGUEZ-SANMARTIN[1], R. WEBSTER[1], and D. ZHANG[1], [1]University of Birmingham, Birmingham, UK, [2]University of Paisley, Paisley, Scotland, UK.
Corresponding e-mail: coch-ph0@wpmail.paisley.ac.uk

High frequency ultrasonic transducers are in demand for medical imaging procedures requiring high spatial resolution. However, cost-effective fabrication for frequencies above approximately 20 MHz is challenging because of the need for a thin layer of active material. For example, PZT 5A ceramic must be approximately 100 μm thick and a typical piezoceramic-polymer composite approximately 80 μm thick to operate at 20 MHz. These thicknesses are difficult because they exceed the capabilities of typical thick and thin film processes but are sufficiently thin that lapping bulk materials is expensive and inefficient. In this paper, the alternative to use net shape ceramic processing is reported. For thin piezoceramic material, the most conceptually simple net-shape processing route is to use viscous polymer processing (VPP) to produce green-state material with rheological properties compatible with calendaring to produce thin sheets which are dried, sintered and can then be cut to shape mechanically or using more sophisticated techniques such as laser machining. This process is also potentially compatible with mechanical shaping, for example to produce a focusing element. The application of electrodes within the net-shape process is also possible, or thin film electrodes can be deposited afterwards. Although such thin specimens are difficult to handle, the immediate addition of a supportive, acoustically-appropriate backing material to lend strength, allows the use of straightforward processes to configure the device into the final ultrasonic transducer. In the present paper, we report piezoceramic made with TRS600FG material finished to thicknesses of 50 μm and 110 μm. The behaviour of the thin samples has been found to be similar to bulk material made with TRS600FG, for example with a thickness mode coupling coefficient, kT, of 0.52 and a relative permittivity, εRS, of 1540. This material has been used as the basis of prototype ultrasonic transducers with element diameters of a few millimetres, corresponding to an electrical impedance in the range 50 - 70 Ω when operated at frequencies approaching 50 MHz. Testing has been performed underwater with a JSR DPR300 Pulser-Receiver, utilising a broadband membrane hydrophone and in pitch-catch mode with two transducers. The successful results suggest that net-shape ceramic manufacturing can overcome the difficulties presently associated with the fabrication of thin piezoceramic.

The authors acknowledge the contribution of G.Dolman to the work reported here.

P1L-5
BROADBAND EMFI ULTRASONIC TRANSDUCER FOR BAT RESEARCH.

A. STREICHER*[1], M. KALTENBACHER[1], H. PEREMANS[2], and R. LERCH[1],
[1]Friedrich Alexander University Erlangen-Nuremberg, Erlangen, Germany,
[2]Antwerp-University Faculty St. Ignatius, Antwerp, Belgium.
Corresponding e-mail: alexander.streicher@lse.eei.uni-erlangen.de

In the field of bat research and robot navigation, broadband air ultrasonic transmitters and receivers are of great importance. For example, in order to investigate the sound as produced by a wide variety of bat species, the transducers have to operate with a frequency range of 20 - 200 kHz and have to match sensitivity (receiver) as well as transmit efficiency (transmitter) of living bats. These requirements can not be achieved by commercially available in-air ultrasonic transducers due to their small bandwidth. Hence, a new transducer technology is required to build up broadband ultrasonic transducers with a good adaptation to air. The most promising transducer material for this is a cellular polymer film called electro mechanical film (EMFi). The cellular structure of the material results in a relatively high piezoelectric constant d_{33} up to 800 pC/N and a resonance-frequency of about 300 kHz.

By utilizing this polymer material different transmitters with a diameter of 1.5 cm were developed for emitting a chirp signal with a sound pressure level up to 90 dB at a distance of 1m for the whole frequency range of 20 - 200 kHz. With the same material, a broadband ultrasonic receiver with a sensitivity of 500 μV/Pa and a low equivalent acoustic noise level of 45 dB was set up. For an optimisation of the transmitter and the receiver we need a deeper understanding of the physical behaviour of the polymer material. Therefore, we applied a 3D finite element simulation by using a piezoelectric material model for a macroscopic description of the EMFi material. However, vibration measurements of the transducer surface show a nonlinear inhomogeneous vibration behaviour at and above resonance frequency. One reason for this is the inhomogeneous structure of the foil. Inside the polymer film the number of cavities as well as their size strongly varies. Because the resonance frequency of each point of the surface depends on the average cavity size at this point, the whole surface vibrates inhomogeneous. Therefore the EMFi material can not be described with a piezoelectric material model and we developed a more complex microscopic model for the precise numerical simulation. To solve this problem we computed the electrostatic and mechanical partial differential equation coupled by the electrostatic forces (Coulomb forces) including the complex geometric structure of the cellular ferroelectric film. To investigate the influence of the geometric structure on the vibration behaviour, models with different void shapes and sizes have been taken into account. For practical simulation of the whole transducer behaviour the microscopic model is not applicable due to computer resources. Therefore, we currently investigate in the development of a macroscopic model for this purpose.

In our paper, we will discuss the simulation results for various designs of transmitters and receivers as well as corresponding measurement results.

P1L-6
BASIC STUDY ON LEAD FREE BNT PIEZOELECTRIC FILM DEPOSITED BY HYDROTHERMAL METHOD.

T. HASEGAWA*[1], N. KAWASHIMA[1], S. TAKAUCHI[1], M. ISHIKAWA[2], and M. KUROSAWA[2], [1]Toin University of Yokohama, Yokohama, Kanagawa, Japan, [2]Tokyo Institutu of Technology, Yokohama, Kanagawa, Japan.
Corresponding e-mail: shin1@cc.toin.ac.jp

PZT piezoelectric poly-crystalline film synthesized by hydrothermal method has been studied actively in order to develop ultra-miniature actuators or sensors in our laboratory. This PZT film has some advantages that it shows piezoelectricity without a polling process, it can be deposited on the titanium substrates with complex shape. However, it is apprehended recently that PZT has malign influences on life and environment, because PZT is chemical compound including lead (Pb). Therefore, we tried to deposit lead free BNT [(Bi0.5, Na0.5) TiO3] piezoelectric film on titanium substrates by hydrothermal method. Bismuth oxide, sodium nitrate and potassium hydroxide were used as source material for lead free BNT piezoelectric film in this study. It was confirmed by SEM image, XRD (X-ray diffraction) pattern and EDS (Energy dispersive X-ray spectrometer) data that the deposited films on the titanium substrate were poly-crystals with perovskit structure. However, the synthesized poly-crystalline film had extremely unbalanced composition rate of Bi 10. We fabricated bimorph vibrators by depositing lead free BNT film on titanium substrate by hydrothermal method. It was found by measurements with laser Doppler vibrometer (LDV) that vibration velocities of the bimorph vibrator with BNT film were about from one fifth to one tenth of vibration velocity of bimorph vibrator with PZT film deposited by hydrothermal method with same size. These results were reported at 2004 IEEE UFFC Joint 50th anniversary conference in Montreal. We repeated the experiments with adjusting Bi concentration in the source material solution after the 2004 conference in Montreal. It was found as a result that composition of synthesized poly-crystalline film could be improved to Bi 20 at the condition of Bi concentration of 0.1 M. It was proved by LDV measurement that a bimorph vibrator using the poly-crystalline film with composition of Bi 20 showed the vibrating velocity of twice the conventional data. We will reports these new considered results in this symposium.

P1L-7
PIEZOELECTRIC PROPERTIES OF $BATIO_3$ THIN FILMS GROWN BY ECR-PLD.

S. ITO, K. NAKAMURA*, and K. ISHIKAWA, Tohoku University, Sendai, Japan.
Corresponding e-mail: nakamura@ecei.tohoku.ac.jp

Ferroelectric (001) $BaTiO_3$ thin films are suitable for generation of high-frequency longitudinal waves, because of the high electromechanical coupling factor k_t of about 0.61 and moderately low dielectric constant of about 56. Epitaxial growth of $BaTiO_3$ thin films has been reported in a number of papers so far. However,

there has been no report on their piezoelectric properties related with the high-frequency thickness-extensional mode. We have recently succeeded in epitaxial growth of high quality (001) $BaTiO_3$ films on conductive La-doped (100) $SrTiO_3$ substrates using an electron-cyclotron-resonance-assisted pulsed laser deposition (ECR-PLD) technique. This paper reports the growth procedure and the piezoelectric properties related with high-frequency thickness-extensional vibrations. The X-ray diffraction analysis revealed that the lattice constant perpendicular to the surface was very close to the *c*-axis lattice constant of bulk crystals. The FWHM of the rocking curve of a (001) $BaTiO_3$ film was as small as 0.09°, which is the smallest among those reported up to now. The electrical admittance response for the thickness-extensional modes in a high-frequency range was measured for the first time. In the 1-8 GHz range, there were observed many large resonance peaks associated with the overtone thickness-extensional vibrations of the whole $BaTiO_3$-film/substrate composite structure. The electromechanical coupling factor k_t of the $BaTiO_3$ film under a 20V dc-bias was evaluated to be 0.41 by comparison with equivalent circuit simulations. The dependence of measured ferroelectric properties on the dc-bias voltage is also presented.

P1L-8
ALUMINUM NITRIDE THIN FILMS ON TITANIUM FOR PIEZOELECTRIC MEMS APPLICATIONS.

S. BOESHORE*, E. PARKER, V. LUGHI, and N. MACDONALD, University of California, Santa Barbara, CA,.
Corresponding e-mail: sethb@engineering.ucsb.edu

Highly-textured aluminum nitride thin films have been deposited onto titanium substrates for the purpose of fabricating piezoelectric MEMS. As a demonstration of this technology, which could lead to radio-frequency devices suitable for harsh environments and broadband high-g accelerometers, trilayer cantilever beams (AlN films sandwiched between titanium bottom electrodes and aluminum upper electrodes) were fabricated using standard MEMS bulk micromachining techniques. We present here the first known demonstration of a piezoelectric titanium MEMS.

Piezoelectric aluminum nitride films were deposited onto bulk polycrystalline titanium substrates using a high-power, low-temperature 40-kHz AC sputter deposition. Because sputtered thin films are polycrystalline the piezoelectric coefficient is controlled by the film texture; in this case, the texture is the alignment of (002) grains normal to the substrate. The deposition parameters were optimized to produce the maximum (002) grain alignment in 1.5- to 2-μm-thick AlN films. X-ray rocking curve analysis of the deposited AlN films showed that full-width half-maxima (FWHM) of under 4° were readily achievable and indicated that the films were suitable for fabricating piezoelectric devices.

To fabricate the trilayer beams, the AlN thin film was etched with a chlorine-based plasma etch followed by a re-entrant deep etch into the titanium substrate to a depth of approximately 10 μm. The beams were then released by an isotropic wet etch in dilute hydrofluoric acid, and finally the top contact layer of 300 nm of aluminum was deposited by electron beam deposition. The released beams measured 60 μm long by 10 μm wide, and had a total maximum thickness of

approximately 4 μm.

Testing of the released trilayer beams was performed using a laser vibrometer to directly measure beam velocities caused by an applied voltage. Because of the piezoelectric coefficient d_{31} , which couples a z-axis electric field to an x-y strain, a voltage across the AIN film created a strain, resulting in beam displacement. An oscilloscope was used to integrate the velocity data into beam displacement. Signal output from the vibrometer was also sent into a vector signal analyzer to record the frequency response of the beams.

The maximum beam tip resonant displacement measured was 3 μm. The resonant frequency of the beams varied from 800 kHz to over 1 MHz. This difference was attributed to processing variations, as all of the cantilevers had the same mask dimensions. The quality factors of the beams were measured at atmospheric pressure and were in the range of 150 to 350. A finite element model of the cantilever was created to compare theoretical results to the measured displacement data. Using an extrapolation method, an AlN film with FWHM of 6.9° was found to have a piezoelectric coefficient d_{31} of 0.80 C/m^2 , roughly half of the reported single-crystal value.

Session: P1M

TRANSDUCER MODELING
Chair: R. Lerch
University of Erlangen

P1M-1
ANALYSIS OF POINT SPREAD FUNCTION IN PHASED ARRAY IMAGING.

MAHMOUD SAKHAEI*, ALI MAHLOOJIFAR, and M. HASAN GHASEMIAN, Tarbiat Modarres uiversity, Tehran, Iran.
Corresponding e-mail: sakhaei@modares.ac.ir

Ultrasound imaging system is generally considered as a linear system and so, it may be mathematically described by impulse response function (IRF) or, in image domain, by point spread function (PSF). It is the subject of many articles to model the ultrasound field in an ultrasound system, but they do not give any analytic expression of IRF or PSF for a wideband ultrasound array. However that expression has been given for single transducer and focal or far field region of an array. So, there is a lack of closed form expression for PSF of an array which is applicable for any excitation and for all regions.

In this paper, we represent an approximate closed form expression of 2-way, 2-dimentional wideband PSF for phased array configuration, which may be used to gain insight to image formation. In addition it is helpful to design the weightings, pulse shape, bandwidth and frequency and so on. Also it may be used for modeling signal statistics and determining system characteristics such as sensitivity, resolution and coherence as well as, image restoration.

The model is established on summation of spherical wave produced by each element and beam spreading and element directivity effects are considered by a convenient scaling factor. It is demonstrated that our model gives acceptable results by comparing it to results obtained by Ultrasound Field Simulation program, FIELDII.

Our model considers the property of spatial shift variant of PSF and is represented for fixed focus in transmit and receive, however it is applicable to any focusing configuration such as dynamic focusing and synthetic aperture techniques. It is known that in each temporal or spatial point, the PSF is a function of focusing point and the point at where the reflector lies. We demonstrate that there is an interesting relation between these points which is that if the places of reflector and focusing point are interchanged, then the new system response is time reversed of primary response.

We show that 2-way PSF is equal to the convolution of one way PSF's inverse filtered by the excitation pulse. Also by analyzing in far field case, it is concluded that our model is consistent to other forms previously proposed and the PSF is shift invariant. Moreover, the effective aperture is convolution of transmit and receive aperture only in far field case.

P1M-2
CONNECTION BETWEEN X-WAVES, FOURIER-BESSEL SERIES AND OPTIMAL MODELLING APERTURE FOR CIRCULAR SYMMETRIC ARRAYS.

P. D. FOX*, INSERM U619 & CIT, CHU Bretonneau, 2 Bis Boulevard Tonnelle, 37044, Tours, France., Tours, Centre, France.
Corresponding e-mail: fox@med.univ-tours.fr

This paper addresses various unresolved issues raised in publications [1], [2], and [3], in connection with the study and application of limited-diffraction and non-diffracting beams. Nondiffracting beams have the property of a constant radial profile with propagation distance, subject to an infinite aperture source, and the related theories advanced in the context of medical imaging have resulted in the possibility of extremely high fame rates. However, all the fundamental theory assumes an infinite-aperture source being available. In reality this is not possible, and when nondiffracting beams are implemented on finite source apertures they become limited diffraction beams. [1], [2], [3] have studied the use of and numerical differences between nondiffracting theory and limited diffraction implementation of such beams for field computation and tuning. In [1], [2] it was shown that an iterative technique could be applied to extend the effective modelling aperture from the physical limits of the transducer (limited diffraction basis functions) towards an infinite modelling aperture (Bessel beams / X-waves), to both tune and compute the emitted field from any given circular symmetric flat array with linear propagation conditions. This technique involved the concept of a modelling aperture spanning the gap between the physical limit of the transducer and infinity, which, when increased iteratively resulted in convergence of the corresponding computed field and source driving function. However, the technique relied on a combination of iterative combinations and

numerical field convergence to within a pre-selected limit in order to terminate the computations at an appropriate point.

In this paper, a formal mathematical connection between the limited-aperture (limited diffraction) basis functions and the nondiffracting infinite aperture theory (Bessel beams / X-Waves) is established as a function of the increasing modelling aperture. The result is that a specific optimal modelling aperture may then be specified as a function of frequency spectrum, spatial field extent to be investigated, and pulse repetition frequency. Consequently the previous iterative technique may be replaced by a single one-shot computation to achieve the same result. As a result, the new technique is significantly more efficient than the previous technique and the specific saving in computation depends on the particular transducer considered, but typically computational reductions are in the order of 50%. The global contribution of the paper is twofold : firstly a formal mathematical connection between limited diffraction beams and nondiffracting beams as function of increasing modelling aperture, and secondly the derivation of the optimal modelling aperture required for computation and tuning of circular symmetric fields with minimal computational demands.

[1] JASA ,Vol. 113, no. 5, pp. 2412-2423, May, 2003.

[2] IEEE Trans. UFFC, Vol. 49, no. 9, pp 1179-1190, Sep 2002.

[3] IEEE Trans. UFFC, Vol. 49, no. 1, pp 85-93, Jan 2002.

This work was partially sponsored by Le Studium, Orleans, France.

P1M-3
FOCUSED AIR TRANSDUCERS: SOUND FIELD COMPUTATION AND FE MODELING.

J. LAN*, S. FRAZIER, and M. CHIASSON, Airmar Technology Corporation, Milford, NH.
Corresponding e-mail: jlan@airmar.com

This paper describes the design of a transducer for air-borne ultrasonic applications. The transducer is highly focused with an F-number approaching one. The application for this air transducer is for non-contact non-destructive testing where a very small focal spot is required. The transducer uses a piezoelectric ceramic as the active element. Key design criteria are to maximize ultrasonic pressure at the focus, optimize depth of field, and be capable of operating over a reasonable bandwidth. Essential to understanding the tradeoffs is FE analysis by which displacements along a curved surface can be accurately predicted (both amplitude and phase). The front of the transducer is composed of syntactic foam with the desired geometric shape, bonded to a flat disk piezoelectric ceramic. Syntactic foam is often used as a quarter-wave matching layer for air transducers. In this application, however, thickness of the syntactic foam ranges from a fraction of a wavelength near the center to tens of wavelengths near the outer edge. Geometry of the emitting surface has the appearance of the interior of a hemisphere. FEA revealed distribution of displacements over the hemisphere, as a function of frequency around the transducer's resonance frequency.

In general a target is working in near sound field and amplitude on radiation surface are not uniform, and are complex number, therefore their sound field are complicated. A group of formulars for calculating sound field distribution and sound pressure along symmetrical axis of surface are derived based on known amplitude on the spherical surface.

Engineering evaluation of the transducer for NDT has demonstrated that good resolution for defects near the surface (which is the system objective).

P1M-4

DIFFERENT APPROACHES TO FINITE ELEMENT MODELING OF EFFECTIVE MODULI OF POROUS PIEZOCERAMICS WITH 3-3 (3-0) CONNECTIVITY.

A. NASEDKIN[1], A. RYBJANETS*[2], L. KUSHKULEY[2], Y. ESHEL[2], and R. Tasker[3], [1]Rostov State University, Rostov on Don, Russia, [2]UltraShape Ltd., Tel Aviv, Israel, [3]TASI Technical Software Inc., Kingston, Canada.
Corresponding e-mail: andrey58@012.net.il

Theoretical aspects of the effective moduli method for an inhomogeneous piezoelectric media were examined. Four static piezoelectric problems for a representative volume that allow finding the effective moduli of an inhomogeneous body were specified. These problems differ by the boundary conditions which were set on a representative volume surfaces: a) mechanical displacements and electric potential, b) mechanical displacements and normal component of electric flux density vector, c) mechanical stress vector and electric potential, and d) mechanical stress vector and normal component of electric flux density vector. Respective equations for calculation of effective moduli of piezoelectric media with arbitrary anisotropy were derived.

Based on these equations and using finite element method (FEM) the full set of effective moduli for PZT porous ceramics having wide porosity range was calculated. Different models of representative volume were considered: piezoelectric cubes with one cubic and one spherical pore inside, cubic volume evenly divided on partial cubic volumes a part of which randomly declared as pores etc. For the modeling of the porous piezoceramics with 3-3 connectivity the representative volume having skeleton structure was considered.

For accounting of inhomogeneous or incomplete ceramics polarization the preliminary modeling of polarization process was performed. To determine the areas having different polarization FEM calculations of the electrostatic problem were executed.

The results of FEM modeling were compared with the theoretical results obtained on the basis of Marutake's effective medium approximation, Bruggeman's formulas and unit-cell models, as well as with the experimental results for different porous ceramics in the relative porosity range of 0-70%. Based on these results

the modeling of high intensity focusing transducers made of “hard” porous PZT ceramics was performed.

P1M-5

THE TEMPERATURE INFLUENCE ON THE PIEZOELECTRIC TRANSDUCER NOISE, MEASUREMENTS AND MODELING.

F. COUTARD*, E. TISSERAND, and P. SCHWEITZER, LIEN, Université Henri Poincaré, Vandoeuvre, France.
Corresponding e-mail: frederic.coutard@lien.uhp-nancy.fr

This work, developed at the Electronic Laboratory of Instrumentation of Nancy (LIEN-France), concerns the characterisation of the electrical impedance and the generated noise of piezoelectric transducers. Special attention is given to the medium of propagation and the temperature on the noise level. Theoretical explanations are proposed to justify the relative thermal stability of the noise level.

This paper is composed of four parts. The first one considers measurements of the complex impedance and the spectral noise density of the piezoelectric transducers and are carried out in water and in air. All measurements are made using the impedance analyser HP4195A and the spectrum analyser Advantest R3131A. Because the noise level of the sensor is very low, we insert an amplifier between the analyzer and the sensor. This amplifier increases the level of signal above the noise floor and adapts the impedances The transducers are made of PZT and their resonance frequencies are situated around 2 MHz. The measurement are realised at a temperature fixed to 298 K. We measure the correlations between the noise spectrum and the impedance.

In the second part, we study the influence of the temperature T on the impedance and the noise spectrum for square transducers in air.The temperature range is 298 to 343 K. In this range, the magnitude of the impedance peak decreases by 0.3 % per K and its relative frequency shifts by 186 ppm per K. The temperature seems to have a little influence on the noise level : the peak magnitude is nearly constant, with a sensibility coefficient equal to 0.08 % per K.

The third part is reserved to suggestions of theoretical interpretations of the observed results. On one hand, the decreasing impedance is explained by the thermal sensibility of certain characteristics of the piezoelectric material such as the dielectric constant. On the other hand, we show that whatever is the origin of the noise delivered by the transducer (intrinsic or noise introduced by the medium), a Johnson noise explains the quasi-stability of the measurements.

If we consider that the noise is generated by the resistive part R of impedance, the noise DSP is proportional to RT. This DSP remains constant because the relative decrease of the resistive part (-13.5 %) compensates the relative increase of temperature (+15 %).

In the last part, we propose a electroacoustic model (type Redwood) which includes an estimate of the transducer noise. Currently, this model implemented

under PSPICE allows to evaluate the signal-to-noise ratio of ultrasonic émission/ réception system.

P1M-6
NONLINEARITIES AND HYSTERESIS PHENOMENA IN RECIPROCAL ULTRASOUND SYSTEMS.

M. WILLATZEN*, L. WANG, and Y. FENG, Mads Clausen Institute, University of Southern Denmark, Grundtvigs Alle 150, DK-6400 Sonderborg, Denmark.
Corresponding e-mail: willatzen@mci.sdu.dk

Results based on a one-dimensional mathematical model of reciprocal ultrasound systems [1, 2] including nonlinearities [3] and hysteresis phenomena are presented. In particular, we consider the constitutive relation for the electric field E to involve, in general, nonlinear terms to third and fifth order in the electric displacement D while linearity in the strain is assumed. The transmitter system consists of a single-layer PZT-5 piezoceramic material layer connected in series to an electrical impedance and a voltage generator. The receiver circuit consists of a single-layer PZT-5 piezoceramic material (similar parameters as for the transmitter) and an electrical impedance (the voltage over the the electrical impedance is the receiver voltage). Results for the E-D curve are presented subject to a given voltage-input scenario and hysteresis phenomena are identified.We also present step-response curves for the transmitter-aperture pressure and the receiver voltage for three cases of constitutive relations: (1) linear constitutive E-D relationship, (2) linear and third-order nonlinear terms in the constitutive E-D relationship, and (3) linear, third-order, and fifth-order nonlinear terms in the constitutive E-D relationship. The present model allows for acoustic and dielectric losses in the piezoceramic layers and the possibility to interconnect a fluid/solid medium between the two PZT transducers.

[1] M. Willatzen, “Ultrasound Transducer Modeling - General Theory and Applications to Ultrasound Reciprocal System,” IEEE Transactions on Ultrasonic, Ferroelectrics and Frequency Control, Vol. 48, No.1 January 2001.

[2] M. Willatzen, “Ultrasound transducer modeling - Received voltage signals and the use of half-wavelength window layers with acoustic coupling layers,” IEEE Transactions on Ultrasonics, Ferroelectrics, and Frequency Control, 46, pp. 1164-1174, September 1999.

[3] L. Wang and M. Willatzen, “Mathematical Modelling of Reciprocal Transducer Systems Accounting for Nonlinear Constitutive Relations,” submitted to Ultrasonics.

P1M-7
PSEUDOSPECTRAL TIME-DOMAIN METHOD TO CALCULATE RADIATION PATTERN OF LENS-FOCUSED TRANSDUCERS.

C. BATIFOL, S. CALLÉ*, P. MARÉCHAL, M. LETHIECQ, and F. LEVASSORT, François Rabelais University, LUSSI, FRE 2448 CNRS, Tours Cedex, France.
Corresponding e-mail: calle_s@med.univ-tours.fr

In ultrasound applications, such as medical imaging or therapy, focusing effect is used to improve both sensitivity and lateral resolution. This is often obtained by the addition of an acoustic lens on the transducer as a final element, in contact with the propagation medium. Previous study on this subject using finite element method (FEM) and an extended unidimensional KLM model [1] shows that the initial assumed plane wave source delivers an heterogeneous spectrum at the lens surface, resulting from longitudinal and transverse waves propagation and also multiple reflections in this lens. The purpose of this study is to describe a pseudospectral time-domain (PSTD) algorithm which takes into account this phenomenon to calculate the radiation pattern of a single-element lens-focused transducer. This method has the main advantage to follow easily the temporal evolution of the displacement or pressure propagated fields, in particular through the lens, and allows to clearly show the different phenomena occurring in this lens.

The PSTD algorithm, which solves time-dependent partial differential equations, combines conventional Fourier pseudospectral method and perfectly matched layers (PML) to avoid reflections and counter the wrap-around effect from the FFTs. The temporal evolution is performed using a 4th order Adams-Bashforth time integrator. The other advantages of the pseudospectral numerical algorithm compared to models based on finite difference or finite element methods are its efficiency to model large-scale problems. It has a better numerical stability and does not require a large number of nodes per wavelength.

To predict the radiated pressure field of a single-element circular transducer, this alternative pseudospectral method has been extended to the 2D axisymmetric case. New conditions according to this configuration are detailed. Validation of this numerical model has been performed for propagation in fluid (water) using a comparison with analytical diffraction models for spherically focused transducers.

Moreover, to study the influence of the lens on plane wave propagation, the model has been updated for wave propagation in an elastic solid. In the particular case of a lens-focused transducer with a 10 MHz center frequency, the pressure field is deduced at the lens surface using the pseudospectral method. This result is compared with those obtained using a finite element method (ATILA) in the same configuration. At the focal point, properties are also in good agreement with standard models and experimental results [1].

Finally, the presented modeling is used to study the influence of several acoustical parameters of the lens such as the acoustical impedance or the shear wave velocity on the radiation pattern, particularly on the electro-acoustic response at the focal point.

[1] P. Marechal, F. Levassort, L.P. Tran-Huu-Hue, M. Lethiecq, *Effect of acoustical properties of a lens on the pulse-echo response of a single element transducer*, IEEE International Ultrasonics Symposium , pp. 1651-1654, 2004.

ORAL SESSIONS

Session: 1A
LOCAL DRUG DELIVERY UCA/THERAPEUTIC
Chair: P. Burns
University of Toronto

1A-1 11:30 a.m.
MECHANISMS OF ULTRASONICALLY-MEDIATED DRUG DELIVERY: HIGH-SPEED CAMERA OBSERVATIONS OF MICROBUBBLES WITH ATTACHED NANOBEADS.

C.T. CHIN*[1], A. VAN WAMEL[2], M. EMMER[2], N. DE JONG[2], C. S. HALL[1], and A L. KLIBANOV[3], [1]Philips Research, New York, [2]Erasmus MC, Rotterdam, The Netherlands, [3]University of Virginia, Charlottesville, VI.
Corresponding e-mail: chien.ting.chin@philips.com

Background: Ultrasonically-triggered drug delivery may be accomplished through the use of microbubble agents modified to carry pharmaceuticals. Understanding of the dynamics and mechanisms of drug release is needed to ensure robust and reproducible delivery of pharmaceutical payloads. The objective of this study was to observe the behavior of lipid-encapsulated microbubbles with attached fluorescently labeled nanobeads within an ultrasonic field.

Methods: Stabilized perfluorobutane microbubbles were prepared by self-assembly of a lipid monolayer shell on the gas-liquid interface; aqueous dispersion of phosphatidylcholine, PEG stearate and biotin-PEG-phosphatidylethanolamine was subjected to 20 kHz ultrasound in the presence of perfluorobutane gas. Microbubbles were purified by flotation. Fluorescent avidin beads were immobilized on the surface of biotinylated bubbles, forming pendant-like structures. The microbubble-bead complexes were immobilized on Petri dish surface and monitored with an epifluorescence microscope equipped with a 40× water immersion objective with a high speed video camera operated at 500 frames/sec (fps). Microbubbles were exposed to an ultrasonic field from a Philips HDI-5000 scanner (MI = 1.5). Observable nanobeads were detached from the bubbles within the time scale (msec) of the experiment. Further detailed observations were made using the Brandaris-128 camera operated at 13 Mfps. The bead-bubble complexes were exposed to ultrasonic pulses (2.0 MHz, 10-cycles, 0.65 MPa peak negative amplitude) from a single-element transducer. Dynamics of the bubble boundary and nanobeads were tracked using automatic and manual image processing tools.

Results: Release and displacement of microbubble-associated fluorescent nanobeads from their original position was observed during insonation. Movement of the nanobeads showed detachment of beads from the bubble shell occurred within 2 to 10 cycles of insonation. Detached beads track the fluid flow induced by the bubble compression and expansion at velocities up to

20 m/sec. The beads motion relative to the bubble surface was due to translational movement of the bubble, the beads or both. The translational and oscillatory movement of detached beads diminishes as the distance between the bubble and the bead increases. At distances more than 10-20 μm, detached beads come to a rest.

Conclusion: This study reveals short time-scale detail of the release of shell-associated material from microbubbles achieved through insonation. The tracked movement of nanobeads in the particular experimental conditions studied infers the mechanism of release may not necessarily involve rapid ejection of the drug payload at near-sonic velocities as some previous models have implied. Therefore, the results did not establish the capability of ultrasound to propel nanobeads to a distance comparable to a few cell layers. Further experiments in a wider range of conditions will be performed to evaluate the additional mechanisms of ultrasound-triggered drug delivery using microbubble complexes.

1A-2 11:45 a.m.
MECHANISMS OF CELL MEMBRANE PERMEABILIZATION WITH ULTRASOUND AND CONTRAST MICROBUBBLES.

T. A. TRAN*[2,3], S. ROGER[2,3], J. Y. LEGUENNEC[2,3], F. TRANQUART[1,4], and A. BOUAKAZ[1,3], [1]Inserm, U619, Inserm, U619, Tours, France, [2]Inserm, E0211, Inserm, E0211, Tours, France, [3]Université F. Rabelais, Université F. Rabelais, Tours, France, [4]CIT Ultrasons, CIT Ultrasons, Tours, France.
Corresponding e-mail: bouakaz@med.univ-tours.fr

Aim: New clinical applications of ultrasound contrast agents extend beyond imaging and diagnostic towards therapeutic applications. A number of experimental findings have now demonstrated evidence of increased cell membrane permeability through sonoporation process. In this study, we explore the mechanisms by which the activation of microbubbles with ultrasound waves breach cell membranes.

Method: An electrophysiological experimental method is set up to explore the cell membrane response in sonoporation conditions. This experimental method consists of measuring the variations in membrane potential which directly indicates the modulation of ion exchange through the cell membrane and thus its conductance. To measure the cell activity during sonoporation, patch clamp technique was used in the “whole cell” configuration where the membrane potential of a single cell is measured. Mammary cancer cells issued from MDA-MB-231 cell-lines were used. Sonovue microbubbles provided by Bracco Research were continuously infused to the cells at a rate of 1ml/min. Ultrasound was applied using single element transducers of 1 and 2.25MHz, both focused at 14 mm. Waveforms of different lengths (20 to 40 cycles), amplitudes (50 to 400 kPa), repetition rates (100 to 500 μs) and exposure times (5 to 20 sec) were transmitted. The microbubbles and cells were simultaneously monitored during ultrasound exposure using a video camera.

Results: The results revealed that during sonoporation, an obvious hyperpolarization of the cell membrane potential occurs during the ultrasound

excitation, indicating the triggering of specific ion channels while the cell and the bubble remain both intact. At the highest acoustic exposure (pulses of 40 cycles at 1 MHz repeated every 100 μs during 20 sec); the membrane potential varied from -30 mV (resting value) to -60 mV and this phenomenon was entirely reversible. This mechanism showed to be dependent on the number of contrast microbubbles in the close vicinity of the cell, but revealed that only cells in direct contact with the bubbles undergo membrane hyperpolarization. Smaller acoustic amplitudes or higher frequency induced only mild hyperpolarization (less than 20mV) while shutting off the ultrasound brings the potential to its resting value. However ultrasound alone does not affect the cell membrane potential.

Conclusions: The results demonstrate that microbubble's oscillations under ultrasound activation entail modifications of the electrophysiological cell activities, by triggering the modulation of ionic transports through the plasmic cell membrane. However, only cells in a direct contact with the microbubbles are impacted. The involved mechanisms are related to activation of specific channels sensitive to mechanical stresses (stretch-activated channels) and possibly non-specific ion channels.

1A-3 12:00 p.m.
TRAPPING OF LOW SENSITIVITY OBJECT BY SEED BUBBLES.

Y. YAMAKOSHI*, Gunma University, Kiryu, Gunma, Japan.
Corresponding e-mail: yamakosi@el.gunma-u.ac.jp

An ultrasonic wave assisted micro object manipulation is a powerful tool, for example, in future Drug/Gene delivery system. Trapping of micro vehicles against blood flow is a targeting technology at desired part. Sonoporation, which makes micro holes through cell membrane by bubble explosion, improves dose to the tissue. In these methods, it is assumed that micro bubbles have enough sensitivity to the ultrasonic waves. It is required that the micro bubbles show large volumetric oscillation so that they receive enough acoustic radiation force for the bubble trapping. It is also supposed that the bubbles explode to make jet flow as a result of nonlinear oscillation. However, these features are not often seen under an actual situation. For example, payloads of bubble harden the bubble shell resulting in decrease of volumetric oscillation. Stiff bubble is difficult to explode. A solution to this problem is to use two kinds of bubbles, which have their own functions. First bubble is a seed bubble, which has higher sensitivity to the ultrasonic wave though it does not carry any payloads. The second bubble is a target bubble, which is an object vehicle though it has lower sensitivity. In this paper, trapping of low sensitivity object by seed bubble is proposed. First, only the seed bubbles are introduced into the ultrasonic wave field. The seed bubbles make bubble aggregation and the aggregated bubbles are trapped. Then, if target bubbles are introduced, the spatial restricted Bjerknes force field, which is produced by the seed bubbles, traps the target bubbles to make bi-layered bubbles mass (Inner layer: seed bubbles, outer layer: target bubbles). Feature of the method is that the target bubbles are trapped under maximum force condition while they are trapped under balance of force condition (zero force condition) in the conventional ultrasonic wave standing wave method. Bubble

mass, which is produced under maximum force condition, is stable for additional forces by, for example, flow turbulence. Second feature is that the produced condensed mass of seed bubble and target bubble is useful in seed bubble based sonoporation, because payloads of the target bubbles are placed by adjoining to the seed bubbles, which are easy to explode under ultrasonic wave radiation. Experiments are carried out using Levovist (Schering A.G.) as a seed bubble and Saccharomyces yeast cells (about 5 μm in size) as an example of target object. It was already proposed that Yeast cell is a vehicle of Drug/Gene delivery system applied in GI tract. Yeast cell is not a bubble but it has some sensitivity to the ultrasonic wave, which may come from micro bubbles produced by fermentation. Ultrasonic wave frequency is from 2.5MHz to 7.5 MHz. The sound pressure is 100 kPa. Flow velocity is set to 5 mm/sec. Three different conditions of yeast cell are examined. It was confirmed experimentally that yeast cells are not trapped when only the yeast cells are introduced into the ultrasonic wave field. However they are trapped as cloud around the aggregated seed bubbles, especially when the yeast cells are prepared in the water of temperature 75 degrees in advance.

1A-4 12:15 p.m.
ULTRASOUND-INDUCED UPTAKE OF DIFFERENT SIZE MARKERS IN MAMMALIAN CELLS.

R. KARSHAFIAN*[1,2], S. SAMAC[2], M. BANERJEE[2], P. D. BEVAN[1,2], and P. N. BURNS[1,2], [1]Medical Biophysics, University of Toronto, Toronto, ON, Canada, [2]Imaging Research, SWCHSC, Toronto, ON, Canada.
Corresponding e-mail: raffik@swri.ca

The delivery of impermeable compounds to cells when exposed to ultrasound have been demonstrated both in in-vitro and in-vivo studies. The physical mechanisms by which this occurs have yet to be elucidated. However, mechanisms due to bubble disruption (formation of microjets and shockwaves) and stable bubble oscillation (acoustic microstreaming) in ultrasonic fields are almost certainly implicated. One of the bioeffects is the formation of pores on the surface of cells. Understanding this process is of vital importance in establishing parameters for drug delivery in-vivo. We hypothesize that the pore size formed in cell membrane depends on bubble disruption phenomenon, with lower and higher acoustic pressures causing smaller and larger pores, respectively. Here, we use a suspension of cells and calibrated ultrasound beams to investigate the uptake of different size markers at various exposure parameters in the absence and presence of microbubbles.

Experiments were carried out on a suspension of cells (KHT-C: murine fibrosarcoma cell line) exposed to a calibrated ultrasound beam, at various acoustic pressures (0 to 1MPa) and frequencies (0.5 and 1MHz), in the absence and presence of microbubbles (7% volume Optison). FITC-dextran was used as a permeability marker with molecular weights of 10, 40, 70 and 500kDa to which a cell membrane is normally impermeable. Flow cytometry and microscopy were used to identify and quantify cell permeability and viability.

The presence of microbubbles is crucial in causing detectable changes in cell membrane permeability; no permeability changes were observed in the absence

of microbubbles even at high pressures (Pneg 1MPa). The sonoporation of the KHT-C cells is a pressure threshold dependent phenomenon. No effect was seen at pressures below 150kPa. The uptake of different molecular weight markers showed similar peak negative threshold values. At lower pressures (<200kPa), the same percentage of cells (6-8%) showed an uptake of FITC-dextran, regardless of the marker size. At higher pressures (>400kPa), however, more cells showed an uptake of the 10kDa (25%) than of the larger markers (13%). The number of permeabilized cells increased with peak negative pressure up to 400kPa, above which a plateau was attained for the higher FITC-dextran sizes.

We hypothesized that bubbles disrupted at low and high pressures would produce smaller and larger pores, respectively. The results indicate that large pores are produced when bubbles are disrupted at low pressures. At higher pressures, more cells showed an uptake of the 10kDa marker only, indicating that small pores were formed in additional cells. The dominating mode of uptake is considered to be passive, although, an increase in the active endocytosis could explain the higher uptake of the 10kDa. Our results imply that the conditions of the ultrasound exposure must be optimized for a range of drug sizes. Future work will continue to characterize the effect of different exposure parameters and bubble combinations on the uptake of bigger size markers.

CIHR

1A-5 12:30 p.m. (Invited)

TARGETED ULTRASOUND IMAGING AND DRUG DELIVERY.

K. FERRARA*, University of California, Davis, CA.
Corresponding e-mail: kwferrar@ucdavis.edu

Molecularly-targeted ultrasound contrast agents and drug delivery vehicles are now in pre-clinical evaluation for applications that include cancer and cardiovascular disease. Here, we review the structure and properties of targeted contrast agents and results of recent performance characterizations. In addition, several classes of drug delivery vehicles are under development including gas bubbles with polymer, lipid, or oil shells, and liquid-filled nanoparticles. High speed photography is used to characterize the oscillations of contrast agents and delivery vehicles with and without a targeting ligand. Ultrasound pulsing is shown to manipulate these particles changing their distribution in vitro and in vivo and improving the transfer of the drug to nearby cells. Selective targeting to cells expressing a specific signature will be demonstrated. Ultrasound can also change the permeability of capillaries within a region, enhancing the delivery of a drug to the desired local region, and the mechanisms associated with the changes will be described.

NIH CA 76062, CA 103828, EB 002952

Session: 2A

STATIC ELASTICITY
Chair: H. Ermert
Ruhr University

2A-1 11:30 a.m.
A SINGLE-ELEMENT FOCUSED TRANSDUCER METHOD FOR HARMONIC MOTION IMAGING.

C. MALEKE, M. PERNOT, and E. KONOFAGOU*, Columbia University, New York, NY.
Corresponding e-mail: ek2191@columbia.edu

Previously, we demonstrated the feasibility of a technique for simultaneous monitoring and generation of ultrasound therapy treatment using two separate focused ultrasound transducer elements [1]. In this study, a new harmonic motion imaging (HMI) technique is developed that estimates tissue displacement induced by harmonic radiation force excitation using a single focused ultrasound element. First, wave propagation simulation models were used to compare the use of one Amplitude-Modulated (AM) focused beam versus two overlapping focused beams as previously implemented for HMI [1]. Simulation results indicated that, unlike the two-beam configuration, the AM beam produced a consistent, stable focus for the applied harmonic radiation force. The AM beam thus offered the unique advantage of sustaining the application of the radiation force on the same tissue region. Experiments were then performed on agar gel phantoms and ex-vivo tissues. The radiation force was generated by a 4.68 MHz focused transducer using a low-frequency Amplitude-modulated (AM) RF-signal. A 7.5 MHz single-element, diagnostic transducer was placed through the center of the focused transducer so that the diagnostic and focused beams were aligned. A bandpass analog filter was used to remove the spectrum of the focused beam. Consecutive RF signals were acquired with a PRF of 1 kHz and the displacements were estimated using a classical cross-correlation algorithm. Absorption coefficients were measured accordingly. The intensity of the focused beam was varied from 26.34 W/cm^2 to 421.44 W/cm^2 allowing us to detect tissue displacements of up to 50 microns with the AM frequency varying between 1 Hz and 100 Hz. The local elastic properties were reconstructed using a Voigt model [2], and the regional elastic moduli were found to be between 680 Pa and 1.3 kPa. Finally, taking advantage of the real-time capability of our method, the change in the elastic properties was monitored during focused ultrasound (FUS) ablation of ex-vivo tissues. In this experiment, the intensity of the focused ultrasound beam was 948.23 W/cm^2 at the focus, in order to simultaneously generate the harmonic radiation force, and the tissue temperature variation and ablation. A decreasing slope of the oscillatory displacements was observed with time due to the change in the speed of sound temperature. Based on the harmonic displacements, their temperature-dependence, and the calculated acoustic radiation force, the change in the regional elastic modulus was monitored during heating. In conclusion, the feasibility of using an AM radiation force for harmonic motion imaging for simultaneous monitoring of tissue elasticity variation

during ultrasound therapy was demonstrated in phantoms and tissues in vitro. Further study of this method will include stiffness and temperature mapping, ex vivo and in vivo.

[1] Konofagou EE, Hynynen K., Ultras Med Biol; 29(10), 1405-1413 (2003).

[2] Krouskop, T., et al., Ultrasonic Imaging 20, 260-274 (1998).

This study was supported by a Special Development Award from the Whitaker Foundation.

2A-2 11:45 a.m.
RECONSTRUCTION OF THERMAL PROPERTY DISTRIBUTIONS - THERMAL CONDUCTIVITY, DIFFUSIVITY, CAPACITY.

C. SUMI* and H. YANAGIMURA, Sophia University, Tokyo, Japan.
Corresponding e-mail: c-sumi@sophia.ac.jp

For various soft tissues, we are developing the ultrasonic strain measurement-based mechanical properties (shear modulus, Poisson's ratio, density) reconstruction/imaging technique. On human *in vivo* liver, and breast etc., we reported the effectiveness as a differential diagnosis technique and a monitoring technique of low invasive therapies such as chemotherapy, cryotherapy, and thermal therapy. On these tissues, we also confirmed the inhomogeneity of thermal-elasticity, for instance, between parenchyma and blood vessels [Trans. on UFFC. (in press)]. Then, we proposed to reconstruct thermal properties such as thermal conductivity, thermal diffusivity, and thermal capacity [1] in addition to these mechanical properties for diagnosis and treatment (planning). Temperature can be measured by ultrasonic imaging and MRI. Provided that the reference values of thermal properties are given in the ROI, by solving the simultaneous first order PDEs (heat transfer equations) having heat fluxes as inhomogeneous coefficients, we can determine the thermal properties distributions. To stabilize reconstruction, regularization is simultaneously applied to each thermal property distribution.

The feasibility was confirmed through simulations and phantom experiments. In simulations, the 3D techniques were evaluated using a cubic phantom (50 mm sides, 36 degrees centigrade) containing a central spherical region (dia., 10 mm) which had twice as high conductivity k and specific heat c as those of the surrounding medium, i.e., 1.0 vs. 0.5 W/(m K), and 8,400 vs. 4,200 J/(K Kg). The density ρ was uniformly 1,000 Kg/m^3. The temperature of the one surface was changed by 12 degrees centigrade in step. The time series of temperature distribution were calculated by the successive over relaxation method. Two cases are considered, i.e., Case 1: two pairs of subsequent temperature distributions of different time were used; Case 2: two paired subsequent temperature distributions having opposite heat fluxes were used. In both cases, the thermal properties were quantitatively reconstructed. Evaluated mean values (spherical region) of thermal properties are shown in table.

For the phantom experiments, an agar phantom was used (3.87 percent; height, 50 mm). A cylindrical inhomogeneous region (dia., 15 mm) was made at the

depth 25 mm using small amount of copper powder. Temperature was measured using our previously developed phase matching method [Trans. on UFFC., vol. 46, pp. 158-166, 1999] by measuring generated strains due to thermal effect [Ebbini]. The phantom was heated by hot water from below side. The inhomogeneous region was detected in respective images of thermal conductivity, diffusivity, capacity [mean value (6.5×5.8 mm) vs. ref. value: conductivity, 0.700 vs. 0.625 W/(m K); diffusivity, 2.20 vs. 1.49×10^{-7} m^2/s; capacity, 3.18 vs. 4.20×10^6 $J/(m^3 K)$].

The demonstrated ability of reconstruction in simulations and phantom experiments is concluded to confirm the potential value of the developed robust reconstruction method.

[1] Sumi, Proc Int Conf on the Ultrason Meas and Imag of Tissue Elasticity, p. 73, 2004.

Evaluated mean values of thermal properties (spherical region).

Case	k [W/(m K)]	rc (´ 10^6) [$J/(m^3K)$]	k/rc (´ 10^{-7}) [m^2/s]
Original	1.00	8.40	1.19
1	1.01	8.59	1.18
2	1.05	9.01	1.17

2A-3 12:00 p.m.
DYNAMIC SIGNAL ARRIVAL CORRECTION FOR VIBRO-ACOUSTOGRAPHY IMAGE FORMATION.

M. URBAN* and J. GREENLEAF, Department of Physiology and Biomedical Engineering, Mayo Clinic College of Medicine, Rochester, MN.
Corresponding e-mail: urban.matthew@mayo.edu

Background: Vibro-acoustography is a recently developed method that uses the radiation force of ultrasound to locally excite an object. Images are formed from the resulting acoustic emission measured by a hydrophone that is in close proximity to the excitation site. In current image formation techniques, we calculate a pixel's value by first applying a static temporal window to the recording of the radiofrequency (RF) signal from the hydrophone, and then calculating some measure such as a root-mean-square of the windowed data. From our experience it has been found that the positioning of the hydrophone relative to the object can affect the overall image contrast because the acoustic emission has to travel a finite distance to the hydrophone from each excitation point. The most common way this artifact manifests itself is as a multiplicative illumination field across the image. **Methods:** To address this artifact a new algorithm has been devised that estimates the relative time delay to the hydrophone for each pixel in the image using an approach based on the Hough transform. We use the shapes of the wavefronts of the acoustic emission data to estimate correction angles for two spatial dimensions, denoted as θ_y and θ_z. Using these two angles,

we create a time delay image that allows us to adjust the location of the temporal window applied to the RF signal in a dynamic fashion. The algorithm finds the maximal response of the acoustic emission data and centers the window about that response and performs the delay correction for each pixel. **Results:** The algorithm has been tested using computer phantoms by varying θ_y and θ_z in the ranges $-65° \leq \theta_y \leq 65°$ and $-65° \leq \theta_z \leq 65°$ in 5° steps, and results show that the mean squared error for the reconstruction using the dynamic window is in almost all cases (98.4%) better than the reconstruction using the static window. Image results will be shown from breast phantom and *in vivo* breast data. The corrected images of the breast phantom show improved contrast of lesions because of the reduction of the multiplicative illumination field. The contrast in the images is calculated using $1/N \, S \, I^{\beta}(m,n)$ where $\beta = 2$ and N is the number of pixels in the image. For breast phantom data, images formed using the dynamic window compared with images formed with different static windows used in current practice show improvement in the image contrast. The percent difference in contrast ranges from 12% to 200%. In *in vivo* data, the contrast improvement in terms of percent difference ranges from 1% to 52%. **Conclusions:** This method correctly chooses the segment of the acoustic emission data to process so that the data is consistent from pixel to pixel despite finite differences in propagation time to the hydrophone. Results using simulated and real data show that image contrast and overall image quality is improved with this algorithm.

This study was supported in part by grants EB002640 and EB002167 from the National Institutes of Health.

2A-4 12:15 p.m.
EVALUATION OF ARRAY SIGNAL PROCESSING METHODS TO ULTRASOUND-BASED ARTERIAL PULSE WAVE VELOCITY MEASUREMENTS ON *IN VITRO* AND *IN VIVO* DATA.

A. DENTINGER*, R. HOCTOR, and K. THOMENIUS, GE Global Research, Niskayuna, NY.
Corresponding e-mail: dentinge@crd.ge.com

The authors have recently developed a model-based signal processing approach to ultrasound PWV estimation and have shown that this method mitigates the effect of arterial reflections on simulated data [1]. Initial application to *in vivo* data produced PWV estimates that were in the proper physiological range but with estimation variances of 30-40%. The present paper investigates modifications to the method to reduce estimation variance for real data, and it describes physical experiments that were conducted to evaluate the new methods.

To perform the experiments, a test ultrasound probe was constructed consisting of six 10 MHz phased arrays, aligned so as to form parallel image planes, and connected in a single cable assembly with multiplexing electronics. A GE Vivid 7 ultrasound scanner was used to control the probe, enabling interleaved color M-mode data to be collected from the six arrays. The data was processed off-line to produce waveforms corresponding to the vessel's rate of distension. A

test tank utilizing a latex tube as a simulated artery was constructed to investigate the sensitivity of the PWV estimation to reflection geometry.

Two PWV estimation methods were evaluated: the least-squares approach described in [1] and one based on eigenanalysis of the spatial covariance matrix of the ultrasound data: the well-known MUSIC algorithm [2,3]. For both methods, the broadband waveforms must be decomposed using the DFT and the PWV estimated for a range of frequency components. A quality metric was developed to automatically combine estimates from the individual frequencies and this led to a reduced variance of the broadband estimates, as compared to the previous trimmed mean approach [1]. The MUSIC method also produced a reduction in the variance when multiple cardiac cycles were used in forming the sample covariance matrix. Misalignment of the ultrasound beam was identified as a source of error, and the impact of amplitude distortions in the distension waveforms from a time-varying Doppler angle was investigated in the test tank and with simulation. It was found that some of the loss in performance due to misalignment could be recovered using amplitude equalization.

In vivo data was acquired on the common carotid artery for subjects in a reclining position. The PWV algorithms were applied and a PWV was estimated for each cardiac cycle. The mean PWV values were in the physiologic range and the estimation variance within the individual data sets was reduced to 5-10%, as compared to previous results [1].

[1] R.T. Hoctor, A.M. Dentinger, and K.E. Thomenius, “Signal processing for ultrasound-based arterial pulse wave velocity estimation,” *Proc. IEEE Ultrasonics Symposium*, vol. 2, pp. 1492-1497, 2004.

[2] R.T. Hoctor, A.M. Dentinger, and K.E. Thomenius, “Array signal processing approaches to ultrasound-base arterial pulse wave velocity estimation,” to be published in *Proc. of 2005 IEEE ICASP*.

[3] D. H. Johnson and D. E. Dudgeon, *Array Signal Processing: Concepts and Techniques*, Prentice Hall: Englewood Cliffs, NJ, 1993.

2A-5 12:30 p.m.
WAVELET TRANSFORM-BASED STRAIN ESTIMATION FOR ELASTOGRAPHY.

L. XU* and J. BAMBER, Joint Department of Physics, Institute of Cancer Research and Royal Marsden NHS Trust, Sutton, Surrey, UK.
Corresponding e-mail: lijun.xu@icr.ac.uk

Background: Elastography is an established method for imaging soft tissue relative strain. Published strain estimators can be divided into two categories: direct and indirect. Indirect estimators first measure tissue displacement and then calculate the strain as the gradient of the displacement. Calculating the gradient amplifies the noise in the measured displacement. Published indirect strain estimators have tended to reduce this by averaging the gradient over time (using many compressions) or space (from a fitted equation, e.g., the least-square (LSQ) method), trading temporal or spatial resolution for improved strain SNR and CNR. We are describing a WT-based approach to indirect strain estimation and evaluate whether it offers improved spatial and contrast resolution.

Method: In the new approach, the wavelet transform has been used to split the displacement image into two spatial bands: an approximate image, which contains the coarse scale information with less noise, and a detail image, which contains fine details of the original image and most of the noise. An approximate strain image is obtained by applying a gradient operator to the approximate displacement image. A detail strain image is obtained by thresholding the detail displacement image followed by a gradient operator. The final strain image is then reconstructed from the approximate and detail strain images. In this approach, only the noise in the approximate displacement image has been amplified by the gradient operator, while the noise in the detail band has been cancelled through wavelet thresholding. Wavelet thresholding has also been implemented into several scales to obtain high SNR and CNR while still retain sharp boundary details of the inclusion.

Results: Zero mean white noise was added to a simulated displacement image obtained by integrating the strain in a homogeneous soft background containing a stiff inclusion of circular cross-section. The strain values in the background and the inclusion were 0.02 and 0.015. Strain images obtained using the direct gradient, LSQ and new estimators were compared. The LSQ estimator (window size 5) produced SNR and CNR values (18.4dB & 9.8) smaller than those obtained using the new estimator (19.0dB & 11.3), and both were substantially better than values obtained with the direct gradient estimator (16.3dB & 8.5). The new estimator, however, retained many of the sharp boundary details of the inclusion that were blurred by the LSQ estimator. Similar observations have been made from tests using real echo data, obtained whilst straining gelatine phantoms that contain stiff spherical inclusions. Another merit of the new approach is that it is much faster than the LSQ method ($\times$2.1 for a 100$\times$100 image and $\times$13 for a 500$\times$500 image).

Conclusion: Wavelet transform-based strain estimation methods hold potential for enhancing contrast, spatial or temporal resolution in elastography. Further work is required to explore alternative approaches to taking advantages of the properties of the wavelet transform, and to determine whether potential concerns, e.g., those arising from noise retained at sharp boundaries, represent disadvantages.

2A-6 12:45 p.m.
ULTRASOUND ELASTOGRAPHY OF RECONSTRUCTED CLEFT LIPS.

C. L. DE KORTE*[1], N. VAN HEES[2], W. F. HUYSKENS[2], G. WEIJERS[1], C. KATSAROS[2], and J. M. THIJSSEN[1], [1]Clinical Physics Laboratory, UMC St Radboud, Radboud University Medical Center, Nijmegen, The Netherlands, [2]Department of Orthodontics and Oral Biology, Radboud University Medical Center, Nijmegen, The Netherlands.
Corresponding e-mail: cldekorte@ieee.org

Background: Evaluation of the reconstruction of a cleft lip is occasionally done by MRI. We have undertaken a study to assess the potentials of ultrasound imaging for this purpose, and more in particular of ultrasound elastography. Using conventional ultrasound, different structures of the lip are visible. The

superficial epidermal layer yields a clear thin echo border and the connective tissue of the lip returns relatively bright echo values, whereas the deeper laying muscles e.g., m. orbicularis oris) are characterized by low intensity echo levels. In a cleft lip, the opposing sides of the interrupted muscle are connected during a surgical intervention. In most of the cases, scar tissue will be formed. The amount of scar tissue and its position are related to functional and aesthetic aspects.

Methods: In this study, elastography is used to identify the presence and the amount of scar tissue in reconstructed cleft lips, as well as to investigate the functionality of the muscle. Elastograms of patients (2) and normal individuals (2) were determined. Rf-data were acquired using a Philips SONOS 7500 live 3D ultrasound system, equipped with an L11 (3-11 MHz) linear array transducer and rf-interface. During the acquisition, the subject was asked to contract the lips by making a “kissing movement”. The data were stored in a computer for off-line processing. Cross-correlation analysis was used to calculate the strain along the ultrasound lines. The strain was determined between frames that were successively acquired in order to keep strain values under 1%.

Results: The strain images of the normal volunteers show a layered structure. The superficial layer is compressing up to 1% while the deeper laying muscle is expanding up to 1%. This expansion is caused by the contraction of the muscle. The compression of the superficial layer is caused by passive stretching due to the pressure of the contracting muscle. Since, the ultrasound lines are perpendicular to the contracting muscle, an expansion is observed. In patients, the original position of the cleft can clearly be distinguished by an interruption in the expanding muscle region indicating scar tissue: this scar tissue region is compressing rather than expanding. On the elastogram a larger scar region can be observed compared to the area indicated in the normal echogram. In the normal echogram, the scar tissue can be observed in the superficial tissue but not always in the muscle layer.

Conclusion: Elastography of cleft lips is feasible and yields information that is additional to the information from conventional ultrasound images. Different contraction patterns in normal and cleft lips are found. The scar tissue can be differentiated from the muscle since compression in stead of expansion is observed. Further validation is required to demonstrate that elastography is an adequate technique to routinely evaluate cleft lip reconstructions.

Session: 3A

BIOSENSORS
Chair: J. Vetelino
University of Maine

3A-1 11:30 a.m.
(Invited)

NOVEL ACOUSTIC BIOSENSORS.

C. R. LOWE*, A. C. STEVENSON, B. ARAYA-KLEINSTEUBER, R. SETHI, and E. KIOUPRITZI, Institute of Biotechnology, University of Cambridge, Tennis Court Road, Cambridge, CB2 1QT, UK.
Corresponding e-mail: c.lowe@biotech.cam.ac.uk

Acoustic biosensors offer a simple, cost-effective sensing platform that responds to a variety of interfacial phenomena, such as DNA hybridisation, antigen-antibody binding and ligand-protein interactions. This lecture will describe a number of approaches to using acoustic principles for sensing applications. Early work involved investigating the sensing properties of surface skimming bulk waves (SSBW). However, it became clear that whilst these sophisticated devices were useful for monitoring biological interactions, they were too expensive to compete with conventional medical diagnostics technologies. The ability to reduce the costs of fabrication of acoustic sensor technology, whilst retaining the substantive advantages of general applicability and ease of use became a major research target. One way to achieve this with acoustic devices was to use less expensive, non-piezoelectric, substrates and eliminate all microfabrication steps, by using remote excitation. This thinking led to the exploitation of magnetic direct generation for the non-contact excitation of acoustic waves in glass plates and an approach for substantially improving the transduction efficiency that utilises continuous wave resonances and thin film generation. These devices use glass plates coated with thin films of aluminium to create free-standing acoustic resonance cavities with high transduction efficiencies and Q factors.

The enhanced magnetic direct generation concept was evolved into a new strategy for chemical sensing based on frequency tunable acoustic devices, the so-called magnetic acoustic resonator sensor (MARS). The device comprises a circular 0.5mm-thick resonant plate fabricated from a variety of non-piezoelectric materials and coated on the underside with a 2.5μm-thick aluminium film. Harmonic radial shear waves over several orders of magnitude frequency range can be induced in the resonant plate by enhanced magnetic direct generation using a non-contacting RF coil and an NdFeB magnet. In a further refinement, a planar spiral coil has been used to induce hypersonic evanescent waves in a quartz substrate with the unique ability to focus the acoustic wave down onto the biorecognition layer. These special sensing conditions were achieved by applying an RF current to a coaxial waveguide and spiral coil, such that wideband repeating electrical resonance conditions could be established over the MHz-GHz frequency range. At an operating frequency of 1.09 GHz, the evanescent wave depth of a quartz crystal hypersonic resonance is reduced to 17 nm, approximately the same as the thickness of a single IgG monolayer, and minimising unwanted coupling to the bulk fluid. The technique has been exploited

to generate a novel bioanalytical technique based on multifrequency acoustic devices, the so-called acoustic spectrophonometer, which develops the concept of the acoustic "fingerprint". In addition, the remote acoustic spectroscopy (RAS) system aims to enhance the characteristics of MARS by reducing the size of the sensing element and making it accessible to electromagnetic interrogation over greater distances (several centimetres) such that it can operate as a truly remote sensing element that is the unique in requiring no antenna, metallization or circuitry, whilst providing MHz-GHz spectroscopic measurements. This simple format lends itself well to biochemical measurements in immersed or subcutaneous samples.

3A-2 12:00 p.m.
A LATERAL FIELD EXCITED ACOUSTIC WAVE BIOSENSOR.

C. YORK*, P. MILLARD, L. FRENCH, and J. VETELINO, University of Maine, Orono, ME.
Corresponding e-mail: chrisjyork@hotmail.com

The rapid sensitive detection of biomolecules, microorganisms and cells is critical to human, animal, and plant health along with food and environmental safety. Available detection techniques such as enzyme-linked immunosorbent assays (ELISA) have high sensitivity but require the acquisition of discrete samples and excessive lab personnel time. The AT quartz crystal microbalance (QCM) offers *in situ* measurements with real time continuous sampling and detection, however the QCM has limitations. The QCM has a gold electrode on the sensing surface to which film overlays must be attached. This electrode prevents the electrical fields associated with the transverse shear mode (TSM) from penetrating the receptor layer. Hence, electrical property changes due to the attachment of a target entity will not be sensed. Recently a lateral field excited (LFE) sensor has been developed [1] which has a bare sensing surface allowing the measurement of electrical property changes in a target analyte selective film. In the present work the LFE sensor is evaluated as a biosensor and the sensor properties are compared to those obtained using a QCM biosensor. The target biological entity is goat antibody directed against rabbit IgG. In order to attach the appropriate film overlays to the LFE and the QCM surfaces an NH_2 bridge moiety is used. This is done through a 45-minute vacuum gas-phase silanization reaction for the LFE and an 8-hour liquid-phase incubation for the QCM. The following biological layers are added: NHS-LC-LC-biotin, NeutrAvidin™, and biotinylated rabbit IgG, which selectively binds the target goat anti-rabbit IgG antibody. Compared to the QCM the LFE exhibited a greater sensitivity and quicker response times to each addition. For example, the LFE resonant frequency shift was over 100% greater than the QCM's shift for the NeutraAvidin™ incubation and for a saturation target concentration the LFE responds 33% faster than the QCM. Finally, tests were performed to determine the sensing surface ensonification area. In the LFE sensor, this area is about 10 times smaller than in the QCM. This leads to the possibility of fabricating an array of sensors on a single wafer. In conclusion the improved sensing properties of the LFE biosensor compared to the QCM biosensor, the simplicity of the LFE sensor structure, and the possibility of realizing a sensor array on a single

substrate, makes the LFE sensor attractive for a wide range of biosensing applications.

**This work is supported by the National Science Foundation under grant 0330100*

3A-3 12:15 p.m.
SHEAR MODE ALN THIN FILM ELECTROACOUSTIC RESONATOR FOR BIOSENSOR APPLICATIONS.

G. WINGQVIST*, J. BJURSTRÖM, and I. KATARDJIEV, Uppsala University, Uppsala, Sweden.
Corresponding e-mail: gunilla.wingqvist@angstrom.uu.se

MOTIVATION The thin film electroacoustic technology has made substantial progress in recent years and is currently used industrially for the fabrication of high frequency telecom components. The high frequency of operation makes such devices suitable for the fabrication of low cost highly sensitive electroacoustic sensors. Typical biosensor applications, however, require that the sensors be operated in liquid media and hence shear mode operation is preferred due to lower losses than the longitudinal mode. The difficulty, however, of growing films with a tilted c-axis hinders their use for the fabrication of shear mode resonators. Often the longitudinal mode is therefore used resulting in high losses in liquids[1,2]. A process for the deposition of highly textured thin AlN films with a non zero mean tilt of the c-axis has recently been developed [3,4].

RESULTS Highly textured thin piezoelectric AlN films with a 30 degrees mean tilt of the c-axis relative to the surface normal have been synthesized on standard 4″ Si wafers with reactive sputtering of an Al target in an Ar/N_2 gas atmosphere. The films have been subsequently used to fabricate for the first time shear mode AlN thin film electroacoustic resonators suitable for operation in liquid media. Classical thin film bulk acoustic resonators (FBAR) with a cavity isolation from the Si substrate have been designed and fabricated using these films. The isolation cavity together with a microfluidic transport system were then formed by etching the Si substrates from the back and top side respectively using a standard Bosch deep Si etch process. The resonator electrodes were made of 200 nm thick Al while a 80 nm thick Au film was subsequently deposited onto the back side of the bottom electrode through the isolation cavity. The latter was finally sealed by gluing a suitable planar substrate to the back side of the Si wafer. The impedance of the resonator thus fabricated was characterised using a HP 8720D network analyzer when operated in air, pure water as well as in varying concentrations of glycerol. The electromechanical coupling of the shear mode was found to be around 1%. The resonator exhibited a Q value of around 300 in air and around 150 in water at a series resonance of about 1.2 GHz. The sensor performance in viscous media was then characterised when operating in contact with different concentrations of glycerol. The glycerol concentration was varied in the range 0 to 64 vol% causing a decrease in Q from 150 down to 70 and a decrease in series resonance with 2.3 MHz. The latter decrease follows the linear relationship with the square root of the viscosity predicted by Kanazawa et al.

[1] Brederlow, R. Biochemical sensors based on bulk acoustic wave resonators, IEDM 03, p. 992-994, 2003.

[2] Zhang, H. Implantable Resonant Mass Sensor For Liquid Biochemical Sensing, MEMS 04, p. 347-350, 2004.

[3] Bjurstrom, J. IEEE Transactions on Ultrasonics, Ferroelectrics and Frequency Control, v 51, n 10, p 1347-53, Oct. 2004.

[4] Bjurstrom, J et al. To be published.

3A-4 12:30 p.m.
A LANGASITE SH SAW O157:H7 *E. COLI* SENSOR.

E. BERKENPAS*, P. MILLARD, and M. PEREIRA DA CUNHA, University of Maine, Orono, ME,.
Corresponding e-mail: mdacunha@eece.maine.edu

The toxigenic *E. coli* O157:H7 bacterium has been connected with hemorrhagic colitis and hemolytic uremic syndrome, which may be characterized by diarrhea, kidney failure, and death. On average O157:H7 causes 73,000 illnesses, 2,100 hospitalizations, and 60 deaths annually in the United States alone. Current methods for the detection and identification of pathogenic *E. coli* typically involve laboratory analyses which are often implemented only after symptomatic illness has been identified. Sensors capable of detecting bacteria rapidly in the field are needed to provide early warning of the presence of these and other dangerous microbes in food and water supplies, with the goal of limiting the exposure of human and animal populations.

Recent research has explored electrochemical, thermal, optical, and acoustic wave techniques for biosensing. Acoustic wave biosensors, in particular, can provide a potentially high sensitivity method for bacterial detection that does not require extrinsic molecular labels. Previous work by the authors used shear horizontal surface acoustic wave (SH SAW) devices fabricated on langasite (LGS) Euler angles (0° 22° 90°) to successfully detect macromolecular protein assemblies. The devices also demonstrated favorable temperature stability, biocompatibility, and low attenuation in liquid environments, suggesting their applicability to bacterial detection.

In this paper, a biosensor test setup utilizing a small volume fluid injection system, stable Peltier temperature control, and high frequency phase measurement is reported, which confirmed the LGS SH SAW device applicability as a bacterial sensor. Delay lines were fabricated and derivatized with a rabbit polyclonal IgG antibody, which selectively binds to *E. coli* O157:H7, in this case a nontoxigenic test strain. To quantify the effect of nonspecific binding (negative control), an antibody directed against the trinitrophenyl hapten (anti-TNP) was also used as a binding layer. Test *E. coli* bacteria were cultured, fixed with formaldehyde, stained with SYTO 13 cell-permeant nucleic acid stain, suspended in phosphate buffered saline, and applied to the antibody-coated sensing surfaces. The biosensor phase of the transmission coefficient ($\angle S_{21}$) was monitored using an Agilent 4396B Network Analyzer to verify the binding of *E. coli* to the anti-O157:H7 antibody. Phase responses of about 14° were measured for the *E. coli* detection, as compared to 2° measured for non-specific anti-TNP binding. Fluorescence

microscopy was used to confirm the selectivity of the antibody surface, indicating a 30:1 *E. coli* binding to the anti-O157:H7 layer when compared to the anti-TNP layer. Bacterial tests were repeated 10 times for both antibody receptors, proving the utility of the antibody-coupled LGS SH SAW device as a selective and sensitive biosensor for *E. coli* O157:H7.

This work was conducted with support from the National Science Foundation (grants ECS-0329913, ECS-0233463, ECS-0134335 and DGE-0139324).

3A-5 12:45 p.m.
MONITORING THE BLOOD COAGULATION PROCESS WITH QCM AND SH-SAW SENSORS.

G. GUHR*, R. KUNZE, G. MARTIN, H. SCHMIDT, and M. WEIHNACHT, Institute for Solid State and Materials Research Dresden, Dresden. Saxony, Germany. Corresponding e-mail: g.guhr@ifw-dresden.de

Blood coagulation time is an important parameter for medical diagnostics of hemostasis. It is also necessary to control blood coagulation during operations and after mechanical heart valve replacement. There is a demand for new, fast, inexpensive and easily applicable measuring methods for these purposes. SAW devices, which are very sensitive to changes of viscosity and other parameters of an adjacent fluid, are capable of meeting these challenges. Before studying the SH-SAW interactions with blood we started with the simpler experimental configuration of the QCM technique using thickness shear mode (TSM) resonators in order to gain a thorough view of the main influences on measuring signals. Besides this, we could also rely on published results of TSM investigations on blood coagulation [1,2]. In the current work, it was discovered that the coagulation process is detectable with all resonator parameters such as resonance frequency, quality factor, impedance response. The best measurement conditions were obtained using a specially constructed cylinder which forms an encased, 0.3 mm thick, disc of blood or plasma lying on top of the TSM resonator electrode. Vaporizing and drying effects causing noisy frequency curves vs. time were suppressed by using this method. Typically, the TSM resonance frequency varies sigmoidally with time during the coagulation process due to the viscosity change of the plasma. Therefore the minimum of first derivative of that curve seemed a suitable definition of coagulation time and was in fact in good agreement with conventional methods for both medically relevant tests such as Quick and activated partial thromboplastin time (aPTT). Investigations have been carried out on human plasma diluted to 15 percent showing a clear relationship between fibrinogen content and change of TSM resonance frequency during coagulation. Next, the smallest plasma volume obtainable under pipet experimental conditions (5 microlitres) was found to give usable signals. Further TSM investigations were extended to higher resonance frequencies for achieving typical SAW frequencies. Starting from the fundamental resonance (9 MHz) the coagulation process could also be measured at the 27th harmonic (243 MHz). The deficiency of the quality factor at high harmonics of TSM measurements was irrelevant in the case of subsequent SAW studies at comparable frequencies. Tests with SH-SAW frequency resonator filters on 36°rotYX-LiTaO3 substrates at 168 MHz mounted in housings resulted in a three

times higher fractional change in frequency compared to TSM experiments. Special attention was paid in avoiding electrolytic corrosion of Al layers due to fluidic contact with noble metal electrodes. We have demonstrated by our investigations, that SH-SAW resonator filters can successfully be used for the detection of blood coagulation.

[1] H.L. Bandey et. al.; Biosensors and Bioelectronics 19 (2004) 1657-1665

[2] H.-C. Chang et. al.; Sensors and Actuators B 66 (2000) 296-298

Session: 4A

PHONONIC CRYSTALS
Chair: J. Brown
JB Consulting

4A-1 11:30 a.m.
APODIZED PHONONIC CRYSTALS.

Y. NELIN*, National Technical University of Ukraine, Kyiv, Ukraine.
Corresponding e-mail: ye_nelin@rtf.ntu-kpi.kiev.ua

Phononic crystals (PC) noticeably improve on parameters of signal processing devices. Phononic band gap formation can be understood as a synergistic interplay between two distinct resonance scattering mechanisms - the microscopic resonance from a single unit cell of the PC and the macroscopic resonance from the geometrical arrangement of repeating unit cells. For requirement characteristics achievement PC apodization is necessary. Such apodization is fulfilled by changing amplitude or (and) phase conditions for locally reflected waves. Under amplitude apodization geometrical periodicity remains, under phase apodization periodicity of the elastic parameters remains.

In this paper we propose two effective methods of apodization - the edge amplitude one and the phase one. Under edge apodization it is necessary to modify cell's parameters only nearby the PC ends. Such locally confined apodization is constructively and technologically noticeably easier than the usual apodization distributed along PC. Three variants of phase apodization are proposed.

The methods are based on cell's parameters control in accordance with the model of the PC's cell/PC's structure interplay. For PCs' analysis the transition line model is used. A comparison of transduction/reflection characteristics of conventional and new designs shows accuracy of the models and noticeably selectivity improvement.

4A-2 11:45 a.m.
IMAGING OF PROPAGATING SURFACE ACOUSTIC WAVES ON PHONONIC CRYSTALS.

D. M. PROFUNSER*, O. B. WRIGHT, and O. MATSUDA, Graduate School of Engineering, Hokkaido University, Sapporo, Hokkaido, Japan.
Corresponding e-mail: dieter@profunser.com

We present the imaging in real time of surface acoustic waves propagating on phononic crystals made up of periodic microstructured patterns. The experiments are performed by ultrashort pulsed optical excitation and detection of the acoustic waves combined with interferometric detection. We obtain images with picosecond temporal and micron spatial resolution. Such a series of images in the time domain gives direct access on Fourier transformation to the complete dispersion relation of the propagating surface acoustic waves.

We first present animations of surface acoustic waves scattered by a one-dimensional periodic pattern made up of copper lines of micron-order in width that are embedded in silicon oxide. This structure is supported by a silicon substrate. The two-dimensional dispersion relation of the surface acoustic waves is analysed and compared to a simple model for propagation perpendicular and parallel to the line pattern. In addition we present animations of surface acoustic waves scattered in a periodic, microstructured two-dimensional copper dot array.

This work should lead to a better understanding of phononic crystals and surface acoustic wave devices based on them.

4A-3 12:00 p.m.
HYPERSONIC BAND GAPS IN TWO-DIMENSIONAL PIEZOELECTRIC PHONONIC CRYSTAL SLABS.

A. KHELIF*[1], B. AOUBIZA[2], S. MOHAMMADI[3], A. ADIBI[3], and VINCENT LAUDE[1], [1]Institut FEMTO-ST, Département LPMO, CNRS UMR 6174, Besançon cedex, France, [2]Laboratoire de mathématiques, UMR 6623, Université de Franche-Comté, Besançon, France, [3]School of Electrical and Computer Engineering, Georgia Institute of Technology, Atlanta, GA.
Corresponding e-mail: abdelkrim.khelif@femto-st.fr

The propagation of elastic waves in inhomogeneous media has attracted a lot of attention over the last years. More recently there has been a growing interest in a special type of inhomogeneous materials, the so-called phononic crystal, whose elastic coefficients vary periodically in space. The interest in theses materials arises mainly from the possibility of having frequency regions, known as absolute phononic gaps, over which there can be no propagation of elastic waves, whatever the polarization and wave vector. There are potential applications in the realization of perfect mirrors, the confinement of acoustic energy in defect modes, and the fabrication of very efficient waveguides. All these functions can be achieved in a very tight space of the order of some acoustic wavelengths.

In this paper, we analyze the propagation of acoustic waves in a phononic crystal slab consisting of metal inclusions placed periodically in a host piezoelectric

material. Our system is composed of a square lattice of tungsten (W) cylinders embedded in an Aluminium nitride (AlN) matrix. It is found that several full band gaps with a variable bandwidth exist for acoustic waves of any polarization and incidence. In addition to the filling fraction, a key parameter for the existence and the width of these full band gaps is the ratio of the slab thickness (h) to the lattice period (a). Especially, we have explored how these absolute band gaps close up and other band gaps appear as the parameter (h/a) increases. Significantly, it is found that the band gaps of a phononic crystal slab are distinct from those of bulk acoustic waves propagating in the plane of the plate and that they are strongly affected by the boundary conditions at both surfaces of the slab. The numerical calculations are performed using the finite element method with periodic boundary conditions derived using the Bloch-Floquet theorem.

4A-4 12:15 p.m.
CHANNEL DROP PROCESS OF ELASTIC WAVE IN A TWO DIMENSIONAL PHONONIC CRYSTAL.

Y. PENNEC*[1], B. DJAFARI-ROUHANI[1], A. KHELIF[2], A. CHOUJAA[2], J. VASSEUR[2], S. BENCHABANE[2], H. LARABI[1], and V. LAUDE[2], [1]LDSMM, Université de Lille1, Villeneuve d'ascq, France, [2]Institut FEMTO-ST, Département LPMO, Besançon, France.
Corresponding e-mail: abdelkrim.khelif@femto-st.fr

We study, both experimentally and theoretically, the transfer of acoustic waves between two waveguides created in a phononic crystal. The experimental setup is based on ultra-sonic immersion transmission technique and the theoretical calculation is made using finite difference time domain (FDTD) method.

The two-dimensional crystal is a square lattice of steel rods in water, with a 3 mm period and a filling fraction of 0.55. Due to the strong contrast between acoustic impedances, this phononic crystal exhibits an absolute band gap extending from 250 to 325 kHz [1]. A full transmission band within the absolute band gap of the perfect crystal is observed when a one period wide straight waveguide is created inside the phononic crystal [2]. Two such parallel waveguides can be coupled through a coupling structure exhibiting two perpendicular symmetry axes [3]. The coupling element is constituted of isolated cavities interacting with stubs located at the sides of the waveguides. The choice of this geometry is based on the fact that both an isolated cavity and a stub coupled to a waveguide display the same resonance frequency at f=290 KHz. From our geometry, we demonstrate that this single frequency at 290 kHz can be transferred from one waveguide to the other.

We are currently investigating possible improvements of the demultiplexing process by changing the size and the nature of the steel cylinders in the coupling element. More generally, we discuss the use of such devices for designing new acoustic or elastic filters and demultiplexers.

[1] A. Khelif, A. Choujaa, B. Djafari-Rouhani, M. Wilm, S. Ballandras, V. Laude, Phys. Rev. B 68, 0214301 (2003)

[2] A. khelif, A. Choujaa, S. Benchabane, B. Djafari-Rouhani, V. Laude, Appl. Phys. Lett. 84, 4400 (2004).

[3] S.Fan, P.R. Villeneuve, J.D. Joannopoulos, and H.A. Haus, Phys. Rev. Lett. 80, 960 (1998)].

4A-5 12:30 p.m.
ANALYSES OF SURFACE ACOUSTIC WAVE PROPAGATION IN PHONONIC CRYSTAL WAVEGUIDES USING FDTD METHOD.

J.-H. SUN* and T.-T. WU, Institute of Applied Mechanics, National Taiwan University, Taipei, Taiwan.
Corresponding e-mail: d89543002@ntu.edu.tw

Phononic crystals consisting of periodic elastic materials had been proved having a property of elastic wave band gaps. Some designs based on the band gaps of phononic crystals were reported, such as elastic wave filters, waveguides, and couplers. Most of the phononic waveguide researches are focused on the bulk acoustic waves, study of surface waves in phononic waveguide is awaited.

In this paper, we adopt the finite difference time domain (FDTD) method to analyze the surface acoustic waves propagating in two-dimensional phononic waveguides. To implement the FDTD program, the Bloch theorem and the absorbing boundary conditions are employed to deal with the periodic boundary condition and the reflection from the numerical boundary. A phononic crystal consisting of circular tungsten cylinders which form a square lattice in a silicon matrix is analyzed first. The dispersion relation is obtained by selecting the resonance frequency of a phononic crystal unit cell and the corresponding transmission coefficient is also calculated to verify to band gaps. The result shows the existence of a total band gap of surface waves and can be utilized to design acoustic waveguides. The eigenmodes of surface wave insides the waveguides are solved with the supercell method. The calculation results show a very confined propagation of the surface waves inside the waveguide.

The authors acknowledge the financial support of this research by the National Science Council of ROC (NSC 93-2212-E-002-025)

4A-6 12:45 p.m.
ANALYSIS OF WAVE PROPAGATION IN PHONONIC CRYSTAL WITH CHANNEL USING THE PLANE-WAVE EXPANSION AND SUPERCELL TECHNIQUES.

Z.-G. HUANG* and T.-T. WU, Institute of Applied Mechanics, National Taiwan University, Taipei , Taiwan.
Corresponding e-mail: huang@ndt.iam.ntu.edu.tw

In recent years, application of photonic crystals is an exciting topic in physics community. Successful application of photonic crystals has led to a rapidly growing interest in the analogous acoustic effects in periodic elastic structures called the phononic crystals. [1,2] In this paper, based on the plane-wave expansion method and the supercell technique, we analyze the defect modes and extended modes of two-dimensional phononic crystals. In addition, with the

supercell technique, the propagating modes of phononic band structures with acoustic channel are studied. The glycerin/mercury and vacuum/silicon band structures are the examples employed in this paper. Couplings of propagating modes and point defect modes are also investigated in phononic crystal with channel. From the calculated results, we can find that the defect modes and extended modes are obvious for not only the bulk acoustic waves but also the surface acoustic waves in phononic crystals. On the other hand, the mode shapes for different defect modes and propagating modes can also be expressed using the plane-wave expansion and supercell techniques. For suitable design, the acoustic filters and waveguides are the possible applications in the two-dimensional phononic crystals.

[1] Tsung-Tsong Wu, Zi-Gui Huang, and S. Lin, "Surface and bulk acoustic waves in two-dimensional phononic crystals consisting of materials with general anisotropy," Physical Review B 69, 094301 (2004).

[2] Zi-Gui Huang and Tsung-Tsong Wu, "Temperature effect on the bandgaps of surface and bulk acoustic waves in two-dimensional phononic crystals," IEEE Transactions on Ultrasonics, Ferroelectrics, and Frequency Control 52(3), 365 (2005).

The authors thank the National Science Council (NSC93-2212-E-002-025) of Taiwan for financial support. Zi-Gui Huang would like to thank Dr. Steven G. Johnson (MIT) for his valuable discussions.

Session: 5A

BAW THIN FILM FILTERS
Chair: R. Weigel
University of Erlangen-Nuremberg

5A-1 11:30 a.m.
A HIGH PERFORMANCE WCDMA HYBRID DIFFERENTIAL BAW FILTER.

C. MULLER*[1], M. A. DUBOIS[1], Y. UESHIMA[2], and K. TAKASUKA[2], [1]CSEM, Neuchatel, Switzerland, [2]AKM, Tokyo, Japan.
Corresponding e-mail: claude.muller@csem.ch

BAW technology has attracted more and more attention over the last few years because of its potential application in wireless communication systems[1-3]. The BAW technology is well suited to cover the 2 to 10 GHz frequency domain where it is destined to substitute the SAW devices. In this work, a BAW interstage differential filter for the Rx WCDMA band centred on 2.14 GHz has been designed, fabricated, packaged and characterised. The architecture of this filter is an hybrid combination of a ladder stage cascaded with a lattice stage [4]. The acoustic insulation of the resonators is made with a Bragg mirror (SMR). The specifications emphasized on a low insertion loss and a high rejection in the Tx band. Characterisation at the wafer level of the mixed-mode differential to differential

S21 parameter shows an insertion loss better than -1.8 dB over the 60 MHz bandwidth of the WCDMA reception band. The ripple over the band is 0.6 dB and VSWR is better than 1.93. The rejection in the Tx band is between -35 and -55 dB. A very close match is observed between measured data and electrical simulations. An RF characterisation of the filter in a ceramic package has also been performed. The packaging induces minor changes of the in-band behaviour while the out-of-band response remains practically unchanged.

[1] K. M. Lakin, "Thin Film Resonators and Filters," presented at IEEE Ultrasonics Symposium, Lake Tahoe, NV, 1999.

[2] R. Aigner, J. Kaitila, J. Ellä, L. Elbrecht, W. Nessler, M. Handtmann, T.-R. Herzog, and S. Marksteiner, "Bulk-Acoustic-Wave Filters: Performance Optimization and Volume Manufacturing," presented at IEEE IMS, Philadelphia, PA, 2003.

[3] R. C. Ruby, P. Bradley, J. Larson, Y. Oshmyansky, and D. Figueredo, "Ultra-Miniature High-a Filters and Duplexers Using FBAR Technology," presented at IEEE International Solid-State Circuits Conference, San Francisco, CA, 2001.

[4] H. K. J. t. Dolle, J. W. Lobeek, A. Tuinhout, and J. Foekema, "Balanced Lattice-Ladder Bandpass Filter in Bulk Acoustic Wave Technology," presented at IEEE MTT-S, Fort Worth, TX, 2004.

The authors would like to thank the CMI center at the EPFL in Lausanne, Switzerland for putting their equipment at their disposal.

5A-2 11:45 a.m.
ABOVE-IC FBAR TECHNOLOGY FOR WCDMA AND WLAN APPLICATIONS.

M.-A. DUBOIS*[1], C. BILLARD[2], J.-F. CARPENTIER[3], P. VINCENT[2], G. PARAT[2], and C. MULLER[3], [1]CSEM, Neuchâtel, Switzerland, [2]CEA-LETI, Grenoble, France, [3]ST Microelectronics, Central R&D, Crolles, France.
Corresponding e-mail: marc-alexandre.dubois@csem.ch

Miniature bulk acoustic wave (BAW) piezoelectric resonators are very promising devices for meeting the needs of modern wireless communication equipment. They can be used advantageously in RF systems operating between 1 and 10 GHz because they feature Q factors much higher than on-chip LC tanks, a large power capability, a low volume, a low cost, and a reasonable coupling coefficient. These properties are all essential when portability is at stake, since they contribute to a reduced power consumption and a greater compactness. Such resonators can be used to create passive high performance filters, or as resonant elements associated with an integrated circuit (IC) to provide specific electronic functions, such as voltage controlled oscillators (VCO) or low noise amplifiers (LNA).

BAW devices have a tremendous advantage over other technologies such as ceramic or surface acoustic wave filters, which is the possibility of being fabricated above integrated circuits, since their materials and thermal budget are compatible with a post-processing approach. Such a co-integration can reduce even further the size and the cost of high performance RF front-ends, and opens the way towards a SoC radio.

This paper describes an FBAR technology based on aluminium nitride which is fully compatible with post-processing above integrated circuits. This technology features low-loss interconnections between the electrodes of the FBARs and the metal lines of the BiCMOS integrated circuits. Resonators fabricated with this technology exhibit a coupling coefficient larger than 6.5 and 6 % respectively at 2.2 and 5.25 GHz, corresponding to WCDMA and WLAN frequency bands. Balanced lattice filters have also been designed and fabricated for these two applications, and are described in the paper. In particular a 60 MHz passband interstage filter designed for the RX chain of a WCDMA mobile phone features moderate insertion loss of -3dB and extreme out-of-band rejection (>-50dB). The latter has been integrated at the wafer level above a BiCMOS zero-IF RF front-end, and in a new type of filtering LNA comprising two broadband amplifiers around the BAW filter, hence demonstrating the feasibility of the above-IC FBAR technology for wireless applications.

This work has been supported by the Swiss Office for Science and Education and the European Commission under the IST-2001-37362 MARTINA project. Part of the processing has been realized at CMI-EPFL.

5A-3 12:00 p.m.
BAW COMPONENTS FOR PCS-CDMA APPLICATIONS.

E. SCHMIDHAMMER*, H. HEINZE, M. WOELKY, M. SCHMIEDGEN, G. HENN, R. BRAUN, and T. METZGER, EPCOS AG, Munich, Germany.
Corresponding e-mail: edgar.schmidhammer@epcos.com

Bulk Acoustic Wave (BAW) technology is highly investigated due to its silicon-based technology for further integration in the RF part of e.g. mobile phones. At the IEEE UFFC Symposium 2004 in Montreal EPCOS AG presented the very first results of a 3838 PCS BAW duplexer using solidly mounted resonator technology (SMR) mounted on a LTCC carrier and packaged using EPCOS' proprietary CSSPlus technology. The new designs show a significant improvement compared to the previous ones with respect to reduced overall losses. Within this one-year periode we have improved the electrical performance in several fields. In particular the temperature coefficient has been improved to be -15 ppm/K for the left skirt and -20 ppm/K for the right skirt, respectively. The broadband behaviour shows excellent attenuation. For the Tx-part we are well below 40 dB up to 4.2 GHz and better than 20 dB up to 6 GHz. Therefore second and third harmonics caused by the PA are well suppressed. In the Rx-part we achieve a value of better than 35 dB up to 5.5 GHz. The isolation is well below 50 dB for both paths (Rx-to-Tx and Tx-to-Rx). The presented duplexer shows full functionality and is almost spec-compliant.

Secondly we have designed single filters (PCS Rx and PCS Tx) using a 2016 HTCC package with standard landing area (footprint) as requested from the market and again using the CSSPlus packaging technology. The achieved process stability allows us meanwhile to present the full matrix of required filters for the design of PCS-CDMA mobile phones.

The Tx-single filter has an insertion loss of 3 dB and nearby selectivities of at least 35 dB on both sides. The Rx-band is attenuated minimum 35 dB. The matched filter has a VSWR of better than 1:1.5 (|S11| and |S22| better than -14

dB). The wideup selection is better than 30 dB up to 5.5 GHz, second harmonic range (3700 - 3840 MHz) is attenuated by at least 45 dB, and third harmonic range (5550 - 5750 MHz) is attenuated by at least 20 dB. The GPS-band is suppressed more than 32 dB, the corresponding Bluetooth-range band is attenuated more than 35 dB.

The Rx-filter has an insertion loss of 4 dB with a nearby selectivity of better than 40 dB on both sides. The Tx-band is attenuated minimum 42 dB. The matched filter has a VSWR of better than 1:2.1 (|S11| and |S22| better than -9 dB). Below the passband the attenuation is better than 38 dB. The Bluetooth-range is suppressed by more than 50 dB, up to 4 GHz the attenuation is better than 40 dB and up to 6 GHz the attenuation is still well below 35 dB.

The presented results show clearly our improvements within SMR-BAW technology. Our process flow using a 200 mm manufacturing line uses only the minimum required process steps by still keeping a high yield in combination with high process stability and high process robustness.

The authors wish to thank the whole EPCOS BAW group for their outstanding work and dedicated effort to make this technology work.

5A-4 12:15 p.m.
A MINIATURIZED FBAR DUPLEXER WITH REDUCED ACOUSTIC LOSS FOR THE W-CDMA APPLICATION.

J. TSUTSUMI*, M. IWAKI, Y. IWAMOTO, T. YOKOYAMA, T. SAKASHITA, T. NISHIHARA, M. UEDA, and Y. SATOH, Fujitsu Laboratories Ltd., Akashi, Hyogo,Japan.
Corresponding e-mail: tsutsumi.jun@jp.fujitsu.com

A miniaturized antenna duplexer for the W-CDMA application has been developed using the modified film bulk acoustic resonator (FBAR) structure and low-loss phase shifters.

Both the FBAR and SAW are the promising technologies for the development of antenna duplexers in the 2 GHz-range systems, such as the US-PCS and the W-CDMA. Although the authors have developed high-performance SAW duplexers for the US-PCS application, we have selected the FBAR technology for the W-CDMA duplexers because of the following two reasons. The first reason is that the W-CDMA system requires extremely low insertion loss with high attenuations, for example 1.5 dB and 2.0 dB for the Tx and the Rx band, respectively. This specification is so severe that it would seem to be beyond the capability of SAW filter technology in the 2 GHz range. The second reason is that the frequency separation between the Tx and the Rx band is relatively wide of 130 MHz, while it is as narrow as 20 MHz in the US-PCS system. This contributes to increase the tolerance of each film thickness, therefore, the FBAR duplexers can be fabricated with a high production yield.

As the required insertion loss is still severe for the FBAR technology, it is necessary to modify the FABR structure to minimize acoustic losses. It is known for the AlN based FBAR that the acoustic energy cannot be confined in the resonant region and leaks in the transverse direction. We proposed to pattern the AlN film along the resonant area to suppress the transverse leakage. It is

observed by the optical probing technique that the leakage was successfully decreased in the modified FABR structure. Also, Ru was selected as the electrode material and the thickness of AlN and Ru was optimized to reduce both the acoustic and the electrical resistive losses. By utilizing above modifications, a minimum insertion loss of fabricated 4-stage ladder type FBAR filter, which is designed for W-CDMA Tx filter, was reduced to 0.4 dB and the effective K2 reached as large as 7.4 %.

The duplexer circuit also has to be optimized to reduce the insertion loss. We have developed the compact and low-loss phase shifter using integrated lumped elements, instead of the distributed transmission line. This enables us to insert the phase shifter in not only the Rx side at the antenna port, but also in the Tx side to minimize the mismatch loss without increase of the duplexer size.

Two FBAR filter dies and the phase shifters were mounted in a 3 mm $\times$ 3 mm ceramic package to form a duplexer. The insertion losses of fabricated duplexers were as small as 1.3 dB and 1.6 dB in the Tx and the Rx band, respectively, with a high isolation between the Tx and the Rx port. In the presentation, the detailed design techniques and the experimental results will be discussed.

5A-5 12:30 p.m.
BULK ACOUSTIC WAVE RESONATORS AND FILTERS - 2D MODELLING AND INDUSTRIALIZATION ASPECTS.

F. VANHELMONT*[1], A. JANSMAN[1], J. RUIGROK[1], R. MILSOM[2], E. VAN DER SAR[3], P. HUISKAMP[3], G. DE BRUIN[3], F. DE BRUIJN[3], J.-W. LOBEEK[3], and A. TUINHOUT[3], [1]Philips Research Laboratories, Eindhoven, The Netherlands, [2]Philips Research Laboratories, Redhill, United Kingdom, [3]Philips Semiconductors, Nijmegen, The netherlands.
Corresponding e-mail: frederik.vanhelmont@philips.com

Bulk acoustic wave (BAW) resonators and filters have established a firm position for use in telecommunication applications at 1-10GHz. 1D models give a reasonable description of the device, appropriate for filter design. Nevertheless, to explain the full resonator and filter characteristics including ripple and insertion loss, the model is insufficient. It has been shown that they are caused by 3D effects associated with electrode edges. These include standing lateral waves inside the resonator and waves carrying energy away from the resonator, which can be modelled adequately in 2D. Various 2D analytical models have been published. Since the dominant behaviour is a 1D thickness extension mode, some of these models assume either that the component of particle displacement parallel to the film-surface can be ignored completely, or at least that the edge boundary condition on this component can be ignored. However, as will be shown in the present paper, lateral modes excited by the 1D electric field show considerable particle displacement in the direction parallel to the substrate surface too. If this is neglected, one can at best achieve a qualitative idea of the 2D effects. In this paper, a quantitative full 2D description developed at Philips Research, will be applied [1,2]. Particle displacement parallel to the surface is shown to be significant. Its effect on resonator admittance characteristics is presented for some real-life examples.

Furthermore the industrialization of the solidly mounted bulk acoustic wave filters within Philips Semiconductors will be discussed. The excellent performance (insertion loss < 2dB, 3dB bandwidth = 65MHz, strong out of band rejection) of processed USPCS filters on die level and completely packaged devices will be shown. Our wafer scale packaging technique will be illustrated and the reliability of the package will be demonstrated.

[1] Comparison of Mode-Conversion, Energy-Trapping and Lateral Acoustic Coupling in FBAR and SBAR, R.F. Milsom, H.-P. Löbl, F. Vanhelmont, A.B.M. Jansman, J-W. Lobeek, A. Tuinhout, 2005 IEEE International Microwave Symposium Proceedings, to be published.

[2] Narrow band Bulk Acoustic Wave Resonators and Filters, H.-P. Löbl, C. Metzmacher, R.F. Milsom, R. Mauczok, W. Brand, P. Lok, A. Tuinhout, F. Vanhelmont, 2004 IEEE Ultrasonics Symposium Proceedings, Vol. 1, p. 411-415.

5A-6 12:45 p.m.
LOW INSERTION LOSS, HIGH REJECTION HANDSET DUPLEXER FOR UMTS-1 WCDMA BAND.

D. FELD*, T. JAMNEALA, and C. WADE, Agilent Technologies, San Jose, CA. Corresponding e-mail: dave_feld@agilent.com

We have developed a duplexer based on thin film bulk acoustic resonator (FBAR) technology for the UMTS-1 WCDMA band (Tx: 1920 - 1980 MHz, Rx: 2110 - 2170 MHz). The worst case Tx-ANT and Rx-ANT insertion loss is typically better than 1.5 dB over an operating temperature range of

-30C to +85C. The typical out-of-band rejection and isolation over the same temperature range are as follows: Tx-ANT/ Rx-ANT rejection: 51/46 dB, Tx/Rx isolation 51/48 dB. The second harmonic rejection for both TX-ANT and RX-ANT is typically better than 20 dBs. The duplexer's low insertion loss and high rejection/isolation enables 3G handsets to operate with low transmit power and high receiver sensitivity in a small package size of 3.8 mm x 3.8 mm x 1.4 mm.

Real estate is at a premium in a 3G handset, given the large amount of hardware that is required for analog and digital signal processing, thus placing the FBAR duplexer at an advantage relative to that of ceramic duplexers which are capable of delivering similar RF performance but in a substantially larger package volume.

Although WCDMA duplexers designed using SAW technology occupy a similar volume to that of the FBAR duplexer, the high Q's of the FBAR resonators comprising the FBAR duplexer give the duplexer a favorable insertion loss - rejection (& isolation) tradeoff over that of SAWs.

We discuss the spec and size constraints, as well as the topologies that we considered that led us to arrive at our final design.

Session: 6A

HIGH FREQUENCY ARRAYS
Chair: S. Smith
GE Global Research

6A-1 11:30 a.m.
PERFORMANCE AND CHARACTERIZATION OF HIGH FREQUENCY LINEAR ARRAYS.

M. LUKACS*, J. YIN, G. PANG, R. GARCIA, E. CHERIN, R. WILLIAMS, J. MEHI, and F. S. FOSTER, Imaging Research, Sunnybrook & Women's College Health Science Centre, University of Toronto, Toronto, Ontario, Canada.
Corresponding e-mail: marc.lukacs@sw.ca

A new approach for fabricating high frequency (> 30 MHz) linear array transducers, based on laser micromachining, has been developed. The capabilities of this approach will be presented using several array devices based on a 30 MHz 64-element, 74-micron pitch design. Each fabricated array has been integrated onto a flex circuit for ease of handling and the flex has been integrated onto a simple custom circuit board for ease of testing.

Examples of measured characteristics of arbitrary array elements are as follows: Electrical impedance, measured in air, of about 100 Ohms with –40 degrees of phase without a lens, and about 160 Ohms with –46 degrees of phase with a lens. A transducer, with individual array elements having a thickness of 62 microns, was acoustically tested using a +/- 30V single cycle drive pulse and a 40μm needle hydrophone. The average center frequency across all 64 elements was found to be 28 +/- 0.7 MHz. The average 1-way bandwidth was determined to be 23 +/- 0.8 MHz. The average peak-to-peak pressure measured at an axial distance of 6 mm from a transducer element (without lens) was 242 +/- 14 kPa. The combined acoustic and electrical cross talk for nearest and next nearest neighbours was determined to be about –30 dB.

Simulations of the array characteristics based on finite element analysis performed with PZFlex show good agreement with experimental results.

Synthesized images based on the measured performance of the array elements for a given fabricated transducer will also be presented.

Key words: linear array, transducer, and high frequency

6A-2 11:45 a.m.
A KERFLESS 30 MHZ LINEAR ULTRASONIC ARRAY DESIGN.

J. CANNATA*, J. WILLIAMS, and K. K. SHUNG, University of Southern California, Los Angeles, Ca.
Corresponding e-mail: cannata@usc.edu

It has been previously reported that kerfless, or non-mechanically diced, linear ultrasonic arrays can provide a simplified alternative to arrays built using

conventional dice-and-fill techniques. This design simplification is most effective when developing high frequency (>30MHz) linear arrays where conventional fabrication techniques can be problematic. However, such a design is limited in use to conventional linear array imaging, where the acoustic beam is not steered, due to reduced element directivity caused by elevated electromechanical cross-coupling between adjacent elements. In this study a 64-element 30 MHz kerfless linear array design is proposed and is compared to a previously built 30 MHz piezo-composite array. A fine grain Navy Type IV was chosen as the active material for both array designs because of its high reported clamped permittivity. A finite element model was used to compare the performance of both arrays. Preliminary results suggest a two-way single element sensitivity increase of 4.7 dB for the kerfless array with two matching layers when compared to the composite array with one acoustic matching layer. This improvement comes with only a slight degradation in pulse shape and bandwidth. However analysis of one-way directivity patterns for single array elements showed a significant reduction in acceptance angle for the kerfless design. The modeled -6 dB acceptance angles were 16° and 22° for the kerfless array element and composite array element, respectively. Based upon these results the effective element width for the kerfless array should be approximately 15% larger than the designed array pitch, or 115 μm, whereas the effective element width of the composite array is approximately 90 μm. Approximately 2.1 dB of the increased echo amplitude observed for the kerfless array can be attributed to a reduction of two-way diffractive loss. Therefore the remaining difference in echo amplitude can be attributed to the improved acoustical matching in the kerfless design.

The authors would like thank the National Institutes of Health (NIH) for providing the funding through grant # P41-EB2182.

6A-3 12:00 p.m.
AN INVESTIGATION OF THE EFFECTIVE WIDTH OF ELEMENTS IN KERFLESS ANNULAR ARRAYS.

C. E. M DÉMORÉ* and G. R. LOCKWOOD, Queen's University, Kingston, ON, Canada.
Corresponding e-mail: cdemore@physics.queensu.ca

Most high frequency (>30 MHz) imaging systems are based on single element transducers. Although transducer arrays could greatly improve the performance of these systems, the difficulty in fabricating miniature arrays (~ 2 mm diameter) has limited their development. We have previously described a method for fabricating miniature 50 MHz annular arrays in which the elements are defined by patterning the electrodes on the surface of the piezoelectric with photolithography [1]. While this greatly simplifies the fabrication process, the resulting kerfless arrays have high mechanical coupling between elements. Despite this high coupling, we have shown both theoretically and experimentally that a satisfactory radiation pattern (secondary lobes < -60 dB), and an excellent pulse shape can be obtained for kerfless PZT transducers with moderate aperture sizes (< 60 wavelengths) [1,2]. Unfortunately, attempts to increase the aperture to improve the resolution, or to image closer than f/2 lead to an unacceptable increase in the secondary lobe amplitude. In this paper we investigate this

limitation of kerfless annular arrays. We explored the extent of mechanical coupling between elements and its effect on imaging performance by comparing the single element radiation patterns calculated by an ideal model (no coupling between elements) and a finite element model of the array. When the same element dimensions are used in both models, there is a significant difference between the predicted radiation patterns. However, we found that the radiation patterns can be made almost identical simply by increasing the width of elements in the ideal model. Furthermore, we discovered that the element width increase required to match the ideal model results to the finite element model results was constant for a given transducer substrate, independent of the aperture size or the number of elements in the array. The increase in element width was also independent of the ultrasound frequency provided the width was expressed in units of wavelengths in the imaging medium. For example, for a transducer with a PZT5H substrate, each element in the array was effectively ~ 2 wavelengths larger than the patterned electrode, while for a PVDF substrate the increase was only ~ 0.4 wavelengths. For a given substrate the effective width for each element can be determined by adding the width of the patterned electrode and the increase required by the ideal model to account for the mechanical coupling in the finite element model. By using effective element widths in an ideal model of the array it becomes relatively easy to predict the imaging performance of a kerfless design.

[1] J.A. Brown, C.E.M. Démoré, G.R. Lockwood, “Design and Fabrication of Annular Arrays for High-Frequency Ultrasound,” IEEE Trans. UFFC, Vol. 51, pp 1010-1017, August 2004.

[2] C.E. Morton, G.R. Lockwood, “Design of a 40 MHz Annular array,” Proc. 2001 IEEE Ultrason. Symp., pp 1135-1138.

6A-4 12:15 p.m.
POLYIMIDE BACKED 40 MHZ PVDF TRANSDUCERS.

J. KETTERLING*[3], O. ARISTIZÁBAL[1,2], and D. H. TURNBULL[1,2], [1]Skirball Institute of Biomolecular Medicine, New York, NY, [2]New York University School of Medicine, New York, NY, [3]Riverside Research Institute, New York, NY.
Corresponding e-mail: oarist@saturn.med.nyu.edu

Single element focused PVDF transducers are widely used for high frequency (> 30 MHz) ultrasound imaging because of their broad bandwidth (BW) and ease of fabrication. A method of fabricating high frequency transducers (both single element and annular arrays) using a copper-clad polyimide (CCP) film epoxy-bonded to PVDF is presented here. To validate this fabrication technique, single element PVDF (9 μm thick) transducers were fabricated using two methods: 1) (TS) Two-sided chromium-gold (Cr-Au) electroded PVDF, spherically focused and epoxy backed; and 2) (TC) PVDF with a Cr-Au electrode on front, and the unelectroded side bonded to CCP, spherically focused and epoxy backed. In addition, an annular array with five rings, 6 mm total aperture and 12 mm geometric focus was assembled using the same techniques as in 2). Transducer performance was compared quantitatively by measuring center frequency, fractional -6dB BW and two-way insertion loss (IL).

A single-sided CCP film was epoxy-bonded to a PVDF membrane and placed on a hollow Teflon plug. For the case of the annular array, the CCP film had an annular circuit pattern etched onto it. The two films were then shaped by press-fitting with a ball, the assembly inverted, and the center bore filled with epoxy and cured overnight. The resulting epoxy plug was joined to an SMA bulkhead coupler and epoxied into a metal housing with the space between the housing and the SMA connector filled with epoxy. The copper (back) electrode was connected to the center pin of the SMA while the gold (front) electrode was connected to ground through the housing.

A single element standard transducer (TS) was compared to a CCP backed transducer (TC) with similar aperture (4.5 mm) and f-number (f/2). Complex electrical impedance measurements showed that at 40 MHz the real components were very similar while there was a greater difference in the imaginary components. KLM model predictions for the two transducers were in reasonable agreement with the measured results, with a closer match to TS than TC, especially in the imaginary components. BW and IL were measured from pulse-echo signals from a quartz plate positioned at the geometric focus. IL measurements were corrected for attenuation in water and for transmission losses at the quartz/water interface. These results are summarized in Table 1. B-mode images of mouse embryos, using a custom scanning system in our laboratory (Aristizabal et al, UMB 24: 1407, 1998) were of equivalent quality. For the annular array transducer, BWs were 33% and, after impedance matching, ILs varied from 29 to 36 dB, increasing from the center to outer annulus. Additional mouse images were acquired to demonstrate the improved depth of field attainable with the annular array.

PVDF transducers fabricated with CCP backing have equivalent performance compared to standard PVDF transducers. This new method provides an easy, efficient method for fabricating high frequency PVDF transducers with complex electrode geometries.

Table 1

	f_o(MHz)	BW(%)	IL(dB)	Z_{meas}(W)	Z_{KLM}(W)
TC	42	86	46	10-*j*26	16-*j*56
TS	44	116	44	10-*j*50	12-*j*44

Research supported by NIH grants NS038461 and EY014371.

6A-5 12:30 p.m.
HIGH FREQUENCY COPOLYMER ANNULAR ARRAY ULTRASOUND TRANSDUCER FABRICATION TECHNOLOGY.

E. GOTTLIEB*, J. CANNATA, C. HU, and K. SHUNG, University of Southern California, Los Angeles, CA.
Corresponding e-mail: egottlie@usc.edu

The annular array ultrasound transducer was fabricated using a 9 μm P(VDF-TrFE) film bonded to an electroded two sided flexible circuit. The flexible circuit consisted of Kapton polyimide film with a top layer equal area pattern of gold annuli electrode apertures separated by a kerf of 30 μm. Each annulus had several 30 μm diameter electroplated vias that connected to electrode traces on the bottom side of the Kapton polyimide film. The total aperture of the array was 3.12 mm. The transducer's performance has been modeled by using the commercial software PiezoCAD based on Krimholtz, Leedom and Matthaei (KLM) model. The transducer's performance was evaluated by measuring the electrical impedance with a HP 4194 impedance analyzer, pulse echo response using a Panametrics 5900 pulser/receiver and crosstalk measurement for each element in the array. In order to improve device sensitivity each element was electrically matched to an impedance magnitude of 50 Ω and 0° phase at resonance. The average round trip insertion loss measured for the array and compensated for diffraction effects was 33.5 dB. The measured average center frequency and bandwidth of an element was 55 MHz and 50% respectively. The measured crosstalk between center and adjacent element at the center frequency was -45 dB in water.

This work was supported by NIH grant P41-EB2182, Ultrasound Transducer Resource Center, University of Southern California, Los Angeles, CA.

6A-6 12:45 p.m.
DESIGN OF SPARSE ANNULAR ARRAYS FOR HIGH FREQUENCY IMAGING.

J. BROWN* and G. LOCKWOOD, Queen's University, Kingston, Ontario, Canada.
Corresponding e-mail: jeremy@physics.queensu.ca

Obtaining better lateral resolution is always desirable in ultrasound imaging. The lateral resolution of an ultrasound imaging system is inversely proportional to the aperture of the transducer. For a linear/phased array, there is a linear relationship between the aperture and number of array elements. If the number of elements is doubled, the image resolution will improve by a factor of two. For an annular array, the aperture is proportional to the square-root of the number of elements. Therefore, four times the number of elements are required for a two times improvement in lateral resolution. Unfortunately, if the aperture is increased by simply enlarging the area of the array elements, higher secondary lobes will result. We have developed an annular array design that allows a significant improvement in lateral resolution, without a corresponding increase

in the number of elements or level of secondary lobes. Instead of expanding the aperture by increasing the area of the array elements, the space between the elements is enlarged. The resulting sparse array provides improved resolution, and since the amplitude of secondary lobes is determined by the area of the elements, an increase in the level of secondary lobes is avoided. It is often assumed that maximizing the active area of an annular array will result in the largest amplitude pulses. This is an incorrect assumption. The on-axis pulse amplitude is maximized at an imaging depth where the phase shift across each element is equal to 180 degrees. Provided this condition is met, the sensitivity of a sparse array can match or even exceed that of an array with larger elements.

In this paper we describe the design of a 35 MHz sparse array. Our goal was to design an array that would provide ≤ 120 micron resolution over an 8 mm imaging depth, while suppressing the secondary lobes at least 60 dB below the main beam. The final design had 10 equal area elements and a 5 mm outer diameter. The array was designed with 110 micron equal width kerfs, resulting in only a 50% active aperture. The simulated performance of the array was compared to a 5 mm diameter, 10-element array operating with a 100% active aperture. The -6 dB beamwidths of the sparse and full arrays were found to increase smoothly from 51 microns at a depth of 6 mm to 120 microns at 14 mm. For the sparse array, secondary lobes were suppressed by more than 60 dB over the entire 8 mm region from 6 to 14 mm. For the fully active array, secondary lobes were suppressed only to -42 dB at 6 mm, and -60 dB lobes were not reached until a depth of 10 mm. The sensitivities of the sparse and full arrays were similar.

Session: 1B

IVUS I
Chair: T. van der Steen
Erasmus MC

1B-1 2:30 p.m.
(Invited)

BIOMEDICAL ENGINEERING IN THE CATHETERIZATION LABORATORY.

P. W. SERRUYS*, Interventional Cardiology Thorax center ErasmusMC, Rotterdam, The Netherlands.

Corresponding e-mail: p.w.j.c.serruys@erasmusmc.nl

Interventional cardiology has made tremendous progress over the last three decades. The inherent boundary conditions make all developments technologically challenging. Whatever diagnostic or therapeutic tool used in interventional cardiology needs to be fit on a flexible catheter with a maximal diameter of around 1 millimeter. Therefore it is not surprising that Biomedical Engineering has played a major role in the developments in this field. It has not been a shear success story. Many technologies did arrive and vanished again.

Therapies like laser ablation, spark erosion, rotablator and radioactive stents did not last. At present the therapies of choice to treat a partially occluded coronary artery are balloon angioplasty and especially drug eluting stents, metal prostheses that are coated with a drug that prevents re-growth of atherosclerotic plaque within the stent (restenosis).

For diagnosis and therapy guidance X-ray angiography and intravascular ultrasound (IVUS) have played important roles. The first one is used for quantitative assessment of the free lumen, the latter one especially for assessing the morphology of atherosclerotic plaque, but also for correct placement of stents.

Currently the main challenges left in interventional cardiology are the identification of vulnerable plaques and therapy guidance during treatment of chronic total occlusion.

A vulnerable plaque is a marginally occluding plaque that consists of a lipid pool covered by a thin fibrous cap. When the cap ruptures the lipid will get in touch with the blood, which can create a thrombus and thus cause an acute myocardial infarction. Vulnerable plaque detection techniques on the horizon are intravascular optical coherence tomography (OCT), intravascular MRI and advanced IVUS techniques like virtual histology, elastography and palpography. Recent results in MRI and multislice Computed tomography give long term hope for non-invasive techniques, which would allow screening.

For the therapy guidance of chronic total occlusion, forward-looking IVUS and forward looking OCT are targeted solutions.

This lecture will put the role of biomedical engineering in state of the art interventional cardiology into a historic perspective and give a glimpse into the future.

1B-2 3:00 p.m.
FORWARD LOOKING IVUS IMAGING USING AN ANNULAR-RING CMUT ARRAY.

F. L. DEGERTEKIN[1], M. KARAMAN*[2], and R. O. GULDIKEN[1], [1]Georgia Institute of Technology, Atlanta, GA, [2]Isik University, Istanbul, Turkey.
Corresponding e-mail: karaman@isikun.edu.tr

Forward-looking intravascular ultrasound (FL-IVUS) can view forward through the front of the catheter and provide Doppler-based blood flow information. Limitations of piezoelectric transducer technology have prevented effective implementation of practical FL-IVUS systems. The latest developments in capacitive micromachined ultrasonic transducer (CMUT) technology enable manufacturing of forward-looking annular-ring (FLAR) IVUS arrays with integrated front-end electronics. To achieve acceptable SNR from FLAR array elements we have recently developed and presented a low-temperature process suitable for building CMUTs directly on CMOS electronics.

In this paper, we present the first volumetric imaging results using a 1.15mm, 64-element FLAR IVUS array based on low-temperature CMUT fabrication process suitable for CMOS electronics integration. We used a test interconnect scheme forming a 32-element array configuration, where 16-element were tied

in transmit and 16-elements were independently used in receive. We collected data sets using point target, plane reflector, and two point targets at different spatial locations, and created to 2D slices of volumetric images.

For comparison of the experimental PSF created using the point target, we also generated both the simulated and theoretical PSFs. For this purpose, we implemented custom software for numerical simulation of wide-band digital FL-IVUS imaging, and we extended the analytical CW PSF expression to the pulsed-excitation by superposing contributions of the signal components within the transducer band. The experimental and simulated PSFs (the receive response due to the non-focused transmitter) fit very well to the theoretical one-way PSF: the first side lobe level was -11dB, whereas the grating lobe level (due to the undersampled aperture) was -17dB.

We also tested the pulse-echo frequency response and SNR performance of array elements using data sets acquired from the plane and point targets. The frequency response for the plane target shows 70% fractional bandwidth around 14MHz, whereas the response for the point target has approximately 67% fractional bandwidth around 13.5MHz. These results were not corrected for frequency dependent attenuation and diffraction loss for fnumber of 5. To estimate the actual pulse-echo SNR values of the array elements, the SNR values calculated using A-scans were normalized by the transmit channel and signal averaging counts, incorporating the case of non-focused transmit array with non-uniform channel gains. The estimation results show that a single element can achieve 22dB and 7dB SNR for the plane and point targets, respectively, even in the case of fnumber of 5 and with more than 10$\times$ parasitic capacitance. Therefore from a single array element with integrated electronics, we expect a minimum of 30dB SNR for planar reflectors and 15dB SNR for point-like targets.

In conclusion, this study demonstrates that FLAR CMUT arrays fabricated with CMOS compatible processes can meet requirements for IVUS imaging in the 10-20MHz range.

This work was supported by the Whitaker Foundation and Boston Scientific Corporation.

1B-3 3:15 p.m.
INTRAVASCULAR PHOTOACOUSTIC IMAGING TO DETECT AND DIFFERENTIATE ATHEROSCLEROTIC PLAQUES.

S. SETHURAMAN[1], S. AGLYAMOV[1], J. AMIRIAN[2], R. SMALLING[2], and S. EMELIANOV*[1], [1]Department of Biomedical Engineering, University of Texas at Austin, Austin, TX, [2]Division of Cardiology, University of Texas Health Science Center, Houston, TX.
Corresponding e-mail: emelian@mail.utexas.edu

Cardiovascular disease continues to be the leading cause of death and disability in the United States and coronary heart disease accounts for more than half of these deaths. High mortality rates result from the rupture of plaques considered insignificant on a coronary x-ray angiographic evaluation. As a result, large emphasis is given on the development of techniques to identify and characterize

the vulnerability of plaques. For example, intravascular ultrasound (IVUS) is one of the imaging tools of the clinical evaluation of atherosclerosis. In this paper, we present and discuss the applicability of photoacoustic imaging method to detect and differentiate atherosclerotic plaques.

Photoacoustic imaging is based on a laser induced optical excitation and subsequent thermoelastic expansion of the incident area. The generated pressure transients are then detected using a high frequency IVUS transducer and time-resolved to form a photoacoustic image. The primary contrast mechanism in intravascular photoacoustic imaging is dictated by the differences in optical absorption between various tissue constituents including water, blood (hemoglobin), fat, etc. In conjunction with high frequency IVUS, photoacoustic imaging may detect and provide vital information on the vulnerability of plaques. In addition, photoacoustic imaging can be used to image intra-plaque hemorrhage and vasa-vasorum. Therefore, simultaneous acquisition of intravascular photoacoustic and ultrasound cross-sectional frames results in automatically co-registered images displaying both structure and functional properties of the plaque.

To evaluate the approach, simultaneous intravascular ultrasound and photoacoustic imaging studies were performed using single element high frequency (20 MHz and 40 MHz) IVUS catheters. Diffused optical excitation for photoacoustic imaging was provided by an Nd:YAG (532 nm and 1064 nm) pulsed laser system. Both vascular phantoms with inclusions and excised arterial samples were imaged. Poly(vinyl alcohol) hydrogel based vascular phantoms with graphite (optical absorbers and ultrasound scatterers) and silica (ultrasound scatterers) particles were used to prove the feasibility of intravascular photoacoustic imaging. Further ex-vivo experiments on excised samples of porcine aorta and rabbit artery with atherosclerotic plaque were conducted to demonstrate the applicability of the photoacoustic imaging to detect and differentiate arterial plaques.

The results of this study suggest that combined intravascular photoacoustic imaging and IVUS is possible. In phantoms, the inclusions were clearly identified in photoacoustic images, while they were not detectable using IVUS alone. Further ex-vivo experiments on arterial samples prove feasibility of the technique. The functional information obtained in photoacoustic images was shown to complement the structural information obtained with IVUS.

Partial support from The University of Texas Center for Biomedical Engineering under Seed Grant Program is acknowledged. The authors also would like to thank Boston Scientific Corporation for their technical support.

1B-4 3:30 p.m.
ARTERIAL LIPID CHARACTERIZATION BY HIGH RESOLUTION TSI.

K. KIM*, R. WITTE, and M. O'DONNELL, University of Michigan, Biomedical Engineering Department, Ann Arbor, MI.
Corresponding e-mail: kangkim@umich.edu

High resolution Thermal Strain Imaging (TSI) using an US microscope was applied to excised porcine tissues. Rupture-prone plaques consist of a large lipid-rich core composed of macrophage foam cells, apoptotic and necrotic cells, separated from the lumen by a thin fibrous cap. It is well known that lipids have a negative temperature dependence of the sound speed, whereas water-based tissues have positive temperature dependence. Controlled local temperature modulation can be used to image the spatial distribution of temporal strain produced by changes in the sound speed. The opposite sign of the two different tissue types creates the contrast required for resolving the lipid-laden pool within a vulnerable plaque from surrounding water-based arterial wall. In-vitro high resolution TSI of an excised porcine fresh bacon and coronary artery covered by fatty tissue were performed. The samples were placed in a temperature controlled water chamber and scanned transversely and longitudinally using a home-built high speed and high resolution ultrasound (US) microscope. 2-D phase-sensitive, correlation-based speckle tracking was applied to map the spatial distribution of temporal strain across the sample. TSI differentiated fatty tissue from the water-based arterial wall and muscle with strong contrast and a spatial resolution of 60 microns for a 50 MHz transducer. Both transverse and longitudinal TSI images compare well with B-scan images of the arterial wall structures, including intima, media, adventitia and covered fatty tissue. Assuming uniform temperature change in the tissue, the temporal displacement was averaged over US beams. For fresh bacon tissue, the thermal strain is estimated to be 0.0047 ± 0.0002 in fatty tissue and -0.0025 ± 0.0001 in muscle, representing temperature rises of 2.8 ± 0.1 degrees and 2.5 ± 0.1 degrees. The temperature change inside the tissue monitored by a thermocouple was from 20.6 to 22.2 degrees. For coronary artery, the thermal strain is estimated to be 0.0047 ± 0.0004 in fatty tissue including adventitia and -0.0024 ± 0.0005 in intima and media, representing temperature rises of 2.8 ± 0.2 degrees and 2.4 ± 0.5 degrees. The temperature change inside the tissue monitored by a thermocouple was from 23.6 to 25.2 degrees. These in-vitro preliminary results demonstrate the feasibility of high resolution TSI with a small temperature change for plaque characterization.

Work supported in part by NIH grants HL-47401 and HL-67647.

1B-5 3:45 p.m.
HARMONIC INTRAVASCULAR CONTRAST ULTRASOUND: A FEASIBILITY STUDY FOR VASA VASORUM IMAGING.

D. E. GOERTZ*[1,2], M. E. FRIJLINK[1], L. C. A VAN DAMME[1], R. KRAMS[1,2], N. DE JONG[1,3], and A. F. W VAN DER STEEN[1,2], [1]Erasmus MC, Rotterdam, [2]Interuniversity Cardiac Inst. Netherlands, Utrecht, [3]Physics of Fluids, Univ. Twente, Enschede.
Corresponding e-mail: d.goertz@erasmusmc.nl

Background The identification of vulnerable atherosclerotic plaques is a central issue in cardiac imaging. It is increasingly recognized that the development of neovascular vasa vasorum is necessary for plaque progression and may promote lesion instability. At present, there are no established clinical tools capable of

high resolution imaging of coronary vasa vasorum. We previously demonstrated harmonic intravascular ultrasound (HIVUS) contrast imaging (subharmonic and second harmonic) in phantoms using an experimental submicron contrast agent. The purpose of this study is to investigate the feasibility of using HIVUS contrast imaging to detect microvessels outside the lumen of a large artery.

Methods A prototype HIVUS system was operated at a fundamental frequency of 20 MHz (F20) to examine second harmonic (H40) signals. A frame rate of 5 Hz was employed, with up to 150 image frames recorded to monitor post-injection agent dynamics. The contrast agents evaluated were i) an experimental small bubble agent (BG2423, Bracco Research, Geneva) and ii) Sonovue™ that was decanted to preferentially exclude larger bubbles. Agent characterization experiments (conc. 1:500) were first conducted to assess contrast-to-tissue-ratios (CTR) as a function of pressure in F20 (25% bandwidth), H40, and F40 (25% bandwidth) imaging modes. Next, a flow phantom was constructed to investigate the situation of an IVUS catheter located within an arterial lumen with a delivery catheter releasing an upstream agent injection. The main lumen was 4 mm in diameter and, to examine small vessels within the wall, a 1 mm side branch vessel was intersected with the main lumen at an angle of 15 degrees. *In vivo* studies were then conducted in an atherosclerotic rabbit abdominal aorta. The IVUS catheter was situated in a region of interest in the aorta and agent was released proximally in the form of a bolus through a second catheter.

Results Agent characterization experiments showed (for pressures ~<0.3 MPa) improvements in CTR in H40 mode relative to F20 and F40 modes. At a depth of 3 mm for example, the improvement in CTR for H40 relative to F20 mode was 9 dB with decanted Sonovue™ and 19 dB with BG2423. The flow phantom experiments revealed the following pattern following the bolus release of agent: first attenuation effects transiently obscured imaging, then agent was imaged towards the periphery of the main lumen, and finally there was a delayed enhancement of the small vessel outside the main lumen. For Sonovue™, the small vessel CTR in H40 was 11 dB. The *in vivo* experimental results followed a similar pattern: agent was first detected within the main lumen, followed by its presence in small adventitial vessels. For both BG2423 and Sonovue™, *in vivo* H40 experiments detected agent, within adventitial or plaque microvessels, following the injection of contrast.

Conclusion These results suggest that HIVUS contrast has potential as a new technique for vasa vasorum imaging.

This work was supported by STW and ICIN. We thank Bracco Research (Geneva) for providing the BG2423.

Session: 2B

BLOOD FLOW
Chair: P. Tortoli
University of Firenze

2B-1 2:30 p.m.
SPECTRAL VELOCITY ESTIMATION USING THE AUTOCORRELATIONFUNCTION AND SPARSE PULSE SEQUENCES.

J. A. JENSEN*, Technical University of Denmark, Lyngby, Denmark.
Corresponding e-mail: jaj@oersted.dtu.dk

Ultrasound scanners can be used for displaying the distribution of velocities in blood vessels by finding the power spectrum of the received signal. It is desired to show a B-mode image for orientation and data for this has to be acquired interleaved with the flow data. This either halves the effective pulse repetition frequency f_{prf}, since the B-mode emissions are interleaved with the flow emissions or gaps appear in the spectrum due to the B-mode emissions. Techniques for maintaining both the B-mode frame rate, and at the same time have the highest possible f_{prf} only limited by the depth of investigation, are, thus, of great interest.

The power spectrum can be calculated from the Fourier transform of the autocorrelation function Rr(k), where the span of lags k is given by the number of emission N in the data segment for velocity estimation. The lag corresponds to the difference in pulse number, so that for lag k data from emission i is correlated with i+k. The autocorrelation for lag k can then be averaged over N-k pairs of emissions.

It is possible to calculate Rr(k) for a sparse set of emissions, as long as all combinations of emissions cover all lags in Rr(k). A sparse set of emissions interleaved with B-mode emissions can, therefore, be used for estimating Rr(k). The sequence [v B v v B] gives 2 B-mode emissions (B) for every 3 velocity emissions (v) and is denoted a 3:2 sequence. All combinations of lags are present k=[0 1 2 3 ..], if the sequence is continually repeated. Many other sequences can be devised with this property giving 3:3, 3:4, and 5:8 sequences.

The approach has been investigated using Field II simulation of the flow in the carotid and femoral arteries. The surrounding walls and their movement have also been included, and the scattering from the quasi stationary signal is 40 dB higher than from the simulated blood. A 5 MHz linear array transducer with 128 elements, a pitch of λ and an element height of 5 mm was simulated. More than 150,000 scatterers in the vessel were simulated, and the pulse repetition time was 15 kHz. Stationary echo canceling was performed by fitting a 3rd order polynomial to the sparse data and subtracting the polynomial fit. The autocorrelation was calculated from the sparse sequence and averaged over a pulse length.

The 1:2 sequence showed a nearly indistinguishable spectrum compared to a Fourier spectrum calculated on the full data. The sparser sequences give a

higher noise in the spectrum proportional to the sparseness of the sequence. The audio signal has also been synthesized from the autocorrelation data by passing white, Gaussian noise through a filter designed from the power spectrum of the autocorrelation function.

The results show that both the full velocity range can be maintained at the same time as a B-mode image is shown in real time, where the trade-off between B-mode frame rate and spectral accuracy can be selected.

This work was supported by grant 9700883, 9700563 and 26-04-0024 from the Danish Science Foundation and by B-K Medical A/S.

2B-2 2:45 p.m.
EXPLOITING THE DEPENDENCY OF THE DOPPLER SPECTRUM ON THE POSITION AND INSONATION DIRECTION OF AN INTRA-VASCULAR DOPPLER WIRE TO ESTIMATE VOLUMETRIC FLOW.

M. MC LAUGHLIN*[1], J. WAUTERS[2], W. HILLEWAERT[3], P. VERDONCK[4], P. DEVOS[3], A. WILMER[2], B. BIJNENS[1], P. SEGERS[4], and P. CLAUS[1], [1]Dept. Cardiology, K.U.Leuven,, Leuven, Belgium, [2]Critical Care Unit, University Hospitals Gasthuisberg, Leuven, Belgium, [3]Dept. INWE, Hogeschool, Ghent, Belgium, [4]Hydraulics Laboratory, Institute of Biomedical Technology, Ghent University, Ghent, Belgium.
Corresponding e-mail: myles.mclaughlin@uz.kuleuven.be

Introduction: Monitoring regional volumetric arterial flow (Q) to estimate organ perfusion could improve patient management in the intensive care unit. Estimation of Q requires the flow velocity distribution (VD) over the cross-sectional area (CA) of the vessel. Commercial intra-vascular Doppler wire (IVDW) systems estimate flow velocities and are highly dependent on wire position. Recently, an algorithm based on the range-gate (RG) dependency of the Doppler power density spectrum (PDS) to measure Q was proposed. The CA is calculated from the RG from which the ratio of the zeroth moments of the PDS (at consecutive RG), remains constant. Q is estimated as the product of the spatial mean velocity (estimated from the PDS) and CA. However, this algorithm assumes the wire is centered in the vessel, which limits its clinical use. Here, we modeled the dependency of the PDS at different RG on the positioning of the wire in a cylindrical tube assuming laminar flow. Q was estimated by fitting the modeled to the measured PDS. This methodology was tested in-vitro.

Methods: In vitro setup: Varying pulsatile flow was generated in cylindrical silicon tubes with diameters of 3 and 4mm filled with a suspension of water and Optison contrast. For each data set (n=11) time collected flow (TCF) was recorded. We used a FloMap system (Volcano Therapeutics, CA, USA) equipped with a .014'' IVDW (12Mhz, opening angle=13°). The audio Doppler signal acquired at a number of RG (4-10mm in steps of 0.13mm) were digitized to estimate the normalised PDS at peak flow described as a function (surface) of frequency and RG.

Theoretical model: The spectral model,contained 5 free parameters: vessel diameter (D), VD (parabolic (po=2) to blunted (po=infinity)), wire position (offset from vessel centre) and insonation direction (two angles). The maximal flow velocity in the center of the tube was calculated from the wire position, insonation direction, VD, and the measured peak velocity (PV). From the resulting velocity distribution in the RG of the beam the normalised PDS was calculated. Transit time spectral broadening was introduced based on the wire characteristics and VD.

Flow estimation: By minimising the RMS difference between the modeled and measured normalised PDS surfaces, the free parameters were estimated. Q was estimated at each point in the cycle from the measured PV, D and VD. The temporal average of Q (Qavg) was compared to TCF.

Results: There was a reasonable correlation between TCF (85-205ml/min) and Qavg (45-168ml/min)($r = 0.82$, $p = 0.001$). Linear regression gave the line of best fit as TCF = 0.88 Qavg + 33 ml/min. In the 3mm tube the estimated D was 3.22 ± 0.78mm and in the 4mm tube D was 4.26 ± 0.34mm. VD was estimated as almost parabolic (po=2.3 ± 0.3).

Conclusion: Volumetric flow can be estimated using a IVDW in combination with a spectral model. The present model neglects the disturbance of the flow caused by the wire. Laminar flow was probably not fully developed at the measured RG, which could partly explain the underestimation of Q.

2B-3 3:00 p.m.
A NOVEL DUAL BEAM APPROACH FOR REMOVING DOPPLER ANGLE AMBIGUITY.

P. TORTOLI*, G. BAMBI, and S. RICCI, Department of Electronics and Telecommunications, University of Florence, Firenze, Italy.
Corresponding e-mail: piero.tortoli@unifi.it

Traditional Doppler methods only measure the axial component of the velocity vector. The lack of information on the beam-to-flow angle creates an ambiguity which can lead to large errors in velocity magnitude estimates.

Different triangulation techniques have been so far proposed, which basically perform multiple measurements of the Doppler frequency shift originated from the same region. In such methods, the performance deteriorates as the angle between the beams is reduced, or when the interrogated sample volumes are not totally overlapped, as it happens especially for large interbeam angles.

In this work, an original approach is proposed, in which two ultrasound (US) beams with known relative orientation are directed towards the same vessel, but only one of them is committed to perform a Doppler measurement, while the second (‘reference’) beam has the specific task of detecting the flow direction. The latter goal is achieved by accurately identifying a 90° reference-beam-to-flow angle through inspection of the backscattered Doppler signal spectrum. In ‘transverse’ flow conditions, in fact, such spectra are expected to be nearly centered on zero frequency, and even a small deviation from the desired 90° orientation causes a noticeable loss of spectral symmetry. Finally, since the

flow direction is known thanks to the reference beam, the velocity magnitude can be directly measured by the other US beam.

Validation of the new method has been performed through in vitro experiments based on a phantom in which it was possible to control the velocity for steady flow conditions. The software of a commercial US machine (Megas, Esaote SpA, Florence, Italy) has been customized to make possible the simultaneous US transmission by two subapertures of a linear array probe. Each transmitted beam could be independently steered at angles of ±6°, ±12° and ±18°. Echo signals backscattered from a sample volume intercepted by both the M-lines have been extracted from the Megas system and sent to a home-made DSP board, computing the Doppler spectra and allowing the related spectrograms to be displayed in real-time on the PC monitor.

The experimental procedure started by accurately setting the reference beam direction until the spectrogram produced by a sample volume in the center of the vessel did not look symmetrical. The Doppler measurement was obtained through the spectrogram produced by the other beam. A set of twenty measurements performed at different velocities and probe-to-vessel angles, have produced velocity magnitude estimates with bias < 4% and standard deviation < 5%.

Preliminary in vivo application of the new method has also been tested. Here, the same common carotid artery of a healthy volunteer was repeatedly interrogated by the dual-beam system with different interbeam angles in the range 18°-30°. The difference between velocity magnitudes estimated in the various cases was <3%.

2B-4 3:15 p.m.
DOPPLER, MULTIGATE MEASUREMENTS OF ULTRASONIC SCATTERING, ATTENUATION AND HEMATOCRIT OF BLOOD IN THE HUMAN ARTERY.

W. SECOMSKI*[1], A. NOWICKI[1], R. OLSZEWSKI[2], J. ADAMUS[2], P. FIDANZATI[3], and P. TORTOLI[3], [1]Institue of Fundamental Technological Research, Polish Academy of Sciences, Warsaw, Poland, [2]Department of Cardiology, Main Military Medical Academy, Warsaw, Poland, [3]Electronics and Telecommunications Department, University of Florence, Florence, Italy.
Corresponding e-mail: wsecom@ippt.gov.pl

The goal of this work was to develop a clinically applicable method for noninvasive determination of hematocrit based on Doppler ultrasound.

Previously published work proved the linear relation between ultrasound attenuation and hematocrit, using a 20 MHz unfocused transducer (2mm diameter) in a pulsed wave multigate Doppler system, capable of simultaneously recording the Doppler signal coming from 128 depths, covering a range of 12.8 mm. The ultrasound attenuation coefficient in blood was obtained by measuring the power of the signal coming from two gates at different depths. Previous results, related to a low number of patients, were sensitive to the selected gates and suffered for a lack of stability and repeatability.

In this work a suitably large amount of in vitro and in vivo data has been collected and a new estimation algorithm is proposed. The new technique evaluates the attenuation coefficient with a robust averaging method using echo-signals from all depths inside the vessel. The resulting attenuation coefficient results stable and the measure is made repeatable.

In vitro measures have been done on porcine blood, with samples of whole blood and separated plasma with hematocrit ranging from 1% to 65%. Steady and pulsatile flow conditions, similar to those existing in the brachial artery, have been simulated with a suitable pump. The attenuation coefficient, determined from the reduction of Doppler amplitude with increasing depth, indicated the linear relation to hematocrit. The resulting correlation coefficient was R = .999 for the continuous blood flow and R = .992 for pulsatile flow.

In-vivo measurements have been performed in the brachial artery in 40 patients with hematocrit in the range 36.4% - 48.6%. The measured attenuation coefficient increased linearly with hematocrit. Correlation coefficient was R = .905.

Preliminary application of the new estimation technique in a first group of 12 patients has produced encouraging results. The mean error has been of only 3% HCT, with a maximum error of 5% HCT.

The proposed method appears to be promising for in-vivo determination of hematocrit, preferred for monitoring changes of hematocrit in patients in traumatic shock or during dialysis.

This work was supported by the KBN grant 5T07B03225

2B-5 3:30 p.m.
VECTOR VELOCITY ESTIMATION USING APERTURE DOMAIN DATA.

H.-L. WANG* and P.-C. LI, Department of Electrical Engineering, National Taiwan University, Taipei, Taiwan, ROC.
Corresponding e-mail: paichi@cc.ee.ntu.edu.tw

Most conventional blood flow estimation methods only measure the axial component of blood velocity vector. In this study, we developed a new method for 2-D velocity vector estimation using aperture domain data (i.e., the data from individual array channels prior to beam summation). Specifically, time shifts resulted from blood motion are calculated for all individual channels using the aperture domain data in the proposed method, whereas the conventional color Doppler technique only calculates the time shift using the beam sum data. Therefore, a time shift profile along the array direction (i.e., as a function of channel index) can be constructed. This profile is then approximated by a first order polynomial. The constant term can be used to determine the axial velocity component and the first order term can be used to determine the lateral velocity component since it is related to steering. Simulations and experiments were performed to verify efficacy of the proposed method. Field II was used in the simulations. In both simulations and experiments, the transducer array had 64 elements, an aperture size of 1.96 cm and a center frequency of 5 MHz. The flow velocity ranged from 5 to 35 cm/s. In the experiments, a programmable array system with 64 system channels (DiPhAS, IBMT, Fraunhofer Institutes,

Germany) was used to acquire the aperture domain data. A gelatin phantom positioned by a 3-D motor system was used to emulate blood motion. The results show that the proposed method had a mean error of 6.7\deg; with the flow angle raging from 15\deg; to 75\deg;, Note that the errors in experimental results may be reduced by increasing the data acquisition speed, since position of the gelatin based phantom may have been moved during data acquisition. One advantage of the proposed method is that it requires a less number of firings (e.g., 4 to 16, depending on the signal-to-noise ratio) than other conventional velocity vector estimation methods (e.g., 64 firings for the spectral broadening technique). The second advantage is that it is less computationally demanding than other methods (e.g., the speckle tracking method). The third advantage is that since the entire time-shift profile is used, accuracy of the axial velocity estimation is also improved over that of the conventional techniques. With this method, the mean error of the axial velocity estimation is 1.4%, compared to 4.7% of the conventional autocorrelation based method.

2B-6 3:45 p.m.
IN-VIVO 2-D BLOOD VELOCITY ESTIMATION USING AN AUTOCORRELATION APPROACH.

J. UDESEN*[1,2] and J. A. JENSEN[1], [1]Center for Fast Ultrasound Imaging, ørsted DTU, Bldg. 348, Technical University of Denmark, Lyngby, Denmark, [2]B-K Medical A/S, Mileparken 34, Herlev, Denmark.
Corresponding e-mail: ju@oersted.dtu.dk

In conventional techniques for blood velocity estimation, only the axial component of the blood velocity vector is found. We have previously shown that it is possible to estimate the 2-D blood velocity vector both in simulations and in flow phantom experiments using a fast and inexpensive method (the transverse oscillation (TO) method) based on an autocorrelation approach. The TO method makes use of a double oscillating pulse-echo field which is created by manipulating the receive apodization function. Two receive beams are beamformed, where the lateral distance between the two beams corresponds to a 90 deg. phase shift in the lateral direction. The TO method works at angles where conventional methods fails to estimate any blood movement, i.e. when the angle between the ultrasound beam and the velocity vector is approximately 90 deg. In this paper the first in-vivo color flow map (CFM) images and movies are presented using the TO method.

A 128 element 5 MHz linear array transducer was used together with the experimental ultrasound scanner RASMUS operating at a sampling frequency of 40 MHz with a pulse repetition frequency of 24 kHz. To ensure that a whole cardiac period was covered the scanning time was 1.8 sec. The number of elements used for each transmit and receive sequence was 64, and 64 emissions were used for each velocity estimate. After sampling the received channel data were beamformed off-line, and a transverse oscillation period of 1.25 mm was created in the lateral pulse-echo field by manipulating the receive apodization function. Echo-canceling was performed by subtracting a line from the sampled data, where the line was a linear fit to the sampled data.

Three different scan areas of a healthy 34 year old male were selected: The common carotid artery, the bifurcation of the common carotid artery and the femoral artery. In all three cases the angle between the ultrasound beams and the blood velocity vector is larger than 60 deg. i.e. the conventional Doppler velocity estimator degrades significantly in terms of standard deviation and bias.

The CFM images from the TO method were compared to the CFM images from a conventional velocity estimation approach derived from the same sampled data. In all three scanning cases it was found that the TO method estimates the 2-D vector velocity at angles, where the conventional velocity estimator fails to detect any significant blood flow. In the case where the carotid artery was scanned, the TO method could estimate the correct angle (85 deg.) of the flow in the center of the artery with a standard deviation of 3.4 deg. and a bias of 1.1 deg.

This work was supported by grant 9700883, 9700563 and 26-01-0178 from the Danish Science Foundation, the Ministry of Science, Technology and Development, and by B-K Medical A/S, Denmark.

Session: 3B
NDE IMAGING AND SIGNAL PROCESSING
Chair: J. Saniie
Illinois Institute of Technology

3B-1 2:30 p.m.
THERMOACOUSTIC TOMOGRAPHY USING INTEGRATING LINE DETECTORS.

P. BURGHOLZER*[1], C. HOFER[1], G. PALTAUF[2], M. HALTMEIER[3], and O. SCHERZER[3], [1]Upper Austrian Research, Linz, Austria, [2]Department of Physics, Karl-Franzens-Universität Graz, Graz, Austria, [3]Department of Computer Science, Universität Innsbruck, Innsbruck, Austria.
Corresponding e-mail: peter.burgholzer@uar.at

Thermoacoustic or optoacoustic tomography (TACT) uses pulses of electromagnetic waves to excite acoustic waves within an optically heterogeneous sample. Spatial variations in optical absorbance lead to variations in generated temperature and thermoelastic pressure, which can be measured as temporally modulated acoustic pressure signals outside the sample. The goal of TACT is to reconstruct the three-dimensional distribution of absorbed energy from the time-varying signals acquired at multiple positions around the sample. The usual approach is to use an array (either a real array or a single detector scanned around the sample) of point like detectors.

Our new approach is to use specially shaped detectors that are larger than the imaged object to acquire acoustic signals. This approach is based on the fact that such a detector receives a signal that is not an approximate projection over a spherical surface but rather an exact projection over an area (or line) that is

determined by the shape of the detector itself. For instance, it can be shown from the properties of thermoacoustically excited waves that a large planar receiver measures a wave as it would be generated in an object in which the initial distribution of absorbed energy (the volumetric energy density) is averaged over planes parallel to the receiver surface. A signal acquired in this way corresponds to the projection of the energy density along those planes, and the time axis multiplied with the speed of sound gives the distance of the projection plane to the detector plane. A set of signals acquired by rotating the plane detector around the object, either around a single axis or around the surface of a sphere, exactly corresponds to the Radon transform of the distribution of absorbed energy density.

Imaging a three-dimensional object requires to rotate the plane detector tangentially around a sphere that encloses the object. Since in practice it is easier to build a device with a single rotation axis, we proposed the fragmentation of the planar detector into a line array perpendicular to the rotation axis as a strategy to obtain images from three-dimensional objects. Single lines as sensitive elements of an ultrasound receiver array can be made using optical sensing technology. Optical methods have the advantage that they allow high bandwidth detection and are relatively insensitive to electrical noise pick-up. First experiments have been done with free beam interferometers in the water surrounding the imaged sample. Ideally a line detector for high-resolution imaging should have a diameter of a few micrometers over a length of centimeters. This is impossible to accomplish with a free beam. Therefore, in order to achieve higher resolution, a fiber-based Fabry-Perot (FP) interferometer is used. Thermal shifts and vibrations are compensated with a fiber stretcher. The resolution and performance of this integrating line detector has been demonstrated in thermoacoustic measurements with line grids (one dimension) and two dimensional objects.

The work of M.H. and O.S. is supported by the FWF Project Y-123 INF

3B-2 2:45 p.m.
ACOUSTIC IMPEDANCE MICRO-IMAGING FOR BIOLOGICAL TISSUE USING A FOCUSED ACOUSTIC PULSE WITH A FREQUENCY RANGE UP TO 100 MHZ.

N. HOZUMI*[1], M. NAGAO[1], S. YOSHIDA[1], K. KOBAYASHI[2], and Y. SAIJO[3], [1]Toyohashi University of Technology, Toyohashi, Japan, [2]Honda Electronics Co. Ltd., Toyohashi, Japan, [3]Tohoku University, Sendai, Japan.
Corresponding e-mail: hozumi@eee.tut.ac.jp

Scanning acoustic microscopy is expected to be a powerful tool for medical application such as intraoperative pathological examination. We recently developed a sound speed microscopy using a nanosecond ultrasonic pulse. The technique made it possible to observe the sound speed profile with a resolution of 20 micrometers, the scanning time for one micrograph being as short as 2 minutes. However preparation of a thin sliced tissue specimen and its fixation on a slide glass were needed for the observation. If a similar microprobe that can observe without slicing and fixing the tissue is realized, an onsite

examination will be made possible, leading to the improvement of efficiency and reliability of operation. Various kinds of biological applications may be considerable as well, if such a microscope is developed.

Based on the above background, we have proposed a new method for two-dimensional acoustic impedance imaging for biological tissue that can perform micro-scale observation without preparing a sliced specimen. As a preliminary experiment, a tissue was attached on a plastic plate. The thickness of the plate was as thin as 0.5 mm. An acoustic pulse with a frequency range up to 100 MHz was irradiated from the “rear side” of the plate, the acoustic beam being focused at the boundary between the tissue and plate. For this purpose, an electric pulse with two nanoseconds in width was applied to a PVDF-TrFE type transducer. The component of echo intensity at an appropriate frequency was extracted from the signal received by the identical transducer. The intensity was interpreted into local acoustic impedance of the target tissue. An acoustic impedance microscopy with 200 x 200 pixels, its view port being 2 x 2 mm, was obtained by scanning the transducer. Quantification of acoustic impedance was performed using water or an appropriate material as a reference. The reference was also in contact with the plastic plate at a different position in the view port.

A rat cerebellum was employed for observation. A cross section of the tissue was attached on the plastic plate. Both sagital and coronal planes were observed. The development of parallel fiber in cerebella cultures was clearly observed as the contrast in acoustic impedance. The acoustic impedance image showed a good agreement with the optical micrograph of the identical tissue after being stained. Another thin sliced tissue was observed by the conventional sound speed microscope. The morphology showed a good agreement with the cross section of the identical tissue observed by the new acoustic impedance microscope. In addition, a good quantitative correlation was seen between acoustic impedance profiles obtained by conventional and new methods. The proposed technique is believed to be a powerful tool for biological tissue characterization, as neither staining nor slicing is required.

This study was supported by Grants-in-aid from Japan Society of Promotion of Science (15300178) and Grants-in-aid from Ministry of Health, Labour and Welfare (H17-nano-001).

3B-3 3:00 p.m.
A NOVEL BACK SCATTERING ARRAYED ULTRASOUND TRANSDUCER FOR NON-DESTRUCTIVE ACOUSTIC IMAGING AND DEFECT INSPECTION.

C.-H. CHUNG* and Y.-C. LEE, Department of Mechanical Engineering, National Cheng Kung University, Tainan , Taiwan.
Corresponding e-mail: n1892136@ccmail.ncku.edu.tw

This research proposes a new type of focusing ultrasound transducer called Analytical Back Scattering Arrayed Ultrasound Transducer (ABSAUT). It is designed for detecting and characterizing internal defects of a sample in an analytic and quantitative way via multiple back scattering ultrasound signals

collection. It essentially follows the basic structure of a conventional focusing ultrasound transducer which has an acoustic lens with a concave spherical surface at one end, and an attached PZT layer for ultrasound generation at the other end. However, an additional PVDF film with patterned electrodes is attached to the concave spherical surface for collecting back scattered ultrasound. The advantages of this novel design are, 1) the PVDF film could act like a matching layer to enhance the wave transmission from acoustic lens to coupling fluid; 2) a number of independent PVDF sensing elements are distributed along the concave acoustic lens surface for measuring the back scattering ultrasound signals; and 3) the transducer is in a pitch-catch mode for wave generation from PZT layer and wave diction form PVDF arrayed hydrophone, hence the corresponding electronics and circuits are greatly simplified. We used an excimer laser to pattern the electrodes on the both sides of the PVDF film which is deformed into spherical concave form to fit the acoustic lens′surface. A number of individual hydrophones are formed and deployed on the spherical concave surface. When the incident acoustic waves are reflected from the sample′s surface and/or scattered from the internal defects inside the solid sample, the back scattering ultrasounds are detected by the PVDF sensing array. The measurement system is constructed under a PC-based configuration. Pulse echo response testing has been carried to verify the performance of this novel transducer. The echoes were obtained from a steel plate target at the focal point of the transducer and the signals were recorded by a digital phosphor oscilloscope for further waveform analysis. Experimental testing of some samples with embedded defects will be carried out with the ABSAUT measurement system. The collected waveforms are used for deriving detail information about the defects in the sample, including defect location, size and other features. Future improvements and applications of the ABSAUT will be addressed.

3B-4 3:15 p.m.
ACOUSTIC IMPEDANCE MEASUREMENT USING PLSR BASED ANALYSIS OF ULTRASONIC SIGNALS.

R. SCHAEFER* and P. HAUPTMANN, Institute of Micro- and Sensor Systems (IMOS), Magdeburg, Sachsen-Anhalt, Germany.
Corresponding e-mail: robert.schaefer@e-technik.uni-magdeburg.de

Ultrasonic measurement techniques play an important rule to many industrial applications as a non-invasive method. A number of those applications use ultrasonic wave propagation time data to derive the wanted quantity and ignore amplitude data contained within the signal shape of the received impulse. In contrast the demand on additional information like the concentration of specific substances within solutions or the density of a medium is increasing according to a growing complexity of industrial processes.

The development of new measurement systems and the integration of new sensors into existing systems respectively are normally associated with a high technological, financial and temporal effort. Considering this aspect and due to a rapidly increasing capability of modern computers a signal processing that extracts additional information by analyzing the shape of ultrasonic impulses

becomes attractive in terms of extending the functional range of existing and approved measuring hardware.

This work introduces a novel signal processing technique for measuring the acoustic impedance Z of a liquid by analyzing the signal shape of transmitted ultrasonic impulses. The applied Partial Least Squares Regression (PLSR) has been implemented as a modified NIPALS algorithm. A through-transmission assembly applying commercial 1 MHz transducers is used as measurement setup.

It is shown that Z is an appropriate quantity to derive material related information. The applicability of the proposed signal processing is demonstrated on measuring the density ρ of an aqueous glycerin solution as well as on determining the glycerin concentration. The adequacy of the transducers in terms of bandwidth- and Q-factor- dependant sensitivity as well as the influence of parasitic drags like temperature changes, noise and particles within the liquid are discussed.

The introduced technique affords precise measurements of Z with a relative error less than 0.5% by using only 6% of all data sets as training input to the PLSR. Significant accuracy improvements can be achieved by comprising more training data and by using optimized transducers. On the basis of Z the glycerin concentration (vol.) was determined with a maximum aberration of 1%. The through-transmission assembly allows acquiring the sound velocity c of the liquid (transit time measurements). Using $\rho=Z/c$ the density was determined with a maximum error of 0.5%. Thus it appears that the PLSR represents a powerful tool to gain valuable additional information by analyzing the shape of ultrasonic impulses.

3B-5 3:30 p.m.
LOW VOLTAGE OPERATION OF 2D ULTRASONIC ARRAYS FOR NDT.

K. STREIBEL*[1], S. COCHRAN[1], K. KIRK[1], D. CUMMING[2], L. WANG[2], and J. WALLACE[2], [1]University of Paisley, Paisley, Scotland, UK, [2]University of Glasgow, Glasgow, Scotland, UK.
Corresponding e-mail: coch-ph0@wpmail.paisley.ac.uk

The use of ultrasonic array transducers for non-destructive testing (NDT) is growing rapidly, supported by several new commercial array controllers. However, practical problems with the flexibility of 1D arrays have been realized. For example, it is impossible to skew the beam on curved surfaces without losing acoustic coupling. As 2D ultrasonic arrays allow 3D beam steering, including skewing, they are thus of major interest for NDT. However, using conventional excitation voltages of the order of 200 V with the many elements in 2D arrays is inconvenient for several reasons. In contrast, low voltage operation allows direct interfacing with digital electronics and low power consumption for portable systems.

The work reported here is focused on array design for low voltage operationg for NDT. A 1D ultrasonic array was first produced, operating at 1.45 MHz for thick section inspection. This was based on a monolithic piezocomposite plate with 36% ceramic volume fraction, made with PZT 5A and epoxy resin. The

plate was bonded to a printed circuit board (PCB) with copper tracks to define the array elements with dimensions 10 mm x 0.28 mm and edge-to-edge separation of 0.4 mm. Acoustic cross-coupling was reduced by aligning the composite pillars diagonally with respect to the elements defined by the PCB tracks. The device was tested with an excitation voltage of 3.3 V on an aluminum test object. Electrical cross coupling of 51.7 dB was found for adjacent elements and the pulse-echo insertion loss, using a signal reflected from the back wall of the 75 mm thick block, was found to be 59 dB. In further work, a 2D ultrasonic array has been produced, with 4×4 elements, using the same piezocomposite material. In this case, the array dimensions are 10 mm $\times$ 10 mm, the element size is 1.2 mm $\times$ 1.2 mm, and the edge-to-edge separation 0.4 mm. The 2D array operates at a frequency of 1.46 MHz. It has also been tested at excitation voltages of 3.3V. In this case, the electrical cross-coupling was found to be –58.3 dB and the insertion loss was 73 dB. Further measurements have been made with laser vibrometry to study acoustic cross-coupling, directly indicating the behaviour related to the diagonal piezocomposite pillar alignment. The results suggest that arrays made with monolithic piezocomposite material have much better performance for NDT than previous arrays made with monolithic ceramic and that low voltage excitation is viable, with low noise amplification and appropriate data analysis.

The authors thank EPSRC for funding this project under Grant GR/T19803. We are also very grateful for the work of Yoan Fernandez in this project.

3B-6 3:45 p.m.
HIGH TEMPERATURE PHASED ARRAY ULTRASONIC SYSTEM WITH INTEGRATED FRONT END ELECTRONICS.

O. VERMESAN*[1], B. FROELICH[2], L. GOMEZ-ULLATE ALVEAR[3], O. MARTINEZ[3], J.-L. GUEY[4], L.-C. BLYSTAD[1], G. FLEURY[4], K. LIANG[5], D. MERCIER[6], R. BAHR[1], P. SCHOEB[7], C. FRITSCH YUSTA[3], and J. MC HUGH[8], [1]SINTEF, Oslo, Norway, [2]Schlumberger-Riboud Product Center, Clamart, France, [3]CSIC, Madrid, Spain, [4]IMASONIC, Besancon, France, [5]Schlumberger-Doll Research, Ridgefield CT, USA, [6]TRONICO, St. Philbert en Bouaine, France, [7]STATICE, Besancon France, [8]BAM, Berlin, Germany.
Corresponding e-mail: Ovidiu.Vermesan@sintef.no

The paper presents a novel phased array ultrasonic imaging system consisting of a cylindrical transducer array with 800 elements and its associated electronics, in a miniaturized package, with the capability of electronic beam scanning and beam focusing. The system can operate in harsh environments with temperature up to 175°C and pressure around 1,400 bars.The system is designed for pipe inspection and can be used in:

-Water distribution

-Oil and gas industry

-Process industry

-Manufacturing plants for the food industry

-Sub sea applications

The system electronics drives the array on transmission and processes the echo signals on reception. The electronics consists of high voltage multiplexers for aperture synthesis, pulsers for generating transmit pulses, integrated front end electronics, FPGA circuits for controlling the array elements, beamforming, filtering, decimation and signal processing, and hardware and software for system management in real time. The receiver is designed as an Applications Specific Integrated Circuit (ASIC) that includes a low noise amplifier (LNA), a programmable gain amplifier (PGA), an output differential amplifier (ODA) and Sigma Delta Modulator (SDM). The front end receiver gain can be programmed by 4 bits in 15 steps from 12dB to 48dB, which give a differential voltage range from 0.5 to 2.0Vpp at the input of the SDM. The LNA input is in the range of 2-500mVpp. The whole receiver architecture is based on SDM data conversion technology, and the signals received from the transducer elements are sampled at a high frequency (up to 48 MHz) within a transmit/receive (T/R) module. This architecture reduces the overall cost, size, and power consumption of phased array front end processing. Digital beamforming is performed on the one bit SDM data output from the T/R module. The implementation is on the cutting edge of high speed SDM ASIC development for digital beamformers in high temperature phased array ultrasound applications. The high speed requirements of the SDM and large scale microelectronics integration are met by using multi chip module (MCM) technology. The MCM technology eliminates many packages and bond wires and improves system reliability. This is valid especially for high temperature applications, where interconnects, metallization, and soldering are areas of reliability concern. The phased array ultrasonic imaging system is very compact and the front end electronics is located in close proximity to the array in order to reduce the parasitics and maintained the required signal to noise ratio. The packaging technology was custom developed for this system to address the demands of integration and harsh environment conditions. MCM technology was employed for electronics components which are mounted on circular multi layer polyimide printed circuit boards that are stack assembled inside a cylindrical housing. The architecture and the design of the electronic system will be shown and temperature characteristics of the performance of subsystems will be discussed.

Work performed in the framework of EC GROW project PharusIT (G1RD-CT-2002-000689).

Session: 4B

OPTICAL INTERACTIONS
Chair: B. Sinha
Schlumberger-Doll Research

4B-1 2:30 p.m.
APPROACH TO INVERSE ACOUSTOOPTIC PROBLEM BASED ON THE COHERENT COMBINING OF SEVERAL OPTICAL BEAMS INTO ONE OPTICAL CHANNEL.

V. PROKLOV*[1], S. ANTONOV[1], and Y. REZVOV[2], [1]Institute of Radio Engineering and Electronics, Russian Academy of Sciences, Moscow, Russia, [2]Novomoscovskii Institute of Radio Chemistry of Technical University, Novomoskovsk of Tula Region.
Corresponding e-mail: proklov@mail.cplire.ru

Majority of traditional acoustooptic (AO) applications are tightly associated with the effect of diffraction of a single-mode laser beam by acoustic waves in solids what results in the significant changes of the output light parameters like the intensity and the propagation directions (in forms of single or multi beams) and etc. Many of those AO implementations might be called as the direct ones.

This paper considers at the first time the possible AO facilities to get salvation so called inverse AO problems, for example to perform the effective coherent combining of several optical light beams into the single one. These transforms are very important for AO implementations in fiber-optic channel demultiplexors, in optical antenna amplifiers and etc. The obtained results offer the theoretical basis and the first successful experimental verifications of the problem.

Under experiments the optical multi-beam field was formed by means of the single mode laser beam diffracted in the instrumental (the additional) AO modulator (AOM-1) which multi-beam output was consequently second time diffracted in the main modulator AOM-2.

Both AOM-1 and AOM-2 were made with use of the anisotropic light diffraction by slow shear waves in TeO_2 , where the light polarization rotation under diffraction have been happened. In both diffraction regimes, Bragg and Raman-Nath, three beams (0,-1 and +1 orders) in case of the first regime and more of five in the second one have been very effectively (about 90%) reconstructed into the single coherent beam in a good agreement with the developed theoretical approach.

This work was supported by the Russian Basic Research Foundation, Project 03-02-16754.

4B-2 2:45 p.m.
ANALYSIS OF SERIAL VERSUS SIMULTANEOUS XY ACOUSTOOPTIC DEFLECTORS.

D. HECHT*, DLH Laboratories, Palo Alto, CA.
Corresponding e-mail: davidleohecht@yahoo.com

Acoustooptic Deflection in two transverse directions (x & y) can be implemented in two ways: 1) serially in which the light passes first through an AO deflector for one direction (x) and then through an AO deflector for the other direction (y) or 2) simultaneously, where acoustic waves induce diffraction in both transverse directions in the same interaction volume. This paper presents comparative analyses and results for the two cases. The first case involves two a two mode (beam) coupled interaction involving deflection in a first direction (x) followed by a pair two mode (beam) coupled interactions involving deflection in the second direction (y); the second case involves one four mode (beam) coupled interaction involving deflections in x and y simultaneously. The interactions considered are Bragg regime with independent arbitrary drive levels in the X and Y directions. The results obtained show that the four output beam intensities I(00), I(10), I(01), I(11), have precisely the same behavior in the two cases, provided that the undeflected beam from the first serial interaction proceeds undisturbed to the second serial interaction. Importantly, the key doubly deflected intensity I(11) is the same in all these cases.

4B-3 3:00 p.m.
HIGH SPEED LASER TUNING USING ACOUSTO-OPTIC TECHNIQUES.

I. C. CHANG*, Accord Optics, Sunnyvale, CA.
Corresponding e-mail: auroraicc@aol.com

High speed tunable lasers operating in the in the infrared are needed in laser radar systems for applications such as the standoff detection of chemical and biological agents. The use of acousto-optic (AO) tuning has shown to be a promising approach for realizing the desired performance goals of high tuning speed, high resolution, small size, and rugged construction of the high speed tunable lasers. There are two basic types of AO tuners: the longitudinal AO tuner that utilizes the wavelength dispersion of an AOTF and the transverse AO tuner that operates on the angular dispersion of an AO Bragg cell. This paper presents a theoretical study of the device characteristics for both types of AO tuners. To be specific the AO tuner is assumed to be a TeO2 device operated in the birefringent diffraction geometry. A primary design goal for the high-speed AO tuner is to realize a large throughput rate defined as the product of the resolution and tuning speed. Achieving a large throughput rate in the infrared region is difficult due to the increasing requirement of the drive power. Optimum designs for to maximizing the throughput rate is obtainable by the wavelength-angular dispersion characteristics of the AO tuner. To simplify the algebra involving in the derivation of the dispersion characteristics of the theoretical analysis of the AO tuner utilizes an elliptical coordinate system for the wave vector representation of the acoustic and optical waves. Another objective of

the theoretical analysis is to determine the performance degradations of the AO tuners caused by the system requirement. For instance, for minimized internal loss in the laser cavity, the AO tuner must operate at the high efficiency regime near 100 percent. This high efficiency operation introduces severe optical beam distortion due to the finite acceptance angle. To evaluate this type of performance degradation the theoretical analysis of the AO tuner is formulated based on strong AO interaction in a divergent optical beam geometry. One technique of minimizing the large signal degradation is to use birefringent AO diffraction operated at non-critical phase matching (NPM) condition. Because of the large angular aperture obtainable at the NPM condition the AO tuner can realize high efficiency and low drive power.

4B-4 3:15 p.m.
HIGH RESOLUTION OPTICAL BEATING BRILLOUIN SPECTROSCOPY OF SOLID AND GAS MATERIALS.

K. SAKAI*, T. YOGI, Y. MINAMI, and K. TAKAGI, Institute of Industrial Science, University of Tokyo, Tokyo , Japan.
Corresponding e-mail: ksakai@iis.u-tokyoa.c.jp

The Brillouin scattering technique is an effective and almost the only method of observing thermally excited acoustic phonons. The light incident to the materials are scattered by propagating phonon, whose propagation is determined by analyzing the power spectrum of light modulated by the Doppler effect through the scattering process. The Fabry-Perot interferometer has been the general tool to analyze the light spectrum, unfortunately however, its frequency resolution is not sufficient to give accurate values of the phonon velocity and absorption. On the other hand, the optical beating Brillouin scattering technique uniquely developed by us enables us to resolve the frequency spectrum with the bandwidth better than 1 kHz, however, the sensitivity in detecting the scattered light has been poor and we can not apply it for hard or dilute materials showing weak scattered light. Recently, we could remarkably improve the sensitivity and it is now possible to observe the phonon spectrum even in the solid glass or air at atmosphere pressure with the resolution as high as 1 kHz. The configuration of the optical heterodyne detection was designed to give the highest correlation between the coherent reference and incoherent scattered lights. In addition, the laser with the power of 10 W was employed together with the high sensitivity photodiode. We could now clearly observe the thermal phonon resonance phenomena even in the solid and gas, whose power spectrum shows fine structure representing the interference of phonons in the confined cavity. The analysis of the resonance spectrum gives quite high accuracy as high as 0.01 % in determining the phonon velocity, which is almost comparable to that expected in the usual ultrasonic measurements. The system would be effective for the investigation of the phase transition among gas, liquid and solids.

4B-5 3:30 p.m.

OPTICAL LABEL RECOGNITION IN SPECTRAL AND TIME DOMAINS WITH COLLINEAR ACOUSTOOPTIC DEVICES FOR PHOTONIC ROUTER.

N. GOTO*[1] and Y. MIYAZAKI[2], [1]Toyohashi University of Technology, Toyohashi, Aichi, Japan, [2]Aichi University of Technology, Gamagori, Aichi, Japan.
Corresponding e-mail: goto@ics.tut.ac.jp

In photonic networks, photonic routing will be an i ndispensable function for processing high-bit rate optical packets over wavelength-division-multiplexed (WDM) large-capacity networks. To develop the photonic routing system, the following issues have to be studied; (i) whole network architecture including photonic routers, (ii) hardware architecture of photonic routers and (iii) control software including packet structure and protocols.

Optical generalized multiprotocol label switching (GMPLS) is a promising technology and has been intensively studied. Routing information is described on the routing label, which is attached to a packet as a header. Various methods of mapping the label information on optical codes have been proposed, which include using the wavelength itself, the subcarrier, the combination of wavelengths, and the optical codes encoded in the time domain or frequency domain.

The authors have studied optical switching and routing systems consisting of collinear acoustooptic (AO) switches for WDM networks. Since multiple WDM optical signals can be processed with a single collinear AO switch by frequency multiplexed surface acoustic waves (SAWs), the switch is applicable to routing of WDM optical packets wavelength by wavelength. Since the switching response is limited to about 1 to 2 micro-seconds by the SAW propagation time over the AO interaction region, the AO switches cannot directly be used for fast packet switching. Integration of multiple AO switches in matrix form can, however, find its application as an optical cross-connect or a matrix switch for photonic burst switching systems since the AO switching time is enough fast for burst switching. The unique feature of WDM signal controllability with a single switch can also be used for spectral encoded label recognition in label routing systems where the label is encoded in the frequency domain. Ziemann et al. demonstrated optical code division multiple access (CDMA) with a collinear AO device. Correlation processing with the AO device can be applied to label recognition for photonic routing systems.

In this paper, we investigate the application of collinear AO switches to the optical correlator for label processing in WDM photonic label routers. This processing system consists of collinear AO switches and optical delay lines, where high-speed switching is not required in the AO switches. This correlator can be used for label recognition and also for label encoding in the time and spectral domains. Since the codes are encoded with optical short pulses at only one or a few wavelengths, the codes can be used for WDM packets. In processing of optical pulses encoded at multiple wavelengths, frequency-multiplexed SAWs are interacted. We discuss the integrated-optic structures for the label processing. The label recognition performance is demonstrated with numerical simulation using the filtering characteristics of the collinear AO interaction.

4B-6 3:45 p.m.

NEW TECHNOLOGY FOR CONTROL OF LIGHT INTENSITY USING ACOUSTICAL ACTIVITY IN GYROTROPIC CRYSTALS.

F. R. AKHMEDZHANOV*, Samarkand State University, Samarkand, Samarkand, Uzbekistan.
Corresponding e-mail: farkhad2@rambler.ru

In present work is proposed the new technology for measuring and control of light intensity, which is differed from all the existing technologies. In the proposed method is used the Bragg light diffraction on the hypersonic wave in gyrotropic crystal. In this case the intensity of diffracted light is dependent on the sound frequency by square law. The light intensity can be changed by modification of generator frequency by which the acoustic wave is excited. As a result, the increasing or decreasing of light intensity is provided electronically, fluently and with high accuracy. Using the standard calibration, it is possible to measure or to change the light intensity to the required value.

In the experiment, Bragg light diffraction on hypersonic transverse waves in ferroelectric crystal $LiNbO_3$ has been used for control and measuring of the laser light intensity. The plane-polarized transverse acoustic waves were excited in the frequency range from 0.9 to 1.1 GHz. Different values of light intensity have been obtained in the range from 0 to the maximum of the diffracted light intensity. These intensities have been used for determination of the specific rotation of the acoustic wave polarization. All necessary calculations have been made for speculation of experimental curves by varying factors, which can be changed in a real experiment.

Session: 5B

THIN FILM BAW MATERIALS I

Chair: K. Lakin

TriQuint

5B-1 2:30 p.m.

(Invited)

PIEZOELECTRIC / FERROELECTRIC FILMS FOR MICROWAVE / MEMS APPLICATIONS: HISTORIC PERSPECTIVE.

S. V. KRISHNASWAMY*, Electronics Sensor Sector, Northrop Grumman Systems Corporation, Baltimore, MD 21090.
Corresponding e-mail: sv.krishnaswamy@ngc.com

This paper surveys the status and recent progress in the growth of piezoelectric and ferroelectric films. Although we discuss the applications of these films

primarily to FBAR resonators and filters some examples of MEMS devices are also included. After a general and historical introduction to bulk acoustic waves (BAWs) and surface acoustic waves (SAWs) a review is given of technologically important materials for microwave acoustic applications with specific reference to FBARs.

Miniature thin film bulk acoustic wave resonator filters rely on obtaining highly oriented thin piezoelectric films. To exhibit piezoelectricity, the crystalline structure of the film must be oriented for alignment parallel with the applied electric field. The electromechanical couplings directly affected by the degree of alignment. Thus, the achievement of processing optimization to obtain this precise ordering of PZ films represents a significant advancement toward low loss microwave filters.

In addition thin films of piezoelectric and ferroelectric materials are also critical in the fabrication of infrared imagers, integrated optic circuits, optical displays, and high-performance semiconductor memories. In this review we discuss recent progress in the control of growth, structure and properties of candidate materials such as ZnO, AlN, PZT-based solid solutions, bismuth titanate. The emphasis of the review is primarily on films grown by physical vapor deposition techniques and on the piezoelectric films for microwave acoustic and RF MEMS applications.

5B-2 3:00 p.m.
C-AXIS INCLINED ZNO FILMS DEPOSITED BY REACTIVE SPUTTERING USING AN ADDITIONAL BLIND FOR SHEAR BAW DEVICES.

M. LINK*[1,2], M. SCHREITER[1], J. WEBER[1], D. PITZER[1], R. PRIMIG[1], M. B. ASSOUAR[2], and O. ELMAZRIA[2], [1]Siemens AG / Corporate Technology, Munich, Germany, [2]Université Henri Poincaré / Laboratoire de Physique des Milieux Ionisés et Applications, Nancy, France.
Corresponding e-mail: mathias.link.1@etumail.uhp-nancy.fr

ZnO thin films where the c-axis is inclined with respect to the surface normal are of interest for the excitation of shear-mode in film bulk acoustic resonators (FBAR), especially when operation in liquids is desired. The growth of ZnO films with inclined orientation is difficult, as the strong trend of the ZnO to crystallize in the perpendicular direction must be overcome. In this work, a technique to deposit inclined ZnO by reactive sputtering using an additional blind positioned between target and substrate is presented. It is shown that oblique particle incidence, which permits inclined film growth, can be achieved without having to tilt the substrate.

400 nm ZnO thin films were deposited reactively with a conventional DC-pulsed magnetron sputtering equipment. Chamber pressure ranged from 0.2 to 0.5 Pa and heater temperature was varied from 150°C to 280°C. A rectangular blind of height varying from 15 to 35 mm was positioned between the substrate and the target. The ZnO films were deposited on the following layered structure: SiO_2 or Al_2O_3 (100 nm) / Pt (100 nm) / Si (400 μm). X-ray diffraction (XRD) and scanning electron microscopy (SEM) have been carried out to obtain information about the film structure. θ-2θ and χ scans confirm that the films have a wurtzite

hexagonal structure with c-axis inclined up to 16° with respect to the surface normal. With this inclination, both shear and longitudinal waves can be excited with comparable electromechanical coupling constants. The most likely explanation for the obtained inclination is oblique particle incidence. The blind positioned near the substrate surface blocks particles with a certain incidence direction yielding an oblique mean incidence angle. Simple geometric simulations performed using MatLab corroborate this explanation. The results of the simulations correspond well to the inclinations measured by XRD.

By depositing a top Pt electrode (100 nm) and structuring it in a ground-signal-ground configuration, highly over-moded FBARs have been obtained. Because a thick Si substrate is used, a series of resonance peaks exist. Between 800 and 900 MHz, the spacing between resonances is about 5.69 MHz, corresponding to an acoustic velocity of 4552 m/s. This is close to the theoretical value of 4674 m/s of the quasi-shear acoustic velocity in (110) Si. An electromechanical coupling constant K of 13 % was obtained for a 16° inclined ZnO film, which is approximately half of the maximum theoretical value that can be reached at this inclination. The lower value may be attributed to a partially opposite adjustment of polar axes.

The described sputtering method produces c-axis inclined ZnO films without the need of an inclination of the substrate. With adapted and geometrically more complex blinds, it will be possible to obtain controlled inclinations over the whole wafer.

This work received financial support from the European Community Information Society Technologies program; project PISARRO (IST-2001-33326).

5B-3 3:15 p.m.
HIGH-Q THIN FILM BULK ACOUSTIC WAVE RESONATOR USING HIGHLY <111>-ORIENTED ALUMINUM ELECTRODE.

R. OHARA*, K. SANO, N. YANASE, T. YASUMOTO, T. KAWAKUBO, and K. ITAYA, Corporate R&D Center, Toshiba Corporation, Kawasaki, Japan., Kawasaki, Kanagawa, Japan.
Corresponding e-mail: ryoichi.ohara@toshiba.co.jp

Recently, FBAR (Film Bulk Acoustic wave Resonator) resonator technologies have become more promising because they provide high performance small passive components, such as filters, making it possible to develop single-chip RF module that contains all the passive and active components.

The choice of the bottom electrode materials of FBARs is an extremely important issues in the fabrication of highly c-axis oriented AlN thin films and in the fabrication of high-Q resonators [1-2]. In this paper, high-Q FBARs using aluminum electrodes are studied. The use of aluminum electrodes in FBARs has advantages as well as disadvantages. The advantages include: (1) low resistivity, (2) compatibility with LSI processes, and (3) similar surface structure of Al(111) and AlN(0001). The disadvantages include: (1) low density thus a low effective coupling constant, (2) low acoustic Q-values and (3) large temperature coefficient of frequency.

It is well-known that there are several methods for achieving highly <111>-oriented Al thin films, such as choosing the suitable substrate and its surface direction appropriately or using an optimized underneath layer. Since the crystallinity of the AlN films depend strongly on that of the bottom electrode, we concentrated on these issues and successfully obtained highly <111>-oriented Al thin films with an Al(111) rocking curve FWHM of 0.7°. The fabricated AlN films showed excellent crystallinity even at the initial stages of the AlN film deposition. For example, the (0002) rocking curve FWHM for the 50nm AlN film was 1.3°. After completion of fabrication and patterning of the top electrode, the cavity was formed by using deep-RIE from the back side of the Si substrate.

The fabricated resonators showed good resonance characteristics, such as high-Q values (loaded-Q ~700) and high effective coupling constants (~6.7%). The impedance ratio (Zmax/Zmin) was more than 1500, corresponding to an FOM (Figure of merit) of 51. These values indicated that aluminum could be a promising electrode material for high-Q FBARs and low loss filters.

[1] S. Mishin et al., Proc. 2003 IEEE Ultrasonics Symposium, p.2028.

[2] T. Yokoyama et al., Proc. 2002 IEEE Ultrasonics Symposium, p.429.

5B-4 3:30 p.m.
VOLUME MANUFACTURING ASPECTS OF BAW FILTERS ON A PRODUCTION CLUSTER SYSTEM.

R. LANZ*[1], C. LAMBERT[1], C. MULLER[2], and M.-A. DUBOIS[2], [1]UNAXIS BALZERS AG, Balzers, Liechtenstein, [2]Centre Suisse d'Electronique et de Microtechnique SA, Neuchatel, Switzerland.

Corresponding e-mail: roman.lanz@unaxis.com

The growing acceptance of Bulk-Acoustic-Wave (BAW) technology for frequency selection devices in the RF front-end of mobile phones and other mobile communication systems calls for increased requirements in terms of properties of the piezo-electric material, metal electrode and, when required, acoustic reflector layers. A highly textured, c-axis oriented, smooth, piezo-electric Aluminum-Nitride (AlN) film with excellent thickness uniformity is paramount to the industrial manufacturing of high performing BAW devices. This can be achieved with reactively, pulsed-DC sputtered AlN thin-films using a high uniformity sputter source showing repeatable, on-wafer AlN thickness uniformity below 0.5% 3s on 150mm wafers. Furthermore, the deposition process of each additional layer of the BAW stack, e.g. electrodes, acoustic reflector layers, seed & adhesion layers, and frequency trimming layers requires dedicated optimization with respect to texture, roughness and stress to minimize acoustic losses and maximize the electromechanical coupling. For the deposition of these layers, a large similarity in process chamber design and operation with respect to the AlN process module is beneficial to production reliability. The requirements on AlN and electrode layer uniformity and quality are such that technology providers have come-up with dedicated equipment and processing solutions in order to meet the manufacturing challenge. In particular, the integration of both sputter deposition and clean-etch processes of multiple layers of the BAW stack into a single manufacturing platform, while maintaining process versatility and

robustness, is an important capability. An efficient optimization of the deposition and etch processes is possible when the link to the electrical properties of the device is clearly established. This raises the need for equipment and technology suppliers to go one step further and come up with demonstrator BAW devices in order to assess and optimize electro-mechanical properties that result from the complex interaction of multiple films in BAW applications.

In this paper, the process repeatability and film properties from our library of BAW processes are presented, including advances for the deposition of AlN, Mo, W and SiO_2 films on 150mm wafers using a single, dedicated, volume production cluster system. The integration of SiO_2 dielectric and W processes is validated through the deposition and characterization of acoustic reflector layers (SiO_2/W/SiO_2/W/SiO_2), achieving a total stack stress close to 0MPa. The smoothing effect of using a soft-etch treatment on the acoustic reflector stack properties is shown. Mo-AlN-Mo layers are subsequently deposited to form Solidly Mounted Resonators (SMR) devices, which are used to demonstrate the on-wafer distribution of electrical properties, in particular a resonance frequency spread across the wafer compatible with RF filter specification requirements. As a next step, the fabrication of SMR filters centered at 1.96GHz is carried out to demonstrate the volume capability of the cluster system for high yield total BAW solutions.

5B-5 3:45 p.m.
IMPROVING MANUFACTURABILITY OF ALN DEPOSITION USED IN MAKING BULK ACOUSTIC WAVE DEVICES.

S. MISHIN*, B. SYLVIA, and D. MARX, Advanced Modular Sputtering, Inc., Goleta, CA.
Corresponding e-mail: dmarx@burgconsulting.com

Bulk acoustic wave (usually referred to as BAW or FBAR) signal filter devices are currently used in more than 50 million CDMA phones produced in the last three years. While it is no longer a great challenge to make limited numbers of wafers employing reactively sputtered piezoelectric AlN films suitable for BAW applications, there are several barriers to making them in a high volume. Control of uniformity, deposition rate, and stress through target lifetimes and from target-to-target variations in are major barriers to high volume production. Novel tool innovations have been successfully implemented to address these issues. Data from production tests show that in-situ laser interferometric thickness monitoring significantly reduces wafer-to-wafer thickness variations due target rate roll-off. Uniform, consistent sputtering target metallurgy is shown to be a critical factor. Use a unique local enhancement of the magnetron magnetic field to compensate for non-radial uniformity profiles eliminates changes induced by variations in target material as well as system asymmetry. Adjustment of stress is achieved though process gas flow control.

Session: 6B
PIEZOELECTRIC SINGLE CRYSTAL TRANSDUCERS
Chair: T. Shrout
The Pennsylvania State University

6B-1 2:30 p.m.
A 7.0 MHZ 0.15MM PITCH PHASED ARRAY ULTRASONIC PROBE USING PMN-PT SINGLE CRYSTAL.

S. M. RHIM*[1], H. JUNG[1], J.-S. JUN[2], and J.-S. HWANG[2], [1]HUMANSCAN Co., Ltd., Ansan, Kyunggi-do, [2]Medison Co., Ltd., Seoul, Korea.
Corresponding e-mail: rms@humanscan.co.kr

PMN-PT single crystal phased array is usually used for low frequency phased array application (1~3MHz) and there are two main reasons in these. First, to get a low frequency single crystal probe is much easier than to get a high frequency probe as single crystal wafer is thick. Second, the attenuation of probe is increased as frequency increasing. However, resolution of ultrasound image is promoting as frequency increasing. Therefore, the image quality of high frequency phased is better than that of low frequency phased array if probe has a high sensitivity. Resently, harmonic imaging technique is used in order to get better image quality in low single crystal phased array using broad bandwidth of single crystal. However, sensitivity of harmonic component is much lower than that of non-harmonic component. Therefore, the penentration of harmonic image is not so good in spite of high resolution than that of fundamental image.

The performance of 64 channel 7.0 MHz phased array ultrasonic probe using PMN-PT single crystal was investigated and compare image quality with low frequency (~3MHz) phased array. The axial resolution of 7.0 MHz phased array is much better than that of 3MHz phased array. The penentration of 5.0 MHz phased array is almost same as 3.0 MHz phased array at the same focal depth. The 6dB bandwidth of this probe is about 100% and directivity is about 95% with respect to theoretical value using CW theory.

6B-2 2:45 p.m.
$PB[(IN_{1/2}NB_{1/2})_{0.24}(MG_{1/3}NB_{2/3})_{0.42}TI_{0.34}]O_3$ PIEZOELECTRIC SINGLE CRYSTAL FOR MEDICAL ARRAY TRANSDUCER.

Y. HOSONO* and Y. YAMASHITA, Advanced Electron Devices Laboratory, Corporate R&D Center, Toshiba Corporation, 1 Komukai, Toshiba-cho, Saiwai-ku, Kawasaki 212-8582, Japan.
Corresponding e-mail: yasuharu.hosono@toshiba.co.jp

The dielectric and piezoelectric properties of $0.24Pb(In_{1/2}Nb_{1/2})O_3$-$0.42Pb(Mg_{1/3}Nb_{2/3})$-$0.34PbTiO_3$ (PIMNT 24/42/34) single crystal (SC) have been investigated in order to improve thermal stability and voltage-proof nature of the electrical

properties. A PIMNT 24/42/34 SC 25 mm in diameter and 30 mm in length was successfully grown by the solution Bridgman method using PbO-B_2O_3 flux; the highest temperature was 1250°C and the growth rate was 0.4 mm/h. The Curie temperature, T_c, and the phase transition temperature between a rhombohedral and tetragonal phase, T_{rt}, were 184°C and 89°C, respectively. The dielectric constant after poling, $\varepsilon_{33}^T/\varepsilon_0$=4,900, electromechanical coupling factors for sliver mode, k_{33}'=80%, piezoelectric constant, d_{33}=2,200 pC/N, and coercive field, E_c=6.8 kV/cm, were confirmed. The k_{33}' value of the PIMNT 24/42/34 SC was very stable until around 80°C because of its relatively high T_{rt}. Moreover, the PIMNT 24/42/34 SC had large E_c due to its high T_c, indicating a good voltage-proof nature. Therefore, the PIMNT 24/42/34 SC may be a promising candidate piezoelectric material for the medical array transducer application in view not only of its excellent piezoelectric properties but also of their good thermal stability and voltage-proof nature.

Multilayer SCs were prepared using the PIMNT 24/42/34 SCs and their dielectric and piezoelectric properties were estimated. Multilayer SCs were fabricated by a bonding method. The 2-layer SC showed about 4 times larger dielectric constant, $\varepsilon_{33}^T/\varepsilon_0$=19,000, and almost the same coupling factor, k_{33}'=78%, compared to those of the single-layer SC.

Simulation results based on the Mason model revealed that the sensitivity of the phased array probe with 2-layer SC was 10.5 dB higher than that of the phased array probe with single-layer SC and the fractional bandwidths of the probes were almost the same.

6B-3 3:00 p.m.
SINGLE CRYSTAL VS. PZT CERAMICS FOR MEDICAL ULTRASOUND APPLICATIONS.

M. LU* and T. PROULX, Siemens Medical Solutions, Mountain View, CA.
Corresponding e-mail: mlu@siemens.com

There has recently been a trend toward commercialization of piezoelectric single crystals (such as PMN-PT and PZN-PT) for sensors, actuators and medical ultrasound transducer applications. Single crystals are notable for having high piezoelectric and electro-mechanical coupling constants (d_{33} ~ 1500pC/N, k_{33} ~ 0.9), which are attractive for producing highly efficient and wide bandwidth transducers. However, these materials also possess a low clamped dielectric constant (K^S_3 ~ 700), coercive field (E_c ~ 2-5KV/cm) and Curie temperature (T_c ~ 120^0C), all of which can seriously limit the range of applications. This paper reviews some of the applications in medical ultrasound for which single crystal has an advantage or limitation compared to conventional PZT ceramics.

First of all, the exceptional fragility and the low sound velocity and coercive field of single crystal material ultimately define a limit on minimum single crystal thickness and therefore maximum frequency. It is effectively impractical to use this material for devices with center frequencies higher than 6 MHz, because of processing or handling constraints and the ability to withstand typical system driving voltages without depoling.

For very low frequency (1-3MHz) arrays with small elements (e.g., phased or multi-D arrays), the element impedance is typically very high for PZT (>500Ω), and impedance mismatch to the cable and system becomes a significant issue. Single crystals face even more challenges than PZT in this application. Typical solutions to the problem involve use of buffer electronics, or multi-layer structures to reduce element impedance. Several 2.5MHz phased arrays of 170um pitch were made with one and two-layer PMN-PT along with triple-layer PZT-5H for comparison. The effects of transformers and pre-amps on the response are also measured or simulated for the one layer PMN-PT array. Results show that performance of the two-layer PMN-PT array approaches that of the multi-layer PZT, but the single layer PMN-PT is significantly worse.

The application for which single crystals can potentially outperform conventional PZT is for transducers with center frequencies in the 3-5MHz range, especially those with larger elements, such as with linear arrays. We present results for a 3MHz PMN-PT array of 300um pitch with 90% fractional bandwidth compared to 75% for the PZT array.

Our experience shows that the benefits of single crystal over PZT for medical ultrasound depend on applications. The optimal uses of single crystals are arrays in the low to mid-frequency (3-5MHz) range, preferably with relatively large elements.

6B-4 3:15 p.m.
ULTRABROADBAND SINGLE CRYSTAL COMPOSITE TRANSDUCERS FOR UNDERWATER ULTRASOUND.

S. COCHRAN*, M. PARKER, and P. MARIN-FRANCH, University of Paisley, Paisley, Scotland, UK.
Corresponding e-mail: coch-ph0@wpmail.paisley.ac.uk

Complex piezoelectric structures exist which show additional resonant harmonics not observed in standard structures. These complex structures can be optimised to have a uniform amplitude of resonance over a number of harmonics in a continuous series. Moreover, with the use of inherently broadband components, such as composites made with PMN-PT single crystal material, and suitable ancillary transducer components, some of these resonances can be combined within a –3 dB amplitude range to give an ultrabroadband device. In the work reported here, results from one-dimensional modelling (ODM) using a matrix solution of the wave equation indicate that a bandwidth improvement by a factor up to four is possible compared with standard piezoceramic transducers. Experimental validation of this theoretical finding has taken place. Due to the lack of consistency of material properties of PMN-PT available commercially, the first stage in this validation involved careful selection of material from a range of suppliers and full characterisation using the commercially available Piezoelectric Resonance Analysis Program (PRAP, TASI Technical, Ontario, Canada). The output data from PRAP were used in ODM and finite element analysis (FEA) with PZ Flex (Weidlinger Associates Inc., CA, USA) to simulate the behaviour of the bulk PMN-PT prior to composite fabrication and good correlation was established. The second validation stage involved the design and fabrication of several composites with different PMN-PT volume fractions

ranging from 30% to 70%. The manufactured composites were tested and disagreements between experimental and theoretical data were reduced by appropriate adjustment of the model parameters. The new parameters were then input into ODM and FEA in the third stage of validation which involved acoustic stack design and optimisation. In this way, several single crystal composites multilayer transducers, designated PAT-UBB, have been made, including appropriate matching layers and housings. Relatively low acoustic impedance backing material was also used. Operating with centre frequencies around 600 kHz and apertures of 10 mm x 15 mm, pulse-echo tests have shown a –6dB relative bandwidth up to 125%, very close to the predicted 135%, with additional good correspondence in terms of ripple within the transducer's frequency range. The results indicate that materials such as PMN-PT can provide very unusually broadband behaviour when combined with complex piezoelectric structures.

This work was carried out under Scottish Enterprise Proof of Concept Award 4/OET-021

6B-5 3:30 p.m.
(Invited)
COMMERCIALIZATION OF PIEZOELECTRIC SINGLE CRYSTALS FOR MEDICAL IMAGING APPLICATIONS.

J. CHEN* and R. PANDA, Philips Medical Systems, Andover, MA.
Corresponding e-mail: j.chen@philips.com

Lead-based single crystals of $Pb(Mg_{1/3}Nb_{2/3})O_3$-$PbTiO_3$ (PMN-PT) and $Pb(Zn_{1/3}Nb_{2/3})O_3$-$PbTiO_3$ (PZN-PT) have become attractive in recent years for electromechanical applications, such as sonar, ultrasound imaging, and actuators. The family of crystal materials offers improved electromechanical properties compared to the existing lead zirconate titanate (PZT)-type ceramic materials, which have been the material of choice for high performance piezoelectric devices for the past 40 years. This paper reviews the discovery and development of piezoelectric single crystals, the advantages of these materials, and the challenges of using these crystal materials in commercial applications.

This work is mainly focused on solving the technical challenges for using piezoelectric single crystals in real devices for ultrasound imaging. The pros and cons of single crystals and ultrasound devices constructed using these materials will be discussed with reference to PZT based devices. Furthermore, this paper also explores the unique properties of <011> oriented single crystals. Single crystal transducer designs with significantly greater bandwidth compared to traditional PZT-based transducers will be discussed. The expanded frequency coverage allows the single crystal transducers to exhibit superior Harmonic imaging over a wider frequency range, and covers the applications of two existing transducers. Finally, the 2D grayscale and color flow cardiac images obtained with the first commercially released ultrasound transducer will be shown to demonstrate the advantage of using piezoelectric single crystals.

This work was partially supported by the Office of Naval Research (ONR).

Session: 1C

IVUS II
Chair: C. De Korte
Nymegen University MC

1C-1 4:30 p.m.
HARMONIC INTRAVASCULAR ULTRASOUND IMAGING WITH A DUAL-FREQUENCY CATHETER.

M. E. FRIJLINK*[1], D. E. GOERTZ[1,2], H. J. VOS[1,3], E. DROOG[1,4], G. BLAQUIÈRE[3,4], A. GISOLF[3], and A. F. W. VAN DER STEEN[1,2], [1]ErasmusMC, Rotterdam, the Netherlands, [2]Interuniversity Cardiology Institue of the Netherlands, Utrecht, the Netherlands, [3]Delft University of Technology, Delft, the Netherlands, [4]TNO-TPD, Delft, the Netherlands.
Corresponding e-mail: m.frijlink@erasmusmc.nl

Background The development of harmonic intravascular ultrasound (HIVUS) instrumentation has the potential to improve the performance tissue and contrast agent imaging with IVUS. Previously, we demonstrated the feasibility of tissue harmonic imaging (THI) in phantoms and *in vivo* using a prototype HIVUS system in combination with a conventional single-element continuously-rotating IVUS catheter (f_c = 30 MHz). In this study we mounted a previously developed dual-frequency transducer element in an IVUS catheter. We then investigated its performance in tissue harmonic imaging mode in phantoms and *in vivo*.

Methods The dual-frequency IVUS catheter was specifically designed for nonlinear imaging in the 20 - 40 MHz range. The catheter was evaluated with a previously reported prototype IVUS imaging system which was operated at a fundamental frequency of 20 MHz (F20) to obtain second harmonic signals at 40 MHz (H40) in pulse-echo mode. Additionally, this system incorporated a novel cascaded passive-active gated limiter circuit which was employed to produce more effective protection of the receive pre-amplifier. Water tank hydrophone measurements were performed to assess the frequency response and sensitivity of both the dual-frequency and the conventional catheters. In order to study the performance of the custom-made IVUS catheter in second harmonic imaging mode, a tissue mimicking phantom with linear scatterers was used. We assessed the signal-to-noise ratios (SNR) in H40 acquisitions with both the conventional and the custom-made catheter, when driven by a F20 pulse with the same amplitude. Finally, *in vivo* feasibility experiments were conducted in atherosclerotic rabbit aortas.

Results The frequency response of the custom-made IVUS catheter showed peaks at both 20 and 40 MHz. The transmit efficiency around 20 MHz was >6 dB higher than the conventional catheter, while around 40 MHz there was no significant difference. The phantom experiments showed a SNR improvement of >5 dB in H40 mode of the custom-made catheter relative to the conventional catheter when the same transmit pulse was applied (90 V_{pp}, 25% bandwidth). We also note that the cascaded limiter avoided saturation of the receive amplifier by suppressing the transmit pulses to below 25 mV peak-to-peak, which in turn

enabled improved imaging in the very near field. The rabbit experiments showed the expected image improvement of H40 imaging *in vivo*.

Conclusion These results indicate that instrumentation developments can improve harmonic IVUS imaging. More specifically, it is shown that an IVUS catheter with a dual-frequency characteristic can improve SNR in H40 tissue harmonic imaging.

Supported by STW and NWO.

1C-2 4:45 p.m.
ON THE POTENTIAL OF THE LAGRANGIAN SPECKLE MODEL ESTIMATOR FOR ENDOVASCULAR ELASTOGRAPHY: IN VIVO HUMAN CORONARY ARTERY STUDY.

R. L. MAURICE*[1], J. FROMAGEAU[1], É. BRUSSEAU[2], G. FINET[3], and G. CLOUTIER[1], [1]University of Montreal Hospital, Montreal, Quebec, Canada, [2]INSERM, Lyon, France, [3]Claude Bernard University, Lyon, France.
Corresponding e-mail: maurice.roch.chum@ssss.gouv.qc.ca

Diagnosis and prognosis of coronary artery atherosclerosis evolution currently rely on plaque morphology and vessel stenosis degree. Such information can accurately be accessed with IntraVascular UltraSound (IVUS) imaging. A severe complication of coronary artery atherosclerosis is thrombosis, a consequence to plaque rupture or fissure, which might lead to myocardial infarction, and sudden ischemic death. Plaque rupture is a complicated mechanical process, correlated with plaque morphology, composition, mechanical properties and with the blood pressure and its long term repetitive cycle. Extracting information on the plaque local mechanical properties and on the surrounding tissues may thus reveal relevant features about plaque vulnerability. According to that, EndoVascular Elastography (EVE) was introduced as a complementary tool to IVUS in the process of coronary artery disease investigations. In this paper, in vivo elastographic data are reported for three patients who were diagnosed with severe coronary artery stenoses. The radio-frequency (RF) data were acquired, in the minutes preceding angioplasty, using a CVIS (ClearView, CardioVascular Imaging System Inc.) ultrasound scanner working with a 30 MHz mechanical rotating single-element transducer. Due to the blood flow pulsation, the vascular tissue was naturally compressed/dilated. The elastograms, or radial strain distributions inside the vessel wall, were computed offline using the Lagrangian Speckle Model Estimator (LSME). This model-based approach considers the speckle as a material property that is, in average, conserved with tissue motion. According to that, tissue mechanical parameters (namely the strain tensor) were inferred from the speckle kinetics. The results showed the potential of the LSME to characterize and to distinguish coronary atherosclerotic plaques from the normal vascular tissue. Namely, atherosclerotic plaques about six times stiffer than the normal vascular wall were observed for two patients (0.8/0.16 and 0.8/0.12 strain ratios, respectively). Inversely, regarding the third patient, radial strain values in the plaque area were found higher than in the disease-free vascular tissue, indicating the potential presence of a lipid pool. In conclusion, these

results confirm that EVE might be a very relevant clinical tool to support IVUS echograms in the characterization of coronary artery. Nevertheless, further investigations are required to fully state on the vulnerability of coronary artery atherosclerotic plaques.

This work is supported by Valorisation-Recherche Québec (group grant #2200-094) and the Fonds de la Recherche en Santé du Québec (National Scientist Award).

1C-3 5:00 p.m.
DEFORMABLE BEZIER CURVES FOR YOUNG'S MODULUS RECONSTRUCTION AND DELINEATION OF VULNERABLE ATHEROSCLEROTIC PLAQUE COMPONENTS.

R. A. BALDEWSING*[1], F. MASTIK[1], J. A. SCHAAR[1], and A. F. W. VAN DER STEEN[1,2], [1]Biomedical Engineering, Thoraxcenter, ErasmusMC, Rotterdam, The Netherlands, [2]Interuniversity Cardiology Institue of the Netherlands (ICIN), Utrecht, The Netherlands.
Corresponding e-mail: r.baldewsing@erasmusmc.nl

Background and Goal Rupture, with subsequent thrombosis, of thin-cap fibroatheroma (TCFA) plaques is a major cause of myocardial infarction. A TCFA has two main components: a large, soft lipid pool and a thin, stiff, fibrous cap covering it. We report on a new tissue characterization method capable of automatically approximating their morphology and stiffness, which is essential for quantifying the effect of any pharmaceutical treatment that aims to stabilize plaques by reducing or stiffening their lipid pool.

Methods From a plaque's strain elastogram it reconstructs an approximation of the plaque′s Young's modulus (YM) distribution. To this end, a minimization algorithm automatically adjusts the morphology and stiffness parameters of a TCFA finite-element-model (FEM), until the corresponding FEM-simulated strain elastogram resembles the measured strain elastogram. The model's morphology parameters are the control-points of two deformable Bezier curves, one curve delineates the lipid pool, the other the cap; these component regions are assumed homogenous and their stiffness is characterized by a YM. The inner and outer boundaries of the TCFA-FEM are contour-detected from the plaque's intravascular ultrasound (IVUS) echogram. To demonstrate the performance of our new tissue characterization method, YM reconstructions were performed from a strain elastogram that was FEM-simulated using a histology-derived computer-TCFA (capYM=1375 kPa, lipidYM=25 kPa), and from a strain elastogram that was processed from radio-frequency data, measured with a 20MHz phased-array IVUS-catheter (Volcano Corp., Rancho Cordova, CA, USA) using a physical vessel-mimicking phantom having an eccentric, soft lipid pool.

Results Visually, the new method showed a much better reconstruction/delineation behaviour for both objects than a previously developed Circular reconstruction method, which used only circles for borders delineation. Using the computer-TCFA, errors in the cap and lipid pool region reconstruction were quantified. The used criteria were errors in: 1) YM, 2) region-overlap (RO), 3)

surface-area (SA) and 4) minimal cap-thickness. The RO-error between reference region A and reconstructed region B was defined as (1-2*[SA of their intersection]/[SA of A + SA of B])*100%.

Using those criteria, the Circular method gave errors of, respectively, 8%(1491/1375 kPa), 40%, -47%, -26%(114/156 μm) for the cap and -96%(1/25 kPa), 27%, 24% for the lipid pool, but the Bezier method merely -8%(1258/1375 kPa), 10%, 8%, -1%(155/156 μm) for the cap and 56%(39/25), 13%, 19% for the lipid pool.

Conclusions Since our new method enables the quantification of both the morphology and stiffness of vulnerable atherosclerotic plaque components, it may evolve into a valuable clinical tool for monitoring plaque progression/regression in vivo.

This research was financially supported by the Dutch Technology Foundation (STW) project RPG-5442 and the Netherlands Organization for Scientific Research (NWO). Feedback by Volcano Corp., Rancho Cordova, CA, USA was greatly appreciated.

1C-4 5:15 p.m.
MOTION COMPENSATION FOR INTRAVASCULAR ULTRASOUND PPALPOGRAPHY FOR *IN VIVO* VULNERABLE PLAQUE DETECTION.

K. Y. E. LEUNG*[1], R. A. BALDEWSING[1], F. MASTIK[1], J. A. SCHAAR[1,2], A. GISOLF[3], and A. F. W. VAN DER STEEN[1,2], [1]Biomedical Engineering, Thoraxcenter, Erasmus MC, Rotterdam, the Netherlands, [2]ICIN, Interuniversity Cardiology Institute of the Netherlands, Utrecht, the Netherlands, [3]Acoustical Imaging and Sound Control, Imaging Science and Technology, Delft University of Technology, the Netherlands.
Corresponding e-mail: k.leung@erasmusmc.nl

Background Intravascular ultrasound palpography can assess the mechanical properties of coronary arteries *in vivo* by radial strain measurements. Validation studies of this technique, previously reported at this conference, have revealed a clear association between high-strain patterns and the number of vulnerable plaques. The strain is measured by cross-correlating RF signals acquired at different systemic pressures. However, catheter motion due to cardiac activity causes misalignment of these signals, so that less strain estimates are obtained. This study reports motion compensation methods to correct for in-plane catheter rotation and translation.

Methods Four motion compensation methods, all based on block matching, were devised. The GRBM (Global Rotation Block Matching) and CMAP (Contour Mapping) methods measured catheter rotation, while LBM (Local Block Matching) and CRT (Catheter Rotation and Translation) estimated displacements of local tissue regions. The methods were validated on nine *in vivo* pullback acquisitions, acquired with a 20 MHz 64 element phased-array transducer (Volcano Corp.) at 30 frames/s. Each frame consisted of 512 circumferential RF lines and 1024 radial samples, which were sampled at 100 MHz. The motion compensation methods were used to align the RF signals of consecutive diastolic frames before

strain calculation. The resulting strain images, i.e. partial palpograms, were aligned and averaged per heart cycle to produce more accurate and robust compounded palpograms. To assess the performance of each method, the number of valid strain estimates in the partial and compounded palpograms was compared with the number without motion compensation. The validity of a strain estimate was determined from the theoretical relationship between strain and decorrelation of the signals: if the decorrelation did not fit the expected value as predicted by the measured strain within a certain bandwidth, the strain estimate was considered invalid.

Results We found that all four methods significantly increase the number of valid strain estimates in the partial and compounded palpograms (P<0.004). For the GRBM, CMAP, LBM, and CRT methods, the average increase in the partial palpograms amounted to 8.1%, 7.0%, 17%, and 11%, while the increase in the compounded palpograms was 5.9%, 4.8%, 15%, and 9.3% respectively.

Conclusions The Local Block Matching method is the best of the four methods investigated. Application of the motion compensation methods leads to palpograms with more valid strain estimates, which will improve the information coming from intravascular ultrasound palpography.

We wish to thank the Dutch Technology Foundation (STW) and Volcano Corp. (Rancho Cordova,CA) for their support.

1C-5 5:30 p.m.
SHEAR STRESS AND 3D INTRAVASCULAR ULTRASOUND PALPOGRAPHY IN HUMAN CORONARY ARTERIES.

F. GIJSEN*[1], J . WENTZEL[1], A. THURY[1], J. SCHUURBIERS[1], J. SCHAAR[1], F. MASTIK[1], A. VAN DER STEEN[1], P. SERRUYS[2], and C. SLAGER[1], [1]Department of Biomedical Engineering, ErasmusMC, Rotterdam, The Netherlands, [2]Department of Cardiology, ErasmusMC, Rotterdam, The Netherlands.
Corresponding e-mail: f.gijsen@erasmusmc.nl

Introduction Currently, it is widely accepted that in the presence of atherosclerotic risk factors, arterial wall locations that experience average low shear stress (SS) are most susceptible to the development of atherosclerosis. Previously, we investigated this relationship in human coronary arteries in-vivo, based on a realistic 3D reconstruction of lumen and wall thickness. The 3D lumen reconstruction served as an input to determine SS with computational fluid dynamics (CFD) and SS was related to the measured 3D wall thickness. To study the more advanced stages of atherosclerosis, including the vulnerable plaque, we need more than morphology alone. Radial strain data can be obtained by means of palpography and serves as an indicator of plaque vulnerability. The fusion of 3D lumen and functional strain data in human coronary artery opens perspectives to perform longitudinal studies to investigate the relationship between SS and plaque vulnerability.

Methods In 12 patients, an untreated coronary artery was imaged with biplane angiography and a sheath-based intravascular ultrasound (IVUS) catheter during ECG-gated pullback. The combination of biplane angiography and IVUS

(ANGUS) makes it possible to explore the 3D lumen and wall thickness. A 64-element phased array IVUS catheter was used during a second continuous pullback to explore the radial strain distribution in the same artery using IVUS palpography. To map the measured strain distribution on the 3D lumen, the two IVUS-based data sets were matched. In both the IVUS recordings corresponding landmarks, including side branches and calcified areas, were used to shift and rotate the data to obtain axial and circumferential matching.

Results We studied 5 right coronary arteries, 4 left anterior descending arteries and 3 left circumflex arteries. The matching procedure was successful in all patients. The average length for the stepped pullback was 57.8 ± 28 mm, and 6.1 ± 2.8 landmarks were identified. Applying a second order fit through the landmarks in two IVUS data sets, we observed a mean distance between the fit and the axial position of the landmarks of 0.52 ± 0.22 mm, and a mean angle between the fit and the circumferential position of the landmarks of 5.3 ± 2.1 degrees.

The results of the matching procedure enable us to map the strain data on the 3D lumen reconstruction from the ANGUS data. In a first analysis, we registered strain data on a realistic lumen of a right coronary artery. We observed 3 high strain spots with strain values larger than 1.2 % at Δp=3 mmHg. All the high strain spots were located in a region with low SS. The relationship between strain, 3D geometry and SS is currently being quantified in the other patients, using the successfully matched data.

Conclusions We demonstrated that the fusion of ANGUS and palpography is feasible in the main human coronary arteries. The combination of ANGUS with CFD renders the SS distribution, opening the possibilities to study the relationship between SS and plaque vulnerability in human coronary arteries in-vivo.

1C-6 5:45 p.m.
A FEASIBILITY STUDY OF INTRAVASCULAR ULTRASOUND ELASTOGRAPHY ON ABDOMINAL ANEURYSMS.

J. FROMAGEAU*, S. LEROUGE, G. SOULEZ, I. SALAZKIN, J. RAYMOND, and G. CLOUTIER, University of Montreal Hospital, Montréal, Québec, Canada.
Corresponding e-mail: j.fromageau@umontreal.ca

Abdominal Aneurysms (AA) occur in 5-7% of the population older than 60 years in industrialized countries. Surgery is presently the standard treatment but the repair by placement of a stent-graft (SG) is a promising minimally invasive alternative. AA is characterized by a dilation of the artery associated with changes of its mechanical and biological properties. Intravascular ultrasound (IVUS) and elastography have been combined to take advantage of the high resolution of this imaging modality to investigate elasticity of the arterial wall of AA.

In this work, the feasibility of the IVUS elastography method for the follow-up of AA pathology and treatment has been studied. Acquisitions were performed at different times, before implantation of the SG, right after implantation, and 3 months later. Several aspects were investigated. First, changes of mechanical properties associated with aneurysms were studied by comparing strain in the

aneurysmal wall to that at the region of the neck before SG implantation. Secondly, we investigated the feasibility of studying possible changes in arterial wall elasticity due to SG constrain after SG implantation. Finally, IVUS elastography was performed 3 months after SG implantation to determine its potential to evaluate the success of the repair and the degree of healing around the implant. In particular, we assessed if IVUS elastography could evaluate the properties of the thrombus formed between the SG and the aneurysmal wall. The elastography method was also considered to detect persistent blood flow in the aneurysm.

Data were acquired in vitro and in vivo on iliac arteries of a canine model, aneurysms were created by surgical construction using venous patches. Images were acquired with a Volcano Therapeutics In-Vision ultrasound scanner and a 20 MHz probe. The probe was coupled to a pullback system to image the whole aneurysm, each acquisition consisted in more that 1000 images. Radio-frequency images were recorded via a Remora data acquisition system and were digitized at 100 MHz with a frame rate of 30 Hz. This frame rate allowed to capture successive images with a small increment of pressure and the small pullback speed of 1 mm s^{-1} permitted to keep a good correspondence between images, which improved the computation of the elastograms.

The preliminary results showed that the artifacts due to the SG's metallic structure are negligible on the IVUS images and on the elastograms. Elastograms in the aneurysm wall showed two distinct areas, possibly the artery and the venous patch, one of these regions had a similar strain (mean strain of 0.5 %) than the strain calculated in the neck, which is normal for this model. Right after implantation, SG rigidity did not allow to estimate coherent elasticity images except in the neck area. After 3 months, a pulsatility was observed around the SG, and elastograms could be estimated highlighting a possible neo-intima.

Valorisation-Recherche Québec (group grant #2200-094) and the Fonds de la Recherche en Santé du Québec (Scholarship awards and National Scientist award).

Session: 2C
ULTRASOUND 19TH CENTURY TO 21ST CENTURY
Chair: J. Greenleaf
Mayo Clinic

2C-1 4:30 p.m.
(Invited)
LORD RAYLEIGH.

P. N. T. WELLS*, Cardiff University, Cardiff, UK.
Corresponding e-mail: WellsPN@cf.ac.uk

John William Strutt was born on 12 November 1842, at Langford Grove in Essex, UK. He was a sickly boy, so his schooling was sporadic. He went up to Cambridge

University 1861, read mathematics and graduated in 1865 with the highest honours in his year. He then obtained a Fellowship at Trinity. In 1871, he married Evelyn Balfour, sister of Arthur Balfour, who later was Prime Minister. Then, in 1872, he suffered a severe attack of rheumatic fever and, to escape the English climate, spent the winter in Egypt and Greece. His father died in 1873 and John William Strutt succeeded to the title as third Baron Rayleigh. He managed the family estate for a few years and combined this with the pursuits of a gentleman scientist. During this period, he published "The Theory of Sound", with volume I appearing in 1877 and volume II, in 1878. The two volumes of this book lay the foundations of all branches of modern acoustics, including medical ultrasonics. In 1879, Rayleigh was appointed second Professor of Experimental Physics and Head of the Cavendish Laboratory in Cambridge; but, in 1884, he returned to his family seat to escape from the distractions of the university and to concentrate on his research. Despite the agricultural depression at the time, Rayleigh was wealthy enough to be able to maintain the momentum of his work. During the period from 1879, Rayleigh investigated optics, vibrating systems, sound, wave theory, color vision, electrodynamics, electromagnetism, light scattering, flow of liquids, hydrodynamics, density of gases, capillarity, elasticity and photography. In all, he published 446 papers. In 1904, he was awarded the Nobel Prize in Physics for his measurements of the density of gases in the air and the discovery of argon. This was the apogee of numerous honors, most notably the Fellowship of the Royal Society in 1873, its Presidency from 1905 to 1908 and the Order of Merit in 1902. Despite these distinctions, Rayleigh was a modest man. He donated his Nobel Prizemoney to Cambridge University to build an extension to the Cavendish Laboratory. Of the Order of Merit, he said "the only merit of which I personally am conscious was that of having pleased myself by my studies and any results that may be due to my researches were owing to the fact that it has been a pleasure for me to become a physicist." In retrospect, it may seem odd that, towards the end of his life, Rayleigh took up an interest in spiritualism: he was President of the Society for Psychical Research in 1919. He died at his home, Terling Place in Essex, on 30 June in the same year.

2C-2 5:00 p.m.
TARGETED CHEMOTHERAPY DELIVERY WITH ULTRASOUND.

M. SHORTENCARIER*[1], T. MATSUNAGA[2], P. SCHUMANN[2], R. LABELL[2], and K. FERRARA[1], [1]University of California at Davis, Davis, CA, [2]ImaRx Therapeutics, Inc., Tuscon, AZ.
Corresponding e-mail: mashort@ucdavis.edu

We demonstrate local drug delivery achieved by ultrasound and modified ultrasound contrast agents used as delivery vehicles. The delivery vehicles are thick-shelled microbubbles that carry a hydrophobic drug. We have previously shown in *ex vivo* studies that combining radiation force and fragmentation pulses can effectively deflect and disrupt gas-filled drug vehicles, depositing the contents on blood vessel walls. The addition of targeting ligands to the shell to improve target specificity is explored here using an RGD peptide sequence to target

expression of $\alpha_v\beta_3$. Static binding assays indicate targeted AALs have a 26.5-fold increase in bound vehicles over non-targeted AALs. To investigate transfer of a drug to nearby cells, two cytotoxicity assays are performed after application of the delivery scheme with vehicles containing the chemotherapeutic drug paclitaxel. Cytotoxicity assays indicate that paclitaxel is delivered to the surface of human melanoma cells and exerts cytotoxic effects, while also demonstrating that the effects of ultrasound alone or ultrasound with delivery vehicles without paclitaxel have a significantly smaller cytotoxic effect. Cells exposed to the delivery pulse sequence with vehicles containing paclitaxel had 10.9-fold less area covered by cell proliferation in culture than the saline control, 10.5-fold less than the ultrasound control, and 8.1-fold less than the ultrasound plus vehicle control. Cells exposed to the delivery pulse sequence with vehicles containing paclitaxel, as well as having targeting ligands incorporated into the shell, had 15-fold less area covered by cell proliferation in culture than saline control, 14.5-fold less than the ultrasound control, and 11-fold less than the ultrasound plus vehicle control. For the delivery vehicle with and without molecular targeting ligands, cytotoxicity after the application of ultrasound was greater than the equivalent conventional paclitaxel treatment. *In vivo* studies with the chicken embryo model (chorio-allantoic membrane model) provide optical real-time imaging of fluorescently-labeled vehicles during insonation. These studies show a local build-up of a fluorescent model drug in the region of the ultrasound beam after a 1 minute application of the drug delivery pulse sequence with a center frequency of 1MHz and peak negative pressure of 50 kPa (radiation force) or 1MPa (fragmentation pulses). At higher transmission pressures the drug can be deposited outside the vessel as well as on the endothelium. The results collectively show promise for this technique by demonstrating that binding via targeting ligands is achievable, the drug is made available to the cells for exertion of bio-activity, and that *in vivo*, drugs are successfully delivered to the endothelium.

This work was supported by NIH CA103828, EB 002952, and ImaRx Therapeutics, Inc.

2C-3 5:15 p.m.
IMPROVING THE USE OF VIBRO-ACOUSTOGRAPHY FOR BONE IMAGING.

F. MITRI*, J. GREENLEAF, and M. FATEMI, Mayo Clinic, Rochester, MN.
Corresponding e-mail: mitri@ieee.org

Background:Ultrasound standing waves in Vibro-acoustography (V.A.) remain a main problem that reduces image quality. The standing wave effect is inherent to Continuous-wave (C.W.) excitation. This effect may occur when the object reflects a portion of the incident ultrasound beam back to the transducer. The transducer surface can then act as a mirror to re-reflect the reflected field towards the object. Depending on the distance between the transducer and the object, and the ultrasound wavelength, these components may interact constructively or destructively. Therefore, the field intensity at the object and hence the resulting image becomes excessively sensitive to the transducer-to-object distance as well as to the frequencies of the ultrasound beams. Artifacts are created and appear as bright and dark stripes in the image.

Methods:V.A. is used in a fundamentally new way to remove the ultrasound standing wave artifact from images. V.A. uses the dynamic radiation force of two C.W.-ultrasound beams to image objects at low frequency. In this technique, the dynamic radiation force is created by means of a confocal focused transducer emitting two ultrasound beams at slightly-shifted frequencies f1 and f2 = f1 + Δf. In response to this force, the object produces an acoustic emission field at the frequency Δf which is used to create an image related to both acoustical and mechanical properties of the object. The process of removing the ultrasound standing wave artifact consists of sweeping the frequencies of the incident ultrasound beams f1 and f2 in a selected bandwidth (i.e.δf) while keeping Δf constant during the sweep. The chirp image is produced by averaging the amplitude of the acoustic emission produced during the sweep.

Experiments:V.A. experiments on excised rabbit scapulas with and without associated muscles were conducted at room temperature. The two scapulas were excised from a euthanized rabbit and immediately immersed in 0.9% saline solution. One of them was carefully cleaned from muscles. They were then kept refrigerated for one hour before the measurements were made. The chirp process was performed in a shorter bandwidth range defined by $0 \leq \delta f \leq 30$ kHz while keeping Δf constant ($\Delta f = 10.8$ kHz). A total of 30 images in increments of 1 kHz were obtained. Each image covered an area of 40 mm by 56 mm, scanned at 0.4 mm/pixel.

Results:The artifacts in the “fixed frequency” images appear as a series of bright and dark stripes at some locations of the scapulas. These artifacts reduce image quality and result in the masking of some details of the bone structure. Some parts of the scapulas are obscured due to the standing wave artifact. The chirp image is the result of averaging N=30 frequency samples acquired during the 30-kHz sweep of the ultrasound frequencies at a fixed $\Delta f = 10.8$ kHz. The resulting chirp images demonstrate remarkable reduction of the standing wave artifact compared to the “fixed frequency” V.A. images.

Conclusion:A new process to remove the ultrasound standing wave artifact is developed. Results indicate that chirp imaging significantly increases the contrast in vibro-acoustography imaging.

2C-4 5:30 p.m.
TISSUE MICROSCOPY USING OPTICAL GENERATION AND DETECTION OF ULTRASOUND.

S. ASHKENAZI*, R. WITTE, K. KIM, Y. HOU, and M. O’DONNELL, University of Michigan.
Corresponding e-mail: shaia@eecs.umich.edu

Optical detection of ultrasound provides a unique and appealing way of forming detector arrays (1D or 2D). Etalon based optical techniques are of particular interest, due to their relatively high sensitivity resulting from multiple optical reflections within the resonance structure. Detector arrays formed by etalon based techniques are characterized by high element density and small element active area, which enables high resolution imaging at high ultrasonic frequencies (typically 10-50 MHz).

Laser generated ultrasound using the photoacoustic effect has been demonstrated in recent years as a powerful imaging modality for medical and biological applications. A short laser pulse illuminates a tissue creating rapid thermal expansion and acoustic emission. Detection of the resulting acoustic field by a detector array enables the imaging of the tissue optical absorption using ultrasonic imaging methods. One of the most appealing features of photoacoustic imaging is that it provides access to tissue composition in the molecular level using multiple wavelength illumination.

In this paper we present an integrated imaging system incorporating laser generated ultrasound and etalon based ultrasound detection. We used a pulsed doubled Nd:YAG laser (λ = 532 nm, pulse width = 12 ns, pulse energy = 30 mJ, pulse repetition rate = 10 Hz) to generate the acoustic excitation. The etalon detector is scanned by a focused CW laser (tunable wavelength range 1440-1590 nm, 4 mW) to form an array of detection positions. Typically, the array aperture is 4 X 2 mm with a corresponding grid size of 200 X 20 points. The effective detection diameter at each point is 20 μm.

High resolution images of phantom targets and biological tissue samples (lobster nerve cord) were obtained. The resolution of these images is better than 50 μm. It is limited by the finite width of the laser excitation pulse (12ns) and by the acoustic response of the etalon structure. An acoustic microscopy system operating at a center frequency of 50 MHz is used to provide a comparison between the two modalities. The additional information of optical absorption obtained by photoacoustic imaging, along with the high resolution detection of the etalon, offer unique advantages for in vitro tissue microscopy and in vivo applications such as intravascular imaging.

2C-5 5:45 p.m.
THE SONIC WINDOW: SECOND GENERATION PROTOTYPE OF LOW-COST, FULLY-INTEGRATED, POCKET-SIZED MEDICAL ULTRASOUND DEVICE.

M. FULLER*[1], E. BRUSH[2], M. EAMES[1], T. BLALOCK[2], J. HOSSACK[1], and W. WALKER[1,2], [1]Dept. of Biomedical Engineering, University of Virginia, Charlottesville, VA, [2]Dept. of Electrical and Computer Engineering, University of Virginia, Charlottesville, VA,.
Corresponding e-mail: mikefuller@virginia.edu

The Sonic Window is a very low-cost, fully-integrated, pocket-sized medical ultrasound device under development at the University of Virginia. It will ultimately consist of a fully-sampled 2D transducer array, receive circuitry implemented on a custom integrated circuit (IC), a DSP to implement our novel beamforming scheme, and LCD for image display, all integrated into a unit the size of a deck of cards. The overall system level design, the low-cost 2D transducer array design, and the DSIQ beamforming algorithm have been described previously. More recently, the first generation system prototype—consisting of a fully sampled 32x32 transducer array and 1024 channels of front-end receive circuitry implemented on a 11" x 11.5" PCB containing 16 custom ICs—was demonstrated to successfully form pulse-echo C-mode images of a wire target and edge

phantom. This paper will focus on the development of the second generation Sonic Window prototype. An array of 3,600 full receive channels—consisting of protection circuitry, a preamplifier, tunable bandpass filter, sampler bank, and 8-bit ADC—is formed by solder bumping twelve identical 300-channel custom ICs onto a double-layer flex circuit substrate. The receive channel pitch is 200 μm x 275 μm and the entire receive circuitry array has a form factor of only 1.9 cm x 1.8 cm. The flex circuit also provides I/O fanout to a beamforming PCB containing bias circuitry, programmable logic, a DSP, and LCD for image display. The receive circuitry array connects through a z-axis electrically conducting interface to a 60x60 element, 300-micron-pitch, fully-sampled transducer array inexpensively fabricated on a double-layer PCB substrate. This prototype will occupy a package the size of a deck of cards and be capable of forming C-mode ultrasound images in real-time. To this end, two custom integrated circuits have been designed and fabricated. The first is a test chip containing individual circuit blocks of the receive channel, including the tunable bandpass filter, sampler bank, 8-bit ADC, and memory. The center frequency of the tunable bandpass filter can be adjusted between 3 - 10 MHz. Experimental test results from this chip are presented. The second chip is the complete 300-channel receive circuitry array IC and will be tested for basic functionality prior to being assembled along with the 60x60 element transducer array, flex circuit, beamforming PCB, and LCD. Initial test results from this second generation Sonic Window prototype are also presented.

This work was supported by the Carilion Biomedical Institute and NIH grant RO1 EB002349.

Session: 3C

NDE-WAVE PROPAGATION
Chair: D. Yuhas
Industrial Measurement Systems

3C-1 4:30 p.m.
DEVELOPMENT OF WIDE FREQUENCY RANGE ULTRASOUND EXPOSURE SYSTEM FOR DISPERSION OF NANO DIAMOND PARTICLES.

T. UCHIDA*, A. HAMANO, N. KAWASHIMA, and S. TAKEUCHI, Toin University of Yokohama, Yokohama, Kanagawa, Japan.
Corresponding e-mail: td10c01@edu.toin.ac.jp

Diamond particles have been used as abrasive agents for high precise polishing or solid lubricants. For example, hard disk substance is polished by diamond particles. Nano-order precise polishing is needed, because of increase of recording density of hard disk. Dispersion stability and dispersibility are important for diamond particles using as abrasive agents. However, most diamond particles are aggregated immediately after manufactured. We considered new dispersion method for diamond particles with shock wave and active oxygen species generated by acoustic cavitation in order to solve such problems like aggregation.

When we irradiated high intensity ultrasound into the diamond particle suspension at 155 kHz and standing wave acoustic field was formed, active oxygen species were generated with generation of acoustic cavitation in the suspension. We proposed the methods that the aggregated nano diamond particles were disaggregated using shock wave from acoustic cavitation and surface of disaggregated particles were modified using the active oxygen species. Consequantly, the disaggregated particles were avoided from re-aggregation. We reported these considered results in 2004 IEEE UFFC in Montreal. However, since the conventional ultrasound exposure system was the narrow frequency band system (fractional bandwidth of 9%) using the Langevin-type transducer, we are apprehensive that the performance of the system became unstable by changing resonant frequency of the transducer due to temperature elevation by long time operation. Therefore, we developed the ultrasound exposure system using PZT piezoelectric ceramic vibrator and acoustic matching layer which is expected to operate in wide frequency range and with high efficiency in this time. There is almost no consideration on the ultrasound exposure system using the acoustic matching layer in the field of sono-chemistry. The bottom plate of the water tank for irradiation of ultrasound into diamond particle suspension is used as the acoustic matching layer, and PZT piezoelectric ceramic vibrator with resonant frequency of 300 kHz was equipped on the bottom plate. It was found by measurement with KI oxidation method and spin-trapping method that active oxygen species like hydroxyl radical and hydrogen peroxide generated by the new ultrasound exposure system was increased twice the amount of those generated by the conventional system. Furthermore, it was proved by measurement of the frequency characteristics of sonochemical luminescence that the new system could generate the active oxygen stably in wider frequency range (fractional bandwidth of 39%) than the conventional system. We obtained the aggregated nano diamond particles with average size of smaller than 100 nm from the aggregated particles with the size of about 5 μm using the new ultrasound exposure system. Zeta potential of sonicated nano diamond particles by new system was increased 50% in the amount of it by conventional system. Evaluated results of the performance of new system and dispersion effects on nano diamond particles by the new system will be reported in this symposium.

3C-2 4:45 p.m.
DEFECT MODES FOR A PROMISING ACOUSTIC WAVE-GUIDE IN TWO-DIMENSIONAL SONIC/ PHONONIC CRYSTALS.

T. MIYASHITA*, Department of Electronics and Informatics, Ryukoku University, Ohtsu, Japan.
Corresponding e-mail: miya@rins.ryukoku.ac.jp

Defect modes, which propagate along a periodical defect of scatterers in a periodic array of scatterers, have been found to be well guided in a frequency range within the full band-gap of such sonic/phononic crystals as arrays of methacrylic resin cylinders in air, steel cylinders in air or in water, and aluminum cylinders in air. These investigations have been made by mean of numerical calculation.

For example, the defect mode along a periodical lacking of every second scatterers in the central line of a periodic array of methacrylic resin cylinders in air has a complete pass-band between 0.54 and 0.59 in the normalized frequency, which is measured by the lattice constant divided by the free-space wavelength.

This defect-mode pass-band locates itself within a full band-gap of the sonic/phononic crystal of methacrylic resin cylinders in air whose frequency is between 0.47 and 0.63 in the normalized frequency.

The level of the acoustic leakage just outside of one of rear side corners of 11 times 11 size of crystal was calculated as -21 to -28 dB.

The defect modes will be promising for effectively well-confined and guided modes alternative to the conventionally investigated modes in a hollow waveguide in a sonic/phononic crystals.

For these theoretical investigations of defect modes in sonic/phononic crystals, we have developed an impulse response FDTD method to obtain precise frequency response of a finite size of periodic structures of acoustic scatterers placed in liquid or gas.

The frequency responses of such typical sonic/phononic crystals have been numerically investigated as those composed of a two-dimensional array of methacrylic-resin cylinders in air, aluminum cylinders in air, and steel cylinders in water.

We have found that the former two crystals may be numerically investigated by our conventional sonic FDTD method with a small normalized frequency difference of 0.01 to 0.02 compared with one by the new elastic FDTD analysis.

On the other hand, it has been found that the latter crystal should be investigated by the elastic FDTD method, because of a large frequency difference of 0.06 to 0.08 compared with the conventional sonic FDTD method.

All results shown in this report have been calculated by means of the elastic FDTD method developed by us.

3C-3 5:00 p.m.
AN EVALUATION METHOD OF BONDING STRENGTH AT A BONDED SOLID-SOLID INTERFACE BY CONTACT ACOUSTIC NONLINEARITY.

D. ZHANG*, J. CHEN, and Y. MAO, Nanjing University, Nanjing,Jiangsu, P.R.China.
Corresponding e-mail: deedez@nju.edu.cn

This paper presents a nondestructive method to evaluate the bonding strength of the interface of bonded solid-solid. It is based on a contact acoustic nonlinearity (CAN) phenomenon produced by a bonded solid-solid interface when a longitudinal wave propagates through the interface. The CAN model is set up to depict a bonded state by the relationship between the bonding strength and the crack width in the interface and the CAN parameter described by the ratio, A_2/A_1, between the amplitudes of the second harmonic and fundamental waves. According to this model, a nondestructive evaluation of the bonding strength

can be established. When the CAN parameter and the crack width are measured, the bonding strength can be evaluated from the model. In this paper, experiments have been done to demonstrate the model and the bonding strengths of some samples are evaluated based on the CAN method, The results (the example of 10.2kg/cm^2)by CAN model are well agree with the bonding strengths (9.89 kg/cm^2) measured by hanging clogs to destroy their interfaces.

3C-4 5:15 p.m.
NONLINEAR INTERACTION OF ULTRASOUND WITH AN UNBOUNDED ROUGH INTERFACE.

P. WU*, Signals and Systems Group, Uppsala University, Uppsala, Sweden.
Corresponding e-mail: Ping.Wu@signal.uu.se

Kissing bonds are one of the specific flaw types in friction stir welds and, in many cases, they are difficult to detect using linear ultrasound. Under the insonification of intensive ultrasound, however, they show nonlinear behavior. This nonlinearity has been exploited to detect such deficient bonds. A kissing bond can be treated as an imperfect interface between rough surfaces in contact (an imperfect rough interface). Motivated by the practical problem, a theoretical model has been developed for calculating the nonlinear interaction of ultrasound with an imperfect rough planar interface. The model is established based on elastodynamic theory. It is a first-order differential equation governing the relation between the interface opening (or thickness) and the ultrasonic (dynamic) force. The relation in general is nonlinear, but it is easy to implement numerically. The solution to the equation is the interface opening, a function of time directly related to the transmitted and reflected nonlinear waves from the interface. The model can be used to deal with various planar interfaces, like smooth interfaces, rough interfaces with either linear or nonlinear relation between Hertzian contact force and interface opening, and rough interfaces with a hysteretic response to ultrasonic load. For smooth interfaces, rough interfaces with linear relation between Hertzian contact force and interface opening, and rough interfaces with piece-wise linear bistability (causing hyteresis), the analytical solutions are available. The proposed model has also been applied to the prediction of the experimental data for a single interface that was made by compressing two copper cylinders together. The results show that it gives a better prediction than the Richardson's theory [1] (for predicting the nonlinearity from a smooth interface) that overestimates the amplitude ratio of the second harmonic to the fundamental.

[1] J. M. Richardson, Int. J. Engng. Sci. Vol. 17, pp. 83–85, 1979.

This work was sponsored by the Swedish Nuclear Fuel and Waste Management Co. (SKB)

3C-5 5:30 p.m.
NUMERICAL STUDY OF THE WIRE FORM FUNCTION VERSUS SURROUNDING LIQUID DENSITY.

J. MATHIEU[1] and P. SCHWEITZER*[2], [1]LAIN, Univ. Montpellier 2, Montpellier Cedex, France, [2]LIEN, Univ. Henri Poincaré, Vandoeuvre-Les-Nancy, France. Corresponding e-mail: schweitz@lien.uhp-nancy.fr

A new ultrasonic measurement method of the density of a liquid has been developed [J. Mathieu and Al., Measurement of liquid density by ultrasound backscattering analysis, Meas. Sci. Technol., 15(5), pp. 869-876, 2004]. It is based on the dependence of the wire form function, or of the ultrasound backscattered by the wire, on the density of the liquid in which it is immersed. To express this dependence, the classic Resonant Scattering Theory (RST) is used.

The principle of the method is to compare the spectrum of the ultrasound backscattered by a wire immersed into the liquid of unknown density to the spectrum obtained with the same wire immerged in a reference liquid (water). The comparison of the spectra provides a characteristic curve of the relative density of the studied liquid with regard to the density of the reference liquid.

The RST provides a non-linear relation between the liquid density and the wire form function. So the resolution of the inverse problem (determining the unknown density) is not obvious. The simple solution is to compared, for example by a least mean square method, the characteristic curve to a set of theoretical ones obtained by RST.

Experimentally, a measurement is divided in four steps and requires two different wires. One of them has a density slightly higher than the one of the studied liquid. The other wire has a much higher density and is used to calibrate the instrumental chain. The four steps correspond to the acquisition of the echoes for each wire in the reference liquid and in the test liquid.

First experiments were made with Nylon 6,6 and copper wires. The estimation gave good results with salted water and milk.

The study of the relation between the wire form function and liquid density is fundamental to optimize measurements and to determine the metrological performance of this new measurement method. We have to choice the wires, in particular their acoustical properties, and the resonance frequency and the bandwidth of the ultrasound transducer accordingly to the size of the wires. The first wire, the measurement wire, must be made with a material for which the wire form function is very sensitive to liquid density. The second wire, the calibration wire, must be made with a material for which the wire form function is practically independent to liquid density. On the same way, the ratio ultrasound frequency / size of the wires must be selected such as the wire form function is very sensitive to liquid density. All these choices are done by a numerical analysis of the partial derivative of the wire form function towards liquid density according to all mentioned parameters.

In this work, the principal results of this numerical analyze are presented. The sensitivity of the form function according to the liquid density :

- increases when the density of the wire decreases ;

- increases when the longitudinal and transversal waves velocities in the wire decrease ;

- is maximal for some wire's resonances or for wave numbers included among about 0.6/a and 0.8/a, where a is the radius of the wires.

3C-6 5:45 p.m.
INTERACTION OF DEFECTS WITH LAMB WAVES IN COMPLEX GEOMETRIES.

D. GREVE*, I. OPPENHEIM, and N. TYSON, Carnegie Mellon University, Pittsburgh, PA.
Corresponding e-mail: dg07@andrew.cmu.edu

Lamb waves have been extensively studied for the detection of defects in plates and cylindrical pipes, to a large degree because they can propagate over considerable distances with low attenuation. We consider here the application of Lamb waves to the detection of cracks in civil infrastructures. Major issues include the detectability of cracks and flaws and the effect of reflections in the complex geometries found in these structures. We have combined experimental studies with finite element simulations to obtain insight into these issues. Time-dependent finite element simulations have been performed in two and three dimen-sions using FEMLAB. These simulations allow us to follow the details of the generation, propagation, and detection of Lamb waves as a function of time and also the interaction of waves with defects and other complex geometries. In previous work, [J.H. Nieuwenhuis, J. Neumann, D.W. Greve, and I.J. Op-penheim, in press] we validated this approach by modeling the generation of A0 and S0 modes by wafer-type transducers and comparing the results with analytic solutions. In the work reported here we have extended this approach to study wave propagation and defects in two and three dimensions. 2D simula-tions show reflection and mode conversion at rectangular slots in a 0.159 cm aluminum plate, consistent with previous published work [Y. Cho, D.D. Hongerholt, and J.L. Rose, 1997] and our own experiments. 2D simulations have also been performed to quantify the reflection of S0 waves at a cracked and un-cracked welded joint between a 0.25" steel plate and a flange of varying thickness. This geometry models the joint found in a plate girder as used in bridge construction. For a pulse center frequency of 200 kHz we find that the reflected S0 energy is less than 20% of the incident amplitude over the range from 0.25" to 1.25" flange thickness, with a minimum reflection near zero at a thickness of 0.75" where the S1 mode in the flange couples strongly with the S0 incident wave. Half-thickness cracks at the weld result in a considerable increase in the reflected energy by more than a factor of two over the entire range of flange thicknesses commonly used. 3D simulations are much more challenging computationally but are neces-sary in order to obtain insight into the detectability of particular flaws. We have investigated wave propa-gation in steel rolled girders and plate girders. We have separately simulated the propagation of A0 and S0 waves down the length of a steel rolled gider. Some of the S0 and A0 wave energy is

coupled into the flanges while a portion of the energy is reflected from the flange at a low angle. This results in a long “tail” to the received pulse. Finally, reflections from cracks in plate girders have been examined using 3D simulations. These simulations show that one particularly attractive transducer location (adjacent to stiffeners) is undesirable because the likely crack geometry results in minimal reflection back toward the transducer. These results will be compared with experiments on a model reduced-scale plate girder with and without flaws.

reflected energy fraction

	0.25	0.31	0.50	.62	0.75	1.00	1.25
no weld bead	0.28	0.23	0.12	0.06	0.01	0.04	0.05
with weld bead	0.21	0.11	0.04	0.03	0.01	0.04	0.05
with 50% crack	0.35	0.43	0.40	0.25	0.23	0.28	0.27

Calculated for 200 kHz S0 wave incident on welded joint between a 0.25

Session: 4C

ULTRASONIC MOTORS
Chair: R White
University of California-Berkeley

4C-1 4:30 p.m.
DESIGN AND TESTING OF ROTORS FOR A CYLINDRICAL MICRO-MACHINED MICRO ULTRASONIC MOTOR.

T. KANDA*, Y. OOMORI, A. MAKINO, K. SUZUMORI, and A. KOBAYASHI, Okayama University.
Corresponding e-mail: kanda@sys.okayama-u.ac.jp

In this paper, a design and testing of rotors for a micro ultrasonic motor using micro-machined cylindrical bulk piezoelectric vibrator is introduced. This motor consists of the vibrator, a glass case and a rotor. The diameter of the piezoelectric vibrator was 0.8 mm and that of the motor case was 1.8 mm. Since the stator transducer is fixed at the end of the cylinder, it is easy to support the vibrator and the structure of the motor was not complicated. In addition, the vibrator and rotor were supported by glass case. This is important for micro ultrasonic motor because it is difficult to support the vibrator when the vibrator was miniaturized. We have fabricated and evaluated some types of rotors for the cylindrical shaped traveling type micro ultrasonic motor using this vibrator.

Three types of rotor were used for the evaluation. The rotor 1 had been already used for the evaluation. This rotor was driven by the inner part of the vibrator. The rotor 2 was generated by the vibration at the outer part of the vibrator. The

rotor 3 had a contact with the end of the vibrator, both inner and outer part.

The vibration velocity of the vibrator is important for the characteristics of the ultrasonic motor. The value of vibration velocity has an effect on the revolution speed of the rotor and the output torque. At the cylindrical vibrator, the vibration velocity of the outer part was larger than that of inner part. By using the rotor 2 or 3, the larger torque would be obtained when the rotor 1 was used for the driving.

The starting characteristics were measured to evaluate the effect of the rotors. The surface vibration speed of the shaft which was united with rotor was measured by using the laser surface velocity meter. The revolution speed of the rotor was estimated from the measured values. The pre-load was given by a spring. The rotor was supported by the needle at the center pivot at upper side. The rotor was pushed by the needle tip and has a contact with the end of the vibrator. The pre-load value was changed by the length of spring. The starting torque can be estimated from the starting characteristics when there is a first order lag relation between the revolution speed and the time.

In this measurement, the driving voltage was changed from 20 $V_{p\text{-}p}$ to 40 $V_{p\text{-}p}$ and the pre-load was constant at 1 mN. Each starting characteristics shows the first order lag condition between the revolution speed and the time.

The plots of rotor 3 were 3 times larger then those of rotor 1. The largest starting torque was estimated to be 1.6 μNm when the driving voltage was 25 $V_{p\text{-}p}$ and the rotor 3 was used.

This work was supported by the Mazda Foundation, and by the Cooperation of Innovative Technology and Advanced Research in Evolutional Area (CITY AREA) of the Ministry of Education, Culture, Sports, Science and Technology.

4C-2 4:45 p.m.
FRICTION DRIVE DYANAMICS OF SURFACE ACOUSTIC WAVE MOTOR.

T. SHIGEMATSU* and M. KUROSAWA, Tokyo Institute of Technology, Yokohama, Japan.
Corresponding e-mail: sgmt@ieee.org

A slider of a surface acoustic wave (SAW) motor has projections at frictional surface. The projections are the only contact points with stator, thus all the driving force is produced hereout. Since a stator of the SAW motor is transparent, we directly measured displacements of one projection through the stator by means of two Laser Doppler Vibrometers (LDVs). In this report we discuss the friction drive dynamics of the SAW motor through this measurement.

A great deal of investigations of friction drive dynamics of ultrasonic motors has been carried out in order to develop design/control method or to improve efficiency. To date, analytical modeling has led the way in the studies due to the difficulty of measurement. However, evaluation of the models was not accurately accomplished only with comparison between calculated and measured mechanical output, such as torque-speed curve, since the mechanical output is a result of complex coupled dynamic system. Some kinds of measurements

hence increase in importance. The SAW motor utilized lithium niobate for the stator, which is a transparent material, so that we could carry out the direct measurement of the frictional interface.

The 5×5×0.3 mm^3 silicon slider had 169 cylindrical projections (50 μm in diameter, 2 μm in height) on frictional surface. The 62x14x1 mm^3 stator was made of double-sided polished 128° y-x lithium niobate. The resonance frequency of IDT for the Rayleigh wave excitation was 9.6 MHz. Through the transparent stator, laser beams of LDVs were incident on a projection at angles of 30 degrees. The normal and tangential displacements of the projection were obtained by composition of measurement vectors. The driving conditions were 20 nm vibration amplitude, and from 5 to 20 N preload.

Time response measurements showed that the projection displaced both in normal and tangential direction followed to each wave vibration. The displacement was increased with preload, i.e., the increase of preload pushed down a balanced position of the projection to an elastic force of the wave, which in turn expanded the contact duration. Trajectories of the projection were tilted semi-elliptic orbits. Taking the trajectory under 15 N preload condition as an example, we would say the projection's motion in one cycle of wave vibration was as follows: on the arrival of wave the projection collided with the wave front, it was then pushed obliquely upward to the wave propagating direction up to the crest of wave. The normal and tangential displacement in the rectilinear trajectory was 20 and 10 nm, respectively. And then the projection descended from the wave crest to the initial position in a slight curvilinear trajectory. The tangential component in the curvilinear trajectory to the slider's traveling direction was owing to the frictional force between elliptically rotating stator's surface particles and the projection, which produced the driving force. It was the first direct measurement of the behavior of frictional interface in ultrasonic motors. That would provide thorough understanding of the friction drive and useful information to reinforce the analytical modeling method.

4C-3 5:00 p.m.
DESIGN OPTIMIZATION ANALYSIS OF A STANDING WAVE ULTRASONIC LINEAR ACTUATOR.

J. M. FERNANDEZ* and Y. PERRIARD, Ecole Polytechnique Fédérale de Lausanne, 1015 Lausanne, Switzerland.
Corresponding e-mail: jose.fernandezlopez@epfl.ch

Ultrasonic actuators are a good alternative to conventional electromagnetic motors since they provide a large output torque but also a braking force without energy consumption. Furthermore, unlike electromagnetic motors that contain an air gap between the rotor and the stator, ultrasonic linear motors are vibratory actuators in which the stator is in frictional contact with the rotor. Thus, the operating principle is based on piezoelectric ceramics that convert electric energy into mechanical energy in the form of vibrations of an elastic body whose surface points perform an elliptic motion with a frequency in the ultrasonic range. The slider, which is pressed against the vibrating body by a prestressing force, can move linearly thanks to the friction forces presented at the interface between the stator and the slider. The standing wave type ultrasonic actuator that is

presented in this paper is composed of a vibratory piece that is connected to two piezoelectric drivers and which tip portion generates flat-elliptical movement. Attached to the slider and if the vibration amplitude is large enough, the two parts loose their contact and impact periodically with the driving frequency of the vibratory piece that provides therefore an intermittent torque.

The goal of the study is to optimize the geometry and materials of the stator (vibratory piece and piezoelectric drivers) to obtain a maximum deformation amplitude and thus achieve a maximum torque. In this paper, the design, optimization and properties of a small prototype standing wave ultrasonic linear actuator are described.

First of all, a numerical model has been built and simulated with Ansys software. To avoid performing a large number of simulations, input parameters like geometrical dimensions, material properties or even boundary conditions can be judiciously chosen in function of their influence on the output parameter (deformation amplitude). In this manner, sensitivity of each input parameter on

the output parameter value can be achieved, in particular using design of experiments. This approach provides for a way of developing a model based on the gathering of data and a way of analyzing the data to compute quantitative and qualitative results which can then be treated to find out the optimal set of parameters for the final design. In this way, Doehlert method, which is generally used for optimization problems, has been chosen. The results found are represented through iso surfaces showing the deformation amplitude variation as a function of the

different input parameters. The method demonstrates that it is absolutely necessary to take into account the quadratic terms in the model because they represent an important effect. Furthermore, the results obtained show also that the optimization technique used makes it possible to improve the actuator's design. The PZT-input to stator-output transfer function has been notably increased compared to the initial design. Finally, experimental measurements make it possible to validate the method and thus obtain a maximum deformation amplitude with the optimized actuator.

4C-4 5:15 p.m.
PERFORMANCE EVALUATION OF TRAVELING WAVE ULTRASONIC MOTOR BASED ON A MODEL WITH FRICTIONAL LAYER ON STATOR SURFACE.

J. QU* and F. SUN, Department of Mechanical Engineering, Harbin institute of Technology, Harbin City, Heilongjiang Province, China.
Corresponding e-mail: qujianjun@hit.edu.cn

The ultrasonic motors have been studied by researchers and companies all over the word. The traveling wave ultrasonic motors (TWUSM) were paid more attention to practical application because they are more wear resistant than the standing wave ultrasonic motors. In study of TWUSM, theoretical model plays an important role in control and optimization of design parameters, and choice of frictional material of the motors.

The earliest quantitative analysis of the contact model between stator and rotor of TWUSM was developed by Kurosawa and Ueha. After that, scholars have set up many kinds of theoretical model in decades. So far the contact model between stator and rotor can roughly be classified as follows:

(1) rigid slider and rigid stator;

(2) compliant slider and rigid stator;

(3) compliant slider and compliant stator.

In this paper; authors proposed a new visco-elastic contact model of TWUSM, i.e. rigid slider and compliant stator. In this model, the rotor is assumed to be rigid body and the friction material on stator tooth surface to be visco-elastic body. The stator contact layer is still divided into two tangential and normal systems independently, but the condition of initial contact boundaries is revised, and then set up corresponding mathematical model. Then the performances of TWUSM as a function of input parameters are deduced and simulated.

Firstly, based on the contact model, effects of thickness h and Modulus of elasticity E of contact layer, frictional coefficient f of contact interface, the applied preload F on the mechanical characteristics and output characteristics of TWUSM are simulated numerically using MATLAB method. The result showed that:

(1) The thinner the frictional material is, the higher the revolution speed of the motor is. But when h is about 0.2mm, the interface conversion efficiency has a maximum;

(2) The higher E is, the higher revolution speed is. At the beginning, the interface conversion efficiency increases with E, but while E is higher than about 1500 N/mm2, it appears as a trend of fluctuating.

(3) f has a little effect on revolution speed and the interface conversion efficiency, but the higher f is, the higher the output power and the stall torque are.

(4) With the increase of F, revolution speed will drop slightly and the stall torque will increase linearly, but the power losses in contact interface will increase quickly at the same time.

Secondly, this model was compared with the compliant slider and rigid stator model. The results shown that under the same condition, the interface conversion efficiency of the two is different, the latter preponderates slightly, but the former will gain bigger stall torque.

Thirdly, the simulated result and the test result were compared, and found that their load characteristics had good agreement. As a result, the validity of proposed model is experimentally confirmed primarily.

The work was supported by the Natural Sciences Key Foundation of China (No: 50235010) and the Multidiscipline Scientific Research Foundation of Harbin Institute of Technology (No. HIT.MD2002.08)

4C-5 5:30 p.m.

A NEW MODELING OF TRAVELING WAVE TYPE ROTARY ULTRASONIC MOTOR BASED ON THREE-DIMENSION CONTACT MECHANISM.

C. ZHAO*, C. CHEN, and J. ZENG, Research Center of Ultrasonic Motors, Nanjing University of Aeronautics and Astronautics, Nanjing 210016,Jiangsu Province, China.
Corresponding e-mail: newraincc@163.com

Traveling wave type rotary ultrasonic motor (TRUM) is a promising type of piezoelectric transducers, whose modeling is always important to improve its design method and performance. Although recently considerable studies were carried out in the field of modeling TRUM, they are based on quite a few assumptions that analyses of the composite stator and contact interface are simplified much. As a result the models cannot describe the dynamical characteristics of motor with enough accuracy. So it is difficult to obtain satisfactory preliminary performance measure and design parameters of the motor. The paper presents a novel model, which allows for more quick and precise performance simulation and optimization of TRUM. First a new modeling strategy for composite stator has been developed and a kind of semi-analytical annular element is applied to mesh its inner web and outer annular plates. In addition each tooth on top of stator is described by hexahedron isoparametric element with 8 nodes, and its dynamical contribution (including stiffness and mass) on the substrate is calculated based on both substructure interface loading theory and Guyan Method. Then the contribution of each tooth is summed up and effects from all teeth can be included. At last the substructure modal synthesis theory is applied to derive the semi-analytical model of the stator. Furthermore authors investigate the more realistic three-dimensional contact mechanism between teeth of stator and friction layer glued on the bottom of rotor, and analyses the distributed contact force not only in the axial and circumferential direction but also in the radial direction. Finally the completed analytical model of the electromechanical-coupled system is derived accordingly. The important performance simulations are yielded and compared against the results from experiments. The model by the paper can simulate and explain the pulsant variety of the revolving speed of the motor, which is shown in experiments too. The speed characteristics make it difficult for ultrasonic motor to drive with precise speed. Then the authors investigate how and why it happens in order to reduce the range of speed variety. Moreover it is turned out that slip friction in the radial direction strongly affects mechanical characteristics of TRUM and leads to considerable waste of energy at the contact interface. In other words the measured performance could not be fitted excellently (almost 10 percent error) if the three dimension contact mechanism was simplified as is shown in some recent literatures. Thus high accuracy of the complete model is demonstrated. At last by simulations it is pointed out that geometric parameters of the teeth will contribute much to the dynamical characteristics of stator and even the motor behavior. In order to cut down the losses from the interface and improve the motor behavior to practical extent, the rotor flexibility in TRUM has to be set properly in the future.

The project was finished with the help from whole research group in RCUM, NUAA. They provided many useful discussions and advice.

4C-6 5:45 p.m.
FREQUENCY CONVERSION STEPPING ULTRASONIC MOTORS.

J. JIN* and C. ZHAO, Research Center of Ultrasonic Motors, Nanjing, Jiangsu, China.
Corresponding e-mail: jjm345@sohu.com

As a kind of ultrasonic motors, stepping ultrasonic motor is a very important member in the USM family. The precise positioners are a key technology and are widely used for optics, robot, aerospace, automatic control, military industry, medical instrument, etc. The stepper piezoelectric or ultrasonic motor has the features both high resolution and large torque. To fabricate a precise positioning actuator, several stepper ultrasonic motors have been proposed by some precursors. These can be divided into two groups. One is achieved by special mechanical structure, such as standing-wave type self-correct ultrasonic motors, whose driving forces are tangent components of the normal forces between the rotor and the stator. It is not easy to obtain a large torque of the motors because the tangent components are small. The other obtains precise positioning by control the drive circuits in several type USMs. Owing to USMs' drive mechanism, however, it is difficult to derive a mathematical model of an USM. Moreover, the control characteristics of USMs are complicated and highly nonlinear. The exact values of the motor parameters cannot be obtained easily, and the motor parameters are time-varying due to increasing in temperature and changing in motor drive operating conditions. A new concept of a frequency conversion stepping ultrasonic motor, based on standing wave driving and rotor tooth grooves positioning, is presented. This motor includes a rotor having 144 projections which extend toward a flexible stator with 9 teeth. Piezoelectric elements are connected to and spaced along the circumference of the stator. A drive control unit applies driving signals to the vibrators to create nodes and antinodes forming substantially a standing waveform on the stator. Two bending vibration mode (B03, B06) are used to produce an oblique line movement of the teeth on the stator. The stator teeth can be divided into three groups. The first group 3 teeth locate on the 3/4 wavelength in the B03 mode and in the B06. The three teeth of the second group located on the 9/16 wavelength in the B03 mode and on the 3/8 wavelength in the B06. The teeth of the third group located on the 3/8 wavelength in the B03 mode and on three nodes of the standing waveform in the B06. When the B03 mode is excited, the teeth of the first group cannot impel rotor to run because of their vibrating direction along axis of the motor. The teeth of the second group form oblique line movement and impel the rotor to turn. The three teeth of the third have no drive force against the rotor. When the second group teeth, drive teeth in the B03 mode, locate on the rotor teeth grooves, the rotor can be driven no longer. In the mode B06 the third group teeth become drive teeth and can drive rotor the second step movement. Thus the step movement can be obtained by exciting the two modes by turns. The opposite direction step motion can be achieved by turning the modes. The new motor is capable of bi-direction step displacements driven by an open-loop control

circuitry, which provides two-phase sinusoidal signal via a switch unit to the vibrator. Its step angler displacement is 1.25°.

Session: 5C

THIN FILM BAW MATERIALS II
Chair: J. Larson
Agilent

5C-1 4:30 p.m.
(Invited)
IS THERE A BETTER MATERIAL FOR THIN FILM BAW APPLICATIONS THAN ALN?

P. MURALT*, Ecole Polytechnique Federale de Lausanne, Lausanne, Switzerland.
Corresponding e-mail: paul.muralt@epfl.ch

Aluminum Nitride is presently the only material considered for industrial fabrication of thin film BAW microwave filters. A number of reasons account for this outstanding role: very reproducible and low-temperature processing, high quality factor (Q), high sound velocity, and excellent chemical compatibility with semiconductor front-end materials. The only point for which the material deserves the mark “sufficient” only is the coupling factor (k_t^2), the factor that determines bandwidth. A larger coupling (bandwidth) would be desirable for increasing production tolerances, to have larger tuning ranges, or for increasing the bandwidth for new applications. For below 2 GHz, a material with smaller sound velocity and larger dielectric constant would help to decrease production costs, as devices would be smaller and the active film thinner. Such properties can be found in ferroelectric materials. These often exhibit much larger coupling factors, and have anyhow higher dielectric constants and smaller sound velocities. In addition, ferroelectrics show a much larger electric field dependence of dielectric constants and piezoelectric coefficients, and thus allow for tuning of the resonance frequency and other properties. However, nobody managed to achieve high enough quality factors to date. The best investigated ferroelectric system is $Pb(Zr_xTi_{1-x})O_3$. While good AlN resonators exhibit a figure of merit Qk_t^2 of around 100, the best reported values of PZT resonators amount to 20, even though k_t^2 may reach 0.25. The reason for the low quality factors in the GHz range is known for PZT ceramics and is due to a relaxation of domain wall motions that are too slow to follow the RF field, resulting in an increase of dielectric loss and mechanical damping, and a decrease of dielectric constant and piezoelectric response. This was indeed found in morphotropic PZT thin films. The material must be suitably modified in order to suppress domain wall oscillations. A very interesting material is $KNbO_3$. As SAW devices have been demonstrated based on this material, BAW devices should work as well, provided one can achieve a thin film quality equivalent to mono-domain single crystals. Unfortunately, there are two phase transitions between growth temperature and

room temperature: The cubic (100)-orientation that can be homogeneously obtained during growth splits up into different domains of (101) and (010) orientations. While (101) is the best possible orientation for a high coupling, the passive (010) grains may destroy much of this coupling owing to their large dielectric constant. It would be necessary to eliminate as much as possible (010) grains by poling. Both examples show that the nice features of monodomain ferroelectrics are counterbalanced by a negative impact of domain wall configurations and dynamics. It must be tried to reduce the effects of ferroelastic domains. Their existence and configuration is very much dependent on the substrate on which the film is grown. Further materials will be discussed and recent experimental results will be presented.

5C-2 5:00 p.m.
SYNTHESIS OF TEXTURED THIN PIEZOELECTRIC ALN FILMS WITH A NONZERO C-AXIS MEAN TILT FOR THE FABRICATION OF SHEAR MODE RESONATORS.

J. BJURSTRÖM*, G. WINGQVIST, and I. KATARDJIEV, Uppsala University, Uppsala, Sweden.
Corresponding e-mail: jobj@angstrom.uu.se

A method for the deposition of thin piezoelectric AlN films with a nonzero c-axis mean tilt have been developed. The deposition is done in a standard reactive magnetron sputter deposition system without any hardware modifications. In essence, the method consists of a two stage deposition process. In the first stage (so called nucleation stage) deposition of the material is done under conditions where the sputtered atoms experience substantial gas phase collisions causing thermalization and randomization of the deposition flux. Thus, the film growth is said to be kinetically limited due to the limited surface diffusivity resulting from the relatively low kinetic energy of the condensing species. This results in a film with a relatively low texture, that is, it consists of small crystallites having a relatively broad crystallographic distribution. During the second stage the process is operated under conditions reducing significantly gas phase collisions which gives rise to two effects. The first one is that the deposition flux at any particular point on the substrate is directional (or anisotropic) arising from the asymmetry in the deposition flux emanated from the circular racetrack and received at the point under consideration. This, of course, is not valid for a small exclusion zone in the center of the wafer. The second effect is that the sputtered particles retain most of their original energy which is of the order of half of the sublimation energy of the target material, and which energy is favourable from enhancing surface diffusion and subsequently crystal growth. The latter now proceeds under competitive growth conditions where crystallographic planes exhibiting relatively high surface binding energies as well as receiving largest flux grow fastest. The resulting film has a distinct tilted texture with the mean tilt of the c-axis varying roughly in the interval 28 to 32 degrees over the wafer excluding a small exclusion zone in the center of the latter. The mean tilt angle distribution over the wafer has a circular symmetry.

A membrane type shear mode thickness excited thin film bulk acoustic resonator together with a micro fluidic transport system have been subsequently fabricated

using the two stage AlN deposition process described above as well as standard bulk micromachining of Si. The resonator consisted of a 2 μm thick AlN film with 200 nm thick Al top and bottom electrodes. The resonator was characterized with a network analyser when operating both in air and water. The resonance frequency was about 1.6 GHz, the extracted device Q is around 350 and the effective electromechanical coupling k^2_{eff} is 2% when operated in air while the latter two dropped down to 150 and 1.8 % respectively, when operated in pure water.

5C-3 5:15 p.m.
EVALUATING ZNO THIN FILM TRANSDUCERS THROUGH CONTACT BONDING OF GLASS BLOCKS.

F. HICKERNELL*, University of Arizona, Tucson, AZ.
Corresponding e-mail: f.hickernell@ieee.org

Evaluating sputtered ZnO thin film piezoelectric transducers for bulk wave applications has included a wide variety of techniques such as structural, electrical, and insertion loss measurements. The measurements can be contradictive because of the nature of the piezoelectric effect and the fiber structure. The actual excitation, propagation, and detection of ultrasonic waves by the transducers remain the most useful criteria for determining transducer performance. By depositing thin film transducers on glass blocks of different thicknesses and contact bonding them, the transducers can be evaluated using transmission and reflection loss measurements. ZnO transducers were deposited on aluminum electroded glass mask plates. A transducer matrix was developed with 20 sets of transducers in a 4 by 5 array on 2.36 mm and 1.57 mm thick plates. Each group had four circular electrodes of equal diameter on top of the ZnO with diameters of 0.89, 1.14, and 1.40 mm consistent with obtaining good impedance levels. The ZnO quality across the area was determined by pulse echo techniques. Those having strong piezoelectric activity, were contact bonded and the transmission insertion loss determined under tuned and untuned conditions. The lowest tuned transmission losses through the bonded glass at 500 MHz were 8 dB indicating an individual transducer loss of less than 4 dB. The loss in the glass plates at 500 MHz was approximately 1.0 dB. By characterizing the transducers under contact bonding conditions, it is also possible to compare the properties of non-permanent and permanent bonds between the blocks in subsequent tests and how well they approach an optimum bond condition.

5C-4 5:30 p.m.
OPTIMIZATION OF ACOUSTIC MIRRORS FOR SOLIDLY MOUNTED BAW RESONATORS.

S. MARKSTEINER*, J. KAITILA, G. G. FATTINGER, and R. AIGNER, Infineon Technologies, Munich, Germany.
Corresponding e-mail: stephan.marksteiner@infineon.com

The overall performance of bulk acoustic wave (BAW) filters is dominated by the effective coupling coefficient and the quality factor of the constituting BAW

resonators. Whereas the effective coupling coefficient and its dependency on the layer stack is quite accurately modeled with a simple one-dimensional acousto-electric model (e.g. Mason's transmission line model), the prediction and optimization of the resonators quality factor — particularly in solidly mounted resonators (SMR) — completely fails with this model: whereas a calculation of the acoustic reflectance of a standard quarter-wavelength mirror stack leads to theoretical Q-factors well above 10000, experimental SMR devices with this type of mirror show values of typically below 700. This discrepancy is commonly explained by either visco-elastic loss in the materials and/or laterally leaking waves leaving the active resonator area. However, we have found a new, far more important loss mechanism relating to shear waves generated in the device. These waves can be created by injection from the resonators border area as well as by reflection/refraction of longitudinal waves at non-perpendicular angle of incidence to a material interface.

In this paper, the influence of the mirror structure on the trapping of both longitudinal and shear wave energy will be discussed based on a very simple approach. Trade-offs with respect to the other important device parameters, such as effective coupling coefficient, temperature coefficient of frequency (TCF) and purity of the electrical response, are analyzed. The usefulness of this approach for the optimization of resonator Q-values will be proven by experimental results demonstrating Q-factors of 1500 and higher.

5C-5 5:45 p.m.
SHEAR MODE COUPLING AND TILTED GRAIN GROWTH OF ALN THIN FILMS IN BAW RESONATORS.

F. MARTIN*[1], M.-E. JAN[1], S. REY-MERMET[1], M. CANTONI[2], D. SU[1], and P. MURALT[1], [1]Ceramics Laboratory EPFL Lausanne, EPFL Lausanne, Switzerland, [2]CIME EPFL Lausanne, EPFL Lausanne, Switzerland.
Corresponding e-mail: Fabrice.Martin@epfl.ch

The crystalline orientation of piezoelectric thin films is a key issue in optimizing the piezoelectric response. For bulk acoustic wave (BAW) RF-filters based on AlN, it is sought to grow films with perfect c-axis orientation in order to excite optimally the longitudinal thickness mode (TL0). For immersed sensor applications, however, shear thickness modes are superior. Physical vapour deposition methods may yield a tilted grain growth owing to an oblique incidence of the directional flux of the vapour. So the question arises, whether such a technique could be useful to grow films in which the polar c-axis is uniformly tilted away from the film normal. In this work, process conditions for the growth of tilted grains have been investigated and the resulting films have been characterized by means of scanning and transmission electron microscopy, X-ray diffraction, and BAW resonator response of solidly mounted resonators.

Polycrystalline AlN thin films were deposited by RF reactive magnetron sputtering on Pt(111)/Ti electrode films. The substrates were tilted by an angle ranging from 40° to 70° with respect to the target normal. A low deposition temperature and a high sputter gas pressure were found ideal for tilted growth. The resulting grain tilt angle amounts to about half the substrate tilt angle. This is in agreement with the early work of Nieuwenhuizen and Haanstra in aluminium films (1966),

and with the general idea that tilting is the result of reduced mobility (low temperature) and shadowing (high pressure). At intermediate process conditions, a transformation from vertical to tilted growth was observed, which is thought to be induced by a mobility reduction due to either increase in roughness with thickness, or decrease in ion bombardment with thickness. TEM investigations revealed that the (001) planes in the tilted grains move only a few degrees out of the substrate plane. The main effect of grain tilting is the formation of grain boundaries where the (001) planes do not fit anymore together, thus form a diffusion barrier for ad-atoms hopping from one grain to the next one. Rocking curve measurements at the (002) X-ray Bragg peaks show a peak width broadening from 1.8° for non-tilted growth to 3.9° for 70° substrate tilt. Hardly any systematic tilt is observed. For coupling evaluation, 5 GHz SMR structures have been realized with an acoustic reflector stack consisting of 5 pairs of sputter-deposited SiO2/AlN $\lambda/4$ thick layers. The tilted grain AlN films exhibited a permittivity in the 9.5-10.5 range (as c-axis oriented AlN) and loss tangent of 0.3%. The SMR resonances were measured with varying film thickness. Two shear modes (TS0 and TS1) as well as the longitudinal mode TL0 could be clearly identified. The coupling coefficient k2 of the fundamental thickness shear mode (TS0) was found to be around 0.4 %, which is compatible with tilt angles of around 6°. In conclusion, we have gained a quite consistent picture of microstructure and properties of tilted grain growth.

Session: 6C
TRANSDUCERS AND MATERIALS MODELING
Chair: M. Schafer
Sonictech

6C-1 4:30 p.m.
A TIME DOMAIN APPROACH FOR THE ANALYSIS OF PERIODIC STRUCTURES USING FINITE ELEMENT ANALYSIS.

S. BALLANDRAS*, V. LAUDE, S. CLATOT, and M. WILM, FEMTO-ST, CNRS, Besançon, France.
Corresponding e-mail: ballandr@femto-st.fr

The theoretical analysis of periodic structures using finite element analysis (FEA) provides numerous data about their properties to efficiently guide or radiate acoustic energy. They are characterized by different figures deduced from their spectrum (harmonic admittance, velocity or displacement). The latter presents poles or pseudo-poles for guided or partially guided or leaky waves guided along the structure, but also second order singularities related to waves radiated when related conditions are met. It is particularly interesting to solve those problems in the spectral domain since these singularities can be defined without ambiguity. The computations can be conducted very accurately whatever the propagation or radiation conditions, but it may required long delays in the most general cases

since the algebraic system to solve must be constructed for each frequency point (in some cases, acceleration procedure can be implemented to reduce this delay).

The time domain analysis is an interesting alternative to spectral domain computations for vibrating structures or wave-guides exhibiting short impulse responses. For linear problems, the algebraic system is built and factorised once and for all and the time dependent solution is obtained simply by solving the factorised system and by matrix-vector multiplications. Commercial FEA codes are able to solve transient problems but none takes into account comprehensive periodic boundary conditions. In this paper, we propose a development allowing for solving periodic transient problems. As for harmonic computations, we mesh only one period of the array and we apply boundary conditions relating its edges one to the others. A periodic excitation coefficient similar to the one used in the spectral domain is defined and use to scan all the possible excitation figures. The excitation versus time is performed via a Dirac impulse. It is then shown how to derive mutual time domain coefficients that describe the way the different cells of the array are coupled together. It is remarkable that in this time domain representation, no singularity arises on the computed signals, yielding very favourable conditions for the derivation of mutual coefficients. This time domain representation may be more accessible for most readers and provides an efficient approach for the characterization of massively periodic devices exhibiting low or moderate quality factors.

6C-2 4:45 p.m.
A FAST ALGORITHM FOR THE OPTIMIZATION OF ARRAYS.

E. KUEHNICKE*, Technical University, Institute Acoustic and Speach Communication, Dresden, Saxonya, Germany.
Corresponding e-mail: elfgard.kuehnicke@ias.et.tu-dresden.de

A separation approach in connection with time harmonic GREEN's functions and a point source synthesis was developed to simulate the transducer generated sound field in complex structures with non-parallel and curved interfaces. In previous works it was demonstrated that there is only a small difference between the time harmonic sound field at center frequency and the transient sound field. Therefore it is possible to optimize transducers for NDT- problems by simulating the time harmonic sound field. For evaluation, the transient sound field is calculated by means of a harmonic synthesis (a superposition of the time-harmonic fields of the different frequencies) and a temporal convolution with the excitation function. This optimized evaluation approach lasts 5 to 20 times as long as calculating the corresponding time harmonic sound field.

So far, this kind of approach has not been applied to broadband ultrasonic arrays. However, the paper advocates it as a fast tool, which takes the extension of the single elements into account and hence it suits much better than a common practice - the approximation of an element by a point source. Time harmonic calculations are applied to optimize both the shape and steering electronics of broadband ultrasonic linear arrays. It is shown that the magnitude of side lobes depends on the width of the single elements. By varying the width of the elements

by 10%, the magnitude of the side lobe alters about 1 dB. Moreover, the paper shows also the optimization of steering time for curved arrays and plane arrays by means of harmonic calculations. It will be exemplified that geometrical calculations don't predict the right steering angle and consequently they predict a false location of the focus.

However, calculating the transient sound field is necessary to predict the angle and magnitude of the side lobes of a broadband array exactly. That is why the angle and magnitude of the side lobes depend on the relation between element size and the various partial frequencies within the transient signal. In the paper the dependence of the angle and the magnitude of the side lobes of the transient field on the duration of the excitation function will be discussed comparing the transient and the time harmonic sound fields. A comparison of magnitude of the maxima for different steering angles shows for harmonic and transient field the same relation, that means that time harmonic calculations predict the intensity loss by the side lobes in dependence of steering angle.

Among focusing mainly on fluids, an example for a two-layered NDT-problem will be discussed also.

6C-3 5:00 p.m.
NUMERICAL PROTOTYPING OF PIEZOCOMPOSITE ARRAYS: FROM MATERIAL CHARACTERIZATION TO ARRAY PERFORMANCES.

G. FERIN*[1,2], D. CERTON[2], F. PATAT[2], R. DUFAIT[1], and N. FELIX[1], [1]VERMON, Tours, France, [2]LUSSI \ GIP Ultrasons, Tours, France.
Corresponding e-mail: g.ferin@vermon.com

The numerical prototyping and optimization of ultrasound arrays for medical imaging applications enable probe designers to perform efficient and thorough studies. The efficiency of such methods directly depends on the characterization of probe's constitutive materials. Whatever the model used: a numerical, an analytical or a FEM/BEM model, accurate input data are required to predict properly the final performances of the probe. This work presents a protocol for transducer arrays numerical prototyping.

From our material database, we have selected matching layers, backing material and a piezocomposite plate in order to manufacture a curved linear array with 3.5 MHZ center frequency for abdominal imaging. Using the experimental and/or theoretical procedure, presented in our previous works [1-2], we determined the complete elastic, dielectric and piezoelectric tensors of the piezocomposite material and elastic properties of passive materials. From these data, an array element was simulated with the model, previously described [3] based on the global matrix method. Complete performances were calculated, i.e. electrical impedance, array normal surface displacement, elementary pulse-echo response, and acoustic directivity pattern.

Simulated performances were compared with manufactured transducer data and results exhibit a very good agreement and validate the numerical prototyping procedure. Two application cases are then presented:

→ The prototyping of a 30MHz with 100µm pitch array for high frequency imaging applications, including comparison between theoretical and experimental performances.

→ A parametric study of the array performance variations with the 1-3 piezocomposite ceramic volume fraction. Results are discussed and trade-offs are commented.

These studies point out the flexibility, and the enhanced value of such a tool for 1-3 piezocomposite ultrasound transducers arrays design and development.

[1] G. Ferin, D. Certon, J. Guyonvarch, and N. Felix, "Inverse Calculation Method for Piezocomposite Materials Characterization," presented at IEEE International Ultrasonics, Ferroelectrics, and Frequency Control Joint 50th Anniversary Conference, Montréal, 2004.

[2] G. Ferin, D. Certon, and N. Felix, "Experimental and Theoretical Determination of 1-3 Piezocomposite Electro-acoustic Tensor," to be presented at World Congress on Ultrasonics, 2005.

[3] J. Guyonvarch, D. Certon, L. Ratsimandresey, F. Patat, and M. Lethiecq, "Analytical 2D model of transducer arrays for predicting elementary electroacoustic response and directivity pattern," presented at IEEE Ultrasonics Symposium, 2002.

6C-4 5:15 p.m.
DERIVATION OF THE IMPULSE RESPONSE OF ULTRASONIC TRANSDUCERS BY EXPERIMENTAL SYSTEM IDENTIFICATION.

T. GEHRKE*, F. CHEIKHROUHOU, and H. M. OVERHOFF, University of Applied Sciences Gelsenkirchen, Gelsenkirchen, Germany.
Corresponding e-mail: tobias.gehrke@fh-gelsenkirchen.de

Introduction Simulation of ultrasound systems requires knowledge of transfer characteristics of transducers. The impulse response of a transducer can be calculated either by analytic approaches like equivalent circuits or it can be derived from measurements. The use of analytic methods is limited by the necessity to know the properties of the piezoelectric crystals and their backing and is in many cases not very accurate. Direct measurement of the impulse responses is difficult due to the inability to create needle-shaped signals (Dirac pulses) and nonlinear transient behaviour. Furthermore the influence of spatial diffraction on the measured impulse response has to be considered. An experimental identification of the impulse response of a transducer element using appropriate excitation signals, i.e. frequency-band-adapted chirps of defined amplitude, is presented. This approach does not require any advance information about the transducer and overcomes the difficulties associated with needle-shaped excitation signals.

Materials and methods A piezoelectric ultrasound transducer was excited with chirp signals of different amplitudes and time characteristics. The echo from a reflecting plane was measured by the same transducer. The influence of spatial diffraction was examined and shown to be small if a plane reflector of large

extends compared to the size of the piezoelectric crystal is placed in the nearfield of the transducer. We identified the scope of a linear model from the proportionality of excitation and reflection signal. A linear time-discrete model (time shifted difference equation) was derived by least-squares minimization of the estimation error, i.e. the difference between measured and estimated response signal. An alternative approach based on the maximization of a likelihood function for the error and taking noise into account was tested and compared to the least-squares-method. A discretised impulse response of the transducer was derived from the time domain model. We evaluated our approach by determining the impulse response of a 5 MHz transducer and simulating different imaging situations using the software Field II. These simulations were quantitatively compared to measurements in ultrasound phantoms.

Results The 5 MHz transducer was modelled by a discrete linear system of order n = 6 which showed bandpass characteristic with a 3 dB-bandwidth of 1.5 MHz. The least-squares and maximum-likelihood-method resulted in nearly equivalent models. Simulated and measured system behaviour agreed well in all tested imaging situations. The sum of squared errors was below 5 % of the signal energy whereby the impulse response derived from the maximum-likelihood-method led to slightly better results than the one derived from the least-squares-method.

Conclusion The approach proved to be useful in deriving a realistic impulse response for the use in ultrasound simulation software. The piezoelectric behaviour could be determined on the basis of easily performed measurements.

6C-5 5:30 p.m.
DESIGN AND CHARACTERISATION OF 1-3 ULTRASONIC COMPOSITES USING ATILA AND ULTRA FAST LASER MEASUREMENTS (20 MHZ).

T. ROEDIG*[1], A.-C. HLADKY[2], and A. SCHOENECKER[1], [1]Fraunhofer - IKTS, Dresden, Germany, [2]ISEN – IEMN Department, Lille Cedex, France.
Corresponding e-mail: thomas.roedig@ikts.fraunhofer.de

Further progress in ultrasonic technology is expected by using custom shape high-quality low-cost ultrasonic transducers. Therefore, 1-3 ultrasonic composites have been developed based on piezoceramic fibers. In order to make use of all advantages of piezo composites effective design and characterisation tools are necessary.

Usually, finite element methods are used. ATILA is one, which is able to simulate coupled piezoelectric, electromechanical and acoustic field problems. ATILA was developed for sonar transducers in the Acoustic Laboratory at ISEN in Lille several decades ago. During further developments ATILA has been expanded to active as well as passive materials in air or other fluids. Actually, it is capable to simulate the entire ultrasonic transducer, in general.

Sound pressure level measurement characterises the ultrasonic transducer behaviour. No detailed informations are obtained from the active material inside. Usually, materials characterisation is based on electromechanical impedance measurement. To measure the mode shapes and the velocity of the surface of

the piezo transducer a newly developed ultra fast scanning laser measurement system such as provided by Polytec is needed. This system measures the out of plane vibration vectored to the scanning laser head. The maximum frequency for this set-up is as high as 20 MHz and the minimum laser spot is as small as 13 μm. For example with this measurement set-up deflection of single piezoceramic fiber or the surrounding polymer of the 1-3 composites can be measured. In the scanning mode the entire 1-3 composite can be measured to detect inactive regions, lateral wave and other disturbing influences. Due to the measurement principle, the ultra fast scanning laser measurement system acquires the in-plane sound field.

The present paper is focused on 1-3 composites. First simulated and measured data, e.g. spectrum, resonant frequency and anti-resonant frequency as well as the mode shapes for different frequencies have been collected. The modelled and measured data have been compared showing an excellent agreement. Furthermore new effects of lateral waves of 1-3 composites have been measured and will be discussed in the paper. The experimental findings gave rise to improve the underlying model in ATILA. More detailed structural information must be included. The improved model will be discussed in the paper. Additionally, showcase sound field measurements showed 1-3 composite to radiate a directed field perpendicular to the surface, as expected.

Finally the paper highlights the opportunities of combined use of the FE-tool ATILA and the ultra fast laser measurement system in the development procedure of 1-3 composites as well as ultrasonic transducer.

6C-6 5:45 p.m.
A METHOD FOR THE MEASUREMENT OF THE *K* FACTOR IN LOSSY PIEZOELECTRIC MATERIALS: FEM AND EXPERIMENTAL RESULTS.

N. LAMBERTI*[1], G. CALIANO[2], A. IULA[2], and M. PAPPALARDO[2], [1]DIIIE University of Salerno, Fisciano, (SA), Italy, [2]DIE University of Roma III, Roma, Italy.
Corresponding e-mail: nlamberti@unisa.it

The most important property of a piezoelectric material for practical applications is its ability to generate and to detect stress waves, i.e. to convert electrical energy into mechanical energy and vice versa. As it is well known, the electromechanical coupling factor k fully characterizes this energy conversion. In previous works we demonstrated that, like in static conditions, it is possible to define the k factor also in dynamic situations (k_w) as ratio of energies: for a piezoelectric element in free oscillation, mechanically and electrically insulated, k_w was defined as the square root of the ratio of the converted electrical energy to the total energy involved in a transformation cycle, i.e. the kinetic energy. We extended this definition to lossy materials ($\mathbf{k_w}$), obtaining that $\mathbf{k_w}$ is a complex quantity proportional to the complex static material coupling factor; the proportionality coefficient is the same of the case without losses and does not depend on the vibration mode. We also developed a method to measure the k factor of lossy materials, based on the k_w definition: by means of a 1–D approximated analytical model we showed that $\mathbf{k_w}$ can be evaluated by measuring

the velocity on the element external surfaces orthogonal to the wave propagation direction, and the voltage across the element. The velocity and the voltage must be measured by supplying the piezoceramic with a current generator, working at the element electrical antiresonance frequency $\mathbf{f_p}$. As it is well known, for lossy materials, $\mathbf{f_p}$ is a complex quantity: as we showed, for low lossy materials both the real part and the amplitude of $\mathbf{f_p}$ can be used as working frequency, while for high losses best results are obtained using the $\mathbf{f_p}$ amplitude. In the present work we use a FEM commercial code (ANSYS) to test the proposed measurement method; the obtained results confirm those obtained by means of the 1–D model and show that the method can be applied to any vibration mode. We also checked if the method can be applied when an AC voltage generator is used to supply the piezoelectric element; it is in fact easier, from an experimental point of view, to supply a piezoelectric specimen by a voltage generator instead of a current generator. The obtained results confirm the validity of the method: $\mathbf{k_w}$ can be computed by measuring the velocity on the element external surfaces at $\mathbf{f_p}$, the clamped capacitance and the mass of the specimen. Finally we applied the method to measure the dynamic coupling factor of a piezoelectric cylinder vibrating in the length extensional (rod) mode. First of all we measured the electrical input impedance, in order to find the antiresonance frequency; secondly we supplied the specimen at this frequency by means of an AC voltage generator and measured the velocity on the element external surfaces by means of a laser interferometer. The application of the proposed method to compute $\mathbf{k_w}$ gives results very close to theoretical previsions.

Tuesday, September 20, 2005

ORAL SESSIONS

Session: 1D

MOUSE IMAGING
Chair: S. Foster
University of Toronto

1D-1 8:30 a.m.
MOUSE EMBRYO IMAGING WITH A 40 MHZ ANNULAR ARRAY.

O. ARISTIZÁBAL*[1,2], J. KETTERLING[3], and D. H. TURNBULL[1,2], [1]Skirball Institute of Biomolecular Medicine, New York, NY, [2]New York University School of Medicine, New York, NY, [3]Riverside Research Institute, New York, NY.
Corresponding e-mail: oarist@saturn.med.nyu.edu

Introduction: Current high frequency ultrasound imaging, or ultrasound biomicroscopy (UBM) systems use fixed-focus transducers, which are limited in depth of field (DOF). For anatomical imaging of mouse embryos, the geometrical extent of many structures of interest, such as cerebral ventricles or vascular structures, can be as much as an order of magnitude greater than the DOF for a fixed-focus transducer. This makes volumetric image analysis, including effective segmentation of three-dimensional (3-D) structures, difficult or impossible in many cases. High frequency annular arrays can provide a solution to this problem, extending the DOF through variable focusing in depth. Previously, we described the fabrication of 5-element, 40-MHz annular array transducers (Ketterling et al, IEEE Trans UFFC 52: 672, 2005), and have recently shown with a wire phantom that the DOF (-6 dB) was increased from 1-2 mm to more than 10 mm with array focusing. The aim of this study was to determine the effective DOF of this transducer for mouse embryo imaging, where the heterogeneous media and attenuation is expected to degrade the annular array performance compared to wire phantom experiments.

Methods: Image datasets were acquired by scanning the transducer with an automated motion system, producing 381 lines with line-to-line separation of 25 μm. For a given image line, each array element was sequentially pulsed and a complete set of rf data (from all 5 elements) were acquired. These data were collected and processed offline using a synthetic algorithm simulating annular array focusing and compared to images produced by directly summing the signals from individual elements to simulate a fixed-focus transducer. Data for a complete (2-D) image were acquired in 30 seconds. 3-D datasets were acquired using a 50 μm separation between image planes. Mouse embryos were imaged at embryonic day (E) 11 and 13. The pregnant mouse was killed immediately before image acquisition to eliminate breathing motion during the long data acquisition times. Selected embryos, intact within the uterus, were exposed through midline laparotomy into saline solution for imaging.

Results: Images acquired at both E11 and E13 show a dramatic increase in DOF and the resulting image quality using annular array focusing. A number of anatomical features, including limb buds, cerebral ventricles, amniotic membrane and spinal cord were much easier to visualize with annular array focusing. For E11 embryos, the cerebral ventricles were readily segmented using a 3-D image analysis program (Amira) after array focusing, while the same algorithms were ineffective in the fixed-focus images. By measuring signal intensity variations through homogeneous regions of E13 embryos, we estimated that the DOF was improved from less than 2 mm (fixed-focus) to more than 6 mm (annular array focusing), covering the entire embryo.

Conclusion: We have verified that annular array transducers significantly improve image DOF and enable effective 3-D analysis, providing strong support for the development of real-time annular array imaging systems for mouse embryo UBM.

Research supported by NIH grant NS038461 and EY014371.

1D-2 8:45 a.m.
3D PERFUSION MAPPING IN THE INTACT MOUSE HEART AFTER MYOCARDIAL INFARCTION USING MYOCARDIAL CONTRAST ECHOCARDIOGRAPHY.

Y. LI*, Z. YANG, B. A. FRENCH, and J. A. HOSSACK, University of Virginia.edu, Charlottesville, VA.
Corresponding e-mail: yinbo@virginia.edu

Due to the widespread availability of transgenics and knock-outs, the murine species provides a very useful and robust model in which to study human cardiovascular disease. Myocardial contrast echocardiography (MCE) using microbubbles as contrast agent has been shown to be an effective tool in characterizing myocardial perfusion in vivo, and it has been employed previously for two-dimensional (2D) myocardial perfusion analysis in mice. However, three-dimensional (3D) analysis, fully encompassing the entire left ventricle (LV), is required for a more complete understanding of the relationship between LV perfusion and function after myocardial infarction (MI). In this work, we studied an intact mouse model of surgically-induced MI resulting from a Left Anterior Descending (LAD) occlusion. Healthy mice which underwent a similar invasive procedure but with no occlusion were also studied as controls. Imaging was performed at 14 MHz using a non-destructive, contrast-specific, imaging mode ('Contrast Pulse Sequences' [1]). The infusion of contrast agent was accomplished at a slow and steady flow rate using a syringe pump driving a 1ml syringe. For each mouse heart, MCE images were acquired in parallel short axis cross-sections of the heart at 1 mm elevational increments. For accurate 3D reconstructions, calibrated ECG gating and a tri-axial adjustable micro-manipulator were used for temporal and spatial registration, respectively. Perfusion analysis was conducted by analyzing the local refilling processes within the LV myocardium. This analysis indicated a significantly slower flow rate in areas of perfusion defects compared to normal areas. MCE images acquired during steady-state perfusion of each 1mm slice of the LV were color-

coded to indicate relative perfusion, with blue corresponding to well-perfused areas and red corresponding to perfusion defects. As a standard for comparison, post-mortem tissue was stained with Phthalo blue and TTC red dyes to identify perfused and ischemic yet viable LV myocardium, respectively. A good correlation ($R^2 > 0.87$) was observed between the MCE-based, in vivo measurements and the tissue-based, ex vivo measurements of % perfused area in each tissue slice. 3D multi-slice models and 3D volumetric models of the distribution of perfusion in each LV were created for improved visualization and quantification of the 3D extent of the perfusion defects. These models demonstrated a promising match with the results of post-mortem tissue staining.

[1] P. Phillips, "Contrast Pulse Sequences (CPS): Imaging non-linear microbubbles," Proceedings of the 2001 IEEE Ultrasonics Symposium, vol. 2, pp. 1739-1745, 2001.

NIH grants EB001826. EB002349, Siemens Medical Solutions, Mountain View, CA and Vermon SA, France.

1D-3 9:00 a.m.
COMPARING CONTRAST-ENHANCED US TO MARKERS OF ANGIOGENESIS IN A MURINE GLIOMA MODEL.

R. RO*[1,2], F. FORSBERG[1], K. LIPCAN[1], J. LIU[1], M. POTOCZEK[1], P. LEWIN[2], and B. GOLDBERG[1], [1]Thomas Jefferson University, Philadelphia, PA, [2]Drexel University, Philadelphia, PA.
Corresponding e-mail: rayro@drexel.edu

The purpose of this study was to compare measures of four contrast-enhanced ultrasound (US) techniques with four markers of angiogenesis in glioma tumors xenografted in rats.

Twenty-one rats were implanted with a glioma (C6) cell line. Tumors, approximately 18 mm in diameter, developed 1 to 3 weeks post-inoculation. The US contrast agent Optison (GE Healthcare, Princeton, NJ) was injected in a tail vein (dose: 0.4 ml/kg). Power Doppler Imaging (PDI), Pulse-Subtraction Harmonic Imaging (PSHI), Flash-Echo Imaging (FEI), and Microflow Imaging (MFI) was performed with an Aplio scanner (Toshiba America Medical Systems, Tustin, CA) and a 7.5 MHz linear array. MFI is a flash-replenishment technique, where 5 high power flash pulses (MI > 1.3) destroys bubbles followed by 5 s of low power pulses (MI < 0.1) demonstrating contrast replenishment. A composite image depicting vascular architecture and blood flow is constructed through maximum intensity capture of temporal data in consecutive low power images. PDI and FEI were performed at framerates of 30 and 1 Hz, respectively. Rats were euthanized, and tumors were surgically removed and placed in 10% buffered formalin phosphate solution. Specimens were sectioned in the same planes as the ultrasound images. Immunohistochemical staining of glioma specimens were made using a polyclonal antibody against bFGF, monoclonal antibody against PECAM (CD31), polyclonal antibody against COX-2, and a monoclonal antibody against VEGF. Digital US clips and immunohistochemical stains of each tumor were assessed with image-processing software (ImagePro

Plus; Media Cybernetics, Silver Spring, MD) to calculate fractional tumor neovascularity as contrast enhanced pixels over total tumor area (for US) and staining over total tumor area (for specimens). Linear regression analysis was performed to compare the US measures of tumor neovascularity to the histologically stained derived markers of angiogenesis. P-values less than 0.05 were considered significant.

The tortuous morphology of tumor neovessels was visualized better with MFI than with FEI. Linear regression analysis yielded a strong correlation between MFI and percent area stained with COX-2 ($r=-0.60$, $p=0.004$), as well as significant correlation of measured fractional areas between MFI and CD31 ($r=-0.45$, $p=0.043$). Significant correlation was also shown between FEI and COX-2 ($r=-0.48$, $p=0.026$). All other comparisons were not statistically significant, $p>0.17$.

There were no significant correlations (at the 0.05 level) between contrast-enhanced ultrasound and the immunohistochemical markers bFGF and VEGF in the C6 cell line. Significant correlations were found between fractional tumor neovascularity obtained with MFI and tumor angiogenesis corresponding to the expression of COX-2 and CD31; and between FEI and COX-2. In conclusion, contrast-enhanced ultrasound measures of tumor neovascularity in the glioma xenograft model C6 appear to provide a noninvasive marker for angiogenesis corresponding to the expression of COX-2 and CD31.

This work was supported in part by NIH CA93907, GE Healthcare, and Toshiba America Medical Systems.

1D-4 9:15 a.m.
HIGH RESOLUTION QUANTIFICATION OF MYOCARDIAL STRAIN IN MICE USING SPECKLE TRACKING.

Y. LI*, Z. YANG, B. A. FRENCH, and J. A. HOSSACK, University of Virginia, Charlottesville, VA.
Corresponding e-mail: yinbo@virginia.edu

Image-based assessment of regional myocardial motion provides important information critical to the diagnosis of various cardiac disease states, the monitoring of disease progression, and the response of disease to therapy. Recently, significant progress has been made in the quantitative assessment of regional myocardial function in mice using MRI techniques. A limited amount of one dimensional strain and velocity calculations have also been performed in mice using ultrasound. In this work, we examined two dimensional myocardial tissue motion in mice using ultrasonic speckle tracking techniques with subpixel resolution. Imaging of the left ventricle (LV) was performed both in normal mice and in mice that had remodeled (i.e., dialated) LVs as a result of experimental myocardial infarction. Images were acquired at 25 MHz using a VisualSonics high resolution imaging system. Midventricular short-axis images of the heart with approximately 0.15 mm lateral resolution and 0.05 mm axial resolution (comparable to that of murine cardiac MRI images) were acquired and then retrospectively assembled into a representative heartbeat composed of over 100 frames per cardiac cycle using the Vevo's "ECG-based Kilohertz

Visualization" capability. Instantaneous regional myocardial deformation velocity over the time course of the entire heart cycle was measured offline using tissue motion tracking on successive frames followed by normalization to the time intervals between these frames. Using a parallel processing technique on a 2.9GHz Pentium IV commodity PC, a time resolution of approximately 5 ms (i.e., 20 samples per heart cycle) and a spatial resolution of approximately 0.12 mm $\times$ 0.12 mm can be achieved for this myocardial deformation measurement in 24 seconds of processing time. Regional myocardial radial strain was then estimated. In the normal mouse heart, physiologically typical values for left ventricular myocardial deformation were obtained from myocardium at the mid-ventricular level: The peak radial strain was approximately 40%, the peak rate of systolic wall endocardial velocity was 23 mm/s and the peak rate of diastolic wall velocity was 39 mm/s in the lateral wall. In the infarcted area at the mid-ventricular level of a remodeled mouse heart, radial strain was less than 10% and the peak rate of both systolic and diastolic wall velocity was significantly reduced while velocities of the septal wall were comparable to that found in normal myocardium. These values are consistent with those measured using conventional, but more expensive and cumbersome, magnetic resonance imaging techniques. In conclusion, ultrasonic strain imaging techniques can be employed to study cardiac dysfunction in mice, and thus can evaluate the effects of genetic manipulation and/or pharmacologic intervention in laboratory mice. The technique can also be extended to the early diagnosis of cardiac dysfunction in human beings by scaling up the image processing techniques employed herein.

Jonathan Lindner M.D. (Cardiovascular Division UVA) provided the Vevo770 ultrasound scanner system used in this work. This work was supported by NIH EB001826.

1D-5 9:30 a.m.
CHARACTERIZATION OF DIGITAL WAVEFORMS USING THERMODYNAMIC ANALOGS: DETECTION OF CONTRAST TARGETED TISSUE IN MDA 435 TUMORS IMPLANTED IN ATHYMIC NUDE MICE.

M. HUGHES*, J. MARSH, A. WOODSON, E. LACEY, C. CARRADINE, G. LANZA, and S. WICKLINE, Washington University, St. Louis, MO.
Corresponding e-mail: msh@cvu.wustl.edu

Background: We describe characterization of backscatter from contrast targeted tumor tissue in vivo using analogs of thermodynamic quantities[1]. We apply these waveform characteristics to detection of tumor neovasculature in MDA 435 tumors implanted in athymic nude mice, which were imaged using a research ultrasound scanner over a two hour period post-injection of $\alpha_v \beta_3$-targeted perfluorocarbon nanoparticles.

Methods: Human MDA 435 cancer cells were implanted in the left hindquarters of athymic nude mice between 10 and 22 days prior to acquisition of data. Nine animals were injected with targeted nanoparticles and seven were injected with nontargeted nanoparticles to serve as controls. Mice were preanesthesitized

with ketamine, an intravenous catheter was inserted into the right jugular vein to permit injection of nanoparticles (either $\alpha_v \beta_3$ targeted, or untargeted). Mice were then placed on a heated platform maintained at 37 C (a diagram of the apparatus is shown in Figure 1), and anesthesia was administered continually with isoflurane gas through a nose cone. Subsequently, mice were injected with 0.030 mL of nanoparticle emulsion (equivalent to a whole body dose of 1.00 mL/kg) and ultrasound data were then acquired at 0, 15, 30, 60, and 120 minutes. RF data were acquired with a research ultrasound system (Vevo 660, Visualsonics, Toronto, Canada). The tumor was imaged with a 30 MHz single element wobbler probe and the RF data corresponding to single frames were stored on a hard disk for later off-line analysis. Each frame consisted of 384 lines of 4096 eight-bit words acquired at 500 MHz sampling rate. Each frame corresponds spatially to a region 2.0 cm wide and 0.61 cm deep. Images were constructed from backscattered ultrasound using three different signal processing techniques: Conventional (log of the signal envelop and Log of the sum of squares, i.e., Log Signal Energy), and a thermodynamic analog (H_c). All images were thresholded to select the brightest 97% of pixels. These values wee then averaged to obtain the mean enhancement as a function of time.

Results: Only the H_c receiver is able to distinguish between 0 and 120 minutes post-injection (p=0.060). Moreover, the mean values at all times change in a roughly linear fashion versus time. Log of signal envelope and log of signal energy, however, remain essentially unchanged over time.

Conclusion: These data demonstrate the ability and complementarity of information-theoretic receivers in conjunction with targeted nanoparticles to elucidate the presence of $\alpha_v \beta_3$-integrins in tumor neovasculature.

This study was funded by NIH EB002168, HL042950, and CO-27031. The research was carried out at the Washington University School of Medicine.

1D-6 9:45 a.m.
COMPARISON OF TWO APPROACHES TO VOLUME QUANTIFICATIONFOR FREE-HAND ULTRASOUND SCANNING OF MOUSE HEARTS.

C. GARSON*, J. HOSSACK, and Y. LI, University of Virginia, Charlottesville, VA,.
Corresponding e-mail: cdg6d@virginia.edu

In mouse ultrasound imaging, it is frequently desirable to produce three dimensional (3D) image data from a set of two dimensional (2D) images for volume visualization and quantification. This is accomplished by tracking the motion of the transducer on a frame by frame basis and later assembling and interpolating the 2D image planes into 3D grid space. Traditionally, motion is tracked by attaching either the transducer or the imaging subject to a motion controller but these approaches are somewhat unwieldy. We explore two different approaches in which transducer motion is tracked while permitting the flexibility and ease of use that a free-hand ultrasound scan provides. One approach involved mounting the transducer on a six-jointed articulated, instrumented arm, (Microscribe-3DX), which tracks transducer position with an accuracy of 0.23

mm while still enabling a full range of motion. A second approach, ("I-Beam"), involves placing 1D auxiliary tracking arrays on the head of the imaging transducer itself, perpendicular to the main imaging array, forming an "I"-shaped configuration. The minimum sum of absolute differences algorithm (MSAD) was used to estimate image movement in the tracking array field of view at multiple depths. This information was then used to estimate the relative translation and rotation of the transducer from one image frame to the next. Both the Microscribe and I-Beam approach were used to examine a small, cylindrical inclusion in a phantom that was 8 mm ± 6% long and had a volume of 464 mm^3 ± 15% (representative of a mouse heart in terms of gross dimensions). The border of the inclusion in each image was detected automatically using active contours ("snakes"). Six trials were conducted using the Microscribe system, resulting in a mean volume estimate of 454 mm^3 (a 2% error compared to the 464 mm^3 estimate) with a standard deviation of 19 mm^3. Similarly, six trials were conducted with the I-Beam system, resulting in a mean volume estimate of 472 mm^3 (2% error) with a standard deviation of 24 mm^3. The Microscribe was also used to compute left ventricle end diastolic volume in a short-axis scan of a murine heart. While our initial phantom studies are remarkably encouraging, we expect that somewhat inferior, but still quite acceptable, accuracy will be obtained when analyzing live mice. Nine scans were performed on live mice, yielding a mean LVEDV estimate of 141 mm^3 with 17 mm^3 standard deviation. Left ventricle length was also estimated from the scan, giving a mean length of 6.23 mm with 0.75 mm standard deviation. This was compared with a left ventricle length estimate of 7.1 mm, obtained by visually inspecting a long-axis image (12% error). In the future, we seek to confirm the accuracy of these length and volume estimates through magnetic resonance imaging and histological validation studies.

This work was supported in part by NIH EB001826, Siemens Medical Solutions, Mountain View, CA, Vermon, SA, France, and Tyco Precision Interconnect, Portland, OR.

Session: 2D

VASCULAR
Chair: L. Masotti
University of Firenze

2D-1 8:30 a.m.
DUPLEX ARTERIAL ELASTIC MODULUS RECONSTRUCTION FROM IN-VIVO STRAIN IMAGING AND PWV.

K. KIM*[1], W. F. WEITZEL[2], H. XIE[1], J. M. RUBIN[3], C. JIA[1], and M, O'DONNELL[1], [1]University of Michigan, Biomedical Engineering Department, Ann Arbor, MI, [2]University of Michigan, Internal Medicine, Ann Arbor, MI, [3]University of Michigan, Radiology, Ann Arbor, MI.
Corresponding e-mail: kangkim@umich.edu

Arterial compliance has been shown to be a strong indicator of vascular disease, cardiovascular disease and peripheral vascular occlusive disease. Stiffening of the arterial wall results in lowering strain and increasing Pulse Wave Velocity (PWV). A non-invasive free-hand ultrasound scanning procedure was performed to measure both strain and PWV. Using a commercial ultrasound probe, transverse scan was performed for strain estimation and longitudinal scan was performed at the same location for the PWV measurement. Based on a simple arterial model, elastic modulus was reconstructed from strain and PWV measurement separately and compared with each other. For both strain and PWV measurements, a correlation-based, phase-sensitive, speckle-tracking algorithm was employed. For the elastic modulus reconstruction from strain image, a simple model is used in which elastic modulus E_1 of the artery wall is related to elastic modulus E_2 of surrounding tissue by $E_1 + K_2 E_2 = K_1 [\Delta p/ \Delta \varepsilon]$ where $K_1$and K_2 are geometric factors, Δp is pulse pressure and $\Delta \varepsilon$ is inter-cardiac strain (i.e., change in strain from systole to diastole). Within an offset proportional to E_2, it is possible to reconstruct the arterial elastic modulus as a function of mean arterial strain from the ratio $[\Delta p/ \Delta \varepsilon]$. To reconstruct elastic modulus from PWV, Moens-Kotewerg equation for tethered elastic tube was employed. In both cases, artery geometrical factors, including inner and outer radius, were obtained from B-scan images and speckle tracking trashograms. For PWV case, the density of the arterial wall was assumed to be 1071-1100 Kg/m^3. Incompressibility was also assumed for both cases. Using a 5.8 MHz linear transducer, in-vivo scan was performed on the left common carotid artery of a 43 year old healthy male volunteer. The inner radius(a) of the carotid artery was 2.9 mm, outer radius(b) was 4.2 mm, and BP measured 119/82 mmHg. Based on an estimated intercardiac strain of 11%, the elastic modulus was estimated to be 85.6 KPa . From the PWV of 4.7m/sec, the reconstructed elastic modulus was 79.2-81.3 Kpa depending on the variation of the arterial density. The same scan was applied to the brachial artery of the same subject. This time a pressure equalization technique was applied. After arterial mean pressure was equalized, the reconstructed elastic modulus of the brachial artery (a and b were 1.3 mm and 2.0 mm) from a measured intercardiac strain of 30.0 % was 30.0 KPa and 28.0 KPa from a PWV measurement of 2.8m/sec. These values are lower by a factor of about 3 compared to the values before pressure equalization i.e., under normal physiological pressure. Assuming a and b can be determined within an error as large as half of the speckle size (0.1 mm), the estimation error in elastic moduli will be within 20 % for the artery sizes in this study. Preliminary results demonstrate that arterial elastic modulus can be determined and monitored using a simple duplex elastic modulus reconstruction procedure

Work supported in part by NIH grants HL-47401, HL-67647, HL-68658 and a grant from the Renal Research Institute.

2D-2 8:45 a.m.

A RETROSPECTIVE METHOD FOR PULSE-WAVE VELOCITY MEASUREMENT IN THE MOUSE.

R. WILLIAMS*[1], A. NEEDLES[1], E. CHERIN[1], Y.-Q. ZHOU[2], and F. S. FOSTER[1,2], [1]Sunnybrook and Women's College Health Sciences Centre, Toronto, ON, Canada, [2]Mouse Imaging Centre, Toronto, ON, Canada.
Corresponding e-mail: williams@swri.ca

Diseases such as hypertension and atherosclerosis can induce abnormalities in vascular function through alteration of arterial compliance. To study such diseases, transgenic mice have been created which develop abnormal vasculature. This has engendered a need to develop techniques capable of quantifying local vascular function *in vivo*. The pulse-wave velocity (PWV) is inversely related to arterial compliance, and therefore provides a useful measure of vascular function. In this study, the local PWV was measured non-invasively in the mouse carotid artery using the flow-area method, in which the PWV is estimated as the ratio between the change in volume flow and the change in cross-sectional area during the reflection-free period of the cardiac cycle. Previously, the cross-sectional area and volume flow in human and canine arteries have been measured indirectly using M-mode and Doppler signals, respectively assuming that the vessel is perfectly circular and that the flow is adequately described by Womersley's theory of pulsatile flow in rigid tubes. Our new approach directly measures the cross-sectional area and volume flow through the vessel using high-frequency Retrospective Colour Flow Imaging (RCFI), a technique recently developed in our lab. The cross-sectional area is determined by integrating over the region of flow in each frame of the RCFI dataset, while the volume flow is calculated by averaging the velocities over the vessel in each frame and multiplying by the corresponding area. Using the flow-area method, a local PWV of 2.77 m/s was observed at the mid-section of the carotid artery in a young CD-1 mouse anesthetized with isoflurane. Average PWV measurements over a 10 mm length of the carotid artery were also performed using time-delay Doppler velocimetry. This technique determines the distributed PWV by measuring the time-delay between Doppler-derived upstrokes at two locations a known distance apart. The distributed PWV was observed to be 3.70 m/s, in agreement with previously published data when using this method. Discrepancies between the local flow-area method and the distributed time-delay method will be analyzed and discussed.

Support for this work was provided by the National Cancer Institute of Canada/ Terry Fox Foundation, the Ontario Research and Development Challenge Fund, and VisualSonics Inc.

2D-3 9:00 a.m.

NEW NON-INVASIVE METHOD FOR INTIMA-MEDIA THICKNESS AND INTIMA-MEDIA COMPRESSION MEASUREMENTS.

M. CINTHIO*[1], T. JANSSON[1], Å;. RYDEN AHLGREN[2], H. W. PERSSON[1], and K. LINDSTRÜM[1], [1]Department of Electrical Measurements, Lund Institute of Technology, Lund, Sweden, [2]Department of Clinical Physiology, UMAS, Lund University, Malmö, Sweden.
Corresponding e-mail: magnus.cinthio@elmat.lth.se

Both in the normal aging process and in atherosclerosis the tunica intima-media layers of the arterial wall grow thicker. Intima-media thickness (IMT) is considered as a valuable marker of early atherosclerosis. However, it is a challenging task to do this accurately since the intima-media normally is only 0.5-1 mm thick and the resolution an ultrasound image is around 0.2-0.3 mm. The IMT is defined as the distance between the lumen-intima echo and media-adventitia echo of the arterial wall. Conventionally only an average value of the IMT for each heartbeat is reported instead of a variation of the IMT over time. We here suggest an algorithm for simultaneously measurements of distension, IMT at diastole and the intima-media compression (IMC) with a new fast, robust, high-resolution, and automatic algorithm utilizing the ultrasonic gray-scale information.

The IMT at diastole, IMC and the distension (the diameter change) were measured over a preselected segment of the arterial wall using B-mode ultrasound. All investigations were performed by a commercial ultrasound system (HDI®5000, Philips Medical Systems, ATL Ultrasound, Bothell, WA, USA). The system was equipped with a 50 mm 5-12 MHz linear array transducer. The B-mode image was average in the lateral direction. The new algorithm detected the demarcation of the vessel by finding the maximum echo of each side of the lumen. Thereafter, the far and the near walls were roughly found by the maximum slope for each wall in the envelope signal. The positions of the different parts of the arterial walls were then refined by finding an intersection between thresholds values and the envelope. Finally, the resolution was improved by solving the equation of a line *(y=kx+m)* between the two samples around the threshold values of each wall. The algorithm was thereafter repeated for all images in the cineloop. The algorithm was evaluated *in vivo* on five healthy subjects with no known vascular disease (2M/3F; age 27-47 years).

The intima-media compression was (68 ± 9 μm; range 59-79 μm) with a standard deviation (range 4-14 μm) within an investigation. The intima-media thickness at diastole was (614 ± 76 μm; range 518-717 μm) with a standard deviation (range 4-16 μm) within an investigation. The distension was (687 ± 246 μm; range 543-1124 μm) with a standard deviation (range 7-92 μm) within an investigation. The lumen diameter at diastole was (6.32 ± 0.91 mm; range 5.31-7.46 mm) with a standard deviation (range 0.01-0.13 mm) within an investigation. The measurement time of one image was approximately 2.7 milliseconds with a Pentium M 1.7 GHz computer.

In conclusion we have developed a fast, robust and automatic algorithm with high resolution for simultaneously measurements of intima-media compression,

intima-media diameter at diastole, arterial distension and lumen diameter at diastole of arterial vessels.

This study was supported by a grant from the Swedish Foundation for Strategic Research via Cortech, and from the Swedish Research Council. We would like to thank Mrs. Ann-Kristin Jönsson for skilful technical assistance.

2D-4 9:15 a.m.
DEVELOPMENT OF NON-INVASIVE VASCULAR ELASTOGRAPHY FOR CAROTID ARTERY PLAQUE ASSESSMENTS.

G. CLOUTIER*[1], C. SCHMITT[1], R. MAURICE[1], S. LANTHIER[2], M.-F. GIROUX[2], and G. SOULEZ[2], [1]University of Montreal Hospital Research Center, Montreal, Quebec, [2]University of Montreal Hospital, Montreal, Quebec.
Corresponding e-mail: guy.cloutier@umontreal.ca

In patients with carotid artery disease, only a minority will experience warning symptoms, the majority having their stroke from previously asymptomatic lesions. Since morbidity and mortality after acute stroke is unacceptably high, it would be very important to recognize and treat patients before they develop any symptoms. In this context, we propose the development of non-invasive vascular elastography to study the mechanical properties of suspected unstable carotid artery plaques.

A new implementation of the Lagrangian speckle model estimator that considers local echogenicity variations was used to assess the strain tensor from either cross-sectional or longitudinal ultrasound scans of carotid blood vessels. The feasibility was first assessed in a flow phantom with polyvinyl alcohol (PVA) cryogel vessels simulating normal and stenosed carotids. Scanning of normal subjects and of a patient with carotid stenoses of at least 50% (diameter reduction) was also performed to further validate the method. Ultrasound radio-frequency data were acquired with a ES500RP system (Ultrasonix, Vancouver, Canada) equipped with a 7 MHz linear array probe. From these data, elastograms were computed from the pulsatile pressure changes induced with a pump for the in vitro data, and from normal pulsing arteries in the case of the in vivo scans. Different indices were extracted from these elastograms: Emax that is the highest peak on the strain-stress modulus histogram calculation, and strain statistics.

Reproducible strain distributions were obtained from the homogenous vascular phantom at three positions along the z-axis and for six consecutive pulsing periods. For the mimicking plaque made of PVA layers with different stiffness, the strain decay compensated elastograms clearly showed a low strain area (1.75%) surrounded by a high strain ring (4.7%). Estimated sizes, locations and stiffness ratios of these structures were in good agreement with those of the moulds and tissue materials used to build the phantom. In vivo elastograms were first computed for three normal subjects. In agreement with the literature, Emax of a 26 years old man was 147 ± 7 kPa (mean strain between peak systole and end diastole of 4.45 ± 0.36%), that of a 43 years old man was increased to 540 ± 111 kPa (mean strain of 2.41 ± 0.31%), and finally the 40

years old women presented a value of 162 ± 30 kPa (mean strain of 5.14 ± 2.48%). For the patient with a calcified internal carotid artery, the mean axial strain between peak systole and end diastole was 0.5 ± 3.2 % for the hard calcified plaque, and the surrounding vascular tissue showed a mean value of 9.3 ± 4.0 %. At the junction between the soft vascular tissue and the hard calcified plaque, the axial shear elastogram showed a maximal strain at 20%.

In conclusion, this study further validates the Lagrangian speckle model estimator that provides axial and lateral strain elastograms, and axial and lateral shear elastograms.

Valorisation-Recherche Quebec (group grant #2200-094) and the Fonds de la Recherche en Sante du Quebec (Research Scholar and National Scientist Awards)

2D-5 9:30 a.m.
AN INSTRUMENT FOR SCREENING FOR CAROTID STENOSES.

D. VILKOMERSON*[1], T. CHILIPKA[1], R. OUTCAULT[2], and K. GOLDMAN[2], [1]DVX, llc, Kingston, NJ, [2]Princeton Surgical Associates, Princeton, NJ.
Corresponding e-mail: dv1dvx@comcast.net

Stroke is the third leading cause of death, and the most common cause of disability in the USA. Most of the 700,000 stroke victims per year (USA) are institutionalized or require assistance in daily living. Stroke occurs without warning 80% of the time.

Plaque in the carotid bifurcation is the cause of about half of strokes. It has been proven that removing significant plaque reduces the rate of stroke by a factor of almost three. Thus, screening for carotid stenoses would reduce the number of strokes significantly; however, the cost of screening with conventional duplex Doppler instruments precludes such screening. We report here on an instrument especially designed to screen for carotid stenoses.

A screening instrument is most effective and lowest in cost when it is used in a primary care setting by non-specialists. The new screening instrument is designed for such use.

A new kind of scanhead was developed for the instrument. It consists of a one centimeter diameter, 5 MHz CW transmitting transducer surrounded by 6 receiving transducers angled downward, so their receive-beams′ intersection with the transmitter′s beam forms a large, cylindrical sensitive volume extending from the skin to 4 cm below. It is a vector Doppler instrument, using the received six Doppler frequencies to calculate the highest blood velocity within the sensitive volume, independently of the spatial orientation of the scanhead or the carotids. As only high velocities are of interest, signals from other vessels in the neck, such as the jugular vein, are rejected.

The operator guides the scanhead up the common carotid to beyond the bifurcation by listening to the audio signal derived from the Doppler signals. The operator seeks the highest frequency, i.e. the region of any stenosis. The instrument is otherwise automatic: all adjustments for gain, velocity range, PRF,

etc are made by the instrument. The operator presses a button to measure the velocity in a region, and the instrument analyzes the data from the previous few seconds and displays the highest velocity.

Any patient with high velocities, e.g. 125 cm/sec or higher, would then be sent for a complete duplex Doppler examination. As a screening system, the instrument is effective even if it produces false positives, e.g. from high velocities in the clinically unimportant external carotid, or from certain configurations of the internal and external carotids that confound the vector algorithm.

A clinical test of the instrument on a series of 34 carotids showed the new instrument's sensitivity (percentage of high-grade stenoses found by the new instrument to those found by conventional Duplex system) is 94%, and its specificity (carotids characterized as normal that were normal) is 91%. The examination time using the new instrument averaged 3 minutes per patient.

The instrument described herein appears to have the potential for being an effective screening system to reduce stroke.

This research was partially supported by an NIH SBIR grant R43HL072534.

2D-6 9:45 a.m.
PHOTOACOUSTIC IMAGING TO AGE DEEP VEIN THROMBOSIS.

A. B. KARPIOUK[1], S. R. AGLYAMOV[1], S. MALLIDI[1], W. G. SCOTT[2], J. M. RUBIN[3], and S. Y. EMELIANOV*[1], [1]Department of Biomedical Engineering, University of Texas at Austin, Austin, TX, [2]Winprobe Corporation, North Palm Beach, FL, [3]Department of Radiology, University of Michigan Medical School, Ann Arbor, MI.
Corresponding e-mail: emelian@mail.utexas.edu

One in every hundred people who develop deep vein thrombosis (DVT) dies - the cause of death is most often a pulmonary embolism, i.e., blockage of an artery in the lungs by a blood clot broken off of DVT. All forms of DVT therapy rely on the age of thrombus. However, there are no established clinical techniques to reliably age DVT. Therefore, there is a definite and urgent clinical need for a technique that can detect and adequately age deep vein thrombosis.

Since maturation of the thrombus results in gradual "bleaching" of the blood clot, the optical properties of DVT change with the age of the clot. Specifically, clot aging is associated with the decrease of optical absorption due to reduced concentration of hemoglobin. Indeed, hemoglobin and other porphyrins are substantially stronger absorbers in near-infra-red spectral range compared to other tissue constituents. Therefore, an imaging technique that measures optical absorption could be ideal for aging DVT. Such imaging technique, known as photoacoustics (or optoacoustics and, more generally, thermoacoustics) exists - the primary contrast mechanism in thermoacoustic imaging is based on tissue absorption of electromagnetic waves. In this paper, we initially test the hypothesis that photoacoustic imaging can quantitatively age DVT.

The experiments were conducted using gel-based phantoms with either artificial or true DVT. The artificial blood clots were made from a solution of polyvinyl

alcohol, saline and different (0 to 50%) concentration of red blood cells (RBC). The samples of acute and chronic thrombi were obtained from a rat-based, stasis-induced model of DVT. Both optical and ultrasonic scatterers were added to the phantom to further mimic corresponding properties of soft tissue. The computerized experimental imaging system was based on a 532 nm and 1064 nm Nd:YAG pulsed laser and a 7.5 MHz single-element, focused ultrasound transducer attached to a 3-D mechanical scanning system. Using this system, both ultrasound and photoacoustic images were acquired.

The photoacoustic images of phantom with artificial clots can clearly distinguish acute (50% RBC solution) from chronic (10% RBC solution) clots. The thermoacoustic response of the acute clot irradiated with 532-nm laser pulse was about 7 times stronger than that from the chronic clot - this is an anticipated result based on the differences in the total hemoglobin concentration between the clots. Finally, photoacoustic images of acute and chronic clot specimens were obtained at both 532-nm and 1064-nm irradiation confirming that photoacoustic response of thrombi changes with age. The results of this study suggest that photoacoustic imaging of blood clots is possible and can be used to age DVT. In addition, the photoacoustic method can be used in conjunction with ultrasound and elasticity imaging to simultaneously detect and diagnose deep vein thrombosis.

Support in part by National Institutes of Health under grants CA110079, CA96018 and HL68658 is acknowledged.

Session: 3D

NDE-GENERAL METHODS
Chair: B. Tittman
The Pennsylvania State University

3D-1 8:30 a.m.
STRAIN MEASUREMENTS ON CARBON-EPOXY COMPOSITES BY LAMB WAVES PIEZOPOLYMER INTERDIGITAL TRANSDUCERS.

A. BULLETTI[1], O. OCCHIOLINI*[1], L. CAPINERI[1], L. MASOTTI[1], and E. ROSI[2], [1]Dept. Electronics and Telecommunications, University of Florence, Firenze, Italy, [2]Alenia Spazio, Laben/Proel, Firenze, Italy.
Corresponding e-mail: omar.occhiolini@tin.it

The importance of composite materials for designing and manufacturing high tech products is a matter a fact. Nowadays we find composite materials employed in spacecrafts, avionics, sport vehicles and sport equipments (cars, motorbikes and bicycles, sailing boats, skis and snowboards).

Several methods are commonly used for Non Destructive Testing (NDT) on Carbon Fiber Reinforced Plastic (CFRP) and recently authors developed a method, based on guided acoustic waves generated/detected with piezopolymer

(PVDF film) interdigital transducers [1][2]. This technology has two key advantages respect to piezoceramic IDT: conformability to non-planar surfaces and easy transducer design and manufacturing with reduction of cost production compared with piezo-IDT.

In this work will be presented the results of a research activity devoted to measure the strain on cross-ply [0°/90°] composite laminates, applying a pure bending on 4 points.

As the composite is subjected to strain, the elastic parameters of the structure change. Since the Lamb wave phase velocity depends on these properties, a time of flight method can be used.

Tests have been carried out using two IDTs in pitch-catch configuration at 160mm distance placed on the composite surface. Our IDTs are characterized by 3 finger pairs, wavelength 15mm, PVDF thickness 100μm, excited with a sine burst at 450kHz on a 4 mm thickness composite. A theoretical analysis of the relationship between the strain states due to pure bending of this laminar structure and the variations of the time of flight (S_0 symmetric Lamb wave mode) has been carried out and then experimentally verified. During load tests, the state of pure bending of the composite sample has been also monitored with standard strain gages method. The latter method has been used for comparison. Results of measurements in static conditions with nominal load have been plotted showing time of flight variation and surface strain express in με (from strain gages) versus the stress. Also results of measurements in dynamic load condition have been carried out and the time of flight variation versus the relative surface deformation has been plotted. We will also show the results obtained with mechanical loading and downloading and both strain measurements method. Within a range of 1000 με the ultrasonic method showed a linear relationship of time of flight, and of the guided wave versus strain states due to pure bending quadratic in the range of 1000-1600 με; the same relationships have been found with strain gages. In conclusions, these results have demonstrated that these type of transducers can measure strain in large composite structure with repeatible performances.

[1]F. Bellan, A. Bulletti, L. Capineri, L. Masotti, F. Guasti, E. Rosi,"Acoustic guided waves interdigital transducers for non destructive testing of carbon epoxy composites for spacecraft structures", AISEM 2004 Proceedings, Ferrara, 8-11 February 2004.

[2] ESA-ESTEC Contract n 16938/02/NL/MV

Keywords: PVDF, interdigital transducers, Lamb waves, carbon-epoxy composites

3D-2 8:45 a.m.
FOULING DETECTION IN FOOD VESSEL USING INTERDIGITAL PVDF LAMB WAVE TRANSDUCER.

J. JINGPIN, G. HAIYAN, H. CUNFU*, and W. BIN, Beijing University of Technology, Beijing, China.
Corresponding e-mail: jiaojp@bjut.edu.cn

Fouling films build up during the processing of many liquid food products. This problem is perhaps most widespread in UHT processing of milk and milk-based products. The presence of a layer of fouling on the internal surface of food vessel may have great influence on products, for example, it may reduce the flow rate of product and the rate of heat transfer, and decrease the product quality and safety. A regular cleaning schedule can solve the problem, but it leads to considerable periods of plant downtime and use of significant quantities of cleaning materials, which result in the reduction of product efficiency and the loss of economic. Early detection and quantification of fouling extent can reduce costs incurred due to wear on the machinery, maintenance of vessel, and production down time. Therefore it is required that the fouling should be detect or monitor in situ using the methods of NDT.

Plate commonly used in the processing of food products is a natural wave-guide that can support different types of Lamb waves. Since fouling can be characterized as a thin viscous or solid film on the surface of plate, it is desirable to use a mode that show maximal sensitivity to viscous coating and minimal sensitivity to fluids loaded. By analysis of wave structure of Lamb in thin plate, A0 mode has minimal radical displacement and maximum axial displacement on the surface of plate, which may be capable of discriminating between liquids and viscous and solid films.

In this paper flexible interdigital PVDF transducer is used to generate Lamb wave and detect fouling in thin plate. The process of designing interdigital PVDF transducer for the generation of single A0 mode is discussed. Fouling detection experiments were conducted in thin plate. A 5mm width film, a 25mm width film and two 15mm width films are pasted on the surface of plate, which are considered as the simulated fouling. Using the interdigital PVDF Lamb wave transducer, the exists of four simulated fouling were testified by the detected waveforms. Using the methods of time-frequency analysis, the waveforms were disposed further, and it also demonstrated the validity of fouling detection experiments.

In this paper, it is demonstrated that Lamb wave detection technique is an effective tool for fouling detection in food vessel.

Key words: Lamb wave, interdigital transducer, fouling detection

Acknowledgments: The research was supported by National Natural Science Foundation of China under contract number: 60404017, and Beijing Natural Science Foundation of China under contract number: 4052008

3D-3 9:00 a.m.
DEVELOPMENT OF BROADBAND, OMNIDIRECTIONAL TRANSDUCERS FOR NDE APPLICATIONS.

O. KEITMANN-CURDES*[1], M. PARUSEL[1], W. WILKENING[2], M. MIENKINA[3], and H. ERMERT[1], [1]Institute of High Frequency Engineering, Ruhr-University Bochum, Bochum, Germany, [2]Krohne Altometer, Dordrecht, The Netherlands, [3]Institute of Medical Engineering, Ruhr-University Bochum, Bochum, Germany. Corresponding e-mail: o.keitmann@ieee.org

In order to image highly reflecting (metallic) surfaces in a water-oil-emulsion under high pressure by means of ultrasound, broadband transducers with a wide opening angle (point-sources, spherical waves) are needed, which are not commercially available. Thus, efforts were made to develop and produce such ultrasonic transducers with the following requirements: less than 10 mm in diameter, 2 MHz center frequency, 75-100% 6dB-bandwidth, more than 120° opening angle and potential resistance against high static pressure of up to 1000 bar.

Most promising for this problem are piezoelectric half-spheres. Such elements generate spherical waves on either side: on the outer (convex) side coming from the sphere's center (virtual source), and on the inner (concave) side focused to the center of the sphere and then propagating further. The latter concept is realized by commercially available transducers (i.e. the focal point of a strongly focused transducer serves as a virtual point source), but only with a limited opening angle of 40-45°.

For better application of backing material to the piezoelectric element, we decided to use the convex side of the half-sphere as the emitting ultrasonic aperture. Our transducer designs incorporate backing material and a two-layer matching to water. Experiments with those transducers were conducted in a virtual environment (PZFlex) as well as in the lab. Different materials (aluminum, brass, tungsten, different epoxies) were investigated regarding their suitability as transducer backing media and regarding their compatibility with the designated ambient conditions. On the aperture side, two matching layers were designed consisting of metal (aluminum, magnesium) and/or metal particles embedded in epoxy. Different combinations of backing and matching materials were simulated, and the simulation results verified experimentally.

We will present different realizations of ultrasonic transducers with 1.3, 2 and 3 MHz center frequencies and different backing and matching materials. Recipes for easy transducer modeling will be provided, and the effects of different materials and geometric dimensions will be discussed. The presented transducers are mainly characterized by 6dB-bandwidths of more than 75% and opening angles of more than 120°.

We would like to thank the German Research Foundation DFG (Deutsche Forschungsgemeinschaft, grant ER 94/26) for supporting this project by grants.

3D-4 9:15 a.m.
3D CONTOUR TRACKING OF SPECULARLY REFLECTING SURFACES.

O. KEITMANN-CURDES*[1], P. KNOLL[2], H. MEIER[2], and H. ERMERT[1], [1]Institute of High Frequency Engineering, Ruhr-University Bochum, Bochum, Germany, [2]Chair of Production Systems, Ruhr-University Bochum, Bochum, Germany.
Corresponding e-mail: o.keitmann@ieee.org

The aim of the presented work is to develop an ultrasonic imaging system for contour detection of specularly reflecting sheet metal surfaces and surface contour tracking during a continuous hydroforming process. The active fluid medium is a water-oil-emulsion at a pressure of several hundred bar. Based on

certain design considerations in context with hardware limitations to obtain on-line information about the state of forming during the whole process a sparsely filled ultrasonic transducer array has been used with a limited number of transducer elements distributed randomly on a 10x10 element position raster of a 2D aperture geometry (10 cm x 10 cm), operating at 2 MHz.

It has been shown before, that “2.5D-geometries” (surface areas with curvatures independent of one direction) could be detected and tracked with a sufficient accuracy (linear aperture, 10 cm width, 21 transducers, error in sound propagation direction less than 1 mm). Full 3D contour imaging turns out to require a much higher number of active transducer elements in the sparse array as well as a higher amount of data to be processed. The respective experiments were performed in an experimental set-up with two 2 MHz transducers and two independent traversing units to generate a 2D aperture. In this way, data acquisition was obtained and, in a first step, image reconstruction was performed with a SAFT (synthetic aperture focusing technique) algorithm. Within the SAFT image, the contour of the metal sheet could be detected by means of active contour elements called balloons. Finally, the 3D contour could be represented by mathematic functions with a limited set of parameters as the reconstruction result.

We will present the design and results of an imaging system for automated detecting and tracking of sheet metal surface contours during the forming process by means of an active contour model. The forming process has been discretized into 8 forming stages. Contour tracking is performed stepwise at present. To achieve a sufficient accuracy in the 3D domain, a priori in process information e.g. starting and final positions of the sheet metal, forming velocity, and preceding instantaneous contour geometries are incorporated into the active model.

All presented results are based on measured ultrasonic data and will be discussed with respect to reconstruction accuracy, hardware requirements and computing time.

We would like to thank the German Research Foundation DFG (Deutsche Forschungsgemeinschaft, grants ER 94/26 and ME 1831/9) for supporting this project by grants.

3D-5 9:30 a.m.
ULTRASONIC STUDY OF ALTERATION PROCESSES IN GRANITES BY FREEZING AND THAWING.

L. M. DEL RÍO*[1], F. LÓPEZ[1], F. J. ESTEBAN[1], M. MOTA[2], J. J. TEJADO[2], I. GONZÁLEZ[2], A. RAMOS[3], and J. L. SAN EMETERIO[3], [1]Escuela Politécnica. Universidad de Extremadura (UEX), Cáceres, Spain, [2]Instituto Tecnológico de Rocas Ornamentales y Materiales de la Construcción (INTROMAC). Consejería de Infraestructura y Desarrollo Tecnológico. Junta de Extremadura, Cáceres, Spain, [3]Departamento de Señales, Sistemas y Tecnologías Ultrasónicas. Instituto de Acústica. Consejo Superior de Investigaciones Científicas (CSIC), Madrid., Spain.
Corresponding e-mail: lmdelrio@unex.es

Ornamental rocks and, particularly, granites, represent one of the most important industrial activities in the region of Extremadura (SW Spain). Therefore, knowledge about the intrinsic properties of this natural formation and its evolution in the environment are required in order to ensure the quality of construction activities based on these types of rocks. In this work, we describe a detailed experimental study which relies on the use of different types of granites, which are repeatedly frozen and thawned in a controlled environment. Through this technique, we can obtain information about the transformation of the rocks after laboratory-based artificial analyses, where the rock is frozen-thawned cyclically, thus allowing a better insight into the quality of the material under study. Specifically, our experiments were based on 56 freezing-thawning cycles, where the temperature was varied from - 12 °C to 20 °C at time intervals of 4 and 12 hours, depending on the type of experiment considered. The ultrasonic wave velocity was measured at the beginning and also at the end of the process. In addition, several measurements were made during the process to characterize the evolution of granites. Prismatic samples of 30x10x5 (cm) in size, corresponding to more than 30 varieties of granites, have been used. A low-frequency transceiver set-up, based on a high voltage BPV Steinkamp instrument and two 50 kHz probes, has been used to measure pulse travel times by ultrasonic through-transmission testing. In complementary fashion, we have also used other techniques to derive a large number of their physical and mechanical properties, according to Spanish regulations in force, such as strength, porosity, absorption, etc. More than thirty species of granites were carefully studied, where their characteristic ultrasound propagation speeds before being used in experiments ranged from 3000 and 6000 meters per second (approximately). Although it was apparent that the analyzed granite samples were not in bad condition after the experiments, we have tested (using the proposed technique) that there was a significant reduction in the ultrasound propagation speed in the samples which, depending on the considered species and the applied cycle-time, can be in the order of a 15%. In addition, we obtained strong positive linear correlations ($r > 0.9$) after plotting the reduction in speed against the differences in propagation speeds in water-saturated and dry granites, before and after being tested. This leads us to believe that, although the porosity of the tested granites was below 2 % before experiments, the freezing and thawing processes can increase the size and number of pores significantly, thus decreasing the propagation speed of ultrasonic waves in the rocky material after several cycles.

This work has been partially supported by Consejería de Infraestructuras y Desarrollo Tecnológico de la Junta de Extremadura (Spain) R&D PR03B021.

3D-6 9:45 a.m.
SPEED OF SOUND MICROSCOPY FOR BIOMEDICAL APPLICATIONS.

Y. SAIJO*[1], N. HOZUMI[2], K. KOBAYASHI[3], N. OKADA[3], H. SASAKI[1], E. SANTOS FILHO[1], T. YAMBE[1], and M. TANAKA[1], [1]Institute of Development, Aging and Cancer, Tohoku University, Sendai, Japan, [2]Toyohashi University of technology, Toyohashi, Japan, [3]Honda Electronics Co. Ltd., Toyohashi, japan.
Corresponding e-mail: saijo@idac.tohoku.ac.jp

In biomedicine, scanning acoustic microscopy (SAM) is useful for intraoperative pathological examination, study of low-frequency ultrasonic images, and assessment of biomechanics at a microscopic level.

Recently, we have proposed a prototype of speed of sound microscopy using a single pulsed wave instead of continuous waves used in conventional SAM systems. In the present study, we construct a compact, commercially available speed of sound microscope and evaluate the biomedical efficiency by visualizing normal and atherosclerotic coronary arteries.

Normal and atherosclerotic human coronary arteries were embedded in OCT (optimal cutting temperature) compound and rapidly frozen by liquid nitrogen at -20°C. The specimens were sliced approximately 10 μm by a cryostat and mounted on a silane-coated glass slides.

A single ultrasonic pulse with a pulse width of 5 ns was emitted and received by the same transducer above the specimen. The central frequency was 100 MHz, and the diameter of the focal spot was estimated to be 20 μm. The reflections were received by the transducer and were introduced into an Analogue-digital (A/D) converter with sampling frequency of 2 GHz and resolution of 8 bit. The transducer was mounted on an X-Y stage and the X- and Y-scan were driven by two linear servo motors. Two-dimensional distributions of ultrasonic intensity, speed of sound, and thickness of a specimen measuring 2.4 $\times$ 2.4 mm were visualized using 300 $\times$ 300 pixels.

The waveform from the tissue area contains two reflections at the surface and at the interface of the tissue and glass, but the two components cannot be separated in time domain analysis. Thus, frequency domain analysis was performed by analyzing the interference between the two reflections. Intensity and phase spectra were calculated by Fourier transforming the waveform. The spectra were normalized by the reference waveform. The waveform at the glass surface without the tissue was used as a reference waveform. The decline of the glass surface was compensated by measuring three different points in the glass area surrounding the tissue.

In case of normal coronary artery, the intima was thin and the speed of sound was 1580 m/s in the intima, 1560 m/s in the media and 1590 m/s in the adventitia, respectively. In case of atherosclerotic coronary artery, the speed of sound was 1820 m/s in the calcification in the intima, 1680 m/s in fibrous tissue of the thickened intima and 1480m/s in the lipid pool, respectively. The values of speed of sound were within same range as our previous measurements.

Speed of sound microscopy based on a single pulse and the Fourier transform to calculate the sound speed was developed. The system can be applied to intraoperative pathological examination because it realized very compact size and user-friendly interface.

This study was supported by Grants-in-aid from Japan Society of Promotion of Science (15300178) and Grants-in-aid from Ministry of Health, Labour and Welfare (H17-nano-001).

Session: 4D

PHYSICAL ACOUSTICS 1
Chair: T. Shiosaki
NARA Institute of Science and Technology

4D-1 8:30 a.m.
(Invited)
IONIC CONDUCTIVITY IN ACOUSTIC CRYSTALS.

E. V. CHARNAYA*[1], CH. TIEN[2], and A. L. PIROZERSKII[1], [1]Institute of Physics, St. Petersburg State University, Petrodvorets, St. Petersburg, Russia, [2]Department of Physics, National Cheng Kung University, Tainan, Taiwan, ROC. Corresponding e-mail: charnaya@mail.ru

A short review of influence of ionic mobility on acoustic properties of crystals is presented. Different kinds of ionic mobility in solids are discussed: acceleration of self-diffusion in insulators at high temperature, mobility of ions in superionic crystals and nature of superionic conductivity, mobile impurities and vacancies. High ionic mobility leads to pronounced acousto-ionic interaction, which has specific temperature and frequency dependences. The main attention is focused on alterations in sound velocity and attenuation due to acousto-ionic interaction in superionic, doped and imperfect crystals possessed high ionic localized and delocalized mobility already at moderate temperatures.

Acousto-ionic interaction in piezoelectric crystals for piezoelectrically active acoustic waves is caused by action of electric fields induced by acoustic strains on mobile charges. Such kind of interaction is described by a modified Hutson-White theory where the susceptance due to localized hopping mobility is taken into account. It leads to relaxation acoustic anomalies, which become apparent against background temperature and frequency dependences. When ionic transport dominates the whole conductivity, the attenuation maximum is seen at a temperature corresponding to $\omega=\omega_c$, where ω is the ultrasound frequency, ω_c is the Maxwell frequency of conductivity relaxation. When polarization contribution prevails, the condition of attenuation maximum is $\omega\tau=\varepsilon_c/\varepsilon_r$ for the Debye model with a single relaxation time τ. Here ε_c and ε_r are the static and high-frequency permittivities, respectively. Acoustic anomalies in the $LiIO_3$, $Li_2B_4O_7$, $LiNbO_3$, SiO_2 crystals are considered as examples.

For non-piezoelectric crystals and for piezoelectrically inactive waves in piezoelectric crystals, acoustic anomalies are mainly caused by relaxation due to the deformation potential. Maximum of sound attenuation should be seen upon the condition $\omega\tau=1$. Relaxation ultrasound anomalies and ionic conductivity in $LiIO_3$, CeF_3, SiO_2, molibdates, germanates, and other crystals are considered as examples.

Relaxation alterations in sound attenuation and velocity can be also seen in the superionic state near the structural superionic transitions. The nature of such effects is similar to that of acoustic relaxation anomalies near any structural phase transitions.

Quite different resonance ultrasound attenuation can be observed in come crystals near the superionic phase transitions which are not accompanied with changes in lattice symmetry, for example, in $LiIO_3$ and CeF_3. Such effects can be treated within the framework of the Landau theory of phase transitions assuming oscillatory dynamics of the order parameter.

We gratefully acknowledge support from RFBI and NSC of Taiwan.

4D-2 9:00 a.m.
THE APPLICATION OF FINITE ELEMENT ANALYSIS IN THE DESIGN OF HIGH INTENSITY ULTRASONIC SYSTEMS.

G. HARVEY*, A. GACHAGAN, and A. MCNAB, Centre for Ultrasonic Engineering. Corresponding e-mail: gerald.harvey@eee.strath.ac.uk

Finite element (FE) analysis has become an invaluable tool in the research and design of ultrasonic devices and transducer systems for disciplines such as non-destructive testing, SONAR and biomedical imaging. The accuracy of the software in simulating the individual requirements of these applications has been well documented and experimentally vindicated. However, the design of high intensity, low frequency ultrasonic systems is one field where the verification of FE analysis proves to be very problematic, typically due to inappropriate, and hence erroneous, measurement procedures employed for theoretical verification. A common approach is to adopt an iterative design process, involving the construction of a number of test cells and their experimental evaluation, which can be very expensive, inaccurate and time-consuming. The use of non-invasive instrumentation for the characterisation of high intensity fields solves many of the problems inherent with conventional hydrophone measurement methods; assists in the corroboration of simulation data and hence, establishes confidence in the use of FE methods in the design process.

This paper describes the application of a non-invasive field measurement approach linked with FE design techniques to optimise the identification and control of pressure node locations (associated with regions of cavitation) within test cells. The measurement technique is based on the interferometric detection of refractive index changes in transparent media due to pressure, coupled with modified tomographic scanning routines, to allow the reconstruction of a three-dimensional map of pressure within cylindrical vessels. Importantly, an adaptive algorithm was developed to control the firing angle of the interferometer in order to compensate for the refractional effects introduced by arbitrary cell structures and hence, maintain the parallel projections essential for reconstruction accuracy. Firstly, a series of commercially available Tonpilz transducers was experimentally characterised and extensively modelled in the PZFlex environment, with excellent agreement achieved. Next, modified tomography was utilised to experimentally measure the fields generated in small liquid filled vessels (e.g. 100mm diameter, 150mm height). These systems were simulated in the FE domain with good correspondence between the optically measured profiles and theoretical profiles established. The validated virtual prototyping platform was then used to design systems with specific field characteristics for increased probability of cavitational

effects. Examples of improved designs utilising variations in cell geometries, transducer arrangements and characteristics are presented and applied to a model chemical process system

4D-3 9:15 a.m.
STABILITY CONSIDERATIONS FOR PERFECTLY MATCHED LAYERS IN PIEZOELECTRIC CRYSTALS.

F. CHAGLA and P. SMITH*, McMaster University, Hamilton, Ontario, Canada.
Corresponding e-mail: smithpm@mcmaster.ca

Time domain methods for simulating the behavior of physical systems are commonly used in many disciplines because they allow non-linear and time-varying effects to be modeled. Of these, the Finite-Difference Time-Domain (FDTD) method has been widely adopted for the simulation of electromagnetic or acoustic wave propagation in isotropic media. The method involves the discretization of the wave equations in both time and space and iteratively solving the equations over a grid extending across the physical space of interest. The need to limit the size of the grid, however, requires that a suitable boundary condition be chosen so that the computations do not introduce ghost reflections from the edges of the grid. Here, the Perfectly Matched Layer (PML) is acknowledged to be the boundary condition that most efficiently eliminates the reflections in isotropic solids. In [1], we extended the concept of PML to piezoelectric crystals and showed that it can also be extremely effective for acoustic wave propagation in non-isotropic solids. Since publishing that work, however, we have found that the PML can experience numerical instabilities when it is applied to solids having polar slowness curves that contain concave sections. For example, simulations of acoustic wave propagation in barium germanate ($Bi_4Ge_3O_{12}$) lead to numerical instabilities in the PML, while similar simulations in barium sodium niobate ($Ba_2NaNb_5O_{15}$) do not. We will show several examples FDTD simulations and use the results to deduce the conditions necessary for stability.

[1] F. Chagla, C. Cabani and P. M. Smith, “Perfectly matched layer for FDTD computations in piezoelectric crystals,” 2004 IEEE Ultrasonics Symposium Proceedings, Montreal, QC, pp. 517-520, 23-27 August 2004.

4D-4 9:30 a.m.
OBLIQUELY INCIDENT RAYLEIGH WAVES AT A VERTICAL EDGE-MEASURED AND SIMULATED REFLECTION COEFFICIENTS.

J. KENT*[1], J. D. LARSON III[2], and J. L. AROYAN[3], [1]Elo TouchSystems Inc, Menlo Park, CA, [2]Agilent Laboratories, Palo Alto, CA, [3]JRJ Simulation & Design, Soquel, CA.
Corresponding e-mail: John_Larson@agilent.com

We present measured and calculated results for the reflection coefficients of a 5.53 MHz Rayleigh wave propagating on a plate, and impinging at non-normal incidence on a vertical sharp edge.

Although the theory of longitudinal and shear acoustic waves at non-normal incidence on a boundary is well known[1], there are few results for the reflection coefficient of Rayleigh waves other than that of normal incidence at a discontinuity[2], e.g., in filters and resonators where normal incidence and shallow grooves are employed. In signal processor and touchscreen applications, Rayleigh waves may be propagated into discontinuities at non-normal incidence where the reflected and transmitted wave amplitudes are of importance. We present a study of the reflection coefficient of Rayleigh waves propagating on non-piezoelectric plates and incident on a plate edge at non-normal incidence.

To do this, Rayleigh waves at 5.53 MHz are excited by a series of wedge transducers bonded to the plate surface, and oriented at anglesΦ ranging respectively from 0 to 45 degrees relative to the line normal to the plate edge. The waves propagate toward the edge. To observe the incident and reflected waves, we use a full-field, non-scanning acoustic imaging method based on laser interferometry[3] to measure the vertical component of displacement. From the time sequence of images made of the Rayleigh waves, it is possible to observe the forward and reflected waves quantitatively and deduce the reflection coefficient, either from the direct image or from the spatial Fourier transform, which measures the amplitude A(k) for the components of the incident and reflected k vectors.

Simulation of these experimental cases was carried out using a finite element method (FEM) ultrasonic code (PZFlex TM). Simulation results were compared to those obtained by imaging interferometry, and found in good agreement. In the talk, we will present examples of the measured image data, the FEM simulations, and the reflection coefficients for non-normally incident Rayleigh waves. The results will be compared to those in the literature.

This exercise demonstrates the power of combining simulation and full-field acoustic imaging measurements to predict and verify the response of an ultrasonic device. Imaging measurements provide the vertical displacement to check that of the simulation. Simulation allows the horizontal displacement, shear displacements, and motion within the interior of the plate to be calculated. The development of simulation code and the laser imaging interferometry enables a powerful combination of analytical and measurement techniques for the research and development of many types of ultrasonic device.

1.B.A. Auld, Acoustic Fields and Waves in Solids, Vol. II, John Wiley, New York, chapter 9 (1973)

2.I. A. Viktorov, “Rayleigh and Lamb Waves—Physical Theory and Applications”, Plenum Press, New York, pp.42-43, (1967)

3.K. L. Telschow, et al, “Full-Field Imaging of GHz Film Bulk Acoustic Resonator Motion”, IEEE Trans. SUFFC, vol. 50, no. 10, 99. 1279-1285, (Oct. 2003)

4D-5 9:45 a.m.
PIECEWISE CONTINUOUS DISTRIBUTION FUNCTION METHOD AND THE KINETIC DESCRIPTION OF ULTRASOUND PROPAGATION IN A RAREFIED GAS.

M. SOLOVCHUK*[1] and S. LEBLE[2,1], [1]Kaliningrad State University, Kaliningrad, Russia, [2]Gdansk University of Technology, Gdansk, Poland.
Corresponding e-mail: solovchuk@yandex.ru

The problem of a wave disturbance propagation in a rarefied gas at the gravity field is explored. There is a significant number of problems of gas dynamics at which it is necessary to use a theory beyond the limits of traditional hydrodynamics of Navier - Stokes. The hydrodynamics is valid by small mean free path(small Knudsen numbers). At big Knudsen numbers we must use the more general kinetic equation. But there are no standart ways of its solving.

We propose a modification of the procedure for deriving hydrodynamic-type equations from kinetic theory. We do not begin in the customary way from an expansion in mean free path, as is usualy done. The system of hydrodynamic-type equations for a stratified gas in gravity field is derived from BGK equation by method of piecewise continuous distribution function. We search for the solution of the BGK equations as combinations of two locally equilibrium distribution functions, each of which gives the contribution in its own area of velocities space.

Multiplying BGK equation on 6 eigen functions we obtain the system of differential equations. The obtained system of the equations generalizes the Navier-Stokes at arbitrary Knudsen numbers. The verification of the model is made for a limiting case of a homogeneous medium. The phase velocity and attenuation coefficient values are in an agreement with former fluid mechanics theories; the attenuation behavior reproduces experiment and kinetics-based results at more wide range of the Knudsen numbers.

Session: 5D
NOVEL SAW DEVICES AND ANALYSIS
Chair: D. Malocha
University of Central Florida

5D-1 8:30 a.m.
ONE-PORT SAW RESONATORS USING NATURAL SPUDT SUBSTRATES.

D. P. MORGAN*[1], S. ZHGOON[2], and A. SHVETSOV[2], [1]Impulse Consulting, Northampton, Northants., UK, [2]Moscow Power Engineering Institute, Moscow, Russia.
Corresponding e-mail: dpm@ieee.org

SAW resonators have widespread applications in oscillators, bandpass filters and sensors. The substrate is usually chosen to be one of the standard SAW cases, such as ST-X quartz. However, other orientations may be of interest in order to modify the characteristics. In particular, for sensors the orientation might be chosen to increase the sensitivity to one environmental factor (e.g. stress or temperature), and reduce the sensitivity to another. In general, such modified orientations will give some degree of directivity, i.e. they will show the NSPUDT effect. In this paper, we consider the design of one-port resonators on substrates showing directivity. In particular, we consider the NSPUDT orientation of langasite, extending the work of Fachberger et al [1]. The transducer is taken to be the single-electrode type, in which internal electrode reflections are significant. Substrate directivity is modelled theoretically by modifying the phase of the electrode reflection coefficient. We consider all possible degrees of directivity, ranging from the purely NSPUDT case to the bidirectional case.

We describe two approaches for the design of these resonators. The first method is based on a previous development for symmetrical substrates. It was shown [2] that a device with symmetrical geometry behaves as a single resonant cavity, though internal reflections in the transducer cause some distortion of the effective cavity length. This approach gives a prescription for the grating placement, such as to give a resonance at any required frequency. For a directional substrate, it is shown here that the same principle may be applied, but in a more restricted sense. The concept is applied for a particular frequency, and the method then gives the grating placements needed for a resonance at this frequency. This method generally gives a symmetrical resonator design. The transducer pitch, grating pitch and resonant frequency can all be chosen independently. In addition, the design is shown to be insensitive to the phase of the electrode reflection coefficient. Hence, provided other parameters remain unchanged, the same design is applicable to an NSPUDT substrate or a symmetrical substrate, or a substrate intermediate between these cases.

The second method applies for a design in which the gratings and transducer all have the same pitch. One of the gratings is placed in a synchronous location, so that its electrodes continue the pattern of the transducer. The other grating is spaced from the transducer by a small gap. It is shown that this gives a resonance at the Bragg frequency of the components. Moreover, the resonance is obtained independently of the phase of the electrode reflection coefficient, as for the first method.

[1]. R. Fachberger et al. IEEE Ultrasonics Symp., 2002, pp.501-504.

[2]. D.P. Morgan. Electronics Lett., vol. 39, p. 1361-1362 (2003).

5D-2 8:45 a.m.
SAW RESONATORS FOR TEMPERATURE STABLE OSCILLATORS.

G. MARTIN*[1], B. WALL[2], and M. WEIHNACHT[1], [1]Institute for Solid State and Materials Research Dresden, Dresden, Germany, [2]Vectron International Telefilter, Teltow, Germany.
Corresponding e-mail: g.martin@ifw-dresden.de

For many years, there have been activities to find solutions of frequency determining SAW components for temperature stable oscillators. On one hand, temperature-stable crystal cuts and propagation directions have been searched. On the other hand, the temperature stability has been enhanced by using design tools. The solution presented by Browning and Lewis [1] belongs to the latter group. They describe a double delay line the single delay lines of which have different propagation directions on ST quartz and their IDTs are connected in parallel in pairs. The main delay line has a zero temperature coefficient of frequency of 1st order (TCF1) whereas the temperature coefficient of frequency of 2nd order (TCF2) of the auxiliary delay line dominates. The application of this principle to SAW resonators has not been found. As known, resonators outplay delay lines because of steeper phase characteristics for a given layout length. Therefore, the purpose of the suggested paper is to present a double two-port resonator by means of which the compensation of the TCF1 as well as the TCF2 is possible. The double resonator is composed of two coupled two-port single SAW resonators. The propagation directions are characterized by opposite and equal signs of TCF1 and TCF2, respectively. The coupling is realized by cascading and using a coupling inductance. In order to explain the TC compensation qualitatively a simplified SAW double resonator with coupling is treated analytically by means of the COM theory. The results show that the TCF1 as well as TCF2 can be compensated when adjusting the aperture ratio of the single resonators and the resonator coupling in a suitable manner. The requirement to coupling can be met by choosing coupling inductance. An example of a double two-port resonator is studied by means of model calculations and experiments. 35.5degree rotYX quartz is used as a wafer material. The propagation angles (angle between the propagation direction and the X axis) of the single resonators are chosen to be larger and smaller, respectively, than the angle A0 in vicinity of 45 degree the TCF1 of which is zero. The frequency f0 the temperature stability of which is studied is defined as frequency belonging to a fixed phase. This phase is kept constant within the entire temperature range. The frequency f0 and |S21| at f0 are calculated and measured as functions of temperature. Not only the theoretical but also the experimental results express the temperature shift of f0 from -30°C until 70°C to be essentially smaller than that in the case TCF1= 0 at the propagation angle A0.

[1] T. I. Browning and M. F. Lewis, Proc. 1978 IEEE Ultrason. Symp., pp. 474-477

5D-3 9:00 a.m.
ANALYSIS OF ACOUSTOMIGRATION AND ACOUSTIC LOSS IN DMS FILTERS EMPLOYING FEM/BEM.

M. MAYER*, H. ZIDEK, T. BAUER, and K. WAGNER, EPCOS AG, Munich, Bavaria, Germany.
Corresponding e-mail: Markus.Mayer@epcos.com

FEM/BEM analysis has proved to be an excellent method for the accurate ab initio simulation of the acoustically active tracks of SAW components, especially DMS filters.

Besides its usefulness for the overall SAW component characterization it permits insight into the underlying physics. Within the FEM/BEM approach the stress distribution in the electrodes is, in contrast to the COM and P-matrix scheme, directly accessible. Thus the detailed field distribution within the fingers is available. Therefrom regions exposed to high stresses and thus suffering from acoustomigration can be identified.

For a DMS filter on lithium tantalate the stress distribution is computed. It is compared with the stress distribution in the P-matrix model which is deduced from the distribution of the kinetic energy as well as to REM-images of acoustomigration.

With the detailed knowledge of all stress and displacement components within the finger, vibration modes are visualized and destruction mechanisms are identified. In addition the performance of the DMS filter is examined within the FEM/BEM approach. Of particular interest are radiation losses into bulk waves which predominantly occur in the resonant cavities between the transducers. By placing transition regions between adjacent tranducers a significant reduction of bulk wave excitation is achieved. An analysis of the angular and spatial distribution of the bulk wave radiation in these devices allows to interpret this behaviour.

5D-4 9:15 a.m.
HEXAGONAL SAW DEVICES FOR ENHANCED SENSING.

S. CULAR*[1], V. BHETHANABOTLA[1], and D. BRANCH[2], [1]Sensors Research Laboratory, Dept. of Chemical Engineering, University of South Florida, Tampa, FL, [2]Microsensor Science and Technology Department, Sandia National Laboratories, Albuquerque, NM.
Corresponding e-mail: cular@eng.usf.edu

We present the design, fabrication and testing of a novel, hexagonal array based on 36° YX lithium tantalate for non destructive evaluation of thin inorganic and biological films. Propagation along the x-axis generates the leaky shear horizontal (SH) mode where off axis propagation excites Rayleigh type surface acoustic waves (SAW). Our approach permits rapid and simultaneous extraction of multiple film parameters. Given that SAW devices are in widespread use for chemical and biological sensing; a need exists to rapidly interrogate the interface for several parameters. This is especially relevant in biological applications when the sample quantity can be very limited. Our design allows for the simultaneous extraction of multiple properties (film material density or thickness, Lamé and shear moduli, sheet conductivity) of a thin film material to achieve a more complete characterization than when a single SAW device is utilized. In sensor applications, this capability translates to better discrimination of the analyte and possibly more accurate determination of the concentration. We present this device as an alternative to a SAW sensor array configuration that does not allow for simultaneous probing and which would require larger devices and packaging. These cost advantages are significant when working with novel piezoelectric materials. The device is based on a double split finger delay-line with widths of 4 μm and a delay path of 197λ. The individual delay path of each

hexagonal device intersects in the center of the die producing a single region for sensor analysis. Additionally, the central region where the acoustic waves intersect is shorted to reduce the number of modes of waves traversing the surface. Initial testing has shown the pass band frequency of the individual delay paths to be centered around 97 MHz. The acoustic velocities of the rotated device have been measured to be 3452 m/s, 3161 m/s, and 3331 m/s, which correspond to the theoretical range of all acoustic waves in the crystal of velocities 3290-4160 m/s. This variation is sufficient to allow for the simultaneous solution of the same wave parameter dependent equation that will allow for the multiple properties of the sensing film to be extracted.

We would like to thank Nancy Saldanha and Dr. Don Malocha of the University of Central Florida for the use of fabrication equipment and insightful discussions. Support for this work has been provided by NSF grant number DGE-0221681 and the University of South Florida CERC.

5D-5 9:30 a.m.
LOW PROPAGATION LOSS OF ATOMICALLY-FLAT SURFACE ALN WITH LOW DISLOCATION DENSITY FOR 5-GHZ BAND SAW DEVICES.

K. UEHARA*, Y. AOTA, S. KAMEDA, H. NAKASE, and K. TSUBOUCHI, Research Institute of Electrical Communication, Tohoku University, Sendai, Japan.
Corresponding e-mail: uehara@lfte.de

SAW device operating in 5-GHz bands with low insertion loss and low temperature coefficient is one of the indispensable devices to construct a mobile terminal with high data rate of more than 100 Mbit/s for a next generation wireless communication system. 5-GHz band SAW device using structure of AlN film on sapphire substrate is fabricated easily because wide line and space are designed due to its high phase velocity at maximum of 6,100 m/s to compare with the other materials. Moreover, AlN has a moderate coupling factor at maximum of 1.0 %.

In previous work, using the atomically-flat surface (0001)AlN film with the thickness of 1.0 μm grown on (0001)sapphire substrate by metal-organic chemical vapor deposition (MOCVD), low temperature coefficient of delay (TCD) of 9 ppm/°C at normalized thickness (kH) of more than 5.9 and low propagation loss of 0.0053 dB/λ at 5.17 GHz were reported. We also reported that 5-GHz bands SAW devices with low insertion loss and good TCD were fabricated using atomically-flat surface (0001)AlN on (0001)sapphire.

In this work, to clarify the growth mechanism of atomically-flat surface AlN epitaxial film using MOCVD, dependences between growth rate and process parameters of MOCVD were investigated. To evaluate the defects in the AlN film with low propagation loss, three-type dislocations were observed by transmission electron microscopy (TEM).

In the result of growth rate at various substrate temperatures, it is found that atomically-flat surface AlN were obtained under the area of growth rate independent on a substrate temperature. In the result of growth rate at various gas flow velocities, gas flow velocity of more than 50 cm/s was indispensable

for growth of atomically-flat surface AlN. It is considered that the high gas flow velocity suppresses a thermal convection above a heated substrate. The thermal convection results in rough surface AlN film. Suppression of the thermal convection results in growth of atomically-flat surface AlN. We observed misfit-type, edge-type and screw-type dislocations in the atomically-flat surface grown under the optimum conditions. Periodical misfit-type dislocation lying only on the 1-nm-thick interface between AlN film and sapphire substrate was observed by high resolution TEM. From a dark-field TEM image focused on a spot for (11-20)AlN, edge-type dislocation propagate from interface to surface. The density of edge-type dislocation in its surface region was 10^{10} – 10^{11} cm^{-2} as low as that reported by Shibata et al. From a dark-field TEM image focused on a spot for (0002)AlN, screw-type dislocation propagating along the direction of c-axis AlN was observed. It is noted that almost propagation of screw-type dislocation stops within the thickness of 0.5 μm. It is found that atomically-flat surface AlN film has low density of dislocations concerning misfit-, edge- and screw-type. Atomically-flat surface AlN with a low number of dislocations contributes to low propagation loss.

This work was supported in part by the IT-program (RR2002) of MEXT, Japan.

5D-6 9:45 a.m.
RAYLEIGH WAVE REFLECTION AND SCATTERING CALCULATION BY SOURCE REGENERATION METHOD.

W. WANG[1], T. HAN[2,1], X. ZHANG[1], H. WU[1], and Y. SHUI*[1,2], [1]State Key Laboratory of Modern Acoustics, Nanjing University, Nanjing, Jiangsu, China, [2]Department of Instrumentation Engineering, Shanghai Jiaotong University, Shanghai, China. Corresponding e-mail: yashui@nju.edu.cn

The analysis and precise calculation of reflection and scattering of Rayleigh wave by electrodes is important for surface acoustic wave (SAW) device, especially for SAW identification (ID) tag design. We present a source regeneration method, which takes the stress and electric charge under electrodes as the source, and the reflection and scattering could be considered as two processes: the incident Rayleigh wave produces a source under the reflector; and the source regenerates the reflection wave, scattering bulk wave, etc. The method utilizes Green's function combined with Finite Element Method (FEM)/ Boundary Element Method (BEM) to obtain accurate values of source, and then, reflection, transmission and scattering coefficients. We take one electrode as the reflector on 128°YX-$LiNbO_3$ substrate to show the results as example. The results are very accurate and are obtained with short computing time. The new analysis way shows its powerful ability for other advanced discussion of SAW devices.

The paper is supported by Natural Science Foundation of China No. 10304012

Session: 6D
ULTRASOUND MEMS TECHNOLOGY
Chair: F. Degertekin
Georgia Institute of Technology

6D-1 8:30 a.m.
(Invited)
CMUTS AND ELECTRONICS FOR 2D AND 3D IMAGING: MONOLITHIC INTEGRATION, IN-HANDLE CHIP SETS AND SYSTEM IMPLICATIONS.

C. DAFT*, P. WAGNER, B. BYMASTER, S. PANDA, K. PATEL, and I. LADABAUM, Sensant Corp., San Leandro, CA.
Corresponding e-mail: daft@ieee.org

Capacitive microfabricated ultrasound transducers (cMUTs) have been shown to be practical for medical imaging. Breakthrough performance requires combining these MEMS transducers with electronics. This paper explores synergies between cMUTs and electronics for 2D and 3D imaging. For example, low-noise receive signal conditioning improves tissue penetration, while transmitters capable of arbitrary waveforms minimize clutter. Bias control circuitry creates simple multi-row arrays for improved 2D contrast resolution. It also can enable 3D scanning with less complexity than current alternatives. Matrix transducer elements for 3D present challenges due to their high impedance, number and density. Monolithically integrated cMUTs can offer unique solutions to these problems, enabling isotropic 3D imaging from fully sampled arrays.

To begin, we present a review of previous work in cMUT imaging and integrated electronics. This covers fabrication methods and linear, convex and contrast-harmonic images. Monolithic manufacturing falls into two categories: concurrent creation of the cMUTs and electronics, and post-processing where the micromachining is subsequent to standard IC production.

Probes for 2D imaging do not require monolithic integration, since it is sufficient (and more economical) to locate signal conditioning electronics in the handle. The signal-to-noise, parasitics and aperture agility can be nearly as optimal as with a monolithic approach. Within the handle, amplification and TGC remove the signal loss from driving a low-impedance cable. Careful attention to transmit-receive switching and other system issues can create a probe which is pin-compatible with the installed base of ultrasound systems.

3D imaging using bias control is a unique cMUT capability. New in-vivo 3D images are presented that were acquired with a simple electronic scanning scheme. Fresnel focusing using bias voltages control elevation beams while the imager scans as usual in the azimuth direction. This approach requires minimal modification to contemporary imagers.

3D imaging with piezoelectric transducers has been commercially achieved either through mechanical probe rocking, or via a matrix of elements with sub-aperture beam formation in the handle. We review these methods and compare to cMUT

capabilities. Monolithic integration benefits cMUT matrix transducers greatly. The reasons for this are discussed, together with interconnect and point-spread function issues related to 3D imaging. We also consider alternatives to monolithic integration, such as through-wafer vias and flip-chip interconnect.

Lastly, we evaluate the system implications of different ways of making arrays for volumetric imaging. Such implications vary from straightforward system modifications to wholesale redefinition of the beam forming architecture. For example, highly parallel beam formation is needed to raise volume acquisition rates to acceptable levels in many clinical settings. cMUTs are well positioned to enable imaging involving high-density electronics situated at the transducer element.

6D-2 9:00 a.m.
THROUGH-WAFER TRENCH-ISOLATED ELECTRICAL INTERCONNECTS FOR CMUT ARRAYS.

X. ZHUANG*, A. ERGUN, O. ORALKAN, Y. HUANG, G. YARALIOGLU, I. WYGANT, D. YEH, and B. KHURI-YAKUB, Stanford University, Stanford, CA,. Corresponding e-mail: xzhuang@stanford.edu

In recent years, researchers have demonstrated fully populated 2-D capacitive micromachined ultrasonic transducer (CMUT) arrays with through-wafer via interconnects. Through-wafer vias provide a means of accessing individual elements from the back side of the wafer. In these implementations, through-wafer vias are etched from both sides of the silicon wafer, and later filled with conductive material. CMUTs are fabricated on the front side of the silicon wafer, and bond pads are formed on the back side. However, residual stress, surface contamination, and roughness caused by the through-wafer via process complicate its use with the silicon-on-insulator (SOI) wafer bonding CMUT fabrication technique. The SOI wafer bonded CMUTs have higher fill factor and better process control when compared to the surface micromachined CMUTs.

This paper introduces a novel method that provides interconnects to individual elements in a CMUT array. Deep trenches are etched into the highly conductive silicon substrate to isolate the elements and create silicon pillars that form the bottom electrode of the membranes. In this study, 16×16 2-D CMUT arrays with trench-isolated interconnects are fabricated. These arrays have a 250-um element pitch, and are designed to operate at 5 MHz in immersion. The trenches are 10 um to 20 um wide. Rectangular membrane geometries are used for improved output pressure and bandwidth. Each array element consists of four membranes. The membranes are 52 um wide, 220 um long, 2.56 um thick, and have cavity heights of 0.2 um. Using the SOI wafer bonding technique, the CMUT cells are fabricated on the front side of a highly conductive silicon wafer. After the membranes are fabricated, the front side of the wafer is temporarily bonded to a carrier wafer to provide mechanical support for later processing steps. Using deep reactive ion etching, through-wafer trenches are etched into the substrate to provide electrical isolation between the individual array elements. The wafer is then diced to separate individual arrays. The bottom electrodes are connected to a custom-designed transmit and receive circuit using flip-chip

bonding. Finally, the carrier wafer that had been used for mechanical support is released.

The trench-isolated interconnects have the flexibility to be implemented on both surface micromachined and SOI wafer bonded CMUTs. Because it requires as few as four masks, the trench-isolated CMUT process reduces the processing complexity significantly; the CMUT process with through-wafer via requires as many as 13 masks. Using this novel process, the silicon substrate can be thinned down to reduce series resistance, and to remove the interference due to substrate reverberations from the frequency band of the system. Moreover, this new technique enables the possibility of folding the arrays to conformably cover a curved surface, thus empowering the CMUT to be used in applications in which curved arrays are required.

6D-3 9:15 a.m.
CAPACITIVE MICROMACHINED ULTRASONIC TRANSDUCER (CMUT) MADE BY A NOVEL "REVERSE" FABRICATION PROCESS.

G. CALIANO*[1], A. CARONTI[1], A. SAVOIA[1], C. LONGO[1], E. CIANCI[2], V. FOGLIETTI[2], and M. PAPPALARDO[1], [1]University Roma Tre - Dept. of Electronics, Roma, Italy, [2]IFN-CNR, Roma Italy.

Corresponding e-mail: caliano@ieee.org

During the last few years it has been widely demonstrated that for generation and transduction of ultrasonic signals the micromachined capacitive technology can represent an excellent chance to improve the performances of echographic systems.

Many different construction technologies of 1D and 2D cMUT have been presented, which only differ from each other in the materials used and the processes involved.

In fact, they all have in common the presence of micro-holes on the surface of the transducer necessary to evacuate the cavities under the membranes or, even in the 2D array, to electrically connect upper to lower pads and to allow the electrical connection to external circuits. The presence of holes for emptying the cavities causes great problems both to the uniformity of the membranes and to the sealing of the lower cavities. Moreover, the holes strongly influence the form-fill, especially for high frequency transducers, limiting the possibility to achieve large bandwidth and good sensitivity. The use of deep trenches for the electrical connection on the back of the device, can introduce problems not easily solvable, and remarkable complications in the fabrication process.

In view of these considerations, the authors of the present work designed and realized a cMUT transducer using a new construction concept. Fabrication does not occur, like in the standard process, growing on a silicon wafer successive layers up to the silicon nitride structural layer of the micro membranes, but inverting the layers sequence. The device is built on the face of a LPCVD silicon nitride layer grown over a silicon wafer, with a standard inverted process and only at the end, when the cMUT is realized, the bulk silicon wafer is completely removed (by KOH process), allowing the nitride structural layer of the membranes

to be completely free. By working on the back of the device, there is no need to use holes in the structural silicon nitride layer to evacuate the cavities. The device is made using a commercial silicon wafer with a low stress high temperature LPCVD silicon nitride layer but the whole process uses temperatures not higher than 350°C so that a large number of materials can be used. Electrical connection pads are already on the back of the die ready to be soldered, avoiding deep trenches or interface circuits.

The first devices made using the described new technology show experimental results which clearly indicate that the process is very promising.

In conclusion, the new technology is able to solve the main problems presented up to now by the standard technology, making the cMUT more feasible for very onerous applications, such as 1D and 2D imaging.

6D-4 9:30 a.m.
DESIGN, MODELING AND FABRICATION OF PIEZOELECTRIC MICROMACHINED ULTRASONIC TRANSDUCERS.

B. BELGACEM*, F. CALAME, and P. MURALT, Ecole Polytechnique Fédérale de Lausanne - Ceramics Laboratory, Lausanne, Switzerland.
Corresponding e-mail: brahim.belgacem@epfl.ch

Piezoelectricity is one of the best principles for transduction in Micro-Electro–Mechanical-System (MEMS). Our work focuses on the realization of ultrasonic transducers for airborne sensors, Non Destructive Testing (NDT) and medical applications, whereby the frequency ranges from 200kHz to 30MHz. The fabricated micro machined ultrasonic transducers (pMUT) were based on piezoelectric laminated plates operating at flexural modes. As piezoelectric material a 4 µm thick lead zirconate titanate (PZT) thin film deposited by a sol-gel method was applied. The latter was based on Pb(C2H4O2)2 3H2O, Zr(OCH2-CH2-CH3)4 and Ti[OCH(CH3)2]4 precursors in 2-methoxy-ethanol solvent. The Piezoelectric layer was deposited on Pt/TiO2/Ti/SiO2/SOI (Silicon On Insulator) substrate that included the 10 µm thick membrane silicon layer. The six masks fabrication included four masks for the definition of the topside structures, and two masks to define the bulk-micromachined features at the backside of the SOI wafer. A crucial issue for arrays is the reduction of cross coupling. For this purpose, a stiffening structure between elements was included by deep silicon dry etching. In order to design the Bimorph pMUT (i.e. frequency), we adapted an analytical model based on the clamped plate theory. We show that this model gives a good prediction of the experimental frequency of the 5-layers pMUT plate resonance. By varying the width of the plates, a wide range of operation frequencies was realized on the same wafer. In order to limit the parasitic capacitance, both the bottom and top electrodes were patterned. Our calculation show that central electrodes need to cover 58% and 33% of the membrane surface for a rectangular and circular membrane respectively to achieve optimal coupling. The plate structures exhibited a capacity corresponding to a permittivity of εr=980. The electromechanical coupling coefficient (k2) and quality factor (Q) were measured as k2=4.4% and Q=145 in air for a low frequency transducer

(250 kHz). The effect of DC bias voltage on frequency and k2 has been studied. The device with unpoled film showed a linear increase of the coupling factor with increasing field until saturation at 100kV/cm. The 17 MHz version yielded values of Q=25 and k2=3%. All values were obtained by fitting an equivalent circuit model to real and imaginary part of the measured admittance curve. Good agreement was obtained using a simple RLC series circuit for the mechanical part.

6D-5 9:45 a.m.
MEMS ULTRASONIC SENSOR ARRAY WITH THICK-FILM PZT TRANSDUCERS.

S. DOERNER*[1], S. HIRSCH[2], V. FERRARI[3], R. LUCKLUM[1], B. SCHMIDT[2], and P. R. HAUPTMANN[1], [1]Sensors & Measurement Technology Group, Institute of Micro and Sensor Systems, Otto-von-Guericke-University, Magdeburg, Germany, [2]Microsystems Group, Institute of Micro and Sensor Systems, Otto-von-Guericke-University Magdeburg, Magdeburg, Germany, [3]Dept. Electronics for Automation and INFM, University of Brescia, Brescia, Italy.
Corresponding e-mail: steffen.doerner@et.uni-magdeburg.de

Summary Thick-film piezoelectric transducers have been produced and tested for implementation into a MEMS ultrasonic sensor array. The arrays are intended to be used for beam forming in sensing applications for fluidics in channels at millimeter or micrometer scale (e.g. flow rate measurement, detection of beads, bubbles). Strip and array aligned elements have been evaluated for one-dimensional and two-dimensional beam steering, respectively. In this contribution we further concentrate on an improved Q-factor as a major requirement of the transducer elements.

Motivation Ultrasonic transducer arrays employing capacitive actuators are available and have been intensively studied in the past [1]. For liquid analytes piezoelectric actuation provides better performance due to higher energy density. Piezocomposite technology that has been mainly used for medical imaging can be impedance-matched to the analyte and driven with high excitation voltages. However, combination of piezocomposite and MEMS technology requires a separate mechanical processing. To our knowledge integration onto a MEMS substrate has not yet been developed.

Combination of thick-film and silicon technology[2] provides both piezoelectric actuation with a piezoceramic layer, micro machining of coupling membranes and integration of driver and amplifier electronics on the same substrate.

Results Membrane shape and thickness have been optimized using ANSYS to reduce cross coupling between single elements while maintaining required stiffness for the fluid channel. Using a dry etching process trenches of different dimensions have been created to analyze inter element decoupling.

First test samples were made by Ti-Pt bottom electrodes on silicon test wafers and structured with a lift-off process. A multi-stage screen printing process allowed creating layers of PZT with variable thickness between 30 µm and 110 µm on corresponding membranes. Top electrodes have been formed by additional

screen printing. Packaging was done by anodic bonding on a Pyrex substrate to form a metering cavity for the injected analyte.

We further report on the influence of technological parameters like poling temperature and poling field strength on the Q-factor, crosstalk between array elements and displacement patterns of the array measured with a scanning laser vibrometer.

[1]X. Jin, Ö. Oralkan, F.L. Degertekin and B.T. Khuri-Yakub, “Characterization of One-Dimensional Capacitive Micromachined Ultrasonic Immersion Transducer Arrays”, IEEE Trans. Ultrason., Ferroelect., Freq. Contr. 48, no. 3, pp. 750-760, 2001.

[2]R. Torah, S.P. Beeby, and N.M. White, “An Improved Thick-Film Piezoelectric Material by Powder Blending and Enhancement Processing Parameters”, IEEE Trans. Ultrason., Ferroelect., Freq. Contr. 52, no. 1, pp. 10-16, 2005.

POSTER SESSIONS

Session: P2A
TISSUE CHARACTERIZATION
Chair: P. Laugier
University of Paris

P2A-1
NEW TISSUE MIMICKING MATERIALS FOR ULTRASOUND PHANTOMS.

T. KONDO*[1], M. KITATUJI[1], Y. SHIKINAMI[2], K. TUTA[2], and H. KANDA[3], [1]Faculty of engineering, Tokushima Bunri Unversity, Sanuki, Kagawa, Japan, [2]Medical Dev., Takiron Co., Ltd., Yasutomi-cho, Hyogo, Japan, [3]Hitachi Medical Corporation, Kashiwa, Chiba, Japan.
Corresponding e-mail: tkondo@fe.bunri-u.ac.jp

Background and Goal: A phantom of tissue-equivalent material is important for quality control of an ultrasound diagnostic equipment. A phantom made of polysaccharide gel (agar) in which powdered graphite is dispersed has been widely used because its acoustic characteristics can be easily controlled in the manufacturing process. However, hydrophilic organic materials such as agar have disadvantages in that bacteria propagate in them and thus their acoustic characteristics change with time. We propose new ultrasound tissue-mimicking materials as a solution to the problem.

Materials: Synthesized segmented polyether-urethane gel containing of EO/PO (Ethylene Oxide/Proppylene Oxide) copolymer segments and branched chains that are liquid at ambient temperature and the oil gel made from ethylene glycol and propylene glycol were mixed. Polystyrene or polymethylenthacrelate powder as a sound scatterer was dispersed in the gel. The powders are commercially available materials and their fractional diameter variations can be precisely

controlled. These industrial materials used there have good reproducibility in their physical properties and dimension. The gelatinizer used for the oil gel is dibenzylidene D sorbitol which is commercially provided.

Method: We can measure the sound velocity and attenuation of various kinds of polyether-uretane gel which are synsethesized under various types of block copolymer, component, EO/PO (mol. ratio) and molecular weight.

Results:We obtaied experimentally sound velocity of those gels from 1450 to 1550 m/s, and the lowest attenuation coefficient around 0.1 dB/MHz cm under experiment of the polyether-urethane gel. The acoustic velocity and attenuation of the material can be increased by dispersing the suspended powder into it as uniform particles. The oil gel made from the mixture of the ethylene glycol and polypropylene glycol whose sound velocity and specific acoustic impedance matched those of human tissue were successfully obtained by adjusting the mixture ratio of the materials.

Conclusion: New tissue mimicking materials for ultrasound phantom are proposed; whose acoustic velocity and impedance matched cam be easily matched to those of human tissue prepared (the acoustic velocity and specific acoustic impedance of human tissue are 1540 ms^-1^ and 1.60 $\cdot 10^6$ kgm^{-2} s^{-1}, respectively). The materials are stable in their physical properties during the past a few month.

This work was supported by the Grant (No.16500320) of Japan Society for the Promotion of Science.

P2A-2

ULTRASOUND HARMONIC BEHAVIOUR OF ARTIFICIAL TISSUES.

S. CASCIARO*[2,1], C. DEMITRI[1,3], R. PALMIZIO ERRICO[1,4], F. CONVERSANO[1,5], G. PALMA[1,5], E. CASCIARO[2,1], and A. DISTANTE[1,2], [1]ISBEM (Euro Mediterranean Scientific Biomedical Institute), Brindisi, Italy, [2]IFC-CNR Lecce Section (National Council of Research - Institute of Clinical Physiology), Lecce University, Lecce, Italy, [3]Innovation Engineering Department, Lecce University, Lecce, Italy, [4]Material Science Department, Lecce University, Lecce, Italy, [5]Bioengineering & Robotics Department, Pisa University, Pisa, Italy.
Corresponding e-mail: demitri@isbem.it

Introduction: During the last years several materials have been used to manufacture tissue mimicking phantoms suitable to carry out ultrasound (US) studies with flowing US contrast agents (CA) [1]. Here we discuss about the US properties of a new cellulose-based hydrogel developed to simulate liver tissue. The production process has been optimized at firs by reproducing the sound velocity in the matter. Aim of this study was to evaluate the mechanical index (MI) effect on relative amplitude of different harmonic components of backscattered US signals. Our approach was to compare an hydrogel sample with a pig liver one.

Materials and Methods: Both hydrogel and pig liver samples were studied in the same configuration having a polyurethane layer as support and insonified through a commercially available echograph (Megas GPX, Esaote Spa, Florence, Italy)

equipped with a linear array transducer (LA532), which was placed in contact with the sample surface using a coupling gel. The ecograph was externally linked to a prototype for radiofrequency (RF) analysis (FEMMINA, developed by Florence University), able to get the full raw signal of the probe. Samples were insonified with 10-cycles US pulses at different frequencies (2, 2.5 and 3.3 MHz) and echograph electrical power was varied for each frequency in order to obtain different MI values, which were estimated by the ecograph assuming an attenuation of 0.3 dB/cm/MHz. For both samples, a sequence of 10 data frames of RF raw data was acquired for each instrument setting and analyzed off-line by means of Fortezza software (supplied by Florence University). An ad hoc implemented Fortezza algorithm was employed to select a rectangular region of interest (ROI) of 50×20 data points (approximately 5 mm^2). Mean Fast Fourier Transform (FFT) curve was calculated within the selected ROI for each acquired frame. Then subharmonic (1/2H), fundamental (1H) and second harmonic (2H) component values were extracted from the obtained curves and averaged over the corresponding frame sequence. Finally these values were plotted versus MI.

Results: A direct relationship between MI and backscatter amplitude is evident for each plotted curve. For every tested frequency, hydrogel curves show the same trends of the corresponding liver ones. In particular, at 2 MHz, hydrogel 1/2H and 1H curves tend to coincide with their corresponding in the liver especially at the lowest MIs.

Conclusions: Since the frequency range and MI suitable for US CA in vivo assessment is of < 2 MHz and > 0.2 we can conclude that cellulose-based hydrogel is a suitable material to design a liver tissue mimicking phantom for US studies, since it showed echogenic properties very similar to those of the liver in the studied frequency range, which belongs to the range typically employed in clinical US examinations of the liver.

[1] BROWNE J.E., RAMNARINE K.V. et al. (2003): 'Assessment of the acoustic properties of common tissue-mimicking test phantoms', Ultrasound in Med. & Biol., 29, pp. 1053-1060

P2A-3

THE EFFECT OF VOLUME FRACTION ON THE BACKSCATTER FROM NUCLEATED CELLS AT HIGH FREQUENCIES.

R. E. BADDOUR*[1] and M. C. KOLIOS[1,2], [1]Dept. of Medical Biophysics, University of Toronto, Toronto, ON, Canada, [2]Dept. of Physics, Ryerson University, Toronto, ON, Canada.
Corresponding e-mail: rbaddour@uhnres.utoronto.ca

Recently, new high frequency ultrasound devices have emerged with better system signal-to-noise ratio characteristics, which make it possible to measure ultrasound scattering in tissues so that small variations in scatterer volume fraction, which can result from changes in tissue microstructure due to cancer therapies, may have a significant impact on the backscattered signal. Although the effect of volume fraction has been studied for non-biological scatterers and

red blood cells, this study addresses the case of nucleated cells. Suspensions with volume fractions up to 70% of acute myeloid leukemia cells (OCI-AML-5 cell line; mean cell diameter 12 μm, mean nucleus diameter 10 μm, as determined by optical confocal microscopy of bisbenzimide-stained cells with ultraviolet illumination) in phosphate buffered saline solution were insonified with broadband (100% 6 dB bandwidth) 20 MHz and 40 MHz pulses at 300 independent positions. The resultant average normalized backscatter intensities plotted as a function of volume fraction demonstrated a better agreement with the Yagi-Nakayama continuum scattering theory rather than the Mo-Cobbold particle scattering model (using hard sphere packing). Normalized backscatter increased with cell volume fraction up to a maximum value (occurring between 20 and 30% volume fraction), varying with frequency and then decreased with further increases in volume fraction. This result has implications in the development of new quantitative ultrasound-based monitoring techniques for cancer therapies.

P2A-4

ULTRASONIC MEASUREMENT OF THE HUMAN ACHILLES TENDON STRESS DURING LOADING : PRELIMINARY EXPERIMENTAL AND THEORETICAL RESULTS.

C. ROUX* and M. DEFONTAINE, GIP Ultrasons - LUSSI, Tours, 37032, France. Corresponding e-mail: roux@med.univ-tours.fr

Tendon pathology diagnosis is essentially based on palpation and imaging (MRI, ultrasound). Ultrasonography associated with a measurement of tendon strain and stress has been used by Kuo et al in order to assess tendon elasticity in vivo. Several in vitro ultrasonic methods have also been developed to evaluate elasticity coefficients in stress-less configuration (Hoffmeister et al).

Our purpose is to present a non-invasive quantitative ultrasound method to measure the level of stress in the human Achilles tendon during effort with the objective of helping, in the future, the diagnosis and particularly the follow-up of the healing. This technique, developed for the equine forelimb tendon by the UMR INRA-ENVA BPLC (Maisons-Alfort, France) and the LUSSI consists in the measurement of the ultrasound celerity using an axial-transmission method along the tendon fibers axis during effort. An ultrasonic pulse is emitted at 2 MHz central frequency. The angle and the aperture of the elementary transducers are determined in order to generate and to receive an echo corresponding to the propagation of a longitudinal wave at the tendon surface and at the tendon celerity at any effort level. This wave is called the lateral wave and has been deeply studied by the UMR 7623 LIP (Paris, France) in a static configuration through cortical bones. The emitter - receivers distance is adjusted in order to have the tendon lateral wave echo in first place in the RF signal. The corresponding tendon celerity is estimated using cross correlation techniques between adjacent RF signals. A dedicated electronic and probe modules have been developed in order to acquire simultaneously the ultrasonic and the force data in the Achilles tendon during effort. Several types of muscular exercises have been tested, and particularly cycles of isometric contraction of the triceps muscle /Achilles tendon complex. As expected, the tendon celerity is highly correlated with the effort.

Different propagation modes and multiple echoes are contributed to the RF signal and make the analysis difficult. Moreover the lateral wave tendon echo amplitude is 30 to 40 dB lower than the direct wave echo. In order to optimize the analysis we have developed a 2D simulation of the tendon wave propagation. This model uses partial differential wave propagation equation solved by pseudospectral method and finite difference, including P.M.L.. It clearly shows the propagation of the lateral wave. However very next to the lateral wave front the simulation shows the presence of another wave, reflected from the bottom of the tendon, which apparent celerity at the receivers is higher than the lateral wave one. Those preliminary findings are very interesting and have contributed to an accurate specification of the Ultrasound probe. The next step of this model is also of great interest, since we intend first to implement an additional external stress modeling the muscle force and secondly to resolve the inverse problem to obtain the elasticity coefficients.

P2A-5

CHARACTERIZATION OF *IN VITRO* HEALTH AND PATHOLOGICAL HUMAN LIVER TISSUE PERIODICITY APPLYING SINGULAR SPECTRUM ANALYSIS TO BACKSCATTERED ULTRASOUND.

C. B. MACHADO*[1], W. C. A. PEREIRA[1], M. MEZIRI[2], and P. LAUGIER[3], [1]Biomedical Engineering Program, COPPE/UFRJ, Rio de Janeiro, RJ, Brazil, [2]Dapartement de Physique, Universita Badji Mokhtar, BP 12, Annaba, Algarie, [3]Laboratoire da Imagerie Paramatrique CNRS, Paris, France.
Corresponding e-mail: wagner@peb.ufrj.br

Ultrasonography has been extensively used in the last three decades providing basically qualitative information for clinical diagnosis. Additional quantitative data from ultrasonic signals can provide an important potential diagnostic improvement and is still a research topic. For tissues with a quasi-periodic architechture, spectral analysis methods have been applied to estimate a specific parameter: the Mean Scatterer Spacing (MSS). The Singular Spectrum Analysis (SSA), used by Pereira and Maciel (2001) for ultrasonic biomedical signals, is a method which can separate the periodic part of the signal and then find the periodicity-related frequency in the spectrum. The present work aims to use SSA to characterize in vitro normal and pathological human liver periodicity using backscattered 20-MHz ultrasound signals. Twenty human hepatic samples (about 7-mm thick), with histological status ranging from normal to three different degrees of fibrosis, were studied. They have been classified according to a French score system (METAVIR) after biopsy. A total of 256 ultrasound backscattered signals were collected from each specimen, and then processed with the SSA method. A discriminant analysis was applied to try to differentiate the histological classification. The best result - accuracy (*Ac*) of 75%, a sensibility (*Ss*) of 78.6% and an Specificity (*Sp*) of 66.70% - was reached using four parameters (MSS average, MSS standard deviation, MSS histogram mode and the average ultrasonic propagation speed in the specimen). The best result with three parameters (MSS mean, MSS standard deviation and ultrasonic speed) was *Ac* of 70%, *Ss* of 71.4% and *Sp* of 66.7%. The MSS average alone does not

have a good discriminant power but the inclusion of other parameters (ultrasonic wave speed and MSS standard deviation) has demonstrated the possibility of an acceptable accuracy in discrimination. For further work, it is recommended the inclusion of more specimens (mainly with fibrosis degree 2, not available in this work), and also investigate the inclusion of other tissue parameters like attenuation and backscattering coefficients.

Keywords: ultrasound, mean scatterer spacing, liver tissue, singular spectrum analysis

References:

PEREIRA, W. C. A. AND MACIEL, C. D. Performance of ultrasound echo decomposition using singular spectrum analysis, *Ultrasound in Medicine & Biology*, 27:1231-1238, 2001.

P2A-6

A FEASIBLE STUDY ON THE DETERMINATION OF BLOOD HEMATOCRIT WITH NAKAGAMI PARAMETER CALCULATED FROM BACKSCATTERED SIGNALS.

P.-H. TSUI*[1,2], C.-C. HUANG[1], and S.-H. WANG[1], [1]Dept. of Biomedical Engineering, Chung Yuan Christian University, Taiwan, [2]Department of Biomedical Engineering, Yuan Pei Institute of Science and Technology, Taiwan. Corresponding e-mail: shyhhau@cycu.edu.tw

This feasibility study is to evaluate the application of Nakagami statistical model calculated from backscattering of blood as a function of hematocrit. Red cell suspensions (RCS) of different hematocrits ranging from 3% to 50% were prepared by mixing the washed porcine erythrocytes with a certain amount of buffered saline solution. Subsequently, the ultrasonic backscattered signals from various hematocrits of blood were acquired using a 5 MHz focused transducer. The Hilbert transform and the logarithmic compression were respectively applied to calculate the uncompressed and compressed envelopes from those digitized ultrasonic echoes for the estimation of Nakagami parameter as a function of hematocrit. Results showed that the probability distributions of the uncompressed backscattered envelopes from all of RCS of different hematocrits remained the Rayleigh statistics, as indicated by the unity Nakagami parameter. On the other hand, the statistics of all compressed backscattered envelopes tended to be post-Rayleigh distributed. Specifically, all of the Nakagami parameter calculated from compressed backscattered envelopes were larger than one and were varying dependent on the hematocrit, in which the average Nakagami parameter increased from 1.39 to 1.68 with the increase of the hematocrit from 3% to 12%. As the hematocrits were increased from 12% to 50%, the corresponding Nakagami parameter however decreased from 1.68 to 1.14. The tendency of Nakagami parameter as a function of hematocrit obtained from the compressed backscattered signals is similar to results of backscattering coefficient. It indicates that different hematocrits can be effectively distinguished by the Nakagami parameter after applying the logarithmic compression on the envelope signals. With it is less computational complication and is easy to carry out measurements,

the Nakagami parameter estimated using the compressed backscattered envelopes has a potential to precisely determine the hematocrit of blood.

This work was supported by the National Science Council of Taiwan of the grants: NSC 92-2218-E-033-002 and NSC 93-2213-E-033-035.

P2A-7
DETERMINATION OF DAMPING AND DISPERSION PARAMETERS WITH A COMBINED MEASUREMENT-SIMULATION TECHNIQUE.

L. BAHR*, M. KALTENBACHER, and R. LERCH, Department of Sensor Technology, Erlangen, Bavaria, Germany.
Corresponding e-mail: Ludwig.Bahr@lse.eei.uni-erlangen.de

Ultrasonic attenuation found in mammalian tissue in the frequency range commonly used in clinical medicine, i.e. 1 to 10 MHz, suggest the use of an attenuative term with a frequency dependency according to a power law. For most soft tissue and biological fluids we find that the frequency power factor lies between 1.0 and 1.5. Also, phase dispersion is observed to occur in tissue. To determine attenuation and dispersion as a function of frequency, we use a broadband through transmission measurement setup. A transducer pair is mounted facing each other in a water tank. Two measurements are conducted, one with a slab of the substance to be measured placed between the transducers, and a reference measurement in water without the substance in the propagation path. We performed measurements with castor oil, an agar based tissue mimicking material (TMM) following the recipe in IEC 60601-2-37 Amd. 1 and a polyacrylamid based TMM. The measurement procedure is repeated several times. For each one, model functions build from Kramers-Kronig relations are fitted to the measured attenuation and dispersion curves. The two parameters, which fully define both model curves, are extracted and averaged over all conducted measurements. We achieve a relative standard deviation of less than 1% for both of our parameters.

In a second step we evaluate the effect of diffraction in our measurement setup using the finite element method. We perform the simulation in the time domain using a linear wave equation including attenuation with a power law frequency dependency. Because the phase shift can be computed from the attenuation factor according to Kramers-Kronig relations, a single term can be built describing both, attenuation and dispersion. To implement this term in our finite element program, we use a fractional derivative approach in the time domain, where we use two different algorithms. The first one is the well-known Gruenwald-Letnikov formula, the second one is a collocation approximation using polynomial splines. We verified the accuracy of our implementation with a one-dimensional channel model, where an analytical solution is known, so that after 10 cm of propagation the relative error is less than 0.1%. To evaluate the diffraction effect we conduct two simulations. First, we use the correct material parameters for the propagation path in water and TMM. In a second simulation we apply the correct damping and dispersion parameters, but for water and TMM the same density and propagation speed values, i.e. the impedances are the same and no diffraction

occurs. In both cases the force acting upon the receiving transducer is calculated and the frequency dependent ratio of both are built. With this ratio we eliminate the diffraction effect in the measured spectrum of the receiving transducer and enhance the accuracy to lower frequencies. The obtained method is compared to the analytical expression for the Lommel diffraction correction integral.

Session: P2B

CONTRAST AGENTS I
Chair: H. Torp
Norwegian University of Science and Technology

P2B-1

NON-LINEAR CORRUPTION OF ULTRASOUND TRANSMISSION BY MICROBUBBLE CONTRAST AGENTS.

R. J. ECKERSLEY*[1] and M. X. TANG[2], [1]Imperial College, London, U.K., [2]Oxford University, Oxford, U.K.
Corresponding e-mail: r.eckersley@imperial.ac.uk

Current techniques for detection of microbubble contrast agents make use of their non-linear behaviour under ultrasound insonation. These techniques have been shown to be successful in separating echoes generated by microbubbles from tissue. However, even at low acoustic pressures (< 100kPa peak negative pressure) microbubbles which lie between the transducer and the target can corrupt the transmission signal through non-linear attenuation of the transmission signal. As a result, both microbubbles at the target and in the transmission path contribute to the non-linearity of the echoes at depth. This can result in imaging artefacts especially at depth in tissues. This paper investigates the non-linear corruption process caused by microbubble contrast agents and the effects on current nonlinear imaging techniques. The corruption is studied through both simulation and experimental measurements. The simulations are based on a modified Raleigh-Plesset model and the results compared with experimental measurements on diluted suspensions of the microbubble contrast agent, SonoVue™. The results show that the corruption is primarily due to the nonlinear attenuation of the transmitted pulses, which is dependent on both the insonating amplitude and phase. The microbubbles can also cause a phase shift in the propagating signal, due to the changes in speed of sound when ultrasound travels through a bubble suspension. The amplitude of non-linear forward scattering was also considered and found to be much smaller when compared with the transmitted signals. Our simulation of the attenuation process corresponds well with our experimental results, with corresponding frequency shifts observed in both the simulation and the real data. Potential imaging errors caused by the nonlinear corruption were quantified through both simulation and experiments. Comparison of signal amplitudes with and without non-linear corruption revealed errors as high as 30% when multi-pulse amplitude and phase

modulated detection sequences are used. By comparison the error introduced through non-linear propagation in water at these low peak pressures is shown to provide a much smaller contribution to this imaging artefact.

R.J. Eckersley is supported by the EPSRC (Grant: GR/S71224/01)

P2B-2

QUADRATIC PULSE INVERSION ULTRASONIC IMAGING.

M. AL-MISTARIHI* and E.S. EBBINI, University of Minnesota, Minneapolis, MN. Corresponding e-mail: mamoun@ece.umn.edu

We have previously introduced post-beamforming second order Volterra filter (SOVF) for decomposing the pulse echo ultrasonic radio-frequency (RF) signal into its linear and quadratic components. Using singular value decomposition (SVD), an optimal minimum-norm least squares algorithm for deriving the coefficients of the linear and quadratic kernels of the SOVF was developed and verified. However, the agent specificity of the standard SVD-based quadratic kernel is sometimes compromised by sensitivity to nonlinear echoes from tissue. We present an ultrasonic imaging approach that combines harmonic-sensitive pulse sequences with a quadratic kernel derived from SOVF model. While pulse inversion has high sensitivity to nonlinear bubble oscillation, it is vulnerable to noise and tissue motion. A quadratic kernel derived from an SOVF model of the PI data preserves the true quadratic components while reducing noise and rejecting linear component. A two-step algorithm for computing the coefficients of the quadratic kernel leading to reduction of linear tissue component and increase the specificity while optimizing the sensitivity to the UCA is presented. In the first step, quadratic kernels from individual singular modes of the PI data matrix are compared in terms of their ability of maximize the contrast to tissue ratio (CTR). In the second step, quadratic kernels resulting in the highest CTR values are convolved. In practice this is limited to two or three modes in order to avoid impractically large kernel size. The approach is demonstrated experimentally using images from in vivo kidney after bolus injection with UCA. Illustrative Images of the kidney of a juvenile pig were obtained before and after infusion of contrast agent (SonoVue, Bracco, Geneva, Switzerland) at various concentrations. For example, at a concentration of 0.01 ml/kg, B-mode images (3 cycles at 1.56 MHz transmit frequency) show no quantifiable change due to the presence of the contrast agent. PI images without second harmonic (SH) filtering showed 10.2 dB enhancement and evidence of residual tissue components due to motion. On the other hand, quadratic images obtained using the standard SVD-based, QPI, and two step QPI (TS-QPI) algorithm produced CTR values of 23.1, 31.1 and 35.9 dB, respectively. Imaging results as well as the spectral contents of QPI data show a significant increase in harmonic sensitivity and reduction in noise levels. Similar results were obtained from imaging flow phantom under a variety of exposure conditions and UCA concentration levels. Implications of this approach on new forms of functional ultrasound imaging are discussed.

This work was funded in part by Esaote, S.p.A., Genoa, Italy.

P2B-3

CONTRAST ECHO PROCESSING FOR VERY WIDEBAND SYSTEMS USING HIGHER ORDER STATISTICS.

D. KRUSE*, Y. SUN, and K. FERRARA, University of California,, Davis.
Corresponding e-mail: dekruse@ucdavis.edu

This abstract does not appear in the online abstracts
at the author's request.
It will appear in the print version.

P2B-4

HIGH FREQUENCY ULTRASONIC IMAGING AND ATTACHMENT OF CONTRAST AGENTS UNDER FLOW CONDITIONS.

M. BUTLER*[1], C. MORAN[1], C. CUNNINGHAM[2], T . ANDERSON[1], J . ROSS[2], K. FOX[3], and N. MCDICKEN[1], [1]Medical Physics, University of Edinburgh, Edinburgh, [2]Centre for Inflammation Research, University of Edinburgh, Clinical and Surgical Sciences, Medical School, Teviot Place, Edinburgh, [3]Cardiovascular Research Unit, University of Edinburgh, Edinburgh.
Corresponding e-mail: m.butler@ed.ac.uk

Background: Targeting of ultrasound contrast agents is an area of research which is continuously expanding. Contrast agents can be targeted to attach to markers expressed at areas of interest within the body. Areas of inflammation and molecules expressed at these areas are associated with unstable plaque in arteries. Techniques to distinguish between unstable and stable plaques are currently unavailable.

Previously a flow chamber was described which allowed high frequency ultrasonic imaging of contrast agents attached to surfaces while subjected to flow. A lipid based contrast agent which can be targeted to molecules expressed at areas of inflammation has been developed and attached to agar, under static conditions, using avidin and biotin. It was shown that the contrast agent remained attached to the agar under shear stresses of up to 3.4 Pa; mean arterial shear stresses are 1.5 Pa. The work presented here has involved attaching the contrast agent under flow conditions.

Aim: To determine how the variation of biotin in the contrast agent shell affects attachment under flow conditions.

Methods: Streptavidin coated agar samples were placed in the flow chamber. Biotinylated lipid contrast agents, 0.5 ml in 50 ml saline, were circulated through the flow chamber for 2 hours at a flow rate of 1.65 ml min-1. The samples were imaged with 40 MHz intravascular ultrasound. Images and RF data were captured before and after circulation of the contrast agent. Contrast microbubbles containing 1%, 3% and 5% biotin were tested. Saline and un-biotinylated contrast agent were also circulated.

Results: On the circulation of saline and un-biotinylated contrast agent over the streptavidin coated agar in the flow chamber, no enhancement was seen in the IVUS images. On circulation of the 1% biotinylated agent, enhancement of the agar surface was seen. After circulation of the 3% and 5% biotinylated contrast agents, again enhancement of the agar surface was seen, however, there was better coverage across the surface of the agar than for the 1% biotin agent. The RF data was used to determine the mean backscatter power from the agar surface, across the surface there was no significant increase seen after circulation of 1% biotin-agent. However, there was an increase in the mean backscatter power for the 3% and 5% biotinylated contrast agents.

Conclusions: Variations in the concentration of biotin within the shell can affect the attaching potential of targeted contrast agent. The agent was seen to attach to an agar surface under low flow rates, with better coverage of the agar sample with increasing levels of biotin.

P2B-5

ACOUSTIC RADIATION FORCE ENHANCES ULTRASOUND CONTRAST AGENT RETENTION TO P-SELECTIN IN VIVO.

J. RYCHAK[1], A. KLIBANOV[2], and J. HOSSACK, [1]University of Virginia Department of Biomedical Engineering, Charlottesville, VA, [2]University of Virginia Department of Internal Medicine, Charlottesville, VA.
Corresponding e-mail: jrychak@virginia.edu

Recent studies in animal models have shown that targeted ultrasound contrast agents can achieve specific adhesion to regions of intravascular pathology. However, *in vitro* investigations of microbubble (MB) contrast agent adhesion have revealed that efficiency of the attachment to molecular targets tends to be low, especially in vigorous blood flow. Additionally, the ability of circulating MB to contact the vessel surface, where the targeted molecular markers of disease are located, may be low, especially in large vessels. The poor delivery of agents to the vessel surface is likely due to the rheology of the gas-encapsulated MB, which exhibit transport kinetics similar to that of erythrocytes and thus may migrate radially toward the vessel center in the shear flow found in blood vessels. It has been hypothesized that the efficacy of targeted contrast-enhanced ultrasound imaging may be improved by increasing the fraction of MB that contact and adhere to the intended endothelial target site. In particular, low-intensity acoustic radiation has been used to cause the directional migration of targeted MB toward that vessel wall in several *in vitro* systems. In the current study we present data that this technique enhances targeted adhesion of MB targeted to the pro-inflammatory endothelial protein P-selectin in the mouse microcirculation. We assessed the retention of MB bearing the anti-P-selectin antibody Rb40.34 in a trauma model of inflammation in the mouse cremaster. The cremaster muscle was prepared for intravital microscopy in a heated superfusion bath, and an ultrasound transducer was secured with an adjustable arm in the bath above the tissue. Wild type or P-selectin knock out mice were injected intraveneously with a bolus of 10^7 fluorescently labeled MB, and acoustic radiation was applied perpendicular to the cremaster preparation at 50 kPa and 2.0 MHz at a pulse repetition frequency of 10 kHz for four minutes post-injection. After cessation of ultrasound, we assessed MB retention, vessel wall shear rate, and leukocyte rolling flux in 10-20 venules of diameter 8-40 μm. Targeted MB exhibited a five-fold greater retention following application of acoustic radiation, and negligible adhesion was observed in knock out mice or wild type mice injected with sham-targeted MB exposed to acoustic radiation. We observed no correlation of MB retention with leukocyte rolling flux fraction or vessel wall shear rate. We did not observe a significant difference in vessel diameter or shear rate in venules due to the application of radiation force. These results suggest that low-intensity radiation force is a viable mechanism for enhancing MB retention for imaging inflammation.

This work was supported by NIH EB001826.

P2B-6
SHELL RUPTURE THRESHOLD, FRAGMENTATION THRESHOLD, BLAKE THRESHOLD.

M. POSTEMA*[1], N. DE JONG[2,3], and G. SCHMITZ[1], [1]Ruhr-Universität Bochum, Bochum, Germany, [2]University of Twente, Enschede, The Netherlands, [3]Erasmus MC, Rotterdam, The Netherlands.
Corresponding e-mail: postema@ieee.org

The disruption of contrast agent microbubbles has been implicated in novel techniques for high-MI imaging and local drug delivery. At MI>0.6, microbubble fragmentation has been observed with thin-shelled agent (~10 nm), and shell rupture with thick-shelled agent (~250 nm). To predict the disruption of these nanoshelled microbubbles, destruction thresholds have been under investigation. In several studies, the Blake threshold pressure was associated with microbubble destruction. The Blake threshold pressure is the peak rarefactional acoustic pressure at which the critical Blake radius is reached, approximately twice the equilibrium radius, above which a bubble behaves like an inertial cavity. We studied the acoustic pressures at which a thin-shelled microbubble fragments and those at which a thick-shelled microbubble cracks. More specifically, we investigated the validity of the Blake threshold for these phenomena. The oscillating and fragmenting behavior of microbubbles with a 10 nm shell was simulated at a driving frequency of 0.5-2 MHz, using a modified Rayleigh-Plesset equation and assuming that fragmentation occurs when the kinetic energy of the microbubble surpasses the instantaneous bubble surface energy. For microbubbles with radii between 1 and 6 μm, the fragmentation thresholds lie between 20 and 200 kPa. Generally, the critical radius is much smaller than twice the equilibrium radius. The moment of break-up during the collapse phase is in agreement with high-speed optical observations that were presented previously.

Furthermore, the shell rupture behavior of microbubbles with a 250 nm elastic shell was analyzed for quasistatic pressure changes (relatively low ultrasonic frequencies), assuming that the shell obeys Hooke's Law. The rupture threshold pressure of -80 kPa had been determined from acoustical data. For shells with the typical Young's modulus 2 MPa and Poisson ratio 0.5, this is in agreement with the observation that the maximal excursion upon rupture of such bubbles is smaller that 0.3 μm.

In conclusion, we may state that the Blake threshold is neither a good estimator for the fragmentation, nor for the rupture of contrast agent microbubbles.

Session: P2C
THERAPEUTICS AND HYPERTHERMIA
Chair: C. Cain
University of Michigan

P2C-1
NONCAVITATIONAL MECHANISMS OF INTERACTIONS OF ULTRASOUND WITH TARGETED PERFLUOROCARBON NANOPARTICLES: IMPLICATIONS FOR DRUG DELIVERY.

N. SOMAN*, J. MARSH, M. HUGHES, G. LANZA, and S. WICKLINE, Washington University School of Medicine, St. Louis, MO.
Corresponding e-mail: nsoman@wustl.edu

We have previously demonstrated that perfluorocarbon nanoparticles consisting essentially of liquid perfluoro-octyl bromide (PFOB) core surrounded by a lipid monolayer can serve as highly specific site-targeted contrast and therapeutic agents after binding to cellular biomarkers. Based on previous findings that ultrasound applied at 2 MHz and 1.9 mechanical index (MI) for a five-minute duration dramatically enhances the cellular interaction of targeted PFOB nanoparticles with melanoma cells in vitro without inducing apoptosis or other harmful effects to cells that are targeted, we sought to define mechanisms of interaction and the safety profile of ultrasound used in conjunction with liquid perfluorocarbon nanoparticles for targeted drug delivery, as compared with conventional microbubble ultrasound contrast agents under identical insonification conditions.

Cell-culture inserts (1.0 μ, 0.33 cm^2, BD BioSciences, PA) were used to grow a confluent monolayer of human umbilical vein endothelial cells (HUVECs). The parameters assessed were transmonolayer albumin permeability, transendothelial electrical resistance (TEER) and cell viability. Definity® in conjunction with continuous wave ultrasound (2.25 MHz for 1 and 5 minutes) caused a significant increase ($p < 0.05$) in the permeability of the HUVEC monolayer to 5.72 (± 1.64) times above the normal along with a 0.6 ± 0.13 ($p<0.05$) fold decrease in TEER (a sign of reduced membrane integrity), and decreased cell viability by 52.3 ± 4.9 % ($p<0.05$). Histological evaluation demonstrated extensive disruptions of cell monolayers. Nanoparticles (both non-targeted and targeted) elicited no changes in these different measures under similar insonification conditions and did not disrupt cell monolayers.

We hypothesize that ultrasound facilitates drug transport from the perfluorocarbon nanoparticles not by cavitation-induced effects on cell membrane but rather by direct interaction with the nanoparticles that stimulate lipid exchange and drug delivery. A non-disruptive method for enhancing the interaction of nanoparticles with cell membranes can thus be utilized to facilitate drug delivery without inducing membrane damage (pore formation) or cell death from destructive cavitation.

P2C-2

REAL-TIME MONITORING TRANSCRANIAL SUB-MEGAHERTZ ULTRASOUND THROMBOLYSIS WITH PHASED ARRAY SCANNER.

J. KUBOTA*[1], M. OGIHARA[1], A. SASAKI[1], T. AZUMA[2], S. UMEMURA[2], K. ANDO[3], J. SHIMIZU[3], T. ISHIBASHI[3], and H. FURUHATA[3], [1]Hitachi Medical Corporation, Kashiwa-shi, Chiba-ken, Japan, [2]Central Research Laboratory, Hitachi, Ltd., Kokubunnji-shi, Tokyo, Japan, [3]Jikei University School of Medicine, Minato-ku, Tokyo, Japan.
Corresponding e-mail: kubota@rd.hitachi-medical.co.jp

[Background] Transcranial ultrasonic thrombolytic system has been developed, for acute ischemic stroke therapy during hyper acute phase. The system aims to have a higher potential for early recanalization in the thrombo-embolism by accelerating the effect of thrombolytic agent with transcranial ultrasonication.

[Method] Sub MHz ultrasound has less attenuation by several orders through cranium than that of more than 2MHz, while it has higher risk of intracranial hemorrhage. In order to avoid the risk, the direction of therapeutic ultrasound (T) beam is targeted at an area around the embolic artery, and in order to minimize mechanical and thermal adverse biological effects, T-beam frequency is selected 500kHz under the condition of MI≤0.25 and TI≤2, the acoustic intensity limited less than the maximum regulation level of the diagnostic ultrasound equipment. The transcranial diagnostic (Doppler or color flow imaging) ultrasound (D) beam at 2MHz is used for monitoring the recanalization. The system irradiates both T- and D-beam alternately in the signal control subsystem through a phased array single compound probe.

[Results] The fundamental specification of the developed system has been verified from in vitro and in vivo experiments. Acoustic intensity of 50mW/cm2 showed significant increase in recanalization rates with the newly developed system compared with thrombolytic agent alone. The diagnostic array in the probe provided the same precise image as the commercialized sector scanning diagnostic phased array. The probe also has supplied T-beam of the maximum acoustic intensity designated by the regulation for the diagnostic equipment. The margin of safety was confirmed through animal experiments.

[Conclusion] It is anticipated from the results that the developed system has a great potential for clinical studies treating the AIS patients.

This work was carried out as the Translational research project of Health and Labour Sciences Research Grants, supported by Japanese Ministry of Health, Labour and Welfare.

P2C-3

QUANTITATIVE RELATIONS BETWEEN ACOUSTIC INERTIAL CAVITATION AND GENE TRANSFECTION RATE/CELL VIABILITY.

C.-Y. LAI*[1], C.-H. WU[2], C.-C. CHEN[2], and P.-C. LI[1], [1]Department of Electrical Engineering, National Taiwan University, Taipei, Taiwan, ROC, [2]Department of Chemistry, National Taiwan Normal University, Taipei, Taiwan, ROC.
Corresponding e-mail: paichi@cc.ee.ntu.edu.tw

Gene therapy is a technique for correcting defective genes. Ultrasound has been utilized to assist gene transfection, as it is non-invasive and has the ability to focus at depth. In combination with ultrasound, microbubble-based contrast agents have also been used to enhance the transfection efficiency by inducing acoustic inertial cavitation. Although microbubbles have been used for gene transfection by several groups, the relations between inertial cavitation and gene transfection rate/cell viability are still unknown. It is therefore the primary purpose of this study to examine such relations experimentally and quantitatively. In the experiments, 2% agarose phantoms were made to contain solution with cells and microbubbles. A 1 MHz cylindrical transducer was used to send out ultrasound pulses and a 10 MHz transducer was used to detect the wideband acoustic signal generated when the bubbles collapsed. A commercial contrast agent Levovist® was used, and the cavitation was represented by the parameter ICD (inertial cavitation dose). The ICD is defined as the cumulated root mean squared broadband noise amplitude calculated in the frequency domain. The relations between ICD and gene transfection rate/cell viability were studied under various acoustic pressures, microbubble concentrations and pulse durations. Concentration of cells (HeLa cells) and DNA (short DNA-FITC molecules) were 10^6 cells/mL and 20 μg/mL, respectively. The ultrasound exposure time was 60 seconds. After exposure, the cells were incubated under 37^0C for 24 hours. The transfection rate was then calculated with a fluorescence microscope and the cell viability was evaluated with the trypan blue assay. Regarding the cavitation results, the ICD increased from 0.16 to 0.73 V-s (Volt-second), 0.21 to 1.05 V-s and 0.14 to 1.15 V-s when the acoustic pressure, microbubble concentration and pulse duration changed from 0.48 to 1.32MPa, 10 to 100mg/mL, and 1 to 10 cycles, respectively. Under these ICDs, the transfection rate ranged between 12-32% and the cell viability ranged between 100-37%. These results also compare favorably with those found in the literature that also used Levovist® as the cavitation nuclei. For example, Sandra Koch et al. achieved a 5.5% transfection rate with 39.3% cell viability in a work published in 2000, and Tieli Li et al. achieved a 5% transfection rate along with 60% cell viability in a work published in 2003. Linear regression was also performed on the transfection rate versus ICD and the cell viability versus ICD. For the transfection, $y=28.95x+5.65$ (x: ICD, y: transfection rate) was obtained ($R^2=0.759$). On the other hand, $y=-73.43x+121$ (x: ICD, y: cell viability) was obtained ($R^2=0.935$) for cell viability. The results show high correlations between transfection rate/cell viability and ICD.

P2C-4

A CYLINDRICAL PHASED-ARRAY ULTRASOUND TRANSDUCER FOR BREAST TUMOR THERMAL THERAPY.

C.-S. HO*[1], K.-C. JU[1], Y.-Y. CHEN[2], and W,-L. LIN[1], [1]Institute of Biomedical Engineering, National Taiwan University, Taipei,Taiwan, [2]Department of Electrical Engineering, National Taiwan University, Taipei,Taiwan.
Corresponding e-mail: r93548042@ntu.edu.tw

Purpose: In this paper, we investigated the feasibility of a cylindrical phased-array ultrasound transducer for producing a conformal heating while preventing overheating or overdosing the ribs and normal tissue for breast tumor thermal therapy.

Methods: In this system, a 1-MHz cylindrical phased-array transducer consisted of 200 elements with a radius of 10 cm and a width of 2 cm. The breast was taken as a 6 cm- radius hemisphere and was surrounded by the transducer. The geometrical center of the transducer was arranged at the center of the target volume. Foci were electrically scanned to cover the entire target volume. In this simulation study, the power deposition patterns were calculated by using the wave equation. A pseudo-inverse method was used to calculate the driving signals for each transducer element. The temperature distributions were obtained by using Pennes transient bioheat transfer equation.

Results: Nine focal patterns, each with 1~4 focal spots, were used to heat a target volume with 1*1 cm^2 section located at the center of the transducer. Each focal pattern with a maximum intensity of 400W/cm^2 was sonicated for 2 sec, without cooling phase, and the total heating time was 18 sec. Simulation results indicate that the region with a thermal dose higher than 240 min (TD240) covers the 1*1 cm^2 section, and has a width about 1 cm. Hence, a 1*1*1 cm^3 cube can be well heated. When the target volume becomes larger, a pattern-based method was proposed as our heating strategy. To heat a 2*2 cm^2 section, it was divided into four 1*1 cm^2 subsections and 36 focal patterns with 170W/cm^2 maximum intensity were used. The resulting heated volume was about 2*2*1 cm^3 . When the target volume was off-axis of the breast, the transducer center was shifted to the center of the target volume. The heating result shows that the TD240 region almost covered the target area, and the width was about 1 cm.

Discussion / Conclusion:In this simulation study, the width of the heated volume is dependent on the width of the transducer. If the width of the target volume is larger than 1cm, the target volume was divided into several stacks and then heated separately to cover the whole target region. The advantage of this system is that the emitted wave from the transducer approximately paralleled the ribs. Therefore, not only the power deposition but also the temperature rise of ribs can be eliminated. It demonstrated that the cylindrical phased-array ultrasound transducer has the ability to conformally heat the target volume without producing undesired overheating even the tumor is close to the ribs.

The authors would like to thank the National Science Council of the Republic of China for partially supporting this research under contract nos. NSC 93-2213-E-002-069.

P2C-5

THE INVESTIGATION OF CONTRAST-AGENT ENHANCED ULTRASOUND THERMAL EFFECT.

Y. S. TUNG*[1], C. C. WU[3], H. L. LIU[4], K. C . JU[1], W. S. CHEN[2], and W. L. LIN[1], [1]Department of Biomedical Engineering, National Taiwan University, Taipei, Taiwan, [2]National Taiwan University Hospital, Taipei, Taiwan, [3]Department of Mechanical Engineering, National Taiwan University, Taipei, Taiwan, [4]Department of Electrical Engineering, Chang-Gung University, Taoyuan, Taiwan.
Corresponding e-mail: wenshiang@ha.mc.ntu.edu.tw

In recent years, high intensity focused ultrasound (HIFU) was shown to have promising effect on ablating both malignant and benign tumors. Despite its unique advantages such as minimal invasiveness and radiation free, the size of the ablation lesion is small and thus the duration for complete tumor ablation is usually too long. In this study, the effect of using ultrasound contrast agent (UCA) to enhance the ultrasound thermal effect, and thus enlarge the lesion size, was studied. Different concentration of UCA ranging from 0% (control), 0.001% to 0.1% (v/v) was mixed evenly with polyacrylamide gel phantoms containing egg white as a temperature indicator. A 1.85-MHz HIFU transducer was used to form thermal lesions inside the 2cm*2cm*4cm phantoms. For the electric power of 50W and 70W, 'cigar' and 'tadpole' shaped lesions were formed inside the control phantoms respectively. The volume enlargement ratio (VER), defined as the ratio of volume formed in phantoms with UCA to the volume without UCA at the same power level, was used to evaluate the effect of UCA on thermal ablation. When the concentrations of UCA were 0.001%, 0.005%, 0.01% and 0.015%, the VER were 9.28, 42.12, 56.07, 77.33 at 50W, and 1.94, 5.63, 11.75, 15.49 at 70W, respectively. The administration of UCA significantly increased the lesion size up to 77 times! UCA also reduced the necessary power to form a lesion of a certain size. For example, 0.001% of UCA at 50W produced a lesion close to controls at 70W in size. Same concentration of UCA at 70W formed lesions equivalent in size for phantoms without UCA at 100W. 30% reduction of the power level was achieved. Complications of overheating could certainly be reduced when the output power decreased. The forward shift of a lesion, defined as the distance of the most heating position to the HIFU focus, was also investigated. When the UCA concentration was 0%, 0.001%, 0.005%, 0.01% and 0.015%, the lesion shifts at 50W and 70W were 0.1, 0.65, 0.95, 1.32, 1.53 cm and 0.62, 0.72, 1.38, 1.99, 2.20 cm, respectively. If the concentration of the UCA was greater than 0.05%, the lesion was basically formed at the surface of the phantom since most of the incident ultrasound waves were reflected. In conclusion, UCA would increase the size of lesion by enhancing scattering, and the lesion size increased with the increase of UCA concentration. However, lesions moved toward the transducer when concentration increased. It would be unable to produce the lesion inside the phantom if the concentration of UCA was too high. Overall, low concentration (0.001%) of concentration agent and low power (50 W) were enough to produce a lesion 42 times larger, and produced minimal lesion movement (0.65 cm).

This work was supported in part by NSC 93-2320-B-002-097 and NHRI ME-093-CP-12.

P2C-6

ACOUSTIC HEMOSTASIS AND THERAPEUTIC ULTRASOUND AT UW, SEATTLE WA: AN UPDATE.

S. VAEZY*, University of Washington, Seattle, WA.
Corresponding e-mail: vaezy@apl.washington.edu

Our work has focused on research and development of ultrasound image-guided High Intensity Focused Ultrasound (HIFU) therapy for applications in hemorrhage control and tumor treatment. Recent efforts in addressing clinically-significant problems have included the following: 1) Transcutaneous sealing of punctured femoral artery in pigs and rabbits, a model for hemostasis therapy of vascular wounds in trauma and catheterization procedures. Results show that B-mode and color-Doppler guided HIFU can be used effectively to close the vascular wound caused by a catheter, in less than a minute. 2) Selective intraoperative liver vessel occlusion in pigs, a model for vascular embolization in tumor treatment and hemorrhage control applications. Veins and arteries, located deep in the parenchyma of liver, within the focal distance range of an ultrasound-guided annular phased array (3-6 cm), were completely occluded, using control software that allows point and shoot HIFU targeting. 3) Hemorrhage control for lacerations on the posterior surface of liver, via an ultrasound image-guided HIFU approach from anterior surface. Complete hemostasis of these lacerations in anti-coagulated pigs was achieved in about 5 minutes. 4) Resection of liver, spleen, and kidney, using high-power HIFU devices. Large sections of tissue (12 cm of a liver lobe, 5 cm of spleen, and lower pole of kidney) were hemodynamically isolated from the rest of the organ by producing a coagulative necrosis wall, in less than 5 minutes of application of HIFU, allowing subsequent bloodless resection. 5) Contrast-agent-enhanced bleeding detection and hemostasis. The results show that ultrasound contrast agents (Optison and homemade albumin shell microbubbles) provide a valuable tool for localization of bleeding sites (alone or in combination with advanced imaging strategies such as pulse inversion harmonic imaging). Additionally, the presence of microbubbles in the HIFU treatment field have resulted in shortening of the duration of HIFU application needed to achieve hemostasis of liver injuries. 6) Uterine fibroid treatment using ultrasound image-guided HIFU. Human uteri containing fibroid tumors, obtained after being excised in hysterectomy, were treated with HIFU, and lesions were formed and visualized using an annular phased array HIFU device, integrated with a transvaginal imaging probe. Engineering developments that have made the above investigations possible include the following: 1) Various single element HIFU devices, integrated with multiple ultrasound imaging probes, using fast prototyping methods of developing application-specific devices that meet particular clinical and engineering requirements. 2) Color-Doppler guided annular phased array HIFU devices. 3) Bleeding detection algorithms, using RF-based measurements of tissue vibrations. Future work includes thin-profile devices for intraoperative applications in tight regions such as the dome of the liver, and HIFU devices incorporating imaging scanheads. The preclinical studies will focus on blood flow occlusion for applications in hemorrhage control as well as tumor treatment.

US DoD, NIH

P2C-7

ULTRASOUND SELF-CALIBRATION AND REAL-TIME QUALITY CONTROL FOR INTERVENTIONS.

E. M. BOCTOR*, G. D. HAGER, and G. FICHTINGER, The Johns hopkins University, Baltimore, MD.
Corresponding e-mail: eboctor@ieee.org

This abstract does not appear in the online abstracts
at the author's request.
It will appear in the print version.

P2C-8

ULTRASOUND IMAGING FEEDBACK OF TISSUE LIQUEFACTION IN ULTRASOUND SURGERY.

T. HALL*, B. FOWLKES, and C. CAIN, University of Michigan, Ann Arbor, MI.
Corresponding e-mail: hallt@umich.edu

Introduction: Previous work has shown that under certain conditions, high-intensity pulsed ultrasound can be used to liquefy tissue. This process is thought to occur as a result of repeated subdivision of tissue through cavitation until the cellular structure of the targeted tissue is completely broken down. We hypothesize that cavitation induced liquefaction of tissue should produce a significant **reduction** in standard B-scan imaging speckle amplitude as tissue is homogenized to a sub-cellular level. This may provide an effective feedback mechanism for treatment efficacy in ultrasound surgery using cavitation.

Methods: Freshly harvested (6-12 hours) porcine liver was cut into 5x7x2.5 cm sections and placed in degassed saline in the geometric focus of a 512 channel therapeutic ultrasound array transducer (Imasonic). A standard diagnostic linear imaging probe (Siemens Elegra) was placed perpendicular to the therapeutic ultrasound propagation path and used to monitor treatments. The therapeutic focus was rapidly scanned electronically over a 1 cm square grid in the plane of the imaging transducer with short (25 us) high intensity (>18 MPa peak negative pressure) pulses at a frequency of 1 MHz and a low duty cycle (0.1 %). The intention was to create spatially well-defined liquefied lesions primarily through inertial cavitation while minimizing bulk thermal effects (therapeutically significant heating). Tissue samples were exposed to 2000 pulses within each location and then formalin fixed and sliced for evaluation. 8 MHz RF B-scan images were collected before and after treatment to measure average speckle amplitude (ASA) changes.

Results: Application of high intensity ultrasound produced highly transient hyperechoic spots on the B-scan image within the intended treatment area. At the end of treatment, this hyperechogenicity rapidly faded leaving a reduced ASA compared to pretreatment images. Regions outside the treatment area did not change significantly in ASA. Median ASA changes within the treatment area were measured to be -13 dB. Gross examination of lesions showed complete homogenization of the target volume. Lesion boundaries were very sharp and did not extend outside the target volume. Microscopic examination revealed complete tissue disruption with no recognizable cellular structures remaining.

Conclusions: Pulsed ultrasound at very high intensities and low duty cycle is effective at creating precise lesions consisting of liquefied tissue. The resulting lesions display substantially reduced backscatter speckle amplitude due to mechanical homogenization on a microscopic scale. This change is easily measured with standard diagnostic ultrasound imaging and is likely useful for non-invasive feedback on treatment efficacy in ultrasound surgery using cavitation.

This research was funded by grants from the Johnson & Johnson Focused Giving Program and the National Institues of Health RR14450.

P2C-9

THE GENERATION OF INERTIAL CAVITATION IN CONSTRAINED MEDIA, IN VITRO AND EX VIVO INVESTIGATIONS.

P. M. MA*[1], W. S. CHEN[2], C. K. YEH[3], and M. S. CHEN[1], [1]Department of Mechanical Engineering, National Taiwan University, Taipei, Taiwan, [2]National Taiwan University Hospital, Taiepi, Taiwan, [3]Department of Electrical Engineering, Yuan Ze University, Taoyuan, Taiwan.
Corresponding e-mail: wenshiang@ha.mc.ntu.edu.tw

Shock wave has been used routinely for the treatment of urolesthesis for decades. Strong evidences suggest that cavitation bubble activity plays an imortant role on the stone breakage. Recently, shock wave was also shown to be effective in the treatment of certain soft tissue disorders such as tendinosis. However, whether or not cavitation occurs in tight tissue and contributes to tendon healing as well as pain relief remain unknown. In order to understand the possible physical mechanism of the shock wave therapy, we focused on searching the evidences of cavitation in tissue during the shock wave treatment, and also the determining factors of bubble generation. It was hypothesized that the shocck-wave induced cavitation was constrained by the space for bubble expansion, and thus occurred more easily in vessels of larger diameters than capillaries, intercellular space and inside cells. To prove our hypothesis, a series of studies was performed to detect the presence of inertial cavitation in soft tissue blocks of various density ex vivo and elastic phantoms embedded with vessels of diferent size in vitro. We found that shock-wave induced bubble generation highly depended on the 'porosity' (equivalen to the perfusion status) of the ex-vivo tissue blocks. The bubble generation in muscle was substantially less than that in liver, and was undetectable in tendon. For vessel phantoms, cavitation occurred easily in vessels with diameters greater than or equal to 0.7 mm when tap water was pumped through. However, no trace of bubble signal was found in smaller vessels under the same acoustic conditions. Size threshold existed. After adding low concentrations of cotrast agent (Definity®) in the flow-through fluid, cavitation threshold dropped substantially. For a vessel of 0.32 mm in diameter, bubble and signal enhancement could be easily obtained even after a single shot of shock wave. Furthermore, the presence of cavitation-induced bubbles significantly enhanced the signal-to-noise ratio of vessels in the B-mode image, compared with the use of contrast agent alone. Concentration as low as 0.005% (v/v) could elevate the B-mode's averaged gray level in the target area up to 76

levels, much higher than the enhancement contributed by contrast agent alone (about 2 to 3 levels in this concentration). Simulation was also performed for further understanding of the possible mechanism of medium constrain on bubble dynamics.

This work was supported in part by NSC grants 93-2314-B-002-130 of Taiwan, ROC.

P2C-10
SELECTIVE LIVER VESSEL OCCLUSION WITH AN ULTRASOUND-GUIDED HIFU PHASED ARRAY.

V. ZDERIC*[1], L. CRUM[1,2], and S. VAEZY[1,2], [1]Center for Industrial and Medical Ultrasound, Applied Physics Laboratory, University of Washington, Seattle, WA, [2]Department of Bioengineering, University of Washington, Seattle, WA.
Corresponding e-mail: vesna@u.washington.edu

Objective. To determine the applicability of an ultrasound-guided HIFU phased array for selective occlusion of blood vessels at different depths inside the liver. **Methods.** An 11-element annular phased array (aperture of 3.5 by 6.0 cm, focal depth of 3.0-6.0 cm, frequency of 3 MHz) was coupled to an ultrasound imaging probe (C9-5, Philips). A water pillow was held against the front surface of the array to enable water circulation for transducer cooling and coupling of the HIFU energy into the tissue. The Labview software was developed to provide control of the HIFU driving electronics and image guidance. The program allowed an operator to choose multiple foci either by defining the focal distance from the transducer (in 3 to 6 cm range) or clicking on the desired position on the ultrasound image (e.g. blood vessel) with a mouse. The device efficacy in producing tissue necrosis was tested in freshly excised pig liver. The tissue lesions were formed beginning at a focal depth of 6.0 cm and moving by 0.5 cm increments to 3.0 cm, and vice versa. Total incident electric power levels were set to 110 W (~ 4,300 W/cm^2, in water) and 165 W (~6,200 W/cm^2, in water), with each focus being treated for 30 and 20 seconds, respectively. Ten liver vessel treatments were performed in a pig model in vivo. In these treatments, HIFU was applied at the input electrical power of 110 W or 165 W, for 20-40 s. The HIFU treatment monitoring was achieved by the observation of hyperechoic region at the focal position in B-mode ultrasound images. The vessel patency was determined using Color Doppler ultrasound. **Results.** At the intensity of 4,300 W/cm^2, the length of the 30-to-60 mm lesions was 25.5 +/- 8.8 mm, compared to 36.9 +/- 1.8 mm for the 60-to-30 mm lesions. At the intensity of 6,200 W/cm^2, the length of the 30-to-60 mm lesions was 26.7 +/- 4.8 mm, compared to 41.0 +/- 3.0 mm for the 60-to-30 mm lesions. Therefore, the treatment patterns that began distal to the transducer and moved proximally produced longer lesions than the patterns that moved distally. The average lesion width was 1 cm. The lesion volumes were 66% larger after HIFU application at the intensity of 6,200 W/cm^2 as compared to the application at 4,300 W/cm^2. During in vivo HIFU treatments for selective vessel occlusion, liver vessels of up to 1.5 mm in diameter were occluded, while vessels of 3 mm in diameter were patent after the treatment (as determined by both Color Doppler monitoring and gross observations).

Conclusion. The ultrasound-guided HIFU array was shown to be effective in monitoring, targeting and occluding small liver vessels located at various depths inside the liver. The application of higher input powers and longer HIFU exposure times may allow occlusion of large vessels. Our device has a potential to be developed into an intraoperative surgical tool for embolization of liver vessels in hemorrhage control and tumor treatment.

P2C-11
DEVELOPMENT OF A HIGH INTENSITY FOCUSED ULTRASOUND (HIFU) HYDROPHONE SYSTEM.

M. SCHAFER*[1], J. GESSERT[2], and W. MOORE[2], [1]Sonic Tech, Inc., Ambler, PA, [2]Sonora Medical Systems, Longmont, CO.
Corresponding e-mail: marks@sonictech.com

In the past few years, High Intensity Focused Ultrasound (HIFU) has developed from a scientific curiosity to an accepted therapeutic modality. Concomitant with HIFU's growing clinical use, there has been a need for reliable, reproducible measurements of HIFU acoustic fields. A number of approaches have been proposed and investigated, most notably by Kaczkowski et al [Proc. 2003 IEEE Ultrasonics Symposium, 982-985]. We have developed a similar reflective scatterer approach, incorporating several novel features which improve the hydrophone's bandwidth, reliability, and reproducibility. For the scattering element, we have used a fused silica optical fiber with a polyamide protective coating. The fused silica core is 73 microns in diameter with a 5 micron thick polyamide coating for a total diameter of 83 microns. The fiber was prepared by cleaving to yield a perpendicular/flat cut. The fiber is maintained in position using a capillary tube arrangement which provides structural rigidity with minimal acoustic interference. The receiver is designed as a segmented, truncated spherical structure with a 10cm radius; the scattering element is positioned at the center of the sphere. Each segment is approximately 6.3 cm square. The receiver is made from 25 micron thick, biaxially stretched PVDF, with a Pt-Au electrode on the front surface. The PVDF is stretched and bonded to the spherically curved segments using a compliant pressing fixture with controlled temperatures and pressures. Each segment has its own high impedance, wideband preamplifier, and the signals from multiple segments are summed coherently. As an additional feature, the system is designed to pulse the PVDF elements so that the pulse-echo response can be used to align the fiber at the center. This is important when the need arises to change the fiber due to, for instance, cavitation damage. The hydrophone can also be designed with a membrane structure to allow the region around the scatterer to be filled with a fluid which suppresses cavitation. Initial tests of the system have demonstrated a receiver array sensitivity of -279 dB re 1 microVolt/Pa (before preamplification), with a scattering loss at the fiber of approximately 39dB, producing an effective sensitivity of -318 dB re 1 microVolt/Pa. The addition of the closely coupled wideband preamplifiers boosts the signal to a range which is sufficient for the measurement of HIFU transducers. The effective bandwidth of the system exceeds 15MHz, through careful design and the use of PVDF as a sensor material. In order to test the system, several HIFU transducers in the frequency

range from 2.0 to 3.5MHz were tested at low output settings using a conventional PVDF membrane hydrophone. The prototype system was then used to characterize the same HIFU transducers at full power. The results showed good correlation between waveforms and cross-axis beam measurements, taking into account the additional shock losses at higher output settings.

Keywords-hydrophone; HIFU; PVDF; dosimetry

P2C-12
EFFECT OF ULTRASONIC INTENSITY ON THE AMYLOID-β INDUCED APOPTOSIS OF PC12 CELLS.

C.Y. CHIU, S.-H. WANG*, S.H. CHEN, and W.-T. LI, Dept. of Biomedical Engineering, Chung Yuan Christian University, Taiwan, Taiwan.
Corresponding e-mail: shyhhau@cycu.edu.tw

Previous studies have shown that the effect of Amyloid-β(Aβ) on the induction of apoptosis could lead neuronal losses to the Alzheimer's disease. The stimulation by physical energy was found able to greatly diminish Aβ induced apoptosis. In this study, the effect of different ultrasonic intensities on the neuronal cells was explored. The experiments were carried out using such precursor neuronal cells as PC12 which was added with Aβ of a 20μM concentration during pre-cultured preparation. These cells were subsequently stimulated by a 20% duty cycle ultrasound of different energies ranged from 50 to 150 mW(SATA) for three minutes. The cellular response under ultrasound exposure was assessed, 7 times within 48 hours after those cells were stimulated, using the microscopic morphology, cell death measured by the typical MTT assay, and DNA fragmentation assay. Results showed that stimulations by ultrasound of lower and higher intensities than 100 mW may respectively diminish and increase the Aβ induced apoptosis compared to those of control groups. Morphological results also indicated that those cells stimulated by higher intensity ultrasounds tended to activate more cellular differentiations in PC12 discerned by morphological changes. This study demonstrated that the proliferation to diminish apoptosis and differentiation of neuronal cells could be regulated with the insonification of an appropriate ultrasonic intensity.

This work was supported by the National Science Council of Taiwan of the grants: NSC 92-2218-E-033-002 and NSC 93-2213-E-033-035.

P2C-13
DEVELOPMENT OF A 50MHZ OPTICAL FIBRE HYDROPHONE FOR THE CHARACTERISATION OF MEDICAL ULTRASOUND FIELDS.

P. MORRIS*[1], A. HURRELL[2], and P. BEARD[1], [1]University College London, Dept. Medical Physics and Bioengineering, London, UK, [2]Precision Acoustics Limited, Dorcherster, Dorset, UK.
Corresponding e-mail: psmorris@medphys.ucl.ac.uk

A wideband fibre optic hydrophone system based on a polymer film Fabry-Perot sensing interferometer (FPI) is being developed for the measurement of medical

ultrasound fields. The sensor's transduction mechanism is based upon the interferometric detection of acoustically-induced changes in the optical thickness of the polymer film. The advantage of this concept is that it offers the prospect of providing sufficiently small element sizes to avoid spatial averaging at frequencies in the tens of MHz range. This is because the sensitive region of the sensor is defined, to a first approximation, by the dimensions of the interrogating laser beam which is less than 10μm for a single mode fibre. Since the detection mechanism is all-optical, the sensor is also immune to electromagnetic interference. A further advantage is the low unit cost of production. This is made possible by vacuum depositing both the polymer film and reflective gold coatings that form the FPI mirrors directly onto the fibre tip, a process which is readily applicable to batch fabrication. It has been previously shown that this type of hydrophone can provide a bandwidth of 20MHz and a wideband noise equivalent pressure of 10 kPa (P Beard, A Hurrell, T. Mills, *IEEE Trans. Ultrason., Ferroelect., Freq.,Cont.* Vol 47, No1, p256-264, 2000). The concept has been advanced by making two key developments. Firstly, a new range of sensors with extended bandwidths, in excess of 50MHz, has been designed. This ensures that the sensors can accommodate the increased bandwidths produced by the elevated centre frequency scan heads that are becoming widely used in modern diagnostic ultrasound systems. Since this increase in bandwidth is achieved, in part, by decreasing the thickness of the polymer film to 10μm, the acoustic sensitivity is reduced. To compensate for this, the reflectivity finesse of the FPI has been increased by developing a numerical model of the transfer function and using it to identify the optimum values of the mirror reflectivities. Secondly, in order to develop a relatively low cost system with the necessary robustness for practical field use, the operating wavelength region of the sensors has been shifted to the 1540-1610nm range. This enables the rapidly tuneable, stable and inexpensive fibre-coupled C-L band lasers developed for optical telecommunications applications to be used as the interrogating source. It is considered that this type of fibre optic hydrophone offers several distinct advantages over PVDF needle and membrane hydrophones. Its small element size, EM passivity and potential disposability lead to a wide range of applications, from the laboratory characterisation of medical ultrasound sources, to *in-vivo* measurement of therapeutic and diagnostic ultrasound.

P2C-14

INTRAVASCULAR ULTRASOUND ARRAY FOR IMAGING AND ABLATION OF ATRIAL FIBRILLATION.

S. WONG*, G. SCOTT, S. CONOLLY, and D. LIANG, Stanford University.
Corresponding e-mail: shwong@stanford.edu

Atrial fibrillation (AF) affects 1% of the population and increases chances of stroke and death. Reentrant electrical pathways near the pulmonary vein often trigger AF. Clinical studies show that circumferential pulmonary vein ablation destroys these pathways, thereby eliminating AF. Currently, radiofrequency (RF) electrodes are used to treat such arrhythmias. Due to difficulties visualizing and

positioning the catheter against the atrial wall, procedures take over 7 hours and have <80% long term success. Fluoroscopic visualization produces projection images with little tissue contrast. Difficulties in registration between image and physical position as well as mechanical difficulties with catheter motion often mean RF burn patterns are discontinuous, leaving electrical pathways intact to trigger AF.

Intravascular ultrasound arrays can be precisely and electronically steered, making it easier to produce continuous burn patterns. Since ultrasound has good tissue contrast, the same array could image the region of interest to position the burn, eliminating registration issues. We propose a 20mm by 2mm intravascular linear ultrasound array on a 7 French catheter. We previously demonstrated that a 20mm by 2mm transducer could create temperature rises (>45C) and intensities (~250W/cm2) necessary for ablation. The paper will show the feasibility of imaging these HIFU lesions.

Instead of using an electronically focused array, we used a single element 10MHz transducer (APC International) with the same total area as the array. To focus the ultrasound, we used a cylindrical reflector (10 mm focal length). We positioned the tissue at the focal point of the reflector and angled the transducer to produce a slightly off-axis burn. The apparatus was submerged in water, and a 10MHz 20W CW signal was amplified by an (AR Kalmus) amplifier and applied to the transducer. A 5MHz SONOS 2500 imaging probe was placed along the direction of ultrasound propagation to view the burn in real-time.

Real-time imaging showed increasing echogenicity during lesion formation. Directly, after lesion formation (post-burn image), the burned region was, on average, 20-30% brighter than in the pre-burn image. The signal to noise ratio (SNR) in the post-burn images was 1.7-2.5. The lesion faded in brightness in 15-45 seconds, but sometimes remained slightly (~5%) brighter than the pre-burn image. In order to exploit the nonlinear effects of thermal heating and bubble formation during ablation, we tried using second harmonic imaging. We also observed increases of echnogenicity in the second harmonic images with intensity fading in 15-45 seconds. The contrast ratio between the burned region in the pre-burn and post-burn images was about the same as images using the fundamental frequency. However, SNR in the post-burn images was 2-3 times greater. These initial results are promising for HIFU lesion detection using ultrasound. We hope to produce brighter and longer lasting lesions with higher intensities at the focal point, which will induce more bubble formation and linear affects.

Thanks to John Pauly for his help and support.

Session: P2D

ELASTICITY IMAGING
Chair: H. Kanai
Tohoku University

P2D-1
ELASTOGRAPHIC IMAGING OF THE ACL-BONE INTERFACES IN VITRO.

E. KONOFAGOU*, J. SPALAZZI, and H. LU, Columbia University, New York, NY.
Corresponding e-mail: ek2191@columbia.edu

The anterior cruciate ligament (ACL) functions as a mechanical stabilizer in the tibiofemoral joint. Over 250,000 Americans each year suffer ACL ruptures and tears, making the ACL the most commonly injured ligament of the knee. A long term goal in tissue engineering has been to regenerate the ACL-Bone interface. To this end, an in-depth understanding of the structural and mechanical properties of the transition zone is needed in order to define relevant design parameters. Song et al. [1], using an Finite-Element Modeling (FEM) model of ACL, predicted that stress was transferred from the ligament to bone at the femoral insertion, and the magnitude of the stress was reduced near the tibial insertion compared to the ACL proper. However, experimental determination of the mechanical properties at the interface have been difficult due the small area (<1mm) involved and limited resolution of standard techniques. The current study uses elastography to characterize the functional properties of the interface under applied load. Tibiofemoral joints were mounted on an Instron MTS 858 Bionix Testing System. The ACL was loaded at different strain rates and tested to failure while RF data was collected at 5 MHz with a Terason (Teratech, Inc.) ultrasound scanner. For both tensile and compression testing, axial elastograms between successive RF frames were generated using cross-correlation and recorrelation techniques using a 3 mm window size and 80% window overlap [2]. When the ACL-Bone complex was tested in the tibial alignment on the MTS system, compressive strains were found to dominate at the tibial insertion. Compressive strains were observed in the ligament proper since the transducer was aligned with respect to the insertion during loading. The distribution of tensile and compressive strain varied as a function of strain rate during testing and between loading and unloading. Elastograms indicate that the strain distribution throughout the insertions is highly complex, with both tensile and compressive strain found at the insertion site. When tested under tension, the strain profile at the interface was predominantly compressive in nature, while tensile strains were found at the ACL as expected. These preliminary results agree with those of prior FEM model predictions [3]. In addition, a narrow band of high strain in the middle of the ACL was detected during compression that is considered to be a softer region of the ACL containing a highly collagenous structure. These preliminary results on ACL geometry and function indicate that elastography can provide important information in understanding the structure and function of both the ACL and the ACL-bone insertion. Ongoing studies focus on in-depth evaluation

of the mechanical properties and the structure-function relationship existing at the ACL to bone insertion.

[1] Song Y et al., J. Biomech.,37(3):383-390.

[2] Konofagou E. and Ophir, Ultras. Med. Biol. 24(8): 1183-1199, 1998.

[3] Matyas et al., J.Biomech., 28(2):147-157, 1995.

This study was supported by startup funds from Columbia University and by a grant from the Whitaker Foundation.

P2D-2
ESTIMATION OF PRESSURE-DISTRIBUTION EFFECTS UPON ELASTICITY IMAGING.

T. MATSUMURA*[1], R. SHINOMURA[1], T. MITAKE[1], H. KANDA[1], M. YAMAKAWA[2], and T. SHIINA[2], [1]Hitachi Medical Corporation, Kashiwa, Chiba, Japan, [2]University of Tsukuba, Tsukuba, Ibaraki, Japan.
Corresponding e-mail: matsumura@rd.hitachi-medical.co.jp

Background: We have already proposed the real-time strain imaging techniques (ca. 12 fps) for stable diagnosis in freehand ultrasound probe manipulation and image classification method for the breast tissue diagnosis (sensitivity of 87%, specificity of 91% and accuracy of 89% for 137 patients with breast diseases). In order to get objective diagnosis, most important problem is come from the fact that the strain image patterns were strongly depending on the magnitude and uniformity of the compression. To this purpose, we investigate the pressure-distribution effects on the elasticity imaging using the tissue-mimicking elastic phantom.

Methods: We manufactured the following 5 types of chemical gel phantom with different stiffness controlled by the concentrations of acrylamide [2]. All phantoms have the same shape of rectangular solid with dimension of 75 mm(Thickness)×100 mm(Lateral)×80 mm(Depth), and #1-#3 have uniform stiffness overall in the rectangular solids and #4-#5 include small rectangular solids with different stiffness from surroundings. Phantom#1, #2 and #3 are mimic fatty, mammary grand and fibrous tissues and contain 6%, 9%, 20% acrylamide, respectively. Phantom#4 and #5 are mimic fatty tissues which include inner rectangular solid (75 mm(T)×10 mm(L)×10 mm(D)) with mimic mammary grand and mimic fibrous tissues, respectively, at 20 mm depth far from the surface. The phantom stiffness was estimated from the distribution of pressure and induced strain using our elasticity imaging system (modified EUB-6500, external PC and pressure-sensing unit).

Results and Conclusion: (1) The Young's moduli of first three phantoms were estimated as 19±3 kPa, 56±8 kPa and 151±31 kPa, respectively. (2) In the case of phantoms#4 and #5, outer parts were estimated as 24±3 kPa and 28±4 kPa, and inclusion parts were measured as 64±38 kPa and 183±59 kPa, respectively. (3) For the special case of above phantoms, we applied non-uniform pressure (3 times difference between each lateral limits). Even in that case, we successfully reduced the effect of non-uniformity from 244% in strain imaging to 10% in elasticity imaging. In conclusion, we believe the pressure information reasonably

enables us to estimate the specific stiffness of the targets and establish the definite imaging diagnosis without depending on the manipulation manners.

We will present in this paper, the details about the elasticity estimation method and experimental results.

[1] T. Matsumura et al., Diagnostic results for breast disease by real-time elasticity imaging system, Proc. of 2004 IEEE Ultrasonics Symp., pp. 1484-1487, 2004

[2] K. Kawabata et al., Tissue mimicking phantom for ultrasonic elatography with finely adjustable elastic and echographic properties, Proc. of 2004 IEEE Ultrasonics Symp., pp. 1502-1505, 2004

P2D-3
FAST RECONSTRUCTION OF QUANTITATIVE TISSUE ELASTICITY IMAGE BASED ON MODIFIED 3-D FINITE-ELEMENT MODEL.

M. YAMAKAWA*[1], T. SHIINA[1], T. MATSUMURA[2], and T. MITAKE[2], [1]University of Tsukuba, Tsukuba, Ibaraki, Japan, [2]Hitachi Medical Corporation, Kashiwa, Chiba, Japan.
Corresponding e-mail: yamakawa@mibel.cs.tsukuba.ac.jp

For tissue elasticity imaging, strain imaging technique is being used in clinical tests. However, strain image corresponds to visualizing the qualitative information about tissue hardness, and is not a quantitative elasticity image. Therefore, in this study, we propose a method for reconstructing tissue hardness (Young's modulus) as quantitatively as possible from ultrasound data using 1-D array ultrasonic probe. In this method, we use a modified 3-D finite-element model, in which object is divided into finite elements as usual on an ultrasonic measurement plane, but it is not divided in the elevational direction. Using this modified 3-D model, it becomes possible to estimate Young's modulus only from the 2-D axial strain distribution and pressure distribution on the body surface. Moreover, since the modified 3-D model has 3-D structure, we can use the more realistic 3-D elastic equations and it is possible to estimate Young's modulus more quantitatively.

In addition, the simulation experiments showed that accuracy is the best when the thickness of this model is the same as the pressure width on the body surface.

We conducted the performance comparison experiments of the method based on the modified 3-D Model and the methods based on the 1-D model, 2-D model and 3-D model, respectively. Consequently, it is checked that the proposed method has 4.0 times precision better than the 1-D model method, 3.0 to 1.5 times precision better than the 2-D model method. (Young's modulus estimation error of modified 3-D model method is 19.2%.) Although the proposed method is slightly inferior to the 3-D model method in accuracy, the accuracy which is equal to the 3-D model method is acquired near the model center. Moreover, the proposed method can attain high-speed processing about 170 times faster than the method using 3-D model.

In addition, also in the phantom experiment, an appropriate result is obtained and it is checked that the proposed method is effective to an actual object.

P2D-4

AUTOMATIC MEASUREMENT OF REGIONAL ELASTICITY OF CAROTID ARTERY INTIMA-MEDIA COMPLEX.

H. HASEGAWA* and H. KANAI, Graduate School of Engineering, Tohoku University, Sendai, Japan.
Corresponding e-mail: hasegawa@us.ecei.tohoku.ac.jp

Artery wall elasticity and intima-media thickness (IMT) are useful markers for diagnosing atherosclerosis. However, the regional elasticity of intima-media complex (IMC) have never been measured. Therefore, we developed a method for imaging the regional elasticity by measuring changes in wall thickness due to heartbeat [Kanai, IEEE Trans. UFFC, 1996; Hasegawa, Jpn. J. Appl. Phys., 2001]. In this method, multiple points are assigned in the wall along each ultrasonic beam with intervals of 75 μm just before ejection of the heart. Then, the displacement of each point is estimated, and the change in thickness, Δh_{d0}, between two points is obtained from the difference between corresponding estimated displacements. The initial distance, $d0$, between two points is assigned to be 375 μm based on the duration of ultrasonic pulse. A spatial distribution of Δh_{d0} is obtained by shifting the combination of two points along each ultrasonic beam with a pitch of 75 μm. The regional elasticity is imaged from strains obtained by dividing Δh_{d0} by $d0$=375 μm. For healthy subjects, IMC is almost homogeneous and is defined by the region between two dominant echoes from the lumen-intima and media-adventitia boundaries (LIB and MAB). Thus, Δh_{d0} between each two points always becomes the change in IMT because only two dominant echoes from LIB and MAB contribute to displacement estimation. To obtain the actual strain, Δh_{d0} should be divided by IMT. In the present study, this error in strain estimation is corrected based on the homogeneity of measured Δh_{d0} and the automatically determined IMT, IMT_{auto}. **Method:** LIB is automatically determined by our method [Hasegawa, IEEE Trans. UFFC, 2004]. MAB is searched in the region deeper than the detected LIB and determined at the point showing the maximum gradient of echo intensity. When the elasticity image between determined LIB and MAB (=IMT_{auto}) is homogeneous (=homogeneous Δh_{d0}) and IMT_{auto} differs from $d0$=375 μm, the elasticity image is recalculated from strains obtained by dividing Δh_{d0} by IMT_{auto} (not $d0$). **Basic exp.:** A rubber plate was cyclically expanded in the longitudinal direction in a water tank. The theoretical value of the change in thickness caused by expansion was 2.5 μm for the entire thickness of 0.5 mm. Two dominant echoes from the near and far interfaces were found as well as echoes from LIB and MAB. Multiple points were assigned along an ultrasonic beam, and Δh_{d0} between each two points were measured. Mean±SD of Δh_{d0} was 2.3±0.2 μm. From these results, Δh_{d0} was homogeneous, and the entire thickness should be used to obtain the actual strain. It is also shown by the fact that measured Δh_{d0} coincided with the theoretical value for the entire thickness. **In vivo exp.:** By applying the method to a human carotid artery, IMT_{auto} was 0.46±0.03 mm (at 46 ultrasonic beams) and differed from $d0$=375 μm. It agreed well with manually determined IMT of 0.43±0.03 mm. Almost homogeneous elasticity was found along each of 46 beams (mean: 130~350 kPa, SD: 0.1~8.8%). Then, the elasticity was recalculated using IMT_{auto}, and the intima-media elasticity was finally determined to be 170~430 kPa.

P2D-5

OUR RECENT ULTRASONIC STRAIN-MEASUREMENT-BASED SHEAR MODULUS RECONSTRUCTION.

C. SUMI*, Sophia University, Tokyo, Japan.
Corresponding e-mail: c-sumi@sophia.ac.jp

We have been developing ultrasonic strain-measurement-based 1D, 2D, and 3D shear modulus reconstruction techniques [1] as diagnostic tools for various *in vivo* tissues, e.g., breast and liver. The strain tensor field is generated by spontaneous heart motion and/or externally applied pressure or vibration. We developed (i) a proper configuration technique for mechanical sources/reference shear modulus regions (materials) [2], (ii) a regularization-based implicit-integration approach utilizing *a priori* knowledge about tissue shear elasticity [2] which is quite robust with respect to unfortunate occurrence of improper configurations and inevitable strain measurement errors.

In this report, we review our developed 1D reconstruction methods. For 1D reconstruction, the calculated ratio of the strains generated in the direction of predominant deformation along the direction can be used as the final estimate of the target's shear modulus value at a normal position where no singularity occurs (change of the sign of strain or numerically infinitesimal absolute strain often occurs at stiff region) [3], and then 1D implicit-integration is performed only at the singular positions which substantially reduces computation time. For 1D reconstruction and 1D strain imaging, a stiff region and stress concentration regions in front of and behind a stiff region, and a soft region and low-stress regions in front of and behind a soft region are erroneously estimated to be softer and harder than the original, respectively [3] However, by setting the reference regions to pass through stress concentration regions and low-stress regions, even a 1D reconstruction can significantly reduce the erroneous artifacts [3]. However, with exception of the case in which reconstruction should be sufficiently regularized for monitoring of thermal treatment, the 1D reconstruction image and 1D strain image are often similar. However, needless to say that the absolute or relative shear modulus value can be directly read throughout a ROI from the reconstructed image of which erroneous artifacts are reduced and singularity is treated. The shear modulus distribution resulting from calculated ratio of the measured strains is also utilized as an initial estimate in 1D, 2D, and 3D implicit-integration. However, since the 2D and 3D methods require a special US data acquisition system to accurately measure the strain tensor field, the 1D techniques utilizing standard US imaging equipment is considered to be clinically useful.

The usefulness is verified by comparing the 1D reconstruction-based imaging to strain imaging for *in vivo* breast and liver. Summarizing, the shear modulus imaging is useful to provide in real-time quantitative information about tissue stiffness with high spatial resolution (< 0.8 mm). Strains at reference region should be stably evaluated. Empirically, low-pass filtering should be applied to inverse of shear modulus distribution. Implicit-integration yields an acceptable, stable reconstruction.

[1] Trans. on UFFC (in press).

[2] Trans. MI, vol. 17, pp. 419-428, 1998.

[3] IEICE Trans. on Fundamental, vol. E78-A, pp. 1655-1664, 1995.

P2D-6
EVALUATION OF SHIFT ESTIMATION TECHNIQUES FOR SPECTRAL-BASED ELASTOGRAPHY.

K. HOYT*[1,2], F. FORSBERG[2], and J. OPHIR[3], [1]Drexel University, Philadelphia, PA, [2]Thomas Jefferson University, Philadelphia, PA, [3]University of Texas Medical School, Houston, TX.
Corresponding e-mail: Hoyt@drexel.edu

Throughout the last fifteen years, elastography has emerged as an effective imaging modality for depicting local strain distributions in soft tissue. Despite exhibiting a high sensitivity for extracting strain information, conventional gradient-based elastographic techniques are known to be susceptible to decorrelation noise sources, which manifest by degrading the tissue displacement estimation process. In an alternative approach, spectral elastography functions by estimating local tissue strain directly from the relative shift between congruent sets of pre- and post-compressed power spectra and has been shown to be more robust than its time-domain counterpart. Despite promising results regarding spectral elastographic performance, computational complexity still constitutes a source of concern for real-time applications.

In this project, we compared the performance of various discrete spectral shift estimators for use in spectral elastography using a 1-D elastographic simulation in MATLAB, namely, the normalized cross-correlation (NCC), sum squared difference (SSD), and sum absolute difference (SAD). Additionally, most shifts encountered in spectral elastography are not exact integer values, and thus, require some form of interpolation strategy in order to increase the density of the samples. Though increasing the Fourier transform length will improve the accuracy of the shift estimator, this requires a large *N*-length Fourier transform and consequently is computationally burdensome since it essentially provides interpolated samples throughout the entire spectrum. Hence, in addition to the above, we investigated the computationally simple parabolic- and cosine-fit interpolation methods for subsample spectral shift estimation using simulations in MATLAB.

Results demonstrate that the SSD method exhibits no marked difference in strain sensitivity, dynamic range or elastographic signal-to-noise ratio (*SNRe*) when compared to the more computationally costly NCC. The SAD method, though computationally less burdening, failed to exhibit performance comparable to that of the NCC and SSD methods. Furthermore, subsample spectral shift estimation techniques using a cosine-fit interpolation method outperformed that of the parabolic-fit method in terms of reduced bias errors and subsample estimate standard deviations. The latter was further analyzed in this study due to computational simplicity, and thus, the role of spectral density was subsequently evaluated without and with parabolic-based subsample interpolation. Based on minimizing computational complexity, it is concluded

that a (low density) spectral SSD strain estimator coupled with parabolic-based subsample estimation is the preferred choice for spectral elastography.

This work supported by National Institutes of Health (USA) Program Project Grant P01-CA64597.

Session: P2E
NDE SIGNAL PROCESSING AND MODELING
Chair: J. Saniie
Illinois Institute of Technology

P2E-1
SPATIO-TEMPORAL DECONVOLUTION OF PULSED ULTRASONIC FIELDS RECEIVED BY A TRANSDUCER OF LINEAR APERTURE: A SIMULATION STUDY.

W. DJERIR[1], T. BOUTKEDJIRT*[1], M. O. SI-CHAIB[2], and H. DJELOUAH[1], [1]Faculté de Physique, Université des Sciences et de la Technologie Houari Boumediene, Algiers, Algeria, [2]Faculté des Sciences de l'Ingénieur, Université de Boumerdes, Boumerdes, Algeria.
Corresponding e-mail: tarek_boutkedjirt@hotmail.com

For the measurement of pulsed ultrasonic fields, the use of piezoelectric PVDF membrane hydrophones is recommended. However, at high frequencies, spatial averaging due to the latter aperture finite size and variations of their frequency response may affect the electric signal delivered. In this work, these spatio-temporal effects are inverted in order to reconstruct the pulsed ultrasonic field with higher spatial and temporal resolution. A solution to such an inverse problem has been proposed for harmonic fields, where, however, only spatial deconvolution had to be considered [Ultrasonics 39(2002) 631-648].

For the development of appropriate deconvolution procedures, the direct problem has been first studied. The pulsed pressure field radiated by a wideband 10mm-diameter planar transducer, with f_c = 2.25 MHz central frequency (λ_c: corresponding ultrasonic wavelength in water), has been simulated. The spatio-temporal impulse response of the receiving chain (hydrophone, cable, oscilloscope...) has also been calculated. The receiver was a 25 μm- thick PVDF membrane hydrophone. The receiving system was supposed to be linear and space- and time-invariant. The hydrophone output voltage could be obtained by convolving this response with the radiated pressure field and supposing a non-correlated white Gaussian corrupting noise.

The study concerned the critical transmitter ′near field′ and was restricted to a linear receiving aperture (Length *L*, width negligible as against *L* and the wavelength). The choice of such an aperture, which may be encountered in ultrasonic imaging systems, restricts the spatial domain studied to one dimension and allows addressing critical parameters influencing the deconvolution process.

The deconvolution of the hydrophone temporal impulse response by inverse filtering has leaded to excellent results for three signal-to-noise-ratios (SNR): 60, 40, and 20dB. In contrast, the spatial deconvolution could not be achieved by using a spatial inverse filter because of drastic noise amplification. This ill-posedness of the problem could be overcome by means of regularization procedures such as using a time-frequency dependent two-dimensional Wiener filter. The latter has been implemented with and without a-priori knowledge of the power spectral densities (PSD) of the sound pressure and of the noise. In the latter case, these quantities had to be estimated from the signal delivered by the hydrophone.

The study showed a strong dependency of the reconstruction quality upon SNR, hydrophone dimensions and axial distance z to the source. For an aperture of length L = 2.6 mm ~ $4\lambda_c$, placed on axis at z = 3 mm, correlation coefficients between the reconstructed pressure and the original one, r_{pp}, of 0.999, 0.986 and 0.655 have been obtained, for SNRs of 60, 40 and 20 dB respectively. For a greater aperture (L = 10.6 mm ~ $16\lambda_c$) and SNR = 40 dB, no useful results could be obtained at this distance (r_{pp} = 0.786). However, at greater axial distances good deconvolution results could be achieved (r_{pp} = 0.893 and 0.985 at z = 20 mm and 50 mm respectively).

P2E-2

EFFICIENT HARDWARE REALIZATION OF FREQUENCY-DIVERSE ULTRASONIC FLAW DETECTION USING ZERO-PHASE IIR FILTERS.

E. ORUKLU*, F. MARTINEZ VALLINA, and J. SANIIE, Illinois Institute of Technology, Chicago, IL.
Corresponding e-mail: orukerd@iit.edu

Ultrasonic imaging has been an essential tool for nondestructive testing and flaw detection in industrial applications. Often, ultrasonic data are acquired, analyzed and processed offline. Recently, there has been an increasing demand for the realization of real-time, online applications of ultrasonic flaw detection. In this study, we aim to address the increased computational demands of real-time ultrasonic data processing by developing an efficient frequency-diverse detection algorithm and architecture. The objective of frequency-diverse ultrasonic detection is to decorrelate clutter echoes and enhance the visibility of defects. In this respect, we have analyzed the frequency-diverse ultrasonic detection methods including Fast Fourier Transform (FFT) based Split Spectrum Processing (SSP) and order statistics processors. Essentially, the SSP method is the same as applying several bandpass FIR (finite impulse response) filters. Substantial computational savings can be obtained if the FIR filters are replaced by IIR (infinite impulse response) filters which involve a much lower number of coefficients with similar filtering characteristics. Our objective is to design IIR bandpass filters, and evaluate their performance in the SSP technique as an alternative. However, the design of IIR filters results in phase distortion which shifts the frequency dependant signal features. This drawback greatly deteriorates the detection performance of the designed IIR bandpass filters. Consequently, for protection against phase distortion, an IIR zero-phase filter

has been designed and presented. The design of the IIR zero-phase filter is performed as follows: first, time-reverse the discrete backscattered ultrasonic signal, then filter it with an IIR bandpass filter, time-reverse the output of the IIR bandpass filter, then filter it again by the same IIR bandpass filter. Analytically, it can be shown that the last output is not phase distorted. Our experimental and simulated results demonstrate that the performance of zero-phase IIR filters for flaw detection in the presence of high scattering clutter is as effective as the FFT based SSP method. For efficient hardware synthesis of the zero-phase IIR filters, a multiplierless implementation based on the primitive operator graph synthesis method has been developed. In particular, a reduced adder graph, RAGn, algorithm replaces the multiplication block of the IIR filter with a directed graph structure. In this structure, only primitive operator functions; shift and addition/subtraction operations are utilized which reduces the logic substantially. Given all the filter coefficients, the algorithm searches through the table and realizes the desired filter by finding common sub-expressions among the coefficients. The outcome is a minimal number of adders for a particular IIR filter implementation. A small number of coefficients inherent to IIR filters and optimal coefficient multiplier implementation using a minimum number of adders provide an optimal architecture suitable for real-time implementation of ultrasonic imaging applications.

P2E-3

APPLICATION OF THE EMPIRICAL MODE DECOMPOSITION TO THE ULTRASONIC ECHO-SIGNAL PROCESSING.

Z. QI*, Q. PEIWEN, L. QINGKUN, and C. TIANLU, Institute of Automatic Detection, Shanghai Jiaotong University, Shanghai, China.
Corresponding e-mail: zhangqi2004@sjtu.edu.cn

Ultrasonic detection is one of the most widely used techniques for nondestructive testing . The ultrasonic waves reflected or diffracted from flaws or boundaries can provide useful information on its integrity. But in ultrasonic nondestructive testing, as a basic testing data, the echo-signal of pulse reflection, is disturbed by electronic noise(such as thermal noise, digitalization noise), and structure noise. Because of these noises it is very difficult to identify the ultrasonic defect signal. Before it is analyzed, the echo-signal of pulse reflection must be denoised. This paper provides a new method based on the principles of empirical mode decomposition to reduce noise for enhancing the signal-to-noise ratio. First, the empirical mode decomposition method is introduced. According to the feature of the ultrasonic echo-signal the principle of the denoising is described. Second, the simulation ultrasonic echo-signal is decomposed by the empirical mode decomposition. Third, this method is applied to the real ultrasonic echo-signal.

The empirical mode decomposition method for analyzing nonlinear and non-stationary signals is first introduced by N.E. Huang et al (1998). With this decomposition method the complicated data are decomposed into a finite number of components, called intrinsic mode functions (IMF) and a residue. The decomposition method is adaptive. The original data can be reconstructed by the sum of the IMF components plus the residue. Each IMF component reflects

a different oscillation mode and with different amplitude and frequency content. The first IMF component has the highest-frequency content, frequency content decreases with increasing IMF component. The useful results can be obtained by analyzing every IMF component. Because Ultrasonic echo-signal is broad-band, narrow pulse signal, the energy of the original signal is concentrated in some IMF components after decomposition. Some IMF components are cancelled by judging every IMF's energy and other IMF components are added to reconstruct the signal.

Computer generated white Gaussian noise was added to the simulation ultrasonic echo-signal, SNR=9.12. Using empirical mode decomposition the simulation ultrasonic echo-signal is decomposed to 8 IMF and a residue. Reconstruction simulation signal is showed judging the energy of Every IMF component to choose some IMF components, SNR=14.67. The signal-to-noise ratio is enhanced clearly.

The real ultrasonic echo-signal is collected by experimental system of ultrasonic data acquisition. Ultrasonic echo-signal is decomposed into several IMF components and a residue. The signal-to-noise ratio is enhanced using this method and it is easy to identify the ultrasonic defect signal. In this paper wavelet decomposition and empirical mode decomposition are compared, the result shows that the empirical mode decomposition method is more adaptive.

P2E-4
A TECHNIQUE FOR ACCURATE TIME IDENTIFICATION OF NOISY AND OVERLAPPING ULTRASONIC NDT ECHOES.

C. TIANLU*, Q. PEIWEN, and L. HUAMING, Institute of Automatic Detection, Shanghai, China.
Corresponding e-mail: chentianlu@sjtu.edu.cn

Accurate arrival times of ultrasonic echoes are sometimes hard to achieve because of overlapping and low SNR. When ultrasonic testing is applied to a thin layer, multiple echoes of diminishing amplitudes due to reverberations of sound can be observed, often overlapping. When a crack locates in the dead zone of TOFD (Time-of-Flight-Diffraction) method (close to the surface), the overlapping of the crack tip diffracted waves and lateral wave is unavoidable. In addition, noise originating from both the measurement system and sample material also increases the difficulty of accurate time identification.

Popular methods used to estimate ultrasonic NDT echo arrival time are mainly based on cross-correlation and wavelet transform. Their performances are limited by or dependent on noise pattern, reference signal or basic wavelet function. A new identification technique is proposed to estimate accurate arrival times of overlapping echoes in the presence of noise. Firstly, decompose an ultrasonic signal into several intrinsic mode functions (IMFs) by modified Empirical Mode Decomposition (EMD, a time-series processing technique proposed by NASA in 1998). Then, reconstruct a new signal with high SNR and enhanced flaw information using selected IMFs. Finally, get the envelope of the reconstructed

signal by Hilbert transform. The peaks of the envelope denote the arrival of corresponding echoes.

EMD is defined by an algorithm and is fully data driven. Therefore, there is no need for a reference signal or a wavelet function, no restriction to noise pattern. Modified EMD algorithm for ultrasonic signal is presented in detail. The IMF selection and signal reconstruction strategy is described by an example. Frequency and energy are major criterions.

Two kinds of simulated and experimental signals are selected to investigate the performance of the time identification technique: signals containing several overlapping echoes, and relatively noisy signals. The technique can identify the arrival times of all echoes effectively if only the difference of their decay factors and the signal SNR are larger than the threshold value. For the raw TOFD signals of eighty vertical cracks (made by EDM) in two thin steel plates (8mm), the time resolution is 0.1us. The average error is 0.08us. The dead zone of TOFD method is reduced to 2.0mm under the surface. The speed, complexity, adaptability and accuracy of this technique are analyzed and compared with wavelet method briefly.

This work is partially supported by National High Technology Research and Development Program of China (863 Program) #2001AA602021

P2E-5
A NEW ULTRASONIC ASCILLOSENSOR AND ITS APPLICATION TO EXTRACTION OF SLEEP STATE.

Y. KAMOZAKI*[1], S. KOBASHI[1], K. KONDO[1], Y. HATA[1], T. SAWAYAMA[2], and K. TANIGUCHI[3], [1]Graduate School of Engineering, University of Hyogo, Hyogo, Japan, [2]New Sensor Incorporated, Hyogo, Japan, [3]Kinden Corporation, Kyoto, Japan.
Corresponding e-mail: er05t015@steng.u-hyogo.ac.jp

The vibration of human vital activity has usually 10Hz or less. The sensor that effectively detects this vibration by high sensitivity is needed in the field of medicine and nursing. We propose an extraction system of sleep state using a new ultrasonic oscillosensor. This sensor consists of part of a sensor and a converter (included an ultrasonic pulsar receiver). The sensor has a cylindrical tank of 26mm diameter filled with water, and an ultrasonic probe (Center frequency: 2MHz) under the bottom of the tank. This sensor detects the vibration of the water surface by obtaining the echo signal reflected from the water surface. Since the sensor is set to the under bar of the bed of a human, we can non-invasivily extract the human vital signal. A conventional vibration sensor is difficult to detect the vibration for all axis of X, Y and Z. However, this sensor can detect all axis low-frequency vibrations. In the addition, the conventional acceleration sensor requires low S/N and velocity sensor has large size in the 10Hz or less band. This sensor has 30dB in the resonance frequency and small size (26 diameter $\times$ 10mm), and has a linear characteristic in a band being lower than the resonance frequency. The resonance frequency of this sensor is 6.8Hz in spite of longitudinal and transverse vibration. This resonance frequency can freely fixed by changing the diameter of this sensor. We propose an extraction

system for counting flop-over and sleeping time of a human by using this sensor. The vibration of the human is converted to amplitude value of the ultrasonic wave (sampling interval 20msec). The amplitude values are quantized to 1024 levels. The difference value between the maximum and the minimum is provided to the personal computer of our system. In the preliminary study, we compare the sleep depth obtained by electroencephalograph with the values of the sensor. Our system can then detect the sleep state as the continuous low signal values and detect the flop-over as the high values for a short time.

We apply our method to a healthy volunteer and two patients (we received the informed consent from the patients). In the experimental results, we extracted the number of flop-over at the 13% error rate and extracted the sleeping time at 3.5% error rate for the healthy volunteer. These error rate are calculated by comparing our result with the truth values. For the two patients one is insomniac and the other is not so, the extracted number of flop-over in the sleeping period was 2.13 times/day and the sleeping time was 3.26 hours for the insomniac. While, the extracted number is 15.25 time/day and the sleeping time was 8.62 hours for the other. Thus, we can successfully extract these sleeping states by the new ultrasonic oscillosensor.

This work was supported in part by the fund from the Foundation for Biomedical Research and Innovation.

P2E-6

PATTERN RECOGNITION METHOD FOR ULTRASOUND-BASED PIDS.

J. PERALTA*, M. CASAS, and A. RUGGERI, Universidad Nacional de Santiago del Estero, Santiago del Estero, Argentina.
Corresponding e-mail: joper38@yahoo.com

Background. We present a way to process ultrasound echoes coming from emitters and detectors driven by microcontrollers, as in a Perimeter Intruder Detection System proposed by two of us in an earlier paper. That is a string of spaced but otherwise serially communicated microcontrollers, driving emitters and receivers which use radar effect, and surveying receiver outputs sequentially. All support a common code for pattern recognition and serial communication. Adequate geometrical configuration of the emitter beam net conforms a redundant source of information.

Methods. Each microcontroller deals with a large number of echoes. Patterns, typified by echoes number and time elapsed since emision of ultrasonic signal, differ for each receiver, since these are at different points and oriented in different directions to conform the net. A Master sends sampling orders and the process is repetitive in time: in steady state situation, units being all equally coded, the pattern of echoes seen by one receiver in a given interval of time is always the same, but different to the observed by others. Once an ultrasound wave pulse is emitted, just one receiver is enabled to detect its echoes during a certain interval of time. Its driving unit runs a pattern analysis based on some echoes, (for ex. 2nd, 4th, 7th and 8th). Results will be different for each unit, since in each case those echoes come from different fixed objects. Late echoes from non-associated

emitters deserve no further considerations, the pattern is repetitive for a given receiver. If a change in relation to the no-intruder, steady state situation, is detected at any unit in the string, a coded signal is communicated to the next. This does a similar task, and after that it retransmits that received signal and its own produced signal to its next neighbour, the third of a triad. According to the result of the pattern analysis made with the three coded data, the decision of triggering an alarm is taken there. Then a very complex pattern is reduced to simpler patterns sequentially analysed.

Conclusions. Our Lab prototype worked at 40 kHZ. A microcontroller enabled reception during 20 ms., determining echoe arrival times and total number of echoes. Trials were made with 10 wavelengths pulses and 20 ms detection time. Echoes were selected by software according to arrival time; this selection is a practical problem, as it depends on space configuration in which the PIDS is working and the geometry of the ultrasonic net. First results indicated that three or four echoes characterized by their time of arrival, properly selected, are sufficient and may be adopted as the steady pattern observed by the receiver. Total number of echoes arriving within the 20 ms may also be included in the steady state pattern. Significant departures from that pattern are observed when an intruder is approaching the PIDS. Work is in progress in the subject of resolution of the method, and to obtain preferential transport speed for an emergency alarm signal and coordinates.

P2E-7

NEW INSIGHTS AND EXTENSIONS OF SPLIT-SPECTRUM ALGORITHMS FROM AN OPTIMUM DISTRIBUTED DETECTION PERSPECTIVE.

I. BOSCH*, L. VERGARA, and R. MIRALLES, Departamento de Comunicaciones, Universidad Politécnica de Valencia, Valencia, Spain.
Corresponding e-mail: lvergara@dcom.upv.es

Split-spectrum (SS) algorithms have been extensively applied to the suppression of grain noise in ultrasonic NDE. Basically, they take advantage of the tuning frequency sensitivity of grain noise, when it is filtered (directly or through frequency domain transformations) by band-pass filters tuned along the grain noise bandwidth. A typical problem where suppression of grain noise is a must, is the automatic detection of echoes due to inner flaws or to other reflectors, embedded in significant levels of grain noise background. The spectral overlapping between the signal (echoes of reflectors) and the grain noise, the lack of knowledge of the signal waveform and the often unsuitability of the Gaussian assumption for the grain noise distribution, imply serious difficulties to the use of optimum matched filter detectors. Thus SS algorithms are used in a pre-processing step to suppress grain noise, and then automatic detection is applied to the “clean” record. Unfortunately, the non-linear nature of SS makes the optimum design of the detector a very difficult problem.

In this paper we approach SS automatic detection from a distributed detection perspective. The basic idea is to implement an energy detector at the output of every band-pass filter, and then to fuse all the detections to generate a final

decision for every time index. The individual detectors are optimally designed by using the subspace matched filter theory (briefly, every band-pass filter is equivalent to the projection into a tuned subspace). The fusion is also optimized by using the well established theory of distributed detection. We call it split-spectrum distributed detection (SSDD). The main contributions of the paper are:

•Proposal of SSDD algorithm for optimum automatic detection of echoes in grain noise background, based on matched subspace and distributed detection theories. We include in then paper the necessary analytical work leading to the equations for fitting a required probability of false alarm and evaluating the (maximized) probability of detection.

•It can be easily verified that SSDD includes as particular cases the well-known minimization and order statistic SS algorithms, when adapted to the automatic detection problem. We also include analytical work showing that optimality is strictly achieved only when grain noise disappears in the presence of signal, thus giving insights into the adequate conditions for the SS based detectors to correctly work. This provides an explanation of the irregular behaviour of SS algorithms observed thus far.

•Comparisons, both analytically and by simulation, with just a gating of the original record under analysis are also given.

•The proposed detection algorithms are applied to the analysis of the ultrasonic NDE of the inner layer structure of the vault of a Spanish basilica, to verify the adequate consolidation of layers after restoration. The results show the interest of the proposed new detection schemes.

This work has been supported by Spanish Administration under grant TIC2002-4643 and by Polytechnic University of Valencia under grant 2003-0554.

P2E-8
AIRBORNE ULTRASOUND DATA COMMUNICATIONS: THE CORE OF AN INDOOR POSITIONING SYSTEM.

S. HOLM*[1,2], [1]University of Oslo, Oslo, Norway, [2]Sonitor Technologies, Oslo, Norway.
Corresponding e-mail: sverre@ifi.uio.no

Ultrasound communications is usually considered to be inferior to radio communications due to its short range and low data rate. Despite this, in nature bats are highly successful in utilizing ultrasound for ranging and navigation. Ultrasound with frequencies just above the audible range also shares most properties with human speech, the communications system which by far has the largest 'installed base' of all. This paper describes an airborne ultrasonic communications system in the 40 kHz range that is used as the core of an indoor positioning system.

Indoor positioning is done by the principle of confinement, not by triangularization as in most RF systems. Confinement positioning uses the insulating properties of walls, so that if an ultrasonic tag is detected it has to be localized in that room. This interfaces well with humans as we find it more natural to position objects

indoors by reference to rooms rather than x,y,z-coordinates. Besides, the positioning is virtually error free unlike RF systems which sometimes can place a tag in an adjacent room. Applications are in e.g. tracking of valuable equipment in hospitals and industrial environments.

Several pilot projects have already been undertaken using the main hardware components which are a tag and a detector. The tag transmits its own unique ID and a multiple access method has also been developed in order to avoid collisions between simultaneous tags. The detector uses digital signal processing to cope with the acoustic environment and its noise, reverberations and Doppler shift and communicates its results over Ethernet or WLAN.

The attainable range for the ultrasonic link is 10-20 meters and by making a comparison with the range for speech and for the Silbo whistling language, we find that the range predictions are consistent with our experience. The channel efficiency of the system is found to be comparable to human speech which also has to deal with a similar acoustic environment. This comparison is done by using the Shannon channel capacity theorem. Finally the output energy of the system is compared to currently accepted exposure limits to ultrasound and found to be safe.

P2E-9
BLIND NOISE CANCELLATION IN ULTRASONIC NDE USING RPS AND ICA: COMPUTER SIMULATION.

Q. LIU*, P. QUE, H. GUO, and S. SONG, Institute of Automatic Detection, Shanghai Jiaotong University, Shanghai,China.
Corresponding e-mail: liuqingkun@126.com

In ultrasonic nondestructive evaluation (NDE), flaw signals are often contaminated by noise. This affects seriously the analysis and identification of flaw signals. Therefore some kind of signal processing technology needs to be applied. Several signal processing techniques have been developed over the years, including split-spectrum processing, wavelet transform, adaptive filtering, wiener filtering et al.

Although much research has been done about noise cancellation in ultrasonic NDE, little work has been done using reconstructed phase space (RPS) and independent component analysis (ICA) on this subject. This paper develops a new framework for blind noise cancellation using RPS and ICA in ultrasonic non-destructive evaluation (NDE). First a RPS is constructed out of a series of delay vectors from the measured ultrasonic signal. The reconstructed phase space (RPS) contains the information we require, but mixed form which therefore needs to be deconstructed. Second independent component analysis (ICA) is performed on the RPS to deconstruct the single channel ultrasonic signal into its underlying ultrasonic signal component and other noise components. Finally blind noise cancellation is realized by identifying and reconstructing the component of ultrasonic signal.

To demonstrate the utility of the proposed framework for blind noise cancellation, much simulation is performed. The ultrasonic signals can be simulated by Gaussian echo model. And then the noise ultrasonic signal can be simulated by

the mixture of simulated ultrasonic signal and white Gaussian noise (WGN). The denoising performance of the proposed framework is tested under different noise level and compared with wavelet transform. Simulation results show that this method not only performs as well as wavelet transform in SNR enhancement but also can restore the ultrasonic signal waveform with fewer detail loss. In particular the noise ultrasonic signal is decomposed into noise free ultrasonic signal component and other noise components using RPS and ICA. Therefore the denoising process is very intuitive. This is the main difference of the proposed method with the present denoising method in ultrasonic NDE.

Session: P2F

BAW PIEZOELECTRIC FILMS

Chair: A. Ballato

U.S. Army

P2F-1

ASSESSMENT OF THE PIEZOELECTRIC RESPONSE OF SPUTTERED ALN FILMS BY X-RAY DIFFRACTION.

E. IBORRA*, A. SANZ-HERVÁS, M. CLEMENT, L. VERGARA, J. OLIVARES, and J. SANGRADOR, Depto. Tecnología Electrónica, Universidad Politécnica de Madrid, Madrid, Spain.
Corresponding e-mail: eiborra@etsit.upm.es

The good piezoelectric characteristics of AlN, along with its chemical stability and compatibility with CMOS technology, have allowed to develop applications such as SAW, BAW, and MEMS devices. For these applications the material must be oriented with the c axis perpendicular to the substrate, as its unit cell is polar along that axis. This requisite is usually assessed through an XRD pattern, which must display (00•2) texture with good intensity and narrow rocking-curve (r-c). Any polycrystalline polar material (ZnO, GaN, AlN, etc.) can contain grains with opposite piezoelectric polarities along the c axis. In this case, the net piezoelectric dipole can be very weak despite the material being good from a conventional XRD standpoint. TEM direct observations or AFM topography after selective wet etching have been employed by some authors to observe the presence of grains with opposite polarities. A simpler method would be very convenient, especially for the routine evaluation of the material.

In this work we report a method for the assessment of the piezoelectric response of AlN films based on the correlation observed between the piezoelectric response and the presence of the 10•2 reflection in conventional $\Theta/2\Theta$ XRD patterns. The AlN films were deposited on bare and Pt-covered Si (100) wafers by reactive RF sputtering under various deposition conditions to achieve material of different crystal quality. We recorded XRD $\Theta/2\Theta$ patterns and r-c around the 00·2 reflection. To evaluate the piezoelectric response, SAW filters were made using Cr IDTs on the AlN films. The electromechanical coupling coefficient k^2 was deduced from the scattering parameters (S_{ij}) through computations based

on a circuital model. All AlN films were (00•2)-textured with Θ/2Θ FWHMs of the 00•2 peak between 0.08° and 0.2° and r-c FWHMs between 1.5° and 15°. Some films also displayed a very weak 10•2 reflection with an intensity below 0.5% of the 00•2 peak intensity. Although high values of k^2 are usually associated to a narrow r-c, we have not found a clear correlation between both magnitudes. For example, many of our samples with r-c FWHM larger than 5° yielded values of k^2 higher than 1.5%. However, some samples with very narrow rocking curves (1.5°-3°) exhibited poorer values of k^2. On the other hand, we have found in many samples a clear relation between low k^2 values and the presence of the 10•2 reflection in the XRD patterns. Samples with an intense 00•2 peak and narrow r-c that exhibited a distinct 10•2 reflection provided a negligible piezoelectric response. The presence of the 10•2 reflection seems, therefore, to signal the occurrence of some kind of defect that is associated with the existence of grains with opposite polarities. The analysis of the XRD pattern around the 10•2 reflection is thus a good method to identify AlN layers with poor piezoelectric response. The conventional criterion based only on the width of the r-c is not completely reliable, as it may reject good piezoelectric material or validate films with poor piezoelectric response.

P2F-2

RESONANT ELECTROMECHANICAL DEVICE FABRICATION WITH NEW THIN FILM MATERIALS.

J. MCPHILLIPS*[1], N. DONNELLY[3], M. GREGG[1], R. BOWMAN[1], A. ABRAR[4], G. MCROBBIE[2], K. KIRK[2], D. CORNEZ[2], and S. COCHRAN[2], [1]Queens University, Belfast, Belfast, Northern Ireland, UK, [2]University of Paisley, Paisley, Scotland, UK, [3]Pennsylvania State University, State College, PA, [4]Pakistan Institute of Engineering and Applied Sciences, Islamabad, Pakistan.
Corresponding e-mail: coch-ph0@wpmail.paisley.ac.uk

There is significant interest in thin film piezoelectric materials for high frequency bulk acoustic wave resonators for applications, for example, in mobile communications systems. The characteristics of relevant conventional materials such as AlN are well known. However, quite poor piezoelectric properties, such as d33 of the order of 5 pm/V, are typical of these materials. In the field of bulk piezoelectric materials, single crystals such as Pb(Mg1/3, Nb2/3)O3 - xPbTiO3 (PMN-PT), offer much higher performance and thin films of such materials are also viable. In this paper, work on AlN and PMN-PT thin films is described. AlN has been deposited by a low-temperature sputtering method and PMN-PT with pulsed laser deposition. Basic characterisation of the electromechanical and acoustic behaviour of thin film structures of Au/PMN-PT/La0.5Sr0.5CoO3 on LaAlO3 single crystal substrates has shown measured characteristics including dielectric constant up to ~2000, d33 ~100 pm/V and Q33 0.01 - 0.09 C^-4 cm^2 [1]. For further comparison of the materials, both have been configured to allow the composite resonator characterisation technique of Zhang et al [2] using spacing of parallel resonant frequencies (SPRF) to be explored. The SPRF technique takes into account that the films are not self supported and that their properties are dependent on the substrate. AlN films up to 6 μm in thickness have been observed in operation at frequencies around 800 MHz on glass and

PMN-PT films up to approximately 1 μm in thickness around 2 GHz on MgO. Using software based on a frequency-domain matrix formulation of solutions of the one-dimensional wave equation and the ANSYS finite element analysis packages, good correlation has been found with appropriate material parameters, allowing further exploration of the suitability of PMN-PT for thin film device fabrication and direct comparison with AlN.

[1] N.J. Donnelly et al, J. Appl. Phys. vol. 93, pp. 9924-9 (2003)

[2] Y. Zhang et al, IEEE Trans. Ultrason. Ferroelect. Freq. Contr., vol. 50, pp. 321-333 (2003)

P2F-3
ZNO FOR THIN FILM BAW APPLICATIONS.

J. MOLARIUS*[1], T. PENSALA[1], A. NURMELA[1], M. YLILAMMI[1], and A. DOMMANN[2], [1]VTT Technical Research Centre of Finland, Espoo, Finland, [2]CSEM Centre Suisse d'Electronique et de Microtechnique SA, Neuchâtel, Switzerland.
Corresponding e-mail: jyrki.molarius@vtt.fi

Thin film BAW (Bulk Acoustic Wave) devices used for rf-bandpass filters for mobile phone applications have been most commonly made from aluminium nitride (AlN). However fair amount of research has also been devoted to zinc oxide (ZnO). In this work ZnO was studied as thin film piezoelectric material for BAW applications.

The aim of this work has been to develop the rf-sputtering process of ZnO in order to achieve highly piezoelectric thin films. This requires high purity, high (0001)-preferred orientation (ZnO has hexagonal crystal structure), and high resistivity film with fine columnar microstructure perpendicular to the substrate. The ZnO films have been deposited using reactive magnetron sputtering from either metallic zinc target or compound zincoxide target in Ar/O_2 atmosphere. Metallic target was used in dc sputtering whereas compound target was utilised in rf-mode (13.56 MHz).

As a test vehicle to measure the piezoelectricity of the ZnO films resonators were fabricated using standard microelectronics photolithography, deposition and etching techniques on 100 mm Corning glass or silicon wafers. Resonators and filters were SMR type (solidly mounted resonator), where the acoustic quarter wavelength mirror consisted of high and low acoustic impedance materials, which were either three pairs of Mo and SiO2 or two pairs of W and SiO_2, respectively. Mirrors were aimed at 1 to 2 GHz frequencies.

Material properties of the ZnO films have been studied by x-ray diffraction (including rocking curve), scanning electron microscopy, and atomic force microscopy. Resonators were measured from 0.5 to 6 GHz using network analyser. The influence of the film deposition process parameters as well as technological boundary conditions (like sputtering system) on film properties will be discussed.

In X-ray rocking curves the FWHM of ZnO (0002) peak (0,4°) indicated very good orientation. In case of AlN Löbl[1] showed that the good orientation of the piezolayer correlates to high coupling coefficient of the resonators. Indeed the

highest acoustic coupling coefficient, kmat = 0,282 (k^2 = 7,95%) at 1.6 GHz, for thin film ZnO was achieved. Also a passband filter fulfilling the complete E-GSM specifications was fabricated using ZnO piezoelectric in the resonators[2]. Although these excellent results were achieved with ZnO piezolayer the repeatability and stability of the sputtering process never fulfilled massproduction requirements. These and other aspects of the processing will be discussed in detail in the paper.

References:

1. Löbl H.P., et al., Materials Chemistry and Physics 79 (2003) 143 and Materials Science and Engineering B (2002).

2. Kaitila J., Ylilammi M., Molarius J., Ellä J., Makkonen T., IEEE Ultrasonics Symposium (2001) 223.

P2F-4

CONTROL OF EFFECTIVE ELECTROMECHANICAL COUPLING COEFFICIENT AND QUALITY FACTOR INA 1.8 GHZ RANGE FILM BULK ACOUSTIC WAVE RESONATOR FEATURING MULTI-LAYERS USING ZNO, SIO_2 AND AL_2O_3 THIN FILMS.

M. TAKEUCHI*, H. YAMADA, H. KAWAMURA, Y. YOSHINO, T. MAKINO, and S. ARAI, Murata Mfg. Co., Ltd., Yasu City, Shiga Pref., Japan.
Corresponding e-mail: takeuchi@murata.co.jp

Both effective electromechanical coupling coefficient (k_{teff}^2) and Quality factor (Q factor) has been controlled in 1.8GHz range film bulk acoustic wave (BAW) resonator featuring a multi-layers using ZnO , SiO_2 and Al_2O_3 thin films. The ZnO / SiO_2 / Al_2O_3 and ZnO /Al_2O_3 / SiO_2 structure BAW resonators were designed on secondary harmonics at about 1.8GHz by finite element method (FEM). The ZnO and SiO_2 thin film were prepared by RF magnetron sputtering. Deposition conditions of the ZnO thin film were optimized for c-axis orientation. Under the optimized conditions the ZnO and SiO_2 thin films have a compressive stress of -100MPa and -150MPa, respectively. The Al_2O_3 thin film was formed by electron beam evaporation and has a tensile stress of +380MPa. Combination of the ZnO and SiO_2 thin films having compressive stress with the Al_2O_3 thin film having tensile one reduces the total stress of a membrane composed of ZnO, SiO_2 and Al_2O_3 thin films. So the membrane has been able to avoid deformation and destruction by the stress. Compared the ZnO / SiO_2 / Al_2O_3 structure with the ZnO /Al_2O_3 / SiO_2 structure, calculations by FEM indicated that the ZnO / SiO_2 / Al_2O_3 structure BAW resonator had a larger k_{teff}^2, but the ZnO /Al_2O_3 / SiO_2 structure had a larger Q. Our experimental results agree with the calculation: The ZnO / SiO_2 / Al_2O_3 structure BAW resonator has the Q of 600 and the k_{teff}^2 of 5.0%. The ZnO /Al_2O_3 / SiO_2 structure has the Q of 900 and the k_{teff}^2 of 4.0%. The order of the SiO_2 and Al_2O_3 thin films under the ZnO thin films has controlled k_{teff}^2 and Q of BAW resonators. We focused on acoustic impedance calculated from young modulus and density of materials. Since acoustic impedance of the SiO_2 thin film is smaller than those of the ZnO and Al_2O_3 thin films, reflection of

the acoustic wave at the interface between the ZnO and SiO_2 thin film works for elastic energy trap in the ZnO thin film. Amplitude of the ZnO thin film of the ZnO / SiO_2 / Al_2O_3 structure estimated by FEM at the resonant frequencies was larger than that of the ZnO /Al_2O_3 / SiO_2. The elastic energy that existed in the ZnO thin film of the ZnO / SiO_2 / Al_2O_3 structure was larger than that of the ZnO /Al_2O_3 / SiO_2 structure. So the k_{teff}^2 in the ZnO / SiO_2 / Al_2O_3 structure is larger than that in the ZnO /Al_2O_3 / SiO_2. These results suggest acoustic impedance of materials and location of elastic energy trap caused by the difference of them are important in BAW resonators design.

P2F-5
ELECTROMECHANICAL COUPLING COEFFICIENT K_{15} OF (11-20) TEXTURED ZNO FILMS.

T. YANAGITANI*, N. MISHIMA, M. MATSUKAWA, Y. WATANABE, and T. OTANI, Doshisha University, Kyotanabe, Kyoto, Japan.
Corresponding e-mail: etd1105@mail4.doshisha.ac.jp

Recently, there has been an explosion of interest in longitudinal mode FBARs using (0002) textured ZnO or AlN films. In contrast, the (11-20) textured ZnO films allow shear mode FBAR with many potential advantages. For instance, the shear mode FBAR has half lower TCF (Temperature coefficient of Frequency) owing to the small temperature coefficient of c_{44}. Furthermore, the electrode area of shear mode FBAR is half smaller than the longitudinal mode FBAR for the same operating frequency. This results in smaller device package. In previous research, we have obtained (11-20) textured ZnO films where crystallites c-axis are unidirectionally aligned in the substrate plane[1]. These films are formed without epitaxial technique using a conventional RF magnetron sputtering apparatus. In this study, we have succeeded in fabricating (11-20) textured ZnO films which have high electromechanical coupling coefficient k_{15}. The thickness of the piezofilms should be uniform in the electrode area for the accurate measurement of resonant spectrum. To obtain ZnO films with uniform thickness, the substrate was moved backward and forward using a vacuum motorized stage while sputtering deposition.

Sample (A) and (B) were prepared with different conditions to form different crystallites orientation. Piezofilm thickness of the sample (A) and (B) were 8.0μm and 9.5μm, respectively. The crystallite orientation of the films was investigated by an X-ray diffractometry. The phi-scan pole figure analysis and the ω-scan rocking curve yield quantitative data on the extent of the crystallite alignment in the substrate plane direction and normal direction, respectively. The full width half maximum (FWHM) of ω-scan rocking curve of the sample (A) and (B) were 1.7 °and 3.0°. FWHM of phi-scan distribution curves of (11-22) poles of (11-22) pole figures were 19.8° and 20.5°, respectively.

Finally, the electromechanical coupling coefficient k_{15} of (11-20) textured ZnO was first determined, considering the structure of the over-moded resonators consisting of Cu electrode film / (11-20) textured ZnO piezofilm / Al electrode film / quart substrate. The procedure of determining electromechanical coupling coefficient was followed by the resonant spectrum method [2]. The real part of Z_{11}

and Y_{11} of the over-moded resonator were measured using a network analyzer (E5071B Agilent technology) with a microwave probe (Picoprobe GGB Industries). No longitudinal mode responses were observed at shear mode resonant frequency. Using SPRF (spacing of the parallel resonant frequencies) and k^2_{eff} distribution curves as well as data of each layer, k_{15} of the (11-20) textured ZnO films were determined. k_{15} of sample (A) and (B) show 0.23 and 0.22, respectively. These values were 88% and 85% of the reported value of single crystal ZnO (k_{15}=0.26). To confirm the validity of the obtained k_{15}, the SPRF and k^2_{eff} distribution curves were simulated. The simulated results show good agreement with the experimental results.

1) T. Yanagitani et al., IEEE Trans. Ultrason, Freq Contr. in press.

2) Y. Zhang et al., IEEE Trans. Ultrason, Freq Contr, vol.50, No.3, pp.321-333, 2003.

P2F-6

HIGHER-ORDER SHEAR MODE FBAR USING POLARIZATION-INVERTED LAYERS OF (11-20) TEXTURED ZNO FILMS.

Y. MIYAMOTO*, T. YANAGITANI, M. MATSUKAWA, Y. WATANABE, and T. OTANI, Doshisha University, Kyotanabe, Kyoto, Japan.
Corresponding e-mail: dte0140@mail4.doshisha.ac.jp

The temperature characteristics of FBAR (Film Bulk Acoustic Resonator) are always required to be highly stable. Temperature coefficients of stiffness constants c_{11} and c_{44} of single crystal ZnO are -1.12 and -0.7 [$\times 10^{-4}$/°C], respectively. Estimated temperature characteristics of longitudinal mode resonator and shear mode resonator using ZnO piezofilms are approximately -62 and -35 [ppm/ °C], respectively. This result indicates that the shear-mode is more suitable for resonator. Without epitaxy we have succeeded in fabricating ZnO films where crystallites c-axis is unidirectionally aligned in the substrate plane [1)]. These ZnO piezofilms are (11-20) textured and enable to realize shear mode FBAR.

On the other hand, the high frequency resonator can be achieved by using second-order mode resonance. Nakamura et al. have reported second-order thickness-mode resonator using an inversion layer of $LiNbO_3$ plate [2)]. We have then first fabricated a second-order mode FBAR consisted of two layers of (11-20) textured ZnO piezofilm. The polarization directions of upper and under layers are opposite each other. Consequently, we could fabricate second-order mode resonator with twice as higher resonance frequency as fundamental order mode resonator. The actual structure of the film is: Cu electrode film / upper (11-20) ZnO piezofilm / under (11-20) ZnO piezofilm / Cu electrode film / quart substrate (25×25×0.8 mm).

(11-20) textured ZnO piezofilms were deposited by a conventional RF magnetron sputtering apparatus. For the uniform thickness, the substrate was moved backward and forward while sputtering deposition. FBAR was then fabricated by peeling off the film layers from quart substrate. Cu electrode film should be thin, however, a thick electrode film was deposited to peel off the piezofilm from

the substrate. Film thickness of the upper electrode film, upper ZnO piezofilm, under ZnO piezofilm and the under electrode film are 0.2, 2.2, 1.8 and 1.1μm, respectively. The input admittance of the sample was evaluated by using network analyzer. Area of the upper electrode was adjusted to the input impedance of 50Ω.
The admittance response data showed the fundamental, second and third order mode resonances at 233, 477 and 735 [MHz], respectively. Small fundamental shear mode resonance was observed. In contrast, we can observe comparatively strong second and third order modes. Here, longitudinal mode resonance was not observed. The strong third-order shear mode seems to result from the thick under electrode film. We can then expect pure second order mode by reducing the under electrode thickness. Effective electromechanical coupling coefficients k^2_{15eff} in the fundamental, second and third order mode resonances were determined as 0.3, 0.6 and 2% from the resonance and anti-resonance frequencies of the real part of input admittance and impedance. These results represent innovative second-order shear mode FBAR using polarization-inverted layers.

(1) T. Yanagitani et al., IEEE Trans. Ultrason, Freq Contr. in press.

(2) K. Nakamura et al., Proc. IEEE Ultrason. Symp. (1986), p. 719

Session: P2G
BAW MATERIALS AND PROPAGATION II
Chair: J. Brown
JB Consulting

P2G-1
PERFORMANCE DEGRADATION EFFECTS IN FBAR FILTERS AND RESONATORS DUE TO LAMB WAVE MODES.

R. C. RUBY*[1], J. D. LARSON, III[2], R. S. FAZZIO[3], and C. FENG[3], [1]Agilent Semiconductor Products Group, San Jose, CA, [2]Agilent Laboratories, Palo Alto, CA, [3]Agilent Semiconductor Products Group, Ft. Collins, CO.
Corresponding e-mail: John_Larson@agilent.com

Film Bulk Acoustic Resonators (FBAR) are thickness mode devices that assume single mode, z-directed dilatational waves as the basis for their operation and analysis. FBARs often exhibit non-ideal behavior, for example, interfering resonances within the pass band and degraded quality factor (Q). For a more complete understanding of FBARs and for suppression of these parasitic effects, one must also include Lamb acoustic waves propagating in the transverse (x or y) directions, as part of the description.

Of the spectrum of possible Lamb wave normal modes, we have identified four members (two symmetric, two anti-symmetric) that are most pertinent to FBAR device performance. For FBAR device design and understanding, these Lamb

wave normal modes are the zero and first order symmetric modes (S0 and S1), and the zero and first order asymmetric modes (A0 and A1). Each mode has its own distinct "personality" and gives rise to particular types of unwanted device degradation.

This paper will present measured vibration data and measured dispersion (ω- k) diagrams for Agilent suspended membrane FBARs as obtained from the Agilent/ INL imaging acoustic microscope, discuss the (ω- k) diagram for each of the four important Lamb modes, and relate this to the behavior of resonators as observed in the frequency domain.

There are several techniques that are utilized to minimize the parasitic effects of the Lamb modes on device performance, including apodization of the device geometry, for example. We will relate observed device performance for FBARs employing parasitic effects suppression techniques to the experimentally observed Lamb modes in these devices.

K.L. Telschow, at the Idaho National Laboratory, Idaho Falls, ID, is acknowledged for help with the acoustic microscope data acquisition.

P2G-2

FABRICATION AND EVALUATION OF AN "ELECTRODELESS" SOLIDLY MOUNTED THIN FILM ELECTROACOUSTIC RESONATOR.

J. ENLUND*, I. KATARDJIEV, and D. MARTIN, Uppsala University, Ångström Laboratory, Uppsala, Sweden.
Corresponding e-mail: Johannes.Enlund@angstrom.uu.se

A solidly mounted resonator (SMR) consists of a piezoelectric thin film, sandwiched between two thin electrodes, fabricated directly onto a carrier substrate. The resonance frequency of the resonator is determined roughly by the total acoustic thickness of the resonance cavity defined by the piezolayer and the electrodes. To acoustically isolate the resonator from the substrate, it is fabricated on top of a classical acoustic mirror, consisting of a sequence of a quarter wavelength layers of low and low high impedance respectively, is used.

We have eliminated the bottom electrode from the acoustic cavity by incorporating it into the acoustic mirror instead. Choosing a low impedance metal as the topmost layer in the mirror, eliminates completely the need for a bottom electrode and brings, in return, a number of significant benefits. Most notably, the ohmic resistance of the resonator is reduced, since the reflector layer is much thicker than the electrode or alternatively the whole stack could be made of conducting materials. Further, the excitation efficiency is also increased since the bottom electrode, which is piezoelectrically "dead", is no longer part of the resonance cavity. Furthermore, if the acoustic reflector layers is made up entirely of metals, an efficient heat path through the mirror is established which reduces thermal resistance and increases the power handling capabilities of the device. By the same token, the top electrode can also be eliminated from the resonance cavity achieving total acoustic isolation of the resonator from its surrounding in addition to doubling the gains described above.

Solidly mounted resonators have been fabricated based on reactively sputtered piezoelectric aluminum nitride films as the active piezolayer and aluminum top electrode. The acoustic mirrors were made of aluminum and molybdenum layers. The devices were electroacoustically characterised and the results compared with standard SMR resonators. The results demonstrate that devices with the proposed design do exhibit improved performance.

This work is suupported by the Swedish Foundation for Strategic Research (SSF) through ICTEA program in microelectronics

P2G-3

DESIGN AND FABRICATION OF A SURFACE MICROMACHINED FREQUENCY TUNABLE FILM BULK AACOUSTIC RESONATOR WITH AN EEXTENDED ELECTROSTATIC TUNING RANGE.

W. PAN*[1,2], P. SOUSSAN[1], B. NAUWELAERS[3], and H. TILMANS[1], [1]IMEC-MCP, Leuven, Belgium, [2]ESAT-INSYS, Katholieke Universiteit Leuven, Leuven, Belgium, [3]ESAT-TELEMIC, Katholieke Universiteit Leuven, Leuven, Belgium. Corresponding e-mail: wanling@ieee.org

Frequency tuning of a surface micromachined film bulk acoustic resonator (FBAR) by electrostatic actuation has been designed and demonstrated in earlier work [1], in which a vertically movable piezoelectric layer with a top electrode is suspended above a bottom electrode, the air gap between the piezoelectric layer and the bottom electrode functions both as a tunable capacitor and as an acoustic isolation. Frequency tuning is realized by applying a DC voltage to electrostatically displace the suspended piezoelectric layer and thus change the air gap capacitance and the frequency response of the device.

This early design has however a relatively small tuning range due to restrictions exerted by pull-in of the piezoelectric cantilever and the maximum continuous tuning range achieved before pull-in was about 2MHz at a resonant frequency of about 6.8GHz (~0.03% tuning) for a DC actuation voltage of 9V. In this paper, we propose a modified design, where the layout of the device remains mostly unchanged, except that the area of the tunable air-gap capacitor is now m (m>1) times the effective area of the piezoelectric resonating layer, as defined by the overlapping area of the electrodes sandwiching it. Pull-in can be avoided if $t/g0 \geq 2\varepsilon/m$, where t is the thickness of the piezoelectric layer, g0 is the zero-bias air-gap distance and ε is the low-frequency equivalent dielectric constant of the piezoelectric layer. The largest possible tuning range is expected when $t/g0=2\varepsilon/m$. In the current technology, t and g0 are of the same order, and ε's of commonly used piezoelectric materials such as AlN and ZnO are around 9. It is thus easier to reach the maximum tuning range for a large m value. If pull-in is not avoidable, a larger area ratio (m) still gives a larger displacement range before pull-in and consequently a larger relative tuning range. In case of an AlN-based FBAR, for m=1,4,8,16, and t/g0=1, the maximum possible continuously tuning ranges are expected to be about 0.12%, 0.35%, 0.52% and 0.7%, respectively, for the AlN quality currently achievable in our pulsed direct current reactive sputtering equipment.

The fabrication of the tunable FBAR can be realized by surface micromachining techniques, as described in previous work [1]. A bottom electrode is deposited on a glass or high-resistivity Si wafer. A polyimide sacrificial layer is spin coated and patterned. An Al seed layer, an AlN piezoelectric layer and a top electrode are then deposited consequently and patterned. After depositing and patterning an Al layer, which functions both as the signal line and as the supporting layer for the piezoelectric cantilever, the final device is realized by wet etching of the sacrificial layer and a releasing step in a CO2 critical point dryer. The temperature in the complete process does not exceed 250°C, and each step is compatible with the standard CMOS technology.

[1] W. Pan, P. Soussan, B. Nauwelaers and H.A.C. Tilmans, A surface micromachined tunable film bulk acoustic resonator, EUROSENSORS XVIII Tech. Digest, 2004, pp.99-100.

P2G-4
DESIGN OF BULK ACOUSTIC WAVE RF RESONATORS AND FILTERS BASED ON ADVANCED BRAGG REFLECTOR.

G. CARUYER*[1], A. DEVOS[2], J. F. CARPENTIER[1], R. VÉLARD[1], N. CASANOVA[1], A. LEFEVRE[3], F. DUMONT[1], G. PARAT[3], and P. ANCEY[1], [1]ST Microelectronics, Crolles, France, [2]Institut d'Electronique de Microélectronique et Nanotechnologie, dept. ISEN, Lille Cedex, France, [3]CEA-LETI, Grenoble, France.
Corresponding e-mail: gregory.caruyer@st.com

Recently much progress has been done in Bulk Acoustic Wave resonators technology for RF filtering applications in wireless systems. AlN based BAW resonators have been demonstrated for filter fabrications on silicon substrates in the GHz range and, many results on PCS duplexers have been shown with very good power handling capabilities and small size.

BAW resonators have to be acoustically insulated from the substrate. This can be done by realizing suspended Film Bulk Acoustic Resonator structures or mounting the resonator on an acoustic reflector, called Solidly Mounted Resonator (SMR). The so-called Bragg reflector used in SMR structure is fabricated alternating quarter-wavelength layers with high acoustic impedance ratio. Couples used for the reflector were W/SiO_2 and Mo/SiO_2 that has a high impedance ratio, but the metal has to be patterned to avoid electromagnetic coupling between resonators. AlN/SiO_2 and Ta_2O_5/SiO_2 have also been used and are fully dielectric, but they require numerous layers due to a quite low acoustic impedance contrast between the materials.

Using the original Picosecond Ultrasonics characterization method, we have identified a new couple of dielectric materials that have a very high impedance ratio and allow the fabrication of Bragg reflector with very good performances. In this new Bragg reflector, a conventional silicon nitride layer is used as the high impedance material and a low k organo-silicate glass (SiOC:H) is used as the low impedance material. WCDMA Rx Mo-AlN-Mo SMR resonators have been realized with 2 SiN/SiOC:H bi-layers and very good performances have

been demonstrated. Electromechanical coupling coefficients up to 6%, a high quality factor and a TCF of -20 ppm/°C have been achieved.

A complete filter for WCDMA Rx application has been realized based on this new SiN/SiOC:H Bragg reflector SMR and very good results have been demonstrated with insertion losses lower than 2.5 dB and Tx frequency rejection better than -40 dB. The effect of the electromagnetic substrate coupling has been investigated, and the advantage of using high resistivity silicon substrate is pointed out.

In addition to these good performances, this new Bragg reflector shows advantages for process simplification (no need to pattern layers, low roughness...) and for thickness measurements (dielectric transparent materials can be optically controlled). Silicon nitride and organo-silicate glass are standard microelectronics materials, opening perspectives for integration of SMR filters and duplexers with active devices in above-IC approach.

P2G-5
SPURIOUS RESONANCE SUPPRESSION IN ZNO BASED THIN-FILM BAW RESONATORS: FEM MODELING AND EXPERIMENT.

T. PENSALA*[1], T. MAKKONEN[2], and M. YLILAMMI[1], [1]VTT Information Technology, Microelectronics, Espoo, Finland, [2]Helsinki University of Technology, Materials Physics Laboratory, Espoo, Finland.
Corresponding e-mail: tuomas.pensala@vtt.fi

Due to the finite lateral size of thin film bulk acoustic wave (BAW) resonators, laterally propagating Lamb wave modes form standing wave resonances within the resonator area. The plate-like geometry of the thin film BAW resonators causes these so called spurious resonances to lie near the main resonance of the device in frequency and to distort its frequency response with ripple in an undesired manner.

An effective method to suppress the spurious resonances employs a ring-like structure which modifies the mechanical boundary conditions of the resonator [1]. Methods to model and analyse the mode spectrum of the resonator include semi-analytical transfer matrix models for Lamb wave dispersion in different regions of the device, and the numerical finite element method (FEM).

In this work, we simulate the effect of the ring-like structure on the behavior of the spurious resonances using two dimensional FEM. We compare the simulation results with electrical measurements of ZnO-based BAW resonators of the solidly mounted type (SMR) utilizing the ring-like structure.

Mode shapes and input impedance are calculated by FEM and the scattering parameter S_{11} is measured by a vector network analyser from the corresponding real devices for varying dimensions of the ring structure. Figures describing the spurious content of the electrical response are calculated as functions of the ring dimensions in both cases. Good correlation between the measured and simulated results is shown. Emergence of the so-called piston mode with simultaneous suppression of the spurious modes at the optimal ring structure

dimensions is demonstrated. Quantitative differences and limitations of the model are discussed.

[1] J. Kaitila, M. Ylilammi, J. Ellä, and R. Aigner, Proc. IEEE Ultrasonics Symposium pp. 84-87 (2003).

P2G-6
BEVELING AT-CUT QUARTZ RESONATOR DESIGN BY AN EFFICIENT NUMERICAL METHOD.

S. Y. PAO*[1], M. K. CHAO[2], C. H. CHIU[2], C. S. LAM[2], and P. Z. CHANG[1], [1]Institute of Applied Mechanics, National Taiwan University, Taipei, Taiwan, [2]TXC Corporation, Ping Cheng City, Taoyuan County, Taiwan.
Corresponding e-mail: sypao@mems.iam.ntu.edu.tw

In recent years, the rapid progress of personal communication system pushes the size of circuit device, including the resonator and oscillator, becomes smaller and smaller. For the miniaturization trend of quartz resonator, the role of an efficient and precision simulation tool is more and more important. Based on Mindlin's 2-D model and Lee-Brebbia's [1] FEA method, Pao [2] et al. presented an efficient numerical method in calculating the electrical impedance different modes of AT-cut quartz crystal resonator. This method considers not only the pure mechanical vibration but also the electrical response, so we can identify different modes easily.

For energy trapping, beveling process in low frequency and small size AT-cut quartz resonator is very important. But it is very different to simulate it by general 3-D piezoelectric model, because it is hard to mesh elements in thickness direction with slight thickness variation. In this paper, we use the efficient numerical method we presented last year and the mass loading effect concepts to develop a program tool to simulate the characteristic of a beveling quartz plate. By this tool, we can easily obtain the electrical gain response and vibration mode shapes which exist physically. At the same time, we can also predict the electrical response change with beveling. We present a real $3.2*2.5mm^2$ quartz resonator design to show how we use this program tool to design the beveling amount and how to suppress the dominated unwanted modes. The simulation results match the experimental data. We verify this method is both precise and efficient enough for beveling quartz plate design.

[1] P.C.Y. Lee, C. Zee, and C.A. Brebbia, "Thickness-Shear, Thickness-Twist, and Flexural Vibration of Rectangular AT-Cut Quartz Plates with Patch Electrides", *Proceeding of the 1978 IEEE International Frequency Control Symposium*, pp. 108-119, 1978.

[2] S.Y. Pao, M.K. Chao, C.S. Lam and P.Z. Chang, "An Efficient Numerical Method in Calculating the Electrical Impedance Different Modes of AT-Cut Quartz Crystal Resonator", *Proceeding of the 2004 IEEE International Ultrasonics, Ferroelectrics, and Frequency Control 50th Anniversary Joint Conference*

Session: P2H
SAW MATERIALS AND PROPAGATION
Chair: R. Potter
Vectron International

P2H-1
ELECTRO-ACOUSTIC SLIP AND GAP WAVES IN PIEZOELECTRIC STRUCTURES OF GENERAL ANISOTROPY.

A. DARINSKII[1] and M. WEIHNACHT*[2], [1]Institute of Crystallography, Moscow, Russia, [2]Leibniz Institute for Solid State and Materials Research, Dresden, Germany.
Corresponding e-mail: whn@ifw-dresden.de

The theory has been developed of the acoustic waves of two types guided by piezoelectric structures: 1) Slip waves (SW) on the perfect sliding contact, metallized (electric potential vanishes) and non-metallized (electric potential and normal projection of electric displacement are continuous); 2) Gap waves (GW) propagating along the air gap between two crystals. The propagation and reflection problems for these waves can be studied analytically by solving explicitly the relevant equations only in the case of SH polarization. In the present work we investigate generally polarized GW and SW in structures constituted of identical crystals of arbitrary crystallographic symmetry. Our considerations have been based on the properties of the impedance and admittance matrices derivable without evaluating the characteristics of plane partial modes. We have analyzed the existence of subsonic SWs and GW, which travel slower than all bulk waves. It has been proved that at most three and at most two subsonic SWs exist on the metallized and non-metallized sliding contacts, respectively. When the structure assumes orientations belonging to certain families, it appears possible to trace the interdependence between the number of SWs and the shape (concave/convex) of the slowness surface of slowest bulk waves. It has been shown that at most four GWs exists at a fixed value of kh, where k is the tangential projection of the wave vector and h is the gap width. We have discussed the interdependence between the existence of GWs and the existence of SAWs on the mechanically free surface of the half-infinite substrate at different electrical boundary conditions. We have also analyzed the existence of the leaky GWs in the vicinity of orientations supporting limiting bulk waves that leave the surface of the half-infinite medium traction free and satisfy certain electrical boundary conditions. In addition, we have considered the behavior of the coefficients of plane mode conversion describing the reflection of bulk waves incident on the gap at angles corresponding to the excitation of a leaky GW. It has been shown that the reflection coefficient can decrease to zero within a narrow interval of angles around a resonance value of the angle whereas it hardly differs from unity outside this interval. The transmission coefficient equals unity at the resonance. The examination of the expressions derived reveals that such a resonance total transmission can occur in structures of arbitrary symmetry provided the piezoeffect is not too weak. The threshold strength of piezoeffect

has been estimated. The results of numerical investigations of the SWs and GWs propagation as well as the resonance transmission in LiNbO3 and LiTaO3 structures have been discussed.

P2H-2
EXPERIMENTAL VERIFICATION OF THE BASIC SCATTERING THEOREM.

G. PASHKEVICH[1], M. SYCHEV[1], I. MITELMAN[2], and B. SVESHNIKOV*[2], [1]Rodos, Ltd., Kiev, Ukraine, [2]Nizhny Novgorod State University, Russia.
Corresponding e-mail: bvs@ieee.org

This abstract does not appear in the online abstracts at the author's request.
It will appear in the print version.

P2H-3
ANALYSIS OF SURFACE ACOUSTIC WAVE'S THERMAL BEHAVIORS ON LANGASITE USING LAGRANGIAN EFFECTIVE MATERIAL CONSTANTS.

T. HAN*, X. JI, and W. SHI, Department of Instrumentation Engineering, Shanghai Jiaotong University, Shanghai, P.R.China.
Corresponding e-mail: than@sjtu.edu.cn

Analysis of thermal behaviors of SAW on langasite is of importance for designing the devices in high-temperature applications, for example, LGS gas sensors up to 500°C.

The SAW properties of LGS in singly and doubly rotated cuts are investigated [1]. However, the theoretical results of TCD are only in accordance with the experimental ones under 250°C.

By using Lagrangian effective material constants model [2], we firstly calculated the TCF of XY-LGS and LGS with Euler angle (0,138.5,26.6). Compared with the published experimental results[3][4], the theoretical results can be in good accordance with them up to 500°C.

The turnover temperatures of Z-cuts and rotated Y-cuts (between 250°C and 350°C) as well as the corresponding electromechanical coupling coefficients((>0.2%) are given. Some of them show the applicability to gas sensors.

There is no temperature compensation cuts even in trebly rotated cuts. Under 500°C temperature bias, we also present some cuts have high electromechanical coupling coefficients (>0.45%) as well as great TCD (25-30ppm), which show the applicability to temperature sensors.

References:

1. X.J. Ji T. Han W.K. Shi and G.W. Zhang, Investigation on SAW Properties of LGS and Optimal Cuts for High-Temperature Applications, (to be published in IEEE UFFC)

2. Bernard dulmer, Roger Bourquin. Lagrangian effective material constants for the modeling of thermal behavior of acoustic waves in piezoelectric crystals. Journal Acoustical Society of America, Vol.110, No.2, 2001: 1792-1807.

3. Thiele, J.A., da Cunha, M.P.. High temperature surface acoustic wave devices: fabrication and characterization. Electronics Letters, Vol. 39 , No.10 , 2003: 818-819.

4. Mrosk J.W., Ettl C.. SAW sensors for high temperature applications. Proceedings of the 24th Annual Conference of the IEEE. Vol.4, 1998: 2386-2390.

Financial support from National Natural Science Foundation of China under grant No.10304012 is gratefully acknowledged. The authors also thank Dr. S. Ballandras of LPMO CNRS Besancon France for his helpful suggestion on SAW theoretical analysis.

P2H-4

TEMPERATURE CHARACTERISTICS OF SH-TYPE ACOUSTIC WAVES IN A ROTATED *Y*-CUT $LiTaO_3$ THIN PLATE.

H. FUJIWARA, D. YAMAZAKI, and K. NAKAMURA*, Graduate School of Engineering, Tohoku University, Sendai, Miyagi, Japan.
Corresponding e-mail: yamazaki@ecei.tohoku.ac.jp

The SH-type surface acoustic wave (SH-SAW) in 36° *Y-X* $LiTaO_3$ has a high electromechanical coupling factor K^2 of about 0.047 and a comparatively low temperature coefficient of delay (TCD) of about 32 ppm/°C[1)], and therefore it has extensively been used for RF-SAW filters in mobile phones. In recent years, however, the demand for lower TCD has increased. The temperature coefficient of the relevant shear stiffness constant for the SH-SAW in 36° *Y-X* $LiTaO_3$ changes its sign if the electric field in the substrate could be thoroughly short-circuited. Therefore the TCD of the 0-th SH-wave propagating in a very thin 36° *Y-X* $LiTaO_3$ plate with surface electrodes is expected to be lower due to the electric-field short-circuiting by the surface electrodes. This paper describes theoretical calculations and experiments on the 0-th SH-wave propagating along the *X*-axis in a θ°-rotated *Y*-cut $LiTaO_3$ thin plate. It is shown that the TCD becomes zero at θ=20.1° and 67.1° for an infinitesimally thin plate. Between these two cut angles the SH-wave has a negative TCD and a high electromechanical coupling factor K^2. In the 36° *Y-X* finite-thickness plate with surface electrodes on its both sides, the TCD becomes zero at a normalized plate thickness of h/λ=0.236 (*h*: plate thickness, λ: wavelength), where the electromechanical coupling factor K^2 is as high as 0.17. Some experimental results on the 0-th SH-wave in 36° *Y-X* $LiTaO_3$ thin plates are also presented and compared with the theoretical results.

1) K. Nakamura, M. Kazumi and H. Shimizu: Proc. IEEE Ultrason. Symp., p.819 (1977).

P2H-5
THEORETICAL AND EXPERIMENTAL INVESTIGATION OF PSAW AND SAW PROPERTIES OF ALN FILMS ON ISOTROPIC DIAMOND SUBSTRATES.

M. BENETTI[1], D. CANNATA'[1], F. DI PIETRANTONIO[1], V. I. FEDOSOV[2], and E. VERONA*[1], [1]Consiglio Nazionale delle Ricerche - Istituto di Acustica, Roma, Italy, [2]Russian Academy of Sciences - Institute of Radioengineering and Electronics, Moscow, Russia.
Corresponding e-mail: enrico.verona@idac.rm.cnr.it

Diamond and AlN are, respectively, the non-piezoelectric and piezoelectric materials showing the highest acoustic velocities. So SAW devices based on AlN/diamond are a promising candidate to operate at the highest frequencies. In this work we analyze both theoretically and experimentally the propagation along this structure of the 0th and 1st SAW modes and of the 1st PSAW mode. To find the PSAW solution, the partial waves for the substrate were selected in accordance with [1]. The phase velocity and *leaky* propagation loss were calculated vs. AlN film thickness normalized to wavelength (h/λ), for different electrical boundary conditions (EBCs) at the AlN surfaces. The changes (Δv) in the phase velocity (v), produced by these different EBCs are reported in terms of $K^2 = 2\Delta v/v$. For AlN/diamond, two different low-loss PSAW conditions (h/λ ~ 0.09 and 0.15) have been observed in the 1st PSAW mode, where the *leaky* loss is below 0.001 dB/λ, i.e. it is possible, that *fast* PSAWs degenerate into SAWs, at these points. The corresponding velocities are ~ 15.9 and 13.4 km/sec with K^2 in the range 0.02 - 1.1 and 0.2 - 2.4 %, respectively. For ZnO/diamond, only one low-loss PSAW condition was found, at h/λ ~ 0.03, with a

velocity of ~ 14.7 km/s and K^2 between 0.09 and 1.25 %, as reported in the literature [2].

Experiments on both SAW and low-loss PSAW propagation have been done using the same delay line configuration on AlN/diamonds, at different AlN thickness. The delay line (λ = 8 mm) consisted of IDTs with 15 pairs of electrodes, placed 440 λ apart. IDT electrodes were located at the free AlN surface, without any conductive layer at the AlN/diamond interface. The isotropic diamond layer, grown on a poly-silicon substrate was 22.4 mm thick (h/λ = 2.8). Low-loss PSAW condition, at h/λ ~ 0.09, was achieved with an AlN layer 0.72 mm thick (f = 2.019 GHz). The 0th and the 1st SAW modes where observed at h/λ ~ 0.27 (AlN thickness 2.16 mm) at frequencies of 1.03 and 1.35 GHz, respectively. A good accordance between experimental data and theoretical predictions was observed for both phase and group velocities. The influence of the finite thickness (2.8 λ) of the diamond film on the acoustic wave properties was also investigated using the compound matrices method [3], which is suitable to investigate thick film layered structures.

[1] S.V. Biryukov, M. Weihnacht, “The Effective Permittivity in the Complex Plane and a Simple Estimation Method for Leaky Wave Slowness”, 1996 IEEE Ultrason. Symp. Proc., p. 221.

[2] M.P. da Cunha, E.L. Adler, D.C. Malocha, “HVPSAW Sensitivity to Film Properties for ZnO/Diamond/Si Structures”, 2000 IEEE Ultrason. Symp. Proc., p. 283.

[3] V.I. Fedosov, V.I. Anisimkin, I.M. Kotelyanskii, C. Caliendo, P. Verardi, E. Verona, “Analysis of Acoustic Waves in Multilayers Using Compound Matrices”, 1996 IEEE Ultrason. Symp. Proc., p. 207.

Work supported by the Fondo Integrativo Speciale Ricerca (FISR) project of the Italian Minister for Education, University and Research and the Russian President grant Scientific School #1391.2003.2.

P2H-6

TEMPERATURE SENSITIVE CUTS FOR TEMPERATURE SENSORS.

V. I. CHEREDNICK* and M. YU. DVOESHERSTOV, Nizhny Novgorod State University, Russia, Nizhny Novgorod, Russia.
Corresponding e-mail: odissey@sandy.ru

Cuts and orientations in various crystal substrates which may be promising for temperature sensor design are investigated. In particular quartz, lithium niobate, lithium tantalate, lithium tetraborate, langasite, langanate, and langatate are looked into. Full contour maps of the temperature coefficient of delay (tcd) and other basic SAW propagation characteristics are calculated and plotted in order to find cuts and orientations, for which temperature coefficient of delay is large and all the other propagation characteristics are close to their optimal values.

It is shown, that such orientations can be found in all the above mentioned substrates. For example in range of orientations on quartz $\Phi = 0°$, $\theta = 60° - 80°$, $\psi = 0°$ (Φ, θ, ψ are the Euler angles) orientations can be found with tcd about -

$27*10^{-6}$/°C, electromechanical coupling coefficient (K^2) close to 0.2 %, zero power flow angle (pfa) and a small value of the second order tcd of about $2.5*10^{-9}$/°C^2.

Orientations on the lithium niobate ($LiNbO_3$) in the range Φ = 0°, θ = 60° - 90°, ψ = 80° - 100° correspond to tcd close to its maximal value of about $98*10^{-6}$/°C, rather large K^2 about 4.7 %, and zero pfa.

Rather good characteristics for temperature sensors can be found also in the range of Euler angles Φ = 0°, θ = 160° - 180°, ψ = 85° - 95° on lithium tantalate ($LiTaO_3$), tcd about $75*10^{-6}$/°C, K^2 about 1.4 %, the second order tcd about $0.8*10^{-9}$/°C^2, and zero pfa.

The lithium tetraborate ($Li_2B_4O_7$) substrate also can be used for temperature sensors. In particular tcd is about $77*10^{-6}$/°C, K^2 about 1.25 %, zero pfa in the area of Euler angles Φ = 0°, θ = 10°, ψ = 20° - 60°.

Contour maps of all the basic SAW propagation characteristics of langasite, langanate, and langatate look almost the same and differ from each other only by values of corresponding characteristics. The area of Euler angles Φ = 0°, θ = 40° - 80°, ψ = 30° - 70° correspond to the best combination of the propagation characteristics for temperature sensors. The tcd value can exceed $-110*10^{-6}$/°C on the langanate, whereas it is about two times less on the langasite and langatate. The K^2 value is 0.15 % - 0.2 %, and pfa = 1.5°- 2° for orientations, corresponding to maximal tcd in these three crystals.

Some other ranges of orientations with rather large tcd in the mentioned crystals are shown too, but they are not optimal from point of view of other propagation characteristics.

P2H-7

APPROXIMATION OF PROPAGATION LOSS IN ROTATED Y-CUTS OF LITHIUM TANTALATE WITH A PERIODIC GRATING.

N. F. NAUMENKO*[1] and B. P. ABBOTT[2], [1]Moscow Steel and Alloys Institute, Moscow, Russia, [2]Sawtek Inc., Apopka, FL.
Corresponding e-mail: nnaumenko@ieee.org

In order to correctly design low-loss resonator filters, which use leaky surface acoustic waves (LSAW) propagating in rotated Y-cuts of lithium tantalate, it is necessary to account for the dependence of propagation loss on frequency and detuning from synchronous resonance in finite gratings. It can be made via numerical integration of complex admittance function around the synchronous resonance, for each frequency, but requires large computaion time. For analytic integration, the propagation loss should be first approximated as a function of frequency and normalized wave number. We report on the method of approximation for propagation loss, based on the comparison of approximated and numerical harmonic admittance of infinite grating. The approximation uses Plessky's two-parameter dispersion equation, to account for LSAW/BAW interaction and the parasitic resonance caused by surface-bulk hybrid mode (SBH). In general, the two-parameter dispersion equation fails to predict accurately the dispersion both around the main and parasitic resonances,

because of gradual transformation of quasi-SH bulk wave into the four-partial LSAW. This transformation was taken into account in the modified dispersion equation derived by Abbott. Since the modified equation combines two different approaches in one dispersion equation, the disperion function, and hence the function which approximates admittance, become too complicated for accurate extraction of propagation loss. Therefore, the original two-parameter dispersion equation is used, but the values of both parameters are assumed to be frequency-dependent, to fit numerical and experimental admittances in the analyzed frequency interval. For open-circuit and short-circuit gratings, all parameters needed for approximation of dispersion equations, are extracted from harmonic admittance. To make it, first three basic frequencies are extracted - two edges of the stopband and the frequency, at which the SBH mode arises from the bulk wave. Using simple analytic equations for these characteristic frequencies, the SBH resonant frequency is found. This frequency plays an important role in the two-parameter dispersion equation but is difficult for direct extraction. After fitting of imaginary parts of both admittances, the propagation loss can be extracted from the real part of numerical function. The described technique was verified for 36-LT and 42-LT, and demonstrated good agreement between numerical and approximated admittance functions, including accurate simulation of SBH resonance.

P2H-8
PRESSURE CHARACTERISTICS OF SPHERICAL BALL SAW DEVICE.

D. Y. SIM*[1], N. TAKEDA[1], S. AKAO[2], N. NAKASO[2], Y. EBI[3], H. KAZATO[3], T. MIHARA[4], and K. YAMANAKA[4], [1]Ball Semiconductor Inc., Allen, TX., [2]Toppan Printing Co., Sugito-machi, Saitama, Japan, [3]Yamatake Co., Fujisawa, Kanagawa, Japan, [4]Tohoku Univ., Sendai, Miyagi, Japan.
Corresponding e-mail: dysim-ball@jp.yamatake.com

Spherical ball SAW(Surface Acoustic Wave) device has many application areas as a physical or chemical sensor device. In this paper, as an example of physical sensor, we introduce a wide range pressure sensor using Φ1mm ball SAW device. The SAW signal on the sphere is excited by an interdigital transducer (IDT) made on an equator of the sphere, propagated along the equator and detected by the identical IDT. This ball SAW device uses a collimation and the collimated SAW on the sphere realizes ultra multiple roundtrips along the equator.

Fabrication of the ball SAW device is based on 3-dimentional Ball Semiconductor/ MEMS technology. A single crystal quartz ball of 1mm diameter is used as substrate material. The IDT electrode having center frequency of 150 MHz is designed on the Z-axis cylinder to realize the multiple roundtrips.

The fabricated device without sensing film was set up in a test chamber, in order to inspect characteristics to the pressure change. The device was tested under two different conditions of room temperature. One is atmosphere to high vacuum of 10^{-5} [Pa] and the other is from atmosphere to high pressure of 0.3 [MPa]. In case of the high pressure, the Φ1mm ball SAW device was pressed by nitrogen gas. We focus on the signal at 150 turns among the multiple roundtrip signals of

SAW on the sphere. For improving S/N ratio, the signal processing technology using digital FIR filter is adapted, and the filter has a passband width of ±20 [MHz] to the center frequency of 150 [MHz]. The temperature in the test chamber is monitored by a thermo-couple.

Amplitude change is more sensitive than delay time change to the pressure change and is not influenced by the temperature. The amplitude signal of the ball SAW device extremely increased and the variation is 6.5 [mV/kPa] between atmosphere and 10^2 [Pa], and it was slowly changed in high vacuum. On the other hand, the amplitude exponentially decreased due to the energy emission to the environment in the high pressure. The measured signal is at 50 turns and it is more sensitive to the high pressure than that at 150 turns. The amplitude to the induced pressure deceases as 0.17 [mv/kPa].

In conclusion, the pressure detection is realized by the leaky loss effect of SAW into environment due to an acoustic impedance change. We presented a wide range pressure sensor from vacuum to high pressure using one chip. An integrated pressure sensor with temperature detecting function will be developed in the future.

This work was partially supported by Ministry of Education, Culture, Sports, Science and Technology.

Session: P2I

SAW DEVICES II
Chair: M. Mayer
EPCOS AG

P2I-1
EFFECT OF SUBSTRATE THICKNESS ON QUASI-LONGITUDINAL LEAKY SAW PROPAGATION ON QUARTZ.

M. OSHIO*, S. KANNA, and K. IIZAWA, SEIKO EPSON Corporation, Suwa-shi, Nagano-Pref., Japan.
Corresponding e-mail: oshio.masahiro@exc.epson.co.jp

Quasi-longitudinal leaky SAWs (QLL-SAWs) have been investigated in many piezoelectric materials due to their high phase velocity. They have a phase velocity higher than the ordinary leaky SAWs, so that they are suitable as a surface acoustic wave propagation mode for higher frequency SAW devices. For quartz substrate, STW (Surface Transverse Wave) has already been utilized to achieve high frequency with high temperature stability. But QLL-SAW is still not applied for practical use.

In this paper, substrate thickness effect of the QLL-SAW on rotated Y-cut quartz substrates is investigated. We find that Q values of the QLL-SAW is strongly affected by the substrate thickness. Experimental Q values of one-port resonator are improved more than twice when the relative thickness of substrate, i.e. the ratio of the substrate thickness to the SAW wavelength, is reduced from 50 to

25 at a frequency of around 700 MHz. By using finite element method, we also confirm that the frequency of spurious modes, excited around the resonance frequency of QLL-SAW, varied with the substrate thickness. The frequency dependency on the substrate thickness and the frequency-temperature curve of resonance frequency are in good agreements with the experimental results. Through this investigation, high frequency SAW devices with high Q-value can be designed by optimizing the thickness of quartz substrate.

P2I-2

INVESTIGATION OF AL/TI METALLIZATION PERFORMANCE IN TERMS OF ACOUSTOMIGRATION STABILITY.

H. SCHMIDT*[1,2], M. PEKARCIKOVA[1], S. MENZEL[1], M. HOFMANN[1], and R. KUNZE[1], [1]Institute for Solid State and Materials Research Dresden, Dresden, Saxony, Germany, [2]VI Tele Filter, Teltow, Brandenburg, Germany.
Corresponding e-mail: h.schmidt@ifw-dresden.de

Power durability of usual Al-based metallizations for SAW devices is limited by acoustomigration, because SAW stress induced material transport results in an irreversible damage of the microstructure of the metal film [1]. As reported in literature the resistance against migration effects can be increased by alloying addition or multilayer structures which result in a better power durability in comparison to pure aluminum electrodes [2, 3]. With regard to this, Al-Ti material systems are typically used for finger electrodes. Although the acoustomigration behavior of Al/Ti multilayer systems was studied in SAW devices, a correlation with underlying processes (e.g. interdiffusion and phase formation) was not studied in detail up to now.

In this paper the performance of Al/Ti metallization systems for power loaded SAW structures was systematically investigated in comparison with a novel copper metallization [4]. For these purposes, a power SAW test structure was fabricated using finger electrodes of different multilayer stacks. In a first sample series a 340 nm Al film was deposited on a 9 nm thick Ti adhesive layer, whereas in a second and a third series the layer stack consist of Al(180 nm)/Ti(40 nm)/ Al(180 nm)/Ti(40 nm) and Al(110 nm)/Ti(20 nm)/Al(110 nm)/Ti(20 nm), respectively. All these layers were deposited by electron-beam evaporation on 128°XY LiNbO3 substrates. The devices were loaded at about 130 MHz with an SAW input power of several Watts to investigate the damage behavior of each metallization system. During this SAW loading the electrical behavior (e.g. peak frequency shift of the admittance curves) of interdigital test transducers was measured as an indicator of acoustomigration. Additionally, in-situ observations by means of optical microscopy as well as scanning electron microscopy were used to correlate the electrical behavior with electrode degradation.

The SAW loading experiments were completed by studies of the behavior of the Al/Ti microstructure during heat treatment with respect to interdiffusion effects as well as to formation of intermetallic phases. It was found, that the Al3Ti phase was only formed due to thermal treatment above 400°C. However, it was not formed by SAW loading at room temperature with up to 4 W, where the

metallization was heated only by acoustic power dissipation. The influence of this Al3Ti phase on the power durability was investigated in comparison to the untreated Al/Ti layer system. Both Al-based metallizations were compared to the copper system which was referred to in an earlier paper regarding to their power durability and lifetime.

[1] K. Wetzig and C.M. Schneider (Eds.): Metal Based Thin Films for Electronics, Whiley-VCH, Weinheim 2003

[2] N. Hosaka et al.: A study of Al-alloy electrodes for high power SAW filters. In: Proc. IEEE Ultrason. Symp. 1987.

[3] M. Furokawa et al.: EP0991186A1

[4] M. Pecarcikova et al.: Investigation of high power effects on Ti/Al and Ta-Si-N/Cu/Ta-Si-N electrodes for SAW devices. To be published in: Trans. Ultrason. Ferroelectr. Frequ. Contr. vol.UFFC-52, (2005) no.5.

P2I-3
EXCELLENT FREQUENCY STABILITY AND HIGH-Q AND SMALL SH-TYPE QUARTZ SAW RESONATORS.

T. OWAKI* and T. MORITA, Toyo Communication Equipment Co., Ltd., Kanagawa, Japan.
Corresponding e-mail: t-ohwaki@toyocom.co.jp

This paper presents small sized surface acoustic wave (SAW) resonators that offer both satisfactory frequency stability and a high Q-factor superior to conventional ST-cut quartz SAW resonators utilizing Rayleigh waves. Intensive research efforts have been made into SAW propagating on quartz substrates. In one such research effort, Lewis et al. proposed a surface skimming bulk wave (SSBW). [1] We studied how to concentrate the SSBW on the surface of the substrate and utilize reflectors to achieve small sized resonators with a high Q-factor. In other words, we focused on shear horizontal type (SH-type) SAW propagating perpendicular to the X-axis on the rotated Y-cut quartz substrate. We investigated how frequency-temperature characteristics of SH-type SAW resonators depend on a cut angle of the substrate, and an aluminum electrode film thickness. We also investigated the reflection coefficient, electromechanical coupling factor, Q-factor, and capacitance ratio γ depend on the aluminum electrode film thickness. As a result of this work, we developed SAW resonators with Q-factor more than 50% higher than from ST-cut quartz resonators, as well as high reflection coefficient advantage for downsizing. We achieved these by utilizing SH-type SAW resonators with a cut angle in the vicinity of -52° (the Euler angle in the vicinity of (0°,38°,90°)) and by optimizing its aluminum electrode film thickness. We fabricated 315 MHz prototype SAW resonators for tire pressure monitoring system (TPMS) using 3×3 mm^2 package and obtained the characteristics with Q of 25,000 and γ of 1,100. The figure of merit (Q/γ) of 23 was obtained, which is more than double that of conventional ST-cut quartz resonators. The frequency stability of our resonators was also superior to the ST-cut quartz. It showed a tertiary frequency-temperature curve with an inflection point of approximately 100°C. Therefore, the wider the temperature range, the greater the advantage against ST-cut with quadratic curve. The frequency

fluctuation in the prototype for TPMS within a temperature range of -40 to +125°C was 100 ppm, which is a reduction to less than 50% that of ST-cut quartz Rayleigh wave resonators.

[1] T.Browning and M.Lewis, “A new class of quartz crystal oscillator controlled by surface-skimming bulk waves”, Frequency Control Symp. Proc.,pp.258-265 (1977)

P2I-4
SAW ANALOGS OF BREWSTER’S ANGLES: THE DEPENDENCE ON THE STRIP SHAPE.

S. V. BIRYUKOV*[1,2] and M. WEIHNACHT[1], [1]Leibniz Institute for Solid State and Materials Research Dresden, Dresden, Germany, [2]Mints Radiotechnical Institute, Moscow, Russia.
Corresponding e-mail: s.biryukov@ifw-dresden.de

The analogs of Brewster’s angles or, in other words, the angles of zero scattering for surface acoustic waves (SAW) were discovered theoretically by one of the authors thirty years ago [1]. Considering at oblique incidence the scattering of classical Rayleigh wave in the isotropic half-space by long topographic irregularities of small thickness like projections and grooves it was found by perturbation method that the reflection coefficient is equal to zero for some angle of incidence. The angle changes with Poisson’s ratio only within a narrow range from 25.9 to 28.5 degrees independently from the shape of irregularities. A lot of following publications confirm the existence of such angles also in more complicated cases (three-dimensional irregularities, periodic structures, layered structures, anisotropic substrates), however the problem was never treated more accurately then by first order perturbation method on a small parameter as the ratio thickness/wavelength. So up to now the existence of a shape dependence for these angles is an open question.

In this work the impedance method was used for a correct investigation of the problem in the case of periodic strips. It was found that in the simplest isotropic case with topographic projections a strong dependence of angle value with increasing of a small parameter above 0.03 is observed. Moreover, a second angle appears and both angles become closer and disappear for thick projections. The aluminum strips on piezoelectric crystals of STX quartz and of 128 YX lithium niobate are also considered. In these cases the behavior of angles keeps the mentioned features in main, but it is more complicated due to both the anisotropy and the contribution to the reflection caused by electrical shorting of substrates, which exists also for vanishing thickness of strips.

[1] S. V. Biryukov. Scattering of surface waves by local irregularities, M. Sc. Thesis, Moscow Institute of Physics and Technology (MIPT), 1975, 37 pp.

P2I-5

TRANSFER EFFECTS OF INDUCED CARRIERS BY SAW.

C. KANESHIRO*[1], K. KOH[1], K. HOHKAWA[1], K. NISHUMURA[2], and N. SHIGEKAWA[2], [1]Kanagawa Institute of Technology, Kanagawa, Japan, [2]Nippon Tetelegraph & Telephone Co., Kanagawa, Japan.
Corresponding e-mail: chinami@ele.kanagawa-it.ac.jp

III-Nitride semiconductor is suitable for optoelectronic devices as well as high power, high temperature transistor and surface acoustic wave devices. In order to find out the possibility of a functional device based on GaN epitaxial film, we examine transfer characteristics of transversal filters with side gate fabricated on unintentionally doped GaN layer on a sapphire wafer. Also, we investigate transport characteristic of photo-induced carriers by the potential well caused by traveling acoustic wave.

The test device consists of transversal filters with Al IDT electrodes and side-gate with Schottky contacts fabricated on an epitaxially GaN layer. The side-gate is isolated from the IDTs. As acoustic waves, we used SAW and guide wave layer mode in GaN thin film and employed MSM detector having the same structure as that of input IDT. An amplitude of center frequency of SAW increased about 6 dB by applying the gate voltage at 20 V. It may be indicated that the carriers due to unintentionally doping interrupt the SAW propagation. By gate bias, excess carriers would be moving under the gate electrode.

Moreover, during the applied gate voltage, we measured the characteristics of propagation wave under UV light irradiation. The DC component signals of propagation wave are obtained at the output diode for both modes. However, we have observed a relatively complicated phenomena, such as change on DC component signal polarity depending on the intensity of UV, trapping effect of carriers. We clarified that excess carrier either electron or hole in transported carrier would reasonably explain these effects.

We present the experimental results and discuss the carrier transfer by acoustic wave. We also mention that the application of GaN SAW device is suitable for UV sensors.

P2I-6

ALN-ON-SI SAW FILTERS: INFLUENCE OF FILM THICKNESS, IDT GEOMETRY AND SUBSTRATE CONDUCTIVITY.

M. CLEMENT*, L. VERGARA, E. IBORRA, A. SANZ-HERVAS, J. SANGRADOR, and J. OLIVARES, Depto. Tecnología Electrónica, Universidad Politécnica de Madrid, Madrid, Spain.
Corresponding e-mail: eiborra@etsit.upm.es

Surface acoustic wave (SAW) filters are currently used for many industrial applications. Compared to conventional piezoelectric materials, such as quartz, lithium niobate and lithium tantalate, AlN films are compatible with monolithic

integration technology, as they can be deposited on non-piezoelectric silicon substrates yielding high SAW propagation velocities. Thin piezoelectric films of AlN show good mechanical properties and resistance to humidity and chemical etching. Moreover, the opposite values of the temperature coefficient of delay in Si and AlN make this pair of materials particularly suitable for implementing thermally stable SAW devices.

The frequency response of the SAW filters depends on the piezoelectric constants of the AlN layer, which determine the value of the electromechanical coupling factor k^2. However, some parasitic effects may affect seriously the performance of the device. Some of them are due to causes external to the device, such as the packaging and the wire bonding. Additionally, in the case of SAW devices implemented on non piezoelectric substrates, other parasitic effects arise from the device itself: for AlN films deposited on conductive silicon these effects are the interaction between the substrate and the IDTs, which causes the apparition of capacitive couplings, and the electromagnetic feedthrough (EMF) through the substrate.

In this paper we analyse the influence of some parameters on the frequency response of SAW filters implemented with AlN layers on silicon substrates: these parameters are the AlN film thickness, the geometry of the IDT contacts and the resistivity of the silicon substrates. AlN films with thickness between 0.3 μm and 3 μm were deposited with a commercial r.f. sputtering system in a mixture of Ar and N_2. Oxidized and bare silicon wafers with resistivities ranging from 0.1 Ω·cm to 8000 Ω·cm were used as substrates. The crystal structure and the preferred orientation of the films were investigated by XRD and FTIR, showing that the films had a high (00·2) texture. To fabricate SAW filters, IDTs of chromium and molybdenum of different geometries were patterned on top of the AlN films. Filters with various wavelengths, widths of the IDTs and separation between them were used for the studies. The scattering parameters (S_{ij}) of the filters were measured with a network analyzer and fitted using a circuital model. The elements of this circuital model take into account all the external and internal parasitic effects along with the theoretical response of the ideal SAW. We discuss the relation of the values of the circuital elements with the physical properties of the SAW device (geometry, substrate resistivity, thickness of the piezoelectric layer etc.) and with the parasitic effects due to the packaging and the wire bonding. The influence of the different physical properties and the parasitic effects on the actual electrical response of the filters is analyzed. Based on this analysis, some guidelines are given for the design of SAW structures with optimum frequency response.

Session: P2J
TRANSDUCER MATERIALS AND COMPOSITE MATERIALS
Chair: K. Shung
University of Southern California

P2J-1
AFM CHARACTERIZATION OF 1-3 PIEZOCOMPOSITE ARRAYS.

F. MARINOZZI[1,4], F. BINI[1], D. PASSERI[2], and A. GRANDONI*[3], [1]Mechanics and Aeronautics Department, Eudossiana, Rome, Italy, [2]Energetics Department, A. Scarpa , Rome, Italy, [3]Transducer Manufacturing Engineer, Industrial Engineering Group ESAOTE S.p.A, Caciolle , Florence, Italy, [4]Neurological Rehabilitation Hospital S. Giovanni Battista ACISMOM, L. E. Morselli , Rome, Italy.
Corresponding e-mail: franco.marinozzi@uniroma1.it

Ceramic polymer piezoelectric composites with 1-3 connectivity have become an important tool in the design and manufacture of thickness mode transducers for medical diagnostic ultrasonic imaging. The major reasons for this are that, relative to piezoelectric ceramics alone, the composite can be designed with higher thickness coupling coefficient and its acoustic impedance can be more closely matched to human tissue. These improvements lead to higher sensitivity and bandwidth in the transducer and reduce ringing due to unwanted vibration modes.

Several characterization methods and performance evaluation already exist: electrical properties measurements are performed with impedance analyzer, cross coupling evaluation are made in the frequency domain with network analyzer and in time domain via electroacoustic characterization. Electroacoustic performances are evaluated by pulse-echo operation on an immersed flat target or in transmission using an hydrophone system. Beam pattern could be evaluated by acoustic or optoacoustic method (Schlieren imaging). In previous work by Felix et al., laser interferometry demonstrates its ability for evaluation of 1-3 piezocomposite material.

Indeed, the Laser Doppler vibrometer (LDV) used by Felix et al. has a 100 mW output power with a 30 micrometers diameter of the laser beam. As a result, the power density in the measurement area is about 14 kW/cm2. Moreover, the LDV used by the authors has a 0,8-1 mW ouput power with a 10 micrometers diameter and a 175 mm focal distance, which corresponds roughly 1,3 kW/cm2. The macroscopic and microscopic damage that a high output power concentration may cause to the transducer is not known a priori. Furthermore, for a maximum change of e.g. 5mm in the LDV to transducer distance, the corresponding change in laser beam diameter is 50 micrometers. This also causes an increase of the spatial average effect when the oscillation of a surface point of the transducers is measured.

As an alternative to commercially available LDV systems, we propose a direct, mechanical method using atomic force microscopy (AFM) for in situ characterization of 1-3 piezocomposite.

AFM involves an atomically sharp probe tip affixed to a cantilevered beam which is raster scanned in close proximity over the surface of interest. Piezoactuators and feedback circuitry maintain a constant level of atomic force between the tip and the surface. The tip deflection is measured by reflecting a laser off the cantilever into a photo-detector. The AFM tip has a vertical resolution on the order of 1 nm or below, it is ideally suited for the local detection of low-amplitude vibrations. The lateral resolution of the AFM measurements can be less than 25 nm due to the very fine AFM tip. The goal of this paper is to compare two characterization methods to predict and verify the behaviour of 1-3 piezocomposite. Preliminary results about oscillation amplitude of parallel rods of PZT ceramic in a passive polymer matrix will be presented.

P2J-2
ACCURATE METHODS FOR PIEZOCOMPOSITE MATERIAL ASSESSMENT.

G. FERIN*[1,2], D. CERTON[2], and N. FELIX[1], [1]VERMON, Tours, France, [2]LUSSI \ GIP Ultrasons, Tours, France.
Corresponding e-mail: g.ferin@vermon.com

Piezocomposite materials are widely used for ultrasound imaging probes design. Such materials exhibit many degrees of freedom that can be tuned to optimize the final performances of probe. Nowadays, many numerical or analytical tools predict electrical, electroacoustic and acoustic performances of transducers. But, the key feature for proper simulations is the accuracy of the active layer full electromechanical tensor.

In this work, we present and compare two methods, an experimental one and a theoretical one, for calculation of the complete equivalent electromechanical tensor of 1-3 piezocomposite material plates.

The experimental method is based on through transmission measurements, enabling by inverse problem the characterization of passive and active layer properties. The forward problem is described with respect to the boundary conditions of the experimental set-up. The minimization process is calibrated using numerical phantom. With this method we characterize a resin plate and a high dielectric permittivity piezoceramic plate. Based on these two materials, we manufactured a 1-3 piezocomposite plate (56% volumic fraction and thickness set to target 3.5 MHz resonance frequency), measured it using the through transmission procedure and evaluated the effective electromechanical tensor.

In order to compare the experimental equivalent electromechanical tensor, we propose a technique based on the Floquet wave analysis [1]. The slowness surfaces of waves in an infinite thickness medium are first calculated, then using an inversion method, they are minimized to the slowness surfaces of an equivalent homogeneous medium. Theoretical equivalent properties of the manufactured piezocomposite have been calculated using the properties of the resin and the piezoceramic materials previously characterized.

The experimental and theoretical equivalent properties are compared, showing a very good agreement. High accuracy of the prediction is obtained particularly for the stiffness coefficients

C^E_{11}, C^E_{31} and C^E_{55}.

These techniques will offer then accurate information, for simulation model input, 1-3 piezocomposite process monitoring, and will provide to ultrasound array transducer engineers flexibility and accuracy in material choice and assessment.

[1] G. Ferin, D. Certon, and N. Felix, "Experimental and Theoretical Determination of 1-3 Piezocomposite Electro-acoustic Tensor," to be presented at World Congress on Ultrasonics, 2005.

P2J-3
MATERIAL PROPERTY VARIATION AS A FACTOR IN COMMERCIAL ADOPTION OF PIEZOCRYSTALS FOR COMPOSITE TRANSDUCER MANUFACTURE.

M. PARKER*[1], P. MARIN-FRANCH[1], S. COCHRAN[1], D. CHOI[2], and M. WALSH[2], [1]University of Paisley, Paisley, Scotland, UK, [2]PCT Ltd, Aberdeen, Scotland, UK.
Corresponding e-mail: coch-ph0@wpmail.paisley.ac.uk

Recently developed single crystal materials such as PMN-PT have shown the first step change improvement in piezoelectric material properties since the introduction of piezoceramics more than seventy years ago. This improvement is likely to feed through to high performance commercial ultrasonic transducers for applications such as non-destructive testing (NDT) and underwater sonar, provided the materials are used in piezocomposite structures with a polymer matrix. However, such commercial reality is presently dependent on a reliable material supply. In this paper, practical experience of material supply and performance is detailed. The investigation was based on a set of more than 20 pieces of nominally identical material, along with specimens shaped for material characterisation with the Piezoelectric Resonance Analysis Program, (PRAP, TASI Technical Software, Ontario, Canada). Evaluation of the samples indicated that physical properties such as density and acoustic velocity, and hence acoustic impedance and stiffness, varied relatively little from piece to piece, but that there were variations as large as ±27% in relative permittivity and ±24% in d33, compared with the average values. These variations are very large, even compared with the typical tolerances quoted for commercial piezoelectric ceramics. To assess the effect of potential material variation on transducer performance, prototype devices with conventional 1-3 piezocomposite elements made with PMN-PT have been manufactured and used as the basis for validation of results of thickness-mode modelling and finite element analysis. The validated models have then been used to explore the acceptable range of material parameters. The results indicate that routine quality assurance is a necessity if some present sources of commercial PMN-PT are to be used and that significant material cost savings may accrue if tolerance to material variation is built into the transducer specification and design.

M.Parker is supported by UK EPSRC Studentship, co-supported by PCT Ltd. P.Marin-Franch was supported by Scottish Enterprise during the work.

P2J-4
ENHANCEMENT OF THE PIEZOELECTRIC RESPONSE IN PEROVSKITES BY EXTERNAL BIAS FIELDS.

M. BUDIMIR*, D. DAMJANOVIC, and N. SETTER, Ecole Polytechnique Federale de Lausanne - EPFL, 1015 Lausanne, Switzerland.
Corresponding e-mail: marko.budimir@epfl.ch

The influence of the uniaxial bias fields (electric field and mechanical stress) on the piezoelectric properties of tetragonal $BaTiO_3$ and $PbTiO_3$ monodomain crystals is modeled in the framework of the phenomenological Landau-Ginzburg-Devonshire theory. It is shown that a compressive stress, or an electric field aplied anti-parallel to the spontaneous polarization, can significantly enhance the piezoelectric response if they are large enough; on the other hand, it is also shown that a tensile stress or an electric field applied parallel to the spontaneous polarization reduce the piezoelectric response. The enhancement effect is due to the flattening of the free energy profile and the corresponding dielectric softening of crystals, caused by the compressive stress or anti-parallel electric field. In $BaTiO_3$ crystals, at temperatures close to the tetragonal-orthorhombic phase transition temperature, the free energy profile flattening and dielectric softening are the largest along axes perpendicular to the polarization direction, facilitating thus the polarization rotation away from the $[001]_c$ polar axis. The resulting enhancement of the shear piezoelectric coefficient is directly responsible for the increase of the longitudinal piezoelectric coefficient along the $[111]_c$ axis. At temperatures deep within the tetragonal phase in $BaTiO_3$, and over the whole ferroelectric region of $PbTiO_3$, the flattening of the free energy profile and the dielectric softening by compressive stress or anti-parallel electric field are the strongest along the polar axis. The resulting enhancement of the longitudinal piezoelectric coefficient is thus the largest along the polar $[001]_c$ direction. These results, which can be applied to other perovskite crystals, have broad implications.

The authors acknowledge financial support of the Swiss National Science Foundation

P2J-5
OPTIMIZATION OF THE TRANSVERSE PIEZOELECTRIC COEFFICIENT BY DOMAIN ENGINEERING.

M. DAVIS*, D. DAMJANOVIC, and N. SETTER, Swiss Federal Institute of Technology (EPFL), Lausanne, Switzerland.
Corresponding e-mail: matthew.davis@epfl.ch

A large transverse piezoelectric coefficient d_{31} is desirable in applications such as flextensional transducers (e.g. bimorphs) and cymbal actuators though should be minimized in biomedical and sonar transducer arrays. 'Domain engineering' is already known to yield large longitudinal piezoelectric coefficients (d_{33}) in

perovskite piezoelectrics: here it is shown how d_{31} can also be tailored by domain engineering. Using room temperature monodomain data, d_{31}* has been calculated for the 6 domain engineered structures formed by poling $0.67Pb(Mg_{1/3}Nb_{2/3})O_3$-$0.33PbTiO_3$ (PMN-33PT), barium titanate (BT) and potassium niobate (KN) along non-polar axes ('*' denotes an off-axis measurement). In general, different domain variants in the structure will contribute different values of d_{31}* to that measured. Furthermore, d_{31}* is found to be strongly dependent on the choice of transverse (vibration) direction (x_1) for the domain engineered crystal: in [101]-poled PMN-33PT d_{31}* varies between +700 and -1600 pC/N for different choices of x_1. Finally, the domain engineered structures formed by tetragonal BT and lead titanate (PT) are compared. Positive values of d_{31}* are apparent in PT for certain orientations, due to its low shear coefficient (d_{15}), but not in BT, which has a much higher dielectric anisotropy: this is an extension of the well-known result for modified lead titanate ceramics. This work will be extremely useful to the design of single crystals for use in a wide range of transducers and actuators.

The authors acknowledge support from the Swiss National Science Foundation

Session: P2K
MICROMACHINED TRANSDUCERS
Chair: C. Daft
Siemens

P2K-1
PHOTOACOUSTIC IMAGING USING A TWO-DIMENSIONAL CMUT ARRAY.

I. WYGANT*, P. KUO, X. ZHUANG, D. YEH, O. ORALKAN, M. FEJER, and B. KHURI-YAKUB, E. L. Ginzton Laboratory, Stanford University, Stanford, CA. Corresponding e-mail: iwygant@stanford.edu

Photoacoustic imaging is a promising complement to pulse-echo ultrasound imaging because it provides contrast between areas with different light absorption characteristics. Specifically, regions with higher blood concentration can be identified, which is useful for the early detection of cancer. Here we present volumetric photoacoustic images of a 1 cm^3 piece of chicken breast embedded with pieces of chicken gizzard. A two-dimensional capacitive micromachined ultrasonic transducer array is used for acoustic detection. The use of a two-dimensional transducer array eliminates the drawbacks of a mechanically scanned system and enables volumetric imaging. To our knowledge, this is the first demonstration of CMUTs applied for use in photoacoustic imaging. CMUT technology enables new types of transducer arrays that would benefit photoacoustic imaging. Fully populated two-dimensional arrays, annular ring-arrays, and high-frequency arrays have all been demonstrated using CMUT technology and have advantages for photoacoustic imaging systems.

For this work, a chicken sample is suspended in an oil tank with thin nylon wires. The transducer array is located 1 cm away, at the bottom of the tank. A Q-

switched Nd:Yag laser illuminates the chicken from the side. The laser has a 1.064-um wavelength, 12-ns FWHM pulse duration, 6-mm $1/e^2$ intensity diameter, and a 10-Hz repetition rate. The laser energy is adjustable with a maximum value of 2.3 mJ. The CMUT array is 16 elements by 16 elements. Each element is 250 um by 250 um. The entire array including bias pads is 4 mm by 4.6 mm. The elements have a center frequency of 7 MHz and 87% fractional bandwidth. Using through-wafer interconnects and flip-chip bonding, the transducer array is attached to a custom-designed integrated circuit that comprises the front-end electronics. Photoacoustic and pulse-echo data are acquired one element at a time for the 256 elements of the array. Preliminary imaging results show strong photoacoustic signals and enhanced contrast for the photoacoustic image.

P2K-2
IMPROVING THE PERFORMANCE OF CAPACITIVE MICROMACHINED ULTRASOUND TRANSDUCERS USING MODIFIED MEMBRANE AND SUPPORT STRUCTURES.

S. ZHOU and J. HOSSACK*, University of Virginia, Charlottesville, VA.
Corresponding e-mail: shiwei@virginia.edu

The high signal bandwidth and consequent improved resolution of Capacitive Micromachined Ultrasound Transducers (CMUTs) have attracted significant interest in the medical ultrasound imaging community. However, one issue with CMUTs is that they exhibit relatively low conversion efficiency. This is due to in part to the fact that the edge region of the membrane has limited deformation because of physical constraint imposed by the practically rigid support walls. To improve cMUT transducer performance, we present two new cMUT structures with the objective of increasing the membrane displacement and making deformation more uniform. Both of new structure designs were analyzed using PZFlex Finite Element Analysis (FEA). In the first design, trenches are formed at the edge region on the membrane in a regular circular-shape cMUT. The maximum membrane displacement on axis was increased by 608% in a 5-trench design under the same DC bias. The edge region on the membrane achieved an even larger increase of the displacement in percentage terms compared with the center region. Thus, the most active membrane area (with deformation more than 90% of the maximum displacement) was increased by 196%, and the on-axis acoustic pressure output close to the cMUT cell was improved by 181% in the 5-trench design. In the second design, the shape of the support structure has been modified into a more flexible ‘dogleg’ shape. The maximum membrane displacement and the acoustic pressure output were increased by 148% and 24% respectively, and the membrane area with deformation more than 90% of the maximum displacement was increased by 135%. In both designs, a figure of merit (FoM) was defined (as the ratio of the average displacement over the maximum displacement) to evaluate improvement on the uniformity of the membrane deformation. It was found the FoM value was improved from 0.38 to 0.54 in the 5-trench design, and from 0.36 to 0.53 in the “dogleg” design. Since the two new designs made the transducer structure more flexible, the resonance frequency became lower. However, FEA simulation demonstrated

that the effective electromechanical coupling coefficient (k) was significantly improved by 438% in the 5-trench design and 172% in the “dogleg” design. Therefore, the fractional bandwidth was increased, the output pulse length was shorter, and consequently, the axial resolution was actually improved.

Paul Reynolds Ph.D. Weidlinger Associates Inc., Los Altos, CA, Funding: NIH EB002349, EB001826, US Army W81XWH-04-1-0240

P2K-3
A LUMPED CIRCUIT MODEL FOR THE RADIATION IMPEDANCE OF A 2D CMUT ARRAY ELEMENT.

A. BOZKURT*[1] and M. KARAMAN[2], [1]Sabanci University, Istanbul,Turkey, [2]Isik University, Istanbul,Turkey.
Corresponding e-mail: abozkurt@sabanciuniv.edu

Recent advances in CMUT fabrication and integration techniques lead to research efforts on the realization of 2D arrays for 3D ultrasonic imaging. Since the Nyquist criteria for spatial sampling of a 2D aperture restricts the element size in both dimensions, the sensitivity of a 2D array element becomes substantially small. This imposes more stringent requirements on the front-end electronics in terms of the parasitics and noise figure. Therefore, the performance of the front-end circuit must be thoroughly analyzed using an accurate circuit model of the transducer element. The Mason equivalent circuit assuming a large transducer size relatively to the wavelength, does not have any reactive part in the radiation impedance. For the case of a 2D array element, however, the radiation impedance has a significant reactive part since the element size is comparable to the acoustic wavelength.

In this paper, we present an approach for the derivation of an equivalent lumped circuit model that accounts for the non-zero reactive radiation impedance of a 2D CMUT array element. Using the finite element method (FEM) we first found the radiation impedance of a 2D array element composed of CMUT cells. The simulation results showed that the element had a complex radiation impedance similar to that of a piston transducer with an effective area having a value between the element’s overall area and the total active area of the CMUT cells constituting the element. As the second step of our analysis, we showed that the complex radiation impedance of the 2D array element can be represented by a simple resonant circuit placed parallel to the real radiation impedance in the Mason’s equivalent circuit. The component values of the reactive lumped elements forming the resonant circuit were determined by fitting the impedance of overall equivalent circuit to the FEM results through an iterative procedure. To test the lumped circuit model, we first performed the FEM analysis of a $200\times200\mu m^2$, 2.5MHz 2D array element composed of 5×5 CMUT cells, and calculated the radiation impedance over a frequency range from 1 to 4MHz. The parallel resonant circuit parameters determined by impedance fitting were C=4.5fF and L=156.4mH, where the resulting radiation impedance approximates the FEM result with 6% accuracy. This approximation was found to be valid for up to 120% fractional bandwidth, independent to the operation center frequency, provided that the transducer size is smaller than half of a wavelength. In conclusion, the lumped equivalent circuit model investigated here can be used for fast and accurate

analysis of 2D CMUT array elements using conventional circuit simulation tools.

Keywords: 2D CMUT arrays, 3D acoustic imaging, transducer model, radiation impedance.

This work is supported by the Turkish Natinal Science and Technical Research Council (TUBITAK).

P2K-4
IMPLEMENTATION OF MASTER CURVES FOR CMUT ARRAYS DESIGN.

F. TESTON*[1], D. CERTON[1], F. PATAT[1], and N. FELIX[2], [1]LUSSI, Tours, France, [2]VERMON, Tours, France.
Corresponding e-mail: francktesto n_info@univ-tours.fr

Capacitive micromachined transducers are competitive candidates for high performance ultrasonic imaging arrays in a wide frequency range. Furthermore, technology offers several degrees of freedom for the design and optimization for such devices. First, at elementary cell scale : the geometrical parameters and mechanical properties of the different layers must be considered in order to adjust electromechanical coupling coefficient, collapse voltage, resonance frequency and capacitance. On the other hand, for array elements, the size and layout of cells are essential for the radiated acoustic field. Through a parametric study, the purpose of this paper is to compare the performances of square and rectangular shapes to commonly used circular and hexagonal shapes.

The simulation of the static and dynamic response of one array element composed of rectangular cells is described. It is based on the model previously described in the case of circular cell [1]. Firstly, the plate equation with non-uniform flexion rigidity and electrostatics is solved using finite difference method. The static regime is solved in order to extract the electromechanical coefficient, the collapse voltage and the static capacitance. Then, the dynamic regime is modelled considering small signal amplitude as compared with the bias voltage. Fluid is taken into account in an equivalent electromechanical scheme by the mechanical radiation impedance of rectangular shape cells with periodic distribution.

The influence, in terms of final performances, of both geometrical parameters and mechanical properties of the CMUT layers have been studied with different rectangular shapes, membrane thicknesses, electrodes and gaps. Then master curves, like the collapse voltage, the electrical anti-resonance frequency, the capacitance and electromechanical coupling factor as a function of geometrical parameters were calculated and compared for each test configuration. Results show that the global behaviour of array elements did not depend on the shape of the elementary cell and geometries but massively on other constituent parameters.

[1] Certon et all., to be published in IEEE-UFFC Special Issue on Micromachined Ultrasonic Transducers, 2005.

This work was performed within the EURIMUS program: MEMSORS, and financed by the French Ministry of Finance and the Direction Generale de l Entreprise (DGE).

P2K-5

THE CHARACTERISATION OF CMUTS AT LOW GAS PRESSURES.

L. DAVIS*[1], D. HUTCHINS[1], R. NOBLE[2], and D. BANFIELD[3], [1]University of Warwick, Coventry, UK, [2]QinetiQ Ltd, Malvern, UK, [3]Cornell University, Ithaca, NY.
Corresponding e-mail: D.A.Hutchins@warwick.ac.uk

There is a need for the measurement of gas flow in low pressure environments. One example is the estimation of wind velocity on the surface of other planets within the solar system, such as Mars. One possible approach to this is to use gas-coupled cMUTs to send ultrasonic signals in counter-propagating directions, and thus measure the time of flight changes. The main challenge to such a measurement is the fact that the pressure at the surface of Mars is low (~6 mbar), and predominantly carbon dioxide. Both of these factors will cause increased attenuation over measurements in air at atmospheric pressure. In addition, the frequency response and sensitivity of the devices will change with pressure. This paper will report results from measurements at low pressures in the laboratory, using a vacuum chamber into which various gases could be introduced. cMUTs with different membrane thicknesses and surface areas were investigated. The experiments indicated that, as expected, the centre frequency of operation reduced with pressure. However, it has been shown that signals can be propagated through gases such as air, carbon dioxide and helium at very low pressures, down to values below 10 mbar. The results are shown to agree with analytical models, which predict the behaviour of the cMUTs as a function of pressure.

Funded by the Worshipful Company of Scientific Instrument Makers and EPSRC.

P2K-6

CMUT DESIGN CHARTS TO MAXIMIZE THE GAIN-BANDWIDTH PRODUCT.

S. OLCUM* and A. ATALAR, Bilkent University, Ankara, Turkey.
Corresponding e-mail: selim@ee.bilkent.edu.tr

Capacitive micromachined ultrasonic transducers (cMUT) have large bandwidths, but they typically have low conversion efficiencies. In this work we define a performance measure in the form of a gain-bandwidth product to investigate the conditions that optimize the gain and bandwidth with respect to device dimensions, electrode size and electrical termination resistance.

For the transmit mode, where the electrical input power is essentially unlimited, we define the figure of merit as the pressure-bandwidth product. With such a measure only the mismatch at the acoustic port is considered. On the other hand, in the receive mode the acoustic input power is limited. In this case, the performance measure is defined as the transducer power gain-bandwidth product to include the effects of acoustic mismatch as well as the electrical mismatch. For transmit mode the applied bias voltage is assumed to be 45% of the collapse voltage while it is 90% for the receive mode.

In the transmit mode, larger and thicker membranes produce a higher pressure but a lower bandwidth. Fully-metallized membranes achieve a higher pressure-bandwidth product compared to partially metallized ones. It is shown that the bandwidth is not affected by the electrode size. However, the output pressure drops with the electrode radius due to the decrease in the total electric field in the gap. For example, a device (50 μm radius, 2.5 μm thickness) with full electrode yields 71 kPa pressure and a band of 1.4 MHz to 13 MHz. The same cMUT with a half electrode yields 56 kPa output pressure with the same bandwidth. The pressure produced by the cMUT increases with the increasing gap height because of the rise in the collapse voltage.

In the receive mode, the matching at the acoustical port is achieved by adjusting the mechanical impedance of the membrane, while the matching at the electrical port is achieved by optimizing the number of cMUTs connected in parallel. We show that the top electrode radius does not affect the bandwidth. The transducer gain can be maximized by optimizing the electrode radius. The maximum gain is achieved when the electrode is between 45% and 55% of the full membrane radius. The simulations show that the optimum dimensions for a receive mode transducer operating around 5 MHz are 83 μm radius, 7 μm thickness and 50% top electrode radius. This optimum device yields 100% fractional bandwidth and -2.3 dB conversion efficiency. It is calculated that the impedance seen by one cMUT cell should be 120 KΩ in order to achieve this performance, i.e. for an electrical load of 1 KΩ, 120 cells should be connected in parallel. We determine that the receive mode performance is independent of the gap height.

We present normalized charts for designing an optimum cMUT cell at the desired frequency for transmit, receive or pulse-echo modes. Design examples are given to clarify the use of these charts.

P2K-7

FABRICATION AND CHARACTERIZATION OF A MICROMACHINED ULTRASONIC TRANSDUCER.

C. JIA*[1], M. WIEMER[2], J. MEHNER[2], T. OTTO[2], and T. GESSNER[1], [1]Center for Microtechnologies, Chemnitz, Germany, [2]Fraunhofer Institute for Reliability and Microintegration, Chemnitz, Germany.
Corresponding e-mail: chenping.jia@zfm.tu-chemnitz.de

This abstract does not appear in the online abstracts at the author's request.
It will appear in the print version.

P2K-8

DESIGN, FABRICATION AND CHARACTERISATION OF CAPACITIVE MICROMACHINED ULTRASONIC TRANSDUCERS BASED ON A 2D-LIKE ARCHITECTURE.

S. CLATOT*[1], P. BLIND[2], V. PÉTRINI[1], L. GAUTHIER-MANUEL[1], M. WILM[1], R. BERRIET[3], J.-C. JEANNOT[1], and S. BALLANDRAS[1], [1]FEMTO-ST, CNRS, Besançon, France, [2]CTMN, Besançon, France, [3]IMASONIC SA, Besançon France.
Corresponding e-mail: ballandr@femto-st.fr

The possibility to excite and detect acoustic waves in fluids using capacitive micro-machined ultrasonic transducers (cMUT) built on silicon using clean room techniques offers attractive opportunities for manufacturing high quality low cost imaging probes. CMUTs developed for acoustic imaging exploit the first flexural mode of very thin and stiff membranes, leading to bandwidth up to 100% and more. Furthermore, their fabrication requires the use of microelectronics processes yielding opportunities for co-integrated devices (electronics and transducers on the same chip). These transducers can be accurately analysed or even designed using mixed finite element analysis/boundary element methods (FEA/BEM). Particularly in the case of massively periodic structures such as MUTs, periodic FEA is flexible enough to allow for the simulation of devices exhibiting complicated shape interfaces and involving materials of different nature, taking acoustic and dielectric losses into account. In that situation too, BEM are particularly well-suited to provide an accurate description of any stacked medium assuming flat interfaces for the radiation area and the layer interface as well. Such simulations can be conducted for 2D and 3D. Numerous information can be derived from these calculations, for example the resonance frequency, the electromechanical coupling coefficient, the quality of the resonance, but

also more advanced and design-oriented parameters such as emission, reception and transmission transfer function, cross-talk between adjacent pixels, directivity, and so on.

In this work, we report on the design and test of a cMUT structure based on a thin silicon membrane shaped in order to comply our modelling assumptions, i.e. long 2D-like cMUT cells able to operate conformably to the simulated operation of an actual 2D structure. The device is designed to operate at 6 MHz in air and to exhibit an operation bandwidth larger than 100% in water. It is shown how to compute the above mentioned transfer functions using our own periodic FEA/BEM code, and a comparison between 2D and 3D simulation results is presented. The 2D-like structure has been built, shaping the edge of the membrane circularly to favour its flexural motion. The silicon membrane is about 1.5 μm thick and the leading lateral dimension is 42 μm. Different parameters of the transducer are then measured and compared to computation results, as for instance the resonance frequency which agrees well with theoretical predictions. This allows for determining the efficiency of the design approach

based on a 2D restriction of the problem, and also to validate the 3D analysis by experimental assessment, particularly checking the correspondence between theoretically predicted and experimentally measured parasitic modes. Cross-talk measurements are performed in air, and finally, the operation of our cMUT in water is tested.

This work is supported by the EC in the MUSTWIN project within the 6th PCRD programm

P2K-9
BACKING REQUIREMENTS FOR CMUT ARRAYS ON SILICON.

S. BERG* and A. RØNNEKLEIV, Norwegian University of Science and Technology, NTNU, Trondheim, Norway.
Corresponding e-mail: sigrid.berg@iet.ntnu.no

This paper will present simulations based on a CMUT array model described by A. Rønnekleiv in an accepted paper to be published in the IEEE-UFFC Transactions special edition on CMUTs later this year. The model is based on a combination of a free acoustic mode description of an isolated CMUT and the coupling of these modes to the fluid outside the CMUTs where waves can be exited or detected. The parameters of the model describing the isolated CMUT is independent of frequency and excitation of adjacent CMUTs whereas the acoustic impedance matrix describing the coupling to fluid will depend both on the excitation of neighbouring CMUTs and frequency. However, since the silicon substrate is not rigid, some of the forces from the membrane vibration will lead to motion of the substrate that may degrade the radiation pattern.

The aim of this study is to quantify the maximum thickness of a well backed silicon substrate that can be used in a CMUT array, without severely degrading the array performance. The effect of using several bonded silicon layers in the substrate is also included. For the substrate, the simulations are based on Adler's matrix method applied to acoustic waves in multilayer structures. As an

approximation, we have assumed that the silicon is isotropic with elasticity parameters: c11=16.57e10 Pa, c12=4.23e10 Pa and c44=6.17e10 Pa, which gives a surface wave velocity of 4689m/s.

We have looked at a structure consisting of circular CMUTs in an infinite array, each with a diameter of 66 μm with a centre frequency of 3.75MHz. An infinite absorbing backing, matched to the silicon for longitudinal waves perpendicular to the CMUT plane is assumed. When the substrate is properly backed the main interaction between the CMUTs and the substrate is with the surface wave in the substrate which is phase matched with the transmitted wave into water at about 15-20 degrees steering angle.

To accomplish less than 0.5dB ripple at 100% bandwidth, the maximum thickness for a compact backed silicon substrate at 3.75MHz centre frequency is 550 μm. Many authors suggest bonding several layers of silicon; this is expected to increase the compliance of the structure. If the bond introduces a compliance of 60fm/Pa or 130fm/Pa, the maximum total silicon thickness is reduced to 450 μm or 350 μm respectively. These compliances correspond to layers of 5 μm or 11 μm Araldite 502/956 from Ciba or a stiff set of bonding pads covering 50% or 25% of the total bonding area for a lateral centre to centre distance between the pads of 200 μm. This is a reasonable distance between CMUT elements at 3.75MHz centre frequency in a 2D array.

At the symposium we will present work incorporating the anisotropy of the silicon and more realistic models of a flip chip bond.

The research is supported by The Research Council of Norway.

P2K-10
BANDWIDTH IMPROVEMENT IN A CMUT ARRAY WITH MIXED SIZED ELEMENTS.

C. BAYRAM* and A. ATALAR, Bilkent University, Ankara, Turkey.
Corresponding e-mail: cbayram@ug.bilkent.edu.tr

A single cMUT cell can not be used as a stand-alone acoustic transducer, since its area is too small. Conventionally, many cMUT cells are connected in parallel to obtain larger size transducers. These arrays are typically fabricated by concatenation of cMUT cells with identical physical dimensions such as radius, a, membrane thickness, t_m, and gap height, t_g. If the interconnect parasitics are negligible, it can be easily shown that the bandwidth performance of the resultant cMUT array is almost the same as the bandwidth of the single cMUT cell.

If the membrane thickness is kept fixed, the radius of the cMUT determines the center frequency of operation. A smaller radius implies a greater center frequency. Therefore, it should be possible to put cMUTs with different sizes in parallel to get a larger bandwidth at the expense of reduced gain. In this work, we investigate the optimization of the bandwidth characteristics of a cMUT array by using mixed size cells in the array.

Due to the fabrication technique of cMUTs, all cells within an array should have the same membrane thickness and the same gap height. In a mixed array, the

cMUTs will have varying radii. It is known that the collapse voltage of the cMUT is inversely proportional to the square of the radius[1]. Hence, the collapse voltages of different sized cMUTs will not be the same. On the other hand, it is desirable to operate the cMUTs very near the collapse voltage to maximize performance. Since all cMUT cells within an array are electrically parallel, we should find a method to equalize the collapse voltages of different sized cMUTs: If the electrodes on different sized cMUT cells are properly dimensioned, it is possible to equalize the collapse voltages.

We chose to work with just two different sized cMUTs in parallel. The number of cells of each kind is optimized to get a flat frequency response over the bandwidth.

With the techniques summarized above we were able to design a mixed size cMUT array with a predicted fractional bandwidth value of about %155. This value is about %55 better than what can be achieved with a uniform size array. Moreover, this method does not sacrifice the gain more than necessary. There is almost no loss in the gain bandwidth product.

The table below summarizes the predicted results for mixed size arrays with a center frequency of 5.4 MHz. The first row presents the gain and bandwidth values for a conventionally optimized cMUT array. The last row shows the values for a mixed size array obtained from cMUTs of rows two (f_c = 7.12 MHz) and three (f_c= 2.98 MHz). It is clear that we obtained a significant raise in bandwidth with a little loss in gain bandwidth product.

Comparison of uniform size cMUT array and mixed size cMUT array

cMUT Array Elements (all dimensions in um)	Gain	Band width GxBW (MHz)	(MHz)f_c	(MHz)$frac_{GxBW}$	$frac_{BW}$	
a=73.4um t_m=7um t_g=0.6um %50-%70						
Electrode	0.421	5.46	3.54	5.45	0.650	%100
a=60 t_m=6 t_g=0.6 FULL						
Electrode $cMUT_2$	0.392	6.49	4.06	7.12	0.570	%91

Reference[1] A. Bozkurt, I. Ladabaum, A. Atalar, B. T. Khuri-Yakub. Theory and Analysis of Electrode Size Optimization for Capacitive Microfabricated Ultrasonic Transducers. IEEE Trans. on UFFC, vol. 46, pp. 1364 - 1374, Nov. 1999.

P2K-11

ENHANCED ECHOGRAPHIC IMAGES OBTAINED IMPROVING THE STRUCTURAL MEMBRANE LAYER OF THE CMUT PROBE.

A. SAVOIA*[1], G. CALIANO[1], R. CAROTENUTO[1], C. LONGO[1], P. GATTA[1], A. CARONTI[1], E. CIANCI[2], V. FOGLIETTI[2], and M. PAPPALARDO[1], [1]University Roma Tre - Dept. of Electrinics, Roma, Italy, [2]CNR-IFN, Roma, Italy.
Corresponding e-mail: savoia@uniroma3.it

The possibility to generate and receive ultrasounds with capacitive micromachined cMUT probes, for medical diagnostic, has been demonstrated by many authors during the last few years.

The quality of the obtained images benefits from the excellent bandwidth characteristic of capacitive probes but, on the other hand, it suffers from their limited sensitivity, if compared to equivalent piezoelectric probes.

The problem of low sensitivity, which is still under investigation in several laboratories, has many causes, ranging from the transducer physics, the non-optimum design and the fabrication technology; in particular the technology used for the deposition of the structural layers of the micro-membranes has often evidenced limits both physical and chemical of deposited material layer, such as elevated porosity, low resistivity, poor sealing of the cavities, etc.

The parameter that summarizes these limits can be the resistivity of the nitride structural film. In the past, we produced a PECVD nitride film with a resistivity of approximately 10^8 $\Omega\times$cm. Recently, in our laboratories a dual-frequency PECVD process has been made available. Such a process uses two frequencies of excitation of the plasma: one at high frequency (HF) and the other at low frequency (LF).

The deposition of the silicon nitride is carried out mainly using the HF generator but, for a variable time (up to some tens of seconds) the LF generator is also used. In this way, the stress of the silicon nitride can be controlled with extreme precision, on a wide range of values, depending on the time of ignition of the LF generator.

The fabricated silicon nitride film shows higher performances from the electrical point of view (the resistivity is increased up to about 10^{14} $\Omega\times$cm) and a lower porosity, in respect to the single frequency PECVD nitride.

The porosity of the obtained dual-frequency PECVD nitride film is extremely reduced, contributing to effectively sealing the underlying cavities of the cMUT membranes.

The improvement of both mechanical and electrical properties of the cMUT structural layer has led to higher transmission and reception sensitivity.

Using this silicon nitride deposition technique, we have fabricated 64-elements, 6-MHz echographic probes featuring 100% bandwidth and superior sensitivity characteristics evidencing a remarkable improvement in the quality of the obtained echographic images.

The authors are grateful to Esaote S.p.A. for their continuous support.

ORAL SESSIONS

Session: 1E
PORTABLE DEVICES AND OTHER NEAT STUFF
Chair: K. Bom
Erasmus MC

1E-1 11:30 a.m.
(Invited)
TELEMEDICINE: WHAT IS IN PLACE TODAY? WHAT ARE THE CHALLENGES FOR THE FUTURE?

J. SOUQUET*, Philips Medical Systems.
Corresponding e-mail: jacques.souquet@mac.com

Imaging is undergoing significant mutations with the impact of digital technology, new data acquisition paradigms and the advent of genomic medicine as it relates to molecular medicine. Furthermore an acute observation of the world indicates that speed (or time) has become a crucial parameter of our lives. Society is in overdrive and wants more, faster and better. This paradigm will be explained in the context of better image quality, faster data acquisition and more efficient integration in the total workflow environment. Telemedicine has become an essential part to address this problem. This presentation will not only deal with what is in place today , but will try to address the challenges we are going to be faced with in the future.

1E-2 12:00 p.m.
RECONFIGURABLE ARRAYS FOR PORTABLE ULTRASOUND.

R. FISHER*[1], K. THOMENIUS[1], R. WODNICKI[1], D. MILLS[1], C. HAZARD[1], S. COGAN[1], R. THOMAS[1], B. KHURI-YAKUB[2], A. ERGUN[2], and G. YARALIOGLU[2], [1]GE Global Research, Niskayuna, NY, [2]Stanford University, Stanford, CA.

Corresponding e-mail: fisher@crd.ge.com

A collaborative effort between GE Global Research and Stanford University is aimed at the development of reconfigurable array technology. The goal is to enable innovative medical ultrasound imagers ideally suited to portable ultrasound and applications such as remote emergency medicine and combat casualty care. Success depends on developing several technologies, the first of which is capacitive micromachined ultrasound transducers (cMUTs). The monolithic nature of cMUTs facilitates close connection with microelectronics. Thus a second technology under development is a switch matrix application specific integrated circuit (ASIC) that will enable the changing of interconnect between cMUT cells. The reconfigurable array concept arises from this ability to dynamically combine cMUT cells to form ideal apertures for a given imaging

target (e.g. annular and phased apertures of various ring widths) and to move these apertures across the reconfigurable array plane [1-4]. Two central hypotheses are being tested: (1) the reconfigurable array can acquire acoustic pulse-echo data in a manner equivalent or superior to todays 1D piezoceramic arrays (2) reconfigurable array technology will enable highly portable ultrasound platforms.

The first steps to prove the hypotheses by demonstrating key technologies have been taken. A Stanford designed and fabricated 20-ring cMUT annular array showed similar performance to a conventional piezoceramic linear array. In addition, piezoceramic reconfigurable arrays have been fabricated. A switch matrix ASIC that interconnects a 16 x 16 array of transducer elements was developed to enable reconfiguration of an acoustic aperture in real-time. Acoustic testing with the static cMUT annular array has excellent agreement with simulated beam profiles, transmit/receive signal bandwidths, and acoustic sensitivity. Comparison of images taken on phantoms shows similar performance with a conventional PZT ultrasound probe, however, with 6x lower channel count. The switch matrix ASIC has been connected to a 256 element PZT array such that various acoustic patterns have been scanned across the array and measurements taken which provide understanding of signal integrity and real-time aperture agility. Detailed comparisons of the reconfigurable array performance with acoustic field simulation and an equivalent PZT device will be discussed.

In conclusion, the ability to achieve image quality using only 20 annular elements comparable to that of high-end transducers with 128 linear elements will be discussed. The result is intended to be a significant decrease in the channel count and the associated signal processing electronics. This is a key step toward establishing the feasibility of highly portable systems.

US Army Medical Research Acquisition Activity DAMD17-02-0181

NIH (NIBIB) R01 EB002485, Low Cost Ultrasound Using Silicon Transduction.

[1] Patent #6,865,140

[2] Hazard, Annular array beamforming for 2D arrays with reduced system channels, 2003 IEEE Ultrasonics Symposium

[3] Bailey, A computer controlled transducer for real-time 3D imaging, Acoustical Imaging, Vol. 18

[4] Patent #4,641,660

1E-3 12:15 p.m.
SCREAM - A DISCRETE TIME MICROBEAMFORMER FOR CMUT ARRAYS.

T. HALVORSRØD*, L. R. CENKERAMADDI, T. YTTERDAL, and A. RØNNEKLEIV, Institute of Electronics and Telecommunication, Norwegian University of Science and Technology, Trondheim, Norway.
Corresponding e-mail: halvoth@ifi.uio.no

It is believed that more than 80% of sudden heart attacks are caused by rupture of vulnerable plaques leading to the formation of blood clots and subsequent

coronary stenosis and infarction. Techniques which could distinguish between plaques of different kind is therefore of great interest. This paper describes system level analysis of an intravascular ultrasound imaging system using SystemC. SystemC is a C++ extension library offering features like structural description, concurrency, communication and synchronization and is perfect for discrete time SoC analysis. The imaging system described is constructed using CMUT for signal sources and clocked mixed-signal microelectronics to realize the active modules. The sampling frequency is 120MHz and the signal center frequency is 30MHz. To practically be able to construct an array imager, some signal processing must be carried out as early as possible in the signal chain. An integrated signal processor doing such a job is referred to as a μbeamformer. The processor must reduce the number of signals without wasting information. A direct beamformer implementation adds up a number of signal channels, each having an individual, programmable and dynamical updatable phase shift. This operation can be done both in the analog and in the digital domain. Digital beamforming offers much higher flexibility than the analog counterpart. Though, analog signal processing is far more power efficient due to the fact that one can avoid high speed, high dynamic range analog-to-digital converters. Analysis of analog sub-systems is traditionally carried out in SPICE. When the number of transistors exceeds several thousand the simulation time increases dramatically. A system as described above will contain several tens-of-thousands discrete circuit elements. Architecture-level SPICE simulations become very time consuming. System C offers a much better framework to simulate such a system through the use of compiled code. Simulation time is strongly reduced. A discrete time μbeamformer using a ring buffer of capacitors to sample and hold the information constructs the core of the system. This is an extremely power efficient way of temporarily storing a history of the analog signals. The presented architecture assumes a source bank of 16 CMUT elements. Based upon beam-steering-angle and focus a channel dependent phase shift is calculated. To save power all elements requiring the same phase shift within the quantization boundaries are connected to the same pre-amplifier. Each pre-amplifier is connected to a capacitive ring-buffer. All ring-buffers are next connected and added through a cross-point matrix to a common, clocked, low-input impedance amplifier. The configuration of the cross-point matrix is controlled by the desired steering-angle and focus. The system level analysis demonstrates functionality and estimates power consumption, chip area, sensitivity and dynamic range. The effects of mismatch and jitter are demonstrated.

The authors acknowledge the Norwegian Research Council through the project ASICs for Microsystems (project number 133952/420) for the financial help to write this paper.

1E-4 12:30 p.m.
DUAL-ARRAYS BRAIN IMAGING PROTOTYPE: EXPERIMENTAL IN VITRO RESULTS.

F. VIGNON[1], J. AUBRY[1], M. TANTER[1], A. MARGOUM[2], J. LECOEUR[3], and M. FINK*[1], [1]Laboratoire Ondes et Acoustique, Paris, France, [2]ESME Sudria, Ivry, France, [3]Lecoeur Electronique, Chuelles, France.
Corresponding e-mail: francois.vignon@loa.espci.fr

Ultrasonic imaging systems assume a constant acoustic velocity in human tissues in the beamforming process. However, in the case of brain imaging, skull aberrations induce distortions in the wave front. Focusing quality behind a skull bone is strongly degraded, resulting in distortion, resolution damage and contrast lowering of transcranial images.

It has been shown that a very accurate focusing can be achieved through the skull by using the Spatio Temporal Inverse Filter (STIF) technique. This method, however, requires the presence of a set of acoustic sensors within the focal region (the brain) and cannot be directly used for medical imaging.

We present here a new electronic prototype with a high sensitivity driving two arrays of transducers located on each side of head. This prototype is made of 128 fully programmable electronic channels coupled to a 256/256 multiplexer allowing to work in transmit or receive mode simultaneously with the 128 elements of the arrays. It has been programmed to image the brain thanks to a non invasive focusing method inspired by the STIF technique. The left array is used to image the right hemisphere contralaterally and vice-versa. In a first step, the two arrays surrounding the skull perform a simplified tomography of the skull, measuring the attenuation and the speed of sound induced by the skull wall in front of each array. In a second step, the STIF technique is used to determine the set of signals that should be sent from the left array to focus optimally on the right array outside the head. In a third step these emission signals are angulated to bring the focal spot back inside the right hemisphere of the brain. The acoustic map of the right skull wall obtained in the first step is used in the angulation process to take into account the fact that the focal spot has to “cross” the right skull wall.

Non invasive adaptive focusing quality has been experimentally evaluated, showing that the non invasive STIF technique improves the focusing quality up to 15db with respect to the non corrected (cylindrical) wave fronts used in the beamforming process of commercial scanners. The technique has been used to acquire in vitro images of tissue phantoms behind a skull wall, exhibiting the image quality enhancement with respect to images obtained with cylindrical focusing.

This work was supported by grant QLG1-CT-2002-01518 (UMEDS: Ultrasonographic Monitoring and Early Diagnosis of Stroke) from the European Commission.

1E-5 12:45 p.m.
IN VIVO ULTRASOUND BIOMICROSCOPY OF SKIN WITH 20 MHZ AND 100 MHZ RANGE ULTRASOUND: INVERSE ECHO SIGNAL FILTERING OPTIMIZATION.

M. VOGT*[1,3], B. PAUL[2,3], S. SCHARENBERG[2,3], R. SCHARENBERG[2,3], and H. ERMERT[1,3], [1]Institute of High Frequency Engineering, Ruhr-University Bochum, Bochum, Germany, [2]taberna pro medicum GmbH, Lueneburg, Germany, [3]Ruhr Center of Excellence for Medical Engineering KMR, Bochum, Germany.
Corresponding e-mail: Michael.Vogt@rub.de

High-frequency ultrasound (HFUS) in the 20 to 100 MHz range fulfills the opposing requirements concerning spatial resolution and penetration depth for in vivo ultrasound biomicroscopy (UBM) of skin. Because transducer arrays are not yet available for the upper range of this frequency band, spherically focused single element transducers are utilized. The spectra of acquired radio frequency (rf) echo signals change over depth because of the sound beam characteristics and the strongly frequency dependent attenuation of tissue. The potential of inverse echo signal filtering for the optimization of pulse echo measurements with spherically focused HFUS transducers is analyzed and validated.

We have implemented a HFUS imaging system with two separate transducers working in the 20 MHz and 100 MHz range. For imaging, mechanical scans are performed and rf echo signals are digitized (100 MHz and 500 MHz sampling frequencies for 20 MHz and 100 MHz range transducers). The system′s point spread function (psf), which is significantly depth dependent, has been analyzed performing phantom measurements (glass plate surface, speckle phantom). Inverse filters are obtained for different depths by fitting Gaussian model spectra to calculated reference spectra in a least mean square error sense and inverting corresponding spectra. B-mode images are obtained applying the proposed inverse filtering and calculating the magnitude of analytical echo signals utilizing the Hilbert transform. In order to validate the proposed method, in vivo measurements have been performed at healthy skin and skin lesions. Clinical images have been acquired with both transducers at each localization.

The design of the implemented UBM system is presented and discussed. With the 20 MHz range transducer, imaging of the skin and subcutaneous fat is facilitated with a minimum 55 μm / 170 μm axial / lateral resolution. For high resolution imaging of the upper skin, the 100 MHz range transducer is utilized. A broadband electronics (pulser: 1.8 ns pulse width, 63 V peak amplitude; receiver: 170 MHz cut-off frequency, 43 dB gain) has been developed to drive the transducer. Utilizing the proposed inverse filtering, imaging beyond the two transducer′s depth of field (DOF: 3.8 mm / 1.1 mm for 20 MHz / 100 MHz range transducers) is optimized. In vivo images show that the new 100 MHz range UBM enables a detailed imaging of the palmar skin and the upper dermis. The delineation of skin tumors and inflammable tissue from the surrounding tissue is significantly improved compared to the 20 MHz range sonography.

The presented UBM system supports both, 20 MHz range sonography, which is already established in dermatology, as well as a new 100 MHz range technique for high resolution in vivo imaging of skin. In combination with the proposed inverse filtering approach, a significantly improvement of HFUS based skin imaging has been proven.

The work is supported by the Federal Ministry of Education and Research, Germany (BMBF), grant 13N8079.

Session: 2E

CARDIOVASCULAR
Chair: M. O'Donnell
University of Michigan

2E-1 11:30 a.m.
A STATISTICAL MODEL-BASED APPROACH FOR THE DETECTION OF ABNORMAL CARDIAC DEFORMATION.

F. AOUED*[1], E. EROGLU[1], L. HERBOTS[1], F. RADEMAKERS[1], and J. D'HOOGE[1,2], [1]Cardiac Imaging Research- Department of cardiology, Catholic University of Leuven, Leuven, Belgium, [2]Medical Image Computing- Department of electrical engineering, Catholic University of Leuven, Leuven, Belgium.
Corresponding e-mail: fathi.aoued@student.kuleuven.ac.be

Introduction: Ultrasound deformation imaging of the heart, i.e. strain rate imaging, has been introduced for the assessment of regional myocardial function. To date, regional function has typically been characterized using deformation parameters such as peak systolic strain rate (SR), end-systolic strain (ε) and post-systolic ε. However, as both ε and SR information is measured over the whole cardiac cycle, this approach does not exploit all data available. The aim of this study was thus to set out a methodology allowing for an optimized use of the data at hand. Hereto, the behavior of the ε and SR curves over both the whole (W) and the systolic (S) part of the cardiac cycle was compared to a statistical model of normal deformation patterns using principle component (PC) analysis.

Methods: Myocardial Velocity Imaging (MVI) data were acquired in 90 normal (N) subjects and in 10 patients with angiographically proven coronary artery disease (CAD) using a GE VingMed Vivid7. For each subject, data were acquired in the apical 2-,3- and 4-chamber views and post-processed using custom software (SPEQLE) in order to extract ε and SR traces in an 18-segment model of the left ventricle (LV). ε and SR curves from 80 randomly selected normal subjects were used to construct the principal modes of variation between normal individuals, i.e. the PCs. Subsequently, the 10 remaining normal subjects and the 10 patients were used for validation of the model. Hereto, a statistical distance from normality, i.e. the reference model, was constructed based on the PCA theory for each LV segment. Several distance measures (D) were compared based on the first three components (indexed ′123′) and based on the second and third components only (indexed ′23′). Moreover, each distance measure was constructed based on the ε and SR behavior over the whole and the systolic part of the cardiac cycle. In order to find the optimal distance measure, the average distance for the normal subjects and the patients were calculated and compared using a student′s t-test. Finally, the optimal distance measure was used to construct bull′s-eye representations of the LVs of these 20 subjects in order to be classified by a blinded cardiologist as either normal or pathologic. Based on these readings, sensitivity and specificity of this representation for the detection of CAD were calculated.

Results: see table

Conclusions: The most promising distance measure for detecting CAD showed to be based on the first three PCs of the S curve. This distance represented in a bull′s-eye plot showed a sensitivity and specificity of 80% and 100% respectively for the detection of CAD. Principle component analysis of ultrasound deformation data might thus offer a new approach towards the detection of abnormal myocardial deformation.

Student's t-test results

	D23eS	D23eW	D123eS	D123eW	D23SRS	D23SRW	D123SRS	D123SRW
N	0.0969±0.0199	0.2147±0.0301	0.2563±0.0430	0.2685±0.0788	1.2293±0.1666	1.7911±0.1058	1.3027±0.1050	1.7429±0.1857
CAD	0.1416±0.0152	0.2422±0.0311	0.4144±0.0580	0.4625±0.0632	1.7642±0.2377	2.0081±0.4334	1.2443±0.1186	1.5993±0.5661
P value	0.0028	0.2218	3.7174e-005	5.1781e-005	0.0229	0.2830	0.2591	0.3922

2E-2 11:45 a.m.
FULL STRAIN TENSOR CHARACTERIZATION FOR ANGLE-INDEPENDENT STRAIN MAPPING IN MYOCARDIAL ELASTOGRAPHY.

E. KONOFAGOU*, W.-N. LEE, and S. FUNG-KEE-FUNG, Columbia University, New York, NY.
Corresponding e-mail: ek2191@columbia.edu

In Myocardial Elastography, 1D (axial) transmural strain is typically imaged transmurally, since the highest precision is obtained in the axial direction. However, axial strain imaging is highly dependent on the angle between the imaging and muscle motion planes, potentially resulting in false-positive diagnoses when applied clinically.

In this paper, we propose a fully angle-independent method for myocardial elastography. The method consists of two main steps. First, the axial and lateral displacements within multiple image (x-y) planes across the left-ventricular volume are iteratively corrected and estimated in order to reduce decorrelation noise. Thus, each strain component is corrected for displacement in the direction perpendicular to that estimated, i.e., prior to the axial strain estimation the post-deformation RF signals are corrected for the lateral displacement and vice versa. From the 2D displacement vector, the longitudinal and shear strain components are calculated in order to fully characterize the strain tensor at each location in the myocardium. Second, in order to obtain angle-independent estimates, the principal components of the strain tensor were estimated through determination of the eigenvalues of the strain matrix, yielding the actual radial and circumferential strains on a simulated short-axis.

In order to test this method, a previously developed 3D finite-element (FEA) model of the canine left ventricle simulating the passive filling phase was used and containing 48 nodes and 24 elements. The finite-element model was defined in prolate coordinates (λ, μ, θ) while the RF images were generated in cartesian

coordinates (x, y, z). Short-axis displacement and strain maps were computed using the FEA model at several slices (i.e., μ = 0- 95) starting with an undeformed representation (0 mmHg) and passively inflating the model up to 5.875 mmHg. A convolutional image formation model was employed in order to generate the corresponding 2D short-axis RF images.

The iterative correction method was successful in obtaining high quality axial and lateral displacement images as well as longitudinal and shear strain components with a very good agreement between the radial FEA and elastographic estimates. The principal strain elastograms accurately depicted the radial and circumferential strains, showing an increasing strain gradient across the myocardial wall (i.e., from the epicardium to the endocardium) in both the radial (0.543% to 2.698%) and circumferential (0.3% to 0.93%) directions. Finally, the angle between the image plane and the deformation plane was varied (between 0 and 45 degrees) while the principal strain elastograms remained unchanged. In conclusion, the feasibility of an angle-independent myocardial elastography was demonstrated on a theoretical model that could render this technique highly reliable for its application in a clinical setting. Future studies will focus on the in vivo application of the method described.

We would like to thank Chris Ingrassia for generating the FEA model data used. This study was supported by the American Heart Association.

2E-3 12:00 p.m.
INTRAVASCULAR SHEAR STRESS IMAGING BASED ON ULTRASONIC VELOCITY VECTOR MEASUREMENT.

N. NITTA*[1], K. HOMMA[1], and T. SHIINA[2], [1]Institute for Human Science and Biomedical Engineering, National Institute of Advanced Industrial Science and Technology (AIST), Tsukuba, Ibaraki, Japan, [2]Graduate School of Systems and Information Engineering, Univ. of Tsukuba, Tsukuba, Ibaraki, Japan.
Corresponding e-mail: n.nitta@aist.go.jp

The factors of plaque rupture in arteriosclerosis are classified into the vulnerability of plaque and the direct triggers (Falk, 1995). As with the assessment of vulnerability by an elasticity imaging and so on, it is important to assess the triggers including the hemodynamic factors such as the blood pressure and the cyclic loading by shear stress. On the other hand, since the shear stress affects the endothelial cell functions, its assessment is also useful for preventing the various vascular diseases. Therefore, we address the intravascular shear stress imaging (SSI) in this study.

A generalized method for SSI is proposed based on the Newton viscosity law, without the conventional assumption of Hagen-Poiseuille flow. Since the pressure terms in the Navier-Stokes equations are eliminated by derivative calculations in the flow field with vorticity, the kinematic viscosity coefficient can be derived by the velocity vector distribution alone. Since the shear rate distribution can be also obtained by differentiating the velocity vector field, consequently, the SSI can be achieved by the only velocity vector field because the shear stress is defined by the product of the viscosity coefficient and the shear rate where it is

assumed that the density of fluid is known. Although this methodology is applicable for 3D velocity vector field, the 2D velocity vector field is treated in this study, because that can be easily estimated in real time by using the Doppler method for beam-axis component and the incompressible condition in fluid dynamics for lateral component.

In order to validate the proposed method, the flow-phantom experiments were performed. A silicone tube with a diameter of 5 mm was set in a water tank, and a step imitating the plaque was laid on the tube wall to create the flow field with vorticity. For investigating the distinguishability of fluid type by the estimated shear stress, two fluids (type A: water, type B: water mixed by PVA) with the scattering source were flowed steadily in the tube at a speed of 1 m/s. As the preliminary measurements of the kinematic viscosity coefficients by the viscometer under the room temperature (21°C), the coefficients of types A and B were 1.5 and 6.2 mm^2/s, respectively. After setting the angle between the tube and the beam axes to 67°, the frame data for Doppler measurement (74 pulses every scan line) were acquired by driving an ultrasonic transducer at a center frequency of 4.7 MHz on the sagittal cross section through the tube axis so that the 2D velocity vector field can be assumed.

As the results obtained by the estimated 2D velocity vector distribution, the ultrasonic estimations of the kinematic viscosity coefficient coincided well with the above viscometer measurements (the averaged error was 9%). Moreover, the shear stress distribution obtained by SSI coincided with the finite difference simulation, and the averaged shear stresses in types A and B were 0.1 and 0.3 Pa, respectively. These results reveal that the proposed method is valid for SSI and the difference of shear stress according to the difference of fluid viscosity can be validly distinguished.

2E-4 12:15 p.m.
TIME-AVERAGED HIGH CONTRAST ULTRASOUND IMAGING WITH MOTION CORRECTION.

H. YOSHIKAWA*, T. AZUMA, K.-I. KAWABATA, K. SASAKI, and S.-I. UMEMURA, Central Research Laboratory, Hitachi Ltd., Kokubunji, Tokyo 185-8601.
Corresponding e-mail: hi-yoshi@crl.hitachi.co.jp

Ultrasound imaging is an indispensable tool in diagnosis and therapy. Because it can be done in real-time, operators can directly observe not only an object's motion but vascularity through the motion of contrast echo signals in the blood flow. Generally, vascularity is contrasted with micro-bubble agents, so a minute vein such as a peripheral vessel is not imaged in just one frame because of its low density. Operators reconstruct the motion of the agent into the line of the vessel using plural images obtained in an ideal space. This reconstructed image cannot be shared with other doctors or patients.

We propose a method to produce a concrete image that is reconstructed in an ideal space with the time-averaging approach using plural image frames. Although an agent in a minute blood vessel appears as a dot in each contrast frame, its motion can be traced by connecting consecutive frames. With the time-averaging approach using plural frames, the vessel can be reconstructed into a line structure by gathering the dot signals in each frame.

The averaged signals in specific regions cannot be described without a method of correcting tissue motion, e.g., breathing or cardiac motion. We studied the feasibility of a method to correct for tissue motion with the least squares approach in an *in vitro* experiment using a tissue-mimicking phantom. The region of interest (ROI) was divided into subregions so small that the deformation in each could be ignored when estimating motion in the image planes. We analyzed the allowable range of displacement perpendicular to the image planes in accurately estimating tissue motion. The results revealed that displacement in the image plane could be detected when the perpendicular displacement between two consecutive frames was as small as 0.4 mm, which is about 20% of the beam size in this direction. We also found that if the subregion was larger than the speckle size, tissue motion could be accurately detected.

We did time-averaged imaging with the motion-correction method in *in vivo* experiments on a rabbit kidney using a contrast agent, and found that minute vascularity in the kidney could be described without cloudiness, which could not be shown in just one frame. Moreover, three-dimensional data could be obtained with the time-averaging approach with the object's motion perpendicular to the image plane. Three-dimensional vascularity such as the intersection of vessels could be described as volume rendering.

We also applied this method to the B-mode images of a human carotid, and found that contrast resolution increased. This was because static signals from the wall vein or tissue were enhanced, and dynamic signals such as random echo signals in the blood flow were removed. Moreover, slight displacement perpendicular to the image plane induced compound efficiency in that dimension, and a high-contrast image could be acquired without speckle patterns.

2E-5 12:30 p.m.
EXACT AND WEAK SCATTERING MODELS FOR THE COMPLEX ACOUSTIC FIELD NEAR TO CYLINDRICAL WALLS AND BOUNDARIES IN TISSUE.

R. S. THOMPSON*, C. MACASKILL, and L. FARNELL, University of Sydney, Sydney, NSW, Australia.
Corresponding e-mail: roset@maths.usyd.edu.au

Differences between the interior and exterior media are important in the ultrasonic investigation of tissue objects such as cavities, lesions or vessels. These are generally assessed on an ad hoc, case-by-case basis, whether we wish to establish that there are no significant differences, or to explicitly differentiate between, say, a benign cyst and a malignant lesion. The aim of this work is to develop a more systematic approach through a theoretical investigation of the complex acoustic field modulations that arise close to tissue boundaries. We are interested in regions which are mid-sized compared to the wavelength, with scaled wavenumber (ka) typically in the range 10 to 100, with physiological sound speed and density variations, i.e. variations of less than ±10%, between fluid media. We have previously developed a simulation method to calculate the exact acoustic pressure field in and around cylindrical and nearly cylindrical vessels, including vessels with walls. These simulations show a range of

characteristic, but complicated, modulations of the magnitude of the pressure field, especially in the shadow zone close to the distal edges of the vessel.

In the present study we developed a weak scattering (Born approximation) model to gain insight into these modulations. This gives a simple integral representation for the complex acoustic field, in terms of the 2D Green's function, that is valid even close to internal boundaries. This approach also allows the effects due to small sound speed and density changes to be identified, and separated from the effects of boundary geometry, in a way that is not possible for the exact field calculations. In this study we focused particularly on the behaviour of the phase of the complex acoustic field remaining after removal of the fast modulation due to the incident wave. It is known that this phase, in the Born approximation, generally behaves in a more regular fashion than magnitude, and we found this to be the case. This regularity is especially interesting near the distal vessel boundaries, in the shadow zone. Our results show that the phase behaviour is readily associated with changes in material properties. Further, by comparing our weak scattering and exact results, we found that the results for phase can be scaled into a parameter regime where the material variations are sufficiently large that the Born approximation fails for the field magnitude. Weak scattering results for objects with multiple boundaries, as in walled vessels or lesions, are easily built up by adding the results for each individual boundary. We present results for cylindrical vessels with and without walls, and simulated lesions, using both our exact and approximate approaches. For mid-sized tissue boundaries, modulations of phase are shown to be associated more directly with changes in material properties than the pressure field magnitude.

This work was supported by the Australian Research Council.

2E-6 12:45 p.m.
WINDKESSEL MODELING OF PULSATILE ULTRASONIC STRAIN WAVE.

L. Y. HUANG*, B. DUNMIRE, J. KUCEWICZ, P. VICINI, and K. BEACH, University of Washington, Seattle, WA.
Corresponding e-mail: huangly@u.washington.edu

A novel modeling technique is developed to analyze ultrasonic pulsatile strain wave due to tissue deformation caused by blood volume changes during the cardiac cycles. A Doppler ultrasound technique, called ultrasonic plethysmography, has been developed to detect the strain wave whose amplitude is around 0.1% and frequency is at around 1 Hz. The shape of the strain wave contains information related to physiological or pathological states of blood flow perfusion. Fourier Transform (FT) and Harmonic Analysis (HA) were previously applied to characterizing the shape of the strain wave by amplitude and phase of each harmonic component; however, the parameters of FT and HA do not have clear physiological interpretation. Tissue strain is believed to be proportional to the blood volume change: the integral of the blood flow rate. The Windkessel model was selected to formulate the blood flow rate for its efficacy in describing pressure-flow relation and capability in relating its parameters to physiological structure.

A two-port Windkessel model was chosen since it is suited to microcirculation. The transfer function of two-port Windkessel model is the summation of two second order functions, corresponding to in-flow from large arteries and out-flow to capillaries and venules respectively. The flow rate was formulated as summation of two attenuated sinusoid functions. The strain wave of the tissue deformation is proportional to the integral of blood flow rate function. The parameters of the strain waveform model were related to the resistance and the compliance of local vasculature.

Validation studies were conducted first using a computer generated model of a normal strain wave. A second series of studies used the brachial artery Doppler blood flow rate and finger photoplethysmographic (PPG) signals. Finally the Windkessel modeling was applied to ultrasonic strain wave obtained from the calf region, using the ultrasound RF data from a real-time ultrasound B-mode imager (Terason™, Teratech, USA). Two sets of ultrasonic strain waveforms, one before and the other after exercise, were collected from the calf and compared.

The accuracy of fit of the model to the data was evaluated by mean square error (MSE) and R-value. The rationality of the parameters in the models was assessed by 95% confidence intervals of the parameters. Consistently the R-value was more than 0.9 and the 95% confidence intervals were less than 10.3% of the estimated parameters. Discriminant analysis showed the difference of the parameters of the strain wave model pre- and post- exercise. The change of the parameters demonstrated a 32.8% decrease in the parameters related to resistance and a 4 times increase in the parameters related to compliance in the-post exercise waveforms compared to the pre-exercise waveforms.

The statistical results demonstrated the efficacy of the modeling technique to characterize the ultrasonic strain wave. The leg-exercise study exhibited the capability of the model in depicting physiological states.

Session: 3E

NDE SIGNAL PROCESSING
Chair: E. Furgason
Purdue University

3E-1 11:30 a.m.
CHIRPLET TRANSFORM FOR ULTRASONIC SIGNAL ANALYSIS AND NDE APPLICATIONS.

Y. LU*, G. CARDOSO, R. DEMIRLI, and J. SANIIE, Illinois Institute of Technology, Chicago, IL.
Corresponding e-mail: luyufen@iit.edu

In ultrasonic nondestructive evaluation (NDE), the patterns of ultrasonic echoes represent valuable information pertaining to the shape, size and orientation of reflectors and the physical properties of the propagation path. However, these echoes are overlapped due to microstructure scattering and closely spaced

reflectors. The resolution (i.e., decomposition) of echoes is a major and challenging problem. Furthermore, the signal loss from scattering and absorption imposes a limit on the detection capability of ultrasonic NDE systems. Therefore, signal modeling and parameter estimation of the nonstationary ultrasonic signal is critical for precise material evaluation. This type of study addresses a broad range of applications including flaw detection, deconvolution, object classification, velocity measurement, and ranging systems.

The chirp signal is a type of signal often encountered in ultrasonic testing of dispersive and/or inhomogeneous materials consisting of complex microstructures. The chirp signal parameters correlate to the physical properties, and the estimation of these parameters leads to the characterization of materials. In this investigation, the chirplet transform is introduced as a means to obtain not only time-frequency representation, but also to estimate the echo amplitude, time of arrival, center frequency, bandwidth, phase, and chirp rate of multiple interfering ultrasonic echoes. This transformation can be used for signal decomposition and successive parameter estimation of multiple interfering echoes. It has been shown that by using both simulated chirp signals and the ultrasonic experimental data, the chirplet signal decomposition algorithm performs robustly, yields accurate echo estimation and results in SNR enhancements. Numerical and analytical results show that the algorithm is efficient and successful in precise signal representation.

The chirplet-based parameter estimation algorithm developed in this study is an effective tool for signal decomposition and the estimation of narrow-band, broad-band, dispersive or nondispersive echoes. Once the signal is decomposed by a family of chirplet echoes, these echoes individually or collectively can be used to describe the nonstationary behavior of the signal and also can be utilized for time-frequency analysis. To demonstrate the superior time-frequency performance of the chirplet transform, ultrasonic flaw echoes embedded in grain scattering, and complex multiple interfering chirplets emitted by a large brown bat have been analyzed. In this study it has been shown that the chirplet transform outperforms conventional time-frequency transformations such as short-time Fourier transform, Wigner-Ville transform, and continuous wavelet transform.

3E-2 11:45 a.m.
COMPUTATIONALLY EFFICIENT SPARSE DECONVOLUTION OF B-SCAN IMAGES.

T. OLOFSSON*, Signals and Systems Group, Department of Engineering Sciences, Uppsala University, Uppsala, Sweden.
Corresponding e-mail: tomas.olofsson@signal.uu.se

The resolution of ultrasonic B-scan images of objects containing closely spaced scattering targets can be improved by synthetic aperture focusing techniques (SAFT) or deconvolution. In NDT applications it is common that the B-scans are acquired from regions residing in the near field. Then, linear minimum mean squared error (MMSE) 2-d deconvolution of ultrasonic images, taking into account spatially variant diffraction effects, show improved resolution compared to SAFT but at the cost of an increased computational time, which limits is practical use for large images. This paper proposes a 2-d sparse deconvolution algorithm

that has a significantly reduced computation time compared to 2-d linear MMSE deconvolution. Sparse deconvolution, which has previously been used only for ultrasonic A-scans, is motivated in many NDT applications, where the scattering targets in the objects are relatively few and that are characterized by having a relatively high impedance contrast to the surrounding medium.

The proposed algorithm is divided into two stages: (i) finding the set of active targets that has the highest probability and (ii) estimating the reflection amplitudes of the targets in this set. Step (ii) is performed by maximum a posteriori estimation assuming Gaussian distributions for noise and scattering amplitudes. In step (i), the algorithm combines an initial SAFT-processing to quickly isolate small regions of interest with a subsequent efficient search procedure to find the optimal set of active targets within these regions. The search criterion used in step (i) is a model selection criterion based on Bayesian inference in which the scattering amplitudes are treated as nuisance parameters.

The performance is evaluated for synthetic and real ultrasonic data acquired from an array system. The results show that the 2-d sparse deconvolution yields images that have improved resolution compared to linear MMSE 2-d deconvolution and the results are arrived at in only a fraction of the time required by the latter method.

3E-3 12:00 p.m.
STEPPED SINE VERSUS CODED PULSE AS EXCITATION SIGNALS FOR ULTRASONIC TRANSDUCER CALIBRATION IN A NON-LINEAR PROPAGATION FIELD.

R. P. B. COSTA-FELIX*[1] and J. C. MACHADO[2], [1]Division of Acoustic and Vibration Metrology, INMETRO, Duque de Caxias, RJ, Brasil, [2]Biomedical Engineering Program, COPPE/UFRJ, Rio de Janeiro, RJ, Brasil.
Corresponding e-mail: rpfelix@inmetro.gov.br

Pure tones are often used as excitation signals to calibrate ultrasonic transducers, the technique known as “stepped sine”. Despite the time consumed by the technique, the assessed magnitude of the transducer signal response is accurate enough over the frequency span, and the signal to noise ratio can be enhanced a lot with the excitation signal voltage level properly driven to the transducer. However, one must be aware about the non-linear propagation field that can easily be developed in water, even for relative low intensities and short acoustical paths. The non-linear distortion parameter, which is proportional to the distance between emitter and receiver and also to the intensity of the generated ultrasonic wave, plays a key role in the characterization of the non-linearity. Because of the nature of the distorted waveform, an amount of the power originally driven in a certain frequency, with a pure tone, is transferred to its harmonics. The typical bell-shaped magnitude of an ultrasonic transducer frequency response leads to different intensities of the pure tones used to calibrate it, even if the drive voltage is equal throughout all stepped sine. So, different distortion parameters arise, and consequently different distortion degrees are assessed for each pure tone. Far from the center frequency, the deviation due to non-linear propagation is

easily more than 10 dB less than in the center frequency. Without corrections, the shape of the transducer frequency response will not be accurately represented. Nevertheless, the corrections are not easily implemented, once the non-linear parameter depends on the intensity close to the transducer surface, which is not easy to measure. On the other hand, a Coded Excitation Pulse (CEP), similar to a chirp but with slightly distinct theoretical approach in its development, can suppress the distortions caused by non-linear propagation. The decoding process employed eliminates all distortions, and the loss due to propagation non-linearity is automatically compensated. The frequency response obtained is as exact as it would be if measured using an ideal digital impulse as excitation signal, which is not possible with any other real physical excitation. A comparison of both excitation signals (stepped sine and CEP) was performed, and arguments to consubstantiate the use of the second one are experimentally validated. This paper will present the results of that comparison, pointing out the advantages of the CEP against pure tones as excitation signal, reinforcing previous work's findings.

3E-4 12:15 p.m.
ADAPTIVE THRESHOLDING TECHNIQUE FOR DENOISING AND COMPRESSING ULTRASONIC SIGNALS.

G. CARDOSO* and J . SANIIE, Illinois Institute of Technology, Chicago, IL.
Corresponding e-mail: cardoso@fnal.gov

In ultrasonic imaging applications, signals acquired with poor signal-to-noise ratio (SNR) are not uncommon. Therefore, before any data analysis can be applied to the signal, some level of noise removal is necessary. In this paper, we analyze the denoising and compression performances of the discrete wavelet transform (DWT), discrete cosine transform (DCT), and Walsh-Hadamard transform (WHT) for low SNR. In particular, we introduce a procedure for obtaining an adaptive thresholding function (ATF) that, when applied to DWT, DCT and WHT coefficients, improves the signal-to-noise (SNR) of ultrasonic signals embedded in noise. The ATF technique is very effective and outperforms the classical thresholding techniques when the ultrasonic signal has a low SNR (below 5dB). Classic thresholding techniques (hard, soft, and Garrote thresholding) are all realized by using a fixed threshold parameter to separate noise from signal. On the contrary, the ATF technique removes the noise from the signal by generating a thresholding function that is obtained from the statistical noise parameters. Hence, each transform coefficient is compared to its own threshold. For signals with uniform noise added to DWT coefficients, the ATF technique achieves SNR improvements around 9dB over classic thresholding techniques; these improvements are above 10dB for Gaussian noise. Data compression is the process of obtaining a more efficient representation of a signal; consequently, it is desirable to use data compression techniques to reduce the ultrasonic data size while maintaining the signal integrity. In this study, data reduction is achieved by removing (i.e., setting to zero) all transform coefficients below a given threshold. The process of removing the transform coefficient with small amplitude leads to a certain level of denoising, as the noise energy spreads

in the transform domain. In this paper, we study the application of a hard thresholding function after the preprocessing of the ultrasonic NDE data with the ATF technique. Results obtained from experimental data show that the ATF preprocessing block leads to a compressed signal with higher SNR. The experimental ultrasonic flaw signals are often embedded in microstructure scattering and measurement noise. Hence, we evaluate how the ATF technique performs in denoising these types of signals in the DWT, DCT, and WHT domains. Processed results show that the DWT has the best performance among the transforms in the group analyzed. The energy packing capabilities of the DWT, along with the time localization of the wavelet kernel, allow a few DWT coefficients to correctly identify the location of the ultrasonic flaw echoes. Such localization is paramount for flaw detection, signal denoising and compression. Thus, the adaptive thresholding function technique presented in this paper offers data compression and denoising capabilities for ultrasonic signals suitable for target detection, pattern recognition, and material characterization.

3E-5 12:30 p.m.
PARAMETRIC MODELING OF WAVE PROPAGATION IN GAS MIXTURES - A SYSTEM IDENTIFICATION APPROACH.

J. MARTINSSON* and J. E. CARLSON, Lulea University of Technology / EISLAB, Lulea, Sweden.
Corresponding e-mail: Jesper.Martinsson@ltu.se

Using ultrasonic techniques, the measurable properties of a gas are characterized by the frequency dependent attenuation and speed of sound. The properties are directly related to the bulk modulus by the wave number. For a non-attenuating and non-dispersive gas the bulk modulus is a real-valued constant containing the equilibrium density and the thermodynamic speed of sound. For dispersive gases, the relationship between the acoustic pressure and the condensation is dynamic, and the bulk modulus connecting these two quantities is both complex-valued and frequency dependent.

The standard approach to describe the dynamics of the bulk modulus is to parameterize it given the physical knowledge of the gas properties under investigation. However, for gas mixtures with complex dynamic behavior and/or unknown components, a complete physical description of the bulk modulus is generally not available. For these situations a common approach is to use non-parametric methods to describe the dynamics. Although non-parametric techniques are easy to apply, they give only moderately accurate descriptions. To obtain higher accuracy, parametric models must be used. When choosing the model structure, two things are desirable: First, the model should capture the dynamics of the system and second, the model parameters should give information about the underlying physical properties.

In this paper, the bulk modulus is parameterized using a rational transfer function (spring-dashpot model). This structure has a well-known connection to some physical properties, while still keeping the number of parameters reasonably low. We use system identification techniques to estimate the parameters and

cross-validation to prevent over-parameterization. The model is validated by analyzing the prediction errors which show that the prediction errors are uncorrelated with the measured echoes. This means that the parametric model is able to capture the dynamics of the true system.

The proposed method is compared with standard non-parametric techniques using pulse-echo measurements in ethane, oxygen, and mixtures of the two. The experimental results show that the variances of the estimates are considerably smaller using the proposed method compared to non-parametric methods, especially for noisy data.

Generous grants from the Swedish Energy Agency and the Kempe Foundation are gratefully acknowledged.

3E-6 12:45 p.m.
HIGH RESOLUTION ULTRASONIC ARRAY IMAGING USING POSITIVITY CONSTRAINTS ON THE SCATTERING AMPLITUDES.

F. LINGVALL*[1] and T. OLOFSSON[2], [1]Department of Informatics, Group of Digital Signal Processing and Image Analysis, University of Oslo, Oslo, Norway, [2]Department of Engineering Sciences, Signals and Systems Group, Uppsala University, Uppsala, Sweden.
Corresponding e-mail: fl@ifi.uio.no

In this paper a beamforming method for ultrasonic array imaging is presented that performs compensation in both the spatial and temporal domain based on a maximum a posteriori (MAP) estimation approach. The presented MAP estimator performs a regularized inversion of the propagation operator for the ultrasonic array system at hand by constraining the scattering amplitudes to be positive which applies in applications where the scatterers have higher acoustic impedence than the surrounding medium. The MAP beamformer accounts for the transmit and receive processes, defined in terms of finite array element sizes, transmit focusing laws and electrical transducer characteristics. The resulting MAP beamformer takes the form of a non-linear quadratic programming problem and is solved using efficient numerical algorithms.

The novel non-linear MAP beamformer is compared to a linear beamformer based on a minimum mean squared error (MMSE) criteria as well as to the traditional delay-and-sum (DAS) beamformer with respect to both resolution and signal-to-noise ratio. The algorithms are compared using both simulated and measured data. The simulated data was obtained using ultrasonic field simulations using the DREAM software and the measured data was acquired using a linear phased array imaging wire targets in water. The results show that the non-linear MAP beamformer has superior temporal and lateral resolution compared to DAS beamforming and the ability to supress noise is better for the non-linear MAP beamformer compared to both the linear MMSE beamformer and the DAS beamformer.

Session: 4E

PHYSICAL ACOUSTICS 2
Chair: G. Mansfield
IREE-Russian Academy of Sciences

4E-1 11:30 a.m.
ACOUSTIC SCATTERING FROM STIFFENED PLATE IMMERSED IN WATER: BLOCH-FLOQUET PHENOMENON.

G. MAZE*, R. LIETARD, and D. DECULTOT, LAUE UMR CNRS 6068, IUT, Place Robert Schuman, Le Havre, 76610, France.
Corresponding e-mail: gerard.maze@univ-lehavre.fr

The acoustic scattering from hollow objects with a simple shape immersed in water shows resonances on acoustic spectra in relation to the propagation of circumferential and helical surface waves. These waves can be compared to the Lamb wave in high frequencies. The Resonance Scattering Theory (RST), developed by H. Überall team, allows to explain the resonance phenomena. Recently some authors have studied, theoretically (M. Tran Van Nhieu, JASA 110, 2001, pp. 2858-66) and experimentally (B. H. Houston et al, JASA 98, 1995, pp. 2851-53), the acoustic scattering from periodically stiffened cylindrical shells. They have highlighted additional phenomena due to the ribs: Bragg diffraction and Bloch-Floquet diffraction. The Bragg diffraction is due to the reflections of the incident wave on the lighting points associated to the join of ribs, this diffraction is a rigid effect. The Bloch-Floquet diffraction is due to an elastic phenomenon. To explain this diffraction, the acoustic scattering from a plate with two parallel ribs taking place at large distance immersed in water is studied. A monostatic and a bistatic experiments are developed to record the time signals rediated from the different parts of the limited stiffened plate. In the low frequencies, only two types of guided waves propagate in the elastic shell immersed in vacuum, the S_0 Lamb wave or compression wave and the A_0 Lamb wave or flexural wave. The S_0 wave has a practically constant velocity superior to the sound velocity in water, if the plate is immersed in water, this wave is weakly coupled with it and the energy exchange between the wave and the water is weak, it is not influenced by fluid. The dispersion curve of the phase velocity of the A_0 wave crosses the sound velocity in water (C_{water}=1470m/s), as seen in the case of cylindrical shell in water, this dispersion curve is divided into two curves, a curve with velocity values inferior to the water velocity, in high frequency the velocity tends to the water sound, and a curve with velocity values superior to the water velocity, the trajectory of the velocity is identical to the A_0 wave except for the values near the water velocity. The first curve is associated to the Scholte wave or A wave or A_0^- wave, the velocity value is always smaller than the velocity value of A_0 wave in vacuum, and the second curve is associated to the A_0^+ wave, this phenomenon is identical to the one observed on the cylindrical shell in water. In the studied frequency domain, as the velocity value of A_0^- wave is smaller than the water velocity, this wave is not coupled with the fluid and the radiation is possible only on the plate extremities and the ribs. The

propagation times of different echoes are calculed, taking into account the velocity of waves, and are compared to the experimental results. The whole results are used to explain the Bloch-Floquet diffraction observed from a plate with periodically spaced parallel ribs.

4E-2 11:45 a.m.
BOREHOLE FLEXURAL WAVES IN FORMATIONS WITH RADIALLY VARYING PROPERTIES.

B. SINHA*, H. P. VALERO, T. IKEGAMI, and J. PABON, Schlumberger-Doll Research, Ridgefield, CT.
Corresponding e-mail: bsinha@ridgefield.oilfield.slb.com

Elastic wave propagation in a fluid-filled borehole is affected by near-wellbore alteration of formation properties. Near-wellbore alteration can be caused by several sources, such as overbalance drilling, borehole stress concentrations, shale swelling, near-wellbore mechanical damage and supercharging of permeable formations. Optimal completions of a well for production require both identification and estimation of the radial extent of alteration in reservoir intervals. Measured borehole flexural dispersions in the presence of radial gradients in formation properties can be inverted to estimate the radial extent of mechanical alteration. However, the presence of a tool structure that carries the acoustic transmitters and hydrophone receivers also introduces certain amount of bias on the measured borehole flexural dispersions. This paper describes the Backus-Gilbert inversion of synthetic borehole flexural data for radial variation in formation shear slowness (slowness is inverse of velocity). The inversion algorithm accounts for the tool bias on the measured data by introducing an equivalent structure of a heavy-fluid column placed concentrically with the borehole axis. This simple structure enables computation of the eigensolution for a reference homogeneous and isotropic formation that are used for calculating the data kernel in the perturbation integral equation. The solution of this integral equation yields the radial variation in the formation shear modulus in terms of fractional differences in the measured and reference dispersion at various wavenumbers. Results are presented for both radially increasing and decreasing shear slownesses away from the borehole.

4E-3 12:00 p.m.
ULTRASONIC AND SONOCHEMICAL REACTION STUDIES OF O-CRESOLS IN DIFFERENT SOLVENT MIXTURES.

S. V. RANGA NAYAKULU*[1], S. VENKATESWAR[2], C. SREENIVASA REDDY[2], and D. LINGA REDDY[2], [1]Tellakula Jalayya Polisetty Somasundaram College, Guntur-522006,Andhra Pradesh,India, [2]Osmania University, Hyderabad-500 007,A.P.,India.
Corresponding e-mail: nayakulu@rediffmail.com

Ultrasonic and sonochemical reaction studies have been carried out by measuring ultrasonic velocities(u) in the mixing of phenols like ortho cresol with

esters like ethyl acetate and Iso amyl acetate as solvents. The ultrasonic velocities(u) were measured using ultrasonic pulse echo overlap technique(Model UX4400) on mixing of o-cresol with solvents at different temperatures. The results are interesting because increase in the acid content in the binary mixture decreases the ultrasonic velocity(u).Another important feature is the effect of solvents like Isoamyl acetate instead of ethyl acetate on the kinetic process. The reaction rate is larger with ethyl acetate as compared to the kinetic rate in Isoamyl acetate. The variation of ultrasonic velocity(u) in the binary mixtures of ortho cresols-Isoamyl acetate system with sonic waves is also studies and it has been dound that the reaction rate decreases due to passage of sonic waves through the medium. Arhenius Parameters have been computed for ortho cresol - Isoamyl acetate system. The free energy of activation($\Delta F^{\#}$)has been computed for o-cresol-ethyl acetate system. It is found that heat of activation(E_a),entropy of activation($\Delta S^{\#}$) and free energy of activation(\Delta;F$^{\#}$) are quite in order for this process.

Key Words: Ultrasonic Pulse echo overlap technique,Reaction rate,Arhebius Parameters

One of the authors (S.V.Ranga Nayakulu) is thankful to Prof.P.S.Radhakrishna Murthy for valuable suggestions and encouragement and also thankful to Head, Dept.of Physics,Osmania University for cooperation and encouragement.

4E-4 12:15 p.m.
EFFECTIVE SUBSTITUTION OF ALUMINUM FOR GALLIUM IN LANGASITE-TYPE CRYSTALS FOR A SENSOR USE AT HIGH TEMPERATURE.

H. TAKEDA*, S. TANAKA, S. IZUKAWA, H. SHIMIZU, T. NISHIDA, and T. SHIOSAKI, Graduate School of Materials Science, Nara Institute of Science and Technology, 8916-5 Takayama, Ikoma, Nara 630-0192, Japan.
Corresponding e-mail: hiro-t@ms.naist.jp

Recently, $La_3Ga_5SiO_{14}$ (langasite, LGS) crystals have attracted the attention as pressure sensor materials usable at high temperature, because LGS has its piezoelectric properties up to its melting temperature. For such sensor applications, a crystal with high electric resisitvity, ρ, at high temperature has been demanded. LGS crystals grown at conventional oxygen-contained atmosphere have the lower ρ value (4.0E+8 Ωcm) at the high temperature (400 °C). The desired ρ value is more than 1E+10 Ωcm at 400 °C for a practical use. Very recently, Taishi *et al.* [1] successfully improved the resistivity of the LGS crystals. The crystals were grown in inert gasses (N_2 or Ar), and the ρ value was 10-10^2 times higher than that of the LGS crystals grown at oxygen-contained atmosphere. However, the crystals need coating in order to shut out outside oxidation atmosphere with high temperaure. We have paid attentions to aluminum-substituted LGS single crystals [2]. In this study, we have grown the $La_3Ga_{5-x}Al_xSiO_{14}$ (LGAS) and isomorphic $La_3Ta_{0.5}Ga_{5.5-x}Al_xO_{14}$ (LTGA) single crystals by the Czochralski technique and compared the electric properties with those of pure LGS and $La_3Ta_{0.5}Ga_{5.5}O_{14}$ (LTG). The size of the crystals grown in <001> direction was 18-23 mm in diameter and 70-100 mm in length.

Piezoelectric measurement was carried out according to the IEEE standard on piezoelectricity. The electromechanical coupling factors and the piezoelectric moduli were evaluated by measuring the resonant and anti resonant frequencies of these resonators. The piezoelectric modulus d_{11} values (6.21 and 6.53 pC/N) of the LGAS and LTGA crystals were slightly larger than that of LGS and LTG ones (5.97 and 6.28 pC/N), respectively. We measured the d_{11} and ρ values from room temperature to 800 °C. The d_{11} values of the LGAS crystals increased with increasing temperature, whereas those of the LTGA crystals were independent of the temperature. The ρ values of the LGAS and LTGA crystals at 400°C were considerably higher than those of the pure LGS and LTG crystals grown at oxygen-contained atmosphere. We found that the aluminum substitution is effective to improve the electric resisitvity of the LGS and LTG, and then that the LGAS and LTGA crystals are superior materials for a pressure sensor use.

[1] T. Taishi, K. Kato, T. Hayashi, K. Fujiwara, N. Banba, T. Fukami, K. Hoshikawa, *Proc. Piezoelectric Mater. & Device Sympo.* (2005) 21 [in Japanese].

[2] H. Takeda, M. Kumatoriya, T. Shiosakit, *Appl. Phys. Lett.* **79** (2001) 4201.

This work was partly supported by a Grant-in-Aid for Young Scientists Research No. 17686058 from the Ministry of Education, Culture, Sports, Science and Technology of Japan.

4E-5 12:30 p.m.
PROBING HIGH FREQUENCY PHONON MODES IN NANOSCALE FEATURES.

C. M. FLANNERY*[1], S. KIM[1], W. JOHNSON[1], and C. S. SOLES[2], [1]National Isntitute of Standards and Technology, Materials Reliability Division, Boulder, CO, [2]National Isntitute of Standards and Technology, Polymers Division, Gaithersburg, MD.
Corresponding e-mail: flannery@boulder.nist.gov

Structures for microelectronic and other applications are becoming increasingly important in the sub-100 nm range. However, structures of such size present serious problems to fabricate and inspect in a reliable and repeatable manner. Mechanical properties of the materials involved can become quite different from bulk or even micron-scale properties, and there is a serious lack of inspection techniques to characterize important properties, such as stiffness and density, as well as the dimensions and uniformity of the fabricated structures. In this work, Brillouin light scattering (BLS) is used to inspect phonon vibrations in sub-100 nm lithographic features (parallel polymer lines and spacings, 50-100 nm height, 30-80 nm width) supported on a silicon wafer and results are used to extract elastic properties.

BLS is a non-destructive, optical technique where incident laser light interacts with phonon modes present in the material inspected and photons are scattered with small changes in energy (or frequency) resulting from phonon-photon collisions. The frequency shifts are in the gigahertz range and indicate the different phonon modes present, which reveal the material's mechanical properties. The phonon wavelengths involved are of the order of the structure dimensions, meaning that a mode's velocity and propagation is sensitive to structure size.

This allows us to probe vibrational modes in structures on a scale smaller than any previously inspected. Finite Element analysis and classical Green's function theory are used to analyze and explain detected modes. We detect several new modes in these nanostructures: These include Lamb-like flexural vibrations confined within the nanostructures themselves, and higher order Rayleigh and Sezawa waves propagating in both nanostructure and supporting substrate. From these we are able to extract the elastic properties of the nanoscale features and study their size dependence. Our results indicate that the mechanical properties do not deviate significantly from their bulk values for feature dimensions inspected here. The ability to detect both flexural modes and surface wave modes in nanowires establishes BLS as a unique and powerful non-contact, non-destructive tool to characterize and understand mechanical properties of nanoscale features. Finite Element and Green's function approaches allow us to develop techniques to better understand phonon vibrations and mechanical properties on the nanoscale.

4E-6 12:45 p.m.
PHYSICAL PROPERTIES OF LANTHANUM GALLIUM TANTALATE CRYSTALS FOR HIGH-TEMPERATURE APPLICATIONS.

S. A. SAKHAROV*[1], A. N. ZABELIN[1], and D. V. ROSHCHUPKIN[2], [1]FOMOS Technology Co, Moscow, Russia, [2]Institute of Microelectronics Technology RAS, Chernogolovka, Moscow District, Russia.
Corresponding e-mail: saharov@fomos-t.ru

Temperature dependence of electrical conductivity and piezoelectric charge constant (d_{11}) of LGT were experimentally investigated.

Lanthanum gallium tantalate (LGT) and lanthanum gallium silicate (LGS) crystals have certain advantages compared to well known piezoelectric materials (piezoceramics and quartz) traditionally used for acoustoelectronic application. They demonstrate the lack of phase transitions up to the melting temperature point, piroelectric effect and hysteresis. Moreover LGT has higher piezoelectric charge constant (d_{11}) and exhibits better temperature stability compared to LGS that allow using it for sensors operating on the direct piezoelectric effect.

The general problem of high-temperature sensors is a noise level increasing via operating temperatures caused by increasing of electrical conductivity in a piezoelectric element.

Electrical conductivity and piezoelectric charge constant (d_{11}) of LGT were investigated in a temperature range up to 500°C. The structural perfection of the LGT crystals was investigated using high-resolution X-ray diffraction and topography as well as main growth defects were determined (growth banding, twins, colorated F-centers, etc).

Session: 5E

RF FILTERS AND MODULES
Chair: C. Ruppel
EPCOS AG

5E-1 11:30 a.m.
(Invited)
TRENDS IN INTEGRATED FRONT-END MODULES FOR CELLULAR HANDSETS.

P. WRIGHT*, TriQuint Semiconductor, Hillsboro, OR.
Corresponding e-mail: pwright@tqs.com

In 2004, nearly 700M handsets were sold globally, making it the largest-volume market for RF semiconductors and SAW filters. In the future, an additional growth engine for this market will be the trend to “universal wireless connectivity.” Laptops, personal computers, cars, appliances, etc. will all be expected to communicate through a wireless interface which will only serve to drive the technological developments even faster. As a result, the cell-phone market has become the driving force for technological innovations in RF semiconductors, SAW, and more recently BAW filters.

Today’s phones are complex multi-band and multi-mode radios, capable of operating in global cellular bands, and increasingly in others such as GPS, Bluetooth, and WLAN. Despite this increase in complexity, both the size and cost of handsets have continued to decline significantly. This has been achieved by increasing levels of integration; CDMA single-band Power Amplifier modules are now as small as 3×3 mm2, and GSM quad-band PA modules are as small as 5×5 mm2. Recent CDMA modules have integrated the SAW duplexer with the power amplifier, and in GSM, antenna switches and transmit filters have been incorporated into the power amplifier module. Future modules will continue this trend and will be multi-standard, as well as multi-band. One consequence of this for SAW filter manufacturers is that the SAW filter cell-phone market is transitioning from one that was predominantly discrete into one that is predominantly modular. This presentation will discuss how the industry is responding to these challenges and likely future directions. In particular, we will present examples of this integration in the RF front end of a cellular handset and the likely evolution of these products in future designs.

5E-2 12:00 p.m.
TEMPERATURE COMPENSATED $LiTaO_3$ /SAPPHIRE SAW SUBSTRATE FOR HIGH POWER APPLICATIONS.

M. MIURA*[1], T. MATSUDA[1], Y. SATOH[1], M. UEDA[2], O. IKATA[2], Y. EBATA[2], and H. TAKAGI[3], [1]FUJITSU LABORATORIES LTD., Akashi, Hyogo, Japan, [2]Fujitsu Media Devices Limited, Yokohama, Kanagawa, Japan, [3]National Institute of Advanced Industrial Science and Technology, Tsukuba, Ibaraki, Japan.
Corresponding e-mail: mmiura@labs.fujitsu.com

A temperature compensated $LiTaO_3$ /Sapphire SAW substrate was developed. The $LiTaO_3$ /Sapphire SAW substrate has several advantages over other temperature compensating methods. The first advantage is that this kind of substrate has almost the same k^2 and Q value as the original $LiTaO_3$. As a result, the $LiTaO_3$ /Sapphire SAW substrate enabled us to create temperature compensated SAW filters with low loss and steep cut-off. The second advantage is that the $LiTaO_3$ /Sapphire SAW substrate has large thermal conductivity. As a result, efficient heat dissipation is brought about, effectively suppressing any heat buildup in SAW chips. They will be superior on two points, especially for SAW filters that are used in high-power applications like antenna duplexers. These points are temperature compensation and migration prevention of the electrode material, or in other words, high power durability. The third advantage is the new SAW substrate has little bow even during heat processes. That brings about as high a yield in SAW filters as in conventional ones. The bonding technique is also an important point for the $LiTaO_3$ /Sapphire SAW substrate. Surface activated bonding (SAB) was optimized and bow-free $LiTaO_3$ /Sapphire SAW substrate was achieved. The $LiTaO_3$ /Sapphire SAW substrate enables the creation of a US-PCS SAW duplexer with low loss and high power durability in a miniaturized PKG, such as one that is 3x3 mm.

5E-3 12:15 p.m.
DESIGN STUDY ON A COMPACT, HIGH PERFORMANCE SAW DUPLEXER.

A. FLECKENSTEIN*[2], J. E. KIWITT[1], F. M. PITSCHI[1], M. JAKOB[1], K. CH. WAGNER[1], and W. MENZEL[2], [1]EPCOS AG, Munich, Germany, [2]Microwave Techniques, University of Ulm, Ulm, Germany.
Corresponding e-mail: fleckens@mwt.e-technik.uni-ulm.de

Regarding the passive integration taking place in the radio frequency (RF) sections of wireless transceivers there is an increasing trend towards combining receiver (Rx) and transmitter (Tx) filters together with a potentially required matching network in one component — the so called duplexer. The filters are connected at the common antenna port and provide separate ports for the following transmitter and receiver stages, respectively. Usually, a matching network is necessary to prevent the filters from influencing each other.

Particularly critical in the design of duplexers is the demand for preferably high selectivity in the Rx and Tx paths in the frequency ranges of the Tx and Rx pass bands, respectively, and for preferably high isolation between Tx input and Rx output. Futhermore, self matching is required on all ports. Duplexers in state-of-the-art mobile phones are mainly realized by acoustic components. They exhibit a small size caused by the low phase velocity of surface acoustic waves. To take advantage of this fact a compact package design is also targeted. Therefore, flip chip technology together with LTCC packaging has been applied to the described duplexer. In order to decrease space requirement within the package while achieving high performance, the design study presents and discusses different novel measures for enhancing the mentioned parameters, selectivity, isolation, and matching, by carefully utilizing electromagnetic effects appearing in the component. These measures allow to reduce the package footprint to a size of only 3mmx2.5mm.

First samples have been manufactured to experimentally verify the measures discussed. They exhibit good performance with the isolation being higher than 50 dB in Tx band, for instance. In order to allow an accurate prediction of the electromagnetic behaviour of the LTCC package, which is one of the crucial parts of this component, the simulation has to be enhanced carefully. With these enhancements measurement and simulation are in good agreement.

5E-4 12:30 p.m.
DOUBLE-RESONANCE SAW FILTERS.

J. MELTAUS*[1], V. P. PLESSKY[2,1], and S. S. HONG[3], [1]Helsinki University of Technology, Materials Physics Laboratory, Espoo, Finland, [2]GVR Trade SA, Bevaix, Switzerland, [3]Samsung Electro-Mechanics Co., Ltd., Suwon, Korea.
Corresponding e-mail: johanna.meltaus@hut.fi

We present SAW filters based on a double resonance appearing in structures consisting of long interdigital transducers (IDT) separated by a λ/4-gap. This type of device was proposed by Plessky et al in 1996 [1]; it was called degenerated coupled resonator filter (CRF) because its topology combines characteristics of CRF and impedance elements. Although COM modeling showed filter response with low loss and small standing wave ratio, experimental results [1] gave unsatisfactory performance with 6-8 dB insertion loss. We show that the loss was caused by scattering and attenuation in the gap, prominent in this type of device with resonant energy concentrated in the gap. Replacing the gap with a distributed gap will radically decrease the loss level [2]. To achieve low loss, the anti-resonance frequency of the synchronous resonance of the long IDTs must coincide with the frequency of the hiccup resonance arising in the gap. The anti-resonance of the IDTs cancels the static capacitance of the structure, self-matching the filter. We describe three variants: a single-ended 2-IDT filter, a 3-IDT filter with balanced output, and a 3-IDT filter with cascaded characteristics.

Topologically, the structures studied here resemble a standard CRF. The operation, however, is not similar to that of a CRF. Long structures give rise to strong reflections that prevent acoustic propagation in the device. In a 2-IDT device, electrical signal is transmitted from input to output by excitation of a synchronous resonance in the first IDT and a hiccup resonance in the gap. Gap resonance transmits a part of the acoustic energy to the second IDT, creating a voltage in the bus bars and a synchronous resonance in the IDT. The hiccup resonance is spatially localized in the gap, as opposed to CRF where resonance modes are distributed over the length of the device. Therefore, we feel that it is more precise to call the structure a double-resonance filter.

Above-described scheme of operation can be applied to situation with more than one gap; e.g., for 3 IDTs separated by 2 distributed gaps, transmission of signal from input at first IDT via center IDT to output at third IDT is possible, if the central transducer is left open-circuited. The characteristics of such a filter are similar to that of two 1-gap filters cascaded. Grounding the center IDT eliminates the uniform resonance in this part of the structure and prevents the transfer of the signal from input to output.

The 3-IDT structure can operate with input in the center and output at sides, typical of a standard CRF. In this case, the resonances in the two gaps are connected in parallel, and the skirts will not be as steep as for the cascaded variant. Such a symmetric structure can be employed with unbalanced input and balanced output.

Measurements confirm the simulations of the described scheme of operation, and experimental data will be presented. The structures described here are ideal for filters with 1...1.5 % bandwidth requiring extremely low loss and small standing wave ratio.

[1] V. P. Plessky et al, 1996 IEEE Ultrasonics Symposium, pp. 25-28.

[2] W. Wang et al, 2004 IEEE Ultrasonics Symposium, pp. 1363-1366.

5E-5 12:45 p.m.
SAW DUPLEXER FOR US-PCS THAT IS COMPOSED OF TEMPERATURE COMPENSATED FILTERS WITH SIO2/IDT/LT SYSTEM.

R. TAKAYAMA*, Y. IWASAKI, K. FUJII, Y. HAMAOKA, H. NAKANISHI, and K. NISHIMURA, Panasonic Electronic Devices Co., Ltd., Kadoma, Osaka, Japan. Corresponding e-mail: takayama.r@jp.panasonic.com

Recently, the well-known defects of SAW filter, such as high insertion attenuation, low power durability, have been improved dramatically by devising design technique and substrate/electrode material. Also, long standing problem of SAW filter, high temperature coefficient of frequency (TCF), has been improved by some researchers using several kind of approaches. One of the approaches is coating the SAW filter with SiO2. This approach has not put into practical because this method degrades the filter characteristics, especially anti- resonant characteristics. In our previous report, we pointed out that the degradation of filter characteristics is large-concerned with the layer-profile of SiO2, and stated that temperature stable SAW resonator without the degradation of anti- resonant characteristics was successfully realized by controlling the layer-profile of SiO2. In the SAW resonator with SiO2/IDT/LT system, anti-resonant characteristics become better with layer-profile of SiO2 becoming flat. But reflection coefficient, which is one of important factors of SAW resonator, becomes so small because the density of SiO2 is nearly equal to the density of Al that is main material of electrode. Then we leave small ridge on SiO2 surface to get good resonator characteristics with enough reflection coefficient. We have developed US-PCS SAW duplexer using ladder type filters, which were composed of these resonators. The coupling constant of these resonators, which has close relation to bandwidth of SAW filter, decrease by SiO2 coated on IDT. Therefore, we apply novel structure of ladder type filter to Tx filter for our US-PCS duplexer to improve its bandwidth. This duplexer show the good insertion attenuation of 2.5dB at the pass band of Tx and of 3.4dB at the pass band of Rx. Concerning isolation characteristics, attenuation at Tx/Rx pass band were larger than 55dB/ 40dB, respectively. Moreover this duplexer has the low TCF of Tx/Rx were -22.8/-12.3 ppm/ ° K.

Session: 6E

CMUTS
Chair: C. Daft
Siemens

6E-1 11:30 a.m.
ANALYSIS AND DESIGN OF DUAL-ELECTRODE CAPACITIVE MICROMACHINED ULTRASONIC TRANSDUCERS.

R. O. GULDIKEN* and F. L. DEGERTEKIN, Georgia Institite of Technology, Atlanta.
Corresponding e-mail: gtg181u@mail.gatech.edu

Although ultrasound imaging arrays based on conventional Capacitive Micromachined Ultrasonic Transducers (CMUTs) have been shown to have adequate performance, the flexibility offered by microfabrication techniques can be exploited to further enhance the capabilities of CMUT arrays. With multiple electrodes embedded in dielectric CMUT membrane, dual-electrode CMUTs that can be considered an example of this approach improving both transmit and receive performance of the CMUTs without relying on collapsed membrane operation [1]. Simple parallel-plate electrical equivalent circuit model suggests that the electromechanical transformer ratio close to collapse depends only on the gap thickness but not on the absolute value of the collapse voltage. The advantage of the dual-electrode structure in the receive mode becomes apparent when non-zero DC bias is applied to the side electrodes reducing the effective gap for the center receive electrode. However, in contrast to the ideal parallel plate CMUT, the maximum improvement with gap thickness reduction is limited in CMUTs with dielectric membranes. As predicted by coupled finite element analysis, when the bias voltage applied to the side electrodes is increased over a certain value, the bottom of the silicon nitride membrane underneath the center electrode makes contact with the bottom surface before the device is forced into unstable collapse region and reach the maximum possible receive sensitivity. Therefore, minimizing the dielectric layer thickness between the receive electrode and the bottom electrode, e.g. eliminating the isolation layer over the bottom electrode, helps improve the receive performance. These predictions are verified by experimental data obtained on dual-electrode CMUTs by recording receive signal amplitude as a function of side and center electrode bias voltage. Dual-electrode CMUT design for transmit performance improvement involves placement of side electrodes and shaping the silicon nitride membrane to increase maximum volume displacement. For example, using 0.4μm deep, 1μm wide notches between 4μm wide center and side electrodes in a 0.9μm thick 20μm wide rectangular silicon nitride membrane improves the overall performance of CMUT by 10.7dB over conventional CMUT. This is achieved while reducing the required maximum (collapse) voltage levels from 90V to 50V for center receive electrode when 70V is applied to the side electrodes. Analysis methods, experimental results, and optimal dual-electrode CMUT designs are discussed in detail in this paper.

[1] R.O. Guldiken, J. McLean and F.L. Degertekin, “CMUTs with Dual-electrode Structure for Improved Transmit and Receive Performance,” submitted to IEEE Trans. Ultrason., Ferroelect., Freq. Contr., 2005.

6E-2 11:45 a.m.
INVESTIGATION OF THE NONLINEAR CMUT BEHAVIOR.

A. LOHFINK*[1,2] and P.-C. ECCARDT[1], [1]Siemens AG, CT PS 8, Munich, Germany, [2]IMSAS, University of Bremen, Bremen, Germany.
Corresponding e-mail: al.ctms2@cert.siemens.de

Due to the electrostatic excitation principle, capacitive micromachined ultrasound transducers exhibit a significant nonlinear behavior. This effect cannot be neglected in case of transmission where CMUTs are driven with high-level signals and are operated near the collapse point. Especially for medical ultrasonic diagnostics, nonlinear distortions of the transmitted sound pressure signals are highly undesirable for harmonic imaging.

This paper will present a comprehensive investigation of the CMUT nonlinearities. The calculations are based mainly on the 1D CMUT model presented in [1]. The model parameters are derived from FEM simulations of an arbitrary CMUT design. This approach guarantees a good description of a large CMUT array operated near the first order membrane mode. Compared to existing equivalent circuit models, which are linearized at the operating point, this 1D model has the advantage of being suitable also for fast nonlinear calculations.

The nonlinear simulations investigate the amplitude of the available sound pressure and the harmonic distortions of the sound pressure signal. Transmitted sound pressure is significantly higher compared to linear calculations. The maximum applicable voltage can exceed the static collapse voltage, resulting in an increased maximum sound pressure. Reason for this behavior is the phase shift between the membrane displacement and the input voltage.

Harmonic distortion of the transmitted sound pressure increases with higher input voltage and depends on the signal frequency. Near and above resonance frequency the nonlinear effect is significantly reduced, as the membrane acts as a mechanical low pass filter. This effect will be will be illustrated by a flow diagram of the nonlinear electrostatic transformer and the linear membrane model. The influence of the feedback loop for the membrane displacement will be discussed. Further reduction of harmonic distortion can be achieved by pre-distorted input signals. An optimizer for the calculation of pre-distorted signals, which is based on the 1D model, will be presented. Results compared to FEM simulations will be discussed.

[1] A. Lohfink, P.C. Eccardt, W. Benecke, and H. Meixner. Derivation of a 1D CMUT Model from FEM Results for Linear and Nonlinear Equivalent Circuit Simulation. In Proceedings of the IEEE Ultrasonics Symposium, Honolulu, Hawaii, October 5-8, 2003.

6E-3 12:00 p.m.

CAPACITIVE MICROMACHINED ULTRASONIC TRANSDUCERS (CMUTS) WITH PISTON-SHAPED MEMBRANES.

Y. HUANG, E. HÆGGSTRÖM, X. ZHUANG, A. ERGUN, and B. T. KHURI-YAKUB*, Stanford University, Stanford, CA.
Corresponding e-mail: hyongli@yahoo.com

Compared to PZT transducers in medical applications, CMUTs reported on so far have broader fractional bandwidth (FBW) but lower transduction efficiency (TX and RX). Most fabricated CMUTs reported on in the literature carried membranes of uniform thickness. Since there is a performance trade-off between transduction efficiency and FBW when designing CMUTs with uniform membrane thickness, there is limited room for performance improvement in these devices. However, wafer-bonding-based CMUT fabrication provides design flexibility by allowing fabrication of membranes with different thickness profiles. Herein, CMUTs featuring piston-shaped membranes are developed to improve device performance.

According to our theoretical predictions, piston-shaped membranes should improve the CMUT performance in terms of output pressure, sensitivity, and broader fractional bandwidth. The large ratio of 2nd resonant harmonic frequency to 1st resonant frequency improves FBW. Increased electric field intensity in the CMUT cavity (due to the larger equivalent spring constant of this membrane, compared to classical membranes) improves TX and RX. The device performance also benefits from a flatter membrane shape that allows greater average membrane displacement and intra-cavity electrostatic pressure.

CMUTs featuring piston-shaped membranes with different geometric shapes were designed and fabricated. In order to make a fair comparison, all designs have a similar first resonant frequency, and all devices are equal in size.

Fabricating CMUTs featuring piston-shaped membranes is a more complex process than fabricating CMUTs with uniformly thick membranes. However, no yield-loss was observed when CMUTs featuring piston-shaped membranes with different geometric shapes were fabricated.

The device characterization was carried out with both pitch-catch (PC) and pulse-echo (PE) immersion tests in oil. These devices achieved ~100% improvement in transduction performance (TX and RX) over CMUTs with uniform membrane thickness. For CMUTs with square and rectangular membranes, FBW increased from ~110% to ~150% and from ~140% to ~175%, respectively, over CMUTs with uniformly thick membranes. The new devices produced a maximum output pressure exceeding 1 MPa. Finally, performance optimization using the geometric shape was the same in both CMUTs featuring piston-shaped membranes and CMUTs with uniform membrane thickness.

6E-4 12:15 p.m.
ANALYSIS OF CROSSTALK BETWEEN FLUID COUPLED CMUT MEMBRANES.

P.-C. ECCARDT*[1], A. LOHFINK[1,2], and H.-G. VON GARSSEN[1], [1]Siemens AG, CT PS 8, Munich, Germany, [2]IMSAS, University of Bremen, Bremen, Germany.
Corresponding e-mail: al.ctms2@cert.siemens.de

Crosstalk between array elements is an important and intensively discussed topic for CMUTs. For operation in fluids crosstalk effects significantly influence the dynamic range at pulse-echo mode, the directivity pattern as well as the frequency response and are highly undesired for medical application. On the other hand, crosstalk effects between the membranes and the surrounding fluid can be used for other CMUT applications like pumping and mixing in micro fluidic channels.

So far, coupling between the membranes and the surrounding fluid was mostly described as Stonely or Scholte waves at the CMUT surface. This paper will present an analytical description of this crosstalk effect between CMUT membranes. The basic idea is that the elastic membranes act on the fluid as a complex load. Waves at such an interface are comparable to gravitational waves at a free water surface.

Considering a homogeneously stiff and mass loaded interface, the speed of sound of an evanescent fluid wave at this interface will be described analytically by a formula for a fluid half space bounded by a complex acoustical impedance. The approach was validated with FEM simulations. The influence of discretisation, size of typical membranes and inactive area between membranes onto the intensity distribution of this surface wave will be investigated. The dependency of the speed of sound on membrane stiffness and membrane mass is discussed. The wave is highly dispersive, its speed of sound increases with increasing stiffness and with decreasing frequency. Both effects are monotonic, but nonlinear for frequencies above the membrane resonance. Near membrane resonance the speed of sound approaches zero.

FEM simulations of typical CMUT membranes show, that these surface waves have a significant influence onto the array behavior and can be well described by the presented analytical approach.

6E-5 12:30 p.m.
IMPROVED PERFORMANCE OF CMUT WITH NONUNIFORM MEMBRANES.

M. N. SENLIK* and A. ATALAR, Electrical and Electronics Engineering Department, Bilkent University, Ankara, Turkey.
Corresponding e-mail: niyazi@ee.bilkent.edu.tr

When capacitive micromachined ultrasonic transducers (cMUT) are immersed in water, the bandwidth is limited by the membrane's second resonance frequency, which causes an increase in the mechanical impedance of the membrane. We propose a new membrane shape to shift the second resonance frequency to higher values, in addition to keeping the impedance of the

membrane as small as possible. The structure consists of a very thin membrane (with a radius of a_1 and thickness of t_{m1}) with a thicker rigid mass at the center (the corresponding dimensions are a_2 and t_{m2}). The stiffness of the central mass moves the second resonance frequency to a higher frequency. The effect of the central portion on the natural resonance (first resonance, f_r) and antiresonance (second resonance, f_a) is investigated using a finite element simulator by changing the thickness of the center, t_{m2}, while keeping the remaining dimensions a_1, a_2 and t_{m1} constant at 26 μm, 20 μm and 0.4 μm, respectively. The results indicate that as t_{m2} is increased from 0.5 μm to 6 μm, f_r initially increases from 3.2 MHz to reach a maximum value of 5.5 MHz (first region), then begins to decrease (second region). Hence, a nonuniform membrane has the same f_r for two different t_{m2} values. The ruling effect in the first region is the stiffness of the membrane, whereas in the second region it is the mass of the membrane. Shift of f_a from 12 MHz to 40 MHz as t_{m2} is increased, promises the possibility of obtaining a higher bandwidth, which cannot be achieved with a uniform membrane.

To make a fair comparison between the performance of the nonuniform and uniform devices, f_r is kept constant around 5.2 MHz. Since it is possible to obtain same f_r with more than one choice of the device dimensions for a given radius, a_1, we chose the membranes that are in the second region, which also gives higher f_a compared to the ones in the first region.

During the receive mode, the cMUT is biased at 90% of its collapse voltage. For a water immersed membrane with a_1=20 μm, a_2=15 μm, t_{m1}=0.3 μm and t_{m2}=1.55 μm, the obtained 3-dB bandwidth is 20 MHz with a transducer gain of -13.5 dB, which is higher than that can be achieved with an optimized uniform membrane (15 MHz with -16.5 dB gain). As a_1 is increased, the impedance of the membrane begins to increase resulting in a decreased bandwidth. However the product of the bandwidth and gain remains nearly the same, which reveals the possibility of the trading the gain and bandwidth efficiently, which is not possible with a uniform membrane.

During the transmission mode, a bias of 0.45 of the collapse voltage is assumed. The excitation is assumed to be sinusoidal with a peak value equal to the bias voltage. For the device described above, the 3-dB bandwidth is found to be 26 MHz with an output pressure of 200 kPa for a gap height of 0.5 μm. On the other hand, an optimized uniform membrane can achieve a maximum bandwidth of 17 MHz with an output pressure of 60 kPa.

6E-6 12:45 p.m.
CHARACTERIZATION OF CROSS-COUPLING IN CMUTS.

B. BAYRAM*, M. KUPNIK, G. YARALIOGLU, D. LIN, A. ERGUN, O. ORALKAN, and B. KHURI-YAKUB, Stanford University, Stanford, CA.
Corresponding e-mail: bbayram@stanford.edu

This paper analyzes element-to-element and cell-to-cell cross-coupling in capacitive micromachined ultrasonic transducers (cMUTs), using optical interferometric displacement measurements. For an array, a single element was

excited periodically, and membrane displacements were measured at different positions along the whole array (linescan). The array was then covered with a polydimethylsiloxane (PDMS) layer, and the cross-coupling measurements were repeated. The cross-coupling levels for conventional and collapsed mode operation of the cMUT were compared. To mimic the acoustical properties of tissue, the cMUTs were immersed in oil during measurement. After the measured values were corrected to eliminate the effect of acousto-optic interaction, the results were reviewed in different representations, i.e. time-spatial and frequency-spatial domains. While collapsed operation generates cross-coupling waves travelling at 1320 m/s, conventional operation generates cross-coupling waves travelling at only 840 m/s. The center frequency of the cMUT shifts from 300 kHz in conventional operation to 700 kHz in collapsed operation. In both modes of operation, cross-coupling dispersion curves predicted a gradual reduction in phase velocity at higher frequencies. At lower frequencies, this phase velocity tended to approach 1480 m/s asymptotically. The element-to-element cross-coupling experiments showed that a 10-μm PDMS layer reduced the measured cross-coupling levels. The interferometer measurement is a useful tool to characterize cross-coupling effects in cMUTs, in addition to its use for absolute displacement measurements.

This work is supported by the Office of Naval Research. Mario Kupnik acknowledges the FWF Austrian Science Fund for financial support.

Session: 1F

ELASTICITY DYNAMIC
Chair: S. Emelianov
University of Texas at Austin

1F-1 2:30 p.m.
PERIPHERAL VASCULAR ARFI IMAGING: *IN VIVO* CLINICAL AND PHANTOM RESULTS.

D. DUMONT*, J. D. ALLEN, E. MILLER, C. MOYER, S. HSU, and G TRAHEY, Duke University, Durham, NC.
Corresponding e-mail: dmd@duke.edu

Non-invasive characterization of focal and diffuse atherosclerosis is difficult with existing techniques, but clinically important in guiding the selection of drug, surgical and other treatments. We describe new non-invasive techniques for monitoring vascular health with ARFI imaging. Custom ECG-gated beam sequencing was implemented on the Siemens SONOLINE Antares scanner to measure radiation force induced displacements for *in vivo* vascular tissue. Techniques are discussed for generating ARFI images and ARFI-based tissue stiffness measurements during systole and diastole. Signal processing methods and factors impacting image quality are discussed for imaging both the proximal and distal arterial walls. Transducer and tissue heating are also evaluated.

We present the results of a clinical pilot study involving twenty-four volunteers

with no predisposition for peripheral vascular disease (PVD), and fifteen patients with diagnosed PVD. The temporal and spatial stability of radiation force induced displacements along the distal and proximal wall of the popliteal artery are described. Vascular wall and plaque contrasts are calculated and compared to conventional ultrasonic imaging, Intima-Media Thickness (IMT) measurements, as well as the Ankle-Brachial Index (ABI).

The results suggest a relatively uniform response for healthy vascular tissue to radiation force with noticeable demarcation seen between the vascular wall and surrounding tissue. Plaques identified in the conventional B-mode images are well visualized in the corresponding ARFI images. The ratio of peak diastolic displacement to peak systolic displacement (DSR) was calculated and found to be 1.75 ± 0.60 for volunteers and 1.23 ± 0.24 for PVD patients; statistical analysis of the data suggests a relationship exists between DSR and PVD.

We have developed layered Cyrogel vessel phantoms to mimic arterial layers as well as embedded plaques in the vascular wall. Custom phantoms with layers of varying stiffness but homogenous echogenicity are statically pressurized to physiological realistic levels in a watertank, and then imaged with acoustic radiation force. Layers are well visualized in the corresponding ARFI images with little contrast seen in the matched B-mode images. Displacement data is examined over a physiological relevant pressure range.

This work has been supported by NIH 1R01HL07548501 and NIH 5T32EB001040. We thank Siemens for in kind support.

1F-2 2:45 p.m.
A COMBINED INDENTER/ARFI IMAGING SYSTEM.

L. ZHAI*, R. BOUCHARD, M. PALMERI, R. NIGHTINGALE, and K. NIGHTINGALE, Department of Biomedical Engineering, Duke University, Durham, NC.
Corresponding e-mail: liang.zhai@duke.edu

Introduction: The goal of this project is to develop an integrated indenter-ARFI (acoustic radiation force impulse imaging) system, which is capable of acquiring matched datasets from ex vivo tissue samples, which will be used to evaluate excised colo-rectal tumors and blood vessels. This system will facilitate correlation of ARFI images in tissue samples with independently characterized material properties. We hypothesize that for a fixed indenter load, the measured tissue displacements will be linearly related to the ARFI generated displacements, which are inversely proportional to the stiffness of the tissue.

Methods: A one-pound load cell connected to a 1.8 mm diameter rod is used as the indenter probe. It is attached to a 3D computer-controlled translation stage. The translation stage has an accuracy of 0.1μm and maximum speed of 5 mm/s in all three axes. A Labview program for automatic 2D stiffness mapping was developed to control the stage and collect the load data in real time. Two control methods, force control and displacement control, were implemented. To correlate the indenter measurements with the ARFI images, a custom designed fixture holds both the load cell and the ultrasound transducer, ensuring alignment of the data. Indenter calibration is accomplished with comparison to compressive

load measurements on an MTS system. For homogeneous media, the material elastic modulus can be estimated using Timoshenko's solution for a point load in a hemi-infinite medium. For heterogeneous and layered media, however, the computed modulus will reflect material and structural information; therefore relative displacements are used for comparison with ARFI data. In this work, matched indenter/ARFI data have been obtained in a tissue-mimicking phantom under varying loads. The gelatin/graphite phantom has 10 mm diameter spherical inclusion located 1mm below the surface. The recipes for the inclusion and background were identical, except the gelatin Bloom strengths were 300 and 100, respectively, which generated a difference in stiffness of approximately 3:1.

Results and Discussion: Matched ARFI and indenter displacement data show good general agreement. The indenter displacement profile exhibited a decrease across the lesion diameter 58%. The diameter of the lesion as measured by the indenter was 8.3 mm. Corresponding ARFI imaging of this lesion showed a decrease in displacement of 52%, and a lesion diameter of 8.7 mm. The ratios of displacements inside and outside of the lesion were 0.42 and 0.47 for the indenter and ARFI data, respectively. The displacement ratios and measured lesion diameters were independent of applied load for both indenter and ARFI data. Future trials with this system will be performed on freshly excised ex vivo tissue samples including rectal tumors and diseased blood vessels.

1F-3 3:00 p.m.
(Invited)
DYNAMIC MR-ELASTOGRAPHY AS A NON-INVASIVE IMAGING MODALITY: IN-VIVO APPLICATION TO BREAST, LIVER AND BRAIN.

R. SINKUS*, Laboratoire Ondes et Acoustique, Ecole Supérieur Physique Chimie Industrielle, Paris, France.
Corresponding e-mail: ralph.sinkus@espci.fr

Elastography is a novel imaging modality which aims to measure locally the viscoelastic properties of tissue. The general idea of dynamic Elastography is to perform an acoustic experiment: the tissue under investigation is exposed to low-frequency acoustic waves (about 50 Hz) and the resulting displacement distribution is measured by means of a motion-sensitized imaging technique. Reconstruction of the shear viscoelastic parameters is done locally by solving the partial differential equation governing the propagation of sound within the material.

Reconstruction faces a severe problem: the presence of the compressional wave in the measured displacement field. Its contribution must not neglected for heterogeneous objects (even in case of pure shear excitation), but its consideration in the partial differential equation fails due to the almost incompressible nature of tissue. The problem is characterized by the enormous difference in magnitude between the shear modulus (about kPa) and the second Lamé coefficient (about GPa) in soft tissue. It can be shown that the remaining compressibility of tissue balances minutely the large magnitude of the second

Lamé coefficient. There are two solutions: on the one hand the so-called Helmholtz-Hodge decomposition allows extraction of the transversal displacement component by solving an additional equation for an unknown vector potential; on the other hand it is possible to apply the curl-operator to the partial differential equation. The drawback of the second technique is the involvement of third-order spatial derivatives, while the difficulty of the first method is it sensitivity to boundary conditions. Either way, both methods enable the removal of the compressional wave and lead to a Helmholtz-type equation with only the shear-viscoelastic parameters as the unknown coefficients.

Initial clinical results for breast and liver MR-Elastography are presented. Here, the diagnostic focus is put on tumor characterization and diffuse liver disease such as fibrosis. In addition, feasibility studies for the application of MRE to brain, prostate and parotids are shown.

Philips Research Hamburg, Germany; University Hospital Tuebingen, Germany; Hospital St. Luc, Brussels, Belgium; Prince of Wales Research Center, Sydney, Australia

1F-4 3:30 p.m.
STRESS FIELD FORMATION FOR MULTIFREQUENCY VIBRO-ACOUSTOGRAPHY.

M. URBAN*[1], G. SILVA[2], R. KINNICK[1], M. FATEMI[1], and J. GREENLEAF[1], [1]Department of Biomedical Engineering and Physiology, Mayo Clinic College of Medicine, Rochester, MN, [2]Departamento de Tecnologia da Informacao, Universidade Federal de Alagoas, Maceio, AL, Brazil.
Corresponding e-mail: urban.matthew@mayo.edu

Background: Vibro-acoustography is a recently developed method that uses the dynamic radiation force (stress) of ultrasound to locally excite an object. Presently, to form the stress field we typically use two ultrasound beams whose frequencies differ by Δf, typically in the kilohertz range. The two beams interfere at the system focus creating the radiation stress at the difference frequency Δf. The system point spread function (PSF) is given as a function of the radiation stress. The object response to the radiation stress may vary significantly as Δf changes due to its internal resonances. Thus, acquiring images with multiple Δf values in one scan would provide more information than using one difference frequency. **Methods:** We propose a multifrequency vibro-acoustography method that uses a multifrequency radiation stress produced by an array transducer driven with N ultrasound frequencies. The N ultrasound beams interfere at the focus of the transducer producing up to $N(N\text{-}1)/2$ unique difference frequencies in the radiation stress. This method can produce a multifrequency image at the different $N(N\text{-}1)/2$ frequencies with only one scan of the region of interest, increasing the information of the scanned region by a factor of $N(N\text{-}1)/2$. The objective of this paper is to present the image formation theory in multifrequency vibro-acoustography systems with experimental validation. The radiation stress generated by sector array and annular array transducer systems is analyzed theoretically. For experimental validation, an eight element sector array transducer driven with four different ultrasound frequencies is used to produce a PSF with six components at different Δf values. A stainless steel sphere with

diameter 0.51 mm embedded in a gelatin phantom was scanned to obtain a measurement of the PSF. A Doppler laser vibrometer is used to measure the vibration velocity of the sphere, which is proportional to the radiation stress upon the sphere. The detected signal was processed using a bandpass filter and lock-in amplifier to extract each of six PSF components. In another configuration, the raw signal from the laser was digitized for off-line digital filtering to insure that each PSF component can be extracted from the raw data set. We compared the measured and the theoretical PSF components through their spatial distribution, mainlobe width at -6 dB, and sidelobe levels. Lastly, we used a computer phantom with small spheres to demonstrate the usefulness of multifrequency vibro-acoustography for microcalcification detection in breast imaging. **Results:** The main lobe width numerically evaluated for a PSF component is 0.91 x 2.06 mm, while the experimental measurement yields 0.98 x 1.94 mm. The theoretical and measured sidelobe levels are -7.29 dB and -7.67 dB, respectively. **Conclusion:** The proposed method holds the potential for a large gain of information with no increase in same scanning time when applied to conventional vibro-acoustography systems.

This study was supported in part by grants EB002640, EB002167, and EB00535-03 from National Institutes of Health, and DCR2003.013 from FAPEAL/CNPq, Brazil.

1F-5 3:45 p.m.
SPATIALLY MAPPING THE ELASTIC PROPERTIES OF THE INTRAOCULAR LENS USING BUBBLE-BASED ACOUSTIC RADIATION FORCE.

T. ERPELDING*, K. HOLLMAN, and M. O'DONNELL, University of Michigan, Ann Arbor, MI.
Corresponding e-mail: terpeldi@umich.edu

Bubble-based acoustic radiation force has been used to measure highly localized tissue viscoelastic properties. In the current study, we use acoustic radiation force applied to laser-induced bubbles to measure the spatial distribution of elastic properties in porcine intraocular lenses. A potential *in-vivo* technique to measure lens spatial elasticity is crucial to understanding the onset of presbyopia and guiding surgical procedures for presbyopia or cataracts. Current techniques to measure lens stiffness are limited to *ex-vivo* procedures that require lens sectioning to achieve spatial localization. Bubble-based acoustic radiation force can measure the spatial elasticity distribution without disrupting the lens capsule or significantly altering intervening tissue. Laser-induced optical breakdown (LIOB) creates microbubbles spaced by 1 mm laterally along the equator of explanted porcine lenses. Optical breakdown occurs when sufficiently high threshold fluence is attained at the focus of femtosecond pulsed lasers, inducing plasma formation and bubble generation. Porcine eyes obtained from a local slaughterhouse are explanted upon arrival and embedded within a gel phantom (5 w/w%). 20 μJ laser pulses from a 800 fs Nd:glass laser generate target microbubbles. A two-element confocal ultrasonic transducer applies 6.7 ms acoustic radiation force-tone bursts with the 1.5 MHz outer element while monitoring bubble displacement within the lens using the 7.44 MHz inner element.

Large differences in bubble displacements are noted at different lens regions. Bubble displacements found in the lens nucleus (N = 5) from the 3 central positions averaged 9 μm, while bubble displacements in the lens cortex from the 4 peripheral positions averaged 40 μm. This suggests the lens nucleus is over 4 times stiffer than the lens cortex. Bubble lifetime, the duration from creation until collapse, also correlates with local lens stiffness. LIOB bubbles not exposed to acoustic radiation force excitation demonstrate much longer lifetimes in the lens nucleus than in the lens cortex. The average bubble lifetime in the lens nucleus (N = 3) was 14.6 minutes, compared to only 2.4 minutes in the lens cortex. This result is consistent with previous findings that longer bubble lifetimes occur in stiffer materials. Both bubble displacements and lifetimes are nearly symmetric about the lens center, as expected and predict that the porcine lens nucleus is several times stiffer than the lens cortex. Bubble-based acoustic radiation force appears well-suited as a potential *in-vivo* technique to spatially map the elastic properties of the lens.

This work has been supported in part by the Whitaker Foundation and the National Institutes of Health grant EY-015876.

Session: 2F
CONTRAST AGENTS: IMAGING I
Chair: A. Bouakaz
University of Tours

2F-1 2:30 p.m.
ULTRASONIC MOLECULAR IMAGING OF PRIMORDIAL ANGIOGENIC VESSELS IN THE PAPILLOMA VIRUS TRANSGENIC MOUSE WITH AVB3-INTEGRIN TARGETED NANOPARTICLES USING INFORMATION-THEORETIC SIGNAL DETECTION.

M. HUGHES*, J. MARSH, J. ARBEIT, R. NEUMANN, R. FUHRHOP, A. WOODSON, G. LANZA, and S. WICKLINE, Washington University, St. Louis, MO.
Corresponding e-mail: msh@cvu.wustl.edu

Background: To detect the binding of molecularly targeted nanoparticles to sparse avb3 epitopes in primordial angiogenesis, we developed novel, nonlinear entropy-based signal receivers based on information theory, which are sensitive to subtle changes in the shape of an rf RF signal as contrasted with conventional signal amplitude processing.

We sought to characterize the sensitivity of information-theory-based signal receivers versus conventional signal power analyses for delineation of early neovascularization in the ears of transgenic mice, which is driven by the papilloma virus.

Methods: Eight K14-HPV16 transgenic mice were treated with either normal saline (n=3) or 0.3 mg/kg i.v. of $\alpha_v\beta_3$ -targeted nanoparticles (n=5) and imaged dynamically for two hours using a research ultrasound imager (Vevo 660 30MHz probe) modified to store digitized RF waveforms. All RF data were processed off-line to reconstruct images using information theoretic and conventional receivers. Image segmentation was performed by thresholding measurements at the 97% level for both data sets. The mean value of pixels segmented was computed at each time post-injection.

Results: The transgenic strain had markedly thickened and stiffened pinnae as compared with the normal animals. With conventional image processing techniques, no targeted contrast signal could be detected in angiogenic vessels in the ears due to the abundance of specular reflections from the skin and cartilage. However, the subtle changes in signal features induced by binding of $\alpha_v\beta_3$-targeted nanoparticles to neovasculature was clearly distinguished from surrounding echoes, and ultrasound enhancement increased over time. Control mice demonstrated no contrast enhancement, regardless of the image processing method applied.

Conclusion: These data demonstrate the ability and complementarity of information-theoretic receivers in conjunction with targeted nanoparticles to elucidate the presence of $\alpha_v\beta_3$-integrins in primordial neovasculature, particularly in acoustically unfavorable environments.

This study was funded by NIH EB002168, HL042950, and CO-27031. The research was carried out at the Washington University School of Medicine.

2F-2 2:45 p.m.
PULSE INVERSION FUNDAMENTAL IMAGING WITH LIPOSOME MMICROBUBBLES AT 25-50 MHZ.

C.-H. LI[1], A.-H. LIAO[1], J.-A. HO[2], and P.-C. LI*[1], [1]Department of Electrical Engineering, National Taiwan University, Taipei, Taiwan, ROC, [2]Department of Applied Chemistry, National Chi Nan University, Nantou, Taiwan, ROC.
Corresponding e-mail: paichi@cc.ee.ntu.edu.tw

Pulse inversion based fundamental imaging was proposed for enhancement of contrast detection in a previous study. Performance of the imaging method was tested with a commercial contrast agent (Levovist®) at 1.5-3 MHz. In this study, we applied pulse inversion fundamental imaging at 25-50 MHz with liposome microbubbles that were produced in-house. The purpose of this investigation is for small animal contrast imaging, which has gained wide interest over the past few years. The pulse inversion technique involves two firings with inverted waveforms. When the returning echoes from the two firings are summed, the residue signal is limited to even-order harmonics for tissue. However, when the returning echoes are from microbubbles, the fundamental signal is not completely cancelled because the reaction of the bubbles under compression is different from that under rarefaction. Thus, with the application of the pulse inversion technique, the signal in the fundamental band can be used to enhance the contrast-to-tissue ratio. In this study, pulse inversion based fundamental B-mode images were constructed with a high frequency imaging platform. A LiNbO3

transducer with a center frequency of 45MHz and a 55% -6dB fractional bandwidth was used. The received signal was amplified, filtered and then digitized at 200 MHz. A computer-controlled positioning stage was used for mechanical scanning. Phantom experiments were performed. Liposome microbubbles were made in-house with a recipe developed in our lab. Compared to conventional fundamental imaging, the contrast-to-tissue ratio was enhanced by 7~18 dB when the transmit signal varied between 25 and 50 MHz. As the number of cycles increased, the contrast improvement also became more significant. Compared to conventional second harmonic imaging, pulse inversion fundamental imaging provides an additional advantage. That is, the bandwidth of the transmit signal is not limited in order to accommodate both the fundamental and harmonic bands within the passband of the transducer. Also, the transmit and receive passbands both can be around the center frequency of transducer. With this technique, the microbubbles can be further developed for small animal molecular imaging.

2F-3 3:00 p.m.
CONTRAST ENHANCED SUBHARMONIC BREAST IMAGING: WORK IN PROGRESS.

F. FORSBERG*[1], C. W. PICCOLI[1], R. J. RO[1], K. J. LIPCAN[1], D. A. MERTON[1], J. B. LIU[1], R. SOPARAWALA[1], W. T. SHI[1], and A. L. HALL[2], [1]Thomas Jefferson University, Philadelphia, PA, [2]GE Healthcare, Milwuakee, WI.
Corresponding e-mail: flemming.forsberg@jefferson.edu

Contrast enhanced subharmonic imaging (SHI) can detect slow, small volume blood flow due to its excellent contrast to tissue signal to noise ratio. Hence, it may be possible to combine imaging and estimation of quantifiable flow parameters such as perfusion from subharmonic signal intensities. In this project in vivo SHI of normal blood flow and breast lesion neovasculature was investigated.

A modified Logiq 9 scanner (GE Healthcare, Milwaukee, WI) operating in grayscale SHI mode (transmitting/receiving at 4.4/2.2 MHz) was used to measure in vivo SHI time intensity curves in 4 dogs. Renal SHI was performed following intravenous injections of the contrast agent Optison (GE Healthcare, Princeton, NJ). Following 3 contrast injections a neutron activation assay technique (BioPhysics Assay Laboratory Inc, Worcester, MA) was employed to quantify the degree of perfusion in 8 sections of each kidney. Digital clips were transferred to a PC and SHI time intensity curves acquired in each section. SHI fractional blood volumes (FBVs) were calculated and the perfusion estimated from the initial slope of the FBV uptake (i.e., rFBV = dFBV/dt). SHI perfusion data was compared to the gold standard using linear regression analysis. As part of an ongoing study women with breast lesions, who subsequently underwent a breast biopsy, participated in a study of mammography and contrast enhanced breast ultrasound. Following baseline scans of grayscale ultrasound and power Doppler, Optison was administrated for power Doppler and grayscale SHI (0.5 and 4.0 ml dosages, respectively). Digital clips were acquired of each injection and transferred to a PC for off-line analysis. Power Doppler and SHI time intensity

curves were determined within each lesion using Image-Pro Plus software (Media Cybernetics, Silver Spring, MD).

In the dogs, 270 SHI time intensity curves were acquired. SHI perfusion estimates correlated significantly with microsphere results ($r = 0.57$; $p < 0.0001$; regression line: $Qp = 0.47 \times rFBV + 1.62$). To date four patients with five benign breast masses have been studied. In SHI there was an almost complete suppression of tissue signals allowing the lesion vascularity to stand out. The internal morphology of the vascularity associated with the breast masses was visualized better with SHI than with power Doppler. SHI perfusion estimates of the breast lesions ranged from 1.67 to 2.46 ml/min/g.

In conclusion, a new contrast specific imaging technique, SHI, has been investigated for in vivo breast imaging and perfusion estimation, but further studies are required to substantiate these preliminary results.

The U.S. Army Medical Research Material Command under DAMD17-00-1-0464 and GE Healthcare supported this work.

2F-4 3:15 p.m.
HIGH FREQUENCY SUBHARMONIC PULSED-WAVE DOPPLER AND COLOR FLOW IMAGING OF MICROBUBBLE CONTRAST AGENTS.

A. NEEDLES*[1], D. E. GOERTZ[2], A. S. BROWN[1], and F. S. FOSTER[1], [1]Sunnybrook and Women's College Health Sciences Centre, Toronto, Ontario, Canada, [2]Erasmus MC, Rotterdam, The Netherlands.
Corresponding e-mail: aneedles@swri.ca

A recent study (Goertz et al, UFFC 2005) has shown the feasibility of subharmonic (SH) colour flow (CF) imaging. In this paper we extend this work by examining the performance of SH CF as a function of transmit pressure and specifically investigate the feasibility of SH pulsed-wave Doppler (PWD). Experiments were performed at a 20 MHz transmit frequency using an adapted VisualSonics (Toronto, Canada) scanner and a 20 MHz (f# 2.1) transducer. Quadrature analog demodulation was performed about the SH frequency (10 MHz) to produce both CF and PWD data. Additional filtering and amplification was used to enable nonlinear imaging, and custom software was used for CF data acquisition. Flow experiments were performed with a 1 mm diameter wall-less vessel cryogel phantom and a 65 degree transducer-vessel angle. Definity™ (0.01% conc.) was flowed at 15 mm/s, first towards and then away from the transducer. CF and PWD experiments used 7 and 10 cycle pulses respectively, and transmit power was varied from 0.1-100%. The peak negative pressure at the focus for 100% transmit was 4.5 MPa, as measured with a needle hydrophone in a water tank. CF experiments were performed at 0.5 and 5 fps (4 mm frames), using a 2D autocorrelator for velocity estimation. For the PWD transmit case, both m-mode CF and audio PWD data were acquired. In all cases, both fundamental frequency (F20) and SH data were acquired. We identify four pressure regimes of behavior in the CF and PWD data sets. At low transmit powers (20%) we observe that both SH and F20 CF velocities are significantly lower than true velocities when flow is towards the transducer and higher when flow is away.

PWD velocity estimates for the towards flow case begin to reduce at >16% transmit power. In this stage we hypothesize that radiation pressure begins to alter microbubble velocities. Finally, as transmit power was increased beyond 20%, there was evidence of disruption or unstable bubble behavior for both the CF (reverse flow pixels) and PWD (broadband spectra). These phantom results therefore show there is an identifiable pressure range where accurate SH CF velocity estimates can be made, supporting the results of a previous feasibility study. Further, the PWD data demonstrates the feasibility of high frequency SH PWD. In vivo studies examining SH blood velocity estimates in small animals will be presented. The ability to suppress tissue signals using SH signals may improve sensitivity to microvascular flow or slow velocities near large vessel walls by eliminating the need for clutter filters.

2F-5 3:30 p.m.
OPTIMIZED CONTRAST AGENT IMAGING CONSIDERING DIFFERENT SOURCES OF NONLINEARITY.

W. WILKENING*[2], TH. HOELSCHER[3,2], CH. HANSEN[1,2], CH. FISCHER[1], and H. ERMERT[1,2], [1]Institute of High Frequency Engineering, Ruhr-Universitaet Bochum, Bochum, Germany, [2]Ruhr Center of Excellence for Medical Engineering, Bochum, Germany, [3]Department of Radiology, University of California San Diego, San Diego, CA.
Corresponding e-mail: Wilko.G.Wilkening@rub.de

We previously proposed an approach to improve contrast imaging with N different (coded) transmit pulses, where the N echoes are processed by N filters with J taps prior to summation and envelope detection. Based on sample data for tissue and microbubbles in tissue, the filter coefficients are determined by solving an Eigenvalue problem. The filters individually adjust frequency and phase responses to improve the contrast and they lower the requirements for the transmitters to correctly reproduce the coded pulses. This processing is most effective for sequences with more than 2 different pulses. Then, the system is under-determined with respect to the cancellation of echoes resulting from linear wave propagation and scattering. The optimal solutions for imaging microbubbles, however, use all degrees of freedom indicating that the nonlinear scattering of microbubbles differs considerably from a 2nd order polynomial.

We now tackled the following issues: 1) Low MI imaging suffers from limited SNR, whereas at higher acoustic pressure levels the nonlinear effects of wave propagation in tissue have to be compensated. 2) The proposed signal processing requires training data. The system should be calibrated with in vivo data that is acquired during an exam. 3) Since long pulse sequences reduce frame rate and increase sensitivity to motion artifacts, short sequences are preferred.

To solve these issues, we 3) went back to a simple phase inversion sequence (0° and 180° pulses). 2) The new Siemens Antares Ultrasound Research Interface was used to acquire in vivo RF data of human brains during contrast studies. Signals from pre- and post-contrast frames representing parenchyma were taken

as sample data for tissue and contrast agent. 1) The aforementioned processing was enhanced to compensate the nonlinear response of the tissue without sacrificing bandwidth: additional virtual echoes are derived from the actual echo signals. Phase inversion results in 2 echoes e_1 and e_2 per beam line. Considering second order nonlinearities, another 3 virtual echoes are calculated: $e_3 = e_1 e_2$, $e_4 = (e_1)^2$, $e_5 = (e_2)^2$. The optimized filtering and summation is then applied to all 5 actual and virtual echoes to cancel out the effect of a second order non-linearity.

In vivo, calibrating the systems with pre- and post-contrast RF data frames worked reliably. Incorporating the nonlinear processing especially helped at higher pressure levels, even with very short filters (1-16 taps). At low pressure levels, where tissue harmonics are negligible, longer filters suppressed noise efficiently. B-mode completely failed to differentiate between perfused and unperfused parenchyma resulting in a classification error of close to 50%. Standard phase inversion imaging (PI) reduced the error to 8% in the best case, and the proposed processing to 2%. The proposed processing extends contrast imaging to higher pressure levels, where lower classification errors were achieved than with low MI PI.

The work is partly funded by the Federal Ministry of Education and Research, Germany (BMBF), grant 13N8079. We thank Siemens Medical Solutions for additional support.

2F-6 3:45 p.m.
PHASE-SHIFT NANOPARTICLE SYSTEM FOR ULTRASONIC IMAGING AND THERAPY.

K.-I. KAWABATA*, N. SUGITA, A. YOSHIZAWA, T. AZUMA, H. YOSHIKAWA, and S.-I. UMEMURA, Central Research Laboratory, Hitachi, Ltd., Kokubunji, Tokyo, Japan.
Corresponding e-mail: kk@crl.hitachi.co.jp

Recently, much attention has been paid to “molecular imaging”, by which biological functions rather than anatomical structures are observed, with medical imaging modalities such as positron emission tomography (PET). With appropriate molecular targeting contrast agents, ultrasound imaging can also be utilized for molecular imaging.

One of the limitations of currently available contrast agents for ultrasound is that they are bubbles of several micrometers in diameter and can only be applicable to targets inside blood vessels. To target other tissues, much smaller contrast agents are needed. As an approach to obtain such agents, we are developing a nanoscale particle system containing volatile organic compounds, which have the potential to change their phase from liquid to gas through ultrasound exposure. Besides its diagnostic application, such a system may also have potential for selective therapies, due to the enhanced ultrasound-energy deposition with the aid of microbubbles.

We are developing nano-particle systems containing two different types of volatile liquids; one possesses boiling points lower than 37ºC and is vaporized directly by the energy of the exposing ultrasound, and the other possesses boiling points higher than 37ºC and is vaporized not by directly being exposed to ultrasound

but via energy deposition by bubbles created through vaporization of the former type of volatile liquid.

We prepared emulsions of phosphatidylcoline containing perfluoropentane (PFP, b.p.: ~30ºC) and 2H,3H-perfluoropentante (2H,3H-PFP, b.p.: ~54ºC) and monitored the phase shifts during the exposure of pulsed ultrasound at a frequency of 3.4 MHz in the acoustic range of 1 to 10 W/cm^2 by using a diagnostic ultrasound scanner (Hitachi Medical Corp. EUB-8500, probe: L53S) both *in vitro* and *in vivo*.

As a fundamental study, the acoustic intensity threshold for producing acoustically detectable microbubbles in water was investigated. It was found that the nanoparticles change their phase to gas upon the ultrasonic irradiation with acoustic intensities at several W/cm^2. The dependence of acoustic intensity threshold on the ratio of PFP in the total perfluorocarbon indicated a multi-step phase shifting, which may increase the safety of phase-shift colloids.

Based on these findings, we determined if our nano-particles could change their phase in colon 26 mouse tumor tissues *in vivo*. Ultrasound exposure under the same conditions as the above *in vitro* experiments was found to induce a phase shift in the particles in tumor tissues. It was also found that focused ultrasound at an acoustic intensity of 20 W/cm^2 contiguously exposed after the phase shift is established in the tumor tissues induce therapeutic effects at the focus. Our results indicated the potential usefulness of the nano-particle system as a versatile agent for ultrasonic diagnosis and therapy.

Part of this work was supported by the Japanese Ministry of Education, Culture, Sports, Science and Technology through a grant-in-aid for the creation of innovations through business-academic public sector cooperation.

Session: 3F

GAS-LIQUID SENSORS
Chair: M. Pappalardo
University of Roma TRE

3F-1 2:30 p.m.
(Invited)
DIFFRACTION-FREE PROPAGATION OF COLLIMATE SURFACE ACOUSTIC WAVE ON A SPHERE APPLIED FOR INNOVATIVE GAS SENSORS.

K. YAMANAKA*[1], D. Y. SIM[2], I. SATOH[3], T. MIYAGISHI[3], H. TANAKA[3], T. FUKIURA[3], H. KAZATO[3], S. AKAO[4], T. OHGI[4], N. NAKASO[4], T. TSUJI[1], T. MIHARA[1], Y. EBI[3], and T. NAKATSUKASA[4], [1]Tohoku University, Sendai, Miyagi, Japan, [2]Ball Semiconductor, Allen, TX, [3]Yamatake, Fujisawa, Kanagawa, Japan, [4]Toppan Printing, Sugito, Saitama, Japan.
Corresponding e-mail: yamanaka@material.tohoku.ac.jp

A thin beam of wave usually diverges due to diffraction and it is a limitation of any device using such waves. However, surface acoustic wave (SAW) on a sphere with an appropriate aperture does not diverge but is collimated, realizing ultra-multiple roundtrips along an equator of the sphere. This effect is caused by the balance between diffraction and focusing on a spherical surface. On an anisotropic single crystal ball, the ultra-multiple roundtrips were realized, and we performed theoretical analysis by using a finite element analysis code specially developed for this purpose. Here we show immediate and far-reaching implications of this effect; First, it realizes a high performance SAW sensors. The advantage of ball SAW is most fully appreciated when applied to a very thin sensing film where the multiple-roundtrip enhances the sensitivity whereas the attenuation loss would not cause a serious problem. It is exemplified in a hydrogen gas sensor using 40-nm-thick palladium alloy sensing film that realizes a wide sensing range of 10 ppm to 100% for the first time. It also realized relatively fast response time of 20 s without heating the sensing film. Application to wide variety of other gasses is feasible. Moreover, this effect could be employed not only in acoustic but also in acoustooptic and/or optical devices.

This work was partially supported by Ministry of Education, Culture, Sports, Science and Technology.

3F-2 3:00 p.m.
DESIGN OF MICROMACHINED RESONATORS FOR FISH IDENTIFICATION.

A. RØNNEKLEIV*[1,3], J. BRUNGOT[3], D. WANG[4], R. BERNSTEIN[4], V. JAHR[3], K. KJØLERBAKKEN[3], L. HOFF[2,3], and S. HOLM[5,3], [1]Norwegian University of Science and Technology, Trondheim, Norway, [2]Vestfold University College, Horten, Norway, [3]VivID AS, Ås, Norway, [4]SINTEF, Oslo, Norway, [5]University of Oslo, Oslo, Norway.
Corresponding e-mail: sverre@ifi.uio.no

The fish ID system described here was developed in order to have a tag with the advantage of RF-tags in that it can be read remotely in-vivo in water, and with the low price and lack of battery of the coded wire tag. This led us to design and test an ultrasound tag based on micromachined resonators. The intended use is for identifying fish as they pass through a tube typical of fish pumping systems in the fish farming industry.

The passive chip and the signal processing system operate in the 200-400 kHz range. The ID chip responds to an ultrasound signal at specific frequencies and the combination of frequencies gives the identity. Each chip may typically contain some 5 or more resonance cavities and the total number of possible resonance cavities available may be about 17, giving a total number of possible ID's of at least 3-4,000. This is adequate for classification at the batch level, as in fish farms or local wild fish tribes.

The resonators consist of thin, nominally 500 nm, Si_3N_4 membranes suspended over separate evacuated cavities. The resonators are made using bulk silicon micromachining from the nitride film on a silicon wafer. The cavities have been etched from the back side of the wafer, and are sealed by bonding the back side of the wafer to a glass plate. Individual ID chips with five resonators per chip are

obtained by dicing this composite plate. The center to center distance between resonators on the chip is about 1 mm, and the dimensions of the chip are about 5 by 1.5 by 0.8 mm.

The resonators were designed using a rough procedure of matching the pressure and volume deflection of a spherical vibration pattern in the water at a reasonable radius, to the volume compliance due to the deflection of the membrane at the same pressure. Interaction between neighbor resonators was neglected. The resonators were designed to have Q-values in the range 26 to 36, decreasing with center frequency. This frequency dependence follows from the fact that all resonators are made from the same nitride membrane.

The resonators were subjected to ultrasound in water in a tank and the resonances were measured from a distance up to about 30 cm. Sharp resonance peaks in fair accordance with the chip design were achieved, and the results were repeatable also with small changes of the chip's angular position in relation to the ultrasound beam. The better resonators showed Q-values about 30 % below the design value. The measurements indicate some interaction between neighbor resonators, and also that resonators at the ends of the chip perform poorer than those in the middle of the chip.

Chips with the same resonance cavities from the same silicon wafer have the same resonance frequencies, whereas chips from different series differ a bit according to deviations in membrane thickness and size. The resonators have also been measured when put inside the abdomen of both slaughtered and live fish with equally good results. Hence additional losses from the fish flesh seem to be reasonably small.

This project has been partly financed by Innovation Norway (SND), The Norwegian Research Council (NFR) and the Science Park at Ås.

3F-3 3:15 p.m.
A LATERAL FIELD EXCITED ACOUSTIC WAVE PESTICIDE SENSOR*.

W. PINKHAM*, L. FRENCH, D. FRANKEL, and J. VETELINO, University of Maine, Orono, ME.
Corresponding e-mail: wade.pinkham@umit.maine.edu

Organophosphate pesticides are commonly used worldwide to control pests in fruits and vegetables. Although these pesticides serve their purpose in protecting crops, excessive pesticide use can have adverse effects on the environment and also jeopardize the health of the consumer. Government agencies in the U.S. limit the amount of pesticides that may be used, however many agricultural products are imported from countries where pesticide use may not be regulated. Therefore, to minimize environmental effects and protect the health of consumers, a need exists for a low-cost portable sensor that will detect harmful pesticide levels. Recently a lateral field excited (LFE) acoustic wave sensor on AT-cut quartz has been developed [1] which is capable of detecting both mechanical and electrical property changes in a film which selectively sorbs a target analyte. In the LFE sensor the transverse shear mode (TSM) is excited by electrodes on the reference surface and the sensing surface is unmetallized and coated only

with the target analyte selective film, resulting in a much simpler structure than the standard AT-cut quartz crystal microbalance (QCM). In the present work a polyepichlorohydrin (PECH) film is evenly spun onto the sensing surface of an LFE sensor to detect the organophosphate pesticide, phosmet ($C_{11}H_{12}NO_4PS_2$), in an aqueous environment with a flow through system. When comparing the LFE sensor to the standard QCM as a pesticide sensor, results show that the LFE sensor has at least 25% greater sensitivity with a lower limit in the parts per billion (ppb) range, 12% shorter response times and more consistent reproducibility. The improvement in sensitivity, response time and reproducibility is most likely due to the absence of the gold film on the sensing surface. In particular the electric field associated with the TSM is able to penetrate directly into the analyte selective film and monitor film electrical property changes resulting in higher sensitivity. Quicker response times and better reproducibility may also be attributed to the absence of the gold film and any aging effects associated with the film. In conclusion, the simplicity in structure and improved sensing properties of the LFE sensor results in a sensor platform which may replace the standard QCM in a wide range of applications.

[1] Y. Hu, L. A. French Jr., K. Radecsky, M. Pereira da Cunha, P. Millard, and J. F. Vetelino. “A Lateral Fiield Excited Acoustic Wave Sensor.” IEEE Transactions on Ultrasonics, Ferroelectrics, and Frequency Control, Vol. 15, No. 11, pp. 1373-1380, November 2004.

**This work is supported by the National Science Foundation under grant 0330100*

3F-4 3:30 p.m.
NANOMATERIAL SENSING LAYER BASED SURFACE ACOUSTIC WAVE SENSORS.

K. SRINIVASAN[1], S. CULAR*[2], V. BHETHANABOTLA[2], S. YUP LEE[3], M. T. HARRIS[3], and J. N. CULVER[4], [1]Department of Electrical Engineering, University Of South Florida, Tampa, FL, [2]Department of Chemical Engineering, University Of South Florida, Tampa, FL, [3]School of Chemical Engineering, Purdue University, West Lafayette, IN, [4]Center for Biosystems Research, University of Maryland Biotechnology Institute, College Park, MD.
Corresponding e-mail: ksriniv3@eng.usf.edu

Bio-nanotechnology is aimed at design and synthesis of novel biological materials. These materials could be used to design optical, biomedical and electronic devices. One such example of nanoscale biological system is a virus. Viruses have been given a lot of attention for assembly of nanoelectronic materials. Tobacco Mosaic Virus (TMV) is a well-known plant virus contagious to tobacco leaves. Strains of this virus have been previously coated with metals, silica or semiconductor materials and formed end-to-end nano-rod assemblies. A genetically engineered TMV with cysteine residues on the outer surface has been utilized to coat the Pd clusters. Palladium clusteres were nucleated and deposited on the engineered TMV surface by the chemical reduction of palladium chloride anions. It was found that wild type TMV do not accept Pd coatings. In this work, the Pd cluster-coated engineered TMV particles are being studied for gas detection with the help of Surface Acoustic Wave (SAW) resonators. The coating of a gas sensing material attenuates the surface wave magnitude, and

shifts the resonant frequency of the SAW resonators. Exposure of the desired gas causes the resonant frequency to shift further due to absorption or reaction with the sensing material. This change can be directly calibrated to determine concentration of gas absorbed. The increased surface area of Pd exposed to gases, a result of decorating TMV with Pd nanoparticles (about 2.3 nm), was seen to enhance sensitivity and improve response. High robustness and stability are observed when compared to conventional hydrogen sensors. Repeatability was also observed when tested for a week using a range of concentration (0-2.5 volume %) of hydrogen. The sensor shows very good response (3-6seconds) and recovery (3-6 seconds) times with shifts of about 250 Hz were observed. Larger frequency shifts may be achieved by increasing the TMV-Pd coating thickness. The frequency of the device was observed to increase upon hydrogen exposure, which is opposite to the expected behavior if hydrogen absorption by Pd (mass-loading) is the mechanism. TMV has a 300 nm long tubular structure with an outer diameter of 18 nm and an axial canal 4 nm in diameter. They are somewhat similar in structure to Multi-Walled Carbon Nanotubes (MWCNT′s) which are about 2-20 nm in diameter and 100 nm of more in length, and are easier to produce in large quantities. These MWCNT′s decorated with Pd will be studied as SAW coatings for their behavior to hydrogen exposures and compared to the performance of Pd-TMV materials.

Prof. Dr Micheal T Harris, School of Chemical Engineering, Purdue, for TMV-Pd samples.

3F-5 3:45 p.m.
CHARACTERIZATION OF PIB AS A CHEMICALLY SENSITIVE LAYER IN LIQUID ENVIRONMENTS USING TSM RESONATORS.

O. AMU*[1], S. SCHNEIDER[1], F. JOSSE[1], J. HOSSENLOPP[2], and Y. JONES[2], [1]Department of Electrical and Computer Engineering, Marquette University, Milwaukee, WI, [2]Department of Chemistry, Marquette University, Milwaukee, WI.
Corresponding e-mail: Susan.Schneider@marquette.edu

The design and analysis of sensor arrays using polymer-coated acoustic wave devices for the detection and identification of analytes in aqueous environments require an appropriate characterization of the chemically sensitive coating. For thin rigid layers, the use of a simple mass loading interpretation has been shown to be sufficient for chemical detection in which case, the analysis is done using only the change in density or thickness of the coating while neglecting the shear moduli of the film[1]. However, for viscoelastic layers, material parameters such as the shear storage and loss moduli, G′ and G″, of the coating can contribute significantly to the sensor's response and when such is the case, the sensor is classified as operating in the non-gravimetric regime. Because most chemical sensors utilize rubbery or glassy polymers as a chemically sensitive layer, the need for the modeling and characterization of the coating$'s viscoelastic properties during detection in liquid environments is important.

In this paper, an analysis and extraction of the viscoelastic properties of thin chemically sensitive layers as well as subsequent changes upon analyte sorption

in the liquid phase is presented. Using 9-MHz AT-quartz thickness shear mode (TSM) resonators coated with different thickness values of poly(isobutylene) (PIB), a rubbery polymer, admittance spectra were measured near resonance as a function of thickness. The PIB coatings were exposed to varying concentrations of aqueous solutions of ethylbenzene and toluene. The spectra are analyzed using the modified Butterworth-VanDyke (BVD) model to simulate the electrical characteristics of the coated TSM resonator. A general model [2] that incorporates a diverse set of single-component loads including the viscoelastic media and fluids resulting in a non-linear relationship between the total surface mechanical impedance and the changes in the characteristic mechanical impedance of the film and the fluid is used to extract the shear moduli G (= G′ + jG″). Preliminary data of the sorption of ethylbenzene in aqueous solution by a 3.2 μm PIB film shows that the storage modulus, G′ decreases by 0.07% for a frequency shift of 1 Hz caused by the analyte while the loss compliance, J″ (= G″/(G′² + G″²)), increases by 0.4% for every increase of 1 ohm caused by the analyte. These results are discussed in terms of polymer-coated sensor design and analysis.

[1] R. Lucklum, C. Behling, P. Hauptmann, Anal. Chem. 1999 Vol. 71, p. 2488-2496

[2] H. L. Bandey, S. J. Martin, and R. W. Cernosek, Anal Chem. 1999 Vol. 71, pp. 2205 - 2214

Session: 4F

MEDICAL TRANSDUCERS I
Chair: K. Shung
University of Southern California

4F-1 2:30 p.m.
DEVELOPMENT AND CLINICAL EVALUATION OF A 10MHZ LINEAR ARRAY CATHETER FOR ENDOBRONCHIAL IMAGING.

O. CLADÉ*[1], F. TRANQUART[2], P. PALANCHON[2], M. OLAR[2], E. HAZOUARD[2], and D. DINET[1], [1]VERMON, Tours, France, [2]CIT Ultrasound, University Hospital-Bretonneau, Tours, France.
Corresponding e-mail: o.clade@vermon.com

Advances in ultrasound transducers in terms of miniaturization and frequency increase open the way to new medical applications such as endoscopic ultrasound imaging from bronchial tubes. Applying endoscopic ultrasound to image external part of bronchial tubes is of great interest and complementary with other imaging methods.

This paper presents the design and acoustical testing of a catheter array for endobronchial imaging as well as results of the clinical study performed with this probe. The probe is a 64 elements ultrasound transducer included in a 7 Fr

(2.4 mm Outer Diameter) catheter in order to be used in an existing bronchofiberscope. The ultrasound array has a 200 µm pitch, a 1.5 mm elevation, and operates at 10 MHz center frequency. The piezoelectric material is based on 1-3 piezo-composite technology and the front layer is selected to act both as a matching and barrier layer. The probe is integrated into the 7 Fr catheter and interfaced to a commercial ultrasound system. It was used in 20 patients without any inconveniences for the patient (in terms of discomfort and time duration which is limited to 10 minutes at the maximum) or the clinicians (easy use, perfect visualisation of the area of interest). The only limitation encountered concerns the presence of air bubbles on bronchial walls which could limit the visualisation of structures. This allowed the characterization of chest tumours (hypoechoic tissue) with possible adjacent lymph nodes (minimal size of 3 mm) which were not described on CT-scan. This identified clearly some underlying vessels to be spared during biopsy. This helps in identifying some regions of tumours which appeared as vascularized to guide the site of biopsy. In conclusion this specific probe is of great value to better image bronchial structures, to depict extension of tumours as well as possible sentinel lymph nodes for a more complete initial diagnosis and guidance of biopsies. This will be used to improve diagnosis and safety of biopsy.

4F-2 2:45 p.m.
2D ARRAYS PERFORMANCES OPTIMIZATION TO ADDRESS HIGH QUALITY VOLUMETRIC IMAGING.

L. RATSIMANDRESY*, N. FELIX, D. DINET, and R. DUFAIT, VERMON, Tours, France.
Corresponding e-mail: n.felix@vermon.com

Over the past decade a lot of advanced studies were performed on 2D arrays from modelling, acoustic design to interconnect technologies both on sparse and fully populated configurations. The main technological issues were interconnecting 100% of the thousands active elements and on the system side: beamforming and image formation with fully populated 2D arrays (typically 64*64). Still, it is essential to advance 2D arrays active elements performances to obtain image quality at the same level than current state of the art 1D phased array images.

In this work, we focus on the array acoustic optimization. To illustrate this we have manufactured sub-apertures of 2D 2.5MHz center frequency, 64*64 active elements and 300µm pitch. The 8*16 elements sub-apertures are composed of an active layer, 2 matching layers, a backing layer, and a flexible interconnect circuit that allows to plug the array to a 128 coaxial cable.

In these arrays, we investigate different configurations of single active elements from bulk to piezocomposite microstructure. We manufactured arrays with different process and material parameters: kerf width - filler material. Once the arrays were packaged and interconnected, we fully characterized them by measuring electric impedance, pulse-echo response, cylindrical coordinate directivity pattern and radiation pattern. All results were synthesised and analysed, then trade-offs on elementary performances discussed.

Finally, the previously determined performances are compared with state of the art 1D phased array commonly used in 2D imaging.

4F-3 3:00 p.m.
CALIBRATED TOMOGRAPHIC SCHLIEREN SYSTEM FOR CHARACTERIZATION OF MEDICAL PROBES.

J. LE FLOC'H*, P. GATTA, G. CALIANO, R . CAROTENUTO, and M. PAPPALARDO, University Roma Tre, University Roma Tre, Rome, Italy.
Corresponding e-mail: lefloch@uniroma3.it

Ultrasound (US) probes in the MHz range are mainly used in the medical field and must comply with specific rules. Their correct behaviour is verified using calibrated hydrophones. This technique is time consuming.

The Schlieren system allows visualising in real time changes in the refractive index distribution of the water due to the propagation of the US wave. The diffracted components of the optical beam, which are proportional to the acoustic intensity profiles, are visualized in terms of luminance on a screen. Real time image of the US field is then obtained; however, no quantitative measurements are available. Works have been performed in [1],[2] to answer this issue using an industrial Schlieren; however, only a relationship between average intensity and gray level was found.

In this paper, the realisation of an experimental set-up of reasonable dimensions $40\times100\times40$ cm^3allowing real time imaging and a quantitative tomographic reconstruction of an US beam in CW mode is reported. We experimentally find the non-linear relationship between pressure measurements, tomographic luminance values and frequency, in order to calibrate our Schlieren system.

The acousto-optic effect is obtained propagating the US beam under investigation in a tank, containing freshly deionized and degassed water, between two small identical lenses (diameter 40mm, F=20cm). The US beam crosses the laser beam and, the diffracted light is then selected using a manually variable aperture. The choice of the aperture depends on the actual frequency of the acoustic beam under investigation.

The optical source is a single mode laser diode (λ=660 nm, fiber core diameter 4μm). The transducer can be vertically translated and rotated by steps of 10μm and 1.8°, respectively, allowing a complete visualization of the acoustic field. A CCD camera continuously captures the light patterns and a frame grabber (768×576 pixels) digitizes the received information, for successive post processing on a PC. By mechanically rotating the transducer 200 projections of the diffracted light are obtained and the corresponding Schlieren images are stored on the PC. The pixels at a given depth $z_{section}$are automatically selected to build an image corresponding to a tomographic view of the US beam. The gray level of a pixel, an approximation of the luminance at a given voxel, is then known. A calibrated needle hydrophone is then used to perform local measurements of the pressure field. Micro controllers accurately control the position of the hydrophone at the depth $z_{section}$with respect to the voxel. Pressure measurements are performed for the full range of the observed luminances. The non-linear relationship between the luminance, the pressure field within a

given voxel and the frequency can then be computed. Experimental results obtained using two transducers excited at 3.5 MHz and 27 MHz are presented.

Ref:

[1] Hanafy A, Zanelli CI Quantitative Real-time Pulsed Schlieren Imaging Of Ultrasound Waves Proc IEEE 1991, p. 1223.

[2] Schneider B, Shung KK Quantitative Analysis Of Pulsed Ultrasonic Beam Patterns Using Schlieren System IEEE TRANS UFFC 1996. 43(6):p. 1181-86

4F-4 3:15 p.m. HIGH-RESOLUTION IMAGING WITH HIGH-FREQUENCY 1-D LINEAR CMUT ARRAYS.

D. YEH*, O. ORALKAN, I. WYGANT, A. ERGUN, J. WONG, and B. KHURI-YAKUB, Stanford University, Stanford, CA.
Corresponding e-mail: dtyeh@stanford.edu

High-frequency arrays can generate high quality ultrasound images for applications in fields such as dermatology, ophthalmology, and cardiovascular medicine. Because of the tradeoff between resolution and attenuation, high-frequency ultrasound is suitable for applications in which the features of interest are small and near the surface. While mechanically scanned high-frequency transducers have been demonstrated, high-frequency arrays, which enable dynamic focusing and higher frame rates, are still a work-in-progress because of the difficulty of fabricating piezoelectric transducer arrays with the fine pitch required for high frequency imaging. In contrast, the characteristics of capacitive micromachined ultrasonic transducers (CMUTs) are well suited for constructing high-frequency arrays. This work demonstrates the enabling potential of CMUT arrays.

The cell-based structure of CMUTs decouples the design of the frequency of operation from the physical dimensions of the transducer element. In addition, the method of building CMUTs, microfabrication, easily defines array elements at the fine pitch needed for high-frequency imaging. CMUTs can be made with either the wafer bonding technology, which is a simpler fabrication process that also results in better uniformity, or surface micromachining, which currently allows for more reliable operation in collapse mode. CMUTs can be designed to operate in high frequency either conventionally, or in collapse mode, which provides higher output pressure.

Two CMUT arrays from the two fabrication technologies were used. The wafer bonded CMUT array has 64 elements with a pitch of 50 um, 195 cells per element, membrane radius of 6 um, membrane thickness of 1.0 um, center frequency in immersion of 41.9 MHz and 87% fractional bandwidth. The surface micromachined array has 64 elements with a pitch of 36 um, 110 cells per element, membrane radius of 6 um, membrane thickness of 0.4 um, center frequency of 25.5 MHz and 72% fractional bandwidth.

The imaging setup consists of 32 adjacent elements of the linear array wire bonded to two integrated circuit dice, each of which comprises 16 pulser/receiver circuits. The wafer bonded array takes a DC bias of 150 V, a unipolar 25-V

pulse, and a pulse width of 15 ns. The surface micromachined array takes a DC bias of 110 V, a unipolar 25-V pulse, and a pulse width of 20 ns. Both devices are biased for conventional operation. The array elements are fired one at a time, and A-scans are collected from all 32 elements at a sampling rate of 2 GS/s. Images are reconstructed offline from the full set of 32x32 A-scans.

Ongoing work includes expanding the system to utilize all the elements of the array and to support real-time imaging. A high-frequency acoustic lens for focusing in elevation is also a subject of current research.

This work was supported by the National Institutes of Health. David Yeh is supported by a National Defense Science and Engineering Graduate Fellowship.

4F-5 3:30 p.m. (Invited)

ADVANCES IN CATHETER-BASED ULTRASOUND IMAGING.

T. PROULX*, D. BERGMAN, D. TASKER, and J. BARTLETT-ROBERTO, Siemens Medical Solutions USA, Ultrasound Division, Mountain View, CA.
Corresponding e-mail: tim.proulx@siemens.com

Conventional transthoracic and transesophageal ultrasound imaging often cannot satisfy imaging requirements for many advanced catheter-based interventional cardiac procedures due to restricted access to the anatomy. Intracardiac echocardiography (ICE) can provide unrestricted access and has been shown to be very effective in accurately guiding interventional cardiac procedures through high quality visualization of anatomy. ICE is steadily replacing transesophageal ultrasound as the preferred imaging tool for device guidance during atrial fibrillation treatment, valve repair and closure of atrial septal defects.

This article provides a history of the ACUSON AcuNav™ Ultrasound Catheter and a review of the expanding range of clinical applications where ICE technology is utilized. Requirements for an intracardiac ultrasound imaging system and catheter-based transducer device are discussed with respect to particular markets, and the performance of ICE is compared to other imaging modalities such as fluoroscopy.

Important technologies applied to catheter-based transducers are described, as well as recent advances in materials, interconnects, cables and arrays. We review critical performance requirements, such as image quality, catheter size and maneuverability, and assess the regulatory environment associated with catheter-based ultrasound and the key elements necessary to ensure patient safety.

Finally, we describe recent innovations in ICE, such as 3D tools for navigation and volume rendering and new imaging modalities like velocity vector imaging (VVI), and we conclude with exploration of emerging applications for catheter-based ultrasound in the field of minimally invasive surgery.

Session: 5F

SAW ANALYSIS
Chair: P. Smith
McMaster University

5F-1 2:30 p.m.
IDENTIFICATION OF NEW LTO HVPSAW ORIENTATIONS CONSIDERING FINITE THICKNESS ELECTRODES.

T. KENNY* and M. PEREIRA DA CUNHA, University of Maine, Orono.
Corresponding e-mail: mdacunha@eece.maine.edu

The continuing trend towards higher operating frequencies in RF communications has strained SAW filter fabrication capabilities, focusing recent efforts on identifying low-attenuated high velocity pseudo-surface acoustic wave (HVPSAW) orientations of quartz, lithium niobate (LNO), lithium tantalate (LTO), and lithium tetraborate (LBO). In particular, LTO is a well established SAW substrate widely used for wireless applications, due to its relatively high electromechanical coupling and moderate temperature sensitivity in comparison to the other substrates previously mentioned. Although HVPSAW propagation directions have been recently identified in the literature for these materials, several show diminished coupling or prohibitively high propagation losses. Others imply the use of heavy mechanical loading by the use of thick electrodes to achieve reduced device loss.

This paper reports on the investigation of LTO HVPSAW excitation and propagation properties, including: phase velocity, propagation loss per wavelength (λ), and electromechanical coupling (K^2) for arbitrary orientations under periodic aluminum (Al), gold (Au), and platinum (Pt) electrodes. The harmonic admittance of periodic electrodes is calculated using orthogonal Chebyshev basis functions in conjunction with the finite element method. The determination of well defined complex poles in the harmonic admittance curve as a function of crystal rotation leads to the identification of low-attenuated and high coupled HVPSAW orientations. For example, along selected orientations of the LTO (0°,120°,ψ) plane, HVPSAWs are identified which exhibit phase velocities around 5000 m/s, propagation losses as low as 0.04 dB/λ, and K^2=0.74 %, for Al and Au electrodes with thicknesses h/λ=9% and h/λ=3%, respectively. For the same electrode materials and thicknesses, the HVPSAWs propagating under a uniform film layer show propagation losses around 0.3 dB/λ, using matrix method calculations. Therefore, the resulting decrease in propagation loss by more than one order of magnitude demonstrates the importance of the grating structure in achieving low loss operational HVPSAW devices. The reported work identifies new LTO HVPSAW orientations, exhibiting high phase velocity, low propagation loss, and high electromechanical coupling, suitable for high frequency, low loss communication and sensor applications.

This work was conducted with support from the National Science Foundation (grants ECS-0233463 and ECS-0134335).

5F-2 2:45 p.m.
OPTIMISATION AND IMPROVED CONVERGENCE OF COUPLED FINITE ELEMENT/BOUNDARY ELEMENT ANALYSES.

S. BALLANDRAS*[1], R. LARDAT[2], V. LAUDE[1], A. REINHARDT[1], M. WILM[1], W. STEICHEN[2], and T. PASTUREAUD[2], [1]FEMTO-ST, CNRS, Besançon, France, [2]TEMEX, Sophia Antipolis, France.
Corresponding e-mail: ballandr@femto-st.fr

The interest of simulation tools based on the combination of finite element analysis and boundary element method (FEA/BEM) now has been established for numerous problems in acoustics. Particularly in the case of periodic structures, the flexibility of FEA allows for the simulation of interfaces exhibiting complex shapes involving materials of different nature whereas the BEM approach provides accurate description of stacked materials (near and far fields as well) assuming flat interfaces. It can be performed in 2D and 3D, accounting for acoustic and dielectric losses. When solving the problem from the FEA side, the computation delay appears as the main drawback of the approach.

As a consequence, the possibility to improve the convergence and to optimise the computation delay of periodic FEA/BEM has been investigated. Different approaches have been implemented in that matter. The first consists in reducing the mesh as much as possible without any loss of accuracy. Previous computations were conducted meshing a small part of the homogeneous substrate supporting the electrodes or more generally the excitation structure. We show that one can suppress this operation without any degradation of the computation precision. The second approach was based on increasing the interpolation degree in the physical description of the FEA. It is found that a 1st degree polynomials interpolation provides the best trade-off between accuracy and computation delay. Finite elements taking into account only the active part of the field also were developed. For instance, pure shear waves are simulated using a 2 degree-of-freedom (dof) element, respectively corresponding to the shear displacement and the electrical potential (this approach also can be generalized to 3D problems). Finally, we introduce a treatment of the asymptotic behaviour of the Green's function in the BEM part. This latter approach is particularly efficient for problems involving several electrodes for instance, or more generally for which the period is much longer than its homogeneous elements. The efficiency of the different developed ways is illustrated using classical structures such as inter-digital transducers and also more complicated periodic devices (recessed electrodes, passivated transducers).

5F-3 3:00 p.m.
ANALYSIS OF SAW PROPAGATION UNDER A PERIODIC MULTI-ELECTRODE-TYPE GRATING.

TH. PASTUREAUD*, R. LARDAT, W. STEICHEN, and P. VENTURA, TEMEX, Sophia Antipolis Cedex.
Corresponding e-mail: thomas.pastureaud@temex.fr

Excitation and propagation of Surface Acoustic Waves (SAW) have been thoroughly investigated in order to manufacture efficient piezoelectric transducers dedicated to pass-band filters and general signal processing applications. The development of low loss, small size, and high performance SAW devices requires the use of more and more complicated cells to meet specifications. To reach that goal, there has been a continuous search for smart electro-acoustic structures that can achieve the following properties: triple transit suppression, maximal directivity, internal reflection and low level of harmonics. Some cells are known for possessing the desired properties (DART, FEUDT, Hamma-Unsiger). These cells are composed of several electrodes having geometries that can vary greatly. To model and simulate such cells, there are two competing approaches:

- use the superposition principle of several mono-electrode periodic cells,

- directly solve the multi-electrode periodic cell.

The latter solution should produces more accurate results but is more complex to develop. Even though some multi-electrode periodic numerical tools have been presented [1], [2], [3], to our knowledge, most of the modelling of these cells is based on periodic mono-electrode-type grating and superposition principle.

In this paper, we will briefly present the numerical model of such multi-electrode periodic software using the now classical FEM-BEM concepts. Validations against different numerical tools and experiments will be given. But emphasis is put on the study of widely used SPUDT cells. In particular, it will be shown that the superposition principle of mono electrode is reasonably accurate for DART cells on Quartz substrate but leads to large error when used on highly coupled material such as Niobate. Moreover, it will be shown that DART cells radiate energy into the bulk, producing a low-level propagation loss. Finally, an extensive study of Hamma-Unsinger cells is presented, showing the presence of two separate Eigen modes, located respectively at the beginning and the end of the stop-band. A discussion is opened concerning the determination of an absolute phase reference that is required for accurate simulation in the case of directive cells placed in a non-periodic environment.

[1] K.Y Hashimoto, “Surface Acoustic Waves Devices in Telecommunication, modelling and simulation”, Springer Verlag ed.,2000

[2] J. Lin, N. Wang, H. Shen, Y. Shui, “Fast precise and full extraction of the COM parameters for Multielectrode type grating by periodic Green’s function method”, IEEE UFFC trans., vol 49 , no 12 ,dec. 2002.

[3] S.V. Biryukov et al, “The impedance method in the theory of surface acoustic waves in periodic structures”, J. Appl. Phys. Vol 96, No 6, sept 2004.

5F-4 3:15 p.m.
3D PIEZOELECTRIC SURFACE GREEN’S FUNCTION.

V. LAUDE*[1], C. JEREZ HANCKES[2,1], and S. BALLANDRAS[1], [1]Département LPMO, Institut FEMTO-ST, CNRS UMR 6174, Besançon, France, [2]CMAP, Ecole Polytechnique, CNRS UMR 7641, Palaiseau, France.
Corresponding e-mail: vincent.laude@femto-st.fr

We consider the computation of the harmonic 3D spatial-domain Green's function of the surface of a piezoelectric substrate. This Green's function represent the response of the surface to a delta-like excitation. The response to more general excitation distributions can be obtained by convolution from this elementary solution. The 3D piezoelectric Green's function is typically needed for the 3D simulation of finite transducers by finite element method/boundary element method (FEM/BEM) type methods. For isotropic materials, it is known that the surface acoustic wave contribution to the surface Green's function is given by the $H_0^{(2)}$ Hankel function. However, general elastic and piezoelectric media are anisotropic and this solution needs to be generalized. The proposed computation of the harmonic spatial-domain Green's function at the surface of a piezoelectric halfspace is based on the known form of the Green's function expressed in the spectral-domain. In the Fourier transform, the singular contributions are isolated and treated separately. It is found that the surface acoustic wave contributions, i.e. poles in the spectral Green's function, give rise to an anisotropic generalization of the isotropic Hankel function $H_0^{(2)}$. The asymptotic behaviour at infinity and at the origin (for the electrostatic contribution) are also explicitely treated. The remaining non singular part of the spectral Green's function is obtained numerically by a combination of fast Fourier transform and quadrature. Illustrations are given in the case of a substrate of Y-cut lithium niobate.

The authors acknowledge support in this work from Temex, France.

5F-5 3:30 p.m.
MODELING LONGITUDINAL LEAKY SAW PROPAGATION UNDER PERIODIC ELECTRODE ARRAYS.

T. MAKKONEN*[1] and V. PLESSKY[2], [1]Helsinki University of Technology, Materials Physics Laboratory, P.O. Box 2200, 02150 TKK, Finland, [2]GVR Trade SA, CH-2022 Bevaix, Switzerland.
Corresponding e-mail: tapani@focus.hut.fi

We have extended our earlier simple model for longitudinal leaky SAW (LLSAW) in isotropic elastic substrate [1] to account for periodic disturbation on the surface. In particular, periodic system of mechanical resonators on the surface is considered. The computed dispersion curves show Bragg stopband for LLSAW as well as stopband due to backscattering of LLSAW to Rayleigh SAW. Furthermore, it is shown that the propagation loss can be made essentially to vanish with suitably chosen parameters of the resonators on the surface such that the ratiation of shear bulk wave into the substrate is suppressed.

It was recently shown that LLSAW modes with low propagation loss exist on YZ-cut $LiNbO_3$ substrate for different thicknesses of the aluminum finger electrodes [2]. These modes can be associated with higher order resonances of flexural waves in the electrodes. Here, simulation of infinite periodic IDT on YZ-$LiNbO_3$ with gold electrodes is carried out using periodic FEM/BEM technique. It is found that, in addition to the flexural mode, other Lamb wave modes propagating in the gold electrode also support LLSAW with low losses. The computed dependence of Q value (attenuation), LLSAW velocity and resonance-

antiresonance-distance on electrode dimensions is presented in detail. These dependencies can be exploited in resonator and, consequently, ladder filter design.

[1] V. Plessky et al., 2001 IEEE Ultrasonics Symposium, pp. 239-242.

[2] M. Solal et al., 2004 IEEE Ultrasonics Symposium, pp. 1207-1212.

M. Solal and W. Steichen are acknowledged for discussions.

5F-6 3:45 p.m.
ANELASTIC RELAXATION EFFECTS AND ELASTIC INSTABILITIES IN CGG-TYPE COMPOUNDS.

J. SCHREUER*[1] and C. THYBAUT[2], [1]Institute of Crystallography, University of Frankfurt, Frankfurt, Germany, [2]Laboratory of Crystallography, ETH Zurich, Zurich, Switzerland.
Corresponding e-mail: schreuer@kristall.uni-frankfurt.de

The elastic and piezoelectric properties of langasite, $La_3Ga_5SiO\{_{14}$ (LGS), langatate, $La_3Ta_{0.5}Ga_{5.5}O_{14}$ (LGT), $Ca_3Ga_2Ge_4O_{14}$ (CGG) and $Sr_3Ga_2Ge_4O_{14}$ (SGG) have been studied between 100 K and 1800 K using resonant ultrasound spectroscopy (RUS) in combination with certain standard methods.

In all investigated members of the CGG-family strong ultrasound dissipation develops in the ultrasonic frequency regime at elevated temperatures. The temperature evolution of the inverse quality factors of the observed vibrational modes show a peak-like behaviour which is characteristic for anelastic defect relaxations. Depending on composition and frequency the loss maximum appears between 900 K and 1300 K. The strength of the attenuation effects suggests a large number of relaxation centers, i.e. they are probably connected with a structural feature like the off-center position of an ion.

In LGT an additional less pronounced loss maximum with an activation energy of the relaxation process of about 1.05 eV was observed at about 800 K in accordance with previous results [1].

At temperatures below the range with strong anelastic relaxation effects we derived sets of accurate elastic and piezoelectric constants as well as their temperature derivatives from experimental resonance spectra. Whereas

the longitudinal elastic stiffnesses and transverse interaction coefficients show no anomalous behaviour, the temperature dependence of the shear resistances is in most cases non-linear with an increase of the temperature coefficient to lower temperatures. In general dc_{66}/dT and dc_{44}/dT vanish close to room temperature and become positive at lower temperatures. This behaviour indicates a structural instability that might lead to a phase transition at low temperatures or high pressures [2].

[1] W. Johnson, S. Kim and D. Lauria, “Anelastic loss in langatate.”, in {\em Proc. IEEE Inter. Freq. Control Symp.}, 2000, pp. 186-190.

[2] A. Pavlovska, S. Werner, B. Maximov, B. Mill, “Pressure-induced phase transitions of piezoelectric single crystals from the langasite family: $La_3Nb_{0.5}Ga_{5.5}O_{14}$ and $La_3Ta_{0.5}Ga_{5.5}O_{14}$" in Acta Crystallogr. **B58**, 2002, 939-947.

The authors would like to acknowledge financial support from the Swiss National Science foundation under grant No. 2000-061482.00/1.

Session: 6F
INDUSTRIAL MEASUREMENTS AND APPLICATIONS
Chair: J. Tsujino
Kanagawa University

6F-1 2:30 p.m.
FINITE ELEMENT SIMULATION OF A LONG NARROW WORKLOAD IMMERSED IN AN ULTRASONIC CLEANING BATH: PRACTICAL COMPARISONS AND IMPLICATIONS FOR CLEANING EFFICACY.

J. P. LEWIS*[1], S. GARDNER[1], and I. CORP[2], [1]University of Glamorgan, Pontypridd, Rhondda Cynnon Taff, United Kingdom, [2]Ultrawave Limited, Cardiff, United Kingdom.
Corresponding e-mail: jamie.lewis@ultrawave.co.uk

Ultrasonic vessels are widely utilised in both medical and industrial settings for cleaning a wide variety of contaminated objects and as a crucial part of sterilization cycles. A paper is presented in which the role of boundary reflections on cleaning efficacy in an ultrasonic cleaning vessel is discussed. A two-dimensional finite element model of such a bath containing a long flat workload is developed and simulated with and without reflection of the radiated sound wave from the tank boundaries by using a time harmonic Helmholtz solution to the wave equation. This specific problem relates to the positioning of items on trays within ultrasonic baths and is part of a wider project on generic 3D modelling for ultrasonic bath design. Unlike many previous studies this paper concentrates on the steady state standing wave field caused by the continuous time harmonic variation in pressure amplitude and reflections. Reflections from the vessel geometry are found to have a positive impact on the pressure profile presented to the upper side of the work piece and hence the cavitation and cleaning efficacy of the vessel. Practical validation of the model is conducted via the foil ablation test and data from a commercially available cavitation probe. Practical results are found to be in reasonable agreement with the simulation output with the location of standing waves within the vessel giving rise to areas of higher cavitational density. Limitations of the current model are discussed along with directions for future development.

The research associate is generously funded by both the Engineering and Physical Sciences Research Council (EPSRC) and Ultrawave Ltd of Cardiff who design and develop ultrasonic cleaning equipment for industry.

6F-2 2:45 p.m.

NUMERICAL SIMULATION OF ULTRASONIC WAVES IN CAVITATING FLUIDS WITH SPECIAL CONSIDERATION OF ULTRASONIC CLEANING.

N. BRETZ*[1,2], J. STROBEL[1,2], M. KALTENBACHER[2], and R. LERCH[2], [1]Robert Bosch GmbH, Stuttgart, Germany, [2]Dept. of Sensor Technology, Friedrich-Alexander-University Erlangen-Nuremberg, Erlangern, Germany.
Corresponding e-mail: Nina.Bretz@lse.eei.uni-erlangen.de

High-intensity ultrasound is widely used in modern industry, one of which is ultrasonic cleaning. Due the strengthened demand on cleaning results, an appropriate design of the cleaning devices is necessary. One important tool to achieve this goal is numerical simulation. As cavitation is considered to be one of the main cleaning mechanisms, not only the propagation of ultrasound but additionally the emerging sites of cavitation bubbles, their dynamics and influence on to the sound field and the cleaning are of interest. A further challenge in this context is the generation of standing waves due to repeated reflections at the fluid boundaries. In terms of numerical simulation this leads to a set-up, which is very sensitive to boundary conditions. In addition, the computational effort increases tremendously, since the transient response of standing waves has to be considered.

A numerical model is presented to calculate the ultrasound propagation in a cavitating fluid. The model is based on a two-phase continuum approach. The conservation equations for the bubbly liquid are linearized and transformed into an extended wave-equation, which is dependend on the bubble-dynamics. Contrary to most cavitation models, a finite element code capable of simulating coupled problems, e.g. acoustic-mechanical problems, is used to solve these equations. The bubble dynamics described by the Gilmore-equation is iteratively coupled to the extended wave-equation via the bubble radius and the pressure of the mixture.

The transient computation of standing waves although possible with the above model is very costly, e.g. already a one-dimensional channel with only 230 elements would need 500000 steps to reach this state. This is not feasible for aimend applications. Therefore, we introduce a two-step procedure. First, the standing wave field is computed in the frequency domain without consideration of cavitation. The simulation results are used as new initial data in the second step which computes the ultrasonic waves and the cavitation using the presented model. These procedure reduces the computational time for the channel from ten hours to two minutes.

The results of the above numerical simulation will be compared with experiments. Therefore, measurements of multi-dimensional standing wave fields and cavitation in a tube are carried out. In addition to the pressure field the cavitation field is investigated with the help of visualisation methods (bubble distribution and sonoluminescence observed by sensitive CCD cameras). Two cases are considered, one without and one with an object to be cleaned introduced into the tube. This object is stained with a reference contamination and the cleaning results are examined. The experiments also provide the input data for the

numerical simulation, such as the velocity of the excitation measured by a scanning laser vibrometer.

Considering the volume fraction occupied by cavitation bubbles numerical simulations and experiments show a qualitative agreement. The implications of the simulated cavitation activity on the cleaning results are discussed.

6F-3 3:00 p.m.
WELDING CHARACTERISTICS AND TEMPERATURE RISES OF VARIOUS FREQUENCY ULTRASONIC PLASTIC WELDING.

J. TSUJINO*, M. HONGOH, M. YOSHIKUNI, H. MIURA, and T. UEOKA, Kanagawa University, Yokohama, Japan.
Corresponding e-mail: tsujino@cc.kanagawa-u.ac.jp

Welding characteristics and temperature rises in plastic welding specimens over frequency range of 27 kHz to 180 kHz are studied. Using 27 kHz, 40 kHz, 67 kHz, 94 kHz, 150 kHz and 180 kHz ultrasonic plastic welding systems, temperature rises at welding surfaces of lapped 1.0-mm-thick polypropylene plates and polymethyl methacrylate plates are measured using thermo-couples inserted between plate specimens, and also temperature rise distributions at cross sections of the lapped plate specimens are measured using a thermo-tracer. Furtheremore, temeperature rise distributions in a thick plastic plate are measured. Required vibration velocities become smaller as vibration frequency becomes higher. As a example, the 94 kHz vibration system made for ultrasonic plastic welding consists of a bolt-clamped Langevin type longitudinal vibration source using four 30-mm-diameter piezoelectric ceramic (PZT) rings, a stepped horn (super aluminum alloy: JISA7075B, vibration velocity transform ratio N = 3.0) and a catenoidal horn (JISA7075B, N = 3.13) with a 8-mm-diameter welding tip. The diameter of 94 kHz vibration system 30 mm is corresponding to about 0.56 wavelength, which is usually designed less than 1/4 wavelength in a conventional vibration system. Maximum welding tip vibration velocity 3.2 m/s (peak-to-zero value) was obtained using four PZT rings. The other vibration systems have similar configurations to the 94 kHz system with exceptions of the diameters 40 mm of 27 kHz and 20 mm of 150 kHz and 180 kHz sytems. Using higher frequency system, temperature rise measured at the welding part are higher. Temperature rises are measured at welding surfaces using thermocouples and temperature distributions in cross sections of the welding part using a thermo tracer, and maximum temperature rise measured was over 330 °C. Temperature rises are highest at welding surfaces compared with the other welding parts.

This study was partly supported by High-Tech Research Center Project from the Ministry of Education, Culture, Sports, Science and Technology, Japan.

6F-4 3:15 p.m.
TORSIONAL WAVE TRANSDUCTION USING OBLIQUELY-BONDED MAGNETOSTRICTIVE NICKEL STRIPS IN CYLINDERS.

C. I. PARK*, S. H. CHO, and Y. Y. KIM, Seoul National University, Kwanak-Gu, Seoul, KOREA.
Corresponding e-mail: 21cforce@idealab.snu.ac.kr

Magnetostrictive transducers become more widely used for guided-wave based non-destructive evaluation. In comparison with more popular piezoelectric transducers, they are cost-effective and capable of generating high-power without direct wiring. As an effort to advance the magnetostrictive transducer technology, a recent study has reported that torsional elastic waves can be generated and measured quite efficiently if a set of thin nickel strips is bonded at an oblique angle relative to the cylinder axis. This transducer uses several rectangular nickel strips, which are bonded obliquely with 45 degrees in the axis direction on a cylinder-like structure. Several nickel strips and two solenoid coils, one for static bias current and the other for dynamic excitation current, comprise the transducer. The bias coil carrying the direct current offsets the magnetic state in the nickel strips. When alternating current is introduced into the actuating/sensing coil, the developed magnetic field deforms the nickel strips because of the magnetostrictive effect of nickel. The dynamic deformation of the strips occurs mainly in their longitudinal direction, which is oblique to the pipe axis, and generates elastic waves in the pipe to which the strips are bonded. In an earlier investigation, experiments were performed that the obliquely angle is 45 degrees on the basis that the strip stretch at 45 degrees to the cylinder axis would result in the largest shear stress along the cylinder axis direction. However, the orientation giving the largest torsional wave signal for a given solenoid coil current, and the reason for it, remain to be determined. The objective of this work is to investigate the transduction efficiency depending on the angle of strip bonding relative to the cylinder axis and to explain the observed phenomena. Several sets of experiments were conducted with various orientation angles of the nickel strip in an aluminum pipe. Excitation frequencies used were between 40 kHz and 100 kHz because the highest transduction was observed for the used nickel strips.

6F-5 3:30 p.m.
WELDING OF THICK COATED WIRE SPECIMENS USING A 19 KHZ ULTRASONIC COMPLEX VIBRATION WELDING SYSTEM.

J. TSUJINO*, T. UEOKA, R. KARATSU, G. KISHIMOTO, and T. KAWASAKI, Kanagawa University, Yokohama, Japan.
Corresponding e-mail: tsujino@cc.kanagawa-u.ac.jp

Welding characteristics of thick coated wire specimens using a 19 kHz ultrasonic complex vibration welding system are studied. Thin wire such as 0.036-mm-diameter polyurethane coated wires were welded previously with almost their

material strength using 40 kHz, 60 kHz and 100 kHz ultrasonic complex vibration welding equipments with elliptical to circular vibration locus. But thick wires such as over 1.0-mm-diameter or 2.0-mm-wide square cross section with polyurethane or polyurethane and polyimide copolymer insuration coating layer are difficult to weld using these rather small vibration capacity systems. 19 kHz large capacity ultrasonic complex vibration systems using complex vibration converter (40 mm in diameter, titanium alloy) with diagonal slitts are developed. The complex vibration systems consisted of a longitudinal-torsional vibration converter which has four welding tips at the free edge, stepped horn for amplifying vibration velocity (transform ratio N = 4) with a supporting flange and a bolt-clamped Langevin type PZT longitudinal transducer (diameter: 60 mm) for driving the complex vibration converter. Longitudinal vibration amplitude of welding tip with elliptical locus 30 μm (peak-to-zero value) is obtained under driving voltage of 50 Vrms. Using the 19 kHz complex vibration, 1.0-mm-diameter or 2.0-mm-wide square cross section wires with polyurethane or polyurethane and polyimide copolymer insuration coating layer are welded directly to copper plates or copper layer on substrates with 70 to 100 W input power in short time. Required vibration amplitudes of 40 kHz, 60 kHz and 100 kHz welding equipments for polyurethane coated copper wires of 0.036 mm in diameter and copper plates are over 4 μm, 2 μm and 1 μm.

The welded specimens were inspected using a tensile strength tester, a digital height gage, SEM and a laser microscope. It is revealed that the copper wire part is completely welded on the copper substrate and the insulated coating material is driven from welded area to outsides of the wire specimens by high frequency complex vibration. Weld strengths obtained were almost the copper wire strength. Deformation of the welded part is smaller as vibration frequency becomes higher. Furthermore, fluctuations of obtained weld strength become smaller as higher vibration frequency is used.

Insulated wires with various plastic coatings are used for various applications in electronics and furthermore microelectronics. If ultrasonic welding of the insulated wires becomes possible, as an example, direct joining without solder of antenna wires installed in various wireless IC cards or thick coated copper wire for DC motors may be applicable. Coated wires are impossible to weld using a conventional welding equipment with linear vibration locus.

This study was partly supported by High-Tech Research Center Project from the Ministry of Education, Culture, Sports, Science and Technology, Japan.

6F-6 3:45 p.m.
27 KHZ SMALL DIAMETER ULTRASONIC COMPLEX VIBRATION SOURCE WITH MULTIPLE TRANSDUCERS.

J. TSUJINO*, T. UEOKA, Y. KIKUCHI, T. AOYAMA, and T. KYUZEN, Kanagawa University, Yokohama, Japan.
Corresponding e-mail: tsujino@cc.kanagawa-u.ac.jp

The ultrasonic complex vibration systems with elliptical to circular locus are effective and essential for new high power applications in various industries

including automobile production. It have been shown that, using a complex vibration weld tip, weld area and weld strength become larger than that obtained using a conventional system with linear vibration locus.

Configurations of 27 kHz large capacity complex vibration sources with four and six bolt-clamped Langevin type PZT transducers (BLT: 40 mm in diameter) and furthermore with eight or tweleve BLT transducers and welding characteristics of metal plates using the complex vibration systems are studied. 40 kHz complex vibration source was developed before, but it was revealed that the vibration capacity of he 40 kHz system with four or three BLT transducers of 30 mm in diameter is a little short for welding of over 2.0 mm thick aluminum alloy or the other material weldig specimens. Therefore, the 27 kHz complex vibration sources with large vibration capacity are developed. The 27 kHz complex vibration sources have similar configurations od 40 kHz systems developed before, and consist of stepped and catenoidal complex transverse vibration horn with a welding tip part and a (2, 1) mode complex transverse vibration disk with four or six driving longitudinal vibration systems installed normally ingle side of the disk between two nodal circles of the disk or with eight or twelve BLT transducers installed both sides of the disk. The driving longitudinal vibration systems consist of stepped catenoidal horns and BLT longitudinal transducers. Quality factors of the complex vibration systems are over 1000. Outer diameters of the 27 kHz complex vibration sources are about half of the diameter 400 mm of the 27 kHz vibration source with a longitudinal vibration disk that was developed previously. Stepped catenoidal complex transverse-vibration horns with a welding tip is installed in the center of the disk and is driven in circular vibration locus at the free edge of the rod (welding tip) using an arbitrary waveform generator with variable phase outputs, transformers, and transformers and two and three 500 W power amplifiers.

Using the complex vibration systems, 1.0-mm-thick aluminum alloy plates were welded with weld strength almost equal to the material strength using welding tip vibration amplitude of 3.5 μm. Weld strength over 2000 N was obtained per one welded spot area. Welding charactersitics of 2-mm-thick aluminum alloy plates were welded with material strength and furthermore under testing.

Using ultrasonic complex vibration welding systems, ultrasonic welding of various metal plates becomes possible which is almost impossible using a conventional system with linear vibration. It have been shown that, using a complex vibration weld tip, weld area and weld strength become larger than that obtained using a conventional system and independent of the welding position.

This study was partly supported by High-Tech Research Center Project from the Ministry of Education, Culture, Sports, Science and Technology, Japan.

Session: 1G

ELASTICITY
Chair: K. Nightingale
Duke University

1G-1 4:30 p.m.
APPLYING *IN VITRO* ELASTICITY IMAGING RESULTS TO OPTIMIZE *IN VIVO* BREAST LESION CHARACTERIZATION USING A COMBINED 3D US/ DIGITAL X-RAY SYSTEM.

R. BOOI*[1,2], P. CARON[1,2], R. ERKAMP[1], H. XIE[1], A. KAPUR[2], G. LECARPENTIER[1], M. ROUBIDOUX[1], J. FOWLKES[1], and M. O'DONNELL[1], [1]University of Michigan, Ann Arbor, [2]General Electric Global Research Center, Schenectady, NY.
Corresponding e-mail: rbooi@engin.umich.edu

Ultrasound-based reconstructive elasticity imaging has great potential for diagnosis and characterization of breast lesions. Applying external strain with a mammographic paddle as part of a combined 3D US/Digital X-ray system provides more uniform deformation and breast stability, offering opportunities to improve image fidelity. In this study, we examined *in vitro* and *in vivo* strain image quality with three GE transducers (M12L, 10L, 7L) each operating at several frequencies between 5-10 MHz and four TPX paddle thicknesses to predict optimal *in vivo* results with the combined system. Out-of-plane motion was measured by translating an ultrasonic transducer across a breast phantom (ATS, model BB-1) in 50μm steps over 400μm. Each image was correlated to the first in the sequence using conventional 2D phase-sensitive speckle tracking techniques to determine the rate of elevational decorrelation. Next, in-plane, strain-limited decorrelation was evaluated by compressing the phantom at 0.15% increments up to 5% strain. Images were correlated at step sizes 0-7 (0-1.05% mean strain) using two-pass 2D speckle tracking algorithms and estimated displacements were accumulated. Adaptive strain estimation (ASE) was applied to maximize CNR throughout the final strain image. Overall, the 10L transducer caused the least decorrelation due to out-of-plane motion (R = 0.97 at 7.5MHz and 400μm elevational translation). In-plane decorrelation was also primarily strain-limited with the 10L transducer at 7.5MHz, with R = 0.9 for a 1.6% strain step. Accumulated strain images after ASE demonstrated a CNR = 3.8 with the M12L transducer at 10 MHz. Using the same post-processing techniques, the 10L transducer at 7.5 MHz demonstrated a CNR = 4.7. Of the four TPX paddle thicknesses (0, 0.25, 1.0, 2.5 mm) used in the *in vitro* study, the 2.5mm paddle created clearer strain images with less artifacts than the thinner paddles under the same experimental conditions, providing more uniform deformation during compression by bowing less than the thinner paddles. Next, we evaluated sources of *in vivo* chest wall motion in 7 subjects to minimize patient motion during the scan. Patients were asked to breathe shallowly during exams as it caused less decorrelation due to chest wall motion (Ravg = 0.96 over 91 frames) than holding

their breath (Ravg = 0.93). *In vivo* results were acquired with the 10L at 7.5 MHz and TPX 2.5mm paddle using continuous compression over 2.1 seconds. Strain images clearly distinguished between tissue types when accumulated up to 4% strain and ASE was applied. *In vivo* results are limited by out-of-plane motion and CNR but are expected to improve significantly with full 3D tracking. These early successes indicate that using elasticity imaging with the combined system shows great potential for characterizing breast lesions that might be malignant, reducing the need for biopsies.

This work was supported in part by NIH grant RO1 CA 091713.

1G-2 4:45 p.m.
3D STRAIN ESTIMATION FOR ISOTROPIC AND ANISOTROPIC MATERIALS.

R. G. P. LOPATA*[1], M. M. NILLESEN[1], I. H. GERRITS[1], J. M. THIJSSEN[1], L. KAPUSTA[2], and C. L. DE KORTE[1], [1]Clinical Physics Laboratory, Radboud University Medical Center, Nijmegen, The Netherlands, [2]Children's Heart Center, Radboud University Medical Center, Nijmegen, The Netherlands.
Corresponding e-mail: r.lopata@cukz.umcn.nl

Background: Strain imaging in ultrasonics has been proven to be a useful tool in assessing the elastic properties of tissues. In previous work, axial and lateral strain are estimated using the raw radio-frequency data (RF) of 2D ultrasonic datasets. In cardiac strain imaging the tissue deformation is due to an active contraction/relaxation process repeating itself each heart cycle. The 3D structure and geometry of the heart is complex and the orientation of muscle fibers is not confined to one single plane. However, since 3D ultrasound imaging is at the rise, new techniques are available for assessing strain in all dimensions. The advantage of 3D strain imaging lies in the possibility of imaging 3D anisotropic strain in a complex structure as the human heart. In this study, the real-time 3D capability is exploited to determine the strain in 3 orthogonal directions.

Methods: Raw (rf) ultrasound data were acquired with a Philips SONOS 7500, equipped with a 4MHz 3D transducer and a RF-interface. An algorithm was developed to estimate the displacement in all 3 directions. First, the axial displacement was estimated using the RF-data. The time-delay of the RF-signal was measured by evaluating the cross-correlation function for signal-windows of both the pre- and post-deformation data. Next, the lateral and elevational displacement was estimated using the B-mode (demodulated) data. Interpolation (16 times) was used to determine additional ultrasound lines in between the acquired lines. A correlation-based search algorithm was used to determine the displacement in lateral and elevational directions. A geometric correction was applied to convert the measured displacements to true displacement values. The strain was determined from the displacement using a moving average procedure in time and in space. The method was validated using simulations and phantom (10%-gelatin, 15 μm SiC-scatterers) experiments and further evaluated in vivo by using a volunteer's calf muscle imaged during passive compression with the transducer and active compression by means of muscle contraction.

Results: The simulation (a non-compression recording was artificially stretched: axial stretch: 1%; lateral stretch: 0.5%, cq. a Poisson-ratio of 0.5)) revealed excellent correlation between applied and measured axial strain. In lateral and elevational direction, a slight overestimation of the applied strain was observed (0.54%). A higher standard deviation was found in lateral (0.18%) than in axial (0.15%) direction. Similar results were found for the phantom studies. The phantom experiment revealed an axial strain of 1.6%. The lateral and elevational strain were similar (0.8%) as might be expected in this homogeneous isotropic material. The in vivo experiment revealed different strain values in lateral and elevational direction due to the anisotropy of the calf muscle.

Conclusion: 3D strain estimation is feasible using a real-time 3D scanner. Additional validation studies in anisotropic phantoms are required to fully validate the technique.

1G-3 5:00 p.m.
A QUANTITATIVE STUDY OF MECHANICAL PROPERTIES OF HUMAN DERMIS IN-VIVO USING 2D HIGH FREQUENCY ELASTOGRAPHY.

Y. MOFID*[1], S. GAHAGNON[1], C. IMBERDIS[2], F. PATAT[1,3], and F. OSSANT[1,3], [1]LUSSI FRE 2448 CNRS, Tours, France, [2]LMARC UMR 6604 CNRS, Besançon, France, [3]University Hospital Bretonneau, Tours, France.
Corresponding e-mail: mofid_y@med.univ-tours.fr

This work was based on 2D high frequency elastography used for the in-vivo study of the mechanical behavior of human dermis in terms of axial strain and lateral displacement. Furthermore, mechanical properties as anisotropy, viscoelasticity, intra and inter-individual variations were quantitatively studied.

In a previous paper [1], it has been shown the potential of 2D high frequency (20MHz) elastography for the qualitative study of the mechanical behavior of skin. The experiment material was the combination of 2 devices. First, the extensiometer [Patent No FR03/09220] developed by LMARC laboratory for in-vivo skin applications using uni-axial stretching stress cycle applied in the plane of the skin in 3 stages : stretching, hold and releasing. Second, our 20 MHz real time sonographer, Dermcup 2020TM (100 MHz sampling frequency, 256 RF A-lines per image, 6mm in width and 6mm in depth). Filtered and Staggered Strain Estimation algorithm was used to produce elastograms with cumulating small deformations over 20 steps.

In this study, in-vivo experiments were conducted with a new generation of Dermcup: 500 MHz sampling frequency and 296 RF A-lines per image. RF image had 3.2mm in depth, which allowed to explore only the dermis. In this case, elastograms was obtained over 50 steps.

To quantify locally the strain-stress relationship in the dermis, kinetic profiles of the axial strain $\varepsilon(t)$ were obtained for homogeneous ROIs in the dermis. Typically, for 24% stretching (stress cycle of 8s) in a zone of the forearm (internal side) the maximum strain induced was in the order of 10%. Kinetic variation showed several characteristics: a non-linearity during stretching and releasing stages, a relaxation phenomenon in the hold step ($\Delta\varepsilon$=-1% in 1.5s), and a time delay in

the releasing stage due to viscoelastic effect. We have also studied the anisotropy of dermis. Kinetic profiles were calculated for stretching along (0°) and through (90°) Langer's lines. We always obtained $\varepsilon(t)90° > \varepsilon(t)0°$ for the same stress.

Inter-individual variations were studied for 12 subjects, with stretching in 0° and 90° directions. The intra-individual variations study was performed for three zones in the forearm area. Results showed a low intra-individual variations (a few %) and a strong dispersion for inter-individual variations.

Finally, we have performed preliminary elastograms at 50 MHz. In this frequency, elastographic axial resolution is 2 times increased which provided more details to comprehend mechanical behavior of the dermis.

These in-vivo results showed the potential of 2D elastography for the quantitative study of the mechanical properties of the dermis at 20MHz and at 50 MHz in perspective work.

[1] Mofid Y, Ossant F, Imberdis C, Josse G and Patat F, "High frequency elastography for in-vivo study of the mechanical behavior of skin", Proceedings of IEEE Ultrasonics Symposium, Montreal, 22-26 aout, (2004)-2.

1G-4 5:15 p.m.
THE INVERSE PROBLEM OF ELASTICITY: A RECONSTRUCTION PROCEDURE TO DETERMINE THE SHEAR MODULUS OF TISSUE.

W. KHALED*[1], S. REICHLING[2], O. T. BRUHNS[2], and H. ERMERT[1], [1]Institute of High-Frequency Engineering / Ruhr-University Bochum, Bochum, NRW, Germany, [2]Institute of Mechanics / Ruhr-University Bochum, Bochum, NRW, Germany.
Corresponding e-mail: Walaa.Khaled@rub.de

Purpose: In the field of medical diagnosis, there is a strong need to determine mechanical properties of biological tissue, which are of histological and pathological relevance. In order to obtain non-invasively quantitative mechanical properties of tissue, we propose in this work an inverse approach by which the spatial distribution of the relative shear modulus of tissue can be estimated only from the measured axial deformation.

Methods and Tools: First, during the solution of the mechanical forward problem the biological tissue was modeled as a linear isotropic incompressible elastic medium and a 2-D plane strain state model was used. Furthermore, to develop an inverse elastography reconstruction procedure, finite element simulations were performed for a number of biological tissue object models. The results obtained from finite element analysis were confirmed in the ultrasonic experiments on a set of tissue-like phantoms with known acoustical and mechanical properties. These phantoms were produced using PVA-Materials with different thaw and freeze cycles so that the relative shear modulus E2/E1 between the inclusions and the the surrounding medium as a reference is nearly 3 (E1=30 kPa, E2=90 kPa). The RF-data was acquired using a standard ultrasound system (SONOLINE Omnia, Siemens AG, Germany) equipped with a 9 MHz linear array probe and a conventional ADC (fs=50 MHz). The axial

displacements were calculated using the fast root-seeking technique (A. Pesavento, A. Lorenz and H. Ermert, Electronics Letters, 35, 1999, p. 941-942). Finally, using numerical solution models and solving the inverse problem using two different methods we calculate the relative shear modulus. The first method is a modified direct method based on solving the equations of equilibrium. The second method is an iterative method for solving the inverse elasticity problem and is based on recasting the problem as a non-linear optimization problem.

Results and Conclusion: The results of an ongoing clinical study on the prostate tumor diagnostic with more than 200 patients show, that our real time ultrasound elastography system is able to differentiate hard lumps from soft tissue, in a qualitative manner. The data collected with our real time elastography system were also used in the reconstruction approaches which seem promising for an additional quantitative differential diagnosis of lesions in biological tissue. The phantom results show that the iterative approach leads to a relative shear modulus ratio of about 2.4 (E2=72kPa for the inclusion), whereas the direct method results in a ratio of 1.9 (E2=57 kPa). The feasibility of both methods was also demonstrated using the measured real time ultrasound data from a tissue-like phantom with multiple inclusions and in vitro data. The proposed methods were compared with respect to the stability of algorithms using numerical simulations and ultrasound measurements. Based on this comparison, an approach is introduced, which is capable of taking into account large deformations, whereas other existing methods are generally based on the theory of linear elasticity.

1G-5 5:30 p.m.
ULTRASONIC MECHANICAL RELAXATION IMAGING AND THE MATERIAL SCIENCE OF BREAST CANCER.

M. INSANA*[1,2], M. SRIDHAR[2], J. LIU[1], and C. PELLOT-BARAKAT[2], [1]University of Illinois at Urbana Champaign, Urbana, IL, [2]University of California at Davis, Davis, CA.
Corresponding e-mail: liujie@uiuc.edu

Material science is the study of relationships between structural properties and function. Ultrasonic imaging is widely used to describe material properties of soft tissues and thus infer functional characteristics. Palpable breast lesions, for example, often appear more hypoechoic and stiffer than their surroundings in sonograms and elastograms, suggesting that edema from compromised lymphatics is a common feature. Nonpalpable malignancies present with less specific image characteristics. Nevertheless, they can be differentiated by imaging mechanical relaxation rates from estimates of time-varying strain. Recent literature on the molecular biology of breast cancer reveals why this occurs. The viscosity of the polysaccharide gel surrounding the collagen fibers in connective tissues of the breast is reduced within malignant lesions and is increased within benign fibrous lesions. Viscoelastic imaging techniques are sensitive to interstitial fluid movements as tissues creep under stress. Despite the wide variability of elastic properties for nonpalpable tumors, preliminary data suggest that visco- and poroelastic properties are specific to lesion type.

Data from 13 patients were combined with measurements on tissue-like gelatin samples to optimize clinical scanners for breast imaging. We used a VF10-5 linear array at 8 MHz and ramp-compress-and-hold techniques with the Siemens Antares URI to acquire RF echo frames. Recording RF frames at a rate between 0.1 and 4 f/s up to 100 s, we generated a time sequence of strain for visualizing viscous creep. A Kelvin-Voigt model is adopted to estimate the relaxation time constants for the bi-exponential creep curves. Experiments show the two components are associated with water flow and crosslink relaxation within the collagen matrix. Gelatin measurements yielded a water-flow relaxation time constant of T1 = 3 s and crosslink relaxation time constant of T2 = 100 s. The mechanisms are independent and separable only under special boundary conditions. For typical clinical scanning conditions with uniaxial handheld compression and unrestricted boundary motion, T1-weighted (water flow) relaxation constants for breast tissues in vivo were measured in the range of 1-2 s for malignant (IDC) tumors, 7-9 s for benign fibroadenomas, and 3-4 s in the regions surrounding the tumors. Although sonograms and elastograms of malignant and benign lesions are similar, the T1-weighted mechanical relaxation images appear distinct. Our conclusions are based on several independent measurement techniques, including strain imaging, that are designed to isolate the elastic, poroelastic, and viscoelastic responses. Measurements in gelatin are presented to verify creep mechanisms and establish find limits for the imaging technique to help interpret clinical findings.

The work was supported in part by NIH R01 CA082497

1G-6 5:45 p.m.
IMAGING ELASTIC NON LINEAR PROPERTIES OF SOFT TISSUES: TOWARDS BREAST CANCER CHARACTERIZATION.

R. SINKUS[1], J. BERCOFF*[1], M. TANTER[1], K. ELKOURY[2], V. SERVOIS[2], and M. FINK[1], [1]Laboratoire Ondes et Acoustique, Paris, France, [2]Institut Curie, Radiology department, Paris, France.
Corresponding e-mail: jeremy.bercoff@loa.espci.fr

To date, elastography techniques are devoted to estimate mechanical parameters linked to the stiffness of tissues. Some of them also assess viscosity or relaxation time. However, elasticity, as known from clinical experience, will probably not be the ultimate parameter to differentiate between benign and malignant lesions. The clinical pertinence of viscosity has not been demonstrated yet.

We propose in this work to estimate a new mechanical parameter: the elastic non linearity of soft tissues that could be of great interest for breast tumor characterization. An ultrasound based methodology to locally estimate elastic non linearity of soft tissues is here investigated. A low frequency monochromatic excitation (~60 Hz) is applied to the tissue by an external vibrator. Induced motion is estimated in a 2D plane by imaging the medium with a 1D linear ultrasound probe and using classical 1D cross-correlation techniques. The ultrasound imaging frame rate is triggered with the mechanical excitation to acquire data at different steps of the monochromatic oscillation. A Fourier analysis is then

performed and the ratio between the second harmonic and the fundamental component is spatially mapped. This elastic non linearity mapping technique has been first studied in vitro on beef samples. Non linearity maps has been computed before and after a local injection of a gluta-aldehyde solution in the beef. Such solution allows a deep change in the tissue architecture of the sample. Results shows a strong non linearity enhancement in the injection zone showing that non linearity is closely related to the tissular matrix properties. According to previous works [1], change in the tissue architecture is a very good indicator of malignancy. Ex vivo studies on several mastectomy specimen presenting localized carcinomas will be presented.

[1] Tissue architecture: the ultimate regulator of breast epithelial function, Cell Biology, 15: 753-762, 2003

Session: 2G
CONTRAST AGENTS: IMAGING II
Chair: K. Ferrara
University of California, Davis

2G-1 4:30 p.m.
INTRAOPERATIVE CONTRAST ENHANCED PERFUSION IMAGING OF CEREBRAL TUMORS.

CH. HANSEN*[1,2], M. ENGELHARDT[3,2], W. WILKENING[2], K. SCHMIEDER[3,2], and H. ERMERT[1,2], [1]Institute of High Frequency Engineering, Ruhr-Universitaet Bochum, Bochum, Germany, [2]Ruhr Center of Excellence for Medical Engineering, Bochum, Germany, [3]Department of Neurosurgery, Ruhr-Universitaet Bochum, Bochum, Germany.
Corresponding e-mail: Wilko.G.Wilkening@rub.de

Objective: In previous publications the capability of transcranial contrast enhanced ultrasound perfusion imaging of the brain has been shown. In clinical studies on stroke patients ultrasound perfusion measurements were conducted by scanning the brain of patients. In this paper we present results of intraoperative cerebral perfusion imaging on patients during tumor resections using Sonovue. The aim is to reliably differentiate between normal tissue and the tumor so that the resection is complete and the damage to vital brain tissue is minimal.

Methods: Every patient was scanned four times: the first time preoperatively in order to detect and classify the tumor transcranially; the second and third time intraoperatively before and after resection of the tumor; the fourth time postoperatively in order to compare results with those obtained preoperatively. All measurements were conducted with a Siemens Sonoline Elegra. For pre- and postoperative imaging a phased array (2.5PL20, 2.5 MHz) was used driven at 2 MHz scanning through the temporal bone window of the human skull. For intraoperative imaging an endocavity transducer (6.5EC10, 6.5 MHz) was used with a transmit frequency of 3 MHz. To detect the nonlinear response of the used microbubbles the ultrasound system was set up to image in phase inversion

mode, i.e. THI-mode, (Tissue Harmonic Imaging, but used for contrast agents) for pre- and postoperative examinations and ECI-mode (Enhanced Contrast Imaging) for the intraoperative scans. The frame rate of the ultrasound system was set to 1 fps to account for the destruction of microbubbles and to save memory for data export. While the transcranial scans were performed with high transmit power to overcome attenuation of the skull, intraoperative scans were conducted with low MI settings in the range of 0.2 to 0.5. Both times images were recorded for 90 s, where imaging started shortly before the contrast agent entered the imaging plane. The recorded data sets were analyzed concerning peak intensity, time-to-peak, and further parameters.

Results: Intraoperatively, tissue perfusion and pulsatile flow in vessels were displayed. The results for cystic tumors correlated well with the preoperative diagnostics (i.e. MRI and CT). A strong rim enhancement of the tumorous tissue around the cyst was observed. After injection of Sonovue, tumor associated vessels and the tumor tissue itself could be differentiated from surrounding cerebral tissue in good correlation to gadolinium enhancement in MRI. The peak intensity of the perfused tumorous tissue exceeded the peak intensity of the healthy tissue by 15 dB. Furthermore, the time-to-peak of the pathological tissue was 3 s smaller than that of the healthy tissue and, thus, corresponded to the arterial cerebral inflow. With this novel approach in brain surgery the opportunity is provided to intraoperatively monitor tumor resections and to better protect the vital brain against damage from the surgery.

The work funded in part by the Federal Ministry of Education and Research, Germany (BMBF), grant 13N8079. We would like to thank Siemens Medical Solutions, Inc. for additional support.

2G-2 4:45 p.m.
IN VIVO CONTRAST-ENHANCED IMAGING OF MOUSE VASCULAR DEVELOPMENT.

D. H. TURNBULL*[1,2] and O. ARISTIZÁBAL[1,2], [1]Skirball Institute of Biomolecular Medicine, New York, NY, [2]New York University, New York, NY.
Corresponding e-mail: oarist@saturn.med.nyu.edu

Introduction: Anatomical and functional mapping of the vascular system in mouse embryos is important for understanding both normal vascular development and for phenotype analysis in a variety of genetically-engineered mouse models (Phoon & Turnbull, Physiol Genomics 14: 3, 2003). In lower vertebrates such as zebrafish, confocal microangiography has emerged as an effective method for imaging vascular development using microinjection of fluorescent dyes or transgenic expression of fluorescent proteins. Unfortunately, lack of optical penetration precludes similar measurements in mouse embryos. We are investigating the potential of micro-bubble contrast-enhanced ultrasound biomicroscopy (UBM) to analyze vascular anatomy in mouse embryos, in utero.

Methods: Mouse embryos staged between embryonic days (E) 11 and 13 were imaged with a 40 MHz Vevo 660 UBM system (VisualSonics). Pregnant mice were anesthetized, and the uterus exposed through laparotomy into sterile saline solution maintained at physiologic temperature (37 degrees), enabling the UBM

image-guided microinjection of an ultrasound contrast agent (UCA, Optison) into the embryonic cardiac ventricles for real-time vascular imaging. UBM cine loops (30 frames per second) were acquired pre and post injection of UCA (1 µl of 1:1 dilution of Optison in a PBS / bovine serum albumin mixture; approximately 250,000 bubbles) over 10 seconds. Quantitative image analysis was performed by drawing regions-of-interest (ROIs) and measuring signal intensity before and after injection of UCA.

Results: At both E11 and E13, small cerebral blood vessels and vascular bifurcations were identified in post-contrast images that could not be resolved in pre-contrast images. ROI analysis showed an increase from 138 ± 30 (pre) to 152 ± 34 (post) in these brain regions. Quantitative data from larger blood vessels as the umbilical artery showed a larger increase in image intensity from 176 ± 23 (pre) to 234 ± 20 (post). Serial images demonstrate the three-dimensionality of the embryonic vascular system. In future we plan to implement real-time 3-D acquisition and volumetric analysis of contrast-enhanced UBM data. In our combined data on both E11 and E13 embryos, 31/59 (52%) embryos survived to four days after contrast-enhanced UBM, which is similar to other (non-cardiac) UBM-guided injection experiments in our lab.

Discussion and Conclusions: Real-time vascular micro-imaging with contrast-enhanced UBM has been demonstrated in mouse embryos, in utero. Future extension of this approach, with 3-D acquisition and analysis, will enable volumetric vascular mapping in mouse embryos. Survival data in these initial experiments indicate that longitudinal studies are feasible. It is likely that UCA enhancement in small blood vessels will also translate into more sensitive detection of blood velocity with UBM-Doppler, which will extend this approach from anatomical to functional vascular mapping of mouse embryonic micro-circulatory systems.

This research was supported by NIH grant HL078665.

2G-3 5:00 p.m.
MICROBUBBLE CONTRAST AGENT DESTRUCTION USING 25 MHZ ULTRASOUND.

E. CHERIN*[1], A. NEEDLES[1], S. STAPLETON[1], R. WILLIAMS[1], J. TAVAKKOLI[1,2], J. MEHI[1,2], and F.S. FOSTER[1], [1]Sunnybrook and Women's College Health Sciences Centre, Toronto, Ontario, Canada, [2]Visualsonics Inc., Toronto, Ontario, Canada.
Corresponding e-mail: emmanuel.cherin@swchsc.on.ca

Microbubble based ultrasound (US) contrast agents have shown great potential in the 1-10 MHz frequency range for the detection and characterization of blood flow in the vasculature, especially in applications related to cancer and cardiovascular disease. The destruction of microbubbles with high intensity ultrasound has played an important role in the development of reperfusion methods. Recently, the use of the 2nd harmonic and subharmonic generated by microbubbles under exposure to 20 to 30 MHz US has been demonstrated in blood flow measurement in vivo in small animals. Under certain circumstances related to flow conditions or microbubble destruction, the efficiency of this technique has exhibited a relatively high variability.

The purpose of this preliminary study is to quantify the destruction of a microbubble contrast agent by 25 MHz US under varying conditions of exposure including acoustic peak-peak pressure (Pr=1.10, 2.08, 3.28, 4.64 and 6.56 MPa), number of cycles (NC= 1, 6, 12) and frame rate (FR= 39, 66, 93 Hz). Experiments were performed in a 1 mm diameter flow phantom, using two Vevo770 scanners (Visualsonics) equipped with an RMV710 probe (25 MHz, diam.= 7.1 mm, F#2.1) for the upstream microbubble destruction and an RMV704 probe (40 MHz, diam.=3 mm, F#2) for downstream linear imaging at 40 MHz. The focal planes of the two probes were separated by 1 cm and the average flow of agent (Definity™, 0.01 % volume fraction) was set to 12 mm/s. Cineloops of the vessel were recorded downstream before, during and after exposure to the 25 MHz beam. The mean pixel grey level (MGL) was measured in each frame of the resulting cineloop in a 0.8 mm diameter ROI centered in the vessel, and the difference in MGL before and during exposure to the destruction beam was calculated for all conditions of exposure.

The MGL measured before and after exposure to the 25 MHz beam was constant over all the experiments (85). A decrease of the MGL was detected during exposure to the 25 MHz beam. This decrease ranged from 10 (Pr=1.1 MPa, NC=1, FR=39 Hz) to 57 (Pr= 6.56 MPa, NC=12, FR=93 Hz). The decrease in MGL became more important as the pressure, the number of cycles, or the frame rate increased. Radiofrequency data are currently being analyzed and will be presented to support the MGL results. This study shows that 25 MHz ultrasound at pressures in excess of 1 MPa is effective in destroying Definity™ microbubbles. In addition expected increases of destruction were observed as the number of cycles in the transmit pulse and the frame rate were increased.

This information could be useful for the measurement of flow at high frequency in the microvasculature in mouse cancer model, in particular for destruction/ reperfusion measurements, using microbubble contrast agents.

Support was provided by the NCIC with funds from the Terry Fox Foundation, CIHR, CFI, ORDCF, and Visualsonics.

2G-4 5:15 p.m.
ACOUSTICAL INVESTIGATION AND SIMULATION OF FREELY MOVING SINGLE MICROBUBBLES.

H. VOS*, F. GUIDI, E. BONI, and P. TORTOLI, Department of Electronics and Telecommunications, Universita di Firenze, Firenze, Italy.
Corresponding e-mail: Vos.Rik@Gmail.com

Predicting the response of microbubbles to ultrasound (US) excitation can be important for new applications of contrast agents (CAs) such as targeted drug delivery. Acoustic observations of CA behavior are typically related to full populations, and little work has been so far reported to characterize individual bubbles that are free of moving in a fluid.

In this paper a new approach is presented to characterize a full population of CA suspended in a water tank, by observing the response of single bubbles to US excitation. In particular, we exploit the fact that the imaging burst induces an US force on the bubble, and hence its displacement, at an extent depending on

the US burst, the bubble characteristics and the medium properties. A bubble model describing both radial and translational motion has been developed to predict the backscattered signal and bubble displacement, which are compared to values measured in various experimental conditions.

Two different types of experiments have been performed to estimate viscoelastic properties and radial dimensions, respectively, of thermoplastic shelled microbubbles (F-04E, Matsumoto Yusi-Seiyaku Co. Ltd., Osaka, Japan). Viscoelastic shell properties have been estimated by comparing the experimental maximum bubble velocities to the velocities predicted for resonant bubbles insonified with a 50 cycles US burst with 2 to 8 MHz frequencies and 280 kPa and 490 kPa rarefactional pressure. The modeled shell properties have then been updated to obtain a good fit between these velocities over all frequencies. In this way we have estimated 12 MPa for the shear modulus and 0.14 Pa.s for the viscosity (at a shell thickness of 2.7 % of the radius). These values are close to those so far obtained through standard backscatter and attenuation experiments for a similar type of encapsulated bubbles (Hoff et al, JASA 107(4), p. 2272, reporting shear modulus 11-13 MPa, viscosity 0.4 - 0.5 Pa.s, at a shell thickness of 5%).

The diameters have been estimated by exploiting the non-linear behavior of single bubbles. In this case, the bubbles have been insonified by a 20 cycle 2 MHz burst with 490 kPa rarefactional pressure. The received relative second harmonic signal level and the bubble velocity are compared to values predicted by simulation for incrementing bubble radii, until a unique radius, and hence the resonance frequency, can be read. In preliminary experiments, we were able to estimate diameters ranging from 5 μm to 9 μm for 10 different bubbles, with about 20% uncertainty (mainly due to pressure uncertainties).

In conclusion, it is shown that model-based investigations of freely moving single bubbles in a population can give advanced knowledge on the bubble characteristics.

2G-5 5:30 p.m.

A NEW MODEL FOR THE ULTRASOUND REFLECTIVITY ENHANCEMENT DUE TO THE PRESENCE OF MICRON-SIZED PARTICLES ON A SURFACE.

O. COUTURE*, P. B. BEVAN, K. CHEUNG, and F. S. FOSTER, Sunnybrook and Women's College Health Sciences Centre, University of Toronto, Toronto, Ontario, Canada.
Corresponding e-mail: olicou@sten.sunnybrook.utoronto.ca

The combination of ultrasound biomicroscopy (UBM) and targeted contrast agents has potential for the assessment and tracking of biomarkers in animal models. It has been reported that submicron particles containing liquid perflurocarbon (PFC) targeted to a thrombus can enhance its ultrasound reflectivity by up to 22.8 dB (Marsh, J.N., et al., IEEE Trans UFFC, 2002. 49(1)). Unfortunately, the one-dimension transmission line model that partly explains this enhancement does not take into account the discrete nature of the source of backscattering.

A model was developed to predict the reflectivity enhancement of discrete particles bound to a surface. This model takes into account surface density, scattering cross-section, pulse bandwidth, driving frequency and transducer characteristics. An impulse response approach in which particles are sparsely and randomly distributed on the surface and sparse enough to limit multiple scattering and stacking is used to calculate the coherent sum of the scattering for all scatterers over the surface.

Experiments confirming this model were first performed with glass beads of a narrow size distribution (5.1 microns in diameter) and narrowband pulses over the frequency range 15MHz to 60MHz. The beads were deposited on a surface of Aqualene (a solid coupling medium Zo=1.46 MRayl) with a surface density varying from 20 to 9000 beads/ mm2. Further experiments were then performed with particles filled of C6F14 with an average diameter of 1.1 micron deposited by centrifugation on an agar surface to obtain a surface density of 3600 to 160 000 particles/mm2

The amplitude of the reflection increased linearly with the number density of glass beads on the surface and corresponded to predicted values. This increase deviated from linearity at a surface density around 6000 beads/mm2, when a confluent layer was determined to be 10000 beads/mm2. A maximum reflectivity enhancement of 25 dB was attained at a surface density of 20000 beads/mm2. Interestingly, at higher density the reflectivity decreased and seemed to enter a regime of interference between the different interfaces between water, glass and Aqualene. Results from the particles filled of C6F14 were more variable, but the increase of reflectivity as a function of surface density is linear. The maximum reflectivity enhancement with respect to agar was 45 dB.

Previous models correctly predict the reflectivity of the surface when the scatterers are confluent. However, they significantly underestimate reflectivity (by 800% at 1000 beads/mm2). The new model presented satisfactorily describes the reflectivity enhancement caused by particles deposited on a surface over both a range of frequencies and a range of surface densities expected to be encountered when particles are targeted to biological markers.

We would like to thank the Canadian Institute of Health Research and the National Cancer Institute of Canada with funds from the Terry Fox Foundation.

2G-6 5:45 p.m.
EXPLOITING STATEFULNESS IN A CONTRAST BUBBLE FOR IMPROVED CONTRAST IMAGING.

J. BORSBOOM*[1,2] and N. DE JONG[1,2], [1]Erasmus MC, Rotterdam, the Nethelands, [2]Interuniversity Cardiology Institute of the Netherlands, Utrecht, the Netherlands.
Corresponding e-mail: j.borsboom@erasmusmc.nl

Detecting contrast agent in the myocardium at low MI poses a challenge due to the low number of contrast bubbles and confounding of tissue and bubble echoes. Currently, methods for low MI imaging mainly exploit the strong non-linear scattering of a contrast agent bubble. Well-known methods like harmonic imaging, power modulation and pulse inversion all use a filtering approach to

extract that part of the spectrum in which the received echo shows the largest difference in power between tissue and contrast agent. However, none of these methods separate the confounded contributions from tissue and contrast agent. We have developed a pulsing sequence that exploits a difference in system theoretical property of tissue and bubbles to selectively suppress the tissue signal and, thus, improve the detection of contrast agent. With this method we are able to separate the confounded signals received from tissue infused with contrast agent bubbles.

Our method is based on the concept of 'state' in a bubble; a concept that is well known in system theory. Due to its resonant nature, a contrast agent bubble is stateful because at least one state variable is needed to model its behaviour. Tissue, on the contrary, does not show resonance and hence, when working in retarded time, is stateless. To exploit this property, we propose a two or three pulse sequence designed to cancel stateless echoes. Thus, we can selectively suppress the tissue part in the received signal. To evaluate the performance of the new technique, a simulation study was performed based on a realistic model for ultrasound propagation (KZK-equation) and contrast agent. Simulation results indicate tissue suppression of more than 40 dB relative to contrast agent in fundamental and second harmonic. In vitro measurements on an agar-agar phantom and an experimental contrast agent confirm suppression of the tissue signal with this method. Relative suppression of 25 dB was obtained for fundamental and 15 dB at second harmonic. In conclusion, the proposed method works in the fundamental mode as well as in the harmonic mode and shows an increase of 15 dB in sensitivity compared to current methods.

Session: 3G

ULTRASONIC FLOWMETERS
Chair: L. Lynnworth
General Electric

3G-1 4:30 p.m.
TRANSIT TIME ULTRASONIC FLOWMETER: VELOCITY PROFILE ESTIMATION.

E. MANDARD*[1], D. KOUAMÉ[1], R. BATTAULT[2], J. P. REMENIERAS[1], and F. PATAT[1], [1]LUSSI FRE 2448, Tours, France, [2]Faure Herman, La Ferté Bernard, France.
Corresponding e-mail: mandar_e@med.univ-tours.fr

Over the last years, improvements in acoustics and signal processing allowed to measure the flow rate with ultrasonic flowmeter at a very high accuracy. Transit time ultrasonic method is based on a well known principle: let A and B be 2 locations of transducers on each side of a pipe, then the apparent difference of the sound speed on the path AB and on the path BA is proportional to the fluid velocity averaged over the path. The estimation of the flow rate needs the conversion of this path velocity to a velocity averaged over the entire cross-

section of the pipe containing the flowing fluid under investigation. Two phenomena have a particularly important impact on flowmeter performance: on the one hand, swirl which is the whole of no flowing transverse velocities and on the other hand, the fluid velocity profile which can be asymmetric downstream an elbow for example. To date, the correct estimation of the fluid velocity profile and the compensation of swirl is not satisfactory solved. For these purposes we investigated two main directions. To overcome the problem of swirl, we have developed a geometrical configuration of flowmeter paths, which fully compensates this phenomenon. Concerning the fluid velocity profile, we have defined a parametric model able to describe both symmetric and asymmetric flow velocity profiles. This theoretical parametric model was tested on numerical simulations and validated on data coming from experimental petroleum set up loop. These results show that our approach is a promising way for performance improvement of existing ultrasonic flowmeter accuracy.

3G-2 4:45 p.m.
ESTIMATION OF THE INFLUENCE OF THE INTEGRAL ULTRASONIC FLOWCELL CONFIGURATIONS ON THE EFFICIENCY OF THE VELOCITY PROFILE AVERAGING.

V. K. HAMIDULLIN*, Laboratory of ultrasonics, VZLJOT, Incorporated, St. Petersburg, Russia.
Corresponding e-mail: hamidullin

Ultrasonic flowmeter technology presents certain advantages, such as the possibility of non-invasive operation with all the after-effects, over traditional equipment for industrial flow measurements (i.e. turbine or orifice plate devices). Nevertheless, there are still problems in obtaining a high accuracy using ultrasonic flowmeters, in particular for dynamic flow conditions and non-uniform velocity profile of the flow. Usually multipath ultrasonic flowmeters are used to solve problems related to the averaging of the velocity profile. The local velocity in each acoustic path (chord) is measured successively in time and then, from received data, an average flow velocity is calculated. Such successive averaging in time is not effective for flows with fast-changing velocity profile, in systems with short straight lengths of pipe lines (in aerospace power control systems, for example, and others). In this paper, an alternative method for increasing the effectiveness of velocity profile averaging is discussed. It is based on the simultaneous interrogation of the flow, throughout the cross-section of the pipe, using integral flowcells of special configurations.

The first configuration of a flowcell was the pipe length with square cross-section and rectangular piezoelements mounted across the width on sides of the pipe.

The second configuration of the flowcell was the pipe length with round cross-section on the surface which two ring-shaped clamp-on transducers were coaxially mounted with the certain space between them. Each transducer comprised a waveguide for appropriate orientation of the emitted / received ultrasonic beams.

The third configuration of the flowcell was the pipe length with round cross-section on the surface which two clamp-on shear mode transducers were mounted. The waveguides were constructed with the specific arc cylindrical footprint surfaces to comprise the flowcell pipe length under the given arc.

Herein the interrogation of moving medium by ultrasonic signals through the pipe walls was carried out using the traditional and Lamb wave approaches. Results of characterization and computer simulation of piezoelectric transducers, ultrasonic fields and flow configurations are presented. Experimental measurements confirmed the idea of such kind of integral flowcells. The accuracy of 0.5 to 1.0% of reading in a dynamic range 1:100 was provided for the pipes of OD from 30 to 50 mm with liquids (water, kerosene, oil, mixtures).

3G-3 5:00 p.m.
A NOVEL BOUNDARY INTEGRAL FORMULATION FOR ACOUSTIC RADIATION IN A NONUNIFORM FLOW: COUPLING TO FEM AND APPLICATIONS.

M. BEZDEK*[1,2], A. RIEDER[2], H. LANDES[1], and R. LERCH[1], [1]Department of Sensor Technology, University of Erlangen-Nuremberg, Erlangen, Germany, [2]Endress+Hauser GmbH+Co. KG, Freising, Germany.
Corresponding e-mail: bezdek@ehfs.de

This paper reports the advances of the research first published in [1]. The novel boundary integral method HIRM introduced in [1] is applicable to acoustic radiation problems in arbitrary nonuniform flows at low Mach numbers. It relies on a generalized free-space Green's function, which approximates a point source solution by means of solving the ray tracing equations between the source and the target point.

For simulation of practical acoustic devices, a hybrid simulation scheme consisting of FEM and HIRM is proposed in [1]. FEM is used for simulation of the solid parts of the device (structure-borne sound), whereas HIRM is applied to the moving fluid (fluid-borne sound).

In order to demonstrate the functionality of this coupled FEM-HIRM scheme, simulation of a realistic transit-time ultrasonic flowmeter is considered here. In this case, the simulation procedure is subdivided into three consecutive stages: generation (in the piezoelectric transmitter), extrapolation (through the interior of the flowmeter pipe) and reception (in the piezoelectric receiver). Generation and reception are operated by FEM, whereas extrapolation is handled by HIRM. The interfaces between these stages (the fluid-structure interfaces) have to be modeled in such a way that they emulate the presence of open exterior domains and, consequently, ensure the validity of the boundary integral within a certain limited time horizon. For this reason, the FEM model of the interfacing regions makes use of an acoustic absorbing boundary condition. In addition, a new type of reflection-free acoustic source is formulated. It allows the injection of HIRM results into the FEM model without causing non-physical reflections associated with common hard acoustic sources.

The coupled FEM-HIRM scheme is first verified by means of an axisymmetric experimental setup consisting of two piezoelectric transducers glued on a water-

filled cylindrical container. It is demonstrated that the received electric signals are determined by both fluid-borne and structure-borne ultrasound traveling from the transmitter to the receiver. The comparison with experimental results confirms that the FEM-HIRM model accounts for all involved physical phenomena and provides a very accurate prediction of the received signals.

Finally, a realistic 3D simulation of a complete transit-time flowmeter is presented for the first time. The corresponding experimental setup is based on a measurement pipe of 100 mm inner diameter and two noninvasive ultrasonic sensors of 500 kHz operational frequency. FEM-HIRM simulations are performed to study the effect of flow on the received electric signals. It is shown that the obtained simulation results again exhibit a very good agreement with the measurements. Thus, the applicability of the novel boundary integral method HIRM to modeling of complex acoustic systems involving moving media is verified.

[1] Bezdek, Rieder, Landes, Lerch, Drahm: “A novel numerical method for simulating wave propagation in moving media,” in Proc. IEEE Ultrasonics Symposium, Montreal, Canada, 2004, pp. 934—937.

3G-4 5:15 p.m.
PHASE VELOCITY MEASUREMENT IN PULP FIBER SUSPENSIONS CONTAINING FIBERS AND FINES.

J. NIEMI*, Y. AITOMÄKI, and T. LÖFQVIST, Department of Computer Science and Electrical Engineering, Luleå University of Technology, Luleå,Sweden.
Corresponding e-mail: jan.niemi@ltu.se

In the manufacturing process of paper the properties and mass fraction of fibres in the pulp suspension is important for the finished paper. The increasing amount of recycled paper in the manufacturing process, where the properties of the fibre are unknown, and also the increased speed in the paper making process demands an on-line measurement. Where ultrasound among other techniques have the capability to achieve it. The objective of this paper is to investigate how phase velocity, an important parameter in ultrasonic measurements, is affected by different concentrations and types of fibres. In this paper we also present a method to determine the phase velocity that addresses the problem of accurately determine the phase velocity. The method proposed here removes the linear part of the phase in the signal and leaves the remaining part that contains the information on the phase spectrum of the signal. The idea is to find a continuous phase spectrum and minimize the likelihood of discontinues is within the bandwidth, this to avoid the phase sheet ambiguity in the unwrapping of the phase.

The signal consists of two echoes, the first from the boundary between the buffer rod and the medium of interest, and the second from the reflection between the medium and a steel reflector. The echoes are divided in two separate sampling windows. The phase without any discontinues and the minimal likelihood of discontinues within the frequency bandwidth of interest is found by circularly shifting each echo sample by sample and calculate the phase using an FFT algorithm. A sign shift of the echo is also carried out, representing a

phase shift of π or 180°, and again circularly shifted and the phase is again calculated with the same method. The results are compared and the phase without discontinues and minimal likelihood of discontinues of these is chosen to calculate the phase spectrum difference.

The total phase difference between the echoes is then the sum of the delay between the windows, numbers of sample shifts and the difference in phase spectrum between the echoes. To further increase the accuracy of the method the effects of diffraction is also compensated for.

The method is validated experimentally on pulp suspensions with different amount of fibre and fines contents. The fibres have a nominal length of 2 mm and diameter of 30 microns and the fines a nominal length of 0.2 mm and diameter of 10 microns. The concentrations vary in mass fraction between 0-1.0% for fibres and 0-0.5% for fines. Pure water is used as a reference medium.

The result of the experiment shows that the phase velocity increases with total mass fraction in the range covered. Both fibre and fines affect the phase velocity. However, the dispersion is higher in suspensions containing only fibres than the suspension containing only fines

3G-5 5:30 p.m.
ON-LINE ULTRASONIC MEASUREMENTS OF FIBER CONSISTENCY IN DILUTE PULP SUSPENSIONS.

Y. JUN* and L. BIN, School of Mechanical Engineering and Automation, Shanghai University, Shanghai, China.
Corresponding e-mail: grandone0529@yahoo.com

In paper industry,fiber consistency is an important property to determine paper quality.Purpose of the article is to give an on-line consistency measurement system for dilute pulp suspensions by the study of ultrasonic attenuation.

Considering fiber as infinitely long isolated isotropy elastic cylinder and ignoring the effects of heat conduction,which are expected to be small in frequency range under study, a simplified scattering model of cylindrical fiber is presented to determine ultrasonic attenuation.Six wave equations at the fiber boundary are solved.According to single scattering theory,the relation between consistency and attenuation coefficient is derivated.

A transducer assembly including a transmitter and a receiver is designed.Each transducer has a diameter of 12mm and consists of front wall,insulating layer,bonding layer,piezoceramic,backing,back cover,seal gasket.The front wall is made of stainless steel so that the transducer assembly is developed to measure the flow of pulp fluid as electrodes of electromagnetic flowmeter.Eight pairs of transducer assembly with different center frequency span frequency range from 0.8 to 5MHz.The two transducers are mounted on a measuring tube with a distance of 80mm.

Most measuring systems in literatures used lab devices,which can’t carry out on-line measurement needed in industry.A low cost and compact electronic system for on-line measurement is designed to measure excess attenuation between suspension and water by CW transmission method.Frenquency and

attenuation amplitude of ultrasonic signal are well controlled and measured.Attenuation is calculated and stored in the system.More detailed description will be given in full length paper.

Fiber suspensions consist of water and bleached birch pulp.Detailed physical parameter will be shown in the table. Fiber suspensions with mass consistency from 0 to 2% are prepared and measured following Greenwood's method.

Experiments are carried out in a recirculation system with constant flow rate and temperature.This system includes a storage vessel,a submersible pump,a stirrer,hot water and cool water supplies,a temperature sensor.The measuring tube is vertically mounted to avoid settling of fibers.Fibers and water are well mixed by the stirrer.

Both experiment results and theory prediction data are plotted.According to calibration data, consistency measurement results are given.Within the frequency range under investigation,attenuation-consistency figures show attenuation is proportional to consistency when mass consistency is below 1.5%,which has an agreement with prediction.Above consistency of 1.5%,attenuation is higher than prediction because of multi-scattering occurs.In attenuation-frequency figures, attenuation increases with frequency.Some deviations between theory and experiment are indicated at lower frequency due to the finite length of the fibers.

Further studies are discussed,such as measuring consistency,flow and temperature with the transducer assembly.Possible causes for the uncertainty of measurement,for example,fiber flocculation,temperature fluctuate and flow rate fluctuate are also analyzed.

Physical Properties of water and fiber (20 degree)

	Water	Fiber
Density(kg/m3)	998.2	1350.0
Fiber average diameter(um)	-	35
Fiber average length(mm)	-	2.5
Fiber Young's modulus(GPa)	-	4.3
Fiber Poission's ratio	-	0.3
Fiber Poission's ratio	-	0.3
Sound speed(m/s)	1400	3200
Sound speed(m/s)	1483	2070

3G-6 5:45 p.m.

BUBBLE DETECTION AND GAS VOLUME MEASUREMENT IN BUBBLE LOADED LIQUIDS WITH PULSE DRIVEN MEASUREMENT DEVICES.

M. GULSCH* and B. HENNING, University of Paderborn, Paderborn, Germany. Corresponding e-mail: Henning@emt.upb.de

Motivation Currently there are pulse based ultrasonic sensor systems used to measure flow, liquid level, concentration or in process monitoring. In several processes the investigated media are a mixture of liquid and solid ingredients . The use of ultrasonic sensor systems will be very complicated if gas bubbles appear at the measurement place caused by chemical reactions, high temperature or fast flow.

Firstly, the appearance of gas bubbles falsifies the measured absorption. Secondly, the measured velocity is influenced by gas bubbles. In [pov97] is visible that a volume fraction of 0.1 ppm of undissolved air decreases the sound velocity by 1.4 m s-1.

Further investigations have shown that pulse driven ultrasonic sensor systems are measuring a higher sound velocity if gas bubbles appear. This measured velocity could even be higher than the velocity of the bubble-free medium. This is inconsistent with the shown relation.

The bubbles inside the liquid media are influencing the sound propagation inside the media and the received pulse will be deformed. The zero-crossing-points of the receiver signal are shifted to shorter measuring time and this cause the measurement of a higher sound velocity.

Goals To make common ultrasonic measurement systems more reliable if gas bubbles are inside the media it is necessary to develop a comprehensive method for the data processing. In addition, this work aims at the determination of sound velocity of the pure liquid and the characterization of gas phase (volume, bubble size, bubble size distribution) simultaneously.

Results Using a modified Wavelet-Transformation (WT), the time of flight for each signal frequency of the broadband receiver pulse could be determined. The effect of dispersion will be good visible if one pulse passes a bubble loaded measuring path. It can be shown that selected frequencies are not or only less influenced by the bubbles. This offers the possibility to determine the sound velocity of the pure liquid in a bubble-liquid-mixture. These results correspond to the published relations of J. W. Povey [pov97]. On the other hand there are frequency ranges showing a clear relation to the bubble size and their size distribution. The important advantage of this data processing method is to measure material properties of liquid phase (concentration, temperature) and gaseous phase (number and size of bubbles, size distribution, gas volume) separately and simultaneously.

This feature improves the reliability of ultrasonic sensor systems significantly.

Conclusion In the contribution, a new method of signal analyses will be presented to determine the sound velocity of the liquid media, even if there are gas bubbles inside. Moreover, it is possible to get reliable information about the volume fraction

and bubble size distribution of gas inside a liquid media by using the WT.

Currently it is investigated whether this method is also suitable to characterize emulsions or suspensions.

References

[pov97] Povey, Malcolm J. W.: Ultrasonic techniques for fluids characterization. Academic Press, 1997

Session: 4G
INTERVENTIONAL ULTRASOUND
Chair: G. Lockwood
Queen's University

4G-1 4:30 p.m.
(Invited)
A GLIMPSE INTO THE FUTURE OF INTRAVASCULAR ULTRASOUND TECHNOLOGY.

S. FRY*, Strategic Business Development, Inc., El Dorado Hills, CA.
Corresponding e-mail: stevefry@comcast.net

Intravascular ultrasound (IVUS), used to examine coronary and peripheral artery disease, is poised for rapid market expansion, based on development of several new technologies that provide more information to the physician, while reducing the cost of catheters and equipment. New transducers, including capacitive machined ultrasonic transducer (cMUT) arrays have the potential to reduce scanner cost and improve reliability, as well as provide new capabilities, such as combined side-looking and forward-looking IVUS and harmonic imaging. New phased array and rotational IVUS catheter technologies, such as distal-tip micro-motor drive and radio frequency identification (RFID) catheter calibration will improve image quality and ease of use. System consoles based on field-programmable gate array (FPGA) technology are becoming smaller, less costly and easier to use. Specialized processing of the RF backscatter signal from an IVUS catheter can now provide tissue characterization ("Virtual Histology"), identification of high strain spots in the vessel wall ("Palpogrpahy", "Thermal Strain Imaging"), and visualization of contrast-enhanced vasa vasorum. 3D volumetric imaging and 3D catheter positioning information can be used to provide virtual road-mapping, and navigation through chronic total occlusions (CTO). Prediction of atherosclerotic lesion progression using IVUS-based shear stress analysis is also an active area of investigation. The ongoing development of these new device technologies and new applications, which provide additional diagnostic information and/or guidance of interventional devices, represents a renaissance in the use of IVUS as an important adjunctive technology in intravascular procedures.

4G-2 5:00 p.m.

3-D ULTRASOUND IMAGING USING FORWARD-VIEWING CMUT RING ARRAYS FOR INTRAVASCULAR AND INTRACARDIAC APPLICATIONS.

D. YEH*[1], O. ORALKAN[1], I. WYGANT[1], M. O'DONNELL[2], and B. KHURI-YAKUB[1], [1]Stanford University, Stanford, CA, [2]University of Michigan, Ann Arbor.
Corresponding e-mail: dtyeh@stanford.edu

Forward-viewing intravascular ultrasound enables new procedures in medicine such as diagnosing severely occluded blood vessels or guiding the placement of stents. Using a forward-viewing transducer in catheter-based applications requires clearance in the center of the transducer for the guidewire, and requires the development of a ring array. It is challenging to design and fabricate piezoelectric transducers of the dimensions needed for forward-looking ring arrays. However, Capacitive Micromachined Ultrasonic Transducers (CMUTs) can be used to develop such arrays. This paper presents the first full synthetic phased array volumetric images from CMUT ring arrays with integrated electronics.

CMUTs offer several advantages over piezoelectric transducers for use in medical imaging. Microlithography is used to make CMUTs and routinely yields the finely controlled dimensions required for high frequency ring arrays. In addition, the CMUT can be switched on-demand between its two modes of operation during the imaging procedure, thereby providing a choice between the low frequency conventional mode for navigation and the high frequency collapse mode for diagnosis.

The CMUT ring array demonstrated in this paper has the following parameters: ring diameter, 2 mm; number of elements, 64; element pitch, 102 μm; element size, 100×100 μm; cells per element, 9; cell membrane radius, 13 μm.

The imaging setup consists of the CMUT mounted in a 209-pin PGA package with the array elements wire bonded to 64 transmit/receive channels in a bank of four integrated circuits. The full synthetic phased array data set was collected by exciting one element at a time, and acquiring signals from the entire array for each transmit element. Each A-scan was acquired at a sampling rate of 500 MS/s for both collapse and conventional modes, with 16 averages, and without averaging. The imaging phantom consists of three steel wires 0.30 mm in diameter. A-scan data indicates that the transducer operates conventionally at 7.5 MHz with a 6-dB bandwidth of 8.5 MHz, and in collapse mode at 19 MHz with a bandwidth of 13 MHz. A conical volume was reconstructed offline from the complete 64×64 set of A-scans, weighted for full-aperture resolution and cosine apodization. The wires are clearly visible in images reconstructed from data taken with no averaging, and demonstrate the good SNR of the CMUT. Because of higher operating frequency and reduced crosstalk, collapse mode produces images with a narrower main lobe than conventional mode imaging.

We have demonstrated 3-D ultrasound imaging with a forward-viewing CMUT ring array using the first full synthetic phased array data taken using a ring array. A fully integrated system with flip-chip bonded electronics will further improve performance and SNR. These results show that forward-looking probes

for intravascular ultrasound are well on their way to becoming reality.

This work is funded by the National Institutes of Health. David Yeh is supported by a National Defense Science and Engineering Graduate Fellowship.

4G-3 5:15 p.m.
COMPONENTS FOR FOCUSED INTEGRATED PMUTS FOR HIGH RESOLUTION MEDICAL IMAGING.

A. FLEISCHMAN*[1], C. CHANDRANA[1,3], J. FAN[1,2], J. TALMAN[1], S. GARVERICK[2], G. LOCKWOOD[4], and S. ROY[1], [1]The Cleveland Clinic Foundation, Cleveland, OH, [2]Case Western Reserve University, Cleveland, OH, [3]Cleveland State University, Cleveland, OH, [4]Queens University, Kingston, Ontario, Canada. Corresponding e-mail: chandrac@ccf.org

Significant improvement in the conventional ultrasonic minimally invasive imaging such as intravascular imaging can be achieved by the use of miniature focused broad band transducers. Polymer piezoelectric materials such as PVDF and PVDF-TrFE are excellent candidates for such transducers but have high impedance and typically require a preamplifier in close proximity to the transducer. Such focused transducers can be integrated with conventional CMOS electronics using batch fabrication techniques and appropriate protection circuitry compatible with CMOS fabrication technology.

Spherically-focused, high-frequency (35-45 MHz) ultrasound transducers, with aperture diameters of 0.75-2.00 mm and focal-numbers ranging from 1.3-4.5 have been developed using micromachining and membrane deflection techniques. Two dimensional radiation contours for various diameter transducers excited by a 40 MHz monocycle were obtained and modeled and close agreement was observed between the experimental and modeled radiation contours. These transducers exhibited diffraction limited focused radiation patterns with 24 μm axial resolution and -6dB fractional bandwidths near 80%. The axial radiation pattern of a 2 mm diameter transducer (geometrical focus at 7.1 mm) excited by a 40 MHz 15 cycle gated sinusoid was compared to the calculated continuous wave axial radiation pattern from an identical spherical ultrasound transducer and shows good agreement (Pearson correlation coefficient of 0.99) over the axial range from 5 mm to 10 mm. The tissue imaging capabilities of the micromachined ultrasonic transducers are demonstrated through successful imaging of human cadaveric aorta.

An ASIC low-noise preamplifier with integrated limiter and sub-microsecond pulse recovery time that provides a matched input impedance was designed to interface with the ultrasonic transducer using a standard 0.35 μm CMOS process. The preamplifier was fabricated and tested and demonstrated to recover to equilibrium condition in 0.6 microseconds after a 70 V_p pulse. The circuit was also able to withstand a 100 V_p excitation pulse at a 2 KHz repetition rate for a total of 57 megacycles with no change in the small signal gain of the amplifier. When fully integrated with the low noise preamplifier, the micromachined ultrasonic transducer chip will be small enough for intravascular and endoluminal imaging applications.

4G-4 5:30 p.m.

AN ENDOSCOPIC ULTRASOUND IMAGING SYSTEM BASED ON A TWO-DIMENSIONAL CMUT ARRAY: REAL-TIME IMAGING RESULTS.

I. WYGANT*[1], X. ZHUANG[1], D. YEH[1], S. VAITHILINGAM[1], A. NIKOOZADEH[1], O. ORALKAN[1], A. ERGUN[1], M. KARAMAN[2], and B. KHURI-YAKUB[1], [1]E. L. Ginzton Laboratory, Stanford University, Palo Alto, CA, [2]Department of Electrical Engineering, Isik University, Istanbul, Turkey.
Corresponding e-mail: iwygant@stanford.edu

Real-time catheter-based ultrasound imaging tools are needed by the medical community for diagnosis and image-guided procedures. The image quality of existing catheter-based ultrasound imaging tools is limited due to the difficulty of fabricating piezoelectric transducer arrays with two-dimensional geometries. With increasing transducer frequencies, the fabrication becomes even more difficult. Using capacitive micromachined ultrasonic transducer (CMUT) technology, transducer arrays with widely varying geometries, high frequencies, and wider bandwidths can be fabricated.

We present a real-time volumetric ultrasound imaging system based on a two-dimensional, 16×16-element, capacitive micromachined ultrasound transducer array. Transducer arrays with operating frequencies ranging from 3 MHz to 7.5 MHz were fabricated. Each element is 250 um by 250 um. The elements are connected to flip-chip bond pads on the back side of the array with 400-um long through-wafer interconnects. Using anisotropic conductive film (ACF) technology, the arrays are flip-chip bonded to a custom designed integrated circuit (IC) that comprises the front-end electronics. Integrating the front-end electronics with the transducer array reduces the effects of cable capacitance on the transducer's performance. The front-end IC contains a 25-V pulser and 10-MHz bandwidth amplifier for each element in the transducer array. In this initial implementation of the system, a single transducer element is active at a time. Signals from the 256 elements are acquired in sequence. An FPGA-based data acquisition system is used to sample and process the data. Advantages of this system include the capability of processing data in parallel at high rates and the ability to reconfigure the hardware to meet different imaging requirements.

Characterization and synthetic aperture imaging results for the system are shown. Results are for a flip-chip bonded array with 255 of 256 connected elements. Pulse-echo measurements for a plane reflector were made for each array element. The mean center frequency of the received signal is 7 MHz with a standard deviation of 120 kHz. The mean fractional bandwidth is 87% with a standard deviation of 3.3%. The standard deviation of the received signal amplitudes is 22% of the mean. Using the bonded arrays, 90°×90°×3 cm volumetric images of a phantom were obtained. These results demonstrate the functionality of a complete imaging system capable of acquiring volumetric imaging data in real time.

This work was supported by the National Institutes of Health. IC fabrication was provided by National Semiconductor.

4G-5 5:45 p.m.
REAL-TIME 3D ULTRASOUND LAPAROSCOPY.

E. LIGHT*, E. DIXON-TULLOCH, S. IDRISS, P. WOLF, and S. SMITH, Duke University, Durham, NC.
Corresponding e-mail: edl@duke.edu

We have previously described 2D array ultrasound transducers operating up to 13.5 MHz for applications including real time 3D transthoracic imaging, real time volumetric intracardiac echocardiography (ICE) and real time 3D intravascular ultrasound (IVUS) imaging. We have recently built a pair of 2D array transducers for real time 3D laparoscopic ultrasound imaging. These transducers are intended to be placed down a trocar during minimally invasive surgery. The first is a forward viewing 5 MHz, 19 $\times$ 11 array with 198 operating elements. It was built on an 8 layer multi-layer flex circuit. The interelement spacing is 0.20 mm yielding an aperture that is 2.2 mm $\times$ 3.8 mm. The O.D. of the completed transducer is 10.2 mm, and includes a 2 mm tool port. The average measured center frequency is 4.5 MHz, and the -6 dB bandwidth ranges from 15% to 30%. The 50 Ohm insertion loss, including the MicroFlat cabling, is -81.2 dB. The second transducer is a 7 MHz, 36 $\times$ 36 array with 504 operating elements. It was built upon a 10 layer multi-layer flex circuit. This transducer is in the forward viewing configuration, and the interelement spacing is 0.18 mm. The total aperture size is 6.48 mm $\times$ 6.48 mm. The O.D. of the completed transducer is 11.4 mm. The average measured center frequency is 7.2 MHz, and the -6 dB bandwidth ranges from 18% to 33%. The 50 Ohm insertion loss is -79.5 dB, including the MicroFlat cable. Both transducers were built using Gore MicroFlat cables consisting of 18 wires spaced at 0.10 mm and attached to a polyimide backing. We grounded every other wire to reduce electrical cross talk along the length of the cabling. Both transducers also have a double grounding scheme that includes an external shield ground wrapping the MicroFlats and the front face of the transducer isolated from the transducer signal return ground. Real time in vivo 3D images of a canine heart have been made including an apical 4 chamber view from a substernal access with the first transducer to monitor cardiac function. In addition we produced real time 3D rendered images of the right pulmonary veins from a supersternal access with the second transducer which would be valuable in the guidance of cardiac ablation catheters for treatment of atrial fibrillation.

Session: 5G

SAW SYSTEM APPLICATIONS
Chair: R. Potter
Vectron International

5G-1 4:30 p.m.
(Invited)
SAW AND OPTICAL SIGNAL PROCESSING.

M. LEWIS*, Consultant, Malvern, Worcs, UK.
Corresponding e-mail: meirionfrancis.lewis@virgin.net

Even in this digital age, SAW and Optical devices remain indispensible analogue signal processing technologies whose operation and success derive from common wave propagation phenomena. In this talk I hope to explain why this is so, and will remain so for the forseeable future.

Historically, the development of both of these technologies arose during the Cold War primarily from the military need for an unsurpassed signal processing capability, although both are now widely exploited in civil applications as well. This paper will begin by briefly reviewing the construction, operation, attractions, and selected applications of the SAW devices developed since the invention of the InterDigital Transducer (IDT) in 1965. These devices include delay lines, bandpass filters, and the first SAW device used in anger, the dispersive delay line which was vital to the realisation of pulse compression radar. I shall also review the attractions of SAW oscillators, which I believe still enjoy an opportunity to contribute to the insatiable military need for improved overall oscillator stability. Following this I will introduce some components and techniques devised by the optics community for signal and image processing since the invention of the laser in 1960,beginning with techniques for pattern recognition and the ingenious technique devised to realise real-time Synthetic Aperture Radar, SAR. More recently, the invention and development of laser diodes and fibre optics by the telecommunications industry has led to the realisation of optical signal processing techniques whose functionality is in many respects complementary to that of SAW devices. In particular, optical techniques are now useful for the generation, delay, sampling, and distribution of signals at higher rf frequencies (and bandwidths) than SAW devices, ie at microwave and mm-wave frequencies and above, leading to the modern field of activity known as Microwave Photonics. I shall briefly describe some current research topics in this field, including stable microwave generation, phased array antenna beamforming, and A/D conversion, each being relevant to future military and civil systems.

I am grateful to Drs David Morgan and Rebecca Wilson for valuable advice on this presentation.

5G-2 5:00 p.m.
ULTRA-LOW POWER UWB COMMUNICATION SYSTEM USING SAW MATCHED FILTERS.

T. SUGIURA*, T. SATO, E. OTOBE, K. TANJI, N. OTANI, H. NAGASAKA, M. HASEGAWA, and T. SHIMAMORI, Samsung Yokohama Research Institute, Yokohama, Kanagawa, Japan.
Corresponding e-mail: tk-sato@ieee.org

Ultra-Wideband (UWB) communication is one of the most promising technologies for next wireless personal area network (WPAN) because of the extremely high data rate. SAW matched filters can be used for high speed signal processing device performing correlation of complex pulse waveforms. They are capable of realizing low power consumption, simplification of the circuit and miniaturization, compared to a digital correlator using semiconductor circuits.

In this paper, we introduce a novel UWB communication system using SAW matched filters which can be operated at low power consumption. The system employs a unique pulse position modulation (PPM) method combined with spread spectrum which is realized by SAW matched filters for modulation and de-modulation. The PPM method uses two impulse signals. One refers to a reference impulse and the other refers to a data impulse. In modulation, the reference impulses are generated at some constant intervals while the data impulses are generated by delayed $+\tau$ or $-\tau$ to the reference impulse in case of sending Data1 or Data0 respectively. Moreover, the reference and the data are spread with orthogonal spread spectrum codes by SAW matched filters to easily distinguish these impulses in a receiver. In de-modulation, the reference impulse and $+\tau$ or $-\tau$ delayed impulse are re-generated in SAW matched filters. Therefore, the system does not need high speed semiconductor circuits operating at high chip-rate because SAW matched filter perform spreading and de-spreading automatically.

The SAW matched filters were designed by full wave simulation to reduce unwanted parasitic effects in GHz-range, and developed a unique spreading code to be suited to this PPM method. We fabricated 4GHz SAW matched filters and implemented UWB module comprising these filters, LNA, AD/DA, Base-band circuit and antenna. 20Mbps real-time video streaming has been realized by the UWB communication system. TX and RX power consumption in RF part were 50mW and 150mW, respectively. The implemented results indicate that this system is suitable for WPAN which requires low power consumption.

5G-3 5:15 p.m.
THE ROUNDED SHAPE SPIRAL TRANSMISSION LINE PHASE SHIFTER FOR MINIATURIZED SAW W-CDMA ANTENNA DUPLEXERS.

O. HIKINO*, M. OHKI, S. KONDO, J. HAMASAKI, T. ENDO, T. SHIBA, and Y. FUJITA, Hitachi Media Electronics Co., Ltd.
Corresponding e-mail: hikino@y01.hitachi-media-el.co.jp

This paper will present the phase shifter implemented in LTCC for W-CDMA antenna duplexers. Low loss and high isolation between Rx and Tx are required for the duplexers. The phase shifter in the duplexer act as the key components for the size and thickness reduction since it is the biggest components implemented in the LTCC package on which SAW filters are mounted. Furthermore, the phase shifter's physical structure is a key issue for the insertion loss and the isolation characteristics for the duplexer since its transmission loss and electro-magnetic field coupling to other components is directly affects to the insertion loss and the isolation of the duplexer, respectively.

We have developed unique structure for the phase shifter; the rounded shape spiral structure without any crossover. The phase shifter has very low transmission loss and very low coupling since the phase shifter is almost completely shielded with the ground plate.

Using the above explained phase shifter we have developed SAW W-CDMA (Wideband Code Division Multiple Access) antenna duplexers for Band1 (2.1GHz), Band2 (1.9GHz) and Band5 (850MHz) with the typical size of 3.0x2.5x0.9 mm^3.

5G-4 5:30 p.m.
SAW EXCITATION ON GLASS PLATES FOR A TACTILE DISPLAY APPLICATION.

M. TAKASAKI*[1,3], H. KOTANI[1], T. NARA[2], and T. MIZUNO[1], [1]Saitama University, Saitama, Japan, [2]University of Tokyo, Tokyo, Japan, [3]JST, Saitama, Japan.
Corresponding e-mail: masaya@mech.saitama-u.ac.jp

Recently, reproduction of human haptic sensation has attracted attention of various fields, such as virtual reality, remote control of robots, computer interfaces and so on. Physiologically, haptic sensation is divided into two parts. One is proprioception, which is sensation of weight, resistance, or the approximate shape of an object, and is perceived at muscles and joints of our bodies. The other is tactile sensation, which is a sense of roughness, friction, or the texture of an object's surface, and is perceived at mechanoreceptors in our finger skins.

Two types of surface acoustic wave (SAW) tactile displays had been developed. One is active type, which needs operators' active rubbing motion to indicate tactile sensation. The other is passive type, which uses SAW linear motor principle to actuate operators' finger to reproduce tactile sensation without relative finger motion. With the displays controlled according to operators' rubbing motion, we could enjoy tactile sensation like roughness sensation while we rub on solid surface.

For the active type, whole transducer consisted of a LiNbO3 wafer and electrodes such as interdigital transducers (IDTs) and reflectors on its edge. In the center of the transducer, standing wave of Rayleigh wave was excited and rubbed through a slider with distribution of steel balls. Friction between the transducer and slider could be reduced by the wave. With rubbing motion on burst SAW, finger skin on the slider vibrated at the burst frequency. The vibration was controlled and perceived as tactile sensation.

Since size of an available wafer was 4-inch, the rubbing area of the previous transducer was limited to 46 mm x 43 mm (electrodes were needed on edges). Our purpose of this research is to expand the area for more natural sweeping motion. To overcome the limit, we proposed novel SAW excitation method on a non-piezoelectric substrate such as a glass plate. If we can use such material, larger and curved tactile display can be supplied to expand application of the display.

The proposed method used combination of a piezoelectric material and a non-piezoelectric material. The transducer consisted of a glass substrate with electrodes and fragments of piezoelectric plate. The glass substrate was shaped into suitable dimension. Then conventional IDT (line and space of 100 microns) was formed on substrate edge. Finally, the piezoelectric plate cut into the size of IDT finger area was contacted with the electrode with a preload. Applying a voltage, stress distribution was generated in the piezoelectric plate and propagates into glass substrate through the electrode fingers. A SAW was generated in the same manner as conventional SAW transducer and propagated on the glass substrate surface.

Characteristics of the fabricated glass substrate transducer were measured. Frequency response of admittance had some peeks around 10 MHz. With the applied voltage of 40 V, vibration amplitude of 3 nm was realized at one of the frequencies. The transducer was applied for the active type SAW tactile display. As a result, the display worked successfully.

5G-5 5:45 p.m.
DROPLET EJECTOR USING SURFACE ACOUSTIC WAVES.

J. BENNÈS*, S. ALZUAGA, F. BASTIEN, J. F. MANCEAU, and S. BALLANDRAS, FEMTO-ST INSTITUTE, LPMO Dept, 32 rue de l'Observatoire 25044 Besançon Cedex France.
Corresponding e-mail: jonathan.bennes@lpmo.edu

The present study aims to investigate droplet ejection using Surface Acoustic Waves (SAW). The interests in droplet ejection microsystems have dramatically grown in recent years due to inkjet printhead demand (Drop-On-Demand). Among several actuating methods (thermal, piezoelectric, etc.), the thermally driven inkjet printhead is most successful (low cost, easy fabrication and high printing quality). Almost all of the current ink jet printers eject ink droplets through nozzles, in which case the ejection direction is always perpendicular to the nozzle surface. This paper describes a new way to eject droplets (water, ink, etc…) using SAW. Surface acoustic waves devices are widely used for frequency filtering and are mainly devoted to cellular phones and telecommunication handset. Nowadays, recently published works have demonstrated the interest of SAW for guiding and positioning small liquid droplet atop a flat surface.

The surface acoustic waves devices used to eject droplets are carried out on lithium niobate substrates (LiNbO3 cut Y+128°, X propagation). The Rayleigh waves are excited using classical inter-digital transducers (IDT).

The design of IDT has been simulated with finite element analysis and boundary element methods. The computations on the design of the IDT have been compared with measurements. The vibration amplitude of the waves (Uw) necessary to droplet ejection is measured using a heterodyne laser probe. The range of the droplets volume ejected is between 50nl and 1µl. The influence of the supply voltage on the ejection is presented.

Mr Thomas Pastureaud from TEMEX-Microsonics.

TEMEX-Microsonics 399 route des Cre^tes – BP 232, 06904 Sophia Antipolis cedex France.

Session: 6G
TISSUE CHARACTERIZATION
Chair: G. Berger
CNRS

6G-1 4:30 p.m.
ULTRASONIC TISSUE CHARACTERIZATION FOR THE DIFFERENTIATION OF PAROTID-GLAND TUMORS.

U. SCHEIPERS*[1], S. SIEBERS[1], M. ASHFAQ[1], F. GOTTWALD[2], A. BOZZATO[2], J. ZENK[2], H. IRO[2], and H. ERMERT[1], [1]Institute of High-Frequency Engineering, Ruhr-University Bochum, Bochum, NRW, Germany, [2]University Hospital for Otorhinolaryngology, University Erlangen, Erlangen, Bavaria, Germany.
Corresponding e-mail: ulrich@scheipers.org

The first ultrasonic tissue characterization system for the computerized differentiation of tumors of the parotid-gland is presented. The system is based on a multifeature tissue characterization approach involving spectrum and texture parameters and using fuzzy inference systems as higher order classifiers.

Baseband ultrasound echo data are acquired during conventional ultrasound imaging examinations of the salivary glands using standard ultrasound equipment (Siemens Sonoline Elegra, 7.5L50 linear array probe). Several tissue-describing parameters are calculated within numerous small regions of interest in order to evaluate local spectral and textural tissue properties. The parameters are processed by an adaptive network-based fuzzy inference system (FIS) using the results of conventional histology after parotidectomy as the gold standard. Cases of parotid-gland tumors and alterations include basal cell adenomas, monomorphic adenomas, pleomorphic adenomas, adenoid cysts, cysts and canaliculous adenomas. The results of the classification procedure are presented as a numerical score indicating the probability of a certain tumor or alteration for each parotid-gland. The score can be presented to the physician during the examination of the patient to improve the differentiation between various types of parotid tumors. Because no user input is needed, the system is completely independent of the examining physician.

In a pilot study, the system was evaluated on 23 cases of benign and malignant parotid-gland tumors of patients undergoing radical parotidectomy. The ROC curve area given as the cross-validation mean and cross-validation standard deviation is A_{ROC}=0.95±0.07 when using four-fold cross-validation over cases and differentiating between various malignant and benign parotid-gland tumors as the first and positive target group and monomorphic adenoma as the second and negative target group. Even some alterations which are of benign nature were counted to the positive group, as they occur too seldom to achieve a high probability for being considered safe if left untreated. An exceptional equal error rate of E_{EER}=0.92±0.08 is achieved for the same setup.

This work is an activity of the Ruhr Center of Excellence for Medical Engineering, Bochum, Germany, supported by the German Federal Ministry of Education and Research (grant 13N8079).

Ulrich Scheipers is now with Resonant Medical Inc., Montreal, Quebec, Canada.

6G-2 4:45 p.m.
NEW DEVELOPMENTS IN TISSUE-TYPE IMAGING (TTI) OF PROSTATE CANCER BASED ON COMBINED ULTRASONIC AND MAGNETIC-RESONANCE METHODS.

E. FELEPPA*[1], C. PORTER[2], S. DASGUPTA[1], A. KALISZ[1], J. KETTERLING[1], S. RAMACHANDRAN[1], D. DAIL[2], M. LACRAMPE[2], D. SPARKS[2], F. ARIAS-MENDOZA[3], T. LIU[3], and P. SCHIFF[3], [1]Riverside Research Institute, New York, NY, [2]Virginia Mason Medical Center, Seattle, WA, [3]Columbia University Medical Center, New York, NY.
Corresponding e-mail: feleppa@rrinyc.org

Our prostate tissue-typing studies is to develop more-sensitive and specific imaging methods for identifying and characterizing cancerous prostate tissue and improving the effectiveness of biopsy guidance, therapy targeting, and treatment monitoring.

We acquired ultrasonic (US) radio-frequency (RF) echo-signal data, and clinical variables, e.g., prostate-specific antigen (PSA), during biopsy examinations. We computed spectra of the RF signals in each biopsied region, and trained a neural network classifiers using data from 64 patients and 617 biopsy specimens; biopsy results served as the gold standard. We generated issue-type images (TTIs) through a lookup table that returned scores for cancer likelihood on a pixel-by-pixel basis from locally computed spectral parameter and global PSA values. ROC curves were generated based on leave-one-patient-out and leave-one-biopsy-out approaches to compare efficacy and to choose the method that minimize the chance of biased classification; in this approach, all the biopsies of an individual patient were placed in the test set, and assignment to training and validation sets was done randomly from the remaining biopsies. ROC curves also were generated using a random means of assigning cases to test and training and validation sets, and using a leave-one-biopsy-out approach that placed only a single biopsy in the test set. A preliminary investigation of the feasibility of combining ultrasound spectral parameters and magnetic-resonance

spectral (MRS) parameters for classification was initiated. MRS classification was based on the ratio of choline to citrate, which tends to be higher in cancerous than non-cancerous prostate tissue.

The ROC-curve area for neural-network-based classification using the values of ultrasound spectral parameters plus PSA level was 0.844 +/- 0.018 (95% confidence: 0.806 to 0.877); in comparison, for B-mode-based classification, the area was only 0.6638 +/- 0.031 (95% confidence: 0.576 to 0.697). The sensitivity of neural-network-based classification was approximately 50% better than the sensitivity of B-mode-based classification at the typical B-mode-guided biopsy sensitivity of 50%. TTIs generated from US data acquired pre-surgically showed tumors that were entirely unrecognized in conventional images and undetected during surgery. 3-D renderings of prostatectomy histology and US-MRS TTIs showed encouraging correlations.

TTIs based on neural-network classification of US and clinical parameters show promise for improving the detection and management of prostate cancer, e.g., for biopsy guidance, staging disease, planning surgery or dose-escalation and tissue-sparing options for radiation therapy, and assessing the effects of non-surgical treatments. Combining MRS parameters with US spectral parameters appears capable of further improving prostate-cancer imaging.

This research was supported in part by NIH/NCI grant CA53561 awarded to Riverside Research Institute. The authors are deeply indebted to the late William R. Fair and Frederic L. Lizzi for their encouragement and knowledge.

6G-3 5:00 p.m.
CYCLIC GENERATION OF STRAIN INSIDE OBJECT USING DUAL ACOUSTIC RADIATION FORCE.

H. HASEGAWA*, Y. NISHIO, and H. KANAI, Graduate School of Engineering, Tohoku University, Sendai, Japan.
Corresponding e-mail: hasegawa@us.ecei.tohoku.ac.jp

There are many studies on evaluation of tissue mechanical properties by applying an acoustic radiation force induced by ultrasound to an object. However, if the object is much harder than the surrounding tissue (such like a tumor in the breast tissue), an acoustic radiation force might generate only the change in position of the object and the strain is hardly generated. Therefore, mechanical properties of the object cannot be evaluated. In this study, two cyclic acoustic radiation forces are simultaneously applied to an object to effectively generate the strain inside the object even under such situations. **Method:** Two focused transducers are used to apply cyclic acoustic radiation forces to an object. Each transducer is driven by a continuous signal which is the sum of f_0 Hz and (f_0+Δf) Hz. An acoustic radiation force is proportional to the square of the sound pressure. Therefore, a cyclic acoustic radiation force at a frequency of Δf Hz is generated at the focal area by each transducer. These two acoustic radiation forces at Δf Hz, whose phase difference is $\Delta\phi$, are applied by setting focal points at the different sites inside the object, and the insonification angles are assigned to θ_1 and θ_2 for respective transducers. **Experimental results:** Two cyclic acoustic radiation forces were applied by setting focal points at the upper surface of an

object made of gel (f_0=1 MHz, Δf=10 Hz). θ_1=22 degree and θ_2=145 degree from the horizontal axis. The horizontal distance between these two focal points was 6 mm. Directions of horizontal components of the two acoustic radiation forces were opposite each other by setting $\Delta\phi$=0. Therefore, the region between two focal points was cyclically compressed along the horizontal axis by these acoustic radiation forces, and the thickness along the vertical axis becomes thick in this region. Movies of the surface of the object were taken at two focal points and the center between two focal points using a high speed video camera. Regions at two focal points were cyclically actuated along directions of insonification of respective ultrasonic beams. When radiation forces became the maximum, regions at two focal points moved toward the center between two focal points. This result shows the region between two focal points was compressed along the horizontal axis. The upper surface at the center between two focal points was observed to move upward at the time of horizontal compression. This result show the thickness of the region between two focal points increased along the vertical axis. Then, the displacement distribution along an ultrasonic beam, which was insonified along the vertical axis at the center between two focal points, was measured. Cyclic displacements at 10 Hz were measured along the ultrasonic beam. When radiation forces became the maximum, the upper surface and the region which is 1 mm deeper than the upper surface moved upward and downward by 1 μm, respectively. These results show that the change in thickness (strain) inside the object was successfully generated by the proposed method.

6G-4 5:15 p.m.
ULTRASOUND DOPPLER FOR IMPROVED DIAGNOSIS OF DISEASE IN THE PARANASAL SINUSES.

T. JANSSON*[1], H. W. PERSSON[1], P. SAHLSTRAND-JOHNSON[2], N.-G. HOLMER[3], and M. JANNERT[2], [1]Dept. of Electrical Measurements, Lund University, Lund, Sweden, [2]Dept of Oto-rhino-laryngology, Malmo University Hospital, Malmo, Sweden, [3]Dept. of Biomedical Engineering, Lund University Hospital, Lund, Sweden.
Corresponding e-mail: tomas.jansson@elmat.lth.se

INTRODUCTION: Many sinus irrigations performed today are unnecessary, as they are based on the diagnosis of presence of fluid in the paranasal sinuses. The irrigation involves penetrating into the sinus cavity with a thick needle, which, needless to say, is very uncomfortable for the patient. If the fluid is then shown to be serous (of low viscosity), the procedure has been unnecessary, as the fluid will resorb spontaneously, whereas only if it is mucous (and thereby highly viscous), irrigation and antibiotics is called for. As sinus infection is a very common diagnosis (>250,000/year in Sweden alone), a significant reduction of cost both economically and ecologically, in terms of reduced need for sick leave and antibiotic treatments, would be expected if the diagnosis could be more specific. We propose to investigate the viscosity non-invasively by means of detecting the magnitude of an induced acoustic streaming in the sinus fluid, using a continuous wave Doppler device.

METHOD: The effect of acoustic streaming is well known, and has been shown to be, among other things, inversely proportional to the viscosity of the fluid. To

test the applicability of the method, an anthropomorphic sinus phantom was manufactured. From a human cranium, a cast was made of the sinus cavity. This “plug” was then used to form the mould of tissue-equivalent material, in which fluid could be filled. As tissue-equivalent material, agar was used with added graphite powder to serve as attenuating component. Measurements were performed using a custom made continuous-wave ultrasound Doppler system. The transducer was a commercially available 4.2 MHz dual element type. The transmitter was driven with a voltage of 13 Vpp, producing a spatial-peak-temporal-average intensity of 79 mW/cm^2. The intensity level was measured using a calibrated needle hydrophone. After placing the ultrasound probe against the wall of the phantom, the mean Doppler shift was recorded from a number of water and glycerol solutions, with varying degree of viscosity. Here, the viscosity was varied between 7 to 47 mPas, which falls in the clinically interesting range. A small amount of Sephadex (G10, Pharmacia, Uppsala, Sweden) was introduced as scattering particles in the fluid contained in the phantom.

RESULTS: There was a linear relationship between the recorded Doppler shift and 1/viscosity, in accordance with theory (R^2=0.94, corrected for the square-law dependence of sound speed variation due to varying glycerol concentration).

DISCUSSION: The results show that it is possible to initiate acoustic streaming in fluids having viscosities in the range of serous to mucoid in a sinus shaped cavity. The acoustic energy necessary to initiate the streaming is below the recommended limit of deposited ultrasound intensity (100 mW/cm^2), even with a realistic acoustic attenuation prior to the cavity. In order to obtain a Doppler shifted signal from a fluid within the sinus cavity, the fluid must contain scattering particles. Whether this is the case is still unknown, even if acoustic streaming has been measured in cysts, which acoustically should have a similar content.

6G-5 5:30 p.m.
DETECTION OF THE MYOCARDIAL BOUNDARY IN THE LEFT VENTRICLE FROM SIMULTANEOUSLY ACQUIRED TRIPLANE ULTRASOUND IMAGES USING MULTI VIEW ACTIVE APPEARANCE MOTION MODELS.

J. HANSEGÅRD*[1], S. URHEIM[2], E. STEEN[4], H. TORP[3], B. OLSTAD[3], S. MALM[3], and S. RABBEN[4], [1]University of Oslo, Oslo, Norway, [2]Rikshospitalet University Hospital, Oslo, Norway, [3]The Norwegian University of Science and Technology, Trondheim, Norway, [4]GE Vingmed Ultrasound, Horten, Norway.
Corresponding e-mail: jogerh@ifi.uio.no

We report a new algorithm for detecting the myocardial boundary in the left ventricle (LV) from simultaneously acquired triplane ultrasound (US) image sequences using Multi View Active Appearance Motion Models (MVAAMM). Coupled boundary detection in three planes can potentially increase the accuracy of LV volume measurements, and also increase the robustness of the boundary detection over traditional methods.

The MVAAMM is an extension of the Active Appearance Motion Models (AAMM) and is capable of generating LV triplane image sequences. The parameters of

the model are optimized iteratively to fit the patient data set, and the myocardial boundary is then extracted from the fitted model. Shape and texture are coupled between the image planes, while the model pose is fitted independently.

A database of triplane image sequences from full cardiac cycles, including the standard apical four chamber, two chamber, and long axis views were established from 20 volunteers, including 12 healthy persons and 8 persons suffering from heart disease. Patient cases with asynchronies were not included. A Vivid 7 scanner (GE Vingmed Ultrasound, Horten) was used for acquisition of the data sets. For each dataset the LV myocardial boundary was manually outlined, and the end diastolic (ED) and end systolic (ES) frames were determined visually for phase normalization of the cycles.

Evaluation of the MVAAMM was done by detecting the LV myocardial boundaries in the test sets. Variation within the data sets is critical when training the model. Therefore, a leave one out approach was used for evaluation, resulting in 20 models where one case was left out from each model. The point distance between the automatically detected myocardial boundary and the manually outlined boundary was found as the mean of the distances between corresponding points along the contours. The detected volumes at ED, mid systole and ES (VolC) were compared to manually determined volumes (VolM). Based on the ED and ES volumes, the Ejection Fraction (EF) was calculated.

Table 1 shows the mean and 1 standard deviation of the point distance, volume error, volume fractional error, EF error, and also the regression line for VolC as a function of VolM. The detected volumes at ED, mid systole and ES correlate well with the manually determined volumes ($R^2 = 0.87$). The correlation between detected EFs and manually determined EFs was poor ($R^2 = 0.29$), this is probably caused by the method's tendency to identify an average motion pattern.

Dropouts are handled well by the MVAAMM, because the shapes and textures of the three planes are coupled. The views with the largest point distances have one or more foreshortened views, resulting in a suboptimal detection. Adding more samples to the training database or coupling of the model's pose parameters between the views may improve the performance in such cases.

Table 1: MVAAMM Results

Mean Point distance (mm)	4.1 ± 1.9
Error (VolM - VolC) (ml)	7.0 ± 14
Volume fractional error (1-VolC/VolM) (%)	13 ± 12
Volume regression (y=VolC, x=VolM) (ml)	y = 1.0x – 11
Volume correlation coefficient (R^2)	0.87

We wish to acknowledge Jan Yee at GE Vingmed Ultrasound for gathering ultrasound data. The project is supported by The Research Council of Norway.

6G-6 5:45 p.m.

TWO-DIMENSIONAL SIMULATION OF GUIDED ULTRASOUND WAVE PROPAGATION IN HEALING LONG BONES.

V. PROTOPAPPAS*[1,2] and D. FOTIADIS[2], [1]Department of Medical Physics, Medical School, University of Ioannina, Ioannina, Ioannina, Greece, [2]Unit of Medical Technology and Intelligent Information Systems, Computer Science Department, University of Ioannina, Ioannina, Ioannina, Greece.
Corresponding e-mail: me00642@cc.uoi.gr

This abstract does not appear in the online abstracts at the author's request.
It will appear in the print version.

Wednesday, September 21, 2005
ORAL SESSIONS

Session: 1H
CONTRAST AGENTS: EFFECTS
Chair: O. Basset
Creatis

1H-1 8:30 a.m.
DOUBLE PASSIVE CAVITATION DETECTION OF OPTISONÔ SHELL RUPTURE.

A. Y. AMMI*[1], R. O. CLEVELAND[3], J MAMOU[2], G. I. WANG[2], S. L. BRIDAL[1], and W. O. O'BRIEN[2], [1]Laboratoire d'Imagerie Paramétrique, Paris, France, [2]Bioacoustics Research Laboratory, Urbana, IL, [3]Boston University, Boston, MA. Corresponding e-mail: ammi@lip.bhdc.jussieu.fr

Shell rupture of ultrasound contrast agent (UCA) microbubbles is a phenomenon whose mechanism requires a better understanding in order to more efficiently use them therapeutically and diagnostically.

The objective was thus to determine both experimentally and theoretically the mechanism of UCA shell rupture by determining rupture thresholds as a function of various excitation ultrasonic parameters.

A double passive cavitation detector (DPCD) was formed from two confocal transducers. A low frequency transducer was used to excite UCAs. A high frequency transducer (13 MHz) was used to receive bubble-related responses. The low frequency transducer was used in pulse-echo mode and could thus passively detect signals from the bubble that it had excited. The two simultaneously measured echoes from a single excitation formed a DPCD. Optison™ microbubbles were gently mixed in a water tank with a pump at a dilution selected so that, on average, only a single bubble was within the confocal region at any given time.

The settings of the incident pulses on the microbubbles were varied, four driving frequencies (0.9, 2.8 , 4.6 and 7.9 MHz) and three pulse durations (3, 5 and 7 cycles) within a range of peak rarefactional pressures from 0.3 MPa to 5 MPa. For each setting and excitation transducer combination, 128 received time traces were recorded (100 MHz sampling, 12 bits).

When Optison™ microbubbles ruptured, the signals from single microbubbles received with the high-frequency transducer showed the presence of post-excitation echoes identified as inertial cavitation and rebounds. Using these signals, the collapse threshold was evaluated as a function of excitation frequency, pulse duration, and pressure amplitude. Evaluation of the low-frequency-transducer echo verified the presence of a single microbubble at the focal region and allowed for the study the signal structure outside of the 13-MHz high-frequency-transducer bandwidth. Frequency-domain analysis of the echo signals was performed to identify the harmonic components of the received

signals. The peak rarefactional pressure threshold for detection of the post-excitation emissions increased with frequency (e.g., 0.53, 0.87 and 0.99 MPa for 0.9, 2.8 and 4.6 MHz, respectively; 5-cycle pulse duration) and decreased with pulse duration.

The modified Herring equation was used to model the bubble response at experimentally determined threshold conditions. These predicted microbubble dynamics were used to determine microbubble rupture indices based on: radial strain, peak velocity and peak acceleration.

Work supported by the cooperative project for biomedical engineering between the University of Illinois at Urbana-Champaign, USA and the Centre National de la Recherche Scientifique

1H-2 8:45 a.m.
THE EFFECT OF BUBBLE SIZE DISTRIBUTION AND DRIVING FREQUENCY ON THE "SUBHARMONIC" RESPONSE FROM DEFINITY MICROBUBBLES.

K. CHEUNG*, O. COUTURE, P. D. BEVAN, P. N. BURNS, and F. S. FOSTER, Sunnybrook and Women's Health Sciences Centre, University of Toronto, Toronto, ON, Canada.
Corresponding e-mail: kcheung@swri.ca

The ability of ultrasound contrast agents to produce coherent subharmonic energy when insonated at 20 and 30MHz has been demonstrated by Goertz *et al* (2005). The origin of this energy, however, is still poorly understood. Numerical solutions to the Keller-Miksis model for the radial behaviour of an encapsulated bubble in an ultrasound field suggest that this energy may be due to bubbles excited at the second harmonic of their resonant frequency. At low amplitudes (< 1MPa peak negative pressure) and a driving frequency of 20MHz, such a bubble has a diameter of 2μm. Although resulting in an echo of half the transmitted frequency, this is not a subharmonic.

Experiments using Definity (Bristol Myers Squibb) measured the ratio of subharmonic to fundamental energy when excited by a narrowband (9%, -6dB bandwidth) pulse with a peak negative pressure of 500kPa. This driving pulse was acoustically verified at 20MHz to be below the threshold for disruption. It was hypothesized that by altering the bubble population by mechanical filtration, this ratio would vary depending on the volume fraction of bubbles excited at twice their resonant frequency compared to the rest of the population. At 20MHz, filtering for bubbles smaller than 5μm in diameter should increase the subharmonic ratio, while filtering for bubbles less than 1.2μm in diameter should decrease the ratio. Mechanical filtration was qualitatively verified with the use of a dark-field contrast microscope (Richardson Technologies), though the filter could not completely exclude bubbles larger than the pore size due to the flexibility of the bubble's shell.

For the 20MHz driving pulse, the corrected subharmonic signal for the native population was observed to be 10.2±0.3dB below the fundamental. Repeated trials (N=6) demonstrate that the 5μm filtered population increases the subharmonic ratio by 2.1±0.3dB, while the 1.2μm filtered population decreases

the ratio by 1.9±0.3dB. This suggests that for 20MHz the bubbles primarily responsible for the subharmonic signal are between 1.2 and 5μm in diameter. As the driving frequency was increased upwards to 40MHz, this trend continued for frequencies below 32MHz, at which point the subharmonic ratio of the 1.2μm filtered population began to exceed that of both the 5μm filtered population and the native population by 1.9±0.3dB and 4.7±0.4dB, respectively. We conclude that for a narrowband 500kPa pulse and frequencies in the 20-40MHz range, the bubbles of Definity that contribute most to the subharmonic signal decrease in size as driving frequency increases. At frequencies greater than 32MHz, these bubbles are smaller than 1.2μm in diameter. The signals appearing at half the excitation frequency may be a mixture of true subharmonics and other complex modes of oscillation.

We would like to thank the Canadian Institutes of Health Research and the National Cancer Institute of Canada with funds from the Terry Fox Foundation.

1H-3 9:00 a.m.
ON THE OSCILLATION OF MICROBUBBLES IN RIGID VESSELS WITH A DIAMETER OF 12 MICRONS.

C. CASKEY*, P. DAYTON, D. KRUSE, and K. FERRARA, University of California-Davis, Davis, CA.
Corresponding e-mail: cfcaskey@ucdavis.edu

To date, little is known about the behavior of microbubble contrast agents during insonation in vessels that are on the same size order of the agents themselves. Since a majority of blood volume is contained within capillary networks, information about microbubble behavior in these vessels is important. Changes in the resonance frequency with vessel size have previously been proposed. The presence of microbubbles reduces the acoustic pressure threshold for bioeffects, although the mechanisms for these bioeffects remain uncertain. Also, drug delivery schemes are under development that would take advantage of changes in capillary permeability produced by microbubble oscillation. Theoretical studies indicate that oscillation is affected by boundaries (particularly rigid boundaries) within ten bubble diameters. We seek to characterize microbubble oscillation during insonation within a rigid phantom vessel with a diameter similar to a capillary (~12 microns), and compare that with oscillation in larger vessels. For insonation at 1 MHz and 1 MPa, we observe the relative expansion during insonation to be reduced from up to 20 fold in a 200 micron vessel to 3 fold in a 12 micron vessel. The center frequency of oscillation can also be increased from 1 MHz to 3 MHz in a 12 micron vessel, as compared with a larger vessel. Neither decreasing the center frequency of oscillation nor increasing the transmission pressure produces the expected increase in oscillation amplitude.

This study was supported by NIH CA 76062 and CA 103828.

1H-4 9:15 a.m.

ESTIMATION OF AMBIENT PRESSURE CHANGES USING NONLINEAR ACOUSTIC PROPERTIES OF ULTRASOUND CONTRAST AGENTS.

D. RAZANSKY*, Y. GANOR, M. SAPUNAR, E. KIMMEL, and D. ADAM, Technion - Israel Institute of Technology, Haifa, Israel.
Corresponding e-mail: dan@bm.technion.ac.il

A reliable tool for noninvasive pressure measurement is of interest since it will provide painless and infectionless measurements of ambient pressure changes within the body. Unfortunately, current noninvasive pressure estimation methods within body cavities and organs, e.g. these based on Doppler ultrasound, do not provide correct and reproducible ambient pressure values.

A fundamental feature of nonlinear microbubble response to acoustic drive is the existence of both the sub-harmonic and the second harmonic components, in addition to the basic frequency response. During in-vivo examinations, tissue reflects the transmitted basic frequency, and may also produce a significant second harmonic signal, in addition to that produced by the bubbles. The sub-harmonic component, however, being significant in microbubble response, can be differentiated from other harmonic components produced by tissues surrounding the bubbles.

The purpose of the current research was to investigate the effects of hydrostatic pressures on the harmonic and sub-harmonic response of a clinically available UCA, Optison™. The UCA suspension in saline, at commonly used in-vivo concentration of 50000 microspheres/cm^3, were subjected to hydrostatic pressure variations between 0 and 20 kPa and to insonations at 150-250 kPa, 9 cycles, PRF of 8 Hz bursts. The total duration of each experiment was 300s. In order to minimize possible dependence of the scattered signals on many geometrical and other time-dependant parameters, the harmonic and sub-harmonic responses were normalized to the basic frequency response of the bubbly cloud. The sub-harmonic-to-basic-frequency (SHBF) intensity ratio was found to the most accurate and robust measure of ambient pressure variations. Two basic configurations were examined. One, utilizing a large liquid volume containing UCA, is associated with the conditions existing in different heart chambers. In this configuration, the importance of taking into account the attenuation effects due to propagation in bubbly suspension was studied. It was theorized and then experimentally validated that, in this case, the maximal SHBF and correlation with the ambient pressure changes are obtained when insonifying at frequencies close to the resonance frequency of the bubbly cloud. The second configuration tested the response of UCA contained in an isolated tube, mimicking a blood vessel conditions. In this case, the optimal excitation frequency was shown to be twice the resonance frequency of the cloud. Effects of resonance frequency shift with time was observed, and helped to define the time (>100 s) for which maximal correlation between ambient pressure changes and the intensity of the half-harmonic is obtained. Microbubble response and SHBF correlation with pressure changes was significantly reduced after >300 s, due to bubble destruction and gas diffusion. The proposed method shows good correlation between the actual ambient pressure variations and the measured

nonlinear bubble response SHBF ratios, thus seems suitable for noninvasive blood pressure estimations.

1H-5 9:30 a.m.
DILUTION SYSTEM IDENTIFICATION METHODS FOR CONTRAST ULTRASOUND EJECTION FRACTION ASSESSMENT.

M. MISCHI*[1], A. JANSEN[2], and H. KORSTEN[2,1], [1]Eindhoven University of Technology, Eindhoven, The Netherlands, [2]Catharina Hospital, Eindhoven, The Netherlands.
Corresponding e-mail: m.mischi@tue.nl

Left ventricle (LV) ejection fraction (EF) measurements require time-consuming geometrical methods based on medical imaging techniques. Indicator dilution methods allow a fast EF measurement, but their application is limited due to the need for cardiac catheterization. An indicator bolus is rapidly injected in the LV and its concentration measured versus time. The EF estimate can be derived from the time constant of the mono-compartment model fit of the LV indicator dilution curve (IDC). The injection of an ultrasound contrast agent bolus allows a non-invasive IDC detection, however, a ventricular contrast injection remains necessary.

We have recently proposed the use of LV dilution system identification methods for a minimally-invasive EF measurement. Only a peripheral intravenous injection is required. In this paper, we present, validate, and compare two least-mean-squares (LMS) algorithms for the LV impulse response estimation and the LV EF assessment. Two IDCs, which are measured in the left atrium (LA) and LV, represent input and output of the LV dilution system. The proposed LMS algorithms minimize the error $\varepsilon(h_{LV})=E[C_{LA}*h_{LV}-C_{LV}]$, where C_{LV}, C_{LA}, and h_{LV} are the LV IDC, LA IDC, and estimated impulse response of the LV dilution system, respectively.

The first algorithm determines h_{LV} as the solution of the *Wiener-Hopf* equation. The estimated impulse response is fitted by a mono-compartment model for the EF assessment. The second LMS algorithm uses the a priori knowledge on the LV system. The LV impulse response is parameterized by a mono-compartment model and the EF estimate is derived from the model parameters that minimize ε. Noise in the IDC is mainly due to flow and pressure variations in the ventricle and can be suppressed by a low pass filter without affecting the IDC information, which is characterized by lower frequencies.

The algorithms are validated by 50 measurements in patients with EF between 10% and 80%. The measurements are compared to echocardiographic bi-plane estimates after contrast opacification. The correlation coefficients are 0.62 and 0.87 and the standard deviations are 12.7% and 8.6% for the first and second algorithm, respectively.

An increasing underestimation for higher EF can be recognized in the first method. This problem can be related to the LV impulse-response frequency spectrum, which for larger EF is characterized by higher frequencies that are not excited by C_{LA}. As a result, the higher frequency components of the impulse

response cannot be estimated and the exponential fit results in larger time constant and smaller EF estimates. This effect, which might be solved by an optimized fitting-interval selection, is not recognizable in the second algorithm. The model parameters are automatically estimated by the low frequency components of the signals. However, this can result in reduced sensitivity of ε to parameter variations. In conclusion, adding a priori knowledge in the system identification algorithm leads to increased accuracy of higher EF estimates.

1H-6 9:45 a.m.
THE LONGEVITY OF CONTRAST ENHANCEMENT FOLLOWING IN VIVO INJECTION IS INFLUENCED BY AN UNSUSPECTED INTERACTION WITH THE LIVER.

M. MATSUMURA[1,3], R. KARSHAFIAN[1], M. BANERJEE[2], and P. BURNS*[1,2], [1]University of Toronto, Toronto, ON, Canada, [2]Sunnybrook and Women's College HSC, Toronto, ON, Canada, [3]Daiichi Pharmaceutical Co, Tokyo, Japan.
Corresponding e-mail: burns@swri.ca

Second generation ultrasound contrast agents use low solubility gas to improve stability. In vivo longevity in the blood stream, however, is still only about 3 minutes, up to 100 times less than the comparable in vitro stability. This ratio also varies between agents. We hypothesize that this is due not only to microbubble composition, but to agent specific uptake by reticuloendothelial system (RES) in the liver, and furthermore, that this is independent of the postavascular enhancement of the liver and spleen recognized to occur with some agents.

Optison (Amersham, Princeton) and Definity (BMS, Boston), both agents which show no liver/spleen postvascular phase enhancement, were diluted with water and flowed through latex tubing. Backscattered intensity of the agents was measured at 5 MHz and MI<0.02 and over 3 hours to assess in vitro stability. To assess in vivo longevity, eight rabbits were injected intravenously with contrast and backscatter measured from the iliac artery in the same way. The main input and output vessels of the liver (the portal and hepatic veins) were also scanned at low MI using pulse inversion imaging (Philips HDI5000, Bothell). Linearized data were stored digitally and time-intensity curves obtained from regions of interest positioned in these vessels. Six further rabbits were treated with gadolinium chloride ($GdCl_3$), which depletes Kupffer cells. Similarly time intensity contrast curves were obtained in these animals.

In vitro backscatter showed very slow decrease in power at a rate of about -6dB in 2 hrs. In vivo iliac artery backscatter decreased much faster than in vitro. Optison decayed faster (-3dB at 30 sec, -6dB at 60 sec) than Definity (-3dB at 120 sec, -6dB at 260 sec). Comparing the hepatic and portal vein enhancement, Optison was cleared significantly by the liver, with a 20:1 loss of integrated power between portal and hepatic veins. The ratio for Definity was 2:1. The ratio decreased in $GdCl_3$ treated rabbits with Optison, indicating that Kupffer cells have a significant role in hepatic clearance of Optison, in spite of the fact that it was not possible to image Optison trapped in the liver parenchyma.

Hepatic clearance of the microbubbles differs between agents and has a significant influence on their longevity in vivo. Definity is less affected than Optison, probably because of its surface coating. We conclude that interaction of contrast agents with RES is a significant determinant of microbubble extraction rate, regardless of presence of postvascular enhancement. This should be accounted for in clinical studies of the liver with ultrasound contrast agents.

Work supported by the Terry Fox Programme of the National Cancer Institute of Canada

Session: 2H
ACOUSTIC PROPERTIES OF CELLS AND TISSUES
Chair: G. Schmitz
Ruhr-Universitat Bochum

2H-1 8:30 a.m.
ULTRASONIC DETECTION OF THE ANISOTROPY OF PROTEIN CROSS LINKING IN MYOCARDIUM.

S. BALDWIN*, M. YANG, K. MARUTYAN, K. WALLACE, M. HOLLAND, and J. MILLER, Washington University in St. Louis, St. Louis, MO.
Corresponding e-mail: slb@hbar.wustl.edu

BACKGROUND: Diastolic dysfunction may arise, in part, because of an increase in myocardial stiffness from cross-linking of extracellular matrix proteins such as collagen. Studies by others indicate that high-frequency (30 MHz to 50 MHz) ultrasound can detect chemically-induced increases in protein cross-linking (C. S. Hall et al., "High-Frequency Ultrasound Detection of the Temporal Evolution of Protein Cross-Linking in Myocardial Tissue," IEEE Trans. Ultrason., Ferroelect., Freq. Contr., vol. UFFC-47, pp.1051-1058, 2000).

OBJECTIVE: The goal of the current study was to measure, as a function of the angle of insonification relative to that of the predominant myofiber orientation, changes in myocardial attenuation resulting from increased protein cross-linking.

METHODS: Through-transmission radiofrequency-based measurements of the attenuation coefficient (3 MHz to 7 MHz), for angles of insonification over a complete rotation relative to the predominant myofiber orientation in 5 degree increments, were performed at room temperature on 36 specimens from 12 freshly excised lamb hearts. These specimens were then fixed in formalin to induce protein cross-linking. After sufficient time had elapsed to ensure that the process of cross-linking had reached completion, measurements were repeated on the identical specimens.

RESULTS: For both freshly excised and formalin-fixed myocardium, the attenuation coefficient was found to increase as a function of frequency in an approximately linear manner. The attenuation varied systematically as a function of angle of insonification, with a minimum perpendicular to, and a maximum parallel to, the direction of the myofibers. Increased protein cross-linking inferred

from fixation resulted in a maximum increase in attenuation at perpendicular insonification. For angles near perpendicular to the predominant direction of the myofibers, the measured slope of attenuation increased from 0.52 ± 0.07 dB/(cm•MHz) (mean ± one standard deviation) for freshly excised to 0.85 ± 0.08 dB/(cm•MHz) for formalin-fixed myocardium. In contrast, for parallel insonification uncertainties exhibit considerable overlap (1.88 ± 0.17 for freshly excised and 1.75 ± 0.19 dB/(cm•MHz) for formalin-fixed myocardium).

CONCLUSION: This study indicates that effects of fixation, and therefore presumably protein cross-linking, in myocardium can be anisotropic, suggesting that the response of the extracellular collagenous matrix to changes in cross-linking is directionally dependent. The anisotropy of ultrasonic attenuation may thus provide an approach for the noninvasive monitoring of the extent and progression of myocardial disease associated with changes in protein cross-linking.

NIH R37 HL40302

2H-2 8:45 a.m.
ULTRASOUND CHARACTERIZATION OF THREE ANIMAL MAMMARY TUMORS FROM THREE-DIMENSIONAL ACOUSTIC TISSUE MODELS.

J. MAMOU*, M. L. OELZE, W. D. O'BRIEN, JR., and J. F. ZACHARY, University of Illinois, Urbana, IL.
Corresponding e-mail: mamou@uiuc.edu

The tissue microstructures responsible for ultrasonic scattering remain unidentified. Identification of these structures would lead to potentially improved methodologies for characterizing tissue and diagnosing disease from ultrasonic backscatter measurements. Accurate three-dimensional (3D) acoustic models of tissue microstructure, termed 3D impedance maps (3DZM) could help to identify scattering sources.

3DZMs were obtained for three mammary tumors (a rat fibroadenoma (FA), a mouse carcinoma (CA), and a mouse sarcoma (SA)). 3DZMs are derived from a 3D histological data set of tissue, and are independent of ultrasonically acquired data. Tumors were fixed (10% neutral-buffered formalin), embedded in paraffin, serially sectioned, and stained with H&E for histologic evaluation. Each section was digitally photographed through the light microscope. 3DZMs were then obtained after contrast equalization of each section, registration of adjacent sections, interpolation of the sections lost during sectioning, and assignment of acoustic impedance values to recognized tissue microstructures (e.g., cytoplasm, nuclei, fat, etc. . .). The Fourier transform of the 3D spatial autocorrelation of the 3DZM was used to estimate the backscattered power spectrum. Spectral estimates (scatterer size and acoustic concentration) were then obtained by fitting an assumed scattering model (form factor, FF) to the power spectrum. At first, a Gaussian FF was used to allow comparison with the in-vivo measurements conducted on the same three tumor tissues. Then, a tissue-specific FF was deduced from each 3DZM and used.

The 3DZM estimates were compared to previous values that were obtained from ultrasonic backscatterer measurements (also using a Gaussian form factor) on the same three tumors. From these three 3DZMs average scatterer diameters of 91 μm, 31.5 μm, and 34.5 μm for FA, CA, and SA, respectively, were determined. Independent ultrasonic measurements yielded average scatterer diameters of 105 μm, 30 μm, and 33 μm, respectively. Using the 3DZM-derived FF, average scatterer diameters of 96 μm, 56 μm, and 37 μm were found.

The 3DZM estimates using the Gaussian FF led to scatterer estimates very similar (within 10%) to those obtained with the independent ultrasonic backscatter measurements. However, it was not possible to clearly distinguish between the sarcoma and the carcinoma using the estimates obtained using the Gaussian FF (3DZM and ultrasound). Clear distinction was finally obtained when the 3DZM-deduced FF was used to obtain estimates. Thus, 3DZMs may be tremendous tools to help identify ultrasonic scattering sites and to develop advanced models and sensitive ultrasonic techniques to diagnose disease.

Work supported by the University of Illinois Research Board.

2H-3 9:00 a.m.
A NEW METHOD TO ASSESS THE KINETICS OF ROULEAUX FORMATION IN HUMAN SUBCUTANEOUS VEINS USING HIGH FREQUENCY PARAMETRIC IMAGING: PRELIMINARY RESULTS.

F. YU*, J.-L. GENNISSON, and G. CLOUTIER, Laboratory of Biorheology and Medical Ultrasonics (LBMU), University of Montreal Hospital, Montreal, Québec, Canada.
Corresponding e-mail: francois.yu@polymtl.ca

Laser erythro-agregameter is considered the gold standard method for *in vitro* red blood cell (RBC) aggregation characterization. With this method, a high shear rate is first applied on the blood sample to disrupt the aggregates and to provide a common reference level prior to the aggregation phases. *In vivo*, it is very difficult to have a standard protocol that would allow studying the kinetics of rouleaux formation following prior disruption of the aggregates. We propose a new approach using low frequency shear waves to initially disrupt the aggregates, followed by the measurement of the kinetics of aggregation with high-frequency ultrasound in a peripheral subcutaneous vein following flow stoppage.

The subcutaneous vein in the forearm was occluded for 30 s proximally and distally of the region of interest, and low-frequency shear waves (~100 Hz) were applied for 5 s over the vessel. Acquisitions of radio-frequency (RF) data were made using a VisualSonic wideband 40 MHz system (Vevo 660, Toronto, Canada). The focal point at 6 mm was positioned inside the lumen of the vessel. Backscatter coefficient (BSC) and spectral slopes (SS) were calculated on sequences of RF images before and during the application of the shear waves. Each RF signal was Fourier transformed, averaged in the spectral domain, normalized with respect to a 6 % hematocrit reference RBC suspension at 37°C, and compensated for attenuation to provide parametric images of BSC and SS.

The attenuation was compensated using an arbitrary standard value of 0.2 dB/MHz/cm.

In sequences of RF images of 7 s duration, BSC decreased from 9.8×10^{-3} $\pm3.6\times10^{-3}$ $cm^{-1}sr^{-1}$ to $5.5\times10^{-3} \pm 1.3\times10^{-3}$ $cm^{-1}sr^{-1}$ (-2.5 dB), when the shear waves were applied on the vein of five normal subjects. SS correspondingly increased from 2.8 ± 0.3 to 3.9 ± 0.3 under these conditions. Reversely, when the shear waves were stopped, BSC gradually increased and SS decreased suggesting the formation of new aggregates.

In conclusion, our results suggest that shear waves could be used to initially disrupt the aggregates and provide a common reference level to measure quantitative parametric indices reflecting the level of RBC aggregation. It is believed that this method could be of clinical significance for reproducible measurements in pathologies associated with hyper-aggregation of erythrocytes.

Canadian Institutes of Health Research (grant #36467), the Fonds de la Recherche en Santé du Québec (National Scientist Award), Nateq master's scholarship and Nserc doctoral scholarship.

2H-4 9:15 a.m.
QUANTIFICATION OF RED BLOOD CELL AGGREGATION USING AN ULTRASOUND CLINICAL IMAGING SYSTEM.

A. AMARARENE*, J.-L. GENNISSON, A. RABHI, and G. CLOUTIER, Laboratory of Biorheology and Medical Ultrasonics-University of Montreal Hospital Research Center, Montreal, Quebec, Canada.
Corresponding e-mail: amararene@yahoo.com

Objectives: An abnormal level of red blood cell (RBC) aggregation is a clinical condition associated with many cardiovascular disorders. Ultrasound techniques hold realistic promises for the diagnostic of these diseases. Unfortunately, few works were dedicated to investigate the RBC aggregation using a clinical imaging system. In this study, we propose to characterize this phenomenon with the backscatter power spectral slope (BPSS) using radio-frequency (RF) data collected from a clinical imaging system.

Methods: A flow loop system was used to characterize porcine blood simultaneously using a nonfocused monoelement transducer (as a gold standard) and a linear probe of a clinical imaging system (GE Vivid Five). The frequency bandwidth of the two transducers ranged between 4 and 8 MHz. They were oriented to the same spot of a vascular phantom tube made of PVA (Polyvinylalcohol) and immersed horizontally in a tank filled with degassed water. Porcine blood circulation in the tube was made using a roller pump. An electromagnetic flowmeter along with a flow probe was incorporated in the loop to monitor the blood flow rate in the vessel. The monoelement transducer was used in a pulse-echo setup. Raw RF data from the monoelement transducer and the linear probe were collected versus blood flow rate that was varied from 0 to 100 ml/min at hematocrits (H) of 45% and 20% as well as in a reference saline solution containing 5% of RBCs. The BPSS from the linear probe data was computed and compared to that of the monoelement transducer.

Results: In the case of whole blood where RBC aggregation was possible, using the linear probe, the BPSS increased from a value of 1.7 to 3.2 as the blood flow rate was increased from 0 to 100 ml/min at a hematocrit of 45%. For H=20%, the BPSS increased from 2.1 to 3.0. In the case of the saline solution with H=5% (where no RBC aggregation was possible), we observed a fluctuation of the BPSS around a constant value of 3.5. The reference method which uses the monoelement transducer exhibited the same behavior for the BPSS with values in the same range.

Conclusion: It is well known that ultrasound parameters such as the backscatter coefficient or the BPSS are discriminate tools to characterize the aggregation of RBCs. In the case of high flow rate where no major RBC aggregation can occur, the ultrasound properties of blood had a Rayleigh behavior and the BPSS were close to 4. Aggregation of RBCs appears as the blood flow rate is decreased, a reduction of the BPSS was observed. For the first time, we showed that it is possible to quantify the RBC aggregation in a flow loop system simulating physiological flow rates with a clinical imaging system. The results were validated by a method using a nonfocused monoelement transducer. Currently, we are undergoing *in vivo* experiments. The first results showed the same blood flow rate dependence of the BPSS for the subcutaneous vein (cephalic vein).

This work is supported by the Canadian Institutes of Health Research (grant 36467) and the Fonds de

la Recherche en Santé du Québec (National Scientist Award).

2H-5 9:30 a.m.
USING HIGH FREQUENCY ULTRASOUND ENVELOPE STATISTICS TO DETERMINE SCATTERER NUMBER DENSITY IN DILUTE CELL SOLUTIONS.

A. TUNIS[1,2], R. BADDOUR[1,2], G. CZARNOTA[2], A. GILES[2], A. WORTHINGTON[2], M. SHERAR[1,2], and M. KOLIOS*[1,3], [1]University of Toronto, Department of Medical Biophysics, Toronto, Ontario, Canada, [2]Ontario Cancer Institute, University Health Network, Toronto, Ontario, Canada, [3]Ryerson University, Department of Math, Physics and Computer Science, Toronto, Ontario, Canada.
Corresponding e-mail: adam.tunis@utoronto.ca

High frequency ultrasound (HFUS) has the potential to monitor structural changes occurring in tissues during cell death. Other than spectroscopic methods, which requires the acquisition of RF data, backscatter envelope statistics can also be used. It has previously been shown in tissue-mimicking phantoms and simulations that the envelope statistics of ultrasound backscatter are affected by changes in the scatterer properties. At higher frequencies the wavelength begins to approach the size of cells and cellular components. We hypothesize that at this scale the envelope statistics of backscattered ultrasound become more sensitive to structural changes within cells. To investigate the relation between the envelope statistics and scatterer properties in a biological system, experiments were performed with cells in dilute solutions. The physical meaning of the fit parameters was evaluated by investigating HFUS backscatter envelope statistics from suspensions of various concentrations of two different cell lines of different sizes.

The two cells lines used were AML cells (diameter ~11 μm) and PC3 cells (diameter ~23 μm). A volume of each type of cells was measured and then diluted with a corresponding volume of phosphate buffered saline (PBS) solution in a sample holder to form suspensions with various volume concentrations of cells, ranging from 0.1% to 1.6% cells per volume. Data were acquired using a commercial HFUS scanner (VisualSonics VS-40B) with a focused transducer (f# 2.35, focal length 20mm, centre frequency 20MHz, bandwidth 100%). B-scan images and radio-frequency (RF) data were recorded from approximately 200 independent locations separated by at least one beamwidth (250 mm) within the solution. The B-scan images were recorded in real-time and the RF data were acquired over a period of approximately 2-3 minutes. Using custom software written in JAVA, RF data were extracted from a homogeneous region-of-interest within the stored data. The maximum likelihood estimation technique was implemented in Matlab to obtain the fit parameter values of the Generalized Gamma (GG) function, one of the functions that can be used to describe the envelope statistics.

As demonstrated in theoretical work by Shankar[1], the a parameter of the GG function depends on the effective scatterer cross-section and the ratio of c/v depends on the effective scatterer number density. Experimental results demonstrated that the a parameter was higher for the larger PC-3 cells than the AML cells (0.5±0.1 vs. 0.09±0.02). Furthermore, the ratio c/v increased with cell number density, with similar values for both cell lines at equal number density independent of cell size. These results confirm the interpretation of the parameters proposed in the theoretical predictions of Shankar[1] and extend the work to the biological model of sparse solutions of cells. This technique demonstrates that HFUS signal statistics can be used to measure cell properties.

[1]Shankar, P. M. (2001). “Ultrasonic tissue characterization using a generalized nakagami model.” IEEE Trans Ultrason Ferroelectr Freq Control 48(6).

Generalized Gamma Fit Parameters

Number Density [cells/mm^3]	AML GG a	AML GG c/v	PC3 GG a	PC3 GG c/v
565	0.09±0.02	0.179±0.006	0.5±0.1	0.25±0.01
1131	0.48±0.05	0.49±0.02	1.7±0.3	0.47±0.02

The Generalized Gamma fit parameters for two cell lines of different sizes (AML~11mm and PC3~23mm) at two number densities.

2H-6 9:45 a.m.

VISUALIZATION OF APOPTOTIC CELLS USING SCANNING ACOUSTIC MICROSCOPY.

S. BRAND*[1,2], E. C. WEISS[3], G. CZARNOTA[1,2], R. LEMOR[3], and M. C. KOLIOS[1], [1]Department for Physics, Ryerson University, Toronto, Ontario, Canada, [2]Ontario Cancer Institute, Princess Margaret Hospital, Toronto, Ontario, Canada, [3]Fraunhofer Institut fuer Biomedizinische Technik, St.-Ingbert, Germany. Corresponding e-mail: bastian200@web.de

The goal of this project is to investigate changes in the acoustical properties of cells undergoing cell death for developing a method for apoptosis detection using high frequency ultrasound (20-60 MHz). A scanning acoustic microscope (SAM) was used for visualization of cells undergoing apoptosis (SASAM, Fraunhofer IBMT, Germany). The use of the SAM offers high resolution (1 μm spot size) and therefore enables the visualization of intracellular components allowing the exploration of acoustical properties of intracellular components as a function of treatment time. The results of this investigation provide a better understanding of changes in the acoustical properties of cells with cell death and thus to the development of a non invasive method for measuring the treatment response of cancerous tissue using acoustic waves.

The scanning acoustic microscope was used for visualizing HeLa and MDCK cells using very high frequency ultrasound in the frequency range of 0.75 to 1.1 GHz. Single cells of both cell lines were scanned before and at several time points after treatment with the chemotherapeutic drug Cisplatin. Cells were stained with H33342 for visualizing condensed chromatin and with DIOC 3(5) for visualizing membranes in fluorescence microscopy. Pellets of these cell lines were imaged and rf data collected with a ultrasound biomicroscope (VisualSonics VS40B, Toronto, Ontario) using acoustic waves using 20 MHz and 40 MHz transducers. Spectral parameters were computed from the rf-signals acquired at several timepoints during treatment therapy of the cells in order to relate the changes in backscatter behaviour to the results of the microscopic visualization methods. Imaging using synchronous acoustic and optical microscopy using the SASAM system clearly enables a differentiation between apoptotic cells and cells not responding to the treatment. Apoptotic cells displayed a higher contrast in the acoustic images and were less regular in shape, a change demonstrating that changes in the acoustic properties occurred. Similarly, in the optical images of the same cells nuclear condensation and membrane disruption were detected. Spectral parameters estimated from the rf echoes of cell pellets from similar adherent cell lines (HEp2) acquired with the UBM show changes over time after treatment. Integrated backscatter coefficients increased by 6dB after 12h exposure with Cisplatin. A significant decrease in the slope of the normalized power spectrum (from 0.8 dB/MHz to 0.5 dB/MHz, 20MHz centre frequency) was observed for the HEp2 cells. The same experiments are currently performed for the cell lines imaged with the SAM.

Imaging of cancerous cells undergoing a chemotherapeutic treatment using a scanning acoustic microscope enables to localize changes in acoustic properties of cells undergoing cell death. We were able to detect changes in acoustic cell properties as a function of exposure to drug using SAM. A better understanding

of these localized acoustic changes is crucial for the development of a non invasive method for monitoring of apoptosis, based on ultrasound spectroscopy of B-mode acquired rf data.

Session: 3H

ACOUSTICAL IMAGING
Chair: R. Maev
University of Windsor

3H-1 8:30 a.m.
FAST NONCONTACT IMAGING OF MATERIAL MICROSTRUCTURE USING LOCAL SURFACE ACOUSTIC WAVE VELOCITY MAPPING.

S. SHARPLES*, M. CLARK, and M. SOMEKH, University of Nottingham, Nottingham, UK.
Corresponding e-mail: steve.sharples@nottingham.ac.uk

The make-up of the material microstructure of multi-grained materials such as titanium alloys and aluminum is of great interest to many in industries such as aerospace. The ability to map the material microstructure - in effect to image the grains - quickly and in a nondestructive manner would be useful from both a process control perspective and in the area of nondestructive evaluation. There are several techniques in the field that are capable of imaging grain structure including simple etching, orientation imaging microscopy and scanning acoustic microscopy; all have their strengths and weaknesses. We present a totally new ultrasonic technique that can directly and quantitatively image the local surface acoustic wave velocity over the surface of a material. Material microstructure can be determined if the phase velocity of the grains varies with grain orientation. The acoustic waves are generated and detected by lasers and as well as being noncontact, the technique is relatively fast, can cope with large samples, and is totally nondestructive.

The new technique involves varying the spatial parameters of the excitation pattern in real time to maximize the generation efficiency of the surface acoustic waves at the phase velocity of the material, in the region of excitation. By repeating this over the sample surface, an surface wave phase velocity map can be produced.

As well as describing the velocity mapping technique in detail, several example results of industrially-relevant materials acquired using our new instrument are presented. The limit to the quantitative lateral resolution of the instrument is discussed, and how this relates to the qualitative lateral resolution. Results indicating the practical limit of the accuracy of velocity measurements are also presented.

We demonstrate imaging on several samples ($40mm^2$) and different materials. This shows that the instrument can reveal the underlying microstructure and

image areas of anomalous grain structure that may be significant for the performance of the material. The instrument currently works on smooth samples but can be extended to work on rough surfaces and components with unprepared surfaces and consequently this has high industrial relevance.

3H-2 8:45 a.m.
AIR-COUPLED ULTRASONIC IMAGING TECHNIQUES FOR PAINTING DIAGNOSTIC.

A. SIDDIOLO*[1] and R. MAEV[2], [1]Dipartimento di Meccanica, University of Palermo, Palermo, Italy, [2]Centre for Imaging Research, Windsor, Ontario, Canada.
Corresponding e-mail: siddiolo@dima.unipa.it

An air-coupled ultrasonic method for analysis and assessment of art pieces, particularly wooden paintings, is being developed. This method can bring drastic changes in the activities carried out by museums, e.g. the assessment of physical conditions of museum inventory.

Ancient paintings can be regarded as layered structures with a support. The latter, because of daily fluctuations of ambient parameters, can experience expansions and contractions, and these deformations can produce large strains and eventually cracks and detachments in the remaining layers. Hence, it is a matter of importance, for conservation purposes, to develop a robust method to evaluate painting integrity and locate incipient defective zones. By means of this method, it will be possible to plan *ad hoc* repair works on wooden paintings, and, as a result, our heritage will be preserved.

Standard procedures to find defects are visual and manual, but these methods do not provide quantitative results. In the last years, several techniques have been developed and applied, such as radiographic techniques, holographic interferometry, electronic speckle pattern interferometry and the Scanning Laser Duppler Vibrometer. For some of these techniques, high costs are involved and for some other ones, stability requirements do not allow *in-situ* measurements.

As first steps, several samples have been realized and different wood supports considered. In order to simulate the presence of various delaminated regions, after the first thin layer of animal glue, proper plastic sheets of various shape and dimension have been embedded. Then, the wood support has been coated with a number of superimposed priming layers made from mixtures of gesso and glue (ground). besides, different defects such as cracks in the ground and in the wood and high curvature of the panel have been simulated. Two different experimental configurations have been adopted: a through-transmission configuration(by using a transducer for each side of the painting) and a single-sided configuration, in which both transducers are located on the same side and positioned as close as possible to increase the final image resolution of the technique. By using these configurations, the simulated defects have been clrealy detected. After the above described teasibility analysis, four 400 year old paintings have been investigated. The developed technique allowed us to unambiguously

locate the presence of inner delaminated regions in sime of the checked paintings by using the above mentioned configurations.

3H-3 9:00 a.m.
SUPPRESSION OF SPURIOUS VIBRATION IN ULTRASONIC ATOMIC FORCE MICROSCOPY AND OBSERVATION OF STRESS-INDUCED DOMAIN SWITCHING IN FERROELECTRIC CRYSTAL.

T. TSUJI*, S. IDE, and K. YAMANAKA, Department of Material Processing, Graduate School of Engineering, Tohoku University, Sendai, Japan.
Corresponding e-mail: t-tsuji@material.tohoku.ac.jp

Ultrasonic atomic force microscopy (UAFM) has realized measurement of both precise topography and stiffness distribution for the first time, and it is now being accepted as a practical tool for non-destructive evaluation of mechanical properties and subsurface defects in MEMS devices. In UAFM and related methods, contact resonance vibration is measured using a cantilever, although spurious vibration (SV) in the resonance spectrum degrades precision of the resonance frequency measurement. Although it has been recognized as a serious problem, origin of the SV has not been clarified so far.

In this situation, we tried to reveal the origin of SV, by changing the length of free part of cantilever base not clamped by a fixing wire to the cantilever holder, and found that the frequency of the SV was decreased as the length of the free part increased. Moreover, this decrease agreed to the calculation using an analytical solution for a deflection vibration of a thick plate. Therefore, we found that the origin of SV is the deflection vibration of the base. Accordingly, we fabricated a new cantilever holder that firmly fixes whole the base and succeeded in removing the SV. Alternatively, a cantilever base using high damping material or structure can be used. These methods will be useful not only in UAFM but also in other AC mode AFMs.

As an application of UAFM, we present observation of the stress-induced ferroelectric domain switching whose importance is now recognized in establishing the reliability of piezoelectric actuators using ferroelectric materials. The stress was applied by nano-indentation (NI) within grains of soft PZT ceramic with a tetragonal structure (unpoled). In UAFM image at the 2nd deflection mode, stripe structures were observed showing periodic variation of the resonance frequency, which were caused by the stiffness anisotropy of the newly generated 90 degree domain structure, because there was no such structure before the NI. It is interesting to note that the stripe structures were not observed by piezoresponse force microscopy (PFM), which may be explained by the following facts; (i) the penetration depth of the UAFM is shallower than that of the PFM since the penetration depth of the stress field is less than that of the electric field and (ii) 90 degree domain switching is localized near the surface. In conclusion, we succeeded in eliminating spurious signal in UAFM, and found that UAFM will provide useful information on the mechanism of stress-induced depolarization in ferroelectric materials.

This work was supported by Grant in Aid for Science Research (No. 13450017, 15656179, 17560627) from the Ministry of Education, Culture, Sports, Science and Technology.

3H-4 9:15 a.m.
IMPULSE ULTRASONIC FIELDS RADIATED BY A LINEAR TRANSDUCER THROUGH A LIQUID-SOLID INTERFACE.

D. BELGROUNE*[1,2], J. F. BELLEVAL[2], and H. DJELOUAH[1], [1]D. Belgroune, USTHB, Algiers, Algeria, [2]J.F. de Belleval, UTC, Compiègne, France, [3]H. Djelouah, USTHB, Compiègne, France.
Corresponding e-mail: m.naima@voila.fr

The propagation impulse ultrasonic wave in a solid medium through an interface liquid-solid is more complicated to formulate theoretically and more difficult to check in experiments than in the case of only one fluid environment. It should be noted that this case is often encountered in many applications, in particular in the field of the non destructive testing when a transducer is immersed in a part to control.

We present in this paper, a numerical prediction of the ultrasonic field diffraction the by the angular spectrum method. Modelling is carried out by a development in impulse mode applied to a linear transducer with uniform and non uniform vibration. The pressure field is calculated in a liquid propagation medium then in a homogeneous and isotropic solid medium after its passage through a plane interface. This is performed with considering the refraction phenomenon during the interface crossing.

The obtained results are interpreted in terms of plane waves and edge waves. The arrival times of the waves and their form are correctly predicted as well in normal incidence as in oblique incidence. Our results are similar with the experimental and theoretical results met in the literature and using the impulse response method. Moreover, we show the distributions improvement of the spatio-temporal field in longitudinal mode and transverse mode; in particular in obtaining a maximum of energy on the refracted transducer axis and especially that the refracted beam slope of is not different from the awaited slope.

3H-5 9:30 a.m.
MORPHO-MECHANICAL ANALYSIS OF THE DENTIN-CEMENT INTERFACE STRENGTH USING A SCANNING ACOUSTIC MICROSCOPE.

L. DENISOVA*[1], R. MAEV[2], F. RUSANOV[1], A. DENISOV[1], E. BAKULIN[2], D. GAVRILOV[1], F. SEVERIN[2], and G. GRAYSON[3], [1]Institute for Biochemical Physics, Moscow, Russian Federation, [2]Windsor University, Windsor, Ontario, Canada, [3]Ultradent Clinical Research Ltd., Windsor, Ontario, Canada.
Corresponding e-mail: deniso@com2com.ru

Up to now caries stays one of the most widely spread human diseases. A carious tooth treatment as a rule includes restoration of the pathologically changed tissue with a dental material cement, amalgam, resin etc. Therefore a restored tooth is a small complicated construction formed of biological tissues and an artificial restorative material. Mechanical strength of such a construction depends of many factors, and one of the most significant is adhesive strength of the contact zone between dentin and dental cement. Cement shrinkage, pores, cavities and voids inside restoration and, particularly, in the interface between dentin and restoration can dramatically influence upon the quality of the treatment. The aim of the present study is to develop experimental approaches to evaluate dentin-cement interface quality using a scanning acoustic microscope.

Human teeth extracted by orthodontic reasons in dental clinics have been used. Special model samples imitating good and failed adhesion have been prepared. The study has been performed with scanning acoustic microscopes Sonix (Sonoscan, USA) and Tessonix (R.G.Maev et al). The acoustic lens providing ultrasound frequency 50 MHz (lateral resolution about 30 microns) has been used. Following the investigation in an acoustic microscope, the teeth and prepared samples have been sectioned in accordance with the scanning position and the results, obtained with acoustic microscope have been verified using a light microscope.

Acoustic impedance of the dental materials, which we use in the study, is quite similar to that of dentin. Therefore in the case of a good bonding strength between the cement and dentin almost all acoustic energy of the focused ultrasound passes from the restoration into dentin. This is why we obtain practically no reflected signal from this interface. If due to the shrinkage there is a void (filled with tissue liquid or with air) in the cement-dentin interface, then the ultrasound signal is reflecting not from dentin, but from the media with comparatively low acoustic impedance; so the largest part of the acoustic energy will be reflected and registered. In this case the interface between cement and dentin will became visible in acoustic images, formed in B- or C-scan mode. A series of the acoustic images of the restored teeth and experimental models demonstrate the difference between the imaging of the good and failed adhesion in the cement-dentin interface.

The morphological data obtained non-destructively in the acoustic microscopes are in a good agreement with the results of the examining of the same samples after sectioning in the optic microscope. The experimental approaches developed in the present study can serve as a basis for the development of new instruments and methods for dental clinical practice.

Keywords: acoustic microscopy, focused ultrasound, dental cement, cement-dentin adhesion, nondistructive evoluation

3H-6 9:45 a.m.

IMPROVEMENT OF VELOCITY MEASUREMENT ACCURACY OF LEAKY SURFACE ACOUSTIC WAVE FOR MATERIALS WITH HIGHLY ATTENUATED WAVEFORM OF V(Z) CURVE BY THE LFB ULTRASONIC MATERIAL CHARACTERIZATION SYSTEM.

Y. OHASHI*, M. ARAKAWA, and J. KUSHIBIKI, Tohoku University, Sendai, Miyagi, Japan.
Corresponding e-mail: ohashi@ecei.tohoku.ac.jp

The line-focus-beam ultrasonic material characterization (LFB-UMC) system is capable of evaluating various materials by measuring propagation characteristics of leaky surface acoustic waves (LSAWs) on the water-loaded specimen surface, viz., phase velocity V_{LSAW} and propagation attenuation α_{LSAW}, with high accuracy. The LSAW propagation characteristics can be obtained from analysis for a V(z) curve which is the transducer output when changing the relative distance z between the specimen and LFB ultrasonic device. Measurement accuracy of V_{LSAW} at around 200 MHz is ±2s=±0.0013% (s: standard deviation) for single crystals such as Gadolinium Gallium Garnet (GGG), $LiNbO_3$, and $LiTaO_3$. For specific glass materials such as silica (SiO_2) glasses, however, the measurement accuracy becomes worse in most cases. It is probably concerned with the waveform attenuation of the V(z) curve (α_0) according to the measurement principle.

In this paper, we investigate a factor affecting α_0 and its effect on the V_{LSAW} measurement and strive to improve the measurement accuracy. (111) GGG single crystal and TiO_2-SiO_2 glass (C-7972) are taken as specimens. The α_0 for C-7972 is lager than that for (111) GGG. Frequency dependences of the α_0 (50 to 250 MHz) are calculated from the α_{LSAW} for each specimen. The results revealed that the α_0 dominantly depends on radiation loss of longitudinal waves due to the water-loading effect on the specimen surface, and that the α_0 becomes smaller with decreasing frequency. 200 V(z) curves were measured for each specimen at three frequencies of 75, 110, and 225 MHz using three kinds of LFB ultrasonic devices with different radiuses of the cylindrical acoustic lens; 2.0, 1.5, and 1.0 mm. The α_0 decreases from 0.129 dB/μm at 225 MHz to 0.048 dB/μm at 75 MHz for C-7972, and from 0.019 dB/μm at 225 MHz to 0.011 dB/μm at 75 MHz for (111)-[-1-12] GGG. The results show that the measurement accuracies of V_{LSAW} become higher with decreasing frequency, exhibiting improved accuracies from ±0.0053% at 225 MHz to ±0.0020% at 75 MHz for C-7972, and from ±0.0013% at 225 MHz to ±0.0010% at 75 MHz for (111)-[-1-12] GGG. The V_{LSAW} is determined from the oscillation interval of the V(z) curve, Δz, of which the accuracy depends on the translation errors of the z-stage, viz., the moving characteristics of the z-stage including the accuracy of the laser interferometer. Because the characterization region for the V(z) curve analysis becomes wider with decreasing the α_0 , the ratio of the translation error to the characterization region becomes smaller, resulting in improving the measurement accuracy of V_{LSAW}. Consequently, we successfully demonstrated that the

measurement accuracy of V_{LSAW} for materials with a large α_0 can be improved by extending the translation distance of the *z*-stage with the larger radius of the acoustic lens and also employing lower frequency.

Session: 4H

BAW RESONATORS
Chair: Y.-K. Yong
Rutgers University

4H-1 8:30 a.m.
THICKNESS SHEAR MODE VIBRATIONS IN SILICON BAR RESONATORS.

H. CHANDRAHALIM*, D. WEINSTEIN, and S. BHAVE, Cornell University, Ithaca, NY.
Corresponding e-mail: hc287@cornell.edu

MEMS resonators are promising replacements to conventional SAW, ceramic and quartz resonators in direct conversion transceivers and chip-scale atomic clocks, demonstrating high resonant frequencies and relatively high quality factors. Air-gap electrostatically transduced MEMS resonators have quality factors (Q) > 10,000, but are limited by their large motional impedance (Rx > 10 kΩ)[1]. On the other hand, piezoelectric FBARs have small motional impedance (Rx < 10 Ω) but relatively low Q (~ 2000)[2].

This paper demonstrates a dielectric transducer for thickness shear mode silicon resonators in which a silicon nitride thin film (κ ~ 9) is sandwiched between polysilicon electrodes and the top surface of a silicon bar resonator. This internal electrostatic transducer enhances both the force density of the actuator as well as the sense capacitance, thereby reducing the motional impedance of the resonator by κ^2 relative to air-gap electrostatic transduction. The transducer configuration also enables excitation of the isochoric thickness shear mode in a silicon resonator achieving higher quality factors than FBARs.

To fabricate the resonators, we started with a 1.8 μm thick device layer SOI wafer and deposited 300 nm of silicon nitride. Then we deposited and patterned 752 nm of polysilicon. This was followed by a reactive ion etch step to define the resonator in silicon and a timed-etch of the buried oxide in HF.

The performance of an 80 μm × 40 μm bar resonator was measured using a DesertCryo microwave probe station before HF release of the structure. The unreleased buried oxide acts as an anchor, preventing motion of the bottom surface of the resonator and enabling excitation of the quarter-wave thickness shear mode. When a DC+AC electric field is applied across the silicon nitride film, the compressive stress on the silicon nitride in the transverse direction is accompanied by a lateral stress along the length. The lateral stress is transferred from the dielectric film to the top surface of the silicon resonator generating a lateral shear drive force. As the resonator vibrates, the top surface of the resonator

is harmonically stretched and compressed yielding a motional current at the sense electrode. The quarter-wave thickness shear vibration mode of the unreleased silicon resonator was measured with a resonant frequency of 713 MHz and *Q* of 1,440. By performing a timed etch of the buried oxide in HF, the overall contact area between the oxide and bottom surface of the resonator was reduced to approximately 30 $\mu m \times 5\ \mu m$. This partially released resonator has a measured resonant frequency of 723 MHz, *Q* of 4,400 in air and Rx of 1.2 kΩ. The resonator's f-Q product of 3 x 10^{12} Hz is within a factor of five of the f-Q product for quartz resonators[3]. Moreover, the 1.2 kΩ motional impedance of this resonator is the lowest motional impedance reported to date for any silicon-based VHF MEMS resonator design.

[1] J. Wang *et al*, MEMS 2004, pp. 641-44.

[2] R. Ruby *et al*, Ultrasonics Sym. 2001, pp. 813-21.

[3] F.P. Stratton *et al*, UFFC Sym. 2004, pp. 27-34.

This work was supported by DARPA CSAC program.

4H-2 8:45 a.m.
ANALYSIS OF THE ACOUSTIC WAVEFIELDS IN BAW-RESONATORS BY SCANNING ELECTRON MICROSCOPY METHOD.

D. V. ROSHCHUPKIN*[1], H. D. ROSHCHUPKINA[1], O. A. BUZANOV[2], S. A. SAKHAROV[2], and S. V. PYATKIN[1], [1]Institute of Microelectronics Technology RAS, Chernogolovka, Moscow District, Russia, [2]FOMOS Technology Co., Moscow, Russia.
Corresponding e-mail: rochtch@ipmt-hpm.ac.ru

The development of acousto-electronic devices based on surface and bulk acoustic waves has been very active in the fields of filters, oscillators, real-time processing systems, and convolvers, etc., which are widely used in new communication systems (mobile phones, radio systems, TV, GPS). This development is accompanied by an increasing need for precise characterization of the acoustic wavefields in these devices. This paper reports the investigation of the bulk acoustic wavefields excitation and propagation in BAW-resonators based on the different cuts of the SiO2, LiTaO3, La3Ga5SiO14 and La3Ga5.5Ta0.5O14 crystals using the scanning electron microscopy method which is very useful for qualitative and quantitative analysis of acoustic radiation fields in piezoelectric materials.

The SEM method in the mode of the secondary electron recording was used as an experimental technique for visualization of the bulk acoustic waves in BAW-resonators since only the low energy secondary electrons with energy of ~1÷3 eV are sensitive to the electric field which accompanies the propagation of the bulk acoustic waves in piezoelectric materials. The bulk acoustic waves were rendered visible in a JEOL JSM-840 scanning electron microscope with an accelerating voltage of E=1 kV and a probe current of I=1 nA. The use of higher accelerating voltage is not possible, because the piezoelectric substrate would be highly charged and thus bring about a distortion of the image because of

deflection of the electron probe and the change in the secondary electron emission from the crystal surface. The principle of the bulk acoustic waves imaging is based on the high-frequency modulation of the low energy secondary electrons by a stationary electrostatic interference field formed above the crystal surface by the interaction between the varying electric field of the bulk acoustic wave and the component, normal to the surface, of the electromagnetic radiation field of the electrodes. The electromagnetic and acoustic waves are mutually coherent, since they are excited by the same source (electrodes) and with the same frequency. Since the wavelength of the electromagnetic wave is large than the acoustic wavelength, the period of the stationary interference field is equal to the acoustic wavelength. Under these conditions, the low energy secondary electrons are modulated by the stationary electrostatic interference field and the image of acoustic wavefields can be visualized in the real-time operation mode.

This scanning electron microscopy method was used for visualization of the bulk acoustic wave radiation fields in BAW-resonators, to measure the wavelengths and excitation frequencies, to study the influence of the crystal dimensions and electrodes structure and dimensions on the process of the bulk acoustic wave excitation, to investigate the process of acoustic wave interaction with the crystal structure defects.

This work has been supported by Russian Foundation for Basic Research (Contract No. 04-02-16456).

4H-3 9:00 a.m.
INTERMEDIATE FREQUENCY RESONATORS USING LAMB WAVES CO-INTEGRATED WITH BULK ACOUSTIC WAVE RESONATORS.

A. VOLATIER*[1,3], G. CARUYER[1,3], E. DEFAY[2], D. PELLISSIER TANON[1], P. ANCEY[1], and B. DUBUS[3], [1]STMicroelectronics, Crolles, France, [2]CEA-LETI/DIHS/LCRF, Grenoble, France, [3]IEMN, Lille, France.
Corresponding e-mail: volatieral@chartreuse.cea.fr

Bulk Acoustic Wave (BAW) resonators exhibit attractive properties in term of power handling capacity and on-chip integration to realize filters in the GHz range. In a BAW resonator, a thin piezoelectric layer (a few μm) deposited between two electrodes is driven in its thickness extensional mode of vibration. To get a high quality factor, this structure is decoupled from the substrate by a multilayer Bragg reflector (Solidly Mounted Resonator: SMR) or a surface micro-machining membrane (Film Bulk Acoustic Resonator: FBAR). A current problem in the design of BAW resonators is the existence of spurious resonances due to Lamb waves propagation close to the thickness extensional mode which generate ripple in the filter passband.

In this work, it is demonstrated that Lamb wave resonances can be used to realize resonators in the 30-250 MHz range with high quality factor by using specific electrode design and electrical excitation.

1D simulation (based on Mason model) is usually sufficient for the design of BAW resonators. In our case, two dimensions behaviour of Lamb waves is

modelled using finite element ATILA code. Design of Lamb wave resonators are performed using modal and harmonic analysis. Typical dimensions of resonator are 100 μm width and 450 μm length (clamped-clamped beam). Influence of electrode geometry and type of excitation (one- or two-phase) upon coupling of fundamental or higher harmonic resonances will be emphasized.

Lamb wave resonators are realized using a surface micro-machining process compatible with Above IC integration. Sacrificial layer is first deposited, patterned and encapsulated by SiN film (600 nm). AlN thin film are elaborated by DC pulsed sputtering and the active stack of the resonator is made of Ti (50 nm) / Pt (100 nm) / AlN (550 nm) / Pt (200 nm). Lateral dimension of resonators is defined by etching of AlN and SiN thin films. The release of the structure is made using dioxygen plasma. According to a completely similar process Film Bulk Acoustic Resonators (FBAR) are processed at the same time.

Symmetrical S0 Lamb wave resonances ranging from 30 MHz to 250 MHz are measured for different electrode geometries and electrical excitations (network analyzer HP 8753E). High quality factors (Q_s and Q_p) of 2000 and k^2~0.8% (k coupling coefficient) are obtained at 92 MHz for 3rd harmonic resonator. These electrical measures agree well with 2D simulations previously described. As for Bulk Acoustic Wave resonators, thickness extensional resonance is measured at 2.4 GHz.

The electrical characteristics of Lamb wave resonator are potentially suitable for channel filtering or oscillator applications and co-integrating Lamb wave and FBAR resonators in one single Above IC process promises to offer great potential for design of resonators and filters in the field of Intermediate (IF) and Radio Frequency (RF) applications.

4H-4 9:15 a.m.
PICOSECOND ULTRASONICS: AN ORIGINAL TOOL FOR PHYSICAL CHARACTERIZATION OF BRAGG REFLECTORS IN BULK ACOUSTIC WAVE RESONATORS.

P. EMERY*[1], A. DEVOS[2], G. CARUYER[1], R. VELARD[1], N. CASANOVA[1], and P. ANCEY[1], [1]ST Microelectronics, CROLLES, France, [2]Institut d'Electronique, de Microélectronique et de Nanotechnologie, Dpt. ISEN, LILLE CEDEX, France. Corresponding e-mail: patrick.emery@isen.fr

Radio frequency and intermediate frequency filters are usually based on surface acoustic wave (SAW) components, which are not compatible with CMOS or BiCMOS process. Piezoelectric thin films resonators can replace SAW technology at high frequencies : thickness mode resonators with much reduced dimensions can be fabricated and connected in a ladder or a lattice network to build bandpass filters.

In order to work properly a BAW resonator has to be acoustically insulated from the substrate. This acoustic insulation can be performed by a Bragg reflector, which is tuned to work around the filter frequency. A Bragg reflector consists on an alternation of high and low acoustic impedance layers whose thicknesses

are tuned at λ/4, where λ is the wavelength in the material for the targeted frequency.

In the radio-frequency range the typical thicknesses of the involved layers fall in micronic and sub-micronic scale. In order to design such reflectors one needs to know the mechanical properties of materials (sound velocity, density,...) at this scale which may be different from those of bulk materials. In order to control the frequency range which is isolated by the reflector one also needs fine measurements of thicknesses.

Picosecond ultrasonics is a pump-probe optical technique using a femtosecond laser to generate and detect very short acoustic pulses. A pump beam impulsion launches a strain pulse in the sample, which modifies locally the refraction index and affects the reflectivity of the sample. A delayed probe beam impulsion is used to measure the transient changes on the sample reflectivity. It is then possible to obtain reflectivity curves versus probe delay, that is to say versus time. Picosecond ultrasonics is a non-contact and non-destructive technique that is well adapted to mechanical measurements in thin films.

Here we first show that Picosecond ultrasonics is helpful for the design of Bragg reflectors through precise sound velocity measurements in thin films whose elastic properties may be much different. Secondly we apply the same technique to the complete reflector and show that it permits to check the accordance of the thicknesses with λ/4 and provides a direct measurement of the reflector's central frequency. We will illustrate the interest of this technique by presenting results obtained in W/SiO2 and SiOC/SiN Bragg reflectors. These results reinforce the fact that picosecond ultrasonics is a powerful tool for the characterization of complex stacks as Bulk Acoustic Wave resonators.

4H-5 9:30 a.m.
EFFECTS OF NON-HOMOGENEOUS THERMAL STRESSES ON THE FREQUENCY-TEMPERATURE BEHAVIOR OF AT-CUT QUARTZ RESONATORS.

M. PATEL*[1], Y.-K. YONG[1], and M. TANAKA[2], [1]Rutgers University, Piscataway, NJ, [2]Seiko Epson Corporation, Suwa City, Nagano Prefecture, Japan.
Corresponding e-mail: yyong@rci.rutgers.edu

Currently, the frequency-temperature (f-T) behavior of a quartz resonator can be predicted quite accurately if the resonator crystal is under an ideal thermal stress-free condition. Under such a condition, the steady state temperature change then induces a homogeneous field of thermal strains in the crystal. The ideal thermal stress-free condition is however seldom achieved practically. In practical devices, thermal stresses are often present with temperature changes. We study the effects of non-homogeneous thermal stresses on the f-T behavior of AT-cut quartz resonators by employing a novel method of superposing the results from three existing methods for calculating (1) thermal stresses, (2) acceleration effects, and (3) f-T curves under a homogeneous thermal strain condition. We assume that for a steady state temperature change, the crystal resonator undergoes not only a homogeneous thermal strain field but also a

nonhomogeneous thermal stress field. The method is as follows; for a given temperature change:

(1) calculate using finite elements the thermal stresses,

(2) incorporate the thermal stresses from (1) into an acceleration effects model to calculate the frequency change, and

(3) calculate using finite elements the frequency change under a homogeneous thermal strain field.

The sum of frequency changes from (2) and (3) gives the effects of non-homogeneous thermal stresses on the resonator f-T curve. We present numerical results compared with experimental results for an AT-cut quartz resonator mounted on glass. The difference between the thermal expansion coefficients of glass and quartz give rise to the thermal stresses. Good comparison between the experimental results and numerical results from our new method is shown. We also investigate and present the use of thermal stresses to improve the f-T behavior of AT-cut quartz resonators.

Session: 5H

SAW PROPAGATION
Chair: M. P. da Cunha
University of Maine

5H-1 8:30 a.m.
LINKS BETWEEN TEMPERATURE STABLE BAW AND SAW CRYSTAL ORIENTATIONS.

M. WEIHNACHT*, Leibniz Institute for Solid State and Materials Research Dresden, Dresden, Germany.
Corresponding e-mail: whn@ifw-dresden.de

For many years quartz single crystals have been used as a key material for frequency control applications due to its temperature stability at low costs. Special cuts were developed to ensure first order zero temperature coefficients of frequency (TCF1) for surface acoustic waves (SAW) or bulk acoustic waves (BAW) device characteristics near room temperature. The link between T-stability of BAW and SAW devices has been recognized in the case of quartz BT-cut (BAW) and STW (SAW) as discussed at different places. Besides, the AT- and SC-cut thickness-shear quartz resonators exhibit a cubic T-dependence of frequency with inflection point near room temperature. Depending on the cut-angle a zero slope can be adjusted for the inflection point, i.e., both the TCFs are zero the TCF1 and the TCF2. A SAW-counterpart to the AT-cut seems to be not identified to this day. Otherwise, a SAW-orientation with lowered TCF2 has been found recently [1], the extensive study of this in-plane rotated 33°Y-cut reveals a cubic behavior at elevated temperatures for certain propagation directions. One can bring together this range of orientations with the AT-cut when using the 32 crystal symmetry of quartz. For example, the angles alpha =

90°, beta = -35° for the BAW propagation direction in AT-cut plates (alpha is the rotation angle about the crystallographic Z-axis normal to the plate, beta is the subsequent rotation angle about the new direction of Y-axis after alpha-rotation) correspond to the Euler angles (120°, 125.53°, 44.81°) with a given 1st angle of 120°. Making use of the threefold symmetry of quartz this is equivalent to (0°, 125.53°, 44.81°) which is very close to the SAW orientations of [1]. Apparently, the absolutely uncommon use of 120° as a first Euler angle for a SAW-cut is the reason for the lack of understanding the identity of the mentioned temperature stable BAW and SAW directions.

The demonstrated link between BAW- and SAW-orientations provides a basis for future search for temperature stable SAW-cuts in quartz and of other single crystals of quartz-like temperature behavior like the members of the langasite group or of quartz-type crystals.

[1] S. Kanna, K. Iizawa, T. Yamazaki, and M. Takagi. Temperature stability of surface acoustic wave resonators on the in-plane rotated 33°Y-cut quartz, in Proc. 2002 IEEE Ultrasonics Symp., pp. 98-101.

5H-2 8:45 a.m.
EXPERIMENTAL AND PREDICTED TCD AND SAW PARAMETERS ON LGT [0°, 132°, Ψ] SUBSTRATES.

N. SALDANHA*[1], D. PUCCIO[1], M. PEREIRA DA CUNHA[2], and D. C. MALOCHA[1], [1]University of Central Florida, Orlando, [2]University of Maine, Orno.
Corresponding e-mail: nsaldanh@ucf.edu

The recent investigations of LGT have shown that it has several attractive properties in comparison to quartz, such as higher electromechanical coupling, lower phase velocity and higher temperature of operation. It has been previously shown that LGT with Euler angles [0°, 132°, 31°] has a turnover temperature of approximately 135°C [1], which is a desirable property for devices working at relatively high temperatures, such as sensors. In this work, characterization of the LGT Y-132° cut was performed, versus propagation angle and electrode metallization, to explore its use at elevated operating temperatures. Theoretical predictions of LGT SAW temperature behavior have been previously made from extracted temperature coefficient constants made around room temperature. It has been found that the agreement between temperature predictions and measurements is poor based on extrapolation, and experimental data was required to determine SAW temperature properties. In this work, scattering parameters are measured over temperature utilizing on wafer RF probing. The temperature fractional frequency variation ($\Delta f/fo$) and temperature coefficient of delay (TCD), power flow angle, coupling and velocity for various propagation angles of LGT on the plane with Euler angles [0°, 132°,Ψ] are presented. The results show a fairly large variation of turnover temperature, in the range of 70°C to 200°C, as well as variation of other important SAW parameters.

Finally, several SAW resonators were analyzed and designed using the extracted SAW material parameters in a COM model. A comparison of the predicted and measured device performance is made and shows good correlation. Three different types of metallization were used in SAW resonators: (1) regular Al

electrodes; and two other types to reduce diffusion effects at higher temperatures, namely (2) the sandwiched metal layered type, which includes titanium, copper, aluminum and gold; and (3) platinum over zirconium. Measured results of the various devices and parameters will be presented and compared to predictions.

References:

[1] M. Pereira da Cunha and D.C. Malocha, ″Experimental and Predicted SAW Temperature Behavior of Langatate,″ in Proc. IEEE Ultrasonics Symposium, 2000, pp. 245-248

5H-3 9:00 a.m.
SILICON PHONONIC CRYSTAL FOR SURFACE ACOUSTIC WAVES.

S. BENCHABANE*[1], A. KHELIF[1], W. DANIAU[1], L. ROBERT[1], V. PÉTRINI[1], B. ASSOUAR[2], B. VINCENT[2], O. ELMAZRIA[2], J. KRÜGER[3], and V. LAUDE[1], [1]Institut FEMTO-ST, Département LPMO, Besançon, France, [2]LPMIA, Nancy, France, [3]University of Sarrebrück, Sarrebrück, Germany.
Corresponding e-mail: abdelkrim.khelif@femto-st.fr

Phononic crystals are periodic structures made of materials with different elastic properties. Under specific geometrical conditions, these structures exhibit full band gaps in which no elastic wave, whatever its polarization and wave vector, can propagate. They will find applications wherever perfect mirrors reflecting all incident energy or wave traps (guides and resonators) from which acoustic waves can not escape are needed. They bear strong analogies with photonic crystals which operate on electromagnetic and optical waves.

In this work, we study the surface-acoustic-wave (SAW) propagation in a two-dimensional phononic crystal fabricated in silicon by surface micromachining techniques. The phononic crystal has a square lattice with void circular inclusions. It was fabricated using deep reactive ion etching (RIE) of silicon using the Bosch method. The holes have a diameter of 15 microns and the pitch is 20 microns, resulting in a filling fraction of 50 %. A full band gap for bulk waves with a fractional bandwidth of 30 % is found by simulation. Generally, the band gaps for bulk waves propagating in the plane of the surface coincide with the band gaps for surface acoustic wave. The phononic crystal is characterized experimentally in two ways. The first experiment is based on the deposition of a piezoelectric thin film on top of the micromachined silicon substrate, and the subsequent generation and detection of surface acoustic waves by interdigital transducers. This electrical characterization gives the transmission coefficient of the finite structure. The second experiment is based on Brillouin light scattering and characterizes the propagation of the phonon modes along the surface of the structure. It measures directly the band structure of the phononic crystal.

5H-4 9:15 a.m.
CHARACTERIZATION OF BONDED WAFER FOR RF FILTERS WITH REDUCED TCF.

B. ABBOTT*[1] and N. NAUMENKO[2], [1]Sawtek, Inc., Apopka, FL, [2]Moscow Steel and Alloys Institute, Moscow, Russia.
Corresponding e-mail: bpabbott@sawtek.com

Cellular handsets manufacturers continue to add features to their phones. To accomplish this, existing materials of the phone must be eliminated or reduced in size. Over the last several years this trend has resulted in ceramic duplexers, below 1GHz, being displaced by SAW duplexers. Recently, this trend has initiated the displacement of ceramic duplexers by FBAR and SAW duplexers for frequencies approaching 2GHz.

In order for SAW duplexers, in the 2GHz range, to successfully meet the stringent requirements of insertion loss and skirt steepness, new technologies are required to reduce the temperature coefficient of frequency (TCF).

SAW duplexer manufacturers are aggressively pursuing different methods to accomplish this reduction in TCF, at the wafer level. Their methods will necessarily result in changes to other properties of importance to duplexer design.

This paper examines the effect on bonding of Lithium Tantalate (LT) to Silicon has on the properties of the leaky SAW. The specific structure to be considered is aluminum electrodes on a wafer constituted by 3 layers of media, LT / SiO_2 / Si. The effect of the thicknesses of both LT and SiO2 on the properties of the leaky SAW are examined. These properties include coupling, capacitance, propagation loss (leakage), SAW velocity, etc.

Empirical data on the degree by which the TCF has been reduced in filters is included.

5H-5 9:30 a.m.
NEW THEORETICAL AND EXPERIMENTAL RESULTS ON HIGH FREQUENCY SURFACE ACOUSTIC WAVES EXCITED ON ORIENTED LINBO3 SINGLE CRYSTAL LAYERS TRANSFERRED ONTO SILICON.

T. PASTUREAUD[2], B. BIASSE[3], B. ASPAR[3], W. DANIAU[1], W. STEICHEN[2], V. LAUDE[1], R. LARDAT[2], A. LAENS[2], J.-B. BRIOT[2], J.-M. FRIEDT[1], and S. BALLANDRAS*[1], [1]FEMTO-ST, CNRS, Besançon, France, [2]TEMEX, Sophia Antipolis, France, [3]CEA-DRT-LETI, Grenoble, France.
Corresponding e-mail: ballandr@femto-st.fr

Previous work has shown the possibility to transfer thin layers of oriented single crystal LiNbO3 onto silicon. A process has been developed by the CEA-Léti to transfer a Y-cut LiNbO3 thin layer (0.5 µm) onto (100) Silicon, based on the association of a ion implantation and molecular bonding. Combining LiNbO3 and Silicon is particularly attractive for the excitation and propagation of strongly coupled transverse modes. Theoretical predictions as well as experimental measurements of the Rayleigh-like and shear waves on a 4" LiNbO3(YX)/Silicon

wafer operating at 1 GHz already have been presented and compared to the state of the art. These preliminary results have shown that this kind of wave-guide represent the most efficient approach for the excitation of guided elastic wave in the RF domain.

Considering theoretical predictions, one can expect a factor of 2 for the coupling and reflection coefficients when exploiting the shear mode at 2 GHz. As a consequence, a new set of resonators has been fabricated on our substrates to reach the expected optimal working point. As in previous experiments, the tested devices consist in single-port synchronous resonators. The mechanical period p was 1 µm, and 3 metallization ratio have been tested (0,4 ; 0,5 ; 0,6) to point out the influence of this parameter on the wave characteristics. The electrode height was set to 100 nm, and an acoustic aperture of 100 µm was chosen to get reed of any unwanted diffraction effect. As expected, the shear mode electromechanical coupling and reflection coefficients are doubled. Also the Rayleigh-like wave properties change significantly : the coupling clearly decreases whereas the reflection coefficient increases. A revision of the theory-experiment assessment enables us to point out that the obtained results may be considered insufficient if the silicon wafer actually exhibits a dielectric nature (i.e. a resistivity close to 1000 Ω.cm), which is not the case in our experiments since the wafer resisitivity was about 14 Ω.cm. Comparing now the experimental results with theoretical predictions assuming the substrate conductive yields an improved agreement between theory and measurements. These new results at 2 GHz (theoretical coupling equal to 14 %, 12.5% measured and 15% for the theoretical and experimental reflection coefficient) clearly prove the interest of the method.

This work was supported by the RNRT (French Research and Education Ministery)

5H-6 9:45 a.m.
ELECTRO-ACOUSTICAL CONSTANTS AND REIGHLY SAW PROPAGATION CHARACTERISTICS OF RARE-CALCIUM OXOBORATE SINGLE CRYSTALS.

T. SHIOSAKI*[1], H. SHIMIZU[1], A. KONDO[1], M. NISHIDA[2], H. TAKEDA[1], and T. NISHIDA[1], [1]Garaduate School of Materials Science, Nara Institute of Science and Technology (NAIST), Ikoma, Nara, Japan, [2]Research Development Division, Sakai Chemical Industry Co., Ltd, Sakai, Osaka, Japan.
Corresponding e-mail: s-hiroyu@ms.naist.jp

Rare-earth calcium oxoborate, $RCa_4O(BO_3)_3$ (*R* = La-Lu, Y; *R*COB), single crystals belong to the monoclinic symmetry, the point group *m* and space group *Cm*. We have paid attention to their piezoelectric and SAW properties from previous reports that GdCOB (*R*=Gd) and YCOB (*R*=Y) crystals exhibit excellent non-linear optical properties. In a previous work, we suggested a determination process (cuts and vibration modes) of electro-acoustical constants (ε, *s*, *d*) for monoclinic crystals of point group *m*. Moreover, we reported 27 independent constants of LaCOB (*R*=La) crystals and their SAW properties investigated by experimental evaluations [1]. However, the determination process included two

improvements in 1) evaluation of d_{11} and d_{33} by resonant measurement using longitudinal effect thickness-extensional mode of bar resonators with high leak of electrical induction and 2) use of longitudinal effect thickness-shear mode generated at high frequency. On the basis of them, we investigated use of d_{33} meter (PM100: PIEZOTEST) for d_{11} and d_{33} in order to improve 1) and transverse effect face-shear mode generated at lower frequency for elastic compliances except for s_{11}^E, s_{22}^E, s_{33}^E in order to do 2). In this study, we report electro-acoustical constants and theoretical analysis of Reighly SAW propagation characteristics in LaCOB, GdCOB and YCOB crystals. We used three vibration modes (transverse effect length-extensional, transverse effect face-shear and longitudinal effect thickness-extensional) and 15 cuts in each crystal. All constants in both LaCOB and GdCOB crystals were obtained and six of 27 constants in YCOB were done until now. As a result, it was revealed that dielectric constants $\varepsilon_{11}^T/\varepsilon_0$, $\varepsilon_{22}^T/\varepsilon_0$, $\varepsilon_{33}^T/\varepsilon_0$ at 25°C increased systematically with increasing ionic radius of *R*-site ion (Y: 0.1019 nm, Gd: 0.1053 nm, La: 0.116 nm). Absolute values of $\varepsilon_{11}^T/\varepsilon_0$ in each crystal (La: 9.87, Gd: 9.45, Y: 9.19) were almost the same as those of $\varepsilon_{33}^T/\varepsilon_0$ (La: 9.87, Gd: 9.27, Y: 9.19). On the other hand, $\varepsilon_{22}^T/\varepsilon_0$ in each crystal (La: 14.3, Gd: 12.98, Y: 11.43) increased more conspicuously than $\varepsilon_{11}^T/\varepsilon_0$ and $\varepsilon_{33}^T/\varepsilon_0$ with the increasing. Moreover, it was also revealed that elastic compliance s_{11}^E, s_{22}^E, s_{33}^E at 25°C increased with the increasing. In other words, diagonal components of elastic compliance matrixes in YCOB crystals are the smallest in *R*COB series. This is associated with the result that SAW velocity 3850m/s of YCOB crystal (*Y* cut at *X*-axis propagation) is the largest in *R*COB series. Reighly SAWs velocities were calculated at fundamental crystalline cuts and propagation directions. From the dependence on propagation direction at *Z* cut of LaCOB, the Reighly SAWs velocities *v* of 3150m/s and 3200m/s were obtained at *X*-axis propagation from measured and theoretical results, respectively. The coupling factors k^2 of 0.12% and 0.20% were obtained at *X*-axis propagation from measured and theoretical results, respectively. The results at other cuts are also reported, and propagation modes are discussed. [1] H.Shimizu et al., Proc. 2004 IEEE Ultrasonics Symp., p.1218

Session: 6H
ENERGY HARVESTING & NOVEL TRANSDUCERS
Chair: Y. Takeuchi
Kagoshima University

6H-1 8:30 a.m.
PIEZOELECTRIC MICRO-MACHINED ULTRASONIC TRANSDUCER (PMUT)FOR ENERGY HARVESTING.

K. DOGHECHE*[1], B. CAVALLIER[1], P. DELOBELLE[1], L. HIRSINGER[1], E. CATTAN[2], D. RÈMIENS[2], M. MARZENCKI[3], B. CHARLOT[3], S. BASROUR[3], and S. BALLANDRAS[1], [1]FEMTO-ST, CNRS, Besançon, France, [2]IEMN, CNRS, Villeneuve d'Ascq, France, [3]TIMA, CNRS, Grenoble, France.
Corresponding e-mail: ballandr@femto-st.fr

Micro-electromechanical devices dedicated to energy scavenging purpose have yield an increasing interest for a few years. In this paper we report on the fabrication of PZT/Si piezoelectric micro-machined ultrasonic transducers (pMUT) first designed to ultrasonic imaging applications that may be used as a mechanical to electrical energy transformer for energy harvesting. This work aims to demonstrate the ability of pMUT to convert inertial energy into electrical energy through the piezoelectric layer deposited atop silicon membrane. The diameter of the membrane ranges from 132 µm to 600 µm and the thickness of silicon and PZT are respectively set to 1 and 2 µm. It is shown that the membrane exhibit a deformed shape, as the PZT is under lateral compression, with a maximum deflection equal to more than 1.5 times the equivalent membrane thickness. We first aimed to design a bistable micro power generator as the device could take two stable states that respectively corresponds to the case of PZT under lateral compression and the case of PZT under lateral extension (the symmetric deformation state). First experiments consist in testing the capability of the pMUT to change from one state to the other by a simple and weak mechanical excitation ranging from 0.5g to 2g acceleration.

The experiment results have demonstrated two typical mechanical behaviours, linear (elastic) and non-linear (bistable). The pMUT device can generate electricity along both mechanical behaviours. The elastic mode has been emphasized as we observed different levels of generated voltages corresponding to different levels of mechanical excitation. The membrane is presumably deformed by the inertial excitation at a level less or equal than the threshold enabling to change state. In this case the membrane should then return to its initial stable state along an elastic behaviour. The bistable behaviour has been emphasized as we observed two state changes, i.e. two very sharp opposite and equal signals (larger than 180 mV on a 1 MΩ input impedance oscilloscope), corresponding to the stress inversion (compression to extension and extension to compression) with both respective flow of generated electrical charges. It should be noted that first results were limited by air damping and electrical damping. As a consequence we have developed a piezoelectric finite element model that takes into account the electrical load in the pMUT design. Further simulations with this finite element model should enable to optimize the impedance load of the pMUT for harvesting the maximum electrical energy.

6H-2 8:45 a.m.
ENERGY HARVESTING USING VIBRATING STRUCTURES EXCITED BY SHOCK.

B. CAVALLIER*, P. BERTHELOT, H. NOUIRA, E. FOLTÊTE, L. HIRSINGER, and S. BALLANDRAS, FEMTO-ST, CNRS, Besançon, France.
Corresponding e-mail: ballandr@femto-st.fr

Energy scavenging research shows a growing interest these last years. This paper aims to demonstrate the ability of micro-machined vibrating structures to store mechanical energy and then to convert it into electrical energy through a piezoelectric plate. Such a micro power generator may be used as a mechanical to electrical energy transformer. The energy conversion consists in a mechanical shock enabling to convert low vibrating energy levels at very low frequencies

(typically below 10 Hz for human being excitation source) to mechanical energy to the vibrating structure for which resonant frequencies are ranging from 10 kHz to 1 MHz. Moreover this basic low frequencies to high frequencies spectrum conversion enables to avoid frequency tuning designing that is required for adapting the frequency spectrum of the excitation source.

Preliminary results demonstrate that more mechanical energy can be harvested if we insert a vibrating beam in the system. Along this approach, we proposed a so-called bell concept by using a silicon cantilever as vibrating energy storage element and mechanical shock as an excitation source. The contribution of the silicon beam has been clearly experimentally pointed out. A new set of experiments has then been undertaken in order to increase the harvested power. We focused on three improvements : first, the vibrating parts of the new device (beryllium bronze and silicon with high intrinsic mechanical quality factors) are mechanically isolated from the packages by two or three contact points to minimize clamping losses. Second, the micro power generator has been packaged under vacuum to enlarge the signal amplitude and the mechanical quality factor by eliminating air damping. Furthermore it should be noted that no attempt was made to match impedance of the piezoelectric system in the first set of experiments. The corresponding electrical damping could be an issue as we try to scavenge low vibration energy levels. As a consequence we have developed a piezoelectric finite element model that takes into account the electrical load in the piezoelectric design. Third the load impedance has been optimized using this finite element model to harvest the maximum electrical energy.

This work has been funded by the European Commission through a research project VIBES (IST-1-507911) (VIBration Energy Scavenging) of the 6th Framework Program.

6H-3 9:00 a.m.
PREDICTIVE ENERGY HARVESTING FROM MECHANICAL VIBRATION USING CIRCULAR PIEZOELECTRIC MEMBRANE.

E MINAZARA*[1], D VASIC[1], F COSTA[1], and G POULIN[2], [1]Système et Applications des Technologies de l'Information et de l'Energie (SATIE), ENS Cachan, 61 av. du Pr$/egrave;sident Wilson, 94235 Cachan cedex, FRANCE, [2]Laboratoire d'Automatique de Grenoble (LAG), LAG - ENSIEG, Domaine Universitaire, BP 46, 38400 Saint Martin d'Hères - FRANCE.
Corresponding e-mail: minazara@satie.ens-cachan.fr

The use of piezoelectric materials in acoustic or electro-mechanic systems is not new but it remained confined in actuator or sensor applications. With the increase of wireless devices, their quality as generator begins to interest many researchers. Because more and more devices are wireless, it becomes necessary to conceive their own power supply. For instance, wireless sensors can be placed in very isolated locations, if the energy of surrouding vibration (for example the vibrations of a bridge) could be harvested, the battery could be reloaded and should not be replaced regularly. This study investigate the ability

of recovering the electrical energy from mechanical vibrations in dynamic environment by using a circular unimorph piezoelectric membrane.The transducer consists of two layers(PZT/brass). For a small magnitude of vibration, a classic massive piezoelectric transducer cannot give a correct performance because the deformation is very small. In this regard, we have chosen to use a transducer working with flexion vibrations. In these conditions, a very small vibration amplitude can bring a consequent deformation of the membrane which consequently would generate a significant electrical energy.

The mechanical and electrical behaviours of the piezoelectric membrane are expressed by using Hooke's law, strength material theory, vibration theory and two linearized constitutive equations namely direct and converse piezoelectric effect. Matrix notations are used in order to facilitate the model′s implementation. A relation between the acceleration and the voltage, respectively the input and the output of the model, was carried out. The model enabled us to express the resonance frequencies, to plot the deflexion and strain shapes of the membrane. We have also established the electric equivalent circuit of the transducer, the output electrical impedance and the voltage gain as well as the predicted power harvested in dynamic operating mode. Over all, the model has enabled us to design easily the transducer's dimensions.

Experiments were performed using a membrane whose total weight is around 6 grams, total radius is R=20.5mm, PZT radius is RP=11.5mm, brass thickness is hb=400mm and PZT thickness is hp=230mm. The brass layer is embedded in a bulky metal chassis all around the circumference by epoxy adhesive. Power versus frequency, resistive load and acceleration were plotted. A power of 2mW was recovered at the resonance frequency of the membrane (2.1kHz) across a 10kW optimal resistor, for a 3.4g acceleration which corresponds to a 0.16N effort in relation with the weight of the membrane. Experimental results reveal that our analytical approach is compatible with measurements. At last, some suggestions are given in order to improve the amount of energy harvested.

This work is financial support by SATIE laboratory (Système et Applications des Technologies de l'Information et de l'Energie)

6H-4 9:15 a.m.
A COMPARISON OF PIEZOELECTRIC AND ELECTROSTATIC ELECTROMECHANICAL COUPLING FOR ULTRASONIC TRANSDUCTION AND POWER GENERATION.

M. ANDERSON*[1], C. RICHARDS[2], D. BAHR[2], and R. RICHARDS[2], [1]University of Idaho, Moscow, ID, [2]Washington State University, Pullman, WA.
Corresponding e-mail: anderson@uidaho.edu

Electrostatic and piezoelectric electromechanical coupling are employed in miniature devices to produce ultrasonic waves or generate power. It has been pointed out in the technical literature that in principle electrostatic devices can be designed to have an electromechanical coupling factor of nearly 100%, while it is thought that the upper limit for piezoelectric devices is significantly smaller. We have recently developed a closed-form model of a thin-film piezoelectric

device to predict the performance of membrane piezoelectric energy converters. The model was used to identify several key design and process parameters that have a substantial effect on electromechanical coupling. This model is general enough to allow a comparison of the two technologies, electrostatics and piezoelectrics, at a lower level of detail. In this paper, the model is used to compare the components of the electromechanical coupling factor; capacitance, stiffness, and actuation force, for the two energy conversion technologies. The comparison shows that the capacitance and actuation force coefficient are drastically different for the two technologies, and are controlled by fundamental material properties and device geometries. Consequences of the differences for the design of ultrasonic transducers and power generation devices are discussed.

6H-5 9:30 a.m.
ADAPTING A CMUT TRANSDUCER TO DETECT ACOUSTIC EMISSIONS.

D. OZEVIN[2], S. PESSIKI[2], D. GREVE*[1], and I. OPPENHEIM[1], [1]Carnegie Mellon University, Pittsburgh, PA, [2]Lehigh University, Bethlehem, PA.
Corresponding e-mail: dg07@andrew.cmu.edu

Acoustic emissions are ultrasonic pulses produced in solids when irreversible damage, such as material yielding or crack extension, occurs under mechanical loading. The most common acoustic emission transducer is an underdamped resonant PZT device. The acoustic emission pulse causes a signal from which the number of counts or crossings of a threshold level are used to quantify the intensity of the acoustic emission event. cMUT transducers usually detect ultrasonic waves incident on the flexible diaphragm, causing that diaphragm to deflect with respect to a fixed substrate, but in this novel application the ultrasonic energy is coupled to the substrate. We report on the design, fabrication, and experimental demonstration of a cMUT transducer specifically designed for measurement of acoustic emission events by detecting ultrasonic waves in the 100 kHz to 1 MHz range. This application requires a very different device design, underdamped and lower in resonant frequency than a cMUT intended for high frequency imaging. By appropriate spacing of etch release holes, we have engineered surface micro-machined MEMS devices that exhibit a behavior similar to the commercial acoustic emission PZT transducers. We have fabricated seven resonant devices on a single MEMS chip, a capability which cannot be matched by single-channel commercial transducers. Spring-supported plates and diaphragms that are underdamped in air with resonant frequencies ranging from 100 kHz to 1 MHz have been fabricated on a chip 1 cm2 in area. Individual transducers were 6.97 mm2 in area and had Q factors ranging from 2.4 (100 kHz) to 22 (1065 kHz). DC bias (typically 5-10 volts) is applied between a plate on the substrate and a suspended plate; vibration of the suspended plate causes a time-varying current, in a similar manner to a cMUT device used for ultrasonic detection. The completed sensor array has been comparison-tested with a commercial acoustic emission transducer (Physical Acoustics Corporation). The cMUT chip and the conventional acoustic emission transducer were attached to a pre-cracked rectangular steel beam specimen 76 cm in length that was loaded

in 4-point bending in a testing machine. Signals from five different cMUT transducers were collected along with the signal from the conventional transducer. Following 20X amplification, the cMUT signals were 10-20 mV in amplitude, and the threshold level for event counting was set at 5.5 mV. Strong acoustic emission events were detected by both types of transducers. Some weaker acoustic emission events (about 40% of the events prior to the first load drop at 23 kN) were not detected by the cMUT transducers due to the high noise levels associated with non-optimal electronics. With improved interface electronics, the cMUT acoustic emission transducer will have comparable sensitivity to PZT transducers. Multiple transducers with different resonant frequencies in one small package provide for redundant detection, and the additional information obtained from transducers with varying resonant frequency will help distinguish acoustic emission events from artifacts such as mechanical noise at support locations.

Properties of resonant transducers

transducer	area [mm2]	resonant frequency [kHz]	Q factor
A	7.23	100	2.4
B	7.16	138	3.2
C	6.73	188	4.4
D	6.32	262	6.2
E	7.51	365	8.7
F	7.53	11.9	501
G	6.29	22.3	1065

6H-6 9:45 a.m.
DNA MICROARRAY FABRICATION USING DIRECTIONAL SELF-FOCUSING ACOUSTIC TRANSDUCER ARRAY.

S. KAMAL-BAHL* and E. SOK KIM, University of Southern California, University of Southern California, Los Angeles, CA 90089, USA.
Corresponding e-mail: kamalbah@usc.edu

This paper presents an ultrasonic, nozzleless ejector array for synthesizing DNA sequences on substrates such as glass, plastic or silicon. A four mer DNA sequence is synthesized by ejecting droplets of DNA bases with an array of self-focusing acoustic transducers (SFATs). An SFAT achieves focusing of the acoustic waves through constructive interference of the waves produced by a phased electrode pattern of annular rings. When a pie sector of the annular ring pattern is cut, the SFAT produces directional ejection of liquid droplets.

A directional SFAT array has been integrated with microchannels and reservoirs for DNA synthesis as follows. After depositing and patterning 0.8μm thick LPCVD SiNx on a silicon wafer, we etch 100μm thick silicon for the active area with KOH, followed by another patterning of the SiNx to open windows for the reservoir areas. The wafer is etched further in KOH to form the silicon nitride diaphragm for the SFAT. The ejectors and reservoirs on chip are connected through microfluidic channels formed using XeF2 isotropic etching. After forming the channels, the SFAT device is fabricated using 0.3μm thick Al, 5μm thick ZnO, and then 0.3μm Al. Finally, the directional SFAT array, channels and reservoirs are covered with 8μm thick parylene with a 200μm diameter opening. The opening is to allow micron sized droplets to be ejected, but is not too large to avoid fast evaporation of the DNA bases during the synthesis process.

A 500MHz sinusoidal signal (corresponding to the resonant frequency of the piezoelectric film in SFAT) is pulsed for 10μsec pulsewidth with a high-speed switch, amplified and passed through an impedance matching network before being applied to the SFATs. A CCD camera with a microscope placed horizontally records the ejection process as an LED is turned on and off stroboscopically.

Activated monomers initially contained in the reservoir are automatically brought to the SFAT through microchannels, and ejected by the SFAT onto a target glass slide. Then the target glass with the mounting station is moved to a wash/dry area to be treated with capping solution, which blocks out the nucleotides that have failed to couple using the standard phosphormidite chemistry. We use a mechanical hinge on the mounting station to avoid the need for alignment of the glass slide with the directional SFAT array each time it is placed over it.

Repeating the above steps n times produces n-mer DNA probes. A Cy3 fluorescence dye is added at the last step to the synthesized DNA. Before fluorescence imaging, the glass slide is washed thoroughly with acetonitrile and dried to remove any residues of the dye attached to the glass substrate. Fluorescence microscopy confirms that DNA has been properly synthesized. DNA hybridization and mass spectrometry are currently being used to confirm the sequence order.

The SFAT array integrated with microfluidic components described in this paper demonstrates the feasibility of a portable DNA synthesis system which allows the geneticist to synthesize any DNA sequence within hours using a computer program at an affordable cost in their own labs.

POSTER SESSIONS

Session: P3A

BEAMFORMING
Chair: J. Hossack
University of Virginia

P3A-1

FAST 3D SIMULATION OF 2ND HARMONIC ULTRASOUND FIELD FROM ARBITRARY TRANSDUCER GEOMETRIES.

S. DURSUN*, T. VARSLOT, T. JOHANSEN, B. ANGELSEN, and H. TORP, Norwegian University of Science and Technology, Trondheim, Norway.
Corresponding e-mail: dursun@stud.ntnu.no

A method for fast numerical simulation of nonlinear wave propagation based on a quasi-linear approximation has previously been presented. In the current study this method has been further developed to yield correct levels of the second-harmonic wave. The method can be used for 3D simulations of second-harmonic fields from arbitrarily transducer geometries. The method has been validated by comparing simulations to results produced by a conventional nonlinear simulation model and to experimental measurements. It has also been compared to a closed-form approximation of the acoustic field in the focal zone.

The reference simulation model was a numerical solution of the KZK equation for a forward-propagating pulse using a operator splitting approach.

Experimental verifications were performed with hydrophone measurements in a water tank. An annular array probe (Vingmed Sound APAT 3.25) with diameter 14.7 mm and ROC=78 mm transmitting at 2.9MHz was used. Experiments were performed for 6 different pressure amplitudes with focal pressures ranging from 0.2MPa to 5MPa. Simulations were performed for the same experimental setup.

Beam profiles and spatial peak pulse averages at the first— and second-harmonic frequency, respectively, were found by filtering the hydrophone signal to a bandwidth of 2MHz. Since the quasi-linear approximation is based on the squared linear field, the amplitude of the second-harmonic field as a function of the transmitted pressure amplitude will increase quadratically, and the simulation will be over estimated for high pressures. The level of the second-harmonic was found, and the relation second-harmonic/first-harmonic was over estimated by less than 2dB for focal pressures up to 1MPa.

Comparisons of the power spectra also showed good agreement for focal pressures up to 1MPa.

The pulse forms were compared, and they were found to be similar for low pressure amplitudes. For higher pressure amplitudes the overestimated second-harmonic field produced some pulse distortion. However, these experiments were performed in water where attenuation of harmonic frequency components

is low. Thus the results represent a worst-case situation for the quasi-linear approximation.

P3A-2
VELOCITY SENSITIVITY MAPPING IN TISSUE DOPPLER IMAGING.

S. AASE*, T. BJÅSTAD, and H. TORP, Department of Circulation and Medical Imaging, Faculty of Medicine, Norwegian University of Science and Technology, Trondheim, Norway.
Corresponding e-mail: sveinaaa@ntnu.no

Tissue Doppler Imaging (TDI) offers simultaneous measurement of velocity and velocity gradients across large parts of the myocardium. Estimating velocity, for instance by the autocorrelation method, results in a weighted averaged Doppler shift originating from an area with relatively large lateral span. The weights are determined by the transducer's pulse echo response and the backscatter coefficients. With tissue Doppler velocity estimation, the backscatter coefficients have a rather large dynamical range. This may cause scatterers from far outside the intended sample volume to contribute to the velocity estimates, especially in areas with weak scattering.

This problem is enhanced when using several parallel receive beams for each transmit beam due to misalignment of the transmit and receive beams. In the worst case, a receive beam is steered to a position midway between two transmit beams. In this work a new method for visualizing the velocity sensitivity region (VSR) influencing the velocity estimate in tissue Doppler imaging is presented. Using this new velocity sensitivity mapping (VSM) method, the extent of the VSR in several tissue Doppler setups was investigated. By using a B-mode image as a scattering coefficient object and combining it with the pulse echo response of a possible TDI scan, a map of the spatial contribution to the velocity estimate was calculated. B-mode images of the left ventricle were recorded using a Vivid 7 scanner with the M3S probe. The pulse echo responses of several possible TDI scan settings were simulated using Field II.

One of the TDI scan settings used in the simulations had a sector of 75° and focus at 13 cm, enough to image an adult left ventricle. With five transmit beams the worst case receive beam had a 7.5° offset compared to the transmit beam. This corresponded to the first side-lobe of the transmit beam. With such settings, the two-way beam profile was only 11 dB higher in the receive direction compared to the transmit direction. In the recorded B-mode images the intensity signal of the pericardium was 15 dB higher than the intensity signal from myocardium. When the transmit beam direction covered pericardium and the corresponding worst case receive direction covered myocardium, signal from the pericardium contributed 4 dB more than the signal from the myocardium (receive direction). Using apodisation on receive, the signal from myocardium was 22 dB above the signal from pericardium. The improvement due to apodisation was also clearly visualized with the VSM method. Without apodisation the VSR extended laterally into the pericardium. With apodisation, the VSR was reduced considerably and stayed focused at myocard. Wider transmit beams were also investigated, but were found impractical due to low SNR.

The VSM method can be used to quickly evaluate signal contribution at spatial positions in a TVI scan using clinical B-mode images as scattering coefficient objects. For situations with large receive beam offset to the transmit beam, receive apodisation can reduce the lateral region which affects the estimated velocity.

P3A-3
COMPARING INTERPOLATION SCHEMES IN DYNAMIC RECEIVE ULTRASOUND BEAMFORMING.

J. KORTBEK*[1,2], H. ANDRESEN[1], K. GAMMELMARK[2], and J. JENSEN[1], [1]Technical University of Denmark, Lyngby, Denmark, [2]B-K Medical, Herlev, Denmark.
Corresponding e-mail: jk@oersted.dtu.dk

In medical ultrasound receive focusing is a core signal processing element used for reconstruction of image points from the received transducer signals, in both conventional and synthetic aperture imaging. In the delay-and-sum beamformer a sample is selected from each of the receive channels corresponding to the echo of the image point target. The sample index is based on the total transmit-receive time-of-flight. Due to the continuous nature of the time-of-flight it will not necessarily intersect with the discrete time indices of the sampled channel data. Thus, some form of interpolation is needed and this heavily influences the image quality and the hardware complexity for implementation.

This paper introduces the beamformation toolbox, BFT2 developed at CFU and investigates the consequences of the choice of interpolation scheme by means of ultrasound simulations of point scatterers in Field II. BFT2 is written in C and has a Matlab user interface. It performs dynamic receive focusing and offers choices between static or dynamic apodization and various interpolation schemes. The interpolation schemes investigated include linear, polynomial, cubic spline and finally upsampling and FIR filtering, with an upsampling factor of 8. Various order polynomials and FIR filters are investigated.

The investigation includes conventional B-mode imaging and synthetic aperture imaging (SA), both using a 192-element, 7 MHz linear array transducer with λ pitch as simulation model and both imaging types comprise 129 image lines. For the evaluation a reference data set is obtained by running all simulations in Field II with a sampling frequency of 1 GHz. The evaluation data is created by decimating the reference data to a sampling frequency of 40 MHz. The evaluation is performed by calculating the full-width-half-maximum (FWHM), the side lobe to main lobe ratio, (SLMLR), and the noise power of the interpolation error. The FWHM and the SLMLR are calculated in the horizontal plane at the depth of each of the point scatterers and compared to the case where the reference data is used.

The FWHM is identical for all interpolation schemes, thus the resolution is not affected by the interpolation. The average SLMLR differences are 7.7 dB, 0.2-4.8 dB and 0.03-6.4 dB for the linear, polynomial, and the upsampling scheme, respectively, when the imaging type is B-mode and 0.15 dB, 0.02-0.35 dB and 0.01 dB when the imaging type is SA. The choice of interpolation thus influences

the contrast of the image. The signal-to-noise ratios for both imaging types are 20 dB for the linear interpolation and between 32 dB and 48 dB for the other interpolation schemes.

By using a proper interpolation scheme it is possible to reduce the sampling frequency and avoid a decrease in performance. When replacing linear interpolation with a more advanced interpolation scheme, a reduction of 7 dB in the SLMLR and an improvement in signal to noise ratio of 28 dB is achieved.

This work was supported by grant 9700883, 9700563 and 26-04-0024 from the Danish Science Foundation and by B-K Medical A/S. The BFT2 toolbox is written by Sara Gustavsson.

P3A-4
FOURIER BBASED IMAGING METHOD WITH STEERED PLANE WAVES AND LIMITED-DIFFRACTION ARRAY BEAMS.

J. CHENG and J.-Y. LU*, The University of Toledo,, Toledo, OH.
Corresponding e-mail: jilu@eng.utoledo.edu

In the past two decades, frequency domain image reconstruction methods have been investigated extensively. Most of these studies are focused on synthetic aperture focusing, which suffers from low transmission power, shallow penetration, and low signal to noise ratio. In some configurations, a mechanical scanning system is required, which limits the achievable frame rate. To overcome drawbacks of synthetic aperture imaging and take advantage of the computation efficiency of the Fast Fourier Transform, a high frame rate imaging method base on limited diffraction beams was proposed where a single plane wave was used in transmission and limited diffraction weightings were used in reception to achieve dynamic receive focusing. Although a high imaging frame rate can be achieved with this method, sidelobe is higher due to the lack of transmission focusing.

In this paper, a Fourier-based imaging method is developed to achieve a variable imaging frame rate. In this method, multiple steered plane waves or limited diffraction array beams are used in transmission and Fast Fourier Transform is applied to received echo signals to construct images of an increased resolution and a lower sidelobe. If one transmission is used, the results produced by the method are similar to those produced by the previous high frame rate method. However, at slightly lower frame rates, image quality may improve significantly. At a lower frame rate such as about 60 frames/s for a depth of 120 mm, the method can construct images with a higher quality than the conventional delay-and-sum method where only one transmission focal distance is allowed to achieve a comparable frame rate.

Both computer simulations and experiments were performed to verify the method. In the experiments, a high frame rate imaging system was used to collect radio-frequency (RF) echo data from an ATS539 tissue-mimicking phantom and from the heart of a healthy volunteer. Images were constructed at different frame rates. The experiment results agree with both the theory and computer simulations.

The authors would like to thank Mr. Jing Wang and Mr. Zhaohui Wang in participating in the in vivo experiments. This work was supported in part by a grant HL 60301 from the National Institute of Health.

P3A-5

ADAPTIVE SIGNAL PROCESSING IN MEDICAL ULTRASOUND BEAMFORMING.

F. VIOLA* and W. F. WALKER, University of Virginia, Charlottesville, VA.
Corresponding e-mail: fv7d@virginia.edu

The application of Wiener filter theory to RADAR and SONAR signal processing led to the development of adaptive beamforming (AB). In AB, the information associated with the data received by an array of sensors is used to determine a set of weights that optimize the beamformer output. The weights are determined by minimizing the energy in the beamsum signal, subject to the constraint that the beamformer must exhibit a given response in the look-direction. The second order statistics of the data are used to generate the weights. These algorithms are able to achieve resolutions far superior to those predicted by diffraction theory, while attaining excellent side and grating lobe reduction. In parallel, a series of adaptive algorithms has also been developed which do not rely on statistical properties of the data and thus can be used on a single realization (or snapshot). In the past fifty years a plethora of algorithms have been developed, each exploiting specific properties of the received data.

In medical ultrasound, bright off-axis targets can seriously degrade image quality by introducing broad image clutter, which would reduce image contrast and resolution. The application of AB can reduce the effects of bright off-axis targets, thus improving the overall image quality. In this paper we apply a subset of adaptive algorithms to ultrasound signals. We have examined statistical AB algorithms such as the Duvall and Frost beamformers, as well as deterministic AB algorithms such as the Single Snapshot Beamformer (SSB) and the Spatial Processing Optimized and Constrained (SPOC) algorithm. These algorithms are well known and recognized in the RADAR/SONAR literature.

We have performed a series of simulations using ultrasound data to test the performance of those algorithms and compare them to the conventional, data independent, beamforming. Every algorithm was applied on single channel ultrasonic data that was generated using Field II. While the Duvall, Frost, and SSB algorithms solve directly for the optimal weights using a linear algebra formulation of the received signal, SPOC takes a different approach. A signal model is first generated to describe the received field from a series of hypothetical sources. The sensors output is then matched to the signal model to solve for the position and intensity of the real sources. For a 64 element linear array operating at 5 MHz, beamplot results show that while the Duvall and SSB beamformers reduce sidelobes by roughly 12 dB, the sidelobes using the Frost algorithm rise by 23dB. Furthermore, the -6dB resolution is improved by 38%, 83%, and 43% in the case of Duvall, Frost, and SSB algorithms, respectively. In the case of SPOC, the imaging field was divided into hypothetical sources separated 20 microns axially and 100 microns laterally. In this case, the beamplot shows a superresolution peak with noise floor at -150 dB. Similar results were

obtained for an array consisting of 32 elements. We also present results that analyze the effects of noise on AB.

This work was supported by the US Army Congressionally Directed Medical Research Program in Breast Cancer grant No. W81XWH-04-1-0590.

P3A-6
COMPUTATION OF STEERED NONLINEAR FIELDS USING OFFSET KZK AXES.

P. D. FOX*[1], A. BOUAKAZ[2], and F. TRANQUART[1], [1]INSERM U619 & CIT, CHU Bretonneau, Tours, Centre, France., [2]INSERM U619, CHU Bretonneau, Tours, Centre, France.
Corresponding e-mail: fox@med.univ-tours.fr

Introduction/Background: Commercial medical scanners utilise electronic beam steering and the second harmonic signals generated by tissue nonlinear processes to form images at the second harmonic frequency. Furthermore, characteristics of nonlinearly generated harmonics within the beam itself contribute to improvements in lateral resolution and quality of the reconstructed image. Fully understanding these harmonic features offers new possibilities for redesigning or optimising array transducers to attain better imaging performances, as well as in other areas such as contrast agent responses and microbubble destruction strategies for drug delivery. However, such an understanding is hindered at present by the computational difficulty in accurately predicting all the nonlinear characteristics of steered beams. This paper addresses this issue, presenting a KZK based method for analysing beams steered at arbitrary angles.

Method: The parabolic KZK equation is often used to study nonlinear characteristics of medical ultrasound beams. This equation is traditionally applied in a propagation direction perpendicular to the surface of the transducer, and has been shown to model the pulse propagation well along the central axis of the transducer [1]. However, its accurate angle of application is restricted to within approximately only 16 degrees away from the central transducer axis due to the underlying approximations employed in the derivation of the KZK equation. This restriction causes a problem for studying steered beams, since typical steering ranges up to the order of 45 degrees away from the transducer centreline. To overcome this problem whilst at the same time exploiting the traditional KZK benefits, we develop an iterative method for displacing the KZK axes away from the central transducer axis to investigate arbitrary beam or field angles of interest.

Results/Conclusions: The implemented algorithm is based on a time domain solution of the KZK equation, on a standard 3GHz PC with 2GB RAM producing runtimes in the order of a few hours per investigation angle. The transducer used is a 64 element linear phased array operating at 1.7MHz (height 10.5 mm, width 0.27mm, kerf 0.065mm) with beam steering at 0 and 45 degrees. Validation of the basic KZK algorithm without steering has been given previously at linear pressures (54kPa) against both experimental measurements and Field II and at nonlinear pressures (700kPa) against measurements described previously in [1]. The KZK axes are swept over a range of angles covering the full spectrum

of -90 to +90 degrees relative to transducer centreline, in order to investigate the entire emitted field for both steered and unsteered beams. Element pitch is then increased to investigate grating lobes. All results are decomposed into first and second harmonic fields to compare relative frequency domain properties. The overall contribution is a better characterisation of linear and nonlinear field characteristics at high angles than is possible with the traditional KZK approach.

[1] IEEE Trans. UFFC, vol. 50(6), pp. 730-735, 2003.

This work was partially sponsored by Le Studium, Orleans, France.

P3A-7
OPTIMIZATION OF FREQUENCY DEPENDENT RECEIVE APODIZATION.

R. SCHWANN*, N. STACHE, and T. G. NOLL, Chair of Electrical Engineering and Computer Systems, Aachen, Germany.
Corresponding e-mail: schwann@eecs.rwth-aachen.de

In conventional pulse-echo ultrasound systems, the echo data from the transducer elements is delayed according to the depth-dependent receive focus and weighted with an apodization factor before the data of all channels are summed up. While the required delay can be calculated from the distance to the focal point, the apodization function has to be optimized with respect to the transducer geometry and the transfer function of the transducer elements.

In this paper, different image quality measures are discussed that allow to quantify the dynamic range and the resolution of an ultrasound system by evaluation of the 2D point spread function.

Two quality measures are chosen that can be easily computed and match the visual inspection of simulated images. With the first one, the dynamic range is measured by the average fill-in of an anechoic region. With the second one, the resolution is measured by a criterion that favors a small mainlobe of the point spread function together with low sidelobe energy. A selection of mainlobe or sidelobe regions by defining image areas or threshold values is not required.

For an automated optimization of the apodization function, the chosen image quality measures are continuous and sufficiently smooth so that a gradient search algorithm can find a global optimum.

Since the apodization function depends on the center frequency of the transducer transfer function, it was assumed that the imaging potential of broadband ultrasound transducers is not fully exploited using a simple apodization factor. Therefore, the apodization factors are replaced by symmetric FIR filters for each beamformer channel to realize a frequency dependent apodization without changing the delay scheme of the dynamic receive beamformer.

An ultrasound simulation tool is used to form the 2D images from the receive data for evaluation. The optimizations are performed using measured ultrasound data from a water tank and using simulated data for comparison.

The signal-to-noise ratio of the proposed imaging scheme is compared to a conventional apodization. It is shown that a symmetric apodization filter with a

low number of taps for each channel of the beamformer is sufficient if it is followed by a single filter after the summation point.

As an example, an optimization accounting for both quality measures was made for a broadband transducer with 5 MHz center frequency and 100% relative bandwidth. The fill-in was reduced by 3.8 dB and the lateral mainlobe width was reduced by a factor of 0.86 using apodization FIR filters of length 3 followed by a single FIR filter of length 11 after the summation point.

Compared to a conventional apodization, the presented beamformer scheme offers a significant improvement in image quality that can be achieved with moderate hardware effort suitable for FPGA based beamformer frontends.

P3A-8

NONLINEAR PULSED PRESSURE FIELD FROM FOCUSED RECTANGULAR APERTURES: EXPERIMENTAL AND NUMERICAL RESULTS.

T. KUJAWSKA*, J. WOJCIK, and A. NOWICKI, Institute of Fundamental Technological Research, Polish Academy of Sciences, Warsaw, Poland.
Corresponding e-mail: tkujaw@ippt.gov.pl

In this paper the nonlinear pulsed acoustic pressure fields from the focused square and rectangular apertures are considered. Experimental results in water of the 4D nonlinear sound field radiated from a 2.8 MHz focused (focal distance F = 80 mm) transducer of a square (20x20 mm) and rectangular (10×25 mm) geometry for various excitation levels (producing the average pressure amplitude of 0.01; 0.1 and 0.2 MPa at the source) are presented. The measurement results are compared with the numerical calculations obtained for the same boundary conditions. The novel numerical algorithm was used to simulate the 4D nonlinear pressure field propagation from nonaxisymmetric focused acoustic sources radiating pulsed waves in the attenuating media. Our theoretical model is based on the Time-Averaged Pressure Envelope (TAPE) method, recently developed in our lab. This method employs the propagated pulsed pressure waveform representation as a quasi-Fourier series, i.e. as a superposition of sinusoidal wavelet-like packets with carrier frequencies equal to harmonics of the initial tone burst, and with envelopes (being functions of space coordinates and time) determined by the TAPE method. The spectrum of the propagating pressure waveform is considered to be a sum of each wavelet spectrum contributions. Our model uses the second-order operator splitting approach with an incremental propagation scheme whereby the effects of combined diffraction and absorption are computed separately from the effects of nonlinear harmonic interactions over incremental steps. The proposed model is free from paraxial approximation, is computationally efficient and capable of predicting the 4D ultrasound field in nonlinear and attenuating media with the arbitrary absorption from pulsed, arbitrary shaped, plane and focused sources (including phased arrays with an angular beam deflection). Using a computational power of a standard PC a computational time required for the full 4D nonlinear field simulation depends on the source dimensions, radiated frequency and excitation level as well as on the medium absorption and nonlinearity strength and can vary from few minutes

to few hours. Comparison between experimental and simulation results clearly show that our numerical model predicts well the structure of the nonlinear ultrasound field for all boundary conditions considered.

The authors thank the National Committee of Scientific Research for the financial support (Grant No 5T07B00924)

Session: P3B

CONTRAST AGENTS II
Chair: W. Wilkening
Ruhr University Bochum

P3B-1

HIGH FREQUENCY CHARACTERISATION OF COMMERCIAL CONTRAST AGENTS.

C. MORAN*, M. BUTLER, V. SBOROS, T. ANDERSON, D. ANDERSON, and W. MCDICKEN, Medical Physics, University of Edinburgh, Edinburgh, United Kingdom.
Corresponding e-mail: carmel.moran@ed.ac.uk

Commercial contrast agents are designed so that the contrast microbubbles resonate at clinically relevant ultrasonic frequencies. However, there is increasing interest in the behaviour of contrast microbubbles at higher frequencies, used for applications such as mouse imaging, despite the fact that these frequencies are far removed from the natural resonance frequency of the microbubbles. At present little data exists on the acoustical properties of the commercial contrast agents at these frequencies. **Aim**: In this work we describe the acoustical characterisation of three commercial contrast agents, Definity (Bristol-Myers Squibb, N. Billerica, MA USA), SonoVue (Bracco International, The Netherlands) and Optison (Amersham Health, UK) over a frequency range of 8 MHz to 28 MHz. **Methods**: The base of an acoustically lined ultrasonic tank was covered with a layer of tissue mimicking material (TMM) and filled with 150ml of degassed water. Each of the three high frequency linear array probes (L8-16, L10-22 and L16-28(prototype)) from a Diasus scanner (Dynamic Imaging Livingston, UK) were mounted over the tank at a distance of 20mm from the surface of the TMM and a frame of ultrasound data collected at 10%, 50% and 90% output powers. In addition the RF ultrasound data was digitised to 8 bits at 250 megasamples/s using a Gage Applied CS8500 data capture card and saved on a PC. 100 μl of each agent was subsequently injected into the 150 ml degassed water and insonated over a period of 90seconds. The ultrasonic data from the first frame and a 90second frame were digitised and saved. This procedure was repeated for three power outputs for each probe. In the analysis two ROIs were chosen. The first was chosen at a distance of 12mm from the probe situated within the contrast pool and the second within the TMM below the contrast pool. A reference reflector was made using a thinly covered layer of paper mounted on a metal slide and used to provide reference echoes at 12mm and 20mm. In addition,

the peak negative pressure was measured at the 12mm depth from all three probes at the three output powers using a 0.2mm membrane hydrophone (Precision Acoustics Ltd, UK). **Results**: Peak negative pressures at maximum power output at 12mm depth were measured as -4.89 MPa, -2.41 MPa and -1.55 MPa for the L8-16, L10-22 and L16-28 probe respectively. All three agents were visualised within the tank at 50% power output over the 8-28MHz frequency range. Maximum backscatter power over the 12mm ROI was achieved by SonoVue at 90% power output (-1.49 dB for probe L8-16, -12.7 dB for probe L10-22 and -21.4 dB for probe L16-28). **Conclusion**: Current commercially available contrast agents can be visualised over a broad range of frequencies beyond their natural resonance frequencies highlighting their potential use for high resolution imaging.

P3B-2

COATING MONODISPERSE MICROBUBBLES FORMED BY A FLOW FOCUSING DEVICE.

E. TALU*, M. LOZANO, P. DAYTON, K. FERRARA, and M. LONGO, University of California, Davis, CA.
Corresponding e-mail: etalu@ucdavis.edu

Lipid-coated microbubbles are important in biomedical applications due to their great potential as ultrasound contrast agents and drug and gene delivery vehicles. Stabilization of microbubbles by lipid coatings creates low-density particles in the field of diagnostic imaging. The solubility of the gas in the microbubble has an important effect on the stability of the microbubble. Microbubbles filled by perfluorocarbon (PFC) gases, which have a higher molecular weight, are more stable in blood than those filled by air. The size and monodispersity are important in diagnostic and therapeutic applications with ultrasound. A new microfluidic device called flow focusing device was designed to mass generate micron size gas bubbles with a perfectly monodisperse and controllable diameter (see for example, Gañán-Calvo and Gordillo, Phys. Rev. Lett., 87, 274501-1 - 274501-4). The stream of gas surrounded by the liquid in the pressure chamber flows out of an orifice of the chamber into a liquid thereby creating monodisperse microbubbles. Uncoated microbubbles of air coming out of the flow focusing device rapidly dissolve or coalesce. Dissolution of the microbubble in an aqueous solution and fluorescence microscopy were combined to study coated microbubbles produced by the flow focusing device. Microbubbles were filled with both air and perfluorobutane gas. The stability and size of the microbubbles was shown by using coulter particle counter. Lipid-coated and air filled microbubbles produced by flow focusing device were stable up to four days.

The authors would like to thank to Dr. Mark Borden for his thoughtful discussions and helpful insight; Gang Pu for his help in fluorescence imaging work. This work was funded by Office of Naval Research Hydromechanics Program.

P3B-3

INVESTIGATING THE POTENTIAL FOR THERMAL DAMAGE POSED BY MICROBUBBLE ULTRASOUND CONTRAST AGENTS: EXPERIMENTAL RESULTS.

E. STRIDE*[1], V. WILKENS[2], and N. SAFFARI[1], [1]University College London, London, UK, [2]Physikalisch-Technische Bundesanstalt, Braunschweig, Germany. Corresponding e-mail: e_stride@meng.ucl.ac.uk

The development of coated microbubble ultrasound contrast agents for use in imaging applications and as carriers in drug and gene delivery applications has intensified the need for a clear understanding of their behaviour and potential bioeffects. Previous studies have focused on the risks posed by unencapsulated bubbles as representing the “worst case scenario”. They have concluded that the risk of thermal damage should be minimal, provided the threshold for inertial cavitation is not exceeded. However, these treatments have ignored the heating effects due to viscous dissipation in the coatings of contrast agent particles. The results from theoretical simulations by the authors indicate that the temperature rise due to this process may be sufficient to generate harmful bio-effects even under conventionally “safe” insonation conditions.

The aim of this work was to make a preliminary experimental examination of the heating effect generated by contrast agents under diagnostic imaging conditions. Fine wire metal resistance thermometers (Siemens Matsushita components Typ K 19 B57019) were embedded in an agar block, with the wire tips protruding into a central cylindrical cavity (diameter 10 mm) into which suspensions of different contrast agents could be injected. Insonation was provided by the probe of a medical diagnostic scanner (Siemens Sonoline Sienna) focused upon the centre of the cavity. The diagnostic machine was run in pulse-Doppler mode without simultaneous B-mode operation, i. e. a non-scanning beam was used. The temperature change in the cavity was recorded before, during and after insonation at a rate of 10 Hz, both in the region containing the contrast agent and further down the cavity to provide control measurements. Measurements were made for a range of negative peak pressures (500 kPa - 2.3 MPa at the focus) and pulse repetition frequencies (1-15 kHz) and for different probe centre frequencies (2.6-7 MHz). Three different types of coated microbubble agent were used: Optison® (Amersham PLC Bucks. UK), Levovist® (Schering AG, Germany) and Expancel®(Casco Products AB, Sundsvall, Sweden).

The results indicate that contrast agents do produce a measurable temperature rise under typical diagnostic conditions which is of the same order of magnitude as that predicted theoretically. There are a number of areas of uncertainty. These include the degree to which the sound field was modified by the presence of the contrast agent and hence the degree to which the probes were directly heated by ultrasound scattered from the microbubbles. If the validity of the results is confirmed by future experiments, however, there may be significant implications for the validity of existing safety guidelines, which are based on the behaviour of free bubbles. It may also be of interest for therapeutic applications in which enhanced heating is beneficial, e.g. ultrasonic ablation of tumours.

P3B-4

HARMONIC IMAGING OF TARGETED CONTRAST AGENTS WITH INTRAVASCULAR ULTRASOUND.

D. E. GOERTZ*[1,2], A. VAN WAMEL[1,2], M. E. FRIJLINK[1], N. DE JONG[1,3], and A. F. W. VAN DER STEEN[1,2], [1]Erasmus MC, Rotterdam, [2]Interuniversity Cardiac Inst. Netherlands, Utrecht, [3]Physics of Fluids, Univ. Twente, Enschede.
Corresponding e-mail: d.goertz@erasmusmc.nl

Background Ultrasound contrast agents targeting markers of atherosclerotic plaques are currently being developed for use with intravascular ultrasound (IVUS). Several reports have demonstrated the detection of targeted agents with IVUS by means of linear backscatter enhancement. It was previously shown that free microbubbles can be imaged with IVUS in second harmonic and subharmonic modes. In this study the feasibility of second harmonic and subharmonic IVUS imaging of targeted microbubbles is investigated.

Methods A prototype harmonic IVUS system was employed using fundamental frequency of 20 MHz (F20; 25% bandwidth) to conduct second harmonic imaging (H40), and a frequency of 40 MHz (F40; 25% bandwidth) for subharmonic imaging (SubH20). The agent examined was an experimental biotinated, lipid encapsulated formulation comprised substantially of micron and submicron bubbles (BG3039; Bracco Research, Geneva). The agent was targeted to an avidin coated agar substrate and imaging experiments were performed with the agar situated at approximately 3 mm from the catheter. A block of tissue phantom was also positioned adjacent to the catheter to provide linear scatterer signals within the imaging plane. Experimentally observed subharmonics in small lipid encapsulated bubbles at high frequencies are not well predicted by current bubble models. We hypothesize that this may be due to the form of the relationship between radial strain and lipid shell viscoelasticity for small bubbles at high frequencies being poorly accounted for in current models. To explore this, a modified Rayleigh-Plesset model is employed in combination with a range of functions for the relationship between radial strain and shell modulus contributions.

Results F20 mode detected bound bubbles with a contrast-to-tissue ratio (CTR) of 3.6 dB; in F40 mode it was -1.3 dB. At a transmit amplitude that produced low propagation harmonics, H40 imaging had a CTR of 15 dB. SubH20 signals were pressure dependant and at 0.6 MPa, for example, produced a contrast-to-noise ratio (CNR) of 16 dB, with tissue signals suppressed to below the noise floor. The acquisition of 150 sequential frames was found to not diminish either the H40 or SubH20 signals, indicating that nondestructive imaging conditions were achieved. These results show that subharmonic and second harmonic signals are possible to generate from bound bubbles at IVUS frequencies. With modeling, it was found that shells that are highly stiff on compression and weak on expansion result in expansion dominated subharmonics, which we have previously observed optically. The variation in shell stiffness during oscillations can lead to substantial phase differences between rarefaction and compression and permits subharmonic development for wider bandwidth (e.g. 25%) Gaussian enveloped pulses.

Conclusions This study indicates that H40 and Sub20 imaging of targeted microbubbles is feasible and results in improved CTR. This may lead to improved sensitivity for high frequency molecular imaging.

This work was supported by STW and ICIN. We thank Bracco Research (Geneva) for providing the BG3039.

P3B-5
MODELING MICROBUBBLE RESPONSE TO CODED, MULTI-PULSE, NON-LINEAR PULSE SEQUENCES.

K. CHETTY* and R. J. ECKERSLEY, Imperial College, London, U.K.
Corresponding e-mail: r.eckersley@imperial.ac.uk

Pulse encoding techniques used in ultrasound imaging aim to preserve axial resolution while allowing a significant increase in signal-to-noise ratio (SNR) without increasing the peak intensity of the insonating pulse. Multi-pulse imaging sequences that combine phase inversion and amplitude modulation (PIAM) have been shown to yield high sensitivity to the non-linear scattering associated with microbubbles. Previously, we have shown through experiments that combining frequency modulated pulses (chirps) with PIAM sequences can further improve the sensitivity of ultrasound to microbubbles, even at low acoustic pressures. However, we hypothesize that the non-linear response of the microbubbles is associated with degradation of the axial resolution. In this study we used a modified Rayleigh-Plesset model to examine tradeoffs between SNR and axial resolution. We investigated the effect of the non-linear response of the microbubble on the sidelobes generated in the compression process and the SNR of the system. Factors affecting the perseveration of non-linear signals in the processing were also studied. The effects of pulse length and frequency sweep were explored in order to determine how they can be optimized to minimize sidelobe generation and improve sensitivity to the microbubble. Resonant frequencies of microbubble sizes were determined using ring down simulations of microbubbles with an initial displacement from its equilibrium radius. A microbubble size of 3 μm with a resonant frequency of 1.75 MHz, similar to the microbubble SonoVue™ was chosen and chirp PIAM sequences were simulated and compared to short pulse PIAM sequences with corresponding bandwidth and amplitude. Results show that the compression processing for the chirp pulses was unable to completely restore the axial resolution. Over the pressure range simulated (25 to 150 kPa peak negative pressure) the FWHM of the measured data was found to increase from the ideal case of 1.4 μs to 1.7±0.2 μs. This loss in resolution arises due to the nonlinear response of the microbubbles. The results also show that the PIAM cancellation process acts to further degrade the axial resolution to 3.0±0.1 μs. The resolution obtained from the FWHM was found to be independent of the driving pressure amplitude; however, the generation of side-lobes in the compression process was dependent on pressure. This acts to further degrade the axial resolution and reduce SNR at higher driving pressures. In agreement with our previous experimental observations, a comparison of chirp PIAM and short pulse PIAM showed that after scattering and compression and pulse cancellation the former retained their advantage of having 6 dB more energy. Signal processing methods for both types of sequences

caused energy losses due to the cancellation of linear signals, with decreasing energy losses for increasing driving pressures due to the presence of more nonlinear components.

This work was supported by the EPSRC (Grant: GR/S71224/01)

P3B-6
LOW MICROBUBBLE CONCENTRATIONS SIGNAL ENHANCEMENT VARYING ECHOGRAPH ELECTRICAL POWER.

R. PALMIZIO ERRICO[1,4], S. CASCIARO*[2,1], C. DEMITRI[1,3], F. CONVERSANO[1,5], G. PALMA[1,5], E. CASCIARO[2,1], and A. DISTANTE[1,2], [1]ISBEM (Euro Mediterranean Scientific Biomedical Institute), Brindisi, Italy, Brindisi, Italy, [2]IFC-CNR Lecce Section (National Council of Research - Institute of Clinical Physiology), Lecce, Italy, Lecce, Italy, [3]Innovation Engineering Department, Lecce University, Italy, Lecce, Italy, [4]Material Science Department, Lecce University, Italy, Lecce, Italy, [5]Bioengineering & Robotics Department, Pisa University, Italy, Pisa, Italy.
Corresponding e-mail: demitri@isbem.it

Introduction: Low power and low concentration ultrasonic contrast agent (CA) studies are becoming more and more important in the development of new ecographic modalities and approaches [1]. Aim of this study is to evaluate signal contrast enhancement of a new phospholipidic CA at different concentrations covering all range suggested by the manufacturer and at four acoustic pressure levels. The resulted signal enhancement is discussed and presented.

Materials and Methods: Microbubble solutions were pumped into the vessel cavities of a new tissue mimicking phantom, made of a cellulose-based hydrogel having a sound propagation velocity very close to that of the human liver. It contained a 1 mm diameter cavities (made of PEG diacrylate-based hydrogel) placed at a stand-off distance of 2 cm from the upper surface of the phantom, connected to an external flow circuit. A saline-diluted suspension of an experimental phospholipids CA (supplied by Bracco Research SA, Geneva, Switzerland) continuously mixed by a magnetic stirrer is driven through the circuit by a gear pump at a costant flow rate of 5 ml/min. Starting by the Bracco suggested maximum value of dilution 1:500000 until 1:20000, eighteen different CA dilutions were insonified through a commercially available echograph (Megas, Esaote Spa, Florence, Italy) equipped with a linear array transducer (LA532) at 3,3 MHz using four echograph electrical power (EEP) values (37%, 50%, 75% and 100%). The CA solutions have been analyzed in terms of absolute concentration and diameter distribution by means of Multisizer™ 3 Coulter Counter® (Beckman Coulter, Inc.) The echograph was externally linked to a prototype for radiofrequency (RF) analysis (FEMMINA, developed by Florence University), able to get the full raw signal of the probe. For every dilution, a sequence of 100 data frames of RF raw data was acquired for each setting described above and analyzed off-line by means of Fortezza software (supplied by Florence University). An ad hoc implemented Fortezza algorithm was employed to select a rectangular region of interest (ROI) of 5×50 data points (1 mm^2). Mean signal amplitude was calculated within the selected ROI for each acquired frame sequence and these data have been plotted versus CA dilution.

Results: Each plotted curve shows a slight growth of backscatter amplitude with CA concentrations, while it is more evident a direct relationship between CA backscatter amplitude and EEP in the whole tested dilution range. Mean signal amplitude presents an increment normalized to its lowest value respectively of 3,3%, 8,5% and 12,4% for each EEP rising step value. We have found a strong linear increasing relationship (r=0.996) between mean backscatter amplitude and EEP.

Conclusions: This study indicates that backscatter amplitude of the investigated ultrasound CA at very high dilutions can be considered almost independent by CA concentration, while it is clearly influenced by incident acoustic pressure values.

References

[1] V. SBOROS et al. (2003): 'The behaviour of individual contrast agent microbubbles', Ultr. in Med. & Biol., 29, pp. 687-694

Session: P3C

BONE
Chair: W. O'Brien
University of Illinois

P3C-1
A 60 DAYS BEDREST STUDY: PRELIMINARY QUS BUA AND SOS CHANGES AT THE CALCANEUS SITE.

M. DEFONTAINE*[1], M. NASSER-EDDIN[1], J. RITTWEGER[2], and M. LAZERGES[3], [1]GIP Ultrasons - LUSSI, Tours, France, [2]Benjamin Franklin Kliniküm, Berlin, Germany, [3]ESTEC - ESA, Noordwijk, Netherlands.
Corresponding e-mail: defontai@med.univ-tours.fr

In the context of manned-space flights, we have developed for ESA, a dry QUS device dedicated to heel bone parametric imaging: Beam Scanner. To that aim, a pair of 2D arrays US probes including 576 elements, at 5OO KHz central frequency (Vermon, Tours, France) and a beam forming and scanning electronic bay (Ultrasons Technologies, Tours, France) have been manufactured. This device calculates and displays two parametric images of BUA (Broadband Ultrasonic Attenuation, dB/MHz) and SOS (Speed of Sound, m/s). The Beam Scanner has been fully validated and has provided non standardized coefficients of variation of 2% and 0.3%, for BUA and SOS respectively. These short-term precision values have been estimated (RMS average) from a population of 80 subjects realizing 3 measurements with interim repositioning. SOS and BUA data were obtained from the automatic positioning of a 14 mm ROI in the posterior and less attenuating region of the Calcaneus bone.

A 60 days bed rest study has been organized in the Benjamin Franklin Universitätkliniküm in Berlin by the Professor Felsenberg and Dr Rittweger, under ESA requirements. It consists in simulating O gravity effects on body physiology,

by lying horizontally in bed for a while. We have participated to that study in order to evaluate the bone changes at the heel site using the Beam Scanner device. 16 young, healthy males (volunteers), aged from 20 to 40 years old, have been including in the QUS protocol. Three QUS acquisitions were performed on each foot with interim repositioning. Measurement sessions were planned before bed rest, every 15 days during the Bedrest, and after 1 month, 3 months, 6 months and 12 months. The subjects were divided in two groups: a control group and an exercise group. The exercise training session was essentially concerning the lower limbs and feet. We clearly have a difference in bone loss between these two groups. The control group bone loss has been estimated superior to 6% for the BUA parameter and is statistically highly significant. The bone loss difference between groups is also statistically significant. Similar results have been obtained with the SOS parameter. However this parameter is more sensitive to soft-tissues thickness changes and provides interesting discussion.

In conclusion it was the first time that a QUS device was used in the context of such a longitudinal bone changes study. Two months bedrest are long enough to provide changes at the lower limbs and it has been demonstrated that QUS measurements are well adapted to follow bone changes over such a period.

P3C-2

NONLINEAR RESONANT ULTRASOUND SPECTROSCOPY (NRUS) FOR BONE MICRO-DAMAGE ASSESSMENT.

M. MULLER*[1], J. TENCATE[2], T. DARLING[3], A. SUTIN[4], R. GUYER[5], M. TALMANT[1], P. LAUGIER[1], and P. JOHNSON[2], [1]Laboratoire d'Imagerie Paramétrique, Université Paris 6, UMR CNRS 7623, Paris, France, [2]Geophysics, Los Alamos National Laboratory, Los Alamos, NM, [3]Materials Sciences and Technology, Los Alamos National Laboratory, Los Alamos, NM, [4]Stevens Institute of technology, Hoboken, NJ, [5]Department of Physics, University of Massachussets, Amherst, MA.
Corresponding e-mail: marie.muller@lip.bhdc.jussieu.fr

Bone micro-damage has a strong influence on bone quality and fracture risk. It is therefore important to develop a non invasive tool for bone micro-damage assessment. Nonlinear Resonant Ultrasound Spectroscopy (NRUS) is a technique exploiting the significant nonlinear behaviour of damaged materials, related to the presence of damage. This study shows for the first time the feasibility of this technique for damage assessment in bone. Two samples of bovine cortical bone were subjected to a progressive damage experiment. After removing soft tissues and marrow, the samples were wrapped in gauze impregnated with saline solution in order to keep them hydrated during the experiment. Damage accumulation was progressively induced in the samples by compressional fatigue cycling in a mechanical testing press. At each damage step, NRUS experiments were performed on the samples in order to study their resonance behavior. Each sample was probed using a step-sweep in frequency around an eigenmode of the sample, at gradually increasing drive levels. The measured resonance frequency shift provided quantitative information regarding the nonlinear behavior of the sample. For independent assessment of damage,

high energy X-ray CT imaging was performed, but only helped in the detection of the prominent cracks. As the quantity of damage accumulation increased, NRUS revealed a corresponding increase in the nonlinear response. The measured change in nonlinear response is much more sensitive than the change in modulus. Indeed, the measured nonlinear parameter, proportional to the frequency shift, revealed a 700% increase and a 1400% increase in the two samples respectively, whereas no quantitative change in the modulus could be measured. The results suggest the inability of linear acoustic parameters to reflect mechanically induced damages and that NRUS could be a potential tool for micro-damage assessment in bone. Further work has to be carried out for a better understanding of the physical nature of damaged bone, and for the ultimate goal of in vivo implementation of the technique.

P3C-3

NUMERICAL SIMULATION OF ULTRASOUND TRANSMISSION AND BACKSCATTERING IN CANCELLOUS BONE.

F. PADILLA*[1], E. BOSSY[2], G. HAIAT[1], F. JENSON[1], and P. LAUGIER[1], [1]Laboratoire d'Imagerie Paramétrique, CNRS UMR 7623 – Université Paris 6, Paris, France, [2]Laboratoire d'Optique Physique, CNRS UPR A0005 – ESPCI, Paris, France.
Corresponding e-mail: padilla@lip.bhdc.jussieu.fr

Quantitative ultrasound (QUS) measurements techniques based on transmission of ultrasound waves through trabecular bones have played, in recent years, an increasing role in the assessment of bone status. However, the physical mechanisms implied in the propagation of ultrasound waves through trabecular bones still remains unclear. Trabecular bone has a very complex microarchitecture composed of a network of solid interconnected trabeculae saturated by marrow in vivo. A description of ultrasound wave propagation in this medium using analytical approaches that would take into account a large number of parameters (complex 3D anisotropic geometry, fluid/solid interaction, etc…) quickly become inextricable. Numerical simulation offers a powerful alternative and the objective of this work is to assess the ability of 3D numerical simulations of ultrasound propagation through trabecular bone to yields features of real experimental measurements. Numerical simulation of wave propagation were performed for 31 trabecular bone samples measured by high resolution synchrotron microtomography. The simulation software uses a finite difference approach based on the Virieux numerical scheme. The simulation algorithm accounts for propagation through both the saturating fluid and the solid bone matrix, modeled as lossless materials. The synchrotron microtomography provided high resolution mappings of the 3D bone structures, which were used as the input geometry in the simulation software. An incident plane wave was propagated on a volume of bone of approximately 5x5x8 mm^3. We show that 3D simulation in transmission can predict phenomena observed experimentally on the same specimens (linear dependence of attenuation as a function of frequency and negative velocity dispersion). The ability of the simulation to predict backscatter phenomena is also demonstrated by comparison of computational

results to experimental data obtained on the same specimens. One sample was rotated to align the main orientation of the trabecular structure with the direction of ultrasonic propagation, leading to the observation of a fast and a slow wave. Numerical simulation based on real bone architecture therefore provides a powerful tool to investigate the physics of ultrasound propagation in trabecular structures. As an illustration, comparison between results obtained on bone modeled successively as fluid and a solid structure demonstrated the major role of mode conversion from the incident acoustic wave to shear waves in bone to explain the large scattering efficiency of trabecular bone.

P3C-4
PRECISION OF THE ESTIMATION OF SCATTERERS SIZE IN CANCELLOUS BONE USING SPECTRAL BACKSCATTER MEASUREMENTS.

F. PADILLA*, F. JENSON, and P. LAUGIER, Laboratoire d'Imagerie Paramétrique, CNRS UMR 7623 – Université Paris 6, Paris, France.
Corresponding e-mail: padilla@lip.bhdc.jussieu.fr

Ultrasonic backscatter measurements can be used to characterize trabecular bone structure and to estimate trabecular thickness (Tb.Th, i.e. the size of the scatterers). Our objective was to evaluate the performance of this estimator as well as others spectral estimators, like the frequency dependence and the mid-band amplitude of the backscatter coefficient. Two factors mainly degrade the performance of these estimators: interference noise due to random positioning of the scatterers and attenuation.

We have simulated rf-lines backscattered from trabecular bone assuming a random positioning of the trabeculae (leading to a fully developed speckle), a Gaussian form factor for the scatterers and a linear-frequency dependent attenuation in the medium. It is found that the variance in the estimation of the frequency dependence of the backscatter coefficient is as high as the variance due the biological variability in Tb.Th, in agreement with the results showed by K Wear (JASA,110,2001). In contrast, the experimental variance on the mid-band amplitude and on the estimated trabecular thickness are not fully explained by the speckle noise. The fundamental precision on estimated Tb.Th is approximately 5 μm, which is lower than the variance due to the biological variability. We also show that the effect of attenuation may be compensated by using an appropriate attenuation-compensation function. Finally, we show that the inverse procedure resulted in an excellent agreement between the actual mean trabecular thickness derived from synchrotron micro computed tomography 3-D reconstructions and averaged over 37 human femur specimens (Tb.Th = 132 ± 12 μm), and ultrasonically estimated scatterer size obtained using a Gaussian autocorrelation function (134 ± 15 μm). These results suggest that the inverse problem can be appropriately addressed.

P3C-5

COMPARISON OF VARIOUS IN VITRO ULTRASONIC VELOCITY MEASUREMENTS IN BONE: EFFECT OF FREQUENCY-DEPENDENT ATTENUATION AND OF VELOCITY DISPERSION.

G. HAÏAT*[1], F. PADILLA[1], R. BARKMANN[2], C.-C. GLÜER[2], R. O. CLEVELAND[3,1], and P. LAUGIER[1], [1]Laboratoire d'Imagerie Paramétrique, France, [2]Medizinische Physik, Klinik für Diagnostische Radiologie, Universitätsklinikum Schleswig-Holstein, Germany, [3]Dept of Aerosp. and Mech. Eng. , Boston University, Boston , MA.
Corresponding e-mail: haiat@lip.bhdc.jussieu.fr

Bone Mineral Density (BMD) measured with DXA techniques is the current gold standard for osteoporotic fracture risk prediction. Quantitative ultrasound techniques (QUS) in transmission measurements have been accepted as an alternative approachBroadband ultrasonic attenuation (BUA) and ultrasonic velocity (UV) measured on the proximal part of the human femur have been shown to be both significantly correlated with BMD. However, a lack of standardization of signal processing techniques used to compute UV complicates the comparison between data obtained with different commercial devices.

In this study, 38 excised human femurs were measured in transmission with a pair of focused 0.5-MHz central frequency transducers. Two dimensional scans were performed and RF signals were digitally recorded at each scan position. BUA was estimated and 8 different signal processing techniques were performed to estimate UV. The resulting difference in measured UV was determined as a function of frequency-dependent attenuation and velocity dispersion. A numerical simulation was employed to explain how attenuation and dispersion impact these different UV measurements. A new method aimed at compensating for the effect of attenuation was devised and led to a significant reduction in the difference between UV values obtained with the various signal processing approaches.

A comparison between different UV and BMD measurements indicated that the best correlation (r^2=0.86; RMSE=0.08 g/cm^2; p<10-4) was reached for UV calculated using a marker located in the early part of the signal. Moreover, we show that a linear multiple regression using both BUA and UV and applied to site matched regions of interest improved the accuracy of BMD predictions (r^2BMD-UV/BUA = 0.95, RMSE=0.05g/cm@). The conclusion is that velocity measurements considering early part of the signal should be preferred for ultrasonic assessment of BMD at this potential fracture site and that highly accurate estimate of BMD are possible using combination of BUA and UV.

This work was supported by the European Commission (Contract no QLK6-CT-2002-02710).

Session: P3D
MODELING AND VISUALIZATION
Chair: J. Jensen
Danisa Tecnical University

P3D-1
SOUND FIELDS FOR CODED EXCITATIONS IN WATER AND TISSUE.

J. LITNIEWSKI*, A. NOWICKI, Z. KLIMONDA, M. LEWANDOWSKI, and I. TROTS, Institute of Fundamental Technological Research, Polish Academy of Sciences, Warsaw, Poland.
Corresponding e-mail: jlitn@ippt.gov.pl

Coded ultrasonography is intensively studied in many laboratories due to its remarkable properties: increased penetration depth, signal to noise (SNR) gain and improved axial resolution. However, no data concerning the spatial behavior of the pressure field generated by coded bursts transmissions were yet reported.

This paper reports the results of investigations of the field structure in water and in degassed beef liver using five different excitations signals: two and sixteen periods sine bursts, 8 μs chirp (1 MHz bandwidth), and sinusoidal sequences phase modulated with 13 bits Barker code and 16 bits Golay complementary codes. For the liver tissue, the beam cross sectional data (pressure) at the output of the tissue blocs of varying thickness, just at the tissue – water interface were recorded. Flat, circular transducer with 15 mm diameter, 2 MHz center frequency and 50% bandwidth was used in all experiments. The data were recorded using PVDF membrane hydrophone (Sonic 804-201 USA) and collected using computerized scanning system developed in our laboratory. The results of measured pressure field distributions before and after compression were compared to those recorded using standard ultrasonographic short pulse excitation.

The comparison clearly indicated increase in the signal to noise ratio of the decoded pressure fields. Also, the modification of the spatial pressure field distribution, especially in the intensity and shape of the side-lobes, was apparent. As coded sequences are relatively long, intuitively, the beam shape or directivity pattern would be expected to be very similar to those produced by a long sine burst. Whereas the outcome of the experiments confirmed that this is correct for non-compressed distributions of the examined signals, in the case of the compressed sound fields, especially those generated for binary Golay sequences, the field patterns exhibited diminishing side-lobes similar to those obtained using short bursts.

The widening of the beam width in far field in the liver tissue was observed for all excitation signals. The high value of attenuation coefficient in the liver tissue explains this effect. Both media, water and liver tissue posses relatively high B/A nonlinear coefficient and considerable amount of energy is converted to higher harmonics during propagation of the wave. In the liver tissue, due to high attenuation, these harmonics are quickly absorbed and only weakened

fundamental wave component is detected. In water, where attenuation is very small all generated harmonics including the fundamental frequency compose the pulse and are measured by the hydrophone. As the harmonics generation depends on the second power of the amplitude the effect is largest along the axis of the transducer.

The differences in the field distribution found in the tissue and in water show that care should be taken when the results obtained from measurements in water are used for explanation of waves behavior in the tissue.

This study was supported by the State Committee for Scientific Research, Poland(grant no. 3T11E02928)

P3D-2

AN EIKONAL EQUATION BASED SCHEME FOR REFRACTION COMPENSATION IN TIME-OF-FLIGHT TOMOGRAPHY.

M. ASHFAQ* and H. ERMERT, Institute of High Frequency Engineering, Ruhr-University Bochum, Bochum, Germany.
Corresponding e-mail: mohammad.ashfaq@rub.de

Background: Acoustic speed in conjunction with the acoustic attenuation has been proven to possess histological relevance in differentiating between malignant and benign breast tumors. With this application in mind, a new setup was designed and constructed to collect the through-transmission data required for the tomographic reconstruction of the two aforementioned parameters with the help of a conventional ultrasound system, the latter being augmented with an add-on module. This add-on module consists of a mechanical setup resembling the helical CT system, and a custom designed supporting hardware and software interfaces to make a through transmission measurement at any position along a helical trajectory via an external wave generator possible. Two 7.5 MHz linear arrays probes were used in the experiments. Whereas the transmitter was fed by an external generator, the receiver was connected to the commercial ultrasound system of type Siemens Sonoline Omnia. As the reconstruction of the speed of sound is based on the assumption of the straight ray model, it is necessary to compensate for the refraction artifacts.

Methods: The correction scheme applied here is based on the solution of the ray equation derived from the eikonal equation. An accurate numerical solver estimates the curved ray paths founded on the parallel beam reconstruction. Two different strategies were developed to solve the ray equation. Besides a direct numerical integration, a perturbation technique was also investigated, the latter may be reduced to the boundary value solution of the eikonal equation. Whereas the computationally intensive direct numerical integration combined with an appropriate data interpolation technique renders very accurate ray paths possible, the boundary value solution of the eikonal equation is substantially faster with acceptable accuracy. An extended back projection scheme adapted to bent rays as well as an arithmetic reconstruction technique was employed to reconstruct the refraction corrected speed of sound tomograms.

Results and Conclusions: The accuracy of estimation of the ray estimation algorithms was demonstrated on Maxwell's fish eye. To demonstrate feasibility of the overall correction concept, experiments were carried out on phantoms with known geometrical and acoustical properties. The parallel ray constructions could achieve in the best case an average reconstruction accuracy of 86% whereas the bent ray correction techniques could be demonstrated to possess an average reconstruction accuracy of 93%, the term average reconstruction accuracy being defined as the mean of the pixel-wise accuracy. A more substantial improvement was however seen in the capability of the correction technique to demarcate the boundaries of the lesions more accurately.

This work is an activity of the Ruhr Center of Excellence for Medical Engineering Bochum (KMR), funded by the German Federal Ministry of Education and Research (bmb+f grant #. 01EZ0206)

P3D-3
COMPUTER MODELLING OF ITERATIVE TECHNIQUE APPLICATION FOR TISSUE THERMAL IMAGING.

K. BOGRACHEV* and W. M. D. WRIGHT, Ultrasonics Research Group,Department of Electrical and Electronic Engineering, University College Cork, Cork, Ireland.
Corresponding e-mail: konstantinb@rennes.ucc.ie

Thermal therapies are effective methods used for cancer treatment. During thermal cancer treatment there are usually small temperature fluctuations of between 37 0C and 43 0C inside the human body. These fluctuations are very important to monitor accurately for quality cancer treatment, preferably with a non-invasive technique.

Through-transmission ultrasonic tomography is a convenient non-invasive technique, which allows internal cross-sectional images of acoustic properties to be obtained; acoustic properties change as the temperature changes, and this allows temperature fields in tissue to be measured.

Computer modeling of temperature fluctuation reconstruction using ultrasonic through-transmission tomography has been carried out. The model considers a fan-bean tomography scheme (60 sensors, 2160 rays in total) and iterative techniques for solving the inverse problem. It also assumes the 2D temperature is being reconstructed in an area of tissue of 60 mm*60 mm size, and the temperature fluctuation size is ~6.5 mm in diameter. Such heated regions can appear, for example, during thermal treatment using high intensity focused ultrasound (HIFU). Algorithms for solving the inverse problem using algebraic iterative methods (including EM, ART and SART) have been investigated. Bilinear interpolation of temperature values was used in between the nodes, in which temperature is being reconstructed. The model takes into account electronic measurement noise and assumes increasing linear dependence of sound speed on temperature, which is approximately correct for the considered temperature range and non-fatty tissue. Circular and ellipsoidal heated regions have been investigated, along with multiple contrasts. It was shown that it is possible to reconstruct temperature fluctuations with a good accuracy.

A reconstruction technique was also investigated for regions of tissue which contain bones or other acoustically non-transparent objects, as these objects cause missing parts in the projection data. A special method for temperature distribution reconstruction from noisy projections with missing data was developed. The developed method reduces the number of unknowns by partial substitution of values obtained by iterative EM technique reconstruction. The accuracy of the developed method was investigated by computer modeling and compared with known expectation maximization methods. It was shown that the developed method gives higher accuracy and less distortion after reconstruction than the expectation maximization method. The developed method, therefore, may give a better opportunity to accurately monitor the thermal cancer treatment of more regions of the human body.

P3D-4
ULTRA-FAST ULTRASOUND 3D IMAGING SIMULATOR.

T. HERGUM*[1], S. RABBEN[2], and H. TORP[1], [1]Norwegian University of Science and Technology, Trondheim, Norway, [2]GE Vingmed Ultrasound, Horten, Norway. Corresponding e-mail: torbjorn.hergum@ntnu.no

Most available ultrasound imaging simulation methods are based on the spatial impulse response approach, basically calculating and adding the contribution from each subresolution scatterer. The execution speed for such a simulation is of the order of days for one heart-sized frame using desktop computers.

However for some applications the accuracy of such rigorous simulation approaches is not necessary. This work outlines a much faster 3D ultrasound imaging simulation approach, which can be applied to tasks like simulating 3D imaging with a matrix probe, 3D speckle-tracking, and the study of de-correlation of 2D speckle-tracking from out-of-plane motion.

A kinematic model of the left ventricle is used as input to the ultrasound simulations. This model provides a dynamic 3D object filled with point scatterers that are moved according to a realistic myocardial deformation during a cardiac cycle. Knowing the exact location of all scatterers at all times makes for an excellent reference e.g. for testing of speckle-tracking algorithms.

The increased speed of the proposed simulation method is based primarily on two approximations. Firstly the point spread function (PSF) is set to be spatially invariant, which is a good approximation in beam-space coordinates. The ultrasound image is found as the convolution of the PSF and an object of randomly distributed scatterers. This is done in the frequency-domain, where convolution reduces to a simple multiplication of the point spread function and the object.

The second approximation is that the randomly distributed scatterers of the object are passed through an anti-aliasing filter before insertion into a regular beam-space grid. This significantly reduces the amount of data which needs to be processed, while maintaining the correlation of the speckle pattern from frame to frame. The time to simulate one full 3D image from an object containing ~1.500.000 scatterers is of the order of 200 seconds, using a desktop computer. Approximately half of the simulation time is used for the anti-aliasing filter.

A comparison with the well-established simulation software package Field II has been made. Simulating a full 3D image using the same input object was found to be of the order of 1000 times slower than the presented method.

One apparent drawback of the proposed method is that the whole volume is imaged at the same time-instance, so there is no time-delay between each beam. However, a scan with arbitrary timing between the beams can be made by first simulating 3D images at a frame rate equal to the pulse repetition frequency (~4000 frames/s). Next the desired image is constructed using these high frame rate images as raw material.

Following these considerations the proposed simulation method can be a valuable and rapid tool for working with 3D ultrasound imaging and in particular 3D speckle-tracking.

P3D-5
FIRST IMAGES WITH A 3D-PROTOTYPE FOR ULTRASOUND COMPUTER TOMOGRAPHY.

N. RUITER*, M. ZAPF, R. STOTZKA, T. MÜLLER, K. SCHLOTE-HOLUBEK, G. GÖBEL, and H. GEMMEKE, Forschungszentrum Karlsruhe, 76133 Karlsruhe, Germany.
Corresponding e-mail: nicole.ruiter@ipe.fzk.de

Introduction Ultrasound computer tomography (USCT) is a novel imaging method capable of producing volume images with both high spatial and temporal resolution. We want to apply this method for early breast cancer diagnosis. In this paper the first volume images obtained are presented and discussed.

Methods To obtain high quality images, we arrange several thousand transducers in a cylindrical array. They enclose a water tank, which contains the object to be imaged. Sequentially, one transducer transmits a spherical pulse while all other transducers are receiving the transmitted, reflected, or scattered signals. The image reconstruction for reflection images is based on a sum-and-delay algorithm.

At the moment our experimental 3D setup (18cm diameter and 15cm high) contains 128 sending and 512 receiving transducers, grouped as a 5cm high ring in the middle of the cylinder. The transducers are almost automatically manufactured to obtain cheap and reproducible results. Their quadratic aperture of $(1.4mm)^2$ was a compromise between the emitted signal amplitude and the desired spherical emission characteristic. The developed data acquisition system used massive parallel processing.

Results For first tests the USCT was filled with water, a thin wire of 1.6mm diameter, and a plastic cup of approx. 10cm diameter filled with oil and containing artificial structures, like drinking straws and nylon threads. All reconstructed images had satisfactory quality and pictured the main structures of the phantoms.

Discussion and Conclusion The new 3D-setup is working and produces satisfactory images. The results show better local contrast than conventional ultrasound methods. That is due to the spatial compounding effect of our system, which average the speckle noise out. Due to the relatively small number of

transducers the contrast and resolution of the imaged structures were suboptimal compared to the results with the 2D setup. To reach the 2D-resolution in 3D, the system will be extended to 384 senders and 1536 receivers. Furthermore a complete cover of the cylindrical surface will be emulated by small rotation steps of the cylinder.

P3D-6

MULTI-VOLUME RENDERING FOR THREE-DIMENSIONAL POWER DOPPLER IMAGING.

R. MANAGULI*[1,2], Y. M. YOO[1], and Y. KIM[1], [1]Image Computing Systems Laboratory, Department of Bioengineering, University of Washington, Seattle, WA, [2]Hitachi Medical Systems of America, Twinsburg, OH.
Corresponding e-mail: ravim@u.washington.edu

Multi-volume rendering (MVR) has been used for better localization of tumors by integrating structural (e.g., Computed Tomography, CT) and physiological/ functional 3D information (e.g., Positron Emission Tomography, PET) in other medical modalities. Similar fusion in ultrasound imaging between B-mode and Power Doppler provides improved visualization and better understanding of the correlation between anatomical structures and blood flow, e.g., heart, kidney, liver. However, little work has been reported in the literature discussing the ultrasound fusion algorithms. Algorithms developed for other imaging modalities (e.g., CT-PET scanner) cannot be applied directly to ultrasound imaging. They need to be modified and adapted for ultrasound fusion.

In this paper, we present three fusion algorithms that we have developed for ultrasound: property fusion (PPF), post fusion (PF) and progressive fusion (PGF). In the PPF, volumes are fused based on properties of B-mode and Power data and are then rendered. In PF, BW and Power volumes are rendered separately and then fused using alpha blending. In PGF, fusion is performed at several stages and intermixing of volumes occurs both during and after rendering. We have investigated these three fusion techniques (i.e., PPF, PF and PGF) using in vivo data acquired from carotid bifurcation, kidney and liver using a commercial ultrasound machine (i.e., EUB-6500, Hitachi Medical Corporation, Japan) with free-hand and mechanical scanning. Correlation between anatomical structure and blood flow can be visualized using all three methods. Advantage of PPF and PGF over PF is that both these algorithms provide depth cue information between anatomical structures and blood flow. However PPF and PGF methods significantly change the rendering pipeline while PF has little effect on the rendering pipeline. Even though the rendered quality of all these three methods depends upon the opacity table chosen, the dependence of PGF on opacity table is much higher than the others. We will present these algorithms along with their computational requirements and discuss relative advantages and disadvantages of each of these methods.

P3D-7

TRACKING OF REGIONAL LEFT VENTRICULAR ROTATION BY TISSUE DOPPLER IMAGING.

J. CROSBY*[1], T. HELLE-VALLE[2], B. H. AMUNDSEN[1], and H. TORP[1], [1]Department of Circulation and Medical Imaging, Norwegian University of Science and Technology, Trondheim, Norway, [2]Department of Cardiology, Rikshospitalet University Hospital, Oslo, Norway.

Corresponding e-mail: crosby@ntnu.no

Background: Left ventricular (LV) torsion has been proposed as sensitive marker of LV function. Speckle tracking techniques on short axis (SAX) views have recently been introduced as an ultrasound-based method for assessment of rotation, as an alternative to MRI tagging. This study presents a complementary method for regional rotation estimation that utilizes the velocity field provided by Tissue Doppler Imaging (TDI).

Method: Assumed that the myocardial wall remains fairly circular in the SAX view through the heart cycle, the motion of LV can be divided into three components: A translation of the centre, a change in LV radius, and rotation. Two circular layers are drawn by the user inside the LV myocardium in one frame; one placed near the endocardium and the other near the epicardium. The software automatically carries out an independent bidirectional frame-to-frame tracking on a set of intervening layers. The tracking procedure searches for the change in global geometric parameters that minimizes the deviations between the observed TDI velocities and the velocities predicted by the model. The remaining deviations are being used as an expression of local differences in angular velocities, which results in regional variations in rotation. The method has been compared with results from commercial speckle tracking echocardiography (STE) software (EchoPAC 2D Strain, GE Vingmed) on six healthy humans.

Results: For valid regions, the peak rotation in degrees viewed from the apex found by TDI and STE was -2.87±5.72° and -2.84±3.64° at the base, 1.09±3.05° and 1.57±3.21° at the level of the papillary muscles, and 4.53±2.20° and 6.79±3.68° near the apex. Time to peak for the two methods was, correspondingly, 0.388±0.055 s and 0.390±0.061 s, 0.280±0.112 s and 0.290±0.101 s, and 0.362±0.087 s and 0.369±0.088 s. The correlation coefficients for peak rotation and time to peak were 0.84 and 0.96, respectively. 14 of 102 regional TDI traces had to be excluded from the analysis, of which nine were from the posterolateral segments where the ultrasound beam were almost perpendicular to the LV circumference.

Conclusion: The assessment of regional LV rotation from the TDI velocity field was shown to be feasible. The preliminary results showed good correlation with results from speckle tracking echocardiography.

Session: P3E

SIGNAL PROCESSING
Chair: W. Walker
University of Virginia

P3E-1
CORONARY PLAQUE CLASSIFICATION THROUGH INTRAVASCULAR ULTRASOUND RADIOFREQUENCY DATA ANALYSIS USING SELF-ORGANIZING MAP.

T. IWAMOTO*[1], A. TANAKA[2], Y. SAIJO[3], and M. YOSHIZAWA[4], [1]Graduate School of Engineering, Tohoku University, Sendai, Miyagi, JAPAN, [2]Faculty of Symbiotic Systems Science, Fukushima University, Fukushima, Fukushima, JAPAN, [3]Institute of Development, Aging and Cancer, Tohoku University, Sendai, Miyagi, JAPAN, [4]Information Synergy Center, Tohoku University, Sendai, Miyagi, JAPAN. Corresponding e-mail: iwamoto@yoshizawa.ecei.tohoku.ac.jp

Intravascular ultrasound (IVUS) is an important clinical tool that provides high resolution cross-sectional image of coronary artery. However, it is difficult to accurately classify plaque composition by conventional IVUS images. In the present study, we apply self-organizing map (SOM) of radiofrequency (RF) signal spectra for automatic plaque classification in IVUS diagnosis.

IVUS data were acquired with a commercially available IVUS system with the central frequency of 40MHz. RF data were digitized and stored in a workstation using by an A/D board with the sampling frequency of 500Msa/s and the resolution of 8 bits. Initially, a software-based band-pass filter (15MHz-105MHz) was applied to the IVUS RF signal data. Then each line in the ROI was scanned by a 128-points width hamming window. The frequency spectrum was calculated for each position of the window using a mathematical autoregressive (AR) model. Akaike's final prediction error method estimated the optimum AR model order was 15 for characterizing plaque components.

Further, the optimized AR spectra were used to compute 18 spectral shape parameters for each ROI, like fundamental wave power, harmonic wave power, slopes and other shape parameters widely used in the literature.

The SOM is one of neural network applications and it is a vector quantization method that places the weight vectors on a regular low-dimensional grid in an ordered fashion. A SOM consists of neurons organized on a grid. Each neuron is a d-dimensional weight vector where d is equal to the dimension of the input data vectors. The neurons are connected to adjacent neurons by a neighborhood relation, which dictates the topology of the map.

In this study, the SOM classifier learned the plaque component type based on spectral parameters. And then the SOM classified windowed area of IVUS data based on these parameters.

ROIs for training data were selected from IVUS B-mode images by an expert medical doctor. Then two plaque types (fibrous and calcified plaque) and four structure types (catheter, guidewire shadow, blood, and media) were defined.

Spectral parameters of these data were used as training data for the SOM.

Color codes were assigned to the plaque component values, and the tissue maps were reconstructed on IVUS B-mode images by our algorithm.

Based on the training data, other123 ROIs were identified in 23 coronary artery images.

ROIs were selected for catheter (n=21), guidewire shadow (n=18), blood (n=15), fibrous plaque (n=11), calcified plaque (n=31), and media (n=27) areas. The SOM learned from the AR spectrum parameters of these ROIs. The sensitivity and specificity of classified ROIs by the SOM were showed in table 1. The overall accuracy was 84.2%.

These results suggest that the proposed technique is useful for automatic characterization of plaque components in IVUS image.

Table 1) Sensitivity and specificity

Tissue components	Sensitivity	Specificity
Catheter	99.2%	99.9%
Guidewire shadow	84.7%	89.3%
Blood	97.3%	99.5%
Fibrous plaque	84.6%	95.9%
Calsified plaque	96.2%	99.9%
Media	36.3%	98.9%

Results from the SOM classifier with spectral parameters

This study was supported by Grants-in-aid from Japan Society of Promotion of Science (15300178) and Grants-in-aid from Ministry of Health, Labour and Welfare (H17-nano-001).

P3E-2
HIGH FREQUENCY IMAGING USING CODED GOLAY TRANSMISSION.

A. NOWICKI*, M. LEWANDOWSKI, W. SECOMSKI, and J. LITNIEWSKI, Institute of Fundamental Technological Research, Polish Academy of Sciences, Warsaw, Poland.
Corresponding e-mail: anowicki@ippt.gov.pl

Sonographically, the normal skin is composed of three layers: an epidermal entry echo, dermis and subcutaneous tissue. Their thickness varies according to the areas of the body and patients age. All three layers: a highly reflecting epidermis, less echogenic dermal layer (depends on the amount of collagen fibers) and finally weekly or non-echogenic subcutis (due to its mainly adipose nature), are rather clearly differentiated using 20-30 MHz ultrasound. However,

deeper structures - part of subcutaneous fatty layer and fascia are rarely visible due to rather high attenuation (>18dB/cm at 30 MHz). The fascia thickness measurement is an important factor in the diagnosis of the scleroderma. In particular, fascia thickening and changes in the echostructure of the subcutaneous tissue are characteristic for morphea en plaque and profound morphea. The morphea involvement in fascia structure can be an early sign of the lesion activity, prior to the liliac ring. The issue of maximizing penetration depth with concurrent retaining or enhancement of image resolution constitutes one of the time invariant challenges in ultrasound imaging. Concerns about potential and undesirable side effects set limits on the possibility of overcoming the frequency dependent attenuation effects by increasing peak acoustic amplitudes of the waves probing the tissue. To overcome this limitation we have used a pulse compression technique employing 16 bits Complementary Golay Codes at the frequencies from 20 to 30 MHz. In comparison with other coded excitation schemes, such as chirp, pseudo-random and Barker, the Golay coding allowed virtually side lobe free operation. The coding and matching filters circuitry were implemented in our high frequency skin and eye scanner. In order to accelerate the overall image formation for Golay excitation, both codes were sent one after another along the same scanning line, with the time span of 40 microseconds corresponding to about 30 mm of the scanning depth. The excitation voltage applied to the ultrasonic transducer for short burst and Golay coded transmission was equal to 50 $V_{p\text{-}p}$ in order to keep the I_{sptp} intensity constant. Scanning was done using 25 MHz (center frequency) $LiNbO_3$ focused, spherical transducer (4 mm in diameter) with varying thickness along the radius. The last resulted in 55% bandwidth, sufficient for efficient coded transmission. The basics of the coding technique including the description of the code generation algorithms will be given. The new system was initially tested using a thread phantom in order to verify the quality of axial and lateral resolution comparing both to the data recorded using a short burst transmission. The in vivo experimental data collected by scanning different skin sites clearly proved almost doubled penetration comparing to the standard short pulse transmission. On other hand we were able to increase the probing frequency up to 31 MHz for coded transmission and keep the same penetration depth as for 20 MHz short burst scanning.

This work was supported by the KBN grant 3T11E02928

P3E-3
INVESTIGATION OF NONLINEAR PROPAGATION IN A TISSUE OF A CHIRP-MODULATED ULTRASOUND PULSE SIGNAL.

Z. BENENSON*, N. KULBERG, A. ELIZAROV, and T. YAKOVLEVA, Computer Center of Russian Academy of Sciences, Moscow. Russia.
Corresponding e-mail: benenson@mtu-net.ru

The results of the investigations of propagation in a tissue of ultrasound pulse signals with chirp modulation have been obtained by calculating. For the case of Gaussian apodization of the signal emitted by the phased array an approximate formula is obtained describing the second harmonic component of the signal

both in 3-dimensional space and in its 3D Fourier transformation. The formula was derived on the basis of the estimation of a wave equation solution relatively the 3D Fourier transformation of the second harmonic signal, the right side of the equation containing 3D Fourier transformation of the second derivative of the first harmonic pulse signal with chirp modulation. The formula obtained allows estimating a signal amplitude, the beam width and an active area of the second harmonic formation, the first and the second harmonics amplitudes ratio.

A technique has been developed for the numerical simulation of nonlinear propagation in tissues of a signal on the basis of the fast three-dimensional Fourier transformation application for the wave equation solution in an iterative regime when the right side of the equation is being corrected in the iterations thus more accurately characterizing the nonlinear term of the wave equation.

The simulation has been implemented for two variants of a transducer. In the first variant a transducer is used consisting of one-dimensional phased array with the changing focal distance along the longitudinal axis of the array and with the constant focal distance along the transverse coordinate. For the phased array with the rectangular aperture of 12x20 mm and the transmitting frequency of 2MHz the second harmonic level is 8dB lower than the first harmonic level at the depth of 10 cm at the absence of chirp modulation. For the case of chirp modulation with the compression coefficient of the pulse of 15 the second harmonic level is increased by 13 dB.

The results for a simple pulse signal were compared with the measurements by hydrophone for the signal propagation in a tank of water. A good coincidence of the data has been obtained.

The data having been calculated by the formula practically coincides with the results of the numerical simulation for the Gaussian signal.

In the second variant a transducer is used consisting of 2 piezo-electric arrays that allows to get 3D images for the diagnostics of the small parts, one of the transducers being transmitting and the second one being receiving.

The simulation was conducted for the transmitting frequency of 3.3MHz. For achieving the acceptable ratio of signal to noise it is necessary to apply a chirp modulation with the compression coefficient of the order of 20-30.

This work was supported by grant 05-01-00325 from RFBR (Russia).

P3E-4
RAPID TRACKING OF SUBMICRON DISPLACEMENTS WITH ULTRASOUND.

G. PINTON*, J. DAHL, and G. TRAHEY, Duke University, Durham, NC.
Corresponding e-mail: gfp@duke.edu

Acoustic Radiation Force Impulse (ARFI) imaging uses short duration acoustic pulses to generate and subsequently determine localized displacements in tissue. Displacements in ARFI imaging are normally orders of magnitude smaller than those encountered in elastography, Doppler flow, or Doppler tissue measurements and thus require different signal processing techniques.

We describe a real-time ARFI imaging system which implements normalized cross correlation, 1D, and 2D autocorrelation. A Siemens Antares scanner was used to acquire the echo data either as downsampled quadrature demodulated (I/Q) data with four parallel receive beams for each transmitted push or as raw rf. The performance of the algorithms is examined in terms of bias and jitter for noise, downsampling factor, computational load, and the ability to resolve a step displacement. For normalized cross correlation, kernel size and interpolation are also taken into account to optimize these parameters for ARFI. The ability to reconstruct displacement images from downsampled I/Q data is demonstrated for quadrature using the Hilbert transform and trigonometric functions. Normalized cross correlation generally performs better than the autocorrelation methods. For example at an SNR of 30 dB, a base displacement of 4.8 μm, and no downsampling, the jitter is 0.43μm for normalized cross correlation and 3.7μm for autocorrelation. However the jitter error becomes similar to the autocorrelation methods' as the I/Q downsampling increases.

ARFI images are produced in real-time by porting the displacement tracking data to an eight node Linux cluster with 3.0 GHz processors and 1 GB RAM over 100 Mbit ehternet. The system calculates displacements down to theoretical limits set by the Cramer-Rao lower bound (0.2 μm) with self balancing master-slave parallel code written with the Message Passing Interface. The parallelization efficiency is 66%. Communications between processors occur over a 1Gbit ethernet network. A linear motion filter reduces artifacts due to physiological motion. Shot noise is reduced using a two-dimensional median filter and a dynamic display range is determined based on the image histogram. A matched b-mode image is displayed along with the displacement image either directly on the ultrasound scanner or on a separate display. The frame rate is computationally limited to 12Hz though transducer heating and patient acoustic exposure restrict the achievable frame rate in most applications.

The authors thank the Ultrasound Division at Siemens Medical Solutions USA, Inc. for their in kind and technical support. This work was supported by the NIH grants R01-HL07548501, 1R01CA114093-01, and R01-EB002132.

P3E-5

THE EFFECT OF INITIALIZATION AND REGISTRATION ON THE ACTIVE SHAPE SEGMENTATION OF THE MYOCARDIUM IN CONTRAST ENHANCED ULTRASOUND.

J. PICKARD*, S. ACTON, and J. HOSSACK, University of Virginia, Charlottesville, VA.
Corresponding e-mail: jep5m@virginia.edu

Unfortunately, ultrasound images inherently include a considerable amount of speckle noise and other image artifacts resulting from various physical phenomena. Frequently, several ultrasound images are averaged together to improve image quality prior to automated processing. However, registration inaccuracy will produce blurred object edges and hamper the segmentation process. For automatic object identification in ultrasound imagery, model-based

segmentation approaches are of particular interest because of their global approach and ability to infer edge-less parts of the object based on a priori information. These models, typically implemented as active contours, are iteratively deformed towards image objects. Segmentation results are strongly dependant on initial contour placement, as the contour often falls into local energy minima when initialized far from the desired image boundary. This paper presents results on the effects of initial contour placement and registration error on the success of an active contour model segmentation of the myocardium from contrast enhanced ultrasound.

An active shape model (ASM), as introduced in [1], was created for the segmentation process. ASM is an active contour which uses a deformable point distribution model, created from a set of training shapes, to iteratively move to find image edges. This model describes not only the expected shape of the training set, but also the variability, allowing global constraints of the contour shape, and ensuring a final segmentation similar to the training set. This model was used for automatic segmentation of 65 echocardiograph studies, the results of which were compared to manual segmentations. Standard accuracy measures – accuracy, sensitivity, specificity, and Root Mean Squared Error (RMSE) – were computed to quantify segmentation results. Variability to initial contour placement was explored by comparison of segmentations resulting from two automatic initialization algorithms to the segmentation resulting from a manual initial contour placement. Similarly, variability to image sequence registration was explored by comparison of segmentation results of automatic segmentation on manually registered data to automatic segmentation results on automatically registered data.

As illustrated in Table 1, segmentation results from manual placement of the initial contour were shown to fall within intra-observer error for manual segmentation. Both automatic initialization algorithms performed worse due to poor initial contour placement. Segmentation success was not as dependant on registration accuracy. The automatic registration algorithm provided registration results with an RMSE of 1.10 pixels (0.63mm), however the segmentation results showed accuracy comparable to segmentation from manually registered data.

This work is supported in part by NIH grant EB001826.

Table 1: Accuracy Results

	Accuracy	Sensitivity	Specificity	RMSE (Pixels)	RMSE (mm)
Intra-Observer	0.98	0.82	0.99	3.9	2.2
Manual Initialization	0.98	0.79	0.99	3.4	2.0
Automatic Initialization 1	0.97	0.71	0.99	5.5	3.1
Automatic Initialization 2	0.97	0.71	0.99	4.3	2.5
Automatic Registration	0.98	0.79	0.99	3.4	1.9

[1] T. F. Cootes, C. J. Taylor, D. H. Coooper, and J. Graham, "Active Shape Models - Their Training and Application," Computer Vision and Image Understanding, vol. 61, pp. 38-59, 1995.

P3E-6

GASEOUS AND SOLID EMBOLI DIFFERENTIATION USING RADIATION FORCE.

G. SOUCHON*[1], M. BIARD[1], J. M. GIRAULT[1], D. KOUAME[1], and F. TRANQUART[2], [1]LUSSI, Tours, France, [2]INSERM U619, Tours, France.
Corresponding e-mail: gregory.souchon@med.univ-tours.fr

Cerebral embolisms represent a major part of all ischemic strokes in occidental countries. It has been found that a good knowledge of emboli (detection, differentiation and sizing), which are foreign particles to blood normal cerebral circulation, remains a promising challenge. Their characterization can be used, in fact, as a diagnostic or therapeutic tool. The most commonly used tool to detect emboli is a transcranial Doppler system.

Clinical studies have shown that patient having a prosthetic heart valve present in the embolic Doppler signature a high frequency modulation index while for patient having atherosclerotic plaque the frequency modulation index is low.

We hypothesis that this high level modulation index is probably induced by the radiation force effect (trajectory modification). We will show in this study that it is possible, by using the radiation force, to discriminate gaseous to particulate emboli. The study is divided into theoretical and experimental parts.

We limited our study to embolus ranging from 10µm to 300µm which seems to be the size range encountered in clinical investigation. We show in a theoretical manner that the displacement induced by the radiation force acting on gaseous emboli is, in this range, always higher than the one produced on solid emboli.

We will show experimentally that the displacement evaluated via the index modulation for gaseous emboli is always higher than the one produced by solid emboli.

The experimental acoustical set up is composed by a gear pump, a PW Doppler system operating at 2MHz (20 cycles,PRF=8.33 kHz), a water tank, a tygon tube. We proposed two types of configurations : with or without skull between the tube and the probe. For the highest power delivered by our Doppler system, the pressure level in the tube is 25kPa without skull and 5 kPa with skull. Gaseous emboli are naturally produced by the gear pump (size<100µm) and solid emboli are peace of pork meal (size ranging from 100 to 300µm). Circulating gaseous or solid emboli are detected when they cross the acoustic beam. For each embolic Doppler signals, we evaluate the frequency modulation index.

As result, we show that without skull the average frequency modulation index is 100Hz/s for solid emboli and 10000Hz/s for gaseous emboli . A threshold of 5000Hz/s allow 90% of discrimination. With the skull, the average frequency modulation index is 700Hz/s for gaseous emboli while for solid emboli the index is around 0. A threshold of 200Hz/s allow 90% of discrimination.

This approach seems to be a good technique to differentiate gaseous to solid emboli and has to be confirmed by a clinical study.

Session: P3F

NDE TRANSDUCERS
Chair: R. Addison
Rockwell Scientific Company

P3F-1
NONLINEAR ULTRASONIC PHASED ARRAY FOR IMAGING CLOSED CRACKS BY SUPER- AND SUBHARMONICS.

Y. OHARA*, R. SASAKI, T. OGATA, T. MIHARA, and KAZUSHI YAMANAKA, Department of Materials Processing, Graduate School of Engineering, Tohoku University, Sendai-City, Miyagi, Japan.
Corresponding e-mail: a4td5601@stu.material.tohoku.ac.jp

Although closed cracks can propagate under applied stress resulting in catastrophic accidents e.g. in atomic power plants, it is difficult to detect them since the intensity of scattering waves is much lower than that from open cracks. Recently, nonlinear ultrasound is expected to have a potential of detecting and evaluating them, and subharmonic wave with half-frequency of input signal is particularly useful because of its selectivity for cracks. Thus far, we have observed subharmonics in closed cracks and developed a model to analytically reproduce the observed waveform [1]. Also, we observed a peculiar wave at the tail part of observed wave and explained it as a free oscillation of cracks [2]. However, fast and reliable test was not realized due to the lack of imaging capability.

In this situation, we propose a fast and reliable method by a nonlinear ultrasonic phased array (PA) using digital signal processing (DSP). Since transducers in conventional PA can not generate an intense ultrasound required in nonlinear testing of cracks, we developed a LiNbO3 single crystal transmitter, which can endure against high voltage input, with an appropriate wedge made of polyimide. It is driven by a short tone burst amplified by a gated amplifier, whereas the PA is utilized as a receiver. Before imaging, DSP extracts linear, subharmonic or superharmonic components. Then, it is necessary to calculate a time shift of the waveforms arriving from focal point, since the transmitter and receiver are different. We defined the coordinates for describing the geometry with single probe as a transmitter and phased array sensor as a receiver, and then, formulate the propagation time and time delay.

To verify the performance of nonlinear PA, fatigue cracks were introduced in aluminum alloy samples by a three-point bending fatigue test under two conditions: (1) a maximum stress intensity factor Kmax of 17 kgf/mm$^{3/2}$ and a minimum stress intensity factor Kmin of 2 kgf/mm$^{3/2}$. (2) Kmax of 14 kgf/mm$^{3/2}$ and Kmin of 2 kgf/mm$^{3/2}$. We conducted the imaging of the crack by extracting linear and nonlinear components respectively, and succeeded in imaging of a crack tip, which had been overlooked before without the PA. In the linear image, the crack tip in sample (1) was clearer than that in sample (2). In contrast, in the subharmonic image, the crack tip in sample (2) is clearer than that in sample (1). Also, second harmonic images were obtained in both, though the intensity

was low due to the frequency response of the PA. In conclusion, we demonstrated that the nonlinear PA with a LiNbO3 single crystal transmitter provides various images representing the crack with different stress history, and it is a promising tool for fast and reliable nondestructive evaluation of closed cracks.

[1] K. Yamanaka, et al. Jpn. J. Appl. Phys. 43 (2004) 3082. [2] R. Sasaki et al, to be published in Jpn. J. Appl. Phys. 44, 6B (2005).

This work was supported by a Grant in Aid for Science Research (No. 15360377, 15656179, 16206071), from the Ministry of Education, Culture, Sports, Science and Technology.

P3F-2

MULTIPLE FLAWS LOCATION BY MEANS OF NDE ULTRASONIC ARRAYS PLACED AT PERPENDICULAR PLANES.

M. A. RODRIGUEZ[1], A. RAMOS[2], and J. L. SAN EMETERIO*[2], [1]Universidad Politecnica Valencia, Valencia, Spain, [2]Instituto Acustica CSIC, Madrid, Spain. Corresponding e-mail: marodrig@upvnet.upv.es

A new procedure for ultrasonic location of multiple flaws using two identical mutually perpendicular arrays is presented. It is a generalization of the method proposed in [1] which was limited to the location of isolated flaws. This previous method is based on the ultrasonic inspection with two broadband transducers arrays located at perpendicular surfaces. The individual transducers work in near field zones and are sequentially operated so that in each shot only one transducer emits and receives. Each elementary area of the inspected piece provides information to be received by two perpendicular transducers. A specially designed digital signal processing algorithm combines the information obtained by each transducer to form a two-dimensional representation of the inspected area. Several algorithms to improve quality in this two-dimensional representation have been previously presented [2, 3]. Nevertheless, this method is valid only for isolated flaws, so that when two flaws are closely located into the same elementary area, two additional flaw indications of phantom type could appear and an ambiguity is produced.

This paper proposes a solution to the location of proximate multiple flaws using information acquired by emitting and adjacent transducers. Thus, in each shot, one transducer emits and three transducers receive (the emitting and the two adjacent ones). A new digital signal processing algorithm has been developed which includes two basic steps: i) in the first step, only the echo-traces received by the emitting transducers are used by means of a time-envelope combination method [1], which produces a first two-dimensional representation; ii) the second step is applied only when two or more flaws are located in the same elementary inspection area, and it is based on the information acquired from adjacent transducers.

To illustrate the procedure, simulation results corresponding to an inspected piece with three flaws will be presented. Two of these flaws are closely located into a common intersection area and the third one is located in other distant zone. After the first combination step, the two flaws of the same area produce

two additional phantom flaws, whereas the third reflector originates only one indication. After the application of the second procedure step, the phantoms are eliminated whereas the real flaws remain.

[1] M.A. Rodriguez, A. Ramos, J.L. San Emeterio. Localization of isolate flaws by combination of noised signals detected from perpendicular transducers, NDT&E International, 2004 (37): 345-352.

[2] M.A. Rodriguez. Ultrasonic Non-Destructive Evaluation with Spatial Combination of Wigner-Ville Transforms, NDT&E International, 2003 (6): 441-445.

[3] M.A. Rodriguez, A. Ramos, J.L. San Emeterio, J.J. Perez. Flaw location from perpendicular NDE ultrasonic transducers using the wavelet packet transform. IEEE Ultrasonic Symposium. Montreal, 2004, Session P3UX-5:L8.

This work was supported by the Spanish Ministry of Education and Science (R&D Project PI2002-00441) and CYTED - CNPq (Research Project 'Pulsets')

P3F-3
DIGITAL PROCESSING FOR AN AIR-COUPLED ULTRASOUND NDT SYSTEM USING CONCAVE ARRAYS.

Y. YAÑEZ*, M. J. GARCÍA-HERNÁNDEZ, A. TURÓ, J. SALAZAR, J. GARCÍA-ALVÁREZ, C. BALLABRIGA, and J. A. CHÁVEZ, Politechnical University of Catalonia, Barcelona, Barcelona, Spain.
Corresponding e-mail: yyanez@eel.upc.edu

Non-Destructive Testing is a growing field of interest for those industries where the development of high-value components implies the need of better quality control. Ultrasonic testing is widely used to test a great variety of materials, but ultrasonic waves need a couplant to get a good transmission coefficient between the inspected material and the ultrasonic transducer. Liquid couplants are widely used but in applications where the inspected material can be altered or destroyed, air-coupled ultrasound is more suitable. However, when air is used as couplant, new problems arise, such as the higher attenuation of ultrasound, specially at high frequencies, and the huge acoustic impedance mismatch between air and transducers. Matching layers are included in the transducer to improve the transmission coefficient,and improvements in the emitter and the receiver are implemented in order to achieve the required dynamic range of the system.

The main benefit which Lamb waves contribute in is the ability to inspect thin plate structures of large area in a short time. The way for coupling ultrasound from air into Lamb waves in the plate is by generating a plain wavefront with an specific angle of incidence. Lamb wave ultrasonic techniques are mostly based on the use of a single element ultrasonic transducer, where the single element is specifically oriented to excite the desired Lamb wave mode. The angular range where Lamb wave modes can be excited is very narrow in air, therefore a system providing high angular resolution is needed. An array system is a good solution to obtain this high angular resolution. It also has two main advantages, transducer arrays allow accurate beam steering, and the signal-to-noise ratio

improves. Nevertheless, the use of transducer arrays supposes a considerable increase of the complexity of emission and reception systems.

This work presents a signal processing subsystem for an air-coupled concave array NDT system, which uses Lamb waves. The main goal of the inspection system is the on-line evaluation of any type of laminate material during the fabrication process. A typical example is the fabrication of paper.

The subsystem is able to equalize, delay and add signals provided by a circular concave array used to receive Lamb waves in laminate materials, such as paper. A Field Programmable Gate Array (FPGA) is used in order to achieve shorter processing time and more flexibility than with Digital System Processor (DSP) systems. Furthermore, a special memory configuration has been implemented in order to accelerate data processing. The array has circular concave shape and hence the delays used to get a plain wavefront are not lineal, thus a table with the delay values must be stored inside the FPGA. The feasibility of the system has been demonstrated with the measurements done.

This work has been supported by the research project DPI2004-02853, of the Ministry of Science and Technology of Spain.

P3F-4
MAGNETOSTRICTIVE GRATING TRANSDUCERS: EFFECTS OF GRATING SIZE AND SHAPE.

I. K. KIM* and Y. Y. KIM, Seoul National University, Seoul, Korea.
Corresponding e-mail: kik@idealab.snu.ac.kr

In many applications, pure shear-horizontal (SH) wave generation is critical because non-dispersive SH waves are very convenient for signal processing. If SH waves are generated and measured successfully in plate structures, one can use the wave transduction method in various non-destructive evaluation applications including bio-MEMS applications. As a preliminary study, we considered somewhat a large-scale SH-wave transducer. As an efficient means to generate and measure SH waves, we considered using the principle of magnetostriction because the energy conversion between magnetic energy and acoustic energy in magnetostrictive material can take place wirelessly. In this investigation, the grating-type magnetostrictive transducer was considered as the first choice; by changing grating size and distance, the SH waves at desired frequencies can be tuned. Our grating-type transducer consists of nickel patches, permanent magnets and coils providing an alternating current. The static bias magnetic field by permanent magnets should be perpendicular to the field generated by the coil.

In our magnetostrictive frequency-tuned transducer, the nickel gratings work not only as the element for generating and sensing ultrasonic waves but also as the path of the magnetic field. Therefore, the shape of the nickel gratings can affect the performance of the magnetostrictive grating transducer. We investigated the effect of the shape and the size of nickel patches on the SH wave transduction efficiency and examined the frequency-tuning characteristics and Q-factor of grating-type transducers. Experiments showed that the bias field strength and the grating width should be selected appropriately not to

generate unwanted wave modes such as the Lamb wave modes but to generate SH waves only. It was also confirmed by experiments that the grating distance controls the center (or tuning) frequency of the grating transducer. To improve the Q-factor significantly, we considered grating shape variations. Interestingly, the Q-factor became maximum for non-rectangular gratings; conventional gratings were rectangular.

P3F-5

INNOVATIONS IN MONITORING FLUID AND PARTICULATE FLOW WITH SPECIAL EMPHASIS ON DRILLING OPERATIONS USING MULTI SENSOR DATA FUSION WITH AN ARRAY OF AE SENSORS AND TEMPERATURE SENSORS.

K. J. ALME[2] and S. MYLVAGANAM*[1,2], [1]Telemark University College, Porsgrunn, Norway, [2]Tel-Tek, Porsgrunn, Norway.
Corresponding e-mail: saba.mylvaganam@hit.no

The usage of acoustic emission in sand detection and monitoring is well proven and widespread in the oil and gas industry. A new type of flange mounted AE sensors has been used in various particulate flow studies. An array of such sensors and the processing of their signals give not only the concentration of particulates but also their average flow velocities. By employing passive AE-sensors, in addition to active ultrasonic sensors used in interrogating pipe integrity and erosion, it has been shown that the flow of particulates in pipelines can be monitored without interrupting the process, thus leading to improved process monitoring and control in the multi-phase flow applications encountered in the oil and gas industry.

A sensor suite comprising multiple AE sensors, active ultrasonic sensors and an array of RTDs have been used successfully in achieving the following in pilot plants consisting of pipelines for liquid transport, gas and particulate flow: concentration of particulate material from signature signals from AE-sensors, flow rate of particulates, liquid/gas flow rate and slip velocity in two phase flow. Some of these measurements have been verified using LDA measurements. Both frequency and time domain analysis are used in the sensor data fusion algorithms. Artificial intelligent technologies involving multivariate data analysis and neural networks are also used in the analysis and presentation of the data. Some results will be shown online during the conference involving selected sensors from the multi sensor suite used in this study by performing remote operations on the rigs used for this study.

The paper rounds up by looking into the possibilities of using these techniques with new types of microsensors and optical sensors used for temperature profiling in drilling operations.

Part of this work is sponsored by the Royal Norwegian Research Council. Part of the PLC based AE sensor system was financed by the EU thematic network 'THEIERE'. Some of the algorithms based on AI was developed by project groups over the last few years.

P3F-6

A NEW TRANSDUCER FOR TORSIONAL GUIDED WAVE GENERATION AND DEFECT DETECTION.

Z.-H. LIU*, B. WU, C.-F. HE, X.-Y. WANG, and S.-M. YANG, Beijing University of Technology, Beijing, People's Republic of China.
Corresponding e-mail: lzhbull@hotmail.com

Different kinds of defects, such as corrosion, crack etc, usually affect operating life of long pipes in the industry. Guided waves are suitable to test these pipes for they can propagate long distance from a single probe position. Two kinds of axisymmetric guided wave modes, longitudinal and torsional modes, are usually used in long pipe inspection. Longitudinal modes are sensitive to circumferential defects but insensitive to longitudinal defects. However, it is possible that torsional modes are suitable for detecting all types of defects including longitudinal defects for their unique wave structures. For exciting torsional mode to detect defects in pipe, a new transducer is developed in this paper. The transducer is made of many shear mode piezoelectric elements. These elements are attached axisymmetrically around a pipe end to form a ring. Their top and bottom segements will vibrate oppositely uniformly, shearing deformations will generate along the circumferential direction of pipe and torsional modes are excited when their electrodes are activated simultaneously. Tone bursts of 10 cycles modified by Hanning window function are excited in a 4-m-long, 60-mm-OD, 3.5-mm-wall carbon steel pipe. It is confirmed that end-reflected waveforms are T(0,1) mode by calculating their propagation velocities. For verifying the feasibility to detect different defects, two kinds of penetrant defects, longitudinal and circumferential defect, are processed successively. Their dimensions are 35-mm-long, 1-mm-wide and 26-mm-long, 1.2-mm-wide and they are 2.5m and 1.5m apart from the pipe end with these elements respectively. The echoes of two defects are found easily in received signals. Results show thickness shear mode piezoelectric elements can excite torsional guided wave to detect defects in pipes.

Thanks are given to National Natural Science Foundation of China (No. 10272007, 60404017 and 10372009) and Beijing Natural Science Foundation (No. 4052008) for their support of this project.

P3F-7

DESIGNING AND EVALUATING TRANSDUCERS FOR NARROWBAND ULTRASONIC SPECTROSCOPY.

M. JONSSON and T. STEPINSKI*, Uppsala University, Signals and Systems, Uppsla, Sweden.
Corresponding e-mail: ts@signal.uu.se

Introduction of new composite materials in airspace applications has created a demand for an efficient NDE technique. Ultrasound resonance inspection is especially suitable for the inspection of multilayered structures. In the narrowband ultrasonic spectroscopy (NBUS), which we developed recently [1], the surface of an inspected structure is scanned with a resonant transducer whose frequency response is monitored in a narrow frequency band. Since a piezoelectric

transducer is an electromechanical device the parameters of its electrical resonance depend on its mechanical load, i.e., the acoustical impedance of the inspected material. Thus, in this kind of test, the resonance spectrum of the inspected structure is not measured directly but through its influence on the resonance spectrum of a narrowband transducer. A feasible way of extracting information about the inspected structure using a narrowband piezoelectric transducer is sensing variations of its electrical impedance caused by the varying conditions of the inspected structure. The electrical impedance for a predefined frequency in the vicinity of transducer's resonance is relatively easy to measure using a vector voltmeter.

The paper is concerned with optimizing the NBUS setup consisting of a piezoelectric transducer coupled to a multi-layered structure. Variations of the electrical impedance of a piezoelectric transducer caused by variations of parameters of the inspected structure are estimated using an equivalent circuit and a finite element based model.

First, the KLM equivalent circuit model which takes into account mechanical loads on both surfaces of its piezoelectric element is used to model the NBUS setup. A simplified model valid for plane longitudinal waves is used to model the inspected multilayered structure.

Second, the results obtained using the finite element model accounting for finite dimensions of the piezoelectric transducer and different elastic waves in the multilayered structure are presented.

Variations of transducer's electrical impedance resulting from the presence of flaws and weak bonds in the multilayered structure are presented in plots in function of frequency. The results obtained using both models are compared with the measurements performed using a network analyzer.

Contrary to common opinions, the presented results show that NBUS inspection of multilayered structures can be effciently performed using transducers with much lower center frequencies than those required in pulse-echo inspection of the same structures.

[1] T. Stepinski and M. Jonsson, "Narrowband Ultrasonic Spectroscopy for NDE of Layered Structures", INSIGHT, J. of The British Inst. of NDT, vol. 47, pp. 220 - 224, 2005.

P3F-8

MEASURING THE INNER BODY TEMPERATURE USING A WIRELESS TEMPERATURE SAW-SENSOR-BASED SYSTEM.

G. MARTIN[1], P. BERTHELOT[1], A. LAMBERT[2], W. DANIAU[1], V. BLONDEAU-PATISSIER[1], and S. BALLANDRAS*[1], [1]FEMTO-ST, CNRS, Besançon, France, [2]INSERM, Strasbourg, France.
Corresponding e-mail: ballandr@femto-st.fr

Sensor systems based on a remote control of a set of passive surface acoustic wave (SAW) devices have been implemented for various purposes. They are particularly used for measuring physical parameters such as temperature,

pressure, etc., in the 433.9 MHz ISM (Industrial, Scientific, Medical) band. A lot of work has been devoted to improve the passive SAW devices used in that matter. If coding is not an issue, the use of SAW resonators is the most simple way to implement such systems. The required information is then provided by the frequency shifts of the resonant sensor, and its resolution is mainly governed by the resonance quality factor. The sensor usually consists in one reference and one proof body. From the electronics side, one must take care of the stability of the interrogation system itself to ensure that the actual sensor resolution can be reached.

In this work, the possibility to measure the temperature of the inner body is addressed. As explained above, the system consists in two SAW resonators wirelessly interrogated using a system that scans the band to detect the device responses. It is based on a Direct Digital Synthesis (DDS) using a Temperature Compensated Crystal Oscillator (TCXO) allowing for a stability of the emitted signal frequency better than 1 ppm/K on the working range 0-75°C. After amplification and filtering, the received signal attacks an IQ detection circuit used to improve the signal/noise ratio. One then tracks the SAW resonator responses on the received signal and stores the corresponding frequencies for exported post-treatments. The SAW sensors are built on YZ-cut of LiNb03 because of its very high sensitivity to temperature and its large coupling coefficient yielding sufficient energy conversion efficiency to fight against the strong insertion losses arising in organics. They also must be packaged to enable ingestion and transit via the digestive canal. This imposes drastic conditions on the antenna which must be small enough to ease the swallowing and capable to receive and emit signals in the used frequency band. A particular antenna design is then proposed, allowing for reducing the whole sensor size down to a 3.5 cm long 0.8 radius PDMS cylinder that contains both the antenna and the SAW resonators. The efficiency of the system is reported and first tests on living animals are discussed.

P3F-9

UNDERSURFACE PHOTOACOUSTIC IMAGING OF PLANE SOLID SPECIMENS BY THE USE OF A LINE LASER BEAM.

T. HOSHIMIYA*[1] and M. SUZUKI[2], [1]Graduate School of Engineering, Tohoku Gakuin University, Tagajyo,, Japan, [2]New Inductrial Creation Hachery Center, Tohoku University, Sendai,, Japan.
Corresponding e-mail: tpth@tjcc.tohoku-gakuin.ac.jp

In this paper, a line laser beam focused on a solid plane specimen was used to perform nondestructive imaging of undersurface defect by photoacoustic microscope. A CT (computed tomography) technique was applied to the imaging of a line-shape undersurface defect fabricated at the welded region of two steel plates by drilling. The diameter of welded region is about 8mm and the steel thickness is 1.5mm each. A second harmonic green laser beam of a LD-pumped YAG laser was expanded and focused on a specimen by concave and cylindrical lenses, respectively. The laser beam scanning to the specimen was achieved by rotating with a mechanical rotating stage controlled by a computer. Rotation

step and the amount of rotation were 1 and 180 degrees, respectively. Laser power and modulation frequency were 28 mW and 8 Hz, respectively. The size of a lser beam on a specimen was 8 mm (length) times 1 mm(width). The detected photoacoustic (PA) signal is proportional to that generated on the plane specimen surface summed along the focused line-shaped laser beam. The PA signal shows a maximum at the defect with the ratio of 1.43 compared to the background. The measurement time used for a single scan was 7 minutes. That was about 4 times shorter than a conventional PA imaging by 2D scanning, which takes 30 minutes. This measurement is the first one in the photoacoustic tomographic trial with a line laser beam.

Session: P3G
GENERAL PHYSICAL ACOUSTICS
Chair: V. Proklov
IREE Russian Academy of Sciences

P3G-1
THEORY OF ONE-DIMENSIONAL ACOUSTIC WAVE PHASE CONJUGATION.

A. MERLEN[2,3] and Q. ZHANG*[1,2], [1]Université des sciences et techniques de Lille, Villeneuve d'Ascq, France, [2]Laboratoire de mécanique de Lille UMR CNRS 8107, Villeneuve d'Ascq, France, [3]Joint European Magneto-Acoustics Laboratory, Villeneuve d'Ascq, France.
Corresponding e-mail: alain.merlen@univ-lille1.fr

The WPC in acoustics or ultrasonics is a non-linear coupling between an incident acoustic wave and an oscillating source of energy. It is the acoustic or ultrasonic equivalence of Brillouin scattering in optics. In parametric resonance conditions, the incident wave is amplified exponentially and, by conservation of momentum, gives rise to a conjugate wave time-reversed and also exponentially amplified. Recently, WPC became of great interest since new technical possibilities were demonstrated particularly in acoustic imaging thanks to magnetostrictive solid materials.

In practice, a magneto-acoustic wave conjugator is generally a cylinder of magneto-strictive material partially submitted to a magnetic field.

The incident wave travels approximately along the axis of the conjugator, hence the most simple theoretical model is the one-dimensional situation.

In ultrasonics, in opposition to optics, the saturation process leading to the end of the exponential growth, does not come from the constitutive law of the medium since the relative variation of the sound velocity with the intensity of the wave is negligible compared with what happens to the refraction index in optics. The non linear processes leading to saturation have been shown to be the feedback from the elastic energy toward electric energy. This happens only when the stress becomes very high and explains why the exponential growth can be

observed during a long time before saturation. Therefore, the linear pumping theory is far much useful in acoustics than in optics. This is why, here, the acoustic or ultrasonic wave phase conjugation (WPC) in active medium is treated in a theoretical and numerical way in one dimension, in the frame of the linear pumping assumption. In other words, the pumping is considered as a small harmonic oscillation of the sound velocity of the medium around a constant value.

Actually, there are few analytical solutions of this problem in the literature except a very general solution obtained by Laplace transform, in the frame of Brillouin diffusion in optics, for a finite active zone in an infinite homogeneous medium. Here the solutions are derived by a multi-scale method in a very practical formulation which could be generalized to the heterogeneous cases. These analytical solutions explain many properties of the phase conjugators (critical threshold, variation of the stress spatial repartition inside the sample) or allow the optimisation of the impedance ratio in order to extract the maximum acoustical energy possible for a given pumping. This is a clue point for medical applications like hyperthermia of cancer cells. Finally, despite of the simplification due to the 1D hypothesis, the conclusions obtained here are very similar to the experimental ones and help for a deeper and quantitative understanding of the phenomenon.

Some of these answers to the questions which were not solved hitherto can have a great importance for the applications of such a time reversal with giant amplification which are numerous in acoustic imaging, non destructive testing ... and for high energy cases, in non-intrusive surgery.

P3G-2
FLOW VELOCITY MEASUREMENTS BY MEANS OF NONLINEAR INTERACTION OF PHASE CONJUGATE ULTRASONIC WAVES.

Y. PYLNOV[1,2], V. PREOBRAZHENSKY[2,3], P. PERNOD*[2], and N. SMAGIN[1,2], [1]Moscow Institute of Radioengineering, Electronics and Automation/LEMAC, Moscow, Russia, [2]Institut d Electronique, de Microelectronique et de Nanotechnologie (IEMN-DOAE UMR CNRS 8520/LEMAC), Lille, France, [3]Wave Research Center of General Physics Institute RAS/LEMAC, Moscow, Russia.
Corresponding e-mail: pylnov@yandex.ru

The application of the method of parametric wave phase conjugation (WPC) of ultrasound in measuring the velocity of flows in liquids is presented in this paper. A fundamental property of phase-conjugate waves (PCW) is their ability to reconstruct the phase of the primary wave at its source. The phase reconstruction is directly connected with the invariance of an acoustic field with respect to time reversal. It allows compensating phase aberrations in the traces of propagation of PCW. In the presence of flows in the propagation medium, this invariance is violated. As was demonstrated in [1,2], the presence of flows in the propagation region leads to an uncompensated Doppler shift in the phase of a phase-conjugate wave at the source, that may be used for measuring the flow velocity with the help of phase conjugation.

Development of the supercritical parametric technique of acoustic WPC, notable for giant amplification of PCW, stimulated the beginning of investigations in the field of nonlinear wave front reversal acoustics. Using of high power ultrasound PCW in ′harmonic imaging′ systems allowed improving characteristics of acoustical images.

In this paper, we consider some new approaches of using the phase-conjugation phenomenon in nonlinear ultrasonic velocimetry of flows in liquids. In the first approach the Doppler phase shift of second harmonic of PCW (fundamental harmonic frequency 10MHz) was used for reconstruction of the velocity profile of liquid jet. The acoustic image of flow obtained by this method is demonstrated. It is shown that the sensitivity of Doppler shift to the flow velocity variations increases twice by using of the second harmonic of PCW.

In the second approach the Doppler phase shift of low frequency emission (LFE) generated by nonlinear interaction of phase-conjugate ultrasonic waves was studied. In this case two co-propagating waves: ultrasonic wave of frequency 11MHz and PCW of frequency 10MHz was used to provide ultrasonic wave of frequency 1MHz. It is shown that the phase shift of the low frequency wave in this case is defined by the high frequency of PCW (10MHz) and is much higher than might be expected for 1 MHz wave.

In the third approach we studied the phase shift of LFE signal (1MHz) generated by nonlinear interaction of the second harmonic of PCW (20MHz) and co-propagating ultrasonic wave of frequency 19MHz. The increase of signal-to-noise merit proportional to the frequency ratio (20 in our experiment) was obtained in this case.

The carried out experiments have shown that by using nonlinear acoustic effects accompanying the propagation of PCW in a moving liquid one can get improvement of characteristics of Doppler imaging systems.

1.Y. Pylnov, O. Bou Matar, V. Preobrazhensky, Ph. Pernod. IEEE Int. UFFC Conf.Aug. 24-27, 2004, Montreal, Canada.

2.Y. V. Pylnov, P. Pernod and V. L. Preobrazhensky. Acoust. Phys., 51, No1, 105-109, 2005

The research described in this publication was made possible in part by Awards No VZ-010-0 of the U.S. (BRHE), PICS program CNRS-RAS N5008, Ecole Centrale de Lille, French Embassy in Moscow (MAE), Interreg IIIa.

P3G-3
TIME REVERSAL INTERACTIVITY: EXPERIMENT AND MODELIZATION.

G. RIBAY*[1], R. K. ING[2], N. QUIEFFIN[2], D. CLORENNEC[1], S. CATHELINE[1], and M. FINK[1], [1]Laboratoire Ondes et Acoustique, ESPCI, Université Paris VII,, Paris, France, [2]Sensitive Object, Research & Development Department, Paris, France. Corresponding e-mail: stefan.catheline@espci.fr

Thanks to the Time Reversal theory, a technique of localization of an impact generated by a simple finger knock on solid objects has been developed. This concept applied in the interactivity field can transform objects in tactile remote control with a very basic equipment: an accelerometer and a personal computer.

From a signal analysis point of view, this adaptive technique can be decomposed in two steps: in a first learning step, acoustic signatures of interactive points are stored in a memory. In the second step, when a user knocks on the object, the acoustic signature is compared to the ones stored and the knock position is determined. The TR theory predicts that this second step can work only if the medium acoustic reciprocity has not been broken by any change in the medium including waves speed variation due to temperature change. Thus we studied the influence of temperature on the ability to localize an impact. During the cooling phase of a plate and a bar from 50°C to 20°C, knocks were given by a vibrator on the object surface at regular intervals. A laser interferometer coupled to a low-frequency demodulator was used to measure the displacements at the surface, thus avoiding the temperature-dependence of the sensors. We observed that the temperature variation leads to a stretching of acoustic signatures. It is shown that a simple contraction can restore the reciprocity which shows the feasibility of the technique for outdoor Time Reversal interactive experiment.

The same laser experiment shows that the frequency range of the wave created by such a knock on 0.1 to 1cm thick plate or bar is less than 20kHz. Now, Lamb waves at such low frequency have not been often studied. Since it is difficult to create monochromatic plane wave at such a frequency, a 2D numerical simulation has been developed and used to deduce the phase-shift of lamb wave at this frequency when reflecting on a free edge: as predicted by the theory, this phase-shift tends to Pi/2 when the frequency tends to 0. Moreover, we could observe that the evanescent waves are confined near the edges, and are negligible at around one centimenter far from the edge. Finally, thanks to the simulation, we could have access to the wave field in the whole depth of a plate, and thus quantify the energy of each of the two possible propagative Lamb mode at these frequencies. It was deduced that with this kind of excitation, the A0 Lamb mode is predominant, and mode conversion at the edges is negligible. Given that the A0 wavelength is much smaller than the S0 wavelength, this explains why we can distinguish two impacts on a 5 mm thick plate separated by one or two centimetres.

This work was financed by the European FP6 IST Project "Tangible Acoustic Interfaces for Computer-Human Interaction (TAI-CHI)". The support of the European Commission is gratefully acknowledged.

P3G-4
ON THE FORCES ACTING IN MICROMANIPULATION OF PARTICLES AT LOW FREQUENCIES.

F. PERALES* and I. GONZALEZ, Acustic Institute, CSIC, Madrid, Spain.
Corresponding e-mail: fperales@ia.cetef.csic.es

Micromanipulation of particles by ultrasound in standing pressure waves has been researched by diverse research programs, but only axial forces have been taken account and the order of magnitude of frequencies was Mhz.

Rayleigh streaming is originated in a resonating chamber when standings pressure waves are established. This streaming drives particles towards nodes or antinodes, depending on their properties, by Direct Radiation Force (DRF).

In addition, some lateral mechanism have been observed but they haven´t been researched yet. A vertical and a horizontal resonating chamber were made for this research. An experimental and theorical study has been developed in this work. Both air bubbles (500 μm of diameter) and aluminum particles (50 μm of diameter) were studied. They were driven towards antinodes or nodes by axial forces and then, they were collected in clumps due to lateral forces.

An expression of these forces had been developed analytically. The movement of particles has been observed and analyzed by a camera. Analytical and experimental results were very similar.

This work is one of the first theorical and experimental results of micromanipulation of particles by lateral forces at a low frequency as 56.7 and 123 KHz. These results could be very useful for macro manipulation of particles or bubbles in a washing machine.

P3G-5
DIRECT OPTICAL MEASUREMENT OF THE Q VALUES OF RF-MEMS RESONATORS.

O. HOLMGREN*[1], K. KOKKONEN[1], V. KAAJAKARI[2], A. OJA[2], and J. V. KNUUTTILA[1], [1]Materials Physics Laboratory, Helsinki University of Technology, Espoo, Finland, [2]VTT Information Technology, Espoo, Finland.
Corresponding e-mail: oholmgre@focus.hut.fi

Micromechanical bulk acoustic mode silicon resonators may offer an attractive alternative for reference oscillators in wireless communication applications; these RF MEMS resonators possess high Q values (130,000) in vacuum, good power handling capacity (0.12 mW) and low phase noise (-138 dBc/Hz at 1 kHz offset from the carrier) [1]. Typically, Q values are determined from electrical measurements. However, a direct measurement of the surface displacements can be used to determine the mechanical Q value of the resonator. Such measurements provide more detailed information on the device operation. In this work, we have determined the Q values of a RF MEMS square-plate resonator utilizing a scanning Michelson laser interferometer [2].

The main vibration mode of the MEMS square plate resonator (13.1 MHz) can be characterized as a two-dimensional plate expansion preserving its original shape [1]. The test resonator also exhibits the Lamé mode (12.1 MHz) in which the edges of the square plate bend in antiphase preserving the volume of the plate. Vibrations in both modes occur parallel to the plate (in plane). However, the surface of the resonator plate also features an out-of-plane vibration component due to the Poisson ratio of the silicon crystal.

High Q values for the resonator are achieved only when operated in vacuum. In atmospheric pressure, the Q value is decreased substantially due to air damping, typically by an order of magnitude. To facilitate interferometric measurements in vacuum, a custom-build sample enclosure has been developed. The MEMS resonator is placed in a small metal case with a quartz window and with a connecting tube to a vacuum pump. The measurement beam of the interferometer passes through the quartz window onto the surface of the resonator.

We have measured in- and out-of-plane vibration components as a function of frequency in ambient air pressure and in vacuum (pressure below 1 mbar) for both the main mode and the Lamé mode. From these measurements, the Q values are determined for each case. For a typical sample, the mechanical Q values in air pressure are close to 5000 while in vacuum they are roughly ten times higher. Results are compared to electrically measured Q values.

[1] V. Kaajakari et al., Electron Dev. Lett., **25**, 173 (2004).

[2] J. V. Knuuttila et al., Opt. Lett. **25**, 613 (2000).

Acknowledgements: O.H. thanks the Research Council of HUT and the Alfred Kordelin Foundation for scholarships, and the Magnus Ehrnrooth Foundation for a travel grant. This research has been supported by the Academy of Finland through the Programme TULE (Future Electronics Research).

P3G-6
ESTIMATION OF THE 3RD-ORDER ELASTIC CONSTANTS OF POLYMERIC MATERIALS USING A BRILLOUIN SCATTERING TECHNIQUE.

K. KADOWAKI* and M. MATSUKAWA, Doshisha University, Kyotanabe, Kyoto, Japan.
Corresponding e-mail: dte0127@mail4.doshisha.ac.jp

The conventional ultrasonic material characterizations stand on the point of the linear elasticity theory. They have then give us the information of ultrasonic wave velocity and attenuation, which can be related to the real and imaginary part of elasticity. The measurement of nonlinear elasticity, however, brings us another feature of the structure, because it is connected with the anharmonic atomic and molecular interaction forces. In case of solid materials, the measurement of nonlinearity results in the observation of higher order elasticity. In many metals, 3rd order elastic constants have been experimentally investigated. However, few studies have treated the polymeric materials and biological tissues, in spite of the importance of nonlinearity characterization of the visco-elastic materials. We have then focused on the non-contact evaluation of the nonlinear elasticity of the isotropic polymeric materials.

There are various ultrasonic methods for the measurement of 3rd order elastic constants. One method is the observation of the distortion of finite amplitude elastic waves, which pass through the materials. This method, however, has many difficult problems resulted from the wave propagation phenomena. On the other hand, Brillouin scattering technique makes us free from the difficulties of the precise wave-form measurements, because this technique enables non-contact measurement of the thermal phonons. In this study, we have measured wave velocities in the polymeric sample under the tensile stress, using a Brillouin scattering technique. In addition, by using 90A scattering optical geometry, we can realize the simultaneous measurements of longitudinal and shear wave velocities in the sample without considering the refractive index. The stable experimental condition has improved the precision of velocity measurements (maximum uncertainty 1%) at the GHz range, in spite of the very weak scattering light.

The experimental system is maintained in the range of 24±0.5 degrees C. Polyvinylchloride (PVC) plate with thickness of 0.5mm was shaped into a dumbbell specimen. The tensile test is performed at the rate of 0.5mm/min. The PVC specimen yielded at the strain of 13%. Here, the true stress is always estimated by using Poisson's ratio 0.353. We have operated both measurements of stress and wave velocities. Especially, longitudinal and shear wave velocities were simultaneously obtained by measuring the Brillouin frequency shifts. We then estimated the complete tensors of 3rd order elastic constants which have 6 elements as a function of strain. 3rd order elastic constants became stable in the strain of more than 4%, showing the negative values. The obtained constants, e.g. c_{111}=-236[GPa], are not contradictory with the reported 3rd order elastic constants of other polymeric materials. However, these elements showed comparatively large uncertainty, which were carefully investigated considering the both Brillouin and stress measurements.

P3G-7
THE INTERACTION OF ULTRASOUND WITH MUD IN BETWEEN HARD SOLID AND IDEAL LIQUID.

N. F. DECLERCQ*, J. DEGRIECK, and O. LEROY, Soete Laboratory, Department of Mechanical Construction and Production, Ghent University, Sint Pieternsnieuwstraat, Gent, Belgium.
Corresponding e-mail: NicoF.Declercq@ugent.be

A liquid, showing Bingham behavior, such as mud, in between a hard solid and an ideal liquid, forms a rheological system in which the physical parameters vary continuously. Moreover, inside this liquid, there is often a transition zone in which the shear wave velocity varies almost exponentially. For mud, this zone is called the nautical bottom and determination of its position is very important for the harbor and dredging industry. First we translate this rheological system into a theoretical rheological model that is numerically susceptible to predict its physical influence on impinging sound. Then, we show theoretically how the interaction of sound with this rheological model is solved. The presented theory is valid for pure homogeneous plane waves as well as for inhomogeneous plane waves. Finally, we present some numerical results for impinging inhomogeneous waves and we show how a bounded beam interacts with this continuously layered system. It is seen form our calculations that a standing wave pattern is generated within the Bingham liquid and that the incident beam bends away from the normal. It is also shown that total reflection might occur on each layer at particular angles of incidence. Furthermore, the position of the nautical bottom, in the case of mud, can be determined by studying the reflected bounded beam profile.

Nico F. Declercq is a Postdoctoral Fellow of the Research Foundation - Flanders (FWO - Vlaanderen)

Session: P3H
BAW MATERIALS AND PROPAGATION I
Chair: J. Brown
JB Consulting

P3H-1
PROPAGATION OF ACOUSTIC WAVES THROUGH PERIODIC STRUCTURES CONTAINING PHASE DISCONTINUITY.

Y. GULYAEV[1], V. PUSTOVOIT[2], G. MANSFELD*[1], and V. DMITRIEV[3], [1]Institute of Radioengineering and Electronics RAS, Moscow, Russia, [2]Scientific and Technological Center for Unique Instrumentation RAS, Moscow, Russia, [3]Institute of System Engineering, St.Peterburg.
Corresponding e-mail: mans@mail.cplire.ru

The report contains the analysis of peculiarities of BAW and SAW propagation through the system of two reflecting Bragg structures (mirrors) separated by a gap or another structure providing non regularity of the phase of acoustic wave. For excitation and detection of acoustic waves two transducers located outside the structure are used (contrary to usual SAW resonator where transducer is located between reflecting structures). Such a structure not only reflects the acoustic waves but also provides the propagation of the wave on resonant frequency to the output transducer. Due to interference of the acoustic waves between two Bragg mirrors their amplitude increases and the level of the wave registered by output transducer became comparable with the level of the wave excited by the input transducer. The resonant propagation of the acoustic waves through the structure is possible in a very narrow frequency range.

The analytical approach to the problem of acoustic wave propagation through such structures has been developed. The results were numerically confirmed for the case of BAW structures where reflecting mirrors were made as quarter-wavelength multilayers (matrix approach) and using COM method for SAW structures (mirrors - gratings).

The analysis showed that the bandwidth depends on the reflecting properties of the mirrors. The bandwidth decreases with the increase in the reflectivity of the mirrors and it comes to the limit depending on the material acoustic losses.

The results of the analysis in the case of SAW structures are confirmed by the results of the experiment. The structures under study were made on the surface of quartz crystalline substrate.

P3H-2
INFLUENCE OF ACOUSTIC WAVE ON FORMING AND CHARACTERISTICS OF SILICON P-N JUNCTION.

J. OLIKH*[1], A. EVTUKH[1], B. ROMANYUK[1], and O. OLIKH[2], [1]Institute of Semiconductor Physics, National Academy of Science of Ukraine, Kiev, Ukraine, [2]Kyiv Taras Shevchenko National University, Kyiv, Ukraine.
Corresponding e-mail: jaroluk3@ukr.net

The p-n junction parameters changing are caused by the influence of the Acoustic Waves (AW) treatment on interaction of Si structural defects with implanted impurity. The forming peculiarities of electrically active impurities (B, As) in silicon at the in-situ AW excitation have been investigated. The AW influences significantly on generated by ion implantation point defect redistribution. It was shown the possibility of control the p-n junction parameters by varying the frequency and intensity of AW excitation. Test structures with p-n junctions have been fabricated and tested.

The phosphorus-doped (12 ohm.cm) and boron-doped (10 ohm.cm) (100)- CZ-Si wafers were used for p^+ and n^+ shallow doped layer formation correspondingly. For implantation we used BF_2^+ and As^+ ions with energies E=33 keV and 50 keV correspondingly and dose of 5.10^{14} cm^{-2}, at implantation through upper silicon oxide layer of d=125 nm (BF_2) and d=30 nm (As) thick. The impurity activation was performed by rapid thermal annealing in the temperatures range of 850-1100°C. A set of structured was fabricated at the AW action during ion doping. The samples were mounted inside the implanter chamber on piezoelectric transducer via acoustics binder. Low amplitude ultrasound vibrations were generated in the wafer by operating the transducer in a resonance vibration mode. The basic resonance frequency was varied from 6 MHz to 14 MHz. The amplitude of the deformation did not exceed 10^{-5} corresponding to an acoustic power of (0.2-0.5) $W.cm^{-2}$.

Current-voltage characteristics of the manufactured p-n junctions were measured. It is shown that the p-n junctions fabricated at the AW action have small leakage currents and relatively high breakdown voltage ($I \sim 10^{-9}$ $Axcm^{-2}$, $U_{bd} \sim$ 50-80 V). The increase of breakdown voltages and decrease of the leakage currents of p^+- n and n^+- p junctions were revealed at ion implantation with in-situ AW. This points out the perspectivity of such process for technology of semiconductor devices and ICs. The model of the in-situ AW influence on the impurity redistribution at ion implantation and subsequent rapid thermal annealing has been developed for explanation of experimental results. Current-voltage characteristics of Si solar structures were studied alongside with the influence of AW on the barrier. The influence on the current via the barrier were established also.

The new technological approach of powerful AW as a tool of the engineering makes its possible to control characteristics of semiconductor devices.

The authors would like to thank Dr. Melnik V. for helpful discussions. The research described in this publication was partially supported by the STCU (Project # 2367).

P3H-3

THIN-FILM COMPOSITE RESONATORS ON CRYSTALLINE SUBSTRATES.

A. BALLATO*, US Army CERDEC, Fort Monmouth, NJ.
Corresponding e-mail: a.ballato@IEEE.org

Telecommunications systems depend on high stability frequency sources. For mobile uses such as cell phones, size and cost are severe additional constraints. This paper describes a class of composite piezoresonators that are comprised of piezoelectric thin films deposited on crystalline plate substrates [1] oriented to obtain very low temperature coefficients of frequency (TCFs) for the composite structure. Specifically described are high-frequency bulk acoustic wave resonators (HBARs) comprised of piezoelectric thin films on AT- or BT-cut quartz substrates. In order to achieve low or zero TCFs, it is necessary to utilize the pure shear plate mode in the quartz. When the film driving the motion consists of material in class 4mm or 6mm, such as a piezoceramic, the pure shear mode is driven when the film is in one of two states: 1) polarization vector in the plane of the film, and excited from electrodes placed on the major surfaces, or 2) polarization vector normal to the plane of the film, and excited by electrodes producing an electric field in the plane of the film [2]. The combination of piezofilm and quartz yields miniature, high frequency devices that are able to be accurately designed, while remaining affordable to produce. Electrical networks containing acoustic transmission lines are used to characterize the frequency-temperature and impedance properties of the HBARS. An example design for a 2.1 GHz composite resonator is provided

[1] A. Ballato, “Multilayer devices comprised of piezoceramic thin films on crystalline dielectric substrates,” Am. Ceramic Soc. Trans., vol. 167, pp. 259-269, 2005.

[2] A. Ballato, “Lateral and thickness excitation of obliquely poled ferroelectric ceramic plates,” Am. Ceramic Soc. Trans., vol. 106, pp. 309-332, 2000.

P3H-4

EXPERIMENTAL PROOF OF TEMPERATURE COMPENSATED CUT IN GAPO4 BEAM RESONATOR VIBRATING IN LENGTH EXTENSION.

F. STHAL*, E. BIGLER, M. BECKER, J. DOPEUX, L. DELMAS, and R. BOURQUIN, FEMTO-ST dept LCEP, ENSMM, 26 Chemin de l’Epitaphe 25030 BESANCON Cedex, Besançon, France.
Corresponding e-mail: fsthal@ens2m.fr

We report progression in modeling and measuring temperature effects in vibrating beam Gallium Orthophosphate (GaPO4) resonators. In addition to the well known thickness-shear AT-cut, temperature compensated cuts exist in GaPO4 for length extensional modes. Experimental evidence of temperature compensated cut in GaPO4 rectangular beam resonator vibrating in length extension is given.

Analytical models of temperature-effect [1] are compared with experimental measurements on devices. Experimental frequency-temperature curves are

given for several orientations. The agreement between theory and experiment is fairly good taking into account that temperature coefficients of GaPO4 have been experimentally tested only for a few thickness-shear resonators.

[1] L. DELMAS, F. STHAL, E. BIGLER, B. DULMET, R. BOURQUIN, "Temperature-compensated cuts for length extensional and flexural vibrating modes in GaPO4 beam resonators", IEEE Transactions on Ultrasonics, Ferroelectrics and Frequency Control, vol. 52, no. 4, April, pp. 666-671, (2005).

P3H-5
THE MASS-LOADING INFLUENCE ON ELECTRICAL CHARACTERISTICS OF GaPO4 AND LGS RESONATORS.

I. MATEESCU[1], C. BRAN*[1], F. KRISPEL[2], K. SCOTT[3], and G. JOHNSON[3]
[1]National Institute of Materials Physics, Bucharest, Romania, [2]Piezocryst Advanced Sonsorics GmbH, Graz, Austria, [3]Sawyer Technical Materials, Conroe, TX.
Corresponding e-mail: imate@infim.ro

The investigations on the mass-loading effect in thickness-shear quartz resonators (AT-cut, SC-cut) and langasite resonators (Y-cut) using Ballato's transmission-line analogs, have shown that the harmonic dependence of resonator characteristics is influenced by the electrodes due to the non-uniformity of the vibratory motion over the electrodes of the crystal. Based on these results, the non-uniform distribution of motion, depending on frequency and electrode parameters (geometry, structure, material) was described in terms of coupling of thickness-shear with thickness-twist modes, as well as interfacial stresses between the electrodes and the piezoelectric substrate. The comparative analysis of the results was realized, on the one side, between the AT-cut and SC-cut quartz resonators and, on the other side, between the AT-cut quartz resonators and Y-cut langasite resonators. The experimental results revealed that the maximum harmonic variation of the SC-cut resonators characteristics for various electrode parameters is significantly lower than that of AT-cut quartz resonators and the mass-loading effect on Y-cut langasite resonators is much lower as compared to AT-cut quartz resonators. This behavior is partially done by the stress-compensated feature of the SC-cut and probably of the Y-cut.

This idea is supported by the new experimental results related to the influence of the electrodes on the electrical characteristics of the Y+45°-cut langasite resonators. These results are presented in this paper. The Sawyer Y+45°-cut plan-parallel polished langasite blanks of 14mm diameter and 5MHz resonant frequency were used in experiments. Ag and Au electrodes with 4.6 and 7mm diameters and 100,125,200nm thicknesses were deposited by vacuum evaporation on Y+45°-cut langasite plates. The analysis of the results revealed that the maximum variation of the effective mass-loading, coupling coefficient and inductance as a function of harmonics for various electrode parameters is significantly lower for Y-cut langasite resonators than for Y+45°-cut langasite resonators.

Based on the previous and the present results we see that the Y-cut langasite and SC-cut quartz resonators present a mass-loading effect much lower as compared to the AT-cut quartz and Y+45°-cut langasite resonators.

The conclusion is that the influence of the mass-loading on the characteristics of crystal resonators is dependent on the plate orientation. The knowledge of the mass-loading effect in various orientations of the piezoelectric crystals allows to do the best choice of resonators used in the specific applications.

P3H-6
REBUILDING OF DEFECT STRUCTURE IN GAMMA-IRRADIATED N-TYPE SI CRYSTALS, STIMULATED BY ULTRASONIC.

J. OLIKH*[1], M. TYMOCHKO[1], V. KHIVRICH[2], and M. PINKOVSKA[2], [1]Institute of Semiconductor Physics, National Academy of Science of Ukraine, Kyiv, Ukraine, [2]Institute for Nuclear Research, National Academy of Science of Ukraine, Kyiv, Ukraine.
Corresponding e-mail: jaroluk3@ukr.net

As ultrasonic waves (USW) are known to interact strongly with crystal defect structure one can use them to study crystal imperfection properties or to control material parameters in general. In the given article the attempt is made for the first time to show the possibility of ultrasonic stimulated rebuilding (namely, changes of configuration and structure and also center charge) of radiation defects (RD) in Si crystals. Monocrystal samples of n-type Si, grown by zone melting with low (140 Ohm.cm, oxygen concentration ~ 10^{15} cm^{-3}), and also by Czochralski method SZ Si (32 Ohm.cm, oxygen concentration ~ $9.5.10^{17}$ c^{-3}), irradiated by gamma-rays of ^{60}Co(D =10^7Gy). Temperature dependences of Hall coefficients, electroconductivity and Hall mobility were studied in the temperature ranges 80 -·300 K and magnetic fields 0,45 Tl. Samples were treated by longitudinal USW (frequency f_{US}= 5 - 17 MHz, intensity W_{US}= 0,5 -·2 $Wt.cm^{-2}$, durations t_{US} =10^3-·10^4 s, T_{US} < 70C) and measured after each treating step. It has been discovered that USW treatment leads to: a) Changes of temperature dependences of all electrophysical characteristics; b) Character of US induced changes is specified by structure of RD in as-irradiated samples and electronic state of appropriate electrically active center during experiment; c) Effect is more expressive at lower temperatures and depends partly on the USW orientation in crystal, changes in [110] direction are a bit stronger than in [100].

It has been stated that active defects with level E_C - 0.17eV±0.01 eV are main for both types of crystals: with high (SZ Si) and with low (zone-melting Si) content of oxygen. However nature of these levels for samples with high and low oxygen concentration are different. The direct testifies of it is a fact that given level can transform during US treatment to the level of E_C- 0.23 eV or E_C- 0.12 eV - for SZ Si or to the level E_C - 0.20 eV - for zone-melting Si.

The work was partially supported by the STCU, Project # 2367.

P3H-7

ANALYTICAL AND EXPERIMENTAL STUDY ON SECOND HARMONIC RESPONSE OF FBAR FOR OSCILLATOR APPLICATION.

W. PANG*, H. ZHANG, and E. S. KIM, University of Southern California, Los Angeles, CA.
Corresponding e-mail: weipang@usc.edu

In the case of a Film Bulk Acoustic Resonator (FBAR) composed of Metal/Piezoelectric-Film/Metal with symmetric top and bottom metals, there are only odd harmonic responses. However, an FBAR with non-symmetric metals or with a support layer (e.g., Metal/ZnO/Metal/SiO_2) has even harmonics in addition to odd harmonics because of the non-symmetric acoustic energy distribution in the piezoelectric layer. As FBAR′ application areas grow to include frequencies beyond 5GHz, FBAR needs to use very thin piezoelectric and electrode films that require a non-piezoelectric support layer. Moreover, in case of a temperature compensated FBAR, SiO_2 is commonly employed as a temperature-compensating layer to achieves a low TCF (<5ppm/°C). Thus, an FBAR with a support layer will be more prevalent in coming years, but the effects of the support layer on the FBAR performance have not been fully investigated.

In this paper, the input impedance equation for a four-layer (Metal/Piezoelectric-film/Metal/Non-piezoelectric-film) FBAR is derived from Mason′s model to study the second harmonic response of the FBAR, especially the effects of the non-piezoelectric layer on the resonator characteristics. We analyze the equation numerically for the second harmonic resonance at 5 GHz, using material parameters (for all the layers) including sound velocity, relative dielectric constant, and acoustic attenuation. We fix the top and bottom metal electrodes, and vary the thickness ratio of the piezoelectric ZnO layer to a supporting layer (three supporting layers Si_xN_y, SiO_2, and Si have been used) to obtain the electromechanical coupling constant K_t^2 and the quality factor (Q) for each ratio.

The numerical analysis shows that by choosing a low loss material for the non-piezoelectric layer and a proper thickness ratio between the piezoelectric layer and non-piezoelectric layer, the Q of a four-layer FBAR can be twice higher than that of a tri-symmetric-layer FBAR. For each of the three different support materials, there exists an optimal thickness ratio for the highest Figure of Merit (FOM, which is the product between K_t^2 and Q). It is found that all the peaks of FOM occur at a thickness ratio that is close to the acoustic-velocity ratio between the ZnO layer and the non-piezoelectric layer. This is reasonable because that condition means that largest acoustic standing wave is generated in both the piezoelectric layer and the support layer.

For experimental verification, we have fabricated membrane-type FBARs with the thicknesses of the bottom and top Al electrodes fixed at 0.1μm and 0.15μm, respectively. The Si_xN_y thickness is varied from 0.2 to 1.2μm, while the thickness ratio between the ZnO and Si_xN_y is chosen to make the second harmonic resonant frequency range between 5.0 and 5.2 GHz. Five variations of FBARs have been fabricated, and measured. The thickness of Si_xN_y affects the K_t^2 and FOM of the

four-layer FBAR, as the numerical analysis predicts. The measured data agree with the calculated results very well.

This material is based upon work supported by (DARPA) under (Chip-Scale Atomic Clock) program.

Session: P3I

SAW FILTERS AND DEVICES
Chair: V. Plessky
Helsinki University of Technology

P3I-1

INVESTIGATION OF HIGH-ATTENUATION CHARACTERISTICS AT LOWER-SIDE FREQUENCY BANDS FOR RF-FILTER-INTEGRATED MODULES.

M. HIKITA*[1], N. SHIBAGAKI[2], and K. SAKIYAMA[3], [1]Kogakuin University, Shinjuku, Tokyo, Japan, [2]CRL Hitachi Ltd., Kokubunji, Tokyo, Japan, [3]Hitachi Media Electronics Ltd., Totsuka, Yokohama, Japan.
Corresponding e-mail: hikitami@cc.kogakuin.ac.jp

Almost all cellular-phone systems have the receiver-frequency bands higher than the transmitter-frequency bands. High attenuation characteristics are required at the transmitter bands, i.e. lower-side frequency bands, for the receiver filters. These requirements are remarkable especially for duplexers used in CDMA systems, where transmission and reception are performed simultaneously. However, in recent miniatures SAW- and FBAR/SMR-filter modules, electrically ideal grounds can not be achieved within the modules. This is because metal-draw-line patterns to the grounds formed between multi-layered ceramic or LTCC sheets of the modules have common resistive/inductive components for the filters, which result in not so good attenuation characteristics at lower-side bands especially for ladder-type filters. In this paper, first we investigated the effects of common resistive/inductive components using computer simulation procedures. Second, we will propose new SAW- and FBAR/SMR-filter configurations, which have additional resonators connected in parallel to serial-arm resonators of ladder-type filters, which provides parallel resonances at lower-side bands. We will not only show the effectiveness of the new configurations by computer simulation but also confirm them by experiments.

P3I-2

USE OF SECOND ORDER INFORMATION IN THE AUTO REGRESSIVE MOVING AVERAGE TECHNIQUE FOR THE DESIGN OF LINEAR PHASE SAW FILTERS.

B. PANWAR*, P. UJALAYAN, and S. JOSHI, Indian Institute of Technology Delhi, Hauz-Khas, New-Delhi, India.
Corresponding e-mail: bspanwar@care.iitd.ernet.in

The design of small size low loss SAW filter utilizes the idea of single phase unidirectionality where distributed reflectors are superimposed on top of a normal SAW interdigital transducer. The impulse responses for these filters are synthesized using unit cells comprising of withdrawal weighted reflection and transduction centers. The reflecting DART/EWC structures in the design of SAW filters have so far been used to provide the directivity on the acoustic ports, which is used to reduce the insertion loss and pass band ripples. In the present case the reflections arising from the DART/EWC structures are used to synthesize a pole in SAW transducer. This makes it possible to implement an IIR transfer function in SAW technology for reducing the size and improving the pass-band and stop band performance of SAW filters.

The present work describes the use of mixed first and second order information, in the form of a finite portion of its impulse response $\{h_0, h_1, ..., h_m\}$ and the autocorrelation sequence $\{r_0, r_1,...., r_n\}$. The objective is to use the second order information to find a lowest order recursive filter which matches the data $\{h_0, h_1,...,h_m, r_0, r_1,...,r_n\}$. This interpolation problem termed as Auto Regressive Moving Average (ARMA) technique facilitates in obtaining the transfer function of a recursive filter matching the frequency response of FIR filter. The desired finite impulse response of the SAW filter is mapped to rational function of order (m,n) of the form $H(z) = P(z)/Q(z) = (b_0 + b_1 z^{-1} +,...,b_m z^{-m}) / (1 +a_1 z^{-1} +,...,a_n z^{-n})$. The coefficients of the numerator polynomial provide the moving average information (transduction centers), whereas the reflection centers using the DART / EWC structures are used to synthesize the poles of the denominator (AR information).

A combination of two reflecting cells is used to describe a set of new 81 cells. This new set of cells, characterized by a rational transfer function, is derived from 9 primary cells with withdrawal weighted transduction and reflection centers. Subsequently, an iterative approach [1] is used to synthesize the poles of the transfer function obtained using the ARMA modeling. This is followed by implementing the modified numerator polynomial obtained by dividing H(z) with the rational function used to approximate the poles. A variety of SAW filters with different fractional bandwidth have been designed using the proposed ARMA technique. The simulation results show smaller ripple size in the pass-band (an inherent property of IIR filters) and reduction in the filter length of more than 50% in comparison with the FIR response of the filter obtained using Remez Exchange Algorithm. This approach is also being explored to split the impulse response for implementing on input/output transducers.

1. Priyanka Ujalayan, S. D. Joshi, B. S. Panwar, 'An iterative approach to design a SAW filter having the desired response', to appear in IEEE Trans. Ultrason. Ferro. Freq. Control.

P3I-3
DESIGN OF SAW FILTERS WITH NONEQUAL INPUT AND OUTPUT IMPEDANCES.

V. S. ORLOV*, V. B. CHVETS, A. O. KUSTOVA, A. L. SCHWARTZ, and V. T. SVIRIDOV, Moscow Radiocommunication Research Institute, Moscow, Russia. Corresponding e-mail: filcrys@rinet.ru

In modern communication systems, SAW filters with nonequal input Z_{in} and output Z_{out} impedances are often required. The coefficient of impedance transformation $K_{TI}=Z_{out}/Z_{in}$ can vary from 1.5 (75Ω/50Ω/) to 5 (250Ω/50Ω/) or even higher. Usually for admittance transformation in SAW filters 3DMS or 5DMS sections on longitudinally coupled resonators are utilized [1]. However, some problems occur, which result from necessity of reducing apertures of IDTs and insertion loss increasing with required K_{TI} value. In the present work, we suggest to use symmetrical [2] and unsymmetrical ladder Γ-type and T-type sections for building single ended and balanced filters with nonequal input and output impedances. We demonstrate that two approaches can be used for design of such filters: with the jump-like or smooth variation of impedances at the boundaries of neighbor ladder sections. In the first case, the higher value of K_{TI} can be realized but it is difficult to provide the reflections at the input and output ports of a filter less than VSWR=2.0-2.5, without application of matching circuits. In the second case, the reflections can be reduced to VSWR=1.5-1.8 but the maximum achieved K_{TI} value is lower. We investigated the dependences of maximum achieved coefficient of impedance transformation, insertion loss and attenuation in the stop band on the number of sections and required bandwidth at fixed reflections VSWR at the input and output ports of a filter. The calculations are confirmed by experimental results for few types of filters with center frequencies about 600 MHz and 1330 MHz, and impedances 50Ω/100Ω single ended; 50Ω/200Ω single ended; 50Ω/100Ω balanced; 50Ω/250Ω balanced.

[1] K. Hashimoto, T. Omori, and M. Yamaguchi, “Application of SAW Devices to Matching Elements in RF Circuits”, IEEE 2003 Ultrasonics Symposium Proc., pp. 407-410.

[2]. V.S. Orlov , A.L. Schwartz, V.B. Chvets, E.I.Fedorov and A.O. Kustova ,’’Design of High Selectivity Low-loss Ladder Filters “ , IEEE 2004 Ultrasonics Symposium Proc.

P3I-4

DESIGN OF LOW-LOSS SAW FILTERS WITH CONSTANT GROUP DELAY USING RESONANT SPUDTS.

H. LI*[1], J. WEN[2], T. OMORI[2], K. HASHIMOTO[2], and M. YAMAGUCHI[2], [1]Venture Business Laboratory, Chiba University, Chiba-shi, 263-8522, Japan, [2]Dept. Electronics and Mechanical Eng., Chiba University, Chiba-shi, 263-8522, Japan. Corresponding e-mail: k.hashimoto@ieee.org

This paper describes the design of low-loss SAW filters with constant group delay in transition bands as well as in a passband. This characteristic can be applied to the development of low-loss switchable filter banks and wideband filters employing slanted IDTs, in which multiple responses with different centre frequencies are used to overlap each other.

The device employs resonant single-phase unidirectional transducers (RSPUDTs). The simulated annealing, one of the stochastic optimisation methods, is used here to find the optimal weighting functions for excitation and reflection properties of the RSPUDTs, and the under-sampling technique is adopted to speed up the optimisation.

Then the designed continuous weighting function is transformed into a discrete withdrawal weighting. In addition to conventional four types of EWC/SPUDT cells, an elementary cell is introduced to take account of the reversal of sign in the weighting functions.

It is shown that the constant group delay and low insertion loss are simultaneously achieved by using an appropriate object function in the optimisation. It should be noted here that because of the limited group delay time, the transition bandwidth gets relatively large and the passband shape becomes similar to that of the sinc function.

A low-loss SAW filter with constant-group delay was designed and fabricated on a 128°YX-$LiNbO_3$ substrate. The Al electrode thickness was chosen to be relatively thick for reduced parasitic resistance. Experimental results were in good agreement with the design; the group delay deviation of 20 ns was realised over the range of +-8 MHz at the centre frequency of 512 MHz. The minimum insertion loss and –3 dB bandwidth were 4.3 dB and 8.5 MHz, respectively.

For the same specifications, filters employing non-resonant SPUDTs were also designed and fabricated for comparison. It is shown how flat group delay can be synthesised by giving partial resonances to the structure.

Finally, the application of this technique is discussed for developing high-performance switchable filter banks and wideband filters employing slanted IDTs.

P3I-5
USE OF NON-SYNCHRONOUS RESONATORS ON LEAKY SUBSTRATES AS IMPEDANCE ELEMENTS FOR LADDER AND NOTCH FILTERS.

J. MELTAUS*[1], V. P. PLESSKY[2,1], and S. S. HONG[3], [1]Materials Physics Laboratory, Helsinki University of Technology, Espoo, Finland, [2]GVR Trade SA, Bevaix, Switzerland, [3]Samsung Electro-Mechanics Co., Ltd, Suwon, Korea.
Corresponding e-mail: johanna.meltaus@hut.fi

In this paper, we will present simulation results for non-synchronous impedance elements on leaky 42°-$LiTaO_3$ and discuss how they can be applied in the design of ladder-type and notch filters.

Structures with long interdigital transducers (IDT) combined with a hiccup-type, resonating λ/4 gap were first proposed by Plessky et al. in 1996 [1]. Although COM simulations predicted excellent performance, experimental devices suffered from high insertion loss due to loss mechanisms occurring in the metallized gap. In [2], Shui et al. showed that the Q-value of a hiccup resonance on leaky 42°-$LiTaO_3$ substrate can be significantly increased using a distributed gap instead of open of metallized gap, i.e., replacing the open gap by a short IDT section having a pitch different from that of the remaining structure. We combine these two concepts to make impedance elements (IE) on leaky substrates, consisting of a long synchronous part combined with a hiccup-type resonator with distributed gap in the middle.

In such a non-synchronous IE, two resonances take place: one arising from the long synchronous IDTs and other occurring in the distributed gap. The

synchronous resonance is typical of the conventional IE, located at the left edge of the reflector stopband. The hiccup-type resonance, on the other hand, is governed by the topology of the distributed gap, and is located in the middle of the stopband.

The use of the hiccup resonance arising in the distributed gap can benefit applications in at least two ways: i) the Q-value of the hiccup resonance can be increased compared to that of a conventional resonator, and ii) the resonance-antiresonance (R-aR) distance of the hiccup resonance can be affected by varying the gap and IDT parameters, resulting in a variable passband width and skirt steepness.

In order to establish the applicability of the structure to improve the performance of ladder and notch filters, we study non-synchronous IEs with varied parameters using Fem/Bem simulations. We will discuss the operation of the devices and show examples of applying them in ladder-type bandpass filter and notch-filter design.

[1] V. P. Plessky, T. Thorvaldsson, and S. Kondratiev, Proc. of the 1996 IEEE Ultrasonics Symposium, pp. 25-28.

[2] W. Wang, X. Zhang, Y. Shui, H. Wu, and V. P. Plessky, Proc. of the 2004 IEEE Ultrasonics Symposium, pp. 1363-1366.

P3I-6
OPERATION MECHANISM OF DMS FILTERS WITH PITCH-MODULATED IDTS AND REFLECTORS.

K. HASHIMOTO*, T. OMORI, and M. YAMAGUCHI, Chiba University, Chiba, Japan.
Corresponding e-mail: k.hashimoto@ieee.org

One of the authors (K.Y.) proposed pitch-modulated IDTs and reflectors [1] for developing low-loss and wideband longitudinally coupled double-mode SAW (DMS) filters.

This paper discusses how wide and flat passband shape is realised by using the pitch-modulated IDTs and reflectors in DMS filters.

The basic idea for DMS filter design is to make the resonance frequency for an even mode coincide with the anti-resonance frequency for an odd mode, or vice versa. This suggests that the filter passband can be extended if the above condition is satisfied at multiple frequencies.

It is shown in the designed device structure that the location of multiple resonance frequencies is adjusted simultaneously by varying an effective reflective position with frequency. The IDTs are pitch-modulated so that the outer portion has slightly larger pitch than the inside, whereas the pitch of outermost reflectors is the largest. Accordingly, higher-order SAW resonances occur between the two pitch-modulated IDTs; the outer portion of each IDT acts as an reflector while the inner portion is mainly responsible for SAW excitation. The first-order SAW resonance occurs between the two reflectors.

This design also offers two distinctive features:

1) Because of the extended IDT acoustic length, the IDT aperture should be made short for impedance matching. This is effective in reducing the electrode ohmic loss.

2) Through the sufficient number of degrees of freedom introduced in the design, structural discontinuities become avoidable. This results in the reduced filter insertion loss caused by BAW scattering.

[1] O.Kawachi, S.Mitobe, M.Tajima, T.Yamaji, S.Inoue and K.Hashimoto: "A Low-Loss and Wide-Band DMS Filter Using Pitch-Modulated IDT and Reflector Structures", Proc. UFFC 50th Anniversary Conference (2004) pp. 298-301.

P3I-7
SAW BAND REJECT FILTER PERFORMANCE AT 850 MHZ.

C.-Y. JIAN* and S. BEAUDIN, Nortel, Wireless Technology Laboratory.
Corresponding e-mail: cyjian@nortel.com

SAW band reject filters constructed of single pole resonators have very low insertion loss and can withstand very high powers in their passband. Also, they can achieve very sharp transition bands. All these features plus the well known SAW device features: small size and low cost are very attractive to the front end of a wireless base station or handset. Since we reported the concept of the SAW band reject filter and its potential applications two years ago, there have been no further reports regarding this technology presented publicly. This paper will show our experimental results regarding the power handling capability of the SAW band reject filter and some measured performances of our actual designs. As a highlight here, our one port SAW band reject filter showed 0.1dB or less insertion loss and ladder type SAW band reject filter consisted of ten SAW resonators showed about 1 dB insertion loss and around 300 kHz wide transition band in 18 dB rejection at 853 MHz. The power handling test showed that the SAW band reject filter can withstand CW signal power as large as 42dBm in its pass band.

P3I-8
AN IMPROVEMENT OF SAW RESONATOR CASCADE CONNECTION BY CAPACITIVE COUPLED RESONATOR.

H. NAKAMURA*[1], S. SEKI[2], K. NISHIMURA[2], and T. ISHIZAKI[1], [1]Device Integration Laboratory, Organization Staff Corporate Components Development Center, Panasonic Electronic Devices Co., Ltd., Kadoma City, Osaka, Japan, [2]Engineering Group 3, Circuit Components Business Unit, Panasonic Electronic Devices Co., Ltd., Kadoma City, Osaka, Japan.
Corresponding e-mail: nakamura.hiroyuki@jp.panasonic.com

Recently, SAW duplexers have been widely used for CDMA mobile phones. The SAW duplexers are required not only low insertion loss and high attenuation but also high power durability. It is popular to use the ladder-type SAW filters in

SAW duplexer because power durability of ladder-type filter is easily improved by design technique. The cascade connection of resonators is one of well-known techniques to improve it. The conventional cascade connection of the resonators, of which bus-bar electrodes are connected mutually. We focused attention on the energy loss of this connected part between resonators. This energy loss comes from the electric resistance of this part and the leak of SAW from waveguide into this part. The authors propose a novel design technique for cascade connection of SAW resonators. We have developed the capacitive coupled resonator, which can realize the cascade connection without bus-bar electrodes.

Our basic idea is adoption of capacitive coupling for cascade connection of resonators. The origin of the capacitive coupling structure is capacitive weighting technique used for transversal-type SAW filter. The capacitive coupled resonator is composed of upper and lower finger electrodes and multi-strip lines. The upper and lower finger electrodes are placed symmetrically, and multi-strip lines are interdigitated to the upper and lower finger electrodes. The upper finger electrode capacitively coupled to the lower finger electrodes through the multi-strip lines. Thus, the equivalent cascade connection of resonators can be realized.

The insertion loss of the capacitive coupled resonator was improved of 0.1dB at 1GHz band, compared with the conventional cascade connection using bus-bar electrode. The capacitive coupled resonator has the potential to realize excellent performance for the duplexer.

P3I-9
DISPERSIVE DELAY LINES BASED ON THE USE OF NARROW OPEN METAL RREFLECTORS AND FAN TRANSDUCERS.

S. M. BALASHOV*[1], V. P. PLESSKY[2], C.-U. KIM[3], C.-W. NAM[4], and V. I. GRIGORIEVSKY[5], [1]SAWDES Ltd, Campinas, San-Paulo, Brazil, [2]GVR Trade SA, Bevaix, Switzerland, [3]C&C Tech Plus, Seoul, South Korea, [4]University of Ulsan, Ulsan, South Korea, [5]IRE RAS, Fryazino, Moscow region, Russia.
Corresponding e-mail: sergey.balashov@gmail.com

In-line dispersive delay line (DDL) demands low and controllable reflectivity of the reflectors, especially if the SAW propagates all long way along the reflecting structure. The metal reflectors are usually too strong and introduced too much attenuation in such a device. A solution of this problem is found based on fan transducers - to separate spatially the acoustic channels for different frequencies and on the use of narrow open metal reflectors - to reduce reflectivity in desired way.

Fan transducers (FIDT), performing distribution of the signal with different frequencies into different channels, are used to construct dispersive delay lines (DDL). Innovative arrangement of FIDT allowed one to minimize the influence of multiple reflections of the SAW in DDL and use 180-deg. reflection of the SAW. Narrow open metal strips (NMS) with metallisation ratio of the order of 20% are used as reflectors with small reflectivity.

These reflectors are suitable for application in DDL: demanded low reflectivity can be easily obtained, while the resistivity losses remain negligible. Due to small metallization coefficient the SAW velocity change caused by mass-loading is also small. Methods of optimization of DDL performance are discussed on the basis of effective aperture of FIDT. DDL are treated as multichannel structures with electrical interaction between channels inside FIDT. COM model was used to simulate the performance of such DDL. New method of analysis of such multichannel SAW devices is proposed. Methods generalizes the notation of the chain matrix on the case of the system with arbitrary acoustic channels (AC) and electrical ports (EP) numbers. Arbitrary acoustic interaction between AC and EP connections could be considered on the basis of the approach proposed. Experimental results for reflectivity of MNS are presented. Experimental performance of the proposed DDL is presented as well as comparison with the results of simulations.

P3I-10
5~10 GHZ SAW RESONATORS AND LOW LOSS WIDE BAND RESONATOR FILTERS USING ZERO TCF HIGH ELECTROMECHANICAL COUPLING SAW SUBSTRATES.

K. YAMANOUCHI*, Y. SATOH, H.I ISONO, and D. KAWASAKI, Tohoku Institute of Technology, Sendai, Japan.
Corresponding e-mail: yamasaw@tohtech.ac.jp

The development of GHz-band surface acoustic wave (SAW) devices has become necessary because of the increasing volume of information and communication media, such as mobile telephone, satellite broadcasting, spread spectrum communications. Especially, zero TCF, wide band and low loss filters with an ultra-small size and high performance are required for mobile communication systems. We developed the SiO_2/Rotated Y-cut, X-Propagating $LiNbO_3$ leaky SAW substrates with a large k^2 (over 0.2) and zero TCF at the very thin thickness of SiO_2 of H_{SiO2}/λ=0.2 (H_{SiO2}:SiO_2 film thickness, λ:SAW wavelength) and zero propagation attenuation in the case of metalized surface.

In this paper, the theoretical and experimental results of SAW resonators and resonator filters in the frequency ranges of 5~10 GHz using the above substrates are described. One of the important things at 5~10GHz-range SAW filters is the thickness effect of IDT electrodes due to decreasing the resistive loss. Therefore the filters were analyzed for the SiO_2/Al-IDT/$LiNbO_3$ substrates. The resonator showed the band width of 1.0~1.3GHz at the center frequency of 10GHz and resonator filters showed the band width of 1.0~ 2.0 GHz and insertion loss of about 2dB in the center frequency of 10GHz at the H_{Al}/λ=0.15(H_{Al}=600A), H_{SiO2}/λ=0.25(Only, H_{SiO2}=1000A). The experimental results show the good agreements to the theoretical ones.

P3I-11
HIGH FREQUENCY SAW DEVICES BASED ON THIRD HARMONIC GENERATION.

L. LE BRIZOUAL*[1], TH. PASTUREAUD[2], F. SARRY[1], O. ELMAZRIA[1], S. BALLANDRAS[3], V. LAUDE[3], and P. ALNOT[1], [1]Laboratoire de Physique des Milieux Ionisés et Applications, Vandoeuvre Lès Nancy, France, [2]TEMEX, Sophia Antipolis , France, [3]Institut FEMTO-ST, Besançon, France.

Corresponding e-mail: laurent.lebrizoual@lpmi.uhp-nancy.fr

Zinc oxide (ZnO) is of great technological interest for the development of passive signal processing devices on different kind of substrate, and particularly Silicon. Many theoretical as well as technological works have been carried out on the ZnO layers deposited on dielectric, semi-conducting or piezoelectric substrates. Furthermore, ZnO has been widely investigated as a piezoelectric material for surface acoustic wave (SAW) devices, mainly because of the strength of its piezoelectric coupling coefficient. The centre frequency (f0) of a SAW device is determined by the phase velocity ($V\Phi$) of the acoustic propagation and the period (p) of the inter-digital transducers such as $f0=V\Phi/p$ (the acoustic wavelength λ is assumed equal to p in a first order approximation). In this work, we demonstrate the interest of the third harmonic generation to obtain high frequency SAW devices based on a ZnO/Si layered structure.

The ZnO films are deposited by a DC planar magnetron sputtering system on silicon Si(100) substrates. Aluminum inter-digital transducers (IDT) with uniform finger spacing and various spatial periods can be patterned by conventional contact UV photolithography and wet etching at the Si/ZnO interface or atop ZnO. The number of IDT pair fingers and the IDT aperture have been respectively fixed at 50 and 2 mm (always more than 100 λ). The metallization ratio (η) of IDT has been chosen to favour the generation of the 3rd harmonic. As a consequence, we show that sub-micrometric lithography is not required to develop SAW devices based on our ZnO/Si structure operating in GigaHertz range.

The experimental frequency characterization of the IDT response was performed using a network analyzer (HP8752A). The measured frequencies are 665 MHz, 971 MHz, 1.54 GHz and 2.47 GHz, corresponding respectively to the mode 0 harmonic 1, mode 1 harmonic 1, mode 0 harmonic 3, mode 1 harmonic 3 of the structure (higher modes have not been characterized).

A theoretical study has been carried out for this device to check the possibility to accurately analysed its operation, with the goal to demonstrate the possibility to efficiently design devices operating on such harmonic modes. It is based on a boundary integral method (BIM) of stacked materials coupled with finite element analysis (FEA) according to the celebrated Ventura's approach. The 4 above-mentioned modes are theoretically found in good agreement with experiments. The resonance frequencies deduced from harmonic admittance curves are predicted with a precision of about 1%, which is satisfactory considering the possible fluctuations of the film properties (process dependent). All the mode parameters are predicted and compared to those obtained experimentally. Moreover, the influence of the electrode on the 3rd harmonic mode parameters

is reported, allowing for a better definition of the optimal working conditions of IDT under the considered operation mode.

P3I-12
INVESTIGATION OF RF LADDER-TYPE SAW FILTERS INCORPORATING PACKAGING EFFECTS.

S. WANG, I. CHEN*, C. TAI, and C. CHOI, Department of Electrical Engineering, I-Shou University, Dashu Township,kaohsiung County, Taiwan R.O.C.
Corresponding e-mail: smwang@isu.edu.tw

Commercial surface acoustic wave (SAW) device typically is fabricated on piezoelectric substrates, such as LiTaO3, LiNbO3, and quartz wafer. Often the device is required to be integrated into a package before it can be used with other circuits. When the operation frequency is low, the parasitic effects due to packaging are insignificant. Those effects can be either ignored or simply accounted for by adding a capacitor between input and output of the device to model the crosstalk. However, as frequency is increased to gigahertz range, the parasitic effects are also increased. Discrepancy in performance, such as passband insertion loss, bandwidth, sideband rejection level, and even center frequency, before and after packaging could be large. Although frequency is a main issue in determining the significance of packaging effects, different design pattern is an important issue in determining if the device is sensitive to packaging effects. In this paper, the sensitivity to packaging effects of two different RF ladder-type filters was studied, one is a GPS RF filter and the other is a GSM RF filter. The GPS filter requires narrow band and high sideband rejection. Therefore, the static capacitance ratio of parallel resonator and series resonator is large. The GSM filter has a relatively wide band and excellent passband insertion loss. The static capacitance ratio is small. Both filters were packaged in 3x3mm^2 packages. A 3D EM wave simulator was applied to obtain the parasitic effects from the package and pattern layout. The performance of one-port SAW resonators in ladder-type was analyzed by Mason's model. By connecting packaging model with resonator model via a high frequency circuit simulator, the performance of packaged filter was then calculated. The simulation results are well matched with measurements. From the simulation and measurement results, the packaging effects on GPS filter is much more significant than that on GSM filter.

The authors would like to thank the National Science Council of the Republic of China for financially supporting this research under Contract No. NSC 93-2213-E-214-014 and ftech corporation for technique support.

P3I-13

A NOVEL WEIGHTED METHOD FOR WIDE-BAND SAW FILTERS USING SLANTED FINGER INTERDIGITAL TRANSDUCERS ON LAYERED PIEZOELECTRIC SUBSTRATES.

Y.-Y. CHEN*, C.-M. LIN, and T.-T. WU, Institute of Applied Mechanics, National Taiwan University, Taipei, Taiwan.
Corresponding e-mail: yychen@ndt.iam.ntu.edu.tw

In contrast to the FM chirp or apodized SAW filters, SAW filters using slanted finger interdigital transducers (SFITs) have an extremely flat pass-band response, an excellent linear phase response across the pass band, and the large out-of-band suppression. Therefore, there are increasing research activities on the SFIT SAW filters applied in the area of telecommunication systems, requested for higher bit rates and more transmitted data. Most of the existing literatures concerning SFIT SAW filters showed how to modify the SFIT geometric shapes to improve their performance of wide-band SAW filters, especially to flatten the inclined pass band caused by the transducers' impedance. In this paper, we proposed a novel weighted method for wide-band SAW filters using SFITs on layered piezoelectric substrates. We calculated frequency responses of SFIT SAW filters based on layered piezoelectric substrates by the coupling-of-modes (COM) model, which is valid for a layered SAW device. According to the calculated results, we found the dispersive electromechanical coupling coefficient or dispersive phase velocity in the layered substrate would affect the pass band greatly. Moreover, we flattened the inclined pass band by choosing the film thickness or SAW wavelength appropriately based on the dispersive electromechanical coupling coefficient relation; we also employed the dispersive velocity relation to increase the bandwidth. Two wide-band layered SAW filters using SFITs on AlN/Silicon were analyzed to verify the accuracy of the proposed methods: one was designed to flatten the inclination of pass band and the other was designed to widen the bandwidth. The results are in very good agreement with the predictions.

The authors thank the financial support of this research from the National Science Council of Taiwan through the grant NSC93-2218-E-002-052.

P3I-14

DESIGN OF SAW BANDPASS FILTERS USING WEIGHTED LEAST MEAN SQUARES (WLMS) TECHNIQUE.

ALEXANDER S. RUKHLENKO*, Institute of Microtechnology, Neuchatel, Switzerland.
Corresponding e-mail: rukhlenko@bluewin.ch

The innovative SAW filter optimization technique is presented that is an alternative to the Remez exchange algorithm or linear programming. The weighted least mean squares (WLMS) technique produces an equiripple minimax

design if a suitable least squares weighting function (unknown a priori) is applied. The WLMS procedure includes two basic steps at each iteration: 1) solution of the standard WLMS problem for a given weighting function; 2) update of the weighting function (reweighting) using the results of the current iteration. A simple and efficient reweighting scheme is proposed. The merits of the WLMS technique are as follows: 1) easy programming and short source code, 2) use of the standard WLMS subroutine (for the prescribed weighting function) as the principal programming block. The algorithm demonstrates fast and stable convergence resulting in the quasi-equiripple design after few iterations. The technique has been generalized and effectively applied to arbitrary magnitude shape and non-linear phase response synthesis problem. As is shown, the WLMS complex Chebyshev approximation is reduced at each iteration to two separate WLMS approximations for the real and imaginary parts with the same updated weighting function. Parameter reduction schemes in time or frequency domain can be applied to reduce the number of the optimized variables and computational time. The baseband frequency response can be approximated using the WLMS technique, with the time response oversampled to recover the required bandpass response. On the other hand, a frequency sampling technique can be directly applied where the relatively small number of the frequency samples is being optimized, while the others are set identically to zero. The WLMS iterative algorithm has been implemented both in Fortran and Matlab using the standard WLMS subroutines. SAW filter design examples are presented which confirm efficiency and flexibility of the WLMS SAW filter synthesis.

This work was partially supported by Sawtek, Inc., Florida, USA.

P3I-15
SINGLE-TO-BALANCED BAW FILTER COMBINING CRF WITH LATTICE FILTER.

T.-Y. WU, T.-K. SHING*, and H.-K. CHEN, Delta Electronics, Inc., Toyuan, Taiwan. Corresponding e-mail: bryan.wu@delta.com.tw

Although FBAR filters have been successfully commercialized in CDMA duplexer market, it still can not displace the SAW filter in general RF front-end filter applications. Most of present cell phone systems like GSM or WCDMA require the filter device to have both single-to-balanced conversion and impedance transformation functions. Current BAW filter with ladder or lattice topology can not satisfy any of these requirements. Therefore the coupled resonator filter (CRF) has gained a lot of attention since it posses the potential to meet all the requirements of state-of-the-art wireless systems.

In the past, CRF needs to be fabricated in a SMR structure with proper selection of reflector layer materials. The purpose of using SMR structure is to suppress the redundant resonant response of CRF. However, comparing with membrane-type structure, the SMR has slightly lower Q and effective K2. In this paper, a new design with topology combining CRF and lattice filter for single-to-balanced conversion applications is proposed. It can help eliminate the need of SMR structure and thus the performance could be improved.

This concept is verified by simulation and the comparison to conventional ones is discussed.

Session: P3J

SAW SYSTEM APPLICATIONS
Chair: J. Kosinski
US Army REDCOM

P3J-1

DEVELOPMENT OF A MONOLITHIC CMOS-SAW OSCILLATOR.

M. FURUHATA*[1], A. YAJIMA[1], K. GOTO[1], H. SATO[1], T. FUNASAKA[1], S. KAWANO[1], T. HIGUCHI[1], M. UENO[1], T. KARAKI[2], and M. ADACHI[2], [1]Seiko Epson Corporation, Suwa, Nagano, Japan, [2]Toyama Prefecture University, Tonami, Toyama, Japan.
Corresponding e-mail: Furuhata.Makoto@exc.epson.co.jp

In recent years, miniaturization and high accuracy of mobile communication systems have been required. Because of the good phase noise performance, SAW clock is qualified for data transmission. However, a SAW oscillator is usually made up of a SAW device and a CMOS-IC separately, so that the large size limited its application to mobile communication systems. In this paper, we succeeded in developing the smallest monolithic SAW oscillator using thin film ZnO deposited on a CMOS-IC. The SAW device and the IC were combined into a single unit, and the total thickness was nearly the same as the IC.

Simulation based on Campbell's method for layered structure SAW device was carried out to calculate velocity dispersion. The results suggested that a Rayleigh wave could be driven with a high coupling factor around kh=1.6. The improved Smith's equivalent circuit method was chosen to design IDT patterns for the layered structure. A high performance Al reflector with a thickness kh>0.1 was set up to minimize the SAW area to 1x1.6mm. To achieve a high gain at a low voltage power source, we optimized the gate size of transistor and the parasitic element for phase adjustment in IC design using the Agilent ADS simulator.

To deposit SAW film on conventional CMOS-IC, flatness of the surface is very important. We used CMP (Chemical Mechanical Polish) to optimize the SAW layout in wafer. Furthermore, this helped the connection between IC and SAW device by Al layered on the surface easily. The high piezo-electronic performance ZnO film was deposited at low temperature by rf sputtering method, since the temperature should be lower than that of CMOS-IC process to avoid damages in IC.

Measurement results showed that the phase noise achieved an excellent value of -120dBc/Hz@10kHz. It indicated the IC performance was not affected by the ZnO thin film.

P3J-2

SWITCHABLE SAW FILTER BANK WITH 78% BANDWIDTH.

S. HE*, J. LIU, S. LI, and Y. LIANG, Institute of Acoustics, Chinese Academy of Sciences, Beijing 100080, China.
Corresponding e-mail: heshitang@mail.ioa.ac.cn

Switchable SAW filters have wide application to frequency synthesis, frequency hopping radio and communication system. In these applications SAW filters are normally asked to operate over wide bandwidth and to perform low loss to make system working in adequate signal-to-noise ratio. In the paper, 16 channel low loss and wideband switchable SAW filter bank will be presented. The total operational bandwidth reaches to 78% of central frequency. To achieve low loss, the individual filter in each channel is made of longitudinally coupled resonator filter. The switches are added to both input and output of filters. The single channel operation mode can make sure the required low loss for application. Three kinds of longitudinally coupled resonator filters are separately adopted in different channels, which are fabricated on 41°LiNbO3 using 1-3 mode, 41°LiNbO3 using 1-2 mode and 64°LiNbO3 using 1-3 mode, to get the same bandwidth possible. The experimental filter bank results in insertion loss of less than 6dB(include the insertion loss of two-stage switch), channel bandwidth 17~23MHz and stopband rejection of more than 40 dB.

P3J-3

PULLING OF SAW RESONATORS FOR WIRELESS SENSOR APPLICATION.

E. GULIYEV and S. KLETT*, Technische Universität Ilmenau, Ilmenau, Germany.
Corresponding e-mail: elshad.guliyev@tu-ilmenau.de

SAW resonators are best suited for passive wireless sensing due to the high Q factor (storage of rf energy), and the possibility to change their resonance behaviour according to the influence by an external measurand (frequency pulling).

The sensor is based not only on the direct physical effect on the acoustic wave but also the electrical effect outside the resonator (e.g. capacitive or inductive).

The sensor signal is determined by the external circuit elements. It leads to a frequency and amplitude shift.

The pulling frequency, the optimum pulling range, and the transmitted power are estimated from both the external reactive circuit elements, and the SAW-Resonator characteristic.

To obtain the maximum power transmission, a matching between the sensor element and the antenna for wireless interrogation is necessary. Simultaneously, one element of the matching network is the sensing element that pulls the frequency.

For well-designed sensors, the parameters of equivalent circuitry of the resonator have to be estimated with a high accuracy, in order to simulate the resonator

pulling in combination with different matching networks. Thus, all the L-, Pi- and T-sections that provide matching and pulling are being tested to ensure the maximum power transmission in a wide pulling range.

This paper presents simulation and experimental results for the design of efficient wireless sensor systems.

P3J-4

SUPER-WIDEBAND HIGH BIT-RATE SAW CORRELATOR.

Y. ABRAMOV*, Soliton, Holon, Israel.
Corresponding e-mail: yuri_a@netvision.net.il

To increase signal-processing gain, SAW barker-correlator is normally applied, wherein the SAW device has two IDTs: input and output. One of the IDTs (for example, output IDT) comprises fingers, forming a barker coding bits, and another (input) IDT is shorter than length of one coding bit, in order not to distort the desired barker coding. However in case, when a high bit-rate is desired, certain design difficulties appear, resulting in the increased insertion loss and inter-bit diffraction. The main reason of the insertion loss increasing consists in shortage of fingers in the short input IDT. Moreover, filling by active fingers the entire inter-bit area in the coding output IDT causes the inter-bit diffraction. This effect is normally neglected, however it becomes important for correlator, having short bits, resulting substantial decreasing the signal-processing gain. To avoid the two problems we have found a decomposition of desired coding pulse characteristic such that now the both IDTs are apodized and the short input IDT is doubly longer than the bit length. The two apodization functions are construed as linear combinations of shifted and weighted barker sequences. Thereby, the method, utilizing simple apodization, allows designing high bit-rate correlator.

Session: P3K
TRANSDUCER FABRICATION TECHNOLOGY
Chair: M. Schafer
Sonic Tech

P3K-1

FIELD INDUCED PIEZOELECTRIC TRANSDUCER FOR GENERATION OF CONTROLLED DIFFRACTION ULTRASONIC FIELD.

M. H. LENTE*[1], A. L. ZANIN[1], D. GARCIA[1], L. LEIJA[2], A. VERA[2], H. CALAS[3], and E. MORENO[3], [1]Universidade Federal de São Carlos - Departamento de Física - Grupo de Cerâmicas Ferroelétricas, São Carlos, São Paulo, Brazil, [2]Seccion de Bioelectronica, CINVESTAV, Mexico, [3]Instituto de Cibernética Matemática y Física - Grupo de Ultrasónica, La Habana, Cuba.
Corresponding e-mail: mlente@df.ufscar.br

Over the last decades, ultrasound imaging has been revealed as a powerful method of obtaining images from inside the human body to improve medical diagnosis as well as for nondestructive testing. Indeed, this technique is a useful way of examining many human's internal organs or failure and stress in materials in real time. In this context, conventional piezoelectric materials based mainly on modified-lead zirconate titanate (PZT) ceramics are undoubtedly the most used materials in medical ultrasonic devices. However, a new concept of ultrasonic transducers based on non-uniformly poled materials have emerged as potential candidates for biomedical ultrasonic transducers, because to enable a better control of diffraction of the radiated acoustic field. Among ceramic materials, ferroelectric relaxor, which can present field induced piezoelectric properties, emerge as the most promising class of materials to construct controlled diffraction piezoelectric transducers. In this work, ultrasonic Bessel transducers were developed using relaxor ferroelectric ceramics based on modified-lead magnesium niobate lead titanate ceramics (PMN-PT). PMN-PT ceramics presented large field-induced electromechanical coupling factors, high piezoelectric anisotropy (kt/kp>>1) and relative high mechanical quality factor at relatively low DC bias field. Based on this ceramics, a Bessel-like transducer (composed of three concentric electrodes) was constructed and its acoustic radiation field for different levels of field induced piezoelectric response was characterized. The experimental results revealed that the acoustic field may be significantly modulated by adjusting the DC bias fields. The results obtained for this tunable Bessel-like transducer are compared with those obtained from PZT ceramics.

The authors thank the Brazilian agencies FAPESP and CNPq for the financial support.

P3K-2
NEEDLE TYPE MINIATURE HYDROPHONE WITH PZT POLY-CRYSTALLINE FILM DEPOSITED BY HYDROTHERMAL METHOD HAVING WIDE DIRECTIVITY.

H. KITSUNAI[1], N. KAWASHIMA[1], S. TAKAUCHI*[1], E. OHDAIRA[3], M. ISHIKAWA[2], and M. KUROSAWA[2], [1]Toin University of Yokohama, Yokohama, Kanagawa, Japan, [2]Tokyo Institute of Technology, Yokohama, Kanagawa, Japan, [3]Musashi Institute of Technology, Setagaya, Tokyo, Japan.
Corresponding e-mail: shin1@cc.toin.ac.jp

Recently, the PZT piezoelectric film deposited by hydrothermal method has been studied actively in our laboratory. The PZT films can be formed on the Ti substrate in the KOH solution with Pb ion, Ti ion and Zr ion under high temperature about 140 degrees centigrade and high pressure about 400kPa using hydrothermal method. This PZT film has piezoelectricity without polling process and it is easy to form the piezoelectric film on the titanium substrate with extremely small size by hydrothermal method. We reported on the manufacturing of needle type miniature hydrophones using PZT poly-crystalline film with thickness of about 10μm deposited on an end of titanium wire with diameter of 0.3 mm, length of

150 mm by hydrothermal method at 2004 IEEE UFFC Joint 50th anniversary conference in Montreal. However, it was found that the hydrophones had some significant problems on their directivity. The receiving sensitivity to the side direction was higher than that to the front direction. PZT poly-crystals are synthesized on the all surface of titanium substrate exposed to the source material solution in the apparatus for hydrothermal synthesis. Therefore, PZT piezoelectric poly-crystalline films were deposited not only on an end surface of titanium wire, but also on the side of titanium wire near the end. Consequently, the problems were occurred in the directivity of receiving sensitivity of fabricated hydrophones. Then, we deposited PZT poly-crystalline films on only an end of titanium wire, not on the side of titanium wire by masking on the side of titanium wire using coating material of poly-flon PTFE enamel. We estimated the performance of the fabricated hydrophone using the titanium wire with PZT poly-crystalline film on only its end. As a result, we could confirm the improvement of its directivity of receiving sensitivity (-6dB ; wider than +/-60deg at 10.0 MHz). We will report on the structure of our new hydrophone and considered results like the frequency characteristics of receiving sensitivity, the directivity, etc. in this symposium.

P3K-3

DESTRUCTIVE AND NONDESTRUCTIVE INVESTIGATION OF BONDLINES FOR HIGH-POWER MULTILAYER ULTRASONIC TRANSDUCERS FOR UNDERWATER SONAR.

Z. WU, S. COCHRAN*, G.. MCROBBIE, and K. KIRK, University of Paisley, Paisley, Scotland, UK.
Corresponding e-mail: coch-ph0@wpmail.paisley.ac.uk

Ultrasonic transducers with prestressed mass-spring structures are often used for high power underwater projection in the 20 - 50 kHz frequency range. However, they provide only limited bandwidth. Multilayer piezoceramic or piezocomposite transducers without prestressing may help solve this problem but will require bondlines able to withstand strong tensile forces. This paper therefore reports, for the first time to the authors' knowledge, a systematic investigation of bondline failure encompassing experimental measurements and theoretical analysis. In this investigation, a series of two-layer PZT-5H piezoceramic structures were manufactured with the original silver electrodes fired onto the material during ceramic manufacture as the bonding surfaces. These structures were designed to mimic practical length-extensional mode transducers. Three different adhesives were investigated, an electronic potting compound, a structural adhesive, and an electrically-conductive adhesive. The specimens were subjected to static tensile testing at ambient temperature and elevated temperatures up to 100°C, with the failure stress and the bonding surface conditions after failure recorded. It was found that the conductive adhesive bondlines were weakest up to 60°C. At ambient temperature, the potting compound and the structural adhesive failed at similar stress amplitudes, of the order of 20 MPa. Partial failure of the ceramic rather than the adhesive was observed from the failure surfaces. At temperatures of 80°C and more, contrary to commercial technical advice, the potting compound was stronger. At the higher

temperatures, all the bondlines failed at significantly lower stresses than at ambient, typically much less than 5 MPa. To correlate the measurements with conditions in realistic devices, finite element analysis was used, first to determine if the roughness of the bonding surfaces was a relevant issue, then to calculate the tensile stress distribution and amplitudes under high levels of static and dynamic electric field excitation. These simulations indicate that the stresses induced by electric fields are much smaller than the depolarization field of the piezoelectric material significantly exceed the measured tensile strengths at some temperatures.

Z.Wu is supported by a University of Paisley PhD studentship. The authors thank E.Knox for her contributions to the work.

Session: P3L
HIGH FREQUENCY TRANSDUCERS
Chair: M. Schafer
Sonic Tech

P3L-1
HIGH FREQUENCY ULTRASONIC TRANSDUCER BASED ON INTEGRATED PIEZOELECTRIC STRUCTURE.

P. MARECHAL*[1], F. LEVASSORT[1], L.-P. TRAN-HUU-HUE[1], J. HOLC[2], M. KOSEC[2], and M. LETHIECQ[1], [1]Francois Rabelais University, LUSSI, Tours, France, [2]Jozef Stefan Institute, Ljubljana, Slovenia.
Corresponding e-mail: levassort@univ-tours.fr

Screen-printing technology has been used to fabricate piezoelectric lead-zirconate-titanate thick films on porous PZT substrate for high frequency transducer applications. The thick film composition was modified with lead germanate to lower its firing temperature to 800°C-900°C. The sintered film has a thickness of 36 micrometers. Porous PZT substrate has been chosen for relatively high acoustical impedance and attenuation, two conditions perfectly compatible with transducer requirements for medical imaging. Moreover, the almost identical chemical compositions of the thick film and substrate minimize chemical and physical interactions such as diffusion and thermal mismatch. For the fabrication of the substrate, ammonium oxalate has been used as temporary additive to obtain reproducible process and to control the porosity with a volume fraction of 14%. Gold material has been used for the bottom electrode. Cross section of multilayer sample and optical analysis have allowed to deduce the thickness of all layers (electrodes, piezoelectric thick film) and the porosity in the piezoelectric thick film. All these parameters have been used as in the KLM model to quantify the effective properties of the active film. This has allowed to minimize the number of unknown variables, and electrodes were taken into account. The film displays a high effective thickness coupling factor of 44%,

comparable to those obtained for bulk ceramics of similar composition. The resonant frequency of the structure is at 25 MHz.

This integrated piezoelectric structure has been used to fabricate a high-frequency single element transducer. For this, electrical contacts and a housing have been made and a lens based on pure epoxy resin has been molded on the front face. According to the diameter of the active element and the acoustical properties of the lens, the focal distance is chosen at 5 mm in water to have a f-number near 3. Stand alone lead-titanate disks (Ferroperm Piezoceramics Pz34) obtained with standard technology for bulk ceramic (pressing) have also been characterized (resonant frequency around 20 MHz) and used to manufacture reference transducers with silver-loaded epoxy backing.

Transducers have been characterized in terms of pulse-echo responses at the focal point (sensitivity, axial resolution) and radiation pattern (lateral resolution and depth of field). Results show that the sensitivity and axial resolution (50 micrometers at -6 dB) for the transducer integrating the screen-printed thick film are high, which shows clearly the interest of this technology.

Finally, these two transducers have been successively integrated in a high frequency medical imaging system to obtain in vivo images of human forearm skin. The image qualities are compared and discussed.

This work was funded by the EU in the FP5 GROWTH project PIRAMID (Contract No. G5RD-CT-2001-00456). Authors thank also Ferroperm Piezoceramics A/S for the fabrication of PT disks.

P3L-2

PMN-PT HIGH FREQUENCY ULTRASONIC NEEDLE TRANSDUCERS FOR PULSED WAVE DOPPLER MEASUREMENTS IN THE EYE.

E. GOTTLIEB*, B. LAI, X. XU, Q. ZHOU, J. CANNATA, and K. SHUNG, University of Southern California, Los Angeles, CA.
Corresponding e-mail: egottlie@usc.edu

High frequency ultrasonic needle transducers were fabricated using a 51 μm thick layer of lead magnesium niobate-lead titanate (PMN-33%PT) as the active piezoelectric material. The active element was bonded to a conductive silver particle matching layer and a conductive epoxy backing material through direct contact curing. An outer matching layer of parylene was formed by vapor deposition. The active element was housed within a polyimide tube and 20 gauge needle housing. The measured center frequency and bandwidth of the device was 44 MHz and 36 % respectively. The electrical impedance magnitude and phase were 74 Ω and - 58° respectively. The intended use of this device is for in-vivo high frequency pulsed wave Doppler detection of blood flow in the posterior portion of the eye. A custom high frequency pulsed wave Doppler system has been developed based on the coherent demodulation and sample and hold techniques. The Doppler system includes: a pulser/receiver board consisting of a 45 MHz oscillator, a timing circuit, a power amplifier, wide-band low-noise amplifiers, quadrature coherent demodulator, sample and hold circuitries, and audio amplification; A/D converter (sound card) and PC. An Initial system test

with a pulse repetition frequency of 44 kHz has shown a Doppler shift frequency of 10 kHz corresponding to an approximate velocity of 175 mm/s for a vessel diameter of 5 mm close to the surface of the forearm. An in-vivo Doppler study of the retinal arterial blood flow will follow on New Zealand white rabbits.

This work has been supported by the Resource Center for Ultrasound Transducer Technology, NIH grant # P41-EB2182-07.

P3L-3
INK-JET MICRO-PRINTING OF PATTERNED P(VDF-TRFE) MICRODEVICES.

S. H. ZHANG, Z. Q. LIANG, Q. WANG, and Q. M. ZHANG*, The Pennsylvania State University, University Park, PA.
Corresponding e-mail: sqz100@psu.edu

Poly(vinylidene fluoride-trifluoroethylene) (PVDF-TrFE) copolymers have been used extensively for ultrasonic transducers, especially for very high frequency transducers. Compared with conventional fabrication process, ink-jet printing provides a low-cost versatile method to fabricate polymer devices such as array transducers. For ink-jet printed array transducers, it is important to understand what control the feature size and how to produce uniform array elements (in ink-jet printing, a coffee stain is often produced due to fast solvent evaporation at and the retraction of the edge during the solvent evaporation, which has a very thick ridge and thin center). In this talk, the influences of driving waveform at the jet head, ink concentration, substrate chemistry, and the solvent quality on the printed P(VDF-TrFE) dots were investigated. It was found that well-defined P(VDF-TrFE) micro-dots with diameter of less than 30 μm and thickness of ~1 μm can be printed by using a mixed solvent system, consisting of a good solvent (such as DMF) with relatively low boiling temperature and a poor solvent (such as DOP) with high boiling temperature, on perfluorinated hydrophobic gold surface. The printed P(VDF-TrFE) micro-dots possess crystallinity comparable to that of the bulk sample, indicating that ink-jet printing technology is a promising micro-fabrication technology for manufacturing P(VDF-TrFE)-based micro-devices.

This research was supported by Pittsburgh Digital Greenhouse, Pennsylvania, USA.

P3L-4
HYDROTHERMAL PZT THICK FILM ULTRASONIC TRANSDUCER FOR 2 TO 40 MHZ FREQUENCY BAND.

M. ISHIKAWA*[1], M. KUROSAWA[1], A. ENDOH[2], T. HASEGAWA[2], and S. TAKEUCHI[2], [1]Interdisciplinary Graduate School of Science and Engineering Tokyo Institute of Technology, Nagatutamati, Midori-ku, Yokohama, Kanagawa, JAPAN, [2]Faculity of Engineering, Toin University of Yokohama, Kurogane-cho, Aoba-ku, Yokohama, Kanagawa, JAPAN.
Corresponding e-mail: m.ishikawa@ae.titech.ac.jp

High frequency, wide band characteristic and high intensity ultrasonic transducer was fabricated by hydrothermal deposition technique of lead zirconate titanate polycrystalline thick film (HPTF-PZT). This ultrasonic transducer radiated ultrasounds in the frequency range from 2 to 40 MHz with a 15 dB deviation. Transmitting sensitivity was 1.2 kPa/V at 30 MHz. Additionally, an electric strength of the HPTF-PZT was over 10 V/μm presently obtained value. The transducer had a 20-μm-thick PZT layer on a 50-μm-thick titanium substrate in an active area of 1.4 mm × 8 mm and the HPTF-PZT ultrasonic transducer was driven by a thickness vibration mode. This is first report of the HPTF-PZT ultrasonic transducer characteristics at over 20 MHz operation.

The 20-μ-thick PZT was deposited on a titanium substrate by solution including Pb^{2}+, Zr^{4}+ and Ti^{4}+ in an autoclave at 160°C. First, a nucleation of the PZT crystals of a few micrometers was formed on the titanium substrate by hydrothermal reaction between the titanium substrate surfaces and the solution. The deposit film of the nucleic PZT crystals had a polycrystalline structure. Next, the nucleic PZT crystals was grown for target thickness by hydrothermal reaction between the polycrystalline PZT surfaces and the solution. Previously the characteristics of the HPTF-PZT obtained has measured. The atomic ratio by EDS was Zr:Ti= 80:20 and the piezoelectric constant d33 by LDV measurement was 54 pm/V, the acoustic impedance from dilatational wave velocity and the bulk density was estimated 8.6 Mrayl. The electric strength was over 10 V/μm.

The ultrasonic characteristics of the HPTF-PZT was measured as follows. The electrode of Au was deposited on the HPTF-PZT surface by the vacuum evaporator on one side in 1.4 mm × 8 mm square area . Driving signals were applied between the Au electrode and the titanium substrate. The HPTF-PZT ultrasonic transducer was fixed at its edges to keep it inside the degassed water for propagation of ultrasonic waves. The radiated the ultrasonic waves from the HPTF-PZT were received by a calibrated hydrophone in frequency range between 1 to 60 MHz. The hydrophone was set the horizontal distance of 20 mm from the HPTF-PZT ultrasonic transducer.

Driving signals of burst wave between 2 MHz to 40 MHz were applied to the HPTF-PZT. The sound pressure received in frequency range from 22 MHz to 40 MHz was in the deviation of 6dB and in wide frequency range from 2 to 40 MHz was 15 dB deviation. Additionally, the peak transmission sensitivity was 1.2 kPa/V at 32 MHz. This peak of 32 MHz was estimated to be the quarter wavelength resonance frequency of the 20-μm-thick HPTF-PZT. These results indicate that the HPTF-PZT has capability for wideband and high intensity operation.

It was found that the hydrothermal PZT thick film was completely meet the various requests on medical ultrasonic transducer. It is expected that this hydrothermal PZT will be utilized for development of medical ultrasonic transducer that serve double duties as assessment and therapy.

This research was supported by Japan Society for the Promotion of Science

Session: P3M

MEDICAL TRANSDUCERS II
Chair: C. Oakley
W. Gore, Inc.

P3M-1

THIN-PROFILE HIFU APPLICATORS FOR INTRAOPERATIVE HEMOSTASIS.

V. ZDERIC*[1], S. BURGESS[1,2], and S. VAEZY[1,2], [1]Center for Industrial and Medical Ultrasound, Applied Physics Laboratory, University of Washington, Seattle, WA, [2]Department of Bioengineering, University of Washington, Seattle, WA. Corresponding e-mail: vesna@u.washington.edu

Introduction. Our objective has been to optimize current HIFU applicators for use in a clinical surgical environment. Ideally, surgical HIFU applicators should be robust, light, and with small dimensions. We have been developing, manufacturing and testing new thin-profile HIFU applicators (thickness of 1 cm) for intraoperative hemostasis. **Methods.** Two types of HIFU applicators were manufactured: a) working at the operating frequency of 6.3 MHz with the focal distance of 3.5 cm, and b) working at the operating frequency of 3 MHz with the focal distance of 5 cm. The applicators consisted of a PZT concave element (diameter of 3.5 cm) and aluminum housing. The design and optimization of different elements of the device were done using SolidWorks. The housing had a spoon-like shape with the central concave disc (diameter of 4 cm, thickness of 1 cm), and a thin tube (diameter of 4 mm) that served for guiding the coaxial cable to the PZT element and as the device holder. The PZT element was air-backed, and a plastic cap was sealed on the back of the housing. The housing front surface had thickness of 1/4 or 3/4 of ultrasound wavelength in aluminum to provide acoustic matching. The resonant frequency and quality (Q) factor of the device were determined with the impedance analyzer. The ultrasound field was observed using Schlieren imaging and hydrophone field mapping. The acoustic power was measured with reflective radiation force balance. The device efficiency for producing tissue necrosis was tested in BSA-polyacrylamide gel phantom and rabbit kidney in vivo. **Results.** The 3 MHz applicator had frequency bandwidth of 0.43 MHz, and Q factor of 9. The 6.3 MHz applicator had frequency bandwidth of 0.17 MHz, and Q factor of 37. Schlieren images showed sharp focusing at the theoretical focus of the applicators. The -3dB width and length of the focal area of the 3 MHz applicator were 0.5 mm and 10 mm, respectively. The -3dB dimensions of the focal area of the 6.3 MHz applicator were 0.6 mm and 2.2 mm in lateral and axial direction, respectively. The efficiency of electrical to acoustic power conversion was 40%. The maximal intensity at the focus was 9,500 W/cm^2 (in water). The HIFU application for 10 s produced lesions in the gel phantom, and rabbit kidney in vivo. **Conclusion.** Thin-profile HIFU applicators have an advantage of simple design, and a small footprint, which facilitates intraoperative access to injured sites. We believe that the success of our initial devices will lead to the design and production of a new surgical tool for HIFU hemostasis.

P3M-2
MULTILAYER PZT ULTRASOUND ARRAYS SHOWING IMPROVED THERMAL PERFORMANCE.

M. ZIPPARO*, Tetrad Corporation, Englewood, CO.
Corresponding e-mail: mzipparo@wlgore.com

This work describes test results for ultrasound arrays designed to have improved acoustic power delivery capability without sacrificing imaging performance. Three layer ceramic stacks of PZT4 and PZT8 were characterized to determine their electromechanical properties as array elements. The resulting electromechanical coupling was 90 to 95% that of a bulk material, with an effective dielectric constant which is nine times that of a bulk material. For example, a 3-layer ceramic fabricated from PZT4 showed a coupling of 0.62 and an effective relative clamped dielectric constant of over 5000. This compares to a single layer of PZT5-H with a coupling of 0.70 and a relative dielectric constant of 1200. Multilayers made with PZT8 showed similar performance relative to bulk properties, albeit the lower coupling of bulk PZT8 resulted in a 3-layer resonator coupling of around 0.55. An array made with the PZT4 3-layer stack showed a round trip sensitivity 3 dB higher than a control array made with a single layer of PZT5-H. The -6 dB bandwidth was 60% for the PZT4 3-layer array, compared with 66% for the control. The sensitivities of the PZT8 multilayer arrays were equal to or slightly better than the control, and the bandwidth was close to 50%. Power tests were performed by driving arrays in pulsed Doppler mode while radiating into air and observing the temperature increase on the face of the array. The arrays tested were identical except for the PZT material, the control having a single layer of PZT5-H and the other having a 3-layer stack of PZT8. Neither array had a front acoustic lens. With equivalent electrical input power, the control array stabilized at 81 degrees C, while the PZT8 array stabilized at 64 degrees C. In summary, arrays fabricated with low loss multilayer PZT showed equivalent or improved acoustic performance and improved thermal performance relative to arrays made with a single layer of PZT5-H.

This work has been funded by NIH.

P3M-3
COMPARISON OF THREE DIFFERENT TRANSDUCER CONCEPTS FOR ACOUSTIC BLADDER VOLUME ASSESSMENT.

E. J. W. MERKS*[1], G. MATTE[1], N. BOM[1], A. F. W. VAN DER STEEN[1,2], and N. DE JONG[1,2], [1]Erasmus MC, Rotterdam, The Netherlands, [2]ICIN, Utrecht, The Netherlands.
Corresponding e-mail: e.merks@erasmusmc.nl

Background: In a preceding study the importance of non-invasive bladder volume assessment was addressed. A new technique to measure the bladder volume on the basis of non-linear ultrasound wave distortion was validated. It was shown that the harmonic level generated at the posterior bladder wall increases for larger bladder volumes.

Objective: The objective is to design an optimal transducer with respect to efficiency and beamforming. The transmit efficiency at fundamental frequency should be such that the generated second harmonic peak pressure due to non-linear propagation in water is at least 40 kPa at 12 cm axial distance. Further, the -6 dB beamwidth at 12 cm should be at least 6 cm to capture a large part of the bladder.

Methods: Three different transducer concepts were compared. The first was an unfocused multi-layer transducer with active radius of 15 mm, using a single element PZT-transducer (2 MHz center frequency, -6 dB BW: 55%) for transmission and a 52 μm thick PVDF top-layer for reception. The second was an unfocused single element 1-3 piezocomposite transducer with active radius of 15 mm. It was designed for optimal transmission at 2.25 MHz and reception of the fundamental, second and third harmonics with fractional bandwidths of 10%. The third transducer consisted of an unfocused air-backed ring element with outer radius of 1 cm and inner radius of 5 mm for transmission at 2.2 MHz, and a broadband unfocused inner element with active radius of 5 mm for reception (4.5 MHz center frequency, -6 dB BW: 61%). All three concepts were subjected to a drive level of 120 V_{pp} and were mutually compared using pulse-echo measurements, in water with a plane reflector and on agar phantoms with and without a water filled cavity, and calibrated hydrophone measurements in water. Identical measurements were performed with an additional acoustic lens (Rexolite) with radius of curvature of 35 mm to obtain the required beamwidth.

Results: All concepts allowed for harmonic imaging when scanned across agar phantoms, indicating sufficient receive sensitivity. Hydrophone measurements in water showed that the multi-layer transducer generated peak pressures of 290 kPa and 50 kPa at 12 cm for the fundamental and second harmonic respectively. The piezocomposite transducer generated peak pressures of 215 kPa and 35 kPa at 12 cm, whereas the ring transducer generated peak pressures of 850 kPa and 405 kPa. Applying an acoustic lens on the first two concepts increased the -6 dB beamwidth at axial distance of 12 cm from 25 mm to 60 mm. The mean fundamental and second harmonic pressures decreased with 8 dB and 13 dB, respectively, for both transducers. The lens in combination with the ring concept gave a complex and fractioned beamprofile.

Conclusions: The results showed that the ring concept has the best efficiency, but a complex beamprofile. Also, its relatively small active area should be put in perspective with the other concepts. Hence, the multi-layer concept was found best.

This research was funded by the Dutch Technology Foundation and Diagnostic Ultrasound Europe.

P3M-4
HIGH ELEMENT COUNT (3600), FULLY SAMPLED, TWO DIMENSIONAL TRANSDUCER ARRAY.

M. EAMES*, S. ZHOU, and J. HOSSACK, University of Virginia, Charlottesville, VA.
Corresponding e-mail: mde3c@virginia.edu

Extending our previous research directed towards fabricating fully sampled, high element count arrays for use in a portable ultrasound system, a 60 × 60 (3600) element 5 MHz 2D array is presented here. Our previously assembled and tested array with 32 × 32 (1024) elements and 4 MHz resonant frequency enabled approximately 0.5 mm resolution images. Among the challenges encountered when fabricating the newer arrays are the finer pitch (300 microns) and reduced PZT thickness (320 microns). The finer array pitch and reduced element thickness necessitates subdicing of the array elements in order to yield close to unimodal thickness mode operation. We have established via finite element analysis (FEA) and practical experimentation that a viable compromise in terms of kerf widths is obtained using 45 micron kerfs between adjacent elements to ensure electrical and acoustic isolation, and subdicing with 25 micron kerfs to maximize residual PZT volume in each element. The thin PZT material makes it increasingly difficult to avoid short-circuits when using silver-loaded epoxy on both sides of the array for connections to a top surface ground return carried by a metallized polyester film and the bottom conducting signal lines. In early fabrication prototyping, we have achieved a high live element yield (approximately 92% without open or short circuits). Electrical connection to the elements is provided by mounting the elements onto a board (typically fiber reinforced plastic) with metallized through holes formed under each element. Contact to a 'fanout' circuit is provided via a Z-axis conductive polymer mounted between the array board and the matching processing board. (Eventually, in a fully developed version, the transducer board and processor board will be reflow soldered together.) FEA impedance data, pulse echo responses and angular beam patterns are presented. Additionally, we have used PZFlex FEA to perform parametric analysis to determine the optimum subdicing depth taking account of element impedance, pulse echo response and angular beam pattern.

Supported in part by NIH EB002349 and US Army W81XWH-04-1-0240

P3M-5
A KNOWLEDGE BASED APPROACH FOR DESIGN OPTIMIZATION OF ULTRASONIC TRANSDUCERS AND ARRAYS.

S. N. RAMADAS* and G. HAYWARD, The Centre for Ultrasonic Engineering, University of Strathclyde, Glasgow, Scotland, UK.
Corresponding e-mail: nishal@ultra.eee.strath.ac.uk

The design of ultrasonic transducers and arrays is reliant traditionally on practical experience, supplemented by performance evaluation via computer modelling. As technology requirements have advanced, transducer complexity has increased dramatically, making intuitive design very difficult. This paper presents a knowledge-based, interactive optimizer for transducer and array design. A rule based expert system shell is used to capture expert knowledge and guide the design and optimization process. The expert system also forms an intelligent front end for the software program, by permitting interactive and flexible user dialogue. The design optimization is carried out using a genetic algorithm based

search procedure. A number of models have been developed to simulate a variety of thickness mode transducer structures, including multi-layers incorporating inversion, parallel and independent configurations. Each is configured to be directly compatible with electronic simulation environments such as PSPICE, enabling design optimization of signal to noise ratio, bandwidth and efficiency, with respect to transducer structure and constituent materials.

Examples of the design optimization process are illustrated. The first of these relates to the implementation of a front face matching layer, designed to promote bandwidth and sensitivity in relatively straightforward thickness mode applications. This is followed by a multi-layered structure comprising different zones of piezoelectric polarisation. A lattice model has been developed and used for simulation purposes, with the number and dimensions of the active layers, along with passive matching layer information being fed as variable parameters for the optimizer. The results are shown to compare very favourably with conventional methods and serve to demonstrate that the knowledge-based approach is a very efficient and attractive alternative. It may be implemented for design and optimization of any kind of thickness mode transducer system, subject to the availability of an appropriate simulator.

P3M-6
BIPLANE ULTRASOUND ARRAYS WITH INTEGRATED MULTIPLEXING SOLUTION FOR ENHANCED DIAGNOSTIC ACCURACY IN ENDORECTAL AND TRANSVAGINAL IMAGING.

N. FELIX*, R. DUFAIT, D. VOISIN, S. MAITRE, and P. AUCLAIR, VERMON, Tours - France.
Corresponding e-mail: n.felix@vermon.com

Biplane endorectal probes are nowadays commonly used in many applications. For example in biopsy procedure in transrectal guidance two orthogonally placed linear and curved ultrasound transducer arrays allow the radiologist to guide and perform accurately the puncture by placing in the transverse plane the body that need biopsy and in the longitudinal plane the needle puncture. It is also very useful for proper placement of brachytherapy devices that is essential for optimal treatment of the targeted tissue without exposure of normal structures.

But biplane probes are very challenging for ultrasound transducer and system engineers, because of the large number of active elements to be managed in these probes. Typically these probes are composed of one highly curved and one linear array inducing more than 256 active elements and then a high number of coaxial cables to be managed both on the system and probe side.

In this work, we present an innovative solution to reduce this high number of cables, by introducing a high speed switching multiplexing system in the probe handle converting then for example 3*96 connections in an equivalent 96 elements probe, allowing a fast switch between arrays with the target to display in real time all image planes.

To illustrate this technology, we present a probe for endocavity applications including 3 ultrasound arrays. The first one is a highly curved, with a 6.5MHz

center frequency and 96 elements. It is positioned in the transverse plane i.e. orthogonally as compared to probe shaft. Two 96 elements 6.5MHz center frequency low curvature arrays are positioned in the longitudinal plane of the probe on both side of the highly curved array. Then the 3 arrays allow to display one transverse image and a longitudinal one obtained by overlapping the two images of the low curvature arrays.

In both case design is discussed and technological choices are justified: ergonomics, power consumption, trade-offs and key design parameters. But introducing electronic circuits between ultrasound arrays and imaging system must not decrease the array and image performances. Arrays are then fully characterized through electrical impedance, elementary pulse-echo response, and acoustic directivity pattern, with and without the multiplexing electronics.

Results are discussed and show that an optimal electronic design doesn't impact array performances. Finally clinical images are presented to highlight performances of these probes.

P3M-7

SPATIAL FOCALIZATION USING TEMPORAL INVERSION IN CHAOTIC CAVITIES: INFLUENCE OF SURFACE ROUGHNESS.

N. PÉREZ[1], C. A. NEGREIRA[1], G. MONTALDO*[2], and M. FINK[2], [1]Facultad de Ciencias, Montevideo, Uruguay, [2]Ecole Superieure de Physique et de Chimie, Paris, Francia.
Corresponding e-mail: nico@fisica.edu.uy

In the last years, the use of time reversal mirrors (TRM) and time reversal chaotic cavities was proposed as a method to focus sharp pulses in fluid media. An important application of those techniques is the formation of 3D echograpic images.

In a recent work, we present a statistical model to predict the spatial focusing of the time-reversed pulse and show the existence of a cut-off in the spatial frequencies caused by the existence of critical angles in the transmission function. In the solid-fluid interface, the high spatial frequencies are not transmitted to the fluid and generate an important limitation in the spatial focusing. A solution to overcome this limitation is to use rough surfaces in the interface. In this case the waves are scattered by surface irregularities and all spatial frequencies are possible.

In this work, we perform a systematical study of the influence of the spatial roughness in the spatial focusing. We use two spatial patterns, corresponding to the longitudinal and shear wavelength and in each case a set of rms roughness. We show the experimental results using hydrophone scanning and the Schlieren pulsed method to determine the focus size. We obtained a focus reducing in the order of 30% and the reduction of side lobes. The results al also supported by numerical simulations using FEM.

This work was supported by PEDECIBA-Uruguay and PICS 2175- CNRS France.

ORAL SESSIONS

Session: 1I
CONTRAST AGENTS FUNDAMENTALS
Chair: N. de Jong
Erasmus MC

1I-1 11:30 a.m.
(Invited)
BUBBLE ACOUSTICS: FROM SEAS TO SURGERIES.

T. LEIGHTON*, Institute of Sound and Vibration Research, University of Southampton, Southampton, Hants, UK.
Corresponding e-mail: tgl@soton.ac.uk

Acoustics affects our lives profoundly and commonly, both as a nuisance and a necessity. Through speech, acoustics has dominated our communications for millennia. It underpins not only recorded music but also live transmissions, from entertainment in theatres and concert venues to public address systems.

Although our experience for millenia has been dominated by audiofrequency sound in air, today we use ultrasound in liquids for biomedical diagnosis and therapy, for sonochemistry and ultrasonic cleaning, and for the monitoring and preparation of foodstuffs, pharmaceuticals and other domestic products. From the Second World War to the present conflicts, acoustics has had an unrivalled role in the underwater battlespace. Underwater sound sources are used to map petrochemical reserves and archaeological sites, as well as to monitor a huge variety of important commercial and environmental features, from fish stocks to climate change. In all these examples, gas bubbles are the most potent naturally-occurring entities that influence the acoustic environment in liquids.

However our experience as humans of audiofrequency sound in air does not equip us with an intuitive appreciation of the acoustic environment in liquids. The mammals with greatest experience of this are cetaceans (whales, dolphins and porpoises). Given the complexity and potency of gas bubbles in liquids, and the potential for their exploitation, this paper addresses the question of whether there is anything we can learn from the acoustical response of cetaceans to the bubbly marine environment. Within the range of observed behaviours, most curious of all is the aptitude of cetaceans purposefully to generate vast clouds of bubbles via their blowholes. This is because, compared to man-made sonar, the sonar 'hardware' of cetaceans is mediocre. Hence if they possess no more understanding than that used by humans in processing sonar signals in bubbly environments, in creating such bubble clouds cetaceans are effectively blinding their own sonar. However certain aspects of cetacean behaviour, particularly when they hunt, suggest that at times the bubbles they generate may be enhancing their acoustic capabilities. The acoustic and mental processing that might be involved is explored through the use of a new model for nonlinear acoustic propagation in bubbly water, in order to explore to what extent these possibilities may reflect upon our own exploitation of bubbles in marine and biomedical ultrasonics.

1I-2 12:00 p.m.

A MODEL FOR LARGE AMPLITUDE OSCILLATIONS OF COATED BUBBLES ACCOUNTING FOR BUCKLING AND RUPTURE.

P. MARMOTTANT[1], S. VAN DER MEER*[1], M. EMMER[2], M. VERSLUIS[1], N. DE JONG[2,1], S. HILGENFELDT[1], and D. LOHSE[1], [1]Physics of Fluids, Enschede, The Netherlands, [2]Erasmus MC, Rotterdam, The Netherlands.
Corresponding e-mail: s.m.vandermeer@utwente.nl

Background: To enhance ultrasound imaging, coated microbubbles are used as ultrasound contrast agents. Coating materials include lipids, polymer, and thick protein shells. The coating modifies the effective surface tension, and this is expected to strongly influence the dynamics. Current models developed to describe coated bubble oscillations implicitly assume small deformations of the bubble surface; however, in practice, contrast agent bubbles produce oscillations with large variations in the surface area.

Goal: To develop a model designed to incorporate the effect of the coating on the microbubble response to ultrasound, and specifically to capture the high-amplitude dynamics.

Method: We focus on phospholipidic monolayer coatings, used in several contrast agent bubbles[1]. The phospholipid molecules naturally adsorb to the interface and shield the gas from the liquid medium, thereby reducing the surface tension to a value lower than that of water (73 mN/m). We propose an effective surface tension s_{eff} of the lipidic monolayer[2], which describes the bubble in three different states: (i) a buckled state, where the effective surface tension remains zero, (ii) an elastic state, where the effective surface tension depends linearly on the bubble area $A=4\pi R^2$, and (iii) a ruptured state, where the effective surface tension is that of pure water. These states are characterized in the model through the use of these parameters: a buckling surface radius, a shell compressibility and a break-up shell tension.

Results: The model describes some recently observed phenomena for ultrasound contrast agents. First, the model accounts for compression-only behavior. This behavior is characterized by a non-linear response at relatively low pressures (100 kPa). During the compression phase the bubble compresses, but during the expansion phase the bubble hardly expands. The model predicts that at the compression phase the bubble will likely buckle, canceling out any surface tension, and during the expansion phase the surface tension will rapidly rise. A second phenomenon that is described by the model is the rupture of the shell at increased acoustic pressures. Here, the shell breaks up uncovering the bubble surface, thereby obtaining the properties of a free gas bubble. In this case compression-only oscillations change to symmetric oscillations.

Conclusion: We present a new model for the dynamical properties of phospholipid coated contrast agent bubbles. It predicts compression-only behavior and break-up of the shell. Possible applications of the model include an improved characterization of coated microbubbles and the description of non-linear acoustic responses for use in e.g. pulse-inversion imaging.

References

1. A.L. Klibanov, “Ultrasound contrast agents: Development of the field and current status”, Top. Curr. Chem. 222, 73 (2002).

2. P. Marmottant, S. van der Meer, M. Emmer, M. Versluis, N. de Jong, S. Hilgenfeldt, D. Lohse, “A model for large amplitude oscillations of coated bubbles accounting for buckling and rupture”, submitted to JASA (2005).

1I-3 12:15 p.m.
CREATING ANTIBUBBLES WITH ULTRASOUND.

M. POSTEMA*[1], N. DE JONG[2,3], G. SCHMITZ[1], and A. VAN WAMEL[3], [1]Ruhr-Universität Bochum, Bochum, Germany, [2]University of Twente, Enschede, The Netherlands, [3]Erasmus MC, Rotterdam, The Netherlands.
Corresponding e-mail: postema@ieee.org

Ultrasound contrast agents have been investigated for their potential applications in local drug and gene delivery. A microbubble might act as the vehicle to carry a drug or gene load to a perfused region of interest. The load has to be released with the assistance of ultrasound. We investigate the suitability of antibubbles for ultrasound-assisted local delivery. As opposed to bubbles, antibubbles consist of a liquid core surrounded by a gas encapsulation. Incorporating a liquid drop containing drugs or genes inside an ultrasound contrast agent microbubble, however, is technically challenging.

An ultrasound-insonified microbubble generates a pressure field that is inversely proportional to the distance from the microbubble. Therefore, an oscillating contrast agent microbubble may create a surface instability with a relatively big bubble at a short distance. For big enough instabilities, a drop may be formed inside the big bubble.

Three different contrast agents were subjected to 0.5 MHz ultrasound, with mechanical indices >0.6. The contrast agents were inserted through an artificial capillary which led through the acoustic focus of the transducer. High-speed photographs were captured at a speed of 3 million frames per second and higher. We observed that ultrasound contrast microbubbles below resonance size may create visible surface instabilities with bubbles above resonance size. With an albumin-shelled contrast agent, we induced a surface instability that was big enough to create an antibubble inside a free (unencapsulated) gas bubble with an 8 μm diameter. The surface instability has been attributed to the presence of a contrast microbubble with a 3 μm diameter. This instability has the form of a re-entrant jet protruding into the gas bubble. The inward protrusion grew and subsequently drained, leaving a droplet with a five μm diameter inside the bubble. In a subsequent recording after 100 ms, only the gas bubble could be detected. Thus, the life-time of the antibubble was less then 100 ms. The presence of a surfactant on the interfaces might lead to an improved stability of an antibubble.

1I-4 12:30 p.m.

OPTICAL INVESTIGATION OF ULTRASOUND INDUCED ENCAPSULATED MICROBUBBLE OSCILLATIONS: THRESHOLD AND HYSTERESIS EFFECTS.

M. EMMER*[1,2], J. BORSBOOM[1], A. VAN WAMEL[1], M. VERSLUIS[2], and N. DE JONG[1,2], [1]Dept. of Experimental Echocardiography, Thoraxcentre, Erasmus MC, Rotterdam, the Netherlands, [2]Physics of fluids, University of Twente, Enschede, the Netherlands.
Corresponding e-mail: m.emmer@erasmusmc.nl

Background: Next to enhancing microbubble stability, the bubble shell also strongly influences its oscillating behaviour. In previous optical studies [1], we have shown that in contradiction to the predictions of current models, microbubbles with similar sizes can respond differently to ultrasound insonification. We hypothesize that by adding a shell to the microbubble, threshold and hysteresis effects are introduced, which have a certain influence on the dynamic behaviour of microbubbles. In order to get more insight in the contribution of the shell upon the microbubble oscillating behaviour, we investigated threshold and hysteresis effects in individual microbubbles using high-speed imaging.

Method: To investigate these effects, two experiments were carried out. Both experiments used the experimental phospholipid encapsulated agent BR14 (Bracco Research SA, Geneva, Switzerland). It was insonified at 2 MHz centre frequency. Images of individual microbubbles were recorded with the Brandaris-128 camera system [2] at a frame rate of 14 million frames per second. The acoustic pressure threshold for bubble oscillation was investigated through recording individual bubbles in twelve sequences of 64 image frames. A single bubble was insonified with twelve cycle sine wave bursts with increasing peak pressures (40 - 300 kPa) in subsequent sequences. For the hysteresis effect, we recorded sequences of 128 frames in which a single bubble was exposed to a Gaussian apodised burst with a full width at half maximum duration of 3.5 μs and a peak pressure of 300 kPa.

Results: In the threshold experiment, it was observed that only bubbles of larger than 3 micrometers in diameter started oscillating for pressures below 60 kPa. For pressures up to 200 kPa, also bubbles larger than 1.5 micrometers oscillated. For pressures up to 300 kPa, the smallest bubbles that were observed to oscillate were 1.2 micrometers. When comparing single bubble responses between the ascending and descending side of the Gaussian burst, we observed that most of the microbubbles above or below resonance size had higher radial amplitudes at the ascending side. The radial amplitude as a function of acoustic pressure of these bubbles described a clockwise hysteresis curve.

Conclusions: Current models do not fully capture the dynamic behaviour of encapsulated microbubbles. Smaller encapsulated microbubbles do not oscillate until the acoustic pressure has exceeded a threshold value, which is inversely related to the initial bubble size. In addition, we found a hysteresis effect in most of the responses of non-resonant bubbles. These findings may have implications in novel detection methods.

[1] Postema et al., Simulations and measurements of optical images of insonified ultrasound contrast microbubbles. *IEEE Trans Ultrason, Ferroelect, Freq Contr*, 50(5):523-536, 2003.

[2] Chin et al., Brandaris 128: A digital 25 million frames per second camera with 128 highly sensitive frames. *Rev. Sci. Instrum.*, 74(12):5026-5034, 2003.

1I-5 12:45 p.m.
MICROBUBBLE NANO-INTERROGATION USING THE ATOMIC FORCE MICROSCOPE.

V. SBOROS*[1], E. GLYNOS[2], M. BUTLER[1], C. M. MORAN[1], J. ROSS[3], S. D. PYE[4], W. N. MCDICKEN[1], and V. KOUTSOS[2], [1]Medical Physics, School of Clinical Sciences and Community Health, University of Edinburgh, Edinburgh, UK, [2]Institute for Materials and Processes, School of Engineering and Electronics, Centre for Materials Science and Engineering , University of Edinburgh, Edinburgh, UK, [3]Clinical and Surgical Sciences, University of Edinburgh, Edinburgh, UK, [4]Medical Physics, Royal Infirmary of Edinburgh, Edinburgh, UK. Corresponding e-mail: Vassilis.Sboros@ed.ac.uk

The Atomic Force Microscope (AFM) is a versatile tool, that provides an unprecedented spatial and force resolution in the order of Angstroms and sub-nanonewtons, respectively; therefore, it is ideally suited to study morphology and mechanical properties of materials at the nanometer scale.

This paper introduces the use of the AFM to study the topography and the mechanical properties of individual microbubbles.

BiSphere® (Point Biomedical Corp, San Carlos, CA, USA) microbubbles were chemically attached to Petri dishes as required for AFM experiments. The Bioscope AFM (Veeco, Santa Barbara, CA, USA) was used for the measurements.

a) Tapping mode AFM was used for imaging, with cantilevers resonating at 5-8 kHz (NP-20, Veeco).

b) Contact mode AFM was used for mechanical measurements using tipless cantilevers (NSC-20, MikroMash, Spain) with spring constants ranging from 0.03-15 N/m. This is done by measuring the deflection of the AFM cantilever during compression of the microbubble and comparing it quantitatively with that of a hard surface.

Topography maps of 15 different microbubbles were acquired and their dimensions were assessed with an accuracy of 50 nm. The resolution of the topography of the microbubble was as small as 20 nm. Such figures are comparable with data from electron microscopy, but AFM provides superior flexibility as it can interrogate microbubbles in various chemical and physical environments (in liquid at a range of different temperatures, pressures and viscosities).

Optimal measurements of the stiffness of 20 microbubbles ranging in size from 1-10 Î¼m was provided by cantilevers between 0.3-0.6 N/m as cantilevers with lower spring constant were too soft for the measurements, and higher spring constant would destroy the microbubbles. The stiffness (effective spring constant)

of the microbubbles ranged between 1 and 5 N/m. These measurements can be translated to shell properties by using an appropriate model for the shape and structure of the microbubbles.

The work is funded by the Engineering and Physical Sciences Research Council UK (EPSRC)

Session: 2I
ULTRASOUND AND THERAPEUTICS
Chair: K. Hynynen
Brigham and Women's Hospital

2I-1 11:30 a.m.
ULTRASOUND INDUCED ANTIVASCULAR THERAPY OF MOUSE TUMORS.

C. M. SEHGAL*, S. ANSALONI, L. S. ZIMER, W. M. F. LEE, M. D . FELDMAN, and A. K. W. WOOD, University of Pennsylvania, Philadelphia, PA.
Corresponding e-mail: sehgalc@uphs.upenn.edu

The oxygen and nutritional needs of cells in growing tumors are satisfied by the stimulation of angiogenesis. The failure of traditional therapies to eradicate tumors, as well as the recognition that tumor vasculature plays an essential role in tumor growth, has led to alternative therapies that target angiogenesis and tumor blood vessels. The goal of this study is to determine if low intensity ultrasound can be used to disrupt tumor vasculature.

K1735 melanomas were grown subcutaneously in 22 C3HeN mice. Once tumors had grown to a minimum size of 1cm, they were insonated with low-level continuous ultrasound at 1 MHz and 2.3 Wcm-2. Four groups of mice were treated for 0, 1, 2, and 3 minutes. The 0 treatment time represented the control group.

Imaging was performed before and after insonation using power Doppler imaging and a contrast agent (0.1 mL , Optison, Amersham Health Inc, Princeton, NJ), injected intravenously through a tail vein. The images of tumors at peak enhancement were analyzed for color. This involved detection of colored pixels and measurement of the color level representing contrast concentration on a relative scale of 0-100. The color level versus fraction of colored pixels covering the tumor was used to construct cumulative histograms. The area under the cumulative histogram (representing the lack of tumor perfusion) was measured. The difference between the area under the curve, before and after treatment was used to quantify the antivascular effect of insonation. After imaging, the animals were sacrificed. Tumors were fixed in 4% paraformaldehyde, embedded in paraffin, sectioned, and stained with hematoxylin and eosin.

The mice recovered normally following the insonation and imaging of the tumor. Prior to insonation, the tumors were highly vascular. On average, all but 6±2% of the tumor was perfused. After treatment with ultrasound, power Doppler images

showed that the contrast medium did not enter all regions of the tumor. Parts of the tumor were now avascular and had lost their normal vascular perfusion. For 1, 2 and 3 minute treatments the avascular area under the cumulative histogram increased to 38±33%, 69±29% and 82±19 %, respectively. In each case the difference between pre- and post-treatment was significant ($P<0.05$). The control group did not exhibit significant difference between the pre- and the post-treatment values ($P>0.1$). With increasing treatment time, the tumors became increasingly avascular at a rate of about 25% for each minute of insonation. Histology showed disruption of the walls of the tumor blood vessels, and tumor cell death in areas of vascular congestion and thrombosis, suggesting it was secondary to ischemia. The predominant effect of insonation appeared to be thermal.

The results of this study show that low-level ultrasound can effectively disrupt tumor vasculature. The sonication with low-level ultrasound shows promise as an antivascular therapy, whether it is used alone or in combination with other treatments.

Acknowledgements: This work was supported in part by NIH grant number EB001713.

2I-2 11:45 a.m.
THE FEASIBILITY OF FOCUSED ULTRASOUND TO TEMPORARILY INHIBIT NERVE CONDUCTION.

V. COLUCCI, F. JOLESZ, and K. HYNYNEN*, Brigham and Women's Hospital, Boston, MA.
Corresponding e-mail: kullervo@bwh.harvard.edu

The non invasive application of thermal and mechanical energy to selective areas of the human anatomy have led to significant advances in treatment and recovery from typical surgical interventions. New areas for focused ultrasound therapy are being explored with increasing rate. In this study the feasibility of using focused ultrasound to inhibit nerve conduction was explored. The sciatic nerves (50 nerves) from the American bullfrog were subjected to focus ultrasound at frequencies of .661 and 1.986MHz and heated ringer solution. In some experiments the nerve temperature was measured with an invasive thermocouple probe (wire diameter 0.05 mm). Nerve stimulation was accomplished with a Grass S48 Stimulator, SIU5 Stimulus Isolation unit, and CP511 AC amplifier and was viewed on a Tektronix TDS 3012 oscilloscope. When the nerve was electrically stimulated while exposing to the ultrasound the action potential was shown to decrease in all experimental combinations except for the application of 1.986 MHz at a one percent burst length and 100ms repetition rate. The recovery rate and magnitude of the nerve action potential following cessation of the treatment was related to the amount of ultrasound power and the recorded temperature. The action potential returned with in a few minutes after the ultrasound exposure however, the full recovery took approximately 90 minutes. By increasing the power levels above the threshold level permanently eliminated the action potential. Similar results were obtained by heating the nerve except that the low frequency sonication produced the nerve block at lower temperatures

than the higher frequency or the heating of the ringer solution. This study extends the earlier studies and suggest that focused ultrasound could be used to produce a temporary nerve block. This may be useful in many clinical applications.

2I-3 12:00 p.m.
FEASIBILITY OF TRANSCRANIAL, LOCALIZED DRUG-DELIVERY IN THE BRAIN OF ALZHEIMER'S-MODEL MICE USING FOCUSED ULTRASOUND.

J. CHOI, M. PERNOT, S. SMALL, and E. KONOFAGOU*, Columbia University, New York, NY.
Corresponding e-mail: ek2191@columbia.edu

Therapeutic agents are difficult to deliver in the brain because of brain's natural defense: the Blood-Brain Barrier (BBB). Recently, it has been shown that Focused Ultrasound can produce reversible and localized BBB opening in the brain when applied in the presence of ultrasound contrast agents [1]. However, a major limitation of ultrasound in the brain is the strong phase aberration and attenuation of the skull bone. Thus, despite the high potential of non-invasive adaptive focusing techniques, no study of ultrasound-targeted drug treatment in the brain has been reported until now. In this study, the feasibility of BBB opening in the hippocampus of Alzheimer's-model mice using focused ultrasound through the intact skull was investigated. A high power focused transducer (1.5 MHz central frequency) was mounted on a 3D positioning system and a 7.5 MHz single element diagnostic transducer was placed through the center of the focused transducer and aligned with the high power beam in order to achieve high precision targeting. In order to investigate the effect of the skull, needle hydrophone measurements were made through an ex-vivo skull. The pressure field showed minimal attenuation (18% of the pressure amplitude was attenuated) and a well-focused pattern (2-mm focal spot) through the left and right halves of the sagittal suture in the parietal bone. Prior to sonication, ultrasonographic contrast agents (Optison; 0.05 ml) and MRI contrast agents (Omniscan; 0.5 ml) were injected in live mice intravenously. The brains of six mice were then sonicated through intact skull and skin within the first hour following sacrifice. Ultrasound bursts with a duration of 20 ms at 20% duty cycle were applied over 30 s using pressure amplitudes ranging of 0.5-3.5 MPa. Contrast-enhanced high resolution T1 and T2-weighted MR Imaging (9.4 Tesla) with an in-plane resolution of 75 μm was able to distinguish opening of large vessels in the region of the hippocampus. Beyond 1 MPa, multiple small cavitation-induced foci could be imaged in the form of low-intensity regions (~150 microns in diameter) on the MRI images. The extent of cavitation damage could be controlled through variation of the pressure amplitude and a quasi-linear relationship between the area of damage measured from the MRI image and the pressure amplitude was observed. In addition, large vessels including the ventricles had increased concentration of gadolinium (i.e., appearing brighter on the MRI scan) as well as increase in cavitation regions. These results demonstrate the feasibility of potentially, locally opening the BBB in the mouse hippocampus using focused ultrasound through the intact skull and skin. Future investigations will deal with testing of this technique for successful delivery of antibodies into the hippocampal

region of Alzheimer's model mice.

[1] Hynynen et al. Noninvasive MR Imaging-guided Focal Opening of the Blood-Brain Barrier in Rabbits, Radiology, 220, 3, 2001.

This study was supported by a Special Development Award from the Whitaker Foundation and DARPA funding.

2I-4 12:15 p.m.
FIBRIN-TARGETED THROMBOLYTIC THERAPY USING ACOUSTICALLY REFLECTIVE PERFLUOROCARBON NANOPARTICLES.

J. MARSH*, A. PAN, G. HU, K. CROWDER, M. SCOTT, M. HUGHES, S. WICKLINE, and G. LANZA, Washington University School of Medicine, St. Louis, Missouri.
Corresponding e-mail: jnm@cvu.wustl.edu

Background: Thrombolytic agents, i.e. "clot-busters" such as tPA, have been shown to be effective therapeutics for acute ischemic stroke. However, systemic administration of such powerful agents may be complicated by increased risk of cerebral hemorrhage and worsening stroke. Targeting of clot-dissolving therapeutics has the potential to decrease the incidence of these complications while simultaneously increasing effectiveness of treatment, by concentrating the available drug at the desired site and permitting a lower overall systemic dose. We have previously demonstrated targeting of liquid perfluorocarbon nanoparticles (NP's) to thrombi *in vitro* and *in vivo*, with concomitant enhancement of acoustic reflectivity from the targeted clot surfaces. In the current study, a traditional thrombolytic enzyme (streptokinase) was incorporated into fibrin-targeted NP's and targeted to plasma clots *in vitro* to demonstrate their use as both an acoustic contrast agent and an adjunctive targeted therapeutic delivery system.

Methods and Results: Human plasma clots were formed on nitrocellulose membranes *in vitro* and targeted with acoustically active NP's by treating the clots sequentially with biotinylated anti-fibrin antibody, avidin, and NP's incorporating both biotin and streptokinase (a plasminogen-activating enzyme) into their outer lipid monolayer. Samples were then individually sealed in a chamber containing either saline ("control" group) or saline mixed with plasminogen solution at 1U/μL ("treated" group). An acoustic microscope (25 MHz) was used to scan the samples on a 100-μm grid at 15-minute intervals for imaging and quantification of acoustic reflectivity. Treated samples exhibited approximately 10% loss of volume after 3 hrs, as well as marked time-dependent variation in surface topography and acoustic reflectivity. The control group exhibited no significant changes over time.

Conclusions Liquid perfluorocarbon NP's were used to specifically enhance reflectivity of surfaces of targeted thrombi and to simultaneously deliver clot-dissolving drugs that dramatically altered the clot morphology, relative to untreated samples. This observation suggests the potential utility of targeted NP's for combined diagnosis and treatment of thrombus-initiated ischemic stroke.

2I-5 12:30 p.m.
1 KHZ LOW POWER SOUND STIMULATES ATDC5 CHONDROCYTES.

H. ARGADINE*, R. KINNICK, M. BOLANDER, and J. GREENLEAF, Mayo Clinic College of Medicine, Rochester, MN.
Corresponding e-mail: argadine.heather@mayo.edu

Background: It has been extensively shown that treatment with 1.5 MHz ultrasound signal (160mW/cm^2 pulse average) at a 200 μs tone burst repeating at 1 kHz can stimulate chondrocytes and lead to accelerated fracture healing [Parvisi J, et al., J. Orthop. Res. 17, 488-494 (1999)]. A current clinical product from Smith and Nephew uses the pulsed 1.5 MHz signal for treating fractures 20 minutes per day. This pulsed 1.5 MHz signal produces radiation force vibration at 1 kHz. It was therefore hypothesized that the radiation force, not the ultrasound, is responsible for the biological effect of the Smith and Nephew system of stimulating chondrocytes. In vitro experiments using the following method indeed showed that treatment with 1 kHz induced chondrogenesis similar to treatment with 1.5 MHz pulsed ultrasound. **Methods:** To expose cells to 1 kHz signal a device was developed, consisting of 6 Panasonic speakers attached to the bottoms of the wells of a 6-well cell culture plate and connected in series-parallel. Cells are plated in 6-well plates, which are then placed on top of the 1 kHz device for treatment. The speakers are driven with a 1 kHz square wave at 18 mV peak to peak with a 20% duty cycle. A scanning laser vibrometer was used to examine the motion caused by the Smith and Nephew in vitro system. The bottom of a 6-well plate was found to move an average of 1 nm. For the 1 kHz apparatus, the voltage used to drive the speakers was adjusted to give an average displacement of 2-4 nm, which was the closest value attainable to 1 nm. A square wave was used because of the harmonics, which help create a drum-like motion. In vitro experiments were performed with ATDC5 cells, a chondrogenic clonal cell line. Cells were treated with either 1.5 MHz pulsed signal or 1 kHz signal for 20 minutes per day for 3 to 7 days. After the final treatment, cartilage nodules were stained with Alcian blue, providing a measure of chondrogenesis. **Results:** Both 1.5 MHz and 1 kHz significantly increased chondrogenesis compared to control. Quantitative image analysis of stained wells showed that treatments with either signal increased number of nodules 2.3-fold ($p<0.02$) and total area of nodules 3-fold ($p<0.02$) compared to controls. Similar experiments varying the start date of 1 kHz treatments and the number of treatments (6 to 11 treatments) showed that nodules formed 5 days earlier than control. For chondrocytes that started 1 kHz treatments on the same day, more treatments led to an increased number and size of nodules. Interestingly, chondrocytes that started 1 kHz treatments the latest had the most nodules, even though they received the least number of treatments. **Conclusion:** This study provides the first evidence for 1 kHz activation of chondrocytes and for the potential mechanisms with which this vibration is sensed in the cell.

Session: 3I
NDE MATERIAL AND DEFECT CHARACTERIZATION
Chair: R. Addison
Rockwell Scientific Co.

3I-1 11:30 a.m.
CHARACTERIZATION ON THE MATERIAL PROPERTIES OF HYDROGEN-CHARGED ZIRCALOY BASED ON A LASER ULTRASOUND TECHNIQUE.

C.-H. YANG* and Y.-A. LAI, Chang Gung University, Taoyuan, Taiwan.
Corresponding e-mail: yang@mail.cgu.edu.tw

Zircaloys are commonly used in several parts in a nuclear reactor core due to their good mechanical and anti-corrosion properties. However, hydrogen embitterment occurs due to the take-up of hydrogen from the circulation water during extensive services in the high burnup, leading towards to the problems of degradation in mechanical properties and threatening the structure integrity.

In this research, a laser ultrasound technique (LUT) is reported for nondestructive characterization of hydrogen concentration (HC) in Zr-4 cladding tubes. Furthermore, material properties such as elastic constants are obtained with a inversion algorism based on the LUT-measurements. With the LUT, ultrasonic waves propagating in the Zircaloy tubes with different HC are generated and detected remotely by optical means. By measuring the dispersion spectra with the LUT, relations between the dispersion spectra and the HC of the Zircaloy tubes are established. HC ranging from 0 to 1200 ppm in the Zircaloy tubes are successfully discriminated by the LUT with a resolution of 200 ppm. Having the advantages of remote, non-contact and point-wise generation/detection, the LUT serves as a competitive candidate for the inspection of HC in Zircaloy cladding tubes generally operated in irradiative and temperature-elevated environments. The elastic moduli are found to be decreasing as the HC increases, while the Poisson's ratio is not sensitive to the HC.

Financial support from National Science Council, Taiwan, through grant No. NSC92-NU-7-182-003 is gratefully acknowledged. Also kindly discussions and efforts for sample preparations and hydrogen measurements by Dr. R. C. Kuo and Dr. C. T. Yang in Institute of Nuclear Research (INER), Taiwan, R.O.C. are acknowledged.

3I-2 11:45 a.m.
AN AUTOMATED INSTRUMENT FOR THE MEASUREMENT OF MECHANICAL PROPERTIES OF THIN MATERIALS.

E. LAFOND*, T. JACKSON, and X. ZHANG, Georgia Institute of Technology, Atlanta, GA.
Corresponding e-mail: emmanuel.lafond@ipst.gatech.edu

Flexural rigidity and shear rigidity of sub-millimeter thin webs can be determined by analysis of zero order antisymmetric (A0) Lamb waves in the MHz range, even when the web thickness is unknown. Using Laser Ultrasonics to excite and detect Lamb waves in webs is advantageous because it is a non-contact technique suitable to both on-line and off-line measurements. Also, compared to bulk materials, a deposited energy of just a few mJ is sufficient to create a disturbance in a web and to produce a large amplitude of motion easily detectable by an optical interferometer. The principle is as follows: a pulsed laser generates a point source disturbance that excites lamb wave propagation in the web. An interferometer detects the resulting out-of-plane motion in the paper at a location remote from the excitation point. The authors have developed an interferometer using an undoped Gallium Arsenide photorefractive crystal. They employed a two-wave mixing technique that is sensitive to displacement amplitudes in the nanometer range. The frequency response to ultrasonic waves is flat and broad. This is especially useful for the A0 Lamb wave propagation in paper, which is dispersive. The frequency dependent phase differences between Fourier components detected at different excitation-to-reception displacements is used to calculate the ratio of flexural rigidity to basis weight (weight per unit area) and the ratio of shear rigidity to basis weight. The interferometer is now part of a laboratory instrument in which both the generation and the detection laser beams are carried through fiber optics. The fiber optics construction allows flexibility in the testing since the generation and detection points can be moved anywhere. The instrument uses several motorized translation stages to manipulate the position and orientation of the web sample. The generation and detection probes are also translated using motorized stages. The instrument is computer-controlled and fully automated using LabVIEW for routine testing of the web samples. The results of measurements demonstrating the wide bandwidth of the instrument and the dispersion of the waves are presented. The probed materials were as different as paper, paperboard, steel/ aluminum/ brass foils and multilayer samples.

3I-3 12:00 p.m.
LASER ULTRASONICS AT TWENTY METERS PER SECOND IN THE PRODUCTION ENVIRONMENT AND ON A BUDGET: FROM DREAM TO REALITY.

T. JACKSON[1], E. LAFOND*[1], P. RIDGWAY[2], G. BAUM[1], X. ZHANG[1], and R. RUSSO[2], [1]Georgia Institute of Technology, Atlanta, GA, [2]Lawrence Berkeley National Laboratory, Berkeley, CA.
Corresponding e-mail: emmanuel.lafond@ipst.gatech.edu

A laser-based ultrasonic system for non-contact and non-destructive measurement of the elastic properties of paper was demonstrated on a paper manufacturing machine during commercial operation. The paper web was moving at approximately 20 m/s. We believe this to be the highest sample traveling speed reported to date for a commercial application of laser ultrasonics. Ultrasonic waves were generated in the paper with a pulsed Nd:YAG laser at 1064 nm wavelength and detected with a Mach-Zehnder interferometer coupled with a scanning mirror/timing system to compensate for paper motion.

Measurements of the flexural rigidity (FR) and out-of-plane shear rigidity (SR) of the paper web were done automatically by fitting of the frequency dependence of the phase velocity of Ao mode Lamb waves to a model equation. Variation in FR and SR across the width the paper sheet (cross-direction profiles), effects of changes in paper manufacturing process variables on measured FR and SR, comparisons with traditional mechanical stiffness tests will be presented. The laser beams of both the generation laser and the detection interferometer were delivered to the measurement area above the web through fiber optic. The sensor head traveled across a 9 m range in the cross-direction continuously during over two weeks without incident. The sensor head is fully optical and thus measures the web properties without any contact. This laser-ultrasonics system combines a reasonable cost with a relatively small footprint and low power consumption due to the low power output of the lasers that is used. Finally, laboratory data indicate that this technology is directly transferable to measurements on sheet metals and possibly other opaque web materials.

The authors wish to thank the U.S. Department of Energy for its support of this project.

3I-4 12:15 p.m.
GUIDED WAVES ATTENUATION DUE TO DEPOSITS ON THE PIPE WALL.

M. EL MOUSSAOUI[1], F. CHATI[1], F. LEON[1], A. KLAUSON[2], and G. MAZE*[1], [1]Laboratoire d'Acoustique Ultrasonore et d'Electronique LAUE UMR CNRS 6068, Université du Havre, Le Havre, France, [2]Dept. of Mechanics, Tallinn Tech. Univ., Tallinn, Estonia.
Corresponding e-mail: mustapha.elmoussaoui@univ-lehavre.fr

The ultrasonic guided waves are of a great interest for the pipe inspection in food and petrochemical industries. Long lengths of pipe can be thus inspected and cracks, corrosion and much of other defects are detected from this means. A viscous deposit on the surface of a pipe is the defect considered in this article. The product transport through the pipe is disturbed by the presence of this one. Such a deposit reduces the effective diameter of pipe and causes a decrease of the flow rate. In order to evaluate this deposit, our interest is taken on the attenuation of the longitudinal waves at particular frequencies when a circular shape deposit consisted of epoxydic resin is present.

Theoretically and experimentally, we consider the propagation of guided waves in a stainless steel tube with an outer radius a = 19 mm, an inner radius b = 17.5 mm (thickness d = 1.5 mm), filled or not with water. The circular shape deposit (ring) is made of an epoxydic resin characterized by different widths. This deposit is placed on the external surface of the tube in order to analyze only the interaction of the Lamb waves with the deposit.

The experimentation is based on the generation of axisymmetric waves either on the tube by a hand-made flexible PVDF comb transducer, or on the section of the tube by a *Panametrics* piezoelectric transducer. The mode of vibration generated in the two cases is the mode n = 0 and the transducer-emitter is excited by gated sinusoids with a frequency f. In a first time, without internal

fluid, the waves A_0, S_0, A_1, S_1 are generated at particular frequencies belonging to the activation line (1.158 MHz, 1.706 MHz, 2.4 MHz, 2.56 MHz) of the comb transducer. These waves are measured with a comb transducer operating as a receiver and placed after the deposit characterized by its width. Five widths are considered; 3mm, 8 mm, 19 mm, 30 mm, 40 mm. The guided waves attenuation is determined and analyzed for each deposit width. In a second time, with water in the cavity and with a deposit width equal to 25 mm, only the symmetrical waves S_0, S_1 are considered. In a general way, each wave, according to its frequency, is characterized by its axial and radial displacements. In our problem, the generated wave must have a radial displacement close to zero at the surface of the shell (S_0 at f = 238 kHz, S_1 at f = 2.565 MHz). Thus, those are sensitive to the presence of the deposit and not to the internal fluid. We observe in low frequency (f = 238 kHz) the reflection (monostatic method) of the S_0 wave on the deposit but no reflection of the S_1 wave is noted at f = 2.565 MHz. On the other hand, in transmission (bistatic method), the S_1 wave (f = 2.565 MHz) is attenuated when the deposit is present. The experimental results are compared with the theoretical results obtained with a finite element method (FEM).

3I-5 12:30 p.m.
EXPERIMENTAL EVIDENCE OF S1 MODE QUASI-RESONANCE IN THIN PLATE USING A LASER BASED ACOUSTIC MICROSCOPE.

C. PRADA*[2,1], O. BALOGUN[1], and T. W. MURRAY[1], [1]AME Department, Boston University, Boston, MA, [2]Laboratoire Ondes et Acoustique, CNRS, Paris, France. Corresponding e-mail: claire.prada-julia@espci.fr

This abstract does not appear in the online abstracts at the author's request.
It will appear in the print version.

3I-6 12:45 p.m.

MICROWAVE INDUCED PHONONS IMAGING BY BRILLOUIN MICROSCOPY.

B. VINCENT*[1,2], J. K. KRÜGER[1,3], O. ELMAZRIA[1,2], L. LE BRIZOUAL[1,2], L. BOUVOT[1,2], M. KOLLE[1,2], D. ROUXEL[1,2], and P. ALNOT[1,2], [1]Laboratoire Européen de Recherche Universitaire : Saarland-Lorraine, Sarrebrücken/nancy, Germany/ france, [2]Laboratoire de Physique des Milieux Ionisés et Applications, Nancy, France, [3]rimentalphysik, Universität des Saarlandes, Saarbrücken, Germany. Corresponding e-mail: brice.vincent@lpmi.uhp-nancy.fr

Surface acoustic wave (SAW) devices are based on inter-digital transducers (IDT) electrodes combined with a piezoelectric material. That's why two main ways have been investigated to optimise these components: the electrodes design and the material properties. Anyway to provide electrodes enhancement, one have to know the acoustic field distribution. Up to now, several techniques have been used in order to visualise acoustic fields like optical interferometry, atomic force microscopy, x-ray spectroscopy and scanning electron microscopy. Obviously methods that measure directly acoustic properties would be the most efficient ones and that holds especially true for the GHz range.

In this paper we demonstrate that Micro-Brillouin, which is well known for the characterisation of the elastic properties of the material (thermal phonons), can also be applied to the detection of piezoelectrically induced phonons.

Brillouin microscopy with RIθA scattering geometry has been applied to the detection and the characterization of surface phonons as well as bulk phonons. IDT have been used to generate acoustic waves by piezoelectric effect in single crystal and thin films at microwave frequencies. Results demonstrate that Brillouin

microscopy allows the determination of the frequency, the polarisation and the propagation direction of the acoustic waves. Moreover, two-dimensional scans and losses measurements have been achieved and results are compared with previous results obtained using other methods.

As example, experiments performed on Y+41°-cut LiNbO3 substrate show that the piezoelectrically induced acoustic field don't exhibit any divergence and the measured losses are of 16.10-3 dB/λ, where λ is the wavelength of the acoustic wave. Note that the spatial periodicity of IDT was fixed to 14 micrometers.

Same experiments have been done with devices based on ZnO thin films deposited on silicon.

Session: 4I

FLUIDIC ACTUATION
Chair: A. Lal
Cornell University

4I-1 11:30 a.m.
OBSERVATION AND INTERPRETATION OF SAW-INDUCED REGULAR AND CHAOTIC DYNAMICS OF DROPLET SHAPE.

B. A. KORSHAK, V. G. MOZHAEV, and A. V. ZYRYANOVA*, M.V. Lomonosov Moscow State University, Faculty of Physics, Moscow, Russian Federation.
Corresponding e-mail: annazyr@mail.ru

The study of physical peculiarities of interaction of droplets of different solutions with surface acoustic waves on piezoelectric substrates is of immense importance to develop high-performance acoustic programmable biochips (see website www.advalytix.de for details on these devices) and such a study is the main focus of the present research. We have observed and recorded as short movies the following four types of different phenomena in the dynamical behavior of droplets of different liquids, including water, white spirit solvent, acetone, and ethyl alcohol, placed on YZ-lithium niobate 15-MHz SAW delay line. (i) Progressive acoustic transport of a droplet. (ii) Vortex acoustic streaming inside a droplet. (iii) The formation of quasi-stationary smoothed peak on the droplet surface under the action of counter-propagating SAWs and its chaotic dynamics on acetone droplet during its evaporation. (iv) Self-sustained oscillation of such a peak on the droplet surface in the case when the substrate has a slight slope with respect to the horizontal. The velocity of acoustic transport of droplets of white spirit solvent in our experiment reaches 15 mm/s for SAW power about 0.1 Wt. The visualization of acoustic streaming inside the droplets is achieved by the use of potassium permanganate crystals as coloring agent. The turning velocity of acoustic vortices of 100-300 degrees per second is detected in droplets of ethyl alcohol. The lowest frequencies of chaotic and regular oscillations of acetone droplet shape are about a few Hertz. The two first mentioned

phenomena, corresponding to traveling-wave mode of operation, are in agreement with the results of observations of other authors. The two last mentioned phenomena, corresponding to counter-propagating wave mode, are new, to the best of our knowledge. Several alternative interpretations of the peak appearance on the droplet surface in the field of counter-propagating waves are discussed including quasi-standing-wave soliton formation, distortion of droplet profile by acoustic radiation force, excitation of thickness resonance or more complex resonances of droplets, focusing of acoustic and capillary waves inside the droplets. The calculation of radiation force generated by two counter-propagating leaky Rayleigh waves at the boundary between solid and liquid half-spaces is presented to support one of suggested interpretations of the found phenomenon. The generalization of the theory of pulse-vibrational mechanism of acoustic transport [1] to the case of multi-frequency wave action is also discussed.

[1] V.G. Mozhaev and A.V. Zyrianova, Analysis of bidirectional vibrational transport of small objects by periodic wave trains of pulses, Proceedings of 2004 IEEE International UFFC Joint 50th Anniversary Conference, pp. 1169-1172.

4I-2 11:45 a.m.
DEVELOPMENT OF SAW THERMOCYCLER FOR SMALL LIQUID DROPLETS.

J. KONDOH*[1], N. SHIMIZU[1], Y. MATSUI[1], M. SUGIMOTO[1], and S. SHIOKAWA[2], [1]Shizuoka University, Hamamatsu-shi, Shizuoka , Japan, [2]SAW&SPR-Tech, Hamamatsu-shi, Shizuoka, Japan.
Corresponding e-mail: j-kondoh@sys.eng.shizuoka.ac.jp

This paper presents a novel thermocycler for liquid by using surface acoustic wave (SAW) devices. When a liquid droplet is placed on a Rayleigh-SAW propagating surface, a longitudinal wave radiates into the liquid. If the SAW amplitude increases, the liquid shows non-linear dynamics, such as vibrating, streaming, flying small droplet, and atomizing. This phenomenon is well known as SAW streaming. During SAW streaming phenomenon, we measured liquid temperature and found that liquid temperature increases (1). It is necessary to know the relationships between liquid temperature and applied signals for liquid heater application using SAW devices. Water droplet was loaded on the center of two interdigital transducers (IDTs). The SAW was generated from the IDTs to avoid SAW streaming. The experimental results show that water temperature is proportional to the duty factor and the squire of the applied voltage. These mean that the liquid temperature can be controlled by the applied signal. As the mechanism of liquid heating is due to radiation of longitudinal wave, high viscosity solution shows high temperature because of viscosity damping. Using glycerol/ water mixture of 80wt.%, temperature of 120 degrees is achieved.

Realization of periodic temperature control, namely thermocycler, is important for actual application. The following temperature control is carried out; 95 degrees $\rightarrow$ 50 degrees $\rightarrow$ 70 degrees $\rightarrow$ 95 degrees. These values are determined from a polymerase chain reaction (PCR). The applied voltage is fixed at 30 VP-P and the duty factor is varied. The results indicate that the expected temperature control is achieved. Therefore, the SAW device can be applied for PCR

thermocycler. As the Rayleigh-SAW device can be applied for a droplet manipulator, it is possible to integrate both droplets moving and heating system on the SAW device. Therefore, multifunctional lab-on-a-chip is realized using the SAW device.

(1) N. Shimizu, et al, Proc of IEEE UFFC 50th Anniversary Joint Conference, pp. 2235-2238, 2004.

4I-3 12:00 p.m.
MICROFUIDIC DEVICE BASED ON SURFACE ACOUSTIC WAVE.

D. BEYSSEN*, L. LE BRIZOUAL, O. ELMAZRIA, and P. ALNOT, Laboratoire de Physique des Milieux Ionisés et Applications, F-54506 Vandoeuvre les Nancy, France.
Corresponding e-mail: laurent.lebrizoual@lpmi.uhp-nancy.fr

Microfluidic systems can be implemented for miniaturization of chemical and biological processes on a sub-millimeter scale. Surface Acoustic Wave (SAW) devices have been widely used in RF electronic system as resonator, filter or delay line, and have thus become the basis of a huge industry in mobile communication. Moreover recently published works have demonstrated the interest of SAW in microfluidic systems. Specifically, Katsumi Chono and al. have used SAW in atomization system [1] while , C. J. Strobl and al. have worked on a mixing system and a fluidic actuator based on SAW [2]. In this study, Surface Acoustic Waves are used to actuate small droplet (from 2 to 20 μl) on planar surface of piezoelectric substrate. In order to improve droplet displacements, hydrophobic film on LiNbO3 substrate was deposited. The question that arises here is, how a wave of few nanometers in amplitude can induce a droplet motion of few millimeters of diameter. The acoustic wave generated by the inter-digited ransducer (IDT) in contact with a liquid, radiates a longitudinal wave into the droplet.

Our SAW devices were performed on a 128° rotated Y-cut X-propagating LiNbO3 2" wafer. Each IDT has fingers of period 100μm. These devices exhibit two center frequencies at 39.92 MHz (in X direction) and 36.40 MHz (in Y direction). This microfluidic device allows the control of the droplet displacement in the above two perpendicular directions. The evolution of the contact angle was observed using a high-speed acquisition camera (360 frames per second) and the droplet velocity was measured with a CCD camera.

We have measured the sliding force for each hydrophobic film. The films a-CFX were deposited using reactive ion etching (RIE) reactor. The Contact angle hysteresis $\theta = \theta a - \theta r$ is a very important parameter when the droplet motion is considered. The PVDF layer appears better than a-CFX for droplet displacement as the former presents a lower sliding force than the latter. Moreover, the force exerted by SAW on the droplet has been measured and compared to the sliding force FS.

We also measure the SAW device efficiencies in the acoustic mixer mode. Intern mixture, produced by the SAW attenuation at the solid/liquid interface, is observed when the applied input RF power reaches -2dBm. To measure the flow movement

and the particles velocity as a function of the RF power, we used a mixture of micrometric aluminium particles in water. The scattered light from a laser beam by tracer particles is recorded with high speed camera. From two consecutive images we can determine the mean velocities of the tracer particles, which correspond to the flow velocity in a case of low particles density. Effect of RF power on mixing speed is discussed.

REFERENCE

[1] Chono K., Shimizu N., Matsui Y., Japanese Journal of Applied Physics, Vol. 43, No. 5b, (2004) 2987-2991.

[2] C. J. Strobl, A. Rathgeber, A. Wixforth, Planar microfluidic processors

4I-4 12:15 p.m.
SURFACE LIQUID DROPLET MOTION ON SILICON ULTRASONIC HORN ACTUATORS.

X. CHEN* and A. LAL, Cornell University, Ithaca, NY.
Corresponding e-mail: xc35@cornell.edu

On-surface automatic precision handling of liquid drop is desired for integrated fluidic analysis systems. Motion of liquid drops on a solid surface have been induced by Marangoni flow set up by thermal gradients[1], or by surface free energy gradients[2]. We report here a new method producing liquid droplet motion on longitudinally vibrating surface. The motion results from acoustic streaming force induced inside the droplet by the vibrating surface. The velocity of the droplet can be controlled by the amplitude and the gradient of the vibration, and also depends on the surface tension of the liquid, the contact angle of the droplet and the viscous drag on the surface.

Silicon ultrasonic horn actuators have been reported before[3] and their advantages in integrating sensors and microfluidic components have been demonstrated. In this work, silicon horn with half-wavelength longitudinal resonance at 38.85kHz is utilized to produce longitudinal vibration. The velocity distribution along the length of the horn is calculated by FEM. Velocities at the tip and end of the horn are measured with laser Doppler vibrometer and fitted to the calculated values to obtain the actual velocity distribution. When liquid drops are dispensed on the surface of the horn, the longitudinal motion is shear-coupled into the liquid and generates streaming force inside the liquid. The force and therefore the motion are toward the lower vibrating velocity. The motion of the liquid was recorded with a 30 frames/s camcorder and droplet velocities were measured at different locations under different driving voltages.

Aqueous solutions of IPA with different concentrations (100%, 90% and 50%) were tested, which presents surface tensions of 21~24mN/m. A 20mm long segment of the horn is chosen for testing where the vibrating velocity per driving voltage decreases from 73mm/s/Vpp to 29mm/s/Vpp, the velocity gradient along the length of the horn decreases from 2.5mm/s/Vpp to 2.0mm/s/Vpp per mm length. For 1μL droplets, velocities in the range of 0.3mm/s to 6.7mm/s were observed for driving voltages 4Vpp~30Vpp. For all three liquid solutions, the droplet velocity at a fixed location increases approximately quadratically with driving voltage initially, then reaches a maximum value and stabilizes, as the

viscous drag force increases, balancing the streaming force. At a fixed driving voltage, the velocity of the droplet decreases as it travels toward the lower vibrating velocity end since the streaming force is decreasing. Under the same fixed driving voltage and at a fixed location, the liquid with lower surface tension traveled at higher velocity, because it has lower density and larger contact area with the vibrating surface, leading to higher streaming force. Motions of liquid drops as small as 50nL were also observed. This work shows surface liquid drop handling by longitudinal silicon actuators that potentially can be integrated into fluidic and assay systems.

[1] K.D.Barton, R.S.Subramanian, J. Colloid Interface Sci. 141, p146, 1991

[2] M.K.Chaudhury, G.M.Whitesites, Science, 256, p1539, 1992

[3] A.Lal, R.M.White, Sensors and Actuators A, 54, p542, 1996

4I-5 12:30 p.m.
EFFECTS OF FLUID MEDIUM ON STATOR AND ROTOR OF ULTRASONIC MOTOR DRIVING FLUID DIRECTLY.

C. XIA*, B. LI, M. WANG, and W. YU, School of Electrical Engineering and Automation,Tianjin University, Tianjin, People's Republic of China.
Corresponding e-mail: elib@tju.edu.cn

The ultrasonic motor driving fluid directly is a new type of non-contact ultrasonic motor whose rotor swims in fluid. Acoustic streaming induced by stator vibration drives the rotor to rotate, so the energy of the stator is transferred to the rotor. The fluid medium plays an important role in the motor, whose effects both on stator and rotor are studied. When it comes to the stator, due to the coupling between it and the fluid, the stator's vibration frequency varies. There are two types of forces on the stator acoustic normal press and shear press caused by viscous fluid. Using ANSYS we analyzed the influence of these forces on the stator's resonance frequency. Simulation and experimental results show that acoustic press is the key factor that affects the stator′s resonance frequency. When it comes to the rotor, on one hand, Reynold's shear stress generates an acoustic streaming which drives the motor's rotating. On the other hand, Reynold's normal stress acts as a holding force when rotor deviates from its balance position. Through the analysis of Reynold's stress in fluid, the relationships between rotor's speed, rotor's stability and fluid parameters such as fluid height and viscous factor are obtained. The experimental results coincide with the theory analysis.

4I-6 12:45 p.m.
CANTILEVER RESONANCE INDUCED IN SITU BY MAGNETOSTRICTION FOR ACTIVE FLOW CONTROL.

O. DUCLOUX*[1], N. TIERCELIN[1], Y. DEBLOCK[1], P. PERNOD[1], V. PREOBRAZHENSKY[1,2], and A. MERLEN[3], [1]LEMAC / IEMN-DOAE – UMR CNRS 8520, Ecole Centrale de Lille, Cité Scientifique - Av Poincaré, Villeneuve d'Ascq, France, [2]LEMAC / Wave Research Center - GPI-RAS, 38, Vavilov street, Moscow,

Russia, [3]LEMAC / LML UMR CNRS 8107, Boulevard Paul Langevin, Villeneuve d'Ascq, France.
Corresponding e-mail: olivier.ducloux@iemn.univ-lille1.fr

Active flow control is at the intersection between the needs of the aerospace industry and the possibilities of microactuators. By controlling the flow on air wings for example, one may decrease dramatically aircraft fuel consumption and/or noise. Such a control can be achieved for example by pulsed air blowing through submillimetric holes distributed at specific locations of the wings of the airplane [1]. To achieve such pulsed jets, a microvalve containing an internal resonant cantilever actuated by a magnetostrictive film has been designed, fabricated and characterized. The microvalve is fed by a pressurized source of air and the resonating cantilever acts as a deflector on the internal fluid flow addressed alternatively to the output hole on the wing's surface or to a recycling output.

Magnetostrictive films were chosen as actuating means for they can provide high induced stress compared to other kinds of active materials, and also because of their remote actuation capability. In this device, artificially nanostructured TbCo/FeCo multilayers were used: in these layers, a large magnetoelastic coupling can be kept while having a well-defined in-plane magnetic anisotropy, with a relatively low saturation field. These characteristics allow the induction of a Spin Transition Reorientation (SRT) state in the layer: the SRT corresponds to a magnetic instability that is used to increase dramatically the magnetoelastic sensitivity[2] and make it compatible with silicon Microsystems : that way, the field produced by the two microcoils is sufficient for the dynamic actuation.

The actual microsystem consists in a 1000 µm long and 1.5 µm thick polysilicon cantilever on which a nanostructured magnetostrictive film is deposited by RF Sputtering: (TbCo/FeCo)xn, total thickness 0.5 µm to 1µm. On each edge of the cantilever, one microcoil has been processed with 4 windings and a wire thickness of 20 µm. Each coil produces the 20 Oe dynamic magnetic field necessary for the actuation. The magnetic field is then transmitted from one coil to the other via the magnetostrictive film, enabling the cantilever's resonance at a 2 kHz frequency.

Characterization of the resonance frequency, amplitude and magnetoelastic coefficient are achieved by interferometric means. Outcoming flow is visualized by conventional strioscopy method using He / Air optical indice difference. The results of these characterizations are presented

[1] Kumar, S.M.; Reynolds, W.C.; Kenny, T.W.; "MEMS based transducers for boundary layer control", Micro Electro Mechanical Systems, 1999. MEMS '99. Twelfth IEEE International Conference on 17-21 Jan. 1999 Page(s):135 - 140

[2] N. Tiercelin, V. Preobrazhensky, P.Pernod, H. Le Gall, J. Ben Youssef, "Nonlinear actuation of cantilevers using giant magnetostrictive thin films", Ultrasonics 38(2000) 64-66

Session: 5I
SAW FILTERS AND TRANSDUCERS
Chair: R. Weigel
University of Erlangen

5I-1 11:30 a.m.
LOW-LOSS SAW FILTER ON $LI_2B_4O_7$ USING NOVEL-SHAPE APODIZED STRUCTURE FOR 1 GHZ RF-ID SYSTEM.

S. INOUE*[1], T. MATSUDA[1], S. MATSUDA[1], M. UEDA[1], Y. SATOH[1], K. WADA[2], S. MITOBE[2], and Y. EBATA[2], [1]Fujitsu Laboratories Ltd., Akashi, Hyogo, Japan, [2]Fujitsu Media Devices Ltd., Yokohama, Kanagawa, Japan.
Corresponding e-mail: shogo@jp.fujitsu.com

This paper describes the longitudinally coupled double mode SAW filter on 45°X-Z $Li_2B_4O_7$ (LBO) substrate for the 1 GHz application. The novel shaped apodized structure, which suppresses spurious responses due to higher order transverse modes and longitudinal modes, is proposed.

LBO has been used in high performance IF filters because it has large coupling coefficient and good temperature stability. In this work, we attempt to develop the narrow band RF filter taking advantage of LBO. This filter aims at the 1 GHz RF-ID system in Japan.

Filters used in RF circuits are required to be self-matched to 50 Ω because external matching networks increase not only the circuit size but also the insertion loss. In other words, the input and output impedance of RF filters should be around 50 Ω. Since LBO has small dielectric constant compared to $LiTaO_3$ or $LiNbO_3$ substrate, the aperture length of the IDT on LBO tends to be wider so that the input and output impedance correspond to 50 Ω. The higher order transverse modes exist in such a wide aperture and cause spurious responses. Generally, to suppress higher order transverse modes in the IDT, the apodized structure is used. However, it turned out that the conventional shaped apodized structure generated notch responses in the pass band due to longitudinal modes. We developed a simulator for the apodized structure dealing the apodized IDT as the multi-track structure and analyzed these longitudinal modes responses. From this analysis, we devised the novel shaped apodized structure, which suppresses spurious responses due to longitudinal modes as well as higher order transverse modes.

We employed the above-mentioned newly proposed apodized structure for the 953 MHz SAW filter on LBO. In spite of such a high frequency near 1 GHz, the developed filter achieved no spurious response in the pass band, minimum insertion loss of 2.1 dB, 2.7 MHz bandwidth at 3 dB and more than 20 dB attenuation without external matching networks. This filter performance is practical level for the RF-ID system in Japan.

5I-2 11:45 a.m.
BALANCE CHARACTERISTICS STUDIES USING WIGNER DISTRIBUTION ANALYSIS FOR SAW DEVICES.

T. SHIBA*, T. ISHIZAKII, and S. OOSAWA, Hitachi Media Electronics Co., Ltd., Yokohama, Kanagawa, Japan.
Corresponding e-mail: shiba@y01.hitachi-media-el.co.jp

SAW has been successfully employed in a number of signal-processing devices, such as RF filters, IF filters, duplexers and other SAW devices for recent digital mobile communications. It is expected to realize a good performance of common-mode noise suppression for mobile terminals. A function of unbalanced and balanced signal transformation is desired for this purpose. The transverse-double-mode IDTs structures are generally used for low loss and high rejection with a function of unbalanced and balanced port transformation.

Common-mode rejection (CMR) characteristics are suitable parameters to evaluate system balance characteristics using various complex load impedances. The CMR parameter and the direct amplitude/phase unbalance value are used for evaluation. Three kinds of DCS double-mode balanced SAW filters are prepared. A first filter has a high CMR and a high balance characteristic. A second filter has a low CMR and a low balance characteristic. A third filter is prepared by setting a parasitic electrical component to first one. Time-domain analysis based on unbalanced scattering matrix elements and Wigner distribution based on CMR characteristics are applied to these samples. A good agreement with time-domain response of each balanced port and a low Wigner distribution response are obtained for first filter. Unbalanced signals of second filter are observed at 63ns and 125ns delay timing and 1975MHz frequency. It can be found that the unbalance origin of second filter is acoustical mode because of concentration of unbalance signal in time and frequency domain. Unbalanced signals of third filter are observed at whole area corresponding to main signal. It can be appreciated that the origin of third filter unbalance is the electrical mode because of spread unbalance signal in time and frequency domain. Consequently it is verified that these time-domain and Wigner distribution methods are effective for analyzing the origin of unbalance.

5I-3 12:00 p.m.
IMPROVED PURE SHSAW TRANDUCTION EFFICIENCY ON LGS USING FINITE THICKNESS GRATINGS.

T. POLLARD* and M. PEREIRA DA CUNHA, University of Maine, Orono, ME.
Corresponding e-mail: mdacunha@eece.maine.edu

Pure shear horizontal surface acoustic wave (SHSAW) orientations exist on trigonal crystals along (0°, θ, 90°). In particular, this mode has been recently considered on single crystal langasite (LGS) for liquid and biological sensor applications, due to: (i) reduced propagation loss in the presence of liquid-loaded surface; (ii) existence of temperature compensated orientations; (iii) high dielectric

constants; and (iv) the relatively strong piezoelectric effect observed when compared to corresponding quartz orientations. A limitation of the pure SHSAW orientations for device applications has been the significant excitation of the shear horizontal bulk acoustic wave (SHBAW) by the interdigital transducer (IDT). The excitation of SHBAW by the IDT compromises the SHSAW transduction efficiency, η_{SHSAW}, defined as the ratio of SHSAW power to total IDT input power, thus increasing SHSAW device loss. Previous work by the authors verified that an infinitesimally thin metallic guiding layer used in the propagation path around the IDT typically increases η_{SHSAW} from less than 1% (no layer) to 60% (infinitesimally thin metallic layer) on LGS, Euler angles (0°, 22°, 90°) for a 60 split finger pair IDT.

In this work a finite thickness periodic grating guiding structure is explored along LGS (0°, 22°, 90°) to further improve the IDT η_{SHSAW}. The structure studied consists of a finite number of IDT electrodes bordered by gratings on both sides. The model implemented uses orthogonal Chebyshev polynomial basis functions in conjunction with the finite element method and harmonic admittance technique to study the SHSAW mode excitation efficiency in the referred structure. The IDT η_{SHSAW} is examined as a function of electrode material and thickness, metallization ratio, and number of active IDT finger pairs. The analysis performed shows a significant difference in η_{SHSAW} if high density electrode gratings, such as gold (Au) or platinum (Pt) are used instead of low density gratings, such as aluminum (Al). For instance, using a 60 split finger pair IDT and surrounding gratings composed of Au or Pt electrodes, with h/λ=1% (h, thickness and λ, the wavelength), results in η_{SHSAW}=99%. If Al is used, a reduced η_{SHSAW}=51% is achieved for the same h/λ=1%. Moreover, to achieve η_{SHSAW}=99%, the required h/λ value for the Al electrodes increases to about 8.5%, a significantly higher metallization thickness. The effects of the metallization ratio (a/p) on η_{SHSAW} have also been studied. For instance, an increase in a/p from 0.3 to 0.7 adds up to 11% in η_{SHSAW}, indicating that higher metallization ratios lead to higher η_{SHSAW}. Numerical and experimental IDT impedances are also compared, validating the analysis performed. The work reported shows that finite thickness gratings can significantly improve the SHSAW IDT performance, reducing the amount of SHBAW excited by the IDT, and thus leading to high efficiency LGS SHSAW devices for communication and biosensor applications.

Funding for this project was provided by The National Science Foundation (NSF ECS-0134335 and ECS-0329913)

5I-4 12:15 p.m.
ENHANCED SPUDT CELLS FOR HIGH COUPLING SUBSTRATES.

J. GALIPEAU* and J. KIM, Sawtek Inc. A Triquint Company, Apopka, FL.
Corresponding e-mail: jgalipeau@sawtek.com

Since the first SPUDT cells were proposed by Hanma & Hunsinger [1] many refinements have been made including DART [2] and EWC [3] SPUDT cells. Compared to Quartz, however, less attention has been given to SPUDTs on high coupling substrates where the reflectivity is dominated by electrical effects. A drawback of the traditional EWC SPUDT cell on Lithium Niobate, for example,

is that the reflectivity is relatively low compared to the regeneration. Therefore practical filters must be mismatched to cancel triple transit resulting in higher insertion loss and lower return loss than optimal.

A COM optimization tool [4] has been used to predict and refine the coupling, reflectivity and phase difference of a single period SPUDT cell. Several SPUDT cells have been analyzed including EWC, DART, and quadrature SPUDTs, at various h/lambda and duty factors. In particular, An EWC type SPUDT cell has been optimized for Lithium Niobate resulting in a substantial increase in reflectivity while maintaining high piezoelectric coupling without the use of floating electrodes [5].

These improved cells have been employed in the design of several tapered SPUDT filters. Results are presented showing a typical reduction in Triple Transit of nearly 8 dB due to an increase in SPUDT reflectivity of 20%, thus confirming the practicality of the optimized cells.

References:

1. K. Hanma, B. Hunsinger, “A Triple Transit Suppression Technique,” IEEE Ultrasonics Symp. Proc., pp. 328-331, 1976

2. T. Kodama, H. Kawabata, Y. Yasuhara, H. Sato, “Design of Low-Loss Filters Employing Distributed Acoustic Reflection Transducers”, IEEE Ultrasonics Symp. Proc., pp. 59-64, 1986

3. C. S. Hartman, B. P. Abbott, “Overview of Design Challenges for Single Phase Unidirectional SAW Filters”, IEEE Ultrasonics Symp. Proc., pp. 79-89, 1989

4. S. Malocha, B. P. Abbott, “Calculation of COM Parameters for an Arbitrary IDT Cell”, IEEE Ultrasonics Symp. Proc., pp. 267-270, 2002

5. K. Yamanouchi, H. Furuyashiki, “Low-loss Saw Filter Using Internal Reflection Types of New Single-Phase Unidirectional Transducer,” IEEE Ultrasonics Symp. Proc., pp. 68-71, 1984

5I-5 12:30 p.m.
SUPPRESSION OF TRANSVERSE MODE RESPONSES FOR ULTRA-WIDEBAND AND LOW-LOSS SAW FILTERS ON A CU-GRATING/15°YX-LINBO$_3$ STRUCTURE.

T. OMORI*[1], N. YOKOYAMA[2], K. MATSUDA[2], K. HASHIMOTO[1], and Y. YAMAGUCHI[1], [1]Faculty of Engineering, Chiba University, Chiba 263-8522, Japan, [2]Graduate School of Science and Technology, Chiba University, Chiba 263-8522, Japan.
Corresponding e-mail: omori@usl.chiba-u.ac.jp

Having used highly piezoelectric Love waves propagating on a Cu-grating/15°YX-$LiNbO_3$ structure[1], the authors have recently shown that ultra-wideband and low-loss filters can be realised in UHF range. Although the relative bandwidth of 14% and insertion loss of 0.9 dB were achieved, the passband shape was badly deformed by strong spurious responses caused by transverse modes.

From this point of view, this paper discusses a technique to suppress the transverse mode resonances in the ultra-wideband and low-loss filters based on Love waves. Although this sort of responses could be suppressed by narrowing the IDT aperture extremely, this makes impedance matching difficult with peripheral circuitry.

The basic idea of the technique proposed here is as follows; (1) inserting dummy electrodes between the bus-bars and interdigital electrodes, (2) designing the dummy electrodes so as to trap all spurious modes in the dummy electrode region, and (3) weighting the dummy electrodes to make the trapped modes non-resonant.

In a structure employing dummy electrodes, the higher-order transverse modes are categorised into modes A and B; the modes A trapped mainly in the dummy electrode region and the modes B in the interdigital electrode region. It is shown that when the dummy electrodes are properly designed, one of the spurious modes B couples with one of the modes A, and their fields significantly penetrate into the dummy electrode region. Accordingly, these two spurious modes are simultaneously suppressed by appropriately weighting the dummy electrodes. Here, the dominant resonance mode, mainly trapped in the interdigital electrode region, is scarcely affected by the weighted dummy electrodes.

As resonant elements for ladder-type filters, ultra-wideband resonators were designed and fabricated on the Cu-grating/15°YX-$LiNbO_3$ structure. For the application of the proposed technique, the metallisation ratio for the dummy electrodes was set at 0.75. The experimental result showed that the proposed technique is effective in suppressing the spurious responses caused by the transverse modes, while the overall resonator performances were scarcely affected. The Q factor and capacitance ratio are 680 and 4.0, respectively.

[1] K.Hashimoto, H.Asano, K.Matsuda, N.Yokoyama, T,Omori and M.Yamaguchi: "Wideband Love Wave Filters in GHz Range on Cu-Grating/Rotated-YX-$LiNbO_3$-Substrate Structure", Proc. UFFC 50th Anniversary Conference (2004) pp.1330-1334.

5I-6 12:45 p.m.
LOW LOSS RECURSIVE FILTERS FOR BASESTATION APPLICATIONS WITHOUT SPURIOUS MODES.

M. MAYER*, A. BERGMANN, G. KOVACS, and K. WAGNER, EPCOS AG, Munich, Bavaria, Germany.
Corresponding e-mail: Markus.Mayer@epcos.com

In SAW filters spurious waveguide modes may seriously effect the performance: Undesired lobes in the upper pass- or stopband and ripples in the group delay are typical for devices suffering from waveguiding effects.

In order to suppress spurious modes and to excite only the fundamental symmetric mode various approaches as overlap weighting or sawtooth shaping of the busbars in order to destroy the waveguide have been applied.

Alternatively recently it was suggested to employ the first antisymmetric mode by splitting up of the acoustic track into two subtracks, which are longitudinally shifted by half a wavelength with respect to each other.

The very reason of the excitation of higher modes is, however, the fact that the excitation profile is of different shape than the fundamental symmetric or antisymmetric mode. In most cases the excitation profile is of rectangular shape while the waveguide modes usually are of sinusoidal shape. While the approaches of prior arts aimed at changing the excitation profile to maximize excitation of the fundamental symmetric or antisymmetric mode we suggest an approach where the waveguide is changed in order to shape the fundamental symmetric mode rectangularly.

The approach is applied to low loss recursive inline filters which are employed as intermediate frequency filters in GSM infrastructure systems. The method proves to be particulary successful in reducing group delay ripple and sidelobes.

Session: 6I

TRANSDUCER MATERIALS
Chair: Y. Roh
Kyungpook National University

6I-1 11:30 a.m.
ADVANCED PIEZOELECTRIC SINGLE CRYSTAL BASED TRANSDUCERS FOR NAVAL SONAR APPLICATIONS.

K. SNOOK*[1], P. REHRIG[1], X. JIANG[1], W. HACKENBERGER[1], R. MEYER[2], and D. MARKLEY[2], [1]TRS Technologies, Inc., State College, PA, [2]Applied Research Laboratory, State College, PA.
Corresponding e-mail: kevin@trstechnologies.com

TRS is developing transducers based on single crystal piezoelectric materials such as $Pb(Mg_{1/3}Nb_{2/3})_{x-1}Ti_xO_3$ (PMN-PT). These crystals exhibit very high piezoelectric coefficients (d33 ~ 1800 to >2000 pC/N) and electromechanical coupling factors (k33 > 0.9), which may be exploited for increasing bandwidth and improving performance. Apart from basic performance, much research has been done on miniaturizing sonar transducers and increasing their output power. Results are presented from two different studies.

High frequency sonar is increasingly important in both defense and civilian applications, such as shallow water operation and underwater cable inspection. There are significant limits on vehicle dimensions and transmit electronics, creating the need for smaller, better transducer systems. Due to its increased compliance, PMN-PT has a much shorter “33” mode stack length in sonar transducers relative to PZT. This is advantageous for size reduction, though it produces a non-ideal aspect ratio, and lower coupling, due to large lateral dimensions. Alternative “31” mode tonpilz elements are proposed to improve performance over these “33” designs. d32 values as high as -1600 pC/N have been measured in oriented plates, and d31 values over -900 pC/N have been measured in single crystal tubes. Since prestress is applied perpendicular to

the poling direction, “31” mode tonpilz elements exhibit lower loss and higher reliability than “33” mode designs. Finite element modeling shows a 7 dB increase in the transmit voltage response of the d32 PMN-PT design over a traditional PZT tonpilz transducer.

The requirements for small, high power sensors are also becoming increasingly demanding. Not only are broad bandwidth and size constraints important, but temperature and prestress stability are paramount in reducing overheating and circuit complexity. TRS used the approach of modifying the composition of PMN-PT to improve the temperature dependence of the material properties. Results show a 50-75% decrease in the low temperature dependence of doped and PT-modified compositions. Two materials showed an increase in the mechanical Q, and coupling remained high (k33 > 0.8). One-dimensional modeling yielded a drop in source level of 1-8 dB for the compositions relative to PMN-32PT, which agrees well with fabricated prototype tonpilz transducers. The temperature stability and high Q should allow higher drive fields which will compensate for the drop in source level.

This work was supported through contracts #N00014-04-C-0114 and #N00014-04-M-0211 from the Office of Naval Research.

6I-2 11:45 a.m.
RELATIONS BETWEEN SINGLE DOMAIN AND MULTIDOMAIN PIEZOELASTIC PROPERTIES IN PIEZOELECTRIC SINGLE CRYSTALS.

T. DELAUNAY*, E. LE CLEZIO, and G. FEUILLARD, LUSSI GIP Ultrasons Université F. Rabelais, EIVL Blois, France.
Corresponding e-mail: gfeuillard@univ-tours.fr

Relaxor-based ferroelectric single crystals, such as (PMN-xPT) and (PZN-xPT) can reach excellent piezoelectric properties due to the formation of engineered domain configurations. The functional properties of macroscopic systems with multidomain structures will directly depend not only on the single domain properties but also on extrinsic contribution of domain walls. This latter effect can largely contribute to effective properties of macroscopic crystals. To predict the effective properties of multidomain single crystals, the interactions in domain structure and orientations and their contribution to macroscopic behaviour have to be quantified as function of both single domain and domain wall properties. Classical approaches assume that the volume average elastic, piezoelectric and dielectric constant coefficients can be calculated from the volume ratio of each domain. In this case, the orientation dependence of piezoelastic properties is revealed but the interactions between domains are neglected. An alternative method consists in developing a quasi static model which calculates all the effective material properties of a twin system from the usual electric and elastic continuity at the interface domain wall. This method was previously successfully applied to Lithium Niobate crystals.

In this paper, we extend this method to determine the effective properties of a multidomain (PMN-xPT) or (PZN-xPT) single crystal from the properties of its single domains, including domain wall contribution. We propose a quasi static

homogenisation model to calculate the effective tensor properties of twin single domains. Defining appropriate electrical boundary conditions on the interface between two domains, the method allows to distinguish the intrinsic contribution to piezoelectricity due to volume domain and to extrinsic domain walls. This model has been used to calculate the multidomain properties of a PMN-PT single crystal in rombohedral phase. First, the 4mm symmetry of multidomain piezoelastic tensor is predicted, and the level of anisotropy on elastic, piezoelectric and dielectric tensors is found in agreement with results published in literature. As expected, $\varepsilon_{33}^{\ T}$ is much greater than $\varepsilon_{11}^{\ T}$ and the ratio depends on the composition. Experimental measurements on PMN-32PT single crystal with [111] and [001] orientations are reported and discussed. For the thickness mode ratio of piezoelastic constants are consistent with previous theoretical results.

This work is supported by the French ministry of research trough the RNTS project : CT 03 B 439.

6I-3 12:00 p.m.
PERFORMANCE OF PERIODIC PIEZOELECTRIC COMPOSITE ARRAYS INCORPORATING A PASSIVE PHASE EXHIBITING ANISOTROPIC PROPERTIES.

A. C. S. PARR*, A. TROGE, R. L. O'LEARY, R. A. PETHRICK, and G. HAYWARD, University of Strathclyde, Glasgow, Scotland, UK.
Corresponding e-mail: agnes@ultra.eee.strath.ac.uk

Piezoelectric composite transducers normally comprise a regular array of piezoelectric ceramic rods embedded in a polymer matrix. When configured as an array, the positioning of the array elements will generally follow a regular spatial pattern. In such structures, the periodicity of the composite substrate and the electrode pattern can contribute to parasitic lamb wave vibrations across the array aperture, degrading array sensitivity and directional response. The elastic character of the constituent materials plays a key role in the extent to which such mechanical cross talk affects array performance. Careful design of the piezoelectric composite substrate such that the frequency of operation occurs within a stop band of the composite plate can limit these influences by designing the substrate accordingly. However, for extremely wideband designs this approach is limited. Alternatively the inclusion of soft, highly attenuative polymer fillers in the composite substrate will reduce unwanted resonant activity. However this is achieved at the expense of element sensitivity, a very major issue in applications such as high frequency sonar, where signal to noise ratio is at a premium.

This paper explores the minimisation of inter-element cross talk in 1-D and 2-D periodic composite array structures through the incorporation of a passive phase exhibiting anisotropic elastic properties. Initially the PZFlex finite element code was used to monitor array aperture response as a function of material properties. It is shown that in array structures comprising passive polymer materials possessing low longitudinal loss and high shear loss, inter-element mechanical cross talk is reduced, without a concomitant reduction in element sensitivity. A

number of polymer materials with the desired properties were synthesised and their elastic character confirmed through a program of materials characterisation. Finally, a range of experimental devices exhibiting improved directional response as a result of a significant reduction in inter-element cross talk are presented and the predicted array characteristics are shown to compare favourably in each case.

6I-4 12:15 p.m.
BISMUTH-LAYER STRUCTURED FERROELECTRIC $(SR,CA)_2BI_4TI_5O_{18}$ CERAMICS FOR LEAD-FREE PIEZOELECTRIC RESONATOR APPLICATIONS.

T. TAKENAKA*, Y. HIRUMA, S. HORIUCHI, and H. NAGATA, Tokyo University of Science, Noda, Chiba-ken, Japan.
Corresponding e-mail: tadashi@ee.noda.tus.ac.jp

A family of bismuth layer-structured ferroelectrics (BLSF) is attractive materials from the viewpoint of their applications for lead-free piezoelectric actuators, resonators and high-temperature sensors. The chemical formula of BLSF is generally represented by $A_{m-1}Bi_2B_mO_{3m+3}$, where A is a combination of mono-, di- and trivalent ions and B a combination of tetra-, penta- and hexavalent ions, and the integer *m* takes any of the values from 1 to 5. BLSFs are characterized by their low dielectric constant, ε, high Curie temperature, *T*c, large anisotropy in the electromechanical coupling factor *k*, high mechanical quality factor, *Q*m, and low temperature coefficient of resonance frequency, *TCf*. In this presentation, dielectric, ferroelectric and piezoelectric properties of BLSF $Sr_2Bi_4Ti_5O_{18}$ (S2BT) - $Ca_2Bi_4Ti_5O_{18}$ (C2BT) solid solution ceramics, that is, $Sr_{2(1-x)}Ca_{2x}Bi_4Ti_5O_{18}$ [SCBT-x] ($0 \le x \le 1$) with *m*=5, were investigated for environmentally gentle lead-free piezoelectric ceramic resonators with high *Q*m and low *TCf*. SCBT ceramics were prepared by the conventional ceramic fabrication technique (ordinarily firing, OF). Effects of grain orientation on their piezoelectric properties are also studied using the grain-oriented samples that were fabricated by the hot-forging (HF) method. X-ray diffraction patterns show the single phase of BLSF with *m*=5. The grain orientation factor, *F*, was calculated from the X-ray diffraction pattern by the Lotgering method. Specimens for piezoelectric measurements were poled in stirred silicone oil under the conditions of applied fields of Ep=7-12 kV/mm, a temperature of Tp=100 °C, and a time of tp= 7 min. Piezoelectric properties were measured by a resonance-antiresonance method on the basis of IEEE standards, using an impedance analyzer (YHP 4194A). A longitudinal vibration of the (33)-mode was measured using a rectangular specimen of 4×2×2 mm^3. The *T*c of SCBT-0 (S2BT) is 290 °C and becomes higher with increasing the amount (x) of Ca. The coupling factor, k_{33} and piezoelectric constant, d_{33}, of $MnCO_3$ (0.4 wt%) doped OF SCBT-0 were 0.15 and 26 pC/N, respectively. On the other hand, the k_{33} and d_{33} of the grain-oriented (HF) SCBT could be obtained first time in this study. The HF SCBT-0 showed relatively high $k_{33}$and d_{33} values of 0.29 and 51 pC/N, respectively. The *F* of HF SCBT system seems to be higher than 0.9. The *Q*m of SCBT show higher than 4000 and become higher with increasing x. The *TCf* of the (33) mode was gradually improved with increasing x, that is, –89.2 ppm/°C for OF SCBT-0 and –66.6 ppm/°C for OF

SCBT-0.5. Furthermore, the *TCf* of HF SCBT-0 and -0.5 were –63.0 ppm/°C and –56.2 ppm/°C, respectively, and become lower with increasing the orientation factor, *F*. These results indicate that the SCBT ceramics will be a superior candidate for lead-free piezoelectric ceramics for resonators and/or filters.

6I-5 12:30 p.m.
PIEZOELECTRIC PROPERTY OF EPITAXIAL LEAD TITANATE ($PBTIO_3$) THIN FILM DEPOSITED BY HYDROTHERMAL METHOD.

T. MORITA* and Y. CHO, RIEC. Tohoku University, 2-1-1 Katahira, Aobaku, Sendai, JAPAN.
Corresponding e-mail: tmorita@ieee.org

Hydrothermal method is a unique method to deposit an epitaxial $PbTiO_3$ film at 150 degrees Celsius in solution. This temperature is lower than Curie temperature; it means the film does not go through the phase transition during deposition process. Therefore, the residential stress becomes very small compared to the other methods that require 600 degrees crystallization. Due to its low reaction temperature, lead evaporation does not occur so that the chemical composition becomes stoichiometric without excessive lead source. Until now, we have already reported about the ferroelectric properties of the epitaxial $PbTiO_3$ thin film deposited by the hydrothermal method. As is well-known, $PbTiO_3$ is one of the basic ferroelectric materials, however, is easy to have a large conductivity and quite difficult to measure the PE hysteresis curve with conventional deposition methods. On the other hand, we realized a high quality crystal film with the hydrothermal and demonstrated 96.5 $\mu C/cm^2$ remanant polarization. The thickness was 100nm and the polarization was perfectly oriented to the thickness direction.

As a next step, the piezoelectric property of the epitaxial $PbTiO_3$ thin film was examined in this study. For sensor and actuator applications, thick film is indispensable, then; by modifying the lead ions concentrations, the thickness was increased to 430 nm. The substrate was $SrTiO_3$ single crystal substrate (100) on which the $SrRuO_3$ epitaxial film was deposited as a bottom electrode. From the X-ray reciprocal mapping and SNDM (Scanning nonlinear dielectric microscopy) observation, the domain structure was examined. There was no secondary phase such as pyrochlore structure even in nano-scale. The domain structure was almost all c-oriented, however a slight a-domain was confirmed. The residual stress due to the 200 degrees drying process after deposition might be the reason for a-c domain structure. The polarization in c-domain was self-aligned during process from bottom to surface. With the platinum top electrode, the piezoelectric property of the film was measured with atomic force microscopy. It is supposed that such measurement of $PbTiO_3$ is the first successful measurement. The butterfly curve showed splendid linear piezoelectric effect and indicated that the deposited film was composed of a single crystal like quality. It is because the inverse piezoelectric effect came from only intrinsic tetragonal crystal deformation without the crystal rotation. Similar to the previous 100nm thickness thin film, the 430 nm thickness film also had small leakage and resulted in a successful measurement. The effective piezoelectric constant $d_{33effec}$ was

97 pC/N, which was larger than the predicted value. The linearity of the piezoelectric displacement is thought to be useful for practical applications, for example, high frequency ultrasonic transducers.

6I-6 12:45 p.m.
CALOTTE PZT THIN FILM STRUCTURES FOR MICROMECHANICS.

F. CALAME* and P. MURALT, Ecole Polytechnique Federale de Lausanne, Ceramics Laboratory, Lausanne, Switzerland.
Corresponding e-mail: florian.calame@epfl.ch

The interest in piezoelectric microsystems (or MEMS) based on piezoelectric films has markedly increased. The technology developed so far is limited to flat geometries, i.e. a thin film is deposited onto flat cantilevers, bridges or plates. The transverse piezoelectric coefficient is exploited to bend the structures. This mechanism is not very efficient with respect to force and mechanical power directed perpendicular to the film plane. In this work, we studied fabrication and properties of 3-dimensional structures coated with piezoelectric PZT thin films in order to improve the piezoelectric coupling into the 3rd dimension. Calotte layers have been chosen as demonstration devices. The base diameters range from 40 to 120 μm, the height varies between 10 to 30 μm. A dynamic, in-situ co-sputtering process allowing for in-situ growth was applied. In order to achieve 3-d structures, micromolds were formed by wet etching in silicon. The etchant was a HNA solution (HF, HNO_3, CH_3COOH) on a silicon dioxide mask. Calottes were obtained with the desired geometry and smooth surface state after few minutes etching time as the solution is very corrosive and reactive. The SiO_2 mask is then removed. The surface of the wafer was grinded down by chemical mechanical polishing (CMP) in order to reduce the slope at the border of the calotte. The silicon surface was oxidized by thermal wet oxidation. The bottom Pt electrode was deposited, on top of which a thin {100}-oriented $PbTiO_3$ seed layer was grown. The bottom electrode was patterned by dry etching, and PZT (100) was grown up to a thickness of 1 μm. A Pt top electrode was deposited and patterned. Deep silicon dry etching is then used to liberate the calotte layer. The SiO_2 was removed by dry etching in CF_4 gas. Pt bottom electrode served as an etch-stop. The calotte-membrane thus consists of Pt bottom electrode, PZT and Pt top electrode. X-ray diffraction confirmed the (100) orientation of the PZT layer. Grain morphology was the same everywhere, the grains growing perpendicular to the local normal inside the calottes. This growth property seems to be astonishing for a sputter process, but is explained by the large mobility of the ad-atoms at the growth temperature of 570 °C. The final structures have been characterized by an impedance analyzer. The dielectric constant and loss tangent of the calotte capacitors amounted to 800 and 5 % respectively (10 kHz). The fundamental resonance frequencies varied between 2.5 and 15.8 MHz, and were found to be inversely proportional to the base radius of the calotte, the proportionality factor being 0.06 $Hz \bullet m^2$. Future evaluations will include amplitude measurements.

This work is supported by the European project MEMSPIE

Session: 1J

QUANTITATIVE CARDIAC IMAGING
Chair: J. Miller
Washington University

1J-1 2:30 p.m.

ELECTROMECHANICAL IMAGING OF THE MYOCARDIUM AT NORMAL AND PATHOLOGICAL STATES.

M. PERNOT and E. KONOFAGOU*, Columbia University, New York, NY.
Corresponding e-mail: ek2191@columbia.edu

The heart is a complex electromechanical pump. Therefore, accurate diagnosis of a number of heart diseases would potentially take advantage of quantitative analysis of the electromechanical coupling mechanisms. However, this is currently limited by the lack of non-invasive imaging techniques of the global electromechanical function of the heart. Using current imaging techniques, the evaluation of the heart function is mainly based on a single mechanical interpretation of the myocardial deformation. However, during the cardiac cycle, electrical waves propagate in the myocardium in order to induce the contraction of the myocardium. The fibers' contraction results in a strong mechanical wave that propagates in the myocardium. Since this wave results from coupling of the electrical excitation and the mechanical response of the tissue, it is hereby named "electromechanical wave". We propose a new method for measuring the electromechanical coupling in the myocardium. Our method is based on imaging and analyzing the delay in small tissue displacements (on the order of 10 microns) resulting from the propagation of the electrical excitation. In-vivo experiments were performed in anesthetized open-chested dogs. The transducer was placed on the anterior wall side of the left ventricle to obtain a short-axis view. Sequences of approximately three cardiac cycles were acquired at a frame rate of 56 images/s. The 2D displacement maps were estimated using a cross-correlation-based technique (windows size: 5mm, 90% overlap). The displacement maps clearly show the propagation of several mechanical waves (shear waves) along the circumference of the myocardium. The wave velocity was found to be approximately 0.6 m/s in the posterior wall, and was corroborated by prior conduction velocity findings [1] as well as through invasive electrophysiological measurements using a matrix of electrodes on a proximal site. Temporary regional ischemia was then induced by coronary artery ligation. The velocity of the electromechanical wave was found to increase up to approximately 1.7 m/s in the ischemic region. This strong increase could be due to an increase of the shear modulus in the ischemic region or a change in the conduction velocity or both. Finally, in vivo experiments were performed on healthy human patients at a frame rate of 170 images/s. Strong electromechanical (or, shear) waves were detected with speed from 0.6 m/s to 1.3 m/s depending on the phase of the cardiac cycle. These results demonstrate the feasibility of imaging in vivo the electromechanical activity of the myocardium. Moreover, since the electromechanical wave speed is a function of both electrical and mechanical

properties of the myocardium, i.e., the electrical conductivity and the shear modulus, this method could potentially be used for early, noninvasive and simultaneous detection of electrical and mechanical dysfunctions in the heart.

[1] Roth, B. J. (2000), Circulation Research 86, E19-E22.

This study was supported by a Scientist Development Grant from the American Heart Association and a Special Development Award from the Whitaker Foundation.

1J-2 2:45 p.m.
IN VIVO VISCOELASTICITY ESTIMATION OF MYOCARDIUM.

H. KANAI*, Tohoku University, Sendai, Japan.
Corresponding e-mail: hkanai@ecei.tohoku.ac.jp

Background: Though myocardial viscoelasticity is essential in the evaluation of heart diastolic properties, it has never been noninvasively measured *in vivo*. **Experimental Results for Examining Potential Model:** By the ultrasonic measurement of the myocardial motion (Kanai et al. IEEE Trans UFFC 43, 1996), we have already found that some pulsive waves are spontaneously excited by aortic-valve closure (AVC) at end-systole (T_0) (Kanai et al. Ultrasound Med Biol 27, 2001). These waves may serve as an ideal source of the intrinsic heart sound caused by AVC. **Method:** In this study, using a sparse sector scan, in which the beam directions are restricted to about 16, the pulsive waves were measured almost simultaneously at about 160 points set along the heart wall at a sufficiently high frame rate. The consecutive spatial phase distributions, obtained by the Fourier transform of the measured waves, clearly revealed *wave propagation* along the heart wall for the first time. The propagation time of the wave along the heart wall is very small, namely, several milliseconds, and cannot be measured by conventional equipment. Based on this phenomenon, we developed a means to measure the myocardial viscoelasticity *in vivo*. In this measurement, the phase velocity of the wave is determined for each frequency component. By comparing the dispersion of the phase velocity with the theoretical one of the Lamb wave (the plate flexural wave), which propagates along the viscoelastic plate (heart wall) immersed in blood, the instantaneous viscoelasticity is determined noninvasively. This is the first report of such noninvasive determination. **In Vivo Experimental Results:** In *in vivo* experiments applied to 5 healthy subjects, propagation of the pulsive wave was clearly visible in all subjects. For the 60-Hz component, the typical propagation speed rapidly decreased from 5 m/s just before the time of AVC (t=T_0-8 ms) to 3 m/s at t=T_0+10 ms. In the experiments, it was possible to determine the viscosity more precisely than the elasticity. The typical value of elasticity was about 24-30 kPa and did not change around the time of AVC. The typical transient values of viscosity decreased rapidly from 400 Pa•s at t=T_0-8 ms to 70 Pa•s at t=T_0+10 ms. The measured shear elasticity and viscosity in this study are comparable to those obtained for the human tissues using audio frequency in *in vitro* experiments reported in the literature. For 4 patients with hypertrophic cardiomyopathy (HCM) and 3 patients with aortic stenosis (AS), similar propagation of the pulsive wave was clearly visible. However, the above method cannot be easily applied to

these patients because there were inhomogeneities in the phase velocities due to the diseased myocardium. **Conclusions:** We found that clear propagation of the pulsive waves along the IVS was recognized for the first time. From the dispersion of their phase velocities, the myocardial viscoelasticity was determined noninvasively for the first time. This method offers potential for *in vivo* imaging of the spatial distribution of the passive mechanical properties of the myocardium, which cannot be obtained by conventional echocardiography, CT, or MRI.

1J-3 3:00 p.m.
THE ULTRASONIC NON-INVASIVE ASSESSMENT OF RADIAL, LONGITUDINAL AND CIRCUMFERENTIAL CARDIAC STRAIN IN NORMAL PIGS.

S. LANGELAND*[1], S. COENEN[1], M. WU[1], F. RADEMAKERS[1], and J. D'HOOGE[1,2], [1]Cardiac Imaging Research - Dept. Of Cardiology, Catholic University of Leuven, Leuven, Belgium, [2]Medical Image Computing - Dept. of Electrical Engineering, Catholic University of Leuven, Leuven, Belgium.
Corresponding e-mail: stian.langeland@uz.kuleuven.be

Introduction: Ultrasonic deformation imaging has been used extensively to study cardiac (patho) physiology in the porcine model. However, to date, only deformation along the ultrasound line can be assessed. This methodological limitation combined with the fact that a closed-chest porcine model has a limited amount of acoustic windows has restricted these studies to investigate radial (R) cardiac function only. Nevertheless, a significant amount of information might be available from the longitudinal (L) and circumferential (C) strain components. To date, these have only been available non-invasively using MRI. In our laboratory, a new ultrasound methodology has previously been developed allowing the measurement of all in-plane strain components. This approach has recently been validated against sonomicrometry in an open-chest sheep model. The aim of this study was to apply this new methodology to a closed-chest porcine model and to test the feasibility of assessing all strain components (R, L and C) non-invasively.

Methods: 13 closed-chest pigs were anaesthetized and imaged using a Toshiba Aplio system. During apnea, radio frequency (RF) data were acquired from a parasternal transducer position in both the long and short axis views. For all data sets, in-plane myocardial velocity vectors were estimated using a sum of squared differences velocity estimator. Subsequently, both in-plane myocardial strain components of the anteroseptal and inferolateral walls were extracted using custom made software (SPEQLE-2D) according to a previously described methodology. In this way, radial-longitudinal and radial-circumferential strains were obtained from the long and short axis data sets respectively.

Results: For all animals, all strain components could be estimated in both myocardial walls and showed normal physiological behavior. The average ± standard deviation of the end-systolic R, L and C strain components of both myocardial walls are given in table 1.

Conclusions: The non-invasive assessment of all strain components of the left ventricular anteroseptal and inferolateral walls was shown to be feasible. This

might open interesting new possibilities to investigate the patho-physiology of different cardiac diseases.

Table 1

	SAX R	SAX C	LAX R	LAX L
Inferolateral wall	83±41%	-20±10%	75±38%	-24±11%
Anteroseptal wall	20±12%	-21±13%	34±16%	-19±7%

R, L and C strain as measured in the two walls.

1J-4 3:15 p.m.
MULTI-DIMENTIONAL STRAIN RATE IMAGING BASED ON VECTOR DOPPLER.

A. CRITON*[1,2], J. POWERS[1], N. MCDICKEN[2], and P. HOSKINS[1], [1]Philips Ultrasound, Bothell, WA, [2]Department of Medical Physics, Edinburgh, UK.
Corresponding e-mail: aline.criton@philips.com

Atherosclerosis accounts for more than 50% of all deaths in the Western world. It is associated with narrowing of the vessel lumen and plaque rupture. These latter create high tissue stresses and tissue under perfusion, which alter local arterial and myocardial wall dynamics and elastic properties. Hence visualization of tissue dynamic and deformation property changes is crucial to detect atherosclerosis in the earliest stages to prevent acute events.

We previously developed two methods to assess one-dimensional tissue deformation and multi-dimensional tissue velocity. This work describes a new technique to estimate the full tissue deformation tensor from multi-dimensional vector velocity estimation. One-dimensional strain rate can be derived from one-dimensional velocity. A strain rate estimator can be derived from the phase difference in between two lag-one autocorrelation estimations along the ultrasound beam divided by the distance in between these two estimates. To describe the deformation of a volume a three dimensional tensor is necessary. This tensor has 9 components: 3 strain rate components along the main axis (on the diagonal of the tensor) and 6 shear strain rate components. The shear strain rate components are characterized by the fact that the deformation occurring is in the plane perpendicular to the direction of velocity, while for strain rate components, the deformation occurs in the direction of velocity. A new estimator has been developed to assess strain rate and shear strain rate components from lag-one autocorrelation estimates derived from multi-dimensional vector Doppler acquisition. These strain rate components are calculated from the phase differences of velocity estimates along each dimension divided by the distance between the estimates. The shear strain rate components are calculated from the phase differences of the velocity estimate in direction perpendicular to the main deformation direction divided by the distances between the estimates.

An experimental setup has been built to qualitatively assess the two-component strain rate. This setup includes tissue-mimicking flow phantom, with a straight tube, a PC driven controller and a DC-motor applied to a fluid gear pump. This phantom is used as a model for carotid application. By applying a cyclic flow pressure variation (via a gear pump) in the flow phantom, a circumferential deformation is applied to the surrounding tissue mimicking. Two-component vector velocity field from the moving tissue is acquired. A software tool has been developed to derive and display two-component strain rate images from two-component TDI velocity estimates. The resulting strain rate and shear strain rate images are showing agreement with the expected deformation patterns.

1J-5 3:30 p.m.
DETECTING BROKEN STRUTS OF A BJÖRK-SHILEY VALVE USING DIAGNOSTIC ULTRASOUND: A FEASIBILITY STUDY.

P. VAN NEER*[1], A. BOUAKAZ[3], E. VLAANDEREN[2], J. DE HART[1], F. VAN DE VOSSE[1], A. VAN DER STEEN[2], and N. DE JONG[2], [1]Eindhoven University of Technology, Eindhoven, Brabant, The Netherlands, [2]Erasmus University Medical Center, Rotterdam, Zuid-Holland, The Netherlands, [3]Inserm, Tours, Cedex, France.
Corresponding e-mail: p.l.m.j.v.neer@student.tue.nl

Background: The Björk-Shiley convexo concave (BScc) mechanical heart valve has been extensively used in surgery between 1979-1986. There is increased occurrence of unexpected mechanical failure of the outlet strut of the valve compared to equivalent valve types, with a high incidence of mortality, when it occurs. Many approaches have been attempted to noninvasively determine BScc valve integrity, such as cineradiography methods or acoustic assessment methods. None however resulted in adequate performance, mostly due to a lack of either sensitivity or specificity demonstrated in in vitro and/or in vivo studies.

Methods: The proposed method analyses the movement of both legs of the BScc valves outlet strut during the cardiac cycle. It is based on the assumption that a broken leg will have increased movement compared to either the intact leg or the flange. BScc heart valves were mounted in the mitral position in an in vitro pulse duplicator system, which is a plexiglass model of the left ventricle that can mimic the hydrodynamics in the ventricle and concomitant forces of heart valves. A focused single element ultrasound transducer (Panametrics V311, Fc 10 MHz, -6dB: 2.5-10 MHz, focal length 7.5 cm) is excited using a sinusoidal wave to direct ultrasound (prf 4 kHz), on a particular leg of the outlet strut. Correlation based time delay estimation is then used to estimate the difference in time of flight of the echoes during the cardiac cycle. These differences are subsequently converted to produce the movement of the outlet strut during the cardiac cycle.

Results: The movement of two valves has been studied, one intact valve and a valve with a single leg fracture with both ends grating against each other

(SLFgrating). No significant difference in movement could be detected between both legs of the intact BScc valve (amplitude of movement 9.2 μm ± 0.1 μm). The amplitude of movement of the broken leg of the SLF valves outlet strut was 12 μm ± 1.6 μm versus 8.6 μm ± 0.1 μm for the intact leg.

Discussion: The detection of a difference in movement between the broken and the intact leg (or flange) is the most difficult in the case of an SLFgrating BScc valve, as broken leg movement is damped the most in this case. Therefore, a larger difference in movement between both legs of the outlet strut (or the broken leg and the flange) is expected for valves with a non-grating type of fracture. In vivo implementation of this method is expected to be possible as well; the main challenge is the handling of motion of the whole valve. However since the majority of strut fractures occur close to the strut flange junction, the measuring positions on a particular leg of the outlet strut and the flange can be located close to each other, minimizing the effects of whole valve movement.

In conclusion, the proposed method has shown to be feasible in vitro and has potential for the in vivo detection of BScc valve outlet strut fracture.

Gratitude goes to C. Pakvis, J. Honkoop, L. Bekkering, L. Baijens, M. Stijnen, C. Lancee and the Trustees for the Bowling-Pfizer Heart Valve Settlement Funds.

1J-6 3:45 p.m.
NON-INVASIVE TWO DIMENSIONAL ELASTOGRAPHY OF THE CAROTID ARTERY.

H. RIBBERS*[1], S. HOLEWIJN[2], J. D. BLANKENSTEIJN[2], and C. L. DE KORTE[1], [1]Clinical Physics Laboratory, UMC St Radboud, Radboud University Medical Center, Nijmegen, The Netherlands, [2]Department of Vascular Surgery, Radboud University Medical Center, Nijmegen, The Netherlands.
Corresponding e-mail: cldekorte@ieee.org

Background: Cardiac disease and stroke are the major cause of death in the Western World. Atherosclerosis of the carotid artery is the most important predictor of stroke. Elastography is a technique to assess the composition and vulnerability of an atherosclerotic plaque. Contrary to intravascular applications, the ultrasound beam and radial strain are not aligned in non-invasive acquisitions. In this study, two dimensional strain estimation methods were developed to reconstruct the radial strain in atherosclerotic carotid arteries.

Methods: rf-data were acquired using a Philips SONOS 7500 live 3D ultrasound system, equipped with an L11 (3-11 MHz) linear array transducer and rf-interface. A homogeneous phantom (20% gelatin, 1% SiC scatterers (10 μm)) was fixed in a water tank with water column system to generate different intraluminal pressures. Additionally, measurements in patients (n=10) were made to evaluate the in vivo applicability of the technique. Longitudinal and cross-sectional recordings were made, both in phantoms and patients.

Strain along the ultrasound beam (axial strain) was determined using cross-correlation analysis for signal-windows of both the pre- and post-compression data. For lateral strain, new ultrasound lines were generated between the acquired lines using interpolation. A cross-correlation based search algorithm was applied to determine lateral displacement and strain.

Results: Longitudinal axial strain images show a decreasing strain from the lumen vessel wall interface to the outer region that can be described by a 1 over r^2 relationship. The lateral strain image shows no strain in this direction indicating a plane strain situation. Plane strain was used in previous studies, but never demonstrated using phantom experiments. In the cross sectional view, compression of the material in regions at 12 and 6 o'clock is observed, whereas expansion is observed in regions at 3 and 9 o'clock. This pattern is in accordance with theory, but can only be partly corrected for: in the transition regions, zero axial strain is measured. The lateral strain image shows a complimentary pattern.

In patients, low strain is observed in non-atherosclerotic artery walls. High and low strain regions were found in atherosclerotic plaques. High quality elastograms were generated both in longitudinal and cross-sectional views. Additional validation is needed to assess the value of this technique to identify plaque vulnerability and composition.

Conclusion: Two dimensional non-invasive elastography of atherosclerotic carotid plaques is feasible. Phantom studies reveal elastograms in accordance with theory.

The support of Philips Medical Systems in providing the linear array transducer is greatly appreciated.

Session: 2J

THERAPY MONITORING
Chair: L. Crum
University of Washington

2J-1 2:30 p.m.
IN VIVO INTRA-CARDIAC ACOUSTIC RADIATION FORCE IMPULSE IMAGING OF RADIOFREQUENCY ABLATIONS.

S. HSU*, P. WOLF, B. FAHEY, G. PINTON, D. DUMONT, and G. TRAHEY, Duke University, Durham, NC.
Corresponding e-mail: sjh6@duke.edu

Radiofrequency ablations (RFA) have been demonstrated to be an effective procedure for the treatment of rapid or irregular heartbeats such as atrial fibrillation. Assessing thermal lesion size and growth with ultrasound has been limited, as the changes within conventional B-mode images often are subtle. Acoustic radiation force impulse (ARFI) imaging is a promising modality to monitor cardiac ablations, as it is capable of imaging the changes in local stiffnesses associated with the developing lesion. However, ARFI imaging of the heart has been limited due to its relative inaccessibility. By using an intra-cardiac probe, the transducer can be positioned closer to the ablation site where quality ARFI images of the developing lesions can be made.

We describe ARFI imaging with the Siemens AcuNav intra-cardiac probe to monitor cardiac ablations *in vivo*. Radiofrequency ablations were performed within the heart of a live ovine subject, while B-mode and ARFI imaging with the AcuNav were used to monitor the developing lesions. The catheters were positioned within the heart using B-mode (from the AcuNav itself) and fluoroscopic imaging. Ablations were performed within the right atrium with the AcuNav monitoring the ablation 1-2 cm away.

ARFI sequence acquisition was triggered off the electrocardiogram (ECG) in order to acquire images during periods where cardiac motion is minimized. This proved to be effective in reducing motion artifacts within the images as long as the ECG was stable. Realtime ARFI imaging was also used to determine suitable regions interests for ablations as well as monitor the progress of the lesions during the ablation. Image calculation and display took less than a second.

Although there was little indication of a developing lesion within the B-mode images, the corresponding ARFI images displayed regions around the ablation site that displaced less suggesting the creation of a lesion. The ARFI images showed a semicircular region of increased stiffness around the ablation site whose maximum displacement decreased from 8.9 ± 2.1 μm before the ablation to 4.6 ± 0.9 μm afterwards. From these results, we discuss the potentials and limitations of ARFI imaging for cardiac ablations.

This research was funded by NIH Grant no.: 1R01-HL-075485 and 5T32-EB-001040, and Biosense Webster. We would like to thank Siemens Medical Solutions USA, Inc. for their hardware and system support.

2J-2 2:45 p.m.
HIGH-THROUGHPUT HIFU TREATMENT FOR INTRAOPERATIVE RESECTION OF SOLID ORGANS.

V. ZDERIC*[1], J. FOLEY[1,2], G. O'KEEFE[3], L. CRUM[1,2], and S. VAEZY[1,2], [1]Center for Industrial and Medical Ultrasound, Applied Physics Laboratory, University of Washington, Seattle, WA, [2]Department of Bioengineering, University of Washington, Seattle, WA, [3]Department of Surgery, University of Washington, Seattle, WA.
Corresponding e-mail: vesna@u.washington.edu

Objectives. 1) To increase HIFU throughput by developing very high power HIFU devices, thus enabling faster treatment of large tissue volumes. 2) To explore a potential new application of HIFU for resection of solid organs (liver, spleen, and kidneys in a large animal model). **Methods.** The HIFU transducer (diameter of 7 cm, focal length of 6 cm, frequency of 3.3 MHz) was driven using a high power amplifier. A water pillow connected to a circulation pump with in-line degasser provided transducer coupling and cooling. The input electrical power was 380 W, corresponding to the acoustic power of 153 W, and focal intensity of 118,000 W/cm^2 (in water). The -3dB cross sectional area of the focus was 0.0013 cm^2. The HIFU device was used for intraoperative resection of solid organs in 8 pigs: 16 resection of liver lobes at approximately 12 cm from the tip of the lobe, 8 spleen resections (4 distal resections at 15 cm from the tip of the spleen, and 4 proximal resections at 30 cm from the tip), and 8 resections

of the lower pole of the kidneys. A reflector (polystyrene foam) was positioned at the posterior surface of the organ, to allow clamping of the organ between the reflector and the HIFU device and also to increase the delivered acoustic power. The resection consisted of several 60 s or 30 s treatments, with the number of treatments judged by the operator based on tissue discoloration. Color Doppler ultrasound was used to observe the blood vessels in the solid organ before and after the HIFU treatment. If some of the vessels (usually 1-2) were still oozing or bleeding after the resection, the additional treatment was performed using an intraoperative solid cone HIFU device for few minutes, at the in situ intensity of 8,000 W/cm^2. **Results.** The blood vessels sizes were 5 +/- 2 mm, 2.8 +/- 1.7 mm, and 3.5 +/- 1.6 mm, in the liver lobes, spleen and kidneys, respectively. The resection of liver lobes was achieved in 287 +/- 54 s of high-power HIFU application and additional 133 +/- 55 s of the application of the solid cone device to seal few remaining patent or oozing vessels. The width of the necrotic region was 4 cm on average. The resection of the distal portion of the spleen was achieved in 165 +/- 54 s of high-power HIFU application. The resection of the proximal portion of the spleen was achieved in 250 +/- 54 s of high-power application, and additional 40 +/- 4 s of solid cone application. Seven kidneys were completely resected after high-power HIFU application for 162 +/- 29 s, and for one kidney additional application of a solid cone device was needed (for 60 s). **Conclusion.** The development of the high power HIFU device allowed the deposition of sufficiently high HIFU energy in relatively short times (within several minutes) to produce resection of solid organs in a large animal model. This method holds promise for future clinical applications in resection of solid tumors and hemostasis of high grade injuries of solid organs.

2J-3 3:00 p.m.
MEASUREMENT OF OUTPUT INTENSITIES OF MULTIPLE-MODE DIAGNOSTIC ULTRASOUND SYSTEMS USING THERMOACOUSTIC SENSORS.

V. WILKENS*, Physikalisch-Technische Bundesanstalt, Braunschweig, Germany. Corresponding e-mail: Volker.Wilkens@ptb.de

Ultrasound exposure measurements for medical ultrasound systems are essential as regards aspects of safety and quality assurance. Spatial-peak temporal-average output intensities of ultrasound machines which have to be declared by the manufacturer according to IEC 61157 or for FDA approval are commonly derived from hydrophone measurements. In the case of modern multiple-mode diagnostic equipment, the required hydrophone measurements are quite cumbersome and expensive. Much effort is necessary to find out the parameter settings and operation modes that produce the highest intensities, and synchronization of the measurement system to all ultrasound pulses incident at the position of interest is a difficult task.

Thermoacoustic sensors are a very simple and low-cost alternative for the determination of local temporal-average intensities. The measurement technique investigated is based on the transformation of the incident ultrasonic energy into heat inside a small-sized cylindrical absorber, and the detection of the

temperature rise on the rear side of the absorber. Here, inclusion of all contributing pulses and temporal averaging is done by the sensor inherently, without the need for synchronization to individual pulses and pulse sequences.

To enable quantitative measurements, sensors with 3 mm and 1 mm absorber diameter are calibrated in the frequency range from 1 MHz to 9 MHz. The calibrated sensors are then applied to acoustic output measurements on a commercial diagnostic ultrasound machine at different parameter settings. The results for M-mode and for pulse-Doppler mode, i. e. for non-scanning beams, are compared with the intensities derived from additional hydrophone measurements, and agreement is found within the typical uncertainty ranges for ultrasound intensity determination. The investigation of more complex scanning modes and of combined modes shows that the sensor technique can be used efficiently to identify the parameter settings of the diagnostic machine which lead to maximum acoustic output. Therefore, use of the measurement technique described can reduce the expenses of the manufacturer for regulatory testing and may improve the results and the reliability of output parameters.

2J-4 3:15 p.m.
A CLASSIFICATION SYSTEM FOR MONITORING THERMAL THERAPIES.

S. SIEBERS*[1], U. SCHEIPERS[1], J. HAENSLER[2], M. FRIESER[2], D. STROBEL[2], C. WELP[3], J. WERNER[3], E. HAHN[2], and H. ERMERT[1], [1]Institute of High Frequency Engineering, Ruhr-University Bochum, Bochum, Germany, [2]Dept. of Internal Medicine, University Erlangen-Nuernberg, Nuremberg, Germany, [3]Institute of Biomedical Engineering, Ruhr-University Bochum, Bochum, Germany.
Corresponding e-mail: stefan.siebers@rub.de

Introduction: Thermal ablation is well accepted for the treatment of tumors in cases where established therapeutic methods such as surgical resection are either inapplicable or ineffective. However, conventional B-mode imaging is often not sufficient due to low contrast between coagulated and healthy tissue. Therefore we propose to apply tissue characterizing features from spatial and spectral domain to characterize coagulated tissue.

In this work, various features are processed by a classification system using linear classifiers. The extracted features include first and second order texture features, estimates of attenuation coefficients, and measures of backscatter (slope, intercept and midband value).

Materials and Methods: Measurements were performed on 15 bovine liver samples in vitro and on 10 pigs in vivo. Coagulation was induced using an RF-ablation device (Elektrotom HiTT 106, Integra ME GmbH, Tuttlingen, Germany). During in vitro experiments, ultrasonic imaging was done using a Siemens Antares diagnostic ultrasound system (3.5 MHz (C5-2) curved array transducer). RF data were acquired using the Siemens Axius Direct Ultrasound Research Interface (URI), which provides RF data at 40 MHz sampling rate and 16 bit resolution. In vivo measurements were performed using a Siemens Elegra system (3.5 MHz, C5-2). Acquisition of RF data was always done immediately after finishing the ablation process.

Afterwards the liver samples were sliced along the imaging plane and photographs of the coagulated zone were taken to serve as a reference. Each RF dataset was subdivided in up to 1700 overlapping ROIs. The size of the ROIs was set to 128 samples (3.9 mm) axially and 16 lines (4 degrees) laterally. B-mode and parameter images of 40 features extracted from each ROI were calculated offline. According to the photographs boundaries of the coagulated zone were delineated in the B-mode images. The boundaries were transferred to the parameter images. Thus two classes ("coagulated" and "noncoagulated") were defined based on the reference.

The Maximum-Likelihood measure was used to classify each ROI separately. Classification was done by total cross validation over cases. The best feature combination found by sequential forward selection was processed by the classifier.

Results and Conclusion: Classification results were visualized in binary coagulation maps. For each coagulation map, sensitivity and specificity were determined as a quality measure of the classification results. In vitro measurements yielded sensitivities and specificities of 0.9 ± 0.12 and 0.84 ± 0.09, respectively. In vivo measurements yielded sensitivities and specificities of 0.86 ± 0.11 and 0.76 ± 0.09, respectively. Superimposing the coagulation maps to conventional B-mode images can advance the visualization of the coagulated zone.

This work is an activity of the Ruhr Center of Excellence for Medical Engineering Bochum. It is supported by the German Federal Ministry of Education and Research (grant 13N8079) and Siemens Medical Solutions, Siemens AG.

2J-5 3:30 p.m.
CONTROLLED SPATIO-TEMPORAL HEATING PATTERNS USING A COMMERCIAL, DIAGNOSTIC ULTRASOUND SYSTEM.

K. FRINKLEY*, M. PALMERI, and K. NIGHTINGALE, Duke University, Durham, NC.
Corresponding e-mail: kdf2@duke.edu

Background: Thermal ultrasound therapy is being investigated as a non-invasive surgical tool with applications in soft tissue tumor and cardiac ablation; as a method for hemostasis; and in the control of thermally-activated drug delivery vehicles. The success of localized ultrasonic thermal therapy depends on image guidance, typically done with a separate imaging transducer, but alignment of these transducers is challenging. A system capable of both functions would be ideal. However, the inherent tradeoff between image quality and power output presents a challenge for dual-function probe design. **Goal:** To investigate the feasibility of using a modified, commercial diagnostic ultrasound system for combined B-mode, Doppler guidance, ARFI imaging, and therapeutic thermal applications. **Methods:** A Siemens Antares™ scanner and transducers (75L40: f_c=5.7 MHz; CH62: f_c=4.4 MHz) were used. Custom pulse sequences were designed to transmit high intensity pulses down a single line of flight using different pulse lengths, amplitudes, PRFs, and F/#s for therapeutic purposes.

These sequences were delivered to *ex vivo* porcine muscle through a waterpath to the focal point where a type T thermocouple was positioned at the water/muscle interface. Transducer surface heating was monitored in a separate experiment for these sequences by centering a thermocouple on the surface of the transducer. The muscle measurements were compared with analytic solutions to the bio-heat transfer equation and FEM models. Transmit parameters were evaluated to determine the optimal sequencing approach for different thermal therapies. **Results:** Temperature rises of 14 ± 0.3 C for ~0.5 s were regularly achieved on the surface of the porcine muscle without damaging the transducers or the system. Temperature measurements at the focus were made for increasing durations of insonification, and were consistent with the bio-heat transfer equation solution (neglecting perfusion). A cooling time constant of 0.26 ± 0.02 s was determined for the porcine muscle (k=0.49 W/m/K). As expected, a longer time constant (3.9 ± 1.7 s) for transducer face cooling was observed. Under some conditions, temperature rises of 20 C for 0.3 s were achieved but caused transducer damage. **Discussion:** According to the thermal dose equation and reported values in the literature, the regularly achieved temperature rise would need to be held 28 times longer than currently achieved or raised by 34% for the 0.5 s time period to induce necrosis in liver. For a thermally-activated drug delivery application, the required temperature rise is only 2-4 C for 1-5 minutes, which is within the capabilities of the diagnostic system. However, these experiments do not incorporate perfusion effects or, more significantly, attenuation of intervening tissue which will be encountered for most *in vivo* applications. Thus, passive cooling modifications are being explored to decrease transducer heating while maintaining good image quality.

Siemens Medical Solutions, NDSEG Fellowship, and Dr. Gregg Trahey.

2J-6 3:45 p.m.
AUTOMATIC TREATMENT PLANNING FOR PROSTATE HIFU THERAPY.

R. FEDEWA*[1], R. SEIP[1], R. F. CARLSON[1], W. CHEN[1], N. T. SANGHVI[1], K. A. DINES[2], M. A. PENNA[3], and R. PFILE[4], [1]Focus Surgery, Inc., Indianapolis, IN, [2]XDATA Corporation, Indianapolis, IN, [3]Dept. of Mathematical Sciences, Indiana University, Indianapolis, IN, [4]CoEval Systems LLC, Indianapolis, IN.
Corresponding e-mail: rseip@focus-surgery.com

Last year, a framework for computer-assisted treatment planning for prostate cancer high intensity focused ultrasound (HIFU) treatments using 3D ultrasound images, user tracing, and 3D models of the prostate, urethra, and rectal wall was presented. This framework provides the input for the current research: the development of a general-purpose HIFU treatment planner module. This module is capable of automatically specifying the prostate HIFU treatment sites using given prostate anatomical information from 3D ultrasound images and HIFU probes, transducer, and elementary lesion parameters stored in a lesion library. The output of the automatic planner module is a complete treatment plan that is executed after interactive physician review. Additional inputs to this module include clinically relevant parameters, such as inter-lesion spacing and treatment margins. Advantages of this approach include a reduction in the overall treatment

time, the ability to easily and accurately plan treatments for complex prostate shapes, and the ability to adapt the planner to other systems and geometries simply by providing a different lesion library specific to that system. The automatic planner module has been integrated into the treatment software of the Sonablate®500 image-guided HIFU device (Focus Surgery, Inc.), and has been evaluated using phantom , canine, and human prostate ultrasound imaging data. Lesion library entries for this system include lesions for different transducer focal lengths and treatment power settings. Preliminary results using lesion libraries with 2 and 54 entries indicate that the planner generates HIFU treatment plans that are equivalent in treatment dose, time, and treatment site locations to those manually generated by physicians in about half the time. The entire treatment planning process will be presented, highlighting the usefulness of the automatic planner module. Planner implementation details, lesion library specifics, and output results will also be shown.

This work was supported by SBIR NIH Grant R44 DK059664.

Session: 3J
MATERIALS CHARACTERIZATION
Chair: W. Arnold
Fraunhofer Institute for Nondestructive Testing

3J-1 2:30 p.m.
(Invited)
SURFACE CHARACTERIZATION USING ULTRASONIC VIBRATION MODES OF ATOMIC FORCE MICROSCOPE CANTILEVERS.

U. RABE*, Fraunhofer Institute for Nondestructive Testing, IZFP, Saarbruecken, Germany.
Corresponding e-mail: ute.rabe@izfp.fraunhofer.de

According to Abbe's limit, the lateral resolution of microscopes is restricted to approximately one wavelength of the involved radiation, here the acoustic wave. Using near-field microscopes the lateral resolution can fall below Abbe's value. An Atomic Force Microscope (AFM) which senses the ultrasonic vibrations in a sample can be considered as a near-field acoustic microscope. Different types of near-field acoustic microscopes derived from AFM were proposed. Here we show how the flexural, torsional and lateral vibration modes of the AFM sensor beams can be used to image surface properties such as elasticity, adhesion and friction. Due to the small size of the sensor beams their resonant frequencies are in the ultrasonic frequency range. When the AFM senor tip is in contact with the sample surface, the resonant frequencies of the beam increase. Furthermore, the shape of the resonance curves changes when nonlinear interaction such as adhesion or friction is involved in the contact. Images will be presented and examples of quantitative contact-resonance spectroscopy will be shown.

Part of this work was supported by the German ministry of education and research (BMBF) in the frame of the research program "Nanoanalytik" under the contract No. FKZ13N8326

3J-2 3:00 p.m.
STATISTICAL CHARACTERIZATION OF METALS FROM ULTRASONIC ABERRATIONS.

J. A. HERNÁNDEZ*, M. CLARK, S. SHARPLES, and M. SOMEKH, University of Nottingham, Nottingham, UK.
Corresponding e-mail: eexjah@nottingham.ac.uk

Materials with random microstructure can have an adverse effect on ultrasonic measurements through scattering and aberration of the acoustic field. We have developed a theoretical and experimental technique for characterizing the effect of the material microstructure on the propagation of acoustic waves. The theoretical method predicts preopagation of the statistical properties in the random medium. Using this model and a novel experimental technique we can extract materials properties from observations of acoustic aberrations. The microstructure has been modelled as having grains randomly orientated and weakly anisotropic. Moreover, individuals grains are treated to be equiaxed. This is summarized by assuming that the correlation function for the wave number has a Gaussian shape. Under this assumption, the approximated power correlation function for the acoustic field has been obtained using the stochastic wave equation for random media, along with numerical simulation using phase screen theory.

The experimental evidence that aberrations are frequency dependent is presented. Multiple c-scans on titanium were performed using a 10MHz transducer as an ultrasonic source. The output of the transducer gives substantial frequency components between 6MHz and 16MHz. The variation of the frequency on a fixed sample enables us to examine different measurement regimes (higher frequencies correspond to large grains).

The statistical analysis and estimated power correlation function from measurements are compared to a modelled power correlation function. The correlation length and standard deviation of the wave number define the power correlation function of the field. This function has been fitted to the estimated power correlation from measurements on titanium 6-4, and values for the variance and correlation length were obtained. The paper demostrates that the stochastic model is capable of quantitative prediction of the predominant wave scattering effect in granular materials.

3J-3 3:15 p.m.

THICKNESS AND VISCOSITY OF ORGANIC THIN FILMS PROBED BY COMBINED SURFACE ACOUSTIC LOVE WAVE AND SURFACE PLASMON RESONANCE.

J.-M. FRIEDT*[1], L. A. FRANCIS[2,3], and S. BALLANDRAS[1], [1]FEMTO-ST/LPMO, Besancon, FRANCE, [2]Université catholique de Louvain, Louvain-la-Neuve, BELGIUM, [3]IMEC, Leuven, BELGIUM.
Corresponding e-mail: jmfriedt@lpmo.edu

The simultaneous measurement of ad-layers from liquids with acoustic and optical methods allows the estimate of the viscosity, the thickness and the solvent content at once. For the present set-up, a Love mode surface acoustic device is combined with a surface plasmon resonance for measurements of the properties of organic thin films adsorbed on gold by means of evanescent acoustic and optical fields.

On one hand, Love mode acoustic waves transmitted at 125 MHz in a guiding silicon dioxide layer on a quartz substrate are used to probe the mechanical properties (density, viscosity) at an unknown thickness of the adsorbed organic film through the change of the acoustic signal (insertion loss and phase shift) travelling along the sensing path. On the other hand, and on the same sensing surface, single wavelength surface plasmon resonance provides an unresolved estimate of the optical index and the thickness of the adsorbed organic film. By the combination of both methods and with help of simulations, the viscosity, the thickness and the solvent content of the organic film are independently identified.

A typical feature displayed by the combined setup is to discriminate between several kinds of organic layers the importance of the viscous interaction in that layer that is function of the solvent content dissolved in the ad-layer.

Experimental analysis was carried on small globular molecules (S-layer, IgG and CTAB - a surfactant -), on a heavily loaded layer with solvent (collagen) and on an intermediate case (fibrinogen). In all cases, the nature of the rigid or viscous interaction is determined by the acoustic measurement through the ratio of the insertion loss to phase shift: a predominantly rigid interaction (low solvent content) has a small ratio (<0.1 dB/rad) while a viscous interaction (high solvent content) has a high ratio (>0.1 dB/rad).

An interesting case is provided by pNIPAM, a polymer whose conformation changes with temperature, with a lower critical solution temperature around 31^o C, switching reversibly from an hydrophilic to an hydrophobic behavior.

Our methodology requires strong modelling of the interaction of the layer with the acoustic and the optical methods and signal processing to combine these signals to uniquely determine the characteristics of the ad-layer. Within that respect, two different modelling approaches were used: one based on transmission lines model (fast, but somewhat not adequate to all material combinations), and one based on a mixed Finite Element Method/Boundary Element Method which requires a full geometrical description of the device, including surface roughness.

L. A. Francis would like to thank the F.R.I.A. (Belgium) for financial support

3J-4 3:30 p.m.

DECOMPOSITION OF THE TIME-REVERSAL OPERATOR APPLIED TO QUANTITATIVE CHARACTERIZATION OF SMALL ELASTIC CYLINDERS.

J. G. MINONZIO*, C. PRADA, and M. FINK, Laboratoire Ondes et Acoustique, Paris, France.
Corresponding e-mail: jean-gabriel.minonzio@loa.espci.fr

The analysis of acoustic scattering is an important tool for object identification. It has applications among non-destructive evaluation, medical imaging or underwater acoustics. The decomposition of the time-reversal operator (DORT method in French) is a new approach to scattering analysis that was developed since 1994 and is applied to detection and focusing through non-homogeneous media. The principle is the analysis of the whole pulse echo responses of an array. The eigenvalues and the eigenvectors of the time-reversal operator (i.e., singular values and singular vectors of the array response matrix **K**) provide information on the scatterers in the insonified medium. Recent experiments showed how DORT can also be used as a characterization method of subwavelength scatterers as elastic cylinders, imbedded in water [Minonzio et al., J. Acoust. Soc. Am. **117** (2), pp 789-798, 2005]. It has been shown that multiple singular values are associated with a single scatterer and that the singular vectors are combinations of the normal modes of vibrations (monopolar, dipolar, quadripolar...). The singular values and the singular vectors of the array response matrix were calculated and experimentally verified.

After a brief presentation of these recent results, we propose to study more precisely the case of small cylinder ($ka < 0.5$), for which the two first normal modes are preponderant. We present experimental results obtained in the MHz range for cylinders of different material and diameters using 128 elements array of transducers. We show that there are two preponderant singular values. They depend on geometrical parameters, and on the cylinder radius a, the compressibility contrast α, the density contrast β between the cylinder and the fluid. We demonstrate that the first singular value is proportional to $k(\alpha + \beta)a$ and the second one is proportional to $k\beta a$. Thus, the linear frequency dependence of the two singular values provides two equations with three unknowns, α, β and a. If one of these three parameters is known (for example, α is about 1 for metals), the two others can be determined.

In the experiment, a calibration is achieved using a known elastic cylinder, which provides a singular value reference level. The geometrical parameters are determined from the phase of the first singular vector. Measurements were carried out for materials of α ranging from 0.6 to 0.99 and β between 0.1 and 1.6. A good agreement between calculated and experimental singular values was observed. These results open a new perspective towards quantitative imaging.

3J-5 3:45 p.m.
COMPENSATION FOR TEMPERATURE VARIATION IN ULTRASONIC CHEMICAL PROCESS MONITORING.

A. KALASHNIKOV*, V. IVCHENKO, R. CHALLIS, and A. HOLMES, University of Nottingham, Nottingham, UK.
Corresponding e-mail: alexander.kalashnikov@nottingham.ac.uk

The monitoring of chemical reactions on the basis of ultrasonic compression wave propagation velocity can achieve sensitivity to changes in chemical composition of the order of 300 ppm [1] provided that the temperature of the reaction vessel does not change by more than a fraction of a degree. The monitoring of exothermic or endothermic reactions can be difficult due to temperature changes in the reaction vessel causing changes in wave speed of similar order to those brought about by the chemical reaction. The use of a separate temperature probe in the reaction vessel enables compensation for these effects although in many circumstances this may not be possible. In this work we have investigated wholly acoustic temperature sensing which avoids the use of a separate probe. The basic monitoring variable was the ultrasonic wave speed obtained from the time of flight (TOF) across the reaction vessel of the received ultrasonic pulse; this was obtained in the pulse-echo configuration, there being an acoustic reflector on the opposite side of the reaction vessel from the interrogating transducer. The principle behind the temperature measurement was to use a thick acoustic reflector and to estimate the wave speed in it - this would be a function of the vessel temperature due to the relationship between the wave speed in the reflector material and its temperature, combined with its thickness expansion. For simple metal reflectors of practical widths this method did not give adequate sensitivity to temperature. However, a compound reflector which incorporated a water filled cavity was found to work well. The high thermal conductivity of the metal part of the assembly ensured thermal equilibrium between the cavity water and the contents of the reaction vessel proper. Individual ultrasonic echoes from the compound reflector corresponded to the reflector front face in contact with the reacting mixture, and from the front and back walls of the cavity. In operation the combined sensor works by computing the TOF/phase velocity from the first echo, and the apparatus temperature from the velocity in the cavity water calculated from the interval between the following two echoes. The apparent wave velocity in the reaction vessel is then corrected for temperature to give the change in velocity attributable to the progress of the chemical reaction. A cavity width of 3mm gave a sensitivity to temperature of 10 time domain samples per degree K when the system sampling frequency was set to 1890 MHz - a temperature resolution of 0.1 K. The new sensor will be used in the first instance to monitor the progress of a number of acid-base titrations, although with further optimization of the compound reflector geometry a broad range of new applications is envisaged.

[1] A.N.Kalashnikov, K.L.Shafran, R.E.Challis, C.C.Perry, M.E.Unwin, A.K.Holmes and V.Ivchenko,

“Super-resolution in situ ultrasonic monitoring of chemical reactions”, *in Proc. IEEE Ultrason. Symp.*, 2004, pp. 549-552.

This research was supported by EPSRC (UK).

Session: 4J
ULTRASONIC MICROFLUIDICS AND BULK EFFECTS
Chair: J. Vig
US Army

4J-1 2:30 p.m.
A SILICON MICROMACHINED ULTRASONIC ATOMIZER BASED ON A LIQUID HORN STRUCTURE.

J. M. MEACHAM*, M. VARADY, A. G. FEDOROV, and F. L DEGERTEKIN, Georgia Institute of Technology, Atlanta.
Corresponding e-mail: levent.degertekin@me.gatech.edu

A micromachined ultrasonic droplet generator is developed and demonstrated for liquid atomization. The droplet generator uses a 1 mm thick bulk ceramic piezoelectric transducer for ultrasound generation, a reservoir for the ejection fluid, and a silicon micromachined liquid horn structure as the nozzle. The pyramidal-shaped horn structures are formed using a simple batch microfabrication process involving wet etching of (100) silicon in a potassium hydroxide solution, and the nozzle openings are defined by dry etching of silicon in an inductively coupled plasma environment. Device operation for various applications is demonstrated by droplet ejection of water, liquid fuels and measles vaccine through 5 -30 μm orifices at multiple resonant frequencies between 1 and 5 MHz. Finite element simulations of the acoustic fields in the cavity and the electrical impedance are in agreement with measurements and indicate that the device utilizes cavity resonances in conjunction with acoustic wave focusing by the horn shaped nozzles to achieve low power operation. Visualization and scaling of drop-on-demand and continuous-jet fluid atomization of water is also presented to elucidate the fluid physics of the ejection process and characterize the modes of operation of the ultrasonic droplet generator. The interactions between focused ultrasonic pressure waves and capillary waves formed at the liquid-air interface located at the nozzle tip are found to govern the ejection dynamics, leading to different ejection modalities ranging from drop-on-demand to continuous-jet [1]. A time scale analysis of the ejection process, which involves period of electrical excitation (process), viscous, capillary and inertial time scales, is used to explain the observed results of high-resolution stroboscopic optical imaging of the liquid-air interface evolution during acoustic pumping and to gain an understanding of the key fluid mechanical features of the ejection process.

[1] J.M. Meacham, M. Varady, F.L. Degertekin, and A.G. Fedorov, “Droplet formation and ejection from a micromachined ultrasonic droplet generator: visualization and scaling,” to be published in Physics of Fluids, 2005.

This work is supported by NASA.

4J-2 2:45 p.m.
AN ULTRASONIC MEMS PARTICLE SEPARATOR WITH THICK FILM PIEZOELECTRIC ACTUATION.

M. HILL*[1], N. R. HARRIS[2], R. J. TOWNSEND[1], N. M. WHITE[2], S. P. BEEBY[2], and J. DING[3], [1]School of Engineering Sciences, University of Southampton, Southampton, U K, [2]School of Electronics and Computer Science, University of Southampton, Southampton, U K, [3]School of Mechatronics, University of Electronics Science&Technology, Chengdu, China.
Corresponding e-mail: m.hill@soton.ac.uk

An ultrasonic resonator has been microfabricated from layers of silicon and Pyrex. A fluid channel of approximately 200μm in depth is etched into the Pyrex and allows particles within the fluid to be moved by acoustic radiation forces into the pressure nodal planes of the ultrasonic standing wave. Depending on the required application this can be used to generate a particle-free fluid sample, to concentrate particles prior to analysis, or to move particles to a surface within the resonator to aid analysis. In previously published work this resonator has been driven using a thickness mode bulk piezoceramic. While this has provided reasonable performance, the adhesion of the piezoceramic plate to the silicon has proved both the least repeatable and the least reliable element of the fabrication process. It has also been a factor in the long-term failure of test devices. To overcome these issues, multilayer thick-film printed actuators have been developed to replace the bulk piezoceramic. Thick-film processing offers an effective means of depositing active materials onto substrates, and the technique is compatible with the microfabrication process, allowing multiple actuators to be printed onto a wafer comprising multiple devices. A variety of structures has been tested on ceramic substrates and shown to provide acceptable acoustic outputs when compared with bulk transducers mounted on identical substrates. A two-layer actuator provides a good performance without excessive complexity and this configuration has been used on the resonator. Further acoustic and flow modelling of the device is described, and this has been used both to improve the channel geometry and to select better operating conditions for the system. It is shown that the thick-film actuated device working at the new operating conditions provides significantly improved performance when compared with the bulk piezoceramic device, and in particular is able to offer a five-fold reduction in concentration for 1μm latex particles, which had previously proved difficult to manipulate successfully.

The authors gratefully acknowledge the help of the Engineering and Physical Sciences Research Council and dstl for funding this work.

4J-3 3:00 p.m.
ULTRASONIC ATOMIZATION USING SILICON-BASED HIGH-FREQUENCY MULTIPLE-FOURIER HORN NOZZLES.

S. C. TSAI[1], Y. L. SONG[2,3], Y. F. CHOU[3], J. H. CHENG[3], N. WANG[2], Y. C. HUANG[2], and C. S. TSAI*[2,3], [1]California State University,, Long Beach, [2]University of California, Irvine, [3]National Taiwan University, Taipei, TAIWAN.
Corresponding e-mail: cstsai@uci.edu

This paper reports on ultrasonic atomization for production of monodisperse drops (mist) and verification of its underlying mechanism. More than 93% of the drops 7.0 μm in diameter were produced using a MEMS-based 0.5 MHz 3-Fourier horn (FH) silicon nozzle 3.66 x 0.38 x 0.11 cm^3 in size. The nozzle is made of a piezoelectric drive section and a silicon-resonator consisting of multiple FHs each with half wavelength in length and magnification of two in longitudinal vibration amplitude [1]. Using the multiple-FH design, a large vibration amplitude gain at the nozzle tip can be achieved with no reduction in the tip cross sectional area for channeling a large flow rate of liquid to be atomized. As water exits from the 200μm x 200μm central channel of the nozzle, a liquid film is maintained at the nozzle tip that vibrates at the resonance frequency of 486.5 kHz and the drive voltage of 5.5 V, resulting in formation of standing capillary waves (SCW) on the free film surface. Temporal instability of these SCW sets in as the tip vibration amplitude exceeds a threshold, and a spray of drops is produced. The vibration amplitude threshold observed is in good agreement with the predicted onset amplitude of the SCW on the free liquid film surface [2]. Thus, the resonance effect of the multiple FHs facilitates the breakup of SCW at the single sub-harmonic frequency generated by the linear electro-mechanical vibration [3]. Monodisperse drops are produced as a result.

Silicon-based ultrasonic nozzles, first realized using MEMS technology at 74 kHz [4], possess a number of advantages over conventional metal-based bulk-type ultrasonic nozzles such as potential for mass production using MEMS technology and the ultrasonic frequency far exceeding the 120 kHz limitation of the bulk-type ultrasonic nozzles. Ultrasonic frequency much higher than 120 kHz is required for production of drops <10 μm in diameter. Drops <10 μm are highly desirable because they can be processed at much lower temperatures and atmospheric pressure, allowing efficient production of nanoparticles. Also, monodisperse drops <10 μm of expensive medicines are particularly desirable because they allow efficient target delivery and alleviate side effects resulting from excess dosage of undesirable drop sizes. Potential applications of such high-frequency nozzles include nanoparticles synthesis, 3-D spray coating for micro electronics, alveolar delivery of medicines, and interfacing with micro-fluidic on-chip reactions.

[1] S.C. Tsai, Y.L. Song, T.K. Tseng, Y.F. Chou, W.J. Chen, and C.S. Tsai, IEEE Trans. on UFFC, 51, 277, 2004.

[2] W. Eisenmenger, Acustica, 9, 327, 1959.

[3] K. Kumar, Proc. Roy. Soc., London, A, 452, 1113, 1996.

[4] A. Lal and R.M. White, Proc. of IEEE Ultrasonics Symposium, 1, 339, 1996.

This work was supported in part by UC Discovery Program, USA and the National Science Council, Taiwan

4J-4 3:15 p.m.
CALIBRATION OF ACOUSTIC RADIATION PRESSURE FIELD INSIDE MICROCHANNELS USING MICROPARTICLE ZETA POTENTIAL MEASUREMENT.

M. ARAZ* and A. LAL, Cornell University, Ithaca, NY.
Corresponding e-mail: mka22@cornell.edu

We have previously presented a low power, small scale ultrasonic excitation of bending waves on a glass capillary microfluidic system by a laser-cut PZT plate [1]. Complex acoustic force field generated by the inertial coupling of standing flexural waves on the capillary body can be used to collect and manipulate cells, silica or polystyrene beads suspended in the fluid. As focusing of particles from 300nm to 10 μm (or larger) size range is possible, separation of particles with respect to size or acoustic impedance is also possible by 2-D radiation pressure fields [1]. While the FEM, and analytical modeling of the actuator dispersion relationships agree with the experimental results for a broad range of frequency regime of the actuation [2], nonlinear affects due to excessive bending leads to parametric excitation of multiple modes, making modeling of acoustic radiation pressure difficult. Since two of the possible proposed applications of the device are controlled biological assays and cell growth in 3-D, a quantitative understanding of the distribution of the radiation force inside the capillary is needed.

Related to the problem given above, we present a new method to estimate the acoustic field inside the capillary. It is known that acoustic radiation force on a spherical object is related to its radius. While radiation force decreases by the size of the particle, small particles collected inside the channel tend to disperse due to Brownian motion and electrostatic interactions of the Debye layer surrounding them. The Debye layer interaction can be quantified by measuring the zeta potential of the suspended particle. While Brownian motion will be only related to the temperature and the viscosity of the suspension, varying the pH of the solution enables control of the zeta potential around the particles. Although, zeta potential change has negligible affect on the acoustic field, it changes the electrostatic interaction between the particles depending on the value of the pH change. In this sense possibility of calculating the dispersion force due to the repelling of charged particles and Brownian motion can be used to estimate the counter balancing ultrasonic force produced by the acoustic field. Our preliminary results show that 500 nm silica beads suspended in pH 7 solution, having about -30mV of measured zeta potential tend to collect in a broader range forming a cloudy structure compared to the same particles in pH 3 solutions. The tightly packed structures form due to smaller zeta potential. The size of the radiation-induced force induced clusters is a sensitive function of the zeta function. Since the radiation force experiments can be run on samples with different zeta potentials, a quantitative value for the radiation forces can be extracted. This extraction procedure and analysis of the limits of the procedure will be presented.

1) M.K.Araz, C.H.Lee, A.Lal, “Ultrasonic Separation in Microfluidic Capillaries” IEEE UFFC, Honolulu, 2003

2) M.K.Araz, C.H.Lee, A.Lal, “Finite Element Modeling of Ultrasonic Separation at the Microscale”,IEEE UFFC, Montreal, 2004

4J-5 3:30 p.m.
IMPROVEMENT IN Q-FACTOR OF AT-CUT QUARTZ CRYSTAL RESONATORS USING SINGLE WALL CARBON NANOTUBES (SWNTS).

A. GOYAL*, S. TADIGADAPA, A. GUPTA, and P. EKLUND, Pennsylvania State University, University Park.
Corresponding e-mail: abhijatgoyal@psu.edu

Use of higher operating frequencies and integration with VLSI circuits and MEMS are driving the need for smaller and thinner quartz crystal resonators (QCRs). Implicit in such scaling is the maintenance of Q-factor of the resonator necessary for achieving the required frequency stability. The intrinsic Q-factor of the resonator is inversely proportional to the resonance frequency, limiting the maximum Q that can be achieved. Recent research in this field has been directed towards attaining as close value as possible to the intrinsic Q in miniaturized QCRs. These include reduction of surface roughness, reduction of support losses by reduction of resonator thickness, making resonator surface convex to increase energy trapping, etc. In this paper we report the first observation of the increase in the quality factor of an AT-cut quartz resonator through deposition of thin layers of SWNTs on its electrodes.

Miniaturized quartz resonators in an inverted mesa configuration were fabricated using Inductively Coupled Plasma (ICP) reactive ion etching with electrode diameters ranging from 100μm to 1mm, and thickness ranging from 33μm (49 MHz) to 90μm (19MHz). This resulted in Q factors ranging from ~500 to ~7500, depending on the geometry of the crystal. The thinner and bigger the crystal, the higher was the value of the Q obtained. An rms surface roughness of less than 2nm was obtained at 350 W of substrate power, 150 W of ICP power, 6 sccm of Ar, 3 sccm of SF6 and a process pressure of less than 3 mTorr. A solution of debundled SWNTs (a mixture of metallic and semiconducting nanotubes procured from Carbolux Inc.) in NMP (N-methyl-2-pyrrolidinone) was prepared. AFM measurements were made to determine the fraction (~80-90%) of SWNTs appearing as single isolated tubes on the substrate. The SWNTs were typically ~1.4nm in diameter and ~ 800nm in length.

Multiple layers of the SWNTs were used causing sequential increase in the Q-factor of the resonator in air and in vacuum, with values of a representative resonator listed in Table as a function of mass of deposited SWNTs. The presence of SWNTs on the surface of the resonator was confirmed using Raman spectroscopy. Equivalent circuit parameters at resonance were extracted and showed a reduction in the motional resistance (Rm) of the oscillator (Table). The quality factor and the amplitude of vibration increased while Rm decreased monotonously when the resonator was kept in vacuum for extended periods of time (24 hours). This is because SWNTs are known to be store house of gases,

desorption of which cause decrease in viscoelastic damping and hence an increase in the Q. Such a process was found to be reversible when the resonators were taken out of vacuum and operated in air.

Gas desorption measurements from SWNTs on micromachined resonators configured as Quartz Crystal Microbalance (QCM) showed femtogram range mass sensitivity owing to their reduced dimensions and increased Q. In addition to the improvement in the Q-factor, SWNTs offer opportunities for functionalization in applications such as (bio)chemical sensors and will be presented in this paper.

Mass of SWNTs (ng)	Resonance Frequency (MHz)		Quality Factor		Motional Resistance (ohms)		Phase Rotation (degrees)	
	Air	Vacuum	Air	Vacuum	Air	Vacuum	Air	Vacuum
0 (As Fabricated)	29.42329	29.42501	579.3	658.06	12084	11004	88.1	96
4.0874	29.41038	29.41268	793.5	900.2	9164.76	8063	103.56	111.63
7.3062	29.40021	29.40476	954	1075.9	7560.88	6784	109.88	115.66
9.5632	29.39223	29.39969	989	1136.6	7346.9	6557	111.55	117.91

4J-6 3:45 p.m.
BULK DETECTION OF SOUND WAVES LAUNCHED BY SURFACE MICROMACHINED BEAM RESONATORS.

S. ARDANUC* and A. LAL, Cornell University, Ithaca, NY.
Corresponding e-mail: sma34@cornell.edu

We investigated the bidirectional coupling between polysilicon beam resonators and an ultrasonic transducer attached to the backside of the die on which the beams were electrostatically actuated. We report on the detection of the sound waves emitted from the anchors of these beams and calculation of the frequency dependent parameters of an equivalent electrical circuit used to represent the overall interaction.

The beams tested were fabricated in the commercial Poly-MUMPS surface micromachining process and consisted of 200 micron long clamped beams with resonance frequencies in the range 200-300kHz and quality factors around 900 at 100mTorr. The ultrasonic transducer used is a 25.4mmx5mmx0.5mm PZT-4 block which was adhesively bonded to die and the circuit board. For one beam, we measured the small signal gain from resonator to the transducer to change from -60dB to -55dB as the polarization voltage used for the electrostatic actuation was increased from 18V to 23V. Spring-mass lumped modeling of the resonator predicts the peak displacement to be between 45nm to 55 nm for this voltage range. Later this mechanical model is incorporated into an equivalent circuit [1] which was generalized to account for asymmetry of the energy loss during the transfer of the power from one port to the other. Parameters of this circuit, which

physically correspond to coupling coefficients, are then extracted from the gain measurements.

This model and experimental setup also allowed us to compare electrostatic actuation and bulk-PZT excitation for a given beam while keeping the capacitive displacement detection scheme unchanged hence leading to a fair comparison for the two actuation methods. We observed considerable difference in piezoelectric actuation of two same type beams which have identical electrostatic response. This indicates the strong position dependency of this type of measurements as well as the room for improvement of piezoelectric actuation against electrostatic actuation by careful placement on the die. Results of this comparison along with the interferometric measurements of bulk vibrations on the die will be detailed in the paper. Possible applications of the piezoelectric pickup scheme to be presented include investigation of anchor loss mechanisms, and optical sensors using self-oscillation [2] without any required wirebond to the die surface

[1] Humad S. etal., “High Frequency micromechanical piezo-on-silicon block resonators”, IEDM 2003, pp:957-960.

[2] Aubin K. etal. ,”Limit Cycle Oscillations in CW Laser-Driven NEMS”, JMEMS 2004, pp:1018-1026.

NSF/IRG-E

NSF/NIRT

Cornell Nanofabrication Facilities

Session: 5J
BAW RESONATOR DESIGN AND ANALYSIS
Chair: E. Schmidhammer
EPCOS

5J-1 2:30 p.m.
OPTIMIZATION OF ACOUSTIC DISPERSION FOR HIGH PERFORMANCE THIN FILM BAW RESONATORS.

G. G. FATTINGER*, S. MARKSTEINER, J. KAITILA, and R. AIGNER, Infineon Technologies AG, Munich, Bavaria, Germany.
Corresponding e-mail: gernot.fattinger@infineon.com

The dominant trend in mobile communication is the reduction of cost and size of the components. Bulk-Acoustic-Wave (BAW) filters are ideally suited to replace conventional RF-filters for all major cell phone standards such as GSM, CDMA and WCDMA. The main advantages are a performance which is unmatched by SAW filters, very low manufacturing costs and the availability of a Wafer-Level-Package.

In order to achieve excellent filter characteristics it is necessary to get rid of the so called “spurious modes”. These are undesired resonances due to the finite

boundaries of the device. This problem can be resolved very efficiently by covering a small portion of the resonator edge with an additional layer, the so called overlap layer. By variation of the width and the thickness of this region, all modes besides the main resonance mode ("piston mode") are suppressed.

However, this scheme only works if the layer stack fulfills some important requirements. The key issue here is to understand the concept of acoustic layer stack dispersion. Basically two types of dispersion relations are possible. The major distinctive feature is the relative frequency position of the longitudinal and the shear resonances. It will be shown, that the overlap scheme can only work with one dispersion type.

Furthermore, the dispersion behavior of the used materials will be discussed. Based on those facts, it can be shown that generally a BAW stack, designed without any precautions regarding the dispersion type will end up with a certain type determined mainly by the piezoelectric material used. Nevertheless, in the case of a SMR (surface mounted resonator) it can be shown, that certain stack modifications can toggle the dispersion type, while maintaining most of the other resonator performance parameters. Electrical and interferometrical measurements will be shown, proving this concept. It will be shown, that without this stack modification a clean response of a high-Q SMR-type BAW resonator is virtually impossible to achieve.

Finally, the basic stack design flow will be outlined and the difference between a successful and an ill-designed resonator stack will be demonstrated using electrical measurements. Moreover, the pros and cons regarding the membrane and the surface mount BAW resonator approach will be discussed with special focus on dispersion type and spurious modes.

5J-2 2:45 p.m.
SUPPRESSION OF SPURIOUS MODES IN MIRROR-TYPE THIN FILM BAW RESONATORS USING AN APPROPRIATE SHAPE OF THE ACTIVE AREA.

A. LINK*[1,2], E. SCHMIDHAMMER[2], H. HEINZE[2], M. SCHMIEDGEN[2], M. MAYER[2], B. BADER[2], K. WAGNER[2], and R. WEIGEL[1], [1]Institute for Electronics Engineering, University of Erlangen-Nuremberg, Erlangen, Germany, [2]EPCOS AG, Munich, Germany.
Corresponding e-mail: andreas.link@epcos.com

Film bulk acoustic resonators (FBARs) have emerged as an important new technology for realization of GHz filter components. They allow a small filter package, a low filter insertion loss and a high filter power durability. Commonly two different technologies are used: bridge-type resonators and mirror-type resonators, so called solidly mounted resonators (SMRs). Bridge-type FBARs are close to the idealized vibrating plate oscillators well known from acoustic resonator theory. They show high quality factors and a high electromechanical coupling, but the needed air interface at both resonator sides complicates the manufacturing process. In contrast fabricating mirror-type FBARs is less critical and can be done nearly with standard CMOS process steps. Here additional layers for an acoustic mirror are necessary, which introduce a more complex

acoustic behaviour and reduce the quality factor and the electromechanical coupling.

Because of the finite resonator dimensions, both bridge-type FBARs and mirror-type FBARs show many unwanted lateral modes beside their main resonance. Like the main mode those lateral spurious modes are standing acoustic waves within the resonator, but they have a non-zero lateral wave number. Filters composed of FBARs, for example bandpass ladder-type filters, suffer from spurious resonator modes: they show a higher insertion loss, a lower bandwidth and several ripples in their passband.

Suppression of lateral spurious resonator modes in bridge-type FBARs by modification of the active resonator area shape has been successfully investigated by applying parallel plate theory. The aim of this paper is to investigate to which extent the same mechanisms can be applied to mirror-type FBARs. By manufacturing and measuring various solidly mounted resonators with distinct shapes and in addition complete filters this question will be answered and the key mechanisms will be identified.

The authors wish to thank the whole EPCOS BAW group for manufacturing test devices and the fruitful discussions.

5J-3 3:00 p.m.
SIMULATION AND EXPERIMENTAL MEASUREMENTS OF HIGH-OVERTONED BULK ACOUSTIC RESONATORS (H-BAR).

S. ALZUAGA*, J.-M. FRIEDT, N. VERCELLONI, J. MASSON, L. ROBERT, N. RATIER, D. GACHON, W. DANIAU, B. GUICHARDAZ, N. BAZIN, and S. BALLANDRAS, FEMTO-ST, CNRS, Besançon, France.
Corresponding e-mail: ballandr@femto-st.fr

During the past twenty years, several acoustic devices have been investigated for filter and source applications. Different kinds of resonators using SAW, SSBAW, BAW have been considered with variable interest considering their skills (i.e performance, cost, complexity, etc). These devices seem to present limitations when the resonant frequency tend to overpass the GigaHertz. The classical techniques of lithography are rising their upper limits in this range of frequencies. Furthermore, the Q.f products obtained are limited to 10^{13}. In this paper, High Overtone Bulk Acoustic Resonators fabricated with different substrates are studied. In the 80s, several papers have emphasized the possibility of HBAR to present high Q at frequencies of several GHz. C-axis normal aluminum nitride (AlN) films were used as a transducer for all the substrates yielding high order longitudinal modes. We have performed simulations of such resonators to optimize their performances. The method used for computation consists in calculating the Green's function of the whole structure, allowing for computing the admittance of the resonator assuming a unit potential excitation applied to the piezoelectric layer. This approach doesn't take into account the finite scale of the electrodes but is able to calculate all kind of contributions and wave polarization in the different layers. The parasitic signals related to the finite dimension of the electrodes are accounted for by finite element

computations. The influence of the electrodes and AlN thickness has been explored. Computational results have been used to matched the thickness with the expected frequency. The performances of the resonators have been also analyzed with regard to temperature from a theoretical point of view. In order to validate the computations, several resonators have been fabricated and tested experimentally. The comparison between calculations and measurements are discussed in the paper. The potential applications of such resonators in term of microwave stabilized sources or filters are examined.

5J-4 3:15 p.m.
SINGLE-CHIP MULTIPLE-FREQUENCY RF MICRORESONATORS BASED ON ALUMINUM NITRIDE CONTOUR-MODE AND FBAR TECHNOLOGY.

G. PIAZZA*, P. J. STEPHANOU, J. P. BLACK, R. M. WHITE, and A. P. PISANO, University of California, Berkeley.
Corresponding e-mail: piazza@eecs.berkeley.edu

This work reports experimental results on a new class of multiple-frequency contour-mode bulk acoustic aluminum nitride resonators that were co-fabricated on the same silicon chip with suspended thin film bulk acoustic resonators (FBAR). The center frequency of this novel contour-mode resonators (either rectangular plates or rings) is set by the in plane dimensions of the device (width of rectangular plate or width of ring) and it is defined lithographically, as opposed to FBAR technology for which the film thickness sets the fundamental frequency. Therefore these contour-mode resonators can span frequencies from 20 MHz up to 650 MHz, showing high-quality factors (2,000-4,000) in air and low motional resistance (50-200 Ω). The same microresonators were arranged in a ladder filter configuration and demonstrated very promising band pass filter response with insertion losses as low as 4 dB at 93 MHz and 8 dB at 236 MHz. The performances of these filters are comparable to the one of commercially available intermediate frequency (IF) SAW filters, but these novel devices provide for 20X reduction in size and improved temperature coefficient of frequency (TCF is -25 ppm/°C versus -35 ppm/°C for uncompensated SAW devices). Also a 224 MHz contour-mode ring resonator was connected in a pierce oscillator circuit, showing phase noise below -110 dBc/Hz at 10 kHz offset, with a power consumption of 3.5 mW. These devices were fabricated on the same substrate with suspended FBAR resonators, which showed quality factors of ~ 2,000 at 1.9 GHz and motional resistance as low as 5 Ω. Substantially we have demonstrated a unique single-chip silicon platform on which the resonant devices can span frequencies in the VHF and UHF range, while maintaining high quality factors and low motional resistance.

The fabrication of these microresonators is based on a simple, four-mask and post-CMOS compatible (Tmax < 400 °C) micromachining process. A thin low-stress nitride is deposited on the silicon wafer to provide for electrical isolation. The thin-film aluminum nitride layer (~ 2 mm thick) is sandwiched between a bottom Pt electrode (patterned by lift off) and a top Al electrode (patterned by dry etching in Cl_2 -based plasma). AlN films are sputter deposited using and AMS PVD tool and show very good rocking curve values (~1.3° FWHM) on the

Pt seed layer. The AlN layer is etched in a Cl_2-based reactive ion etching process, which provides for fairly straight sidewalls (~16° from vertical). The structures are selectively released by removing part of the silicon and low-stress nitride underneath the device using a dry XeF_2 process. This dry release process eliminates stiction forces, therefore reducing yield issues generally associated with wet etching techniques.

The authors believe that this work provides a fundamental step forward towards a single-chip RF module solution in which the resonant devices dedicated to RF and IF filtering and clock functions are all fabricated on the same substrate and could ultimately be integrated with existing CMOS.

5J-5 3:30 p.m.
FINITE ELEMENT ANALYSIS OF MONOLITHIC FILTERS.

M. PATEL* and Y.-K. YONG, Rutgers University, Piscataway, NJ.
Corresponding e-mail: yyong@rci.rutgers.edu

We present a novel approach in selecting the resonator configurations for a monolithic filter based on the results obtained from three-dimensional finite element analysis of the whole filter itself. The primary concern in the design of monolithic filters for high frequency is the complexity involved in tuning control circuits in order to achieve small fractional bandwidths. The bandwidth of the resonating system depends on many parameters but the main parameter affecting the bandwidth is the quality factor of the resonating structure. Thus the performance characteristics of monolithic filters is based on the “energy trapping” in the electrode region and the region between the electrodes (acoustic gap). Here we have studied the performance of the monolithic filters as a function of the energy trapped within the designed structure of electrodes and the acoustic gap.

The design of monolithic filter consists of two or more pairs of electrodes fabricated on a single quartz plate. We have developed a three-dimensional finite element model for a two-port monolithic filter using a 40 MHz AT-cut quartz crystal. In order to understand the acoustical behavior of the monolithic filters, eigen-frequency analysis is carried out for varying aspect ratios of the output and the input electrodes along with varying acoustic gap. Based on these finite element results we present the frequency spectra for monolithic filters which serve as an aid in selecting the resonator configurations. Frequency response curves with the desired bandwidth are then obtained for the determined resonator configurations.

5J-6 3:45 p.m.
AN ISOPARAMETRIC SPLINE METHOD FOR THE VIBRATIONS OF PIEZOELECTRIC RESONATORS.

S. SRIVASTAVA*, Y.-K. YONG, and M. PATEL, Rutgers University, Piscataway, NJ.
Corresponding e-mail: yyong@rci.rutgers.edu

A new method of analysis for piezoelectric resonators and filters is presented: an Isoparametric Spline Method (ISM). The method has certain advantages over the finite element method which is now the most widely used method for the analysis of piezoelectric resonators and filters. One immediate advantage of our isoparametric spline method is that it uses the same spline functions and control data employed in the prototype CAD (computer aided design) drawings of resonators and filters. A pre-processing finite element graphical software would be needed to produce a separate finite element mesh model of the prototype if the finite element method analysis was used. The process of creating a finite element mesh could be a tedious and time consuming task, especially if the prototype has a complex geometry with many parts. Our isoparametric spline method would not need a separate mesh, but would instead use directly the existing CAD data.

The Non-Uniform Rational B-Splines (NURBS) are most commonly used for representation of curves, surfaces and volumes in CAD drawings. NURBS basis functions which demonstrate the variation diminishing property when performing interpolation over discontinuous data have a distinct advantage over the finite element Lagrangian shape functions that show heavy oscillations when interpolating discontinuous data. This could induce inaccuracies in modeling high frequency vibration modes such as the thickness shear mode and its harmonic overtones in quartz plate resonators. Also, since the actual geometry is modeled when using NURBS basis functions there is an overall reduction in the minimum size of problem required to accurately model the quartz resonators. This reduces the overall memory required. Thus, the isoparametric spline method for analysis of piezoelectric quartz resonators provides us with a viable alternative to the conventional finite element methods whilst consuming less memory and providing more stable and accurate results. The term isoparametric refers to the use of the same NURBS basis functions for interpolating the mechanical displacement and electric potential variables as those for the geometry. The theory and derivations of an isoparametric spline method are presented. Numerical results for the frequency spectra and vibrations mode shapes of AT-cut quartz resonators using the isoparametric spline method and finite element method are compared and presented. Also, the numerical results are in good agreement with the experimental results, and the comparisons are presented.

Session: 6J

BEAMFORMING II
Chair: K. Thomenius
GE

6J-1 2:30 p.m.
MINIMUM VARIANCE ADAPTIVE BEAMFORMING APPLIED TO MEDICAL ULTRASOUND IMAGING.

J. SYNNEVAAG*, A. AUSTENG, and S. HOLM, Department of Informatics, University of Oslo, Oslo, Norway.
Corresponding e-mail: johanfr@ifi.uio.no

Medical ultrasound images are in practice always formed using a delay-and-sum beamformer. The beamformer supresses energy from all off-axis directions without consideration of the actual wavefield recorded, limiting the achievable resolution. Adaptive methods attempt to increase resolution by adaptively selecting complex weights on the array elements, placing zeros in directions of interfering reflections, and allowing large sidelobes in directions where there is no energy. We propose a way to enable use of the amplitude-preserving version of the minimum variance (MV) adaptive beamformer in medical ultrasound imaging. The broadband nature of ultrasound acquisition prevents direct use of the beamformer as it was derived for narrowband signals, since propagation delays between array elements can not be expressed as a vector of complex exponentials. Our method consists of prefocusing in the direction of the transmitted beam, aligning reflections from that direction, and then applying the minimum variance beamformer to each time sample. This broadband version does not suffer from the limitations of its narrowband counterpart, which is unable to resolve coherent signals. However, the few samples available for estimating the covariance matrix required in the method gives a poorly conditioned matrix. Preprocessing the data by spatial smoothing solves this problem: The transducer array is divided into sub-apertures which are averaged to form the sample covariance matrix, increasing its rank.

We have demonstrated the performance of the MV beamformer on both simulated and experimental data. We simulated a 4 MHz, 96 element transducer, imaging a number of pairwise reflectors located at depths ranging from 30 to 80 mm. The MV beamformer shows superior performance compared to the conventional delay-and-sum: The -6 dB beamwidth is reduced by at least a factor 4 for all targets. For the closest reflectors the maximum side-lobe level is reduced by between 5 and 10 dB. For the deepest targets where resolution is poorest, the targets are only resolved by 3 dB for delay-and-sum, but are still resolved by 15 dB for the MV beamformer.

We also applied the method to an experimental RF data-set from a heart-phantom acquired with a 64 element, 3.5 MHz transducer. The narrow beamwidth and low sidelobes of the MV beamformer results in sharper edges in the final image, which is seen by improved definition of the ventricular walls.

Because of the high resolution of the MV beamformer at high SNR, a large number of scan lines may be required to avoid angular undersampling and ensure reliable amplitude estimates. Several methods exists where some resolution is sacrificed to gain robustness in the amplitude estimates, avoiding an exhaustive scan. These methods do not fully capture errors in assumed acoustic velocity since they were derived for far-field conditions, and ultrasound data are acquired in the extreme near-field. However, initial studies on robustness shows that the MV beamformer performs well when the velocity estimate errors are small.

6J-2 2:45 p.m.
EXPERIMENTAL COMPARISON OF THE (LINEAR) 2F FIELD TRANSMITTED WITH FULLY REALIZED TWO-DIMENSIONAL EFFECTIVE APODIZATION AND THE (NONLINEAR) 2F HARMONIC FIELD.

J. MILLER*, T. KRUEGER, M. HOLLAND, and K. WALLACE, Washington University in St Louis, Saint Louis, MO.
Corresponding e-mail: kirk.wallace@wustl.edu

BACKGROUND: Phase and amplitude variations resulting from propagation through aberrating media such as chest or abdominal walls appear to be the source of significant degradation of diagnostic ultrasound images, especially in obese patients. Nonlinear (harmonic, 2f) imaging often results in improvements in image quality relative to that obtained with linear (fundamental, 1f) imaging. Results presented at previous IEEE Ultrasonics Symposia demonstrated that, in a non-aberrating medium, the field obtained by transmitting (linearly) at 2f with an “effective apodization” applied only in the azimuthal direction with a 1D transmitting array produces a field in the azimuthal plane that is nearly identical to the field generated at 2f by a finite amplitude signal originally transmitted at 1f. However, this 1D approximation to the 2D effective apodization is not adequate in the presence of significant aberration, presumably because the aberrators compromise the independence of the azimuthal and elevational planes. OBJECTIVE: The goal of the present work is to design and construct mechanical apodization plates to permit a fully-realized two-dimensional effective apodization and to investigate the resulting ultrasonic fields. METHODS: Matched pairs of precisely contoured lossy apodization plates were constructed of RP-6410 polyurethane (Freeman Manufacturing & Supply, Avon, OH). One plate from each pair was tapered more aggressively to achieve the effective apodization corresponding to the nonlinearly generated 2f field resulting from the application of the other. Results of our measurements on flat and parallel control specimens indicate that this polyurethane has a 1.04 g/cm^3 mass density, 1550 m/s speed of sound, and attenuation coefficient of 22.3 dB/cm at 1f = 2.3 MHz and 62.2 dB/cm at 2f = 4.6 MHz. The two-component liquid precursor of the solid polyurethane is cast in aluminum molds that are machined (to a tolerance of better than 1%) to the dimensions describing the apodization profiles. The two-dimensional apodizations were achieved by affixing each plate to the face of a circular cross-section, planar, broadband transducer of 3.5 MHz center frequency (-6 dB bandwidth 2.2 to 5.5 MHz). RESULTS: One matched pair of plates consisted of

a rectangular window apodization and the corresponding effective apodization. Detailed measurements of the resulting ultrasonic fields were obtained by scanning a point-like receiver in transverse planes at both 3.6 cm and 6.0 cm from the source to mimic a two-dimensional receiving array of 61 by 61 elements at 0.5 mm spacing. These measurements were in good agreement with results predicted by a previously described Burgers equation enhanced, nonlinear angular spectrum simulation tool. CONCLUSIONS: For plates approximately 1 cm in thickness, measurements of the difference in signal strength between the center and the outer edge of the apodized source demonstrate the feasibility of this approach for achieving the desired two-dimensional apodization using plates of realistic dimensions.

NIH R01 HL072761

6J-3 3:00 p.m.
APPLICATION OF A CYSTIC CONTRAST BASED RESOLUTION METRIC TO GUIDE ULTRASOUND SYSTEM DESIGN.

K. RANGANATHAN*[1] and W. WALKER[1,2], [1]Dept. of Biomedical Engineering, University of Virginia, Charlottesville, VA, [2]Dept. of Electrical and Computer Engineering, University of Virginia, Charlottesville, VA.
Corresponding e-mail: kr6u@virginia.edu

We have previously described a metric that characterizes the 3D spatial resolution of broadband ultrasound systems [1]. Resolution is expressed as the size of a spherical anechoic cyst, embedded in a speckle-generating medium, that is required to generate a specified contrast. The contrast of the cyst relative to the background depends on the ratio of the system point spread function (psf) energy outside the cyst to the total psf energy.

In this work, we extend our formulation to include the effect of electronic noise. We then apply it to guide the design of a low-cost, C-scan system being developed at the University of Virginia, demonstrating the utility of our formulation in the optimization of system parameters. It is difficult to optimize parameters using beamplots or psfs because each set of parameters yields a multidimensional (up to 4D) response that is hard to interpret. In comparison, our formulation yields a single curve for each set of parameters that characterizes the cystic contrast as a function of cyst size. Using our formulation, parameter optimization reduces to the straightforward task of picking the value that yields the maximum contrast at the cyst size of interest, or alternatively the value that yields the required contrast with the smallest cyst. We simulated the impact of electronic noise, quantization in the analog to digital converter (ADC), f/#, apodization, and crosstalk on our current prototype system. Since we are primarily interested in cysts of radii between 1.5 to 2.5 mm for our system, we chose the parameter values that combined maximal contrast at this range of cyst sizes with the least associated system complexity and cost.

We evaluated the impact of electronic noise on our system by varying the SNR per channel from -10 dB to +20 dB. We also quantified the tradeoffs associated with quantization by using bit precisions ranging between 6 and 16 bits per real

sample. We optimized the f/# by investigating the effect of f/#s between 0.75 and 1.75. The individual and combined effects of acoustic crosstalk (experimentally determined to be -25 dB with a delay of 215 ns on the nearest neighbor) and electrical crosstalk (assumed to be -25 dB on the nearest neighbor) were examined. Finally, we investigated the effect of apodization by evaluating some windows commonly used in signal processing.

The results of our analyses indicate that an SNR of 0 dB per channel, along with 10 bit precision, yield adequate image quality in our system. Higher f/#s yield better contrast for large cysts, but lower contrast for small cysts; an f/1 system is a good compromise across the cyst sizes of interest. The Nuttall window yields the best contrast among the investigated apodization windows. Crosstalk reduces the detectability of small cysts and increases the detectability of large cysts, but has a surprisingly negligible overall effect.

[1] K. Ranganathan and W. F. Walker, “A new performance analysis metric for medical ultrasound,” Proc. IEEE Ultrason. Symp., vol. 3, pp. 23-27, 2004.

Acknowledgements - NIH grant EB002349 and US Army CDMRP awards DAMD17-01-1-0443 and W81XWH-04-1-0590.

6J-4 3:15 p.m.
ABERRATION ESTIMATION USING FDORT: INSIGHTS AND IMPROVED METHOD FOR SPECKLE SIGNALS.

J.-L. ROBERT* and M. BURCHER, Philips Research USA, Briarcliff Manor, NY. Corresponding e-mail: jean-luc.robert@philips.com

Clinical ultrasound imaging is degraded by tissue velocity inhomogeneities that reduce resolution and contrast. The Focused DORT (French acronym for decomposition of the time reversal operator) method, here denoted FDORT, was presented last year as an aberration estimation method. FDORT uses per-channel received RF data obtained from several focused transmissions. An aberration profile is estimated using a singular value decomposition method. The advantage of FDORT over a cross-correlation based method was its ability to identify individual wavefronts in complex RF regions. Both methods exhibit good results with point targets but significant residual rms errors (between applied and estimated aberrator) in speckle regions (typically 15ns for a 45ns aberration). This study aims to explain the behavior of FDORT in speckle and the origin of the error (consisting of a bias and a variance). This explanation is then used to improve the method; reducing both the bias and variance of the estimation.

In speckle, the FDORT matrix can be interpreted as a cross-spectrum matrix of the backscattered signal. Masoy et al. [JASA 117 (1) 2005] obtained a similar matrix that required different realizations of the speckle medium. By contrast, FDORT averages over different transmissions in the same medium, and is therefore compatible with medical ultrasound data. Originally, the first singular vector was used for the estimation: it contained the amplitude and delay law that maximized the speckle brightness. The origin of the bias can be explained using the van Cittert Zernike theorem: it results from the fact that the transmit itself is aberrated. We propose a method to reduce the bias to a linear shift by using a combination of all eigenvectors. A new scheme is introduced to reduce

the variance: for each transmit, it uses the signal originating not only from the focal depth but also from several different depths. This modification typically reduces the variance by a factor of 2. Finally, we introduce a non-biased estimator by forming a tensor from a full synthetic aperture data set. Its first singular vector maximizes the speckle brightness by correcting both transmit and receive - this is equivalent to an FDORT estimation when the aberration is completely corrected in transmit and provides the lowest error.

We performed Field-II (Jensen) simulations using a 45ns, 4mm FWHM near-field phase screen on a speckle phantom with point targets and cysts. This aberration reduces the cyst contrast from 23 dB (non-aberrated) to 4 dB (aberrated). After receive-only correction, cyst contrast is 16 dB using the 1st eigenvector (original FDORT implementation), 19 dB ns for the linear combination, 19 dB for the tensor, and 14 dB for a correlation-based method. The residual rms errors are 17 ns, 4 ns, 2 ns, and 15 ns respectively. In-vivo aberration estimation results are also presented. The theoretical understanding of the speckle behavior in FDORT has led to improved performance and further insights into using statistical-based approaches for aberration measurement.

6J-5 3:30 p.m.

BEAMFORMING USING SPATIO-TEMPORAL FILTERING.

J. LIU*, K. KIM, and M. INSANA, University of Illinois at Urbana Champaign, Urbana, IL.
Corresponding e-mail: liujie@uiuc.edu

Roger Zemp showed last year that (Wiener) spatial filtering (SF) of unfocused echo signals in the nearfield of low f-number apertures is an ideal beamforming strategy for detecting low-contrast lesions. The advantages of SF over dynamic receive focusing (DRF) include greater echo signal-to-noise ratio (eSNR) and improved lateral resolution. Disadvantages include sidelobe growth and a loss of eSNR gain in the farfield. Performance of SF beamforming exceeds that of DRF when the pulse-echo impulse response (IR) function is known so that sidelobes are minimal and the space-bandwidth product is larger than one for improved eSNR. Temporally coded pulses enhance eSNR at all depths, but generate the lowest range sidelobes in the farfield. Temporal codes are distorted in the nearfield of low f-number apertures, unless filtering is applied to individual receive channels. In this paper we combine the best of both techniques with the goal of enhancing low contrast breast lesion visibility. Beamforming is achieved in the nearfield by transmitting standard broadband pulses and matched filtering the received echoes with a depth-varying IR. In the farfield, phase-modulated codes are transmitted, DRF is applied, and the beamformed echoes are decoded using an inverse filter.

Data were recorded from a Siemens ANTARES system with the VF10-5 linear array transmitting a 10 MHz base sequence. The short pulse and 7-bit and 15-bit Barker coded pulse sequences transmitted were programmed into the Antares pulser. The URI provided echo data summed across the aperture. Performance was measured using lateral beamwidth, contrast and contrast-to-noise ratio (CNR) estimates.

An ATS phantom was scanned to compare the performance of beamforming with the spatio-temporal filter (STF) to conventional DRF. We found that STF images had superior spatial resolution compared to DRF images. Far from the focal region, the -6dB beamwidth of the image was reduced by a factor of 3 at 20mm and by a factor of 2.5 at 30mm. The matched filter increased sidelobes by 10 dB, which lowered CNR from 2.36 for DRF to 1.81 for STF for lesion targets >4mm. However, for smaller targets, where visibility is limited by spatial resolution, the STF images outperformed DRF images. The contrast and CNR of 2mm cyst targets were 0.63 and 1.96 for STF images but only 0.28 and 0.67 for DRF images. In the far field, the 7-bit Barker code reduced noise and increased penetration 1 cm. Lengthening the code length to 15 bits increased penetration another 1 cm and enabled us to clearly visualize the deepest cysts.

Experimental results clearly show improved spatial resolution and increased penetration over conventional beamforming techniques with some loss of contrast for targets larger than 4mm. These improvements are worthwhile for enhancing breast lesion detection on an early stage. The technique is also promising for higher frequency imaging where electronic beamforming is difficult and frequency dependent attenuation is large.

6J-6 3:45 p.m.
SPATIAL COMPOUNDING WITH TISSUE HARMONIC IMAGES AND MONOSTATIC SYNTHETIC APERTURE RECONSTRUCTION.

M. ASHFAQ, C. HANSEN*, W. WILKENING, and H. ERMERT, Institute of High Frequency Engineering, Ruhr-University Bochum, Bochum, Germany.
Corresponding e-mail: mohammad.ashfaq@rub.de

Background: A high precision mechanical add-on system was realized to implement a tomography system around a commercial ultrasound system. A Siemens Antares was used for this work, which allows the acquisition of RF data of high quality B-scans and tissue harmonic imaging (THI) over the Axius Direct Ultrasound Research Interface (URI). This possibility was exploited to explore some more intricate processing options. One of the two new strategies for compounding consists of calculation of a compound image from the THI data, as the latter is known to possess a better contrast and lateral resolution. While the RF data acquired from various transducer positions provides all the necessary input for monostatic synthetic aperture focusing (SAFT), the other strategy was to implement SAFT imaging.

Methods:

Experimental Setup: A Siemens Sonoline Antares equipped with URI was used for data acquisition providing 16 bit beamformed data at 40 MHz sampling rate. A convex array (C5-2, 3.5 MHz center frequency driven at 2.22 MHz and 50° field of view) was used. Three focal zones per image were set to 2, 4 and 6 cm, respectively. The range for data acquisition was set from 1.5 to 8 cm. The transducer was rotated about the object with a computer controlled servo-motor whilst the data acquisition was triggered with the Physio module over the LPT port of the same PC. At each transducer position, one frame in THI-mode using the phase inversion technique was taken.

Data Analysis: Each recorded data frame contained 6 RF echoes per line (3 foci, 2 pulses with 0° and 180° carrier phase). Focal zone blending was applied after envelope detection. In THI-mode, phase inversion echo pairs were summed before envelope detection, in B-mode thereafter. For the SAFT reconstruction, the RF data was quadrature demodulated to base-band. The phase of the complex signals was corrected to account for different path-lengths prior to summation. SAFT images were reconstructed with and without phase inversion. The problem arose that phase aberrations introduce severe interference artifacts. Thus, a standard compound image formed from data after envelope detection served as a reference for realignment of the base-band data. This procedure does not correct geometric distortion but reduces interference artifacts.

Results: Scanning of a wire phantom, a boiled egg, and a porcine kidney showed that THI-mode-compounding outperformed the standard compounding. The strong depth dependence of THI was leveled out by the tomographic approach. Expectedly, THI images improved the resolution by a factor of 1.5 in average. SAFT imaging without phase inversion resulted in the best resolution but was sensitive to incorrect calibration of the system and to phase aberrations that occurred in the kidney. THI SAFT turned out to be unreliable. This is easily explained by different harmonic signal generations due to different paths leading to interference artifacts.

This work is an activity of the Ruhr Center of Excellence for Medical Engineering Bochum (KMR), funded by the German Federal Ministry of Education and Research (bmb+f grant #. 01EZ0206)

Session: 1K

3D/4D CARDIAC IMAGING
Chair: T. Thomas
Siemens

1K-1 4:30 p.m.
DYNAMIC 3D ECHOCARDIOGRAPHY IN VIRTUAL REALITY.

A. VAN DEN BOSCH*[1], A. KONING[2], J. MCGHIE[1], F. MEIJBOOM[1], P. VAN DER SPEK[2], and A. BOGERS[3], [1]Department of Cardiology, Erasmus MC, Rotterdam, The Netherlands, [2]Department of Bioinformatics, Erasmus MC, Rotterdam, The Netherlands, [3]department of Thoracic surgery, Erasmus MC, Rotterdam, The Netherlands.
Corresponding e-mail: a.e.vandenbosch@erasmusmc.nl

Background: Objective three-dimensional echocardiographic images of the heart greatly facilitate the diagnosis of unknown and complex pathology. However, its full 3D potential cannot be used in the currently available setting, since the 3D data can only be presented on a flat 2D screen. Virtual dynamic techniques, known as virtual reality, can assist with the interpretation of 3D echocardiographic images of the heart.

The purpose of this study is to evaluate 1) the feasibility to visualise 3D echocardiographic data in a virtual reality and 2) if the 3D echocardiographic heart model has the potential to advance virtual reality visualization to a clinically useful tool for the planning of cardiac interventions.

Methods: 3D echocardiographic data sets from 2 normal subjects and from 4 patients with a mitral valve pathological condition were included in the study. The 3D data sets were acquired with the Hewlett-Packard Sonos 7500 echo-system. The cartesian 4D image data was stored on CD-ROM in DICOM 3.0 format and

transferred to the SGI Onyx4 UltimateVision computer driving the I-space. The BARCO I-space is installed at the Erasmus MC. To investigate the time series of 3D ultrasound images, we used the CAVORE (SGI OpenGL Volumizer library) volume rendering application. In the I-space all this results in an animated "hologram" of the dataset being visualized, floating in space in front of the viewers. With a stylus tracker, the hologram can be turned in every desirable angle and a clip plane tool cuts away the part of the model between the user and the clip plane. This is performed in real-time, and the clip plane can be freely chosen. Ten independent observers assessed the six 3D data sets with and without mitral valve pathology.

Results: After 10 minutes instruction in the I-Space, all of the observers could use a stylus tracker and make the necessary cut planes in the hologram. We found that in the normal heart, tilting of the hologram leads to better perception of mitral valve motion. In the generated 3D hologram of a patient with localised prolaps of the posterior leaflet, the mitral valve is seen from a left atrial view, the exact localisation of the prolaps of the posterior mitral valve leaflet was easy visualised. Within 10 minutes, the 10 independent observers correctly assessed the normal and pathological mitral valve in the holograms.

Conclusion: The present report of the use of dynamic holographic imaging in patients with normal and abnormal mitral valve function demonstrates the feasibility, applicability and use-fullness of this technology in clinical cardiology, particularly in valve disease, for which the visual perception of motion is fundamental in making the correct diagnosis. Virtual reality is a novel approach for visualization of dynamic 3D echocardiographic data.

1K-2 4:45 p.m.
A NOVEL DYNAMIC PROGRAMMING BASED SEMI-AUTOMATIC ENDOCARDIAL BORDER DETECTION METHOD FOR 4D CARDIAC ULTRASOUND.

M. VAN STRALEN*[1,3], M. M. VOORMOLEN[1,2], G. VAN BURKEN[1,3], B. J. KRENNING[1], R. J. M. VAN GEUNS[1], E. ANGELIÉ[3], R. J. VAN DER GEEST[3], C. T. LANCÉE[1], N. DE JONG[1,4], A. F. W. VAN DER STEEN[1,2], J. H. C. REIBER[2,3], and J. G. BOSCH[1,3], [1]Thoraxcenter, Erasmus Medical Center, Rotterdam, The Netherlands, [2]ICIN, Interuniversity Cardiology Institute of the Netherlands, Utrecht, The Netherlands, [3]Leiden University Medical Center, Leiden, The Netherlands, [4]University of Twente, Enschede, The Netherlands.
Corresponding e-mail: marijn.vanstralen@erasmusmc.nl

Background: Quantification of left ventricular (LV) volume and function is a clinically important and common task. 3D ultrasound (3DUS) can provide quick access to these important diagnostic values, provided that suitable analysis tools are available. We propose a semi-automatic endocardial border detection method for LV volume estimation in 4D (3D + Time) cardiac ultrasound images requiring minimal user interaction. We compare our results with MRI.

Methods: Cardiac apical ultrasound images are acquired with our own developed fast rotating ultrasound (FRU-) transducer and recorded with a GE/VingMed Vivid 5 ultrasound system. Images are acquired at 1.8 MHz, at ~ 100 frames/s over 5 - 10s with a rotation speed of 240 - 480 rotations/s. ECG is recorded simultaneously. Our method exploits the relatively high resolution in individual images of this 3DUS technique, but is generally applicable to other techniques, like matrix array transducers. Detection is performed in an optimal subset of images at a number of equidistant rotation angles and cardiac phases, selected using multi-beat fusion.

From four manually drawn contours (in approximately 2- and 4-chamber views in end-diastole and end-systole), models for LV shape and endocardial edge pattern are generated. Using these models, optimal contours are detected in all the images by applying pattern matching of the edge patterns from the model, constrained by the LV shape model by using dynamic programming. The 3D endocardial surface is then reconstructed from the detected contours, resulting in full-cycle LV volumes. Corrections can be applied to the detected contours if needed, which improve the shape and edge pattern models for the redetection and iteratively result in a superior detection.

We evaluated the method by comparing results on 10 patients, with semi-automatic tracings of short-axis MRI images of the same patients. MRI was traced independent from the 3DUS study by one observer. 3DUS was traced by two observers independently. We compared the average of the two 3DUS observers against MRI on full-cycle LV volumes, and the interobserver variability between the two 3DUS observers.

Results: Good correlations were found between 3DUS and MRI tracings without (r=0.92, y=0.68x - 32.9 ml) and with corrections (r=0.94, y=0.72x - 30.3 ml). A low interobserver variability was found between the 3DUS observers without (r=0.94, y=1.08x - 16.0 ml) and with corrections

(r=0.94, y=1.11x - 16.8 ml).

Conclusions: Our method provides precise full-cycle volumes requiring little user interaction. Although correcting contours visually improved the detection, quantitative results did improve only slightly. Systematic differences were found with and without applying corrections against MRI volumes. 3DUS tends to estimate lower MRI volumes well, but under-estimates larger MRI volumes. This may be caused by differences in tracing conventions between MRI and 3DUS, or by the different views in which was traced: apical long-axis for 3DUS vs. short-axis for MRI.

This work has been supported by the IOP (Dutch Ministry of Economic Affairs IBVC02003)

1K-3 5:00 p.m.

REAL TIME VOLUME STITCHING IN 4D ECHOCARDIOGRAPHY.

S. BREKKE*[1], S. RABBEN[2], E. STEEN[2], G. HAUGEN[2], A. HAUGEN[2], and H. TORP[1], [1]Norwegian University of Science and Technology, Trondheim, Norway, [2]GE Vingmed Ultrasound, Horten, Norway.
Corresponding e-mail: svein.brekke@ntnu.no

Three-dimensional (3D) echocardiography is challenging due to limitation of the data acquisition rate caused by the speed of sound. When recording data with a 2D array probe at a rate of 30 volumes per second at a depth of 12 cm, approximately 6400 pulse firings may be done to acquire each volume. This only suffices to a 15 by 15 beams volume data set yielding approximately one beam per cm in lateral direction at depth 10 cm in a full scan of the left ventricle - a resolution inadequate for clinical use. Multi-line acquisition with four parallel beams would double the beam density, but it would still result in poor image quality.

The aim of this work was to provide adequate frame rate in real time 3D ultrasound imaging and to avoid geometrical distortion of the images due to time lag between ultrasonic pulses within one data volume.

We present a volume stitching algorithm that merges data from N (2 to 10, typically 4) consecutive heart cycles into a volume data set. The data from each cycle was taken from a different 3D position. Only the merged data was shown on the display, and both stitching and presentation were performed in real time during scanning. The change in the 3D scan position was triggered by the R-wave detected from the patients ECG signal. The stitching algorithm was implemented in the Vivid 7 Dimension scanner from GE Health Care.

In-vivo, stitched volume data acquired over 2, 4 and 8 cycles were compared to unstitched data, and an evident gain in image quality was demonstrated.

One of the promised achievements of 3D ultrasound compared to 2D, is more reliable volume measurements of the left ventricle. However, with frame rates as low as 10 frames per second, the geometrical distortion within one single 3D volume may become substantial and affect the volume measurements. To investigate errors in volume estimates, synthetic ultrasound data was created by applying realistic scan patterns at a kinematic model of the left ventricle. Stitched data sets filling a 64 by 64 pyramidal volume were created with 2, 4 and 8 cycle scan patterns, yielding three data sets with realistic time lag between beams and volume rates of 12, 24 and 48 volumes per second. Volume measurements were performed on each frame in each data set with the EchoPAC software application from GE Health Care, and the measured volumes were compared to the true volumes of the model.

The measured volumes showed good agreement with the true volumes at 48 volumes per second (average error: 2.5%, peak difference: 6.6% over-estimation), not quite as good agreement at 24 volumes per second (average error: 4.2%, peak difference: 9.7% over-estimation) and poor agreement at 12 volumes per second (average error: 17.0%, peak difference: 49.7% over-estimation).

We conclude that real time stitching is an adequate technique for increasing frame rate in 4D ultrasound imaging at a given spatial resolution, and that the volume estimation errors due to geometrical distortion decreases substantially for data with higher volume rate.

1K-4 5:15 p.m.
IMPROVED SPATIOTEMPORAL VOXEL SPACE INTERPOLATION FOR 3D ECHOCARDIOGRAPHY WITH IRREGULAR SAMPLING AND MULTIBEAT FUSION.

J. G. BOSCH*[1,3], M. VAN STRALEN[2,3], M. M. VOORMOLEN[1,2], B. J. KRENNING[1], C. T. LANCÉE[1], J. H. C. REIBER[3,2], A. F. W. VAN DER STEEN[1,2], and N. DE JONG[1,4], [1]Erasmus MC, Rotterdam, The Netherlands, [2]ICIN, Utrecht, The Netherlands, [3]LUMC, Leiden, The Netherlands, [4]University of Twente, Enschede, The Netherlands.
Corresponding e-mail: j.bosch@erasmusmc.nl

Background: A fast rotating linear array can be used to acquire images of the left ventricle covering 3D space over the full cardiac cycle in near-real time. Image quality within the 2D image planes is superior to matrix array transducers, but these planes are spread sparsely and irregularly over space and time. We developed a novel spatiotemporal interpolation technique to tackle the complex problem of generation of optimal voxel sets.

Methods: Cardiac apical images are acquired with a fast rotating ultrasound (FRU) transducer developed in our laboratory and recorded with a GE/VingMed Vivid 5 ultrasound system. Images are acquired at ~100 frames/s over 5-10 seconds with a rotation speed of 240-480rpm. ECG is recorded simultaneously. After acquisition, exact rotation angle and cardiac phase (time offset from R-peak) is calculated for each 2D image frame. Due to the fast rotation and varying beat length, individual 2D images have a complicated 3D shape and beams are irregularly distributed over rotation angle and cardiac phase. We developed a novel multi-beat fusion technique using a special 4-dimensional (3D+time) interpolation for sparse, irregularly sampled data (ISI), giving 3D image quality superior to classical techniques, and reducing motion artifacts. The technique is parallelizable and suitable for fast implementations. ISI was tested quantitatively by simulations on synthetic data of a pulsating ellipsoid representing the beating left ventricle. It was compared to spatiotemporal nearest neighbor interpolation (STNI). From the synthetic data, spatiotemporal sampling errors D of both methods were calculated by sampling a distance function from the beating ellipsoid's surface and subtracting the true (known) distance at the exact desired time and spatial position. Target resolutions for the rotational image sets were 32 angles and 32 phases within the cardiac cycle (resolutions of about 11 degrees, 25 ms). ISI voxel space generation was tested qualitatively on a phantom and in-vivo cardiac images of 10 patients, compared to a classical temporal binning with spatial trilinear voxel interpolation.

Results: Nearest neighbor sampling showed temporal errors of -1.1 ± 13.8 ms (mean ± standard deviation) and angular errors of -0.2 ± 4.8 degrees. Mean and

SD of absolute errors were 10.2 ± 9.4 ms and 3.8 ± 3.0 degrees, respectively. From the synthetic data simulations, ISI showed distance errors D of 0.16 ± 1.95 mm ; this was considerably lower than for STNI (D=0.31 ± 4.58 mm). Absolute distance errors were 1.23 ± 1.52 mm for ISI vs. 3.45 ± 3.03 mm for STNI. In the in-vivo images, the resulting voxel sets showed reduced motion artifacts, suppression of noise and interpolation artifacts and better delineation of structures.

Conclusion: The proposed interpolation technique (ISI) improves the quality of 3D+T images acquired with a fast rotating transducer in simulated and in-vivo data. The technique may also prove useful in similar cases where multibeat fusion, irregular sampling and/or phasic motion artifacts induce image errors, e.g. freehand 3D ultrasound.

1K-5 5:30 p.m.
AN OPTICAL REGISTRATION METHOD FOR 3D ULTRASOUND FREEHAND SCANNING.

C. POULSEN*[1], P. PEDERSEN[1], and T. SZABO[2], [1]Worcester Polytechnic Institute, Worcester, MA, [2]Boston University, Boston, MA.
Corresponding e-mail: pedersen@ece.wpi.edu

Three-dimensional ultrasound is emerging as an important adjunct to conventional 2D scanning, in particular in obstetrics and cardiology. 3D scanning can be implemented with a mechanically scanned array transducer or with a 2D array, both confined by a limited field of view. Alternatively, 3D ultrasound can be carried out as free hand scanning, which can be augmented with a registration system in the form of an optical or EM source, mounted on the transducer and corresponding sensors placed in the room. In terms of portable ultrasound, free hand scanning is the only practical way to acquire 3D scans.

This paper presents a new and very compact type of optical registration system, which tracks a position of the transducer on the skin surface. The motivation for the 3D registration system is to develop a portable ultrasound system with better visualization capabilities for trauma injuries. A CCD array captures an image of a small area (typically 1 mm^2) of the skin 1500 times per second, and the sequence of images are continuously cross-correlated to yield the relative position of the ultrasound transducer. The implementation is based on an optical fiber bundle with associated lenses, which couples image information at the skin surface to the CCD array, and an LED light source, which illuminates the area of the skin underneath the optical fiber bundle. Using an optical fiber bundle allows an unhindered movement of the ultrasound transducer over the skin surface. This method makes it possible to compensate a regular 3D freehand scanning for offsets from scan path and speed variations with highest achievable (theoretical) resolution of 0.09 mm, as measured on the skin surface.

The 3D image reconstruction is performed with software that runs on a standard Windows-PC. Images are digitally and losslessly transferred from a 2D scanner software (Terason) to a 3D reconstruction software (Sonocubic). In a synchronized fashion, a position is acquired from the CCD-array driver through a Windows-DLL. Using a nearest neighbor interpolation algorithm 8 points are

selected by the 3D reconstruction software and a new correctly placed scan plane is generated in the 3D volume. The interface to the position sensor can be easily modified so that existing software implementations for transducer mounted transmitters (e.g. Flock of Birds) can be used.

To validate the method a vessel phantom was scanned in a highly uneven scan path. Here it could be seen that the compensation algorithm was working as expected. By measuring the deviation from the straight path it was observed that the deviation in the uncompensated scan was 31.5 mm while it in the compensated was reduced to 4.5 mm. The error is inversely proportional to a socalled SQUAL (Surface QUALity) value. This value is a measurement of the number of distinct features visible to the CCD array. A skin surface produces a higher SQUAL value and therefore gives a lower error than the surface of an ultrasound phantom does. When a protective, transparent window is used underneath the optical sensor, the presence of acoustic coupling gel does not interfere with the estimation of the position.

1K-6 5:45 p.m.
EFFICIENT QUANTIFICATION OF THE LEFT VENTRICULAR FUNCTION FROM 3D-ECHOCARDIOGRAPHY.

M. M. VOORMOLEN*[1,2], B. J. KRENNING[1], R. J. VAN GEUNS[1], C. T. LANCÉE[1], W. B. VLETTER[1], F. J. TEN CATE[1], J. R. T. C. ROELANDT[1], A. F. W. VAN DER STEEN[1,2], and N. DE JONG[1,2], [1]Thoraxcenter, Erasmus MC, Rotterdam, The Netherlands, [2]ICIN, Interuniversity Cardiology Institute of the Netherlands, Utrecht, The Netherlands.
Corresponding e-mail: m.voormolen@erasmusmc.nl

Background: Present-day 3D-echosystems can record a full volume within a few heart cycles with sufficient spatial and temporal resolution for volumetric evaluation of the left ventricle. In this study we determined the minimum number of 2D long axis images, extracted from the 3D-dataset, to be used for accurate quantification of the left ventricular volume. Minimizing the number of 2D-images minimizes the tracing time, which is required for routine use of quantitative 3D-echocardiography in the clinical practice. In addition, this will reduce the number of cardiac cycles needed for acquisition, which, in turn, will reduce possible artefacts resulting from beat-to-beat variability.

Method: Both MRI and 3D-echocardiographic recordings of the left ventricle were made from 15 patients with various cardiac pathologies.

For the echo recordings our custom developed fast rotating ultrasound (FRU-)transducer was used. The array of the transducer contains 64 elements and has a center frequency of 3.2 MHz with a bandwidth of about 86 % (-6 dB) which makes the transducer highly suitable for tissue and contrast harmonic imaging. The array is rotated continuously at a speed ranging from 240 to 480 rpm. The typical acquisition time for a densely sampled 3D-dataset is less than 10 s, which has proven to be conveniently short during clinical application.

End diastolic and end systolic volumes were determined with the commercially available 4D LV Analysis software from TomTec (Munich, Germany) featuring a

semi-automated border detection algorithm. The volumes were determined using 16, 8, 4, and 2 equidistant long axis images that were randomly orientated around the imaging axis.

Result: A strong correlation was observed between volumes obtained with MRI and 3D-echo using 16 long axis images (r=0.99; y=0.95x + 3.3 mL; SEE=7.1 mL). When comparing 16 slice echo with 8, 4 and 2 slice echo it was found that 4 and 2 slice echo were significantly different ($p<0.005$). However, when the slices were not randomly orientated but had a predetermined relation to the left ventricular axis this was only the case for 2 slice echo ($p<0.001$).

Conclusions: Accurate left ventricular volume quantification can be performed with as little as 8 equidistant long axis images. With the FRU-transducer, this makes LV volume measurements even possible with images from one single cardiac cycle. By selecting the correctly orientated image set, the number of images can be brought down to 4, which will reduce the tracing time even further. Together with short acquisition times, advanced quantification software and the general advantages of echo this makes three-dimensional echocardiography, and specifically the FRU-transducer, highly suitable for determination of the left ventricular function in the daily clinical practice.

This work has been supported by the Technology Foundation STW (RKG.5104).

Session: 2K

CAVITATION
Chair: T. Matula
University of Washington

2K-1 4:30 p.m.
AN INTEGRATED HIFU SYSTEM FOR THE TREATMENT OF BREAST CANCER.

A. SHRESTHA*, H. YAO, and E. S. EBBINI, University of Minnesota, Minneapolis, MN.
Corresponding e-mail: emad@umn.edu

Advances in ultrasound transducer technology make HIFU an attractive modality for the treatment of breast cancer, especially in early stages. We have designed and investigated two HIFU systems for potential use as image-guided treatment of Primary breast cancer. The first is a 64-element dual-mode array system with therapeutic and imaging capability that we have reported on previously. The second is an integrated system utilizing a diagnostic system for guiding the HIFU by imaging cross sectional plane(s) orthogonal to the axis of the HIFU beam. The imaging system is equipped with a research interface allowing for capture of RF data suitable for speckle tracking for temperature estimation as well as tissue strains. The HIFU transducer is synchronized with the frame and line sync signals of the imaging system. This allows for precise control of sub-therapeutic HIFU beams used for assessment of thermal and mechanical tissue

response in the focal region. The HIFU transducer is mounted on a motorized unit that is also synchronized with the imaging array. Short-duration (~ms) HIFU pulses are used to cause localized shear waves that allows for measurement of absorption and shear modulus. In addition, low power beams with longer duration (~0.2 s) are used to cause a small (~ 1°C) temperature change. The transients of the heating profile at the HIFU focus allow for absorption (from initial heating rate) and perfusion (from initial rate of decay) at the focus. A complete series of experiments for validation of both forms of measurements at multiple locations in each sample were performed. In addition to freshly excised tissue samples used in lesion formation, tissue-mimicking phantoms with hard inclusion were used for validating the SWEI approach. For example, a soft tissue mimicking phantom with ~0.1 kPa modulus was made with a10.7 mm-diameter hard inclusion (~1.6 kPa). A series 0.25 ms HIFU beams were used to push the tissue along a line just outside the inclusion (barely visible on the B-mode image). M-mode data at 4300 fps was collected before, during and after the pushing pulse and peak displacement images were recorded. The inclusion was clearly visible on the displacement image (Inclusion: mean=1.9, sd =0.43 um. Soft Tissue: mean = 17.1, sd = 5.6 um). Thermal lesions in *in vitro* exhibited transient behavior (peak displacement very large after 3 minutes probably due to increased absorption), but showed more contrast in the time to peak after cool down (20 % reduction measured at 12 and 20 minutes). This indicates that the tissue stiffness increases after thermal lesion formation as expected. We present an approach that combines the absorption measurements from low-power and short-duration HIFU beams as means of increasing the robustness of shear modulus measurements during the treatment. This may allow for more reliable monitoring of the state of the tissue undergoing irreversible damage during HIFU treatments.

Funded by Grant DAMD 17-01-1-0330.

2K-2 4:45 p.m.
A NUMERICAL STUDY OF PULSED SONICATION FOR REDUCING THERMAL DEPOSITION IN THE SKULL DURING TRANSCRANIAL FOCUSED ULTRASOUND SURGERY.

X. YIN and K. HYNYNEN*, Department of Radiology, Brigham and Women's Hospital, Harvard Medical School, Boston, MA.
Corresponding e-mail: xyin@bwh.harvard.edu

Transcranial focused ultrasound surgery has been demonstrated by researchers as a potentially promising noninvasive treatment for brain tumor patients. The obstacles to the transcranial beam focusing and steering due to skull inhomogeneity have been overcome by phase correction techniques using phased arrays. However, the absorption of ultrasound energy by skull bone inevitably leads to thermal deposition in skull during a sonication. Excessive heating in skull bone could damage not only the skull but also the adjacent scalp and brain tissue. Maximizing the beam penetration area through the skull surface, large area arrays are proposed to reduce the risk of hot spot in skull. Although beneficial for accumulating thermal dose in the focal zone in brain

tumor, the continuous wave (CW) sonication may not be an optimized scheme for minimizing thermal deposition in skull. In this study, a pulsed wave (PW) sonication scheme was proposed to allow extra cooling between sonicating pulses so that the accumulated heat in skull would dissipate from the skull surface to the surrounding low temperature coupling water. A simulated homogeneous brain tissue was placed inside a digitized skull that was constructed from a raw CT scan data set of a cadaver skull. Using a 0.6 MHz, 500-elemnt and 300-mm-diameter hemispherical transducer array, the ultrasound beam intensity distribution in the brain and skull bone was calculated from a large-scale 3D finite difference time domain (FDTD) acoustic simulation with distributed client/server computing techniques. The consequent thermal responses of the brain and the skull were calculated by an FDTD bioheat transfer equation solver. The speed of sound and acoustic attenuation coefficient variations in skull bone were incorporated into both the acoustic and thermal simulations. An active exchange of 15°C chilling water was used to cool the skull before sonication. The CW case had a 20-s sonication followed by a 40-s cooling time. Several PW sonication sequences were tested to evaluate the peak temperature and peak thermal dose in the skull bone in comparison with those of the CW case. One typical PW case had 10 identical pulses with 2-s sonication and 2-s cooling time in each period, then followed by a 20-s cooling time. To reach a 70°C peak temperature at focus in brain tissue, the CW and PW cases had peak temperatures of 45.6°C and 44.4°C in the skull bone, respectively. The peak cumulative equivalent minutes at 43°C in the skull bone of the CW and PW cases were 13 and 4 min, respectively. The skull peak thermal dose of the PW case was 69% lower than that of the CW case. The results suggest that the pulsed sonication scheme may be useful in reducing thermal deposition in the skull bone during the noninvasive transcranial focused ultrasound surgery.

Work supported by NIH Grant No. EB003268

2K-3 5:00 p.m.
RADIATION FORCE IMAGING FOR DETECTION OF IRREVERSIBLE CHANGES CAUSED BY HIGH INTENSITY FOCUSED ULTRASOUND.

T. AZUMA*, K. SASAKI, K.-I. KAWABATA, and S.-I. UMEMURA, Central Research Laboratory, Hitachi Ltd., Kokubunnji, Tokyo, Japan.
Corresponding e-mail: t-azuma@crl.hitachi.co.jp

High Intensity Focused Ultrasound (HIFU) therapy requires image guidance for targeting and monitoring the tissue to be treated. Mapping of tissue temperature changes during treatment based on echo time shifts has been studied and its potential for monitoring focused ultrasound treatment has been demonstrated[1]. The echo shifts can be affected by various changes within a targeted area. Thermal changes in the speed of sound, thermal expansion of tissues, irreversible changes in tissue properties and radiation force generated by HIFU can cause echo time shifts. Visualizing the profile of the treated area with HIFU is one of the most important purposes of monitoring. Since tissue coagulation is dependent not only on the temperature but also the HIFU exposure time, and since it is difficult to establish this time for each localized area in the target due to tissue

motion during the exposure, the temperature itself does not provide sufficient information to obtain the profile for the treated area.

In this study, we focused on the detection of irreversible changes. We used two approaches, an amplitude modulation sequence of HIFU[2] and the split focus approach. The amplitude modulation sequence consisted of three parts: radiation force monitoring under pre-treatment conditions with low intensity HIFU, HIFU treatment at sufficient intensity to create lesions, and radiation force monitoring under post-treatment conditions with low intensity HIFU. By comparing displacements under pre-treatment and post-treatment conditions, irreversible changes in echo shift could be separated from other changes. The experimental system consisted of a HIFU transducer with driving circuitry, an ultrasound scanner, and a digital capture board to store RF data after beamforming. Each HIFU exposure at 3.25 MHz with a duration of 6 ms was synchronized with an imaging frame at a repetition period of 14.7 ms. The peak intensities of HIFU were 3.2 kW/cm^2 for monitoring and 5.6 kW/cm^2 for treatment. An excised swine liver lobe submerged in a water tank was exposed to HIFU. The echo shift in pre-treatment was less than the resolution of the system, 24 μm, and the echo shift in post-treatment was 100 μm when the treatment exposure was continued for 7 s. The same magnitude of echo shift was observed immediately and 10 min after the treatment exposure. The irreversible tissue changes induced by HIFU treatment were detected by radiation force through the proposed sequence.

To separate the effect of radiation force from other changes, we used a split focus technique[3], with which the peak for ultrasonic intensity could be shifted from that for tissue temperature. Tissue displacement caused by radiation force was not detected with a split HIFU beam with large separation. In contrast, focal tissue displacement away from the transducer was observed with a narrow HIFU beam, where the effect of radiation force might have exceeded that of expansion.

[1] C. Simon et al., IEEE Trans. UFFC, Vol. 45, pp. 1088- 1099, (1998).

[2] U.S. Patent 6488626.

[3] S. Umemura et al., Proc. IEEE Ultrason. Symp., Vol. 2, pp. 1431- 1434, (1998).

2K-4 5:15 p.m.
TARGETED DISRUPTION OF THE BLOOD-BRAIN BARRIER WITH FOCUSED ULTRASOUND: ASSOCIATION WITH INERTIAL CAVITATION.

N. MCDANNOLD*, N. VYKHODTSEVA, and K. HYNYNEN, Brigham and Women's Hospital, Harvard Medical School, Boston, MA.
Corresponding e-mail: njm@bwh.harvard.edu

Purpose: To see whether blood-brain barrier (BBB) opening produced by focused ultrasound in the presence of an ultrasound contrast agent is always associated with inertial cavitation.

Methods: Locations were targeted 10 cm deep in the brain of 10 rabbits with pulsed focused ultrasound sonications (pulse length: 10 ms, repetition frequency: 1 Hz, duration: 20s) using a spherically curved transducer (frequency: 260 kHz,

diameter/radius of curvature: 10/8 cm). At least ten days before sonication, a craniotomy was performed in order to simplify the experiments. Four locations were targeted per brain. Approximately 10 s before each sonication, a bolus of ultrasound contrast agent (Optison®) was injected IV via the ear vein at a dosage of 0.05 mL/kg. Acoustic power levels of 0.04-1.7 W were tested (estimated peak pressure amplitudes in brain: 0.1-0.6 MPa). A ring-shaped focused hydrophone surrounding the transducer served as a passive cavitation detector. Acoustic emission (time signal) was recorded with a digital oscilloscope at a sample rate of 10 MS/s for the first pulse and for 3-4 additional pulses during each sonication. The frequency spectrum of the emission was later reconstructed via FFT. The sonications were targeted under MRI guidance, and any resulting BBB disruption was detected in contrast-enhanced T1-weighted images (contrast agent: Magnevist®). Animals were sacrificed 4 h after sonication and histological evaluation was performed (N=4).

Results: BBB opening started to occur at a pressure amplitude of 0.3 MPa. Wideband acoustic emission was observed for locations sonicated at a peak pressure amplitude of 0.6 MPa. Below this value, the BBB disruption was observed without this wideband emission. Enhanced emission at higher harmonics was observed during sonication with BBB opening in many cases. No lesions were found in the histology study.

Conclusions: BBB opening using this method can apparently be achieved without wideband acoustic emission, which is a signature for inertial cavitation. The pressure amplitude where wideband acoustic emission was found was accompanied by more extravasated erythrocytes scattered in the sonicated area. At lower values, no or only a few extravasations were found in the sonicated area. Thus, these results may indicate that the extravasations observed in our experiments could have been due to inertial cavitation. We are currently investigating whether the emission observed at higher harmonics can be used as a marker for BBB opening, which would be useful for guiding this procedure, a potential method that could allow targeted drug delivery of large molecular agents in the brain.

This work was supported by NIH grant EB000705

2K-5 5:30 p.m.
THERMAL EFFECTS OF HIFU AT SOFT TISSUE-AIR INTERFACE IN THE POST-FOCAL REGION: A SAFETY CONCERN, AND A POTENTIAL SOLUTION USING CAVITATION.

S. VAEZY*[1], V. ZDERIC[1], J. FOLEY[1], W. LUO[1], F. STARR[1], and A. LEBEDEV[2], [1]University of Washington, Seattle, WA, [2]Mirabilis Medica, Seattle, WA.
Corresponding e-mail: vaezy@apl.washington.edu

Introduction: The thermal effects of HIFU on tissues adjacent to high impedance mismatch interfaces such as air or bone in the post-focal regions could be of concern if the temperature increase at the interface is large enough to cause tissue damage. We measured the temperature at an air interface, in the post-focal region of a HIFU beam, and tested the feasibility of reducing the thermal

energy deposited at the interface, by producing endogenous bubbles in the focus. **Methods:** The HIFU transducer was a 3.5 MHz, 3.3 cm diameter, concave element, with a radius of curvature of 3.5 cm. In-situ intensities in the range of 450-15,000 W/cm2 were used to produce focal lesions, either based purely on thermal effect or involving cavitational effects. Duration of treatment was 30 s in all cases. An ultrasound imaging probe was used to detect the formation of bubbles at the focus, appearing as hyperechoic in the image. An infrared thermal camera was used to image a 5 cm x 7 cm cross sectional plane, perpendicular to the HIFU acoustic axis, at 2 cm post-focus. The studies were performed in-vitro in turkey breast (n=42), and in-vivo in rabbit liver (n=4) and muscle (n=11). Gross examination, immediately after the treatment, was performed to confirm the presence of thermal and cavitational lesions in tissues. **Results:** The in-vitro results showed that when cavitation lesions were formed, the temperature at the air interface increased by approximately 5 C above the baseline of 20 C during the first 3 s of HIFU application, and decreased continuously afterward, to an end temperature of 22.7 C. When thermal lesions were formed, the temperature increased continuously throughout the HIFU application to a final temperature of 25 C. Similar results were obtained in-vivo. The temperature of the liver at the air interface rose from 34 C to 62 C within the first 3 seconds in the case of cavitational lesions, and then decreased continuously to 44 C at the end of treatment. For the lesions that involved immediate cavitational effects, the temperature rose to 70 C within the first 10 s when the lesions were purely thermal, decreased as cavitation started, and continuously dropped to an end temperature of 50 C. In muscle, very similar patterns, with results shifted to lower temperatures, were obtained. **Conclusions:** This study showed that thermal effects of HIFU at a post-focal tissue-air interface, such as bowel, could result in clinically-significant increases in temperature. A temperature increase of 7C, the maximum temperature recorded in our in-vivo experiments, could lead to protein denaturation and tissue death. Bubble formation at the focus appears to provide a method to reduce this thermal effect by blocking the wave propagation beyond the focus, and shielding the post-focal region from potential tissue damage. Implications in image-guided therapy are favorable since cavitation bubbles at the focus appear as hyperechoic regions in B-mode images, providing a valuable method for guidance and monitoring of HIFU treatment, an added advantage of cavitation at the focus.

US DoD

2K-6 5:45 p.m.
QUANTIFYING INERTIAL CAVITATION PRODUCED IN *IN VIVO* RABBIT EAR VESSELS WITH OPTISON®.

J. TU, J. HWANG, A. BRAYMAN, T. MATULA*, and L. CRUM, Center for Industrial and Medical Ultrasound, Applied Physics Laboratory, University of Washington, Seattle, WA.
Corresponding e-mail: juantu@u.washington.edu

Inertial cavitation (IC) is a very important mechanism for ultrasound (US)-induced bioeffects. Previous *in vitro* studies have shown that the US-induced mechanical bioeffects with the presence of ultrasound contrast agents (UCAs) are highly

correlated with IC "dose" (cumulated root mean squared broadband noise amplitude in frequency domain). The IC dose has also been used to quantify IC activity in ex vivo perfused rabbit ear vessels. The current set of *in vivo* experiments conducted here using a rabbit ear vessel model are designed to: (1) detect and quantify IC activity in vivo within the constrained environment of rabbit auricular veins with the presence of Optison®, and (2) Measure the temporal evolution of microbubble IC activity and the ICD generated during insonation treatment, as a function of acoustic parameters. New Zealand white rabbits are used for these studies based on NIH guidelines under a protocol approved by the University of Washington IACUC. The pre-selected region of interest (ROI) in the rabbit ear vein is exposed to pulsed focused ultrasound (1.1 MHz, 1-Hz PRF). Experimental acoustic variables include peak negative acoustic pressure (P^-; 1.1, 3.0, 6.5 or 9.0 MPa), and pulse length (20, 100, 500 or 1000 cycles). The ICD is quantified based on passive cavitation detection (PCD) measurements. The results show that: (1) The arrival time of microbubble IC activity is relatively consistent, approximately 20s, (2) After reaching its peak value, the IC activity will decay exponentially and the half-life decay coefficient ($t_{1/2}$) increases with increasing P^- and pulse length, and (3) the normalized IC "dose" generated by pulsed ultrasound exposure increases significantly with increasing P^- and pulse length.

Key Words: *In vivo* inertial cavitation, Passive cavitation detection, Ultrasound contrast agents, Microbubbles, Optison®, Inertial cavitation dose

The authors wish to convey their gratitude for the helpful assistance offered by Frank Starr and Dorothy Lowell. This work was funded in part by NIH R01 CA14325-04.

Session: 3K

ACOUSTIC SENSORS
Chair: J. Kushibiki
Tohoku University

3K-1 4:30 p.m.
BEAM SPLITTER FOR BALL SAW DEVICE USING DIFFRACTION BY A TWO DIMENSIONAL METAL DOT ARRAY.

T. MIHARA*[1], K. ATSUMI[1], N. NAKASO[2], S. AKAO[2], D. Y. SIM[3], and K. YAMANAKA[1], [1]Tohoku University, Sendai, Miyagi, Japan, [2]Toppan Printing, Kitakatsushikagun, Saitama,Japann, [3]Ball Semiconductor, Kanagawa, Japan. Corresponding e-mail: mihara@material.tohoku.ac.jp

The ball surface acoustic wave (SAW) sensor utilizing multiple roundtrips of SAW along the ball surface has a high S/N ratio because no diffraction loss occurs, and is promising for compact and highly accurate sensors [1]. Furthermore, if multiple routes on a single ball are employed, multiple-gas

sensors and/or automatic temperature compensation will be realized. However, fabrication of multiple interdigital transducers (IDTs) on different routes is not straightforward because of the need for precise alignment and of the limited space for conductive line connection.

In this situation, we propose a novel approach using a SAW beam splitter by diffraction dot array fabricated on one of the propagation route. The diffracted beam is propagated along another route and returns to the original one after one roundtrip, thus enabling detection by the IDT on the first route. If a second sending film is deposited on the second route, two different gas sensing is realized by one IDT on the first route. To design this dot array, precise analysis of the diffraction on a curved surface of anisotropic crystal is needed. It is performed by a three dimensional finite element method (FEM) simulator using elements defined in polar coordinates, thus enabling efficient calculation of complex phenomenon [1].

Before implementing on a ball, a piezoelectric crystal plate was used to evaluate the design of the beam splitter. Single crystal of 128 degree Y cut LiNbO3 was used as a substrate and two pairs of IDT to transmit and receive 50MHz SAW were fabricated where SAW is propagated both parallel and normal to the X-axis. Moreover, 30x30 square metal dot array with each dot of $\lambda/4$ in side length were arranged at intervals of λ on the delay line for each IDT pair, where λ is a wavelength of SAW. The Bragg angle of diffraction was set to 90 degrees.

In the propagation towards 90 degree from X-axis, a pseudo-SAW was observed and the amplitude of transmitted SAW was smaller than that of X-axis propagation. The diffracted wave amplitude was -35dB of the transmitted wave for X-axis propagation, and -20dB for perpendicular to the X-axis. In addition, it did not depend on the thickness of metal dots and enough amplitude was obtained even for the 40nm thick dot array. On the contrary, it was larger for Au on Cr dot array than that for Cr dot array. These results suggest that the diffraction by dots is mostly due to the electric loading rather than the mass or elastic loading. In conclusion, the proposed beam splitter will be promising as a device which branches SAW transmission, applicable to a multiple SAW sensor on a single ball.

[1] K. Yamanaka et al, “Diffraction-free propagation of collimate surface acoustic wave on a sphere applied for innovative gas sensors”, (INVITED), this symposium.

A part of this research was supported by a grant from the Ministry of Education, Culture, Sports, Science and Technology.

3K-2 4:45 p.m.
BULK ACOUSTIC WAVE RESONATOR OPERATING AT 8 GHZ FOR GRAVIMETRIC SENSING OF ORGANIC FILMS.

S. REY-MERMET*[1], R. LANZ[2], and P. MURALT[1], [1]Ecole Polytechnique Fédérale de Lausanne, Ceramics Laboratory, Lausanne, Switzerland, [2]Unaxis Balzers, Balzers, Liechtenstein.
Corresponding e-mail: samuel.rey-mermet@epfl.ch

Gravimetric sensing is a proven technique for the measurement of the mass deposited in thin film deposition, and has a large potential in bio-medical diagnosis to detect mass and viscosity changes resulting from specific bio-chemical processes such as antigen-antibody reactions. Usually such sensors are made of quartz crystal working in the range of 3-10 MHz. With the use of thin films it is possible to reduce the thickness of the whole resonator in the sub-micron range and to increase the resonant frequency to over 1 GHz. This leads to a major increase in the sensitivity of the sensor and can be a great improvement for medical science and drug testing. The mass sensitivity of aluminium nitride (AlN) thin film resonators operating in air at 6 to 8 GHz has been investigated in theory and experiment. The sensors are made of 30×30 µm wide resonators including a 180 to 300 nm thick, highly oriented AlN thin film, bottom and top electrode (aluminium or platinum), and an acoustic reflector made of five AlN/SiO2 bi-layers. The mass sensitivity is defined as the ratio of the shift in frequency over the product of the resonant frequency times the mass added per area. The top electrode was loaded by defined polymer layers to test sensitivity and simulation model (Novotny,Benes 1987). The model agrees very well with the experimental points and demonstrates the impact of type and thickness of the top electrode. It is possible to increase the sensitivity of the resonator by 20% when a SiO2 layer is added on top of the aluminium electrode as impedance matching layer. 10 to 20 nm thick PMMA coatings served to demonstrate sensitivity with a getter gel in form of spontaneous adsorption of acetone from the vapour phase. During absorption of acetone, the resonant frequency drops by 15 MHz to reach a stable value corresponding to a saturated state. This frequency shift corresponds to an added mass of 1.35 pg and the sensitivity equals 1250 m2/kg. When the sensor is removed from the acetone atmosphere the resonant frequency rapidly increases and returns to the former level showing the complete desorption of acetone. Finally, a self-assembled monolayer (SAM) of 11-mercaptoundecanoic acid was formed on a platinum top electrode for the demonstration of a sub-monolayer sensor in air showing that pico-grams of such SAM could be detected with a sensitivity up to 1000 m2/kg. Comparison with literature data confirms the expected linear increase of sensitivity with frequency.

3K-3 5:00 p.m.
SENSOR FOR AMBIENT PRESSURE AND MATERIAL STRAINS USING A THIN FILM BULK ACOUSTIC RESONATOR.

J. WEBER*, M. LINK, R. PRIMIG, D. PITZER, and M. SCHREITER, Corporate Technology, Siemens AG, Muenchen, Germany.
Corresponding e-mail: phd-ferro2-ctmm2@mchp.siemens.de

Monitoring the pressure of gas and fluids is a task that is required in nearly all industrial sectors (for example fluidic systems or chemical processes). Measuring the internal stress of materials on the other hand is frequently desired in material testing and fabrication. Film Bulk Acoustic Resonators are devices that are small, mechanically rugged, CMOS integrable and can be driven at very high frequencies (several GHz). Their resonance frequency can be read out easily

and with high precision and is influenced by factors like the resonator thickness, mass density and the elastic constants of the resonator composing material. When an external stress is applied to these devices, the elastic constants are being altered and a frequency shift can be observed. This opens a wide field of new applications. Two principle configurations for a stress sensor are possible, depending on the sensing purpose.

The first configuration comprises a piezoelectric resonator with two electrodes which is solidly mounted on an acoustic bragg mirror that serves for confining the energy in the resonator. Being attached onto a substrate the resonator can then be used to monitor changes of the substrates internal stress.

In the second configuration the resonator and the electrodes form a membrane. This membrane fulfills two functions in one: first of all it ensures a confinement of the acoustic energy. Secondly the difference between the pressure of the gas / fluid on one side of the membrane and a reference gas / fluid on the other side leads to a deformation of the membrane and thus the pressure of the former can be measured. Through dimensioning the resonator according to its lateral size and thickness an amplification of the sensor response can be reached.

The great potential of an FBAR-pressure-sensor lies in its silicon compatibility which enables an integration of the sensor with a readout circuit as well as in the possibility of a measurement with fine spatial resolution as the FBAR-sensor can be made relatively small (in the range of some µm).

In this study the feasibility of such a sensor is demonstrated. Therefore an FBAR on the basis of a ZnO thin film solidly mounted on a silicon substrate was realized. The pressure sensitivity was experimentally evaluated by inducing a static strain through bending of the FBAR device. The resulting stress could be straightforwardly calculated and thus the sensitivity of the device could be quantified to about 0.03 Hz / Pa which is about in the range or slightly better than for SAW-devices.

Further investigations were made to examine the influence of frequency, wave mode and resonator parameters like form and size on the stress sensitivity. It could be shown, that the frequency shift can be mainly attributed to a change in the elastic constants.

This work received financial support from the European Community Information Society Technologies program; project 'PISARRO' (IST-2001-33326).

3K-4 5:15 p.m.
DUAL MODE, MULTIPLE ELECTRODES QUARTZ SENSOR.

A. IVAN*[1,2], R. BOURQUIN[1], and B. DULMET[1], [1]FEMTO-ST/ Dep LCEP, Besancon, France, [2]FIE-UVT, Targoviste, Romania.
Corresponding e-mail: rbourquin@ens2m.fr

High frequency bulk acoustic waves piezoelectric resonators are used as frequency-output sensors for direct measurement of force or related quantities such as acceleration or pressure. The performances of such sensors on wide temperature ranges are generally limited by their frequency-temperature

sensitivity, even when the crystals are realized in (quasi) thermally-compensated cuts. A way to avoid this limitation is to use the quartz as its own temperature sensor to compensate the residual variation of frequency due to temperature change. This can be done by operating the resonator at two resonant modes of different families (B and C) and by extracting the useful information from the two frequencies of modes. The treatment is simplified if the corresponding transfer matrix is quasi-diagonal.

Then one mode must be essentially sensitive to the force, while the other must be essentially sensitive to the temperature. Electronic operation can be achieved by using a single pair of electrodes systems and appropriate filtering. In that case, main overtone modes, so-called (n,0,0) and belonging to different thickness-propagation families (B and C) are systematically used. The use of a pair of anharmonic modes offers a better way with superior optimization, since, in that case, one can efficiently connect the two oscillators to separate electrode systems on the sensing resonator which greatly simplifies the design of the electronics. This can be achieved if the vibration amplitudes of the two modes are mainly located in separate regions in the plane of the resonator. Taking advantage of spatial symmetry properties of well-chosen pair of modes (for instance using C-mode (3,0,1) and B-mode (3,1,0)) leads to a dual-mode design which virtually eliminates the intermodulation between the two oscillator signals, while keeping the transfer matrix as nearly diagonal as possible. This approach efficiently combines the designing effort on the crystal and driving electronics in order to make dual-mode multiple electrodes sensors competitive in comparison with the more complicated electronically discriminated dual-mode sensors relying on a single pair of wires.

We present here a method to design the shapes of electrodes derived from the knowledge of modes patterns corresponding to given mode family, overtone number and rank of anharmonic. These ones are obtained experimentally by using X-Ray topography and laser amplitude measurement. Then data is employed in association with the analytical model of Stevens and Tiersten to get the precise amplitude distribution of mechanical displacement for the design of electrodes and to compute the force sensivity of the sensor. Practical application is made for a plano-convex SC cut. Using two independent low-cost oscillators connected to a microcontroller, a precise measurement system of force is implemented.

This work is supported by EU Contract QxSens

(G6RD-CT-2002-00648)

3K-5 5:30 p.m.
ULTRASONIC SENSOR DEVELOPMENT FOR THE SEMI-SOLID METAL WORKING PROCESS.

B. TITTMANN*, M. HUANG, C. MOOSE, and A. NIESSNER, Penn State University, University Park, PA.
Corresponding e-mail: brt4@psu.edu

Semisolid Metalworking (SSM) is a hybrid manufacturing process that incorporates the advantages of both casting and forging. However, high volume

commercial production has suffered from inadequacies in process monitoring and control. A key process parameter is the SSM solid-liquid fraction, which is a sensitive indicator of the deformation and flow behavior of the material during forming. Unfortunately, no sensor currently exists to provide an in-situ measurement of this important parameter. Here we present preliminary results for an advanced ultrasonic sensor to measure solid fraction. With the aid of metal alloy phase diagrams the binary alloy Sn-Bi was chosen to simulate behavior of Al/Si (e.g. 300 series) alloys. The phase diagram was used to provide the value of solid fraction at any given temperature. Measurements with longitudinal ultrasonic waves at 1 MHz in the selected alloy heated to different solid fractions were performed with a combination of commercial transducers and quartz buffers penetrating into a temperature controlled furnace. Five compositions were used ranging from 83% to 100% -Bi in the binary Sn-Bi alloy. Presented are measurements of longitudinal wave velocity as a function of temperature across the entire range from totally solid to semi-solid to liquid states in both heating and cooling runs. The curves show the characteristic phase transitions. A quasi-static viscoelastic model based on Atkinson, Kytomaa and Berryman was prepared and modified for the SSM application. The comparison of the model calculations with the experimental results were in reasonable agreement. With the recent development of high temperature ultrasonics our results provide a potential solution to the development of an ultrasonic sensor for SSM.

3K-6 5:45 p.m.
ACOUSTICAL AND OPTICAL CHARACTERIZATION OF AIR ENTRAPMENT IN PIEZO-DRIVEN INKJET PRINTHEADS.

J. DE JONG*[1], H. REINTEN[2], M. VAN DEN BERG[2], H. WIJSHOFF[2], M. VERSLUIS[1], G. DE BRUIN[1], N. DE JONG[3], and D. LOHSE[1], [1]Physics of Fluids, University of Twente, Enschede, The Netherlands, [2]Océ Technologies B.V., Venlo, The Netherlands, [3]Dept. of Experimental Echocardiography, Thoraxcentre, Erasmus MC, Rotterdam, The Netherlands.
Corresponding e-mail: jos.dejong@tnw.utwente.nl

Air entrapment leads to malfunctioning of jet formation in a piezo-driven inkjet printhead. The entrapped air bubbles disturb the acoustics and in many cases cause the droplet formation to stop.

Here we will focus on piezo-electric inkjet devices where a voltage pulse applied to a piezo-electric element causes an ink-filled channel to deform, thereby creating a pressure waveform in the ink. Fluid acoustics are involved to guide the waveform energy towards the nozzle, and to create pressure and velocity profiles needed for the droplet jetting process. Droplets are jetted every 50 μs and it is essential that the droplet formation remains stable for an extensive period. Though the droplet forming process is very stable for literally millions of droplets, from one to the next actuation cycle there may be an occurrence giving rise to a malfunctioning of the droplet formation. A notorious problem in piezo-acoustic inkjet systems is the formation of air bubbles during operation. Here

we detect air entrapment, reveal the air entrapment process, and the time evolution of the entrapped air bubble.

The acoustical signal is monitored by using the piezo actuator as a sensor to measure the pressure in the channel after the pulse is applied. The optical measurements are performed with a range of high speed imaging cameras up to 1 Mfps, including the Brandaris 128 camera system [1]. The nozzle diameter is 30 μm or less. Typically the firing frequency is 20 kHz.

When a droplet is fired correctly, the acoustical signal is perfectly reproducible. The variations in the amplitudes of the signals stays well within 0.1%. This signal is employed to monitor deviations in the droplet formation and to trigger the optical setup. In particular, it detects the presence of an air bubble inside the ink channel, as an air bubble modifies the acoustical signal in a characteristic way. Once entrapped, the air bubble has an initial radius of 10 μm and oscillates with a frequency near 200 kHz. The radial growth of the bubble is found to be 0.3 μm/ms and the bubble reaches velocities up to 20 mm/s inside the ink channel.

In conclusion, the acoustical signals from the piezo actuator can be used to detect air bubbles inside the printhead and disturbances, which can result in air entrapment at the nozzle. The optical results will be implemented in numerical and theoretical models for entrapped bubble growth, displacement and oscillations.

[1] C.T. Chin et al, Brandaris 128: a 25 million frames per second digital camera with 128 highly sensitive frames. Review of Scientific Instruments, 74, 5026-5034 (2003).

This study is being financed by the Fundamenteel Onderzoek der Materie (FOM) of The Netherlands under Grant. No. 02MFS39 and by Océ Technologies B.V.

Session: 4K

PHYSICAL ACOUSTICS III
Chair: M. Fink
ESPCI-Universite-Paris VII

4K-1 4:30 p.m.
NEW METHOD OF CHANGE IN TEMPERATURE COEFFICIENT DELAY OF ACOUSTIC WAVES IN THIN PIEZOELECTRIC PLATES.

I. KUZNETSOVA*[1], B. ZAITSEV[1], S. JOSHI[2], and A. KUZNETSOVA[3], [1]Institute of Radio Engineering and Electronics of RAS, Saratov Branch, Saratov, Russia, [2]Marquette University, Milwaukee, WI, [3]Saratov State University, Saratov, Russia. Corresponding e-mail: iren@ire.san.ru

As is well known the coefficient of electromechanical coupling (K^2) and temperature coefficient of delay (TCD) of acoustic wave are very important for development of various acoustic devices and sensors. One of the modern lines

of investigation in acoustics is the search of such wave types and crystallographic orientations of wave-guides for which the value of K^2 is maximal and value of TCD is minimal. At present there exist the papers showing that fundamental shear-horizontal (SH_0) acoustic waves in thin (in comparison with wavelength) piezoelectric plates possesses by significantly more electromechanical coupling coefficient than surface acoustic waves (SAW). For example, it has been shown that SH_0 wave has K^2=34% and 44% for hf = 500 m/s (h/λ~0.15) in YX and 30Y-X $LiNbO_3$ plate, respectively (h=plate thickness, f=wave frequency, λ =wavelength). However, the values of TCD in these cases are equal 66 ppm/C and 55 ppm/C, respectively that are less than for SAW but is not enough for development of temperature stable devices. In this paper the new method of decreasing TCD at keeping high value of electromecanical coupling coefficient is suggested. It is known that velocity of SH_0 wave in lithium niobate plate always decreases when the temperature increases. From other hand it has been found that the velocity of SH_0 wave in plate always increases when dielectric permittivity of contacting media decreases. It is well known also that dielectric permittivity of most liquids decreases with temperature increase. At that the presence of weakly viscous liquid does not change significantly the attenuation of SH_0 wave. So, by using the structure containing liquid with certain value of dielectric permittivity one can significantly decrease TCD of SH_0 wave (until to 0). In this paper the theoretical analysis of temperature influence on velocity of SH_0 wave in YX lithium niobate plate (hf=500 m/s) contacting with nonviscous and nonconducting liquid from one side of plate has been carried out. As contacting liquid we used chlorbenzol, methyl acetate, benzol, butyl acetate, etc. Calculation showed that in case of contact of plate with such liquids as butyl acetate ($C_6H_{12}O_2$) and methyl acetate ($C_3H_6O_2$) the TCD of SH_0 wave are equal 0.7 ppm/C and –0.8 ppm/C respectively. In both cases the value of K^2 is about ~30%. This result was confirmed by experiment. The analysis also shows that for given liquid the value of TCD can be changed by selection of plate thickness. In whole the obtained results open the real prospective of use of SH_0 wave in thin piezoelectric plates for development of temperature stable acoustic devices for signal processing and high sensitive sensors.

This work is supported by NSF grant and RFBR grant #05-02-16947. Dr. I.Kuznetsova thanks Russian Science Support Foundation for help.

4K-2 4:45 p.m.
IN-PLANE AND OUT-OF-PLANE PARTICLE VELOCITY MEASUREMENT USING ELECTROMAGNETIC ACOUSTICAL TRANSDUCERS.

X. JIAN*, S. DIXON, and S. B. PALMER, University of Warwick, UK.
Corresponding e-mail: x.jian@warwick.ac.uk

Ultrasonic waves can be generated by many different physical approaches including piezoelectric transducers, laser or electromagnetic acoustical transducers (EMATs). Out-of-plane particle velocity fields can be investigated using miniature piezoelectric transducers while the out-of-displacement field can be investigated by laser interferometer. In our EMAT measurements we verified that only out-of-plane particle velocities were picked up by comparing

the measured refraction coefficient curve with the theoretical curve. EMATs can be used to preferentially measure particle velocities in a particular direction (in-plane or out-of-plane). Incoming ultrasonic waves interact with the static magnetic field, producing eddy currents in the skin-depth of the electrically conductive sample. The eddy currents will in turn induced current in the detection coil and in this way, the ultrasonic waves are detected. The signal picked up by an EMAT is proportional to the vector product of the particle velocity of the coming ultrasonic waves and the static magnetic field and a model has been developed to predict the EMAT signal measured on the detection coil. By arranging the static magnetic field in a particular direction, we can measure the particle velocity component perpendicular to the static magnetic field. If the static field is parallel to the sample surface, out-of-plane particle velocity can be measured; if the static magnetic is perpendicular to the sample surface, in-plane particle velocity can be measured. The waveforms corresponding to the of in-plane and out-of-plane components of EMAT measured particle velocities of the zero order symmetric Lamb waves (S_0) are different to those of the zero order anti-symmetric mode (A_0). The elastic response of the Lamb waves are calculated using a Finite Element Method (FEM). The measured particle velocities from the two Lamb wave modes will have in-plane and out-of-plane components are compared to the FEM predictions. The waveforms of the measured particle velocity components which are thought to be in-plane and out-of-plane agree well with that predicted by FEM. This demonstrates that it is clearly the in-plane and out-of-plane particle velocities that are measured using EMATs.

The work is supported by the EPSRC funded UK Research Centre for Non-Destructive Evaluation (RCNDE). We thank professor Fradkin LJ, London South Bank University for useful discussion over Rayleigh scattering by a crack.

4K-3 5:00 p.m.
DECOHERENCE OF LAMB WAVES BY ROUGH INTERFACE.

B. MORVAN[1], A.-C. HLADKY*[2], D. LEDUC[1], M. BAVENCOFFE[2], and I. JEAN-LOUIS[1], [1]LAUE UMR CNRS 6068, Le Havre, France, [2]IEMN UMR CNRS 8520, Lille, France.
Corresponding e-mail: bruno.morvan@univ-lehavre.fr

The propagation of Lamb waves on one-side rough elastic plates has shown an attenuation which can be interpreted as a phenomenon of decoherence. It means that all the partial waves (longitudinal and shear waves) cannot interfere constructively at each interface. In order to verify this hypothesis, a simplified model is considered in order to exhibit this decoherence. A fluid plate with a limited periodic grating on one interface is studied by a finite element method (ATILA). An antisymmetric Lamb mode is excited before the grating. The pressure is studied under the grating along the median plane of the plate, where it is equal to zero for the homogeneous plate. Depending on the spatial periodicity grating, a pressure can be observed or not on the median plane. In the general case, when the wavelength of the Lamb wave is close to the grating spacing, reflected waves are observed and a phonon relation is written between the incident signal, the converted mode and the phonon related to the grating. When

the phonon condition is not fulfilled, the recorded pressure in the median plane is the trace of incoherent waves. For the incident wave, the main effect is caused by the first groove even if the others play a role. But this role is less and less important : this fact can be interpreted as a progressive adaptation of the Lamb wave. If a phonon is excited, a reflected converted Lamb mode is clearly exhibited. In the two cases, there is one outgoing wave from the grating corresponding to the attenuated incident wave.

The authors acknowledge CNRS GDR 2501 for financial support.

4K-4 5:15 p.m.
OPTICAL MEASUREMENT OF ACOUSTIC RADIATION STRAINS IN SOLIDS.

X. JACOB[1], R. TAKATSU[1,2], C. BARRIÈRE*[1], and D. ROYER[1], [1]Laboratoire Ondes et Acoustique, Université Paris 7, Paris, France, [2]Doshisha University, Kyoto, Japan.

Corresponding e-mail: christophe.barriere@espci.fr

The existence and physical meaning of radiative acoustic stresses in a solid are not well established. For example, Brillouin concluded to a zero value of the induced static strain in solids and laterally confined fluids, whereas Chu and Apfel identified an acoustic straining associated with the radiation pressure. The first direct experimental evidence of the acoustic radiation-induced static strain in a solid is reported in a paper by Yost and Cantrell (Physical review B, vol. 30, p. 3221, 1984) following a theoretical paper by Cantrell (Physical review B, vol. 30, p. 3214, 1984). Using an optical heterodyne interferometer, we investigate the radiation-static-strain associated with propagating acoustic longitudinal waves in solids. Acoustic tone burst with carrier frequencies in the range 20-30 MHz were launched in duraluminum and fused silica bars of various lengths. The phase detection circuit of the optical probe has been adapted and calibrated, for measuring separately fundamental (HF) and static (LF) displacement components. The output filter bandwidth has been carefully chosen to not disturb the LF waveform. Duraluminum and fused silica have non-linear coefficients of opposite signs: $\beta_{dural} = 11.8$ and $\beta_{silica} = -7.4$. For HF displacement of order 1nm, a LF displacement equal to a few tens of pm was measured at the free end of the bar. We determined some characteristics of this displacement:

i) The amplitude of the LF pulse is proportional to the square of the HF displacement

ii) For duralumin and silica samples the sign are opposite

iii) The waveform of the LF pulse is similar to the envelope of the tone burst

iv) The amplitude does not depend on the tone burst duration

v) In the case of a non-absorbing material, such as fused silica, the LF amplitude grows roughly as the sample length.

The first assessment is in agreement with the proportionality of radiation stress to the acoustic energy density. The second one confirms that the radiation stress depends on the nonlinearity coefficient β. However, third and fourth points are in

contradiction with previous results obtained by Yost and Cantrell. Experiments are in progress in order to obtain quantitative agreement with theoretical results.

4K-5 5:30 p.m.
STRONG ON-AXIS FOCAL SHIFT AND ITS NONLINEAR VARIATION IN LOW-FRESNEL-NUMBER ULTRASOUND BEAMS.

Y. N. MAKOV[1], V. ESPINOSA[2], V. J. SANCHEZ-MORCILLO*[2], J. RAMIS[2], J. CRUAÑES[2], and F. CAMARENA[2], [1]Moscow State University, Moscow, Russia, [2]Universidad Politecnica de Valencia, Grao de Gandia, Valencia, Spain. Corresponding e-mail: victorsm@fis.upv.es

The study of ultrasonic beams has greatly attracted the attention of researchers in different fields. Sound beams are interesting just as objects of theoretical (analytical and numerical) and experimental investigations since are usually regarded as multifunctional instruments in many applied technologies, for example, in medical therapies, nondestructive testing, and others. For all that the possibility of focusing of ultrasound beams for the creation of very high intensity in small and accurately controlled volumes is a subject of great importance. For the investigation of these problems and the prediction of the corresponding effects many theoretical calculations and experimental measurements of the acoustic field distribution in beams radiated from different focused transducers have been carried out. In these cases the effects related with focusing, diffraction and nonlinearity must be taken into account. One of the most remarkable effects observed in high intensity focused beams is a dependence on the maximum pressure (focal) point on the intensity and geometrical parameters of the source. However, a precise interpretation and quantification of this effect is absent. In this work we perform a detailed analysis of the phenomenon of maximum pressure shift in focused beams, and its dependence on different factors (the geometry of transducer and the driving power). The effect of the geometry is considered in terms of the Fresnel number of the transducer (beam), which is equal to the ratio between the focal and diffractional lengths divided by π. The results of our investigation show the strong effect of the linear gain value on the axial location of pressure maximum, showing a pronounced variation from the geometrical focal point for low-Fresnel-number focused transducers (beams). An analogous effect exists in optics, and is known as focal shift. We have also observed and characterized that, as the driving transducer voltage is increased, the position of the point of maximum pressure shifts in the beginning (for moderate driving) from its initial linear position towards the geometrical focus, but this tendency is inverted and the motion is backwards as the nonlinear regime become stronger. From these results, it follows that the real position of focal point is not determined solely by the geometry of the transducer, but also depends nontrivially on the strength of the driving. The parallel observation of the temporal waveform (profile) and its modifications served as the best indicator of nonlinearity degree. For the assurance that such dynamics of pressure maximum point results only from the above-mentioned three factors but not on others (e.g. thermal effects) the experimental results

were confirmed by numerical solutions of the KZK equation, which accounts for focusing, diffraction and nonlinearity.

This work was supported by the Russian Foundation for Basic Research (grant # 04-02-17009), and by the CICYT of the Spanish Government, under the project BFM2002-04369-C04-04.

4K-6 5:45 p.m.
NUMERICAL METHODS FOR AXISYMMETRIC AND 3D NONLINEAR BEAMS.

G. PINTON* and G. TRAHEY, Duke University, Durham, NC.
Corresponding e-mail: gfp@duke.edu

Linear theory provides a suitable approximation for small amplitude waves and although in many cases this approximation is sufficient, a higher order description is necessary where large amplitudes or long propagation lengths and small attenuation is involved. Several numerical methods have been implemented to solve equations that describe nonlinear wave propagation but significant challenges remain in modeling certain pulses and geometries at the initial condition surface.

The axisymmetric Khokhlov—Zabolotzskaya—Kuznetsov (KZK) equation has been solved in the time domain using implicit centered differences and the Crank-Nicolson scheme for both the integral form of the diffraction and absorption operator, and a distorted time solution for the nonlinearity. Here, in addition to these methods, we consider solutions of the KZK equation in axisymmetric and Cartesian coordinates with a number of different numerical techniques. The diffraction is solved using the differential form of the operator for pulsed unfocused waves and focused plane waves. The nonlinearity is solved with the Lax-Friedrichs and Lax-Wendroff methods. These are applied separately to each term in the equations and compared to known solutions for pulsed unfocused waves and continuous focused waves or to frequency domain solutions. Then the combined effect for first and second order operator splitting are determined and compared.

The integral formulation performs better for broadband pulses whereas the differential formulation had less error for narrowband pulses. Methods for the nonlinear step are analyzed with reference to the frequency domain solution. The Lax-Wendroff scheme had the least amount of rms error for all depths. For example at shockwave propagation distance of 0.5 the error is 0.0048 for the Lax-Wendroff scheme, 0.023 for the distorted time method, and 0.16 for the Lax-Friedrichs scheme. Second order operator splitting has a faster convergence to the solution by a factor of five though the slope is the same as first order splitting. Beamplots are presented with numerical calculations based on the optimal methods for narrowband or broadband pulses.

The authors are grateful to J. Trangenstein for discussions on the numerical algorithms. This work was supported by the NIH grant R01-CA43334.

Session: 5K
MICROMECHANICAL AND SAW RESONATORS
Chair: D. Hauden
FEMTO-ST/LPMO

5K-1 4:30 p.m.
SMALL % BANDWIDTH DESIGN OF A 431-MHZ NOTCH-COUPLED MICROMECHANICAL HOLLOW-DISK RING MIXER-FILTER.

S.-S. LI*, Y.-W. LIN, Y. XIE, Z. REN, and C. T.-C. NGUYEN, University of Michigan, Ann Arbor, MI.
Corresponding e-mail: ssli@umich.edu

Notching and low-velocity coupling design strategies are described and demonstrated that yield the first UHF vibrating micromechanical hollow-disk ring mixer-filters with IF bandwidths down to 0.05%, while still retaining reasonable passband shapes. Specifically, a 431-MHz mixer-filter, comprised of two mechanically coupled resonators exhibiting *Q*'s in excess of 10,000, has been successfully demonstrated with a flat passband bandwidth of only 202kHz. Like a previous 34-MHz mixer-filter based on clamped-clamped beam resonators [Wong, *et al*., JMEMS, Feb. 2004], the much higher frequency device of this work is capable of performing both mixing (via capacitive transducer nonlinearity) from an RF frequency down to its IF passband centered at 431MHz, then very small percent bandwidth filtering, e.g., to remove unwanted interferers in the receive path of a communication handset. With *Q*'s >10,000, the resonators in the filter portion of the mixer-filter are well-suited to achieving low insertion loss even for percent bandwidths as small as 0.05%. Such a small percent bandwidth would make possible RF channel-selecting filter banks capable of greatly enhancing the robustness and lowering the power consumption of future wireless transceivers.

The mixer-filters fabricated for this work are composed of two micromechanical hollow-disk ring resonators coupled by a quarter-wavelength longitudinal-mode mechanical spring. The center frequency of the filter portion is determined by the resonance frequency of the constituent resonators, while its bandwidth is set by the coupling spring dimensions and its attachment locations between the resonators. In micromechanical filters, the coupling spring and resonator dimensions are generally on the same order, so the masses of the springs can add to that of the resonators, producing a shift in their designed frequencies. To prevent this, quarter-wavelength coupling is often used on this micro-scale, but this can limit the minimum bandwidth achievable by a given filter. This bandwidth limitation can be circumvented if the coupling beams can attach to the resonators at low velocity locations, i.e., closer to nodal locations. In this work, points closer to nodal locations are accessed by cutting notches into the ring structure of the hollow disk resonators, to allow access to low velocity points close to the nodal circle at the center of the ring.

Using coupling beams attached at notched locations, a 431-MHz hollow-disk micromechanical mixer-filter accepting a 446MHz RF input signal and 15MHz local oscillator achieves a measured percent bandwidth as low as 0.047%, while retaining a relatively flat passband and good combined conversion-insertion loss. The 202kHz bandwidth achieved by this filter is quite close to the intended 200kHz of its design, verifying the precision with which notched-coupling can be used to set filter bandwidth. In addition, equivalent circuits modeling filters using notch-coupling are quite accurate in their predictions.

5K-2 4:45 p.m.
LOW NOISE SILICON MICROMECHANICAL BULK ACOUSTIC WAVE OSCILLATOR.

V. KAAJAKARI*[1], J. KOSKINEN[1], T. MATTILA[1], P. RANTAKARI[2], J. KIIHAMÄKI[1], M. KOSKENVUORI[2], I. TITTONEN[2], and A. OJA[1], [1]VTT Information Technology, P.O.B. 1207, 02044 VTT, Finland, [2]Micronova and Center for New Materials, Helsinki University of Technology, Espoo, Finland.
Corresponding e-mail: ville.kaajakari@vtt.fi

Low phase noise frequency references are required in wireless communications for improved sensitivity and frequency selectivity. Quartz crystal resonators have good short and long term stability (phase noise and drift) but the large size makes the quartz devices unsuitable for on-chip integration. Micromechanical resonators have been researched as a potential alternative to the size consuming quartz crystals. Silicon bulk acoustic wave (BAW) resonators have been demonstrated to have comparable power handling capacity (drive level) as the macroscopic quartz resonators leading to the oscillator floor of -150 dBc/Hz at 13 MHz [1]. Noteworthily, the demonstrated power densities with silicon resonators are orders-of magnitude higher than obtainable with shear mode quartz resonators. Recently narrow gap (d < 200 nm) micromechanical resonators and custom integrated electronics have been used to realize oscillators with bias voltages less than 20 V [2,3].

This paper reports on a 13-MHz micromechanical oscillator design based on a narrow gap BAW resonator. Pierce type oscillator topology is chosen as it provides low phase noise with just a single stage amplifier thus enabling very low power consumption. The sizings of circuit elements are discussed with respect the oscillator stability, power consumption, and phase noise. The critical optimization parameters and design trade-offs are identified. The oscillator performance is simulated using harmonic balance circuit simulation. For the phase noise analysis, a highly efficient and accurate simulation method for a quantitative noise analysis in closed-loop oscillator applications is presented. The 1/f-noise aliasing to carrier side-bands is investigated. The noise multiplication processes in both the amplifier and MEMS resonator are included in the analysis. It is found that the nonlinearities in the electrostatic transduction affect the oscillator near-carrier phase noise performance. The simulated oscillator performance is compared to the experimental oscillator with oscillator core power consumption of 90 μW and noise floor of of -147 dBc/Hz at 13 MHz.

[1] V. Kaajakari, T. Mattila, A. Oja, J. Kiihamäki, and H. Seppä, IEEE Electron Device Lett., 25, 173-175 (2004).

[2] Y.-W. Lin, S. Lee, S.-S. Li, Y. Xie, Z. Ren, and C. T.-C. Nguyen, IEEE J. Solid-State Circuits, 39, 2477–2491, (2004).

[3] P. Rantakari, V. Kaajakari, T. Mattila, J. Kiihamäki, A. Oja, I. Tittonen, and H. Seppä, in Transducers'05, 2005.

5K-3 5:00 p.m.
NANOIMPRINT LITHOGRAPHY FOR RF SAW MANUFACTURE.

W. LIU*, Wuhan Research Institute of Post &Telecommunications, Wuhan, Hubei, China.
Corresponding e-mail: liuwen@wri.com.cn

Nanoimprint lithography technologies have made impressive progress in the last few years. The 10nm line width was reported already. Although nanoimprint lithography technologies haven't been adopt for semiconductor integrated circuit(IC) industry so far, because of the multilayers process issue, the possibility to employ them for the surface acoustic wave (SAW) manufacture has been probed because that most of SAW (surface acoustic wave) device only need one metal layer pattern. The nanoimprint lithography can provide a few benefits for the SAW industry development. At first, to achieve the sub-micro meter process ability, the equipment investment will be significant lower with nanoimprint lithography comparing with the traditional optical method; Secondly, not a SAW company can't afford the 150nm process line so far, because of the SAW device market size isn't that big like the IC demand, but now a low cost nanoimprint lithography fabrication line can do the 150nm work at high production yield, which means the 6~8GHz RF SAW would be available without really heavy investment. The frequency range above 3GHz is the range that SAW technology become weaker when it comparing with dielectric and the FBAR (film-bulk acoustic resonator) filters right now. The nanoimprint lithography technologies also make the RF SPUDT (Single Phase Unidirectional Transducers) SAW filter becomes possible. The author discusses a possibility that with slant SPUDT RF SAW, the RF filter shape factor will be significant improved and a big portion globe frequency resource can be saved for many other wireless applications. The author try to make RF SAW with the nanoimprint lithography process, 70 and 100nm linewidth metal grating strip by nanoimprint lithography were realized. In addition, an embody metal grating strip structure was realized and reported together which we believe will enhance the SAW device high power tolerance.

5K-4 5:15 p.m.
LOW TEMPERATURE BONDING OF INTERFACE ACOUSTIC WAVES RESONATORS ON SILICON WAFERS.

H. MAJJAD*, V. LAUDE, and S. BALLANDRAS, Université de Franche-Comté, Institut FEMTO-ST (UMR 6174), Département LPMO, Besançon, France.
Corresponding e-mail: hicham.majjad@lpmo.edu

High frequency passive devices used in wireless telecommunications are mainly based on surface acoustic wave (SAW) components. The use of interface acoustic waves (IAW) [1], also termed boundary waves, in place of SAW is promising to push back the current limitations (electromechanical coupling, propagation velocities and losses). The IAW principle consists in guiding elastic waves with a polarization similar to those of the bulk waves (pure shear or longitudinal compression) at the interface between two materials; one at least is piezoelectric to allow for the excitation and detection. These interface waves vanish in the depth of the substrates from both sides of the interface with the acousto-electric energy confined at the interface. From this perspective, the realisation of high frequency passive devices based on the coupling of piezoelectric transducers with semiconductor components is attractive. We developed a process which enables the bonding of a 3 inches processed lithium niobate wafer with a silicon substrate. In order to prevent thermal strain due to the thermal expansion coefficients mismatch in the stack, a low temperature wafer bonding (125°C) is performed by enhancing energy surfaces thanks to chemical surface activation. The aluminium interdigital tranducers (IDT) are buried inside the lithium niobate wafer. The problems inherent in surface pollution and the effects of the mechanical vibrations are solved by the self-encapsulation of the component. IDT resonators with 10 μm, 20 μm and 30 μm pitch were manufactured. Back side collective wet etching of the Si wafer in KOH enables access to the pad contacts for measurements. We use a finite element analysis/ boundary integrated method (FEA/BIM) model to discuss the experimental results obtained for the Y-cut and 128° Y-cut LiNbO3 wafers.

Keywords: interface acoustic waves, wafer bonding, lithium niobate, FEA

[1] R. Stoneley, “Elastic waves at the surface of separation of two solids”, Proc. Roy. Soc., vol. A-106, pp. 416-428, 1924.

This work was partially supported by DGA/STTC under contract no. 04.34.017

5K-5 5:30 p.m.
TEMPERATURE COEFFICIENT OF ELASTIC CONSTANTS OF SPUTTERED TEO2 THIN FILM FOR ZERO TCD SAW DEVICES.

N. DEWAN*, M. TOMAR, V. GUPTA, and K. SREENIVAS, Department of Physics and Astrophysics, University of Delhi., Delhi, India.
Corresponding e-mail: namratad20

Temperature stability is found to be very important for the fabrication of high frequency narrow band pass surface acoustic wave (SAW) devices, however, most of the well known piezoelectric materials such as $LiNbO_3$ or $LiTaO_3$ possess high positive temperature coefficient of delay (TCD). Possibility of TCD compensation exists by integrating the device with a negative TCD material of appropriate thickness. SiO_2 and AlN are the only known materials in thin film form having negative temperature coefficient of delay. However, requirement of thick film and low deposition rate, restricts their use to make high frequency (>200 MHz) devices temperature stable. Recently, we have reported that TeO_2 over layer is a very good alternative material for making even low frequency SAW devices temperature stable.

In the present work TeO_2 thin film, sputtered under varying oxygen pressure using a metallic tellurium target, has been deposited on prefabricated 128° Y-X $LiNbO_3$ SAW device (a positive TCD device) operating at 36 MHz center frequency. It is found that TeO_2 film deposited under O_2 + Ar (60% + 40%) gas environment is most suitable as an over layer to yield a temperature stable device at reasonably low thickness. The SAW propagation and TCD characteristics of the TeO_2 /IDTs/128° Y-X $LiNbO_3$ layered structure have been studied. It is found that ~ 0.01 λ thick TeO_2 over-layer reduces the TCD of the device from 76 ppm $°C^{-1}$ to almost zero (~ 2 ppm $°C^{-1}$) without deteriorating its efficiency. Various material parameters of the deposited TeO_2 thin film are determined. The density (ρ) is determined separately by weight gain and thickness measurements, and the elastic constants (C_{11} , C_{44}) and their temperature coefficients (TC (C_{11}), TC (C_{44})) are estimated by fitting the experimental results on velocity and TCD to the theory. The values of elastic constants C_{11} , C_{44} and their temperature coefficients are found to be 1.5 x 10^{10} Nm^{-2} , 6.8 x 10^9 Nm^{-2} , 4.0 x 10^{-2} $°C^{-1}$ and 4.4 x 10^{-2} $°C^{-1}$ respectively, and are deviated in comparison to their respective bulk values. In summary the TeO_2 thin film deposited under 60:40::O_2 :Ar sputtering gas mixture could be utilized as an attractive alternative to conventional materials (SiO_2 or AlN) for temperature compensation of SAW devices.

5K-6 5:45 p.m.
DESIGN OF ASYNCHRONOUS STW RESONATORS FOR FILTERS AND HIGH STABILITY SOURCE APPLICATIONS.

J.-M. FRIEDT*, S. ALZUAGA, N. RATIER, N. VERCELLONI, R. BOUDOT, B. GUICHARDAZ, W. DANIAU, V. LAUDE, and S. BALLANDRAS, FEMTO-ST/ LPMO, Besancon, France.
Corresponding e-mail: jmfriedt@lpmo.edu

The development of high frequency (>500 MHz) resonators and filters requires the use of surface acoustic waves propagating at higher velocity than Rayleigh modes: Shear Transverse Waves (STW) are investigated here in the development of high frequency resonators and filters.

We focus on the effects of varying the shape of the electrodes of the interdigital transducers (IDTs) and mirror grating of the resonator on its transfer function. We have investigated the influence of the metalization ratio (ratio of the width of the fingers to the wavelength) on the operating mode of the resonator, avoiding any period rupture as usually performed in standard asynchronous STW resonators. This approach intends to reduce mode perturbation due to possible conversion from STW to bulk modes when varying the period and hence the operating conditions of the wave.

We demonstrate that the asynchronous configuration — in which the fingers in the cavity are narrower than the fingers in the IDT structure — leads to the reduction of spurious side-modes next to the primary resonance on both the STW and Rayleigh configurations. This effect is expected from modelling using a mixed matrix method. However, the quality factor for resonators applications

is not improved with this configuration. This technique is effective even for resonators above 1 GHz for which theoretical and experimental results are reported.

We display results concerning the transfer functions of synchronous and asynchronous devices for high frequency (ranging from 450 to 1100 MHz) source applications, noise spectra obtained by using these resonators in oscillators and compare these results with models of noise contributions.

This work was supported by the French Direction Générale de l'Armement (DGA) under grant number 04-34-029-00-470-75-65

Session: 6K
MEDICAL SIGNAL PROCESSING AND CONTRAST
Chair: W. Walker
University of Virginia

6K-1 4:30 p.m.
SEPARATING FETAL DOPPLER SIGNALS IN PREGNANCY USING INDEPENDENT COMPONENT ANALYSIS: APPLICATION TO THE EXTRACTION OF FETAL HEART RATE AND GLOBAL MOVEMENT.

A. KRIBECHE*, F. TRANQUART, and L. POURCELOT, INSERM U619, Tours, France.
Corresponding e-mail: ali.kribeche@med.univ-tours.fr

Aim: Fetal heart rate (FHR) monitoring is an integral part of fetal monitoring before and during labour. It contains important indications about the health conditions of fetus, and could become a diagnostic tool of particular importance. Recording fetal movements requires an effective transducer with wide beam. We presented last year a new pulsed Doppler system (called ACTIFOETUS) based on 12 independent transducers placed against the maternal abdomen by means of a supple probe holder. Each transducer detects Doppler signals at 5 different depths between 2 and , and all the output signals are then stored on the hard disc of a personal computer (PC). A major problem caused by the acqusition of such a large amount of data is how to process it and detect and descriminate effectively between the various sources such as FHR, mother heart rate and breathing movements. This paper shows the potential of relevant criteria selection and independent component analysis (ICA) approaches to classify the different sources.

Method: To separate the fetal heart rate, fetal breathing movement and global movement from other sources measured on the maternal body surface, a method employing ICA technique based on Maximum Likelihood (icaML) has been developed in this study. The number of independent observations available is significant (120 low frequency signals : 12×5 generating 60 complex Doppler signals). For this purpose we use Bayesian Information Criterion (BIC) to estimate

the number of relevant sources in a mixture of sources. Consequent signal and data processing techniques have then been implemented for extracting the relevant required parameters needed for characterizing fetal rhythms in line with the objectives of the study. Recording duration for each examination was between 20 and 25 minutes each. The algorithm was tested using simulations and in-vivo ata recorded from 40 pregnant women (32-35 weeks pregnancy) that were enrolled in the ACTIFOETUS study.

Results: The algorithms using ICA technique and implemented on the ACTIFOETUS system were validated successfully on the simulated data and on the 40 in-vivo recordings for computing fetal heart rate and detecting global movements on signals given by each ultrasonic transducer. The results showed a successful separation between the FHR from the other sources aush as Mother Heart Rate and fetal breathing (typical range for MHR is 60 to 100 bpm). The rate of success was 100% in the simulated data and 85% in he in-vivo data.

Conclusions: The ICA-based algorithm showed to be robust enough to be implemented on the ACTIFOETUS system and useful in discriminating between the numerous sources present in the Doppler signal mixture.

The ACTIFOETUS system will serve as a new mean for studying fetal response to its environment and also for detecting anomalies related to fetal suffering.

This work was supported by the Centre Regional Council, the French Institute of Health and Medical Research (INSERM) and Ultrasons Technologies Company, France.

6K-2 4:45 p.m.
WAVEFORM SYNTHESIS AND FILTER DESIGN FOR HIGH FREQUENCY IMAGING OF TISSUE ENGINEERED HEART VALVES.

D. LIU*, H. LEE, and E. S. EBBINI, University of Minnesota, Minneapolis, MN. Corresponding e-mail: emad@umn.edu

A high frequency ultrasound system for imaging tissue-engineered cardiovascular valves for aortic valve replacement is being developed. The goal is to image and characterize the elastic properties of the fibrillar biopolymer gel (type I collagen or fibrin) at various stages of development. In the early stages, the ultrasound backscatter signal from entrapped tissue cells and the fibrin is too small to provide a measurable signal to noise with conventional pulse-echo technique. Therefore, we have employed multi-waveform coded excitation and filter-bank receive processing for improving the contrast of the imaging system while maintaining the axial resolution. Both PZT (20 MHz, 70% BW) and PVDF (25 MHz, 100 % BW) transducers were used in conjunction with a 13-bit 200 MS/sec arbitrary waveform generator and a custom-designed 50 MHz broadband amplifier. The system also has servo-based sector scanning capability with synchronized data collection with motor position. The system employs a finite number of coded waveforms with good compression properties (e.g. linear and quadratic chirps with Gaussian amplitude modulation). A filter bank at the receiver side decomposes and compresses the received signal and recombines the samples using a local SNR-based weighting algorithm. The resulting compressed

RF signal shows significant reduction in both near-end and far-out sidelobes without loss in axial resolution. Images from wire targets, Plexiglas flat reflector, tissue-engineered valves as well as *in vivo* from the palm of a human volunteer. In every case, comparisons of the reconstructed RF signal with RF signals resulting from conventional pulse-echo and conventional compression of coded waveforms was made. As an example, when using a combination of 4 microsecond chirps (linear and quadratic with increasing and decreasing frequency), the range near-end and far-out range sidelobes were reduced by 7 dB and 5 dB, respectively. It should be noted that averaging compressed echoes from any one code results in reduction of far-out sidelobes only. The 6-dB and 20-dB resolution was the same as the conventional pulse-echo and better than conventional pulse compression with a linear chirp excitation. *In vitro* and *in vivo* images obtained from the multi-waveform transmission exhibited improved penetration depth (compared with conventional pulse-echo and conventional compression) and retained the fine speckle characteristics of the tissue being image. The mathematical basis for the waveform selection and the filter-bank reconstruction will be described and discussed with illustrative *in vitro* and *in vivo* imaging examples.

Funded by NIH Grant R01 HL71538.

6K-3 5:00 p.m.
PHASE CORRECTION OF SKULL ABERRATION WITH 1.75-D AND 2-D ARRAYS USING SPECKLE TARGETS.

J. J. DAHL*, N. M. IVANCEVICH, C. G. KEEN, G. E. TRAHEY, and S. W. SMITH, Duke University, Durham, NC.
Corresponding e-mail: jjd@duke.edu

Imaging the brain with ultrasound is a difficult process because the skull has a significantly higher speed of sound (approximately 3000 m/s) than soft tissues (nominally 1540 m/s). At such a large discrepancy in sound speed, the phase and amplitude of the ultrasound wave become severely distorted, resulting in significant degradation in beam focusing and image quality. Compensation for phase distortion in the skull can restore image quality; however the lack of point targets and the low SNR in the brain parenchyma make aberration correction difficult.

We present images with polymer casts of skull bone aberrators that have been improved with near-field phase correction algorithms using speckle targets for estimation of the phase profile. A tissue-mimicking phantom with 4 mm spherical voids (RMI 408) was used as the imaging medium, and a section of skull was placed between the transducers and the phantom to generate an aberrating layer. Multi-lag cross-correlation and multi-lag speckle brightness algorithms were used to perform phase correction on a Siemens Antares™ scanner using a 3.5 MHz, 1.75-D transducer (8×96 elements yields an aperture of 8 mm × 19.4 mm)(Tetrad Corp., Englewood, CO). Phase correction with the 1.75-D array was performed in less than 1.4 seconds.

For example, measurements of an aberration profile induced by the skull indicated an aberrator with an rms strength of 66.7 ns and correlation length of 4.2 mm

using the multi-lag cross-correlation algorithm. The contrast-to-speckle ratio (CSR) of the spherical voids was computed in the control, aberrated, and phase corrected images in order to compare image quality. The mean CSR of 24 visible lesions in the control image was 1.57 ± 0.36. In the aberrated image, 6 lesions were visible with a mean CSR of 1.16 ± 0.39. With receive-only phase correction applied, 11 lesions were visible with a mean CSR of 1.52 ± 0.37 using the multi-lag cross-correlation algorithm.

Using a 2.5 MHz, 14 mm diameter 2-D array of 440 transmit elements and 256 receive elements on a real time 3-D scanner (Volumetrics Medical Imaging Inc, Durham, NC) and the same RMI phantom, the skull aberrator was measured with the multi-lag cross-correlation method on four different image lines (θ, ϕ = ± 7°), and had an average RMS phase-error of 50.5 ns and average correlation length of 1.6 mm. Again, CSR was used as a metric of image quality. In this experiment, the average CSR measured over four lesions improved from 1.02 ± 0.37 to 1.41 ± 0.53.

This research is supported by the NIH with grant R01-CA43334 and with technical support by the Ultrasound Division at Siemens Medical Solutions USA, Inc.

6K-4 5:15 p.m.
ABERRATION AND SECOND HARMONIC IMAGING.

T. VARSLOT*, S. E. MÅSØY, and B. A. ANGELSEN, Norwegian University of Science and Technology, Trondheim, Norway.
Corresponding e-mail: varslot@math.ntnu.no

Simulations are presented which indicate that imaging at the second harmonic frequency does not solve the problem of wavefront aberration. The nonlinearity of acoustic wave propagation in biological tissue is routinely exploited in medical imaging, since the larger signal-to-noise ratio leads to better image quality in many applications. The major sources of noise in ultrasound images are aberration and multiple reflections between the transducer and tissue structures (reverberations), both of which are the result of large spatial variations in the acoustic properties of the tissue. These variations mainly occur close to the body surface, i.e. the body wall. As a result, the nonlinearly-generated second harmonic is believed to alleviate both reverberations and aberrations. However, in the case of aberration, the second harmonic is generated by an aberrated pulse. Thus the second harmonic will also experience considerable aberration even if it is generated at a greater depth. Propagation of the acoustic backscatter through the body wall will expose the pulse to further aberration, equivalent to that of linear fundamental imaging.

A 3D numerical experiment was conducted using a simulation setup capable of capturing nonlinear propagation and absorption in heterogeneous tissue. An ultrasound pulse of 2.5 MHz, using an aperture of 2.0 cm focused at 6.0 cm, was propagated through a body wall model with aberration characteristics comparable to published measurements of the human abdominal wall. In the focal region the forward propagating pulse was scattered by a uniform distribution of point scatterers. The acoustic backscatter was then propagated back through the body wall model, forming a simulated transmit/receive beam. For comparison, a linear simulation was performed with a 5.0 MHz transmit pulse.

In comparing transmit-beam profiles in the focal plane, somewhat reduced side-lobe levels were observed for the second harmonic at 5.0 MHz compared to that of the 5.0 MHz linearly-propagated transmit-pulse. This is explained mainly by the fact that a lower frequency will experience less aberration than a higher frequency. Thus the transmit-pulse of 2.5 MHz is less aberrated than the 5.0 MHz transmit pulse.

The receive beam-profile for the second harmonic is similar to that of the linearly-propagated 5.0 MHz pulse. The total aberration of the combined transmit-receive beam is therefore also significant for harmonic imaging.

Furthermore, in an imaging system where the signal level of the second harmonic in the focal zone may be 20dB lower than that of the fundamental, the influence of aberration of the second harmonic will be more significant than for the fundamental. The presented results indicate that the observed improvement in image quality using harmonic imaging is associated with the reduction of reverberations, rather than reduced aberration.

Aberration correction will, however, restore the beam profiles just like it does for linear imaging modes.

Funding for this work was provided by the Norwegian University of Science and Technology.

6K-5 5:30 p.m.
QUADRATIC B-MODE (QB-MODE) IMAGING WITH CHIRPTRANSMIT WAVEFORMS.

D. CECCHINI, H. YAO, and E. S. EBBINI*, University of Minnesota, Minneapolis, MN.
Corresponding e-mail: emad@umn.edu

QB-mode imaging employs second order Volterra filters to separate quadratic components from beamformed RF data resulting in images with improved contrast and increased dynamic range. QB-mode imaging does not require pulse

sequences to separate linear from nonlinear echo signal components thus preserving the frame rate of the imaging system. Furthermore, quadratic Volterra kernels can be obtained from imaging data and have been shown to detect any quadratic interaction ($f_1 + f_2 = f$) throughout the bandwidth of the transducer. This means that, unlike harmonic imaging, wideband transmit pulses can be used thus preserving the resolution of the imaging system. In this paper, we present the first demonstration of the use of QB-mode imaging with coded waveforms. Image data were collected from a flow phantom using linear and quadratic chirp waveforms of 6.5 μs duration. BR14 UCA microbubbles (dilution 1:100000) were circulated in one channel while cellulose microspheres (linear scatterers) were circulated in a parallel channel. Chirp waveforms with very low to low MI (~ 0.02 - 0.1) covering the frequency band of 1.5 - 3.7 MHz using the CA421 abdominal probe on the Technos MPX (Esaote, S.p.A., Genoa, Italy).

Sensitivity to UCA at the given dilution was established with and without compression. Conventional matched filter compression achieved a slight, but measurable increase in specificity. QB-mode images were formed after

conventional pulse compression and have shown significant increase in specificity. This was quantified by

evaluating the contrast-to-tissue ratio (CTR) for the UCA channel. For example, with linear chirp waveform, the average CTR from 18 frames was 3.2, 5.4, and 14.3 for the uncompressed, compressed, and quadratically filtered compressed data. On the other hand, the average linear-scatterer to tissue ratio (LSTR) was -1.2, -2.8, and -4.7 for the uncompressed, compressed, and quadratically filtered compressed data. Resolution measurements from a CIRS Model 40 quality assurance phantom give a 6-dB axial resolution of 2.06, 0.75, and 0.79 mm for the uncompressed, compressed, and the quadratically filtered compressed data. We will show that the nonlinear bubble oscillations ocurred primarily at 2 MHz, i.e., within the fundamental band of the transmit waveform. We explain these results by showing the underlying 2D frequency response of the quadratic kernel. The results show that the kernel is sensitive to interactions at the ± 2 and 4 MHz frequency components. We show that the kernel adds up these sum and difference frequencies in a way that is unique to quadratic filtering, i.e. not possible with harmonic filtering.

Funded by a grant from Esaote, S.p.A., Genoa, Italy.

6K-6 5:45 p.m.
ULTRASOUND CONTRAST AGENTS FOR BLEEDING DETECTION AND ACOUSTIC HEMOSTASIS.

V. ZDERIC*[1], L. CRUM[1,2], and S. VAEZY[1,2], [1]Center for Industrial and Medical Ultrasound, Applied Physics Laboratory, University of Washington, Seattle, WA, [2]Department of Bioengineering, University of Washington, Seattle, WA.
Corresponding e-mail: vesna@u.washington.edu

Objective. To investigate the potential use of ultrasound contrast agents (UCA) in both therapeutic and diagnostic aspects of ultrasound-guided HIFU therapy. **Introduction.** In our previous experiments, HIFU-induced hemostasis was achieved faster in the presence of UCA Optison. In the current studies, we investigated mechanisms of enhancement of HIFU-induced hemostasis in the presence of Optison as well as UCA-enhanced detection of bleeding. **Methods.** In bleeding detection experiments, triangular incisions (3 cm long, 0.5 cm deep) were made in the posterior liver surface in heparinized rabbits. Bleeding detection was performed with Color Doppler ultrasound, before and after injection of UCA Optison (~0.1 ml/Kg). In HIFU therapy experiments, incisions were produced in the anterior surface of the rabbit liver. A HIFU applicator (5.5 MHz, 6,400 W/cm^2 in situ) was scanned over the incision until hemostasis was achieved. Optison solution (0.8, 1.2, or 1.8 ml) was injected into a mesenteric vein, 20 s before the start of HIFU application. The tension strength of the hemostatic incisions was determined as the applied force at which the incision started to bleed. Temperature was measured using infrared thermal camera and a thermocouple (0.13 mm in diameter) positioned at 3 mm from the HIFU focus. The broadband noise, an indication of inertial cavitation activity, was measured in the frequency range of 18-21 MHz. **Results.** *Bleeding Detection:* Hidden bleedings could not be detected before Optison injection. First appearance of color enhancement localized at the bleeding liver site occurred 15 s after Optison injection, and

lasted for a minute. *Hemostasis:* The tension strength at which the hemostatic liver incisions started to bleed was 1.3 +/- 0.8 N, 1.3 +/- 0.5 N and 0.8 +/- 0.3 N for HIFU, Optison+HIFU, and electrocautery treatments, respectively. Histological observations showed similar appearance of the HIFU lesions produced in the presence of Optison and control HIFU lesions. The concentration of free hemoglobin in blood (indication of blood hemolysis) was 19 +/- 18 ml/dL after HIFU treatment, and 76 +/- 46 ml/dL after HIFU+Optison treatment. The coagulum formation times were 9, 7, 5 and 4 s at Optison concentrations of 0, 0.8, 1.2 and 1.8 mL, respectively. The coagulum surface temperature was on average 76 deg C (independent on Optison concentration). The maximal temperature inside the bleeding liver incisions was 18 deg C higher during HIFU+Optison treatments as compared to HIFU only treatments (71.4 +/- 9.7 deg C for HIFU only treatment, 89.4 +/- 15.8 deg C for HIFU+Optison treatment, $p<0.05$). The broadband noise measured during HIFU sealing of liver incisions appeared to be 45% higher in the presence of Optison. **Conclusion.** The enhancement of HIFU-induced hemostasis in the presence of Optison appeared to be due to a combination of mechanical and thermal mechanisms. The presence of UCA resulted in both better visualization of bleeding sites and faster formation of the coagulum over the liver incisions during acoustic hemostasis.

NSBRI

ALL AUTHOR INDEX

Please Note:
The Author Index is created directly and automatically from the abstracts. If an author's name is typed differently on multiple abstracts, the entries in the author index will reflect these discrepancies.

DE DOELEN FLOOR PLAN

ground floor

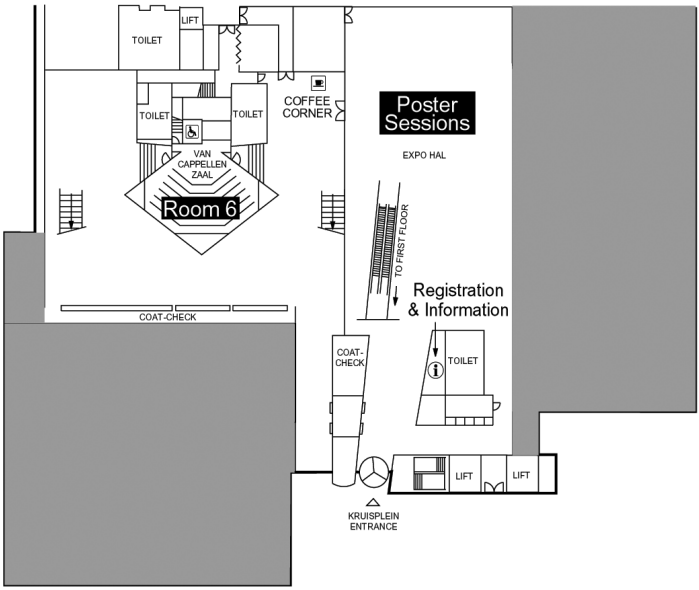

first floor

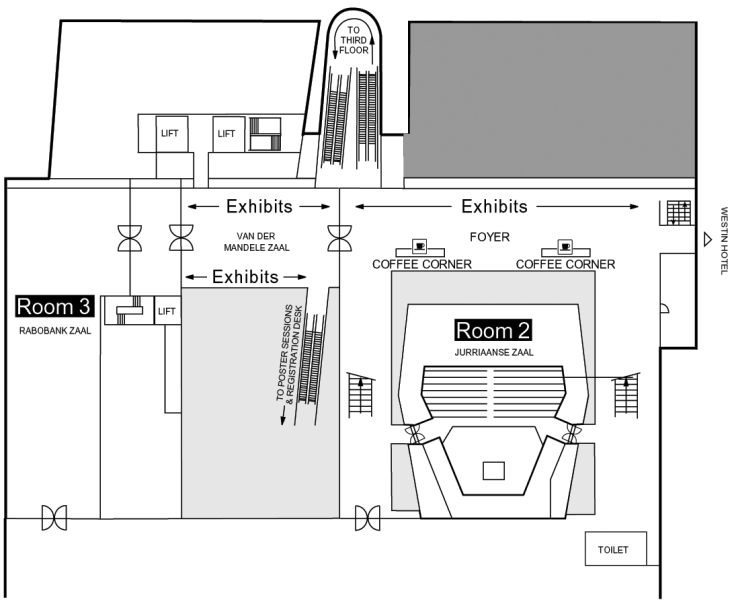

third floor

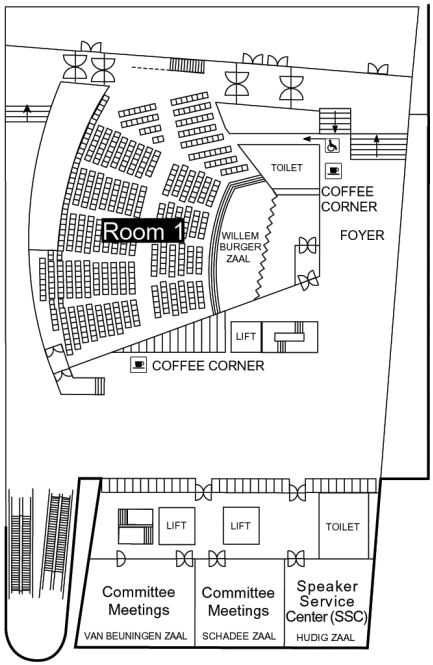

fourth floor